



Proceedings from
the 9th International Conference on
Pedestrian and Evacuation Dynamics

August 21-24, 2018
Lund, Sweden

RISE Research Institutes of Sweden AB
ISBN: 978-91-89049-84-0
DOI: <http://dx.doi.org/10.17815/CD.2020.26>
Borås

Preface

It is our pleasure to hand over to you this book of proceedings for the 9th international conference on pedestrian and evacuation dynamics, held on August 21-24, 2018 in Lund, Sweden. The conference was organized by RISE Research Institutes of Sweden in collaboration with Lund University. The three-day conference hosted about 135 participants.

Every day at the conference was introduced by a keynote lecture. The first lecture Putting the Pedestrian back into PED: the need to reunite our diverging field held by Dr. Aoife Hunt, Associate Director and specialist in crowd planning at Movement Strategies AS. The second day was opened with the lecture Pedestrian movement in buildings using BIM (Building Information Modelling) by Jan Karlshøj, Associate Professor at the Technical University of Denmark. The topic of day three was Universal design - accounting for people by Per Olof Hedvall from Associate Professor at Lund University and head of Certec, the center for Rehabilitation Engineering and Design.

The scientific program of the PED conference included many topics related to pedestrian dynamics as well as evacuation. The parallel sessions covered the following areas:

- Data collection
- Experimental evacuation
- Human behaviour
- Model development
- Simulations

The papers peer reviewed and published as open source by RISE and Collective Dynamics. We are very proud to present the peer reviewed papers. The publications demonstrate a significant scientific depth and also a high societal relevance.

Anne Dederichs, Gerta Köster, Andreas Schadschneider

Table of Contents

DATA COLLECTION

- Pedestrian flow characteristics at upstream and downstream of bottleneck for unidirectional flow under normal conditions 12
Siddhartha Gulhare, Aparna P M & Ashish Verma
Department of Civil Engineering, Indian Institute of Science, Bangalore, India
- Data archive for exploring pedestrian dynamics and its application in dimensioning of facilities for multidirectional streams 19
Maik Boltes, Stefan Holl & Armin Seyfried
Institute for Advanced Simulation, Forschungszentrum Jülich, Jülich, Germany
- Lane formation beyond intuition - towards an automated characterization of lanes in counter-flows 27
Luca Crociani¹, Giuseppe Vizzari¹, Andrea Gorrini¹ & Stefania Bandini^{1,2}
¹*Complex Systems and Artificial Intelligence research center, University of Milano-Bicocca, Milano, Italy*
²*Research Center on Advanced Science and Technology, The University of Tokyo, Tokyo, Japan*
- Accurate pedestrian localization in overhead depth images via height-Augmented HOG 35
Werner Kroneman, Alessandro Corbetta & Federico Toschi
Eindhoven University of Technology, Department of Applied Physics, Eindhoven, The Netherlands
- Anomaly detection of pedestrian flow: A machine learning method for monitoring-data of visitors to a building 43
Kentaro Kumagai
Graduate School of Management, Kyoto University and Disaster Prevention Research Institute, Kyoto University, Kyoto, Japan
- Analysis of distracted pedestrians' waiting time: Head-Mounted Immersive Virtual Reality application 48
Arash Kalatian¹, Anae Sobhani² & Bilal Farooq¹
¹*Ryerson University, Toronto, Ontario, Canada*
²*Utrecht University, Utrecht, The Netherlands*
- Compression of pedestrian crowd in corner turning - subject experiment-based analysis of walking trajectories 55
Mineko Imanishi¹ & Tomonori Sano²
¹*Fire Protection Engineering Group/Takenaka Research & Development Institute, Inzai, Chiba, Japan,*
²*Faculty of Human Sciences/Waseda University, Tokorozawa, Saitama, Japan*
- A large-scale real-life crowd steering experiment via arrow-like stimuli 63
Alessandro Corbetta¹, Werner Kroneman¹, Maurice Donners², Antal Haans³, Philip Ross⁴, Marius Trouwborst², Sander Van de Wijdeven², Martijn Hultermans², Dragan Sekulovski², Fedosja van der Heijden², Sjoerd Mentink² & Federico Toschi¹
¹*Department of Applied Physics, Eindhoven University of Technology, NL*
²*Philips Lighting, Eindhoven, NL*
³*Human Technology Interaction, Eindhoven University of Technology, NL*
⁴*Studio Philip Ross, Eindhoven, NL*
- Field theory in practice 71
José Méndez Omaña
Beuth-Hochschule für Technik Berlin, Berlin, Germany
- Experimental study on the evading behaviour of single pedestrians encountering an obstacle 79
Xiaolu Jia¹, Claudio Feliciani², Daichi Yanagisawa^{2,3} & Katsuhiro Nishinari^{2,3}
¹*Department of Advanced Interdisciplinary Studies, School of Engineering, The University of Tokyo, Tokyo, Japan*
²*Research Center for Advanced Science and Technology, The University of Tokyo, Tokyo, Japan*
³*Department of Aeronautics and Astronautics, Graduate School of Engineering, The University of Tokyo, Tokyo, Japan*

Unidirectional and bidirectional flow in a narrow corridor with body rotation <i>Daichi Yanagisawa^{1,2}, Claudio Feliciani¹ & Katsuhiro Nishinari^{1,2}</i> ¹ Research Center for Advanced Science and Technology, The University of Tokyo, Tokyo, Japan ² Department of Aeronautics and Astronautics, School of Engineering, The University of Tokyo, Tokyo, Japan	87
Grouping behaviour and decision making in road tunnels evacuation in smoke conditions - Experimental approach <i>Jarosław Wąs¹, Jakub Porzycki¹ & Natalia Schmidt – Polończyk²</i> ¹ AGH University of Science and Technology, Institute of Applied Computer Science, Faculty of Electrical Engineering, Automatics, Computer Science and Biomedical Engineering, Kraków, Poland ² AGH University of Science and Technology, Faculty of Mining and Geoengineering, Kraków, Poland	95
Single-file movement of ants stressed by a high temperature <i>Qiao Wang^{1,2}, Weiguo Song¹, Shujie Wang¹ & Siuming Lo²</i> ¹ State Key Laboratory of Fire Science, USTC, Hefei, China ² Department of Architectural and Civil Engineering, CityU, Hong Kong, China	100
A study of evacuation efficiency of a hopper-shape exit by using mice under competition <i>Lin Peng, Wang Guoyuan, Wu Fanyu & Gao Dongli</i> <i>Faculty of Geosciences and Environmental Engineering, Southwest Jiaotong University, Chengdu, China</i>	109
Social group behaviour of triads. Dependence on purpose and gender <i>Francesco Zanlungo¹, Zeynep Yücel² & Takayuki Kanda^{1,3}</i> ¹ ATR IRC, Kyoto, Japan, ² Okayama University, Okayama, Japan, ³ Kyoto University, Kyoto, Japan	120
Experimental study on the influence of background music on pedestrian movement in high densities <i>Guang Zeng^{1,2}, Andreas Schadschneider², Jun Zhang¹ & Weiguo Song¹</i> ¹ State Key Laboratory of Fire Science, University of Science and Technology of China, Hefei, China ² Theoretical Physics Institution, University of Cologne, Cologne, Germany	128
Can we learn where people go? <i>Marion Gödel^{1,2}, Gerta Köster¹, Daniel Lehmbert^{1,2}, Manfred Gruber¹, Angelika Kneidl³ & Florian Sesser³</i> ¹ Munich University of Applied Sciences, Munich, Germany ² Technical University of Munich, Munich, Germany ³ accu.rate GmbH Institute for crowd simulation, Munich, Germany	136
EXPERIMENTAL EVACUATION	
Evacuation data from a hospital outpatient drill: the case study of North Shore Hospital <i>Anass Rahouti¹, Ruggiero Lovreglio², Phil Jackson³ & Sélim Datoussaïd¹</i> ¹ Faculty of Engineering / UMONS, Mons, Belgium ² School of Built Environment / Massey University, Auckland, New Zealand ³ Waitemata District Health Board / WDHB, Auckland, New Zealand	144
Investigation of pedestrian evacuation scenarios through congestion level and crowd danger <i>Claudio Feliciani¹ & Katsuhiro Nishinari^{1,2}</i> ¹ Research Center for Advanced Science and Technology, The University of Tokyo, Tokyo, Japan ² Department of Aeronautics and Astronautics, Graduate School of Engineering, The University of Tokyo, Tokyo, Japan	152
HUMAN BEHAVIOUR	
Comparing different metrics quantifying pedestrian safety <i>Arne Hillebrand, Han Hoogeveen & Roland Geraerts</i> <i>Department of Information and Computing Sciences, Utrecht University, Utrecht, The Netherlands</i>	160

Effect of architectural adjustments on pedestrian flow at bottleneck <i>Jianyu Wang¹, Jian Ma¹ & Peng Lin²</i> ¹ <i>School of Transportation and Logistics/Southwest Jiaotong University, Sichuan, China</i> ² <i>Faculty of Geoscience and Environmental Engineering/Southwest Jiaotong University, Sichuan, China</i>	169
The development of drunk behaviour during evacuation <i>Simeon A. Doychinov¹ & Anne S. Dederichs^{1,2}</i> ¹ <i>Dept. Civil Engineering, Technical University of Denmark, Copenhagen, Denmark</i> ² <i>RISE Research Institutes of Sweden, Borås, Sweden</i>	175
Movement parameters of persons with disabilities on evacuation by lifts <i>Martin Szénay & Martin Lopusniak</i> <i>Institute of Architectural Engineering, Faculty of Civil Engineering, Technical University of Kosice, Kosice, Slovak Republic</i>	183
Crowding and queuing in entrance scenarios: Influence of corridor width in front of bottlenecks <i>Juliane Adrian¹, Maik Boltes¹, Stefan Holl¹, Anna Sieben² & Armin Seyfried^{1,3}</i> ¹ <i>Institute for Advanced Simulation, IAS-7: Civil Safety Research, Forschungszentrum Jülich, Jülich, Germany</i> ² <i>Chair of Social Theory and Social Psychology, Ruhr-Universität Bochum, Bochum, Germany</i> ³ <i>School of Architecture and Civil Engineering, University of Wuppertal, Wuppertal, Germany</i>	191
Safe evacuation for all. A top 10 list of requirements <i>Laura Künzer, Gesine Hofinger & Robert Zinke</i> <i>Team HF Human Factors Research and Training, Hofinger, Künzer & Mähler PartG, Ludwigsburg, Germany</i>	199
Evacuation guidance design: An experimental study based on eye tracking devices <i>Ning Ding¹, Tao Chen² & Yuan Liu³</i> ¹ <i>School of Criminal Investigation and Counter-Terrorism, People's Public Security University of China, Beijing, China</i> ² <i>Institute of Public Safety Research, Department of Engineering Physics, Tsinghua University, Beijing, China</i> ³ <i>Institute of Economics, School of Social Sciences, Tsinghua University, Beijing, China</i>	207
Dynamic guidance by colored running lights and affordance: Route choices of adults and older children <i>Laura Künzer, Robert Zinke & Gesine Hofinger</i> <i>Team HF Human Factors Research and Training, Hofinger, Künzer & Mähler PartG, Ludwigsburg, Germany</i>	216
Estimating social relation from trajectories <i>Zeynep Yucel¹, Francesco Zanlungo², Claudio Feliciani³, Adrien Gregorj¹ & Takayuki Kanda^{2,4}</i> ¹ <i>Okayama University, Okayama, Japan,</i> ² <i>ATR IRC, Kyoto, Japan</i> ³ <i>University of Tokyo, Tokyo, Japan,</i> ⁴ <i>Kyoto University, Kyoto, Japan</i>	224
Experimental study on variation strategies for complex social pedestrian groups in conflict conditions <i>Xiaolei Zou¹, Xiaoyi Qu² & Ruihua Xu¹</i> ¹ <i>College of Transportation Engineering, Tongji University, Shanghai, China</i> ² <i>College of Public Safety Management, Shanghai Open University, Shanghai, China</i>	232
Measuring social influence and group formation during evacuation process <i>Adriana Balboa, Arturo Cuesta & Daniel Alvear</i> <i>University of Cantabria, Los Castros, Santander, Spain</i>	240
The influence of physical and mental constraints to a stream of people through a bottleneck <i>Paul Geoerg¹, Jette Schumann², Maik Boltes², Stefan Holl² & Anja Hofmann¹</i> ¹ <i>Bundesanstalt für Materialforschung und -prüfung, Berlin, Germany</i> ² <i>Forschungszentrum Jülich GmbH, Jülich, Germany</i>	248

Evacuation characteristics of preschool children through bottlenecks <i>Jun Zhang, Hongliu Li, Yanghui Hu & Weiguo Song</i> <i>State Key Laboratory of Fire Science, University of Science and Technology of China, Hefei, Anhui, China</i>	255
Analysis of built environment influence on pedestrian route choice behavior in Dutch Design Week using GPS Data <i>Yanan Liu, Dujuan Yang, Bauke de Vries & Harry J.P. Timmermans</i> <i>Built Environment, Eindhoven University of Technology, Eindhoven, The Netherlands</i>	264
The Modelling of Pedestrian Vehicle Interaction for Post-Exiting Behaviour <i>Peter J Lawrence, Veronica Pellacini & Edwin R Galea</i> <i>Fire Safety Engineering Group, University Of Greenwich, Old Royal Naval College, London, UK</i>	273
MODEL DEVELOPMENT	
Modelling and simulation of urban mobile agents for analyzing mixed flows in urban pedestrian space <i>Toshiyuki Kaneda¹, Masahiro Shohmitsu¹, Wataru Sasabe¹ & Yuanyuan Liu^{1,2}</i> <i>¹Graduate School of Engineering, Nagoya Institute of Technology, Nagoya, Japan</i> <i>²College of Architecture and Urban Planning, Tongji University, Shanghai, China</i>	282
An artificial neural network framework for pedestrian walking behavior modeling and simulation <i>Peter M. Kielar & André Borrmann</i> <i>Chair of Computational Modeling and Simulation, Technische Universität München, Munich, Germany</i>	292
A method for joint estimation of homogeneous model parameters and heterogeneous desired speeds <i>Fredrik Johansson</i> <i>Swedish National Road and Transport Research Institute (VTI), Gothenburg, Sweden</i>	301
Analysis of alighting and boarding movement laws in subway using modified social force model <i>Feng Chen^{1,2}, Yongxin Gao¹, Zijia Wang¹ & Yan Liu¹</i> <i>¹School of Civil Engineering, Beijing Jiaotong University, Beijing, China</i> <i>²Beijing Engineering and Technology Research Center of Rail Transit Line Safety and Disaster Prevention, Beijing, China</i>	309
Concept of a decision-based pedestrian model <i>Cornelia von Krüchten¹ & Andreas Schadschneider^{1,2}</i> <i>¹Institut für Theoretische Physik, Universität zu Köln, Cologne, Germany</i> <i>²Institut für Physikdidaktik, Universität zu Köln, Cologne, Germany</i>	318
Pedestrian collision avoidance with a local dynamic goal <i>Rafael F. Martin¹ & Daniel R. Parisi^{1,2}</i> <i>¹Instituto Tecnológico de Buenos Aires, Lavardén 315, C. A. de Buenos Aires, Argentina</i> <i>²Comisión Nacional de Investigaciones Científicas y Técnicas (CONICET), Argentina</i>	326
The difference between individuals and social groups in multidirectional movement <i>Yanghui Hu, Jun Zhang & Weiguo Song</i> <i>State Key Laboratory of Fire Science, University of Science and Technology of China, Hefei, China</i>	334
Parameter calibration in crowd simulation models using approximate Bayesian computation <i>Nikolai W.F. Bode</i> <i>Department of Engineering Mathematics, University of Bristol, Bristol, UK</i>	342
Movement characteristics of processions <i>Petros Polichronidis & Michael Schreckenberg</i> <i>Physik von Transport und Verkehr/Universität Duisburg-Essen, Duisburg, Germany</i>	350
Noise-induced stop-and-go dynamics in pedestrian single-file motion <i>Andreas Schadschneider¹ & Antoine Tordeux²</i> <i>¹Institut für Theoretische Physik, Universität zu Köln, Köln, Germany</i> <i>²Institut für Sicherheitstechnik, Bergische Universität Wuppertal, Wuppertal, Germany</i>	358

Tsunami evacuation facility choice behavior model in flat area and rias area considering possibility to remain at home <i>Hiroyuki Yoshihara & Tatsuya Kishimoto</i> <i>Graduate School of Science and Technology, Keio Univ., Yokohama City, Japan</i>	366
Modelling emergency evacuation of classroom with different age profiles <i>Lakshmi Devi Vanumu¹, Aditya Arya², Hari Krishna Gaddam³, K. Ramachandra Rao⁴</i> <i>^{1,2,3,4} Indian Institute of Technology, Delhi, Hauz Khas, New Delhi, India</i>	374
Interdependence of flows when merge in rail tunnel evacuations <i>Adriana Balboa, Daniel Alvear & Orlando Abreu</i> <i>University of Cantabria, Santander, Spain</i>	382
Bridging the gap - why we need to enhance common simulation models <i>Angelika Kneidl</i> <i>Accu:rate GmBH, Munich Germany</i>	390
SIMULATIONS	
Determination of pedestrian's personal space in mass religious gatherings - A case study of Kumbh mela <i>Aparna P M, Karthika P Sobhana & Ashish Verma</i> <i>Department of Civil Engineering, Indian Institute of Science, Bangalore, India</i>	396
Understanding Crowd Dynamics in Processions during Mass Religious Gatherings - A case study of Shahi Snan in Kumbh Mela <i>H Gayathri¹, Siddhartha Gulhare², Ashish Verma^{3*}</i> <i>¹Research Scholar,</i> <i>² ex- Project Associate, Department of Civil Engineering, Indian Institute of Science (IISc), Bangalore 560012,</i> <i>³ Associate professor, Department of Civil Engineering and Robert Bosch Centre for Cyber Physical Systems, Indian Institute of Science (IISc), Bangalore 560012, India</i>	404
Investigating pedestrians' obstacle avoidance behavior <i>Abdullah Alhawsawi^{1,2}, Majid Sarvi¹, Milad Haghani¹ & Abbas Rajabifard¹</i> <i>¹Transport Engineering Group, School of Engineering, Department of Infrastructure Engineering, The University of Melbourne, Victoria, Australia</i> <i>²Hajj and Umrah Institute, Umm Al-Quran University, Makkah, KSA</i>	414
A Markov-chain activity-based model for pedestrians in office buildings <i>Sanmay Shelat¹, Winnie Daamen¹, Bjorn Kaag², Dorine Duives¹ & Serge Hoogendoorn¹</i> <i>¹Department of Transport and Planning, Delft University of Technology, Delft, The Netherlands</i> <i>²Argosonic, The Netherlands</i>	424
Incorporation of elevator evacuation from a specific floor - A numerical study of an office building <i>Johanna Hammarberg¹, Håkan Niva² & Axel Mossberg³</i> <i>¹Briab – Brand & Riskingenjörerna AB, Stockholm, Sweden</i> <i>²Briab – Brand & Riskingenjörerna AB, Malmö, Sweden</i> <i>³Brandskyddslaget AB, Stockholm, Sweden</i>	432
Thermodynamics of a gas of pedestrians: theory and experiment <i>Claudio Feliciani¹, Francesco Zanlungo², Katsuhiro Nishinari^{1,3}, Takayuki Kanda^{2,4}</i> <i>¹ Research Center for Advanced Science and Technology, The University of Tokyo</i> <i>4-6-1 Komaba, Meguro-ku, Tokyo 153-8904, Japan,</i> <i>² Advanced Telecommunications Research Institute International 2-2-2 Hikaridai Seika-cho, Sorakugun, Kyoto 619-0288, Japan</i> <i>³ Department of Aeronautics and Astronautics, Graduate School of Engineering, The University of Tokyo, 7-3-1 Hongo, Bunkyo-ku, Tokyo 113-8656, Japan</i> <i>⁴ Department of Social Informatics, Graduate School of Informatics, Kyoto University</i> <i>36-1 Yoshida-Honmachi, Sakyo-ku, Kyoto 606-8501, Japan</i>	440

- Towards real-time monitoring of the Hajj 448
Muhammad Baqui & Rainald Löhner
CFD Center/George Mason University, VA, USA
- POSTERS**
- A Case for Identity Hierarchies in Simulating Social Groups 457
Platt A.¹, Kneidl A.²
^{1,2}accu:rate GmbH Rosental 5, Munich, Germany
- A new framework for high-resolution pedestrian data processing using rule-based algorithms and real-time alarm systems 460
Michael Moos¹, Basil Vitins², Mirwais Tayebi³, Lukas Gamper⁴, Julia Wysling⁵, Uri Schtalheim⁶
^{1,2,3,4,5,6}ASE AG, Zurich, Switzerland
- Agent Based Modelling and Simulation of Pedestrian Crowds in Panic Situations 463
Mohammed M. Alrashed & Jeff S. Shamma, King Abdullah University of Science and Technology (KAUST), Computer, Electrical and Mathematical Science and Engineering Division (CEMSE), Thuwal, Saudi Arabia 23955-6900
- Application of Ensemble Kalman Filter to Pedestrian Flow 467
Fumiya Togashi¹, Takashi Misaka², Rainald Löhner³, Shigeru Obayashi⁴,
¹Applied Simulations Inc. 10001 Chartwell Manor Cr., Potomac, MD 20854, USA
²Frontier Research Institute for Interdisciplinary Science, Tohoku University 2-1-1 Katahira, Aoba-ku, Sendai 980-8577, Japan
³George Mason University 4400 University Dr., Fairfax, VA 22030, USA
⁴Institute of Fluid Science, Tohoku University 2-1-1 Katahira, Aoba-ku, Sendai 980-8577, Japan
- Congestion in Computational Evacuation Modelling 471
Volker Schneider¹, Rainer Könnecke²,
^{1,2}IST GmbH, Feuerbachstraße 19, 60325 Frankfurt, Germany
- Decentralized Control for Self-driving Cars That can Freely Move on Two-dimensional Plane 474
Takeshi Kano¹, Mayuko Iwamoto², Daishin Ueyama³, ¹Research Institute of Electrical Communication, Tohoku University, Sendai, Japan tkano@riec.tohoku.ac.jp ²Interdisciplinary Faculty of Science and Engineering, Shimane University, Matsue, Japan miwamoto@riko.shimane-u.ac.jp
³Faculty of Engineering, Musashino University, Tokyo, Japan d.ueyama@gmail.com
- Efficient Quantification of Model Uncertainties When De-boarding a Train 477
Florian Künzner¹, Tobias Neckel¹, Hans-Joachim Bungartz¹, Felix Dietrich², Gerta Köster³
¹Technical University of Munich, Department of Informatics, Munich, Germany
²Johns Hopkins University, Department of Chemical and Biomolecular Engineering, Baltimore, MD, USA
³Munich University of Applied Sciences Munich, Germany
- Empirical Findings from an Ascending Stair Evacuation Exercise in a Subway Station 480
Helmut Schrom-Feiertag¹, Thomas Matyus¹, Martin Stubenschrott¹, Stefan Seer¹
¹Center for Mobility Systems, AIT Austrian Institute of Technology GmbH, Giefinggasse 2, 1210 Vienna, Austria
- Experimental Investigation of Pedestrian Dynamics in Circle Antipode Experiments 483
Yao Xiao, Rui Jiang, Ziyou Gao, Xingang Li, Yunchao Qu, School of Traffic and Transportation, Beijing Jiaotong University, Beijing, China
- Network-Based Continuous Space Representation for Describing Pedestrian Movement in High Resolution 486
Wataru Nakanishi¹, Takashi Fuse²,
¹Tokyo Institute of Technology, 2-12-1-M1-20 Ookayama Meguro, Tokyo, Japan
²The University of Tokyo, 7-3-1 Hongo Bunkyo, Tokyo, Japan

- Experimental study on mixed traffic flow of bicycles and pedestrians 490
Ning Guo¹, Rui Jiang², SC Wong³, Qing-Yi Hao⁴, Shu-Qi Xue², Yao Xiao², Chao-Yun Wu⁴
¹*School of Automotive and Transportation Engineering, Hefei University of Technology 230009, Hefei, P.R. China*
²*Key Laboratory of Transport Industry of Big Data Application Technologies for Comprehensive Transport, Ministry of Transport, Beijing Jiaotong University 100044, Beijing, P.R. China*
³*Department of Civil Engineering, The University of Hong Kong Pokfulam Road, Hong Kong, P.R. China,*
⁴*School of Mathematics and Computational Science, Anqing Normal University 246133, Anqing, P.R. China*
- Extracting Crowd Velocities at High Density 493
Muhammad Baqui and Rainald Löhner, CFD Center/George Mason University, 4400 University Avenue, MS 4C7, Fairfax, VA 22030, USA
- Follower-Leader Concept in Microscopic Analysis of Pedestrian Movement in a Crowd 496
Jana Vacková¹, Marek Bukáček²,
^{1,2}*FNSPE, Czech Technical University in Prague, Břehová 7, Prague, Czech Republic*
- Forecasting Visitors' behaviour in Crowded Museums 499
Caterina Balzotti¹, Maya Briani², Alessandro Corbetta³, Emiliano Cristiani², Marina Minozzi⁴, Roberto Natalini², Sara Suriano⁵, Federico Toschi^{2,3},
¹*Dipartimento di Scienze di Base e Applicate per l'Ingegneria, Sapienza Università di Roma, Rome, Italy,*
²*Istituto per le Applicazioni del Calcolo, Consiglio Nazionale delle Ricerche, Rome, Italy,*
³*Department of Applied Physics, Eindhoven University of Technology, Eindhoven, The Netherlands,*
⁴*Galleria Borghese, Rome, Italy,*
⁵*Dipartimento di Matematica, Sapienza Università di Roma, Rome, Italy*
- Human stampedes at mass gatherings: An overview 502
Lakshmi Devi Vanumu¹, Laxmikant², K.Ramachandra Rao³,
^{1,2,3}*Department of Civil Engineering, Indian Institute of Technology, Delhi, Hauz Khas, New Delhi, India,*
- Influence of Obstacles on the Use of the Danger Zone on Railway Platforms 505
Jasmin Thurau¹, Nicolas Keusen²,
¹*SBB AG, Technologic Asset Management, Hilfikerstrasse 3, 3000 Bern 65, Switzerland,*
²*BAV, Dept. of Security, Ittigen, Switzerland*
- Modeling Environmental Operative Elements in Agent-Based Pedestrian Simulation 508
Luca Crociani¹, Giuseppe Vizzari¹, Stefania Bandini^{1,2},
¹*Complex Systems and Artificial Intelligence research center, University of Milano-Bicocca, Milano, Italy,*
²*Research Center on Advanced Science and Technology, The University of Tokyo, Tokyo, Japan*
- Multiscale Pedestrian Dynamics and Infection Spread Model for Policy Analysis 512
Sirish Namilae^{1}, Pierrot Derjany¹, Dahai Liu¹ Anuj Mubayi² and Ashok Srinivasan³,*
¹*Embry-Riddle Aeronautical University, Daytona Beach, Florida, USA,*
²*Arizona State University, Tempe, Arizona, USA*
³*University of West Florida, Pensacola, Florida, USA*
- Pedestrian Evacuation Modelling with Dynamics Congestion Avoidance 515
Zongzhi Wang¹, Tao Chen²,
^{1,2}*Institution of Public Safety Research, Tsinghua University, Beijing, China,*
- Using Agent-based Simulation for Safety: Fact-finding about a crowd accident to improve public space design 519
Yuanyuan Liu^{1,2}, Toshiyuki Kaneda¹,
¹*Graduate School of Engineering, Nagoya Institute of Technology Nagoya, Japan,*
²*College of Architecture and Urban Planning, Tongji University, Shanghai, China,*

Pedestrian flow characteristics through bends: Effects of angle and desired speed <i>Jiahua Zhang¹, Charitha Dias², Majid Sarvi³, Miho Iryo-Asano⁴,</i> <i>^{1,2}Institute of Industrial Science/The University of Tokyo, 4-6-1 Komaba, Meguro-ku, Tokyo, Japan,</i> <i>³Department of Infrastructure Engineering/The University of Melbourne, Building 176, Victoria 3010,</i> <i>Melbourne, Australia,</i> <i>⁴Graduate School of Environmental Studies/Nagoya University, Environmental Studies Hall, Furo-cho,</i> <i>Chikusa-ku, Nagoya, Japan</i>	522
Pedestrian Models for Robot Motion <i>Francesco Zanlungo¹, Florent Ferreri¹, Jani Even^{1,2}, Luis Yoichi Morales³, Zeynep Yücel⁴, Takayuki</i> <i>Kanda^{1,2},</i> <i>¹ATR IRC, Kyoto, Japan,</i> <i>²Kyoto University, Kyoto, Japan,</i> <i>³Nagoya University, Nagoya, Japan,</i> <i>⁴Okayama University, Okayama, Japan</i>	525
Social Force Modeling of the Pedestrian Motion in the Mataf <i>Rainald Löhner¹, Eberhard Haug², Britto M. ²,</i> <i>¹Center for Computational Fluid Dynamics, George Mason University, Fairfax, VA, USA,</i> <i>²SL Rasch Kesslerweg 22, Oberaichen, Germany</i>	528
Toward dynamical crowd control to prevent hazardous situations <i>Tomoichi Takahashi, Department of Information Engineering, Meijo University , Nagoya, Japan</i>	531
Virtual Reality approaches for evacuation simulation of various disasters <i>Naohiro Takeichi¹, Takeshi Katagiri², Harumi Yoneda³, Shusaku Inoue⁴, Yusuke Shintani⁵</i> <i>¹Advanced Design Department/Takenaka Corporation, Tokyo, Japan,</i> <i>^{2,3,4,5} Research and Development Institute/Takenaka Corporation, Chiba, Japan</i>	534
Vulnerable People in Microscopic Evacuation Modelling <i>Rainer Könnecke¹, Volker Schneider²,</i> <i>^{1,2}IST GmbH, Feuerbachstraße 19, 60325 Frankfurt, Germany,</i>	537

Pedestrian Flow Characteristics at Upstream and Downstream of Bottleneck for Unidirectional Flow under Normal Conditions

Mr. Siddhartha Gulhare¹, Ms. Aparna P M², Dr. Ashish Verma³

^{1,2,3}Department of Civil Engineering

Indian Institute of Science

Bangalore, India.

siddharthagulhare89@gmail.com; aparna.pras@gmail.com; ashishv@iisc.ac.in

Abstract - The study of pedestrian flow characteristics at upstream and downstream of bottlenecks is important from level of service and evacuation perspective. Many controlled laboratory experiments have been conducted to study pedestrians' behavior at bottlenecks. However, it is unclear whether experiments can reproduce real crowd flow characteristics. In this paper, real field data was collected at normal conditions for unidirectional pedestrian movement at Mahakaleshwar, a Hindu temple at Ujjain, India during Mahashivaratri, a festival day on which a large number of pilgrims visited the temple. Along the corridor there is a width reduction at a U-turn which creates a bottleneck. It is necessary to study pedestrian flow characteristics at bottlenecks to ensure desired level of service at temple premises during heavy flow. The speed-density relationships of upstream and downstream sections were compared and it was found that flow behavior at both the sections of bottleneck severely differ from each other. Pedestrians in the upstream are either at free flow speed for very low density values or moving slowly for intermediate to high range of density values. From the speed-density relationship, it can be concluded that pedestrians at upstream had visual clues of congestion ahead at bottleneck (pedestrian could also see the downstream flow through barricades). Therefore, pedestrians wait at their position, stay in their comfort zone and do not push each other. Thus, even at intermediate local density, pedestrians have such low speeds. This violates the general assumption that pedestrians change their speed only at the shockwave boundary. The movement of pedestrians at upstream is governed by local density and information of congestion status ahead, whereas pedestrian movement at downstream is governed by factors like density, side friction and pedestrians' willingness to compensate for the delay at bottleneck. This study is expected to have application in planning and operation of pedestrian facilities.

Keywords: Bottleneck, Pedestrian Flow Characteristics, Speed-Density Relationships

1. Introduction

India is a country, which celebrates many religious festivals every year. Being the second most populous country in the world with majority of them having faith in religion/tradition and improved transportation facilities are some of the reasons why India witnesses mass religious gatherings, especially during festival days. This in turns impose huge challenges to organizers to manage such large crowd and to avoid any crowd risk situations.

The current practice of crowd management and crowd control is based on experience or "rule of thumb".. Many event managers including festival organizers in temples, create very long and narrow makeshift corridors to channel pedestrian flow and to avoid random movement of pedestrians in the premises. However, a proper scientific guideline can significantly aid crowd management. With the advancement in computing, it is also feasible to use pedestrian simulation tools to assist in crowd control. The simulation tools can also aid in evaluating various crowd management strategies in advance, prior to the event.

One significant hindrance to steady pedestrian flow is the presence of bottlenecks. A bottleneck typically refers to a limited area (in general sense) of reduced capacity or increased demand such as on-ramp [1]. Pedestrian bottlenecks are generally formed due to capacity reduction. It is necessary to study pedestrian flow characteristics at bottlenecks to ensure desired level of service at temple premises during heavy flow. Simulation tools can quantify the impact of bottleneck on pedestrian flow and aid in exploring solutions to reduce its impact. These simulation tools need to be calibrated and validated with empirical data before application. However, there is a lack of pedestrian empirical data around bottleneck in real conditions. This paper attempts to study the pedestrian flow characteristics at the upstream and downstream of bottleneck in a real crowd situation for unidirectional flow.

The outline of this paper is as follows. The next section discusses the review of literature. The section 3 discusses about site condition and data collection. The data analysis is mentioned in section 4 and results are discussed in section 5

2. Review of Literature

The study of pedestrian bottleneck is crucial from the perspective of level of service and evacuation. In the last few years, bottleneck and its impact on flow characteristics of pedestrians have gained significant attention. Several controlled experiments in laboratory conditions have been performed at normal conditions to gain more insights [1-3]. Some experimental studies were performed at various stress levels, as an attempt to replicate real field conditions [4]. However, the ability of participants in such experiments to reproduce real behavior and motivation levels of crowd even at normal condition is doubtful. Also in a laboratory setup, one can test combinations of experimental variables, whereas in a field data collection the conditions may not always be favorable.

Pedestrian flow characteristics at bottlenecks are sufficiently researched, but little is known about pedestrian flow characteristics at upstream and downstream of bottlenecks, especially under real conditions. [5] have quantitatively shown that pedestrians' behavior at upstream severely differs from the behavior at downstream and that density and walking velocity are not always linearly related to each other. However, their results were derived from a controlled experiment, where a group of participants were instructed (repeated many times) to move from a waiting area to the other side of the wall through an opening of different widths of bottleneck. In their experiment, while movements upstream of a bottleneck is governed by their information with respect to the traffic state in the bottleneck ahead of them, their movements downstream of the bottleneck seem to be governed by the physical restrictions of the current local situation only. [4] indicated that participants in upstream respond to the visual clues of traffic congestion at bottleneck. [6] studied the flow characteristics at upstream of bottleneck of real pedestrian movement in a tapering walkway. Their results indicate that pedestrians recognized that, a faster speed would hasten their joining at the rear of the queue and maintaining a low speed provided comfortable low density conditions. When congestion was forming, speed in each section of the study area began to decrease before density began to rise and they concluded that the pedestrians respond to the visual downstream congestions. From the review of literature, it was learnt that the impact of bottleneck at upstream and downstream of real continuous pedestrian flow (with varying flow rate with time) has not been quantitatively studied so far. This study attempts to examine flow characteristics at upstream and downstream for real pedestrian flow.

Researchers have reported that pedestrian flow characteristics are influenced by physical and psychological characteristics such as age and gender [7, 8], culture [9], luggage-carrying [10] etc. Some other factors include geometrical and environmental conditions such as roughness or gradient of surface [11], indoor/outdoor walkway [12] etc. The present study compares the speed-density relationship to comprehensively understand the differences in the macroscopic behavior of pedestrian at upstream and downstream. Since, both upstream and downstream sections are studied for the same time period; same set of pedestrians had crossed both sections. Therefore, psychological and physical characteristics of pedestrians is same for both the sections. Similarly, environmental conditions and surface characteristics were also same for both the sections. It was also crosschecked that no other bottlenecks are present ahead

in the downstream. The pedestrian flow rate at exit of temple was checked and found to be approximately equal to rate of flow at the study area. This also confirms the absence of any other obstruction in the downstream which might have impacted the outcomes. Hence, any difference in speed-density relationship at upstream and downstream must be attributed only to the presence of bottleneck.

3. Site Description and Data Collection

The video graphic data was collected at the Mahakaleshwar Temple, which is the main attraction in the city of Ujjain, India. The data was collected at the temple on Mahashivaratri, a festival day on which large number of pilgrims visited the temple. Makeshift corridors were temporarily installed at the entrance of temple to channelize the crowd. Pedestrians were made to walk in long, narrow corridors in order to accommodate more pedestrians and thereby increase the capacity. A GoPro camera was installed right above the pedestrian flow so as to capture two adjacent corridors, where width of the corridor reduces from 1.6 m to 0.75 m at the U-turn. Figure 1 shows the study area enclosed by a rectangle and the direction of pedestrian flow. Figure 2 shows the screenshot of both the study sections. The reduction in width has led to the formation of bottleneck at the U-turn. The video had captured both upstream and downstream of the bottleneck simultaneously. The length of both the study sections below the camera are 2.3m. The corridors are separated by strong barricades. Pedestrians can see the crowd in front as well as in the adjacent corridors through the barricades to get visual clues of pedestrian flow on the other side i.e. pedestrians at upstream can see pedestrian flow at downstream. A video of 38 minutes was analyzed in which nearly 2300 pedestrians (flow rate 3600 ped/hr) passed through the study sections.

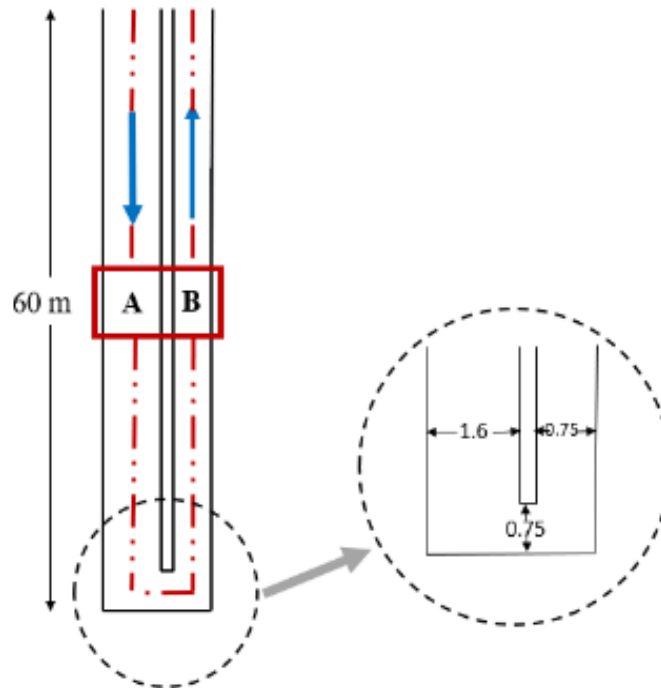


Figure 1 Schematic diagram of pedestrian flow (all dimensions are in meters)

Traps of known dimensions were annotated on the video using Swordsoft Screenink tool to mark the study area and entry and exit times of all the pedestrians passing through the study sections were extracted manually. The entry and exit time of all pedestrians were recorded from video using head as the reference

i.e. a pedestrian was considered to have entered the study section, if at least half of the head of a pedestrian is inside. Similarly, the exit times were also recorded. The entry and exit times were used to calculate the speed of individual (which later gave average speed) and density at every second. Therefore, density has a limitation that it can only take discrete values, based on the number of pedestrians in the study area. The modified density, as mentioned in equation 1 of [13] was chosen, which is as follows.

$$\Theta_i(t) = \begin{cases} \frac{t - t_i^{in}}{t_{i+1}^{in} - t_i^{in}} & : t \in [t_i^{in}, t_{i+1}^{in}] \\ 1 & : t \in [t_{i+1}^{in}, t_i^{out}] \\ \frac{t_{i+1}^{out} - t}{t_{i+1}^{out} - t_i^{out}} & : t \in [t_i^{out}, t_{i+1}^{out}] \\ 0 & : \text{otherwise} \end{cases} \quad (1)$$

Where,

$\Theta_i(t)$ = fraction to which the space between person i and person $i+1$ is inside
 t_i^{in} = entrance time
 t_i^{out} = exit time



Figure 2 Screenshot of the study area from overhead video

4. Data Analysis

The speed-density relationship can be used to quantitatively analyze any pedestrian facility. The inter-quartile graph of speed-density relationship for upstream and downstream section were plotted as shown in Figure 3. (The inter-quartile graphs did not change its behavior for varied range of bin size and bin positions).

In speed-density relationship of upstream, free flow speeds are achieved at low density, which is logical and as expected. For density more than 1 ped/m², the speed of the pedestrians showed a sudden drop followed by a gradual decrease. The lack of intermediate speed points in the graph can also be visualized with help of Figure 4. For density more than 1 ped/m², speed values are very low, even for the intermediate density values. The region of low speed stretches from intermediate to high values of density. This suggests that pedestrians in the upstream are either at free flow speed for very low density values or moving slowly for intermediate to high range of density values. The period of transition between free flow to congestion is sudden. From the speed-density relationship, it can be concluded

that pedestrians at upstream had visual clues of congestion ahead at bottleneck (pedestrian could also see the downstream flow through barricades). Therefore, pedestrians wait at their position, stay in their comfort zone and do not push each other. Thus, even at intermediate local density, pedestrians have such low speeds.

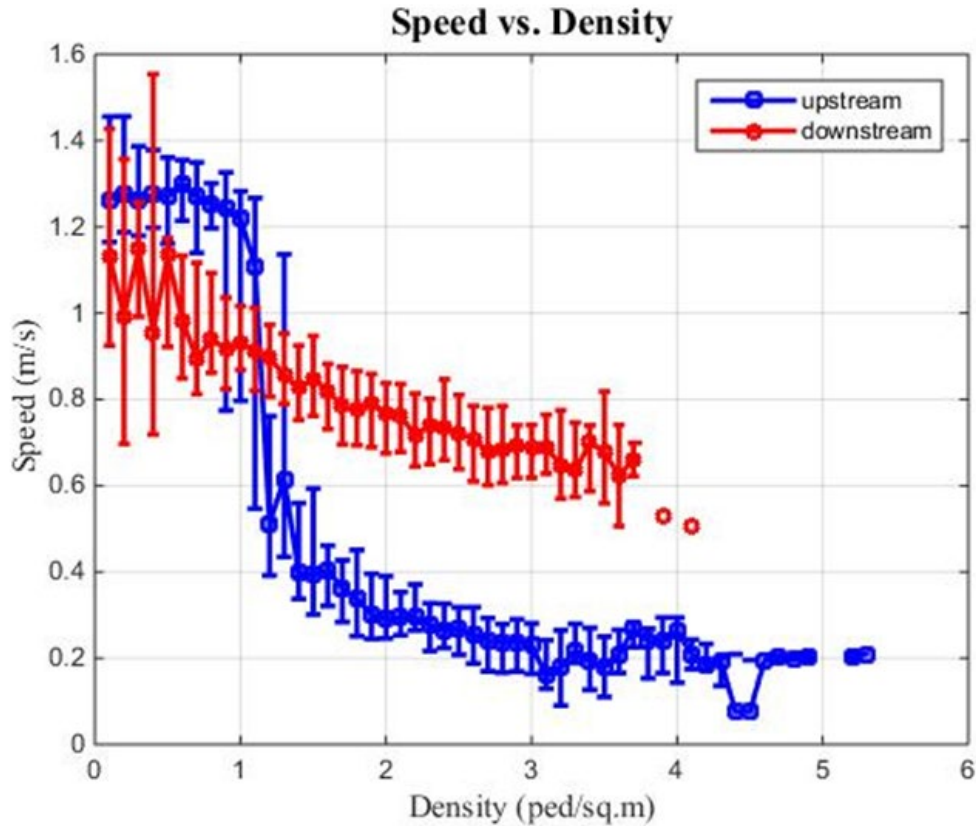


Figure 3 Speed-Density relationship for upstream and downstream section

After crossing bottleneck, pedestrians enter into the downstream section. There were no bottlenecks or obstacles ahead. The free flow speed values are slightly lower because of the presence of side friction from barricades. Since, the channel was very narrow; pedestrians could only enter one after the other from bottleneck section. In downstream, pedestrian had to walk in single file due to constrained motion in the lateral direction. However, the rate of decrease of speed with increase in density was very less. One of the reason is pedestrians had to compensate for the delay at bottleneck. Hence, even increased density could not reduce the speed as expected or mentioned in literature. The density mainly varied between 1 ped/m² to 2 ped/m², the histogram of density can be seen in Figure 4. The high peaks between these ranges, all indicates that bottleneck was saturated for most of the time.

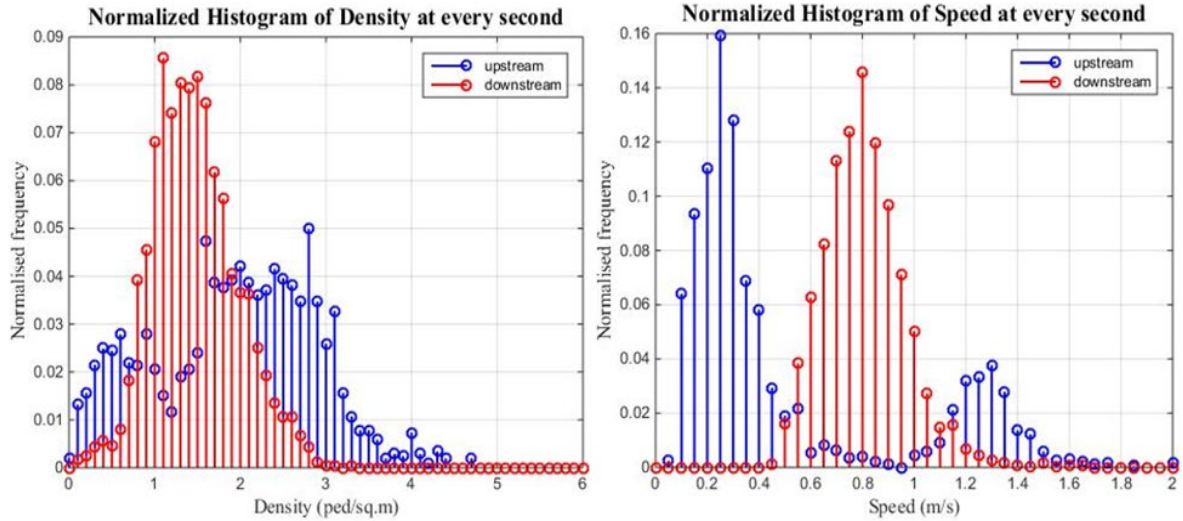


Figure 4 Frequency of density and speed values as upstream and downstream

5. Conclusion

The paper observes the continuous real pedestrian flow characteristics at upstream and downstream of the bottleneck. It quantitatively shows that pedestrian flow characteristics at upstream is different from that of downstream. It can be concluded that pedestrian flow in downstream is governed not only by local factors like density and side friction, but also by pedestrian's willingness to compensate for the delay occurred due to bottleneck. On the other hand, slow moving speed at intermediate density suggest that pedestrian flow at upstream is not only governed by density but possibly also by other factors such as visual clues of congestion status ahead. The results are limited to the pedestrian flow at normal condition; there was no state of panic in the crowd. The study also hints that a single speed-density relationship does not apply to the entire length of the section. There are factors, apart from density, which affects the flow characteristics. The study also suggest that pedestrians in upstream anticipate the visible changes in downstream and slow down. The assumption that speed of pedestrians will reduce only at shockwave interface is also violated. The paper compares the upstream and downstream section characteristics of continuous pedestrian flow, at a macroscopic level, which may have certain limitations. The results can be used for calibration and validation of simulations involving pedestrian movement through long and narrow makeshift corridors for crowd gathering events. In future, comparison based on microscopic characteristics can yield more contrasting differences between upstream and downstream characteristics.

Acknowledgements

The work reported in this paper is part of the project titled "The Kumbh Mela Experiment: Measuring and Understanding the Dynamics of Mankind's largest crowd," funded by the Ministry of Electronics and IT Ministry of Communication and Information Technology, Government of India (MITO-0105), Netherlands Organization for Scientific Research, NWO (Project no. 629.002.202), and Robert Bosch Center for Cyber Physical Systems, Indian Institute of Science, Bangalore. (Grant No. RBCO001). The authors also express their gratitude towards Kumbh Mela administration and government of Madhya Pradesh, India for providing constant support and official permissions to carry out research work and establish Indo-Dutch collaboration research camp at Kumbh Mela 2016.

References

- [1] Kretz, T., Grunebohm, A., & Schreckenberg, M. (2006, October). Experimental study of pedestrian flow through a bottleneck. *Journal of Statistical Mechanics: Theory and Experiment*.
- [2] Daamen, W., & Hoogendoorn, S. P. (2003). Experimental Research of Pedestrian Walking Behavior. *Transportation Research Record, 1828*, 20-30.
- [3] Rupperecht, T., Klingsch, W., & Seyfried, A. (2011). Influence of Geometry Parameters on Pedestrian Flow through Bottlenecks. *Pedestrian and Evacuation Dynamics* (pp. 71-80). Springer.
- [4] Daamen, W., & Hoogendoorn, S. (2010). Emergency Door Capacity: Influence of Population Composition and Stress Level. *Fire Technology, 48*(1), 55-71.
- [5] Duives, D., Daamen, W., & Hoogendoorn, S. (2014). Anticipation behavior upstream of a bottleneck. *Transportation Research Procedia, 2*, pp. 43-50.
- [6] Virkler, M. R., & Elayadath, S. (1994). Pedestrian Density Characteristics and Shockwaves. *Proceedings of the Second International Symposium on Highway Capacity*, (pp. 671-684).
- [7] Tarawneh, M. S. (2001). Evaluation of pedestrian speed in Jordan with investigation of some contributing factors. *Journal of Safety Research, 32*, 229-236.
- [8] Rastogi, R., Ilango, T., & Chandra, S. (2013). Pedestrian flow characteristics for different pedestrian facilities and situations. *European Transport, 53*, 5.
- [9] Chattaraj, U., Seyfried, A., & Chakroborty, P. (2009). Comparison of pedestrian fundamental diagram across cultures. *Advance in Complex Systems, 12*, 393.
- [10] Older, S. J. (1968). The speed, density and flow of pedestrians on footway in shopping streets. *Traffic Engineering and Control, 10*(4), 160-163.
- [11] Lam, H. K., Morall, J. F., & Ho, H. (1995). Pedestrian flow characteristics in Hong Kong. *Transportation Research Record, 1487*, 56-62.
- [12] Ye, J., Chen, X., & Jian, N. (2012). Impact analysis of human factors on pedestrian traffic characteristics. *Fire Safety Journal, 52*, 46-54.
- [13] Seyfried, A., Steffen, B., Klingsch, W., & Boltes, M. (2005). The fundamental diagram of pedestrian movement revisited. *Journal of Statistical Mechanics, P10002*.

Data archive for exploring pedestrian dynamics and its application in dimensioning of facilities for multidirectional streams

Maik Boltes, Stefan Holl, Armin Seyfried

Institute for Advanced Simulation, Forschungszentrum Jülich
Leo-Brandt-Straße, 52428 Jülich, Germany
m.boltes@fz-juelich.de; st.holl@fz-juelich.de; a.seyfried@fz-juelich.de

Abstract - In this paper an overview of an open data archive with data from experiments investigating pedestrian dynamics is presented. As an example of the use of this data the analysis of recently published data about the capacity of crossings is shown.

Keywords: data archive, experiments, trajectories, multidirectional, dimensioning

1. Introduction

To understand and thereupon to model pedestrian dynamics reliable empirical data is needed. In cooperation with the University of Cologne, Wuppertal and other organizations, we performed 15 experimental series with more than 1500 runs in total and up to 1000 participants in a single run since 2005. We share the data in an open-access archive to ensure transparency and openness and to allow further analysis and the use for model calibration and validation. The data is published as soon as a project is completed.

An example of the use of our data sets is the development of methods dimensioning facilities for multidirectional pedestrian traffic. Based on the trajectories from the research projects Hermes [1] and BaSiGo [2], it was possible to investigate the performance of crossings [3].

2. Data Archive

The open access data archive can be found at

<http://ped.fz-juelich.de/da>

The data hosted in the archive is the native data used by ourselves. Most of this data include a description or a paper motivating and outlining the experiments, overhead video recordings and (except experiment No. 1 of Tab. 1) trajectories of every single person with a high temporal and spatial resolution [4]. All experiments were performed under laboratory conditions to focus on the impact of a single variable (e.g. geometry, motivation, density) with as few undesired influences as possible. Tab. 1 shows a list of experiments stored in the current data archive. The list includes the place (if no country is specified, the experiment has been conducted in Germany), the scenario, the maximum number of persons in a single run, the number of runs, the project in which context the experiments have been conducted, the first or most important paper to this study and a URL linking to the data (see Sec. 2.2). Fig. 1 shows snapshots of a choice of experiments in the data archive. The list of experiments ends in 2015, but data from studies with people with disabilities in 2017 and about entrance scenarios in 2018 will be added when the associated projects are finished.

The archive is also open to the community. We started to collect data or references to external data from other research groups to create a starting point for experimental studies on pedestrian dynamics:

<http://ped.fz-juelich.de/extda>

Table 1: Experiments in the pedestrian dynamics data archive

No.	Year	Place	Scenario	# Pers.	# Runs	Project	Pub.	URL
1	2005	Jülich	single-file	34	6		[9]	singleFile
2	2005	Jülich	bottleneck	60	15		[11]	bottleneck
3	2006	Düsseldorf	single-file	70	13	DFG	[10]	singleFile
4	2006	Düsseldorf	bottleneck	200	13	DFG	[11]	bottleneck
5	2009	Düsseldorf	stairs outside stadium	200	7	Hermes	[12]	stairsOutside
6	2009	Düsseldorf	mouth hole	300	8	Hermes	[12]	mouthHoleUpper
7	2009	Düsseldorf	mouth hole	300	8	Hermes	[12]	mouthHoleLower
8	2009	Düsseldorf	stairs inside stadium	300	14	Hermes	[12]	stairsUpper
9	2009	Düsseldorf	stairs inside stadium	300	9	Hermes	[12]	stairsLower
10	2009	Düsseldorf	bottleneck	350	5	Hermes	[13]	bottleneck
11	2009	Düsseldorf	T-junction	350	11	Hermes	[14]	Tjunction
12	2009	Düsseldorf	corner	150	16	Hermes		corner
13	2009	Düsseldorf	corner, free flow	150	3	Hermes		cornerFree
14	2009	Düsseldorf	bidirectional flow	200	6	Hermes	[15]	bidirAsym
15	2009	Düsseldorf	bidirectional flow	300	13	Hermes	[15]	bidirSym
16	2009	Düsseldorf	bidirectional flow	300	5	Hermes	[15]	bidirFree
17	2009	Düsseldorf	unidirectional flow	230	24	Hermes		unidirClosed
18	2009	Düsseldorf	unidirectional flow	350	31	Hermes	[16]	unidirOpen
19	2012	Wuppertal	bike, single-file	33	10		[17]	bike
20	2013	Düsseldorf	entrance	319	1	BaSiGo	[18]	entrCorridor
21	2013	Düsseldorf	entrance	319	1	BaSiGo	[18]	entrSemicircle
22	2013	Düsseldorf	crossing 120°	926	16	BaSiGo	[3]	crossing120
23	2013	Düsseldorf	crossing 90°	603	45	BaSiGo	[3]	crossing90
24	2013	Düsseldorf	bidirectional flow	926	16	BaSiGo	[3]	bidirectional
25	2013	Düsseldorf	unidirectional flow	916	9	BaSiGo	[3]	unidirectional
26	2013	Düsseldorf	single-file	58	6	BaSiGo	[19]	singleFile
27	2013	Düsseldorf	social groups	12	18	BaSiGo	[20]	socialGroups
28	2014	Wuppertal	social groups, pupil	51	132	DFG	[21]	socialGroups
29	2014	Wuppertal	single-file, pupil	58	105	DFG	[22]	singleFile
30	2015	Tianshui, China	single-file, age	71	34		[23]	singleFile

2.1. Data Collection

The extraction of individual paths of each participant has been done automatically in most cases with the free software PeTrack [5]. For the extraction of the code marker additional software [6] has been used. Often a manual review and correction of the resulting data has been conducted to increase the quality. The set of trajectories of all pedestrians enables the measurement of quantities like velocity, flow, density and individual distances at any time and position, thus for example lane formation and local densities can be analyzed [7]. Beside the detailed analysis of pedestrians' movement also microscopic models can be designed, calibrated and verified with the data provided [8].

Sometimes the trajectories are enriched with additional global (e.g. distribution of age and gender) or individual (e.g. body size, head orientation) information. The height of the body often was obtained by special marker or 3D sensors like stereo cameras. In experiments where structured marker were used, the head orientation could be extracted. Extensive global individual information could be gathered using code marker and questionnaires as it was realized in experiments No. 19 to 27 of Tab. 1. Here additional information about human factors like gender, weight, age, togetherness, living environment, experiences in dense crowds and much more was gathered.

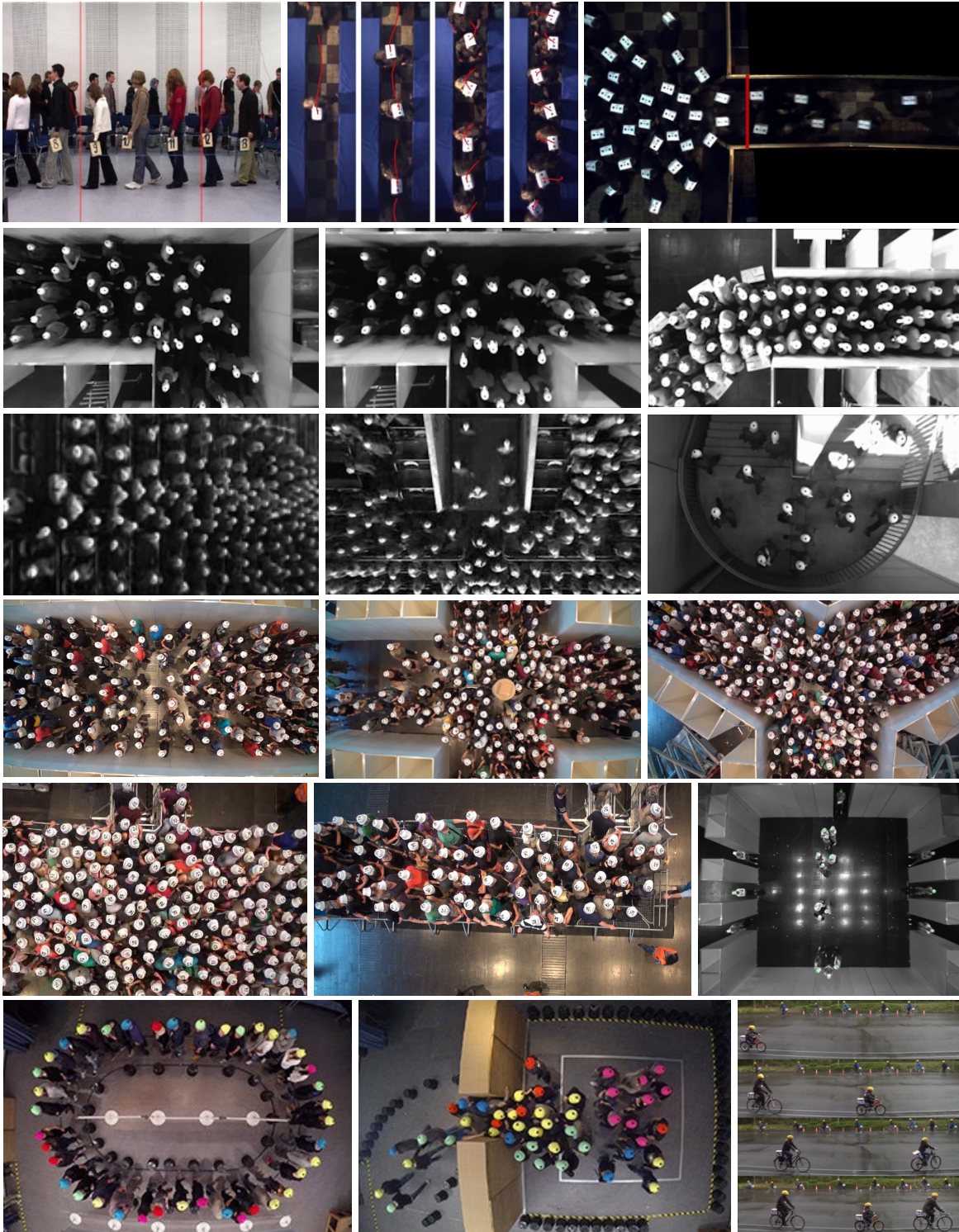


Fig. 1: Snapshots of a choice of experiments for which the data is available in the presented data archive (from left to right, top down): single-file (No. in Tab. 1: 1, 3), bottleneck (4), corner (12), T-junction (11), closed unidirectional flow (17), stairs inside stadium (8, 9), mouth hole (6, 7), stairs outside stadium (5), bidirectional flow (24), crossings (22, 23), entrances (20,21), room with social groups (27), pupil in single-file (29) and at a bottleneck (28), bicycle (19)

2.2. Citation

The use of the data is free, but you are asked to quote the source by citing the corresponding paper of Tab. 1 or if no paper is specified citing [5] describing the collection of the trajectories. To link to a special dataset of the data archive you can use the permanent address build up as follows:

<http://ped.fz-juelich.de/da/YearURL>

whereby Year and URL are the corresponding columns of Tab. 1. Thus, for the experiment No. 23 discussed in Sec. 3 the web address is <http://ped.fz-juelich.de/da/2013crossing90>. More paper and associated videos of the experiments are listed in Tab. 4.3 in [24].

3. Multidirectional Pedestrian Traffic

The data obtained by the experiments make it possible to determine characteristic values for the dimensioning of building facilities. The types of pedestrian streams studied in Hermes [1] and BaSiGo [2] are shown in Fig. 2: (a) unidirectional stream, (b) bidirectional stream with two separated lanes, (c) bidirectional stream with multiple lanes, (d) intersecting stream with two orthogonal directions, (e) crossing stream with four orthogonal directions, (f) confluence of two streams at the T-junction, (g) unidirectional stream at a corner, (h) multidirectional stream at triangular intersection.

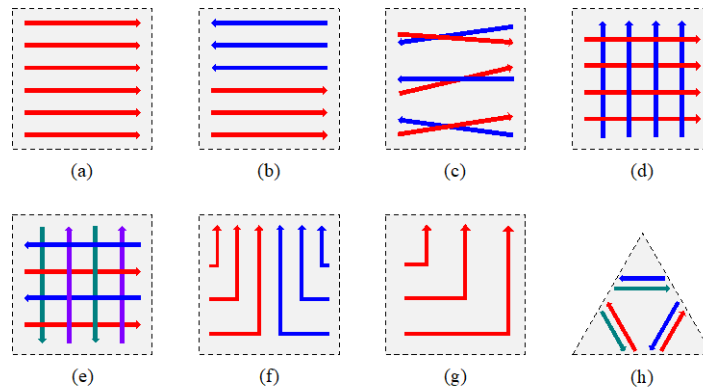


Fig. 2: Types of streams studied in Hermes and BaSiGo [3]

The results of the intersection analysis (structure type e) are presented below by way of example.

3.1. Configuration of the experiment for intersection traffic

For the experiment with multidirectional streams at intersections the crossing was built from 2.5 meter high wooden walls with four entrances arranged at an angle of 90 degrees (see Fig. 3). This spatial structure is referred as CROSSING_90. Each entrance had a clear width of four meters. Above each of the entrances a monitor was mounted. On this it was possible to display roundabout signs as they are known from vehicular traffic. The length of the entrances was 5.00 m and 5.24 m, respectively, followed by a three-meter-wide exit (labeled "OUT" in Fig. 3) on the left and right. In the center of the core area, a column ($\varnothing = 0.6$ m) could be positioned.

For the participation a daily fee of 50 Euro was paid. Most of our test persons were students with a mean age of 24.8 years \pm 4.4 years. The ratio between men and women was 55:45. The experiment was carried out on two days in variants A to G. On the first day (variants A, B, C) 319 and on the second day (variants D, E, F, G) 603 test persons participated.

In variants A, B and C, the test persons were evenly distributed over the four entrances, so about 80 people from each side streamed into the intersection. In order not to obstruct the inflows, the persons who had already passed the measuring area were given the opportunity to leave the corridor laterally.

The test persons were asked to use the exit assigned to their feature (even or odd cap number or yellow or red wristband). In variant A there was no column and no signs were displayed on the monitors. In variant B, there was also no column, however, the monitors showed the roundabout sign and the subjects were instructed to follow the instructions on the monitors. In variant C, the pillar in the center of the intersection was additionally set up, the display of the roundabout sign and the instruction to the test persons corresponded to variant B.

In variants D and E, the test persons were admitted into the intersection only by two entrances arranged at right angles to each other, so about 300 persons streamed in through each of these entrances. In variant D there was no column and no signs were displayed on the monitors. There was also no column in variant E, but the monitors showed the roundabout sign and the subjects were again asked to pay attention to the information on the monitors.

Variants F and G correspond to C and B respectively, whereby the width for the inflow has been increased up to 4 m. About 151 people were equally distributed.

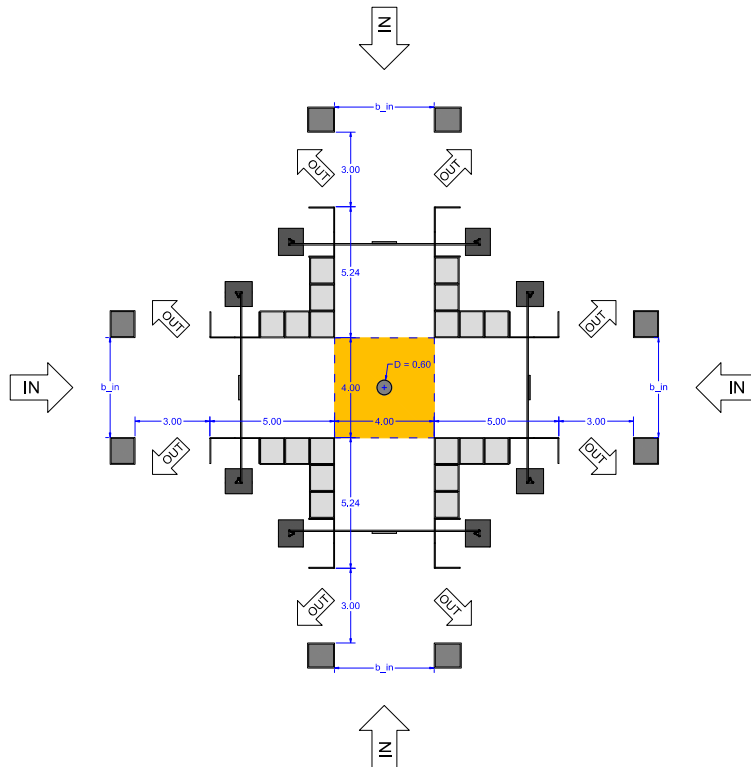


Fig. 3: Setup of experiment CROSSING_90 [3]

3.2. Analysis of the experiments

For the intersection with four entrances and multidirectional flows, the BaSiGo experiment CROSSING_90 is analyzed in variants A to G. Fig. 4 shows a picture and Fig. 5 an example of the trajectories for a run with a column in the center of the intersection.



Fig. 4: Execution of experiment CROSSING_90 [3]

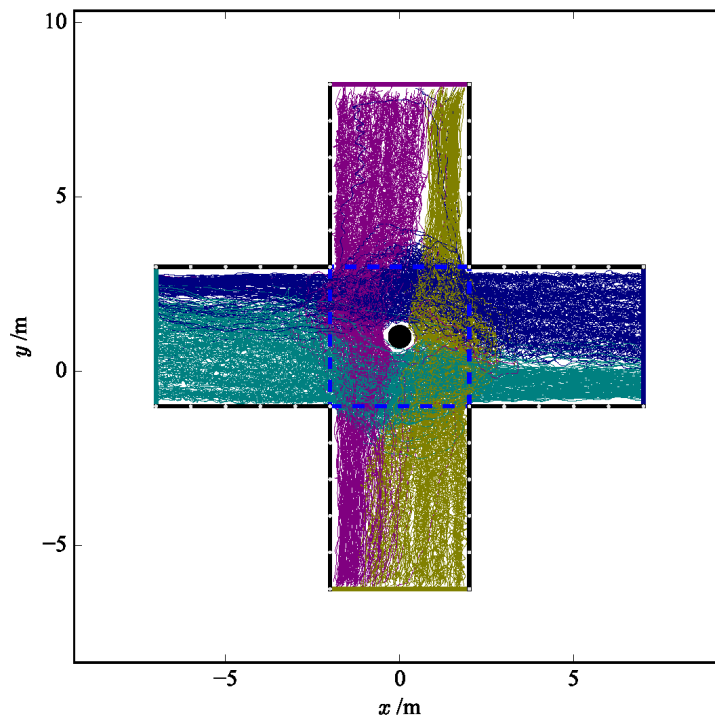


Fig. 5: Trajectories of a single run with four entrances and a column in the center of the intersection [3]

For our analyzes, a measurement method following [25] was used that allows to calculate density ρ , flow J and speed v in a multidirectional traffic system as averages over the same place and time [3, 26]. Fig. 6 shows the fundamental diagrams $v(\rho)$ and $J_s(\rho)$ for the measurement area shown as dashed blue line in Fig. 5. The specific flow J_s is calculated as the product of the mean velocity v and the mean density ρ . The data show no significant differences in the variants of the experiment. Both for the number of accesses used (two accesses in variants D and E, four accesses in all other variants) as well as for the column in the center of the crossing (variants C and F) there is no significant influence on the fundamental diagram in the

density regime covered in the experiments. Noteworthy are the high densities of up to seven people per square meter.

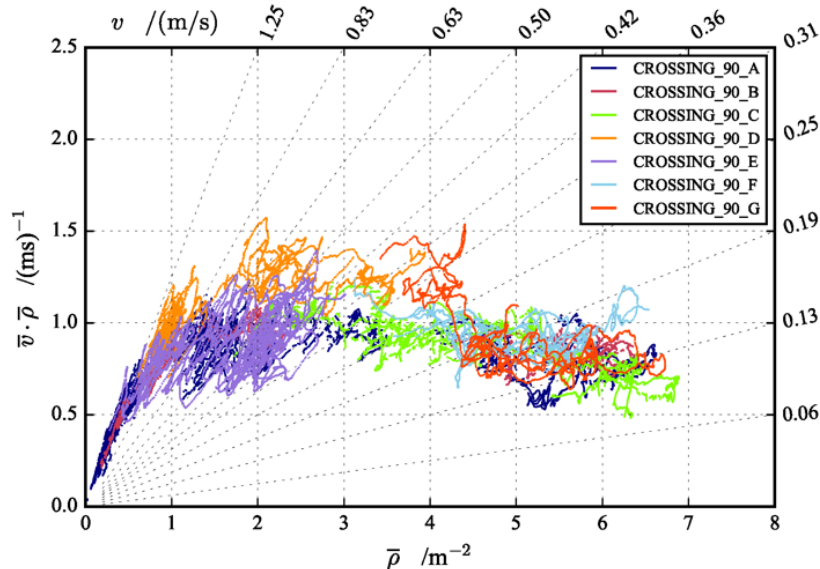


Fig. 6: Fundamental diagram for crossing pedestrian traffic [3, 26]

Acknowledgements

Most of the experiments have been performed within projects funded by the German Research Foundation (DFG-Grant No. KL 1873/1-1, SE 1789/1-1 or No. SCHA 636/9-1) or Federal Ministry of Education and Research (BMBF) (e.g. Hermes, BaSiGo). For the design and performance of the experiments we collaborated with various universities, especially the Universities of Wuppertal, Cologne and Siegen.

References

- [1] S. Holl, A. Seyfried, “Hermes - an evacuation assistant for mass events”, in *inSiDe*, vol. 7, 2009, pp. 60–61.
- [2] S. Holl, M. Boltes, A. Seyfried, “Level of Safety Concept for Major Events”, in *Proceedings of Traffic and Granular Flow 2015*, 2016, pp. 337–344.
- [3] S. Holl, “Methoden für die Bemessung der Leistungsfähigkeit multidirektional genutzter Fußverkehrsanlagen“, in *Schriften des Forschungszentrums Jülich, IAS Series*, vol. 32, 2016.
- [4] M. Boltes, S. Holl, A. Tordeux, A. Seyfried, A. Schadschneider, U. Lang, “Influences of Extraction Techniques on the Quality of Measured Quantities of Pedestrian Characteristics”, in *Proceedings of Pedestrian and Evacuation Dynamics 2016, Collective Dynamics*, 2016, pp. 540–547.
- [5] M. Boltes, A. Seyfried, “Collecting pedestrian trajectories”, *Neurocomputing*, vol. 100, 2013, pp. 127–133.
- [6] W. Mehner, M. Boltes, A. Seyfried, “Methodology for generating individualized trajectories from experiments”, in *Proceedings of Traffic and Granular Flow 2015*, 2015, pp. 3–10.
- [7] J. Liddle, A. Seyfried, B. Steffen, “Analysis of bottleneck motion using Voronoi diagrams”, in *Proceedings of Pedestrian and Evacuation Dynamics 2010*, 2011, pp. 833–836.
- [8] B. Steffen, A. Seyfried, M. Boltes, “Reliability issues in the microscopic modeling of pedestrian movement”, in *Mathematical results in Quantum Physics*, 2011, pp. 254–259.
- [9] A. Seyfried, B. Steffen, W. Klingsch, M. Boltes, “The Fundamental Diagram of Pedestrian Movement Revisited”, in *J. Stat. Mech.: Theory Exp.* P10002, 2005.

- [10] A. Seyfried, M. Boltes, J. Kähler, W. Klingsch, A. Portz, T. Rupperecht, A. Schadschneider, B. Steffen, A. Winkens, “Enhanced empirical data for the fundamental diagram and the flow through bottlenecks”, in *Proceedings of Pedestrian and Evacuation Dynamics 2008*, 2010, pp. 145–156.
- [11] A. Seyfried, T. Rupperecht, O. Passon, B. Steffen, W. Klingsch, M. Boltes, “New insights into pedestrian flow through bottlenecks”, in *Transportation Science*, 43, 2009, pp. 395–406.
- [12] S. Burghardt, A. Seyfried, W. Klingsch, “Performance of stairs – Fundamental diagram and topographical measurements”, in *Transportation research, C 37*, 2013, pp. 268–278.
- [13] L. Weichen, A. Seyfried, J. Zhang, M. Boltes, X. Zheng, Y. Zhao, “Experimental Study on Pedestrian Flow through Wide Bottleneck” in *Transportation Research Procedia*, vol. 2, 2014, pp. 26–22.
- [14] M. Boltes, J. Zhang, A. Seyfried, B. Steffen, “T-junction: Experiments, trajectory collection, and analysis”, in *Proceedings of International Conference on Computer Vision 2011 (Workshops)*, 2012, pp. 158–165.
- [15] J. Zhang, W. Klingsch, A. Schadschneider, A. Seyfried, “Ordering in bidirectional pedestrian flows and its influence on the fundamental diagram”, in *Journal of statistical mechanics: theory and experiment*, P02002, 2012.
- [16] J. Zhang, W. Klingsch, A. Schadschneider, A. Seyfried, “Transitions in pedestrian fundamental diagrams of straight corridors and T-junctions”, in *Journal of Statistical Mechanics: Theory and Experiment*, P06004, 2011.
- [17] J. Zhang, W. Mehner, S. Holl, M. Boltes, E. Andresen, A. Schadschneider, A. Seyfried, “Universal flow-density relation of single-file bicycle, pedestrian and car motion”, in *Physics Letters A*, vol. 378, issue 44, 2014, pp. 3274–3277.
- [18] A. Sieben, J. Schumann, A. Seyfried, “Collective phenomena in crowds — Where pedestrian dynamics need social psychology”, in *PLOS one*, 2017.
- [19] V. Ziemer, A. Seyfried, A. Schadschneider, “Congestion Dynamics in Pedestrian Single-File Motion”, in *Proceedings of Traffic and Granular Flow 2015*, 2016, pp. 89–96.
- [20] N. W. F. Bode, S. Holl, W. Mehner, A. Seyfried, “Disentangling the Impact of Social Groups on Response Times and Movement Dynamics in Evacuations”, in *PLOS one*, 2015.
- [21] C. von Krüchten, F. Müller, A. Svachiy, O. Wohak, A. Schadschneider, “Empirical Study of the Influence of Social Groups in Evacuation Scenarios”, in *Proceedings of Traffic and Granular Flow 2015*, 2016, pp. 65–72.
- [22] J. Wang, M. Boltes, A. Seyfried, J. Zhang, V. Ziemer, W. Weng, “Linking pedestrian flow characteristics with stepping locomotion”, in *Physica / A* 500, 2018, pp. 106–120.
- [23] S. Cao, J. Zhang, D. Salden, J. Ma, C. Shi, R. Zhang, “Pedestrian dynamics in single-file movement of crowd with different age compositions”, in *Phys. Rev. E* 94, 012312, 2016.
- [24] M. Boltes, “Automatische Erfassung präziser Trajektorien in Personenströmen hoher Dichte“, in *Schriften des Forschungszentrums Jülich, IAS Series*, vol. 27, 2015.
- [25] L. C. Edie, “Discussion of traffic stream measurements and definitions“, in *Proceedings of the Second International Symposium on the Theory of Traffic Flow*, 1965, pp. 139–154.
- [26] S. Cao, A. Seyfried, J. Zhang, S. Holl, W. Song, “Fundamental diagrams for multidirectional pedestrian flows“, in *Journal of Statistical Mechanics: Theory and Experiment*, P033404, 2017.

Lane Formation Beyond Intuition

Towards an Automated Characterization of Lanes in Counter-flows

Luca Crociani¹, Giuseppe Vizzari¹, Andrea Gorrini¹, Stefania Bandini^{1,2}

¹ Complex Systems and Artificial Intelligence research center
University of Milano-Bicocca, Milano, Italy
{name.surname}@unimib.it

² Research Center on Advanced Science and Technology,
The University of Tokyo, Tokyo, Japan

Abstract - Pedestrian behavioural dynamics have been growingly investigated by means of (semi)automated computing techniques for almost two decades, exploiting advancements on computing power, sensor accuracy and availability, computer vision algorithms. This has led to a unique consensus on the existence of significant difference between unidirectional and bidirectional flows of pedestrians, where the phenomenon of lane formation seems to play a major role. The collective behaviour of lane formation emerges in condition of variable density and due to a self-organisation dynamic, for which pedestrians are induced to walk following preceding persons to avoid and minimize conflictual situations. Although the formation of lanes is a well-known phenomenon in this field of study, there is still a lack of methods offering the possibility to provide an (even semi-) automatic identification and a quantitative characterization. In this context, the paper proposes an unsupervised learning approach for an automatic detection of lanes in multi-directional pedestrian flows, based on the DBSCAN clustering algorithm. The reliability of the approach is evaluated through an inter-rater agreement test between the results achieved by a human coder and by the algorithm.

Keywords: pedestrian dynamics, lane formation, analysis, clustering

1. Introduction & Literature Review

Pedestrian dynamics have been growingly investigated by means of (semi)automated computing techniques for almost two decades, exploiting advancements on computing power, expressiveness of languages and models, sensor accuracy and availability, computer vision advances. We are witnessing a transition from time-consuming manual counting and/or post-processing tasks (e.g. [1], [2]) to computer supported analyses involving automated tracking algorithms such as [3], characterization of the pedestrian population (e.g. group identification [4]), identification of typical trajectories for the definition of origin/destination matrices [5].

A relevant example of useful outcomes of this kind of analyses is represented by [6], which deeply discusses the physics of bi-directional flows of pedestrians in corridor settings: in particular, it is quantitatively observed that the dynamics significantly differ for uni- and bi-directional flows at least for densities between 1 and 2 ped/m², in contrast with previous studies. While this experiment brings relevant findings about the bi-directional dynamics, it does not fully explain how the lane formation phenomenon emerges, how it can converge to a stable state and whether the dynamics differ at a very microscopic level depending on, e.g., the lane width. The dynamism of the phenomenon, on the other hand, increases the difficulty of defining tools or formulas for its analysis. Counter-flow movements represent thus one of the situations that can be further fruitfully investigated by means of computer supported analyses.

Currently, besides intuitive characterizations of the lane formation phenomenon, some mathematical formulations for aggregated analysis of lane formation have already been defined in the literature [7]. A well-known criterion is described by the order parameter [8], which is achieved by superimposing a discrete representation of the observed environment to aggregate the number of pedestrians moving in each direction for each row of the grid (overall direction of movement is supposed to be parallel to the x-axis of the grid). Values of this observable close to 0 indicate overall chaotic dynamics in the analysed

time window. Vice-versa, an order parameter equal to 1 means that the dynamics is perfectly ordered and each row of the grid only contains pedestrians moving in the same direction. This metric, however, is of limited applicability due to the need of discretizing the analysed environment and assuming that lanes and flows are perfectly aligned with the corridor.

Another kind of analysis of the lane formation phenomenon is based on the notion of rotation, or turbulence of trajectories within a given time interval [9]. This aggregate observable increases its value with the number of changes in direction of tracked pedestrians and it can be considered an aggregated indicator of the quantity of head-on conflicts in the observation.

These mathematical formulations, on one hand, are already able to quantitatively describe the dynamics observed in controlled situations (e.g. bidirectional flows in straight corridors), but they provide aggregated indicators not actually very informative on the number of lanes and their relevant features, such as width, number of included pedestrians, duration of the phenomenon. This kind of more detailed characterization could be employed as an additional element for the validation of simulation models.

A more generally applicable approach, based on a technique from the machine learning area, has been proposed in [10]. In the paper, authors describe performed experimental observations and analyses employing a clustering algorithm to support the identification of pedestrian lanes in the video. The approach is a simple customization of the well-know DBSCAN algorithm [11] (Density Based Clustering Analysis) and it aggregates the instantaneous information about the position and velocity of pedestrians to form the clusters. Although results are preliminary, the adoption of an unsupervised machine learning technique seems particularly suited to this kind of problem. Moreover, a similar approach providing an automatic characterization of the flows in the scene is proposed in [5]. The described algorithm is capable of aggregating positions and velocity vectors of pedestrians and identify origins and destinations of main pedestrian flows in the scene, but the scope of the analysis is not as microscopic as to characterize the possible pedestrian lanes.

The present paper builds on these results trying to provide both a general method for the analysis of the lane formation phenomenon as well as an approach to evaluate its effectiveness. To estimate the precision and reliability of the proposed algorithm for the automated characterization of lanes, we use the video and tracking results collected during the execution of controlled experiments focused on pedestrian counter flows dynamics described in [12]. More precisely, we tested the level of inter-rater agreement between the results achieved by the automated tool and by an expert human coder through a series of Cohen's Kappa statistical analysis [13].

The paper breaks down as following. Section 2 described the methodology and the clustering algorithm, with details on the two steps of the process; Section 3 presents an overview of results, and describes reliability test procedure. The paper concludes with final remarks and future works.

2. A Clustering Algorithm to Characterize Lane Formation

In the vein of [10], we propose a novel clustering-based approach able to identify lanes in arbitrary settings. The algorithm is based on a hierarchical two-steps application of DBSCAN, with distance metrics and respective parameters specifically tailored to deal with this problem. The aim is to achieve clusters that are in tune with the intuitive conception of the lane formation phenomenon.

We briefly introduce the main concepts of DBSCAN to enable the reader grasping the main concepts of the proposed approach. The algorithm identifies an arbitrary number of clusters, of any given shape (even concave) in the dataset, identifying “dense” and well separated zones according to three elements: (i) the assumed distance metric $\phi(\vec{x}_i, \vec{x}_j)$ between points; (ii) a threshold θ for the maximum distance among points that can be considered neighbours and therefore members of the same cluster; (iii) the minimum size of a relevant cluster $minPoints$. While the first element relates to the choice of a function to compute distance between pair of points, the other two are the actual parameter of the algorithm for the final identification of clusters. For the computation of the output, DBSCAN assigns a label to each point specifying whether the point is of type *noise*, *border* or *core*. The first label is assigned to points which do not have enough neighbours (less than $minPoints$) and which are not neighbours of a *core* point.

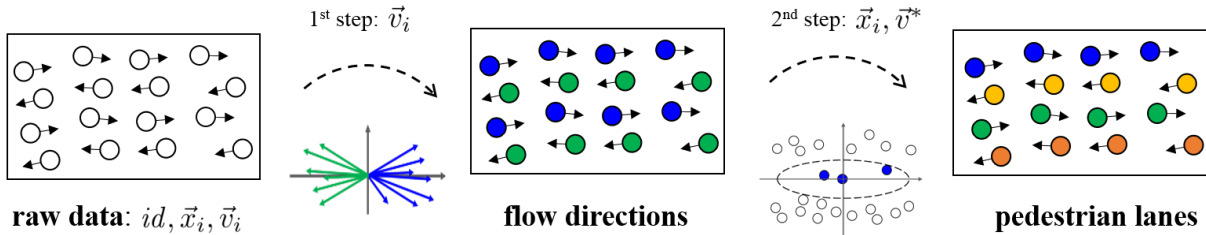


Figure 1: Workflow of the hierarchical clustering algorithm to characterize the lane formation.

Otherwise, a point is labelled as *border* point if it is neighbour of a core point but that does not have enough neighbours. A point is labelled as core, then, if it has at least *minPoints* neighbours and, thus, defines a dense area of the dataset. Finally, according to DBSCAN a cluster is composed of the set of all neighbour core points, plus their neighbour border points.

In the customization of DBSCAN proposed in this paper, the characterization of the lane formation phenomena is computed by means of a hierarchical approach, in which two distinct distance metrics are applied with different thresholds; for the context of application, we assume that the parameter *minPoints* is shared in the two procedures. In particular, this parameter is set to 3 to allow the characterization of lane for a situation in which three persons walk in a river-like pattern, that we consider as the simplest case of lane.

An intuitive description of the two-steps of the overall algorithm is shown in Figure 1. In the first step velocity vectors from the input raw data are used to identify big clusters associated to the main directions of flow, using a distance function which accounts for the *angular distance* between vectors. A second step of DBSCAN is further performed on the output clusters, considering the global average velocity of pedestrians within the cluster and the coordinates of pedestrians to finally characterize the lanes. In this second step, the distance metric is more complicated, since it must consider additional information, and it will be formally described in Sect. 2.2, but it basically considers pedestrians' positions with respect to the positions of neighbouring members of the same flow-cluster.

The algorithm works on almost instantaneous data, potentially allowing the implementation on real-time systems: by means of an aggregation with mobile average, mean positions and velocity vectors of pedestrians related to short time windows (less than half second) are calculated. The two sequential procedures will be now discussed in the following subsections.

2.1 Recognition of main directions of movement

Predominant directions of flow are recognized to identify the potential counter-flow situation as well as to achieve relevant information for the second step of the procedure, where the average velocity of pedestrians walking in the same direction is relevant for the computation of distance.

This process takes as input the set of velocity vectors \vec{v}_i of observed pedestrians in the current frame and analyse the differences in their orientation. The magnitude of the velocity vector is not influencing the result in this case: the emergence of locally higher densities in counter-flow situations, in fact, can lead to sensible differences among the speeds of pedestrians, and then to errors in the clustering process. To avoid this bias, the distance metric ϕ_v for a pair of velocity vectors (\vec{v}_i, \vec{v}_j) is defined as:

$$\phi_v(\vec{v}_i, \vec{v}_j) = \arccos\left(\frac{\vec{v}_i \cdot \vec{v}_j}{\|\vec{v}_i\| \cdot \|\vec{v}_j\|}\right)$$

where the numerator denotes the dot-product between the two vectors. This distance describes the inner (i.e., minimum) angle between \vec{v}_i and \vec{v}_j and a unique threshold $\theta_v \in [0,180]$ is introduced to calibrate the range of neighbourhood (i.e. below this angular distance, the pedestrians are considered members of the same major flow); in the experiments presented in the next section, θ_v is configured to about 50 degrees. While this could be considered as a rather substantial value, two considerations must be introduced. On one hand, given the hierarchical structure of the process we prefer a looser definition of

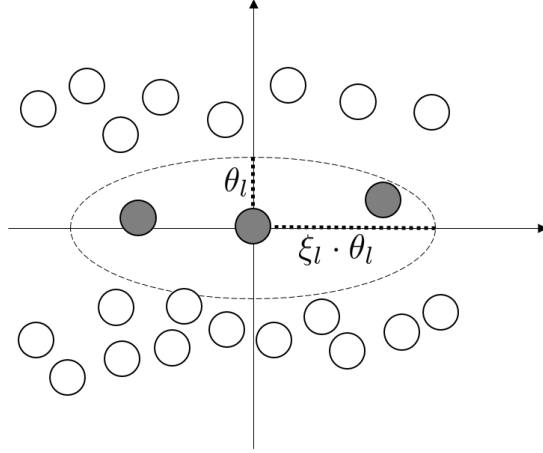


Figure 2: Example of neighbourhood of a pedestrian according to the distance metric ϕ_l . The limits of the neighbourhood are indicated by the drawn ellipse, configurable with parameters θ_l and ξ_l as described. For simplicity, it is assumed that $\vec{v}^* = (1,0)$.

neighbourhood at this stage and refining the output in the next task. Secondly, a thorough calibration on the parameters of the algorithm is still an ongoing work and the results later presented are referred to a calibration that was chosen because it generated visually stable and plausible results (fact that is also endorsed with the Kappa analysis shown in Figure 3). As exemplified in Figure 1, this process produces output clusters that describe pedestrians headed towards the same direction of movement.

2.2 Characterization of lane formation

The second step works sequentially on the individual clusters identified with the previous task, by performing density-based clustering using only their points. It takes as input the actual positions of pedestrians \vec{x}_i and the average velocity vector of the clustered pedestrians \vec{v}^* which is used for the computation of distance. The aim is the final identification of pedestrian lanes in the given frame, and this objective is pursued with the definition of a particularly tailored distance metric to compose clusters describing pedestrians which are not only relatively close, but also in an arrangement that can be associated to a form of queueing situation. With this purpose, in fact, a function able to differentiate distances according to the movement direction of the pedestrian is required. We then configure a function ϕ_l for a pair of points (\vec{x}_i, \vec{x}_j) as to compute distance values asymmetric with respect to the axis of the representation of the analysed environment; the rationale is that this measure grows more substantially along one axis of the 2-dimensional space (we consider the y-axis by assumption):

$$\phi_l(\vec{x}_i, \vec{x}_j) = \sqrt{\left(\frac{\hat{x}_{ij}}{\xi_l}\right)^2 + (\hat{y}_{ij})^2}$$

where \hat{x}_{ij} and \hat{y}_{ij} are the x- and y-coordinates of the relative position of pedestrian j with respect to i (the evaluated point), after being rotated according to the average velocity \vec{v}^* of clustered pedestrians at the first step. ξ_l is the calibration parameter of this function. The vector rotation is performed to align pedestrian positions according to the average direction of movement, for which the distance grows slower in order to aggregate positions describing queueing pedestrians. Formally, it is described with the following equation:

$$(\hat{x}_{ij}, \hat{y}_{ij}) = \odot \left(\vec{x}_j - \vec{x}_i, -\angle \left(\vec{v}^*, (1,0) \right) \right)$$

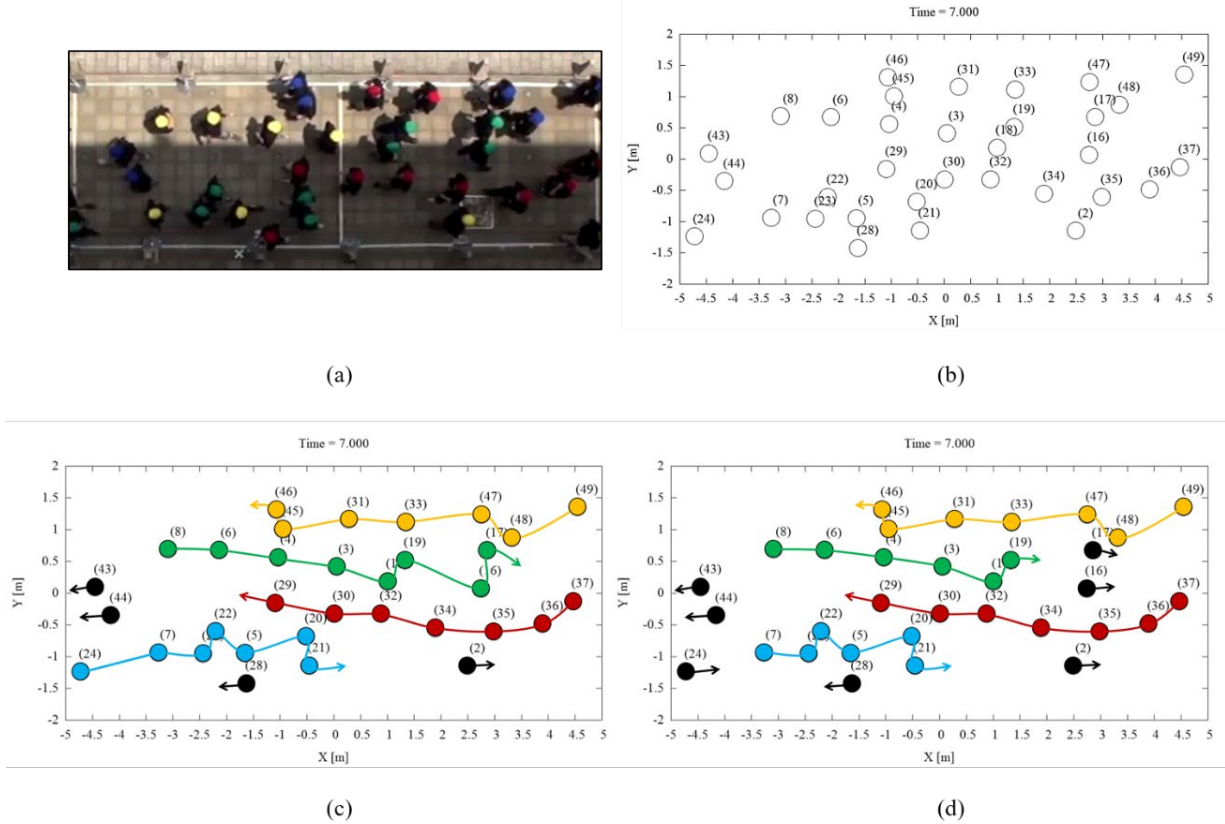


Fig. 3: (a) A frame of the video of the experiment. (b) Numerical identifiers and positions of pedestrians after the tracking process. Characterisation of lanes by our algorithm (c) and by the human coder (d) in the particular frame. Colours indicate the belonging of pedestrians to a lane (black is used for not belonging), while arrows highlighting the movement direction have been added afterwards.

with \odot being the rotation operator, \sphericalangle the function computing the counter-clockwise angle between two vectors and $(1,0)$ a unit vector to align the orientation of the movement direction \vec{v}^* along the x-axis, by rotating neighbour points accordingly.

The functioning of this part of the algorithm is also graphically exemplified in Figure 2. The function ϕ_l defines the neighbourhood of points with an elliptical shape, whose long side is aligned toward the average direction of movement \vec{v}^* : this allows pedestrians that are walking in a river-like formation to be considered as members of the same lane although there is a certain distance between them, whereas if they walk in a line abreast formation the same distance might be considered more relevant. The dimensions of the ellipse are provided by the threshold θ_l and the parameter ξ_l , which acts as a multiplier to define the proportion of the long side. In this way the algorithm provides clusters with a shape that follows the direction \vec{v}^* and aggregating points referring to queueing pedestrians.

3. Reliability Test between the Clustering Algorithm and a Human Coder

To test the reliability (i.e. *internal validity*) of the above described tool for the automated characterization of lanes, we use the video and tracking results collected during the execution of controlled experiments focused on pedestrian counter flows dynamics, thoroughly described in [12]. We focused one of the performed experiments, based on the analysis of fully-balanced bidirectional pedestrian flows. Then, we executed a cross-checking analysis between the results achieved through a preliminary calibration of the algorithm and the results achieved by a human coder, expert in the field of pedestrian crowd dynamics.

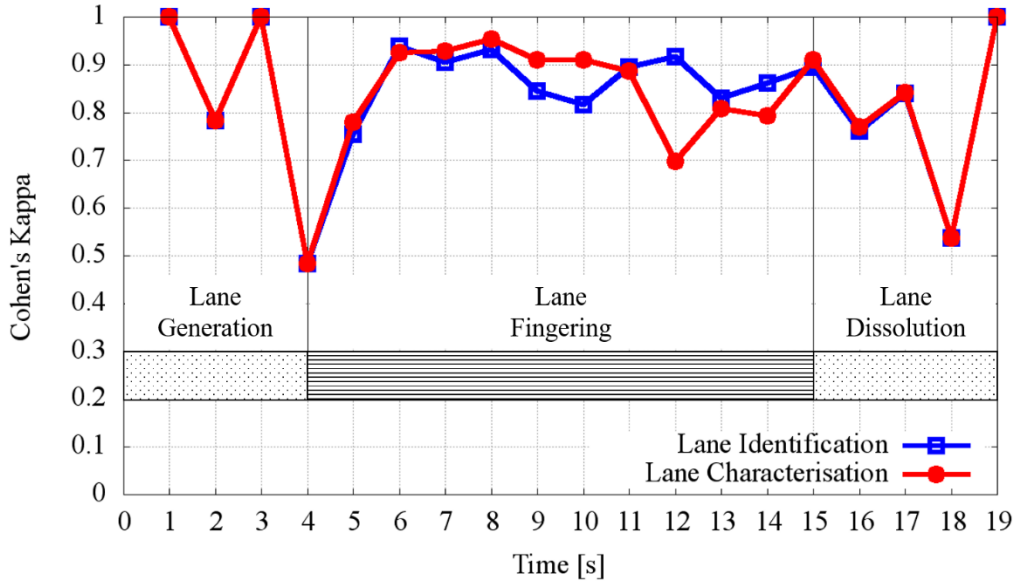


Figure 4: Level of agreement between the algorithm and the human rater in lane identification (blue line) and lane characterisation (red line). The chart illustrates also the three phases of the observed lane formation phenomenon.

Although the formation of lanes is a well-known phenomenon in this field of study, there is still a lack of formal definition for its quantitative characterization. As a general guideline, we started from drafting a common-sense definition of the lane formation phenomenon for sake of human rater analysis, as follow: “a lane is a group of three or more pedestrians, walking in the same direction with a river-like spatial arrangement, avoiding collision with counter flows”.

Then, the human coder was asked to analyse both the video images of the experiments and a video-clip where position and IDs of pedestrians (see Fig. 3(a) and (b)): the video clip has been prepared with the positions of the tracked pedestrians participating the above described experiments, annotated with a numerical identifier to allow human coder to identify pedestrians walking in lanes. To facilitate manual annotation of ID of the lane, the coder was asked to analyse the images of the two synchronised videos starting from the bottom-right part of the screen. To more thoroughly evaluate all these indicators the coder was also asked to rewind the video and take the necessary time to classify pedestrian lanes.

According to the above described methodology, the video of one experimental procedure was analysed by annotating the situation every 30 frames and by describing the observed lane formation phenomenon in the last second. Pedestrians have been classified with a univocal numerical identifier considering:

- their condition of “walking out of any lane” or “walking in a lane” (i.e. *gross classification*);
- their belonging to a certain lane (i.e. *granular classification*).

More in details, the coder was asked to annotate the following information for each second of the video: (i) time of the video; (ii) numerical identifier of pedestrian; (iii) numerical identifier of lane. The conventional value -1 was assigned to identify the condition of “walking out of any lane”, while values greater or equal to zero were used to assign the ID of the lane the pedestrian belonged to in that time frame.

The described data analysis procedure had the objective to cross-check the results about lane formation phenomena achieved through the clustering algorithm and the support of a human coder. To measure the level of reliability of the tool, we tested the level of inter-rater agreement between the two

methods by means of a series of Cohen's Kappa statistical analysis [13]. The Kappa statistics measures the level of inter-rater agreement between two coders in classifying a certain object/subject by using categorial variables. It has a maximum value of 1, when agreement is perfect, 0 when agreement is no better than chance. Other values can be roughly interpreted as: < 0.20 poor; < 0.40 fair; < 0.60 moderate; < 0.80 good agreement. Results (see Figure 4) showed a high agreement on average between the two independent coding methods in both gross classification ($K = 0.837$, $SD 0.144$) and granular classification ($K = 0.841$, $SD 0.139$), confirming the consistency of results and empirically corroborating the reliability of the clustering algorithm.

As introduced by other works present in the literature (e.g., [9, 14]), we analysed the observed pedestrian counter flow situations as subdivided into three phases (see Figure 4): (i) *lane generation* (from the first frame in which pedestrians are separated according to their movement direction, to the moment in which the two flows physically interact and lanes start to emerge); (ii) *lane fingering* (bidirectional flow characterised by the consolidation of the emerged lanes); (iii) *lane dissolution* (lanes are being dissolved). According to this consideration, Cohen's Kappa results has been further analysed considering the lower level of inter-rater agreement in case of lane generation and lane dissolution situations (see Figure 4), due to an effectively more ambiguous situation among the observed phenomenon. Moreover, the trend within the central time window although always over the moderate agreement threshold (and almost always above the good one) is not stable, but it rather reflects transient turbulences in which the number of lanes and their position in the corridor was changing. This seems reasonable, since these transient situations represent a sort of phase change between more stable configurations, that the human coder can foresee, also being able to rewind and look back at the past, a situation analogous to automated trackers taking a global perspective on the analysed video compared to those based on a limited-temporal-locality assumption [15].

5. Conclusions

The paper presented an unsupervised learning approach for an automatic detection of lanes in multi-directional pedestrian flows, based on the DBSCAN clustering algorithm. We also presented a method for the evaluation of its reliability employing an inter-rater agreement test between the results achieved by a human coder and by the algorithm. Achieved results are promising and they will support a further calibration of the overall workflow, that will also consider additional datasets from the literature and potentially consider multiple human coders.

Even though there are many future works in this line of research (first of all, the impact of the presence of groups on the overall phenomenon, which is considered a potentially relevant factor [16]), the central goal is to achieve a characterisation of lanes throughout the whole analysed video and time frame, whereas the current approach only considers relatively small time windows. The basic idea to aggregate current results into a global description of identified lanes is to connect local lanes within different time windows whenever the Jaccard distance among them (considering them as sets of pedestrian identifiers) is greater than a certain threshold. This will allow us to have a more comprehensive characterisation of a lane, granting the possibility to evaluate its persistence in time, average cardinality, length, and potentially other aggregated measures.

Acknowledgements

The authors thank Prof. Katsuhiko Nishinari, Prof. Daichi Yanagisawa and Dr. Claudio Feliciani for their contribution in the design and execution of the experiments referred in this paper. The authors thank also Dr. Yiping Zeng for his contribution in the implementation of the algorithm.

References

- [1] S. J. Older, "Movement of Pedestrians on Footways in Shopping Streets", *Traffic Eng. Control*, 1968.
- [2] J. J. Fruin, *Pedestrian Planning and Design*. New York, Metropolitan Association of Urban Designers

and Environmental, 1971.

- [3] M. Boltes and A. Seyfried, “Collecting pedestrian trajectories”, *Neurocomputing*, vol. 100, 2013, pp. 127–133.
- [4] F. Solera, S. Calderara, and R. Cucchiara, “Socially Constrained Structural Learning for Groups Detection in Crowd”, *IEEE Trans. Pattern Anal. Mach. Intell.*, vol. 38, no. 5, 2016 pp. 995–1008.
- [5] S. D. Khan, S. Bandini, S. Basalamah, and G. Vizzari, “Analyzing crowd behavior in naturalistic conditions: Identifying sources and sinks and characterizing main flows”, *Neurocomputing*, vol. 177, pp. 543–563, 2016.
- [6] J. Zhang, W. Klingsch, A. Schadschneider, and A. Seyfried, “Ordering in bidirectional pedestrian flows and its influence on the fundamental diagram”, *J. Stat. Mech. Theory Exp.*, no. 2, 2012, p. 9.
- [7] A. Schadschneider, W. Klingsch, H. Klüpfel, T. Kretz, C. Rogsch, and A. Seyfried, “Evacuation Dynamics: Empirical Results, Modeling and Applications”, in *Encyclopedia of Complexity and Systems Science*, New York, NY: Springer New York, 2009, pp. 3142–3176.
- [8] J. Dzubiella, G. P. Hoffmann, and H. Löwen, “Lane formation in colloidal mixtures driven by an external field”, *Phys. Rev. E - Stat. Physics, Plasmas, Fluids, Relat. Interdiscip. Top.*, vol. 65, no. 2, 2002.
- [9] C. Feliciani and K. Nishinari, “Empirical analysis of the lane formation process in bidirectional pedestrian flow”, *Phys. Rev. E*, vol. 94, no. 3, 2016.
- [10] S. Hoogendoorn and W. Daamen, “Self-Organization in Pedestrian Flow”, in *Fifth International Conference on Traffic and Granular Flow*, 2003, pp. 373–382.
- [11] M. Ester, H.-P. Kriegel, J. Sander, and X. Xu, “A Density-Based Algorithm for Discovering Clusters in Large Spatial Databases with Noise”, in *Proceedings of the Second International Conference on Knowledge Discovery and Data Mining*, 1996, pp. 226–231.
- [12] A. Gorrini, L. Crociani, C. Feliciani, P. Zhao, K. Nishinari, and S. Bandini, “Social groups and pedestrian crowds: experiment on dyads in a counter flow scenario”, in *8th International Conference on Pedestrian and Evacuation Dynamics (PED2016)*, 2016, pp. 179-184. Also available as *arXiv Prepr. arXiv1610.08325*.
- [13] J. R. Landis and G. G. Koch, “The measurement of observer agreement for categorical data”, *Biometrics*, 1977, pp. 159-174.
- [14] D. Helbing, P. Molnár, I. J. Farkas and K. Bolay, “Self-organizing pedestrian movement”, *Environment and planning B: planning and design*, 28(3), 2001, 361-383.
- [15] A. R. Zamir, A. Dehghan and M. Sha, “GMCP-tracker: Global multi-object tracking using generalized minimum clique graphs”, in *Computer Vision–ECCV*, 2012, pp. 343-356.
- [16] L. Crociani, A. Gorrini, C. Feliciani, G. Vizzari, K. Nishinari, S. Bandini, “Micro and macro pedestrian dynamics in counterflow: the impact of social groups”, in *12th International Conference on Traffic and Granular Flow - TGF 2017*, in press. Also available as arXiv preprint arXiv:1711.08225.

Accurate pedestrian localization in overhead depth images via Height-Augmented HOG

Werner Kroneman, Alessandro Corbetta, Federico Toschi

Eindhoven University of Technology

Department of Applied Physics

Postbus 513, 5600 MB, Eindhoven, The Netherlands

w.kroneman@tue.nl; a.corbetta@tue.nl; f.toschi@tue.nl

Abstract – We tackle the challenge of reliably and automatically localizing pedestrians in real-life conditions through overhead depth imaging at unprecedented high-density conditions. Leveraging upon a combination of Histogram of Oriented Gradients-like feature descriptors, neural networks, data augmentation and custom data annotation strategies, this work contributes a robust and scalable machine learning-based localization algorithm, which delivers near-human localization performance in real-time, even with local pedestrian density of about 3 ped/m², a case in which most state-of-the-art algorithms degrade significantly in performance.

Keywords: real-life pedestrian dynamics measurements; depth-based localization; machine learning; augmented HOG features; high-density localization

1. Introduction

In order to design more pedestrian-friendly environments or improve the evacuation performance of buildings, developing reliable quantitative models of crowd behavior is paramount. The formulation and validation of models demands the acquisition of accurate, real-life, experimental data, e.g. in the form of individual trajectories. Due to the variability of pedestrian behavior, large data volumes are required to robustly isolate average behaviors and obtain resolved statistics of fluctuations and rare events [1,2].

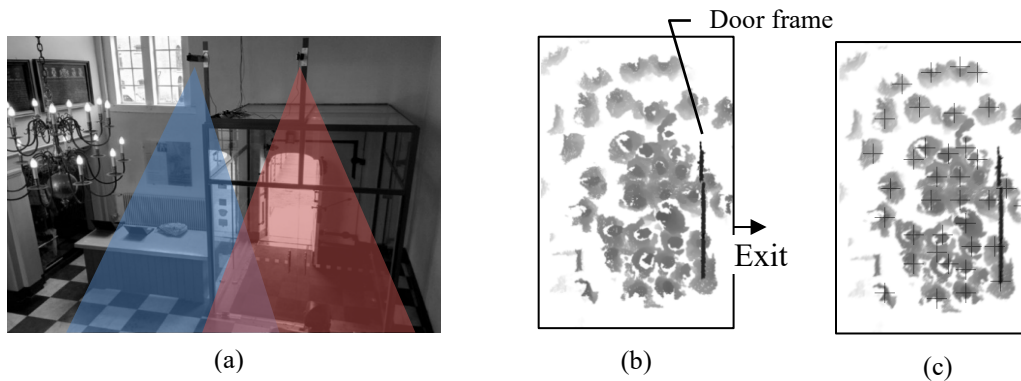


Figure 1: (a) Depth-based tracking system composed of two overhead depth sensors (Microsoft Kinect®) [3] deployed at the entrance of the Pesthuis at the Naturalis Biodiversity Center in Leiden (photo by AC). (b) Sample of a depth image. The depth field is colorized such that points of lower depth, i.e. closer to the sensor and higher above the ground, are in a darker shade. This depth image is taken a moment before a school group leaves through the door. As can be seen in (b), extremely high crowd densities occur at this site, and individual localization is difficult even for a human expert. Pedestrian positions are reported in (c) as output by the HA-HOG method introduced in this paper. This method delivers near-human-quality localization in these conditions, considerably improving upon the state of the art.

However, for the strong variability in pedestrian shapes and environments, achieving quantity and quality of measurements while operating in real-life conditions is a substantial technical challenge. Moreover, privacy regulations for public spaces dictate that recorded images of pedestrians must be anonymous.

Since 2013, overhead depth sensing has shown remarkable capabilities for real-life pedestrian localization, and has been employed in a number of recent experiments [2, 4, 5, 6]. Depth images map the distance between each point and the camera plane. Their usage, in place of color images, allows one to bypass difficulties related to varying light and color as the depth maps directly capture the 3-dimensional shape of pedestrians. Besides, as can be seen in Figure 1b, depth images also contain insufficient information to personally identify pedestrians, which ensures anonymity. Typically, sensors (e.g. Microsoft Kinect® [3]) are placed overhead, facing downwards, to avoid mutual pedestrian occlusions in the captured signals. Multiple cameras can be combined in grid-like configurations to cover larger areas as in Figure 1 or in [4, 7].

Individual tracking is typically implemented as a two-step process: 1. localizing pedestrians in consecutive depth images; 2. linking these detections across time into tracks. So far, the localization step has been a challenge. Especially in dense crowds where pedestrians walk or stand closely together, the most commonly-used method, clustering [6], exhibits a substantial performance degradation, producing errors such as those depicted in Figure 2. Besides, achieving high-frequency localization is paramount to minimize tracking error, so high algorithmic and implementation efficiency is a must.

In this contribution, we present a robust and scalable localization method based on a Histogram-of-Oriented-Gradients-like [8] feature descriptor and a neural network classifier, which remains accurate even at high density. This paper is structured as follows: in Section 2, we elaborate on bottlenecks in state-of-the-art techniques. In Section 3, we introduce our method whose performance is discussed in Section 4. A final discussion concludes the paper.

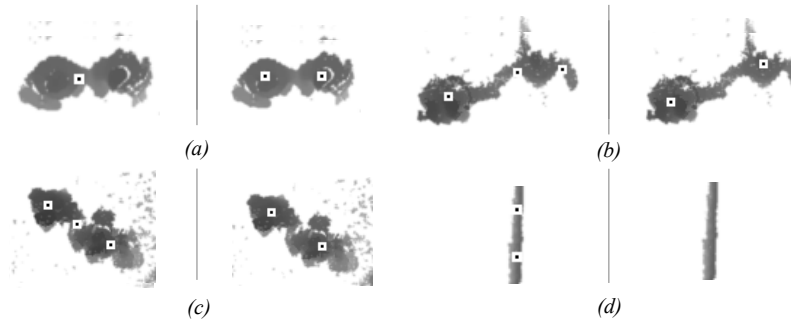


Figure 2: (left panels, a-d) Common errors made by overhead depth-map-based localization algorithms (here considering the clustering method in [6]), (right panels, a-d) ground truth. Specifically: (a) two pedestrians detected as one, (b) a single pedestrian detected multiple times, (c) a hand detected as a pedestrian and (d) a wall confused for a pedestrian. Such errors are made because the clustering algorithm has almost no notion of pedestrian shape, and therefore cannot easily distinguish pedestrians when standing so close together, nor tell the difference between pedestrians and other objects.

2. Related work

To the best of our knowledge, the only techniques employed to localize pedestrians in real-life depth-based crowd dynamics investigations are clustering-based (e.g. [2, 4, 5, 6]). Typically, these techniques involve, first, foreground/background separation based on a height threshold. Then, the point clusters that are left in the foreground are interpreted as persons. At low density, such a pedestrian-cluster association is very effective as wide mutual distances ensure that never two people are clustered together. Besides, clustering is a simple method, with most clustering algorithms only requiring a small number of parameters. However, the accuracy drops severely at higher pedestrian densities, exhibiting problems as shown in

Figure 2. Moreover, clustering becomes computationally expensive as the size or complexity of the depth map increases, as stated in [9].

Awareness of pedestrian shape is necessary to bypass the bottlenecks of clustering (Figure 2), and thus segment pedestrians standing close together. However, countless exceptions are encountered in real-life data, which result from variations in pedestrian shape or imperfections in the depth image. Hence, writing a shape-aware algorithm which achieves sufficiently high localization performance is extremely difficult, with constant requests for the treatment of newly-discovered exceptional cases.

One possible solution to this problem, recently exploding in popularity, is the use of deep learning models [10]. These models are trained end-to-end by annotated examples, and can then generalize towards cases they were never presented with. This, however, requires a large set of depth images manually-annotated with pedestrian positions, incredibly labor-intensive to obtain. To bypass this problem, in [11], a convolutional neural network is trained end-to-end employing synthetically-generated training data. Although the method is reported to have better performance than clustering-based approaches, precision and recall values still dropped below 0.95 at higher pedestrian densities, which is lower than achieved with our method. Besides, synthetically generating realistic high-density depth images is likely a highly non-trivial task.

In the next section, we present a technique inspired by “classic” machine learning approaches which combines learning by examples and traditional localization algorithms. This ensures both robustness against exceptions and low cost of training.

3. HA-HOG localization

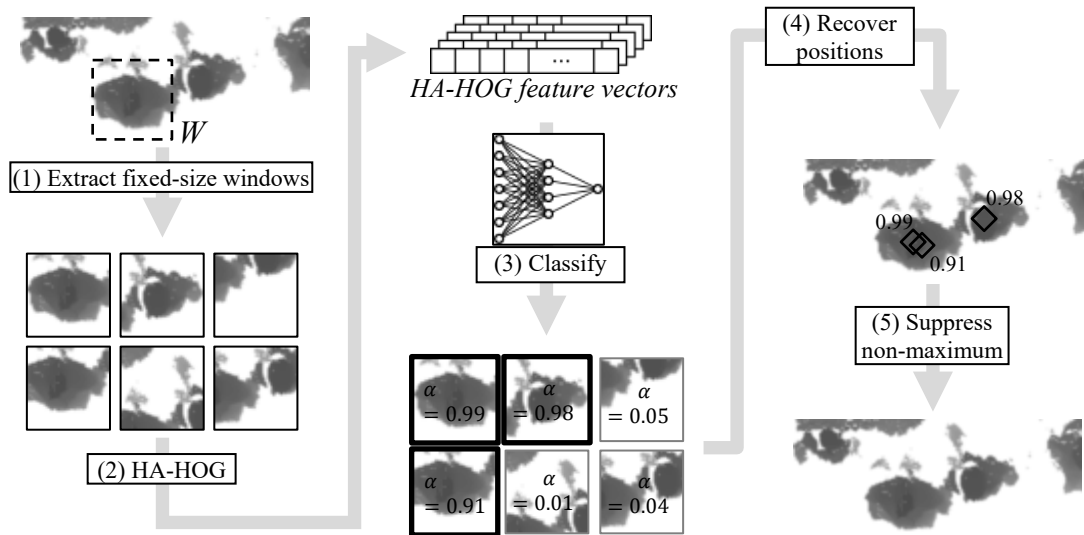


Figure 3: Outline of the localization process. (1) Slide a window with a fixed size slightly larger than a pedestrian over the depth map and process the content separately. (Only a small number are shown here for illustration purposes.) (2) Compute the HA-HOG of each of these samples (3) and present these feature vectors to a neural network, which assigns a score to each sample based on whether it is centered on a pedestrian or not (the score is approximately 1 or 0 in each case, respectively). By applying a threshold, translate this score to a binary “positive” or “negative” decision. (4) Next, associate the positively-classified samples with positions in the depth map. (5) Since multiple windows can be roughly centered on the same pedestrian, this pedestrian may be detected multiple times. Therefore, apply non-maximum suppression to remove duplicate detections. Finally, return the resulting set of positions as the set of detected pedestrian locations within the depth image.

In order to localize pedestrians in a depth image, we slide a fixed-size window throughout the image and classify its content depending on whether it is centered on a pedestrian or not. The process is illustrated in Figure 3 and explained in the next sections. Specifically, in Section 3.1 we present the HA-HOG feature

descriptor and in Section 3.2 we explain its usage for localization. Training and implementation details are provided in Section 3.3.

3.1. HA-HOG Feature description computation

“Image descriptors” are methods that take an image and return a summarized representation, isolating information relevant to the problem. Such simpler representations require less complex statistical models (and therefore training data) when it comes to content classification. In our method, we adapt a simplified version of “Histogram of Oriented Gradients” (HOG), originally introduced by Dalal and Triggs [8] for the detection of humans in color images. Let W be the content of a window sliding through a depth image. The HOG features of W are computed as follows:

1. compute the gradient field $\vec{G} = \nabla W$ (e.g. using the second order finite differences method);
2. compute the polar representation of \vec{G} , (G_r, G_φ) , such that:

$$\vec{G} = (G_x, G_y) = G_r \cdot \begin{pmatrix} \cos G_\varphi \\ \sin G_\varphi \end{pmatrix} \text{ and } 0 < G_\varphi < 2\pi;$$

3. partition \vec{G} into a grid of small, non-overlapping cells. In our case, these cells are square and five or six pixels wide. In each cell, make a histogram of the gradient vectors, binned using G_φ and weighted by G_r . Finally, the histogram is normalized to have unit L2-norm. In formulas, the HOG feature of a cell reads:

$$HOG_{cell} = \frac{Histogram(G_\varphi, weights = G_r)}{|Histogram(G_\varphi, weights = G_r)|};$$

4. concatenate the HOG of each cell in the window to yield the HOG descriptor of the window W .

$$HOG(W) = [HOG_{cell}(c_1), HOG_{cell}(c_2), \dots, HOG_{cell}(c_n)].$$

To further increase the classification accuracy (see Section 3.2), we integrate height information in the feature descriptor, the result of which we call Height-Augmented HOG (HA-HOG), i.e. algorithmically

5. compute a histogram of the depth values over W , which we then concatenate with the HOG:

$$HA-HOG(W) = [HOG(W), Histogram(heights in W)].$$

Step 5 is aimed at allowing the classifier to avoid the misclassification of objects that are similar in shape to pedestrians, but differ significantly in height distribution.

3.2. Classification and localization

After computing the HA-HOG of each image window W , the resulting feature vectors are presented to a multilayer perceptron ([12], see [13] for an example of HOG used in combination with a neural network classifier). The neural network is trained through back-propagation to return a value α , with $0 \leq \alpha \leq 1$, near 1 for samples that contain a pedestrian in the middle (“positive”), and near 0 for ones that either do not contain a pedestrian or are not centered on one (“negative”). All windows for which $\alpha \geq t$ ($t \cong 0.9$) are retained and their center is considered as a candidate for a pedestrian location.

Since the window is moved in strides which are much smaller than the size of a person, multiple consecutive windows may be roughly centered on a pedestrian and be classified as positive. This results in a pedestrian detected multiple times. To prevent this, non-maximum suppression is applied on the resulting

set of positions: for pairs of locations that lie closer to each other than a certain threshold, the location with a lower α is discarded. This process is repeated until no such pairs of locations exist. The resulting set of locations is then interpreted as the locations of pedestrians within the image.

3.3. Training and implementation details

Creating a sufficiently large set of annotated training examples by manually annotating thousands of examples is labor-intensive human work. To bypass this bottleneck, we rely on image augmentation: in our case applying random mutations to image samples such as rotations of 90 degrees and noise insertion, effectively yielding a much larger set of training examples, also done in [14, 15]. Moreover, we also developed a tool which runs the algorithm on a random image and presents the result to a human expert, who can then quickly extract new training examples based on a visual comparison of the set of detected pedestrian locations and the original depth map, thereby targeting weaknesses in the training set. This is essentially a form of hard-mining or bootstrapping [16].

In order to reduce the computational cost of the HOG computation, setting the window stride to a multiple of the HOG cell size will cause many windows to have a large number of overlapping HOG cells, which will only have to be computed once. In our implementation, HOG cells are computed at once over the whole image, and then concatenated in overlapping blocks corresponding to the samples that would be taken by a sliding window on the original depth map.

We compute the HOG features of the image in TensorFlow [17] so as to be able to use the GPU. We implement, train and evaluate the neural network itself using the Keras machine learning framework [18]. Using the GPU capabilities of TensorFlow and Keras, the method can detect pedestrians at over 20 fps on a GT-1030 graphics card, even on depth images as large as those collected during the Glow 2017 campaign (see Figure 4 and [7]).

4. Performance

In order to assess the quality of the localization provided by HA-HOG, we manually annotated a set of depth images (disjoint from the training set), and compared our method against classic HOG and an implementation of the clustering-based method (cf. Section 2) used in [1, 2, 4].

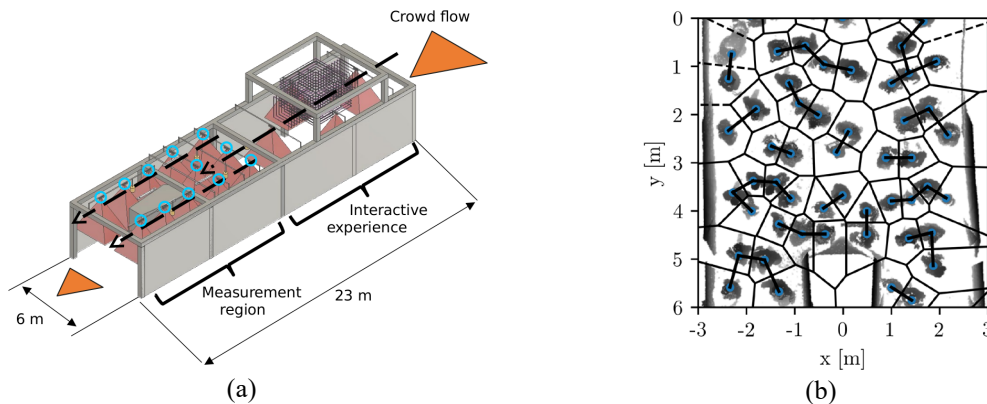


Figure 4: (a) Diagram of the “Moving Light” exhibit at the Glow 2017 light festival in Eindhoven [Glow 2017]. It features a long, mostly continuous stream of people who walk through a large, grid-like set-up of twelve depth cameras (Microsoft Kinect®), circled in blue. Our GPU implementation of HA-HOG can localize pedestrians in this data with high accuracy while still running at over 20 fps. (b) Example of a depth map from the dataset collected at the exhibit annotated with pedestrian positions. A Voronoi tessellation of these annotations is provided and nearest-neighbor relations are displayed as well. All false-positives, false-negatives and true positives are associated with a ground truth position based on the Voronoi cell they fall into, and are thus assigned a nearest-neighbor distance. See Section 4.2 for details.

4.1. Dataset description

We benchmark the algorithm against data from 2 real-life locations:

- The Glow festival in Eindhoven during November in 2017 [7], see Figure 4, featuring a set of twelve cameras, yielding a challenge for computational performance. For instance, the clustering method becomes too computationally expensive to use on images of this size without severely compromising localization accuracy. This data features many people walking close together in small groups in which individuals can be hard to tell apart;
- The entrance of the Pethuis of the Naturalis Biodiversity Center in Leiden between January and May 2018, see Figure 1, featuring extremely high crowd densities and complex scenes, a real challenge for localization even for human experts;

From both datasets, about 80 full-scale frames with high crowd densities were extracted, and annotated by hand (containing a total of, respectively, 1059 and 600 annotations). No training samples are taken from these frames to ensure that the results do not merely result from over-fitting.

4.2. Density-dependent performance analysis

We localize pedestrians in the hand-annotated test frames (see Section 4.1) using HA-HOG, classic HOG and complete linkage clustering, the result of which is then compared to hand-annotated positions, from which we identify true positive (TP), false positive (FP) and false negative (FN) localizations. Let r_{nn} be the distance between each manual annotation and its nearest neighbor. We use the density ρ_{nn} , evaluated as $\rho_{nn} = 1/(\pi \cdot r_{nn}^2)$, as an indication of localization difficulty. In this case, high density values directly imply close vicinity of the nearest neighbor (see Figure 4b). We bin each TP, FP and FN by ρ_{nn} (taken from the closest manual annotation). Then, for each ρ_{nn} bin, let #TP be the count of true positives in that bin (and analogously for #FP and #FN). We evaluate localization performance in terms of density-dependent F-score, defined as $2 \cdot (\text{Precision} \cdot \text{Recall}) / (\text{Precision} + \text{Recall})$, where precision and recall are defined as $(\#TP) / (\#TP + \#FP)$ and $(\#TP) / (\#TP + \#FN)$ respectively.

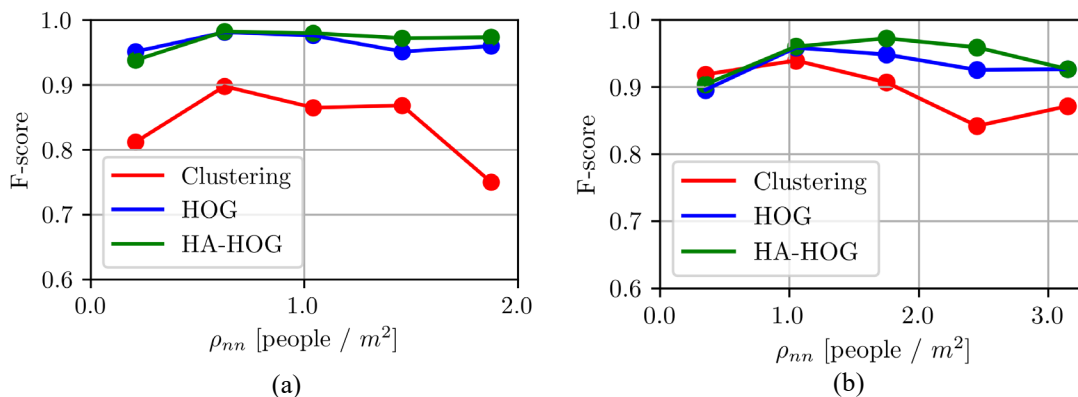


Figure 5: F-score of the localization methods as a function of the distance between closest pairs of pedestrians, when performing on (a) the Glow 2017 dataset and (b) on the Naturalis dataset. Both datasets are presented in Section 4.1. Nearest-neighbor distance is plotted on the horizontal axis with distance decreasing, and difficulty increasing, from left to right. For definitions and a discussion of the results, see Section 4.2.

On the Glow dataset (Figure 5a), HA-HOG performs comparably to HOG, and significantly outperforms clustering at all densities, especially around $\rho_{nn} = 2$ ped/m². On the Naturalis dataset, on the other hand, HA-HOG shows a significant performance gain over both classic HOG and clustering especially at particularly challenging conditions occurring for $\rho_{nn} > 2$ ped/m².

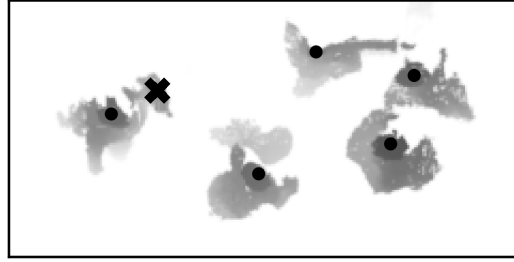


Figure 6: Depth map annotated with pedestrian positions using HA-HOG, with a dot for true positives, and a cross for false positives according to a comparison with manually-annotated positions. Note the false positive on the left: from looking at this depth image, it is difficult to tell whether this is really a false positive. The height and size roughly correspond to a small child, so the output of HA-HOG may be justified in this case despite it counting against the F-score.

At the lowest density bin, one may notice the F-score of HA-HOG dropping below 0.9. Part of this can be attributed to statistical noise, as the number of ground-truth annotations for this bin is only around 50. Besides we found that cases where even human experts fail to find agreement in annotation (cf. Figure 6) are generally associated with positive localization by HA-HOG, whilst being generally ignored by clustering. This causes a higher density-dependent F-score for the clustering method.

5. Discussion

In this paper, we presented HA-HOG, a technique for localizing pedestrians in overhead depth images robust even in high-density cases. The technique extends the classic Histogram of Oriented Gradients feature descriptor to include information about height distribution easily accessible from depth images. The method leverages awareness of shapes to achieve localization, which allows to outperform current approaches based on clustering, especially in high-density conditions. Furthermore, being trained by examples, the method remains robust against exceptions in shape, ubiquitous in real-life data. As annotated example are used just to train a final classifier, rather than the whole feature extractor (as done in deep learning-based approaches), they can be produced with limited human labor (few hours).

To evaluate performance we employed two datasets acquired in two real-life experiments in both of which our method showed near-human performance, with F-score above 95% at around 2.5 ped/m². Finally, unlike clustering, HA-HOG can be efficiently parallelized, e.g. on a GPU, with the computational cost scaling only linearly with the number of pixels.

Acknowledgements

This work is part of the JSTP research programme “Vision driven visitor behavior analysis and crowd management” with project number 341-10-001, which is financed by the Netherlands Organization for Scientific Research (NWO). We acknowledge the support of Naturalis Biodiversity Center for hosting our measurement setup. We thank all contributors of the Moving Light experiment (in Figure 4a) for which we acknowledge the support of NWO, 4TU, Glow, Philips Lighting and Student Hotel Eindhoven. Figure 4a is made in collaboration with Bert Maas.

References

- [1] A. Corbetta, C. Lee, R. Benzi, A. Muntean and F. Toschi, “Fluctuations around mean walking behaviors in diluted pedestrian flows,” in *Physical Review E*, vol. 95, no. 3, 032316, 2017.
- [2] A. Corbetta, L. Bruno, A. Muntean and F. Toschi, “High Statistics Measurements of Pedestrian Dynamics,” *Transportation Research Procedia*, vol. 2, pp. 96–104, 2014.
- [3] Microsoft Corporation, “Kinect for Xbox 360,” Redmond, WA, USA.
- [4] A. Corbetta, J. Meeusen, C. Lee and F. Toschi, “Continuous measurements of real-life bidirectional pedestrian flows on a wide walkway,” in *Proceedings of Pedestrian and Evacuation Dynamics*, pp. 18–24, 2016.
- [5] D. Brscic, T. Kanda, T. Ikeda and T. Miyashita, “Person Tracking in Large Public Spaces Using 3-D Range Sensors,” in *IEEE Transactions on Human-Machine Systems*, vol. 43, no. 6, pp. 522–534, 2013.
- [6] S. Seer, N. Brändle and C. Ratti, “Kinects and human kinetics: A new approach for studying pedestrian behavior,” in *Transportation Research Part C: Emerging Technologies*, vol. 48, pp. 212–228, 2014.
- [7] A. Corbetta, W. Kroneman, M. Donners, A. Haans, P. Ross, M. Trouwborst, S. vd Wijdeven, M. Hultermans, D. Sekulowski, F. vd Heijden, S. Mentink and F. Toschi, “A large-scale real-life crowd steering experiment via arrow-like stimuli,” in *Pedestrian and Evacuation Dynamics*, 2018 (accepted).
- [8] N. Dalal and B. Triggs, “Histograms of Oriented Gradients for Human Detection,” in *IEEE Computer Society Conference on Computer Vision and Pattern Recognition (CVPR05)*, 2005, pp. 886–893
- [9] A. Corbetta, “Multiscale crowd dynamics: physical analysis, modeling and applications,” Ph. D. thesis, Eindhoven University of Technology, 2016.
- [10] J. Redmon, S. Divvala, R. Girshick and A. Farhadi, “You Only Look Once: Unified, Real-Time Object Detection,” in *2016 IEEE Conference on Computer Vision and Pattern Recognition (CVPR)*, 2016, pp. 779–788.
- [11] A. Corbetta, V. Menkovski and F. Toschi, “Weakly supervised training of deep convolutional neural networks for overhead pedestrian localization in depth fields,” in *14th IEEE International Conference on Advanced Video and Signal Based Surveillance (AVSS)*, 2017, pp 1-6.
- [12] R. Collobert and S. Bengio, “Links between perceptrons, MLPs and SVMs,” in *Proceedings of the Twenty-first international conference on Machine learning - ICML 04*, 2004.
- [13] Q. Xia, H.-D. Zhu, Y. Gan and L. Shang, “Plant Leaf Recognition Using Histograms of Oriented Gradients,” in *Intelligent Computing Methodologies Lecture Notes in Computer Science*, pp. 369–374, 2014.
- [14] D. Ciresan, U. Meier and J. Schmidhuber, “Multi-column deep neural networks for image classification,” *Proceedings of the 2012 IEEE Conference on Computer Vision and Pattern Recognition*, 2012, pp. 3642-3649.
- [15] L. Perez and J. Wang, “The Effectiveness of Data Augmentation in Image Classification using Deep Learning,” arXiv:1712.04621, 2017.
- [16] K.-K. Sung, “Learning and example selection for object and pattern detection,” Ph. D. thesis, Massachusetts Institute of Technology, 1996.
- [17] M. Abadi, et al, “TensorFlow: Large-Scale Machine Learning on Heterogeneous Systems,” *Proceedings of the 12th USENIX conference on Operating Systems Design and Implementation (OSDI’16)*, 2016, pp 265-283.
- [18] F. Chollet, et al, “Keras,” 2015. Available: <https://keras.io>.

Anomaly Detection of Pedestrian Flow: A Machine Learning Method for Monitoring-Data of Visitors to a Building

Kentaro Kumagai^{1,2}

¹Graduate School of Management, Kyoto University
Maskawa Bld. for Res. and Ed., Kitashirakawa-Oiwake, Sakyo, Kyoto, 606-8502, Japan
kumagai.kentaro.3e@kyoto-u.jp

²Disaster Prevention Research Institute, Kyoto University

Abstract - Many public facilities such as community halls and gymnasiums are supposed to be evacuation sites when disasters occur. From the viewpoint of managing such facilities, it is necessary to monitor the usage and to respond immediately when an anomaly occurs. In this study, an integrated system of IoT sensors and machine learning for anomaly detection of pedestrian flow was proposed for buildings that are expected to be used as emergency evacuation sites in the event of a disaster. For trial practice of the system, infrared sensors were installed in a research building of a university, and data of visitors to the fourth floor of the building was collected as a time series data of pedestrian flow. As a result, it was shown that anomalies of pedestrian flow at an arbitrary time of a day with an occurrence probability of 5 % or less can be detected properly using the data collected.

Keywords: anomaly detection, pedestrian flow, integrated system, IoT sensor, machine learning

1. Background

Many public facilities such as community halls and gymnasiums are supposed to be evacuation sites when disasters occur. From the viewpoint of managing such facilities, it is necessary to monitor the usage and to respond immediately when an anomaly occurs. However, it is inefficient for humans to monitor the facilities for 24 hours. In this study, we investigate an integrated system of IoT sensors and machine learning for anomaly detection of pedestrian flow. The system monitors pedestrian flow by using IoT sensors, transmits monitoring data to a digital storage on the web in real time, detects anomalies of pedestrian flow automatically, and supports human judgment.

2. Integrated System of Anomaly Detection of Pedestrian Flow

Fig. 1 shows the configuration of the integrated system of anomaly detection as a conceptual diagram. IoT sensors are installed at an entrance of a building to monitor pedestrian flow. When the sensor detects visitors who enter to the building, an occurrence time of an event is recorded and the data of pedestrian flow is sent automatically in real time to a digital storage on the web. Subsequently, a computer with machine learning program analyses the data (Fig. 2): The computer performs a classification of the time-series data of the past data up to the previous day, into some classes based on

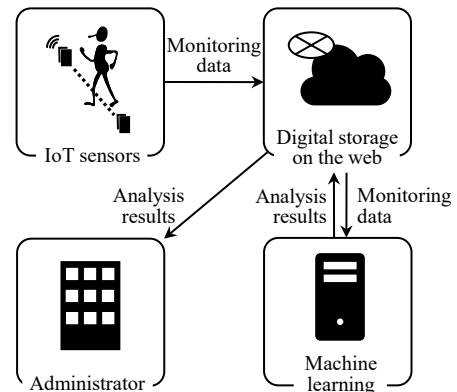


Fig. 1: Configuration of Integrated System.

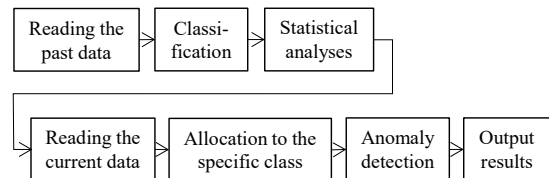


Fig. 2: Flow diagram of Machine learning.

characteristics of the data. And the computer conducts statistical analyses on the data of each class. After the process is finished, the computer allocates the current day's data to the specific class based on the similarity, and performs anomaly detection on the data. Here, "the current day's data" means a set of time-series data of pedestrian flow from the start of the day up to the current time. As the time passes, a data set of "the current day's data" is updated, and the computer repeats the above process iteratively, based on the latest information. At each time step during the day, the computer automatically outputs results and informs them to an administrator when abnormality of pedestrian flow is detected, to support human judgement.

2.1. Trial Practice of the system

The author conducted trial practice of the system as follows: A pair of infrared sensors was installed

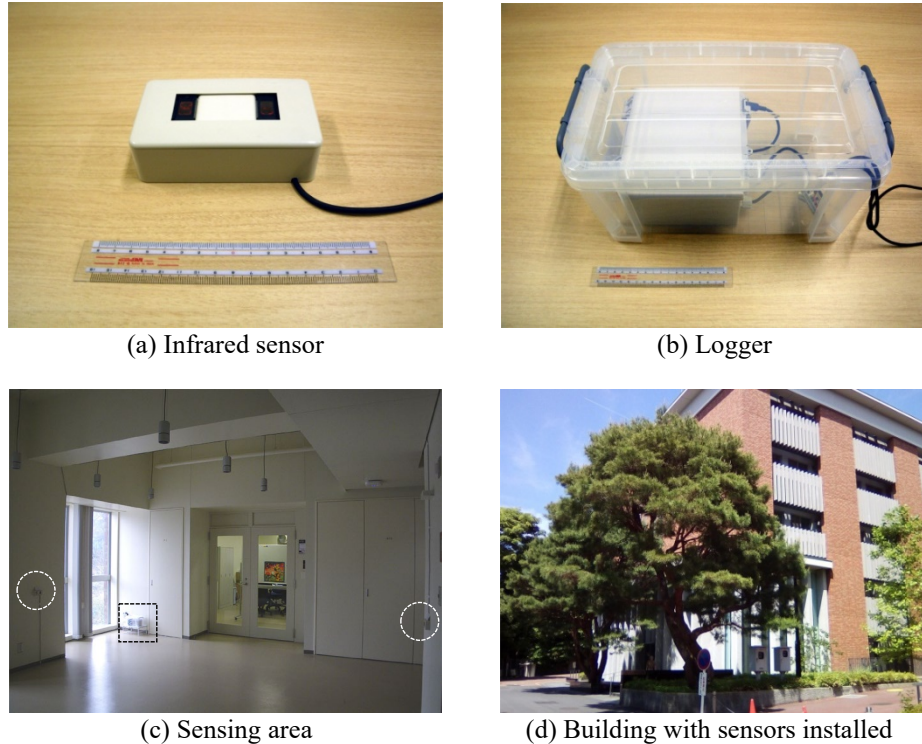


Fig. 2: Infrared sensor, Logger and Building with sensors installed.

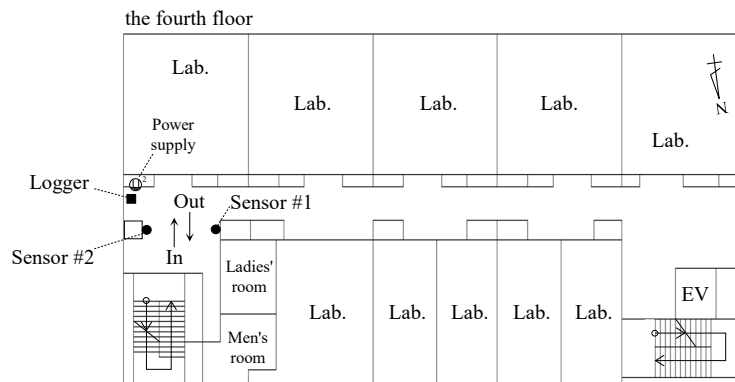


Fig. 3: Plan view of the sensing area in the building

at an entrance of the fourth floor of a research building in Kyoto University. The sensors and a logger (Fig. 2(a), (b)) were products of Scanmatic Marketing Co., Ltd., 'i-trend mini' package. The sensors were attached on the wall at the height of 1 m from the floor, and the sensors were possible to detect the visitor walking through the space between the two sensors. Because a pair of sensors included two irradiation units, the sensor was possible to detect walking direction of the visitor. The minimum resolution in time of this sensor was approximately 0.3 s per event. Each sensor was connected to the logger by cables. Fig. 2(c) shows the sensing area, two white dotted circles on the photo indicate the sensors respectively, and the black dotted square indicates the logger. Fig. 3 is a plan view of the sensing area. The logger saves an occurrence time into a SD memory card, when the sensor detects visitor in 'IN' direction of the figure. The electricity consumed by the sensors and the logger was very low.

Data collected was classified manually into two classes, such as data of weekdays and data for school holidays. A FORTRAN program was written for calculation of the statistical values from data for each class. After the mean value μ and standard deviation σ were calculated for each class by using the past data

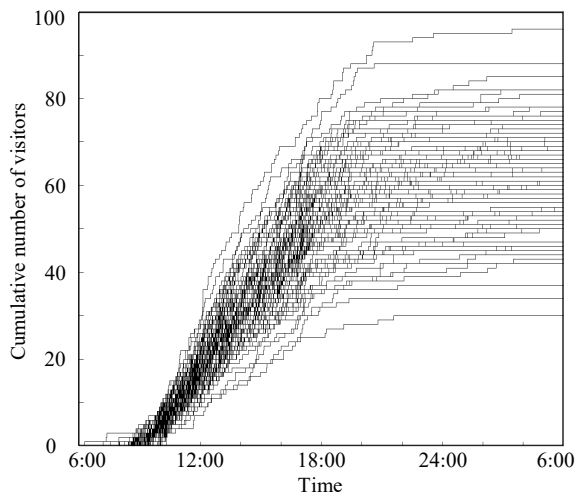
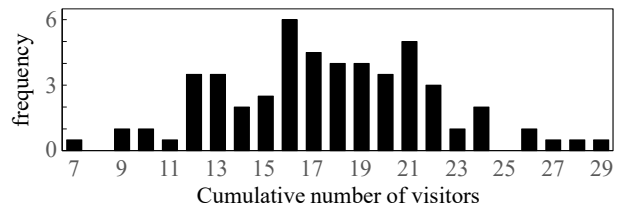
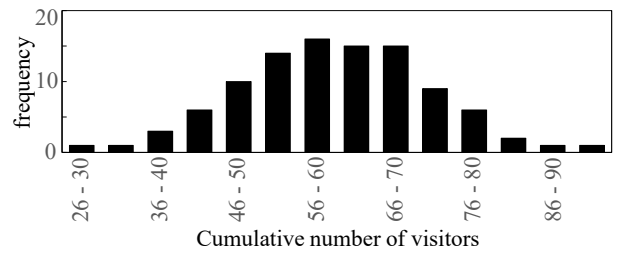


Fig. 4: Time-series of the cumulative number of visitors on weekday.



(1) At 12:00



(2) At 24:00

Fig. 5: Histogram of the cumulative number of visitors.

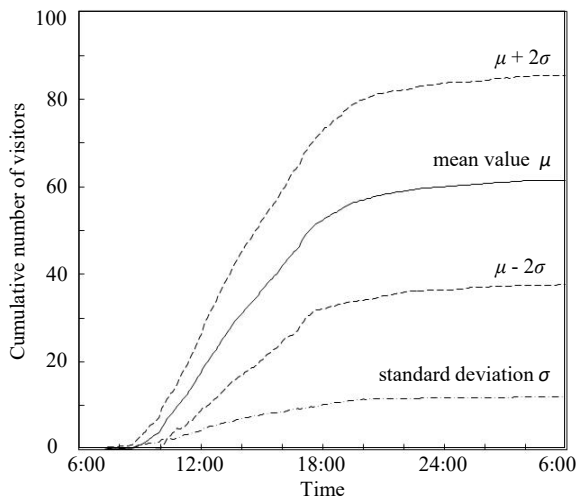


Fig. 6: Mean value μ and standard deviation σ .

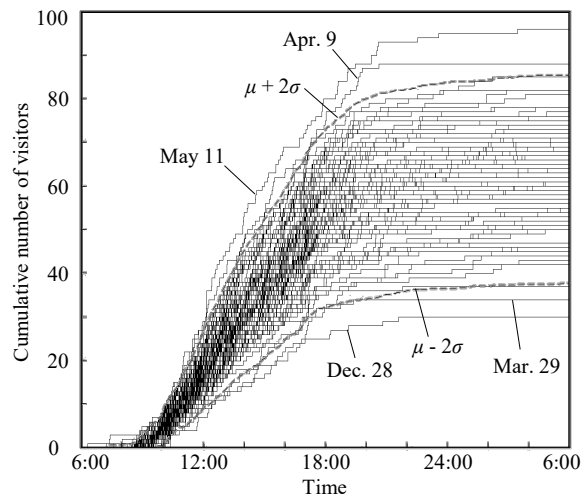


Fig. 7: Superimposing $\mu+2\sigma/\mu-2\sigma$ on Fig. 4.

up to the previous day, the program checked "the current day's data" of pedestrian flow at every five minutes, in view of that the value was in the range of $\mu - 2\sigma$ to $\mu + 2\sigma$ or not.

2.2. Results

Based on the data collected for 152 days, from December 11, 2017 to May 11, 2018, the cumulative number of visitors per day was seemed to be different between weekdays and school holidays. On weekdays, the cumulative number of visitors was in the range of 30 to 95 persons per day. In contrast, that on school holidays was 20 or less. Therefore, it seems to be reasonable to divide the acquired data into two classes, such as data of weekdays and data of school holidays. Here, it should be noted that the word 'a day' means twenty four hours from 6:00 am to 5:59 am of the next day, in this section and the following sections.

Fig. 4 draws the time series of the cumulative number of visitors of weekdays during the above period. The numbers of weekdays were a hundred. The horizontal axis means time, and the vertical axis means the cumulative number of the visitors. It was also possible to draw the distribution of the cumulative number of visitors at an arbitrary time of a day. As an example, Fig. 5(1) and (2) are the histograms of cumulative number of visitors at 12:00 and at 24:00 on weekdays, respectively. In Fig. 5(2), the values were distributed among 30 to 95. Although a strict validation has not been done yet, it seems to be possible to assume that the number of visitors at 24:00 follows a normal distribution. The mean value μ and the standard deviation σ were 61.5 and 12.0, respectively. Fig. 6 shows time-series of μ and σ in a solid line and a dot-dash line, respectively, calculated at every five minutes from 6 am. In the figure, the other two broken-lines showed values of $\mu + 2\sigma$ and $\mu - 2\sigma$, respectively. Assuming that the number of visitors at an arbitrary time of a day follows a normal distribution, if a value exceeding $\mu + 2\sigma$ or a value below $\mu - 2\sigma$ is observed at an arbitrary time of a day in pedestrian flow, it can be judged in real time to occur an anomaly with 5 % or less probability. In Fig. 7, time zones such as almost whole day of December 28, March 29, April 9 and May 11, respectively, should be detected as anomalies.

2.3. Discussions

Dynamic algorithm for automatic classification: To conduct the anomaly detection, information about a class which the current day belongs to is necessary. In the sections 2.1 and 2.2, allocation to the two classes, i.e. weekday or school holiday, was done manually. In case that the target facility is a school, school holidays are often known in advance. However, there are possibilities that irregular holidays may occur depending on facilities. For such facilities, a dynamic algorithm will be requested for automatic classification which allows a user of the system to sort automatically training-data and "the current day's data" up to the current time to an appropriate class dynamically. Since the system is intended to be applied to real-time anomaly detection of pedestrian flow, further consideration is necessary for that point.

Periodic variation: Fig. 8 is a power spectrum of the time-series data of the cumulative number of visitors per day for 152 days, from December 11, 2017 to May 11, 2018. The horizontal axis shows a period of time in the log scale, and the vertical axis shows a density of the power spectrum. The highest peak was at 6.91 day, and this fact means that the strongest periodic fluctuation components included in the data set was a period of approximately one week. In Section 2.2, we focused on weekdays. It was

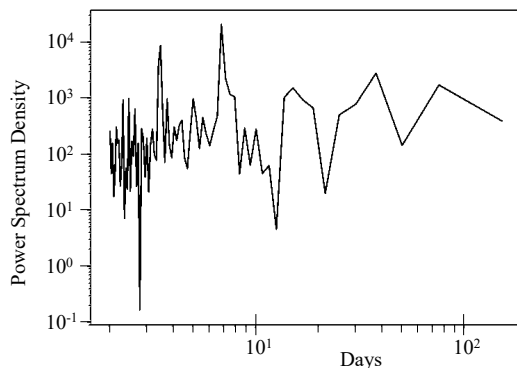


Fig. 8: Power Spectrum

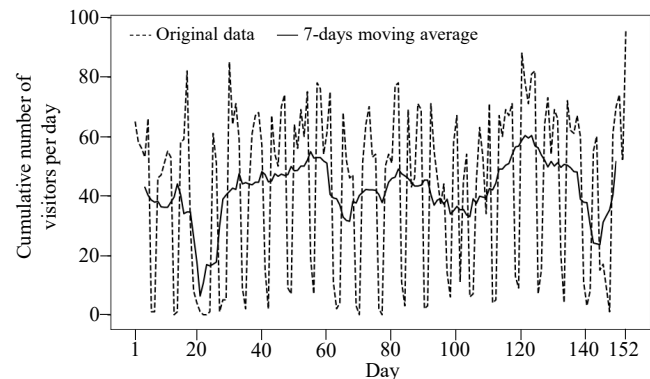


Fig. 9: 7-days moving average

consistent with the fact that the strong periodic fluctuation component of one week.

Fig. 9 shows 7-days moving average of the same data set. The horizontal axis shows number of days since measurement started, and the vertical axis shows the cumulative number of the visitors per day. The broken line and the solid line are the original value and the 7-days moving average, respectively. The broken line obviously showed periodic fluctuation in approximately one week. The solid line showed that the values of the 7-days moving average were at the range of 40 to 60 in many days, but there were four small valleys. The first valley corresponded to the holiday season of year-end of 2017 and beginning of 2018. The second and the third valleys were at the middle of February and the middle of March, respectively. These are both included in the end term of school year of Japan. And the last valley corresponded to another holiday season in May. Since data after the period used in this paper has not been acquired yet, long-term periodic fluctuation, such as monthly, quarterly and yearly, is unknown. Data acquisition is ongoing, and further consideration is necessary when the data becomes available.

3. Conclusion

In this study, an integrated system of IoT sensors and machine learning for anomaly detection of pedestrian flow was proposed for buildings that are expected to be used as emergency evacuation sites in the event of a disaster. For trial practice of the system, infrared sensors were installed in a research building of a university, and data of visitors to the fourth floor of the building was collected as a time series data of pedestrian flow. As a result, it was shown that anomalies of pedestrian flow at an arbitrary time of a day with an occurrence probability of 5 % or less can be detected properly using the data collected.

Acknowledgements

The author would like to express appreciation to Prof. Tomihiro Watanabe, Dr. Masashi Ogawa and Miss Misato Hiraoka of Graduate School of Management, Kyoto University for their support of data collection by sensors at the Maskawa Building for Research and Education of Kyoto University.

References

- [1] T. Ide, Introduction of Anomaly Detection by Machine Learning - Practical Guide by R, Corona Publishing Co.,Ltd., ISBN 9784339024913, 2015.
- [2] T. Ide and M. Sugiyama, Anomaly Detection and Change Detection, Machine Learning Professional Series, Kodansha Ltd., ISBN 9784061529083, 2015.
- [3] M. Jin, Data Science by R - from the Foundation of Data Analysis to the Latest Method, Morikita Publishing Co., Ltd., ISBN 9784627096028, 2017.

Analysis of distracted pedestrians' waiting time: Head-Mounted Immersive Virtual Reality application

Arash Kalatian¹, Anae Sobhani², Bilal Farooq³

^{1,3} Ryerson University
Toronto, Ontario

arash.kalatian@ryerson.ca; bilal.farooq@ryerson.ca

² Utrecht University
Utrecht, Netherlands
a.sobhani@uu.nl

Abstract – This paper analyzes the distracted pedestrians' waiting time before crossing the road in three conditions: 1) not distracted, 2) distracted with a smartphone and 3) distracted with a smartphone in the presence of virtual flashing LED lights on the crosswalk as a safety measure. For the means of data collection, we adapted an in-house developed virtual immersive reality environment (VIRE). A total of 42 volunteers participated in the experiment. Participants' positions and head movements were recorded and used to calculate walking speeds, acceleration and deceleration rates, surrogate safety measures, time spent playing smartphone game, etc. After a descriptive analysis on the data, the effects of these variables on pedestrians' waiting time are analyzed by employing a cox proportional hazard model. Several factors were identified as having impact on waiting time. The results show that an increase in initial walk speed, percentage of time the head was oriented toward smartphone during crossing, bigger minimum missed gaps and unsafe crossings resulted in shorter waiting times. On the other hand, an increase in the percentage of time the head was oriented toward smartphone during waiting time, crossing time and maze solving time, means longer waiting times for participants.

Keywords: pedestrian, crossing waiting time, proportional hazard model, immersive virtual reality

1. Introduction

Pedestrian crossing behaviour is a topic of interest as it gives insights into traffic lights design, pedestrian safety, roadway layouts design and traffic flow optimization. This study aims at exploring one of the attributes of pedestrian street-crossing behaviour: waiting time. Research on pedestrian waiting time analysis have gained popularity as pedestrian-vehicle accidents result in a large proportion of total accident deaths. Pedestrian violations, i.e. J-waling, disobeying pedestrian lights and failure to yield to vehicles, have been a major source of traffic injury and fatality in recent years [1]. Despite implementation of various safety measures, widespread educational programs, etc., rate of pedestrian-related fatalities and injuries in Canada has increased in the last decade. According to the Canadian Motor Vehicle Traffic Collision Statistics, proportion of fatal accidents involving pedestrians to all fatal accidents has increased from 11.8% in 2005 to 15.2% in 2015 [2,3]. A reason for this increase can be traced back to the rise of smartphones and their applications in everyday life. Pedestrians are becoming more distracted in recent years, using their phones for talking, texting, surfing the web, looking for directions, or playing games [1].

In order for a pedestrian to cross an unsignalized intersection, individuals should wait for a gap that, based on each pedestrian's abilities, allows safe crossing of the street. An individual waiting to cross an unsignalized intersection is required to concentrate and evaluate whether each gap satisfies the spatial and temporal requirements of a safe cross. Pedestrian waiting time has a significant impact on unsafe crossings. Studies suggest a positive correlation between waiting time before initiating a cross and the violations caused by pedestrians [4]. Using mobile phones and the distraction caused by them negatively affects

pedestrians' ability to cross and thus, increases the pedestrian-related accident rates [5,6]. By implementing safety solutions, waiting time can be affected for distracted pedestrian.

This paper investigates the effect of smartphone distraction on pedestrians' waiting time by adapting a head mounted immersive virtual reality environment. In conventional field experiments on pedestrian behaviours, it is often difficult to implement different scenarios as the results may be disastrous in terms of participants' safety. In addition, it may be expensive or unsafe to repeat an experiment with the exact same traffic conditions to capture the effects of an implemented safety measure. To overcome such problems, pictures, videos and photomontages can be used to assess participants perception. With the development of interactive computer-generated experiences, Virtual Reality (VR) experiments have gained popularity in various research fields. Using a head mounted VR display device, virtual scenes can be directly projected to the participants so that they will be immersed in the simulated environment [7]. Scenarios used in experiments may be unsafe or expensive to apply on real roads, due to reasons such as dangerous implementations or lack of infrastructures. VR simulator allows running such scenarios, along with scenarios containing new technologies or services that participants have limited mental image of.

Data collection procedure for this study involves a virtual immersive reality environment (VIRE). To investigate distracted pedestrians' waiting time before crossing an unsignalized intersection, we asked participants to cross a simulated unsignalized intersection in VIRE in three different simulation tasks: Task 1. no distraction, Task 2. distraction by a maze on a smartphone, and Task 3. distraction by a maze game on a smartphone with flashing LED lights installed on the crosswalk as a safety encounter. After data collection and conducting a descriptive analysis of the data, a cox proportional hazard model is adopted to further explore the effects of different sociodemographic and traffic parameters on pedestrians' waiting times.

This paper is organized as follows: in Section 2, we review the previous works on the subject. In Section 3 data collection procedure is described. Section 4 discusses the model structure. Moreover, variables derived from data and a descriptive analysis on them are then explained in Section 5. Proportional Hazard model and its implementation on the data is then elaborated in Section 6. In the end, conclusions and future research plans are covered in Section 7.

2. Background

Despite the growing interest in pedestrian behaviour in the literature, pedestrian waiting time at intersections especially for unsignalized and mid-block crosswalks has yet to be widely discussed. For unsignalized intersections, Hamed [8] developed a cox proportional hazard model to identify factors affecting waiting time and number of unsuccessful attempts required before a safe crossing. Their Results suggest that having accident experience, car ownership, number of people on the crosswalk, age, gender, type of trip and vehicle gap time are important factors in determining wait time before crossing. However, waiting time at signalized intersections has drawn more attention in the literature, mainly by looking into calculation of signal timings based on pedestrians' waiting times. In 2003, Keegan and O'Mahony [9] studied the effects of different countdown timers on pedestrian waiting time at signalized intersections. In 2013, Li [10] developed a model for intended waiting time at signalized intersections taking into account bounded waiting times. Results showed that a large proportion of pedestrians cross the street immediately after they arrive at the intersection. In terms of the effects of waiting time on pedestrian violations, Brosseau *et al.* [4] analysed video data of signalized intersections and identified several factors that contribute to dangerous crossing, including maximum waiting time and clearance time.

Data in the aforementioned studies were collected either by questionnaires or by observing pedestrians for a short period of time. In addition, most studies on the subject consider waiting time at signalized intersections, mainly to explore the thresholds of pedestrian crossing signal timings. However, as it may be unsafe to track the pedestrian behavior while they are distracted using their phone, the distraction caused by smartphones has not been studied widely in previous literature.

Recent developments in virtual reality technology have made it possible to analyze different behaviours of pedestrians with minimal risks. Studies suggest that spatial knowledge developed in virtual environments resemble that of the actual physical environments [11,12]. Virtual Reality has been used in

transportation studies in fields such as route choice or evacuation behaviour. However, these studies often lack the interaction element that can be implemented in Virtual Immersive Reality Environments (VIRE). Using VIRE, participants are immersed in an environment where vehicles respond to their actions. For instance, when a pedestrian walks in front of a car, the cars start to slow down, and if necessary, stop for the pedestrian to cross. Although experiments conducted in laboratory environments may lack the realism that is necessary for data collection, VIRE provides researchers with a safe environment that is close to real life situations. Considering the advantages of utilizing virtual reality environment for pedestrian-related experiments, data collection procedure was designed based on a virtual reality-based tool developed by LiTrans and introduced in [7].

3. Data Collection

In this study, an in-house developed tool, Virtual Immersive Reality Environment (VIRE) [7], is used to collect participants' data while they were waiting on the sidewalk to cross an unsignalized intersection. The simulated unsignalized intersection is part of an existing congested street in Montreal, Canada. After an initial familiarization with VIRE, participants were asked to engage in three waiting conditions mentioned earlier. To capture the repetition concern, each task was conducted in 10 random simulation scenarios. Each trial would finish when the participant successfully crosses the street, with maximum allowable time of 60 seconds [13]. Out of 42 participants, 17 were Females, the average age was 26, with 9 participants aged more than 30. Different variables were then generated based on participants collected data. As for the traffic simulation, car-following model and social force model were implemented for vehicular and pedestrian traffic, respectively. In Fig. 1, VIRE set-up and a couple of participants in the experiment can be seen.

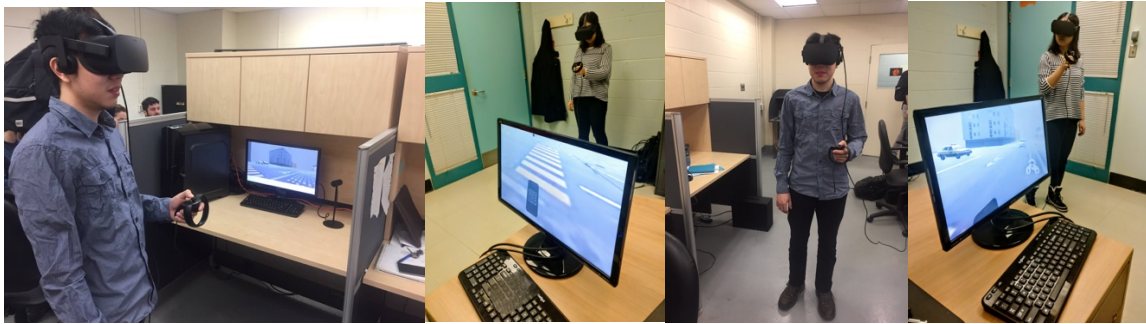


Fig. 1: VIRE setup and environment

4. Model Structure

Developed by Cox in 1972, Cox proportional-hazards model is essentially a regression model mainly used in medical research to identify the relationship between survival times of patients and predictor variables [14]. In this study, hazard function, denoted by $\xi(t)$, is defined as the rate of failure to initiate a cross at time t . Hazard function is written as:

$$\xi(t) = \frac{\lim_{\Delta t} \Pr[t \leq T \leq t + \Delta t | T \geq t]}{\Delta t} \quad (1)$$

To analyze waiting time before a cross, cox proportional hazard model is used, as the most common method for analyzing individuals' survival. Considering the effects of covariates on the baseline hazard, hazard function is written as:

$$\xi(t|\mathbf{R}) = \bar{\xi}(t) e^{\sum_{i=1}^k \chi_i R_i} \quad \text{and } 0 \leq \xi(t|\mathbf{R}) < \infty \quad (2)$$

In Eq. (2), R is the vector of covariates, χ is the vector of coefficients that need to be estimated, and $\bar{\xi}(t)$ is the baseline hazard [8]. Equation (2) gives the risk at time t for pedestrian i , where the baseline hazard expresses hazard or risk for a pedestrian at all time points regardless of the covariates ($R=0$). To estimate model parameters, partial derivatives of the log-likelihood function is taken. As all the pedestrians finally cross the street at some point, our sample data is considered to be uncensored. To estimate parameters of the model, package “survival” in R is used in this study [15].

5. Data

Five types of variables were generated from the collected crossing behaviour data: 1) crossing variables: crossing duration (time from initiating the crossing until the crossing was completed), waiting time duration (the time from the start of the trial where the participant was standing on the sidewalk until the crossing was initiated), crossing speed, and initial walk speed, 2) distraction attributes: percentage of the time the head was facing the smartphone during wait time, percentage of the time the head was facing the smartphone while crossing, number of times the head was facing the smartphone over the total trial duration, maze solving time (the time it takes for a participant to solve one maze in the smartphone), 3) safety measures: TTC (calculated for each second between vehicles and the pedestrian as the time until they would collide if their direction and speed remain unchanged), PET (the time difference between when the pedestrian departs the conflict point and the time vehicle arrives at that point), average and maximum acceleration and deceleration, the percentage of successful and time-out trials, 4) sociodemographic information: age, gender, number of years they owned a smartphone, having a driving license, and 5) gap variables: missing gaps before initiating crossing, and chosen gap for crossing. Table 1 presents the mean value of the attributes. As it can be seen in this Table, in the sample data collected, waiting time increases when participants are distracted. In the sample being studied, LED lights have caused females to wait slightly longer before crossing while distracted. However, Males waiting time has decreased a bit using LED lights. In all three scenarios, females have longer waiting times.

Table 1: Pedestrian behavioural attributes across three crossing conditions

Variable	Task	General	Female	Male
Waiting time (s)	1	18.0	20.9	16.0
	2	21.0	23.9	19.4
	3	21.0	24.3	19.2
Crossing time (s)	1	4.4	3.9	4.7
	2	4.2	4.1	4.3
	3	3.8	3.7	3.8
Minimum gap missed (s)	1	2.72	2.67	2.76
	2	2.68	2.66	2.70
	3	2.67	2.64	2.69
% of time head was oriented toward smartphone during waiting time (s)	2	72.9	68.0	76.2
	3	74.7	69.8	78.0
% of time head was oriented toward smartphone during crossing (s)	2	73.5	73.1	73.7
	3	69.6	71.5	68.3
Initial walk speed (m/s)	1	1.6	1.5	1.6
	2	1.5	1.4	1.6
	3	1.6	1.6	1.6
Minimum PET (s)	1	1.2	1.1	1.2
	2	1.0	1.1	1.0
	3	1.1	1.2	1.1

Crossing success rate %	1	76.9	7.6	81.2
	2	61.4	64.7	59.2
	3	68.8	65.9	70.8
Maximum acceleration m/s^2	1	6.1	4.8	6.9
	2	5.1	4.5	5.5
	3	5.2	5.5	5.0
Maze solving time (s)	2	0.81	0.76	0.87
	3	0.87	0.84	0.92

6. Model Results

To capture changes in waiting time pattern across the three conditions, and also estimate the effects of generated variables on waiting time, cox proportional hazard model is adopted. It should be noted that, in addition to estimating a variable's impact on waiting time, deviations of reasonable variables were evaluated and estimated through interaction variables, for example (Female) * (Maximum acceleration), (Female) * (Percentage of the time the head was oriented toward smartphone during waiting time), etc. Model specifications were calculated through a systematic process of removing statistically insignificant variables and combining variables when their effects were not significantly important. In safety analyses, survival analysis is the most common practice in modeling. In this study, we fit multivariate cox proportional hazard model to analyze the joint impact of factors on survival time. To better fit the model, dummy variables in different ranges were created for continuous variables. Each variable is categorized in two or three groups, based on the distribution of the variable. Category thresholds were set in a way that each group contains at least 25 percent of participants. Crossings with a PET of less than 1.5 seconds were considered as dangerous or unsafe [16]. Table 2 provides estimated parameters of the significant covariates. The first column in this table presents variables that appeared to be significant. It should be noted that a positive coefficient sign means that the chance of starting a cross is higher, and thus, waiting time is shorter. The hazard ratio greater than one, indicates that as the value of the variable increases, the event's hazard increases and thus waiting time decreases.

As it can be seen in Table 2, the Task variable presents the differences of waiting time for Tasks 2 and 3 and Task 1. The positive value of this variable shows that waiting time in the tasks with smartphone involved is less than waiting time for non-distracted Task 1, meaning that smartphone usage has resulted in less waiting on the sidewalk, but the LED treatment has smoothed this negative impact. The second variable which has a significant effect on pedestrians' waiting time at an unsignalized intersection is gender with a negative impact for males. However, gender is not significant for separate tasks, implying that smartphone distraction does not change the behaviour of waiting time for any gender. Additionally, results show that pedestrians with higher crossing speeds (i.e. more rush to cross) waited less on the sidewalk. Analysing the distraction parameters values in Table 2 (i.e. head orientations toward phone while either waiting on the sidewalk or crossing a street) indicates that distracted pedestrians while waiting, spend more time on the sidewalk before initiating a cross, especially when there is no LED safety treatment implemented. On the other hand, distracted pedestrians, even while crossing the street, waited less at the sidewalk. Gap times that participants missed before crossing is reflected in minimum gap missed variable. In general, in all three waiting tasks, longer gap times have led to less waiting time. In task 1, more crossing duration means more waiting time, but this is not necessarily true for Tasks 2 and 3. In Tasks 2 and 3, in which participants are distracted with their phones, crossing duration may increase due to smartphone usage while crossing. Dangerous crossing, i.e. PET below 1.5 seconds, has a significant effect on pedestrians' waiting time for Task 1. Individuals with safer crossing tend to wait longer in task 1. However, this variable is removed in Task 2 and Task 3, which may be because of longer waiting times due to phone usage, instead of waiting for safe gaps. In the end, for each participant, as the time it takes to solve a maze increases, waiting time increases as well. This may be linked to the lack of concentration on road crossing on those participants who solve the maze faster.

Table 2- Results of multivariate proportional hazard model

Variable		Coefficient	Hazard Ratio	p-value
Task	2	3.08	21.86	0.001
	3	2.93	18.82	0.001
Female	General	-0.55	0.58	0.118
Initial walk speed > 1.9 m/s	General	0.33	1.38	0.121
% of time head was oriented toward smartphone during waiting time >85%	General	-1.16	0.20	0.001
	Task 2	-0.96	0.38	0.012
% of time head was oriented toward smartphone during crossing > 85%	General	0.68	-1.97	0.009
Minimum gap missed > 3.1 s	General	2.64	14.01	0.001
	Task 1	1.42	4.17	0.001
	Task 2	1.57	4.83	0.001
	Task 3	1.16	3.21	0.028
Crossing time > 5 s	Task 1	-0.98	0.37	0.089
PET < 1.5 s	Task 1	1.08	2.94	0.002
Maze solving time > 1.1 s	Task 2	-1.21	0.30	0.003
	Task 3	-2.27	0.10	0.001

7. Conclusions and Future Work

By developing an immersive virtual reality-based method for collecting data of pedestrian waiting time in street crossing paradigm, data can be collected in a safe and controlled environment. To observe the effects of various distraction parameters on pedestrian waiting time, cox proportional hazard model was adopted for the modelling purpose.

With regards to the model, results show higher minimum missed gap, dangerous PET (i.e. less than 1.5 seconds), crossing duration, initial crossing speed, percentage of time head orientation towards the phone during wait time and crossing, and gender.

Our study is not without limitations which can be addressed in future studies. Eye movements, brain activity and heart beats can be measured as indicators of participants' stress and distraction level. Other types of distraction can also be added to the experiment. In terms of dataset, larger datasets can be collected and analysed to remove the possible biases. Other safety measures can also be explored and compared to each other to better analyse the effect of different safety measures. Finally, waiting time for different types of intersections can also be studied.

References

- [1] Transport Canada, "Un bref aperçu des usagers de la route vulnérables qui sont victimes d'accidents mortels," 2010.
- [2] Transport Canada, "Canadian Motor Vehicle Traffic Collision Statistics: 2005," 2005.

- [3] Transport Canada, “Canadian Motor Vehicle Traffic Collision Statistics: 2015,” 2015.
- [4] M. Brosseau, S. Zangenehpour, N. Saunier, and L. Miranda-Moreno, "The impact of waiting time and other factors on dangerous pedestrian crossings and violations at signalized intersections: A case study in Montreal," *Transportation research part F: traffic psychology and behaviour*, vol. 21, pp. 159-172, 2013.
- [5] S. E. Banducci, N. Ward, J. G. Gaspar, K. R. Schab, J. A. Crowell, H. Kaczmarek, A. F. Kramer, “The effects of cell phone and text message conversations on simulated street crossing,” *Human factors*, vol. 58, no. 1, pp. 150–162, 2016.
- [6] M. I. B. Lin and Y.P. Huang, “The impact of walking while using a smartphone on pedestrians’ awareness of roadside events,” *Accident Analysis and Prevention*, vol. 101, pp. 87–96, 2017.
- [7] B. Farooq, E. Cherchi, A. Sobhani, “Virtual Immersive Reality for Stated Preference Travel Behaviour Experiments: A Case study of Autonomous Vehicles on Urban Roads,” *Transportation Research Record : Journal of Transportation Research Board*, vol. 2672, pp. 35-45, 2018.
- [8] M. M. Hamed, “Analysis of Pedestrians’ behavior at pedestrian crossings,” *Safety Science*, vol. 38(1), pp. 63-82, 2001.
- [9] O. Keegan, M. O’Mahony, “Modifying pedestrian behaviour,” *Transportation Research Part A: Policy and Practice*, vol. 37 (10), pp. 889-901, 2003.
- [10] B. LI, “A model of pedestrians' intended waiting times for street crossings at signalized intersections,” *Transportation Research Part B: Methodological*, vol. 51, pp. 17-28, 2013.
- [11] M. J. O’Neill, “Effects of familiarity and plan complexity on wayfinding in simulated buildings,” *Journal of Environmental Psychology*, vol. 12, no. 4, pp. 319–327, 1992.
- [12] R. A. Ruddle, S. J. Payne, and D. M. Jones, “Navigating buildings in ‘desk-top’ virtual environments: Experimental investigations using extended navigational experience,” *Journal Experimental Psychology: Applied*, vol. 3, no. 2, pp. 143–159, 1997.
- [13] A. Sobhani, B. Farooq “Impact of smartphone distraction on pedestrians’ crossing behaviour: An application of head-mounted immersive virtual reality”, *Transportation Research Part F: Psychology and Behaviour*, pp. 228-241, 2018.
- [14] T. Therneau, P. Grambsch, “Modeling Survival Data: Extending the Cox Model,” *Springer*, 2000.
- [15] T. Therneau, “A Package for Survival Analysis in S,” version 2.38, Available: <https://CRAN.R-project.org/package=survival>, 2015.
- [16] M. Zaki H and T. Sayed, “Exploring Walking Gait Features for the Automated Recognition of Distracted Pedestrians,” *IET Intelligent. Transport Systems*, vol. 10, no. 2, pp. 106-113, 2016.

Compression of Pedestrian Crowd in Corner Turning

Subject experiment-based analysis of walking trajectories

Mineko Imanishi¹, Tomonori Sano²

¹Fire Protection Engineering Group/Takenaka Research & Development Institute

Otsuka 1-5-1, Inzai, Chiba, Japan

imanishi.mineko@takenaka.co.jp

Faculty of Human Sciences/Waseda University

Mikajima 2-579-1, Tokorozawa, Saitama, Japan

sano-t@waseda.jp

Abstract - In this study, pedestrian crowd dynamics at corner turns were investigated by analyzing pedestrian trajectories in a subject experiment for building more reliable, general-purpose, pedestrian simulation models. An experiment under laboratory conditions was conducted wherein a pedestrian crowd walked straight for a short distance before turning into a right-angled corner built with partition walls; the opposite sides were unwallled. Trials were performed with different widths and densities of initial participant positions. Finally, the trajectories of the pedestrians were extracted from a video through computer image analysis. The results demonstrated that pedestrian behavior at corner turns depends on lane position, lane distance (from the wall), and crowd density.

Keywords: experiment, crowd dynamics, trajectory, data-set

1. Introduction

1.1. Background

Pedestrian crowd simulations have mainly been developed in the field of architecture for evacuation safety evaluation and space capacity estimation. For such purposes, flow rates at a bottleneck and congestion in crowded situations play a major role. Meanwhile, the rise of multi-agent simulation over the last decades has led to more visual and realistic simulations in detailed architectural plans. However, visual presentations of pedestrian simulations often depict unnatural-looking agent behaviors in relatively uncrowded situations, which have been made light so far. A typical example of such cases is crowd behavior at a corner. In some evacuation simulation models with potential fields, agents congest too heavily—or even stack—at a corner because they move straight toward an exit, ignoring other possible conditions. These false stacks eventually preclude the correct congestion evaluation of a plan. Crowd behavior at a corner should be modelled based on real pedestrian behavior.

With regard to the pedestrian model at a corner, Chraïbi et al. [1] developed a traditional social force model by introducing a “virtual” goal while turning at a corner. They identified a parameter that can control the level of congestion at a corner. However, this mathematical model has yet to be validated using real human behavior. Meanwhile, Dias et al. [2–3] conducted a subject experiment. Their study reported on the walking characteristics (of a single or small pedestrian mass) at a corner by comparing walking speeds and different corner angles. Their results could be strengthened by testing under more natural conditions with a larger pedestrian group to solve the current issue of pedestrian congestion at a corner.

1.2. Aim

This study aimed to elucidate pedestrian dynamics at corner turns through a subject experiment for more reliable, general-purpose pedestrian simulation models.

2. Methodology

2.1. Subject Experiment

In this study, the authors conducted an experiment under laboratory conditions in which a pedestrian crowd of 24 participants started walking 7.2 m before a right-angled corner, turned at the corner naturally, and then continued walking straight for over 4 m. Partition walls of 1.8 m height were arranged to form the corner, while the adjacent spaces were unwallled (Fig. 1).

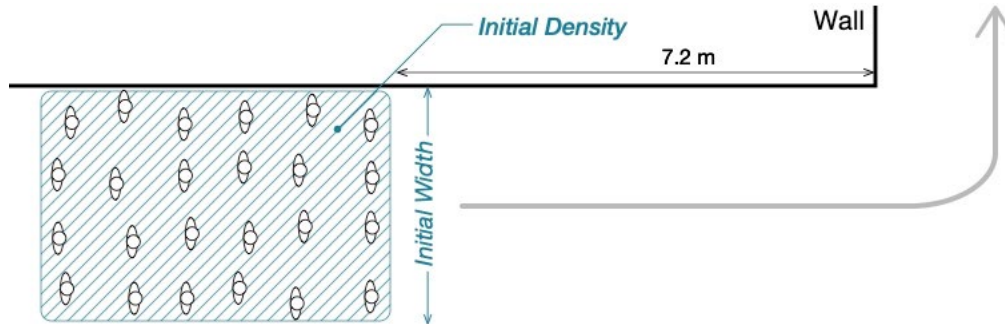


Fig. 1: Schematic of the experiment.

Figure 2 and Table 1 show the experimental conditions. Trials were performed with different widths and densities of initial participant positions. To reproduce a natural situation, the positions were randomized (as shown in Figure 2) by the following process: the participants first lined up along evenly distributed grids marked on the floor with tape; then, they moved one step (or a half-step in high-density conditions) in their desired direction, simultaneously, at a cue from a staff member. Each condition was repeated three times by changing the order of the participants as well as some members. Before the experiment, the participants were instructed: “In these trials, turn left at the corner there (pointing the corner), assuming your destination is beyond the bend. You do not need to maintain formation while walking, and you can overtake others freely. Please behave normally, as though you are walking in a station or shopping mall.”

gh

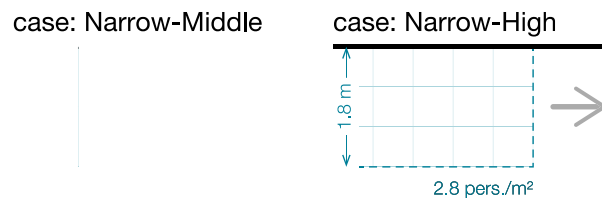


Fig. 2: Initial distribution of participants in each case.

Table 1: Experimental conditions.

Case name	Width	Density	Participants
Low	3.6 m	0.7 pers./m ²	24 persons
Middle		1.2 pers./m ²	
High		2.8 pers./m ²	
Narrow-Middle	1.8 m	1.2 pers./m ²	
Narrow-High		2.8 pers./m ²	

Different participants were chosen for each trial from a pool of 60 participants (male: 41, female: 19). All participants were between 18 and 26 years of age and had no walking disabilities. Fig. 3 shows the population of the participants.

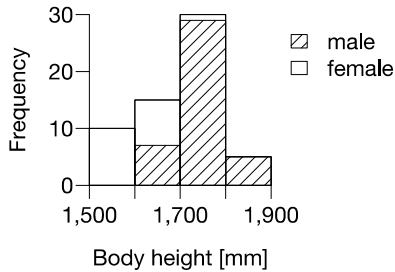


Fig. 3: Distribution of participants according to body height and gender.

The experimental procedure was approved by the Research Ethics Committee at Waseda University, Japan.

2.2. Data Processing

The experiment was recorded using a 2.7K-quality video camera, installed at a height of 15.2 m from the floor (Figure 4). Colour-tape markers were placed on the head of each participant. Each participant wore one of four possible combinations of tape colors—according to their height—so that the coordinate gaps in still frames due to body height differences could later be corrected using a program. The marker coordinates were obtained by an authors' program [4] that uses OpenCV—an open-source image processing library. Subsequently, the marker locations in the still frames were translated into real-world coordinates by taking the camera lens distortion and participant height differences into account. As such, very accurate coordinates could be obtained at 30 frames per second.

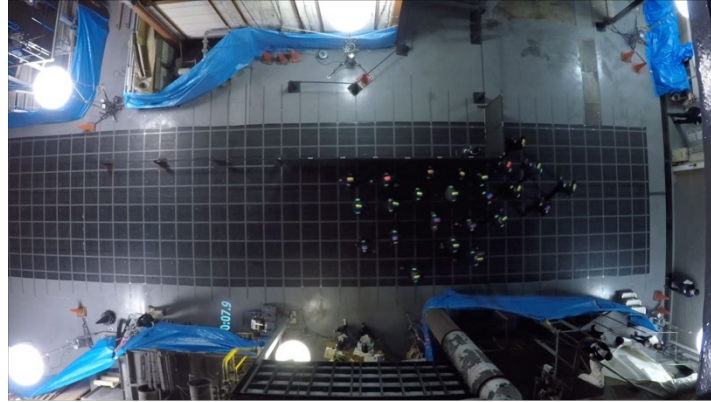


Fig. 4: A still frame from the experiment video.

3. Results

3.1. Compression of pedestrian crowd

Figures 5–7 show the raw participant trajectories in represented trials of some cases. They illustrate that the pedestrian crowd was compressed once at the corner and then gradually dispersed. The compression ratio of the crowd outline increased as the crowd density decreased. That is, participants preferred to go toward the inside lane (when there was space) to avoid a needless detour. Conversely, participants next to the wall appeared to maintain a regular distance from the wall, regardless of the experimental conditions. Furthermore, those participants momentarily came nearer to the wall when passing the corner. Consequently, the entire pedestrian crowd shifted to the outside of the wall under narrow conditions, whereas the crowd absorbed the inside lane shift under wide conditions.

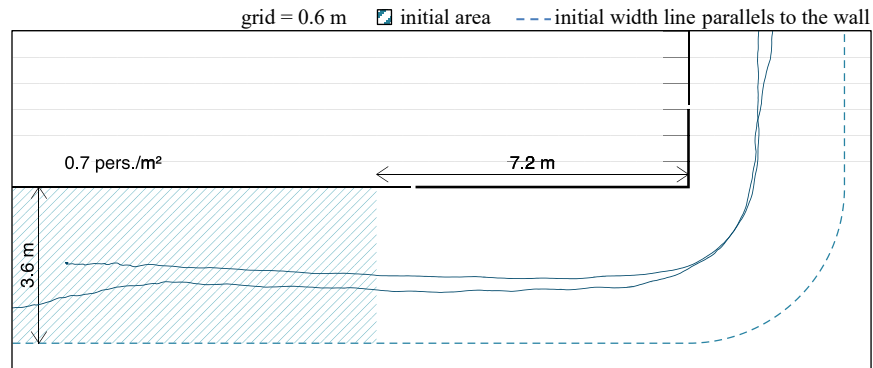


Fig. 5: Walking trajectories of case *Low*.

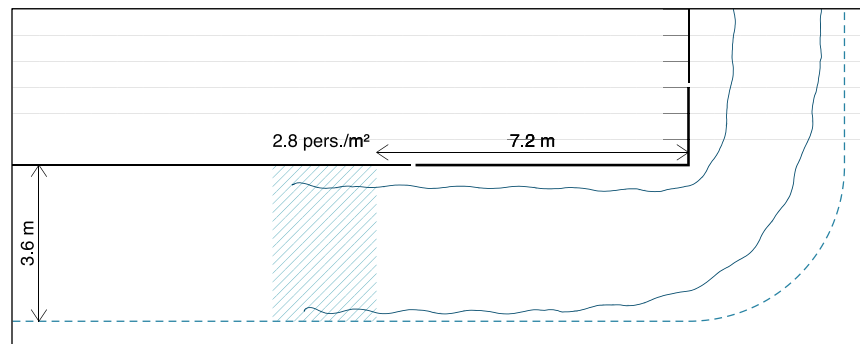


Fig. 6: Walking trajectories of case *High*.

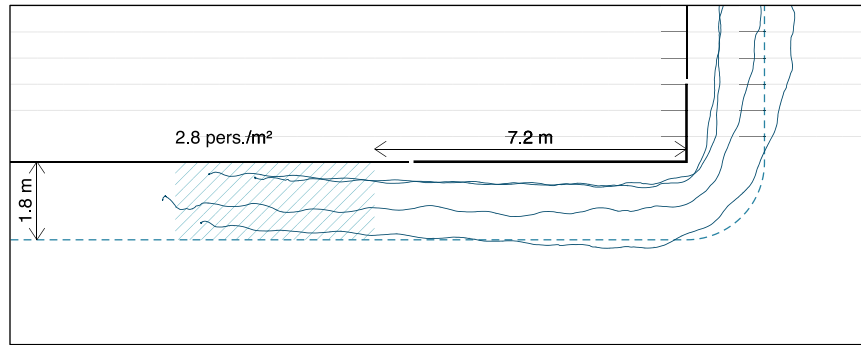
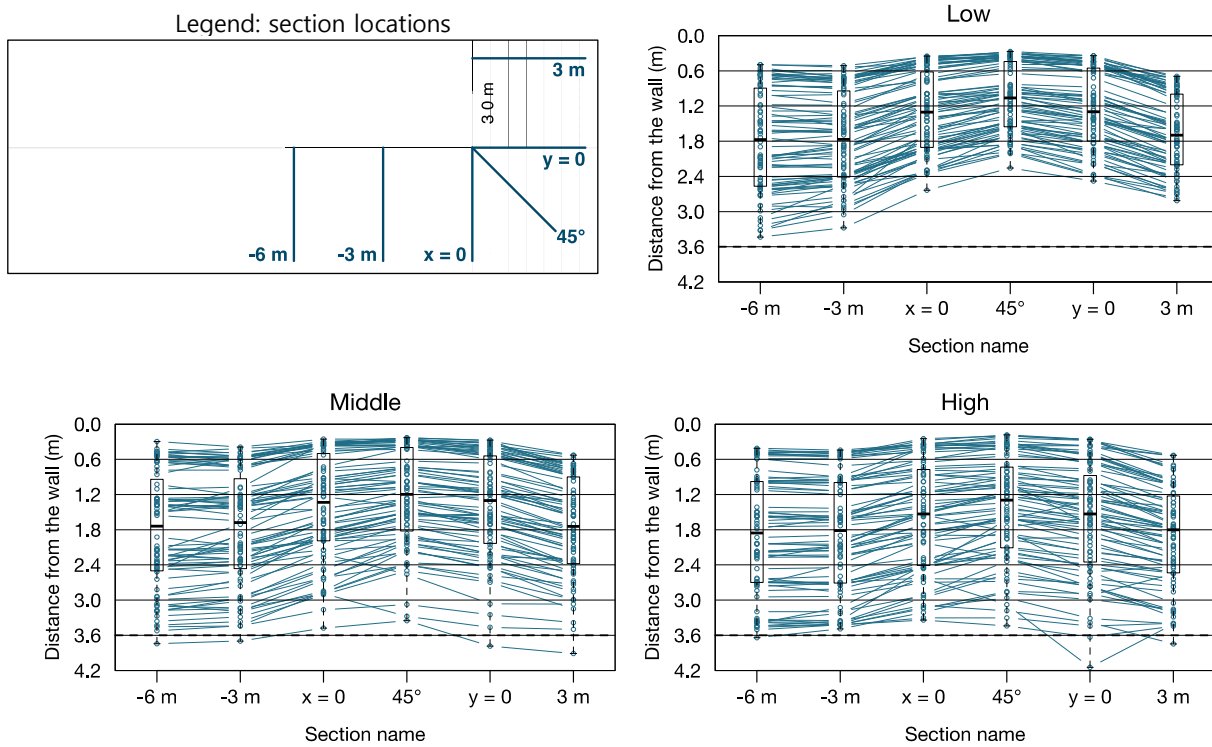


Fig. 7: Walking trajectories of case *Narrow-High*.

Figure 8 shows each participant's distance from the wall as they passed specific sections defined in the legend plan. Each graph contains all three trials of the respective experiment condition. It indicates that the crowd was compressed—particularly at the middle of the turning phase (45° section). The pedestrian distribution in the recovery phase (after turning) varied among conditions. It appears that participants did not maintain their original distance from the wall, but rather found a comfortable position by preserving distance from others.



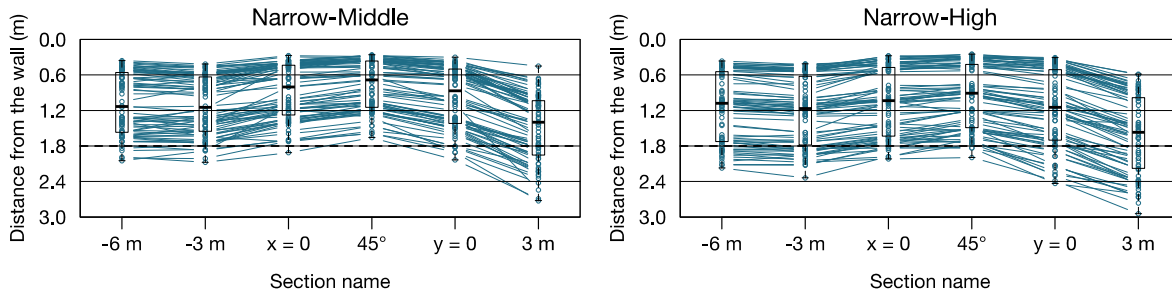


Fig. 8: Distance from the wall at represented sections.

Figure 9 shows the positional relationship between when participants entered ($x = 0$) and exited ($y = 0$) the corner. According to the figure, participants did not change their lane dynamically at the corner. However, the higher the crowd density, the larger the lane variation. This result may suggest that participants were unable to follow their preferred path due to obstacles—other pedestrians. Additionally, in all conditions, the pedestrians concentrated at the edge of the corner because it is the shortest path.

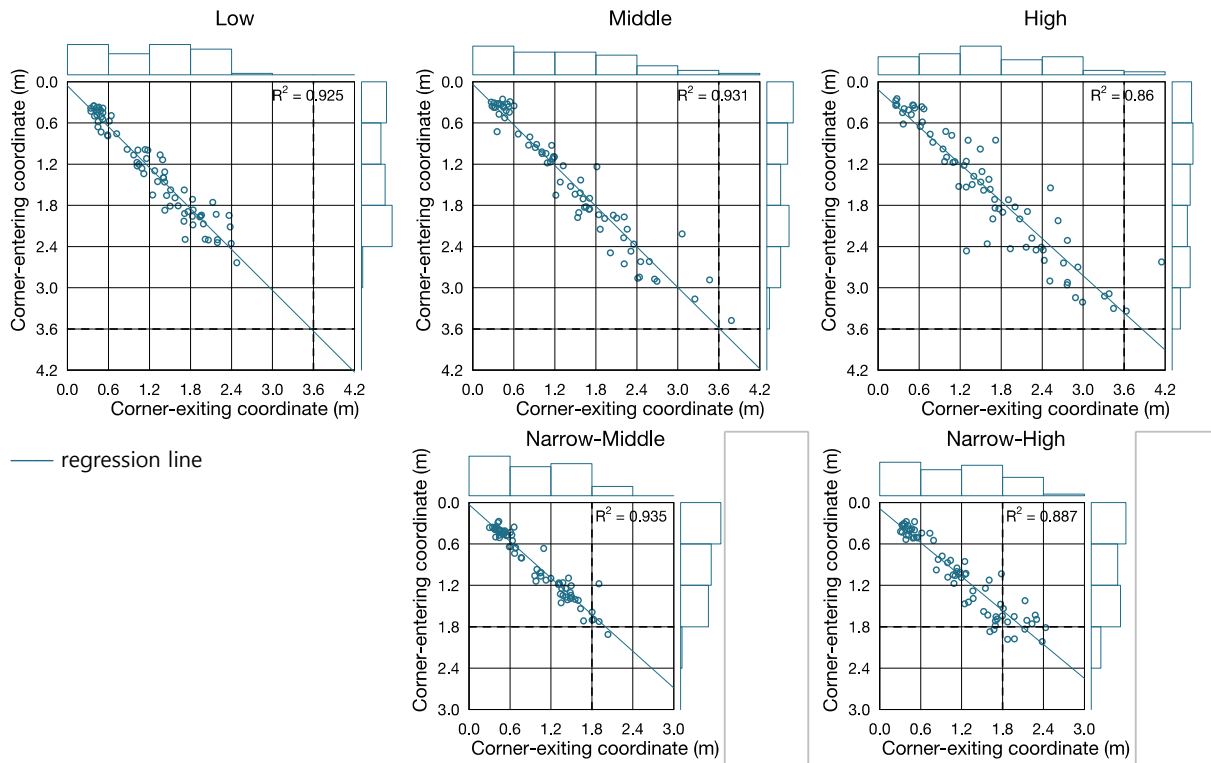


Fig. 9: coordinates perpendicular to the wall when entering and exiting the corner.

3.2. Pedestrians' walking state differences among location

Figures 10 and 11 indicate the mean walking directions at each 0.6-m mesh, representative of two complete trials. According to the figure, pedestrians in the outside lane started changing their walking direction earlier than those near the wall.

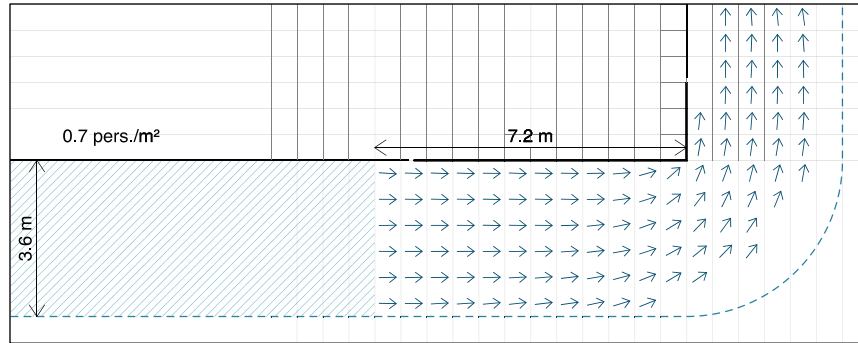


Fig. 10: Distribution of mean walking direction in case *Low*.

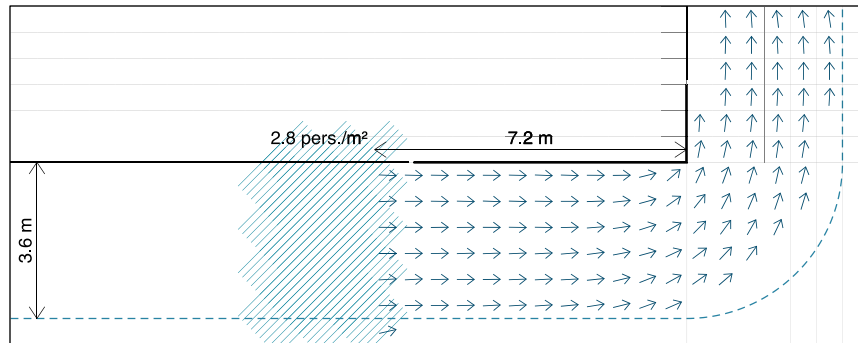


Fig. 11: Distribution of mean walking direction in case *High*.

Figures 12 and 13 indicate the mean walking speeds of the trials in Figures 10 and 11, respectively. Here, the walking speed of a pedestrian at a location was defined as the moving distance from the location to the location one second later. Participants in the inside lane reduced their speed on turning, while those in the outside lane accelerated. It appears that such variations were induced by a change in crowd density due to the stream direction alternation. Furthermore, the higher the density, the larger the difference between lanes. However, the width reduction was observed to be negligible and far from stacking, even in high-density conditions.

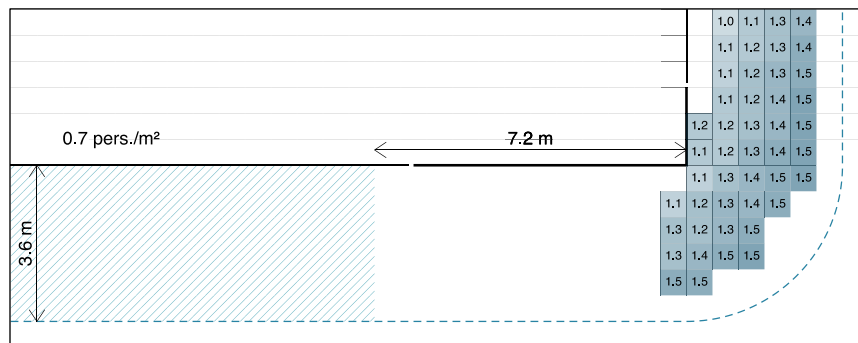


Fig. 12: Distribution of mean walking speed (m/s) in case *Low*.

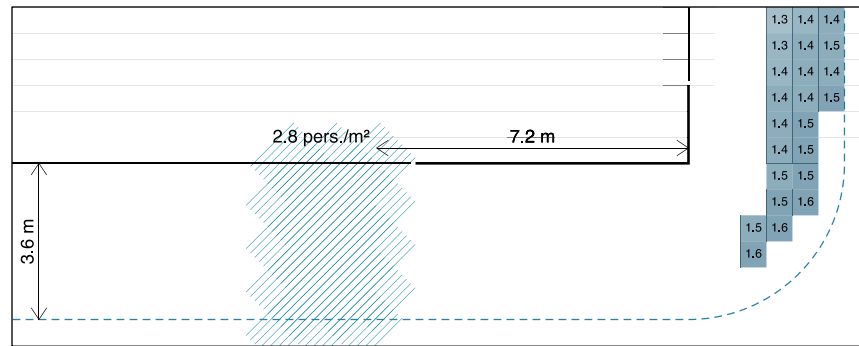


Fig. 13: Distribution of mean walking speed (m/s) in case *High*.

4. Conclusion

Pedestrian crowd dynamics at corner turns was clarified by analyzing pedestrian trajectories in a subject experiment. The results showed that pedestrian behavior at corner turns depends on lane position, lane distance (from the wall), and crowd density.

Further analysis will be performed on these trajectory data to find a quantitative model that describes crowd behavior at a corner.

Acknowledgements

This experiment was conducted under a collaborative research agreement between Akeno Facility Resilience Inc., FDM Corporation, Kajima Corporation, National Research Institute of Fire and Disaster, Obayashi Corporation, Shibaura Institute of Technology, Shimizu Corporation, Taisei Corporation, Takenaka Corporation, Tokyo University of Science, and Waseda University (in alphabetical order). This study was supported by the Joint Usage/Research 2017 by the Research Center for Fire Safety Science, which is part of the Organization for Research Advancement of the Tokyo University of Science.

References

- [1] M. Chraibi, M. Freialdenhoven, A. Schadschneider and A. Seyfried, “Modeling the desired direction in a force-based model for pedestrian dynamics,” in *Traffic and Granular Flow '11*, V. Kozlov, A. Buslaev, A. Bugaev, M. Yashina, A. Schadschneider, M. Schreckenberg, Ed. Berlin: Springer, 2013.
- [2] C. Dias, M. Sarvi, N. Shiwakoti, and O. Ejtemai, “Experimental Study on Pedestrian Walking Characteristics through Angled Corridors,” in *Proceedings of 2013 Australasian Transport Research Forum*, 2013, pp.1–11.
- [3] C. Dias, O. Ejtemai, M. Sarvi, and M. Burd, “Exploring pedestrian walking through angled corridors,” *Transportation Research Procedia*, 2014, vol. 2, pp.19–25.
- [4] M. Tange, M. Imanishi, T. Sano, and Y. Ohmiya, “Pedestrian Tracking with Two Different Color Labels for Large Scale Evacuation Experiments,” in *12th International Symposium of Fire Safety Science: Book of abstracts posters*, Art. P109, June 2017.

A large-scale real-life crowd steering experiment via arrow-like stimuli

Alessandro Corbetta^{1,*}, Werner Kroneman¹, Maurice Donners², Antal Haans³,
Philip Ross⁴, Marius Trouwborst², Sander Van de Wijdeven², Martijn Hultermans²,
Dragan Sekulovski², Fedosja van der Heijden², Sjoerd Mentink², Federico Toschi¹

¹Department of Applied Physics, Eindhoven University of Technology, NL

²Philips Lighting, Eindhoven, NL

³Human Technology Interaction, Eindhoven University of Technology, NL

⁴Studio Philip Ross, Eindhoven, NL

*corresponding author. E-mail: a.corbetta@tue.nl

Abstract - We introduce “Moving Light”: an unprecedented real-life crowd steering experiment that involved about 140.000 participants among the visitors of the Glow 2017 Light Festival (Eindhoven, NL). Moving Light targets one outstanding question of paramount societal and technological importance: “can we seamlessly and systematically influence routing decisions in pedestrian crowds?” Establishing effective crowd steering methods is extremely relevant in the context of crowd management, e.g. when it comes to keeping floor usage within safety limits (e.g. during public events with high attendance) or at designated comfort levels (e.g. in leisure areas). In the Moving Light setup, visitors walking in a corridor face a choice between two symmetric exits defined by a large central obstacle. Stimuli, such as arrows, alternate at random and perturb the symmetry of the environment to bias choices. While visitors move in the experiment, they are tracked with high space and time resolution, such that the efficiency of each stimulus at steering individual routing decisions can be accurately evaluated a posteriori. In this contribution, we first describe the measurement concept in the Moving Light experiment and then we investigate quantitatively the steering capability of arrow indications.

Keywords: Steering pedestrian dynamics; crowd management; high-statistics measurements

1. Introduction

Developing effective management strategies for the motion of pedestrian crowds is a compelling issue in the course towards highest safety and comfort standards in civil infrastructures. Crowd management involves routing pedestrian flows to ensure designated Level-of-Services [1]. This includes an ample spectrum of scenarios in terms, e.g., of crowd density, whose extreme cases are the prevention of dangerous overcrowdings in public gatherings/trafficked hubs (stations, stadiums, etc.) and the establishment of comfortable and uniform floor usage in leisure locations (museums, commercial areas, etc.).

Crowd steering is generally relegated to on-site stewards that, depending on necessities, sort the flow or route it via indications or - in extreme conditions - via physical barriers. Automatizing such steering procedures could be greatly beneficial: actions can be triggered in absence of or with less human supervision, the request for on-site manpower can be diminished, and the spatial granularity of guiding mechanisms can be increased, e.g. for fine-scale floor usage optimizations.

Automating steering is about influencing individual route choices which, in turn, depend on available information about alternative directions. Apart from the geometric characteristics of the environment, also the presence of signage and the relative density of the surrounding crowd plays a role. Currently, experiments comparing these factors have mostly been performed in virtual environments (e.g. [2,3,4]) and with single individuals or at low crowd densities. As of today, empirical evidence on their impact on the crowd movement as a whole is scarce and shows mixed and often contradictory results [5]. Quantitative real-life analyses of the effectiveness of visual stimuli at influencing individual routing decisions are thus a must toward automated steering. Comparing with a wide variety of crowding

conditions (e.g., density levels) as well as ensuring high statistical resolution in the measurements are furthermore paramount, given the high variability in pedestrian behaviour [6].

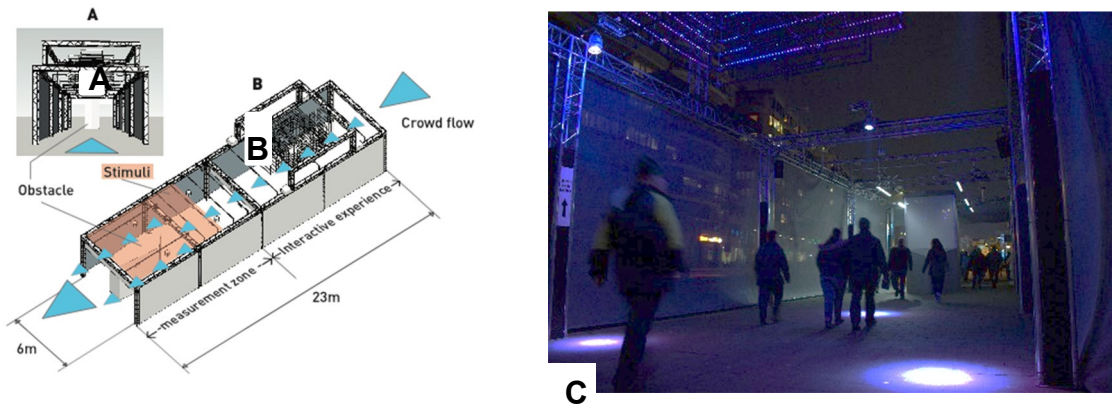


Figure 1: The “Moving Light” real-life pedestrian steer and tracking experiment. We run it as an exhibit at the Glow Festival in November 2017 (Eindhoven, The Netherlands, cf. [7]). (A) Sketch from frontal view as seen by an entering visitor; (B) aerial view - the light blue triangles indicate the direction of the crowd flow. (C) Picture of the exhibit in action (view from the right corner of the entrance).

The scientific core of the facility lays in its second half: the “measurement zone”. There the visitors, while being tracked at high resolution (cf. Figure 3), faced the decision to pass either on the left or on the right side of the central obstacle in order to leave the exhibit. We swayed this decision – otherwise expected left-right symmetric – with stimuli randomly changing every 3 minutes (cf. Figure 2).

We introduce here “Moving Light”, a real-life experiment in which we targeted, in quantitative terms, a prototypical case of automated crowd steering: swaying – by means of visual stimuli – the route choice of pedestrians between two symmetric exits (Figure 1).

The experiment took place as one of the exhibits in the week-long 2017 Eindhoven Glow Light Festival [7]. The Glow Festival, occurring every year and running in the evenings, involves a city-wide uni-directional route in which visitors – in the order of hundreds of thousands – walk through exhibits related to illumination design and light art. In 2017, the event took place in the period 11th - 18th November. The unique experimental nature and the high attendance makes the festival a perfect location for analysing crowd dynamics.

In the Moving Light experiment, for the entire duration of the event, we subjected the visitors stream to stimuli which periodically changed every three minutes and which were chosen randomly from a pool of 18 (one stimulus appeared at once, stimuli were e.g. based on arrow indications or on illumination).



Figure 2: Arrow based stimuli (A, B) and related symmetric control conditions (C, D) employed to sway individual routing decisions for either. Each stimulus appeared on a LED matrix on the front side of the obstacle for intervals of three minutes and changed at random. (A,B) arrows pointing to the left or the right aimed at steering pedestrians to, respectively, the exits on the left or on the right side of the obstacle. (C, D) Neutral control conditions encompassing, respectively, a doubly-sided arrow and absence of signage (no arrow displayed). In the following, these four stimuli are indicated in symbols for brevity respectively as “ \leftarrow ”, “ \rightarrow ”, “ \leftrightarrow ”, “ \emptyset ”.

About 140.000 of the festival visitors crossed our installation: we tracked them individually at high space and time resolution aiming at quantifying the impact of the stimuli on their individual trajectories and on their final exit choice. Visitors were not aware, or at least not notified, that trajectories were recorded and thus we can assume that no bias originated from the experimental setting (note that no feature, visual or otherwise, allowing personal identification was employed or stored in the process).

In this manuscript we analyse the steering performance of arrow stimuli as shown in Figure 2 (these form a subset of 4 stimuli in the pool of 18). Specifically, this contribution is structured as follows: in Section 2 we describe the Moving Light experimental setup. This includes the crowd steering hypothesis testing rationale and the tracking technologies employed. Then, in Section 3, we focus on the dynamics triggered by arrow stimuli and quantify their effectiveness and action range. Section 4 contains a closing discussion.

2. The Moving Light real-life experiment

The Moving Light installation, placed on a wide sidewalk, is framed as a 23m x 6m corridor

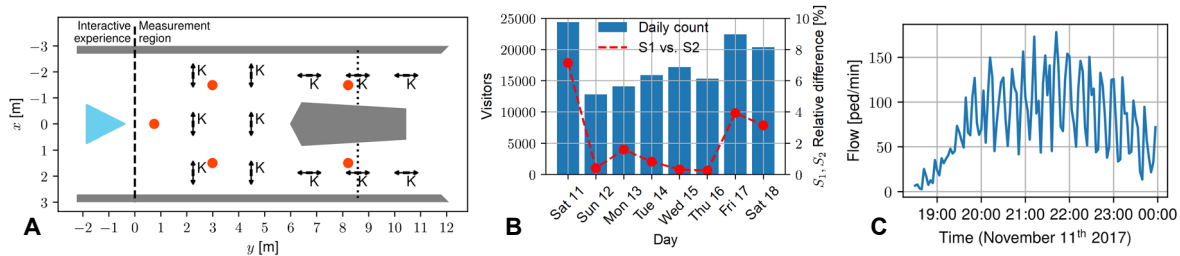


Figure 3: (A) Measurement systems at the Moving Light experiment. Pedestrian tracking has been operated via a Microsoft Kinect™ based system (S1, grid of 12 units, indicated with a “K” and with major Field-of-View angle aligned with the arrows) and via a Xovis AG commercial system (S2, sensor locations indicated by orange dots). See Figure 4A for a depth field image by the Kinect system grid. (B) Visitors count of the Moving Light per festival evening. Bars: average count between the two measurement systems: Kinect-based (S1) and Xovis-based (S2). Dashed line: absolute difference among the counts of the two systems relative to the mean. (C) Visitors flow (ped./min) during the first evening (readings on windows 3 minutes long). The count fluctuation (period: about 15 minutes) is due to a periodic light show located a few hundred meters upstream

(demarcated on either side by 3 meters high semi-transparent fabric fences), and it is formed of two adjacent zones, namely the “interactive experience” zone and the “measurement zone”. These are consecutive along the visit and each one measures 11.5 m x 6m (i.e. half of the full length). The “interactive experience” comes first. It encloses the artistic contribution of the installation as well as it serves the precise scientific aim of grouping visitors in “batches” of 1 minute. At the beginning of every minute, an overhead structure made of LEDs lights up. The motion of visitors underneath influences the illumination patterns creating an interactive show. This brings visitors to stay within the “interactive experience” zone until when, about 50 seconds after the start, the show terminates in darkness (see [8] for further information).

Visitors, in a now almost dark environment, make then their way into the “measurement zone”, the scientific core of the installation. Here, individuals choose between two symmetric exit ways. The exits are defined by a central obstacle which resembles, in shape, a liquid drop with squared sides. The obstacle measures about 5m in length, more than 3m in height, and 2m in width in its largest section – thus, it divides the corridor transversally into three even segments and the exits remain identified by its side ways.

As the flow is unidirectional and visitors have clear sight on the empty sidewalk past the installation, we expect a 50:50 choice rate between the exits, with possibly a slight preference for the right side due to

cultural preferences (e.g. [9,10]). As mentioned, we apply stimuli to break the symmetry in the scenario aiming at influencing the route choice, which we measure by high-resolution individual tracking.

2.1 Arrow stimuli

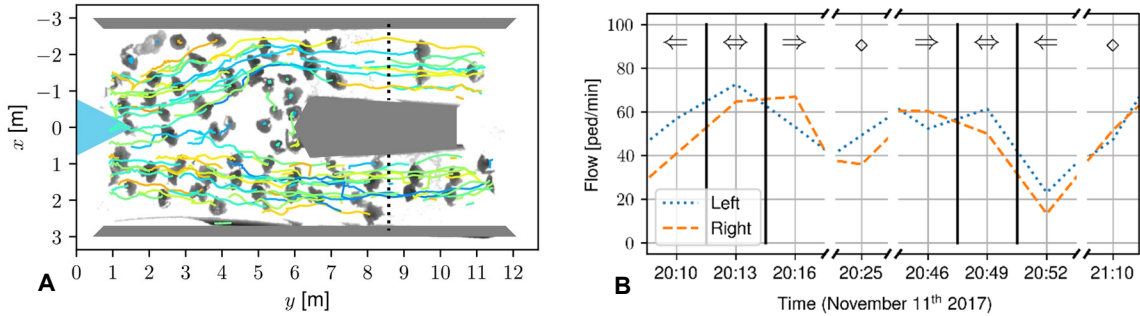


Figure 4: A depth-map collected by the Kinect-based measurement system with superimposed individual trajectories. Depth maps from the 12 sensors (cf. Figure 3A) are undistorted and merged following the procedure in [11]. The dotted line (coordinates $y = 8.5m$) reports the count line we used to evaluate instantaneous flows in Figures 5A and 7. Lateral fabric fences and central obstacle have been added manually in grey colour for reference. (B) Example measurements of pedestrian flows (ped./min) at the two sides of the obstacle as different stimuli (reported atop the lines) were applied. In the vast majority of cases, the left-right symmetry breaks with larger flow in the direction of the arrow as in the cases reported.

An arrow indication is possibly the simplest among the stimuli that can be employed to steer a crowd. Arrow indications were presented to the visitors through a squared LED matrix placed on the frontal face of the obstacle (size about 2m x 2m, cf. Figure 2). The presence of the arrow breaks the symmetry in the installation and comes with the obvious expectation for a quick preference shift for the side indicated. To check the effectiveness of the arrow stimuli we compare its effect against symmetric control conditions, specifically: an arrow pointing both ways and a stimuli-free condition where no arrow is displayed (see Figures 2CD).

2.2 Measurements

To quantify the effect of the stimuli we tracked automatically and with high-space-and-time-resolution each visitor crossing the measurement zone. To this aim we employed two independent technologies:

- S1. A state-of-the-art tracking system developed for pedestrian dynamics research. The system is based on a grid of overhead depth sensors (12 Microsoft Kinects™ [12], cf. Figure 3A) and on ad-hoc localization and tracking algorithms [6,11,13] (see also similar implementation in [14]).
- S2. A commercial pedestrian tracking system produced by Xovis AG, and here deployed in 5 overhead stereo cameras [15].

In Figures 3ABC we report, respectively, the sensors distribution, the number of visitors that crossed the installation each evening (inclusive of measurement differences between S1 and S2), and, as a sample, the time history of the pedestrian flow during the first evening.

Because the tracking systems S1 and S2 produced close results in the counts - especially in the conditions treated in this paper - and given the possibility of the system S1 of comparing the measurements directly with the recorded depth maps (cf. Figure 4A), in the following we will address only measurements by the system S1 (Kinect-based).

2.3 Steering ratio

We quantify the steering effect $S(j)$ of a stimulus j as the ratio between the number of pedestrians that exited the installation by the left side (say $\#(L|j)$) and the total number (i.e. the sum of passages on the left and on the right, say $\#(L|j) + \#(R|j)$). The counting is restricted to time periods in which j was active).

In formulas, this reads

$$S(j) = \frac{\#(L|j)}{\#(L|j) + \#(R|j)} \quad (1)$$

which, in a frequentist interpretation of probability, quantifies the probability of using the left exit conditioned to the presence of j . Operatively, we evaluate $S(j)$ by counting the crossing events of a transversal count-line (i.e. with coordinates $y = y_s = \text{const}$, cf. dashed line in Figure 4A). Passages with $x < 0$ identify a preference (or a choice in case of the position of the count-line in Figure 4A) for the left exit (and vice versa for the right case). An overall crowd-level preference for the left side thus yields $S(j) > 0.5$. Considering different count line positions (i.e. varying y_s) enables us to analyze the evolution of the side preference as a function of the distance to the obstacle.

3. Steering effect of arrow stimuli

During the festival, the four stimuli (left/right arrow, double arrow and no-arrow, cf. Figure 2) were activated in intervals of three minutes, respectively 61, 62, 60 and 52 times. Each one was thus active for about three hours, during which, a total of, respectively, 9017, 10060, 9895 and 8801 pedestrians crossed the facility.

As expected, we could generally observe a stabilization to a side preference following the arrow indication, or, for the control stimuli, to a roughly symmetric flow. In Figure 4B, we report, as an

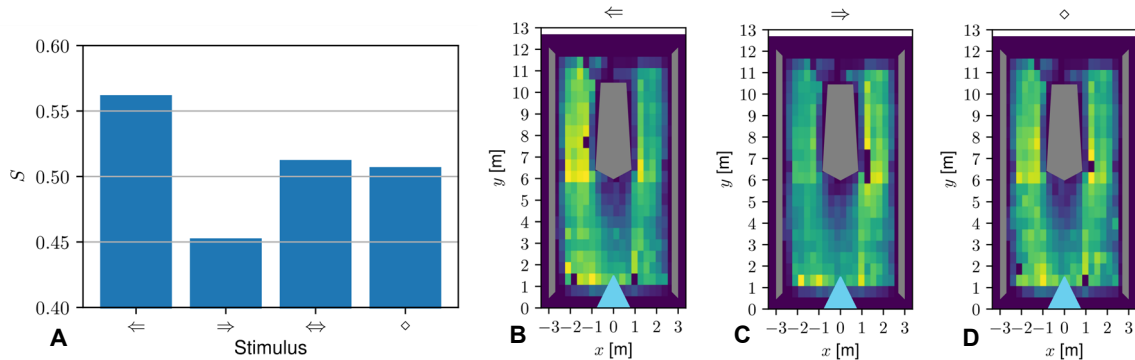


Figure 5: (A) Overall steering effect $S(j)$ (cf. Eq. 1) achieved by the considered stimuli (Figure 2) in presence of the stimulus j ($j \in \{\leftarrow, \rightarrow, \leftrightarrow, \diamond\}$, cf. Section 2.3). The left and right arrow stimuli yield a nearly symmetric effect and varied the preference for the left side of about $\pm 6\%$ (in relation to the average neutral condition response, i.e. 1% preference for the left side). (B-D) Probability distribution function of pedestrian positions in form of heatmaps, respectively in combination with a left, a right and a no-arrow stimulus. The routing preference reported in (A) is here noticeable as the side of the obstacle indicated by the arrow is used more, than in the neutral case.

example, the readings of the pedestrian flow per minute as different stimuli were presented. Although in the figure the effect remain appreciable, instantaneous readings are generally noisy, as affected by the stochasticity of individual behaviours. A side preference, instead, robustly emerges as we consider the measurements as an ensemble, i.e. discarding the time variable, and compute the ratios $S(j)$ globally (see Figure 5A).

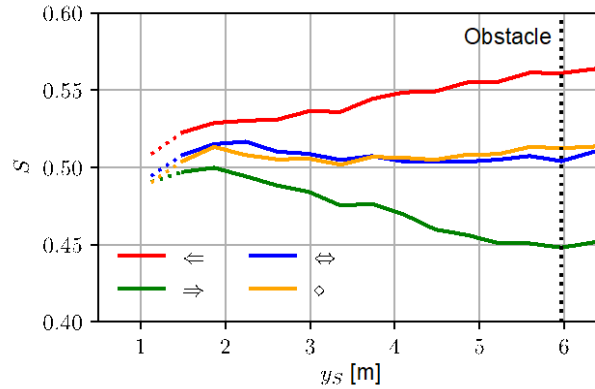


Figure 6: Steering ratio $S(j)$ (cf. Eq. 1) as a function of the count line coordinate y_S (i.e. line $y = y_S$, $y \approx 0$ denotes the entrance of the measurement zone while the obstacle begins at $y \approx 6m$. we report the case $y_S > 1.5m$ as the trajectory reconstruction quality at the boundary of the measurement zone is lower). At $y_S = 1.5m$, the steering ratio of arrow signs is about $\pm 1.5\%$ (in comparison to control conditions), and grows almost linearly up to $\pm 6\%$ (in comparison to control conditions) as one gets closer to the obstacle. Extrapolating from the trend shown, we expect that around $y = 0$, no reaction to the stimuli is observable (i.e. $S(j) \approx S(\text{control})$).

In the case of neutral stimuli, we observe a slight, yet surprising, preference for the left side (about, on average, 1% - i.e., $S(j) - 0.5 \approx 1\%$). This is necessarily connected with the environment: the rightmost fabric fence of the exhibit was about two meters far from a building, while the leftmost fence was bounding a large street (closed to the car traffic during the festival). Since these fabric fences were semi-transparent, we imagine, but we are not sure, that this could pass to the visitor impressions of higher prospect and/or of higher motion freedom on the left side thus the slightly higher preference. These ratios, in any case, define the baseline for our steering measurements and the reference with which we compare the steering ratios in case of arrow signs.

As we display arrow indications, routing choices, as expected, deviated from this baseline. We recorded an almost symmetric response for the left and right arrows in comparison with neutral conditions: in both cases the preference for the left incremented or, respectively, decremented by 6%. This effect remains qualitatively observable also in the position heatmaps in Figure 5BC, where the indicated side display higher position probability, i.e. most chosen in comparison with the neutral case in Figure 5D.

In Figure 6 we report the value of $S(j)$ as we move the count line position, parametrized by y_S , between the beginning of the measurement zone and the obstacle location. We notice that the side preference establishes within the measurement zone, in fact $S(j) \approx S(\text{control})$ at the entrance of the zone ($y \approx 0$). In other words, despite the fact that the obstacle and the indication can be seen from farther away, it is only about when pedestrians enter the measurement zone that deviations from uniform left-right distributions, as to pass around the obstacle, establish. Furthermore, the side preference shows an almost linear growth as we approach the obstacle in presence of directional arrow stimuli.

We observe further a dependence of individuals' "steerability" on the entrance position. Steering effects are in fact stronger if a pedestrian faces the obstacle at the entrance (around $x = 0$ in Figure 4A). In these conditions, they do not have a straight way to the exits and a side movement is necessary. Considering only pedestrians entering in the central segment $x \in [-0.5, 0.5]m$, we measure steering ratios $S(\Leftarrow) \approx 63\%$ and $S(\Rightarrow) \approx 37\%$ (cf. Figure 7), considerably higher than in the global case (Figure 5A). On the opposite, pedestrians that entered more to the sides of the installation, i.e. close to one of the lateral fabric fences, changed their path to follow the arrow indication only with very small probability.

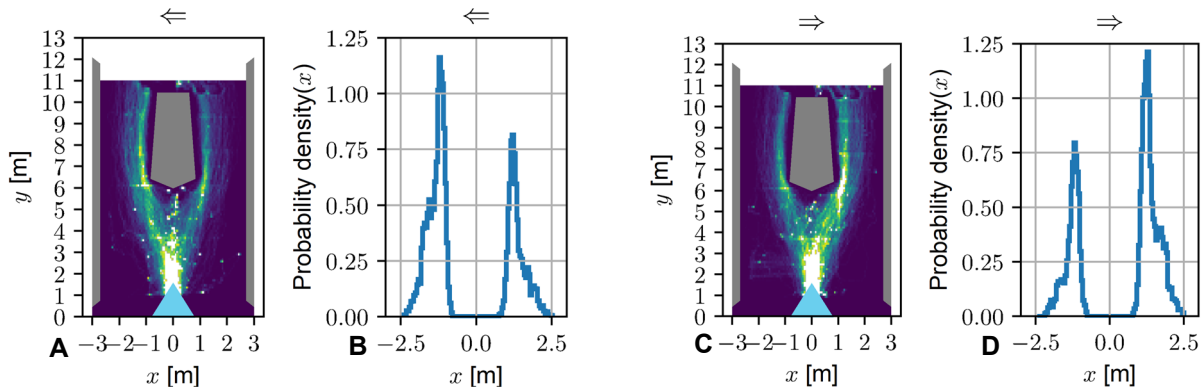


Figure 7: Position distribution of visitors entering at the middle of the corridor (i.e. facing the obstacle, $x \in [-0.5, 0.5]$). (A, B) Case of left arrow stimulus, (C, D) case of right arrow stimulus. (A, C) position heatmap (as in Figures 5B-D). We observe that pedestrians remain close to the middle line and tend to stay close to the obstacle sides. (B, D) probability distribution function on counting line in Figure 4A; the corresponding steering ratios are $S(\Leftarrow) \approx 63\%$ and $S(\Rightarrow) \approx 37\%$. In these conditions our steering capability increases from 6% to ...

4. Discussion

In this paper, we introduced the “Moving Light” real-life experiment, in which we aimed at quantifying the effectiveness of visual stimuli in automatically steering crowd flows. In a week-long campaign held during Eindhoven Glow Festival 2017, we displayed stimuli to bias the decision of the over 140.000 visitors of the exhibit for one of the two otherwise symmetric exits. Our analysis of the stimuli effectiveness has been based on the exhaustive collection of all the visitors’ trajectories through automatic high-resolution tracking methods. Gathering high volume of trajectories is a crucial aspect in our investigation and aims at ensuring high statistical resolution in the observations to build robust conclusions encompassing the randomness of individual behaviours.

We focused here on stimuli based on signage and, in particular, on arrow indications pointing toward one of the exits. Arrows are possibly the simplest stimulus one can devise to steer a choice between alternative directions. Despite the full freedom of choice, and the possibility to see past the installation, arrow indications generated higher pedestrian flows towards the indicated exit. Overall, we measured an increment of the flow of about 6% (with respect to the control conditions) in the direction pointed, and a symmetric response to the left and to the right arrows. Such a 6% increment generated within the measurement region (i.e. within 6m from the obstacle) and translates into having about 27% more people in the designated side with respect to the non-designated side (where $27\% = S(j)/(1 - S(j)) - 1 = (56\% - 44\%)/44\%$).

We notice that this ratio strongly increases as we just consider the individuals that face the obstacle when entering, and who thus cannot exit in a straight line; in this case $S(j) \approx 63\%$, and 70% more people pass by the designated side than by non-designated one. On the opposite, route choices of pedestrians entering along the sides of the installation are hardly affected by the arrow stimuli; instead, they tend to keep to the side on which they entered until the exit. We expect thus higher steering performance in corridors relatively smaller in width with respect to the obstacle. Besides, local density is likely to play a role in steering performance, which we will investigate in forthcoming studies.

We see the Moving Light experiment as a first step toward unmanned crowd steering devices leveraging on visual stimuli to influence individual route choice. This aims at solutions that enhance safety and comfort in civil infrastructures via optimized crowd routing. We established here an experimental

benchmark for quantifying the effectiveness of steering stimuli, and we employed it to analyse the performance of arrow indications. As this paper is written, we are investigating the effects of the entire pool of stimuli considered in the Moving Light experiment. The results of these investigations will be reported on in future publications.

Acknowledgements

This work is part of the JSTP research programme “Vision driven visitor behavior analysis and crowd management” with project number 341-10-001, which is financed by the Netherlands Organization for Scientific Research (NWO). We acknowledge the financial support of TU/e Intelligent Lighting Institute (ILI), 4TU and Philips Lighting, and the logistic support of Student Hotel Eindhoven. Moving Light has been possible also thanks to the contribution of M. Hoekstra, I. Iuncu, T. LeJeune, B. Maas, R. Nuij, S. Schippers, W. Willaert.

References

- [1] J. Fruin, *Pedestrian planning and design*. Elevator World Inc., 1987.
- [2] N. Bode, E. Codlin, “Human exit route choice in virtual crowd evacuations,” *Animal Behav.*, 86(2), pp. 347-358, 2013.
- [3] E. Vilar, F. Rebelo, P. Noriega, J. Teles, C. Mayhorn, “The influence of environmental features on route selection in an emergency situation,” *Appl. Ergon.*, 44(4), pp. 618-627. 2013.
- [4] Ronchi, E., Nilsson, D., Kojić, S. et al., “A Virtual Reality Experiment on Flashing Lights at Emergency Exit Portals for Road Tunnel Evacuation,” *Fire Technol.* 52, 623, 2016.
- [5] M. Haghani, M. Sarvi, “Crowd behaviour and motion: Empirical methods,” *Transport. Res.B-Meth.*, 107, pp. 253-294, 2018.
- [6] A. Corbetta, C. Lee, R. Benzi, A. Muntean and F. Toschi, “Fluctuations around mean walking behaviors in diluted pedestrian flows,” *Phys. Rev. E*, 95, 032316, 2017.
- [7] Glow Festival Eindhoven, official website <https://www.gloweindhoven.nl/en>. Online reference for 2017 edition: <https://www.gloweindhoven.nl/en/projecten/projects-2017>.
- [8] B. Maas, “Moving Light @ GLOW 2017,” *ILI GLOW Magazine*, 8, pp. 8-9, 2017.
- [9] M. Moussaïd, D. Helbing, S. Garnier, A. Johansson, M. Combe, G. Theraulaz, “Experimental study of the behavioural mechanisms underlying self-organization in human crowds,” *Proc. Roy. Soc. Lond. B Biol. Sci.*, 276, pp. 2755-2762, 2009.
- [10] A. Corbetta, C. Lee, A. Muntean, F. Toschi, “Asymmetric pedestrian dynamics on a staircase landing from continuous measurements,” in *Traffic and Granular Flow'15*, pp. 49-56, Springer, 2016.
- [11] A. Corbetta, J. Meeusen, C. Lee and F. Toschi, “Continuous measurements of real-life bidirectional pedestrian flows on a wide walkway,” in *Proceedings of Pedestrian and Evacuation Dynamics*, pp. 18-24, 2016.
- [12] Microsoft Corporation, “Kinect for Xbox 360,” Redmond, WA, USA.
- [13] W. Kroneman, A. Corbetta, F. Toschi, “Accurate pedestrian localization in overhead depth images via Height-Augmented HOG,” in *Pedestrian and Evacuation Dynamics*, 2018 (accepted).
- [14] S. Seer, N. Brändle, C. Ratti, “Kinects and human kinetics: A new approach for studying pedestrian behavior,” *Transport. Res. C-Emerg. Technol.*, 48, pp. 212-228, 2014.
- [15] Xovis AG., “Xovis PC2”, Zollikofen, CH.

Field Theory in Practice

José Méndez Omaña¹,

¹Beuth-Hochschule für Technik Berlin
Berlin, Germany
mendez@beuth-hochschule.de

Abstract - The aim of this paper is to present K. Lewin's Field Theory in practice, applying it to evacuation simulations. The construction of the field is discussed from the scratch in order to define the psychological space of a social event. Then, we illustrate the interplay of the physical and the psychological aspects of a mathematical model of human behavior presenting and discussing evacuation simulations of one event. At first we simulate the physical situation and then we calculate an evacuation time applying an elementary microscopic model. An empirical plausibility control is presented. When we apply mathematical modeling or cybernetic methods to social sciences we are said to be careful. Nevertheless, a social event might be considered, on a natural way, as a set of time series, from the point of view of statistics. In this paper we restrict ourselves to introduce probabilities of random variables associated to the physical and the psychological space and define a measure for the evacuation simulation: The entropy of the event, merging the physical and the psychological spaces.

Keywords: Field Theory, Mathematical Models of Human Behaviour, Social Event Entropy

1. Introduction

Any mathematical model applied in evacuation simulations includes, or should do, implicitly or explicitly, psychological aspects due to its purpose: modelling human behaviour. Data and mathematical concepts are required, but we are told: "For a good statistic of society, we need long runs under essentially constant conditions" [12]. This statement of N. Wiener, inventor of cybernetics, continues: "Thus the human sciences are very poor testing-grounds for a new mathematical technique". We are in the need of interdisciplinary expertise. This is the reason why, Lewin's field theory is interesting. K. Lewin was a psychologist who used mathematical theory, set-theoretic topology and vectors, to express human behaviour [4] and, as we reportedly know, participated in meetings organised by Wieners work group [12]. Concerning pedestrian dynamics the link to psychology exhibits a diversity of forms. For instance: Helbing's Social Force Model [2] includes explicit reference to the work of Lewin and the hydraulic model of Predtetschenski and Milinski [8] presents an implicit solution based on empirics. Let us argue briefly about this assertion: When we work out a task applying this method, the working parameters may suggest psychological aspects play no role. Nevertheless, when the authors introduce the velocity as a function of density and sort of way, they assert that for the same density (on the same track) the values of the velocity may differ strongly and this because of the individual characteristics of each person. The authors introduce explicitly an extended definition of the velocity as a function of three variables: density, sort of way and psychological factors. Nevertheless, for the calculations, we find the velocity as univariate function of the density. Almost 3600 empirical measurements and a statistical data treatment justify the simplification [8]. The question about a good statistic of society rises from at least two points of view and concerns not only this model: Do we have long runs under essentially equal conditions? If we have a good statistic of one society, is it a good statistic of another society?

An important discussion of some psychological aspects of evacuation simulation can be found in [10].

The paper consists of two sections: Field Theory and Introducing Entropy. In the first section we present some basics of Lewin's Field Theory aiming immediate application. In order to accomplish this object and according to the material bounds of this paper one simple case study is presented. The aim of the second section is the introduction of a kind of measurement of a social event: the concept of social event entropy. This happens following strictly Shannon's idea: to define a measurement for uncertainty [11].

2. Field Theory

Field theory is a method of analysing causal relations and of building scientific constructs (systems of a priori concepts) and can be expressed in the form of certain general statements about the nature of the conditions of change of the life or psychological space of a person [6]. Behaviour is any change in the psychological space. A basic construct states that the behaviour b at the time t is a function of the situation S at the time t and only and this time. This can be written as follows: $b_t = F(S_t)$. Thus, modelling the behaviour of a person requires defining her/his life space at a given time. The life space of a person is the totality of possible psychological events. Another expression for behaviour in Lewin's papers is $B=f(PE)$, behaviour as a function of the state of the person and of the environment [4].

In order to explain the constructive procedure of representing the life space of a person and its environment we start excerpting from [4] and later present a rather schematic procedure:

1. "The fundamental constructs which we use in representing the situation must consist of concepts from which one can derive, unambiguously, certain events as "possible", others as "not possible". Instead of classificatory concepts one has to use constructive ones which have a direct relationship to laws."
2. "It should be possible to derive from such a representation all forms of anamneses which actually occur. This stringency of the *derivation of the totality* of possible cases is valid not only for the anamneses of the person within the situation but also for the possible changes of the person or the situation itself."
3. "Such a derivation of the totality of possibilities can only be accomplished if one proceeds from the life space *as a whole*."
4. "The center of interest shifts from *objects to processes*, from states to changes of state. If the life space is a totality of possible events, then "things" that enter the situation, especially the person himself and psychological "objects", have to be characterized by their relationship to possible events."

An important remark has to be made: if we read possible case, then we eventually associate a probability to this case. In this context we have to be aware of the theory and consider that only the subjective probability should be taken into account for predicting behaviour [6]. This means, only what a person knows, plays a role.

In the following we shall speak only about psychological space including the life space concept. As far as we know, the distinction is of historical nature. In the early papers Lewin speaks about life space and psychological space, later about psychological and hodological space.

The rather formal aspects of field theory as the comparison of the mathematical concept of topological space with the hodological space concept might be found in [4] or [7]. Here we merely mention that the Euclidian space concept, say the everyday space with the usual distance, is not suited to describe psychological events. The hodological space is a concept representing an empirical (psychological) space. This is a diversity of facts showing specific forms of interaction at some time [5]. Etymologically explained, hodological space means something like the space where you find the paths (Greek: ὁδός, path, way). The hodological space is set consisting of regions also called cells. The regions may be adjacent or not and they may contain subregions. The regions represent domains of the psychological world of a person or a group of persons. Two regions are said to be independent if a change in one of them does not induce a change in the other one. A point is not a region. Two points may be connected by a path and direction and distance are defined by specified paths. The distance between two regions a and b is defined as the minimal number of regions crossed by a path from a to b . There is also a concept of connectivity as in topology. A change of position in the hodological space is called locomotion and corresponds to the

behaviour. It should be considered at a given time. At this point we have to say, that in the field theory a given time t means often an interval of time and not a point on the time scale. The reason why: we need to know the context of the psychological event and this is practically impossible if we consider only an instant. In practice we could also speak about frames but we are not going to do it.

Before we present a schematic procedure for the psychological space set up, we would like to say that, from the point of view of psychology, there are two approaches for this task: the one is of historical nature, anamneses, and the other diagnostic tests of the present. The first one can't be applied in the standard event management and moreover, following Lewin, won't produce the desired results. Hence, we propose a diagnostic test procedure:

Step 1 Enter the time interval $[0, T]$, the total event time duration. Define the length of the time sub-intervals for diagnostic test and determine, if needed, a frequency.

Step 2 Define the relevant variables.

Step 3 For the first subinterval: attempt to find an answer to the question: What is possible? (Based on the actual situation)

Step 4 For the first subinterval: proof the values of the relevant variables

Step 5 For the first subinterval: sketch the hodological space

Step 6 Return to Step 3 for the second subinterval and so on until required.

We finish this part of this section with two remarks: the proof of the relevant variables may have consequences in the physical world and vice versa. The second remark is, may be, much more than a remark: The diagnostic tests of the present includes elements of the past as the 'habits' of the visitors. This is well known to all event managers.

2.1. Field theory in practice: Example

We apply a quite simple microscopic model developed on our own. For a solution to this kind of problems based on a force field model see [1]. The estimated path of each person or group of persons is given by a curve. Beziér-Curves or splines are in some cases useful. The direction field of a linear, first order ODE with constant coefficients is, in other cases, good suited, because it is easy to obtain solutions for given boundary values. Some of the solutions are used as boundary paths of the pedestrian flow and some other represent special paths. The adequate kind of mathematical objects depends on the geometry and specific characteristics of the venue and event. The area bounded by the boundary paths is calculated and, depending on the flow, we estimate the density at a given time. The quotient of the arc length of a curve or a differential equation solution and a locally suited velocity, according to the density, provides a time estimate.

We illustrate the method by a very simple example: a group of 56 persons, 55 students, one of them using a wheelchair and requiring personal assistance, evacuates a hall. We focus only on the last part of the evacuation namely the specific flow through the door and the flow on the area in front of the door. The width of the door amounts 1.09 m and we consider 2 m in front of. Because of the extension limit of this paper we omit a sketch but the Fig.1 may fill the gap: Imagine the door between the upper right corner, this is the point with the coordinates $(2, 0)$, and the point $(2, -1.09)$. From this point downwards to $(2, -3)$ we have a wall. The upper horizontal axis should be seen as a wall. The remaining lines, from $(0, 0)$ to $(0, -3)$ and from this point to $(2, -3)$ are open, inside of the hall. We choose the direction field of the differential equation $y' = 0.3x - y$ on the closed interval $[0, 2]$ for the independent variable x and on $[-3, 0.04]$ for y . The reason why is the geometry of this special part of the track: a relatively short non-linear path showing eventually high density. The exact solution of this equation is $y = Ce^{-x} + 0.3x - 0.3$, with $C = -2.22$ for the boundary condition $y(2) = 0$, $C = -10.12$ for $y(2) = -1.07$. This are the solutions used as bounds for the pedestrian flow. The area enclosed by the graphs of this functions, the bottom horizontal line passing through $(0, -3)$ and the perpendicular to this line passing through $(2, 0)$ amounts 3.22 m^2 . A third solution $C = -6.65$ for $y(2) = -0.6$ is given, in order to simulate a frequently used path towards and through a point slightly to the right of the midpoint of the threshold of the door. The arc lengths amount 3.28 m and 2.08 m for the upper and for the lower bound respectively. The third arc length amounts 2.71

m. The shape of the pedestrian flow shall be “narrow, wide, narrow”, expressed on a qualitative way, based on empirical knowledge. Quantitatively we assume the pattern 1+1+1+2+2+3 persons, then 9 times 4 and lastly 3+3+2+1+1. For the first three we set $v=1.34+0.26=1.6$ m/s obtaining $t=1.69$ s following the path in the middle. For the next four persons we set $v=1.34$ m/s, also on the path in the middle, and this yields to $t=2.02$ s. We are aware of the pattern, this means: after $3.71+e=1.69+2.02+e$ seconds, where e is an error, 7 persons went along the path in the middle, due to the low density. We recall: the door width amounts 1.09 m. If we assume that, in average, less than two persons but more than one may cross the threshold of the door, then, from now on, the flow sticks in traffic. Moreover, we dare to make a first prediction: If 1.5 persons per second would cross the threshold of the door then we estimate $t_1=56/1.5=37.3$ s for the whole group. After this remarks we continue the calculation: For the coming three persons we set $v=1.23$ m/s and we have $t=2.51$ s. For the four persons groups we set $v=1.11$ m/s and calculate two rather on the upper bound $t_1=3.28/1.11=2.95$ s and two rather on the lower bound obtaining $t_2=2.08/1.11=1.87$ s. The mean of this values is $t=2.41$ s. We add up and obtain $3.71+2.51+9\cdot 2.41=27.9$ s and 46 persons. For the last groups consisting of three persons we set $t=2\cdot 2.51=5.02$ s, hence we have until now $t=32.92$ s and 52 persons. For the group consisting of two persons, one of them on the wheelchair we set $v=0.8$ m/s on the path in the middle and obtain $t=3.39$ s. The last two persons have to adapt their individual velocities to the one of the persons there are behind of and define in fact a two persons group. The result is $t=39.7+e$ s.

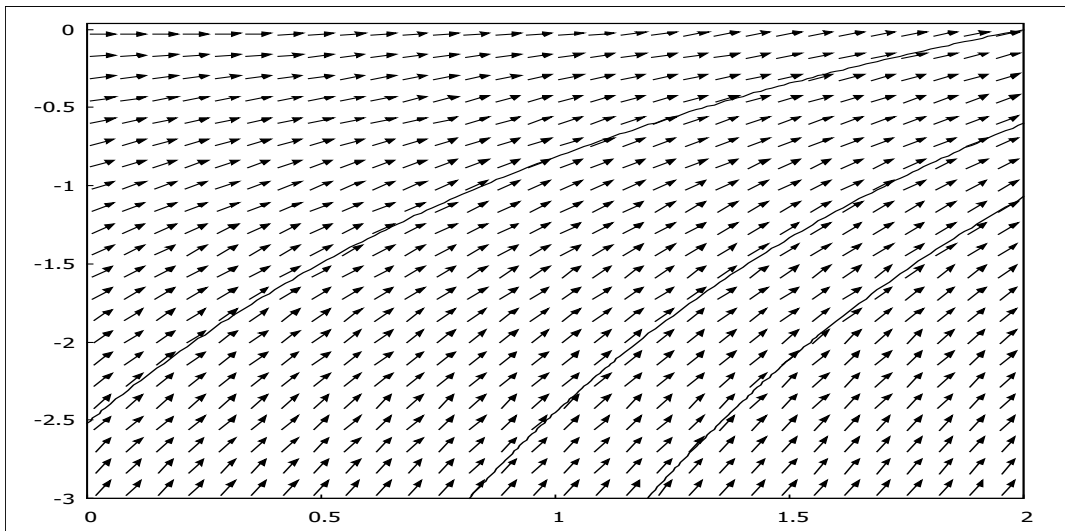


Fig. 1: The direction field of a differential equation and some solutions as paths representation tool

In order to estimate the error we consider the number of “groups” multiplied by a factor, namely $(6+9+4) \cdot 0.25$ s = 4.75 s. This is coming from the transitions between the groups. The applied velocities for three and four persons were determined empirically, but not in this concrete simulation. All in all we have a second forecast: $t=39.7+4.75=44.45$ s and recall the first one $t=37.3$ s. An empirical plausibility control value $t=37$ s had been obtained and based on this time we have the flow rate 1.51 persons per second. The images in Fig 2 may offer an impression of the empirical data collection. Modelling the pedestrian flow applying any CA-model or macroscopic model would have been in fact more comfortable, but we do it on this way, bearing in mind future developments. We have actually simulated the physical part and calculated an evacuation time. Now, we dedicate our efforts to the psychological one. We proceed to implement one diagnostic test, including one hodological space.



Fig. 2: From the left: the pedestrian flow beginning, in between and to the end

In this case we apply some knowledge of the group obtained during the event. Knowledge obtained before shall not be taken into account. For the complete simulation we thought of 90 s but we focus only on the bottleneck situation at the end and think of 45 s. based on the mathematical simulation of the physical aspects. Because of the need for control concerning the shape of the flow applied in this model and the presence of a person on a wheelchair we set $T=45$ and no subinterval division. A rather relaxed attitude due to more experience may induce a definition of subintervals, say breaks, while updating the values of the relevant variables:

Step 1 Time interval: $[0, 45]$. (seconds)

Step 2 Relevant variables: A, attention paid to announcements (0 poor, 1 average, 2 highly concentrated), C social connectivity leading to clusters (0 none, 1 to one person, 2 to more than one person), Coh cohesion tendency in the group (0 no, 1 yes), D diffusion tendency in the group (0 no, 1 yes), M motor-perceptual region accessible (0 non-directly 1 directly), PA potential angeriness (0 no, 1 yes)

Step 3 For the continuous interval: The answer to the question: What is possible? (Based on the actual situation) : No unexpected changes assumed

Step 4 For the continuous interval: proof the values of the relevant variables:

A: 18 x 0, 22 x 1, 16 x 2; C: 18 x 0, 32 x 1, 6 x 2; Coh: 1 x 0; D: 1 x 0; M: 1 x 0, 55 x 1; PA: 56 x 0;

Step 5 Sketch the hodological space: We have no breaks, we start at $t=0$. Although Lewin describes the method to be used as approximation from the general topological space to the specific hodological one, we will construct the hodological space on another way, for the sake of a simpler, rather accessible presentation. At first we define a representation of one person and then we embed it into the model of the life space (hodological space) of this person:

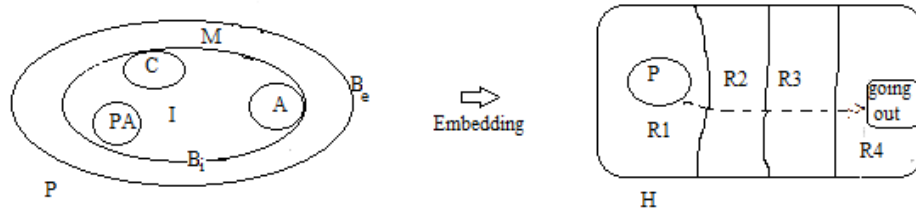


Fig. 3: The representation P of one person and its respective hodological space H

In order to represent one person we introduce a set P including two subsets: the subset I, representing the inner-personal region and the subset M representing the motor-perceptual activities. B_e is the boundary between P and the environment. B_i is the boundary between the motor-perceptual region and the inner-personal one.

As M includes information concerning the bodily interaction of the person and the environment, it is very important for the event management as it concerns the free accessibility of the event. In our example the

subset M of one person representation includes the information wheelchair and assistance required. The value of the variable M set to $M=0$, meaning non-directly accessible. For all other set $M=1$. We are aware of the use of M as subset name and as variable but we do it in order to simplify the notation. The subset I shall be poorly differentiated. Only the variables C (social connectivity), A (attention paid) and PA (potential angriness) are taken into account. As we see, Lewin's application of topology means on the one hand applying point set topology and on the other curves and no Venn-Diagrams for the graphical representation of psychological concepts. In the original papers a boundary is represented by a Jordan curve and the enclosed region is a set or subset. Then we embed P in a superset H and define subsets (regions) building a partition of H . The partition might be coarse or fine, depending on what do we expect: if we do not expect social tensions or another kind of difficulties (an unexpected physical barrier or the behaviour of some person could produce potential angriness) then we set a coarse partition. We define a coarse partition because we do not expect any kind of tensions. Only because of the bottleneck situation we consider more than one subset, say region, to go through. One oriented path from P to the goal has been sketched. The choice of the expression "going out" instead of "exit" for the goal obeys the principle of underlining the fact we are dealing with the psychological and not with the physical world. As the distance in the hodological space is given by the number of regions to be crossed, it is obvious that fine partitions lead to longer distances. We have 56 such sets representing persons and we store the estimated variables values for each person at a given time. Now we define the group made out from all persons. Formally we could simply build the union set G including the 56 subsets, but we may not forget, following again Lewin, the group is not simply the union set but a different entity. Therefore, we define a set G inheriting all information included in the 56 sets representing persons, include some other subsets and embed it in the respective hodological space:

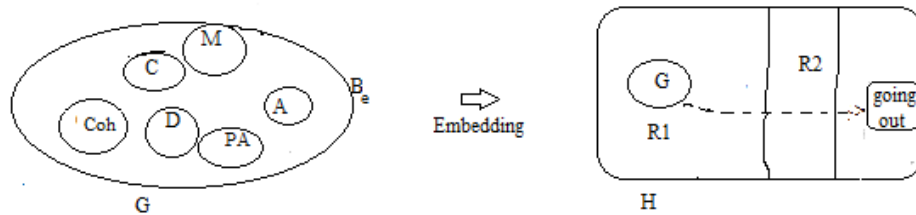


Fig. 4: The representation G of the group and its respective hodological space H

The subsets C , M , A , PA include all information from the individual subsets. The boundary B separates again the set G , the psychological world of the group, from the environment. The common intension of all persons to take part in the event builds up the group and defines also the boundary. We include the new variables Coh and D giving account of cohesion and diffusion tendencies in the group as a whole. C or Coh could show clustering tendencies. Changes in C , D or Coh could deal to a change of the parameter density, independently of the model. For the hodological space we define a partition which is coarser than the one defined in the individual example given above because we do not expect any complicated situation and because of the reduced number of choices for a behaviour change in case of the group.

Step 6 Return to Step 3 We recall: attempt to find an answer to the question: What is possible? (Based on the actual situation) In our example this leads to a continuous update of the variables values and of the partition of the hodological space.

In practice, in order to sketch the hodological space we could have already a template based on a data basis and/or empirical knowledge. The values of the variables is rather difficult to obtain. Start values

may be taken from empirical data collections and adjusted by inspection. The values assumed here are taken from empirical knowledge. It is important to remark: no mean values should be taken as basis for decisions. In some cases (M) only once the value 1 and 55 the value 0 leads to an entirely different situation. Empirical if possible, but any way highly specific diagnostic analysis should be performed in order to make decisions. In our example, the observed and updated values did not lead to new calculations in the physical model.

3. Introducing Entropy

There are concepts of entropy applied to human sciences as Bailey's Social Entropy Theory, or von Cube's Social Group Entropy, which we do not include as reference in this paper because they play no role in our social event entropy concept. They find a mention at this place only for the sake of the interested reader. At this point seems to be adequate to say, that in this section we distinguish between a social event and an event as subset of a probability space. We shall construct the social event entropy concept directly and based exclusively on Shannon's theory [12].

Shannon's mathematical theory of communication was developed in the context of the fundamental problem of communication and from the point of view of engineering: reproducing a message independently of semantics. In contrast to the irrelevance of semantics we have: "the significant aspect is that the actual message is one selected from a set of possible messages" [12]. We proceed to present the definition of a communication system and then we apply a part of it to our aim, namely, the construction of a suited mathematical model of a social event which allows the definition of entropy.

A communication system is a system consisting of five parts: information source, transmitter, channel, receiver and destination. The information source produces a message and is the only part of importance to us. Following an interdisciplinary point of view, we introduce informally the mathematical model of the information source, as Shannon does. The mathematical description of an information source is a stochastic process, a discrete Markov process. Imagine a discrete information source as a message generator which generates a message symbol by symbol. The symbols are chosen, step by step, constrained by some probabilities which depend, on the one hand on the previous choice and on the other on the particular symbol. Quoting Shannon we state: "A physical system or a mathematical model of a system which produces such a sequence of symbols governed by a set of probabilities, is known as a stochastic process". In order to present a formal definition we should introduce a set X_t of discrete random variables. The idea is to consider a social event as an information source producing messages. The messages we are interested on are, on the one hand, made out of quantities from the physical world and other hand made out of quantities from the psychological world. From the physical world we think of a five-dimensional vector with the components t , time, $x(t)$, $y(t)$, position coordinates, $v(t)$ velocity magnitude and $\varphi(t)$ velocity angle. Formally, we should consider the product of some spaces, but in this paper we will not develop the theory in full strength. We just focus, in order to illustrate the idea, on the component velocity magnitude. So we consider the velocity magnitude as a value of a random variable attached to a person or a group at a given time. Then we find out the corresponding probability and calculate the entropy for the given time. For more details concerning the following entropy definition see [12]. The only slight difference between this definition and the classical one is the time aspect. We have for each visitor or group of visitors a probability at a given time. K might be used as norming factor. Any base may be applied but we prefer sometimes the natural base because the velocity, as function of the density, is an exponential function for this base. We write:

$$H_t = -K \sum_{i=1}^n p_{it} \log_b p_{it} \quad (2)$$

It is easy to calculate entropies. Therefore, we close this paper with one example and an application. If we have $N=18$ visitors and the velocity is uniformly distributed, then we obtain in computer simulations almost always 18 different values. Therefore, the entropy with $K=1$ will be $18(1/18) \cdot \log_2(18) = 2.89$, the maximal value. If we set 18 times the same velocity we obtain $H=0$. If we set 7 groups having 7 different

velocities and the group sizes are 3, 6, 5 and 4 members plus 4 one person groups we obtain $H=1.66$. Vice versa, for a given entropy, we could imagine a group structure, as well in the psychological world.

4. Conclusion

The introduction of a systematic diagnostic analysis attempts to offer some answers to questions due to the interdependence of the physical and the psychological world concerning event management. Many of the problems are solved in practice by experienced event managers. Our concern is to improve mathematical models of human behaviour. As the example showed we obtain always a unified overview. There are methods for the analysis of the effect of uncertainty in an evacuation process [11]. The social event entropy may find an application field because of the level on which it works. The level is a kind of meta-level allowing uncertainty measurements on the physical and on the psychological world.

Acknowledgements

The author would like to acknowledge the contributions of Siegfried Paul, Arnim Bautz and students at the Beuth-Hochschule für Technik Berlin for making possible the empirical simulation.

References

- [1] M. Chraïbi, A. Schadschneider and A. Mackens, “Quantitative Description of Pedestrian Dynamics with a Force-Based Model”, arXiv: 0910.2343v1 [physics.soc-ph], 2009.
- [2] D. Helbing and P. Molnar, “Social Force Model for Pedestrian Dynamics,” in *Physical Review E*, vol.51 (5), pp. 4282-4286, 1995.
- [3] H. Klüpfel, T. Meyer-König and M. Schreckenberger, “Models for crowd movement and egress simulation”, in *Proceedings of Traffic and Granular Flow '03*, Berlin, 2004a, pp. 357-372.
- [4] K. Lewin, *Principles of Topological Psychology*, New York: McGraw-Hill, 1936.
- [5] K. Lewin, *Field Theory in Social Sciences*, New York: Harper & Brothers, 1951.
- [6] K. Lewin, “Defining the field at a given time (1941)”, in *Psychological Review* 50(3), pp. 292-310, 1989
- [7] J. Méndez Omaña, “Field Theory and Quantitative Models for Pedestrian Dynamics”, in *Transportation Research Procedia*, vol. 2, pp. 442-445, 2014
- [8] W.M. Predtetschenski and A.I. Milinski, *Personenströme in Gebäuden, Berechnungsmethoden für die Projektierung*, Köln-Braunsfeld: Rudolf Müller, 1971.
- [9] A. Schadschneider and A. Seyfried, “Validation of CA Models for Pedestrian Dynamics with Fundamental Diagrams”, in *Cybernetics and Systems: An International Journal*, vol. 40 5, pp. 367-389,
- [10] I. von Sievers, A. Templeton, F. Künzner, G. Köster, J. Drury, A. Philippides, T. Neckel and H. Bungartz, “Modeling social identification and helping in evacuation simulation”, in *Safety Science*, vol. 89, pp. 288-300, 2016.
- [11] C. E. Shannon, “A Mathematical Theory of Communication”, in *The Bell System Technical Journal*, vol. 27, pp. 379-423, 623-656, 1948.
- [12] N. Wiener, *Cybernetics: Or control and Communication in the Animal and the Machine*, Cambridge MA: M.I.T. Press, 1948.

Experimental study on the evading behaviour of single pedestrians encountering an obstacle

Xiaolu Jia¹, Claudio Feliciani², Daichi Yanagisawa^{2,3}, Katsuhiro Nishinari^{2,3}

¹ Department of Advanced Interdisciplinary Studies, School of Engineering, The University of Tokyo
4-6-1 Komaba, Meguro-ku, Tokyo 153-8904 Japan
xiaolujia@g.ecc.u-tokyo.ac.jp

² Research Center for Advanced Science and Technology, The University of Tokyo
4-6-1 Komaba, Meguro-ku, Tokyo 153-8904 Japan
feliciani@jamology.rcast.u-tokyo.ac.jp

³ Department of Aeronautics and Astronautics, Graduate School of Engineering, The University of Tokyo
7-3-1 Hongo, Bunkyo-ku, Tokyo 113-8656, Japan
tDaichi@mail.ecc.u-tokyo.ac.jp; tknishi@mail.ecc.u-tokyo.ac.jp

Abstract –Present simulation and experimental research still have deficiency in depicting the evading behaviour of single pedestrians confronting with an obstacle, which is the basis for the study of crowd dynamics affected by obstacles in real life. Therefore, this study will conduct experiments with a bar-shaped obstacle in the middle of a corridor and explore the corresponding general and particular features of single pedestrians. Particularly, the variation of pedestrian velocity and trajectory under different-sized obstacles will be illustrated. By taking the average velocity and trajectories of the 32 participants, it could be concluded that pedestrians would walk at a velocity of about 1.5 m/s without being affected by the size of obstacle. Besides, pedestrians tend to pass a location about 0.4 meters away from the obstacle edge that is perpendicular to walking direction. Furthermore, pedestrians tend to begin and finish evading the obstacle at locations respectively about 4.40 meters and 4.85 meters away from the obstacle. We also found a heterogeneity in the evading behaviour and pedestrians could be classified into four types accordingly. Results of this study are expected to provide reliable evidence for agent-based modelling in the future.

Keywords: evading behaviour; obstacle size; velocity variation; evading trajectory; individual experiments

1. Introduction

Most walking facilities, such as sports venues, traffic terminals, and residential complexes, are composed of obstacles including walls, pillars, and fences for pedestrian traffic. Understanding the way in which obstacles affect pedestrian behaviour is essential to the optimization of architectural layouts and pedestrian organization schemes for better evacuation efficiency, comfort, and security. Bar-shaped obstacles such as walls, in particular, are practical for better pedestrian traffic management because they can be used either as architectural boundaries or as obstacles to fulfil certain service functions. In this study, we will explore the influence of bar-shaped obstacle on pedestrian behaviour.

The effects of obstacles on the evacuation behaviour of crowded pedestrians are often simulated by agent-based modelling, which could reproduce mass behaviour through setting certain movement rules to single agent. The most widely applicable microscopic simulation models include the cellular automata (CA) model [1], social force model (SFM) [2] and velocity obstacle method (VO) [3,4,5] in the state-of-the-art research. The CA model divides the space into discrete grids and its agents could only choose to move to the neighbouring grids or stay still, which greatly decreases calculation burden through limiting the moveable direction and velocity of pedestrians. In SFM, pedestrians are regarded as particles driven by psychological and physical forces from obstacles or other pedestrians, so they could enjoy more freedom in choosing walking direction and velocity. In VO model, the collision-avoidance behaviour of pedestrians is also affected by relative velocity except for relative location, and pedestrians could choose optimal collision-free velocity when confronting with obstacles.

The three types of models could reproduce interesting phenomena. For instance, some studies showed that placing a circle-shaped or bar-shaped obstacle at certain distance away from the exit could help improve flow rate [6] or decrease evacuation time [7]. However, these models are not necessarily able to reproduce the real evading behaviour of single pedestrian before an obstacle. To be specific, although some simulation models could emulate individual pedestrians evading obstacles [8,9] and even reproduce varied evading behaviours controlled with parameters [10], experimental evidence to validate the simulations remains insufficient.

Therefore, many scholars have conducted experiments that could help verify whether the modelling rules were in accordance with real pedestrian evading behaviour. Some studies set a static pedestrian as the obstacle in the middle of the corridor and numerically depicted the features of evading behaviour [11,12]. The distance between the centroids of individual pedestrian and the obstacle when the pedestrian began to change his movement direction ranged from 0.5 m to 4.25 m in [11] and from 1.5 m to 4 m in [12]. However, pedestrian behaviour may change when confronting real obstacles instead of static pedestrian, making the experimental results difficult to apply when bar-shaped obstacles are present.

Moreover, the existing experimental analyses of evading behaviour are not adequate. Most studies only depicted pedestrian trajectories and provided an average velocity of single pedestrians without an in-depth analysis on the effect of obstacle size on the heterogeneity of pedestrian evading behaviour. Therefore, through conducting experiments using real obstacle, this study will explore the common and particular features of the evading behaviour of different pedestrians and illustrate the influence of obstacle size variation on evading behaviour.

2. Experimental setup

Experiments have been conducted to investigate the way in which the size of bar-shaped obstacles will affect the evading behaviour of single pedestrians. The experiments were held on November 4th, 2017 in the Lecture Hall of RCAST Building 4, the University of Tokyo, Japan. 32 male students, whose ages ranged from 20 to 24, have participated in the experiments.

A camera was set above the horizontal axis of the corridor and fixed at 6 meters above the ground. Recording of the camera was adjusted to full HD mode (1920×1080 pixel) with a frame rate of 30 fps. With the videos of the experiments as raw data, the recognition and tracking of pedestrian locations under each frame could be achieved by using PeTrack software (version 0.8) [13], and the variations of velocity and trajectory in different scenarios could be obtained accordingly.

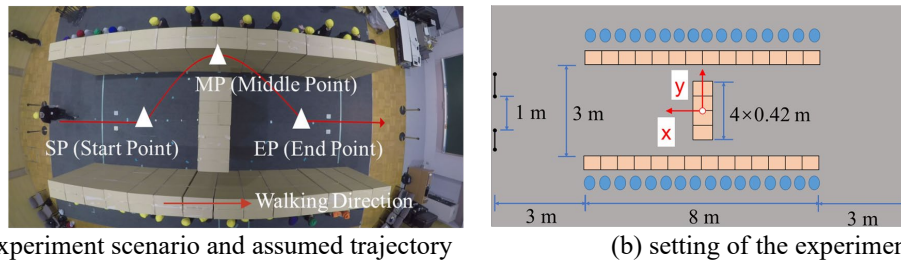


Fig. 1: Experimental scenario with a bar-shaped obstacle formed from four cardboard boxes ($box=4$) in the middle of the corridor. The width, depth, and height of each box is 0.42, 0.46, and 2.1 meters respectively.

As shown in Fig. 1(a), we constructed the walls of a corridor and an obstacle in the middle of the corridor using cardboard boxes. The sizes of the corridor and obstacle can be seen in Fig. 1(b). In order to explore the influence of obstacle size on pedestrian behaviour, the size of obstacle would be changed through adding the number of boxes that comprised the obstacle. As a result, five scenarios have been tested with the number of cardboard boxes comprising the obstacle being zero (without obstacle), one, two, three, and four boxes (i.e., $box=0, 1, 2, 3, 4$).

Pedestrians were asked to wear coloured knitted hats so that they could be easier recognized. During the experiments, pedestrians need to traverse the corridor one by one from the left exit to the right exit.

Besides, each pedestrian was asked to begin to walk only after his former pedestrian passed by the obstacle, and the heights of the boxes were set higher than human height. As a result, a pedestrian could not observe or copy the movement of other pedestrians and would take actions under his own willingness.

Each of the five sub-experiments that corresponded to the five scenarios would finish after all the 32 pedestrians traversed the corridor. Using the video data of the experiments, five sets of location data were obtained. Each set of data contained the real-time locations of 32 pedestrians, and the corresponding trajectories and velocities could be deduced accordingly.

3. Experimental results

When there is no obstacle in the corridor, a pedestrian can walk at his desired/free velocity. However, when there is an obstacle in the corridor as shown in Fig. 1 (a), a pedestrian has to evade the obstacle to traverse the corridor. In the evading process, he will decelerate in the horizontal direction and accelerate in the perpendicular direction, making it possible for us to investigate how the trajectory and velocity of a pedestrian would change during the evading process. In this study, we will analyse both the common and particular features of the evading process of single pedestrians.

3.1. Velocity variation

Through processing the video data, the location of each pedestrian at each frame can be obtained. In each data set (totally 5 sets of data), the velocity variation of 32 pedestrians could be calculated according to the location data. We assume that the location of a pedestrian at certain frame n is \vec{p}_n , the time at frame n is t_n , and the corresponding velocity v_n can be calculated according to the locations of pedestrians during a five frames interval (except for the first and last two frames of each sub-experiment) as below:

$$v_n = |\vec{p}_{n+2} - \vec{p}_{n-2}| / (t_{n+2} - t_{n-2}) \quad (1)$$

After calculating all the v_n at location \vec{p}_n of 32 pedestrians, we divided the x-axis by 0.1 meters into many x-sections, and the average value of the velocity points that fall into the same x-section is defined as the average velocity of this x-section. Therefore, the variation of average velocity with x-axis can be seen in Fig. 2. Please note that compared with normal coordinate system, the x axes of all the following figures have been reversed according to definition of x and y axis in Fig. 1 (b).

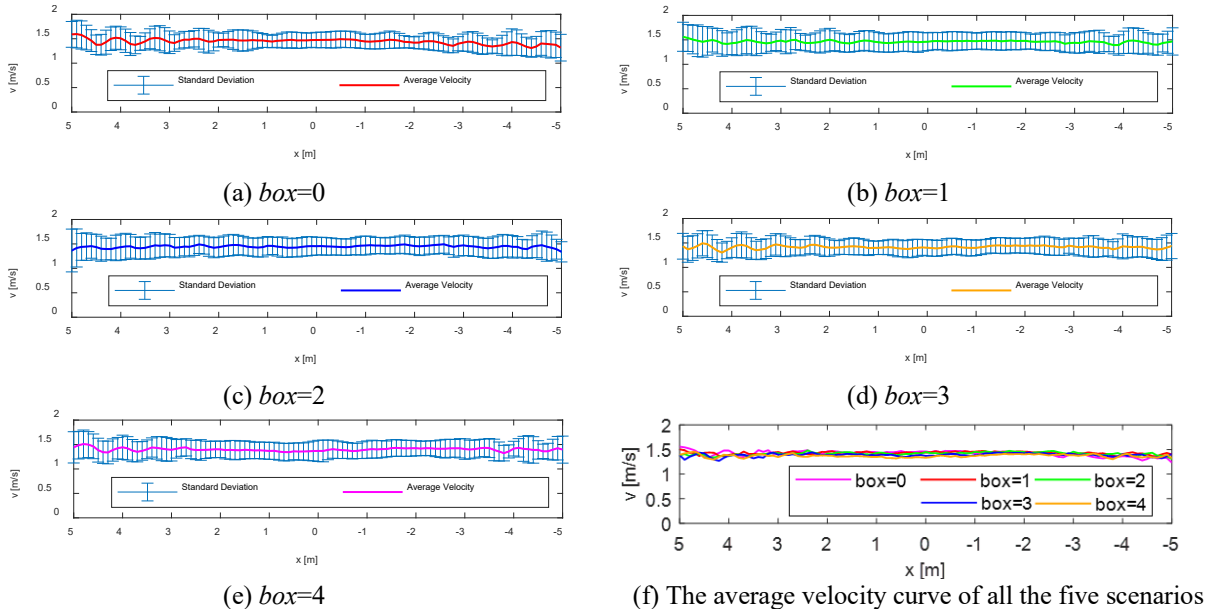


Fig. 2: Variation of average velocity and error bar at different positions along the corridor for five scenarios.

Through observing figures (a)-(e) in Fig. 2, it can be seen that the average velocity falls into 1.5 ± 0.2 m/s most of the time. Besides, the average velocity will not change a lot with the variation of x coordinate although pedestrians have to change the walking direction before and after evading the obstacle. Therefore, it can be deduced that pedestrians tend to keep walking at the desired velocity when evading an obstacle. Meanwhile, Fig. 3 (f) is plotted to compare the average velocity under the five scenarios. It can be seen that the average velocity under different obstacle sizes are nearly the same, which indicates that the existence or size of the obstacle will not affect the velocity of single pedestrian.

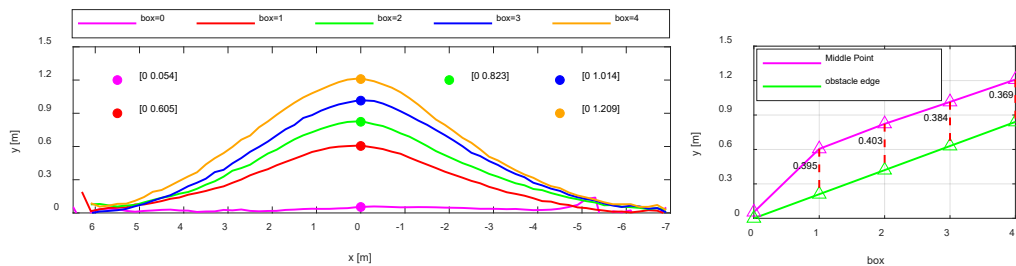
3.2. Variation of trajectory

Although a pedestrian tends to walk at constant velocity when encountering with an obstacle, he has to change his walking direction because he is physically unable to stride the obstacle. In this section, we analyse both the general and the particular features of pedestrian trajectories under different obstacle sizes.

Through observing the experiment process, we assume that pedestrians tend to follow the trajectory shown in Fig. 1 (a) when evading an obstacle. (This assumption will be proved by the linear curve fitting results afterwards.) When entering the corridor, a pedestrian tended to walk straight and then changed his walking direction to evade the obstacle. After passing by the obstacle, he would change his walking direction again until going back to the middle axis and then go straight to pass through the exit. The three critical locations that a pedestrian changed his walking direction are defined as Start Point (SP), Middle Point (MP) and End Point (EP) in this study.

The straight-walking process before SP and after EP is different from the common sense that pedestrians would choose the shortest path for least effort. We presume the psychological motivation behind the straight walking is our participants were not urgent to leave the corridor. As a result, they were probably more affected by the inertia to walk straight or just needed some time for reaction before evading the obstacle, and preferred a more comfortable walking direction before the exit.

To observe the general features of SP, MP and EP under each scenario, we first calculated the average trajectories of 32 pedestrians. The average trajectories and the MPs corresponding to the five average trajectories under five scenarios can be seen in Fig. 3 (a). Please note that the obstacle formed two bottlenecks with the walls in the corridor. Half of the participants passed by the obstacle from the upper bottleneck ($y > 0$) and the other half passed by from the lower one ($y < 0$). To obtain the average trajectory under each scenario, we reversed the trajectories of pedestrians who passed by the lower one by y-axis, and the y-coordinate of MP in Fig. 3 (a) is actually the average absolute values of all the MP coordinates of single pedestrians.



(a) average trajectories and MPs (b) y-coordinate of MP and obstacle edge
Fig. 3: The average trajectories of 32 pedestrians under five scenarios.

It can be seen from Fig. 3 (a) that the average trajectories of the five scenarios are smooth and symmetrical around the axis through $x = 0$, which is the location of the obstacle. Besides, the y-coordinate of the MP will increase with the rise of obstacle size. To illustrate the variation of MP more clearly and show the relation of MP with obstacle width, Fig. 3 (b) has been plotted.

Fig. 3 (b) shows that when there is an obstacle in the corridor ($box \geq 1$), the y-coordinate of MP will linearly increase with the rise of obstacle size. Meanwhile, the distance from the centroid of pedestrian to the obstacle edge that is perpendicular to the initial walking direction of pedestrians is also illustrated in Fig. 3 (b). Through comparison, we found that the distance from the MP to the edge of obstacle will always be

about 0.4 meters despite the variation of obstacle size. Analogously, Weidmann [14] already found that pedestrian tended to keep a distance from walls in the range of 0.2 – 0.45 meters depending on the type of wall. The results of our experiment are in well accordance with his findings.

On the other hand, although the location of MP can be achieved directly from the average trajectories, it is a little hard to get the coordinates of SP and EP directly. Therefore, we use a linear function in Eq. (2) to fit the average trajectories. An example for curve fitting is shown in Fig. 4, which illustrates the original and fitted trajectory of a certain pedestrian before the obstacle.

$$y = \begin{cases} a & (|x| \geq d) \\ bx + c & (|x| \leq d) \end{cases} \quad (2)$$

In Eq. (2), x and y respectively represent the x and y coordinate of the fitted curve, and a , b , c and d represent experimentally determined parameters. When $|x| \geq d$, the fitting equation actually equals to a . When $|x| \leq d$, the fitting equation actually equals to $bx + c$. The location point whose $|x|$ is closest to d among all the points before or after the obstacle is defined as SP ($x > 0$) or EP ($x < 0$) as shown in Fig. 4.

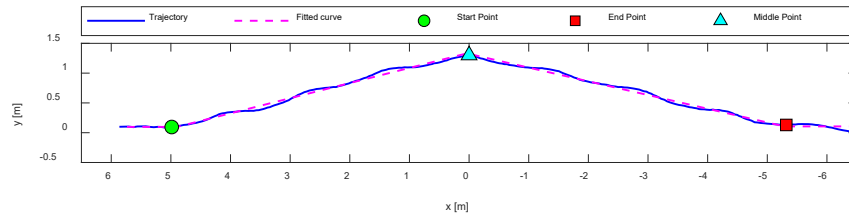


Fig. 4: Example for the curve fitting of trajectory, SP, MP and EP. ($box=4$, $R^2=0.9614$)

Based on Eq. (2), totally 128 trajectories (32 trajectories and four obstacle types) have been fitted. The R^2 of all the fitted curves are around 0.9810 ± 0.0144 , which can illustrate that the accuracy of this trajectory fitting method is high and the observed pedestrian evading pattern shown in Fig. 1 (a) is in accordance with real pedestrian movement. Therefore, the corresponding SPs and EPs can also be regarded as reliable. For better illustration, we define the distance from a SP to the obstacle as L_1 and the distance from an EP to the obstacle as L_2 . The distribution of L_1 and L_2 under the four obstacle sizes can be seen in Fig. 5.

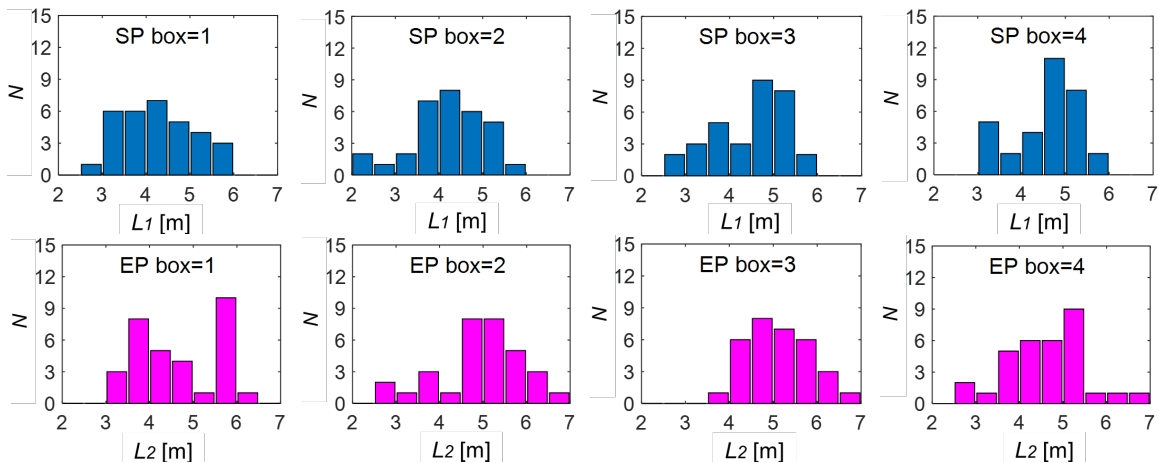


Fig. 5 Distribution of L_1 and L_2 of 32 pedestrians under four different obstacle sizes.

It can be seen from Fig. 5 that L_1 ranges from 2.0 to 6.0 meters and L_2 ranges from 2.5 to 7 meters. Besides, most L_1 are about 3.5 ~ 5.5 meters and most L_2 are about 4.0 ~ 6.0 meters. For further analysis, we calculate the average L_1 and L_2 under the four scenarios as shown in Table 1.

Table 1. Average L_1 and L_2 of 32 pedestrians under four obstacle sizes.

	$box=1$	$box=2$	$box=3$	$box=4$	Average
L_1 (m)	4.27	4.23	4.46	4.61	4.40
L_2 (m)	4.64	4.92	5.11	4.63	4.83

It can be seen from Table 1 that the average distance from SPs to the obstacle, i.e. average L_1 , is 4.40 meters. Besides, it can be seen that when box is small ($box=1$ and 2), L_1 will not change too much. Nevertheless, when the obstacle size is relatively large, L_1 will basically increase with the rise of box . We presume the reason is that when the obstacle size is small, people do not have to detour too much, and the variation of obstacle size has little influence on the evading behaviour of pedestrians. While when the obstacle size is large enough, pedestrians have to detour a longer distance, which might make them feel necessary to evade earlier either to walk more comfortably or evade with a shorter distance.

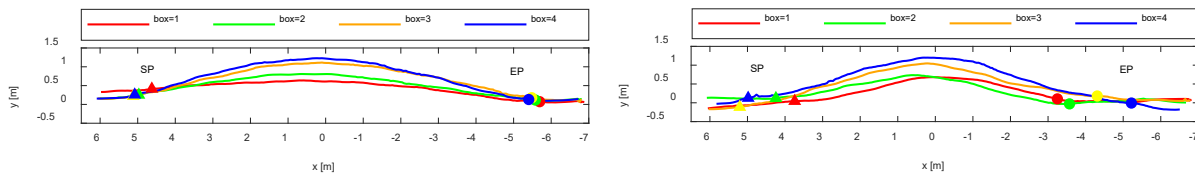
On the other hand, it can be seen from Table 1 that the average distance from EPs to the obstacle, i.e. L_2 , is 4.83 meters. Besides, L_2 will increase with the rise of obstacle size when box is 1, 2 and 3, which may be explained that the distance from the MP to the middle axis becomes larger with the rise of obstacle size, making pedestrians need to walk a longer distance in y direction and thus more or less increase the value of L_2 in x direction. However, when obstacle becomes too large ($box=4$), L_2 suddenly dropped about 0.5 meters, which shows that pedestrians prefer to return to the middle axis earlier when obstacle size is large enough, although the motivation of this movement is still not clear to us.

3.3 Classification of pedestrian behaviour

Despite that we have obtained some general features of the evading behaviour through calculating the average velocity and trajectories, we also found that different pedestrians show some particular features when encountering different-sized obstacles. Compared with the average trajectories in Fig. 3, trajectories of individual pedestrians are not always smooth or symmetric, which may be caused by the heterogeneity of pedestrians' perception and reaction to different walking environment.

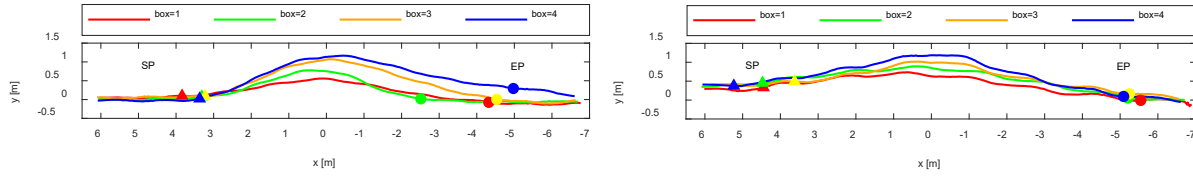
To each pedestrian, the location of SP and EP under each obstacle size can be obtained. However, the change of obstacle size has different influence on the change of SP and EP to different pedestrians. To better classify the heterogeneity of evading behaviour, we categorised pedestrians into four types based on the cluster degree of SPs and EPs under different obstacle sizes. With the variation of obstacle size, pedestrians belonging to Type 1 have similar SPs and EPs, pedestrians belonging to Type 2 have different SPs and EPs, pedestrians belonging to Type 3 have similar SPs but different EPs and pedestrians belonging to Type 4 have different SPs but similar EPs. Please note that we only focus on the x-locations of SPs and EPs while ignoring the y-locations. Besides, we assume that the SPs (or EPs) are similar when the mutual distances of x-locations are all smaller than gap meters. The value of gap is actually the critical distance that could distinguish the similarity of SPs and EPs.

Assuming $gap = 1.2$ m, we could obtain that among the 32 participants, the numbers of pedestrians belonging to Type 1, Type 2, Type 3 and Type 4 are 9 (28.1%), 12 (37.5%), 8 (25.0%) and 3 (9.4%) respectively. Fig. 6 shows the detailed trajectories, SPs and EPs of a certain pedestrian of each type.



(a) Type 1: with similar SPs and EPs

(b) Type 2: with different SPs and EPs



(c) Type 3: with similar SPs but different EPs (d) Type 4: with different SPs but similar EPs
Fig. 6: Illustration of the trajectories, SPs and EPs of pedestrians of four types with $gap = 1.2$ m.

Through reflecting on the whole moving process of pedestrians, we can assume that the evading behaviour begin when a pedestrian passes by the location of SP and terminate after passing the location of EP. Different pedestrians have different recognitions and reactions to the change of walking environment, making them make different decisions on where to start and finish the evading behaviour.

For pedestrians of Type 1 who tend to start and finish the evading behaviour at similar locations, we presume that they tend to follow certain stereotypes and the increase of obstacle size has little influence on their decision-making. For pedestrians of Type 2, they do not seem to follow certain evading pattern and the locations of their SPs and EPs are relatively dispersed. For pedestrians of Type 3, they tend to begin evading the obstacle at similar locations but finish the evading behaviour at different locations. For pedestrians of Type 4, pedestrians would begin to evade the obstacle at different locations but finish the evading behaviour at similar locations. However, the proportion of pedestrians of Type 4 is apparently smaller than that of the other three types. On the other hand, the value of gap also has influence on judging the similarity of SPs and EPs. Therefore, we depicted the variation of pedestrian number under each type with the value of gap increasing from zero to four meters, which can be seen in Fig. 7.

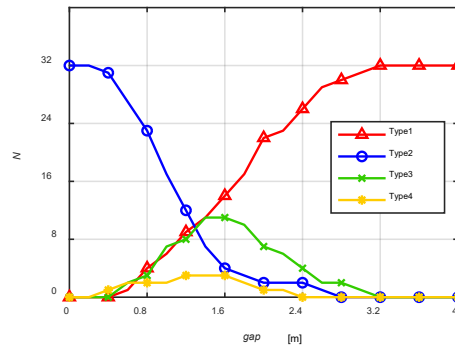


Fig. 7. Variation of pedestrian number of the four types with the increase of gap .

It can be seen from Fig. 7 that the value of gap will greatly affect the proportions of the four pedestrian types. When $gap = 0$ m, all the pedestrians belong to Type 2 because the SPs and EPs of a pedestrian cannot be exactly the same. When $gap = 3.2$ m, all the pedestrians belong to Type 1 because the maximum mutual distances of SPs and EPs of each pedestrian is not larger than 3.2 m. When $0 < gap < 3.2$ m, the critical distance to judge similarity becomes less rigorous than that when $gap = 0$ m and four types of pedestrians exist at the same time. Through comparison, we could see pedestrians of Type 1, Type 2 and Type 3 tend to have large pedestrian numbers. However, pedestrians belonging to Type 4 are always small, which means few people will have different SPs but similar EPs despite the value of gap .

4. Conclusion

This paper illustrates both the general and particular characteristics of the evading behaviour of single pedestrians in front of different-sized obstacle. Generally, a pedestrian tends to maintain his desired velocity and follow certain evading trajectories when encountering an obstacle. Besides, through calculating the average trajectory and accordingly obtain the average Middle Points, it can be seen that the distances from Middle Points to the edge of obstacle is always about 0.4 meters without being affected by the variation of

obstacle size. Moreover, the average value of the distances from SPs to the obstacle centroid (L_1) tends to show a rising trend with the increase of obstacle size. On the other hand, the average value of the distances from EPs to the obstacle centroid (L_2) also tends to increase with the rise of obstacle size but would suddenly decrease when obstacle size is large enough.

On the other hand, a heterogeneity in the evading behaviour has also been indicated. Through comparing the similarity of Start Points and End Points, pedestrians are classified into four types. Different types of pedestrians are supposed to have different perceptions and reactions to the obstacle. Although the critical mutual distance (*gap*) that defines the similarity of Start Points and End Points would affect the proportion of each pedestrian type, it seems that the number of pedestrians belonging to Type 4 is mostly the least despite the variation of critical mutual distance. Both the general and particular features are expected to contribute to developing more realistic evading rules in future related modelling and simulation.

Acknowledgements

This work was supported by JST-Mirai Program Grant Number JPMJMI17D4, Japan and JSPS KAKENHI Grant Number 15K17583. The first author is financially supported by Chinese Scholarship Council. In addition, the author would like to thank the team of Nishinari group for the assistance during the planning and conduction of the experiments in this paper.

References

- [1] V. Blue and J. Adler, "Modeling four-directional pedestrian flows," *Transportation Research Record*, vol. 1710, no. 1, pp. 20-27, 2000.
- [2] D. Helbing, I. Farkas and T. Vicsek, "Simulating dynamical features of escape panic," *Nature*, vol. 407, no. 6803, pp. 487-90, 2000.
- [3] P. Fiorini, "Motion planning in dynamic environments using velocity obstacles", *International Journal of Robotics Research*, vol. 17, no. 7, pp. 760-772, 1998.
- [4] C. Fulgenzi, A. Spalanzani, and C. Laugier, "Dynamic obstacle avoidance in uncertain environment combining PVOs and occupancy grid," *Proceeding of the IEEE International Conference on Robotics and Automation*, Rome, France, 2007, pp. 1610-1616.
- [5] Z. Zhou, Y. Liu, W. Wang, et al., "Multinomial logit model of pedestrian crossing behaviours at signalized intersections", *Discrete Dynamics in Nature and Society*, vol. 2013, pp. 1-8.
- [6] D. Yanagisawa, A. Kimura, A. Tomoeda, et al., "Introduction of frictional and turning function for pedestrian outflow with an obstacle", *Physical Review E*, vol. 80, no. 2, pp. 036110, 2009.
- [7] G. Frank and C. Dorso, "Room evacuation in the presence of an obstacle," *Physica A*, vol. 390, pp. 2135–2145, 2011.
- [8] M. Tang, H. Jia, B. Ran, et al., "Analysis of the pedestrian arching at bottleneck based on a bypassing behaviour model," *Physica A*, vol. 453, pp. 242–258, 2016.
- [9] S. Seer, N. Brändle and C. Ratti, "Kinects and human kinetics: A new approach for studying pedestrian behaviour," *Transportation Research Part C*, vol. 48, pp. 212-228, 2014.
- [10] X. Jia, H. Yue, X. Tian, et al., "Simulation of pedestrian flow with evading and surpassing behaviour in a walking passageway," *Simulation*, vol. 93, pp. 1013–1035, 2017.
- [11] M. Moussaïd, D. Helbing, S. Garnier, et al., "Experimental study of the behavioural mechanisms underlying self-organization in human crowds," *Proceedings of the Royal Society Biological Sciences*, vol. 276, no.1668, pp. 2755-2762, 2009.
- [12] W. Lv, W. Song, J. Ma, et al., "A two-dimensional optimal velocity model for unidirectional pedestrian flow based on pedestrian's visual hindrance field," *IEEE Transactions on Intelligent Transportation Systems*, vol. 14, no. 4, pp. 1753-1763, 2013.
- [13] M. Boltes and A. Seyfried, "Collecting pedestrian trajectories," *Neurocomputing*, vol. 100, pp. 127-133, 2013.
- [14] U. Weidmann, "Transporttechnik der fussgänger," *ETH Zürich*, vol. 90, 1992.

Unidirectional and bidirectional flow in a narrow corridor with body rotation

Daichi Yanagisawa^{1,2}, Claudio Feliciani¹, Katsuhiro Nishinari^{1,2}

¹ Research Center for Advanced Science and Technology, The University of Tokyo,
4-6-1, Komaba, Meguro-ku, Tokyo, 153-8904, Japan

² Department of Aeronautics and Astronautics, School of Engineering, The University of Tokyo,
7-3-1, Hongo, Bunkyo-ku, Tokyo, 113-8656, Japan
tDaichi@mail.ecc.u-tokyo.ac.jp

Abstract - In this paper, we developed a new pedestrian model, where pedestrians are represented with three circles and rotate their body to avoid others. In most pedestrian models, the body posture of pedestrians is statically connected with the walking direction; however, they may become different in our model, in other words, pedestrians can walk sideways. We conducted simulation on bidirectional flow in a narrow corridor where body rotation is necessary to avoid collisions and succeeded to reproduce realistic fundamental diagram.

Keywords: collision avoidance; body rotation; fundamental diagram; unidirectional; bidirectional

1. Introduction

Straight sections are common features in many facilities accommodating pedestrian traffic. Corridors, walkways or crosswalks are the most representative example of this class of structures. The movements of pedestrians inside this particular geometry are constrained by boundaries which limit the lateral motion either in a physical way (i.e. walls in corridor) or by visual means (i.e. lines in the crosswalks).

Pedestrian dynamics inside those structures therefore becomes movement along the longitudinal direction with limited lateral motion. In general, there are two types of flow situations which are possible in such straight sections: unidirectional and bidirectional flow. The first is characterized by a group of people moving in the same direction, while the second has a portion of the crowd moving in the opposite direction.

The unidirectional motion has very close characteristics with the vehicular traffic, and its properties have been known for a long time [1]. Although lane changing is less frequent in the case of vehicles (compared to pedestrians), we consider that a group of pedestrians moving in a corridor can be viewed in the same way as vehicles moving over a multi-lanes highway. In both cases, the fundamental diagram is not much different from the single-file dynamics [2], with the case of bicycles also showing strikingly similar characteristics [3]. The similarities between the two different types of fundamental diagrams are clearly seen by comparing Fig. 1(a) [2] and the scatter plot with red-circle markers relative to the unidirectional flow in Fig. 1(b) [4-6]. Although units for density and flow are different (several lanes are possible in the case of Fig. 1(b)), both shows very similar profiles.

While also simple in its nature, the properties of bidirectional flow have been more difficult to explain. In this case, it is not possible to compare with vehicular traffic, since collision avoidance is only present in pedestrians. Although there have been several simulation models and methods which tried to reproduce the mechanisms when pedestrians walk in different directions ([7-9] are the oldest and most known), there are still several aspects which are not clear. For instance, a different fundamental diagram is obtained in the bidirectional flow with peculiarities which are not shown in the unidirectional case [10, 11]. Moreover, the flow-peak is observed at larger density, and the decrease of flow in the jamming-phase is less marked in the bidirectional flow than in the unidirectional flow (Fig. 1(b)).

Some simulation models managed to reproduce the experimental results by employing enhanced algorithms and making use of several parameters and succeeded to achieve accurate results [12-14]. In addition, a theoretical study [15] managed to highlight the different properties of the uni- and bidirectional fundamental diagram, and the authors were able to describe both fundamental diagrams analytically.

Corridor width in these studies is much larger than the sum of the shoulder width of two pedestrians, thus, pedestrians can avoid others by changing their walking direction if density is not very large. However, when pedestrians need to pass each other in a narrow corridor or in a very high-density situation, they need to rotate their bodies and walk sideways to avoid collisions [16-17].

Although body rotation is considered in some pedestrian models, the body posture of pedestrians is statically connected with the walking direction, thus, pedestrians do not walk sideways [18, 19]. Therefore, we developed a model, where pedestrians can walk sideways, and validated it by comparing the fundamental diagrams depicted from our simulations and experiments.

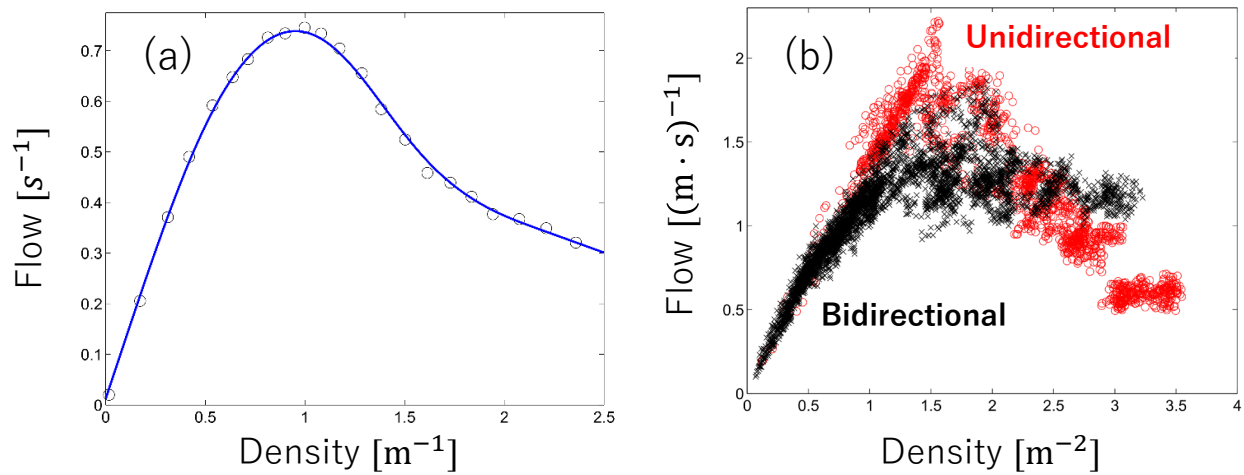


Figure 1: (a) Single lane experimental fundamental diagram [2]; the fitting curve is a common smoothing spline. (b) Experimentally obtained fundamental diagram for the unidirectional and bidirectional flow when multiple lanes are possible. Both plots have been drawn by analysing data from the Julich Research centre [4-6]. Note that the units of density and flow are different in the left and right figures.

2. Pedestrian model for passing in a narrow corridor

In this section, we developed a pedestrian model for passing in a narrow corridor. We consider that pedestrians rotate their body and decrease their effective width by walking sideways when they need to avoid collisions with opponent pedestrians; therefore, we implemented such mechanism in our model.

2.1. Walking speed function without body rotation

To model pedestrian movement and depict fundamental diagram, first, the speed-headway relation should be considered in addition to the body-rotation model. We assumed that the walking speed without body rotation $|v_0|$ is given by the following piecewise-linear function:

$$|v^0| = \begin{cases} 0 & (0 \leq h \leq h_0), \\ |v^{\max}| \frac{h - h_0}{h_1 - h_0} & (h_0 \leq h \leq h_1), \\ |v^{\max}| & (h_0 \leq h \leq h_1), \end{cases} \quad (1)$$

where h [m] is the headway distance. The maximum speed $|v^{\max}|$ [m/s], h_0 [m], and h_1 [m] are the parameters of the walking-speed function. We exploited the experimental data of unidirectional flow in Fig. 1(b) and determined these three parameters through the least squares method. The results were

$|v^{\max}| = 1.39$ m/s, $h_0 = 0.49$ m, and $h_1 = 1.46$ m. Figure 2 shows the plots of the experimental data and the calibrated walking-speed function (1), which were confirmed to agree well with each other ($R^2 = 0.73$).

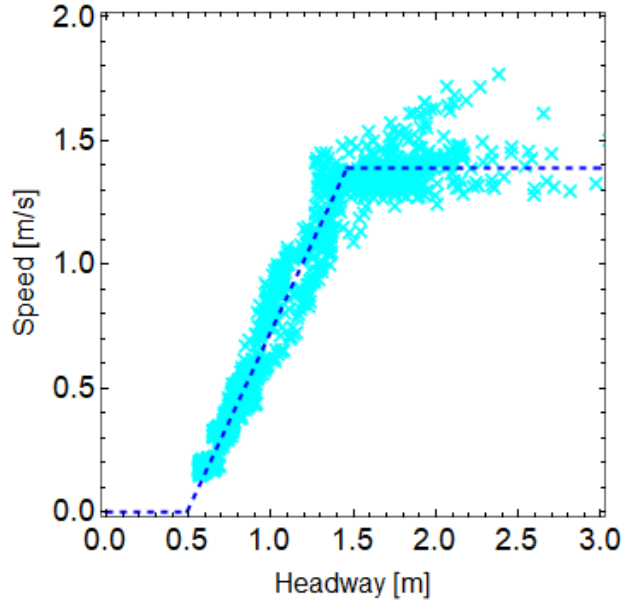


Figure 2: Speed-headway relation in unidirectional flow. The cyan crosses and blue-dashed plot represent the result of the experiments in [4-6] and the calibrated walking-speed function (1), respectively. The parameters are set as $|v^{\max}| = 1.39$ m/s, $h_0 = 0.49$ m, and $h_1 = 1.46$ m.

By using the calibrated walking-speed function (1), we performed the unidirectional-flow simulations in the periodic corridor (circuit), whose length and width were $L = 10$ m and $W = 0.5$ m, respectively. We controlled the number of pedestrians N from 1 to 17 by 1 and positioned them at equal intervals in the corridor at the beginning of the simulations. Overtaking was not considered, therefore, evading or body-rotational behaviours were not observed. Thus, the walking-speed function (1) dominated the system. As we can see from Fig. 6(a), the experimental and simulation results agree well each other in the flow-density relation as well as the speed-headway relation (Fig. 2).

2.2. Evasion and body rotation to avoid opponent pedestrians

Next, we explain the evasion and body rotation mechanism in our model. Each pedestrian was modelled with three circles. Their shoulder width and bust depth are $2a$ [m] and $2b$ [m], respectively, as in Fig. 3(a). Then, pedestrians are no more rotationally symmetric to their centre, so that pedestrians can control their effective width d [m] by rotating their body by θ [deg] as in Fig. 3(b). In our model, pedestrians do not change their walking direction when they rotate their body. In other words, pedestrians walk sideways when they need to avoid opponent pedestrians

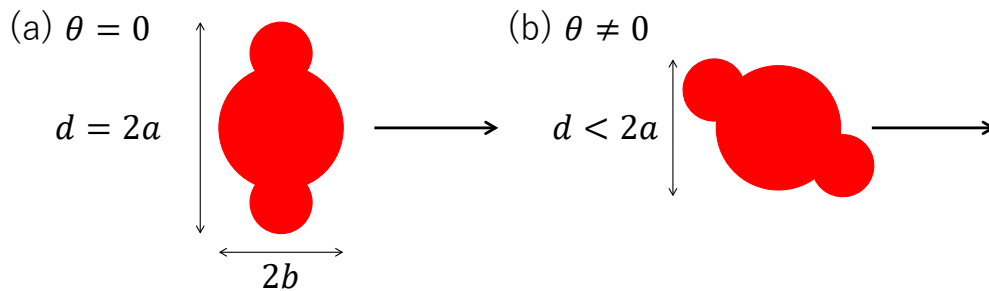


Figure 3: Schematic view of effective width of pedestrians in our model. (a) When pedestrians do not rotate their body, i.e., $\theta = 0$, the effective width is equal to the shoulder width of pedestrians, i.e., $d = 2a$. (b) On the other hand, $2b \leq d < 2a$ when pedestrians rotate by $\theta (\neq 0)$.

Pedestrians avoid collisions with their opponent pedestrians in bidirectional flow by both evasion and body rotation as follows. The position and rotational angle of pedestrian i are represented by (x_i, y_i) and θ_i , respectively. When an opponent pedestrian j come close to pedestrian i , i.e., $|x_i - x_j| \leq s_{cr}$, both pedestrians try to evade each other in the perpendicular direction (y) to their moving direction (x) and rotate their body to decrease the overlap length l as in Fig. 4. (Pedestrians start evading and rotating at the same time.) Thus, pedestrians gradually control their position y_i and rotational angle θ_i proportional to the overlap length l . Furthermore, the walking speed of pedestrians becomes smaller during walking sideways. (We assumed that walking speed becomes zero at $\theta_i = 90^\circ$ and 270° .) Therefore, the equations of motion of pedestrians before passing are described as follows:

$$\frac{dx_i}{dt} = v_i^0 \cos \theta_i, \quad (2)$$

$$\frac{dy_i}{dt} = k_y^A l \cdot \text{sign}(y_i - y_j), \quad (3)$$

$$\frac{d\theta_i}{dt} = k_\theta^A l, \quad (4)$$

where, v_i^0 is the walking velocity without body rotation determined from (1). The parameters k_y^A and k_θ^A are sensitivity parameters for the overlap length. The function $\text{sign}(z)$ gives the sign of the argument z .

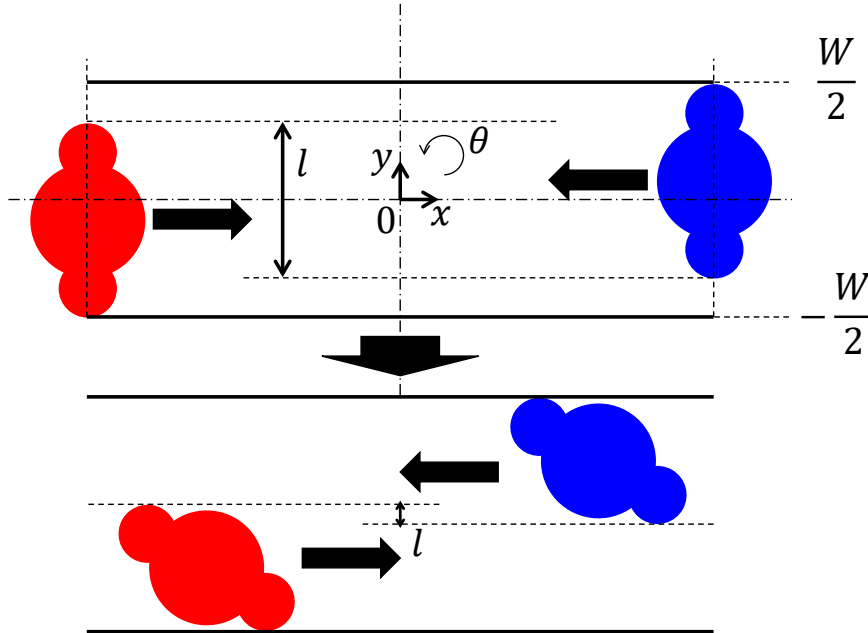


Figure 4: Schematic view of collision avoidance by evasion and body rotation.

When there are no opponent pedestrians close to pedestrians i or after passing, pedestrian i tries to restore his/her body postures and move as fast as they can. We assume that the restoring behavior is proportional to the evading distance and the rotational angle, so that the equations of motion of y and θ after passing are described as follows:

$$\frac{dy_i}{dt} = -k_y^R (y_i - y_j^0), \quad (4)$$

$$\frac{d\theta_i}{dt} = -k_{\theta}^R(\theta_i - \theta_i^0), \quad (5)$$

where, k_y^R and k_{θ}^R are sensitivity parameters for the deviation from the initial position (y_i^0) and the initial rotational angle (θ_i^0), respectively.

The parameters in the model were calibrated by using the experimental data in [17]. Their values are $a = 0.249$ m, $b = 0.155$ m, $s_{cr} = 1.5$ m, $k_y^A = 9.0$ m/(m·s), $k_{\theta}^A = 6.0$ deg/(deg·s), $k_y^R = 5.0$ m/(m·s), and $k_{\theta}^R = 7.0$ deg/(deg·s).

2.3. Bidirectional flow simulations

By using the calibrated model, we conducted bidirectional-flow simulations. We considered a straight corridor, whose length $L = 10$ m, with periodic boundary condition (the left end and the right end of the corridor were connected). The corridor width was controlled from $W = 0.8$ m to 1.0 m by 0.1 m. The number of total pedestrians N was controlled from 2 by 2 until the density achieved 3.4 m^{-2} . The number of the right-going (red) and left-going (blue) pedestrians were the same ($N/2$). Both types of pedestrians were positioned at equal intervals in the corridor at the beginning of the simulations. The sum of the shoulder widths of the two pedestrians $2 \times 2a = 0.996$ m was larger than $W = 0.8$ and 0.9 m, therefore, the pedestrians needed to evade others and rotate to pass each other in such narrow corridors. Figure 5 shows a schematic view of the bidirectional-flow simulation.

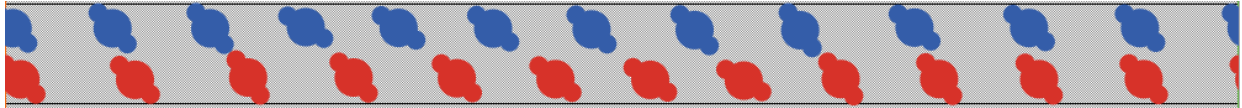


Figure 5: Schematic view of simulation on bidirectional flow. There are two kinds of pedestrians. Red pedestrians are moving from left to right, and the blue pedestrians are moving from right to left. We see that pedestrians rotate their body to avoid collisions with opponent pedestrians.

3. Fundamental diagram

The results of the bidirectional-flow simulations ($W = 0.8$ m) are presented with those of experiments [4-6] in Fig. 6(a). We can see that the simulation results are in agreement with the experimental results.

By comparing the experimental results of the unidirectional and bidirectional flows, we can observe that unidirectional flow achieves larger value of flow than bidirectional flow when the density is smaller than the critical density ($\approx 2.3 \text{ m}^{-2}$). When the density is greater than the critical density, the values of bidirectional flow become larger than those of unidirectional flow. These characteristic phenomena were successfully reproduced in our simulation results. In the low-density situation, pedestrians can move freely in unidirectional flow; however, they have to interact with opponent pedestrians to avoid them in bidirectional flow. Thus, flow is greater in unidirectional flow than in bidirectional flow. In the high-density situation, interactions with other pedestrians are unavoidable in both flows. Overtaking is difficult in unidirectional flow because pedestrians cannot see behind themselves. It is difficult for them to give way to fast followers. Thus, the fundamental diagrams are mainly dominated by the simple speed-headway relation. In contrast, pedestrians can see opponent pedestrians, give way, and pass by each other through evasion and rotation in bidirectional flow. Due to these avoidance behaviours, flow of bidirectional flow remains larger than those of unidirectional flow in the high-density situation. Our simulation model succeeded in reproducing this phenomenon by introducing avoiding behaviours, i.e., evasion to the perpendicular direction and body-rotation. Further, we would like to mention that the introduction of evasion alone was insufficient for bidirectional-flow simulations in a narrow corridor.

Since the sum of the shoulder widths of the two pedestrians $2 \times 2 a = 0.996$ m was larger than the corridor width $W = 0.8$ m, body rotations were necessary to avoid deadlocks.

Figure 6(b) shows the fundamental diagrams of bidirectional for various corridor width ($W = 0.8, 0.9$ and 1.0 m) depicted from the results of the simulations. We see that the flow become larger (smaller) as the corridor width increases when the density is smaller (larger) than the critical density ($\approx 2.3 \text{ m}^{-2}$). The density for the same number of pedestrians decreases when the corridor width increases because the area of the corridor (circuit) increases. Thus, the fundamental diagram just shifts to left if the longitudinal movement of pedestrians does not change at all by the corridor width. In fact, the fundamental diagrams do not simply shift from right to left as the corridor width increases, and the increase of flow cannot be explained by this effect. Therefore, longitudinal movement of pedestrians changed by the corridor width.

When the corridor width $W = 1.0$ m, which was larger than the sum of the shoulder widths of the two pedestrians $2 \times 2 a = 0.996$ m, pedestrians did not need to evade or rotate to pass each other. This situation can be considered that there were two independent corridors whose width is 0.5 m for right- and left-going pedestrians, respectively. Therefore, the flow achieved similar values as in the unidirectional flow. When the corridor width became smaller than 0.996 m, pedestrians had to evade and rotate to avoid their opponent pedestrians. Body rotation forced the pedestrians to walk sideways and decreased the walking speed by (2). Thus, the flow decreases as the corridor width decreases when the density is smaller than the critical density.

When the density is larger than the critical density, the flow becomes larger as the corridor width decreases. In this case, the effect of density-increase due to the decrease of corridor-width overwhelms the effect of speed-decrease due to sideway-walking.

If the corridor is much larger than the sum of the shoulder widths of the two pedestrians, minor change of the corridor width may not greatly affect the fundamental diagram because pedestrians can control both longitudinal and lateral distances with other pedestrians and avoid continuous sideway-walking. However, when the corridor width is small, pedestrians have to keep walking sideways to avoid collisions. Hence, the flow decreases due to the reduction of the walking speed. This result indicates that the value of flow in bidirectional flow is not only determined by the density, but also affected by the corridor width.

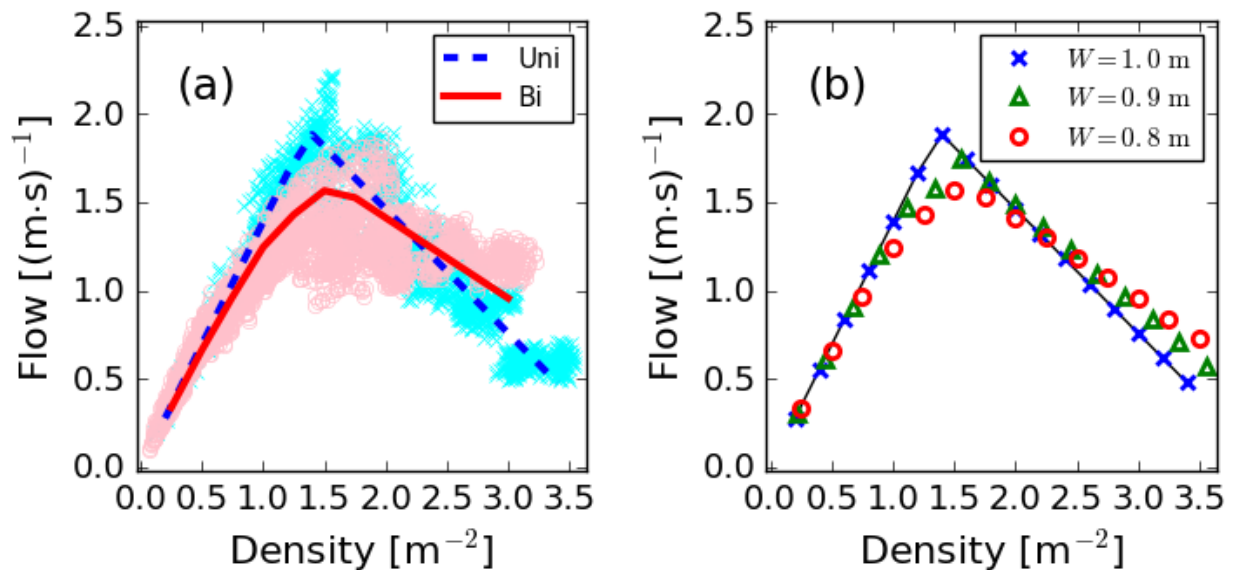


Figure 6: (a) Fundamental diagram obtained from the experiments in [4-6] and our simulation when $W = 0.8$ m. The legends are as follows: cyan crosses: experimental unidirectional flow, pink circles: experimental bidirectional flow, blue-dashed line: simulation unidirectional flow, red-solid curve:

simulation bidirectional flow. (b) Fundamental diagram obtained from our simulation for various corridor width. The legends are as follows: black line: unidirectional flow, blue crosses: bidirectional flow ($W = 1.0$ m), green triangles: bidirectional flow ($W = 0.9$ m), red circles: bidirectional flow ($W = 0.8$ m).

4. Conclusion

In this research, we developed a model, where pedestrians rotate their body to avoid others. In our model, the body posture is not statically connected with the walking direction. Hence, pedestrians walk sideways when they rotate their body. Then, we conducted simulation of both the unidirectional and bidirectional flow and depicted the fundamental diagram. The result of our simulation and that of the experiment agree well each other. Since the corridor width in the bidirectional simulation was smaller than the sum of the shoulder width of the two pedestrians in the simulation, introduction of the body-rotation mechanism (sideway-walking) was necessary to perform simulation. If the pedestrians cannot rotate their body and walk sideways, deadlocks occur in the corridor.

We also investigated the effect of corridor width on the fundamental diagram. Our simulation results show that the flow decreases (increases) as the corridor width decreases even at the same density when the density is smaller (larger) than the critical density ($\approx 2.3 \text{ m}^{-2}$). This result indicates that the value of flow in bidirectional flow is not only determined by the density. The difference of corridor width has influence on the flow when the corridor width is small.

In the future, we are planning to extend our model to perform simulations in more complex scenarios such as cross-flow incorporating with pedestrians' body rotation to investigate the effect of body rotation on congested situations.

Acknowledgements

This work was partially supported by JST-Mirai Program Grant Number JPMJMI17D4, JSPS KAKENHI Grant Number 15K17583, and MEXT as "Post-K Computer Exploratory Challenges" (Exploratory Challenge 2: Construction of Models for Interaction Among Multiple Socioeconomic Phenomena, Model Development and its Applications for Enabling Robust and Optimized Social Transportation Systems) (Project ID: hp180188).

References

- [1] A. Schadschneider, D. Chowdhury, K. Nishinari, *Stochastic transport in complex systems: from molecules to vehicles*, Elsevier, 2010.
- [2] A. Jelić, C. Appert-Rolland, S. Lemercier, J. Pettré, "Properties of pedestrians walking in line: Fundamental diagrams", *Phys. Rev. E*, vol. 85, no. 3, 036111, 2012.
- [3] J. Zhang, W. Mehner, S. Holl, M. Boltes, E. Andresen, A. Schadschneider, A. Seyfried, "Universal flow-density relation of single-file bicycle, pedestrian and car motion", *Physics Letters A*, vol. 378, no. 44, pp. 3274-3277, 2014.
- [4] S. Holl, "Methoden für die Bemessung der Leistungsfähigkeit multidirektional genutzter Fußverkehrsanlagen", Universität Wuppertal, 2016
- [5] S. Cao, A. Seyfried, J. Zhang, S. Holl, W. Song, "Fundamental diagrams for multidirectional pedestrian flows", *J. Stat. Mech.*, vo. 2017, no. 3, 033404, 2017.
- [6] Forschungszentrum Jülich, "Data archive of experimental data from studies about pedestrian dynamics", <http://ped.fz-juelich.de/db/> (accessed May, 2018).
- [7] D. Helbing, P. Molnár, "Social force model for pedestrian dynamics", *Phys. Rev. E*, vol. 51, no. 5, pp. 4282-4286, 1995.
- [8] V. J. Blue, J. L. Adler, "Cellular automata microsimulation for modeling bi-directional pedestrian walkways", *Transp. Res. Part. B Meth.*, vol. 35, no. 3, pp. 293-312, 2001.
- [9] C. Burstedde, K. Klauck, A. Schadschneider, J. Zittartz, "Simulation of pedestrian dynamics using a two-dimensional cellular automaton", *Physica A* vol. 295, pp. 507-525, 2001.

- [10] J. Zhang, W. Klingsch, A. Schadschneider, A. Seyfried, “Ordering in bidirectional pedestrian flows and its influence on the fundamental diagram”, *J. Stat. Mech.*, vol. 2012, no. 2, P02002, 2012.
- [11] C. Feliciani, K. Nishinari, “Empirical analysis of the lane formation process in bidirectional pedestrian flow”, *Phys. Rev. E*, vol. 94, no. 3, 032304, 2016.
- [12] C. Feliciani, K. Nishinari, “An improved Cellular Automata model to simulate the behavior of high density crowd and validation by experimental data”, *Physica A*, vol. 451, pp. 135-148, 2016.
- [13] W. G. Weng, T. Chen, H. Y. Yuan, W. C. Fan, “Cellular automaton simulation of pedestrian counter flow with different walk velocities”, *Phys. Rev. E*, vol. 74, no. 3, 036102, 2006.
- [14] S. Nowak, A. Schadschneider, “Quantitative analysis of pedestrian counterflow in a cellular automaton model”, *Phys. Rev. E*, vol. 85, no. 6, 066128, 2012.
- [15] G. Flötteröd, G. Lämmel, “Bidirectional pedestrian fundamental diagram”, *Transp. Res. Part. B Meth.*, vol. 71, pp. 194-212, 2015.
- [16] C. Feliciani, K. Nishinari, “Pedestrians rotation measurement in bidirectional streams”, in *International Conference on Pedestrian and Evacuation Dynamics 2016*, W. Song, J. Ma, L. Fu, USTC Press, 2016, pp. 76-83.
- [17] H. Yamamoto, D. Yanagisawa, C. Feliciani, K. Nishinari, “Body-rotation behavior of pedestrians for collision avoidance in passing and cross flow”, *Transp. Res. Part B Meth*, vol. 122, pp. 486–510, 2019.
- [18] J. Waś, B. Gudowski, P. J. Matuszyk, “Social Distances Model of Pedestrian Dynamics”, *Lecture Notes in Computer Science (Cellular Automata)*, vol. 4173, pp. 492–501, 2006.
- [19] M. Chraïbi, A. Seyfried, A. Schadschneider, “Generalized centrifugal-force model for pedestrian dynamics”, *Phys. Rev. E*, vol. 82, no. 4, 046111, 2010.

Grouping behaviour and decision making in road tunnels evacuation in smoke conditions Experimental approach

Jarosław Waś*¹, Jakub Porzycki¹, Natalia Schmidt-Polończyk²

¹AGH University of Science and Technology

Institute of Applied Computer Science

Faculty of Electrical Engineering, Automatics, Computer Science and Biomedical Engineering
Kraków, Poland

²AGH University of Science and Technology

Faculty of Mining and Geoengineering

Kraków, Poland

* e-mail : jarek@agh.edu.pl

Abstract - We have performed a set of evacuation experiments in a road tunnel. In each experiment pedestrians were gathered in a bus, the bus was stopped in the tunnel, next the tunnel was filled with artificial smoke and pedestrians had to evacuate. We compared evacuation times and behaviours for different levels of visibility, defined by extinction coefficient C_s range.

Keywords: Evacuation experiments, grouping behaviour, decision making, artificial smoke

1. Introduction

It should be stressed that the experimental approach is very important in evacuation modelling. This makes it possible to estimate behaviours of evacuees in different conditions. However, organization of such tests is not an easy task due to ensuring safety of participants, the high costs of such projects and support required from different services like the fire brigade and ambulance service. One has to select only some scenarios, and the “surprise effect” can only be observed once for each group of participants, as in subsequent trials one can identify the influence of the learning effect on pedestrian behaviour. Anyway, experimental results are necessary both for a better understanding of evacuees’ behaviour as well as in the calibration and validation of computer models of evacuation or risk assessment.

2. Related works

There are a number of works on tunnels evacuation, as well as pedestrian behaviour and decision making.

Seike et al. in [1] analysed influence of the extinction coefficient on walking speed of individual pedestrians in a tunnel. Nilsson et al. in [2] took into account behaviour of motorists in a road tunnel during an unannounced evacuation. Wang et al. in [3] presented experimental research of an evacuation of pedestrians walking blindfolded. Nilsson et al. discussed in [4] how research can be connected to large infrastructure tunnel projects taking into account fire safety issues.

The simultaneous modelling approach is present in research on evacuation dynamics. Ronchi et al. [5] presented virtual experiments on evacuation trajectories, while Lovreglio et al. [6] introduced an evacuation decision model taking into account perceived risk, social influence and behavioural uncertainty. Ronchi et al. in [7] analysed walking speeds in smoke in evacuation models.

3. Description of experiments

In this paper we take into consideration the decision-making process during evacuation in tunnels, as well as grouping behaviours. We have performed a set of full-scale evacuation experiments with artificial smoke in the “Emilia” road tunnel located in the south of Poland.

We gathered 50 participants in a bus, (Fig 1 and Fig 2). The group consists of 34 males and 16 females. The average age is 21 years (21.32, $\sigma = 1:477$.) age span is in this case 19 to 24 years. In the experiment 1, the participants have not received any instructions as to the purpose of the experiment

how to behave in case of smoke, infrastructure of the tunnel namely the location of the evacuation cross - passages as well as the position of the bus in the tunnel. The bus has been directed into the tunnel without stopping, in order to ensure an element of surprise among the participants. The position of the bus in this experiment has been in the middle of the tunnel, just like in the experiments 2 and 3.

Artificial smoke generators were used in order to investigate grouping behaviours [8] and the decision making process for different visibility levels. In each case a vehicle with pedestrians was stopped in a tunnel and artificial smoke was generated around them (Fig 1). Then the pedestrians initialized evacuation from the vehicle and the smoke filled road tunnel. In all cases, the driver was instructed to be passive, namely not to instruct passengers about escape routes and further proceedings, or to get up from seats and evacuate.



Fig 1. Our coach with participants in the “Emilia” tunnel filled with artificial smoke – pre-movement phase of evacuation

During experiments participants evacuated from the main tunnel (road tube), filled with artificial smoke, to the evacuation tunnel, situated parallel to the road tube.



Fig 2 Participants in the coach before experiments in the “Emilia tunnel”

As scientific methodology we applied analyses based on video recordings with standard and infrared cameras, direct observations, segment measurements using UHF technology and questionnaires filled by participants. Participants had assigned numbers, cards with numbers were placed on their clothes (Fig 2).

4. Sample results

In the “Emilia” tunnel we performed the following experiments using different range of visibility coefficient C_s , namely the extinction coefficient based on the Lambert–Beer equation [1].

Tab 1. List of experiments with different levels of visibility, tunnel familiarity of evacuated group of participants and expressed task.

Experiment number	Visibility Cs - range	Tunnel Familiarity	Task for pedestrians
1	0.1-0.2m ⁻¹	No	No expressed task
2	0.4-0.5m ⁻¹	Yes	To evacuate
3	0.8-0.9m ⁻¹	Yes	To achieve the best personal time

Regarding movement speed we observed different velocities in the main tunnel during our experiments. Taking into account pedestrian flow in smoke during three experiments in the “Emilia” tunnel we observed the following distributions of velocities (Fig 3 and Tab 2). In the first experiments the observed speed was relatively low, because it was a new situation for participants and they had to make decisions about evacuation path. Despite the increase of smoke in subsequent experiments, the speed of the first persons increased markedly – “learning effect” was observed.

It should be stressed that in the third experiment we asked participants for to achieve potentially the best individual evacuation time. As a result we observed more competitive behaviour, however due to lower level of visibility the velocities were lower than in experiment 3.

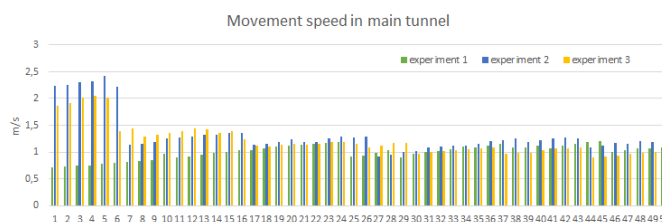


Fig 3. Movement speed of particular pedestrians in the “Emilia” tunnel experiments in three consecutive experiments.

Tab 2 Movement speed for experiments 1-3 - overall statistics.

Experiment Number	Min.	Max.	Mean	Std. deviation
1	0.895	1.211	1.056	0.083
2	0.917	2.422	1.321	0.375
3	0.893	2.044	1.221	0.295

Additionally we checked the time spans between the first and the last evacuees at the following checkpoints: the bus doors and exits from main tunnel (smoke filled area).

Tab 3. Comparison of time span between the first and the last evacuee at each checkpoint for experiments 1-3

Experiment Number	Bus door Checkpoints	Main tunnel exits checkpoints
1	First: 35.81s Last: 130.92s	First: 84.21s Last: 162.73s
2	First: 5.39s Last: 85.03s	First: 20.9 Last: 113.86s
3	First: 2.92 s Last: 67.65s	First: 21.16 s Last: 102.04 s

As we can see in Tab 3, familiarity with a situation and previous experiment cause significantly shorter evacuation times between the second and the first experiment. We observed very interesting results when we compared the results of experiments 3 and 2. Limited visibility (reduction from 0.4-

0.5 m-1 to 0.8-0.9 m-1) should potentially cause longer evacuation time, however one can notice the effect of mobilization due to increasing level of competitiveness.

Regarding decision making, pedestrians tried to identify the nearest evacuation exit. The tunnel is equipped with evacuation signs, which point out the distance to the nearest exit (Fig 4). This information was important in the context of decision making.



Fig 4. Evacuation signs with the distance to evacuation exits from the main tunnel



Fig .5 Pedestrians during evacuation in experiment 3. Double line patterns are observed.

According to different levels of visibility we identified different grouping behaviours and different patterns formed by evacuees. During evacuation of a group in low and moderate level of smokiness (when $C_s < 0.5 \text{ m-1}$) we observed multi-line patterns created by pedestrians. Only the first group of passengers engaged in active decision making, while during heavy smokiness $C_s > 0.7 \text{ m-1}$ we observed characteristic double-line patterns (Fig 5.).

5. Conclusions

Experiments show two potentially dangerous behaviours: group/leader following and delaying of the decision to begin the evacuation. Despite signals to begin evacuation (like appearance of smoke and siren alarm), participants remain in their seats until they hear a voice message. Following the leader and following the group behaviour occurs in both cases: decision on evacuation start and path choice. Evacuees have a strong tendency to follow the group, if only they can see each other.

On the one hand we have gathered statistics on pedestrians' velocities in a smoke filled tunnel (the first phase of the evacuations) and an evacuation tunnel without smoke (the second phase of evacuation). This makes it possible to compare velocities in smoke and the desired velocity for particular pedestrians.

Additionally, in questionnaires participants pointed out different issues related to decision making, well-being during the evacuation, and an assessment of technical infrastructure in the tunnel and so on.

Acknowledgements

This research is supported by grants no 11.11.120.859 and 15.11.100.078.

References

- [1] Miho Seike, Nobuyoshi Kawabata, Masato Hasegawa, Experiments of evacuation speed in smoke-filled tunnel, *Tunnelling and Underground Space Technology*, Volume 53, 2016, Pages 61-67, <https://doi.org/10.1016/j.tust.2016.01.003>.
- [2] Daniel Nilsson, Maria Johansson, Håkan Frantzich, Evacuation experiment in a road tunnel: A study of human behaviour and technical installations, *Fire Safety Journal*, Volume 44, Issue 4, 2009, Pages 458-468
- [3] Shu-jie Wang, W. g. Song and W. Lv, "Moving characteristics of "blind" people evacuating from a room," 17th International IEEE Conference on Intelligent Transportation Systems (ITSC), Qingdao, 2014, pp. 548-553
- [4] D. Nilsson, H. Frantzich, E. Ronchi, K. Fridolf, A. L. Walter, and H. Modig. Integrating evacuation research in large infrastructure tunnel projects - experiences from the Stockholm bypass project. *Fire Safety Journal*, 2017.
- [5] Enrico Ronchi, Max Kinateder, Mathias Müller, Michael Jost, Markus Nehfischer, Paul Pauli, Andreas Mühlberger, Evacuation travel paths in virtual reality experiments for tunnel safety analysis, *Fire Safety Journal*, Volume 71, 2015, Pages 257-267, <https://doi.org/10.1016/j.firesaf.2014.11.005>.
- [6] R. Lovreglio, E. Ronchi, and D. Nilsson. An evacuation decision model based on perceived risk, social influence and behavioural uncertainty. *Simulation Modelling Practice and Theory*, 66:226 – 242, 2016
- [7] E. Ronchi, S. M. V. Gwynne, D. A. Purser, and P. Colonna. Representation of the impact of smoke on agent walking speeds in evacuation models. *Fire Technology*, 49(2):411–431, 2013.
- [8] Jarosław Waś, Experiments on Evacuation Dynamics for Different Classes of Situations, *Pedestrian and Evacuation Dynamics 2008* Springer Berlin Heidelberg, pages="225

Single-file Movement of Ants Stressed by a High Temperature

Qiao Wang^{1,2}, Weiguo Song^{1,*}, Shujie Wang¹, Siuming Lo²

¹State Key Laboratory of Fire Science, USTC

No.96, JinZhai Road Baohe District, Hefei, China

qw2014@mail.ustc.edu.cn; wgsong@ustc.edu.cn; sj573@mail.ustc.edu.cn

²Department of Architectural and Civil Engineering, CityU

Tat Chee Avenue, Kowloon, Hong Kong SAR, Hong Kong, China

bcsml@cityu.edu.hk

Abstract - Single-file movement is a universal pattern in both nature and human society. In this paper, we investigate single-file movement of ants (*Camponotus japonicus*) driven by a high temperature in a narrow channel. Here, ants were placed in a chamber. The chamber was connected to a narrow channel which was 10 cm long and 0.6 cm wide so that the ants can escape through it one by one. Both chamber and narrow channel were in high temperature environment. In the channel, the random pause was observed due to the characteristic of ants. Moreover, ants were inclined to following the preceding one and trying to overtake it, which is different from the movement in natural investigation. On the other hand, the speed increased with distance headway when the distance headway is less than 0.26 cm, that is less than the body size of an ant. Furthermore, touching phenomenon was observed. When the following ants touched the preceding one, they could reduce speed, stop or move backward. On the contrary, the preceding ants increased their speed. Thus, the touching effect in multiple ants experiment can enhance the evacuation efficiency.

Keywords: single-file movement, ant, high temperature, speed-distance headway, touching effect

1. Introduction

Single-file movement, which is one of the simplest system for exploring the relationship between velocity and density, had been studied by conducting controlled experiments with pedestrians [1]. In the experiments of single-file pedestrian movement [2], it was found that velocity had a linear relation with the inverse of density. For the different agents such as pedestrians, bicycles and cars, a consistent flow-density relation could be obtained after simple rescaling [3]. In the field of vehicle traffic, single-file is replaced by single-lane, and models [4-7] and experiments [8, 9] have been conducted to study single-lane movement in vehicle traffic.

Similar with pedestrian and vehicle traffic, the single-file movement in natural traffic occurs frequently, for example in case of ants. Ants, which are social insects, have a trail system that is similar to vehicle traffic. This has drawn many researchers' attention [10]. In the process of foraging, ants move forward along the pheromone that is dropped on the ground by the leaders [11] so that the single-file movement is formed. Through observing ants' behaviors carefully, researchers indicated that a clear lane segregation formed (segregated into inbound and outbound) during the foraging process, in order to avoid head-on collisions [12]. Thus, unidirectional flow is formed in ant traffic. In collective unidirectional movement [13], average velocity did not rely on density and its flow increases monotonically with the density. Ants, with their small size and relatively less aggressiveness, are easy to be controlled. Therefore, they are available for controlled experiments.

In an controlled experiment, faster-is-slower effect and mass behavior are common phenomena of escape panic [14], which is different from the behavior of crowd under normal conditions. Thus it is interesting to study the behavior of ants under emergency conditions. Considering the influence of stress produced by citronella, Soria et al. [15] performed experiments of the carpenter ant *Camponotus mus* (Roger) to study the "Faster-is-Slower (FIS)" effect. In their work, the evacuation of ants was compatible with FIS effect because of a minimum evacuation time observing at intermediate citronella concentration.

However, FIS effect of ants was different from the result presented in social force model [16]. In the process of escaping from a chamber with stimulation of citronella, no jamming and clogging appeared near an exit and the exponential decay of the frequency distribution of time intervals could be observed [17]. In addition, high temperature, as a new aversive stimuli for ants, was used to stress ants escaping [18]. In this work, authors observed that higher temperature resulted in faster evacuation.

Many researchers studied single-file movement of pedestrians, bicycles and cars through experiment and observation [1-3, 9, 19]. Nevertheless, the single-file movement of ants in stressed conditions was studied rarely. In the experiment conducted by Wang *et al.* [20], the speed of ants driven by citronella was approximately constant with the increasing density in a straight passageway.

In this work, we will further investigate the single-file movement of ants under stressed conditions and compare the difference between individual and collective motion. Here, high temperature is used to drive ants to pass through a narrow channel. Both single-file movement of multiple ants and single ant movement are investigated.

2. Materials and Methods

2.1. Ants

A colony of *Camponotus japonicus* was captured in the wild in Shaanxi Province, China, and then transported to our laboratory using centrifuge tubes. This colony with approximately 500 workers was placed in a non-transparent plastic box (51 cm long, 35 cm wide and 33 cm high) that was coated by Fluon to prevent ants from escaping. The box was shaded by a lid on it. Ants were raised in a box with a constant temperature (24 ± 2 °C) and suitable humidity under natural light/dark cycles. When no experiment is conducted, ants can move freely in the box with sufficient food (honey) and water supplying.

The length of *Camponotus japonicus* is usually between 0.8 and 1.4 cm. In this experiment, we only adopted the workers whose body size was more than 1 cm.

2.2. Experimental Device

We built a chamber connected to a narrow channel which was 10 cm long and 0.6 cm wide on the testbed, as shown in Fig. 1. The chamber resembles a funnel that is contributed to guide ants into channel. The 10 cm long channel ensures that the temperature in whole channel can stress ants to left this area. Considering the size of ants' limbs and antennae, the width of the channel was set to be 0.6 cm to avoid the phenomena of crawling side by side and U-turn motion. The chamber and channel composed of tasteless rubber were 0.6 cm high. They were covered by a PMMA (polymethyl methacrylate) lid, in order to prevent ants overlapping and record the experiment by video mounted over the device. A hole was existed in the lid to guide ants into the chamber. The bottom of the device was a copper plate, and there were two copper pipes under two ends of the plate. Water heated by two thermostatic bathes to different temperatures was poured into these two pipes to heat the plate. In this way, a temperature gradient formed as shown in Fig.1 (b), which could successfully induce the ants to escape from the chamber and move in channel one by one spontaneously. Hence, the entrance of the narrow channel was at a high temperature, the end of the channel (i.e., the final exit of the chamber) was at a low temperature. As the temperature of the chamber was high, it could hurt ants for a long time stay. Thus, this high temperature could drive ants to enter the unidirectional channel and form single-file movement.

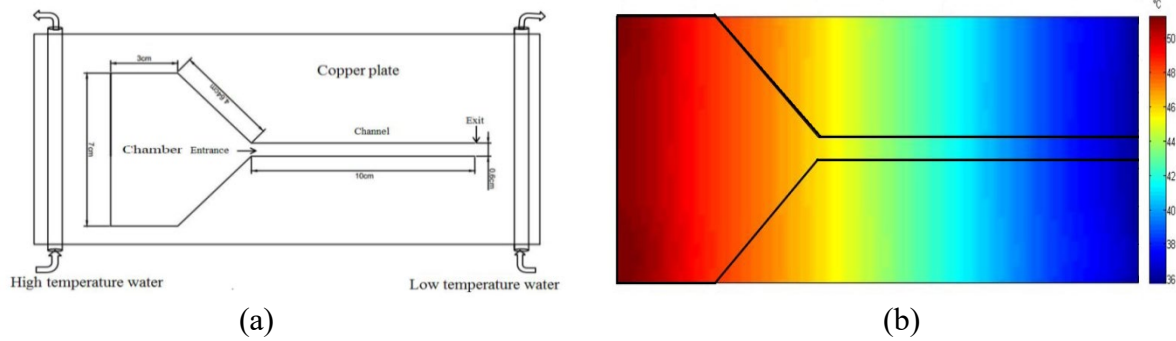


Fig. 1. Experimental device. (a) the investigation region is the unidirectional channel which is 10 cm long and 0.6 cm wide, and the chamber resembles a funnel with an area of 33.5 cm². (b) temperature gradient of chamber and narrow channel is shown.

2.3. Experimental Protocol

The experiment comprised of two parts: single-file movement of multiple ants and single ant movement. Each ant was exposed to a high temperature only once. First, the room temperature was 23 °C, and the entrance of the narrow channel was blocked. Then, two thermostatic bathes were employed to heat the water to different temperatures. Highest and lowest temperatures of water were respectively 75 °C and 30 °C. After two temperatures of the water were satisfied, it was used to heat the copper plate circularly. Consequently, highest temperature in the chamber was 51 °C, and temperatures at the entrance and exit of the channel were 45.8 °C and 35.8 °C, respectively. Therefore, temperature gradient was formed in the chamber and channel. When the temperature gradient of chamber and channel was stable, 15-30 ants with a similar size were quickly guided into the chamber, and then a transparent plastic sheet was used to cover the hole. Finally, we opened the entrance of the narrow channel, and began to record single-file movement of ants. The moment of opening the entrance was the beginning of the experiment. In the experiment of single-file movement of multiple ants, when all normal ants (besides injured ants) passed the exit of the channel, one trial was finished. This experiment was repeated 14 times under the same conditions. The movement of ants in the narrow channel was recorded by a digital video camera (digital sampling rate is 25 fps). Image analysis was implemented through the slow-motion mode of video-playing software. The coordinates of ants' heads in the narrow channel were extracted every two frames (0.08 seconds).

In the experiment of single ant movement, only one ant was introduced into the chamber in each trial. A total of 18 tests were performed. Each trial started when the ant entered the chamber, and was accomplished when the ant left the channel or was injured in the chamber.

3. Results and Discussion

3.1. Single-file Movement of Multiple Ants

In the light of the size measurements of 88 selected ants randomly, the body size is 1.23 ± 0.14 cm (average \pm standard deviation). The temporal evolution of each ant passing through the narrow channel was extracted from video records and in this way the coordinate of a head of an ant was obtained. Due to the restriction of width of channel, ants moved in the narrow channel with one-dimensional motion. Thus, we calculated the instantaneous speed in x-axis every eight frames (0.32 seconds) to relieve data fluctuation and data error caused by too short time interval. The instantaneous speed $V(t)$ at time t is given by

$$V(t) = \frac{S(t+\Delta t/2) - S(t-\Delta t/2)}{\Delta t} \quad (1)$$

where $S(t)$ denotes the abscissa of an ant's head, namely the moving distance in t seconds in the narrow channel. Δt represents the time interval which equals to 0.32 seconds in equation (1). In order to exclude outliers, pauta criterion was used in speed statistics for all ants.

In the field of vehicle traffic [9] and pedestrian [21] dynamics, the speed increases with distance headway until the desired speed is reached. In this work, we are also interested in the relationship between speed and distance headway that is defined as the distance from one ant's head to the tail of a preceding ant. When ants entered the channel, they moved in the channel one by one due the restraint of the width of channel. The instantaneous speed for the leader ant, preceding ants and following ants and the distance headway between two successive ants evolution with time are plotted in Fig. 2. The scattered dots represent the instantaneous speed for each time. Then these dots were connected by a smooth curve with Savizky-Golay method, from which the variation trend of speed with time can be obtained. For the leader ants, there is no interference in front, and the instantaneous speed is influenced by some unknown reasons that cannot be observed from video, which resulted in random pause or deceleration. As shown in Fig. 2(a), the instantaneous speed of leader ants is varying with time. Moreover, the value of the speed has larger fluctuation. Similar with leader ants, the instantaneous speed of following ants changes with time. When the distance headway is large enough, the following ants reduce their speed sometimes. On the other hand, the speed of following ants is influenced by not only some unknown reasons, but also the distance headway as illustrating in Fig. 2(b). From Fig. 2(b), we can see that the following ant decreased the speed once the distance headway is approximate to zero. However, in other case, if the distance headway is less than zero, which means the head of following ant overtakes the tail of preceding one, the following ants could also continue to move ahead as displayed in Fig. 2(c).

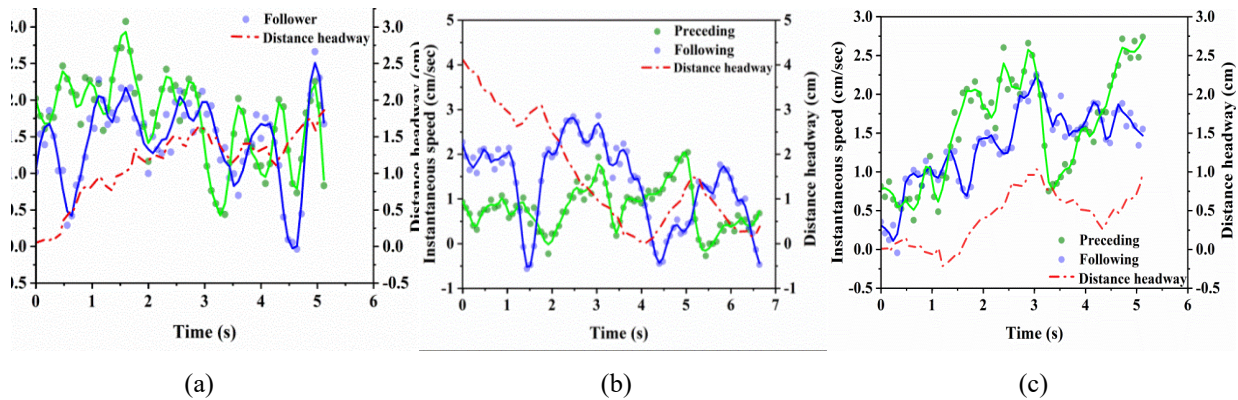


Fig. 2. The time-series of instantaneous speed (green dots for preceding ants and blue dots for following ants) and the distance headway (red dashed line). (a) shows the first ant in one trail and it's follower. (b) and (c) display two successive ants in middle of experiment process.

The results obtained from Fig. 2 indicate that the value of distance headway is less than zero for escaping quickly in some cases. Here, we counted the frequency distribution of distance headway for all the ants moving in the channel as shown in Fig.3. By using the Gaussian fit, the average distance headway μ is 0.3 cm, and the standard deviation $\sigma = 0.32$. This result implies most ants prefer to follow their preceding one closely when passing through the channel, as they are urgent to escape from the high temperature area. In addition, negative values of distance headway also account for a certain proportion.

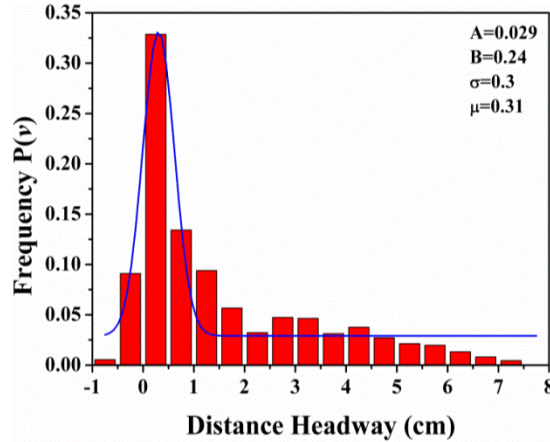


Fig. 3. Distance headway frequency distribution of all ants. The blue solid line represents the Gaussian fitting. The coefficient of determine R^2 is 0.894.

Due to the stress caused by the high temperature, the following ants tried to overtake the preceding one. Thus, following ants were apt to follow the leader one closely, namely less distance headway existed between them. As shown in Fig. 4, there are some special discrete points with distance headway < 0 or speed < 0 . During the experimental process, it was observed that some ants (which we call activists) preferred to overtake its front one when the front one moved with low speed or stopped, in order to escape from the chamber quickly. However, they failed because of the limitation of the channel width. In this case, they can move with the uniform speed sequentially by following the preceding one, as a result of their heads paralleled with the tail of preceding ant. On the other hand, some other ants named as pacifists just decelerated or moved backward once they touched the preceding one. Hence it can be explained that when the distance headway is less than 0, the speeds have both negative and positive values. In addition, we also observed the backward motion (speed < 0) in spite of large available distance which existed in front. Under stressed conditions, it is common for the ants that the distance headway is not more than zero.

The instantaneous speed of a single ant displayed in Fig. 4 is scattered whatever the distance headways are, which is consistent with the result shown in [13, 20]. In order to obtain the relation of the speed-distance headway, we applied a binning procedure [22] to this scattered data, i.e. dividing the whole data of speed into a series of bin per 0.1 cm/sec, and then calculating the peak value of frequency histogram that is obtained from the data of the distance headway falling into each bin firstly. Next, we fitted the peak values by means of linear fitting. The results presented in Fig. 4 show that the speed increases with the distance headway when the value of distance headway is less than 0.26 cm. The result of the linear fitting is 6.4 for the slope. The inverse of slope that is interpreted as a sensitivity to the distance headway [22] is 0.156 in present work. It indicates that ants are sensitive to distance headway. When the distance headway is small, ants can move with both high speed and low speed, and they have strong ability to control their speed.

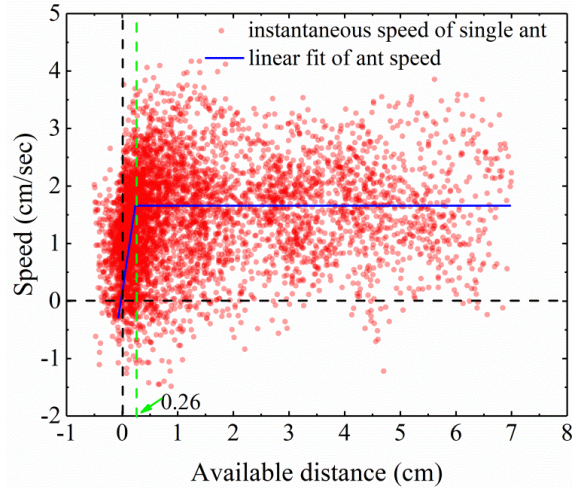


Fig. 4. Relationship between speed and distance headway. The fitting results are $y=6.4*x$ and $y=1.65$. y and x represent speed and distance headway respectively.

3.2. Comparison of Single Ant and Single-file Movement Experiment

In single-file movement experiment, multiple ants were used to investigate the collective motion in the narrow channel. We also employed single ant experiment to study individual motion with the same condition. The single ant movement using the same protocol with single-file movement experiments was conducted. It was repeated 18 times and 15 ants succeed in escaping from the chamber through the narrow channel. Three ants were injured because of long stay in high temperature, which resulted in failed escape. In order to investigate the single ant movement and compare the results with single-file movement of multiple ants, speeds of single ant were obtained with the same methods as above.

Single ant entered the channel driven by high temperature, and in single ant experiment, for each trial, only one ant moved in channel. The relations of speed-time for three ants are plotted in Fig. 5. From this figure it can be seen that the instantaneous speed of ant is fluctuant with time. Sometimes, ants moved in channel with high speed, but after a while, they decreased their speed to zero, even moved backward. The specific reason needs to be studied furtherly in the future.

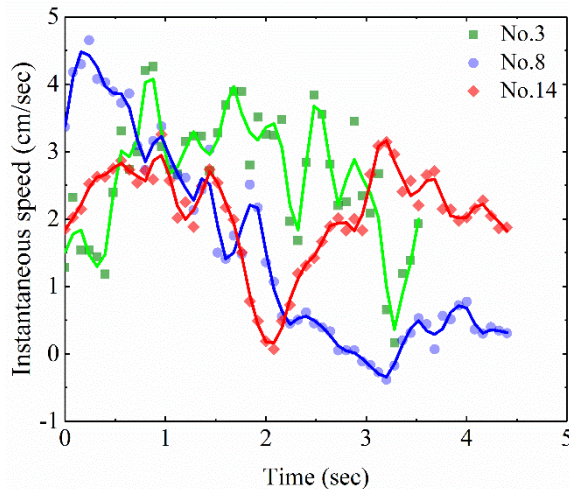


Fig. 5. Variation of speed with time for three single ant in the channel.

First of all, we compared the average speed for both single-file movement and single ant experiments. The speed distributions of all ants moving in the narrow channel for single ant and single-file movement experiments satisfy the Gaussian distribution, as illustrated in Fig. 6. The average speeds of these two experiments are 1.48 and 0.85 cm/sec, respectively. This comparison of the results manifests that the

multiple ants moved in channel can improve the average speed of ants. In the process of experiment, touching phenomenon was observed in single-file movement experiment in which the ants were stressed by high temperature. Attempting to escape from the chamber quickly, it is observed that the following ant touched (expressing as pushing behavior) the preceding one and tried to overtake it if the preceding ant was slower. This pushing behavior led to the increasing of speed of preceding ant. However, this phenomenon is not observed in natural trail of monomorphic ant [13]. From another point of view, the existence of touching behavior in single-file movement experiment is the reason that results in higher average speed (1.48 cm/sec) than in single ant experiment (0.85 cm/sec) in narrow channel. Generally, touching behavior improves the movement efficiency of passing channel.

The standard deviations of single ant and single-file movement experiments are 1.01 and 0.9, which is obtained by means of Gaussian fitting. Actually, the standard deviation reflects the degree of dispersion among individuals in one group. Comparatively speaking, the standard deviation ($\sigma = 1.01$) in single ant experiments is larger than single-file movement experiments ($\sigma = 0.9$), which means that the movement of single ant in channel are more arbitrary. Without the pushing from the following ant, ants moved according to their own characteristic.

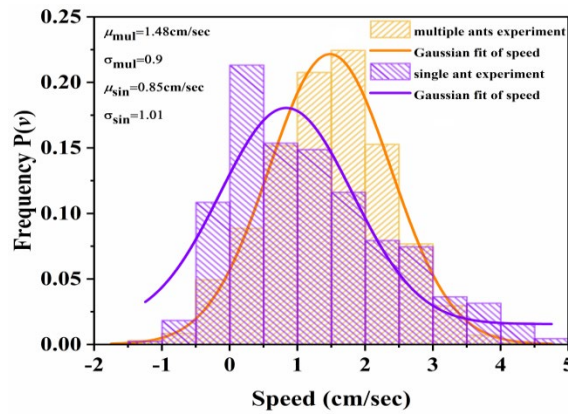


Fig. 6. Speed distribution of ants for single-file movement and single ant experiments.

Trajectories of ant moving in the channel both of single-file movement and single ant experiments are presented in Fig.7. All of the trajectories are tortuous, which signifies the moving ants do not walk forward along a straight line in the narrow channel. This finding is identical with the single-file movement of pedestrians [2]. However, the periodic oscillating was not observed from their trajectories. In these two experiments, the short pause and backward motion were observed in the trajectories of ants. On the other hand, in single ant experiment, there is significant difference between different ants for trajectories. As plotted in Fig. 7(b), the upper trajectory (blue line) displays a relatively smooth line, which presents a fluent movement process. Nevertheless, the bottom one (red line) shows a slow speed. From the bottom of Fig. 8(b), it can be seen that the ant hovered in the distance of 7 to 9 cm away from the entrance of channel for a long time.

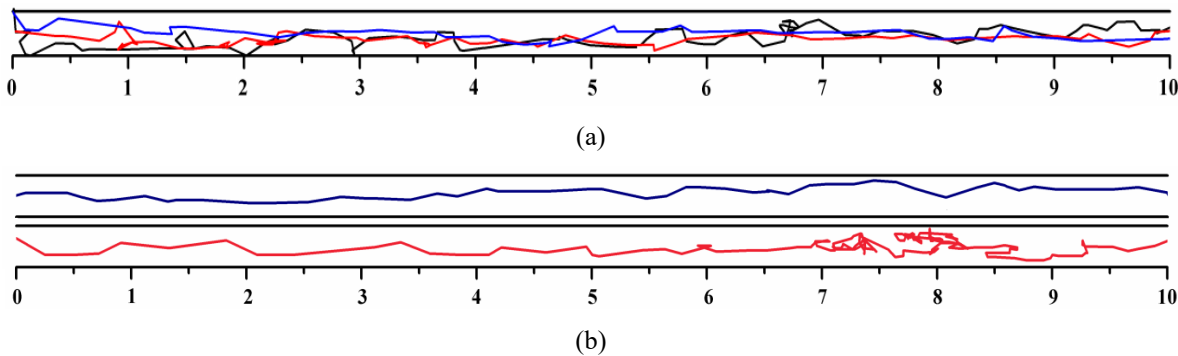


Fig. 7. Trajectories of ants in unidirectional channel for (a) single-file movement experiment and (b) single ant experiment.

Summarily, through comparing these two experiments, it was found that the pushing behavior plays an important role on single-file movement experiment which can promote preceding ants to move ahead or increase their speed. By this way, the efficiency of evacuating from a chamber by passing a long channel has improved.

4. Conclusions

In this work, we investigated single-file movement and the interaction between ants in the narrow channel under high temperature conditions. Under the stimulation of high temperature, ants preferred to follow the front one closely for escaping quickly. In the channel, touching behavior played a main role on escape. It was expressed that the average speed of ants in the single-file movement experiment was faster than that in the single ant experiment. In addition, similar to pedestrian and traffic, the speed of ants was dependent on a certain critical distance headway. Here, the critical distance headway for ant is 0.26 cm due to high ability to control their speed. The trajectories of ants presented a wavy form, which is similar to pedestrian in single-file movement, and whether an amplitude of ants is decreasing with increasing speed like pedestrian needs to be studied in the future work.

Generally, the single-file movement of ants has common characteristics with pedestrians and traffic in some respects. In the future, it is necessary to make a quantitative comparison between ants and pedestrian and vehicle traffic in single-file movement. Furthermore, in the ant trail model studying the ant movement under dangerous conditions, the long body size of ant and touching effect observed in this experiment should be considered in the future.

Acknowledgements

This research was supported by Key Research and Development Program of China (2016YFC0802508), and Fundamental Research Funds for the Central Universities (WK2320000035).

References

- [1] A. Seyfried, B. Steffen, W. Klingsch, and M. Boltes, "The fundamental diagram of pedestrian movement revisited," *Journal of Statistical Mechanics: Theory and Experiment*, vol. 2005, p. P10002, 2005.
- [2] X. Liu, W. Song, and J. Zhang, "Extraction and quantitative analysis of microscopic evacuation characteristics based on digital image processing," *Physica A: Statistical Mechanics and its Applications*, vol. 388, pp. 2717-2726, 2009.
- [3] J. Zhang, W. Mehner, S. Holl, M. Boltes, E. Andresen, A. Schadschneider, *et al.*, "Universal flow-density relation of single-file bicycle, pedestrian and car motion," *Physics Letters A*, vol. 378, pp. 3274-3277, 2014.
- [4] S. Wolfram, *Theory and applications of cellular automata* vol. 1: World scientific Singapore, 1986.
- [5] A. Schadschneider, "The nagel-schreckenberg model revisited," *The European Physical Journal B-Condensed Matter and Complex Systems*, vol. 10, pp. 573-582, 1999.
- [6] M. Fukui and Y. Ishibashi, "Traffic flow in 1D cellular automaton model including cars moving with high speed," *Journal of the Physical Society of Japan*, vol. 65, pp. 1868-1870, 1996.
- [7] M. Bando, K. Hasebe, A. Nakayama, A. Shibata, and Y. Sugiyama, "Dynamical model of traffic congestion and numerical simulation," *Physical review E*, vol. 51, p. 1035, 1995.
- [8] R. Herman and R. B. Potts, "Single lane traffic theory and experiment," 1900.
- [9] G. F. Newell, "Nonlinear effects in the dynamics of car following," *Operations research*, vol. 9, pp. 209-229, 1961.
- [10] E. Wilson, "The insect societies (Belknap, Cambridge, USA, 1971); B. Hölldobler and EO Wilson," in *The ants*, 1990.
- [11] E. O. Wilson, "The insect societies. Belknap," *Harvard, Cambridge MA*, 1971.

- [12] I. D. Couzin and N. R. Franks, "Self-organized lane formation and optimized traffic flow in army ants," *Proceedings of the Royal Society of London B: Biological Sciences*, vol. 270, pp. 139-146, 2003.
- [13] A. John, A. Schadschneider, D. Chowdhury, and K. Nishinari, "Trafficlike collective movement of ants on trails: Absence of a jammed phase," *Physical review letters*, vol. 102, p. 108001, 2009.
- [14] D. Helbing, I. J. Farkas, and T. Vicsek, "Simulating dynamical features of escape panic," *Nature*, vol. 407, pp. 487-490, 2000.
- [15] S. Soria, R. Josens, and D. Parisi, "Experimental evidence of the “Faster is Slower” effect in the evacuation of ants," *Safety science*, vol. 50, pp. 1584-1588, 2012.
- [16] D. R. Parisi, S. A. Soria, and R. Josens, "Faster-is-slower effect in escaping ants revisited: Ants do not behave like humans," *Safety science*, vol. 72, pp. 274-282, 2015.
- [17] S. Wang, W. Lv, and W. Song, "Behavior of Ants Escaping from a Single-Exit Room," *Plos One*, vol. 10, p. e0131784, 2015.
- [18] S. Boari, R. Josens, and D. R. Parisi, "Efficient egress of escaping ants stressed with temperature," *Plos One*, vol. 8, p. e81082, 2013.
- [19] U. Chattaraj, A. Seyfried, P. Chakroborty, and M. K. Biswal, "Modelling single file pedestrian motion across cultures," *Procedia-Social and Behavioral Sciences*, vol. 104, pp. 698-707, 2013.
- [20] S. Wang and W. Song, "Experimental Study of Ant Movement in a Straight Passageway under Stress Conditions," *Journal of Insect Behavior*, vol. 29, pp. 735-743, 2016.
- [21] W. Lv, Z. Fang, X. Wei, W. Song, and X. Liu, "Experiment and Modelling for Pedestrian Following Behavior Using Velocity-headway Relation," *Procedia Engineering*, vol. 62, pp. 525-531, 2013.
- [22] A. Jelić, C. Appert-Rolland, S. Lemercier, and J. Pettré, "Properties of pedestrians walking in line: Fundamental diagrams," *Physical review E*, vol. 85, p. 036111, 2012.

A study of evacuation efficiency of a hopper-shape exit by using mice under high competition

Lin Peng*, Wang Guoyuan, Wu Fanyu, Gao Dongli

Faculty of Geosciences and Environmental Engineering, Southwest Jiaotong University,
Chengdu, China

Corresponding author. Email: drag76@63.com

Abstract - Exit is the bottleneck of an evacuation from a room and the flow rate through an exit is believed to be depended on its width. A series of experiments were conducted in a bi-dimensional container where mice were driven to pass through two kinds of exit of the identical width, i.e., a conventional exit and a hopper-shape exit. The evacuation efficiency of the two exits was experimentally compared by using mice under competition. The results showed that a hopper-shape exit reduces the escape time by 25% compared with a conventional exit. Further study was conducted with the presence of a column in front of the two exits. The presence of a column in front of the conventional exit increases the escape time by 22.5%. On the contrary, the placement of column in front of the hopper-shape exit reduces the escape time by 48%. The study showed that the escape efficiency could be greatly improved by appropriately redesigning configuration of exit.

Key words: hopper-shape exit, mice evacuation, mean escape time, column in front of an exit

1. Introduction

The over-congested crowd, if not managed properly, could lead to disasters[1,2]. For example, 35 people were stampeded to death in the Bund Shanghai on 1st January 2015 and a stampede in Hajj pilgrimage killed around 2177 people on 24th September 2015. Frank and Dorso[3] found the pillar-like obstacle could reduce the evacuation time and the size of the obstacle should be of the order of a pedestrian and the position should be at a distance of 2 or 3 pedestrian sizes. Silo is typical industrial equipment, in which gravity-particles discharge through an outlet. Groups of particles through a narrow exit lead to the spontaneous development of clogs[4]. Full scale experiments [5, 6] in silo showed that the presence of an obstacle above the outlet can significantly reduce the clogging probability of granular matter. The physical mechanism behind the clogging reduction is believed to be the obstacles in front of the outlet partially undertake the force of particles, thus the pressure on the outlet decrease significantly. Numerical simulations of gravity-driven granular flow through an hourglass hopper was conducted[7] and it was found that the flow rate across a bottleneck actually increases if an optimized obstacle is placed before it. A number of full-scale experiments[8] by using different inserts in front the outlet were conducted to study their impact on the mass flow and the results suggested that the minimum horizontal distance between the silo hopper and inserts should be twice larger than the silo outlet diameter. Shiwakoti[9-11], Soria[12] and John[13] conducted a series of evacuation experiments using ants as agents. Apart from ants, a group of students were also made as agents in an room evacuation experiment by Garcimartin[14]. Moreover, Garcimartin[15] and Zuriguel[16] presented an experimental study of a flock of sheep passing through a narrow door. Video monitoring of daily routines in a farm was collected by measuring the time lapses between the passages of consecutive sheep, some features of the flow regime can be assessed and the effect of increasing the door size and the performance of an obstacle placed in front of it were evaluated. Lin et al[17,18] and Chen et al[19] conducted a series of experiments by driving the mice to pass through an exit, with or without an obstacle before it. The study shows that the presence of an obstacle in front of an exit can improve or deteriorate the evacuation efficiency depending on the nearby geometry. In this paper, a series of experiments with mice were conducted at a bi-dimensional space. The objectives of the paper is on one hand, to assess the performance of a hopper-shape exit by comparing with a conventional exit, and to evaluate the impact of column before the two exits on the throughput on the other hand. This paper is structured as follows: the experimental set-up is presented in the subsequent section, and the experimental results will be included in the Section 3. The conclusions will be drawn in Section 4.

2. Experimental set-up

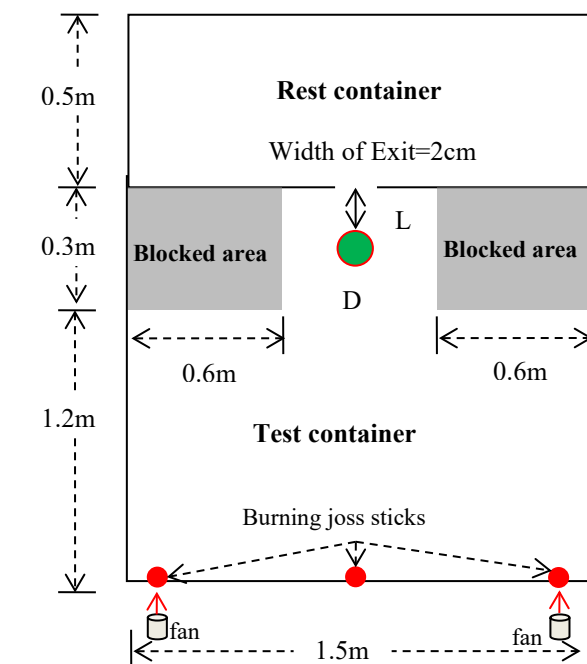
The experiment set-up was introduced by Lin et al [17]. For the completeness, the experimental set-up was only briefly introduced. The experimental setting, as shown in Fig. 1, is composed of two rectangular containers, one is test container for mice evacuation test and the other is rest container to provide food/water/rest for the mice. The two containers are connected by an exit with width of 2 cm. The sizes of the test container are 1.5m long, 1.5m wide and 2.5cm high. The height is only slightly higher than the height of the mice so as to prevent the overlap of mice during evacuation. To increase the competitiveness of the exit, the test container is occupied by two blocks with the sizes of 0.6m*0.3m, which are inaccessible for the mice. The sizes of the rest container are 0.5m long, 1.5m wide and 0.3m high. The wall and floor of the two containers are made of PVC and the ceiling is made of 6mm transparent PMMA for observation during experiment. The column with diameter of D is placed at distances of L to the exit as shown in Fig.1.

Two kinds of exits, i.e., a conventional exit and a hopper-shape exit, were studied respectively. Conventional exit is the benchmarking study for comparison and hopper-shape exit is the proposed alternative design. For both exits, the exit width was the same at 2 cm. Experimental process was recorded with two digital video cameras. All experiment scenarios are shown in Table 1.

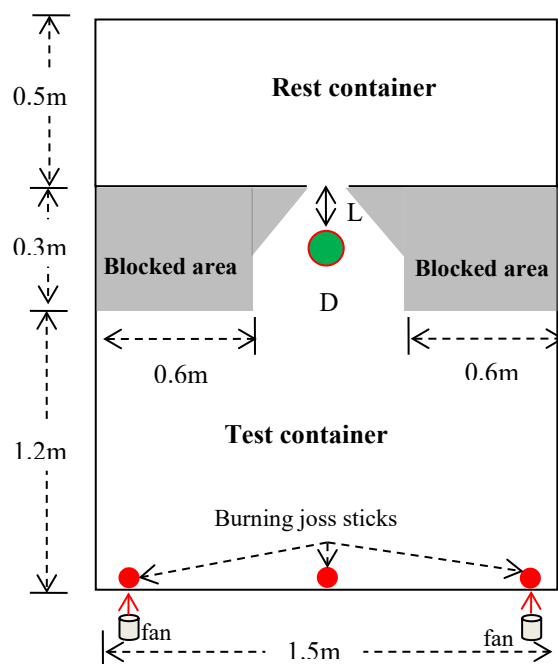
The mice used in the experiment are described as follows: 90 female mice, in the ages of 3~6 weeks, their body parameters are: width of 2.8~3.2 cm, height of 2.3~2.4cm, length of 9.5~10cm, and weight of 25~35g. The mice were trained for weeks to familiar with the location of exit and they escaped toward the exit as far as the burning joss sticks were inserted into Zone A. To produce different levels of stimulus, joss sticks as introduced by Lin et al [17] were used to drive the mice to escape. The experiment showed that when the number of joss stick was increased to 96, the mice desperately competed with each other and the competition is extreme high. We defined they are in a stressed state. Under this very high smoke concentration, the mice neither lost the direction to escape nor lost their ability to escape.

Table 1. Scenarios of experiment

Scenario	Exit Type	Obstacle
I	Conventional	No
II	Hopper-shape	No
III	Conventional	Yes
IV	Hopper-shape	Yes



(a) conventional exit



(b) hopper-shape exit

Figure.1 The plan of the experimental set-up (not to scale, the exit width is 0.2cm for both exits. The burning joss sticks were placed at three points as indicated. D is the diameter of obstacle, L denotes the distance from the closest boundary of the obstacle to the exit.)

3. Experimental results

To minimize the randomness of evacuation process, a number of repeated tests were conducted for each scenario. The number of mice participated in each test varied from 80~95. Each time, a few mice may leave at the test container and only the mice passing through the exit were considered in the estimation of evacuation time.

In scenario I, the evacuation tests were conducted in the test chamber with conventional exit and the escape times were used as benchmarking for further comparison. The evacuation process is recorded as shown in Fig.2. When the mice were placed into the test container, most of them accumulated at the area close to the exit, others distributed randomly along the boundary of the test container. After the inserting of the burning joss sticks, all mice quickly accumulated at the area close to the exit. 4 repeated tests were carried out and a summary of the results for this situation is included in Table 2 and Fig.3. The time lapses ranged from 1s to 20s as shown in Fig.3. The mean evacuation time taking for a mouse through the exit was approximately $4.0 \pm 0.4s$. The total evacuation time is not taken as the main measure due to the unstable number of mice passing the exit in different runs of experiment.

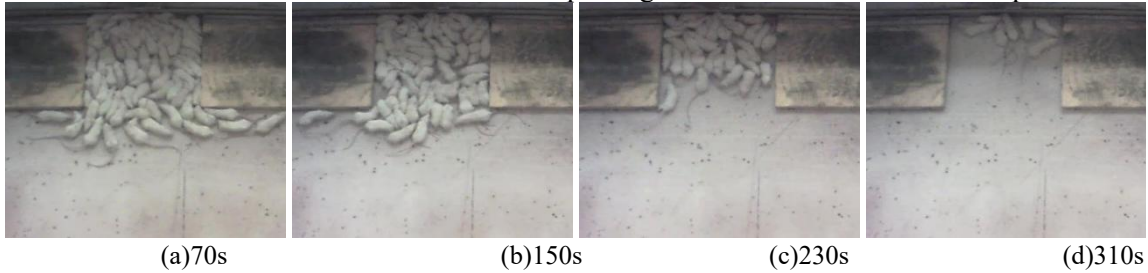


Fig. 2 Recorded escape pattern in scenario I-1

Table 2 Experimental result for scenario I

Test No.	Escape time per mouse (s)	Average evacuation time per mouse (s)	Standard error (s)
I-1	3.9		
I-2	4.0	3.7	0.3
I-3	3.3		
I-4	3.4		

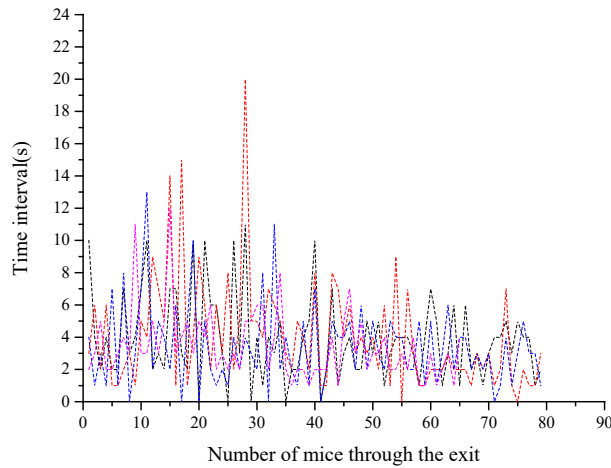


Fig. 3. Number of mice through the exit for Scenario I (The dashed lines with different colors as black, red, blue and magenta represents for scenario I-1, I-2, I-3 and I-4 separately.)

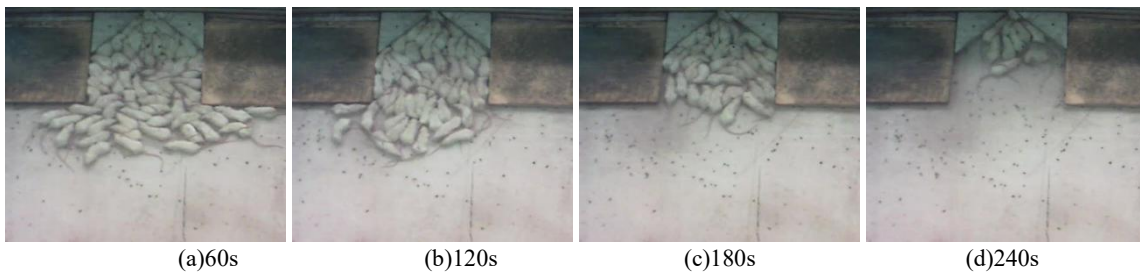


Fig. 4. Recorded escape pattern in scenario II-1

In Scenario II, similar experiments were conducted in the test chamber with the introduction of two triangles as shown in Fig.1(b). The evacuation process is recorded as shown in Fig.4. 4 repeated tests as shown in Table 3. The time lapses ranged from 1s to 18s as shown in Fig.5. The mean evacuation time taking for a mouse through the exit was approximately 3.2 ± 0.5 s. Compared with the results with conventional exit, i.e., Scenario I, the average evacuation time taking for a mouse passing through the exit is reduced by 25%. Clearly, a hopper-shape exit can greatly improve the flow rate.

Table 3. Experimental results for scenario II

Test No.	Escape time per mouse (s)	Average evacuation time per mouse (s)	Standard error (s)
II-1	3.2		
II-2	2.7	3.2	0.5
II-3	3.8		
II-4	3.0		

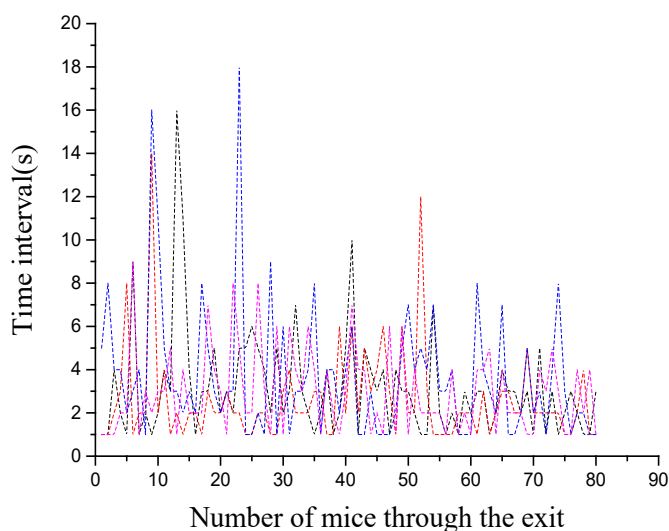


Fig.5. Number of mice through the exit for Scenario II (The dashed lines with different colors as black, red, blue and magenta represents for scenario II-1, II-2, II-3 and II-4 separately.)

Based on previous study in crowds flow, the size of the obstacle is typically of the order of a pedestrian and the position is generally close to the exit (at most at a distance of 2 or 3 pedestrian sizes) and the minimum distance between the silo hopper and column should be twice larger than the silo outlet diameter so as to improve the flow rate. The exit width is 2cm and the body width of mouse is around 2.8cm~3.2cm. Therefore, a column with a diameter of 3.2cm were placed at a distance of 2~4cm (around 1~ 2 times of the exit width) away from the exit. The column was firstly placed in front of the conventional exit at a distance of 2cm away from the exit. Experiment was conducted and the results shown that the mice flow was over-crowded due to the presence of the obstacle and the flow was totally clogged. After 10 minutes, less than 20 mice passed through the exit, the experiment was suspended. Two mice close to the exit crushed to death, which lead to the blockage of the exit. A second test was conducted and similar phenomenon was observed and the experiment was suspended after 5 minutes to avoid casualties. Based on initial tests, the presence of column at a distance of 2cm (around 1 time of the exit width) cannot improve the flow rate. On the contrary, it significantly reduces the flow rate.

In Scenario III, a column with a diameter of 3.2cm was relocated at a distance of 4cm away from the conventional exit. The evacuation process is recorded as shown in Fig.6. 4 repeated tests as shown in

Table 4. The time lapses ranged from 1s to 42s as shown in Fig.7, which is significantly increased compared with Scenario I. The mean evacuation time taking for a mouse through the exit was approximately $4.9 \pm 0.3s$.



Fig. 6. Recorded escape pattern in scenario III-1

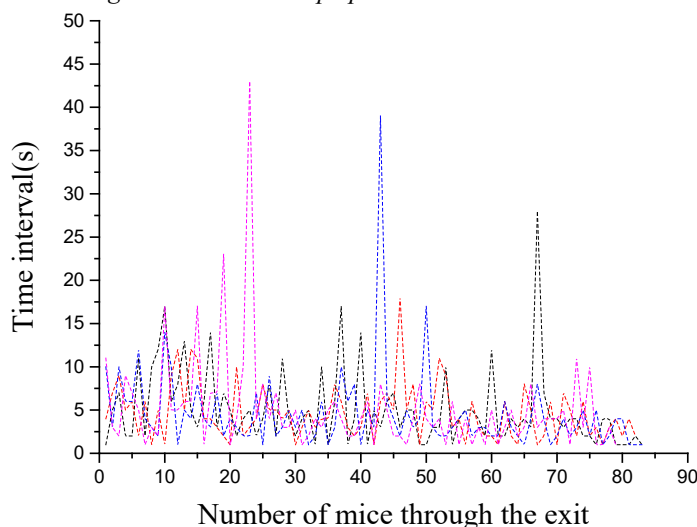


Fig.7. Number of mice through the exit for Scenario III (The dashed lines with different colors as black, red, blue and magenta represents for scenario III-1, III-2, III-3 and III-4 separately.)

Table 4. Experimental results for Scenario III

Test No.	Escape time per mouse (s)	Average evacuation time per mouse (s)	Standard error (s)
III-1	5.1		
III-2	4.6		
III-3	4.7	4.9	0.3
III-4	5.2		

Compared with the results in Scenario I, the introduction of an obstacle makes the average evacuation time taking for a mouse passing through the exit increase by 22.5%. The placement of an obstacle in front of conventional exit cannot improve the flow rate. On the contrary, it reduces the flow rate. The result is beyond our previous understanding as we presumed the presence of obstacle should improve the flow rate and reduce the escape time.

In Scenario VI, the column with a diameter of 3.2cm was further placed in front of the hopper-shape exit at a distance of 4cm above the exit, similar to Scenario III. 4 repeated tests as shown in Table 5 were conducted. The evacuation process is recorded as shown in Fig.8. The time lapses ranged from 1s to 12s as shown in Fig.9. The mean evacuation time taking for a mouse through the exit was approximately $2.7 \pm 0.3s$. Compared with the results in Scenario II, the mean evacuation time per

mouse reduces by 18.5%. That is to say, the presence of an obstacle in front of a hopper-shape exit increases the flow rate and the result is basically consistent with the findings in silo flow. To exploit the flow characteristics of mice flow through the exit at different scenarios, let τ be the time lapse between two consecutive mice, which reflects the clogging characteristic of mice passing the exit.

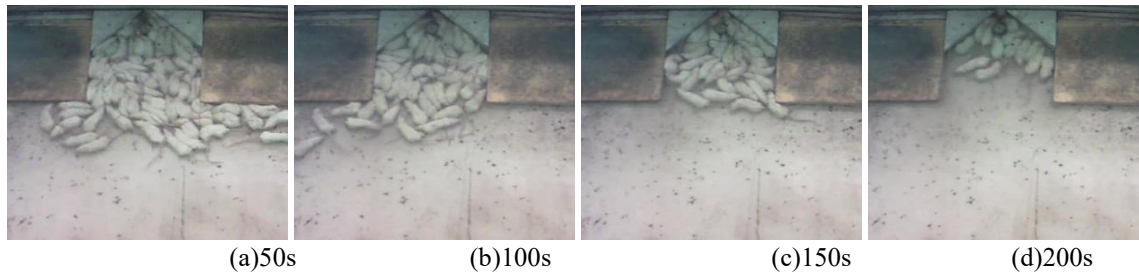


Fig. 8 Recorded escape pattern in scenario IV-1

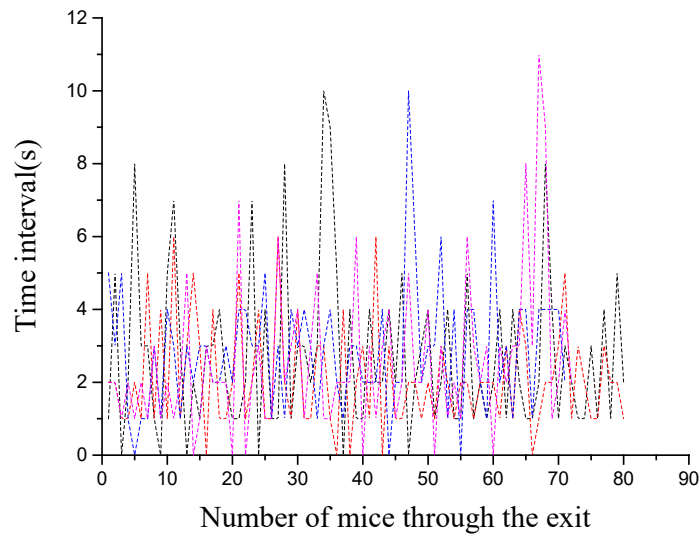


Fig.9 Number of mice through the exit for Scenario IV (The dashed lines with different colors as black, red, blue and magenta represents for scenario IV-1, IV-2, IV-3 and IV-4 separately.)

Table 5. Experimental results for scenario IV

Test No.	Escape time per mouse (s)	Average evacuation time per mouse (s)	Standard error (s)
IV-1	2.8		
IV-2	2.2	2.7	0.3
IV-3	3.0		
IV-4	2.6		

The time lapses of two consecutive mice for the four scenarios were studied and probability distribution of the time intervals is presented in Fig. 10. The distribution of time lapse follows $P(\Delta t) \sim \tau^{-\alpha}$. Garcimartin[14] suggested that alpha is an indicator of the degree of clogging through the exit and a larger of the Alpha, the smoother of the flow through an outlet. A rigorous mathematical tool as suggested by Clauset et al[20] was used to estimate the alpha for each scenario and the results were presented in Figure 10.

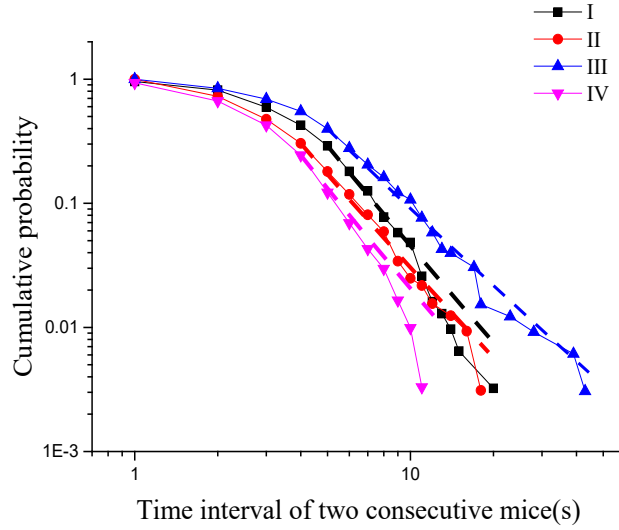


Fig.10 Probability distribution of time intervals (the dashed line is the associated Alpha)

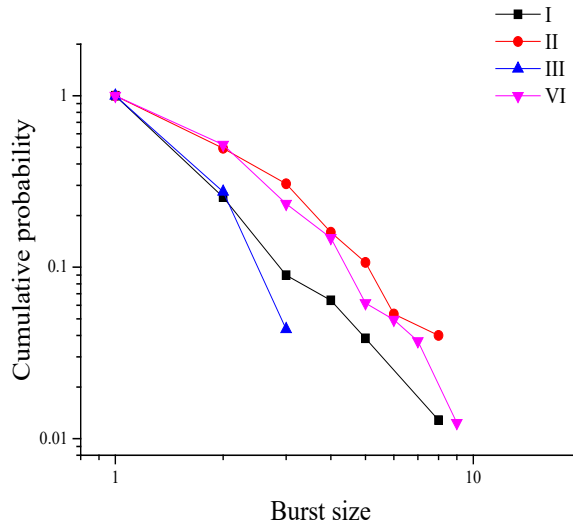


Fig. 11 Probability distribution of burst sizes

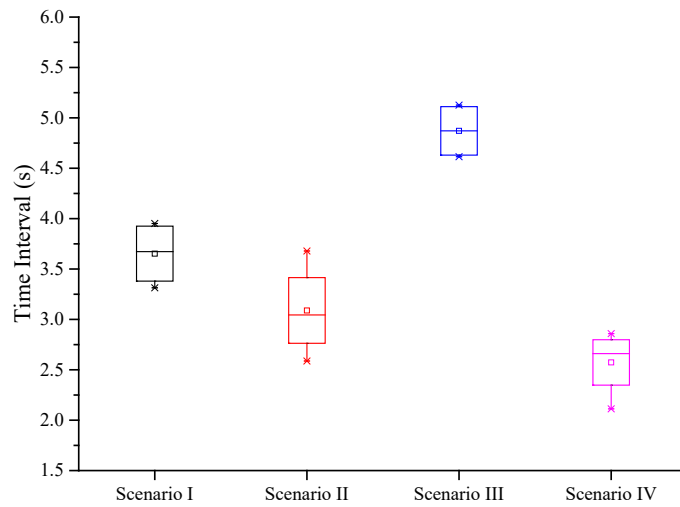


Fig. 12 Mean evacuation time intervals with quartiles of different scenarios

$\alpha_1=3.5$ for scenario I, $\alpha_3=3.5$ for Scenario II, $\alpha_2=3.46$ for Scenario III, and $\alpha_4=3.5$ for Scenario IV. No clear relationship between alpha and evacuation efficiency is observed. Our study showed that the alpha is not an indicator of the degree of clogging through the exit. The clogging is defined as no mice passing the exit within 2 seconds. The burst sizes, defined as the continuous number of mice passing through the exit between two clogs, described the properties of intermittent flow through the exit. The burst sizes displayed an exponential behavior as shown in Fig.11.

4. Discussions and conclusions

In this paper, a series of experiments with mice under high competition condition were conducted at a bi-dimensional space. The use of mice avoids the ethical and legal issues. To make the test consistency, a group of mice were used in this experiment. The mice were trained a few weeks to learn the skill of evacuation. The evacuation process was video-recorded for further analysis.

Two kind of exits of same width, one is a conventional exit and the other is a hopper-shape exit, were experimentally evaluated by using the mice under strong stimulus. The results are shown in Fig 12, and it is found that the hopper-shape exit reduces the mean escape time by 25% compared with the conventional exit.

Cohen's d is defined as the difference between 2 means divided by a standard deviation. For scenarios I and II, the value of d is 1.65, indicating a very large difference between the two scenarios.

The presence of obstacle increase the average evacuation time per mouse by 22.5% with a conventional exit, whilst the presence of obstacle reduce the average evacuation time per mouse by 18.5% with a hopper-shape exit. The presence of the obstacle in front of the hopper-shape exit increases the flow rate and this phenomenon agrees with the observation in silo flow. The impact of the obstacle on flow rate through the exit is totally contrary. The value of Cohen's d between scenarios I and III is 4.69, indicating a huge difference between the two scenarios, whilst it is 1.50 between scenarios II and IV, still showing a very large difference.

With a conventional exit, all mice compete to pass through the exit and they are moving in different directions. The strong competition makes the efficiency of exit decreases greatly. With the hopper-shape exit, all mice in the space move unidirectionally toward to the exit and the competition at the exit is much attenuated. Therefore, the evacuation time is much reduced. In gravity-driven flow, the driven force is unidirectional. Whilst in mice flow, the driven force is multi-directional. The strong interaction of multi-directional mice flow close to the exit leads to a totally distinctive effect of obstacle on the throughput of exit. In the hopper-shape exit, the mice flow is channeled as unidirectional flow close to the exit, similar to that of silo flow. The interaction of mice is much attenuated as they move in the same direction.

Before the experiment gets started, the mice are trained to get familiar with the position of the exit, so that they would not be wandering in the experiment platform.

In the evacuation experiment conducted by Garcimartín[14], it can be found that the evacuation time interval of competitive evacuees is $0.38 \pm 0.04s$, which is shorter than the mean time interval of mice, and the total evacuation time is nearly 28s for 80 evacuees, apparently shorter than that of mice, and the value of the power-law exponent is $\alpha = 5.0 \pm 0.1$, which is larger than that of mice. This might due to the limitation of human experiment in which the evacuees are not in an emergency, and that the evacuation could not reflect the phenomenon under dangerous conditions.

Since the hopper-shape exit can improve the evacuation efficiency, it is essential to dig further to find a best angle minimizing the damage caused by emergency, so a series of hopper-shape exit with different angles are going to be tested and analyzed in the future.

Acknowledgement

The authors greatly acknowledge the valuable comments from anonymous reviewers, the financial support from China Fundamental Research Funds for Central Universities No.2682016cx082 and a number of students who participated the mice experiments.

References

- [1] D. Helbing, I. Farkas, T. Vicsek, Simulating dynamical features of escape panic, *Nature*, 66 (2000) 487-490.
- [2] A.Johansson, D.Helbing, Analysis of Empirical Trajectory Data of Pedestrians, in: *Pedestrian and Evacuation Dynamics 2008, 2010*, pp. 203-214.
- [3] G.A. Frank, C.O. Dorso, Room evacuation in the presence of an obstacle, *Physica A*, 390 (2011) 2135-2145.
- [4] P. Lin, J. Ma, S.M. Lo, Discrete Element Crowd Model for Pedestrian Evacuation Through an Exit, arXiv:1510.07126v1, (2015).
- [5] I. Zuriguel, A.Janda, A.Garcimartín, C.Lozano, R. Arévalo, D. Maza, Silo Clogging Reduction by the Presence of an Obstacle, *Phys. Rev. Lett.*, 107 (2011) 1-5.
- [6] L. Celia, J. Alvaro, G. Angle, M. Diego, Z. Iker, Flow and clogging in a silo with an obstacle above the orifice, *Phys. Rev. E* 86 (2012).
- [7] F. Alonso-Marroquin, S.I. Azeezullah, S.A. Galindo-Torres, L.M. Olsen-Kettle., Bottlenecks in granular flow: When does an obstacle increase the flow rate in an hourglass?, *Phys. Rev. E*, 85, (2012) 020301(R).
- [8] J. Tejchman, *Confined Granular Flow in Silos Experimental and Numerical Investigations*, Springer, 2013.
- [9] N. Shiwakoti, M. Sarvi, M. Burd, Using non-human biological entities to understand pedestrian crowd behavior under emergency conditions, *Safety Science*, 66 (2014) 1-8.
- [10] N. Shiwakoti, M. Sarvi, G. Rose, M. Burd, Animal dynamics based approach for modeling pedestrian crowd egress under panic conditions, *Social and Behavioral Sciences* (2011) 438-461.
- [11] N. Shiwakoti, M. Sarvi, G.Rose, M. Burd, Enhancing the safety of pedestrians during emergency egress: can we learn from biological entities?, *Transp. Res.Rec*, 2137 (2009) 31-37.
- [12] S.A. Soria, R. Josens, D.R. Parisi, Experimental evidence of the 'Faster is Slower' effect in the evacuation of ants, *Safety Science*, 50 (2012) 1584-1588.
- [13] A.John, A.Schadschneider, D.Chowdhury, K. Nishinari, Trafficlike collective movement of ants on trails: absence of jammed phase, *Physical Review Letters*, 102 (2009) 108001.
- [14] A. Garcimartín, I. Zuriguel, J.M. Pastor, C. Martín-Gómez, D.R. Parisi, Experimental Evidence of the 'Faster Is Slower' Effect, in: *the Conference on Pedestrian and Evacuation Dynamics 2014 (PED 2014)*, Delft, The Netherlands, 2014, pp. 760-767.
- [15] A. Garcimartín, J. M. Pastor, L. M. Ferrer, J. J. Ramos, C. Martín-Gómez, I. Zuriguel, Flow and clogging of a sheep herd passing through a bottleneck, *PHYSICAL REVIEW E*, 91 (2015) 1-7.
- [16] I.Zuriguel, D.R.Parisi, R.C. Hidalgo, C.Lozano, A. Janda, P.A. Gago, Clogging transition of many-particle systems flowing through bottlenecks, *scientific reports*, 4 (2014) 7324.
- [17] P.Lin, J.Ma, T.Y.Liu, T.Ran, Y.L.Si, T.Li, An experimental study of the "faster-is-slower" effect

- using mice under panic, *Physica A*, 452 (2016) 157-166.
- [18] P.Lin, J.Ma, T.Y.Liu, T.Ran, Y.L.Si, F.Y.Wu, G.Y.Wang, An experimental study of the impact of an obstacle on the escape efficiency by using mice under high competition, *Physica A*, 482 (2017) 228-242.
- [19] J. M. Chen, P. Lin, F. Y. Wu, D. L. Gao, G. Y. Wang, Revisit the faster-is-slower effect for an exit at corner, manuscript accepted by
- [20] A. Clauset, C.R. Shalizi, M.E.J. Newman, Power-Law Distributions in Empirical Data, *SIAM Rev.*, 51 (2009) 661-703.

Social group behaviour of triads. Dependence on purpose and gender

Francesco Zanlungo¹, Zeynep Yücel², Takayuki Kanda^{1,3}

¹ATR IRC

Kyoto, Japan

zanlungo@atr.jp, kanda@atr.jp,

²Okayama University

Okayama, Japan

zeynep@okayama-u.ac.jp

³Kyoto University

Kyoto, Japan

Abstract - We analysed a set of uninstructed pedestrian trajectories automatically tracked in a public area, and we asked a human coder to assess their group relationships. For those pedestrians who belong to the groups, we asked the coder to identify their apparent purpose of visit to the tracking area and apparent gender. We studied the quantitative dependence of the group dynamics on such properties in the case of triads (three people groups) and compared them to the two pedestrian group case (dyads), studied in a previous work. We found that the group velocity strongly depends on relation and gender for both triads and dyads, while the influence of these properties on spatial structure of groups is less clear in the triadic case. We discussed the relevance of these results to the modelling of pedestrian and crowd dynamics, and examined the possibility of the future works on this subject.

Keywords: group behaviour, social relations, dyads, triads

1. Introduction

Researchers in the fields of pedestrian behaviour and crowd modelling have become recently more and more aware of the necessity of studying and modelling the behaviour of social groups. Groups represent an important, if not predominant, portion of urban pedestrian crowds [1,2], and they exhibit group-specific behaviour [3,4,5,6] and thus understanding and modelling them is necessary to reproduce crowd behaviour in normal and emergency conditions [7]. As a result, a few statistical studies, mathematical and numerical models of group behaviours have been developed [3,8,9,10,11,12,13,14]. It is nevertheless clear that, being related to human social behaviour, group dynamics is probably influenced by the composition of the group and by the relation between the members [6,15,16].

In [17], we studied the dependence of dyad group dynamics on purpose, relation, gender, age and height, along with the interplay of these factors. Our analysis was able to quantitatively confirm some intuitive properties, such as a larger interpersonal distance and walking velocity in workers compared to leisure oriented pedestrians, in colleagues compared to friends and couples, and in males compared to females. Groups including tall pedestrians were also observed to walk faster, as did groups composed of active age adults, when compared to groups with children or elderly people. More surprising results were related to the behaviour of families, which appeared to walk in a less organised (non-abreast) way than other groups, and exhibit counter-intuitive features such as walking faster in high density settings. This behaviour was found to be due to the irregular motion of children.

In this work we extended the statistical analysis performed in [17] on dyads to groups formed by three people.

2. Data set and definitions

Our analysis is based on a data set of trajectories of unconstrained and uninstructed groups, moving in an “ecological” environment (a building in Osaka, Japan, where shopping areas, offices, a monorail station and a ferry terminal are present). The pedestrian trajectories (including pedestrian height) have been automatically tracked using 3D range sensors, while group relation and group composition have been manually determined by human coders through video analysis (see [4,17] for the details of the tracking system and the reliability of human coding, i.e. agreement between coders).

In the current work, we focused on the behaviour of triads. Following [17,18], we defined and analysed their *intrinsic properties* as

- **purpose** of movement
- **relation** between the members
- **gender** of the members
- **age** of the members
- **height** of the members

Regarding the **purpose**, we divided the groups in the *work oriented* and *leisure oriented* classes; regarding the **relation** in *colleagues*, *families* and *friends* (couples, analysed in [17], are absent in triads); regarding the **gender** we considered the *number of females* (from 0 to 3); while regarding the **age** and the **height** we analysed the *average*, *minimum* and *maximum* value assumed by these properties in each group. Nevertheless, due to the limited space, in this work we will show only the results concerning the purpose and gender, which are of relatively easy interpretation and comparison to the dyadic case.

In order to analyse in a quantitative way the triad dynamics, we first, following [17], defined the group velocity as

$$\mathbf{V}^{g^3} = \sum_i \mathbf{v}_i / 3$$

and used a reference frame whose y axis is aligned with \mathbf{V}^{g^3} to measure the components (x_i, y_i) of all pedestrians (Figure 1 left). The labels are chosen in such a way that $x_1 \leq x_2 \leq x_3$.

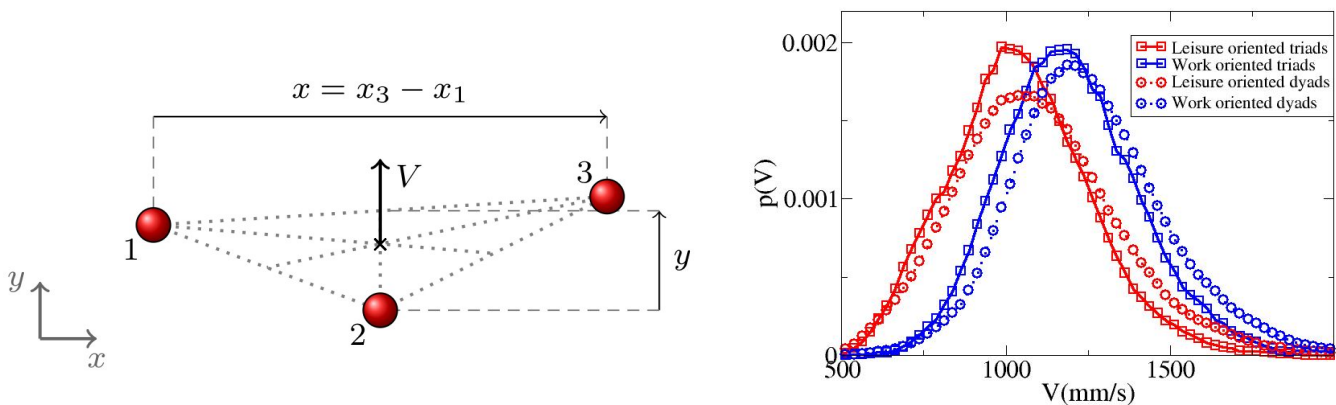


Figure 1: Left: observable definition. Right: comparison between triadic and dyadic V probability distribution function dependence on purpose.

Our quantitative analysis will be based on the following observables:

1. group velocity, defined as $V^{g3} = |\mathbf{V}|$,
2. group width, defined as $x^{g3} = x_3 - x_1$,
3. group depth, defined as $y^{g3} = |y_3 + y_1 - 2y_2|/2$.

In the previous equations, the superscript $g3$ is used to differentiate these observables from their two people equivalent, defined and analyzed in [17] as

1. group velocity, defined as $V^{g2} = |\sum_i \mathbf{v}_i/2|$,
2. group width, defined as $x^{g2} = x_2 - x_1$,
3. group depth, defined as $y^{g2} = |y_2 - y_1|$.

In [17], we also analysed the distance between pedestrians r^{g2} , but such a quantity has not a straightforward triadic generalisation and will not be analysed in this work.

For each observable, we provided the number of groups analysed N , its average value, standard deviation and standard error. We compared the values assumed between different classes giving an ANOVA based "statistical significance" p value (strongly dependent on the number of groups observed) along with an effect size [17] (comparing average value difference to standard deviations, not strongly influenced by the number of observations). We also showed for each observable and class the overall empirical probabilistic distribution functions (pdf), to compare actual variable distribution beyond their average values.

3. Results concerning purpose

Table I shows the observable dependence on the purpose classes in triads, while the results for dyads are copied from [17] and reported in Table II. A standard ANOVA shows that the influence of purpose on velocity is extremely significant, the one on x is still significant but reduced with respect to V , while no significant effect is present for y . In dyads, the purpose had a significant effect on all variables (particularly strong on V and x), although the analysis was based on a larger data set. To correct for the difference in sample size, we may observe that the effect size analysis shows again a large effect on velocity

TABLE II
OBSERVABLE DEPENDENCE ON PURPOSE FOR DYADS. LENGTHS IN MILLIMETRES, TIMES IN SECONDS.

Purpose	N	V^{g2}	x^{g2}	y^{g2}
Leisure	716	1118 ± 7.3 ($\sigma=195$)	628 ± 6.1 ($\sigma=162$)	383 ± 12 ($\sigma=334$)
Work	372	1271 ± 8.2 ($\sigma=158$)	713 ± 8 ($\sigma=154$)	332 ± 15 ($\sigma=289$)
p		$< 10^{-8}$	$< 10^{-8}$	0.0126
effect size		0.832	0.533	0.16

p		$< 10^{-8}$	0.0248	0.818
effect size		1.01	0.363	0.037

(even stronger than the one on dyads), a reduced one on x and a negligible one on y .

A direct comparison of the triad and dyad probability distribution functions for the V observable is shown in Figure 1 (right), while the corresponding distributions for x and y are shown in Figure 2. The effect of the purpose on velocity appears indeed to be very similar in triads and dyads, with a shift between the leisure and work distribution of roughly 150 mm/s regardless the number of the pedestrians in the group, as can be verified from the average values in Tables I and II (for an explanation of the difference in velocity between dyads and triads, refer to [3]). The comparison of x and y pdfs between triads and dyads is obviously less straightforward, since these quantities roughly scale with the group size. Nevertheless, we may see that the tendency of workers to assume a larger abreast distance, that was observed in dyads (roughly 80 mm more, according to table 2), is confirmed also in triads (roughly 100 mm more according to table 1). The y distribution for dyads suggested that workers have a more regular abreast configuration than leisure oriented pedestrians (higher peak), while in the triadic case we were not able to observe any clearly different pattern.

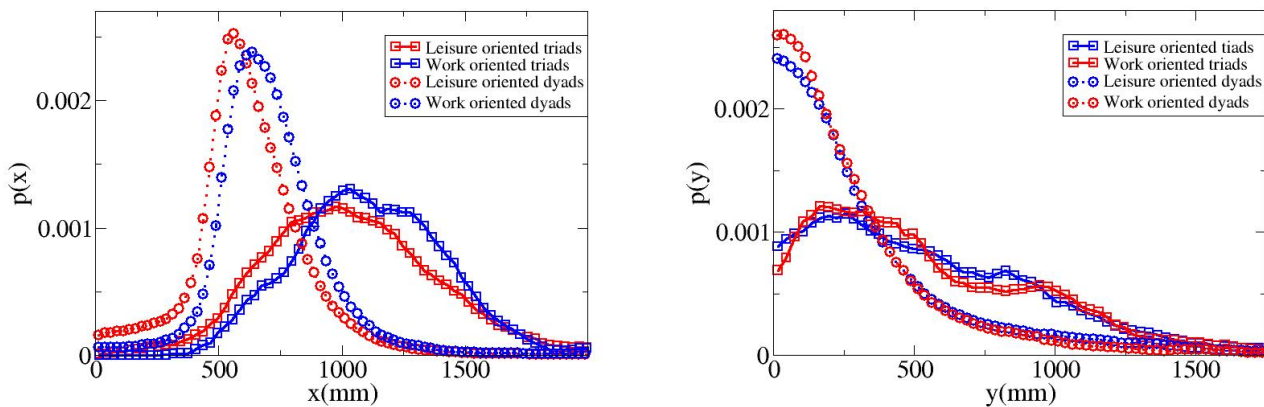


Figure 2: Left: comparison between triadic and dyadic x probability distribution function dependence on purpose. Right: equivalent comparison for the y pdf.

4. Results concerning gender

Table III shows the observable dependence on the gender, while the results for dyads are copied from [17] and reported in Table IV. The ANOVA shows again a very strong statistical significance for the effect of gender on velocity, while no statistical significance is observed for the spatial observables, in contrast to the dyadic case, in which all observables presented statistically significant differences due to the gender of the groups. As previously discussed, these results may be strongly influenced by the smaller statistical sample used for triads. For this reason, we analysed also the effect size, which shows again that the effect on velocity is much stronger than that on spatial observables (and, again, even stronger than in the dyadic case). Furthermore, the effect size on x is strongly reduced in triads (while that on y is similar on triads and dyads).

TABLE III
OBSERVABLE DEPENDENCE ON GENDER FOR TRIADS. LENGTHS IN MILLIMETRES, TIMES IN SECONDS.

Gender	N	V^{g3}	x^{g3}	y^{g3}
Three females	44	1060 ± 21 ($\sigma=140$)	1030 ± 39 ($\sigma=256$)	565 ± 51 ($\sigma=338$)
Two females	26	1008 ± 28 ($\sigma=142$)	1087 ± 57 ($\sigma=289$)	524 ± 76 ($\sigma=386$)
Two males	27	1053 ± 29 ($\sigma=152$)	1028 ± 45 ($\sigma=236$)	621 ± 47 ($\sigma=245$)
Three males	72	1210 ± 19 ($\sigma=165$)	1093 ± 34 ($\sigma=285$)	602 ± 41 ($\sigma=352$)
p		$< 10^{-8}$	0.545	0.696
effect size		1.26	0.237	0.303

TABLE IV
OBSERVABLE DEPENDENCE ON GENDER FOR DYADS. LENGTHS IN MILLIMETRES, TIMES IN SECONDS.

Gender	N	r^{g2}	x^{g2}	y^{g2}
Two females	252	1102 ± 12 ($\sigma=193$)	647 ± 7.8 ($\sigma=123$)	321 ± 20 ($\sigma=311$)
Mixed	371	1111 ± 9.5 ($\sigma=183$)	613 ± 9 ($\sigma=174$)	416 ± 18 ($\sigma=350$)
Two males	466	1254 ± 8.3 ($\sigma=178$)	699 ± 7.7 ($\sigma=166$)	349 ± 14 ($\sigma=293$)
p		$< 10^{-8}$	$< 10^{-8}$	0.000484
δ		0.825	0.51	0.282

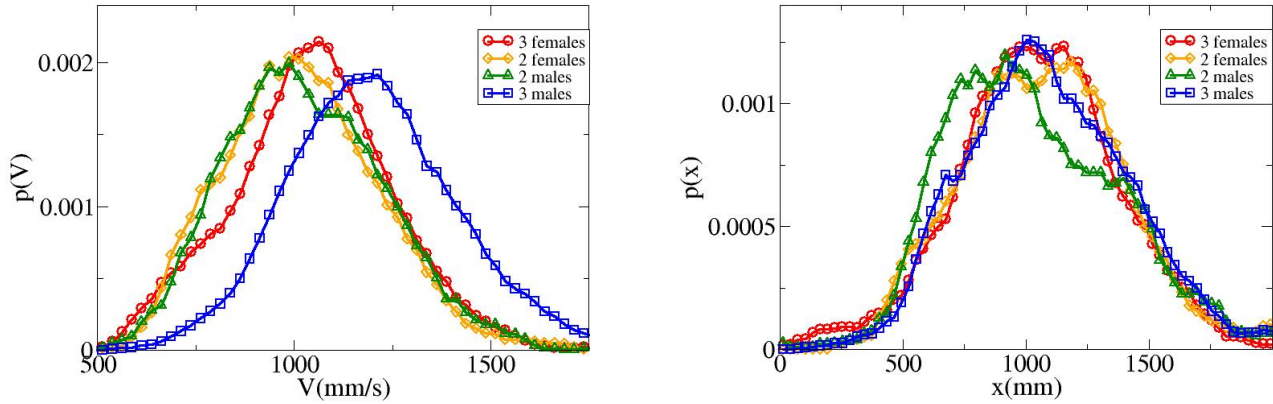


Figure 3: Left: dependence of V^{g3} (triads) pdf on gender. Right: dependence of x^{g3} (triads) pdf on gender.

The dependence of triadic probability distribution functions on gender is shown in Figures 3-left, 3-right and 4-left for, respectively, the V , x and y observables. The comparison to the dyadic case is limited, for simplicity's sake, to same gender groups (i.e. 2 females or 2 males for dyads, 3 females or 3 males for triads) and shown in Figures 4-right, 5-left and 5-right for, respectively, the V , x and y observables.

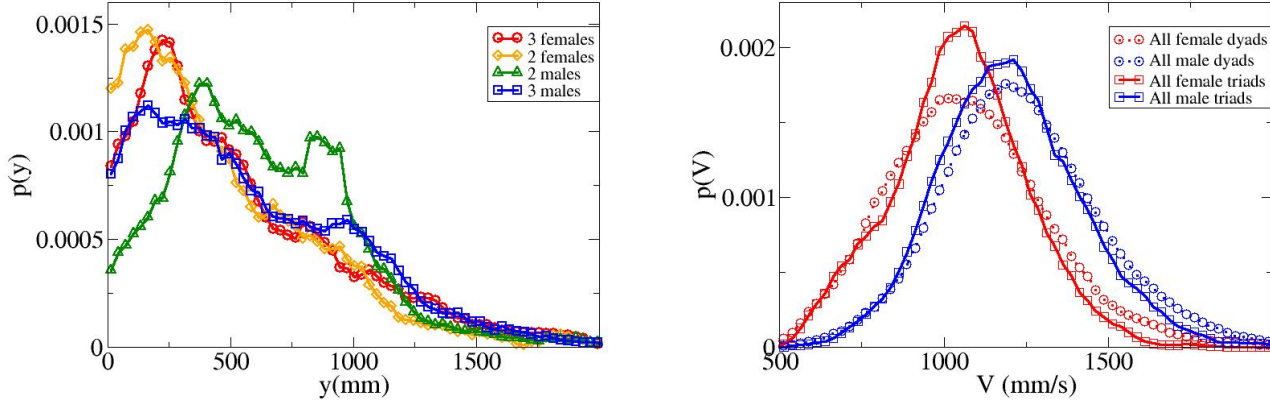


Figure 4: Left: dependence of y^{g3} (triads) pdf on gender. Right: Comparison between triadic and dyadic V pdf dependence on gender.

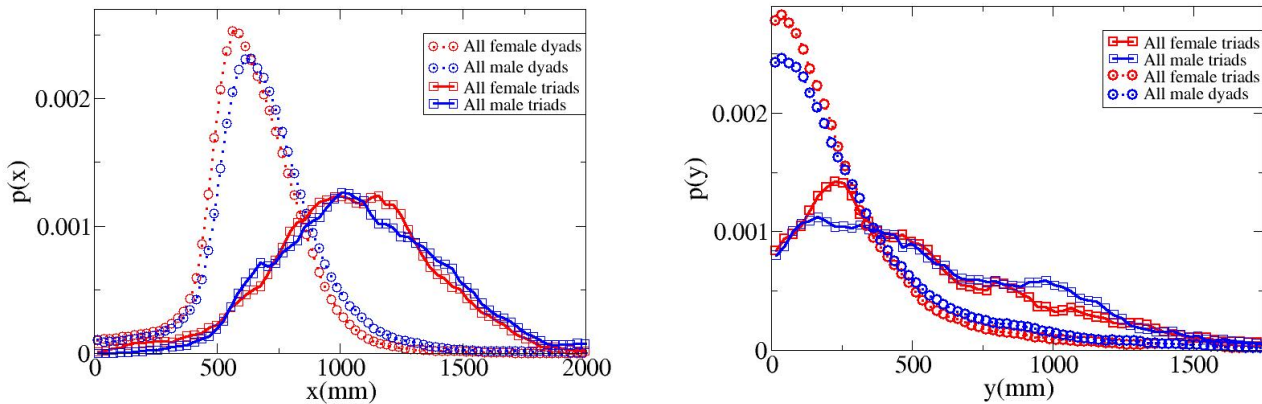


Figure 5: Left: Comparison between triadic and dyadic x pdf dependence on gender. Right: Comparison between triadic and dyadic y pdf dependence on gender.

Both from Figure 4-right and Tables III and IV, we may see that males walk roughly 150 mm/s faster than females regardless of group size (dyads being again faster than triads of 40 mm/s). On the other hand, the tendency of females to walk closer in abreast distance (Figure 5-left), and males in more ordered way (Figure 5-right) is observed in dyads but not in triads.

Concerning the behaviour of mixed gender triads, we may, from the qualitative analysis of the distribution functions, see that they appear to walk slightly slower than female groups (Figure 3-left), and that the spatial distribution of groups with two males appears to have features clearly different from the others. As discussed in the conclusions, without expanding the sample and studying in more detail the relation and age properties of these groups, it is impossible to understand the meaning and significance of these observations.

4. Conclusions

We have observed for triads the same velocity patterns (larger in workers and males) as the patterns observed for dyads, and with similar effect size and statistical significance. While not explicitly reported in this work, we also observed that the effect of relation, age and height on velocity is very similar between two people and three people groups. For dyads we observed also clear patterns in spatial observables, namely males walked at a larger abreast distance and in a more ordered abreast configuration (narrower y distribution). While the effect of purpose on x was observed also for triads, evidence confirming the other effects has not been found. These observations seem to suggest that the geometrical shape of three people groups (V formation, [3]) has some specific features that are more resilient to differences in intrinsic group properties than the simple abreast walking of dyads. An alternative explanation may be that dyadic interactions are of stronger nature than triadic ones, and thus affect more the geometry of groups. Furthermore, triads, by being spatially larger, may suffer more the influence of the surrounding environment (other pedestrians and architectural structures), and as a result the effect of intrinsic features may be reduced.

In [17] we provided a cross-analysis of the effect of different intrinsic features on group behaviour. For example, we observed that although, in our observed sample, work oriented dyads are mainly composed of two males, the effect of gender and purpose were still present when isolated (e.g. comparing two female worker groups to two male ones). Furthermore, we verified that some specific features of mixed gender groups were better explained when couples were isolated from parent-child dyads. A similar analysis will be extremely useful also in the triadic case, but in order to provide it, we will need to expand our statistical sample.

The findings of this work, in particular if confirmed and better elucidated by the analysis of larger set of triads, may help in the development of better group models and, as a consequence, crowd simulators.

Acknowledgments

This work is based on results obtained from a project commissioned by the New Energy and Industrial Technology Development Organization (NEDO).

References

1. M. Schultz, L. Rößger, F. Hartmut and B. Schlag, *Group dynamic behavior and psychometric profiles as substantial driver for pedestrian dynamics*, in *Pedestrian and Evacuation Dynamics 2012*, U. Weidmann, U. Kirsh and M. Schreckenberg, Vol II, pp. 1097-1111 (2014).
2. M. Moussaïd M, N. Perozo, S. Garnier, D. Helbing, and G. Theraulaz, *The walking behaviour of pedestrian social groups and its impact on crowd dynamics*, PLoS One, 2010, 5, 4, e10047.
3. F. Zanlungo, T. Ikeda, and T. Kanda, *Potential for the dynamics of pedestrians in a socially interacting group*, Physical Review E, 2014, 89, 1, 021811.
4. F. Zanlungo, D. Brščić and T. Kanda, *Spatial-size scaling of pedestrian groups under growing density conditions*, Physical Review E 91 (6), 062810 (2015)
5. F. Zanlungo and T. Kanda, *A mesoscopic model for the effect of density on pedestrian group dynamics* Europhysics Letters, 111, 38007 (2015).

6. L. He, J. Pan, W. Wang and D. Manocha, *Proxemic group behaviors using reciprocal multi-agent navigation*, 2016 IEEE International Conference on Robotics and Automation (ICRA), 292--297.
7. S. Bandini, L. Crociani, A. Gorrini, and G. Vizzari, *An agent-based model of pedestrian dynamics considering groups: A real world case study*, IEEE 17th International Conference on Intelligent Transportation Systems (ITSC), 2014, 572--577.
8. N. Bode, S. Holl, W. Mehner, and A. Seyfried, *Disentangling the impact of social groups on response times and movement dynamics in evacuations*, PLoS one <http://dx.doi.org/10.1371/journal.pone.0121227>.
9. G. Köster, F. Treml, M. Seitz, and W. Klein, *Validation of crowd models including social groups*. In Ulrich Weidmann, Uwe Kirsch, and Michael Schreckenberg, editors, *Pedestrian and Evacuation Dynamics 2012*, pages 1051-1063. Springer International Publishing, 2014
10. X. Wei, X. Lv, W. Song, X. Li, *Survey study and experimental investigation on the local behavior of pedestrian groups*, Complexity, Volume 20, Issue 6, July/August 2015, Pages 87–97.
11. I. Karamouzas, and M. Overmars, *Simulating the local behaviour of small pedestrian groups*, Proceedings of the 17th ACM Symposium on Virtual Reality Software and Technology, 183-190, (2010)
12. Y. Zhang, J. Pettré, X. Qin, S. Donikian and Q. Peng, *A Local Behavior Model for Small Pedestrian Groups*, Computer-Aided Design and Computer Graphics (CAD/Graphics), 2011 12th International Conference on, 275-281 (2011)
13. A. Gorrini, L. Crociani, C. Feliciani, P. Zhao, K. Nishinari, S. Baldini, *Social groups and pedestrian crowds: experiment on dyads in a counter flow scenario*, Proceedings of the 2016 Pedestrian and Evacuation Dynamics Conference
14. M. Seitz, A. Templeton, J. Drury, G. Köster, and A. Philippides, *Parsimony versus reductionism: how can crowd psychology be introduced into computer simulation?*, Review of General Psychology, 21(1), 95, 2017
15. Z. Yücel, F. Zanlungo and M. Shiomi, *Modeling the impact of interaction on pedestrian group motion* Advanced Robotics, 1-11 (2018).
16. M. Costa, *Interpersonal distances in group walking*, Journal of Nonverbal Behavior, 34, 1, 15-26 (2010)
17. F. Zanlungo, Z. Yücel Z, D. Brščić, T. Kanda T and N. Hagita, *Intrinsic group behaviour: Dependence of pedestrian dyad dynamics on principal social and personal features*, PLoS One, 2017, 0187253
18. D. Bugental, *Acquisition of the algorithms of social life: A domain-based approach*, Psychological bulletin, 126, 2,187, 2000

Experimental study on the influence of background music on pedestrian movement in high densities

Guang Zeng^{1,2}, Andreas Schadschneider², Jun Zhang¹, Weiguo Song¹

¹State Key Laboratory of Fire Science, University of Science and Technology of China

Jinzhai Road 96, Baohe district, Hefei 230027, China

²Theoretical Physics Institution, University of Cologne

ZuelpicherStrasse 77, Cologne 50937, Germany

gzeng@mail.ustc.edu.cn; as@thp.uni-koeln.de;

junz@ustc.edu.cn; wgsong@ustc.edu.cn

Abstract: It is interesting to investigate the effect of background music on pedestrian movement. This paper investigates the properties of crowd motion with external rhythms. With rhythm, pedestrians stop more frequently than without any rhythm. The stopping also increases with the increment of the tempo. Velocity and flow with rhythms are lower than that without any rhythm at high densities due to the more frequent stopping. Stepping behavior analysis shows that the step frequency with rhythms is smaller than that without any rhythm, especially at high densities. Dynamic coordinated behavior is weakened by music, which also affects the stepping behavior. Our study will be helpful for understanding the effect of background music on pedestrian movement.

Keyword: background music; stop-and-go; fundamental diagrams; stepping behavior

1. Introduction

Although crowding is often observed especially in large cities, it is still not clear how to control crowd motion effectively. Yanagisawa et al.[1] found that a rhythm below the normal step frequency can improve pedestrian flow if pedestrians are instructed to follow the rhythm. Therefore it is interesting to investigate the influence of rhythm on pedestrian motion in more detail, e.g. the effect of rhythm without explicit instructions or of background music.

With instruction of following the rhythm, Styns et al.[2] analyzed isolated pedestrians movement and found that the velocity will increase with the increment of rhythm tempo until 114 BPM and then keep steady. Yanagisawa et al.[1] proposed and verified that pedestrians following the rhythm slower than pedestrian normal step frequency, can improve pedestrian flow. It was explained by cognition science that the rhythm could promote cognitive processes, which results in coordinated pedestrian flow motion[3]. However, there is few work about the influence of background music on pedestrian movement, especially at high densities. In a city environment, different types of music have different effects on pedestrian velocity: a pedestrian walks more quickly when listening to motivational music, while he/she walks more slowly when listening to non-motivational music[4]. Mendonca et al.[5] found that the step frequency is not influenced by music when a pedestrian walks on a treadmill. Sejdic et al.[6] also found that music does not have a natural influence on the walking behavior of pedestrians when a pedestrian walks on the ground. The effect of background music on pedestrian movement is not clear. How different tempos of rhythms influence pedestrian movement when pedestrians are not instructed to follow the rhythm, has not been investigated so far. In this study, we

focus on the effect of different rhythms (different tempos) on pedestrian dynamics. A series of single-file experiments, six experiments with six different rhythms and one without any rhythms, are conducted to study pedestrian movement influenced by different rhythms. These rhythms include 90BPM, 120BPM and 150BPM rhythms from a pure music of a song called “Fade” and 90BPM, 120BPM and 150BPM rhythms produced by electronic metronome.

Single-file experiments, in which pedestrians are only influenced by the purely longitudinal interactions, are commonly used to study pedestrian dynamics. Seyfried et al.[7] studied the fundamental diagram and explained the linear relation between headway and velocity in the view of stepping. Jelic et al.[8] carried out a single-file experiment in a circle corridor and found there are three different regimes in the relation between headway and velocity. Cao et al.[9] found three different regimes of the relation in mixed age group, but only two in young group by analyzing pedestrian movement.

The remainder of the paper is organized as follows: in the second part, the experiment setup will be introduced in detail. The results of the experiment and the analysis will be presented in the third part. At last, the paper will be summarized with a conclusion.

2. Experiment setup

To investigate the effect of background music on pedestrian dynamics, we conducted a series of single-file experiments in Hefei, China. The sketch of the scenario is shown in Fig.1. The scenario is an oval ring corridor with a central circumference of 21.93 m and two 5 m long straight corridors. The width of the corridor is 0.8 m, which is wide enough for pedestrians to walk freely, but does not allow overtaking. 40 college students (18 male and 22 female) took part in the experiment. Different runs with 2, 5, 10, 20, 30 and 40 participants were conducted to realize different global (one-dimensional) densities ranging from 0.09/m to 1.82/m. In each run, pedestrians were given the same instructions to walk as normally without overtaking preceding pedestrians. They walked 5 rounds or at least 3min each run to ensure that enough data for stationary movement can be extracted. Six experiments with different rhythms and an experiment under normal conditions (without any rhythms) were designed for the experiment. The former were carried out with music of 90 BPM, 120 BPM and 150 BPM and 90 BPM, 120 BPM and 150 BPM with a rhythm from an electric metronome, respectively. The music is pure music of a song called “Fade” whose original music tempo is about 108 BPM. We transformed it to three different tempos (90 BPM, 120 BPM and 150 BPM) with Adobe Audition CS6. To avoid interference of these different conditions, different runs for the same rhythm condition were conducted consecutively before the rhythm condition was changed. A total of 77 runs of the experiment were performed. For more details of the experiment we refer to [10].

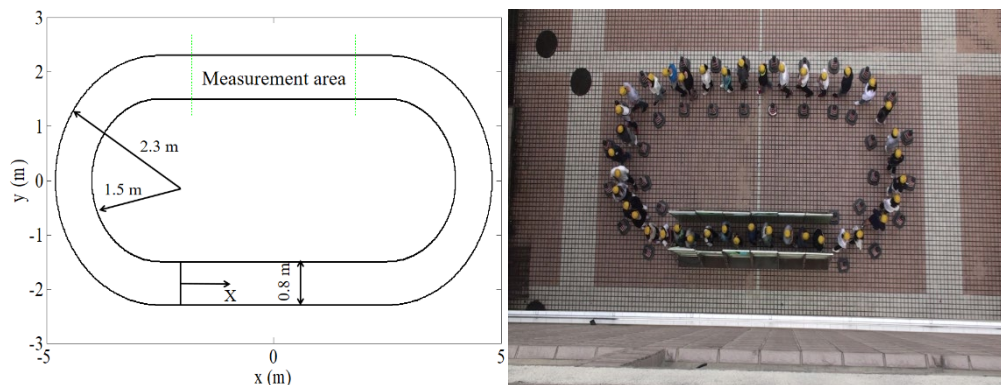


Fig.1 Schematic illustration of the scenario and a snapshot from the experiment

3 Results and analysis

To analyze the data, the 2D coordinate is transformed into a 1D coordinate in Fig.1. The origin 0 of the 1D coordinate is at the center of the starting line of the straight corridor. The maximum length of the coordinate is 21.93m. The coordinate below will be described with the 1D coordinate, if there is no special explanation. To compare the results with different rhythms, only the data in the steady state were analyzed.

Instantaneous velocity is the average velocity in a short time interval. A Voronoi headway is defined as half of the distance between the centers of his following pedestrian and followed pedestrian. Local density is the inverse of the Voronoi headway. They can be calculated as Equation 1. Fundamental diagrams are measured in the measurement area (11.67m, 15.27m) which is shown in Fig.1. Macroscopically, Density and velocity in the measurement area are calculated as Equation 2.

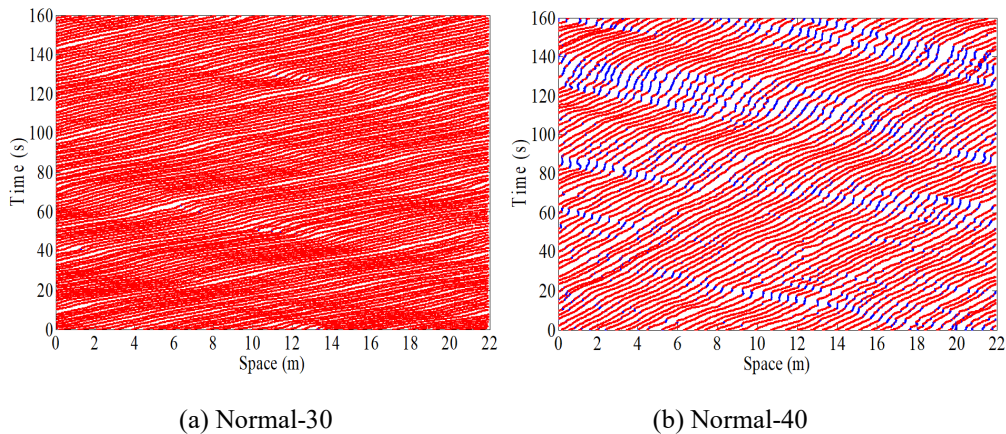
$$\rho(X, t) = \frac{1}{\frac{X_{i+1}(t) - X_i(t)}{2}}, v(X, t) = \frac{X_i(t + \frac{\Delta t}{2}) - X_i(t - \frac{\Delta t}{2})}{\Delta t} \quad (1)$$

$$\rho(t) = \frac{\int \rho(X, t) dX}{l_m}, v(t) = \frac{\int v(X, t) dX}{l_m} \quad (2)$$

Here $\rho(X, t)$, $v(X, t)$, $\rho(t)$ and $v(t)$ represent local density, instantaneous velocity, average density and average velocity, respectively. $X_i(t)$ is the 1D coordinate of pedestrian i at time t . Δt is a time interval chosen here as 0.4 s. l_m represents the length of the measurement area.

3.1 Time-space diagram

Time-space diagram can show characteristics of pedestrian movement. To make it more clearly, we define moving and stopping here. When instantaneous velocity of a pedestrian is beyond 0.1m/s, the pedestrian is regarded as moving, otherwise, he is stopping. Time-space diagrams at high densities (1.37 ped/m and 1.82 ped/m) are shown in Fig. 2, where the red and blue line represent the moving and stopping state, respectively. We can find that stop-and-go starts to appear apparently when the density is 1.82 ped/m (corresponding to the runs with 40 pedestrians) with and without rhythms. However, it is obvious that pedestrians stop more frequently under rhythm conditions.



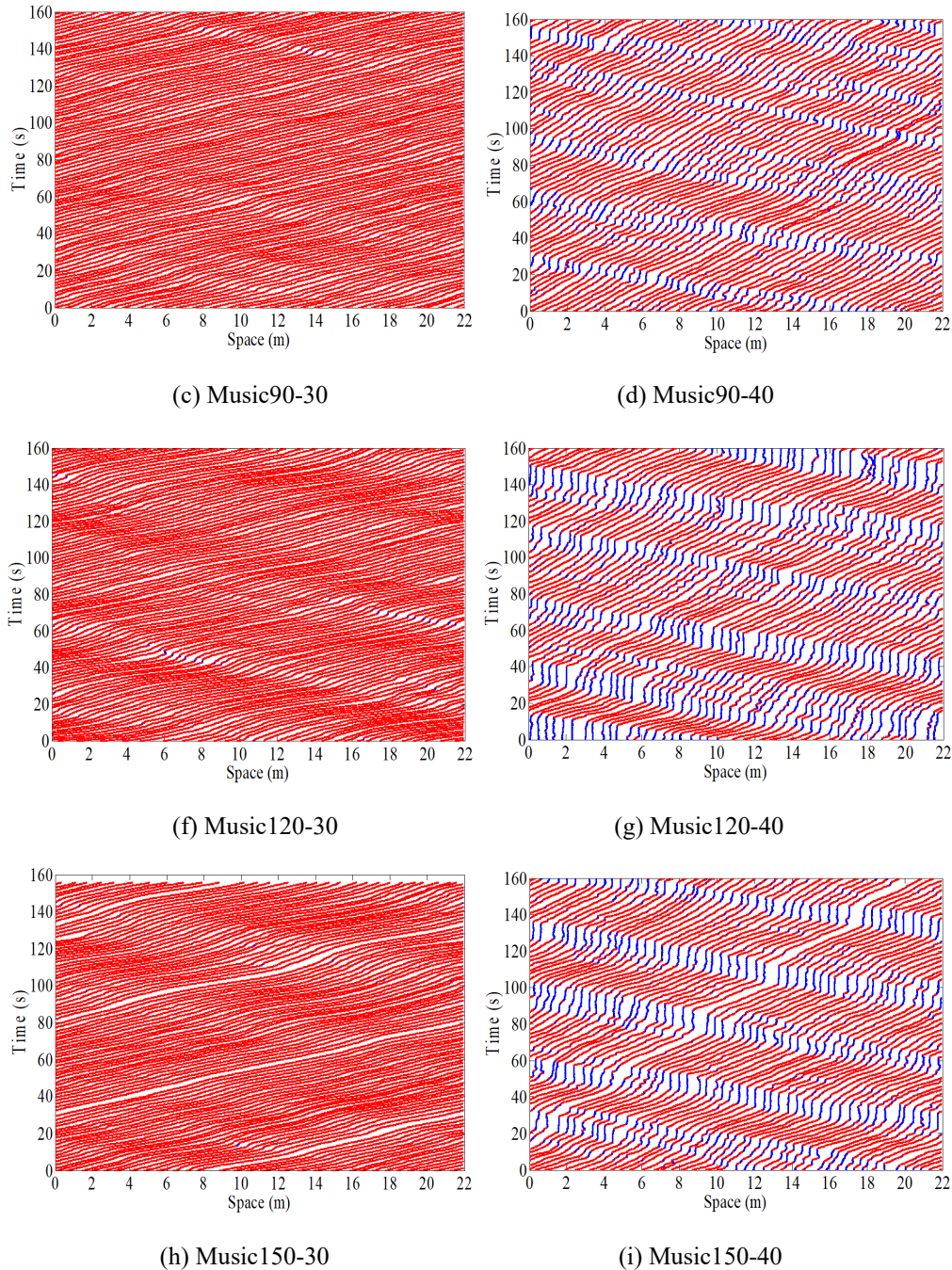


Fig.2: Time-space diagrams for high densities. The red and blue line represent moving and stopping, respectively. Normal-30 represents the run of 30 pedestrians without any rhythm. Music90-30 means the run of 30 pedestrians with rhythm of 90BPM.

Stopping duration is defined as the length of the time interval during which a pedestrian is not moving. It allows to compare pedestrian movement with rhythms and without any rhythm quantitatively. The distributions of stopping duration with rhythms and without any rhythm are shown in Fig.3. Considering the noise and the influence of stopping, we focus on the stopping duration longer than 0.4s. The ratio beyond 3.6s without any rhythm is 1.23%, while those are 3.88%, 12.64%, 11.67% with 90BPM, 120BPM and 150BPM, respectively. We can find that the ratios of stopping duration beyond 3.6s with rhythms are higher than that without any rhythm. Meanwhile, that with 120BPM

rhythm is higher than that with 90BPM rhythm. With rhythms, pedestrians stop longer and the stopping duration increases with the tempo.

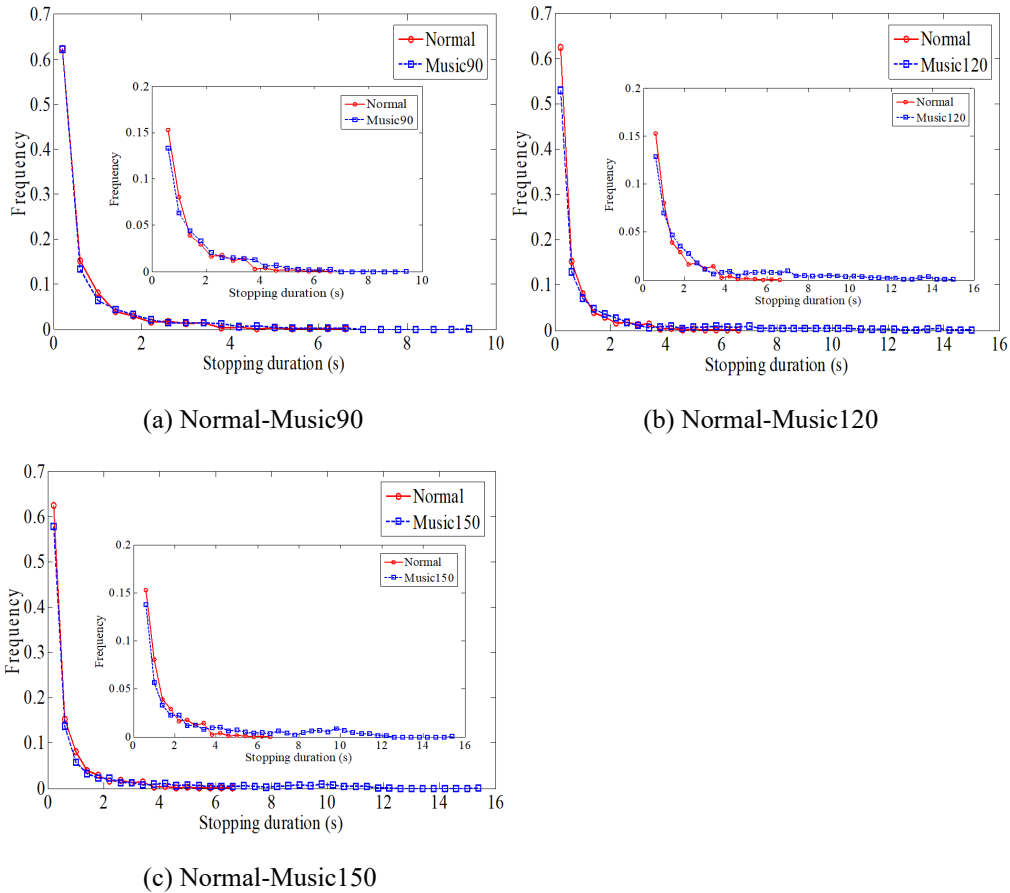


Fig.3: Distribution of stopping duration with rhythms and the normal condition. The inset shows the part of distribution longer than 0.4s.

Stopping headway and restarting headway are defined to analyze the reason for this behavior in more detail. The headway is the distance between the centers of a pedestrian and the frontal pedestrian. Stopping headway is the headway at the frame when pedestrians start to stop. Restarting headway is the headway at the frame when pedestrians start to move again. It shows that pedestrians start to stop at a bigger headway (F-test, $P < 0.001$) with rhythms. They also start to move after stopping at a bigger headway (F-test, $P < 0.001$) in Table 1. It is the reason for pedestrians stopping more frequently with rhythms and the longer stopping duration. The restarting headway with 90BPM rhythm is bigger than that without any rhythm, but less than that with higher tempo rhythms. This may explain the stopping duration increases with the increment of the tempo.

Table 1: Stopping headway and restarting headway with rhythms and without any rhythms

Condition	Stopping headway(m)	Restarting headway(m)
Normal	0.50±0.11	0.53±0.11
Music-90	0.51±0.10	0.54±0.10
Music-120	0.51±0.11	0.55±0.11
Music-150	0.51±0.11	0.56±0.12

3.2 Fundamental diagram

In this section, we will focus on the fundamental diagrams. The tendency of fundamental diagrams with rhythms and without any rhythms are similar(Fig.4). However, we can also find that velocity and flow with rhythms are lower than that without any rhythm at high densities. To make it more clearly, binning procedures[8, 9] are made by dividing density into intervals per 0.1/m from 0/m in Fig.6. Mean value and standard deviation in every interval are calculated. It shows that velocity and flow with rhythms are smaller than that without any rhythm at high densities. With rhythms, velocity and flow with 120BPM rhythm are less than that with other rhythms in high densities. Compared to mean value of velocity(per 0.1/m) at high densities(from 1.5/m to 2.1/m), it decreases 15%, 42% and 21% on average with 90BPM, 120BPM and 150BPM, respectively. The increase of stopping results in the decrease of velocity and flow at high densities.

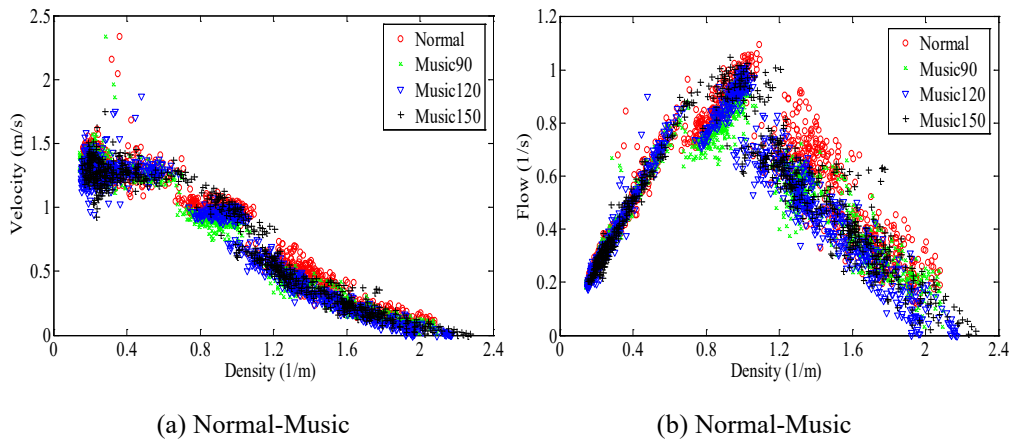


Fig.4: Fundamental diagrams with rhythms and without any rhythms

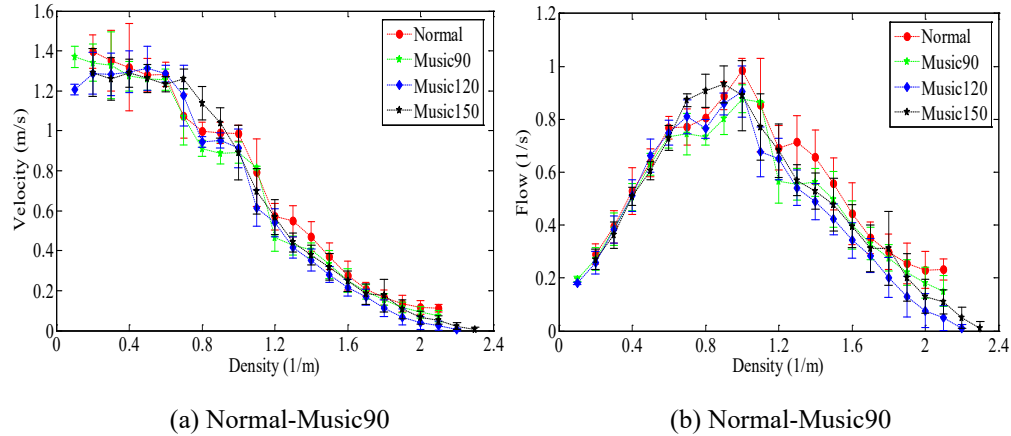


Fig.5: Binning procedures fundamental diagrams with rhythms and without any rhythm.

3.3 Stepping behavior

Stepping is the fundamental property of pedestrians. It can be used to explain the macroscopic properties, such as the fundamental diagram. Eight or ten pedestrians were selected to count the number of steps of each round for runs with 2, 10, 20 and 30 pedestrians with the videos of experiments. The step is roughly defined as the process of one foot touching the ground to the other touching the ground. Step length (sl) and step frequency (sf) are calculated as Equation 3.

$$sl = \frac{L}{SN}, \quad , \quad sf = \frac{T}{SN} \quad (3)$$

Here L means the length of the corridor, which is 21.93m. SN and T represent step number and

the time for these steps.

The results for step length and step frequency with rhythms and without any rhythms are shown in Table 2. It indicates that the step frequency with rhythms is slightly less than that without any rhythms except for that of the run with 20 pedestrians with 150BPM rhythm at low and medium densities. At high densities, the step frequency with rhythms decreases a lot compared to that without any rhythms. Lang et al.[11] found that music will weaken dynamic coordinated behavior, which results in finishing successive behavior with more time. Therefore, it can be explained that pedestrians need more time to step in the presence of music, especially at high densities.

Table 2: Step length and step frequency with rhythms and without any rhythms

Condition	Step length(m)	Step frequency(Hz)
Normal-2	0.74 ± 0.05	1.97 ± 0.10
Music90-2	0.73 ± 0.05	1.93 ± 0.08
Music120-2	0.73 ± 0.06	1.94 ± 0.09
Music150-2	0.76 ± 0.07	1.97 ± 0.09
Normal-10	0.68 ± 0.03	1.92 ± 0.08
Music90-10	0.66 ± 0.03	1.89 ± 0.07
Music120-10	0.68 ± 0.03	1.91 ± 0.08
Music150-10	0.67 ± 0.03	1.89 ± 0.07
Normal-20	0.58 ± 0.04	1.63 ± 0.10
Music90-20	0.56 ± 0.03	1.56 ± 0.07
Music120-20	0.60 ± 0.03	1.62 ± 0.09
Music150-20	0.60 ± 0.03	1.66 ± 0.09
Normal-30	0.38 ± 0.04	1.38 ± 0.15
Music90-30	0.36 ± 0.03	1.11 ± 0.11
Music120-30	0.39 ± 0.03	1.10 ± 0.11
Music150-30	0.38 ± 0.02	1.11 ± 0.08

4. Conclusion

To study the effect of background music on pedestrian movement, we conducted a series of single-file experiments. The trajectories were extracted by PeTrack[12]. With the trajectories, time-space diagrams and fundamental diagrams are analyzed.

Stop-and-go behavior appears apparently at global density 1.82/m with rhythms and without any rhythm. However, compared with pedestrian movement without any rhythm pedestrians stop more frequently with rhythms. Stopping duration will also be longer with rhythms and increases with the increment of the tempo.

With rhythms and without any rhythm, there is a similar tendency in fundamental diagrams. However, velocity and flow with rhythms are lower than that without any rhythms. The mean value of velocity (per 0.1/m) from 1.5/m to 2.1/m decrease 15%, 42%, and 21% on average for 90BPM, 120BPM and 150BPM rhythm, respectively. Stopping contributes to the decreasing of velocity and flow.

With rhythms, dynamic coordinated behavior of pedestrians will be weakened, which will increase pedestrian stepping time. Due to it, the velocity at low density is lower than that without any rhythms. With the increasing of density, pedestrians will also be influenced by the interaction with the

frontal pedestrians. Coupled with them, step frequency will decrease more quickly, which contributes to the sharp decrease of velocity and flow at high densities. When the step frequency cannot decrease any more, pedestrians will stop. This may explain that the stopping headway with rhythms is higher than that without any rhythms. The effect of rhythms will increase with the increment of tempo.

In the future, the stepping behavior needs to be investigated, which will be helpful for understanding the effect of background music more clearly.

Acknowledgement

The authors acknowledge the foundation support from Key Research and Development Program(2016YFC0802500), German Science Foundation (grant SCHA 636/9-1), the National Natural Science Foundation of China (Grant No. 71704168), the Anhui Provincial Natural Science Foundation (Grant No. 1808085MG217) and the Fundamental Research Funds for the Central Universities (Grant No. WK2320000040) and the China Scholarship Council(CSC).

Reference

- [1] D. Yanagisawa, A. Tomoeda, and K. Nishinari, "Improvement of pedestrian flow by slow rhythm," *Phys Rev E Stat Nonlin Soft Matter Phys*, vol. 85, p. 016111, 2012.
- [2] F. Styns, L. van Noorden, D. Moelants, and M. Leman, "Walking on music," *Hum Mov Sci*, vol. 26, pp. 769-85, 2007.
- [3] S. Ikeda, T. Nozawa, R. Yokoyama, A. Miyazaki, Y. Sasaki, K. Sakaki, *et al.*, "Steady Beat Sound Facilitates both Coordinated Group Walking and Inter-Subject Neural Synchrony," *Front Hum Neurosci*, vol. 11, p. 147, 2017.
- [4] M. Franek, L. van Noorden, and L. Rezny, "Tempo and walking speed with music in the urban context," *Front Psychol*, vol. 5, p. 1361, 2014.
- [5] C. Mendonca, M. Oliveira, L. Fontes, and J. Santos, "The effect of instruction to synchronize over step frequency while walking with auditory cues on a treadmill," *Hum Mov Sci*, vol. 33, pp. 33-42, 2014.
- [6] E. Sejdic, B. Findlay, C. Merey, and T. Chau, "The effects of listening to music or viewing television on human gait," *Comput Biol Med*, vol. 43, pp. 1497-501, 2013.
- [7] A. Seyfried, B. Steffen, W. Klingsch, and M. Boltes, "The fundamental diagram of pedestrian movement revisited," *Journal of Statistical Mechanics: Theory and Experiment*, vol. 2005, pp. P10002-P10002, 2005.
- [8] A. Jelic, C. Appert-Rolland, S. Lemerrier, and J. Pettre, "Properties of pedestrians walking in line: fundamental diagrams," *Phys Rev E Stat Nonlin Soft Matter Phys*, vol. 85, p. 036111, 2012.
- [9] S. Cao, J. Zhang, D. Salden, J. Ma, C. Shi, and R. Zhang, "Pedestrian dynamics in single-file movement of crowd with different age compositions," *Phys Rev E*, vol. 94, p. 012312, 2016.
- [10] G. Zeng, A. Schadschneider, J. Zhang, S. Wei, W. Song, and R. Ba, "Experimental study on the effect of background music on pedestrian movement at high density," *Physics Letters A*.
- [11] M. Lang, D. J. Shaw, P. Reddish, S. Wallot, P. Mitkidis, and D. Xygalatas, "Lost in the Rhythm: Effects of Rhythm on Subsequent Interpersonal Coordination," *Cogn Sci*, vol. 40, pp. 1797-1815, 2016.
- [12] M. Boltes and A. Seyfried, "Collecting pedestrian trajectories," *Neurocomputing*, vol. 100, pp. 127-133, 2013.

Can we learn where people go?

Marion Gödel^{1,2}, Gerta Köster¹, Daniel Lehmborg^{1,2}, Manfred Gruber¹, Angelika Kneidl³,
Florian Sesser³

¹Munich University of Applied Sciences
Lothstrasse 64, 80335 Munich, Germany

Marion.Goedel@hm.edu, Gerta.Koester@hm.edu, Daniel.Lehmborg@hm.edu,
Manfred.Gruber@lrz.fh-muenchen.de

²Technical University of Munich,
Boltzmannstrasse 6, Munich, Germany

³accu:rate GmbH Institute for crowd simulation
Rosental 5, 80331 Munich, Germany
ak@accu-rate.de, fs@accu-rate.de

Abstract – In most agent-based simulators, pedestrians navigate from origins to destinations. Consequently, destinations are essential input parameters to the simulation. While many other relevant parameters as positions, speeds and densities can be obtained from sensors, like cameras, destinations cannot be observed directly. Our research question is: Can we obtain this information from video data using machine learning methods? We use density heatmaps, which indicate the pedestrian density within a given camera cutout, as input to predict the destination distributions. For our proof of concept, we train a Random Forest predictor on an exemplary data set generated with the Vadere microscopic simulator. The scenario is a crossroad where pedestrians can head left, straight or right. In addition, we gain first insights on suitable placement of the camera. The results motivate an in-depth analysis of the methodology.

Keywords: (4-8) pedestrian dynamics, predictive simulation, machine learning, random forest

1. Introduction

It is a shared goal of crowd simulation experts to look into the future for at least a few minutes to predict dangers like extremely high densities that might evolve. State-of-the-art microscopic models are, in principle, capable of producing correct crowd flows in many relevant situations, provided they get correct input parameters. The basic idea of predictive crowd analysis is to gather these input parameters online from sensors. Many relevant parameters, like positions, speeds and densities can be obtained from cameras, even if the speed and accuracy with which the data is acquired may be insufficient for prediction at the moment. However, some essential input parameters cannot be observed directly: chief among them are destinations where people go.

Agent-based microscopic crowd simulations use destinations to navigate pedestrians. This holds especially for all simulations based on a floor field. The floor field indicates for each position of the scenario the distance to the destination(s). As a consequence, destinations are a crucial input parameter for the simulation. Nevertheless, in reality destinations are often unknown. They need to be chosen according to experience or statistics. In addition, a previous study has shown that the destinations of pedestrians have a high impact on the simulation output [1].

This work is performed in the context of the S²UCRE research project (www.s2ucre.de). The goal of the project is to set up a control cycle that performs short-term predictions which are continuously compared to the latest video footage. Every time the simulation is started, a destination needs to be assigned to each pedestrian.

To our knowledge, currently only very few publications are available on retrieving information about pedestrian's destinations [2]. In practical applications of pedestrian simulations, there are several ways to

assign the destinations: First, for simulations of evacuation scenarios, known gathering points, emergency exits or simply the closest exit can be chosen. Second, for festivals or events as well as museums and infrastructural buildings, destinations can be assigned based on experience of the organizer, timetables or visitor surveys. Unfortunately, none of these approaches is reliable enough to establish quantitative alignment within a control cycle.

Pedestrian density heatmaps will be available at a later stage of the S²UCRE project as an input to the simulation. In addition, methods of density estimation, the derivation of heatmaps from video footage is expected to become state-of-the-art at some point [3]. That is why we use heatmaps as a basis. Our goal is to extract information about pedestrians' destinations from such heatmaps deploying machine learning techniques. In fact, the research question is: Is there enough information in the heatmaps to predict the distribution of destinations?

Machine learning has become very popular over the last years. There are first approaches to apply machine learning models in the context of pedestrian dynamics. The applications range from crowd counting and density estimation [3] to the prediction of pedestrian movement [4]. Furthermore, destination prediction aims to predict the destinations of people of a certain audience based on trajectories and prior knowledge of possible destinations [5,6]. In our case, the destinations are predicted solely based on a dataset of density heatmaps and our knowledge about possible destinations. We do not utilize user-dependent data.

Our solution proposal for destination prediction is data-driven. That means deploying information from videos or other sources for simulation. This ansatz has already been employed for traffic dynamics. There are two main approaches of data-driven modelling: First, deriving a model from a data set instead of using an equation or rule-based model. Second, complementing existing rule-based models with parameters derived from videos. For the former, [7-11] are of particular interest in our context. The latter was carried out in [12] together with the Social Force Model. In our application, we want to predict macroscopic traffic quantities, such as density and flow, through simulations with an explanatory microscopic model, the Optimal Steps Model [13,14]. The simulation is complemented with parameter learning for the destination distributions from video footage.

For a proof of concept, we will use heatmaps generated from simulations using the simulation framework Vadere [15] instead of actual video footage. We focus on scenarios that appear relevant in the context of the research project S²UCRE. More specifically, we analyse a crossroad in a pedestrian area. A Random Forest predictor is trained on the snapshots to predict decision distributions at the crossroad.

2. Methods and Configuration

Our simulations are performed using the Optimal Steps Model within the Vadere framework. The choice of the next step consists of three parts: First, for each destination a floor field which indicates the distance towards the destination is calculated. Second, at every time step and for each pedestrian repulsion from obstacles and other pedestrians is added to the static floor field. Thus, the ensuing floor field codes negative utility, or cost, of a position. Third, agents find the best next position with respect to the floor field within a circle of their step lengths. A detailed description can be found in [14]. This procedure for choosing the next step explains why targets are a crucial input parameter.

We chose Random Forest [16] as machine learning algorithm to predict the destination distribution based on the density heatmap. A Random Forest is a collection of decision trees whose results are aggregated into one final result. Random Forest is known to be a robust algorithm and easy to apply as there are only few tuning parameters [16,17]. Furthermore, it can be used directly for high-dimensional problems. In addition, Random Forest often works well without heavy tuning of parameters [18].

This study is conducted using the Python implementation provided by scikit-learn [19]. Computations are performed on a platform with an Intel(R) Xeon X5672 CPU with 3.20GHz 4 Cores and 16 GB DDR3 RAM.

In the following, we describe our configuration to adapt the methods for the chosen problem.

2.1. Scenario

A simple, symmetric scenario is chosen for the proof of concept. See Fig. 1. The pedestrians walk from an origin to one of three destinations (left / straight /right). The camera cutout used as baseline for the heatmap generation is shown in red. For an arbitrary time step, the positions of the pedestrians are indicated in blue. In addition, the trajectories for all pedestrians in the scenario at the chosen time step are shown. The scenario only serves to simulate the trajectories, which are used to generate the heatmaps and derive the corresponding destination distribution.

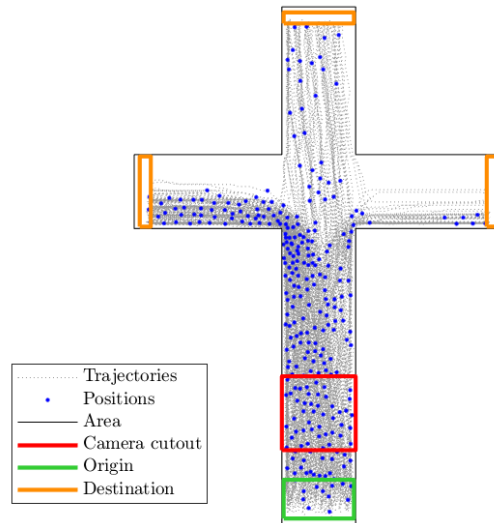


Fig. 1: Scenario for the proof of concept. Pedestrians (blue) walk from an origin (green) to one of three destinations (orange). The camera cutout is indicated in red.

2.2. Density heatmaps

The heatmaps are generated from a set of positions for each time step for a defined camera cutout. At an arbitrary time step, there are n pedestrians at positions x_i located within the cutout. The Gaussian density at position z is calculated as

$$D_p(z) = \frac{d_p^2 \sqrt{3}}{4\pi S^2} \sum_{i=1}^n \exp\left(-\frac{\|x_i - z\|^2}{2S^2}\right) \quad (1)$$

with torso diameter $d_p = 0.195$ m for each pedestrian and scale factor $S = 0.7$ [13,20]. In Fig. 2 a set of five consecutive density heatmaps is shown.

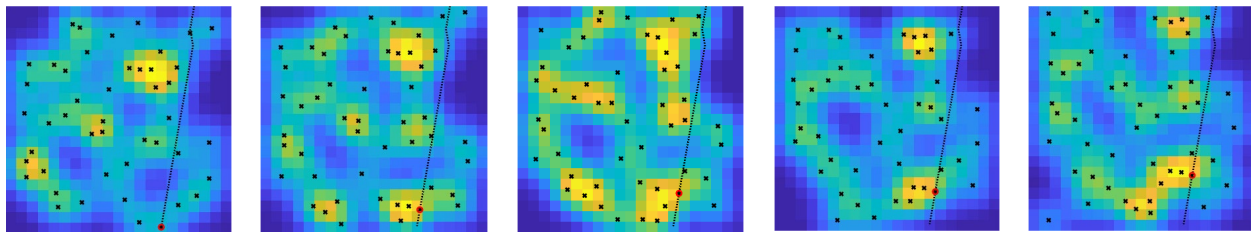


Fig. 2: Five consecutive density heatmaps for a camera cutout of 10x10 m with a resolution of 0.5 m. Pedestrian positions are indicated as black crosses. For one exemplary pedestrian the trajectory is shown as dotted line.

2.3. Configuration of Random Forest

The actual density values describing the two-dimensional heatmaps are rearranged to a vector (row-wise). The combination of one vector and the corresponding destination distribution forms a sample for the Random Forest model. As a consequence, each pixel value in the heatmap serves as a feature. Table 1 shows the response corresponding to the samples visualized in Fig. 2. The response are the percentages of pedestrians within the cutout heading in the three directions. One can see that the heatmaps differ significantly even though the distribution of the pedestrians on the destinations varies only slightly. As a result, one cannot simply derive the destination distribution by looking at a heatmap.

Table 1: Response for Random Forest: Actual percentage of pedestrians heading left (L), straight (S) and right (R).

Percentage of pedestrians heading			Percentage of pedestrians heading			Percentage of pedestrians heading			Percentage of pedestrians heading			Percentage of pedestrians heading		
L	S	R	L	S	R	L	S	R	L	S	R	L	S	R
28.3	39.1	32.6	28.0	40.0	32.0	32.0	38.0	30.0	32.6	41.3	26.1	32.0	40.0	28.0

The problem is posed as a multi-dimensional regression problem. The number of response dimensions is the number of identified destinations. In the considered crossroad scenario, there are three destinations. The advantage of this configuration compared to a classification problem is twofold: First, the responses are not a finite set of classes but continuous between zero and one. Consequently, one would have to design classes that are small enough for the application and large enough to contain enough samples in order to use classification. Second, applying a regression, Random Forest can predict destination distributions that were not part of the training set. The drawback of a multi-dimensional response configuration is that the destination distributions do not necessarily add up to 100%. We overcome this problem by normalizing the model predictions.

2.4. Performance measure

The Random Forest routines can provide an out of bag error estimate as well as the coefficient of determination. However, both quantities are applied before the model predictions are normalized. Therefore, we split our dataset into a training and a test set and compare the prediction on the test set to the corresponding response to evaluate the model. In a first step, we evaluate the Euclidean norm of the difference vector. In the second step, we derive a relative error. Since we normalize the prediction, the maximum error

$$e_{max} = \sqrt{2 \cdot 100^2} \approx 141.42 \quad . \quad (2)$$

occurs if we predict that all pedestrians within the cutout head left while, in fact, they head right (or straight): The relative error is then

$$e = \frac{y - \hat{y}}{e_{max}} \cdot 100 \quad , \quad (3)$$

where y is the response on the test set and \hat{y} is the prediction on the test set. Thereby we obtain a relative error of the prediction that is easy to interpret. Thus, the relative error is used as a measure.

3. Results and Discussion

We predict the percentage of pedestrians heading in three directions: left, straight and right. The scenario used for the simulation is shown in Fig. 1. The simulation serves as a basis for the heatmap generation. All results are obtained using the same data set of simulations described in the following. The heatmaps are generated from 50 simulation runs, each of 500 seconds, performed with Vadere. The first

12 seconds are cut off in order to let the system settle and to observe a well filled camera cutout. In total, we obtain 3050 heatmaps. The available dataset is split into a training set (80%) and a test set (20%).

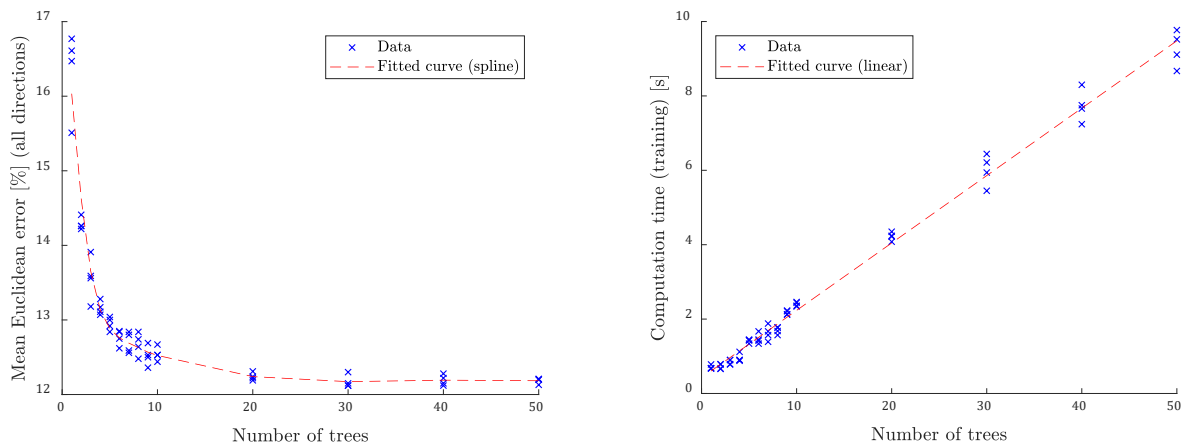
Each pedestrian in the simulation is randomly assigned one of the three destinations according to the current destination distribution. The destination distribution is altered with the generation of every 100th pedestrian. Thus, we make sure that a variety of destination distributions is considered. For each direction, we train one separate Random Forest model. In principal, Random Forest can handle multi-variable responses, but, with separate models, we observe an improvement over using one model that predicts all directions.

The goal of this paper is to offer a proof of concept that one can indeed extract information about destinations from the density heatmaps. As preparation for practical application on real video data, we vary the size and position of the camera cutout and analyse the impact on the accuracy and on computation time.

3.1. Proof of concept

The camera cutout is placed as shown in Fig. 1. Its dimensions are 10 meters \times 10 meters. The resolution of the heatmaps is set to 0.5 meters. Consequently, the heatmaps consist of 20×20 pixels. The correlation between the heatmaps is minimized by choosing a framerate corresponding to the time that pedestrians need to pass the camera cutout. Since the camera cutout is of length 10 meters and the mean free-flow velocity is 1.34 m/s, pedestrians need roughly 7.46 seconds to cross it. Thus, we choose a frame rate of 0.05 Hz, that is, one heatmap every eight seconds. Therefore, a pedestrian is typically considered in only one heatmap.

Fig. 3 shows the performance and computation time in dependency of the number of trees per model. The computation time increases linearly with increasing number of trees while the Euclidean error decreases up to roughly 20 trees. As a result, we use 20 trees for the proof of concept. We perform the split of training and test set, as well as training and test of the Random Forest predictor five times. We obtain a mean Euclidean error of 12.24% and standard deviation 6.93%. Thus, the method is able to predict where people are heading at the crossing with an accuracy of roughly 88%. The average computation time to train the forests is 4.28 seconds.



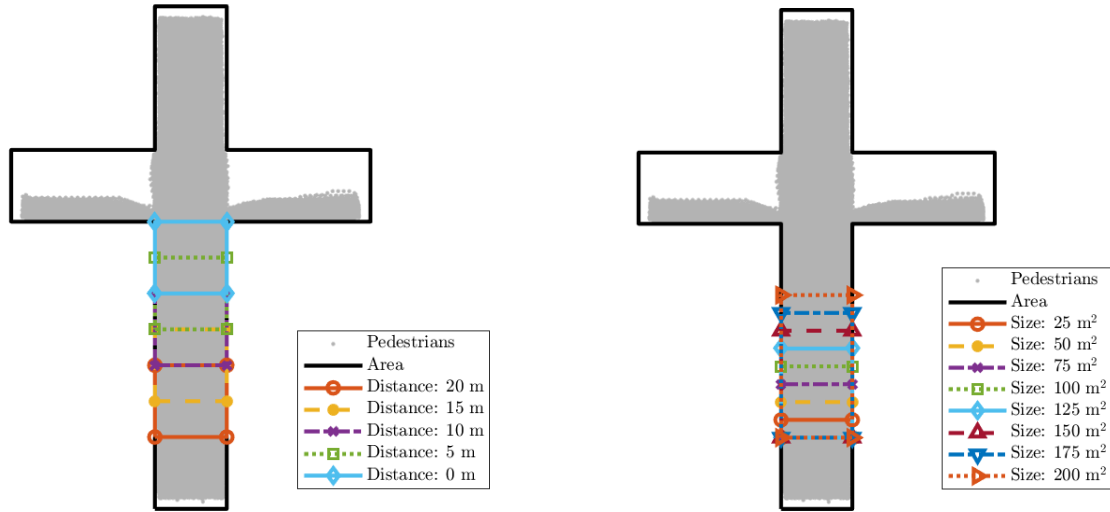
(a) Mean Euclidean error of the prediction on the test set.

(b) Computation time necessary to train the forest.

Fig. 3: Results of Random Forest for different numbers of trees per forest.

3.2. Placement of the camera cutout

Since the proof of concept was successful, we take a closer look at the parameters. One vital parameter for the application of the method on real video footage is camera placement. First, we vary the distance of the camera cutout to the crossing and analyse the impact on the quality of the prediction. Figure 4 (a) shows the varied positions of the camera cutout. In the second step, we analyse the impact of the size of the camera cutout on the predictions. We limit ourselves to cutouts that cover the whole width of the street. Fig. 4 (b) shows eight sizes used for the analysis.



(a) Position of the camera cutout in the corridor.

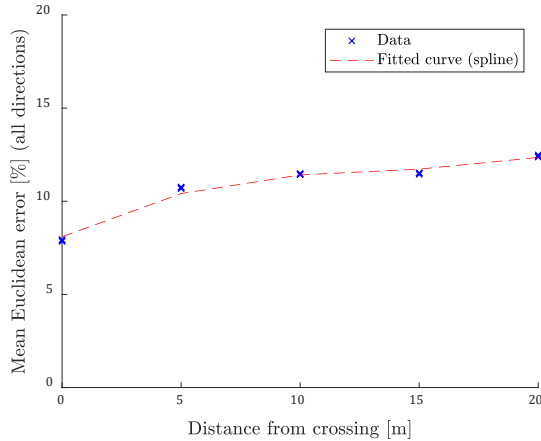
(b) Size of the camera cutout.

Fig. 4: Variation of the camera cutout.

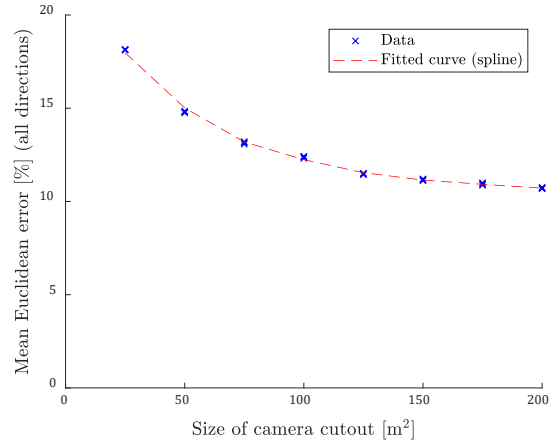
Fig. 5 (a) shows the mean Euclidean error in dependency of the position of the camera cutout. The positions are defined by the distance of the upper edge of the cutout to the lower position of the crossing. We observe that the quality of the prediction only slightly increases when placing the camera cutout closer to the crossing. Thus, the camera does not have to be placed directly in front of the crossing for a sound prediction. That is a big advantage for the practical application, since camera positions are often determined by the space where equipment can be mounted. Also, monitoring an area further away from the crossing, gives us the necessary time frame for the prediction.

In Fig. 5 (b) the results for different sizes of the camera cutouts are depicted. Since the number of features increases with the size of the cutout, the computation time increases as well. We observe a linear increase. The results reveal that the quality of the prediction is highly dependent on the size of the camera cutout. Therefore, in this scenario, the camera cutout should cover at least 75 m². This size yields a mean Euclidean error of 13.15%. Nevertheless, one has to keep in mind that these results are based on simulated heatmaps not on actual video footage.

Besides the insights that we have gained on the impact of the placement of the camera, both variations also serve as plausibility checks. As expected, the quality of the prediction increases both with placing the camera cutout closer to the crossing and with increasing the size of the camera cutout. In combination with alignment between two independent implementations, this verifies our code.



(a) Different positions of the camera cutouts.



(b) Different sizes of the camera cutout.

Fig. 5: Performance of Random Forest for different camera cutouts. The position represented by the distance of the upper edge of the cutout to the lower position of the crossing. For each position and for each size, five runs were performed.

4. Conclusion and Outlook

In this publication, we deliver a proof of concept for configuring a machine learning method to obtain the destinations of pedestrians based on density heatmaps. It was carried out based on a data set of pedestrians' trajectories generated with our simulation framework Vadere. The chosen method (Random Forest) is able to predict the distribution of pedestrians on destinations with an accuracy of up to 90%. In addition, we performed plausibility checks by modifying the size and position of the camera cutout. Coincidentally, we gained insight on the impact of the camera placement: While the position of the camera cutout within the street seems to have little effect, the size of the camera cutout has a significant influence on the quality of the prediction. Consequently, the camera cutout should be chosen as large as possible. In both cases, the camera cutout was selected such that the whole width of the street is covered.

These first results show that the methodology has great potential. We plan to further investigate the approach. In the next step, one could adapt the method to different scenarios to analyse the robustness of the technique. In addition, one needs to study the effect of parameters such as the number of pedestrians in the scenario. Also, we did not exploit the time dependency of adjoining snapshots in this contribution. We expect the prediction quality to profit from adding a time component to the input data. One approach is to use a group of heatmaps instead of a single heatmap. Furthermore, while Random Forest has proven to be robust in this scenario, there are many other machine-learning algorithms. In particular, Convolutional Neural Networks are able to process images as the density heatmaps directly as input and might be able to exploit the topological information. Finally, the main goal is to adapt the methodology for the application on real video footage.

Acknowledgements

The authors would like to thank the students who have carried out first investigations within a project study at Munich University of Applied Sciences: Julian Bauer, Rebecca Brydon, Patrick Gabler, Katja Gruenewald, Lisa-Marie Grundmann, Hubert Hager, Sebastian Klohn, Carsten Kruse, Tim Lauster, Julia Maier, Sarah Nesner, Do Nhu Nguyen, Luca Spataro, Anita Steinberger, Veronika Zwickenpflug. This work was funded by the German Federal Ministry of Education and Research through the project S2UCRE (grant number 13N14464). The authors acknowledge the support by the Faculty Graduate Center CeDoSIA of TUM Graduate School at Technical University of Munich and the research office FORWIN at Munich University of Applied Sciences.

References

- [1] M. Davidich and G. Köster, “Predicting Pedestrian Flow: A Methodology and a Proof of Concept Based on Real-Life Data,” *PLoS ONE*, vol. 8, no. 12, pp. 1-11, 2003.
- [2] P. M. Kielar, A. Borrmann, “Modeling pedestrians' interest in locations: A concept to improve simulations of pedestrian destination choice,” *Simulation Modelling Practice and Theory*, vol. 61, pp. 47-62, 2016.
- [3] V. A. Sindagi and V.M. Patel, “A Survey of Recent Advances in CNN-based Single Image Crowd Counting and Density Estimation,” *Pattern Recognition Letters*, vol. 107, pp. 3-16, 2018.
- [4] Y. Ma, E. W. M. Lee and R. K. K. Yuen, "An Artificial Intelligence-Based Approach for Simulating Pedestrian Movement," in *IEEE Transactions on Intelligent Transportation Systems*, vol. 17, no. 11, pp. 3159-3170, 2016.
- [5] J. Krumm and e. Horvitz, “Predestination: Inferring destinations from partial trajectories,” in *Proceedings of the 8th International Conference on Ubiquitous Computing UbiComp '06*, pp. 243-260, 2006.
- [6] J. K. Laurila et al., “The mobile data challenge: Big data for mobile computing research,” in *Proceedings of the Workshop on the Nokia Mobile Data Challenge, in Conjunction with the 10th International Conference on Pervasive Computing*, p. 1-8, 2012.
- [7] A. Bera, S. Kim, D. Manocha, “Online parameter learning for data-driven crowd simulation and content generation,” *Computers and Graphics (Pergamon)*, vol. 55, pp. 68-79, 2016.
- [8] N. Bisagno, N. Conci, B. Zhang, “Data-Driven crowd simulation”, in *14th IEEE International Conference on Advanced Video and Signal Based Surveillance*, Lecce, Italy, 2017, pp.
- [9] F. Dietrich, “Data-Driven Surrogate Models for Dynamical Systems”, Ph. D. dissertation, Dept. Scientific Computing, Technical University of Munich, Germany.
- [10] S. Kim et al., “Interactive and adaptive data-driven crowd simulation,” in *Proceedings of IEEE Virtual Reality*, Greenville, SC, 2016, pp. 29-38.
- [11] J. Porzycki et al., “Dynamic data-driven simulation of pedestrian movement with automatic validation,” in *Traffic and Granular Flow '13*, Jülich, Germany, 2013, pp. 129-136.
- [12] B. Liu et al., “A social force evacuation model driven by video data,” *Simulation Modelling Practice and Theory*, vol. 84, pp. 190-203, 2018.
- [13] M. J. Seitz and G. Köster, “Natural discretization of pedestrian movement in continuous space,” *Physical Review E*, vol. 86, no. 4, 2012.
- [14] I. von Sivers and G. Köster, “Dynamic Stride Length Adaptation According to Utility and Personal Space”, *Transportation Research Part B: Methodological*, vol. 75, pp. 104-117, 2015.
- [15] Vadere Crowd Simulation (2016) [Online]. Available: <https://gitlab.lrz.de/vadere/vadere>
- [16] L. Breiman, “Random Forests,” *Machine Learning*, vol. 45, no. 1, pp. 5-32, 2001.
- [17] A. Cutler, D.R. Cutler, J.R. Stevens, “Random Forests” in *Ensemble Machine Learning*, C. Zhang, Y. Ma, Ed. Boston, 2012, pp. 157-175.
- [18] A. C. Müller and S. Guido, „Introduction to Machine Learning with Python – A Guide for Data Scientists”, O’Reilly Media, Inc., 2017, p.89.
- [19] F. Pedregosa et al., “Scikit-learn: Machine Learning in Python,” *Journal of Machine Learning Research*, vol. 12, pp. 2825-2830, 2011.
- [20] D. Helbing, A. Johansson, H. Z. Al-Abideen, “Dynamics of crowd disasters: An empirical study,” *Physical Review E*, vol. 75, no. 4, 2007.

Evacuation Data from a Hospital Outpatient Drill The Case Study of North Shore Hospital

Anass Rahouti¹, Ruggiero Lovreglio², Phil Jackson³, Sélim Datoussaïd⁴

^{1,4}Faculty of Engineering / UMONS
Place du Parc 20, Mons, Belgium
anass.rahouti@umons.ac.be

²School of Built Environment / Massey University
Auckland, New Zealand

³Waitemata District Health Board / WDHB
Auckland, New Zealand

Abstract – Assessing the fire safety of buildings is fundamental to reduce the impact of this threat on their occupants. Such an assessment can be done by combining existing models and existing knowledge on how occupants behave during fires. Although many studies have been carried out for several types of built environment, only few of those investigate healthcare facilities and hospitals.

In this study, we present a new behavioural data-set for hospital evacuations. The data was collected from the North Shore Hospital in Auckland (NZ) during an unannounced drill carried out in May 2017. This drill was recorded using CCTV and those videos are analysed to generate new evacuation model inputs for hospital scenarios. We collected pre-movement times, exit choices and total evacuation times for each evacuee. Moreover, we estimated pre-movement time distributions for both staff members and patients. Finally, we qualitatively investigated the evacuee actions of patients and staff members to study their interaction during the drill. The results show that participants were often independent from staff actions with a majority able to make their own decision.

Keywords: Hospital Evacuation, Human Behaviour, Pre-evacuation, Unannounced Evacuation Drill.

1. Introduction

Many egress models have been developed in the recent decades and they are used worldwide to assess the fire safety of buildings. To date, egress model users need to specify input values such as pre-evacuation times, evacuee speeds and evacuee actions, to define an evacuation scenario depending on the occupancy of the building. This is done by selecting those values from existing databases, when available, (see for instance [1-3]) or by making reasonable assumptions. Evacuation data is therefore needed to model and simulate occupants' behaviour [4, 5] as well as to validate existing and new evacuation models [6, 7].

Many drills have been carried out in a wide range of building types, such as schools, apartments, stores and cinemas to collect egress data (reader can refer to [1] for a comprehensive list of those drills). However, only few studies investigated healthcare facilities and hospitals. Moreover, existing studies, carried out in healthcare environments, have been mainly conducted to evaluate the movement data such as evacuee walking speeds in horizontal planes [8-9] and in stairways [9-12]. Only two studies [13, 14] have been carried out to quantify the pre-movement times and evacuees' behaviours in case of an emergency happens in such buildings. For example, the study by Gwynne *et al.* [13] performed at a Londoner hospital outpatients' facility which showed that in a hospital the onus is really on staff members. In fact, it was found that the patients observed and studied the staff members actions and made decisions based on their perception. One of the social behaviours that was observed in this study is that patients only evacuated once a figure of authority had instructed them to do so. Later, Folk *et al.* [14] conducted an announced fire drill at a retirement home in Canada. They attempted to develop a baseline for the behaviour and actions of elderly people during pre-movement and travel phases of the engineering

evacuation timeline model [1]. They observed through this study that some residents exhibited information seeking behaviours, either exiting their rooms or opening their room doors to observe the situation. It was also shown that the residents were dependent on staff members. Even the residents who were fully ambulant did not evacuate until a staff member went to their room, prompted them to leave, and walked with them to the fire doors.

The goal of this paper is to expand existing data on hospital evacuation by analysing evacuee behaviours during an unannounced evacuation drill recorded using the closed-circuit television (CCTV) videos. The drill was carried out in one of hospital outpatients' areas of the North Shore Hospital in New Zealand (see Fig. 1 and 2) and it involved 55 evacuees. Two participants had disabilities: a wheelchair user and a patient with a walking stick. A behavioural analysis was performed to study evacuees' decision-making and behaviours. Moreover, different quantitative measurements were also made by analysing those videos such as pre-movement times, exit choices and total evacuation times. Finally, we propose new pre-evacuation distributions and compare them with the existing data provided in [13].



Fig. 1 – CCTV shot showing evacuees in the corridor and main waiting room



Fig. 2 – CCTV shot showing evacuees targeting the main exit

2. Experimental Methods

The drill was part of the routine evacuation drills conducted twice a year at the hospital according to NZ regulations [15]. This drill was unannounced and involved both staff members and patients. There were two classes of staff members: the staff who had a procedural role and the staff who had not. Staff members with a procedural role swept each of the rooms, forcing the occupants to leave the building and informed them of the path they should follow. It should be noted that the patients were in majority capable of evacuating the building without any help from the staff. Only about 4% of patients with disabilities were involved into the drill. In general, patients took part into the drill in the same manner as other participants excepting those who needed for assistance. Upon the completion of the drill, video images were analysed, frame by frame, using a video software (i.e. using Avidemux) and results were transcribed onto a spreadsheet file (i.e. using Excel).

Approval was obtained from Waitemata District Health Board (WDHB) committee to analyse the CCTV recordings of an evacuation drill held in May 2017. The drill was carried out in the outpatients' area of the hospital. This area extends over three floors and is currently used for a variety of purposes. However, only the ground floor is accessible to the patients. The upper floors include offices, stores, kitchens and teaching rooms allocated to the University of Auckland and for administrative purposes. Fig. 3 shows the configuration of the ground floor. This floor houses mostly clinic rooms, staff offices and waiting areas and has three exit points: the main exit (Exit A in Fig. 3) and the emergency exits (Exits B and C in Fig. 3), while the upper floors have two emergency exits (the staircases in Fig. 3).

Eight CCTV cameras were used to collect data relating to the starting position of evacuees, their actions, their pre-evacuation times, their exit choices and their total evacuation times. These cameras are permanently located throughout the building at each final exit, waiting rooms and corridors (see Fig. 3 for their locations) and are normally used for security issues. Given the permanent positions of those cameras with a majority not located within rooms (excepting the one located in the main waiting room), the

pre-movement time of evacuee is defined as the time from the beginning of the alarm signal to the time the person left the applicable room. This approach is consistent with previous studies such as [16], [17], [18] and [19].



Fig. 3: building configuration, CCTV cameras and exits locations

3. Results

3.1. Pre-movement time

For the analysis of pre-movement time, a subset of total population (i.e. 55 evacuees) could not be investigated because their initial positions were not covered by the surveillance system as those cameras are located only on the ground floor. In total 30 pre-evacuation times were measured from the drill: 14 staff members and 16 patients. The pre-movement times of the observed population are categorised according to the different areas: main waiting room, sub-waiting room, pathology area, lift lobby area and corridor area as reported in Table 1.

Table 1: Pre-evacuation times in seconds for the staff members and the patients

Area	Staff		Patients		All	
	Mean (St Dev)	Range (Sample size)	Mean (St Dev)	Range (Sample size)	Mean (St Dev)	Range (Sample size)
Main Waiting Room	63.6 (29.0)	25.0 - 95.0 (5)	36.1 (10.2)	22.0 - 52.0 (9)	45.9 (22.6)	22.0 - 95.0 (14)
Sub-Waiting Room	12.0*	12.0 - 12.0 (1)	33.0*	33.0 - 33.0 (1)	22.5 (14.8)	12.0 - 33.0 (2)
Pathology	34.0 (24.0)	17.0 - 51.0 (2)	57.5 (7.8)	52.0 - 63.0 (2)	45.8 (19.9)	17.0 - 63.0 (4)
Lift Lobby	12.0*	12.0 - 12.0 (1)	NA	NA	12.0*	12.0 - 12.0 (1)
Corridor	49.8 (21.3)	33.0 - 87.0 (5)	17.5 (11.3)	7.0 - 33.0 (4)	35.4 (23.8)	7.0 - 87.0 (9)
All	47.1 (27.7)	12.0 - 95.0 (14)	33.9 (15.3)	7.0 - 63.0 (16)	40.1 (22.6)	7.0 - 95.0 (30)

*Using the formula $\sqrt{\frac{\sum (x-\bar{x})^2}{(n-1)}}$ for the standard deviation of a sample, it is not possible to obtain a numerical value for only one participant

NA means no patient was in this area

There were seven patients in the “main waiting room” when the alarm signal was sounded. The video recordings showed that those patients started to seek information by looking around and at the staff members. However, none of them evacuated prior to being instructed to do so. These observations are consistent with the studies [13] and [14]. Two other patients evacuated from adjacent clinic rooms without necessarily being dependent upon the staff actions. The average patient pre-evacuation time observed was 36.1 seconds, while the average staff pre-evacuation time observed was 63.6 seconds. At the beginning of the drill, there was only a staff member in the main waiting area. Despite their presence, no instruction was given to the patients present there to evacuate before seeing other people leaving the building. From the video footage, it was apparent that the average staff pre-evacuation time was increased by the late evacuation of two fire wardens who swept the areas of the building to encourage individuals to evacuate. Also, due to the presence of a few vulnerable people, some staff members showed an assisting behaviour (e.g., helping an elderly to rise or assisting a wheelchair user to leave the building) which increased the average staff pre-evacuation time.

Two occupants were initially in the “sub-waiting room”: one patient and one staff member. The staff member was in an adjacent clinic room to this area. S/He started the evacuation after 12 seconds, whereas the patient started the evacuation after being instructed to do so by a fire warden who appeared into the area after 20 seconds. Hence, the average patient pre-evacuation time observed was 33 seconds while the average staff pre-evacuation time observed was 12 seconds.

There were four participants in the “pathology area”: two staff members and two patients. The average staff pre-evacuation time was 34 seconds while the average patient pre-evacuation time was 57.5 seconds. After 57 seconds, a fire warden appeared in the area but he did not see the patient who was not in her/his field of view. Hence, the presence of the fire warden in this area had no impact on reducing the pre-movement time of the patient.

Only one staff member was in the “lift lobby area”. S/He took 12 seconds to start the evacuation.

There were 5 staff members and 4 patients in the “corridor area”. The staff members were seen to act after 2 seconds (e.g., searching for their warden vest). However, the first one started to evacuate only after 33 seconds when being sure that no patient is still in the area. The mean staff pre-evacuation time

observed was 49.8 seconds, while the mean patient pre-evacuation time was 17.5 seconds. The mean staff pre-evacuation time was increased by the late evacuation of some staff members who did not have a procedural role. Some of them waited in the corridor and started to move only after being instructed to do so by a colleague. Other staff members stayed at their room (e.g. clinical room or office) until they have been notified by another staff member. Another staff member who had a procedural role (i.e., a fire warden), started to evacuate only after 95 seconds.

3.2. Exits usage

Table 2 reports the exits used by staff members and patients during the drill as well as their initial positions and the closest exits to their initial positions. The reader can refer to Fig. 3 to locate each of the positions. It can be seen from Table 2 that all evacuees (i.e. 30 occupants) inside the ground floor evacuated through the main entrance (i.e. Exit A), the same door which they walked in, even those who were close to the emergency exits (18% of the participants), while all participants who were inside the first floor (i.e. 25 occupants) evacuated through the staff entrance (i.e. Exit B). The exit routes were therefore the normal routes for the evacuees. It seems that occupants were guided by familiarity. To be more efficient, staff members should familiarise themselves with the use of alternative exits.

Table 2: Exits usage

Initial Positions	Closest exits	Staff	Exits Used	Patient	Exits Used
ADMIN	Exit A	2	Exit A	1	Exit A
VAccWC	Exit A	-	-	1	Exit A
MW	Exit A	1	Exit A	7	Exit A
NS020	Exit A	2	Exit A	-	-
SW058	Exit B	-	-	2	Exit A
SW032	Exit C	-	-	1	Exit A
R016	Exit B	1	Exit A	-	-
CR023	Exit C	1	Exit A	-	-
CR044	Exit C	1	Exit A	-	-
CR048	Exit A	1	Exit A	-	-
CR050	Exit B	2	Exit A	-	-
CR056	Exit B	1	Exit A	1	Exit A
CR060	Exit B	1	Exit A	1	Exit A
CR064	Exit B	1	Exit A	2	Exit A
1stLevel	Exit B or C	25	Exit B	-	-

3.3. Evacuation curve and exits flow rate

Fig. 4 shows the relation between the number of evacuees and arrival time for all the occupants, including the fire wardens who were last to leave the building. The reader should be aware that the arrival time is the sum of the pre-movement time and travel time. This means, that it doesn't include the detection and warning times of the engineering evacuation timeline model. As seen in Fig. 4, the first person reached an exit after 11 seconds. It should be also noted that the arrival time was increased by the late arrival of two fire wardens who were checking that everyone is out of the building and this can be seen from the long tail of the curve in Fig. 4. After 2 min 13 seconds, all the occupants were evacuated. In addition, it should be noted that about 75% of occupants left the building between 37 seconds and 1 min 23 seconds.

This data can also be broken down according to the arrival time for exit A (i.e. main exit) and exit B (i.e. emergency exit) because the flow rate of each exit was different. Exit C was not used by occupants. Thus, the flow rate is equal to zero and it is not reported in Fig. 5. According to Fig. 5, a general trend was that participants who were initially in the ground floor left the building earlier compared to those initially located in the first floor. This might be the result of lower pre-movement time values or lower travel distances. Unfortunately, these assumptions cannot be verified as it was not possible to collect data on the pre-evacuation quantities of the first-floor occupants neither their starting positions. To garner a greater understanding of factors influencing the evacuation time of this subset of occupants and to investigate their pre-evacuation activities, cameras in the first floor are desirable.

Another observation is that most participants (about 87%) who took exit A were evacuating in “one large group”, between 37 seconds and 1 min 15 seconds. For those who were initially in the first floor, it can be identified that at least three groups of people evacuating together at different time intervals (see the red marks in Fig. 5) were formed. The first group evacuated between 52 and 54 seconds. The second one evacuated between 68 and 83 seconds. The last group evacuated between 102 and 107 seconds.

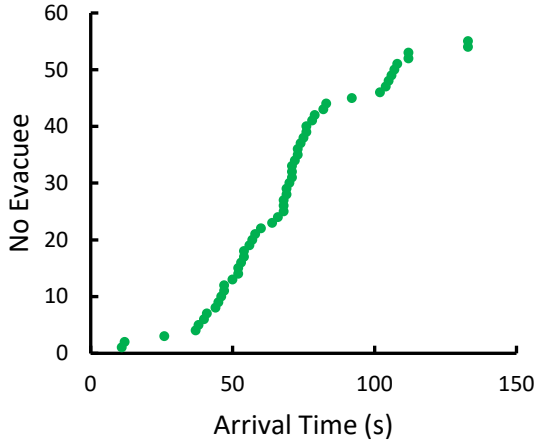


Fig. 4: Evacuation curve. The arrival time (x-axis) starts from the fire alarm.

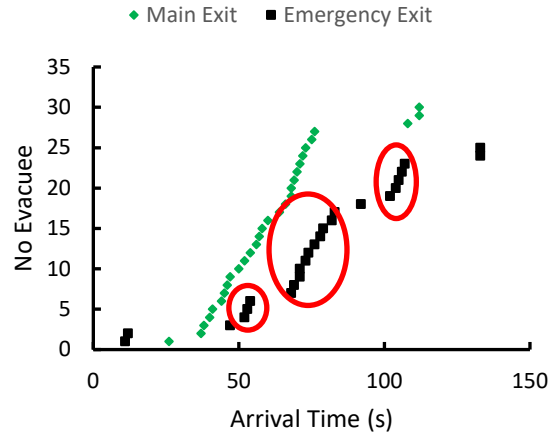
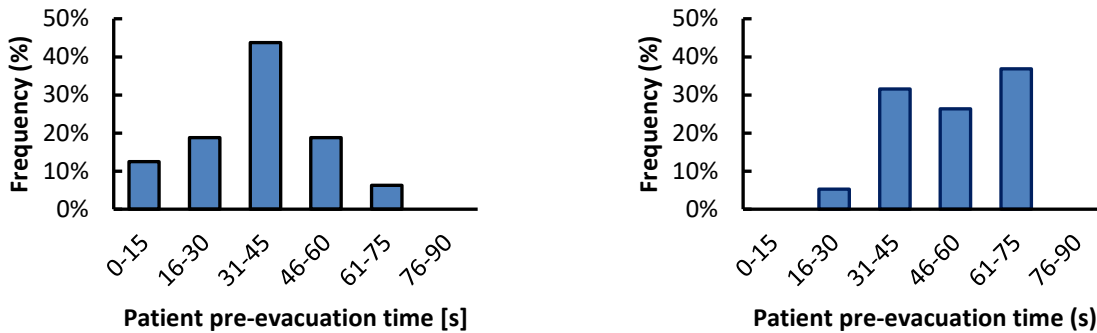


Fig. 5: Arrival time for the exits used during the drill. The red marks identify three groups of people evacuating together.

3.4. Comparison of collected pre-evacuation data with previous studies

Fig. 6 and Fig. 7 show patients and staff members pre-evacuation times distributions retrieved from the present study and from a previous study by Gwynne *et al.* [13] using a class limit of 15 seconds. According to Fig. 6a, it is apparent that very long pre-evacuation times were rare. In fact, most patients responded between 0 and 60 seconds. In the study by Gwynne *et al.* [13] (see Fig. 6b), most patients responded between 30 and 75 seconds. It was concluded from [13] that this reflected the time for the staff to instruct patients to evacuate and for patients to collect their personal goods, more than the time it took them to process the alarm signal information or to perform other pre-evacuation behaviours. The difference in patient pre-evacuation times distribution may be explained this way: in the current study not all the patients were dependent upon staff actions; some of them evacuating with no prior prompting; whereas, in the study by Gwynne *et al.* [13], the patients’ movement was fully dependent upon staff members action. The data presented in the current study gives a better understanding on how patients behave in a hospital outpatients’ area as most of them acted following their own decisions.



a- Current study

b- Previous study by Gwynne *et al.* [13]

Fig. 6: Frequency distribution of patient pre-evacuation times

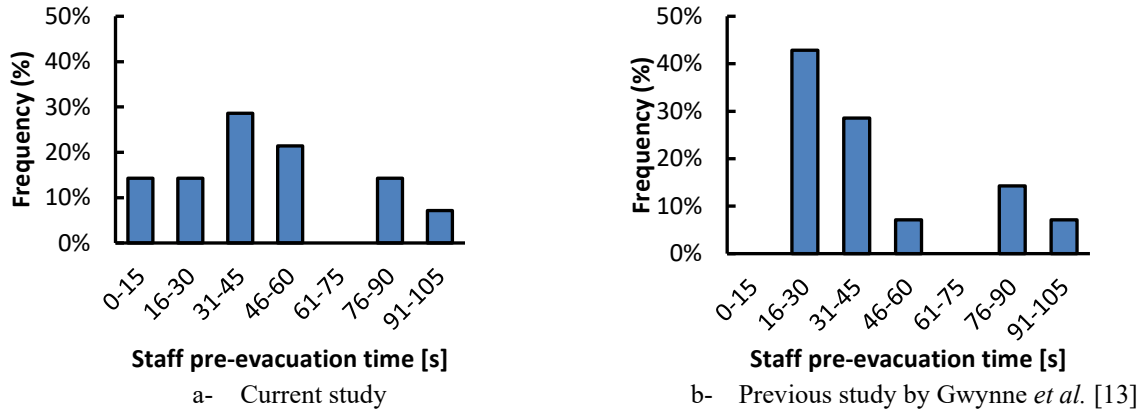


Fig. 7: Frequency distribution of staff pre-evacuation times

4. Conclusion

This study presented new evacuation data of 55 occupants evacuating one of the North Shore Hospital outpatients' areas (Auckland, NZ) based on the recordings of an *unannounced* fire drill. This drill involved a heterogeneous population consisting of staff members and patients. Pre-movement times of a subset of the population were obtained as well as the exits choice, the drill evacuation curve and exits flow rate. From the collected data, new pre-movement time distributions for patients and staff were estimated and compared with the data provided in [13]. These new distributions are useful to feed evacuation models to simulate hospital evacuations. However, the model users should be aware of the context of this data and its limitations. The data was collected to be used for hospital evacuation simulations and specifically for outpatients' area evacuation simulations.

The pre-movement time calculations showed differences in patient pre-evacuation time distributions between the current study and the previous one by Gwynne *et al.* [13]. Indeed, the patients in the current study were less dependent upon staff members action.

We recommend that staff members should familiarise themselves with the alternative emergency exits (i.e. exits B and C). In fact, all the participants, including staff members, made their exit choice based on their habits with the building. The routine usage of the doors to get in the building was one of the reasons leading to these observations. However, the staff having a procedural role, reacted and acted efficiently. They were the last to evacuate the building and often made prompt decisions asking people to move as quick as possible and showing the routes to follow for getting out. In addition, when help was needed, the assistance of at least one staff member was essential.

The drill was completed reasonably fast (i.e. 2 min and 13 seconds). However, the occupants who were inside the ground floor evacuated faster than those who were inside the first floor. This may be explained by three different reasons: 1) The travels distances of occupants of the first floor were greater than those of the ground floor; 2) walking speeds were lower than those of the occupants of the ground floor; 3) their pre-movement time was greater than the one of the occupants of the ground floor. Unfortunately, these hypotheses cannot be verified due to the absence of cameras in the first floor. Cameras in this floor and inside rooms are desirable to garner a greater understanding of factors influencing the evacuation time of occupants and to investigate their pre-evacuation activities.

Acknowledgements

The authors would like to acknowledge the management staff of WDHB for allowing the use of the CCTV recordings analysed in this paper.

References

- [1] S.M. V. Gwynne and K.E. Boyce, “Engineering Data,” in: SFPE Handb. Fire Prot. Eng., Springer New York, New York, NY, pp. 2429–2551, 2016. doi:10.1007/978-1-4939-2565-0_64.
- [2] R. Lovreglio, E. Kuligowski, S. Gwynne, K. Boyce, “A Pre-Evacuation Database for Use in Egress Simulations”, under review.
- [3] Shi, Long, et al. "Developing a database for emergency evacuation model", *Building and Environment* 44.8 (2009): 1724-1729.
- [4] R. Lovreglio, E. Ronchi, and D. Nilsson. "A model of the decision-making process during pre-evacuation." *Fire Safety Journal* 78 (2015): 168-179.
- [5] R. Lovreglio, E. Ronchi, and D. Nilsson. "An Evacuation Decision Model based on perceived risk, social influence and behavioural uncertainty." *Simulation Modelling Practice and Theory* 66 (2016): 226-242.
- [6] A. Cuesta, et al. "School egress data: comparing the configuration and validation of five egress modelling tools." *Fire and Materials* 41.5 (2017): 535-554.
- [7] R. Lovreglio, E. Ronchi, and D. Borri. "The validation of evacuation simulation models through the analysis of behavioural uncertainty." *Reliability Engineering & System Safety* 131 (2014): 166-174.
- [8] K.E. Boyce, T.J. Shields, G.W.H. Silcock, “Toward the characterization of building occupancies for fire safety engineering: capabilities of disabled people moving horizontally and on an incline,” *Fire Technology*, 35, pp. 51–67, 1999.
- [9] A. Hunt, E.R. Galea and P. Lawrence, “An Analysis and Numerical Simulation of the Performance of Trained Hospital Staff using Movement Assist Devices to Evacuate People with Reduced Mobility,” *Fire and Materials*, 2013, doi:10.1002/fam.2215.
- [10] S.A. Lavender, G.E. Hedman, J.P. Mehta, P.A Reichelt, K.M. Conrad and S. Park, “Evaluating the physical demands on firefighters using hand-carried stair descent devices to evacuate mobility-limited occupants from high-rise buildings,” *Applied ergonomics*, 45, pp. 389-397, 2013.
- [11] J.P. Mehta, S.A. Lavender, G.E. Hedman, P.A Reichelt, S. Park and K.M. Conrad, “Evaluating the physical demands on firefighters using track-type stair descent devices to evacuate mobility-limited occupants from high-rise buildings,” *Applied ergonomics*, 46, pp. 96-106, 2014.
- [12] S.A. Lavender, J.P. Mehta, G.E. Hedman, S. Park, P.A Reichelt and K.M. Conrad, “Evaluating the physical demands when using stair descent devices to evacuate mobility-limited occupants from high-rise buildings,” *Applied ergonomics*, 50, pp. 87-97, 2015.
- [13] S.M.V. Gwynne, E.R. Galea, J. Parke and J. Hickson, “The collection of pre-evacuation times from evacuation drills involving a Hospital Outpatient area and a University Library facility,” *Fire Safety Science*, 7, pp. 877-888, 2003.
- [14] L. Folk, J. Gales and M. Kinsey, “Evacuation Simulation of the Elderly: Data collection and Model Validation,” in *Proceedings of the 8th International Conference on Pedestrian and Evacuation Dynamics, (PED2016)*, Hefei, China, Oct 17-21, 2016.
- [15] S. Cartwright, “SR2006/123: Fire Safety and Evacuation of Buildings Regulation, New Zealand Regulation”, 2006 (reprint as at 1 July 2017)
- [16] V.V. Kholshchevnikov, D.A. Samoshin, A.P. Parfyonenko, I.P. Belosokhov, Study of children evacuation from pre-school education institutions, *Fire Mater.* 36 (5–6) (2012) 349–366.
- [17] A.R. Larusdottir, A.S. Dederichs, Evacuation of children: movement on Stairs and on Horizontal plane, *Fire Technol.* 48 (1) (2012) 43–53.
- [18] E.D. Kuligowski, et al., *Movement on Stairs During Building Evacuations (Technical Note 1839)*, US Department of Commerce, National Institute of Standards and Technology, 2014.
- [19] G.N. Hamilton, P.F Lennon and J. O’Raw, “Human behaviour during evacuation of primary schools: Investigations on pre-evacuation times, movement on stairways and movement on the horizontal plane”, *Fire Safety Journal*, 91, 937-946, 2017.

Investigation of pedestrian evacuation scenarios through congestion level and crowd danger

Claudio Feliciani¹, Katsuhiro Nishinari^{1,2}

¹ Research Center for Advanced Science and Technology, The University of Tokyo
4-6-1 Komaba, Meguro-ku, Tokyo 153-8904, Japan
feliciani@jamology.rcast.u-tokyo.ac.jp

² Department of Aeronautics and Astronautics, Graduate School of Engineering, The University of Tokyo
7-3-1 Hongo, Bunkyo-ku, Tokyo 113-8656, Japan

Abstract – In this paper, we present two quantities aimed at numerically describing the level of congestion and the intrinsic risk of pedestrian crowds. The congestion level allows to assess the smoothness of pedestrian streams and recognize regions where self-organization is difficult or not possible. This measure differs from previous attempts to quantify congestion in pedestrian crowds by employing velocities as vector entities (thus not only focusing on the absolute value). The crowd danger contains elements related to congestion, but also includes the effect of density, consequently allowing to assess the risks intrinsically created by the dynamics of crowds. Details on the computational methods related to both quantities are described in the paper and their properties are discussed. As a practical application, both measures are used to investigate supervised experiments where evacuation (or similar conditions) are considered. Results for small room sizes and limited number of pedestrians show that the crowd danger distribution over the space in front of the exit door has similar patterns to typical quantities used in the frame of pedestrian dynamics (density and flow) and symmetrical shapes are obtained. However, when larger scenarios are considered, then congestion map and crowd danger become unrelated from density and/or flow, showing that both quantities express different aspects of pedestrian motion.

Keywords: evacuation, congestion, intrinsic crowd risk, collective motion, experimental investigation

1. Introduction

Evacuations are one of the most common scenario studied in the frame of pedestrian dynamics and also one of the most critical situation involving pedestrians. Although evacuations represent a relatively simple case in terms of geometry, there are still many unknown aspects which need further investigations.

In the past, a number of experiments and field studies have been performed to analyse the behaviour of people during evacuations. Both humans [1-3] and animals [4,5] have been employed in experiments and granular matter [6] has been also taken as a comparative case to better understand human behaviour. Simulation models have also reached a considerable level of maturity in reproducing dynamics observed in reality (possibly due to the existence of a single common destination which makes calculations easier), thus allowing to study simple correlations between experimental conditions and evacuation time [7].

However, although several aspects have been investigated so far (influence of door width and exit location, behaviour of groups, role of leaders...) most of the studies only used the average evacuation time as a measure for effectiveness. As some researchers already pointed out, the evacuation time may not be appropriate to describe evacuation efficiency and related risks, especially considering that troubles may appear if a clog develops at the door leading to critical situations where casualties are caused by asphyxiation related to pressure waves from multiple directions [5,8].

More in general, assessments in pedestrian dynamics are still based on simple quantities such as velocity and density (flow is also used which is usually defined as the product of both). While both are important and help understanding several properties of pedestrian motion, they do not allow a complete and throughout analysis since velocity is typically used as a scalar quantity and density is static by definition. For instance, a dense crowd moving in the same direction may be treated in the same way as chaotic motion

caused, for example, by a perceived danger. If the area considered and the number of people involved are the same, then density is equal by definition, thus not accounting for the differences in motion. On the other side, when velocity is employed, then also directionality should be considered, but no agreement has been found on which method/equation should be used on this purpose.

Over the years there have been several quantities which have been proposed to describe particular properties of pedestrian motion. In particular, the bidirectional flow has attracted a lot of attention because of its capacity to form organized lanes and its similarity with physical systems. The band index [9] and the order parameter [10] have been proposed to assess the degree of stratification between different lanes, thus allowing to measure the capacity of crowds to organize themselves in efficient structures. While both are useful for analysing bidirectional streams, they are not applicable to more complex streams which are very often found in urban environments.

Alternative definitions to the classical vision of density have been also considered (a complete review is given in [11]). Among them, the Voronoi diagram has been often employed to allow defining the local density with better accuracy [12] and has become a common practice to analyse pedestrian crowds. While there are no doubts that definitions for crowdedness more proper to humans are needed, most of the proposed definitions are static by definition, therefore limiting the scope of application.

In this regard, to some extent, the work by Helbing et al. [8] has been an inspiration in developing a new quantity for pedestrian crowds. After studying the motion of pilgrims during an accident at the Hajj in Makkah, the authors came to the conclusion that so-called crowd turbulence was the leading cause to death. To assess the intrinsic risk of crowds (i.e. the amount of risk created by the crowd itself) they came up with a measure which they called “crowd pressure”. By using this quantity, the researchers were able to link the moment and the location where casualties occurred with high levels of crowd pressure, thus showing that it allows to account for the dangerous effects of shock waves (which were observed and studied in detail and were found being a primary cause of injuries).

In this work, we will introduce two new quantities which are particularly useful to better understand collective behaviour during evacuations: the “congestion level” and the “crowd danger”. The congestion level allows to measure the degree of organization in any kind of pedestrian flow (from unidirectional to complete random motion), while the crowd danger (also labelled as intrinsic crowd risk) helps assessing the intrinsic criticality of pedestrian crowds. Both quantities will be compared with traditional approaches using density and flow by considering controlled experiments from different authors.

2. Congestion level and crowd danger definition

Calculation of the congestion level makes use of velocity in the vector form and therefore, as a first step, it is necessary to obtain a vector field describing the motion of the crowd in any given moment. Two important quantities consequently need to be defined to allow the generation of the velocity vector field: grid (mesh) size and sampling time interval.

Grid size is simply the dimension assigned to each cell which will contain the velocity vector representing the average speed and direction in any location of the investigated surface. In continuous fluids, size of the mesh is not so important (or less relevant) since it is possible to measure the speed in any point. However, pedestrian crowds are more closely related to granular matter and size of the mesh need to be determined based on the particles’ dimensions.

In the case of pedestrians, velocity vectors are typically extracted from trajectories (as shown in the left side of Figure 1) and therefore the portion considered also plays an important role. When very long time intervals are considered trajectories from multiple pedestrians will overlap, thus making the description of the local motion not representative of the observed dynamics.

To allow an accurate description of crowd motion with a sufficient spatial and temporal resolution, but yet capture dynamics at different densities, the combination of both mesh size and sampling time interval is fundamental. Also considering the typical size of human body and the typical range of walking speed, we concluded that a mesh size of 0.2 m and sampling time interval of 2.5 s is the most appropriate set of parameters (details of the selection are given in [3]).

Using the above settings, a grid is generated following the steps provided in Figure 1 (on the left side). The portion of trajectory relative to the considered time interval is extracted and local velocity vectors are obtained by differentiation. Finally, an average value is obtained considering all the vectors contained in a single cell.

After obtaining the velocity vector field, the rotational (curl) is applied on the whole surface (a central differences scheme is applied) resulting in vector quantities $\vec{\omega} = [0,0,\omega]$ where only the direction perpendicular to the plane takes non-zero values (hence the first two dimensions are given as 0). Those non-zero values represent the vorticity, which already provides a first-instance estimation of the smoothness of motion. However, the curl returns both positive and negative values depending on the sense of rotation and high values are not necessarily synonym of high congestion. For instance, a couple dancing may return high values of rotation beside the very organized movement.

To avoid the above issues a Region of Interest (ROI) such as the one shown on the right side of Figure 1 is defined to allow a local estimation of motion dynamics. With ω as the only non-zero value of vorticity in the perpendicular direction, the level of congestion in a single ROI is defined as:

$$Cl = \frac{\omega_{max} - \omega_{min}}{|\vec{v}|} \quad (1)$$

with ω_{max} and ω_{min} being respectively the maximum and minimum values of vorticity and $|\vec{v}|$ being the average absolute velocity; all relative to the considered ROI. As for the ROI dimension we found that a circular-like shape with 7 cells (1.4 m) in diameter (see right side of Figure 1) allows to describe with sufficient accuracy local changes in congestion.

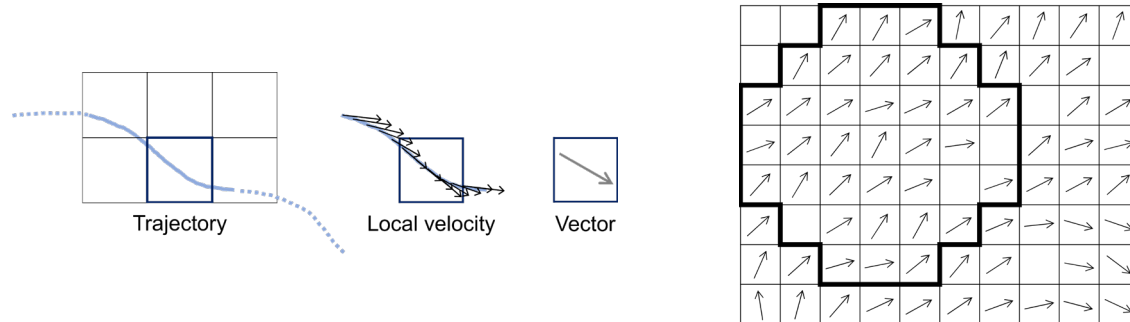


Fig. 1: Steps required to obtain a velocity vector field of moving crowds (left) and a typical vector field showing the computational ROI with thick black lines (right).

The above definition of the congestion level allows to locally measure the smoothness of motion taking into account the self-organization into groups moving in similar directions and the slow down caused by high densities. Also, since the difference between maximum and minimum values of vorticity is used, only positive values are obtained. However, while the congestion level may allow to indirectly consider the effects of density (through a reduction in velocity), it is not explicitly accounted for.

We may therefore define the crowd danger as the local product (considering the ROI again) of the congestion level with density ρ as given by:

$$Cd = Cl \cdot \rho \quad (2)$$

This measure allows to take into account both the collective motion (and the corresponding degree of organization) and the pressure spread in a crowd due to its density. Considering that both the amount of crowdedness and the way people are moving are accounted for, it can be a measure of the intrinsic crowd risk and hence the name crowd danger.

3. Calibration using controlled experiments

To understand the properties of congestion level and crowd danger several characteristic experiments from multiple sources have been analyzed (details are given in [3]). In particular, three types of experiment were considered for comparison: unidirectional, bidirectional and chaotic (multidirectional) motion. Those cases were chosen because of their scientific significance and the availability of experimental data.

The three cases are schematically depicted in Figure 2 using different colors for each class of pedestrians moving in a particular direction. In unidirectional streams, people all move in the same direction and, although overtaking is still possible, a very smooth motion is usually observed. In the case of bidirectional streams interactions become stronger, but lanes are typically formed (if possible) to reduce collisions with the counter-flow. Finally, multidirectional streams are usually chaotic, especially if densities are high, since trajectories often intersect with other pedestrians.

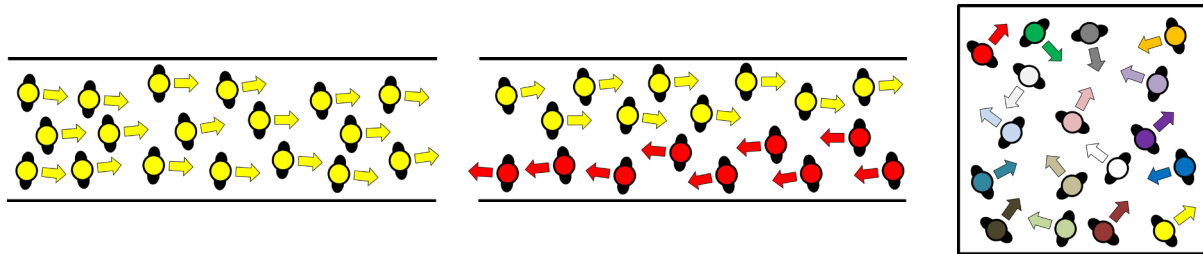


Fig. 2: Different types of pedestrian streams: unidirectional, bidirectional and chaotic (multidirectional) motion (from left to right). Colours are used to distinguish each group of pedestrians based on their destination.

Literature data have been used for the unidirectional and bidirectional case (considered studies are described in [13] and data are available in [14]), while own experiments were performed for the chaotic case (details are given in [3,15,16]). For the latter, two different configurations were tested: in one case participants were simply asked to move inside a room (free chaotic motion) while in a second case some additional people were asked to traverse it in different directions (forced chaotic motion), thus making the formation of organized structure more difficult (and almost impossible).

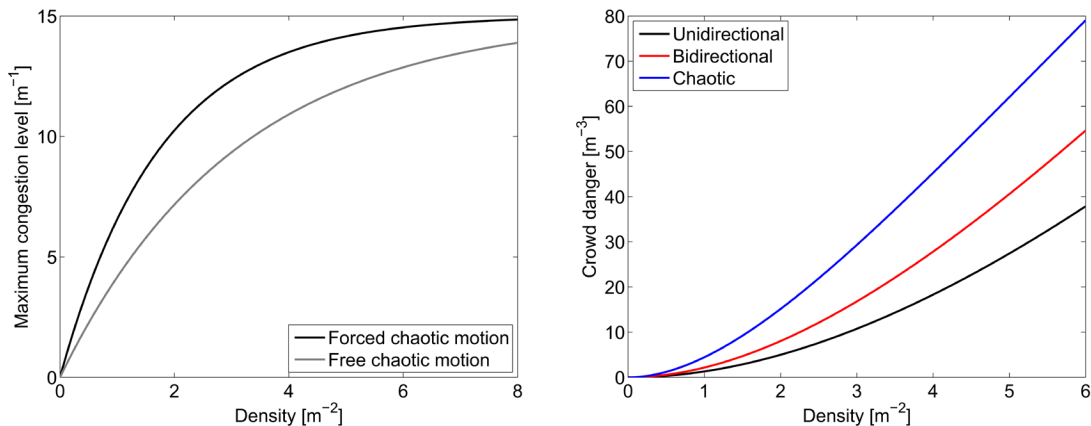


Fig. 3: Maximum congestion level measured at different densities in the chaotic experiment for different configurations (left). Crowd danger evolution for different types of pedestrian streams (right). In all the cases numerical values are derived from experiments (with details provided in [3]). Chaotic curve in the right graph also considers additional chaotic experimental conditions not accounted for in the left graph.

Figure 3 (left) shows the congestion level measured at different densities for the two chaotic experiments described earlier. Results showed that there is a typical maximum value of congestion level

associated with a particular density and experimental configuration. Also, we noticed that the maximum congestion level converged toward a plateau of 15 m^{-1} . While experimental evidence may not be sufficient to come at final conclusions, it may be possible that this value represents a property of pedestrian crowds, in a sort of cognitive process which reduce speed to limit the consequences of collisions which are getting more frequent at higher densities.

When typical values of the crowd danger were computed for different types of flow, we noticed that they all followed an exponential-like behaviour as given on the right side of Figure 3. As the graph shows, the intrinsic crowd risk grows slowly (in relation to density) when unidirectional motion is considered, because movements are synchronized among individuals. However, in case of a crowd moving in multiple directions there is a steeper increase in crowd danger, since movements are more random and collisions (or very close interactions) are frequent. While we have not been able to provide a characteristic cautionary value for crowd danger (also because of the exponential nature of the function), we speculate that above 75 m^{-3} attention is required as accidents are more likely.

4. Results

To further demonstrate the properties of the congestion level and the crowd danger, show possible applications and better study evacuation dynamics, we considered three experiments from different contexts. A representative image of each experiment is given in Figure 4 and similarities/differences among the different cases will be shortly discussed before introducing the results.

The first set of experiments (left in Figure 4, details are provided in [1]), were performed in a squared room 5 m in side length. In the centre of it a smaller area 3 m in side length (clearly visible in Figure 4) was used to gather participants at the beginning of the experiment. After the “start” was given, people rushed to the exit and left the room following a predetermined wide path (i.e. the area in front of the exit was unobstructed allowing a smooth evacuation). Exit door had a variable width of 0.8 m and 1.2 m. This research particularly focused on group behaviour during evacuations and therefore groups of several sizes (from 2 to 8 members) were created among participants (interactions within the social groups also varied among each experimental run). Also, it is important to notice that participants were all children of different ages (from 10 to 12 and from 15 to 17 years old). Number of participants varied from a minimum of 22 to a maximum of 50 people. In total 51 experimental runs are considered. Beside the differences in each case, after examining the videos, we determined that for the scope of this study, the whole set of experiments can be regarded as a single scenario, especially due to the similarity of the experimental geometry.

The second set of experiments (centre in Figure 4, details provided in [3]) consisted in a room of 4 m in width and 7 m in length, with a 0.8 m exit located in the middle of the longest side. Participants (university students in their 20s) gathered concentrically around the exit before the evacuation order was given. A variable number of participants was considered, with 3 runs having 25 participants and 5 runs with 43 participants. All people behaved individually. Also in this case, we deemed appropriate to consider the 8 experimental runs altogether since geometry had not been varied.

The last experiment considered (right in Figure 4, details provided in [17]) consists in a large-scale reproduction of the entrance of a music event. While in this case motivation was not for leaving the room, but rather for entering it, it still represents an interesting case for a bottleneck geometry. 273 young people aged between 20 and 30 gathered for the experiment. In contrast to the previous cases, two small paths allowing only one person each were made available for “evacuation” (both are visible in Figure 4). For this experiment only one execution was performed and participants were specifically asked to imagine that their idol is present at the concert, thus having them trying to enter quickly to get the best places. As a result, pushing and forced motion were frequently seen in different moments of the experiment.

For each experimental run, several heat maps for density, flow, congestion level and crowd danger were computed and are presented in Figure 4. To increase the accuracy for the maps representing the congestion level (and consequently crowd danger) the 2.5 s sampling interval discussed earlier was used, but it has been moved in 0.1 s steps, thus generating a large number of maps also for short experimental runs. In all the cases, densities have been computed by using the Voronoi method [12] and flow was obtained by multiplying local speed (taken over 5 frames) with corresponding density. Mesh size is of 0.2

m as a result of the previous discussion on the computational method of the congestion level. Each experimental run is considered from the moment where the first person exits the room until the last one pass through the exit. Finally, a generic filter has been used to remove outliers resulting from tracking inaccuracies (difference with unfiltered results was judged minimal, thus allowing its use).

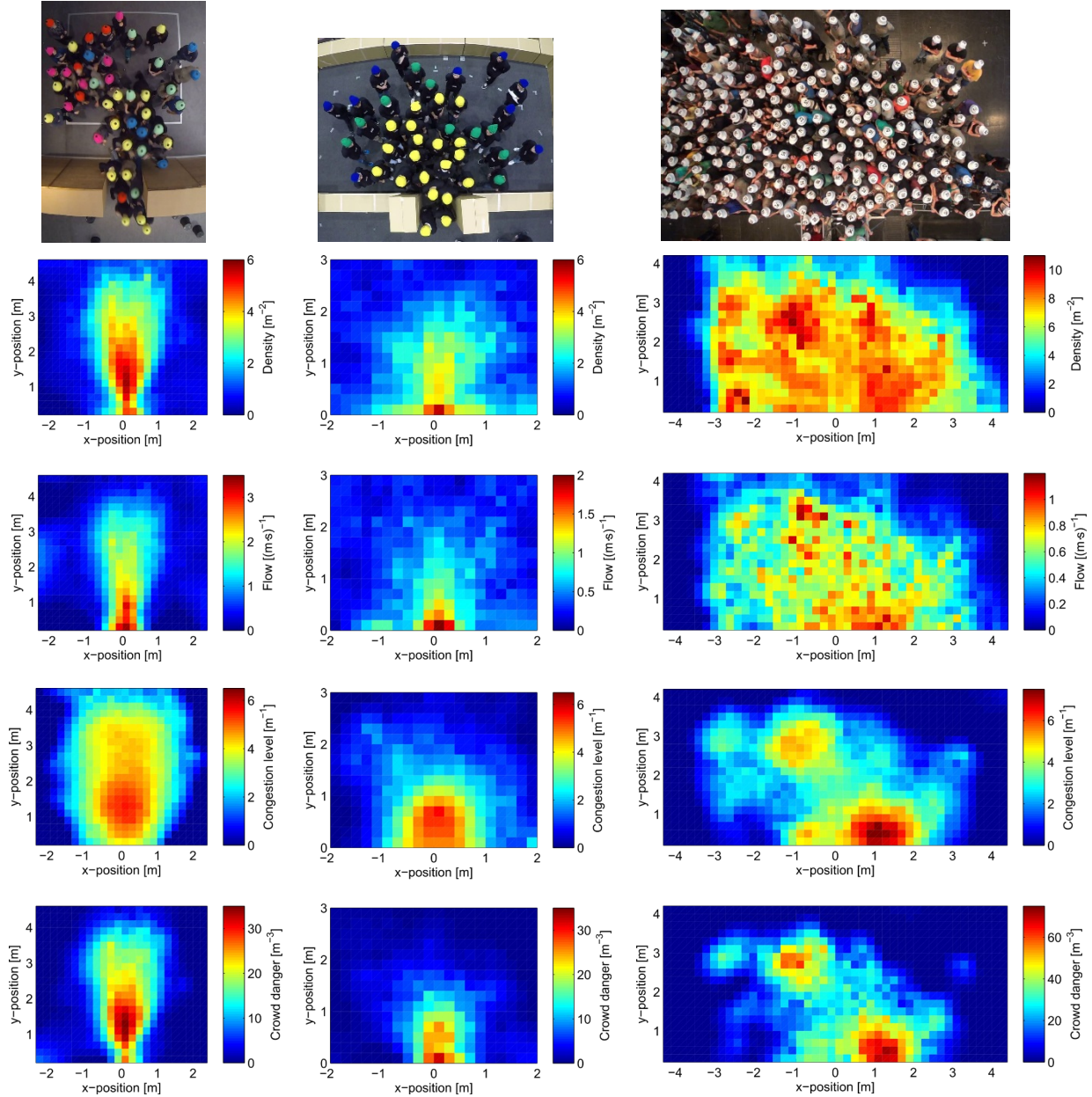


Fig. 4: Heat maps for different quantities (density, flow, congestion level and crowd danger) for the three experimental scenarios considered. In all the cases, the exit (or the centre of it) is located at the origin (0,0). Figures are cropped to focus on the region in front of the exit (complete experimental area is bigger).

Results from Figure 4 show quite different patterns depending on the quantity considered and the experiment being investigated.

In the experiment involving children provided on the left, it is seen that from a qualitative point of view the 4 considered quantities are similar. Density, congestion level and crowd danger all show

their maximum in a location about 1 – 1.5 m in front of the exit. Only the flow shows a quite different shape by peaking right in the location of the exit. In particular, a very close similarity is found between the density map and the one for the crowd danger, which could be partially explained considering that density is involved in the calculation of the latter. The congestion level shows the largest distribution, with comparatively high values of congestion also found where density and flow are low. In interpreting those results one should be reminded that children gathered in the centre of the room before the experiment was started and this could partially explain the high values found in inner parts of the room.

When the second set of experiments is considered, whose results are given in the central part of Figure 4, then a partially different picture is obtained considering evacuation dynamics. While the congestion level still shows a large dispersion roughly centred in a location around 0.5 – 1 m in front of the exit, all the other quantities show their maximum right in the place of the exit. This could be partially associated with the method employed to compute the Voronoi cells, which, although it partially considers the opening created from the door, may still overrepresent the density right in front of the exit. Nonetheless, both experiments involving children (left) and young adults (centre) employ the same method in computing Voronoi density, so this could not be the only cause explaining the high values observed at the exit. An interesting observation can be done by comparing the flow for the case with children (left) with the one for adults (centre). The maximum flow for children is considerably higher than typical figures from the literature [18] (usually in the range of 2 – 2.5 pedestrians (m·s)⁻¹). While this could be explained with partially different definitions for flow, the smaller body size of children is a more possible reason.

Finally, the large experiment relative to the concert entrance, whose results are given on the right of Figure 4, is discussed. In this case, a very different image is obtained among the different quantities and also compared to the previous cases. While high density values are found throughout the whole experimental area, congestion level and crowd danger both have two peaks found close to the right “exit” and in a region lying far from the egress location. The different distributions found show that congestion level has a different nature compared to density and flow and it possibly allow to determine the self-organization of motion for pedestrian crowds. When the crowd danger is considered, then higher values (more than doubles) are obtained compared to the previous case. This is a combination of the higher densities and higher values of congestion and it qualitatively reproduce well the general impression obtained by visioning the video of the experiment.

As a final remark, it is seen that in most of the cases the most congested region lied at a distance similar to the width of the exit door right in front of the exit. Previous studies (involving granular matter, humans and sheep) already found that the flow is increased by placing an obstacle in this region [2,5,6], which may cause an overall reduction in congestion.

5. Conclusion

In this study, evacuation experiments for different types of pedestrian crowds have been studied employing typical quantities usually associated with pedestrian traffic (density and flow) and newly defined measures to assess the level of congestion and the intrinsic risk created by the motion of the crowd.

Results showed that while there are common characteristics among the scenarios involving a small number of participants in clearly defined and symmetric contexts, all defining a congested region right in front of the exit, the situation changed when a more realistic case was studied.

This shows that while it is possible to prevent accident by focusing on hotspots which are generally considered as dangerous, in reality each situation needs to be considered separately and crowd monitoring and management are important aspects to guarantee safe and smooth mass events.

The methods presented in this work may found applications in several contexts involving pedestrian traffic, with evacuation being only an example. In particular, the congestion level and the related crowd danger can be useful for designing pedestrian facilities since dangerous and congested regions are easily recognized. In addition, a use in conjunction with simulation models may also help analysing the results and identify locations which need improvements.

Although both quantities work best on large database of similar experiments (as presented in this study), it may be also possible to employ them for real-time crowd analysis, for example during mass events,

when simple but yet meaningful information are important to highlight location which need a prompt intervention by security personnel.

Acknowledgements

This work was financially supported by JST-Mirai Program Grant Number JPMJMI17D4, the Doctoral Student Special Incentives Program (SEUT RA) and the Foundation for Supporting International Students of the University of Tokyo. In addition, we are grateful to the researchers who openly shared their data.

References

- [1] C. von Krüchten, F. Müller, A. Svachiy, O. Wohak, A. Schadschneider, “Empirical study of the influence of social groups in evacuation scenarios”, in *Traffic and Granular Flow '15*, L. V. Knoop, Springer International Publishing, 2016, pp. 65-72.
- [2] D. Yanagisawa, A. Kimura, A. Tomoeda, R. Nishi, Y. Suma, K. Ohtsuka, K. Nishinari, “Introduction of frictional and turning function for pedestrian outflow with an obstacle”, *Phys. Rev. E*, vol. 80, no. 3, 2009.
- [3] C. Feliciani, K. Nishinari, “Measurement of congestion and intrinsic risk in pedestrian crowds”, *Transp. Res. Part. C Emerg. Technol.*, vol. 91, pp. 124-155, 2018.
- [4] P. Lin, J. Ma, T. Liu, T. Ran, Y. Si, T. Li, “An experimental study of the “faster-is-slower” effect using mice under panic”, *Physica A*, vol. 452, pp. 157-166, 2016.
- [5] A. Garcimartín, J. M. Pastor, L. M. Ferrer, J. J. Ramos, C. Martín-Gómez, I. Zuriguel, “Flow and clogging of a sheep herd passing through a bottleneck”, *Phys. Rev. E*, vol. 91, no. 2, 2015.
- [6] I. Zuriguel, D. Ricardo Parisi, R. C. Hidalgo, C. Lozano, A. Janda, P. A. Gago, J. P. Peralta, L. M. Ferrer, L. A. Pugnaloni, E. Clément, D. Maza, I. Pagonabarraga, A. Garcimartín, “Clogging transition of many-particle systems flowing through bottlenecks”, *Sci. Rep.*, vol. 4, 2014.
- [7] L. Lu, C. Y. Chan, J. Wang, W. Wang, “A study of pedestrian group behaviors in crowd evacuation based on an extended floor field cellular automaton model”, *Transp. Res. Part. C Emerg. Technol.*, vol. 81, pp. 317-329, 2017.
- [8] D. Helbing, A. Johansson, H. Z. Al-Abideen, “The Dynamics of Crowd Disasters: An Empirical Study”, *Phys. Rev. E*, vol. 75, no. 4, 2007.
- [9] K. Yamori, “Going with the flow: Micro--macro dynamics in the macrobehavioral patterns of pedestrian crowds”, *Psychol. Rev.*, vol. 105, no. 3, 1998.
- [10] S. Nowak, A. Schadschneider, “Quantitative analysis of pedestrian counterflow in a cellular automaton model”, *Phys. Rev. E*, vol. 85, no. 6, 2012.
- [11] D. C. Duives, W. Daamen, S. P. Hoogendoorn, “Quantification of the level of crowdedness for pedestrian movements”, *Physica A*, vol. 427, pp. 162-180, 2015.
- [12] B. Steffen, A. Seyfried, “Methods for measuring pedestrian density, flow, speed and direction with minimal scatter”, *Physica A*, vol. 389, no. 9, pp. 1902-1910, 2010.
- [13] J. Zhang, W. Klingsch, A. Schadschneider, A. Seyfried, “Ordering in bidirectional pedestrian flows and its influence on the fundamental diagram”, *J. Stat. Mech.*, vol. 2012, no. 2, 2012.
- [14] Forschungszentrum Jülich, “Data archive of experimental data from studies about pedestrian dynamics”, <http://ped.fz-juelich.de/db/> (accessed May, 2018).
- [15] H. Yamamoto, D. Yanagisawa, C. Feliciani, K. Nishinari, “Modeling body-rotation behavior of pedestrians for collision avoidance in a narrow corridor”, *Transp. Res. Part. B Meth.*, 2018 (submitted).
- [16] C. Feliciani, K. Nishinari, “Estimation of pedestrian crowds’ properties using commercial tablets and smartphones”, *Transportmetrica B*, 2017 (submitted).
- [17] A. Sieben, J. Schumann, A. Seyfried, “Collective phenomena in crowds—where pedestrian dynamics need social psychology”, *PLoS ONE*, vol. 12, no. 6, 2017.
- [18] A. Seyfried, O. Passon, B. Steffen, M. Boltes, T. Rupperecht, W. Klingsch, “New insights into pedestrian flow through bottlenecks”, *Transp. Sci.*, vol. 43, no. 3, 2009.

Comparing Different Metrics Quantifying Pedestrian Safety

Arne Hillebrand, Han Hoogeveen, Roland Geraerts

Department of Information and Computing Sciences, Utrecht University
Princetonplein 5, 3584CC, Utrecht, the Netherlands
A.Hillebrand@uu.nl; J.A.Hoogeveen@uu.nl; R.J.Geraerts@uu.nl

Abstract - The quantification of pedestrian safety is an important research topic. If reliable quantification is possible, it can be used to predict and prevent dangerous situations, such as the crowd crush at the 2010 Love Parade. To quantify safety, we can use several metrics like density, velocity, flow and pressure. Unfortunately, there are several methods to evaluate these metrics, which may give different results. This can lead to different interpretations of similar situations. Researchers compare these metrics visually or search for trends in fundamental diagrams. This is inherently subjective. We propose an objective methodology to compare these methods, where we emphasize the different quantifications of peak “dangerousness”. Furthermore, we refine existing methods to include the obstacles in environments by replacing the Euclidean distance with the geodesic distance. In our experimental analysis, we observe large differences between different methods for the same scenarios. We conclude that switching to a different method of analysing crowd safety can lead to different conclusions, which asks for standardisation in this research field. Since we are concerned with human safety, we prefer to err on the side of caution. Therefore, we advocate the use of our refined Gaussian-based method, which consistently reports higher levels of danger.

Keywords: pedestrian safety, metrics, analysis, density, velocity, flow, pressure

1. Introduction

At the 2010 Love Parade [6], 21 people were crushed to death and hundreds got injured. In 2006 and 2015 hundreds of pilgrims got trampled during the Hajj to Mecca due to dangerously overcrowded situations [7]. Motivated by such disasters, researchers study ways of preventing these from happening again. By studying metrics like density, velocity, flow and pressure, early warning signs for potentially dangerous situations can be found.

In this paper, we refer to density, velocity, flow and pressure as *metrics*. Different *methods* exist to evaluate them. For density, the best-known method is the grid-based method [5]. A regular grid is superimposed on the environment, dividing the environment into cells. Another way of determining density uses Gaussian distributions [7,12]. Such methods place two-dimensional Gaussian distributions on the pedestrian’s locations. By adding the Gaussian distributions together, a density field is formed. A third method to determine local density uses Voronoi diagrams [13]. A Voronoi diagram is a division of the environment in cells, such that all points within a cell are closest to a single pedestrian. The density within each cell is 1 divided by the area of the cell. Details for these methods can be found in Section 2.1.

It is possible to determine the velocity by using density [15]. Using the density and velocity, both flow and pressure can be determined [7]. We describe their implementation in Section 2.2.

Fruin [5] computes the danger level based on the value of these metrics within a (small) region of the environment, which is mapped to six non-overlapping intervals. This method is called *Level of Service* (LoS). The different intervals encode situations from safe to dangerous. The exact boundaries of these intervals depend on different factors, such as the measurement location and even culture [1].

When using LoS, the outcome of the safety evaluation is dependent on the measurement location and on how obstacles are handled. Quantifying these different outcomes is no easy task. One way to compare different methods is by visually inspecting the results. An example of two density fields is given in Figs. 1(a) and 1(b). We can observe a difference between the two images, but this difference is hard to quantify. The absolute difference between the two fields (Fig. 1(c)) only emphasizes that differences exist.

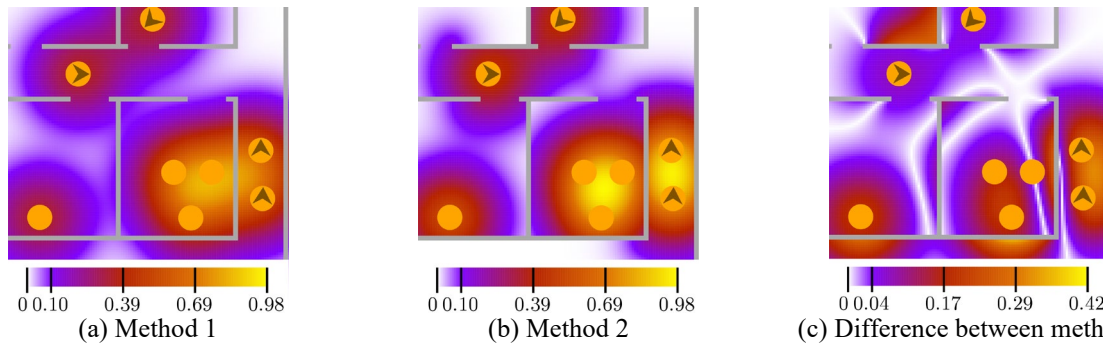


Fig. 1: An environment with pedestrians, represented by orange discs. The environment measures $6m \times 7m$. An arrow symbolises a pedestrian's direction of movement, while a stationary pedestrian does not have an arrow. (a) and (b): Two density fields determined by using different methods. (c): The absolute differences between the two methods.

Duives et al. [4] compare density methods using *fundamental diagrams*. For different scenarios they formulate what trends they expect to be present in these diagrams, and look for them. One drawback of this method is that it requires expert knowledge about what trends are to be expected. Furthermore, it is inherently subjective due to the human classification step.

Duives et al. [4] also propose an objective measure of similarity between density methods called *scatter*. The scatter is the range of measured velocities for non-overlapping density intervals. One downside of this measure is the interdependency between these metrics. A small change in the density method can result in a large shift in the measured scatter due to the potential recategorization of measured velocities.

1.1. Our Contribution

In this paper, we propose an objective methodology for comparing methods that compute safety metrics. We also refine existing methods to consider obstacles in the environment. We achieve this by replacing the Euclidean distance by the geodesic distance [10]. The resulting differences are showcased in Fig. 1. Method 1 uses the Euclidean distance, whereas method 2 uses the geodesic distance.

We also performed experiments on environments to test if our methodology yielded new insights into the differences between methods. We conclude that the classification of a situation as being safe depends on the method that is used, and that our refined methods consistently classify situations as more dangerous.

1.2. Overview

In Section 2, we discuss the different methods used for evaluating the metrics. Here we also introduce our refinements of two methods. Next, in Section 3 we give details of the four measures used to quantify the differences between the methods. These measures are used in Sections 4 and 5 to evaluate the different methods on three basic environments and several scenarios. We end with a conclusion in Section 6.

2. Methods for Measuring Safety

As discussed in Section 1, different metrics exist. Furthermore, there are different methods for computing each metric. In Section 2.1, we discuss different density methods. The considered methods are either grid-, Voronoi- or Gaussian-based. How the resulting density fields can be used to determine velocity, flow and pressure fields will be discussed in Section 2.2.

2.1. Density methods

The *grid-based* method was first defined by Fruin [5]. Intuitively, this method counts the number of pedestrians in a cell C_i , where the cells are defined by a regular grid which is placed over the environment. This grid does not consider the obstacles in the environment. Next, this number is divided by the area A_i of the cell to get the local density. All the pedestrians are considered to be

points, and can therefore only be in one cell at a time. The only parameter for this method is the width w of a cell.

A problem with this method is that obstacles, such as walls, have no effect on the measured density. This can be seen in Fig. 2(a). The large jumps in density when a pedestrian moves to the next cell cause another problem. This last issue can be partially alleviated by modelling pedestrians as discs and measuring the fraction of the disc in a cell.

Steffen and Seyfried [13] take another approach at minimizing these large jumps in density. Their *Voronoi-based* method describes the free space that is available to a pedestrian by using Voronoi diagrams. A Voronoi diagram of n input points is the partitioning of the environment into n cells, such that every position within that cell is closest to exactly one point. Steffen and Seyfried [13] use the locations of the pedestrians for calculating a Voronoi diagram as the input points. After obtaining this diagram, the density within each Voronoi cell i is defined as $1/A_i$. Here, A_i is the area of Voronoi cell i . Next, this Voronoi cell density is used to calculate the density within grid cells by using a weighted average of all the Voronoi cells that intersect that grid cell.

One drawback of this method is that the area of a Voronoi cell can be large, while it is locally very dense (e.g. pedestrians on the perimeter of a dense group). To this end, Steffen and Seyfried suggest a limit of 2 square meters on the area of a Voronoi cell. Furthermore, it is not mentioned how the obstacles should be handled. In our experiments with the Voronoi method, we will remove the area of a cell that is covered by obstacles. As a result, higher (more accurate) densities are reported.

However, only removing obstructed regions from a Voronoi cell can still give the illusion of too much free space. We show an example of this in Fig. 2(b). Here, a Voronoi cell is split into two disconnected pieces by an obstacle. To remedy this, we propose to use a geodesic Voronoi diagram [10], which accounts for the obstacles in an environment. This also changes the shape of the Voronoi cells. We exemplify this in Fig. 2(b) and (c). Some line segments are replaced by curves, because of the nearby obstacles.

Gaussian-based methods measure density for points instead of areas. Here, the contribution of a pedestrian to a point depends on the distance between the pedestrian and the point. This distance is used as input for a function f that determines the contribution. More formally, the density at point l is defined as $\rho(l) = \sum_{p \in P} f(ed(l, p))$. Here, P is the set of all pedestrians and $ed(l, p)$ is the Euclidean distance between point l and pedestrian p .

One of the first methods that uses this is due to Helbing et al. [7]. They use the following function:

$$f(x) = \frac{1}{\pi R^2} e^{-\frac{x^2}{R^2}} \quad (1)$$

This equation is a variation of a Gaussian distribution. Here, x is the distance between a pedestrian and a point. R is the only parameter of this method. It influences the pedestrian's contribution to the perceived density. Duives et al. [4] point out that R influences the contribution and should be picked carefully.

Plaue et al. [12] suggest a method that bypasses this issue altogether. Instead of having R as a fixed parameter, it is dependent on the current locations of the pedestrians at time t . With all locations given as $P(t)$, the function used to determine R for a pedestrian at location p is

$$d^q(p) = \left(\sum_{p' \in P(t), p \neq p'} ed(p, p')^{-q} \right)^{\frac{1}{q}} \quad (2)$$

In their experiments the parameter q is set to 4.

In addition to using a dynamic value for R , Plaue et al. also take obstacles into account. They do this by setting $f(x) = 0$ for points that are inside obstacles. The volume of the Gaussian distribution that would normally fall inside the obstacles is redistributed amongst the obstacle-free points. As a result, the contribution to the density of a pedestrian in closed-off places increases,

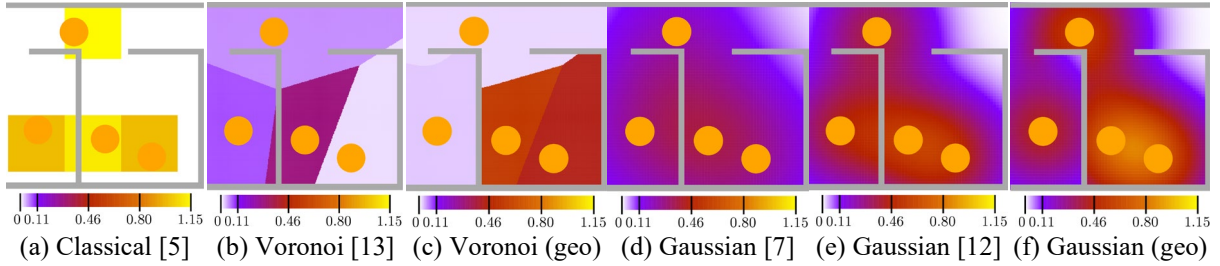


Fig. 2: Different density fields. The orange disks represent pedestrians. (a): Fruin's classical density [5] with $w = 1m$. (b) and (c): The Voronoi diagram as used by Steffen and Seyfried [13] and the geodesic Voronoi diagram. (d), (e) and (f): The Gaussian-based density method by Helbing et al. [7] with $R = 1m$, the method proposed by Plaue et al. [12] and a Gaussian density method using the geodesic distance.

resulting in higher local densities. This becomes clear when we compare Figs. 2(d) and 2(e). However, this method still increases the density at the opposite side of an obstacle. In our example, we can see that there is a region with higher density close to walls because of the presence of pedestrians at both sides.

To further take the obstacles into account, we use the geodesic distance. When two pedestrians have the same Euclidean distance to a measurement point, they should not always contribute equally to the local density, because one or more obstacles may cause a detour for the pedestrian. The geodesic distance takes this detour into account. Such a geodesic Gaussian density field can be seen in Fig. 2(f).

2.2. Derived Metrics

Although density is an important metric for determining pedestrian safety, it is not the only one available. We mentioned velocity, flow and pressure in Section 1 and gave an intuitive definition. In this section, we will show how these metrics can be determined.

To compute (local) velocities, we use an adaptation of the method described in Helbing et al. [7, Equation 6]. In this method, the local velocity is defined as:

$$\vec{V}(l, t) = \frac{\sum_{p \in P(t)} \vec{v}_p f(l, p)}{\sum_{p \in P(t)} f(l, p)} \quad (3)$$

Here, l is a location, t is the current time, $P(t)$ is the set of locations of the pedestrians, \vec{v}_p is the velocity of the pedestrian at location p and $f(l, p)$ is a weighing factor. Helbing et al. use a Gaussian distance-dependent function for the weighing factor. This is the same function as given in Eq. 1.

Since we used different density methods, we will have $f(l, p)$ reflect this. That is, we use different definitions of $f(l, p)$ for the grid-, Voronoi- and Gaussian-based methods respectively. We do this to better reflect the underlying division of the environment in regions. These functions are given in Eqs. 4 through 6. In these equations, p is the location of a pedestrian, C_i is a cell used by the density method, l a point and A_p is the area for the Voronoi cell V_p . Finally, the function $d(l, p)$ is the geodesic distance $gd(l, p)$ when evaluating our refined method, and the Euclidean distance $ed(l, p)$ in the other situations.

$$f_{Grid}(C_i, p) = \begin{cases} 1, & \text{if } p \in C_i \\ 0, & \text{otherwise} \end{cases} \quad (4)$$

$$f_{Voronoi}(l, p) = \begin{cases} \frac{1}{A_p}, & \text{if } l \in V_p \\ 0, & \text{otherwise} \end{cases} \quad (5)$$

$$f_{Gaussian}(l, p) = \frac{1}{\pi R^2} e^{-\frac{d(l, p)}{R^2}} \quad (6)$$

The flow is calculated with the usual equation $\vec{Q}(t, l) = \vec{\rho}(t, l) \vec{V}(t, l)$ for location l at time t . Since we have different definitions of ρ , we will also use the corresponding definition of V . For calculating the pressure, we use the definition given in Helbing et al. [7, Equation 9]. That is, the pressure is defined as $P(l, t) = \rho(l, t) \text{Var}_{l,t}(\vec{V})$, with $\text{Var}_{l,t}(\vec{V})$ the variance of velocity around location l at time t . It is defined as $\text{Var}_{l,t}(\vec{V}) = \langle \vec{V}(l, t) - \langle \vec{V} \rangle_C \rangle_C$. Here, $\langle X \rangle_C$ is the average of X of the points in region C .

3. Comparing different methods

From Fig. 2 it is clear that different methods can give different results, but are these differences significant? We will look at four measures for comparing these methods to try and answer that question.

When we analyse a method M , we will look at a region of interest R within the studied environment. This area is divided into a set of cells C_i for $1 \leq i \leq N$. These cells follow from the method we choose. The value for such a cell is given by $v(C_i, M)$.

First, we look at the *maximal* value for M within R , which enables us to compare measured peak densities, velocities, flows and pressures. We also look at the *maximal difference* between two methods. They are given in Eqs. (7) and (8).

$$\max(M) = \max_{1 \leq i \leq N} v(C_i, M) \quad (7)$$

$$\max(M_1, M_2) = \max_{1 \leq i \leq N} |v(C_i, M_1) - v(C_i, M_2)| \quad (8)$$

These two measures do not offer more information than a visual inspection. The differences are accentuated, but other information is lost. For that reason, we introduce two new measures. For these measures it is important that R is centred within the area we want to study. This, however, should not be a problem since we are interested in local values. We call the first one the *quadratic score* (qs). We define it as follows:

$$qs(M) = \frac{1}{A_R} \sum_{i=1}^N \left(\frac{v(C_i, M)}{\max(M)} \right)^2 A_i \quad (9)$$

Here, A_i is the obstacle-free area of cell C_i and $A_R = \sum_{i=1}^N A_i$ is the obstacle-free area of R . The resulting value is a number in the range of 0 to 1. A value of 1 denotes that all N cells are at the maximal value. When qs gets closer to 0, it means that a large area of R has low values. This function ensures that regions which are closer to high (i.e. dangerous) values are emphasized. Furthermore, this method evaluates to simple scalars. Therefore, it is possible to use existing statistical methods to determine if there is a statistically significant difference.

The last measure we discuss is a comparison based on how the industry often interprets the values from the metrics. Usually, a certain threshold value is used or categories are specified. An example is the LoS concept [5]. Eq. 10 calculates the difference in categorization between two different methods.

$$bd(M_1, M_2) = \frac{1}{A_R} \sum_{i=1}^N (bin(C_i, M_1) - bin(C_i, M_2))^2 A_i \quad (10)$$

Here, $bin(C_i, M)$ is a function that maps $v(C_i, M)$ to the category's number. For example, when a single threshold t is given, a value $v(C_i, M) < t$ maps to 0 and all other values to 1. A higher score means that there are many differently classified cells. The difference between the classifications is squared to emphasize larger differences.

4. Experimental Setup

We performed experiments to test whether there are statistical differences between the methods. To that end, we implemented all the methods and measures described in Sections 2 and 3 in the Utrecht University Crowd Simulation framework [14]. The different parameters we used for the

Table 1: Overview of the settings for determining the fields used in the experiments.

Method	Settings
Grid-based [5]	$w = 1$ meter
Gaussian-based [7]	$R = 1$ meter; Sampling distance = 0.1 meter
Gaussian-based [12]	$R = 0.7$ meter; Sampling distance = 0.1 meter
Gaussian-based (geodesic)	$R = 0.7$ meter; Sampling distance = 0.1 meter
Voronoi-based [13]	$w = 1$ meter; Max. Voronoi cell area = 2 meter
Voronoi-based (geodesic)	$w = 1$ meter; Max. Voronoi cell area = 2 meter

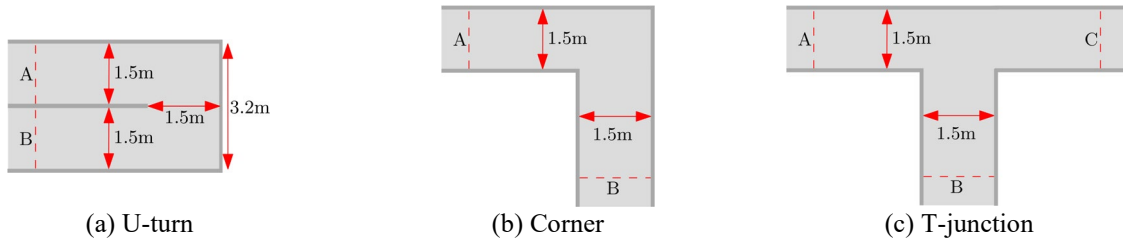


Fig. 3: Visual representations of the three basic environments used in the experiments.

methods are shown in Table 1. The Voronoi-based method is the one that Steffen and Seyfried [13] refer to as D_V .

We tested the methods on the three environments depicted in Fig. 3. These environments are building blocks for larger environments and are frequently used in studies [2,3]. For both the U-turn and corner environment, simulated pedestrians (agents) moved from line *A* to line *B*. For the T-junction environment, we tested two different variations. One with one entrance at line *A* and two exits located at *B* and *C* (scenario 1), and one variation where the agents entered from *B* and *C* and moved towards *A* (scenario 2). The agents were created at a random position behind the starting lines. The rate at which the agents were added was varied from 0.5/s to 2.5/s. The agents' preferred speed was set at 1.4 m/s.

We recorded the location and velocity of the pedestrians every tenth of a second for 10 simulated minutes, starting 2 minutes after the first pedestrian reached the exit. We used this data to calculate the different fields. We also calculated the time-average fields over a timespan of 1s, 10s and 60s.

5. Results

The analysis of the results is split into three parts. First, we look at how the size of the averaging window influences our analyses. Second, we will perform an in-depth analysis for the U-turn environment to show what information can be extracted using the discussed measures. Third and last, we make general observations for all the different environments tested. We only discuss the qs and bd measures. Other results are available on the author's website [9].

5.1. The Size of the Averaging Window

We analysed the effect of different averaging windows. The size of the averaging windows seems to be of little effect for the Gaussian-based methods when looking at the maximum values. Furthermore, the shape of the curves for the reported maxima stay the same. In case of the quadratic score, some details disappear when we increase the size of the averaging window. We found that averaging windows larger than 10s are not needed. Therefore, we will report all results for an averaging window of 10s.

5.2. In-depth Analysis of the U-turn Environment

We summarized the results in Figs. 4 and 5. At first glance, it seems that the results for qs for the Voronoi-based density methods give unexpected results for lower inflows: the entire environment is at the peak density. When the inflow is increased, it steadily declines. This is an artefact of how the Voronoi-based method is defined. Steffen and Seyfried [13] defined a minimal density within all Voronoi cells. When the cells are large enough, the reported local density value is only determined by this maximal area. When the inflow is increased, this setting becomes less and less influential on the maximal measured values.

Table 2: The categories used for the bd measure. These are based on the Levels of Service by Fruin [5].

Level	Density	Velocity	Level	Density	Velocity
A	[0,0.31]	(∞ , 1.3]	D	(0.72,1.08]	(1.22, 1.14]
B	(0.31, 0.3]	(1.3, 1.27]	E	(1.08, 2.17]	(1.14, 0.76]
C	(0.43, 0.72]	(1.27, 1.22]	F	(2.17, ∞)	(0.76, 0]

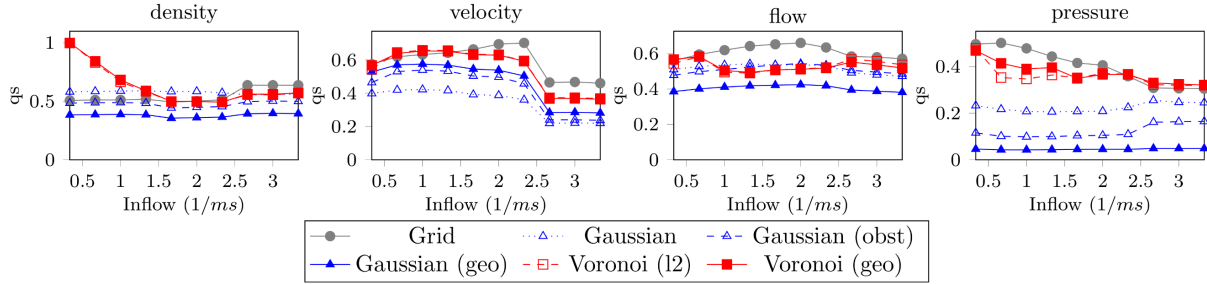


Fig. 4: The different qs values for the U-turn environment. The averaging window is set to 10 seconds.

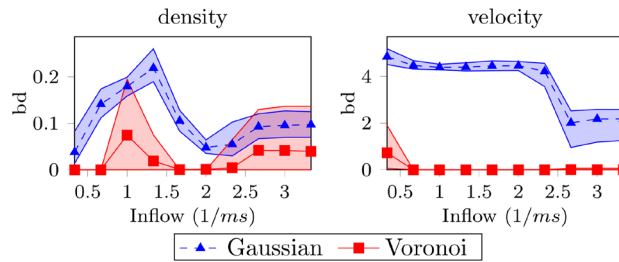


Fig. 5: The different bd values for the U-turn environment. The averaging window is set to 10 seconds. Upper and lower borders show the 5 and 95 percentiles.

Another interesting observation is the ordering of the different Gaussian-based methods. For the density, flow and pressure, the qs score is always lower, but for velocity it is always higher. This is a result of the use of the geodesic distance. The Gaussian-curves are more localized around the locations of the pedestrians in our version. As a result, less of the curves are on the opposite side of the obstacle and opposing velocities do not cancel each other out near the obstacle. This means that the geodesic Gaussian does not influence the area on the opposite side of the walls.

We also determined the bd for density and velocity measurements. The bins that were used are shown in Table 2. In case of the Gaussian method, it is interesting to note that the differences according to the velocity measurements were much bigger. It is also interesting to see that the Voronoi-based methods also show differences, although the qs was similar for all different inflows. However, at what inflow these differences register differs greatly on what metric we use. Further research is needed to determine what metric is more suitable or if more metrics should be used in conjunction.

5.3. Analyses of All Environments

For all tests for statistical significance we used ANOVA with a significance level of 0.05. For each environment, we performed statistical analyses for qs and bd . This reported that there were differences between the different methods. Using Tukey-HSD post-hoc analyses, we found that at almost all flows, all methods were different from each other at almost all levels of inflow.

The situations where these differences were insignificant were at the lower inflows for the Voronoi-based methods. This is probably a result of the maximal Voronoi cell size, as discussed in Section 5.2. For the other environments, similar results were found. That is, the geodesic Gaussian consistently reports higher values than the other Gaussian-based methods. The two Voronoi-based methods seem to generate similar results (although the differences are still significant).

Therefore, we cannot simply use one cut-off point for determining if a situation is safe. This is already widely known when looking at different situations and cultures, but to the best of our knowledge it was not yet shown for different methods. This asks for standardisation in this research field.

6. Conclusion

In this paper, we have discussed different metrics for evaluating pedestrian safety. Each metric can be evaluated by several different methods. We described a refinement for existing methods, namely the usage of the geodesic instead of the Euclidean distance, which takes obstacles into account. We have shown experimentally that this change results in significantly higher densities, flows and pressures.

Furthermore, we discussed four measures for comparing different methods. The maximum (*max*) and maximum difference (*maxdiff*) are already used to show differences between two methods. We introduced the quadratic score (*qs*) and bin distance (*bd*) to better show the differences between methods. We analysed all methods by using these four measures and concluded that the differences between the methods are significant. Since we are concerned with human safety, we prefer to err on the side of caution. Therefore, we advocate the use of our method, which consistently reports higher levels of “danger”.

One major selling point of analysing the differences between different methods using *max*, *maxdiff*, *qs* and *bd* is that it leaves no room for subjective interpretation of the results. As a result, any researcher performing a similar study should be able to end up with similar conclusions.

6.1. Future Work

Although the measures described in this paper show that there is a difference between different methods, it is still not easy to explain what causes them. Therefore, it stays important to look at renderings of the respective fields. It would be interesting to research if there is an automatic classification possible that captures what causes the differences. Furthermore, we only tested on smaller environments. We still need to determine if these measures are effective for larger environments, such as a building or a city.

It would also be interesting to see how the geodesic distance influences the measurements for the different metrics on multi-layered environments [8]. Previously, this was difficult because the Euclidean distance for pedestrians in multi-layered environments is not well defined, but the geodesic distance is. Therefore, it is possible to use the two methods described in this paper for multi-layered buildings.

References

- [1] U. Chattaraj, A. Seyfried and P. Chakroborty, “Comparison of pedestrian fundamental diagram across cultures,” *Advances in Complex Systems*, vol. 12, no. 3, pp. 393–405, 2009.
- [2] M. Creasemeyer and A. Schadschneider, “Simulation of Merging Pedestrian Streams at T-Junctions: Comparison of Density Definitions,” *Traffic and Granular Flow '13*, pp. 291-298, 2015
- [3] C. Dias and R. Lovreglio, “Calibrating cellular automaton models for pedestrians walking through corners,” *Physics Letters A*, vol. 382, no. 19, pp. 1255-1261, 2018
- [4] D.C. Duives, W. Daamen, and S.P. Hoogendoorn, “Quantification of the level of crowdedness for pedestrian movements,” *Physica A: Statistical Mechanics and its Applications*, vol. 427, pp. 162–180, 2015.
- [5] J.J. Fruin, “Pedestrian planning and design,” Technical report, 1971.
- [6] D. Helbing and P. Mukerji, “Crowd disasters as systemic failures: analysis of the love parade disaster,” *EPJ Data Science*, vol. 1, no. 1, 2012.
- [7] D. Helbing, A. Johansson, and H. Z. Al-Abideen, “Dynamics of crowd disasters: An empirical study,” *Physical review E*, vol. 75, no. 4, 2007.
- [8] A. Hillebrand, M. van den Akker, R. Geraerts, and H. Hoogeveen, “Performing multicut on walkable environments,” *International Conference on Combinatorial Optimization and Applications*, Hong Kong, 2016, vol. 10043, pp. 311–325.
- [9] A. Hillebrand. (2018, June 1). [Online]. Available: <https://research.arnehillebrand.nl/publications.html>

- [10] R. Kimmel, A. Amir, and A.M. Bruckstein, “Finding shortest paths on surfaces using level sets propagation,” *IEEE Transactions on Pattern Analysis and Machine Intelligence*, vol. 17, no. 6, pp. 635–640, 1995.
- [11] J. Mitchell, “Shortest paths among obstacles in the plane,” *International Journal of Computational Geometry & Applications*, vol. 6, no. 2, pp. 309–332, 1996.
- [12] M. Plaue, G. Bärwolff and H. Schwandt, “On measuring pedestrian density and flow fields in dense as well as sparse crowds,” *Pedestrian and Evacuation Dynamics 2012*, Zurich, 2014, vol. 1, pp. 411–424.
- [13] B. Steffen and A. Seyfried, “Methods for measuring pedestrian density, flow, speed and direction with minimal scatter,” *Physica A: Statistical mechanics and its applications*, vol. 389, no. 9, pp. 1902–1910, 2010.
- [14] W. van Toll, N. Jaklin, and R. Geraerts, “Towards believable crowds: A generic multi-level framework for agent navigation,” *ASCI.OPEN*, 2015.
- [15] F.L.M. van Wageningen-Kessels, S.P. Hoogendoorn and W. Daamen, “Extension of edie’s definitions for pedestrian dynamics,” *Transportation Research Procedia*, vol. 2, pp. 507–512, 2014.

Effect of architectural adjustments on pedestrian flow at bottleneck

Jianguo Wang¹, Jian Ma^{2, *} & Peng Lin³

^{1,2}School of Transportation and Logistics / Southwest Jiaotong University, Sichuan, China.

³Faculty of Geoscience and Environmental Engineering / Southwest Jiaotong University, Sichuan, China.

*majian@mail.ustc.edu.cn

Abstract – In the last decades, a series of terrible accidents happened within pedestrian crowds, which makes crowd dynamic a significant issue to be investigated. Literature reviews show that pedestrian flow presents different features within different architectural layout. In this paper, pedestrian movement properties at bottleneck are studied by carrying out series of experiments under laboratory condition. The influence of door sizes and exit locations on pedestrian crowd flow is investigated. It was found that larger door width resulted in shorter evacuation time and faster flow rate. By comparing the fundamental diagram among crowd evacuation, the average velocity increases as the width increases under the same density condition. Interestingly, the influence of the boundary layer, as well as the effective width on pedestrian crowd dynamic, was clearly observed. Our results suggest that the combination of exit width and location resulted in a synergistic effect, but the exit widths gradually became the most important factor influencing the flow rate.

Keywords: pedestrian crowd dynamics; door width; exit position; specific capacity; time interval.

1. Introduction

The occurrence of serious accidents within gathering pedestrians in the last decades attracted researchers from different disciplines focusing on crowd dynamics. Studies on crowd accidents show that a series of complex behaviors such as clogging, trampling and crushing at bottlenecks can be observed. It was found that the specific capacity J_s , capacity per meter width, is one of the most important characteristics of pedestrian dynamics at the bottleneck.

Summarizing earlier related studies, it can be found that several researchers have performed controlled experiments or empirical observations to collect pedestrian movement data. Kretz *et al.* [1] studied the pedestrian flow through a bottleneck with 0.40m depth. The J_s was calculated based on passing time of participants, and were about $2.20\text{m}^{-1}\cdot\text{s}^{-1}$ in 0.40m width and $1.85\text{m}^{-1}\cdot\text{s}^{-1}$ in 1.00m width. Daamen *et al.* [2] performed controlled experiments on the ingress of the crowd into a channel bottleneck with various doorway widths, population composition, stress level and presence of an open door. It was found the average capacities are for all widths lowest for the lowest stress level and highest for the highest stress level, and up to $3.31\text{m}^{-1}\cdot\text{s}^{-1}$ with a greater part of children. Garcimartin *et al.* [3-5] conducted controlled experiments where a group of students exits a room through a door with three competitive levels. The average specific flow measured in all the scenarios around $J_s=4.00\text{m}^{-1}\cdot\text{s}^{-1}$, and the maximum specific flow in high competitive condition was up to $4.50\text{m}^{-1}\cdot\text{s}^{-1}$.

For ethical and moral reasons, sometimes we cannot use people to perform laboratory experiments. As a consequence, biological entities have also been employed in structured experiments to investigate collective dynamics. This kind of method is effective due to the ease of handling and the simplicity of the equipment. Shiwakoti *et al.* [6-10] studied factors including the escape space, exit position, the placement of cylindrical obstructions and funnel-shaped exit on ants' collective movement. It was found when the exit is placed at the edge of a wall, the evacuation efficiency is higher when compared with the situation when the exit is placed in the middle of a wall. It was also found an appropriate size barrier placed in front of exit can promote evacuation. Pastor *et al.* [4] investigated the herd of sheep rushing through a door craving for food. The competitiveness among sheep was stimulated by warm days and cool days. Lin *et al.* [11] conducted a series of experiments with mice in a bi-dimensional space. A varying number of joss sticks were used to produce different level of stimulus to drive the mice to escape.

Although it was found that pedestrian flow presents different features within different architectural layouts, the impact of exit position and varying door widths still needs systematic investigation. What is more, studies performed with biological entities need to be verified with human movement data. Thus in this study, real people will be recruited to participate in structured experiments controlling exit positions and widths in a bi-dimensional building. The aim of this study is to systematically analyze the influence of the bottleneck width and position on pedestrian crowds during emergency condition. In this way, it can contribute to deepening our understanding of the evacuation process. Further, the data and results can be applied to construction design, pedestrian model validation, and even crowd management.

2. Experiment setup

In total 131 college students including 80 boys and 51 girls were recruited as participants in this research. All the participants wore white clothes and each one was given a red hat with a white marker in the center. In this way, these participants can be easily identified, and their trajectory data can be extracted. The design of the experiment was inspired by the researches performed by Pastor [4, 5] and Shiwakoti [6]. We considered more practical pedestrian facility layouts in our experiments. All the participants were ordered to evacuate as fast as possible. During the evacuation process, soft pushing as a way to make their way out was allowed for these participants. In our experiment, we made three architectural adjustments, as presented in Fig. 1(a), (b) and (c).

- Exit in the middle of the wall (Exit in the middle)
- Exit at the corner (Exit at the corner)
- The center of the exit located 1 m away from the side wall (Side exit)

For each architectural adjustment, we tested three different door widths, i.e., 0.6m, 0.8m, and 1.0m. To minimize the impact of randomness in the experiment, six repeated runs were conducted. Therefore, $3 \times 3 \times 9 = 54$ group experiments were conducted in all. Table 1 provides the details of these runs.

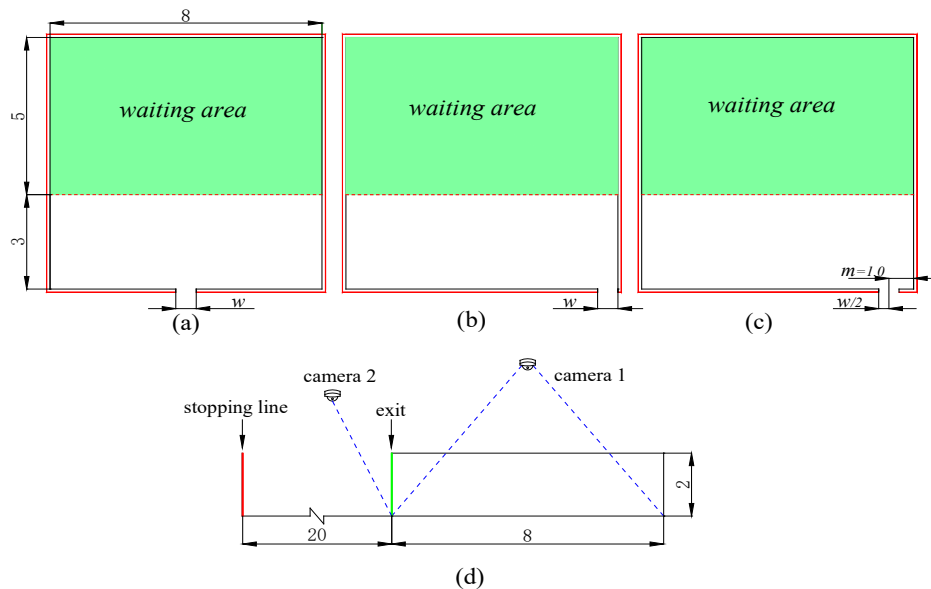


Fig.1: Experimental setups for the crowd egress experiments. (a) middle exit; (b) corner exit; (c) side exit; (d) the side view of experiment site; where w represents the width of the exit, and m refers to the distance from the edge wall. The unit in this figure is m.

The experimental process was recorded by two high-resolution cameras as shown in Fig. 1(d). Cam. #1 was mainly to capture all the chamber and record pedestrians' movement information during the experiments. Cam. #2 was to record the time participants passed through the exit. The film of the evacuation had a resolution of 1920×1080 pixels registered at 25 frames per second. From the

experimental video recording frames, we first marked out a green line at a height of 1.70m at the exit. In this way, we could manually extract the exact time each person's head passed this line. Thus, the time error of each participant passing the exit can be controlled within 0.04s.

Table 1. Details of the experiment runs.

Scenarios number	Exit widths (m)	Condition
1	0.6	Exit in the middle
2	0.6	Exit in the middle
3	0.6	Exit in the middle
4	0.8	Exit at the corner
5	0.8	Exit at the corner
6	0.8	Exit at the corner
7	1.0	Side exit
8	1.0	Side exit
9	1.0	Side exit

3. Result and analysis

The total evacuation time for different scenarios is shown in Fig.2. From Fig.2 we can see that the data show distinct variation feature. When the exit width was 0.8m, one or two particular evacuations in the condition of side exit can be faster than those of other conditions. Moreover, the exit position has an effect on the total evacuation time on all the evacuation scenarios. Finally yet importantly, the group evacuation time obviously decreases with increasing door width.

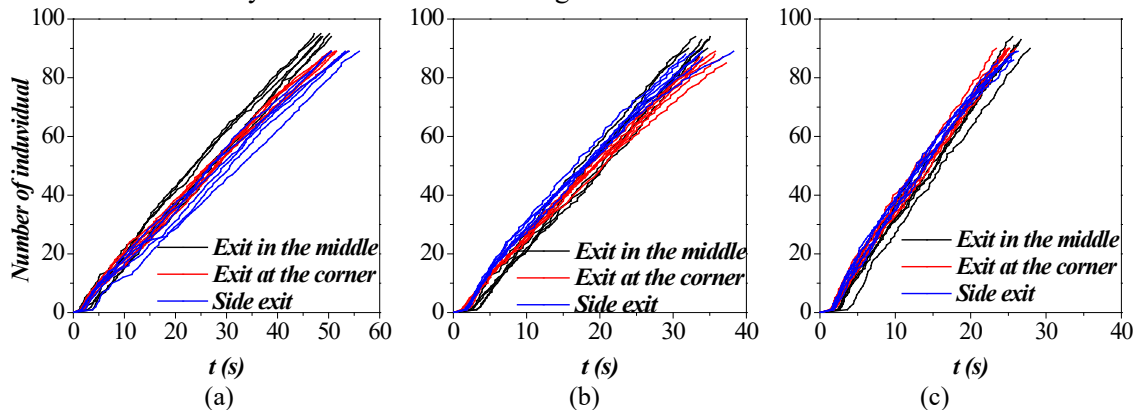


Fig. 2: Cumulative number of evacuated pedestrian through the exit. (a)-(c) correspond to 0.60 m, 0.80 m and 1.00 m door width, respectively.

Then, the total evacuation time was statistically analyzed, as presented in Fig.3. With increasing the door width, the mean evacuation time for the three conditions decreases. When the door width was 0.6m, the fastest movement time was about 48.93s for the scenarios where the exit was located in the middle. This value is approximately 4.9% and 9.5% less than that of the other two conditions. While in the 0.80m width and 1.0m width conditions, the differences among the three physical setups can be neglected. For the 0.80m door width, the average time was in the range of 33.57s to 35.60s. For the 1.00 m exit width, the average time ranged from 25.20s to 26.16s.

We then check the temporal evolution of the instantaneous flow rates at the bottlenecks. The average specific flow rates for all the experimental scenarios are shown in Fig.4. It should be noticed that the flow rate was calculated according to the time a group of 15 consecutive pedestrians needed to pass by the exit. In terms of the average flow rate in the experiments, there is a common observation that the measured specific capacity increases from 0.6m width conditions to 1.0m width conditions. When the door width was 0.60m, the specific capacity was $3.61\text{m}^{-1}\cdot\text{s}^{-1}$ for the middle exit condition, which is

obviously higher than that of the corner exit ($3.18\text{m}^{-1}\cdot\text{s}^{-1}$) and the side exit condition ($3.09\text{m}^{-1}\cdot\text{s}^{-1}$). When the door width was larger (0.8m), the biggest specific capacity was $3.92\text{m}^{-1}\cdot\text{s}^{-1}$ also in the middle condition, followed by $3.66\text{m}^{-1}\cdot\text{s}^{-1}$ in other condition and $3.39\text{m}^{-1}\cdot\text{s}^{-1}$ in exit at the corner condition. As the door width increased to 1.0m, the specific capacity was about $4.00\text{m}^{-1}\cdot\text{s}^{-1}$ for middle exit design and side exit design, while it is just $3.60\text{m}^{-1}\cdot\text{s}^{-1}$ for corner exit design.

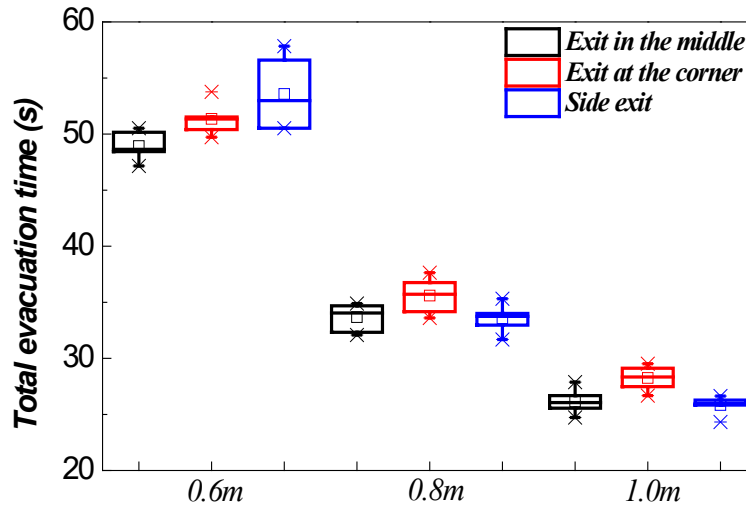


Fig.3: Comparison of evacuation time in various conditions

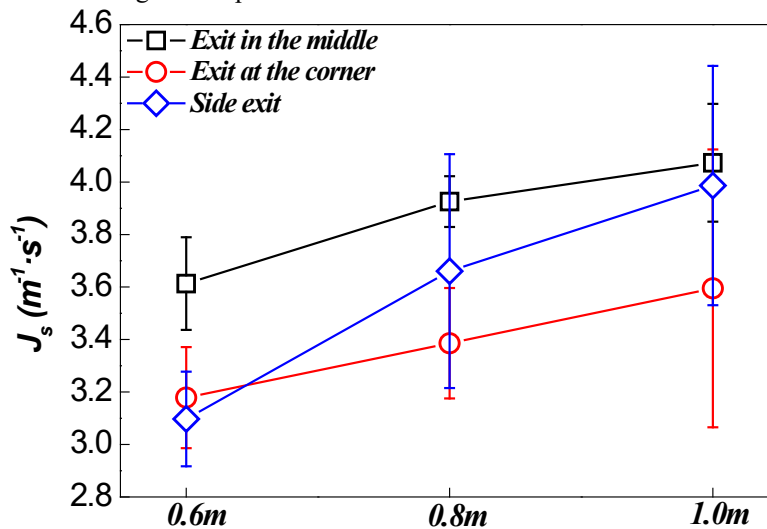


Fig.4: The average flow rate for 0.6m, 0.8m, and 1.0m, calculated based on the measured specific capacity between the first and last window. The error-bar illustrates the uncertainty of the mean flow rate at the bottleneck.

Interestingly, the average specific capacity from 0.6m to 1.0m width for corner exit scenarios was only about 90% of the ones for the middle exit condition. This may be due to the decrease of the effective width, a result of boundary layer effect. Meanwhile, the average specific capacity of the side exit condition was about 87% to 97% of that in the middle exit condition. This indicates that the combination of exit width and location resulted in a synergistic effect, but the exit widths gradually became the most important factor influencing the flow rate. Further experiments need to be performed to prove this discussion.

To further investigate the architectural adjustments on pedestrian crowd flow at the bottleneck, the trajectories for all the runs were extracted by PeTrack [12]. Fig.5 shows the trajectories of the head of each pedestrian in the experiments. From these trajectories, pedestrian characteristics, as density and

velocity are determined. It was found that in Fig.6 the average velocity decreased as the density increases in lower density area and kept around 0.11m/s, 0.14m/s and 0.18m/s from 0.6m to 1.0m door width when the density was large than 4.0per/m². In other words, the changes of the bottleneck width have an influence on pedestrian fundamental diagram under room evacuation condition. This is different from the findings in Zhang et al.'s [13] experiments, which is carried out in a long corridor. Reasons for the difference between these two experiments still need further investigation.

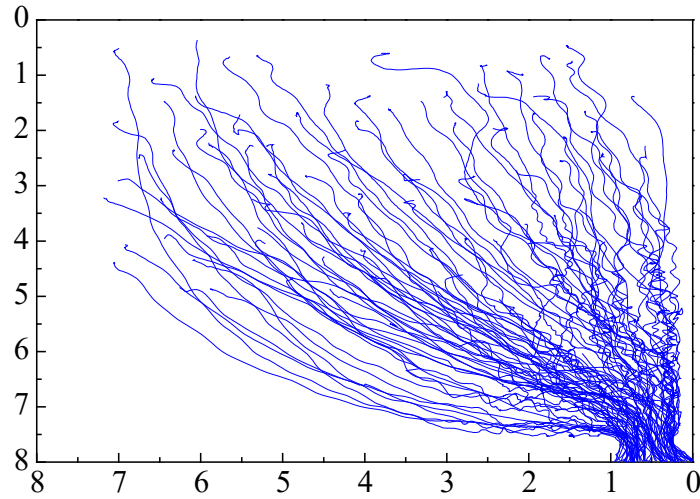


Fig.5: The extracted full trajectories of all subjects from exit at the corner with 1.0m door width.

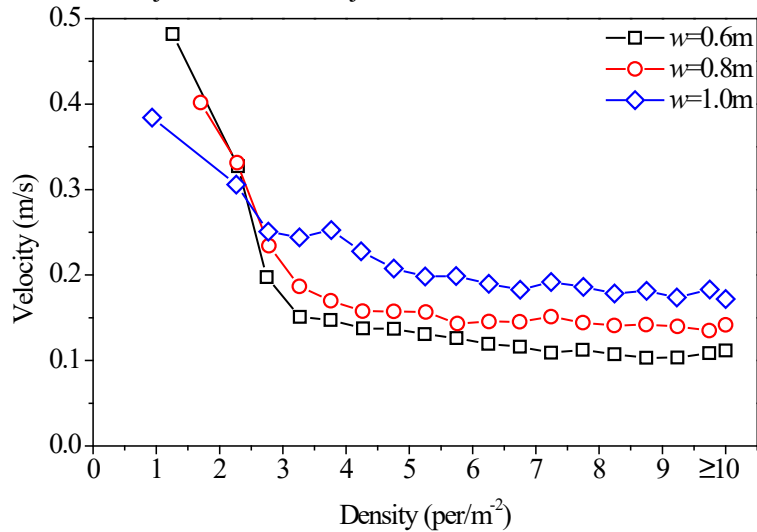


Fig.6: Comparison of fundamental diagrams among the three-door sizes in exit at the corner.

4. Conclusion

In this study, we present a series of laboratory pedestrian experiments to analyze the effect of architectural adjustments on pedestrian flow at bottlenecks. In total, 54 runs were performed by changing the door width and exit position. The whole process of the experiments was recorded by cameras and the pedestrian trajectories were extracted by PeTrack. It is found that irrespective of the exit locations, the greater width cases resulted in shorter movement time in all the repeated experiments. Based on the calculation of instantaneous flow rate, the measured specific capacity J_s are 3.09-3.61m⁻¹·s⁻¹, 3.38-3.92m⁻¹·s⁻¹ and 3.59-4.07m⁻¹·s⁻¹, respectively for 0.6m-1.0m door width. In comparison to previous studies, these values provide a more comprehensive and more practical foundation for competitive

evacuation. Moreover, the influence of the boundary layer (i.e. the effective width) on the evacuation process was clearly observed in our experiments. Here, we can hypothesize that the combination of exit width and location resulted in a synergistic effect, but the exit widths gradually became the most important factor influencing the flow rate. The final observation of this study is that the average velocity increases with the increase of exit width under the same density condition. This may challenge the former assumption that pedestrian fundamental diagram is barely influenced by building layout. It should meanwhile be noted that our findings are restricted to the limit door sizes and locations. In order to identify the transition point and optimum architectural adjustments, more evidence is needed and the author will conduct new sets of experiments in subsequent studies.

Acknowledgments

The supports from the National Natural Foundation of China under Project Nos. 71473207 and 71871189 are deeply acknowledged.

References

- [1] Kretz T, Grünebohm A and Schreckenberg M 2006 Experimental study of pedestrian flow through a bottleneck *Journal of Statistical Mechanics: Theory and Experiment* P10014-P
- [2] Daamen W and Hoogendoorn S P 2010 Emergency Door Capacity: Influence of Door Width, Population Composition and Stress Level *Fire Technology* **48** 55-71
- [3] Garcimartín A, Pastor J M, Martín-Gómez C, Parisi D and Zuriguel I 2017 Pedestrian collective motion in competitive room evacuation *Scientific Reports* **7**
- [4] Pastor J M, Garcimartin A, Gago P A, Peralta J P, Martin-Gomez C, Ferrer L M, Maza D, Parisi D R, Pugnali L A and Zuriguel I 2015 Experimental proof of faster-is-slower in systems of frictional particles flowing through constrictions *Phys Rev E Stat Nonlin Soft Matter Phys* **92** 062817
- [5] Garcimartín A, Parisi D, Pastor J, Martín-gómez C and Zuriguel I 2016 Flow of pedestrians through narrow doors with different competitiveness *Journal of Statistical Mechanics: Theory and Experiment* **13** 043402
- [6] Shiwakoti N, Sarvi M and Burd M 2014 Using non-human biological entities to understand pedestrian crowd behaviour under emergency conditions *Safety Science* **66** 1-8
- [7] Burd M, Shiwakoti N, Sarvi M and Rose G 2010 Nest architecture and traffic flow: large potential effects from small structural features *Ecological Entomology* 464–8
- [8] Shiwakoti N and Sarvi M 2013 Understanding pedestrian crowd panic: a review on model organisms approach *Journal of Transport Geography* **26** 12-7
- [9] Shiwakoti N, Sarvi M, Rose G and Burd M 2011 Animal dynamics based approach for modeling pedestrian crowd egress under panic conditions *Transportation Research Part B: Methodological* **45** 1433-49
- [10] Shiwakoti N, Tay R, Stasinopoulos P and Woolley P J 2017 Likely behaviours of passengers under emergency evacuation in train station *Safety Science* **91** 40-8
- [11] Lin P, Ma J, Liu T, Ran T, Si Y and Li T 2016 An experimental study of the “faster-is-slower” effect using mice under panic *Physica A: Statistical Mechanics and its Applications* **452** 157-66
- [12] Boltes M, Seyfried A, Steffen B and Schadschneider A 2010 *Automatic extraction of pedestrian trajectories from video recordings* Springer 43-54
- [13] Zhang J, Klingsch W, Schadschneider A and Seyfried A 2012 Ordering in bidirectional pedestrian flows and its influence on the fundamental diagram *Journal of Statistical Mechanics: Theory and Experiment* **2012** P02002

The development of drunk behaviour during evacuation

Simeon A. Doychinov¹, Anne S. Dederichs^{1,2}

¹ Dept. Civil Engineering, Technical University of Denmark

² RISE, Research Institutes of Sweden

Abstract - The intoxication of the occupants is hardly considered in the fire safety design, due to the lack of data on the subject. Recent research experiments into the influence of alcohol on evacuation have shown evidence that there might be a correlation between the development of drunk behaviour and the surroundings or context in which the occupants are situated. That is why the experiment in this report investigated the development of drunk behaviour in a group of people within a party environment, independently of alcohol, with the use of non-alcoholic beer as a placebo. The participants were put through 3 identical exercises, which were aimed at testing their balance, reaction times, concentration, hand to eye coordination, problem solving skills, cognitive skills and cooperation. In addition to that they performed 2 evacuations that were used to interrupt their 'drunk behaviour' and test their reaction, decision and overall evacuation times. They were also analysed for signs of drunk behaviour with video and sound recordings. The results showed clear reduction of performance in the tests for concentration, hand to eye coordination, problem solving skills, cognitive skills and cooperation after the consumption of the beer, but little change in the balance tests. Apart from that, some of the participants showed signs of drunk behaviour, such as playfulness and increase in noise after the alcohol was consumed and these were reduced after the environment changed. Based on this it was concluded that even with non-alcoholic beer some of the participants developed drunk behaviour, like that observed in previous experiments with the use of alcohol.

Keywords: evacuation, drunk behaviour, placebo, experiment, fire safety

1. Introduction

Fires at venues where alcohol is consumed have had high consequences in terms of loss of human life and some of the deadliest ones on record have occurred in recent years [1]. Large amounts of people tend to concentrate at such places, and these go beyond night clubs and bars. People number in the thousands at football stadiums, for example, such as the Bradford City stadium where a fire claimed the lives of 56 people, while some of the intoxicated crowd were seen laughing and many moving or standing by with their drinks in their hands [2].

The risks at such places are further increased due to the higher possibilities of reckless behaviour by the participants when they are under the influence of alcohol. Despite this, intoxication of the occupants is not considered in the design process for areas and rooms where alcohol consumption is expected, mainly due to the lack of data on the subject. Consequently, the venues that serve alcohol today might pose a greater risk than is currently expected even if they follow current fire safety regulations.

Recent research experiments into the influence of alcohol on evacuation at DTU have given some new insights and raised many new questions [3] [4]. They have shown evidence that there might be a correlation between the development of drunk behaviour and the surroundings or context in which the occupants are situated. If this correlation is found to be significant enough, it could be used to improve the reliability of further research into the subject and to develop useful methods of crowd control for intoxicated people. That is why the experiment which this report analyses investigates the development of drunk behaviour in a crowd of people within a party environment, independently of alcohol, with the use of non-alcoholic beer as a placebo.

1.2. Knowledge on the effects of alcohol on human behaviour

The lack of research on the effects of alcohol is not isolated to the field of fire safety. As described in [5], research into the effects of alcohol on human behaviour has for a long time had its progress impaired by the disproportionate focus on problems like violence, affecting only a small minority of drinkers, while the study of 'normal' drinkers has been neglected.

A large contribution to this is the fact that nations with a strong temperance tradition and ambivalent attitudes towards alcohol have dominated the field of alcohol studies, while cultures in which drinking is not perceived as a problem have seen little need to conduct extensive research on the subject, as observed by [6].

Nevertheless, there is some useful research that sheds some light on the various effects alcohol could have on people. Both comparative studies and controlled experiments have demonstrated that, while ethanol produces well-understood neurochemical changes, the wide variations in social and behavioural outcomes of drinking can mainly be explained with reference to cultural factors, and to culturally determined beliefs about the effects of drinking [7-13].

1.3. Previous research

Research at DTU on the influence of alcohol on evacuation is still in its early stages and it has predominantly provided insight on the research methods to be used for organizing experiments.

Each experiment has been built on the previous ones and expanded the knowledge on participant behaviour. The current experiment uses insights from its predecessor "Reaction and decision time of evacuees, A study regarding the influence of alcohol on the reaction and decision time" by Poul Brinck Rask [3] and both rely on data obtained from an experiment from 2015, which compares participants performing tests under the influence of alcohol and while wearing Fatal Vision® Impairment Goggles, which simulate drunkenness [4]. Madsen and Hansen give convincing evidence that participants behave differently while wearing the goggles compared to when they are under the actual influence of alcohol.

That is why the experiment by Rask used alcohol to obtain its results. These results indicate that the participants' level of intoxication might be significantly influenced by their surroundings, which raises the question whether a certain level of alcohol intoxication by itself might not be enough to cause drunk behaviour. Therefore, this latest experiment investigates the influence of surroundings on the development of intoxication with the use of placebo alcohol.

All of these research experiments use testing methods that are connected to evacuation of buildings in different ways in order to provide further knowledge on the topic, along with knowledge on the behaviour of people.

1.4. Objective

The experiment from this report investigated the development of drunk behaviour in people as a consequence of the setting and context of the situation they are in. To do that, it was devised in such a way as to assess how the occupants' mental states are changing, what makes them change and what are the consequences of that in relation to the evacuation process. This is done by recreating a party-like environment, like that of a night club or bar, while serving non-alcoholic beer and observing its effects on volunteers and how they are affected when the environment changes.

2. Methods and Experiment Set-up

To accomplish the objective the experiment environment was set up to facilitate a mood of intoxication for the participants, similar to that of a party or a bar; non-alcoholic beer was served. The participants were only briefly brought out of this environment with two evacuations. They performed exercises chosen to measure their coordination, concentration, reaction times, cooperation and balance and were recorded with cameras with audio recording.

The participants were volunteer students from DTU campus. They were of various nationalities and their ages ranged from 19 to 37, although the majority were between 21 and 28 years old. This was a characteristic sample of DTU students and such a mix of ages and backgrounds is a common sight at campus social events.

The experiment was run in the course of 2 hours. Each exercise served as a reference to the next one. Thus, the first exercise was not intended to be a reference to the third (Figure 1).

The goal of this experimental set-up is to have the participants complete the same tasks in 3 different mental states. The only difference between the first and the second exercise is that the second one is done after the consumption of the beer during the scheduled 30 minutes 'party time'. The first evacuation also serves as a reference to the second one and is done before the drinking. It additionally serves as a transition to the 'party time'.

The use of the evacuations as transitions is done because they force the participants to briefly move out of the test environment to interrupt their mood and make them mentally distinguish the 'party time' from the other parts of the experiment. This is especially important for the second evacuation, since it aims to interrupt the participants' drunk behaviour.

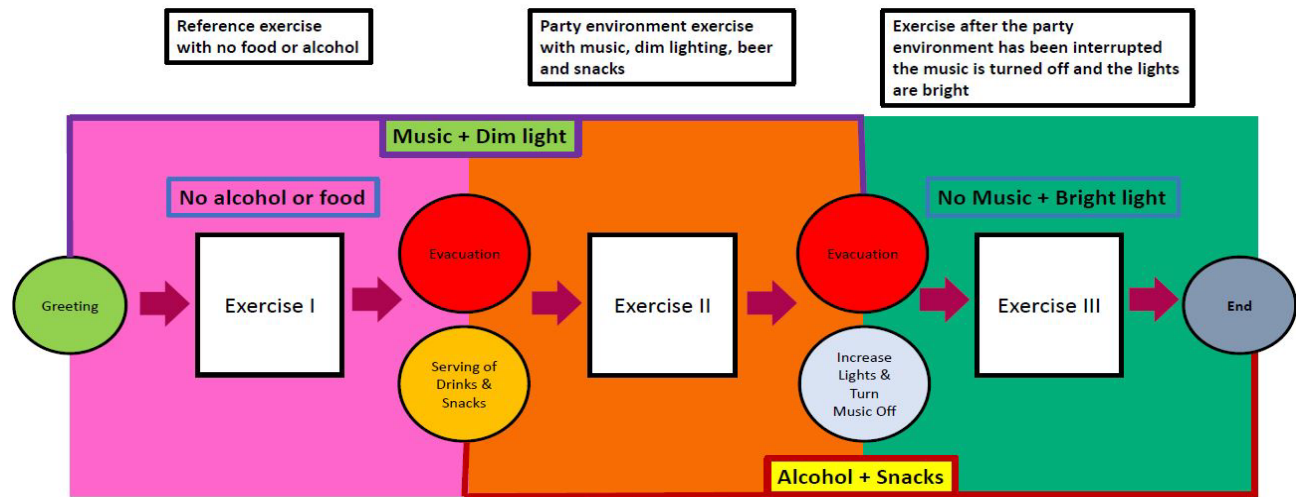


Figure 1 Experiment visualisation

Each exercise contained 3 tasks. The tasks were identical for all 3 exercises. Each participant also had to write down the amount of drinks they have had before the exercise.

The first task was to complete a printed maze of medium difficulty with a pen as fast as possible, while trying to avoid touching the maze walls. The data collected from this task was the time it took each person to complete the maze, the amount of wrong turns each person made and the amount of times they touched the walls of the maze. This type of task engages the participants' patience, cognitive process, hand-eye coordination, problem solving, concentration and, as research has shown, parts of the brain that are connected with orientation are active while solving mazes [14 -16].

The second task in each exercise was the Flamingo test. This is a popular test that requires the participants to stand on one leg for 60 seconds. Every time the person lost their balance and needed to touch the ground to restore the balance the timer was paused until the person restored the balance on one leg. The result was the number of times the person touched the ground. Additionally, it was to be noted down if the person swayed while balancing, used arms for balance or hopped; and it was encouraged to give additional comments if needed.

The third task of each exercise was the Up & Go Test. This is a test of both reaction time and balance. In it two people take turns to test each other - one of the participants sits on a chair and the other stands 2.5 m from them at a marked spot with a timer, see Figure 2.4. When the participants have assumed their

positions, the standing person gives the signal 'GO' and starts the timer, upon which the sitting person has to get up and run as fast as possible around the standing person and sit back on the chair. As soon as they have done that they should yell 'STOP'. When the signal 'STOP' is given the standing person should stop the timer and write down the recorded time. Additionally, they are encouraged to give extra comments on the performance.

The amount of people that participated in the experiment was low, so in order to make more accurate assumptions of the general population based on the data from this experiment the t score formula was used (Mason, Gunst, and Hess 2003).

The formula was applied for a two-tailed distribution of two samples with unequal variance. The final outcome of this calculation is the percentage of certainty with which it can be claimed that the two samples are significantly different. When that percentage is over 95% it is statistically safe to assume that the samples are significantly different.

The participants in the experiment were between the ages of 19 and 37, with the majority being in their mid-twenties. Therefore, they are most representative of this age group.

Another source of error is the gender ratio imbalance, similar to previous experiments. There were 3 times more men than women, so the results might be more indicative of male behaviour.

Additionally, due to the limited amount of people, the same people had to complete all the evacuations and exercises, which means that with every next repetition they gain a certain level of skill in performing them, which affects their results.

To make sure that the experiment did not violate any ethical laws, the National Scientific ethical Committee and the scientific ethical committee at Hovedstaden were provided with detailed information about it. They informed the organizers that if the experiment does not conduct medical experiments it is not required to consult them.

Furthermore, the campus services were consulted about the safety rules that needed to be followed while using the campus facilities for the experiment. Concerning the video recordings, the Danish Data Protection Agency's website states that permission from them is not needed when the data is used in a master's thesis study and with participant consent [17]. The recordings were stored according to university sensitive data storage rules.

The participants were informed about all aspects of the experiment, except the exact alcohol content of the beer. They were given an experiment timetable and were asked to sign a form of consent before participating.

6. Results and Discussion

The participants were divided into three groups based on the amount of beer they drank and whether they drank it throughout the experiment or only in the beginning of the 'drinking time'. These groups are given the names 'high beer consumption group', 'medium beer consumption group' and 'low beer consumption group' (Figure 2).

Beers	Ex2	3	5	5	6	4	5	4	2	2	2	2	2	3	2	2	3	3	3	2	2	3	3	2
	Ex3	5	6	6	8	7	6	5	3	3	3	3	3	4	3	2,5	3,2	3,5	3	2	2	3	3	2,5

Figure 2 High, medium and low beer consumption groups in green, red and blue respectively and the amount of beer each person drank by the first and by the second exercises.

6.1. Maze Task Results

Firstly, the scores from the participants were compared between the 3 groups within each exercise. The difference between the low and medium consumption groups has the highest percentages, but still 86% is the highest one. The percentages are highest in Exercise 1, before the participants consumed the drinks, and get lower with each consequent one.

After the consumption of the alcohol the standard deviations increase, which makes the certainty drop. This may mean that some people experienced the placebo effect while in others it was weaker or did not develop at all, which results in the increasingly different performance. From Figure 3 the differences between the mean scores can be seen.

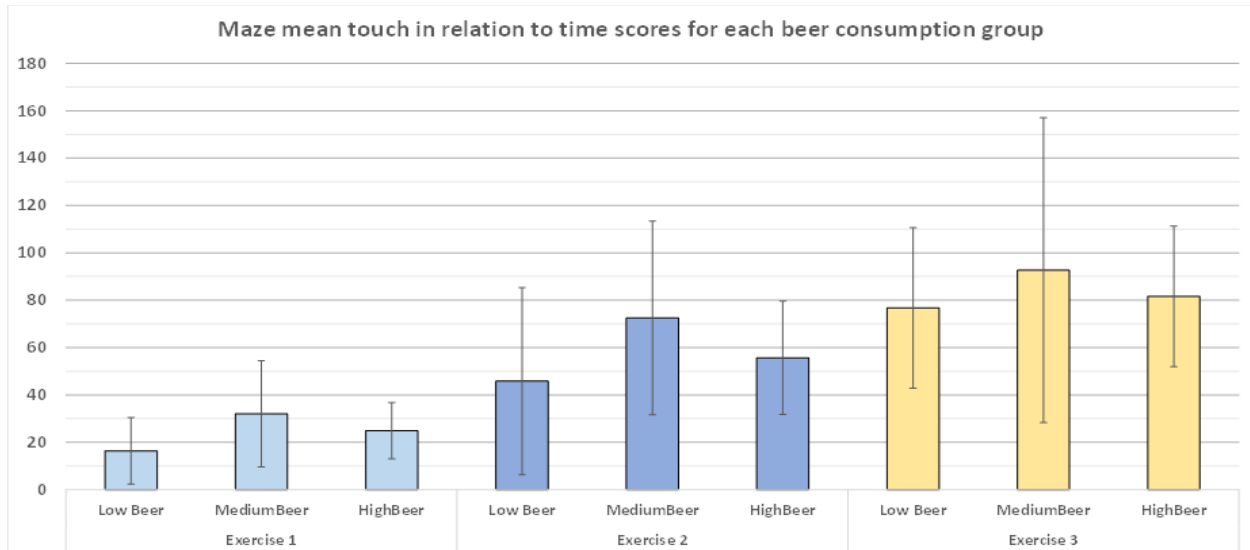


Figure 3 Maze mean touch/time results for each group in each exercise

On Figure 4 the results of each participant are displayed for each exercise based on how much beer they drank by the end with a trend line for each exercise's results. Thus, if a person drank 5 beers in total, their results of each exercise would be at 5 beers and only the scores would change. Two people failed the task in the second exercise, one of which had drank 6 beers and the other 7, so they are missing from the chart.

From the chart it can be clearly seen, that the performance of the participants is dropping as their touches increase in each consecutive exercise and the differences between them are becoming more exaggerated after the consumption of the alcohol but at the same time follow a similar curve.

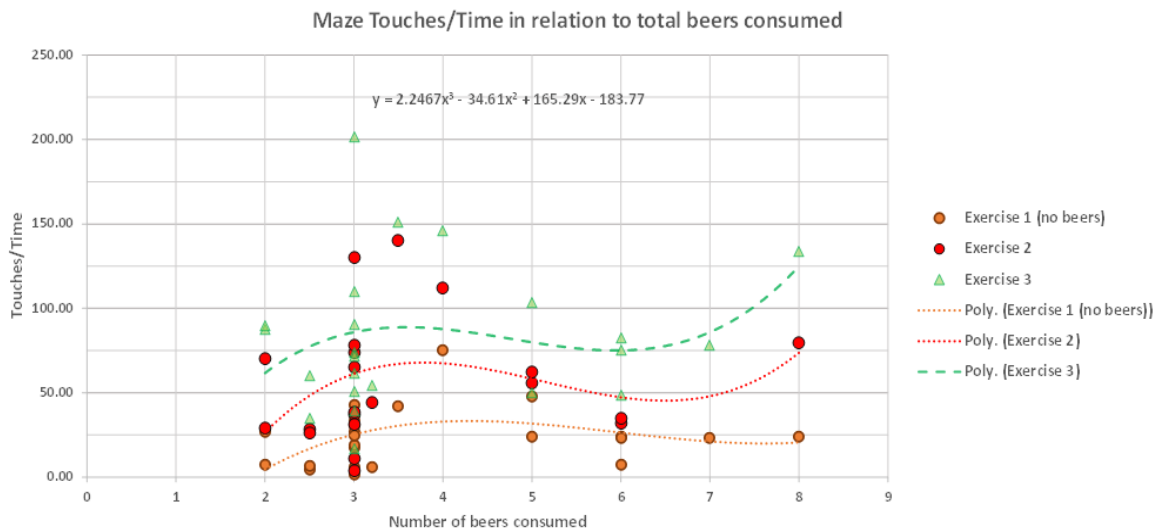


Figure 4 Maze touches per minute scores in relation to beers consumed

In another comparison, the percentages are checked for each group, comparing the group's results from exercise 1 against the results from exercise 2 and, likewise, exercise 2 against exercise 3. From these comparisons the differences in scores are much more certain when compared between exercises, especially

between the first and second exercises. The individual group performance differences between Exercise 1 and 2 are above 95% with the exception of the low consumption group, which is 94%. And when all participants are grouped together the differences are above 95% for both exercises.

From Figure 3 & Table 1 it is visible that the mean scores markedly increase with each consecutive exercise and the standard deviations follow this trend as well, except for the low beer consumption group's third exercise scores, where the deviation slightly decreases.

Table 1 Maze mean touch/time results for all people together and their standard deviations (SD)

	Mean	SD
Exercise 1	23.743	17.1
Exercise 2	56.396	36.744
Exercise 3	83.069	42.853

An additional note should be made about the two people who failed to complete the task in the second exercise. Because in this task the lower the values are the better the performance is and there is no limit to how high the values could go, there is no way to consider the failures into the statistics. That is why the failures are mentioned here separately.

The amount of wrong turns taken is highly dependent on the maze route. Thus, the amount of wrong turns per minute is calculated for each participant and then the means from these results are compared between the different groups only within each exercise.

From the t-test scores the percentages are too low for these results to be conclusive. Only in the comparison between the low and high consumption groups in Exercise 2 there seems to be a very high percentage of 93%, but still lower than the 95% certainty requirement.

What additionally should be noted about these results is that, just as in the touch/time results, the differences that were present between the groups became more pronounced, except that in this case their results are better with each consecutive exercise.

6.2. Up & Go Task Results

The times of the completion show little variation and based on the statistical analysis this variation cannot be used to prove significant differences. The participants, on average, performed the same or only slightly better every next exercise. This can be seen also in a previous experiment that was done with the use of real alcohol. It is not clear to what extent these results are because of the alcohol and to what extent because of learning, but the latter is considered the more probable.

One thing that is clear from both the previous experiment and this one is that drinking between 2 and 8 beers has little to no negative effect on the performance of the participants in this task.

Apart from the time scores of the participants this task also allowed them to make additional comments. There was only one comment in the first exercise, four in the second one and one in the third. While in the first and last exercises the single comments are strictly related to issues with the participants' performance in the task and in the case of the first exercise it was written by an assisting organizer, in the second exercise two of the comments are 'funny' comments.

This suggests not only a slightly higher rate of failure of the participants to perform in the task during the second exercise, but also a more playful and relaxed attitude among some of them.

6.3. Flamingo Task Results

In the Flamingo task the mean number of errors varies very slightly throughout the experiment for each group and at the same time the standard deviations were large, from which no significant differences could be deduced.

These results are in some ways similar to the results from Madsen and Hansen. However, in that experiment the performance becomes worse after consuming the beer, whereas in this experiment the

performance of the medium and high beer consumers worsens in the second exercise and improves in the third while the performance of the low beer consumers improves in each consecutive exercise.

6.3. Crowd behaviour and observations

During the exercises the participants tended to become quiet during the maze task, which required them to focus. During other tasks they tended to converse and make noises due to movement. This was later confirmed with an analysis of the sound recordings of the experiment.

During Exercise 1 they were generally quiet and focused on completing the exercise and the only noise they made was when asking questions on how to perform the tasks. Then, after the first evacuation, they started consuming the beer and became noticeably louder and more relaxed. Some of them started playing drinking games or just games for fun. This changed after the second evacuation. After it was complete they became increasingly quieter and focused on completing the exercise, though some of them were still noisy, especially the ones that continued to drink and drank the most. Their performance during the two evacuations was almost identical.

The magnitudes of the noise in the midst of the participants were extracted into charts and trend lines were generated. Then it was observed from the magnitudes and clearly seen from the trend line that the noise level peaks during the middle of the drinking time and subsides when Exercise 2 begins and then more when at the start of Exercise 3, although it is still higher afterwards than it was during Exercise 1. This is visible on all 3 recordings and is considered as conclusive evidence that the participants became louder with the consumption of the beers.

7. Conclusion

The experiment from this report has tested the development of drunk behaviour, without the consumption of alcohol, in a group of 23 people from a mix of cultural backgrounds for the purpose of evacuation. This was achieved by recreating a 'party-like' environment within the experiment area and using non-alcoholic beer in the hopes of inducing a placebo effect and then test whether this effect influences the participant's evacuation capabilities.

None of the participants showed any signs of suspicion about the alcohol content of the beer and the majority drank continuously throughout the second two thirds of the experiment. During that time several distinct changes were observed in them.

Firstly, the mean maze touch/time results of the participants showed reduced performance in each consecutive exercise. This points to a reduction of hand to eye coordination and focus, which could be either due to inebriation or due to a reduction in the amount of effort put to complete the task successfully. In addition to that, there was an increase in frivolity and emotional behaviour during the second exercise after the consumption of the beer, judged by the comments and notes for all tasks, some of which were irrelevant or 'funny', and two of the participants gave up on completing the task during the exercise. In one of these cases the participant scratched up the maze angrily.

Furthermore, the participants displayed increased contrast in performance, resulting in increased standard deviations after the consumption of the beer and an increase in noise level, which peaked during their drinking time and gradually decreased as the experiment was ending.

At the same time there were things that did not change after the consumption of the beer. The performance from the balance tasks and the evacuations showed little to no change or even very slight improvement, which was in some ways consistent with previous experiments that used normal alcoholic drinks to conduct similar tests.

Overall, the experiment results are in many ways similar to previous experiments with alcohol and show some definite signs of the development of drunk behaviour independently of alcohol. Additionally, there is proof that drunkenness, whether caused by alcohol or a placebo, causes significant changes in cooperation, willingness to follow instructions, focus and mood in some people and it might cause opposite effects in others. There is no proof yet that it impairs the overall group movement capabilities, but there is evidence that the decision making, and course of action of the group and individual might be significantly altered.

References

- [1] “Deadliest public assembly and nightclub fires,” *N. F. P. Association*, 2017. [Online]. Available: <http://www.nfpa.org/public-education/by-topic/property-type-and-vehicles/nightclubs-assembly-occupancies/deadliest-public-assembly-and-nightclub-fires#outside>. [Accessed: 01-Nov-2017].
- [2] FSUK, “The Bradford City Football Fire,” *Fire Service UK*, 2014. [Online]. Available: <https://web.archive.org/web/20130216013625/http://bradfordcityfire.co.uk:80/>.
- [3] P. B. Rask, “Reaction and decision time of evacuees A study regarding the influence of alcohol on the reaction and decision time, Indflydelse af alkohol på reaktions og beslutningstid i forbindelse med evakuering,” 2017.
- [4] A. Madsen and M. W. M. Hansen, “The effect of alcohol related impairment on evacuation characteristics,” 2015.
- [5] D. Morris, “Social and Cultural Aspects of Drinking,” *Rep. to Eur. Comm.*, no. March, p. 102, 1998.
- [6] K. Mäkelä, “Consumption level and cultural drinking patterns as determinants of alcohol problems,” *J. Drug Issues*, 1975.
- [7] L. T. Midanik, “Drunken comportment: A social explanation,” *Addiction*. 2002.
- [8] M. Marshall, *Weekend warriors: alcohol in a Micronesian culture*. California: Mayfield, 1979.
- [9] G. A. Marlatt and D. J. Rohsenow, “Cognitive processes in alcohol use: expectancy and the balanced placebo design,” in *Advances in Substance Abuse: Behavioral and Biological Research*, K. Mello., Greenwich: JAI Press, 1980.
- [10] H. L., D. L.J., and M. J.K., “Drinking contexts, alcohol beliefs and patterns of alcohol consumption: evidence for a comprehensive model of problem drinking. *Journal of Drug*,” no. 25, pp. 783–798, 1995.
- [11] S. Peele, “Utilizing culture and behaviour in epidemiological models of alcohol consumption and consequences for Western nations,” *Alcohol Alcohol*, 1997.
- [12] D. B. Heath, “Cultural variations among drinking patterns,” in *Drinking Patterns and their Consequences*, I. M. Grant and J. Litvak, Eds. Washington: Taylor & Francis, 1998.
- [13] H. D.B. and R. H., “Community reactions to alcohol policies,” in *Drinking Patterns and their Consequences*, I. M. Grant and J. Litvak, Eds. Washington: Taylor & Francis, 1998.
- [14] P. Kirsch *et al.*, “Brain activation during mental maze solving,” *Neuropsychobiology*, 2006.
- [15] R. W. Skelton, S. P. Ross, L. Nerad, and S. A. Livingstone, “Human spatial navigation deficits after traumatic brain injury shown in the arena maze, a virtual Morris water maze,” *Brain Inj.*, 2006.
- [16] J. D. Van Horn *et al.*, “Changing patterns of brain activation during maze learning,” *Brain Res.*, 1998.
- [17] “The Danish Data Protection Agency.” [Online]. Available: <https://www.datatilsynet.dk/english/the-danish-data-protection-agency/introduction-to-the-danish-data-protection-agency/>. [Accessed: 20-Sep-2017].

Movement parameters of persons with disabilities on evacuation by lifts

Martin Szénay, Martin Lopušniak

Institute of Architectural Engineering, Faculty of Civil Engineering, Technical University of Kosice
Vysokoskolska 4, 042 00, Kosice, Slovak Republic
martin.szenay@tuke.sk; martin.lopusniak@tuke.sk

Abstract - In 2010 it was defined five challenges for the solution of evacuation of persons in buildings to 2020. One of the challenges is to implement helpful technologies during evacuations from buildings – lifts. Needed steps for fulfilling this challenge are also quantification of missing data which are dealing with evacuation of persons with disabilities. From 2002 all public buildings in Slovak Republic have to be also accessible to persons with disabilities, but it is also a global problem. In present exists just small number of informations of movement parameters of persons with disabilities during evacuation by lift. There for, this work was focused on collecting these informations. The data collection was realized by using an in-situ experiment. The aim of the work was to quantify the phase stages of evacuation by elevators for persons with disabilities (speed, time, movement and capacity parameters). Person's movements were monitored during the measurements, arrival to lift, cabin entry and exit from the cabin, including leaving the bounded area. Arrival to lift included movement in the bounded area in front of the lift, until the moment of pushing the button was pressed to call the lift. The time of cabin entering includes the time from the beginning of opening the lift doors to the beginning of closing of the lift doors. The exit from the cabin includes the time from opening the lift doors, passing through the lift doors to leaving the bounded area. In total, ten participating persons in the experiments imitated wheelchair movement and movement with leg fracture. Measurements were made on two lifts, where person evacuating himself or with the help of another person. Everyone performed each measurement three times. A total of 720 measurements were performed in the work. According to the results of the experiment it can be stated that cabin entry is longer for a person on the wheelchair than for a person with a leg fracture, but the difference is even bigger during exit from the cabin, including leaving the bounded area. During the experiment, various movement techniques have been observed that may affect their overall the time of cabin entry and exit from the cabin. Obtained results can extend existing evacuation model to the possibility of using the lift. The obtained results quantify the individual phase stages of entering to the lift and exiting of the lift for persons with limited movement.

Keywords: Lift evacuation, Experiment, Movement parameters, Persons with disabilities, Evacuation time

1. Introduction

Passenger lifts are not used to their full potential [1]. Passenger lifts are allowed for evacuation except in exceptional cases and under specific conditions. In most cases related to buildings, people are forced to use staircases for evacuation. In this way buildings represent a series of challenges for safe evacuation, mainly based on 2 reasons – limitations of movement from the point of view of persons mobility impairments [2][3], or fatigue during movement downstairs [4]. According to the Slovak standard, three groups of people movement properties are taken into account. The first group includes persons able to move alone. The “persons of limited mobility” belong to the second group. Persons, whose evacuation is more demanding than in the case of other persons. Old people, children, disabled persons of limited mobility are an example of this group. The third group includes “immobile persons”. Persons, whose evacuation is possible only with help of other persons. For example, mentally affected persons, in-patients at clinics with serious health states, persons temporarily unable to move, infants,

toddlers and the like belong to this group. According to the Statistical Office [5], almost 20% of inhabitants are persons in the old pension age (62 years and more), and 12% of inhabitants are persons of the school age (4 to 15 years) in Slovakia in 2017. Altogether at least one third of inhabitants of the Slovak Republic can be considered persons of limited mobility in the case of the proposal of escape routes. Evacuation using stairs is difficult and practically impossible without assistance of other person for the persons of limited mobility, for example on wheelchair. Lifts are inevitable for evacuation of persons of limited mobility. This leads to shortening of the overall evacuation time.

In 2010, Averil [6] defined several necessary steps to cope with large challenges presented by the solution of evacuation in buildings. The quantification of missing data dealing with evacuation of persons using lifts is one of these steps. Up to the present day, several papers and studies on evacuation of persons using lifts were carried out based on simulated calculations or in-situ experiments. In their paper, Ding N. et al [1] established objectives to ascertain how evacuated persons behave and factors affecting their behaviour during fire and evacuation. They decided to carry out a real experiment using simulated conditions of fire, where the lift should be used by persons for evacuation. In this way this study was able to obtain data about time of get in and get out of the lift, time of opening and closing the lift door and behaviour of persons during the formation of a queue. According to results of the study, time of getting into the lift was shorter than time of opening and closing the door. They have also ascertained that the number of evacuated persons affects their behaviour, but presence of smoke not. The shape of queue of persons has influence on time of passage of persons through the lift door – the shape of a curve is quicker than the shape of a line. Study by Ding Y. et al [7] can served as another example in this field, where simulation software was used to ascertain, beside others, which ratio of persons using the lift and staircase has the most favourable effect on the course of evacuation. Therefore they modelled in their work 28-storey building with the staircase and 2 lifts. Their work also included different age groups of people. They said that the simulation results show that the optimal percentages of the occupants evacuated by the lifts, when achieving the shortest evacuation time, is almost not related to the number of evacuated persons and floors. Further, when focusing on age groups, it was ascertained that if older persons used the lift, the staircase will not be significantly overloaded. At the same time, if the lift is used by children, the rate of its use will be improved. Therefore the selection of portion of persons by age categories, who should be evacuated by the lift can reduce congestions on staircase, and effectively speed up the evacuation process. Papers by Heyes [8], Kinsey et al. [9] and Jönsson et al [10] paid attention to waiting problems and they have demonstrated that people prefer the use of lifts during evacuation instead of staircases, but they are not willing to wait for the lift too long. It is anticipated that 90 to 97% of people will not wait longer than 5 minutes. The choice to wait is increased with the increasing height of the building – people are willing to wait for a longer period of time on higher floors than on lower ones. For example in the next study using the simulation tool, Andrée et al [11] focused on the high-rise building, selection of exits and waiting time for evacuation lifts. Their objective was to examine, inter alia, effect of the lighting system on the selection of exits and to quantify waiting time for lifts. The study resulted into the fact that the well and simply designed system of marking escape routes will affect the selection of an exit. This system can also be used for increasing the portion of people, who will decide for the evacuation lift as the first choice of escape. Further, their results have demonstrated that people were willing to wait for the lift up to 5 minutes, but if they decided to wait, their waiting is usually extended to 20 minutes and more. When evacuating by lift it's needed to focus on people for whom the lift is a necessary device – person with limited mobility . Galea et al. [12] and Hedman [13] dealt with the details of the persons movement with limited mobility to stairs and floors. The evacuation movement of under six years children was studied by Larusdottir a Dederichs [14]. These studies have shown that the movement speed of persons with limited mobility is different from that of healthy persons.

In general, the evacuation process using lifts consists of phases. For example time of getting in or getting out can considerably differ during evacuation from normal conditions. In this way, during the existence of danger, the entire process of evacuation can be decelerated, for example evacuated persons do not want to leave the lift cabin, when overload signal is indicated [7]. Results of previous examinations have demonstrated potential of lifts for evacuation of persons. However, in all aforementioned papers

they call attention to the need of quantification of other movement parameters and description of the entire process using a suitable algorithm that could be used for simple, but also complex calculation models.

As it was stated above, approximately 30% of inhabitants in the Slovak Republic are person of limited mobility. According to laws, they should have available accessible evacuation routes that do not prevent their movement. Therefore lifts are inevitable for the solution of evacuation. But no relevant information on movement parameters of persons of limited mobility exists for assessment of calculations. This is why our work was focused on collection of this information, particularly on the quantification of selected phases of evacuation using lifts – time of movement for persons of limited mobility. The in-situ experimental method was used for collection of data, where movements of persons were monitored – time of arrival to the lift, time of getting into the cabin and time of getting out of the cabin including leaving the defined area.

2. The method used

The lift evacuation process consists of phase stages. The total evacuation time consists of walking and moving movements that are directly related to the lift. Lift-related movement involves both walking and moving the lift cabin. The movement of lifts mechanisms cannot be affected by persons. Conversely, the behavior of persons may affect the time of entry or exit from lift.

2.1. Description of experiment and scenarios

Ten persons participated in experiment (7 men and 3 women) and imitated the movement of people with limited mobility – the movement in a wheelchair and the movement of an injured person (broken leg). None of the participants involved in the experiment had experienced using a wheelchair prior to the experiment. In contrast, three participants confirmed that they had to use a crutch or a support stick at least once in their lives. We examined two different alternatives of evacuation. In the first alternative, the person with limited mobility moved alone, without any assistance from another person. The second alternative included an accompanying person assisting the person with limited mobility. In this case, the accompanying person had no mobility limitation. The task of this person is to push the person on wheelchair and to support the person with broken leg. In all measurements, persons moved like during dangers – evacuation behaviour. During experiment, two passenger lifts were selected in the university building – identified as L1 and L2, respectively. Dimensions of the lift cabin L1 are 1.00×1.26 m and the clear width of the door is 0.78 m (Fig. 1). The prescribed maximum capacity of this lift is 6 persons. Dimensions of the lift cabin L2 are 1.10×1.40 m and the clear width of the door is 0.78 m (Fig. 1). The prescribed maximum capacity of this lift is 8 persons. A measurable area was marked in front of both lifts representing the nearest surrounding of the lift, where change of movement nature occurs (slowing down, change of direction and the like). Dimensions for the L1 lift were selected as 2.35×3 m and for the L2 lift 3×3 m (Fig. 2).

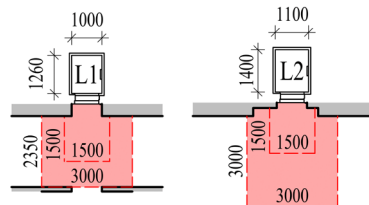


Fig. 1: Scheme of measurable areas and dimensions of lifts L1 and L2

The entire experiment included 8 scenarios. All persons carried out each measurement 3 times. In total, 720 measurements were carried out for 8 scenarios and three monitored phases. Normal mechanical wheel chair was used for the imitation of movement of the person on the wheel chair. This wheel chair belongs to the category of standard wheel chairs with folding frame and seat width of 0.4 m. Crutches of two different sizes and ortheses were used for imitation of movement of the injured person. These means

should ensure that the person's leg was fixed against movement, and could not be bent in the elbow. This fixation of the leg can represent for example the broken leg in plaster.

2.2. Description of experiment

The objective of measurement was to quantify time values of selected phases:

- Arrival to the lift
- Getting into the lift cabin
- Getting out of the lift cabin and leaving the area

The work was focused only on the determination of values of movement time under standard conditions. Areas were sufficiently lighted by day and artificial lighting. Times of travelling in the lift from one floor to another one were also not monitored. This is why the experiment was carried out only on one floor of the building, where movements were monitored during phases.

Arrival to the lift – time No. 1 “D1” (Fig. 2): This time included motion in the measured area. The procedure was as follows: The person with disabilities stood outside the measured area, where he/she started his/her movement towards the lift. Subsequently, this person crossed the boundary of the area, which represents the beginning of measured time D1. In this way, the person could autonomously move in this area in order he/she could get as soon as possible to the lift door with the panel intended for opening the door. The person standing in front of the door had to slow down his/her movement, and subsequently to stop. As the last, he/she had to press the button on the lift panel to call the lift or to open the lift door. The moment of pressing the button means the end of measured time D1.

Getting into the lift cabin – time No. 3 “D3” (Fig. 2): This period included time of door opening and time of movement of the person to inside of the lift cabin. The procedure was as follows: The person with disabilities stood in the measured area in front of the closed lift door prepared for opening the door. Subsequently, this person opened the lift door by pressing the button on the lift panel, which represents the beginning of measured time D3. This person had to wait until the door is fully opened, and he/she could start his/her movement towards inside of the cabin. When this person passed through the door, and was present in the cabin, he/she had to stop his/her movement before the cabin panel. This person, as the last one, had to press buttons located on the cabin panel, by which he/she selected the exit station, and closed the lift door. The moment of pressing the button intended for closing the door represents the end of measured time D3.

Getting out of the lift cabin – time No. 5 “D5” (Fig. 2): This period included time of door opening and time of movement of the person from the lift cabin up to outside the measured area. The person with disabilities stood in the lift cabin with the closed door prepared for opening the door. Subsequently, this person opened the lift door by pressing the button on the cabin panel, which represents the beginning of measured time D5. This person had to wait until the door is fully opened, and he/she could start his/her movement out of the cabin. The person on wheel chair had to reverse, because the cabin space does not allow any turn on the wheel chair. When this person got out of the cabin, he/she had to stop his/her movement, and had to turn by approx. 90° in the direction, in which he/she wanted to leave the measured area. Subsequently, the person started his/her movement, and passed through the area boundary. On the contrary, the person with injured leg can stand face the door, because dimensions of the cabin allow turning of this person. Subsequently, the person started his/her movement in the cabin and passed through the area boundary without necessary stop and turning. The moment of passing the area boundary represents the end of measured time D5.

If the person on wheel chair is accompanied by another person, movement was provided just by this accompanying person. In the case of the person with injured leg, the accompanying person served as a support during movement. In this way the pressing of button was based on free will of participants.

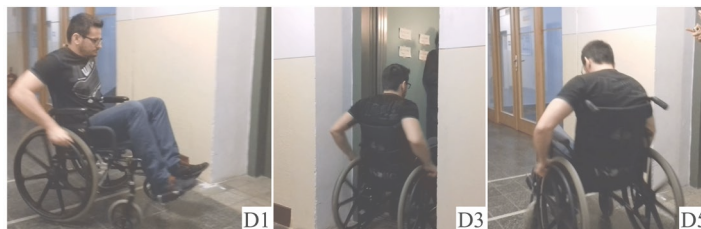


Fig. 2: A specimen of measurements of selected phases

3. Results and discussion

During measurements, the following values of time of phases were obtained for the person on wheelchair without accompanying person and with accompanying person, for the injured person without accompanying person and with accompanying person. In addition to the above, average, maximum and minimum measured time values of phases are depicted for the person on wheelchair and the injured person (Tab. 1).

Tab. 1: Average, maximum and minimum measured times for person on wheelchair and injured person; (1p – persons without the accompanying person; 2p – with the accompanying person)

Persons on the wheelchair	D1-1p	D3-1p	D5-1p	D1-2p	D3-2p	D5-2p
Average time	3.84 s	7.00 s	10.00 s	2.44 s	5.57 s	6.78 s
Maximum time	7.80 s	11.55 s	15.25 s	3.29 s	7.44 s	8.18 s
Minimum time	1.98 s	4.95 s	6.80 s	1.38 s	4.35 s	2.28 s
Max. and min. difference	5.82 s	6.60 s	8.45 s	1.91 s	3.09 s	5.90 s
Injured persons	D1-1p	D3-1p	D5-1p	D1-2p	D3-2p	D5-2p
Average time	3.40 s	5.51 s	5.89 s	3.16 s	5.98 s	6.72 s
Maximum time	5.53 s	7.13 s	8.70 s	4.36 s	8.18 s	8.49 s
Minimum time	2.30 s	3.06 s	4.14 s	2.16 s	4.73 s	4.63 s
Max. and min. difference	3.23 s	4.07 s	4.56 s	2.20 s	3.45 s	3.86 s

When measuring arrival to the lift, time of movement for the person on wheelchair was longer than for the injured person. This can be caused by the fact that the person must manoeuvre with the wheelchair during movement. For example, closely in front of the lift door, it was necessary slightly slew the wheelchair in order the person would face the lift. This results in slowing down during movement. On the contrary, the injured person moved straightly to the lift practically without noticed interruption. This person slowed down only in front of the lift door. In the case of the person on wheelchair, average time of getting into the lift cabin was longer than for the person with leg injury (Fig. 6a; difference was 1.5 s – 21%). This was caused by the fact that the person on wheel chair had tight conditions for passage through the lift door against the injured person. During manoeuvring, some persons on wheelchair bumped into the frame and lift door, by which they slowed down their movement, and sometimes they even had stopped. Maximum time of 11.55 s for getting in was recorded, when the person stood in the door for almost 4 s, and could not move. In the contrary, the injured person could adapt his/her width during passage through the door facilitating the getting in process – the maximum measured time value was 7.13 s. In the case of getting out of the cabin, the difference against the getting in was twofold (Fig. 6a; 4.11 s – 41%). The reason was based on the fact that the person had to reverse out of the cabin, stop in the measured area, turn, and only then he/she could to continue in movement to the area boundary. Problems with bumping the frame and door of the lift occurred like in the case of getting into and getting out of the cabin. This is why the maximum time achieved the value of 15.25 s, when the person was nipped by the lift door during his/her passage trough the door. On the contrary, the injured person could move practically without any interruption of movement directly to the area boundary – maximum measured time value of movement was 8.70 s. In the case of immobile person with accompanying person (Fig 6a),

time differences in the nature of limitation were smaller than in previous cases. Differences were as follows: In the case of arrival to the lift this was 0.71 s (23%). In the case of getting into the lift this was 0.41 s (7%). In the case of getting out of the lift this was 0.05 s (1%). It is possible to conclude that time values for getting in and getting out with the accompanying person are almost the same both for the person on wheelchair and the injured person.

In the case of arrival to the lift, it is possible to speak about negligible influence of the accompanying person on time of movement of the injured person, because the difference is only 0.25 s (7%) in favour of the case with the accompanying person (Fig. 6b). The presence of the accompanying person had influence on shortening the time of movement for the person on wheelchair (Fig. 6b). Difference was 1.40 s (36%) for arrival to the lift, 1.43 s (20%) for getting into the lift and 3.22 s (32%) for getting out of the cabin. It was caused by the fact that the person on wheelchair without accompanying person moves slower. But the accompanying person can push the person on wheelchair without any apparent movement problems – higher acceleration, higher speed, higher slow down. When getting into the lift cabin, the accompanying person almost always manoeuvred with wheelchair without bumping the frame of lift door. When getting out of the lift cabin, the accompanying person could reverse more quickly, turn and start up with the wheelchair. However, the presence of the accompanying person influences time of getting in and out for the injured person. Difference was 0.48 s (8%) for getting into the lift, 0.83 s (12%) for getting out of the lift. The main reason is based on the fact that two persons must pass through the lift door with the width of 0.78 m. During normal movement, the injured person and accompanying person stood next to each other, and walked ahead. During passage through the lift door, both persons had to slow in order they could get into the lift door. The crutch hampered movement, for example it was caught by the door near the floor, and the person had to manoeuvre more with it. Both facts resulted in slowing down the movement. The single person passed almost always without slowing down, because width of the door is sufficient for his/her.

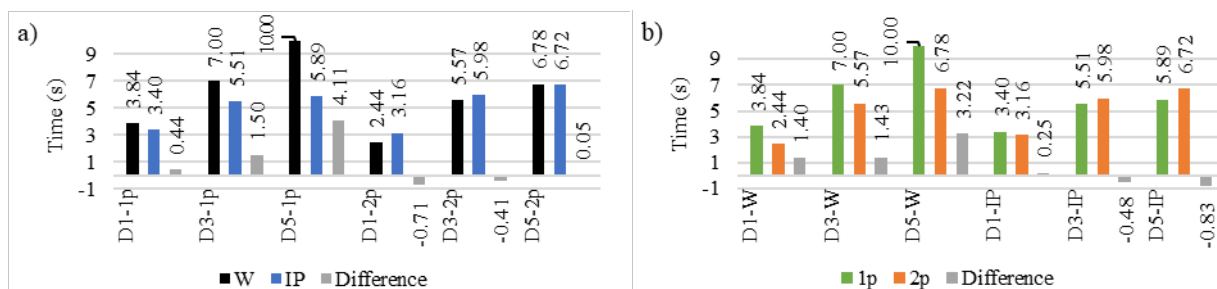


Fig. 6: Comparison of average times – a) persons on wheel chair (W) and injured persons (IP); b) persons without the accompanying (1p) person and with the accompanying person (2p)

When comparing gender of persons with disabilities, it was ascertained that time of movement of women was longer than time of movement of men, if persons with disabilities had not any accompanying persons (Fig. 7). Maximum difference was 1.43 s (29%) and minimum difference was 0.24 s (4%). On the other hand, time of movement of women was shorter than time of movement of men, if the persons with disabilities had accompanying person (Fig. 7). Maximum difference was 0.44 s (8%) and minimum difference was 0 s (0%). The accompanying person declared that pushing and braking the wheel chair with sitting woman was easier than with sitting man. This was valid even in the case of transfer of weight from the injured person to the accompanying person. The accompanying person declared that it was physically more demanding to support a man weighing from 70 to 90 kg than a women weighing from 50 to 70 kg.

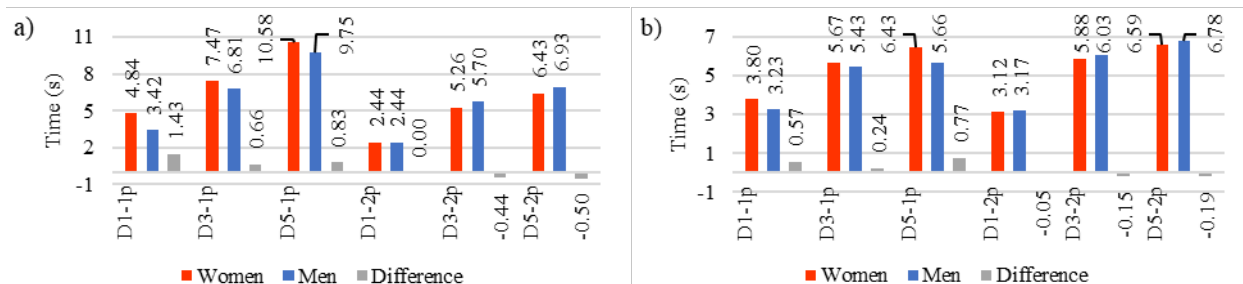


Fig. 7: Average times for – a) person on wheel chair; b) injured person; (1p – persons without the accompanying person; 2p – with the accompanying person)

Different techniques of movement of persons on wheelchair were observed during measurements. Some persons had problem with movement during passage through the door. Therefore they decided, in other trials, to grasp the lift door with hands, and to draw subsequently into the cabin (Fig. 8a). In this way the person could avoid bumping by the wheel chair to the lift door. The situation related to the accompanying of the person on wheelchair during arrival to the lift was another interesting thing. This interesting thing is based on the fact, which person would press the button on the lift panel. If the button was pressed by the person with disabilities, no delay of movement occurred (Fig. 8b). On the contrary, when the button was pressed by the accompanying person, slowing down by approx. 0.5 to 1 s was observed. This happened because the accompanying person had to stop the wheel chair, to bypass it or to lean. Even then the accompanying person could press the button on the lift panel (Fig. 8c).

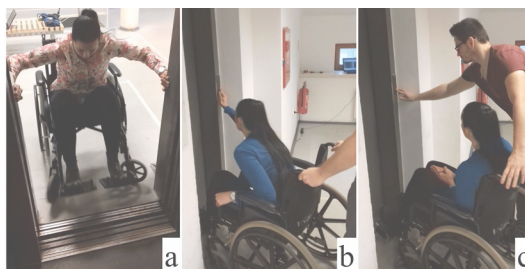


Fig. 8: a) – Getting into the cabin using hands, b) – the person with disabilities is pressing the button, c) – the accompanying person is pressing the the button.

4. Conclusion

The work is focused on obtaining time value of phases of movement for persons with disabilities. Phases were analysed, particularly arrival to the lift, getting into the lift cabin and getting out of the lift cabin. Phase stage of getting into the lift and getting out of the lift also include time of opening the door. Average time of getting into the lift was for the person on wheel chair longer by 21% than for the injured person. In the case of getting out of the cabin, this difference was up to 41%. If any hesitations occurred during passage through the door, resulting time was longer against average time by 65% for the person on wheel chair and by 48% for the injured person. It has also been ascertained that the presence of the accompanying person had effect on shortening the time of movement for the person on wheel chair by 36%. However, in the case of injured person, time was expanded by 12%. Different methods of movement of women and men were observed during the measurements. This was reflected in the mean movement time, which was 30% longer for women than for men.

Measured data apply to persons who may suddenly lose the ability to move without restriction. The sample of persons examined was from 26 to 40 years old and at the same time, they were physically healthy without movement limitation. These persons have never had a experience to movement on wheelchair. Selected lifts did not allow the turning of persons on wheelchair. In the future, it will be

necessary to expand results by the use of larger lifts (for example for two persons with disabilities). It is also necessary to focus on the other types of movement limitation.

Acknowledgements

This work was supported by grant project 2/0042/17 “Solar energy influences and integrated envelopes on the quality of the environment in buildings and cities.”

This paper was created thanks to the financial support from the EU Structural Funds, through the R&D Operational Program and project OPVaV-2008/2.2/01-SORO “Architectural, engineering, technological and economic aspects of the design of energy efficient buildings”, codenamed ITMS: 26220220050; which is financed by EC funds.

References

- [1] N. Ding, T. Chen, H. Zhang. “Experimental Study of Elevator Loading and Unloading Time During Evacuation in High-Rise Buildings” *Fire technology*, vol. 53, is. 1, pp. 29-42, May 2016.
- [2] K.E. Dunlop, T.J. Shields. “Real fire emergency evacuation of disabled people” in *Proceedings of CIB W14 International Symposium and Workshops on Engineering Fire Safety in the Process of Design Equivalency*, 1993, pp. 157-164.
- [3] T.J. Shields, K.E. Boyce, N. McConnell. “The behaviour and evacuation experience of WTC 9/11 evacuees with self-designated mobility impairments” *Fire Safety Journal*, vol. 44, is. 9, pp. 881–893, May 2009.
- [4] J. Averill, D. Mileti, R. Peacock. “Federal Building and Fire Safety Investigation of the World Trade Center Disaster: Occupant Behaviour, Egress, and Emergency Communication” Internet: https://ws680.nist.gov/publication/get_pdf.cfm?pub_id=101046, December 01, 2005 [May 17, 2018].
- [5] “Statistical Office of the Slovak Republic” Internet: <https://slovak.statistics.sk>, [May 17, 2018]
- [6] J.D. Averill. “Five Grand Challenges in Pedestrian and Evacuation Dynamics” in *Pedestrian and Evacuation Dynamics*, 2011, pp. 1-11.
- [7] Y. Ding, L. Yang, F. Weng, Z. Fu, P. Rao. “Investigation of combined stairs elevators evacuation strategies for high rise buildings based on simulation” *Simulation Modelling Practice and Theory*, vol. 53, pp. 60-73, February 2015.
- [8] E. Heyes. “Human Behaviour Considerations in the Use of Lifts for Evacuation from High Rise Commercial Buildings” PhD. thesis, University of Canterbury, Christchurch, New Zealand, 2009.
- [9] M.J. Kinsey, E.R. Galea, P.J. Lawrence. “Stairs or lifts? A study of human factors associated with lift/elevator usage during evacuations using an online survey” Internet: http://www.fseg.gre.ac.uk/fire/fseg_ped2010_liftstairchoice_paper_distrib_final_final.pdf, [May 17, 2018]
- [10] A. Jönsson, J. Andersson, D. Nilsson. “A risk perception analysis of elevator evacuation in high-rise buildings” In *Proceedings of the 5th International Symposium on Human Behaviour in Fire*, 2012, pp. 398–409.
- [11] K. Andrée, D. Nilsson, J. Eriksson. “Evacuation experiments in a virtual reality high-rise building: Exit choice and waiting time for evacuation elevators” *Fire and Materials*, vol. 40, is. 4, pp. 554-567, May 2015.
- [12] E.R. Galea, A.P.M. Adams: “An Experimental Evaluation of Movement Devices used to assist People with Reduced Mobility in High-Rise Building Evacuations” In *Pedestrian and Evacuation Dynamics*, 2011, pp. 129-138.
- [13] G.E. Hedman: “Travel Along Stairs by Individuals with Disabilities: A Summary of Devices Used During Routine Travel and Travel During Emergencies” In *Pedestrian and Evacuation Dynamics*, 2011, pp. 109-119.
- [14] A.R. Larusdottir, A.S. Dederichs: “Evacuation Dynamics of Children – Walking Speeds, Flows Through Doors in Daycare Centers” In *Pedestrian and Evacuation Dynamics*, 2011, pp. 139-147.

Crowding and Queuing in Entrance Scenarios: Influence of Corridor Width in Front of Bottlenecks

Juliane Adrian¹, Maik Boltes¹, Stefan Holl¹, Anna Sieben², Armin Seyfried^{1,3}

¹Institute for Advanced Simulation, IAS-7: Civil Safety Research, Forschungszentrum Jülich
Jülich, Germany

j.adrian@fz-juelich.de; m.boltes@fz-juelich.de; st.holl@fz-juelich.de

²Chair of Social Theory and Social Psychology, Ruhr-Universität Bochum,
Bochum, Germany

Anna.sieben@rub.de

³School of Architecture and Civil Engineering, University of Wuppertal,
Wuppertal, Germany

a.seyfried@fz-juelich.de

Abstract - In this paper, we present results of an entrance experiment investigating the effect of the corridor width in front of a bottleneck on the density. The idea is based on a previous study suggesting that a guiding system in front of an entrance can reduce pushing of the waiting people and thus the density at the entrance. In our study we aim to find out to what extent the corridor width has an impact on crowding or queuing behavior and with that on the density. The results of the presented experiment suggest that the transition takes place between a corridor width of 1.2 m and 2.3 m. The total duration of each experimental run is not significantly influenced by the corridor width but by the width of the entrance itself, the number of participants and partly by the motivation. In general, the density in front of the gate as well as the area of high density is increased by widening the corridor and by intensifying the motivation of the participants. However, the results also suggest that also the number of participants significantly influences the occurrence of pushing and the level of density.

Keywords: crowd management, entrance scenario, queuing, crowding, experiments

1. Introduction

Understanding the behavior of crowds in entrance scenarios is important to draw up or to adapt safety regulations for buildings and events. This understanding is based on observations, field studies and experiments as well as simulations. In a recently performed experiment we studied the transition between crowding and queuing behavior in entrance scenarios depending on the width of the corridor located in front of a bottleneck. The objective was to identify a relationship between density in the crowd and width of corridor, as well as the justness of the entrance procedure.

In a previous study, two entry situations were investigated using different types of spatial barrier structures positioned in front of a bottleneck [1]. In the first scenario, no barriers were used to guide the participants in front of the entrance. In this case, the participants were able to position themselves freely before the gates were opened. This resulted in a semicircle arrangement of the participants. In the second situation, barriers were used forming a corridor perpendicular to the entrance forcing the participants to arrange themselves in loose lanes before the gates were opened. After opening the gates, the participants in the semicircle setup showed crowding behavior. The crowd contracted as soon as the signal for entering was given. In case of the corridor setup, the participants formed loose lanes indicating the formation of an ordering structure, rather showing a queuing than a pushing behavior. On the one hand, the comparison between the distances from the entrance with the times in which the entrance is reached indicates that the semicircle setup is more just than the corridor setup. This is basically a consequence of the high densities in the semicircle setup which make it impossible to overtake persons in front. On the

other hand, the high density makes the semicircle setup less safe, decreases the participants' well-being and leads to the perception of less justness. These results let to the question whether there is a critical corridor width limiting queuing behavior and stimulating pushing behavior instead. In order to investigate this question, we present density analysis and a comparison between waiting time versus distance to target for different corridor width and different motivation.

2. Methods

The presented experiments were carried out at the University of Wuppertal, Germany in January 2018. For each study, between 20 and 75 students were recruited as participants. The participants had to imagine a situation in which they want to enter a concert of their favorite artist. Each group had to perform two runs. In the first run, the motivation was higher than in the second run. This was communicated as follows: In the first run they had to imagine that an undisturbed view of the stage is only guaranteed for the first persons to enter. In the second run, the motivation was decreased by the announcement that all persons will have an undisturbed view of the stage, but nevertheless, the participants were told to enter quickly because they want to be close to the stage.

The experimental setup included an entrance gate with a width of 0.5 m and a corridor leading

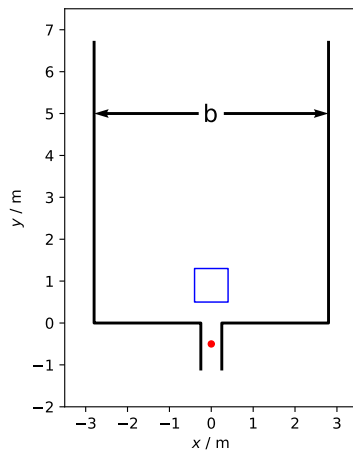


Figure 1: Sketch of the experimental setup. The corridor width b is varied between 1.2 m and 5.6 m. Target is the entrance gate at $x = 0$ m, $y = -0.5$ m (red dot) with a width of 0.5 m. Blue rectangle: measurement area.

Table 1: Overview runs with different corridor width b , number of participants N and motivation h (0: high, -: low).

Run	110	120	230	240	270	280	050	060	030	040
b	1.2 m		2.3 m		3.4 m		4.5 m		5.6 m	
N	63		42		67		42		75	
h	0	-	0	-	0	-	0	-	0	-

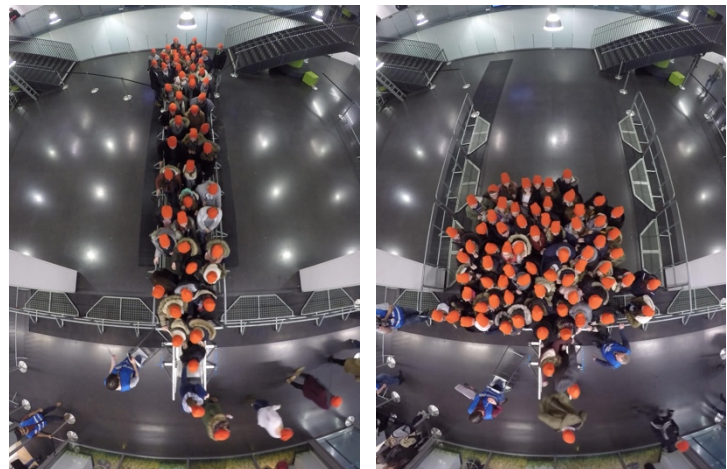


Figure 2: Snapshot for $t = 5$ s of Run 110 (left) and Run 030 (right).

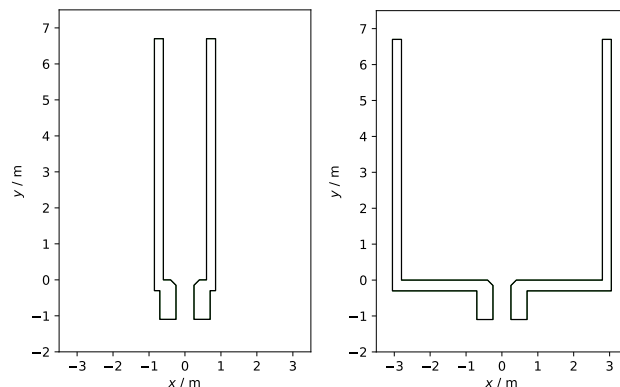


Figure 3: Trajectories of Run 110 with $b = 1.2$ m, $N = 65$ (left) and Run 030 with $b = 5.6$ m, $N = 75$ (right).

straight to the gate (see Figure 1). For different runs, the width of the corridor b was varied between $b = 1.2$ m and $b = 5.6$ m to analyze the transition between low and high state. The number of persons

passing the bottleneck has not been limited additionally. An overview over the corridor width and the number of participants is listed in Table 1 for a representative set of runs.

As an example, Figure 2 shows a screenshot for time $t = 5$ s after the start signal for two runs, one with the smallest corridor width $b = 1.2$ m (Run 110) and one with the largest corridor width $b = 5.6$ m (Run 030). It is clearly seen that the narrow corridor forces the participants to queue with a maximum of two to three persons side by side. The line of sight of all participants, and with that the preferred direction of movement, is oriented along the y-axis towards the target. Therefore, it is expected that most of the pressure is oriented in the same direction and the effective area is generally the area in front. In contrast, the participants in Run 030 are not forced into any formation because of the wide corridor. They arrange themselves in a semicircle in front of the entrance. This leads to a preferred direction of movement with a radial orientation.

Trajectories of individual participants were determined by automatic extraction from video recordings [2]. Figure 3 displays the trajectories corresponding to Runs 110 and 030. As expected from the snapshots in Figure 2, the trajectories of Run 110 show characteristics of lane formation whereas the trajectories of Run 030 show crowding characteristics after a contraction phase being the initial phase in which the crowd contracts from an initial density up to a local density maximum.

3. Results

Data analysis, such as density, velocity and flow measurements, were performed according to [3] using JuPedSim [4,5]. The results presented in the following concentrate on a representative set of runs, listed in Table 1.

3.1. Voronoi Density

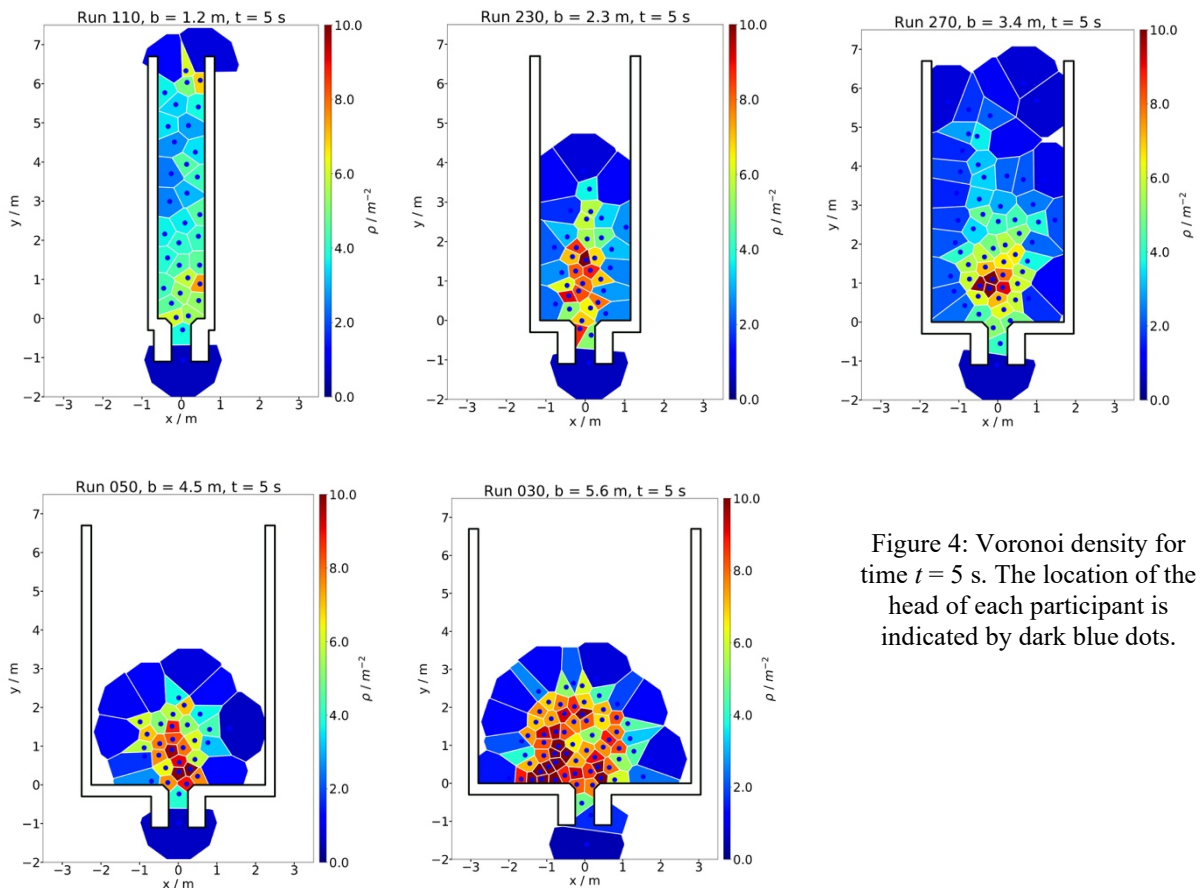


Figure 4: Voronoi density for time $t = 5$ s. The location of the head of each participant is indicated by dark blue dots.

Figure 4 shows the Voronoi cells and the location of each participant for $t = 5$ s after the start signal. At the chosen time, the contraction has already taken place. The color of the polygons indicates the density which is given by the reciprocal of the size of the individual Voronoi cell.

As seen in Figure 2, the narrow corridor of 1.2 m in Run 110 forces the participants into a rather ordered queuing arrangement. The densities within 3 m distance to the target are around 5 m^{-2} . In Runs 230 ($b = 2.3$ m) and 270 ($b = 3.4$ m), the arrangement of the participants in short distance to the entrance is rather v-shaped than a queue. Highest densities of partly more than 10 m^{-2} are found within a limited area in ca. 1-2 m distance to the target. For both, Run 050 ($b = 4.5$ m) and Run 030 ($b = 5.6$ m), the wide corridor favors a semicircle arrangement in front of the entrance gate. This leads to densities of partly more than 10 m^{-2} within 2 m distance to the target. In case of $b = 5.6$ m, these high densities are found in a larger area which is extended towards the left and right of the entrance gate. The participants form a semicircle clearly indicating crowding behavior.

3.2. Density time-series

The development of the density within the measurement area over time is shown in Figure 5 for runs

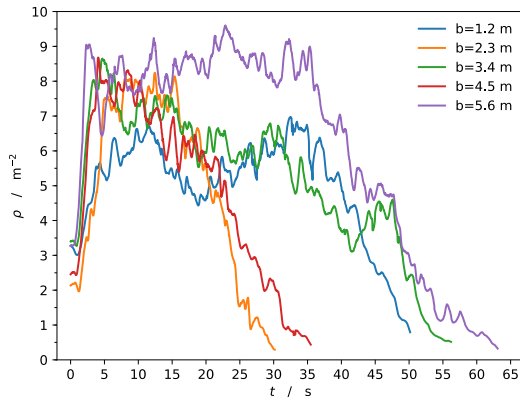


Figure 5: Time-series of density within the measurement area; high motivation.

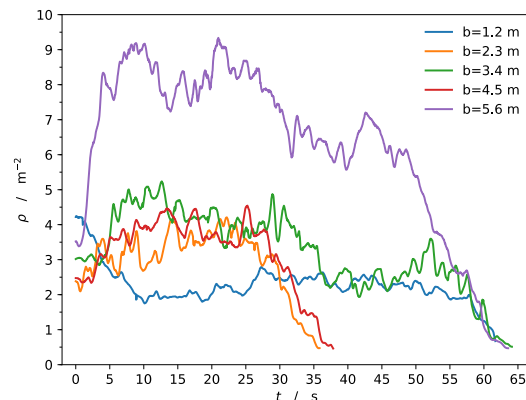


Figure 6: Time-series of density within the measurement area; lower motivation.

with high motivation and in Figure 6 for runs with lower motivation. The size of the measurement area is 0.8 m by 0.8 m and its closest border is located in 0.5 m distance from the entrance of the gate (see Figure 1). The dimension and location of the measurement area is chosen so that it covers the area with highest density for all runs.

In case of high motivation, a contraction phase is indicated by a density increase within the first 5 s after the starting signal. The corresponding local density maximum is lowest for the smallest corridor width of 1.2 m. For the widest corridor ($b = 5.6$ m), the density stays at one level between 8 m^{-2} and 9 m^{-2} for about 40 s. The densities of the runs with $b = 4.5$ m, $b = 3.4$ m and $b = 2.3$ m reach a similar local density maximum as the run with $b = 5.6$ m. However, the density only shortly remains at one level and decreases afterwards. In comparison to $b = 4.5$ m and $b = 2.3$ m, the density time-series for $b = 3.4$ m does not decrease as rapidly. It reaches two more local maxima before decreasing to zero. For $b = 1.2$ m, the density increase takes longer than for the other runs indicating the absence of a rapid contraction. It reaches a maximum of 6.5 m^{-2} after ca. 15 s. Afterwards, it decreases to a minimum of 5 m^{-2} at $t = 20$ s and increases to a second maximum at $t = 35$ s before it finally decreases.

As seen in Figure 6, the maximum density is lower in case of lower motivation. This is true for all runs except for the widest corridor ($b = 5.6$ m). Here, the maximum is similar to the run with high motivation. For the smallest corridor ($b = 1.2$ m), however, the density even decreases from an initial density of 4 m^{-2} to a level of only ca. 2 m^{-2} . For all corridor width, the slope of the initial density increase (or decrease) is not as steep as in Figure 5 with the high motivation. Multiple local maxima, as seen in Runs 110 and 270, indicate sequences of pushing and non-pushing. The slope of the density decrease at

the end of the runs seems to be similar for all datasets. This indicates that the density time-series corresponding to the last persons is only controlled by the outflow through the entrance gate and not by the corridor width.

Another aspect that needs to be considered when comparing different runs, is the varying number of participants. In order to emphasize this assumption, Figure 7 displays density time-series measured in several runs with $b = 1.2$ m. The number of participants N ranges from 11 to 63. It shows that not only the length of the run is dependent on the number of participants but also the maximum and mean density is.

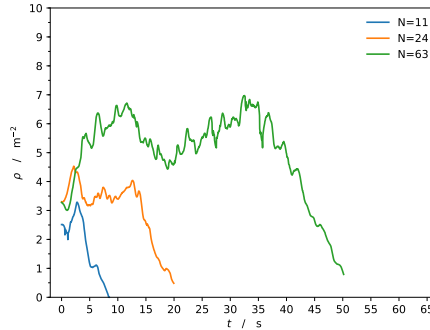


Figure 7: Time-series of density for varying number of participants N within the measurement area; high motivation, $b = 1.2$ m.

Going back to Figure 5 and Figure 6, similarities between the time-series for $b = 2.3$ m and $b = 4.5$ m could be identified, such as maximum density, duration of the run and general curve shape of the time-series. This might be due to the fact that the same amount of people ($N = 42$) participated in these runs (see Table 1). In this case, the corridor width apparently has no big influence on the density. In contrast, in the runs with $b = 1.2$ m ($N = 63$) and $b = 3.4$ m ($N = 67$) nearly the same amount of people participated, but the density time-series show clear differences, especially for low motivation. Therefore, it is assumed that several factors, i.e., number of participants, corridor width and motivation, play a role. But, the influence of the individual factors cannot be quantified, based on the data at hand.

The density time-series for the largest width $b = 5.6$ m stands out. It shows the largest maximum density and the density is higher than for the other runs for a prolonged period of time. It is the run with the most participants ($N = 75$), but the difference in participants is only slightly higher than that for $b = 3.4$ m. Thus, it is more likely that those high densities stem from the difference in corridor width rather than from the difference in number of participants.

3.4. Influence of Corridor Width and Number of Participants on Mean Density

Since it is not suitable to define a steady state for all runs, we decided to use a 5 s interval from $t = 5$ s to $t = 10$ s to determine a mean density (gray area in Figure 5 and Figure 6). We assume that the contraction phase has already taken place after $t = 5$ s. Figure 8 displays the mean density in the 0.8 m by 0.8 m measurement area (see Figure 1) within this time-interval for all runs. In general, the mean density increases with increasing corridor width. For high motivation, it increases from ca. 6 m^{-2} for Run 110 ($b = 1.2$ m) to ca. 8 m^{-2} for $b = 4.5$ m (Run 050, 280) and only slightly less for $b = 5.6$ m (Runs 030, 150). Furthermore, there is a density gap of ca. $3\text{-}4 \text{ m}^{-2}$ between the runs with high motivation (h0) and the corresponding runs with low motivation (h-). This does not hold for the Runs 170, 070 and 190, which were conducted with high motivation. In Figure 8, the mean density of these runs fits to the group of low motivation rather than to the group with high motivation. The reason for these exceptions becomes clear in Figure 9. Here, the mean density is plotted versus the number of participants showing a clear relation. The number of participants in the mentioned runs is low in comparison to the other runs. Therefore, the density is also lower which fits to the findings of the density time-series (see Figure 7). According to Figure 9, the influence of the number of participants on density are not to be neglected. It seems that a certain amount of people is needed for the phases of contraction, congestion and release to fully build up.

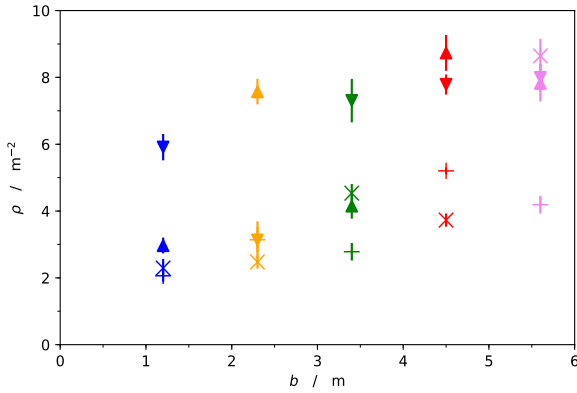
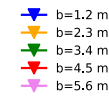
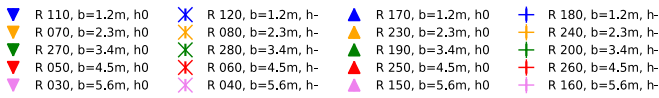


Figure 8: Mean density (determined from $t = 5$ s to $t = 10$ s) in the measurement area against corridor width including error bars. Triangles refer to high motivation, crosses and x to lower motivation. The color indicates the corridor width.

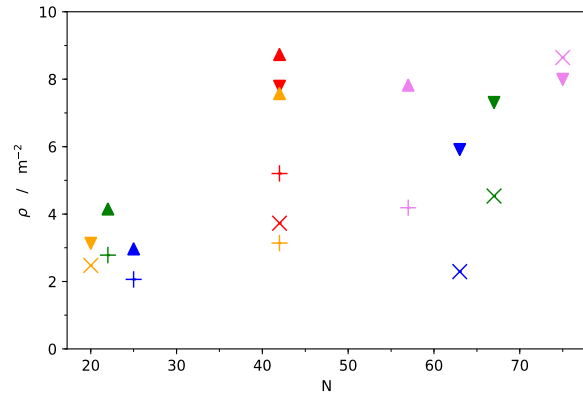


Figure 9: Mean density (determined from $t = 5$ s to $t = 10$ s) in the measurement area against number of participants. Triangles refer to high motivation, crosses and x to low motivation. The color indicates the corridor width (see Fig. 8).

3.5. Waiting Time and Distance to Target

Another characteristic of the entrance process which is helpful to distinguish between queuing and pushing behavior is the time to target. Figure 10 compares the time to target in dependence on the distance to the target for a narrow corridor of $b = 1.2$ m (left) with the corridor width of $b = 2.3$ m (center) and with the widest corridor of $b = 5.6$ m (right). For each participant, the blue dots represent the starting position in terms of linear distance to the target, which lies within the entrance gate (red dot in Figure 1), and the total time to reach the target. Please note that the trajectories were extracted within a limited area only. The maximum extension in y-direction was ca. 7.5 m. Therefore, the starting position of participants who gathered outside this area corresponds to the position where they stepped into the area of interest (see Runs 110 and 120).

During the first seconds after the start signal, two opposite behaviors or initial phases are observable: a rushing or contraction phase on the one hand and a waiting phase on the other hand.

The contraction phase is most obvious in case of high motivation and can be observed for all shown corridor width: The individual lines run from the initial blue dot to the left nearly parallel to the x-axis. This indicates that the distance to the goal is reduced in a short period of time. Or with other words: The participants directly started moving in the direction of the target until all interspaces are filled and a certain (maximum) density is reached (see Figure 5 and Figure 6).

In contrast, the waiting phase is indicated by lines parallel to the y-axis meaning that the distance to the target does not change significantly within a certain period of time. In this case persons start their movement only if the person in front has moved indicating queuing. Like in the transition from a stop wave to a go wave, it takes some time until the stop phase has resolved. This waiting phase is most obvious in case of the narrow corridor with low motivation (Run 120). In some runs, we observe a combination of both phases, e.g. in Run 040. However, in these cases the waiting phase is very short and the contraction phase is predominant.

After the initial phase, the participants find themselves in a congestion, i.e. they can only move forward when the persons in front are moving because all interspaces are filled. This intermediate phase is indicated by a high concentration of individual lines. The mean slope within the congestion phase represents the mean velocity of the individuals in direction of the target. The steeper the intermediate

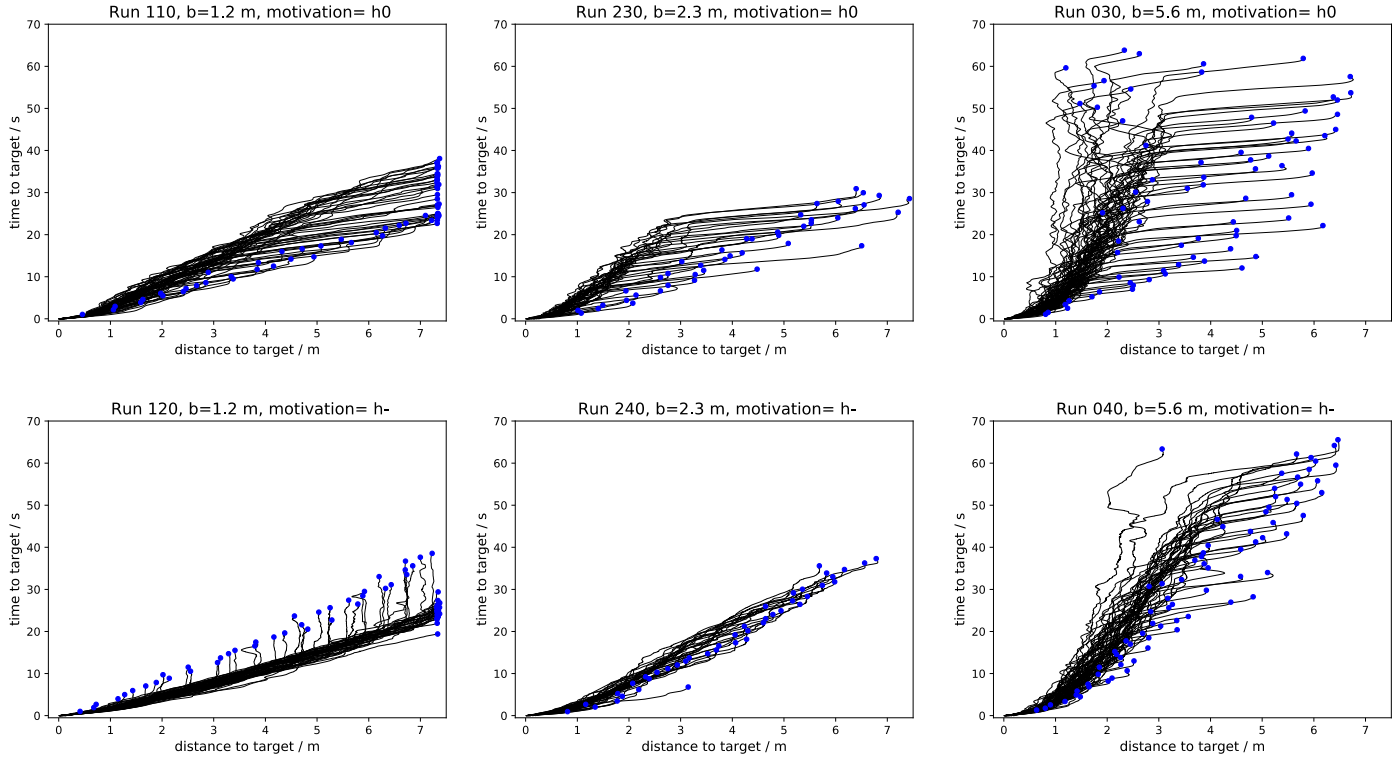


Figure 10: Individual time to target versus linear distance to target. Blue dots indicate individual starting position and complete time to target. High motivation is indicated by h0, low motivation by h-, respectively. The target is located at $x = 0$ m, $y = -0.5$ m.

phase is, the lower is the velocity indicating the progress to the target, the gentler the slope is, the higher is the velocity.

The final phase corresponds to the last 1 m in front of the target. The velocity is increased because the participants are less blocked by the congestion, i.e. there are less people between the release of the gate and the participant himself. This leads to a gentler slope in contrast to the intermediate phase meaning that more distance is made in a shorter period of time. This velocity increase can be seen in all presented runs.

In the following, differences or similarities between the different runs are examined to determine to what extend corridor width and motivation influences the waiting time in connection with the distance to the target entrance. Apparently, high motivation leads to a pronounced contraction phase. In contrast, low motivation leads to a shorter contraction phase and facilitates a waiting phase which might be either additionally or instead. This indicates that the participants are willing to accept a higher density when being highly motivated. For high motivation, the slope within the intermediate phase is steeper than that for the corresponding run with low motivation. In case of the narrowest corridor of $b = 1.2$ m, the slope of the intermediate phase is the shallowest whereas the slope is the steepest in case of the widest corridor ($b = 5.6$ m). Concerning the initial phase in Run 030 ($b = 5.6$ m), the following is observed: Some people are more active than others. This behavior shows in two ways: On the one hand, there are persons who are rushing in the very first seconds, but then enter a waiting phase meaning that they stand behind. On the other hand, the range of individual total runtime is quite broad for persons who started at a similar initial distance to the target. That means that some people are rushing quickly in the beginning to overtake some persons in front. Then they are slowed down when they reach the congestion. The waiting time plots for $b = 2.3$ m (Runs 230 and 240) show more similarities with the ones corresponding to $b = 1.2$ m than $b = 5.6$ m. Except that the waiting phase in the run with low motivation is not that pronounced.

4. Discussion and Conclusions

We investigated the influence of the corridor width in front of an entrance gate and the motivation on the behavior of participants in terms of arrangement, density and waiting time. Understanding this influence could help during the planning process and risk assessment for future building structures and for crowd management of events.

One of the main findings is that the corridor width and the motivation of the participants are important factors when determining whether people queue or start pushing. Furthermore, the density analysis revealed that the number of participants also has a significant influence on the maximum and mean density. This is true even for the narrowest corridor with a width of $b = 1.2$ m. Since the participants were recruited directly after their lesson, it was impossible to guarantee the same amount of participants for each run. In future experiments, the number should either be strictly controlled to ensure comparability or the number of participants should be used as additional parameter which is varied on a controlled basis.

The results of this study clearly reveal differences between wide and narrow corridors and also between different degrees of motivation. In case of the smallest corridor width of $b = 1.2$ m, the participants are forced into a queue with moderate densities. After the contraction phase, the participants have a rather large distance to the target, but they are constantly moving in target direction. Furthermore, the participants' well-being is maintained thanks to the comparably low densities. Overtaking is not necessary because of the constant movement. Therefore, social norms apply avoiding overtaking. In case of the widest corridor of $b = 5.6$ m, we observed a crowding behavior. The participants form a semicircle with high densities in front of the entrance gate but also to the left and right of the gate where people were pushed against the barriers. During the contraction phase overtaking was possible, but after that all interspaces were filled. In comparison to the narrow corridor, the individuals are closer to the target after the contraction, but then, during the intermediate phase, they spend more time in a congestion than with significant movement in target direction. The participants' well-being is reduced due to the high densities they are willing to accept.

The characteristics of the runs with intermediate corridor width, even for the second largest width of $b = 2.3$ m, indicate a pushing behavior rather than a queuing behavior, although the arrangement directly in front of the gate is mostly v-shaped instead of a semicircle. Generally, densities increase with increasing corridor width and increasing motivation.

Based on the presented results, it is assumed that the transition between pushing and queuing behavior takes place. At which width the transition takes place depends on the motivation, the number of people and on the width of the queuing system in front of the entrance. Therefore, we suggest to investigate more intermediate steps of corridor width in future experiments. Besides corridor width, motivation and the already mentioned number of participants, we suggest to consider heterogeneity of the group and to conduct more repetitions to ensure comparability and reproducibility and to increase the statistical reliability in order to derive the relation between the influence of the mentioned factors.

References

- [1] A. Sieben, J. Schumann, A. Seyfried, Collective phenomena in crowds-Where pedestrian dynamics need social psychology, *PLoS ONE* 12(6): e0177328 (2017).
- [2] M. Boltes, A. Seyfried, Collecting pedestrian trajectories, *Neurocomputing* 100 (2013) 127–133.
- [3] B. Steffen, A. Seyfried, Methods for measuring pedestrian density, flow, speed and direction with minimal scatter, *Physica A* 389 (2010) 1902-1910.
- [4] M. Chraibi, U. Kemloh, C. Liao, E. Andresen, A. Graf, *JuPedSim/JuPedSim: JuPedSim v0.8.3*. Zenodo (2018, June 20). <https://doi.org/10.5281/zenodo.1293784>
- [5] A. U. Kemloh Wagoum, M. Chraibi, J. Zhang, G. Laemmel, *JuPedSim: an open framework for simulating and analyzing the dynamics of pedestrians*, 3rd Conference of Transportation Research Group of India (3rd CTRG), Kolkata, India (Dec 2010).

Safe Evacuation for All

A top 10 List of Requirements

Laura Künzer, Gesine Hofinger, Robert Zinke

Team HF Human Factors Research and Training

Hofinger, Künzer & Mähler PartG

Ludwigsburg, Germany

laura.kuenzer@team-hf.de; gesine.hofinger@team-hf.de; robert.zinke@team-hf.de

Abstract

Evacuations are an important aspect of emergency planning. Many persons with special needs could reach a safe area on their own or with assistance by other people around, if evacuation planning and guidance considered them. The so-called self-rescue is crucial for safe evacuation, as fire services and other first-responders need some time to arrive at the scene. In general, people should find the conditions to arrive at a safe area on their own.

In many buildings and infrastructures today, self-rescue is difficult for persons with special needs, e.g. wheelchair users. Sometimes it appears that designers and fire safety engineers only think of “average”, healthy and agile people in evacuations. But for safe and effective evacuations, different groups of people and their needs have to be considered.

The paper suggests a top 10 list of requirements for safe evacuation and improvement of self-rescue from a psychological point of view. Universal Design or Design for All in evacuation has become more relevant in recent times, since accessibility as a political goal has made it possible for persons with special needs to participate more easily in public life. Nonetheless, regulations focus on how people enter a building but not on how to evacuate safely. Preparing for safer evacuations requires knowledge about different occupant groups and their needs. Requirements for different phases of evacuations are discussed and their implications for simulation and modelling, e.g. the potential impact of physiological requirements. The need for a multi-method approach to gather and integrate data, factors to foster safe evacuations, just as practical and design requirements are included. When self-rescue is not possible, assisted evacuation will rely on good leadership fostering social motivation. Last but not least, implementing design for all will help everyone to evacuate safely.

Keywords: Universal Design, Design for All, evacuation, psychology, requirements, special needs

1. Motivation and objective

In case of fire or other incidents, evacuation has to take place as fast and as safe as possible. As fire services need some time to arrive at the scene, self-rescue of occupants is important for safe evacuation of buildings, transport systems and other infrastructures. This is documented in laws, fire codes, and other regulations (e.g. for Germany [1, 2]). If evacuation planning and guidance include persons with special needs, more people could reach a safe area on their own or assisted by other people around.

“Self-rescue should be possible for everyone!”. This is not only an ethic imperative but a practical necessity: As inclusion of persons with special needs encourages that more and more persons with mobility or perception impairments use public infrastructures such as transport systems. But often, efforts are made to let people enter an infrastructure, but not for evacuations on their own.

First responders or fire services are often not prepared to ensure timely rescue of large numbers of persons with special needs. Also, fire services have to contain and fight hazards. If self-rescue is possible for (nearly) everyone, fire services can use their resources for firefighting. But still, not all occupants will be able to evacuate on their own. Rescue or support by others are necessary in special cases, or particular evacuation measures such as safety areas will be required.

In assessing the requirements for self-rescue of persons with special needs, the authors found that there are only few empirical studies on the subject, e.g. [3]. However, single studies explicitly including people with certain special needs can be found for high-rise buildings [4, 5], work places for handicapped persons [6] or day care centers [7].

The paper suggests a top 10 list of requirements for safe evacuation and improvement of self-rescue including a psychological point of view. Furthermore, the top 10 requirements are discussed for their use in simulation and modelling, e.g. the potential impact of physiological requirements.

2. Background

This paper reports recent results from the authors' studies on evacuation from subway stations [8, 9] and from previous research projects reaching back to 2008 [e.g. reported in [10–13]]. A mixed-method design was used in order to gather as many aspects on safe evacuation as possible. Data comes from field studies, surveys, observations, interviews, passenger counts, walk-arounds/ field visits and experiments in the context of underground transportation, but is generalized for other infrastructures using findings from the literature. Participants included wheelchair users, elderly, families, and people with visual impairments [14] (see section 3.1 and 3.3).

Studies (see also [9, 11, 15]) aimed to describe requirements for the design of evacuation routes and evacuation guidance. This included identifying different groups of subway users with special needs, describing their route choice behavior, their strategies in evacuations as well as their knowledge, e.g. knowledge about fires, how they would behave in case of a fire, and what they need to be able to evacuate safely [16].

3. Top 10 Requirements for safe evacuations

3.1 A portfolio of qualitative and quantitative methods is needed for research on special needs

No single method suffices to get insights on the requirements of different groups. Instead, several qualitative and quantitative methods are necessary, as well as an integrated analysis design (triangulation) [17, 18].

For example, persons with visual impairments cannot fill in a questionnaire on their own. Also, the standardized form of a questionnaire can be experienced to disregard their special situation. So, the authors also choose interviews for acquiring self-reported data. Field studies, such as walk-arounds/ on-site visits with persons with visual impairments, wheelchair users and parents of young children in subway stations helped to discover specific requirements. As many persons cannot verbalize their evacuation strategies or route-choice behavior, observations in field experiments were used as an additional method. Data was first analyzed by explorative data analysis and then weighted for detailed and integrated data analysis.

For some research (or most research with humans), study designs and documentation needs to be reviewed by an ethic committee. That might lead to delays in the realization of a study. Consequently, persons incapable of giving informed consent should receive special protection and should not participate studies unless the benefits outweighs potential risks.

3.2 Four factors fostering safe evacuation

Events that lead to evacuations are usually not rooted in isolated causes, they are influenced by the setting. To determine safe and purpose-built evacuation measures, the following four factors should be included [12, 19]:

1. the type of hazard or the triggering event, e.g. a fire or a gas leak;
2. the environment or infrastructure, considering structural properties such as length and accessibility of escape routes, e.g. in a subway station or office building;
3. the reason and occasion why people are in a particular place or building poses different challenges in evacuations, considering an event hall used e.g. as a concert hall for a rock concert or as a convention center;
4. the persons involved (occupants), their competencies, mental and physical abilities, needs and their actual emotional state; e.g. their fitness and excitation.

These four factors interact with each other and make evacuation planning even more complex. But if these factors are systematically considered for each venue, evacuation measures can be identified for persons with special needs and become more effective.

3.3 Persons with different special needs have different requirements for safe evacuation

The authors use the term “special needs” because fast and safe evacuation is not only a challenge for persons with impairments. There are many different kinds of occupants who have conditions that affect their fitness and mobility, and therefore their abilities to evacuate. In order to specify evacuation measures, different groups need to be identified. Results of own research lead to the following differentiations:

- persons with permanent handicaps, e.g. persons using a wheelchair, people with auditory or visual impairments;
- persons with temporal reduced mobility or impairments of perception, such as leg injuries, eye injury, intoxication by alcohol or drugs;
- persons with physical conditions like obesity or heart diseases;
- persons with other conditions that may also impede or prolong self-rescue: pregnancy (especially in third trimester), accompanying small children, lack of local knowledge (tourists) or not understanding local languages;
- persons or groups that may need exceptional assistance for self-rescue and are usually accompanied, e.g. small children or persons with mental disabilities.

Some of the “special needs” do not count as impairment in everyday life (and might even not be easily observable), may also prolong or impede evacuation, for example the ability to climb stairs. Note that each differentiation also has to be determined in more detail and definitions are not always distinct. In most evacuation concepts wheelchair users are considered. But there is a great variation between the impairment and mobility of wheelchair users and consequential movement speed, required space and their need of assistance in evacuations [5, 20].

Research with persons with impairments can be “troublesome” for researchers: Recruitment of participants, valid differentiation of groups (some persons have several impairments) and getting informed consent might be difficult, especially for children or persons with mental disabilities.

3.4 Design for All is relevant for using and evacuation transport systems

Wheelchair users’ needs are different from those of persons with visual impairments. But the authors found that the different groups have some requirements in common. This is true for everyday life but should also be applicable for evacuation. For some years, the idea of Universal Design or Design for All [21] has spread. Even if designs (here: evacuation routes and guidance) cannot suit everybody perfectly, it should be possible to design measures that suit a broad range of people. This leads to the formulation of principles that can help all occupants to evacuate safely. Universal Design principles, e.g. intuitive design, accessibility, equitable use, give the theoretical frame for the design of alarming systems and evacuation routes and are already discussed in the contexts of evacuations [8, 22].

Design for All (or barrier-free design) in evacuation has become more relevant in recent times, since accessibility as a political goal has made it possible for persons with special needs to participate more easily in public life. But often, regulation focus on how people enter a building but not how to evacuate safely.

3.5 Build a shared understanding and bring together different perspectives

Planning that strictly adheres to regulations is a start. But when considering safe evacuation, it is necessary to test practical implications of evacuation routes and guidance. Ideally, measures should be tested together with persons with special needs

In research and practical planning, round-table workshops seem a good method to bring together different perspectives and develop a shared understanding: What is relevant for persons with special needs? Which of their requirements can be usefully implemented in simulation models? How to deal with

conflict between different groups, e.g. tactile guidance systems on the floor for blind people may be a problem for persons using walking aids - at the same time fire safety regulations often focus single needs without considering the side effects of actions for other impairments.

Involving persons with impairments in research studies is sometimes not easy. Researchers need to allow more time for participant acquisition than in studies with students. It can be helpful to make contact via organizations or support groups. Also, data collection often might not follow researchers' expectations: For example, in an interview on evacuation people may tell the researchers all the problems they have with the public transport system and demand improvements. But research with the persons concerned is worth the effort as they are the ones who know their needs best.

3.6 Reduce response time by appropriate alarms

Warnings and fire alarms are used to initiate evacuations. Responses to these alarms are always influenced by individual evaluation, recognition and motivation. However, studies on fire evacuation exercises or case studies [11, 23] show that people often only start to evacuate with hesitation and delays or even refuse to evacuate. To reduce response time or pre-movement time, five phases of perception and information processing that influence compliance behavior to an alarm need to be considered [12, 24]:

1. **Perceive**, e.g. hear or see an alarm: Even if an alarm is transmitted by a public address system, it cannot be assumed that all intended recipients will take notice, even if they have the physical ability. To avoid this, the audibility, legibility and visibility of an alarm should be tested in a particular environment (see 3.2). Also, installed technology such as speakers need to drown out surrounding sounds by soundscapes or speech transmission index [25]. It is also advisable to reach out for more recipients by addressing at least two senses, e.g. by combining visual and acoustic information (redundancy by multi-sensory-principle and multi-channel principle).
2. **Understand**: The perception of an alarm cannot be equated with the understanding of the alarm itself and the comprehension of the importance of this alarm. A fire alarm constitutes an acoustic warning signal which might transmit an ambiguous meaning. The warning signal may be received as urgent by the recipients due to its tonal properties, but the present hazard and intended actions might not be explicitly clear, especially if the recipients never heard the alarm before.
3. **Authenticate**: Responses to alarms are influenced by evaluation of factors such as credibility, urgency and severity of the alarm. In the context of fire alarms the so-called Cry Wolf-syndrome can be observed [26, 27]. Previous "false alarms", because alarms were presented in fire exercises, might decrease the credibility of an alarm and recipients might take alarms no longer seriously ("This is just an exercise..."). Lack of authentication may lead to ignoring the alarm, continuing current activities or even refusing to evacuate. As it is not advisable to neglect exercises, the problem of alarm recognition should be addressed in organizational guidelines and debriefings of exercises. The more credible the alarm the sooner people will start to evacuate. Independently of the infrastructure, live announcements have the strongest effect in reducing response time in evacuation [28].
4. **Consider as relevant**: Personal risk assessment and credibility of an alarm play crucial roles in evacuation warnings. Only if people consider themselves to be the intended recipients of an alarm ("That's an actual fire alarm, which is now important for me!"), they will respond appropriately, e.g. by leaving the building. If possible, specific information concerning the actual hazards and instructions help to increase the relevance of an alarm.
5. **Response**: If a person has successfully completed phases 1 to 4, the person has to decide how to react to the alarm. Studies show that people responses may include [11, 19]:
 - waiting for further instructions ("wait and see")
 - actively searching for further information in order to make a more informed decision
 - helping/ supporting others to evacuate
 - showing attempts to extinguish fire

- actually leaving the infrastructure

Beside features for the design of warnings and alarms, e.g. volume, choice of words, etc., additional features for different requirements should also be included in the design process, e.g. for visitors who do not speak the local language. Paying attention to these features may reduce response time significantly and, thus, should be considered in the application of evacuation time calculations.

3.7 Adequate design of infrastructures can speed up movement time

Movement speed of occupants with special needs are influenced by architectural elements. If their maximum moving speed is to be guaranteed, three elements need to be considered:

1. **Required space, movement areas and accessibility** are especially relevant for occupants with walking impairments. Their requirements exceed the spacial needs of unimpaired users, e.g. up to the factor 2.5 in width. In order to enable their free movement and changes of directions, doors widths and required space need to be considered, e.g. for wheelchair user or occupants using crutches.
2. **Stairs and ramps** have to fulfil special requirements especially for occupants with walking or seeing impairments, e.g. steps should not overlap or exceed 15 cm to 17 cm in height. Wheelchair users will need movement areas at the start and the end of a ramp. The incline of the ramp influences motion and should avoid steep ascending slopes, e.g. up to 6%.
3. **Elevators** may be the only means of reaching a safe area quickly, occupants in wheelchairs exclusively rely on elevators if they want to reach a different level inside an infrastructure on their own. Impaired occupants, e.g. in walking or seeing, may walk the staircase – furthermore slowing down their own movement and reducing the capacity of escape routes for others waiting to pass them. In contrast to the widespread warning: “do not use in case of fire”, elevators can be equipped with a smoke-protection housing and will still operate. But, as most infrastructures do not integrate such elevators yet, future planning and implementations have to give insights of the use of those elevators and their influence on evacuation time.

3.8 Design of evacuation routes and evacuation guidance

Evacuation routes have to be designed according to the requirements of all occupants of an infrastructure (and not only for the sake of regulations). For evacuation simulations it is sometimes assumed that all available (emergency) exits are evenly used. Interviews and case studies show that people tend to use routes which can be considered as the common path of travel [27] e.g. people use the same routes to enter and exit a building. Passenger counts from field studies support these findings [10]. These can lead to an unequal distribution of evacuees and an increase in evacuation time [11].

A more even use of all exists can be reached, if design and guidance features support evacuees based on knowledge on psychological needs, on their wayfinding behavior and route choice strategies [13, 15]. Among these strategies people displayed and reported, the following appear most relevant, often also found in combination [10]: “Use the next possible way up that you can see”, “Follow the green exit-signs displaying a running man”, “Use your knowledge” (local and general to get out), “Avoid jamming and use the local shortest path”; “use quickest path”; “use comfortable way”.

Some of these strategies are being considered in fire safety regulations and even in present evacuation simulations, yet not consequently. Additional strategies were reported by people with special needs, e.g. from a person with visual impairments: “avoid walking in the middle of a group” [29]. – while accessibility and visibility are commonly of high relevance [20], e.g. high-contrast pictograms, commonly used word-based signage, tactile guidance systems.

Exits and level-transitions inside an infrastructure, e.g. stairs and elevators, have to be marked and visible along the evacuation routes. Signage should display accessibility restrictions, e.g. pointing out barrier free routes. This will enable persons with special physical needs, e.g. persons using wheelchairs, travelling with children in a pram, or having other mobility restrictions, to choose an appropriate route quickly, not having to rely on the support by others. It must be kept in mind, that understanding signage depends on evacuee’s knowledge and culture.

3.9 When help is needed – assisted evacuation

Many persons with special needs will be able to evacuate safely if they receive appropriate information and if structural design allows for self-rescue. Someone who doesn't understand the local language, e.g. in loudspeaker announcements, can use other persons as a source of information [16]. Here, herd-like behavior is useful.

But sometimes help is needed: A person may need assistance by others, e.g. guidance. This may be the case when a blind person has to walk unknown routes without tactile information. Another example for assisted evacuation is a family with several small children – others may help by carrying a child. A person with leg injury may be able to climb stairs when supported.

Sometimes, assisted evacuation is not possible and a person may have to be carried – e.g. in old buildings without ramps, smoke-proof elevators or safe spaces, wheelchair users have to evacuate via the stairs. In this case evacuation chairs may be helpful, but still two or more helpers are needed to succeed.

In any of these cases people rely on other people's help. Luckily, in many societies people will support each other in emergencies, e.g. [30]. In crowds, leadership may be necessary as people often do not know if they can and should help, they may need encouragement. Sometimes leadership only evolves as emergency services arrive on scene [31]. Organizations Evacuation planning in organizations should prepare their staff to take over leadership so that everyone in need will be assisted quickly.

3.10 Safe evacuation for all needs knowledge and practice

If safe evacuation for all is to be a realistic goal, knowledge and practice need to be considered in several different areas:

- Authorities need knowledge about users' characteristics and needs, e.g. movement times, space requirements, speech perception. And they should know available organizational and technical solutions. They should insist on plans for barrier-free evacuation.
- Fire fighters need trainings and practice how to evacuate different occupants, e.g. wheelchair users, blind persons. Some need only assistance, some need to be carried. Yet do date, there are very few studies that could support the planning of staff and technical resources. From what is known, it is clear that first responders or fire services cannot rescue all persons with mobility impairments, especially not in an aging society and when barrier-free access is granted. So, safe spaces, where persons can wait, are to be planned. This must come together with organizational solutions and communication strategies.
- Persons with mobility impairments should be included in evacuation drills. In drills where the authors participated or observed, wheelchair users often stayed in the building as it was assumed that evacuation could be too stressful or dangerous for them.
- Technical solutions like evacuation chairs are only useful if building occupants, traffic users and others know how to utilize them and how it "feels" to help a person to evacuate with one of those chairs.
- In the context of evacuations, the term panic is readily used. Practitioners and researcher sometimes assume to cause panic, e.g. by alarms. The (psychological or sociological) concept of mass panic has still not been sufficiently investigated. There is little empirical evidence for competitive or irrational behavior patterns. A sense of duty, helpfulness and altruism has been found [30, 32, 33]. Even if there seems to be a number of events which are in retrospect referred to as mass panic, real mass panic occurs very rarely. Although scientific literature agrees on this, the basic assumption is tenacious.

4. Conclusion

Safe evacuation includes many persons that currently are not adequately considered in evacuation research. Due to the lack of data and statistical numbers it is still a challenge to implement agents

with special needs in simulation models. Today, participants in field studies and experiments are usually healthy, young volunteers. The authors hope that in future studies, also persons with special needs are included whenever this is possible without putting them at risk.

Considering persons with special needs will not only help these persons to evacuate safely. It will also make evacuation easier and faster– including different occupant groups, enough space, understandable and visible signage, information via several sensory channels in several languages, elevators equipped to be used in case of fire, and other (technical and organizational) solutions are essential requirements. Implementation of Design for All will help everyone to evacuate safely.

Acknowledgements

This research was partly funded by the German Ministry for Education and Research (BMBF) contract No. 13N13266 (project ORPHEUS). The authors also would like to thank all persons with mobility impairments who shared their needs and requirements with the project team. Dr. Mareike Mähler, Anna-Lisa Mews and Hendrik Soffner helped to gather and analyze data.

References

- [1] Normenausschuss Bauwesen (NABau) and Normenausschuss Medizin (NAMed), “Barrierefreies Bauen - Planungsgrundlagen: Teil 1: Öffentlich zugängliche Gebäude,” 18040-1, Berlin, Oct. 2010.
- [2] G. Famers and J. Messerer, ““Rettung von Personen” und “wirksame Löscharbeiten” - bauordnungsrechtliche Schutzziele mit Blick auf die Entrauchung,” *DIBt Mitteilungen*, vol. 40, no. 1, pp. 10–12, 2009.
- [3] K. Boyce, “Safe evacuation for all - Fact or Fantasy?: Past experiences, current understanding and future challenges,” *Fire Safety Journal*, vol. 91, pp. 28–40, 2017.
- [4] K. Butler, E. Kuligowski, S. Furman, and R. Peacock, “Perspectives of occupants with mobility impairments on evacuation methods for use during fire emergencies,” *Fire Safety Journal*, vol. 91, pp. 955–963, 2017.
- [5] D. Boenke, H. Grossmann, and K. Michels, *Organisatorische und bauliche Maßnahmen zur Bewältigung von Notfallsituationen körperlich und sensorisch behinderter Menschen in Hochhäusern und öffentlichen Gebäuden mit hoher Benutzerfrequenz: [Abschlussbericht]*. Stuttgart: Fraunhofer IRB Verlag, 2011.
- [6] R. Block, W. Heister, and P. Georg, “Sicherheit in Werkstätten für Menschen mit Beeinträchtigungen,” *FeuerTRUTZ Magazin*, no. 6, 2017.
- [7] A. R. Larusdottir and A. S. Dederichs, “Evacuation Dynamics of Children – Walking Speeds, Flows Through Doors in Daycare Centers,” in *Pedestrian and evacuation dynamics*, R. D. Peacock, E. D. Kuligowski, and J. D. Averill, Eds., New York, NY: Springer, 2011, pp. 139–147.
- [8] L. Künzer and Gesine Hofinger, “Barrierefreie Alarmierung und Fluchtweggestaltung - für alle,” *FeuerTRUTZ Magazin*, no. 1, pp. 46–49, 2018.
- [9] G. Hofinger *et al.*, “Evakuierung für alle: Einige Ergebnisse aus ORPHEUS,” Berlin, Jan. 18 2018.
- [10] G. Hofinger, R. Zinke, B. Schröder, E. Andresen, and L. Künzer, “Human Factors in Pedestrian Simulation: Field Studies in Underground Stations.,” in *Proceedings of the 8th International Conference on Pedestrian and Evacuation Dynamics: PED 2016*, Hefei, 2016, pp. 41–48.
- [11] G. Hofinger, R. Zinke, and L. Künzer, “Human Factors in Evacuation Simulation, Planning, and Guidance,” (en), *Transportation Research Procedia. The Conference on Pedestrian and Evacuation Dynamics 2014 (PED 2014), 22-24 October 2014, Delft, The Netherlands*, vol. 2, pp. 603–611, 2014.
- [12] L. Künzer, “Myths of Evacuations,” *FeuerTRUTZ International*, no. 1, pp. 8–11, 2016.
- [13] R. Zinke, G. Hofinger, and L. Künzer, “Psychological Aspects of Human Dynamics in Underground Evacuation: field Experiments,” in vol. 2, *Pedestrian and Evacuation Dynamics 2012*, U. Weidmann, U. Kirsch, and M. Schreckenberg, Eds., Cham: Springer, 2014, pp. 1149–1162.
- [14] L. Künzer and A.-L. Mews, “Wer rein kommt, kommt auch raus?,” *Barrierefrei planen & bauen*, vol. 1, no. 2, pp. 28–31, 2017.

- [15] E. Andresen, R. Zinke, G. Hofinger, M. Chraibi, and A. Seyfried, “The Impact of Perception and Wayfinding on Pedestrian Movements,” in *Proceedings of the 8th International Conference on Pedestrian and Evacuation Dynamics: PED 2016*, Hefei, 2016, pp. 290–298.
- [16] L. Künzer and G. Hofinger, “Das Verhalten von Menschen in Rauch,” *FeuerTRUTZ Magazin*, no. 5, pp. 57–59, 2016.
- [17] N. W. H. Blaikie, “A critique of the use of triangulation in social research,” *Qual Quant*, vol. 25, no. 2, pp. 115–136, 1991.
- [18] W. Olsen, “Triangulation in Social Research: Qualitative and Quantitative Methods Can Really Be Mixed,” *Developments in Sociology*, vol. 20, pp. 103–121, 2004.
- [19] L. Künzer and G. Hofinger, “7.12 Psychologische Einflussfaktoren in Räumungen und Evakuierungen und Hinweise zu Flucht- und Rettungswegen,” in *Handbuch Brandschutzatlas: Grundlagen - Planung - Ausführung*, L. Battran and J. Mayr, Eds., 4th ed., Köln: FeuerTrutz, 2018.
- [20] K. E. Boyce, T. J. Shields, and G. W. H. Silcock, “Toward the Characterization of Building Occupancies for Fire Safety Engineering: Capability of People with Disabilities to Read and Locate Exit Signs,” *Fire Technol*, vol. 35, no. 1, pp. 79–86, 1999.
- [21] M. F. Story, J. L. Mueller, and R. Mace, *The Universal Design File: Designing for People of All Ages and Abilities*. Raleigh: The Center for Universal Design, NCSU, 1998.
- [22] J. Göbell and S. Kallinowsky, *Barrierefreier Brandschutz: Methodik - Konzepte - Maßnahmen*. Köln: Rudolf Müller, 2016.
- [23] E. D. Kuligowski, “Human Behavior in Fire,” in *SFPE Handbook of Fire Protection Engineering*, M. J. Hurley et al., Eds., New York, NY: Springer New York; Imprint; Springer, 2016, pp. 2070–2114.
- [24] C. Fitzpatrick and D. S. Mileti, “Public risk communication,” in *Disasters, collective behaviour, and social organisation*, R. R. Dynes and K.J. Tierney, Eds., Newark: University of Delaware press, 1994, pp. 71–84.
- [25] Normenausschuss Ergonomie (NAErg), “Ergonomie - Barrierefreie Gestaltung: Schalldruckpegel von gesprochenen Ansagen und öffentliche Lautsprecheranlagen,” DIN EN ISO 24504, Berlin 24504, Oct. 2016.
- [26] S. Breznitz, *Cry wolf: The psychology of false alarms*. Hillsdale, N.J: Lawrence Erlbaum Associates, 1984.
- [27] J. S. Tubbs and B. J. Meacham, *Egress design solutions: A guide to evacuation and crowd management planning*. Hoboken, NJ: John Wiley & Sons, 2007.
- [28] *Fire safety engineering in buildings. Guide to the application of fire safety engineering principles*: British Standards Institution, 2013.
- [29] P. Geörg, L. Künzer, R. Zinke, S. Holl, and A. Hofmann, “Bewegung besonderer Personengruppen: Berücksichtigung von Barrierefreiheit,” *Technische Sicherheit*, vol. 8, no. ½, pp. 38–43, 2018.
- [30] J. Drury et al., “Cooperation versus competition in a mass emergency evacuation: A new laboratory simulation and a new theoretical model,” (en), *Behavior Research Methods*, vol. 41, no. 3, pp. 957–970, <http://dx.doi.org/10.3758/BRM.41.3.957>, 2009.
- [31] B. Latané and J. M. Darley, “Group Inhibition of Bystanders Intervention in Emergencies,” *Journal of Personality and Social Psychology*, vol. 10, no. 3, pp. 215–221, 1968.
- [32] R. F. Fahy, G. Proulx, and L. Aïman, “Panic or not in fire: Clarifying the misconception,” (en), *Fire and Materials*, vol. 36, no. 5-6, pp. 328–338, 2012.
- [33] I. von Sivers, A. Templeton, G. Köster, J. Drury, and A. Philippides, “Humans do not Always Act Selfishly: Social Identity and Helping in Emergency Evacuation Simulation,” (en), *Transportation Research Procedia. The Conference on Pedestrian and Evacuation Dynamics 2014 (PED 2014), 22-24 October 2014, Delft, The Netherlands*, vol. 2, pp. 585–593, <http://www.sciencedirect.com/science/article/pii/S2352146514001355>, 2014.

Evacuation Guidance Design: An Experimental Study Based on Eye Tracking Devices

Ning Ding¹, Tao Chen², Yuan Liu³

¹ School of Criminal Investigation and Counter-Terrorism
People's Public Security University of China, Beijing, China
dingning_thu@126.com

² Institute of Public Safety Research, Department of Engineering Physics
Tsinghua University, Beijing, China
chentao.a@tsinghua.edu.cn

³ Institute of Economics, School of Social Sciences
Tsinghua University, Beijing, China
liuyuan_thu@163.com

Abstract - It is a crucial issue whether evacuees follow the evacuation guidance during evacuation. Good evacuation guidance is necessary to be designed to help the evacuees follow the guidance. In this paper, evacuation experiments based on wearable eye tracking devices were carried out to study the design effect of the evacuation guidance. Three factors were considered in these experiments: 1) the position of the evacuation guidance; 2) follow guidance or follow other evacuees; 3) follow a stranger or a familiar person. The results show that more participants noticed the guidance with low position and ground position than the guidance with up position. The evacuees intend to follow others rather than to follow the guidance, i.e. most evacuees act as “follower”. Eye tracking evacuation experiments can also be used to test the effectiveness of evacuation guidance signs.

Keywords: evacuation guidance; experiments; eye tracking devices; leader-and-follower

1. Introduction

With the continuous development of modern architecture, both the structure and the function of a building are gradually becoming more complicated. Thus, evacuation of people under emergency circumstances becomes an important research topic nowadays. Complex indoor places are usually enclosed environments with internal obstacles and multiple exits. They have features such as large scene area, complex internal structures, and multiple exits, such as supermarkets, movie theaters, and gymnasiums. Unlike pedestrian evacuation modeling in a simple environment (access, barrier-free rooms) whose focus is on research at the operational level, pedestrian evacuation modeling in complex indoor places needs to consider behavioral characteristics at the tactical level^[1]. How do evacuees choose the route in the evacuation process? How to make a decision? Do they follow the evacuation guidance? Only solving the problems of evacuation behaviors can provide a strong basis for the design of building evacuation signs and the establishment of evacuation simulation models.

In general, it is necessary to conduct evacuation experiments to study the crowds' evacuation behavior. The reason is that the evacuation data in fire disasters cannot be collected or the collection is incomplete, and we cannot ignite a building to conduct evacuation experiments. The experiment to study the crowds' evacuation behavior is divided into five types: (1) global evacuation drills^{[2] - [5]}; (2) local evacuation experiments^{[6] - [9]}; (3) controlled pedestrian flow experiments^{[10] - [13]}; (4) computer simulation evacuation experiments^{[14] - [18]}; (5) virtual reality experiments^{[19] - [22]}. Other research methods include the use of animals and insects for evacuation studies^[23], and in particular research on evacuation in panic situations^{[24] - [25]}. However, these experimental studies mainly focused on the microscopic and macroscopic characteristics of pedestrian flow, and they did not fully grasp the decision-making process of the crowd. In

order to further analyze the evacuees' psychology and behavior, eye tracking devices can be introduced in evacuation experiments.

Eyes are an important way for humans to obtain information. They can reflect people's psychological activities to some extent. The eye movement technique is to extract the data such as the gaze point, the gaze time, the number of gazes, the saccade distance, and the pupil size from the records of the eye movement trajectory, so as to study the intrinsic cognitive process of the individual. In recent years, eye tracking devices have also received some attention in evacuation experiments. Cosma^[26] combined VR technology with eye tracker to build a smoke-filled railway tunnel evacuations scene. A green LED lighting system was installed on the road surface. The crowd path selection behavior under different lighting conditions were studied through virtual reality evacuation experiments. It was found that the lighting system has a significant positive impact on the crowd's safety evacuation. Andree^[27] built a virtual high-rise building through VR technology. Through experiments, they studied the export selection behavior of crowds during the evacuation process and the waiting time when using elevators for evacuation. It was found that green evacuation indicators can effectively guide evacuees to choose elevators. However, there are still few experimental studies using eye trackers in evacuations.

In this paper, experiments were carried out to study how the position of the evacuation guidance sign influences evacuees' way-finding behaviors, and the impact of leader-and-follower on the way-finding choices during evacuation. In order to study these issues, we carried out 7 experiments with the use of wearable eye tracking glasses. The building layout and the procedure of the experiments are introduced in Section 2. The results of these experiments, including the ratio of different way-finding choices and the fix-action, are shown in Section 3. In the Section 4, the comparison of these results and some interesting phenomena during the experiments are discussed.

2. Experiment

In this paper, 7 experiments were carried out in a complex building. The objectives of these experiments are: (1) the impact of the positions (high, low, ground) of the evacuation guidance sign on the way-finding behavior; (2) when facing to a guidance sign and another evacuee (a stranger or an acquaintance), how does the participant make his/her choice? (3) when facing to an acquaintance and a stranger, the participant tends to follow which person?

The experiments were carried out in a complex building in People's Public Security University of China. This building is used for police and student training, and there are several rooms, crossroads and staircases. The Room 8 on second floor was used for the experiments, and the layout of the second floor is shown in Fig.1. When a participant arrived at this floor, he/she was blindfolded, and an experimenter guided him/her to a room. Then the eye mask was removed, and the experimenter helped him/her wear the eye tracking glasses (the device is SMI ETGTM). The eye tracking glasses is shown in Fig.2(a), and this glasses is connected with a mobile phone (shown in Fig.2(b)), which is used to storage the experimental data. Participant can easily wear the glasses with the mobile phone in his/her pocket. After calibrating the eye tracking glasses, the participant was asked to stand back to the door with 3 meters. When he/she hears the alarm sound, the experiment is started immediately, and when the evacuee (Participant A) finds the stairwell, the experiment is terminated. In an experiment involving other evacuees (Participant B), participant B stood near the door but did not obstruct the sight of participant A. In order not to introduce interference to the experiments, participant B and participant C were asked to wear the same clothes and pants.

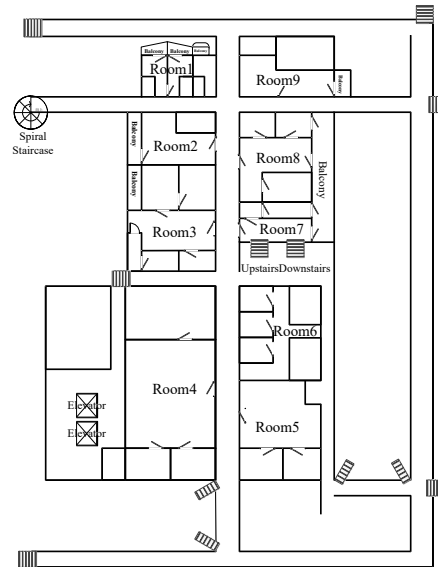


Fig. 1: Layout of the second floor.

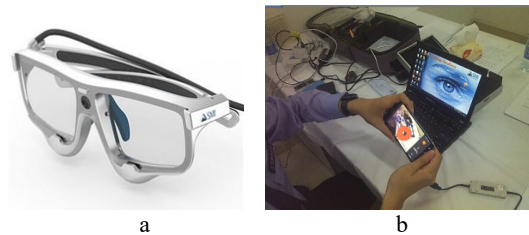


Fig.2 Eye tracking devices.

Before the experiment begins, the participant is asked if he knows which room he is in. If he knows the room, the experiment is considered invalid. The subjects of this experiment were all undergraduates of the School of Criminal Investigation and Counter-Terrorism, People's Public Security University of China. Each experiment includes 50 volunteers, and a total of 300 students participated in the 6 groups of experiments.

The experiment procedure is as follows:

- 1) Experiment 1: the guidance sign is set 30cm higher than the ground on the wall.
- 2) Experiment 2: the guidance sign is set 200cm higher than the ground on the wall.
- 3) Experiment 3: the guidance sign is set right ahead of the door threshold on the ground.
- 4) Experiment 4: the guidance sign is set 30cm higher than the ground on the wall, and a stranger stood around the door inside the room. The stranger was asked to go to the opposite direction of the guidance sign.
- 5) Experiment 5: the guidance sign is set right ahead of the door threshold on the ground, and a stranger stood around the door inside the room. The stranger was asked to go to the opposite direction of the guidance sign.
- 6) Experiment 6: there is no guidance sign at the door. The stranger (Participant B) and a person (participant C) familiar with the evacuee (Participant A) waited in the room before the experiment. When the experiment started, B moved to the left, and C moved to the right. Participant A was behind B and C before the evacuation began.

3. Results

3.1. Analysis Standard

Eye tracking devices are used during evacuation. Because the background is a dynamic picture, the analysis method is different from that for static pictures. This experiment is mainly to test the relationship

between the way-finding behaviour and eye movement in the evacuation process. In general, in experiment 1-3, eye movement characteristics of evacuees during evacuation can be divided into two categories: 1) the evacuee did not look at the guidance sign; 2) the evacuee looked at the guidance sign. Then the evacuees who looked at the guidance signs can be divided into people following the guidance sign and people not following the guidance sign. In experiment 4-5, the eye movement characteristics during evacuation can be divided into four categories: 1) the evacuee only looked at the guidance sign; 2) the evacuee only looked at participant B; 3) the evacuee looked at the guidance sign and also looked at participant B; 4) the evacuee did not look at the guidance sign, and did not look at participant B. The fourth category of evacuees make their own decision without the influence of the sign or participant B, so there is no need to analyse whether their evacuation direction is in accordance with the direction the sign indicated. Category 1-3 will be analyzed later.

In Experiment 6, the eye movement characteristics during evacuation can also be divided into four categories: 1) evacuee only looked at participant B; 2) evacuee only looked at participant C; 3) evacuee looked at participant B and also looked at participant C; 4) evacuee did not look at participant B, and also did not look participant C. Similar to the analysis of experiment 4-5, the fourth category is the independent decision of the evacuee. There is no need to analyze whether the evacuee follows the participant B or the participant C, and the other three categories need further analysis.

The data of the eye tracker mainly analyzes the time when evacuee looks at the sign: 1) if evacuee looks at the guidance sign, the time starts to count from when the evacuee's gaze falls on the sign, and stops when the gaze point is removed from the sign; 2) if evacuee looks at other participant, when evacuee begins to follow a stranger or opinion leader, the timing begins. When the gaze point moves away from the other participant and turns to another place (such as an intersection) during the evacuation process, the timing stops.

In the course of the experiment, some of the participants' eye movement data was invalid, mainly due to the fact that the eyeglasses were loose during the evacuation process and the fix-action was inaccurate. Another reason is that they mentioned previously that they knew the location of the room they were in.

3.2. Results of Experiments 1-3

A snapshot of experiment 1 is shown in Fig.3, and Table 1 shows the results of experiment 1-3. For the lower, upper, and ground signs, the percentage of people who could see the sign is 42.55%, 16.67%, and 47.73%, respectively. The guidance signs used in this experiment are evacuation indicators without light-assisted lighting. It can be seen from the experimental results, the percentage of evacuees who can see evacuation guidance sign is less than 50%, where the sign in lower and ground position is more likely to attract evacuees' attention than signs in upper position.

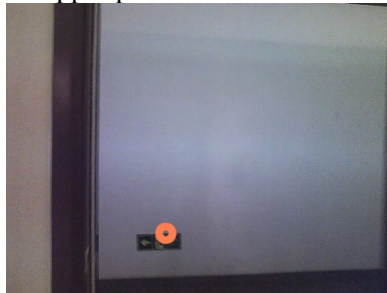


Fig.3: A snapshot of experiment 1.

Table 1. Results of experiment 1-3.

Experiment	Number of valid participants	Sign position	Number of participants who see the sign	Follower	Average gaze time	Non-follower	Average gaze time (s)	Follow-then-backtrack	Average gaze time
1	47	Low	20	12	0.54	6	1.04	2	0.48
2	42	High	7	5	0.53	2	0.52	0	-
3	44	Ground	21	14	0.61	6	0.42	1	0.76

Among people who saw the guidance sign, 60.00%, 71.43% and 66.67% chose to follow the sign, respectively. It can be seen that 60%-70% of those who saw the sign chose to follow direction the sign indicates. There are also individual participants who chose to follow the evacuation signs to evacuate and then went back to the other direction. In terms of the gazing time of the evacuation guidance sign, the average time of the follower in experiment 1 was only half that of the non-follower. However, in experiment 3, the follower's average gaze time is longer than that of the non-follower. It can be seen that there is no significant feature in the gaze time.

3.2. Results of Experiments 4-5

Snapshots of experiment 4 are shown in Fig.4, and Table 2 shows the results of experiment 4-5. In experiment 4-5, most evacuees only saw the evacuation guidance sign or participant B. In both sets of experiments, most of the people who only saw the sign and only saw participant B would choose to follow the directions of the sign or participant B respectively (depending on what they saw). Only in experiment 5, although 2 evacuees only saw the evacuation guidance sign, they did not follow the direction the sign indicated. Among the evacuees who saw the sign, the proportion of evacuees following the signs in experiments 4 and 5 was significantly higher than that in experiment 1-3.

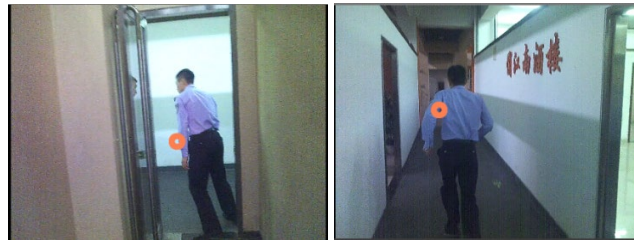


Fig.4: Snapshots of experiment 4.

Table 2. Results of experiment 4-5.

Experiment 4, 36 valid data 36 persons, sign position: low					
Category	Persons	Persons following the sign	Average gaze time (seconds)	Persons following participant B	Average gaze time (seconds)
Only saw sign	10	10	0.74	0	-
Only saw participant B	15	0	-	15	3.75
Saw both	6	6	0.66	0	3.58
Saw now	5	-	-	-	-
Experiment 5, valid data 43 persons, sign position: ground					
Category	Persons	Persons following the sign	Average gaze time (seconds)	Persons following participant B	Average gaze time (seconds)
Only saw sign	10	8	0.77	2	0.79 (time gazing at the signs)
Only saw participant B	18	0	-	18	2.88
Saw both	2	1	0.66	1	0.61
Saw now	13	-	-	-	-

In both sets of experiments, the number of persons who only saw and then followed participant B was significantly higher than the number of people who only saw evacuation signs and followed. The average time of the gaze (3.75 seconds and 2.88 seconds) was much higher than that of participants who only saw the evacuation signs (0.74 second and 0.77 second). The reason is mainly because when evacuees follow other people for evacuation, they will follow this person and watch for a long time.

In experiment 4, six participants saw both the evacuation guidance sign and participant B, but they all chose to follow the direction the sign indicated. It can be seen from their time of fixation that they look at

participant B much longer than when they watch the evacuation sign. In experiment 5, due to the small sample size, there were no significant features.

3.2. Results of Experiments 6

Table 3 shows the results of experiment 6. In experiment 6, the number of evacuees who only saw participant B (stranger) or participant C (acquaintance) are close. And there is no significant difference between the gaze time between the two categories. Of the 15 evacuees who both saw participant B and C, 7 of them chose to follow participant B (stranger), and 8 chose to follow acquaintance. In terms of gaze time, the time to gaze an acquaintance is obviously greater than the time to look at strangers. In addition, there were four people who did not look at familiar people or strangers and made their choices based on their own judgment.

Table 3. Results of experiment 6.

Experiment 6, valid data 6 persons					
Category	Persons	Persons following participant B	Average gaze time (seconds)	Persons following participant C	Average gaze time (seconds)
Only saw participant B	14	13	3.02	1	0.7 (the time gazing at B)
Only saw participant C	13	2	0.43 (the time gazing at participant C)	11	3.76
Saw both	15	7	participant B: 2.01 participant C: 2.43	8	participant B: 1.70 participant C: 3.09
Saw now	4	-	-	-	-

4. Comparison and Discussion

4.1. Comparison

As stated earlier, in experiments 1 and 4, the guidance sign is set 30cm higher than the ground on the wall, in experiment 2 is set 200cm higher than the ground on the wall and in experiment 3 and 5 right ahead of the door threshold on the ground. By comparing the proportions of evacuees who gazed at the guidance sign in experiments 1-5, as shown in Fig.5, results indicate that it is harder to be noticed when the position of the sign is higher. And only 16.67% of evacuees noticed the guidance sign set 200cm above the ground which is the highest sign position in all the six experiments. In contrast, the effect of an evacuation sign set in a lower position is relatively good. However, the evacuation signs used in this experiment were not light-assisted. In other VR evacuation experiments, it was found that the green LED evacuation guidance signs had good effect. In future experiments, we will also consider light-assisted evacuation indicators^[26, 27].

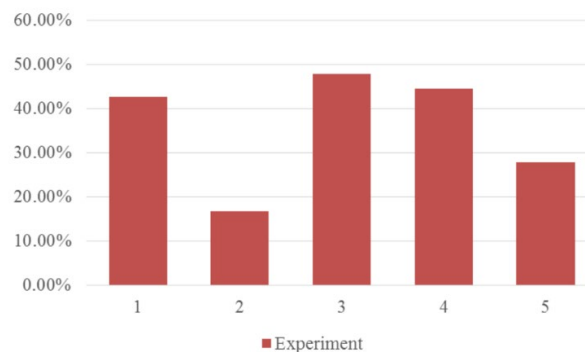


Fig.5 Proportions of evacuees who saw guidance sign in experiment 1-6.

The evacuees' average gaze time in experiment 1-6 was as shown in Fig.6. In all the 6 experiments the duration of gazing at the guidance sign was relatively short, concentrating between 0.5s and 1s. In contrast, the duration of gazing at people is longer because evacuees who follow people kept gazing at them during the evacuation. In experiment 6, the time duration of gazing at acquaintances is longer than at strangers.

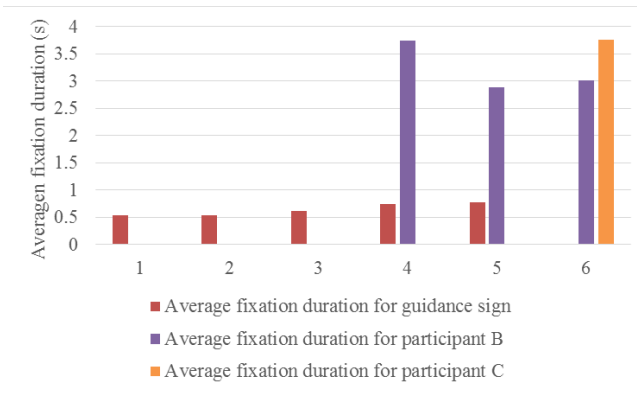


Fig.6 Average gaze time of the evacuees in experiment 1-6.

In the experiment, the proportion of evacuees who only saw the evacuation guidance sign or only saw another participant and acted as follower is shown in Fig.7. It shows that among the evacuees who only saw the guidance sign or another participant, the proportion of choosing to follow another participant is higher than that to follow the signs. By comparing experiments 1 and 4, experiments 3 and 5, it was found that although the location of the evacuation sign was the same, the proportion of evacuees who chose to follow the evacuation sign is higher when participant B is involved in the experiment. In addition, in the experiment 4-6, participants have a higher probability of following the target (guidance sign or other participants) they saw, and in experiments 4 and 5, the percentage of following strangers is 100%. In the experiment, directions of the sign and participant B are opposite. If the directions are the same, the probability that the crowd will follow the guidance sign may increase, and further studies will be conducted in later experiments.

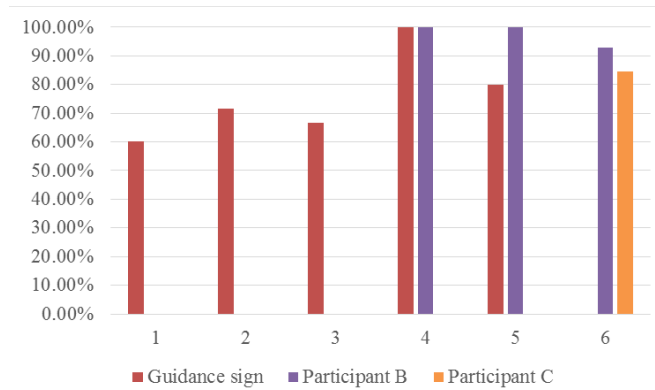


Fig.7 The proportion of evacuees following the target they saw.

In Fig.8 we compare the number of evacuees who only gazed at evacuation guidance signs and at other participants in experiment 4 and experiment 5. The number of evacuees watching strangers was higher than the number of evacuees watching the evacuation signs. It can be seen that in the process of evacuation, the attraction of the other people is greater than the attraction of the guidance signs to the evacuees.

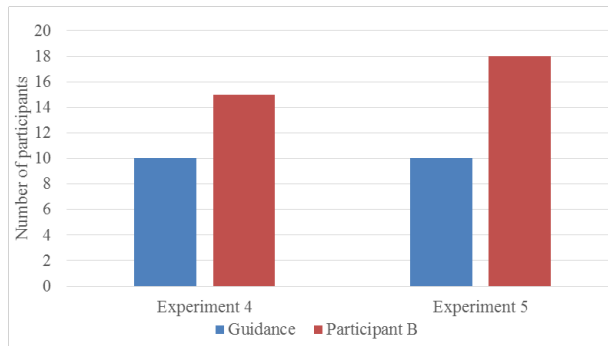


Fig.8. Number of evacuees who only saw the sign or other participants.

4.2. Limitations

There is a gap between experiments and real emergency evacuation events. The participants in our experiments were all Chinese students and well-educated; the type of participants and Chinese culture may have impact on the experimental results.

5. Conclusion

In this paper, 6 experiments were carried out. According to the results of experiments, it is found that more participants noticed the guidance with low position and ground position than the guidance with up position. The evacuees intend to follow others than to follow the guidance. Most of the evacuees play the role of a “follower”. Eye tracking evacuation experiments can be used to test the effectiveness of evacuation guidance signs. In our future work, more features should be tested based on experiments, such as social influence or social bond, guidance sign with lighting.

Acknowledgements

This work is supported by National Key R&D Program of China (No. 2017YFC0803300), the National Natural Science Foundation of China (71373139, 91646201).

References

- [1] Hoogendoorn, S., and W. Daamen. "Self-organization in pedestrian flow." *Traffic and Granular Flow* 2003:373-382.
- [2] Peacock, R. D., B. L. Hoskins, and E. D. Kuligowski. "Overall and local movement speeds during fire drill evacuations in buildings up to 31 stories." *Safety Science*, vol. 50, no. 8, pp. 1655-1664, 2012.
- [3] Huo, F., et al. "Experimental study on characteristics of pedestrian evacuation on stairs in a high-rise building." *Safety Science*, vol. 86, pp. 165-173, 2016.
- [4] Cheng, X., et al. "Study of announced evacuation drill from a retail store." *Building & Environment*, vol. 44, no. 5, pp. 864-870, 2009.
- [5] Kobes, M., et al. "Building safety and human behaviour in fire: A literature review." *Fire Safety Journal*, vol. 45, no. 1, pp. 1-11, 2010.
- [6] Ma, J., et al. "Experimental study on an ultra high-rise building evacuation in China." *Safety Science*, vol. 50, no. 8, pp. 1665-1674, 2012.
- [7] Fang, Z., et al. "Experiment and modeling of exit-selecting behaviors during a building evacuation." *Physica A Statistical Mechanics & Its Applications*, vol. 389, no. 4, pp. 815-824, 2010.
- [8] Fang, Z., et al. "Experimental study on evacuation process in a stairwell of a high-rise building." *Building & Environment*, vol. 47, no.1, pp. 316-321, 2012.
- [9] Liao, Y. J., et al. "A Study on People's Attitude to the Use of Elevators for Fire Escape." *Fire Technology*, vol. 50, no. 2, pp. 363-378, 2014.
- [10] Isobe, M., T. Adachi, and T. Nagatani. "Experiment and simulation of pedestrian counter flow." *Physica A Statistical Mechanics & Its Applications*, vol. 336, no. 3, pp. 638-650, 2004.

- [11] Kretz, T., A. Grünebohm, and M. Schreckenberg. "Experimental study of pedestrian flow through a bottleneck." *J.Stat.Mech.* (2006) P10014.
- [12] Seyfried, A., et al. "New Insights into Pedestrian Flow Through Bottlenecks." *Transportation Science*, vol. 43, no. 3, pp. 395-406, 2009.
- [13] Zhang J, W. Klingsch, A. Schadschneider, et al. "Experimental study of pedestrian flow through a T-junction." *Traffic and Granular Flow 11*. Springer Berlin Heidelberg, 2013: 241-249.
- [14] Liu, S. B., et al. "Modeling Movement Direction Choice and Collision Avoidance in Agent-Based Model for Pedestrian Flow." *Journal of Transportation Engineering*, vol. 141, no. 6, pp. 1-8, 2015.
- [15] Wei, J., et al. "Experiment of bi-direction pedestrian flow with three-dimensional cellular automata." *Physics Letters A*, vol. 379, no. 16-17, pp. 1081-1086, 2015.
- [16] Isobe, Motoshige, T. Adachi, and T. Nagatani. "Experiment and simulation of pedestrian counter flow." *Physica A Statistical Mechanics & Its Applications*, vol. 336, no. 3, pp. 638-650, 2004.
- [17] Helbing, D., et al. "Self-Organized Pedestrian Crowd Dynamics: Experiments, Simulations, and Design Solutions." *Transportation Science*, vol. 39, no. 1, pp. 1-24, 2005.
- [18] Hu, J., et al. "Experiment and simulation of the bidirectional pedestrian flow model with overtaking and herding behavior." *International Journal of Modern Physics C*, vol. 26, no. 11, pp. 1-12, 2015.
- [19] Kinatader M., E. Ronchi, D. Nilsson, et al., "Virtual reality for fire evacuation research." *IEEE Federated Conference on Computer Science and Information Systems (FedCSIS)*, 2014, pp. 313-321.
- [20] Ronchi, E., et al. "A Virtual Reality Experiment on Flashing Lights at Emergency Exit Portals for Road Tunnel Evacuation." *Fire Technology*, vol. 52, no. 3, pp. 623-647.
- [21] Marsh K L, Wilkie C T, Luh P B, et al. "Crowd Guidance in Building Emergencies: Using Virtual Reality Experiments to Confirm Macroscopic Mathematical Modeling of Psychological Variables." *Pedestrian and Evacuation Dynamics 2012*. Springer International Publishing, 2014: 197-212.
- [22] Lu X., P.B. Luh, K.L. Marsh, et al. "Guidance optimization of building evacuation considering psychological features in route choice." *Intelligent Control and Automation (WCICA), 2014 11th World Congress on. IEEE*, 2014: 2669-2674.
- [23] Lin P., J. Ma, T. Liu, et al. "An experimental study of the "faster-is-slower" effect using mice under panic." *Physica A Statistical Mechanics & Its Applications*, vol. 452, pp. 157-166, 2016.
- [24] Shiwakoti, N., and M. Sarvi. "Enhancing the panic escape of crowd through architectural design." *Transportation Research Part C*, vol. 37, no. 3, pp. 260-267, 2013.
- [25] Shiwakoti, N., et al. "Animal dynamics based approach for modeling pedestrian crowd egress under panic conditions." *Transportation Research Part B* 45.9(2011):1433-1449.
- [26] Cosma, G., E. Ronchi, and D. Nilsson. "Way-finding lighting systems for rail tunnel evacuation: A virtual reality experiment with Oculus Rift®." *Journal of Transportation Safety & Security*8.sup1(2016):101-117.
- [27] Andrée, K., D. Nilsson, and J. Eriksson. "Evacuation experiments in a virtual reality high - rise building: exit choice and waiting time for evacuation elevators." *Fire & Materials* 40.4(2016):554-567.

Dynamic Guidance by Colored Running Lights and Affordance: Route Choices of Adults and Older Children

Laura Künzer, Robert Zinke, Gesine Hofinger

Team HF Human Factors Research and Training

Hofinger, Künzer & Mähler PartG

Ludwigsburg, Germany

laura.kuenzer@team-hf.de; robert.zinke@team-hf.de; gesine.hofinger@team-hf.de

Abstract

Guidance to emergency exits play an important role for safe evacuation. Dynamic route guidance by colored flashing lights and strobe lights at emergency exits has been tested [1–3], but the effects of dynamic lights to support route choices need to be determined in more detail. Also, the guidance effects of different colors need to be examined and the reaction of various groups of evacuees.

The paper analyzes the effects of red and green running lights on route choice in subway stations comparing adults and older children (10 to 12 years old). Data was gathered in a laboratory experiment, focusing on the concept of affordance [4, 5]. Participants were asked to make a decision about the safest direction between two alternative directions. Their choice was either unsupported or supported by red or green running lights.

In general, an interaction between color and direction of the running light was found. Green running lights influenced route choices of both participant groups and led participants clearly into the direction indicated by the lights. Red running lights influenced route choices of both participant groups, but red lights lead to ambiguous decisions. Architectural elements such as stairs influenced route choices of both participant groups (functional affordance). But green running light offered a stronger indication to a safe route (cognitive affordance) than a visible staircase (functional affordance). Green lights even led participants to modify their route preference. In contrast, red running lights had an aversive effect: older children chose against the lights and preferred the other direction than the red lights were directing to. Implications for design of dynamic route guidance are discussed. This includes colored running lights to lead evacuees to a safe exit and to implement the influence of running lights on route choice and movement in simulations.

Keywords: evacuation, guidance, red and green lights, route choice, adults, older children, emergency exit

1. Motivation of the study and the concept of affordance

In case of fire, guidance to the safest emergency exits plays an important role in evacuations. In order to support wayfinding and route choice of evacuees, the design of emergency routes has to fulfill requirements. Requirements defined in fire regulation codes include number of exits, length and special dimension of escape routes as well as emergency lighting. Yet, additional design aspects and features could be considered in order to foster wayfinding and quick decision making.

In this regard, the possibility of dynamic route guidance by colored flashing lights and strobe lights at emergency exits has been tested [1, 2]. For example, it is known that “running lights” can create a sense of direction [6]. But the effects of dynamic lights to support route choices still need to be determined in more detail. Also, the effect of different colors needs to be examined in more detail as well as the reaction of various groups of evacuees.

This study focuses on the colors green and red because both colors are used to indicate emergency exits. Results of previous studies indicate meanings of colors: green to indicates “safe” or “go”; red represents “stop” or “danger” [8]. Depending on the country and infrastructure, the use of color for guidance in the context of danger varies to some extent. While the green pictogram of a “running man” indicates a safe

emergency route or exit in most European and Asian countries e.g. [7], the red “EXIT”-sign is used for the same purpose in parts of the USA.

In this paper, the effects of red and green running lights on route choice were analyzed comparing adults and older children from Germany, the latter ranging from 10 to 12 years in age. Older children were chosen to participate because in some countries children at this age use public transport on their own and therefore will also need to understand dynamical guidance features. Younger children are expected to be accompanied by parents or other adults.

The comparison of data from both participant groups focuses on the theoretical concept of affordance [4]. “Affordance” has different notions. In the user-centered design view by Norman [9], affordances result from a mental representation based on knowledge and past experiences. This means that specific characteristics of an object are related to specific actions and knowledge of a user. For example, a person may have encountered “stairs” before and may have made the experience that using them leads upstairs or downstairs. Three kinds of affordances are differentiated: sensory, cognitive and functional affordance [5, 10]. Within this study all three kinds of affordances are taken into consideration:

- “Sensory affordance” helps users with sensory actions (e.g. seeing, hearing, or feeling) and therefore detecting information. Running lights can attract attention. In this study, sensory affordance of green and red running lights was tested with route choices against a baseline without running lights.
- “Cognitive affordance” as a design feature helps interpreting the intended function of a design element. With respect to cognitive affordance, one objective of the study is to determine if a green running light indicates movement into a specific direction.
- “Functional affordance” combines both sensory and cognitive affordance. It allows to identify how and for what aim (usage and utility) an object can be used. The functional affordance of stairs was assumed to be “upstairs” or “outside” in this study.

Affordance in general depends on knowledge and experience of the individual. Since experience also varies with age, results were compared among children and adult participants.

2. Method

2.1. Item design

Pictures of five intersections were taken in subway stations in Berlin and were digitally edited for the purpose of the study. The intersections were presented on a laptop computer as motion pictures in graphics interchange format (GIF). Dynamic guidance was presented in the GIFs by green and red running lights, pointing into a certain direction, e.g. starting from the left and moving to the right. The running lights were moving with a frequency of 200 ms either to the left or to the right.

Each item was designed without any lights (baseline; examples fig. 1-3), and with either green or red running lights (examples fig. 4 and 5). In total, 25 different item designs were used (table 1).

Table 1: Items designs for intersections 1 to 5, no lights (baseline), color of light and direction of running lights, 25 items in total.

Intersection	No lights	Color of lights	Direction of running light
Intersection 1	Baseline	Green	Left ← Right →
		Red	Left ← Right →
Intersection 2	Baseline	Green	Left / upstairs ↖ Right / along platform →
		Red	Left / upstairs ↖ Right / along platform →
Intersection 3	Baseline	Green	Left ← Right / upstairs →
		Red	Left ← Right / upstairs →
Intersection 4	Baseline	Green	Left ← Right →
		Red	Left ← Right →
Intersection 5	Baseline	Green	Left ← Right →
		Red	Left ← Right →
Sum of Items	5		20

The design of the presented intersections was “equivalent” for intersections 1, 4 and 5 (figures 1-3). These intersection, when presented without running lights (baseline), offered equivalent route options for the symmetric left and right directions. Equivalent means that both routes had the similar length and there were no stairs on the route to the exit. Also there was no signage in either direction. So, they were equivalent considering the fastest route to a safe exit. On the other hand, for intersection 4 and 5, the participants’ position was assumed to be on a staircase or escalator, so one of the routes was a bit shorter.

The designs of the remaining intersections 2 and 3 were “not equivalent” as the choice was between a near staircase and route along the platform (intersection 2, see fig.6) or between stairs and a longer route to the left that also led to another, hardly visible, staircase (intersection 3, see fig. 7).

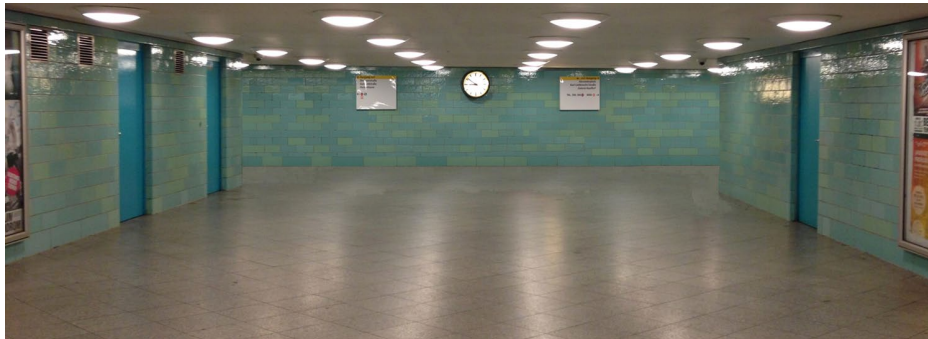


Fig. 1: Intersection 1 without lights (baseline) and equivalent route options for symmetric left and right direction.

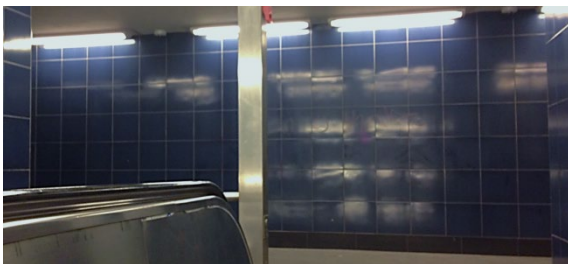


Fig. 2: Intersection 4 without lights (baseline) and equivalent route options for symmetric left and right direction but with a shorter route on the right side.



Fig. 3: Intersection 5 without lights (baseline) and equivalent route options for symmetric left and right direction but with a shorter route on the left side.

2.2 Participants

50 participants took part in the study, 31 adults and 19 older children. The age of the adults ranged from 20 to 31 years with an average of 24.87; SD = 2.86. The age of the children ranged from 10 to 12 years with an average of 10.79; SD = .63.

The study was conducted in German. All adults were Germans, as were 14 of the older children, the others five older children stated to be from Bulgaria (2), Romania (1) and Turkey (2). All older children confirmed that they were able to easily understand and follow the German instructions of the study. Only two of the participants were left-handed. Due to this small number, a possible effect of handedness was not further examined. 25 of adult participants were bachelor or master students. No participant had a professional background related to colored light or signals, so effects of professional background were also not further examined. All participants stated to have normal or corrected eye vision.

2.3 Procedure of the study

All participants were informed about the procedure and risks of the study. Additional information about the research project ORPHEUS was provided. Then informed consent was obtained from all participants. Informed consent for the older children were signed by their parents. The study with the older children was conducted at a school in the presence of the children's parents. The study with the adults was conducted in a real subway station accompanying another field study [12].

Participants filled a questionnaire about socio-demographic data, e.g. age, nationality, eye vision including their experience with subway systems. The participants were then seated in front of a laptop computer. The items and additional questions were presented in a digital format.

Participants were instructed to imagine that they were in a subway station when the station had to be evacuated due to a fire alarm. They were told that several pictures showing two alternative exits are to be presented in sequence and that their task for every picture was to choose the safer of the two exits. Their choice, e.g. for intersection 2 to turn right or to go upstairs (see fig. 6) was either unsupported (baseline) or supported by red or green running lights.

Participants stated their decision via keyboard. The five items without any lights were presented first in randomized order as a baseline. Then the 20 items with green or red running lights were presented in a randomized order. Finally, the participants answered a questionnaire about the green and red lights.

3. Research questions and results

The study included the following research questions:

1. Is there a preference of direction when no running lights influence route choice?
2. How are route choices influenced by green or red running lights?
3. Is there an effect of functional affordance by architectural design on route choice?
4. Is the effect of running light (sensory affordance) stronger or weaker than the functional affordance of architectural design?
5. Are there any differences between the choices of adults and older children?

Items of intersections 1, 4 and 5 (equivalent options) were included for research question number 1 and 2. For question 3 and 4, the items of intersections 2 and 3 were included.

To allow for comparisons (research question number 5), all items were statistically analyzed separately for adult and older children. The comparisons will be discussed as supplementary part of research questions 1 to 4.

3.1 Is there a preference of direction when no running lights influence route choice?

As most participants were right-handed and Germans, there was the expectation that there would be a preference for the right side when there is no guidance by signage or light and when route options have an architectural equivalence. This kind of "natural" preference of direction was analyzed by the items of the baseline condition without any running lights (equivalent intersections 1, 4 and 5). Tests of binomial-distribution were used to analyze "natural" preferences.

No “natural” preference for the left or right direction was found for participants’ choices in intersection 1 (see fig. 1) and intersection 4 (see fig. 2). Also, no “natural” preference was found in older children’s choices for intersection 5 (see fig. 3). Thus, data supported the assumption of equivalent intersection design. Also, the right-handedness and nationality of most of the participants do not influence their route choice in the condition of architectural equivalence.

A “natural” preference to turn right (25 out of 31) was only found in the data of the adults for intersection 5 (see fig. 3). Intersection 5 has symmetric route options, and at the same time has a possible slight affordance for the left side due to the escalator on the right side impeding view, as stated above. Only for this item in the baseline condition the assumed “natural” preference was found. This is surprising because in this item there was even slight functional affordance suggesting the left hand option. Why this is the case remains unclear from the data available.

3.2 How are route choices influenced by green or red running lights?

The effect of lights was analyzed by data comparison of the baseline and participants’ route choices with green or red running lights. McNemar tests were used to analyze “changes” in route choices when lights were included in the equivalent intersections 1, 4 and 5.



Fig. 4: Intersection 5 with green running lights moving to the left (movement was achieved by using GIF).

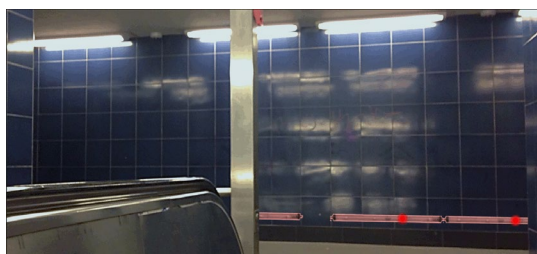


Fig. 5: Intersection 4 with red running lights moving to the right (movement was achieved by using GIF).

Green running lights influence route choices of both participant groups leading participants into the direction the light is moving to.

For intersection 1 and 4, where no “natural” preference was found in the baseline condition, both participant groups’ route choices changed significantly to the direction the green running lights were moving to. This effect was found to be independent of the direction of the green running light: Most participants distinctly chose the direction of the running lights, no matter if the green light moved to the left or to the right. The same effect was found for intersection 5 for most older children’s choices. For intersection 5 (see fig. 4), where a “natural” preference “to the right” was found for adults, most adults also significantly preferred to follow the green lights, even when the lights were moving to the left.

Red running lights influence route choices of both participant groups, but effect of red lights is different for adults and older children

For intersection 1 (equivalent routes), most participants in both groups chose not to follow the direction of the red running light. Instead, they preferred the other route possibility, e.g. most participants chose to turn to the left if the red running light pointed to the right.

Results for intersections 4 and 5 (see example in fig. 5) showed differences between both participant groups: around 60% of the adults chose the direction the red lights were moving to. Also around 60% of the older children chose not to follow the directions of the red running lights and instead opted for the other direction.

In summary, running lights clearly influence route choice compared to the baseline. Comparing results for red and green lights, it can be stated, that participants’ choices to follow the green lights were found to be significant more often (compared to the baseline and the red running lights). Results were also clearer than choices to follow the red running lights. Some adults chose to follow red lights which could be explained by sensory affordance: “movement of lights leads to a safe exit” regardless of the color of the

running light. For older children, the red running light led to a decision against the direction the red light was moving to. The color red represents “stop” as in traffic lights or “danger” [8]. Older children might have projected this concept from their knowledge to the red running lights (cognitive affordance). So, it can be concluded that the conflict between the cognitive affordance of the color red and the sensory and cognitive affordance of the movement of the light into a certain direction overall leads to a less definite, more ambiguous decisions.

3.3 Is there an effect of functional affordance by architectural design on route choice?

Intersections 2 and 3 without any running lights (baseline) were used to analyze the influence of functional affordance offered by “architectural elements”. Examples can be found in figures 6 and 7 that show intersections 2 and 3 (note that both intersections were presented in different items with all variations of green and red running lights moving to the left or to the right).

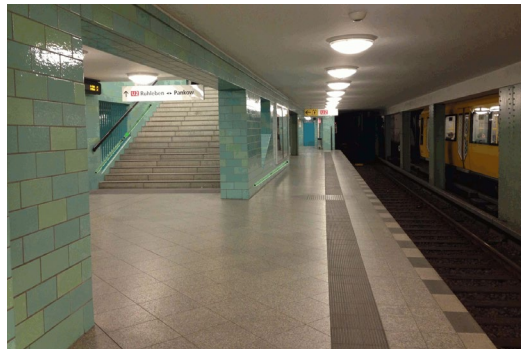


Fig. 6: Intersection 2 with green running lights moving to the left/ upstairs.

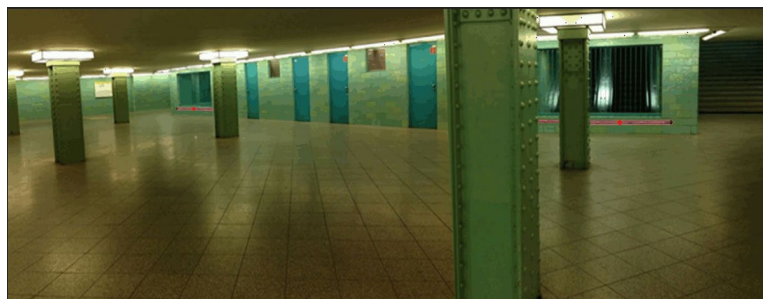


Fig. 7: Intersection 3 with red running lights moving to the right/ upstairs.

“Stairs” influence route choices of both participant groups but in different ways.

Overall, the architectural element “visible stairs” was statistically more often chosen as safest route. This was in accordance with expectations, as the staircase in both items is clearly visible and nearer than the other exit. Also, a staircase might be known to lead “up” or “outside” the subway station thereby indicating “a safe route” (functional affordance).

Differences are found between the groups: Older children chose significantly more often to walk upstairs in intersection 2 whereas no significant effect was found for the adults. One possible explanation is that for adults climbing up stairs is more exhausting and therefore some of them chose the longer route without stairs.

On the other hand, adults chose significantly more often to walk upstairs in intersection 3 whereas no significant effect was found for the older children. Here, one possible explanation is that the children didn’t recognize the staircase that was hardly visibly on the left.

Despite the effects we found, data of this study do not allow generalized interpretations to how staircases and perceived distances influence route choices.

3.4 Is the effect of running light (sensory affordance) stronger or weaker than the functional affordance of architectural design?

The green running light had a stronger influence on participants' choices (cognitive affordance) than the visible staircase (functional affordance) and even led participants to modify their route preference.

By comparing the baseline (no running lights) of intersections 2 or 3 with items including running lights (green or red), interaction effects of cognitive affordance and functional affordance were analyzed using binomial tests. Examples of items with colored running lights can be found in figures 6 and 7.

For intersections 2 and 3, most adults choose the direction the running lights were moving to. Detailed analysis showed that green lights had a significant effect on route choice. The cognitive affordance of the green lights led to a more definite route choice than the functional affordance of the stairs. If the green running light moved “upstairs”, the positive effect by green lights increased and even more participants decided to walk upstairs. The effect, redundancy gain [11], can be explained by congruence of the cognitive affordance of the green light and the functional affordance of the viewable staircase.

Another statistically significant effect was found for intersection 2 in the condition of green lights directing “along the platform”. Around 84% of the adults chose to follow the direction of the running green lights. This is change in route choice compared to the baseline (where they mostly “walked” upstairs) was caused by the sensory and cognitive affordance of the green light. This same effect was found for intersection 3 where adults even chose to walk to the left instead of going directly upstairs (to the right) which had been their choice in the baseline condition. Thus, sensory and cognitive affordance of the green running lights seems to be stronger than the functional affordance of the stairs.

Results from older children also show a strong significant effect of green running lights guiding to the direction of movement of the lights. With green running lights moving in the upstairs direction, most older children still chose to walk upstairs. But when the green running lights were moving along the platform, older children also chose the route along the platform in intersection 2 – which meant a change of route choice in favor of the direction of the green moving lights. This same effect was found for the adults.

Red lights lead to a greater variability of route choices. Interaction (or better interference) between cognitive and functional affordance and the red running light was found. For intersection 2, with a red light moving upstairs, participants more often chose to walk along the platform. When the red light moved along the platform, adults still chose to walk along the platform. Although some adults chose to follow the red running lights, some changed their route choice against the direction the red running lights moved to. With respect to following or avoiding the direction of movement of the red running lights, no statistical evidence was found for either one of the two route choice preferences. In contrast, for the older children red running lights had an aversive effect: they avoided the direction of movement of the red lights and preferred the other route available.

Summarizing results, it can be said that the effect of red running light in comparison to distances or stairs cannot easily be determined. On the other hand, for both participant groups, cognitive affordance of the green running lights seems to be stronger than the functional affordance of the stairs.

4. Limitations of the study and further research

Only five different, but modified intersections were included. Also the intersections were only shown in an experimental setting on the laptop computer. Future studies should be carried out in architectural settings, e.g. subway stations using actual guiding lights. Also, the effects of different saturation or lightness of the colors green and red and combinations of colors and pictographs, e.g. green arrows; red crosses, should be determined.

The study included only two participant groups. To establish a generalization of the findings, further research will include different participant groups, e.g. elderly, differences in gender and cultures, and groups with special conditions, e.g. people with color-blindness. Also, a greater number of participants for each group should be included, because the sample discussed here allowed only non-parametrical testing. Some effects should be investigated based upon a greater sample, e.g. a preference for a direction of people from countries with left-hand traffic, or possible effects of handedness of participants. To examine

redundancy gain effects and to include more participant groups, e.g. people with impaired vision, sensory affordance by guiding lights should be combined with guiding sounds.

5. Conclusions

In the study presented, strong effects of running lights and several types of interactions between color, direction if the light and architectural elements were found. Green running lights influence route choices of both, adult participants and older children, and lead into the direction of movement of the green lights. Green running lights were even stronger than functional affordance proposed by the design of architectural elements in the intersections. Conclusions for evacuation guidance and simulations are as follows:

- Installation of running lights at emergency routes is advisable and can lead evacuees to a safe exit.
- Variability in the interpretations of the color red indicates that dynamic guidance with running lights should use green lights. The exact color values of green are yet to be determined.
- Furthermore, the influence of running lights on route choice and movement should be implemented in simulations: modelling pedestrian flows for the evacuation from an infrastructure could gain an increased level of realism with respect to evacuees' route choice by including route choice preferences in favor of the movement of green running lights. This in return could make evacuation simulation more effective for predicting flows and required capacities of escape routes when using dynamic route guidance by green running lights.

Acknowledgements

This research was funded by the German Ministry for Education and Research (BMBF) contract No. 13N13266 (project ORPHEUS). The authors also would like to thank all participants of the study, especially the children and their parents. Prof. Dr. Andreas Pflitsch and his team encouraged their students to take part in the experiment. Anna-Lisa Mews and Lisbeth Balters conducted the children's' study.

References

- [1] D. Nilsson, H. Frantzych, and W. Saunders, "Coloured Flashing Lights To Mark Emergency Exits - Experiences From Evacuation Experiments," (en), *Fire Safety Science*, vol. 8, pp. 569–579, 2005.
- [2] L. Künzer, G. Hofinger, and R. Zinke, "The Influence of Colored Running Lights on Route Choice – Dynamic Guidance and Affordance," in *Proceedings of the 8th International Conference on Pedestrian and Evacuation Dynamics: PED 2016*, Hefei, 2016, pp. 167–172.
- [3] E. R. Galea, D. Cooney, and L. Filippidis, "Active dynamic signage system: A full-scale evacuation trial," *Human Behaviour in Fire*, 303-314,, 2015.
- [4] J. J. Gibson, *The ecological approach to visual perception*. Boston: Houghton Mifflin, 1979.
- [5] R. Hartson, "Cognitive, physical, sensory, and functional affordances in interaction design," *Behaviour & Information Technology*, vol. 22, no. 5, pp. 315–338, 2003.
- [6] E. B. Goldstein, *Wahrnehmungspsychologie*, 2nd ed. Heidelberg: Spektrum, 2002.
- [7] Bundesanstalt für Arbeitsschutz und Arbeitsmedizin, "Technische Regeln für Arbeitsstätten ASR A2.3: Fluchtwege, Notausgänge, Flucht- und Rettungsplan" (Technical workplace regulations for escape routes, escape exits and escape route plans). GMBI. Nr.45 vom September 2007, die zuletzt im Januar 2017 geändert wurde," 2007.
- [8] L. Künzer, "Alarmstufe Rot!" oder „Alles im grünen Bereich!": Farben im Kontext von Gefahr und Sicherheit," ("Red Alert" or "Green is Safe" Colors in the Context of Danger and Safety), Dissertation, Universität Regensburg, Regensburg, 2016.
- [9] D. A. Norman, "Affordances: Commentary on the Special Issue of AI EDAM," *AIEDAM*, vol. 29, no. 03, pp. 235–238, 2015.
- [10] E. Carattin, R. Lovreglio, E. Ronchi, and D. Nilsson, "Affordance-Based Evaluation of Signage Design for Areas of Refuge," *Interflam 2016. Fire Science and Engineering Conference*, pp. 781–786, 2016.
- [11] C. D. Wickens and J. G. Hollands, *Engineering psychology and human performance*, 3rd ed. Upper Saddle River, NJ: Prentice Hall, 2000.

Estimating social relation from trajectories

Zeynep Yucel¹, Francesco Zanlungo², Claudio Feliciani³, Adrien Gregorj¹, Takayuki Kanda^{2,4}

¹Okayama University
Okayama, Japan

zeynep@okayama-u.ac.jp; gregorja@s.okayama-u.ac.jp

²ATR IRC

Kyoto, Japan

zanlungo@atr.jp

³University of Tokyo

Tokyo, Japan

feliciani@jamology.rcast.u-tokyo.ac.jp

⁴Kyoto University

kanda@i.kyoto-u.ac.jp

Abstract - This study focuses on social pedestrian groups in public spaces and makes an effort to identify the social relation between the group members. We particularly consider dyads having coalitional or mating relation. We derive several observables from individual and group trajectories, which are suggested to be distinctive for these two sorts of relations and propose a recognition algorithm taking these observables as features and yielding an estimation of social relation in a probabilistic manner at every sampling step. On the average, we detect coalitional relation with 87% and mating relation with 81% accuracy. To the best of our knowledge, this is the first study to infer social relation from joint (loco)motion patterns and we consider the detection rates to be a satisfactory considering the inherent challenge of the problem.

Keywords: Dyads, interaction, pedestrian groups, recognition, social relation.

1. Introduction

Crowd has a heterogeneous structure, i.e. it may be constituted of various components (e.g. individuals, groups, commuters, shoppers) with distinct dynamics. Although autonomous agents (e. g., wheelchairs or robots) have recently started to take part in public spaces, in this study we restrict ourselves to crowds constituting of only autonomously walking pedestrians. In that respect, we assume the basic building blocks of the crowd to be (i) individuals and (ii) pedestrian groups.

In the field of pedestrian movement and evacuation dynamics, locomotion of individuals has been studied since a long time. However, the motion of pedestrian groups has started attracting attention only recently, even though they are an important component of crowd dynamics [1,13].

The importance of pedestrian groups is due to their specific dynamics, which distinguishes them from a mere collection of (unrelated) individuals. Moreover, depending on the public space (and thus the context or the scenario), groups may constitute up to more than half of the crowd [1], which increases their significance.

Profiling of groups is important for understanding and analyzing the state of the crowd, for instance for detecting stability, collectiveness or conflict [2, 3]. Moreover, automatic resolution of social relation may eliminate or reduce the need of human labeling in the collection of research or application oriented datasets, and can be used by assistive robots providing services to pedestrians (by allowing recognition of targets for such services, e.g. automatically recognizing potential customers such as families, etc.)

2. Background

In order to understand the dynamics of pedestrian groups, we need to take a closer look into their composition. Namely, several intrinsic features of the group, such as purpose, age, or gender are shown to play a crucial role in their locomotion [4]. In this study, among those intrinsic features, we choose to focus on social relation between the peers.

According to McPhail and Wohlstein, pedestrian groups are people engaged in a *social relation* to one or more pedestrians and move together toward a common goal [5]. Due to the diversity of the social situations, there is no consensus on a universal, concrete and exhaustive list of social relations. Nevertheless, several categorizations of fundamental forms of social relation have been proposed [6, 7, 8, 9]. While these social science studies define relations using concepts such as benefit of exchange or social domain, in more application oriented fields (e.g. simulation, robotics), the concept of social relation is defined and interpreted in direct relation to (i) the empirically available data and (ii) the specific purpose of utilizing the relation information.

Namely, in such domains, images or videos constitute the data used in identification of social relation. For such reason, the data is often subject to computer vision analysis. Several applications include resolution of kinship relation [10], recognition of domain related roles, such as birthday child and guests, understanding of hierarchical relations between leader/subordinate and interpretation of different social circles such as bikers, hippies, clubbers, etc. [11].

In this study, we choose to focus on social relations which commonly occur among pedestrians in a public environment, trying to use an approach that may fit both to theoretical (social or natural science) studies and to practical applications (automatic recognition for crowd analysis, simulation, robotic applications).

From a collective point of view of the above listed considerations, the approach of Bugental is regarded to be the most convenient model in categorizing social relations [9]. Namely, Bugental proposes a domain-based approach and divides social life into five non-overlapping domains defined as: attachment, hierarchical power, mating, reciprocity and coalitional [9]. When applied to walking pedestrian group classification, the reciprocal domain corresponds to friends, the attachment one to families, the mating one to couples and the coalitional one to colleagues (the hierarchical domain corresponds to a situation that does not fully apply to moving pedestrians in a public space, such as presenter-audience relationship in a seminar room or teacher-pupil relationship in a classroom).

Furthermore, in this study, as a first step to identification of social relation from locomotion, we contain ourselves to two kinds of social relations: mating and coalitional. We examine dyadic groups, which are in one of those relations, and propose an algorithm to distinguish them using a set of observables derived from 3D range data originating from our previous works [4] and [12]. In the future, we aim expanding our scope to the relations of reciprocal and attachment.

3. Dataset

The dataset used in this study is already introduced by [13] and is freely available at [14]. In what follows, for the integrity of the manuscript, we briefly provide relevant information on the dataset but refer the interested reader to [13] and [4] for a through discussion. The dataset is recorded in an indoor public space covering an area of approximately 900 m² in a one year time window. The public space is the ground floor of a business center, which is connected to a train station, a ferry terminal and a shopping center. Therefore, it is populated with pedestrians coming from a diverse background.

Over the course of the data collection campaign, range information is registered for over 800 hours using 3D depth sensors. Using the algorithm of [15], pedestrians are automatically tracked and their position (on 2D floor plane) and height are computed, which can be all downloaded freely from [14]. As a result of the tracking process, the cumulative density map of the environment is found as in Fig. 1(a).

In addition to the range information, we also collected video footage for labeling purposes. Based on the video, three coders (non-technical staff members of one of our institutions) label the dataset with respect to several intrinsic group features. One specific feature refers to the apparent relation, where the possible options are friends, family, couples and colleagues, which correspond to the domains of reciprocal, attachment, mating and coalitional, respectively [9].

Identification of social relation from videos is obviously difficult and subjective. For confirming the inter-rater reliability of the labeling process, we use the following procedure, whose details are reported in [4]. To reduce the work load on coders, we asked to two of them to label only part of the dataset, while the third coder labeled the entire dataset. Inter-rater reliability is evaluated based on the data analyzed by all coders. Using several prominent statistical measures such as Cohen's κ , Fleiss' κ and Krippendorff's α , the coders are found to be in considerable agreement [16, 17, 18, 4], and thus we decided to use the labels of the third coder as the basis of our study [4]. As a result, the relation between dyads is distributed as follows: 358 coalitional, 96 mating, 216 attachment and 318 reciprocal.

In this preliminary study, we tried to differentiate between coalitional and mating relations (i.e. "colleagues" and "couples"). This choice is established based on the observations presented in [4], which suggest that coalitional and mating relations present the most distinct features among all combinations of relation pairs. Namely, [4] illustrates that work-oriented dyads move with a significantly larger velocity in comparison to not work-oriented dyads (i.e. mating, attachment, reciprocity relations). On the other hand, [4] proves that the variation on distance between the peers is distributed over a range of values, where coalitional relation is associated with the largest expected value and mating relation is associated with the smallest expected value. In other words, among all relations, on the average, colleagues move with the largest distance, whereas couples move with the smallest distance between peers.

From these dyads in coalitional or mating relation, we require a minimum observation duration of 15 secs (this threshold was introduced to assure that the tracking and interaction time were enough stable, and it is based on considerations relating the nature of the environments, e.g. length of the corridor), which we regard to be sufficiently long to speculate on the social relation. Therefore, we initially consider the 358 dyads in coalitional relation and 96 dyads in mating relation. In addition, from the trajectories of these dyads, we eliminate the portions with unexpected or irregular behavior (such as stopping and waiting or meeting, splitting etc.) using similar criteria to [13]. Specifically, we require a minimum average group velocity of 0.5 m/sec and a maximum interpersonal distance of 2 m. After eliminating the portions of trajectories, which are not in line with our requirements, we derive and contrast several observables from the remaining portions. The details of the definitions of observables and the cumulative empirical observations are presented in Section-4.

4. Observables and Empirical Distributions

In examining the joint behavior, we focus on the following observables: interpersonal distance, group velocity, velocity difference and height difference of the peers. In what follows, we provide the definitions of these observables on a sample pair (p_i, p_j) depicted in Fig. 1(b).

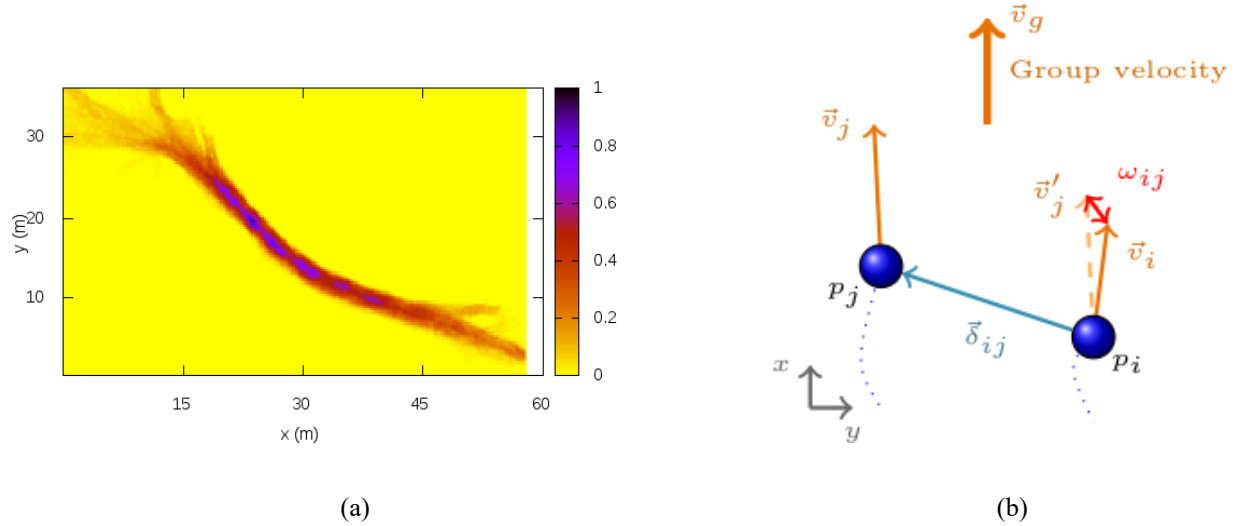


Fig. 1: (a) Cumulative density map of the environment and (b) The observables depicted on a sample dyad .

4.1. Definition of Observables

The data-set introduced in [4] is based on the tracking system [15], that uses laser range sensor to track pedestrian position in 3D (i.e., including pedestrian height). Based on our previous works [4,14] we decided to use the following observables (x and y are defined, respectively, as the direction of motion of the group, determined by the average velocity, and the “abreast direction” orthogonal to the velocity). Namely, the observables depicted in Fig. 1(b) are defined explicitly as follows:

- (i) Interpersonal distance $\delta_{ij} = \sqrt{(\delta_{x(i,j)}^2 + \delta_{y(i,j)}^2)}$
- (ii) Group (average) velocity $v_{g(i,j)} = |(\vec{v}_i + \vec{v}_j)/2|$
- (iii) Velocity difference of the peers $\omega_{ij} = |\vec{v}_i - \vec{v}_j|$
- (iv) Height difference of the peers $\Delta\eta_{(i,j)} = |\eta_i - \eta_j|$, where η_i and η_j stand for the height of p_i and p_j , respectively.

Henceforth, we drop the indices i and j for the simplicity of notation.

4.2. Empirical Distributions of the Observables

The cumulative distribution of interpersonal distance δ , relating the entire set of dyads in coalitional and mating relation is presented in Fig. 2(a). It is clear that mating dyads stay in closer proximity than coalitional dyads and that their behavior is more “stable” (i.e. less spread) (Fig. 2(a)). In other words the values regarding mating dyads are distributed around a smaller mean and with a lower deviation.

We also took a closer look into on the projections of interpersonal distance along and perpendicular to motion direction [4]. Namely, we denote the projections of δ_{ij} on x -axis and y -axis with δ_x and δ_y , respectively (see Figure1-(b)). Here, δ_x corresponds to the *depth* of the group, whereas δ_y corresponds the *abreast distance* of the peers. Between coalitional and mating dyads, group depth δ_x is found to have no significant difference; while abreast distance δ_y and δ are found to present a similar degree of statistical difference [4], and thus, taking in consideration also computational economy, we decided to consider only the absolute distance observable while ignoring, in this preliminary work, its components.

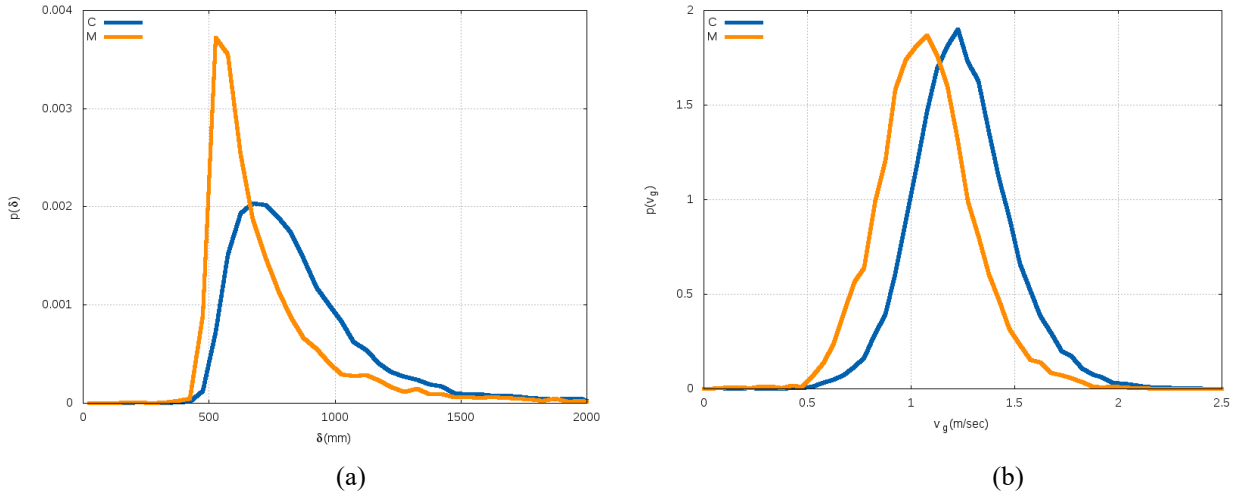


Fig. 2: Empirical distribution of (a) interpersonal distance and (b) group velocity in coalitional (C) and mating (M) relation.

As presented in Fig. 2(b), group velocity v_g of the mating dyads is on average lower than that of the coalitional groups. Moreover, despite being less clear than the distinction of group velocity, also the absolute difference of velocities ω is found to be different between two social relations as shown in Fig. 3(a) (and confirmed by an ANOVA, as reported below and treated in more detail in [4]) due to the lower maximum and heavier tail.

The last observable of interest, height difference of the peers, $\Delta\eta$, depicted in Fig. 3(b), does not depend on the motion of the peers but rather on their gender in an indirect way. Namely, mating relationship often refers to a heterosexual pair, whereas it is not uncommon for coalitional groups to be composed of same gender peers. In this respect, height difference turns out to be a discriminating feature, since it is higher for mating relation than for coalitional relation (although its effectiveness may depend on cultural factors, i.e. ratios of same gender couples or mixed gender coalitional dyads).

Here, we would like to point out to one certain advantage of using height difference instead of height. Height of individuals strongly varies between societies, while sexual dimorphism (i.e., the tendency of males to be taller) is reported in all human societies [19]. Therefore, using $\Delta\eta$ instead of η makes the method more flexible and generalizable over different societies.

In addition to these subjective evaluations, we carry out an ANOVA (following the analysis performed in [4]) to confirm the inferences mentioned above. All observables of δ , v_g , ω , and $\Delta\eta$, are found to have a p-value smaller than 10^{-4} . Adopting the widely accepted threshold value of 0.05 for statistical significance [20], we can say that there exists a considerable distinction between coalitional and mating relation in terms of all observables.

5. Recognition of Social Relation

In this section, we describe our method for discriminating coalitional and mating relations using the observables introduced in Section 4. Specifically, we take a Bayesian stand-point similar to [21] and

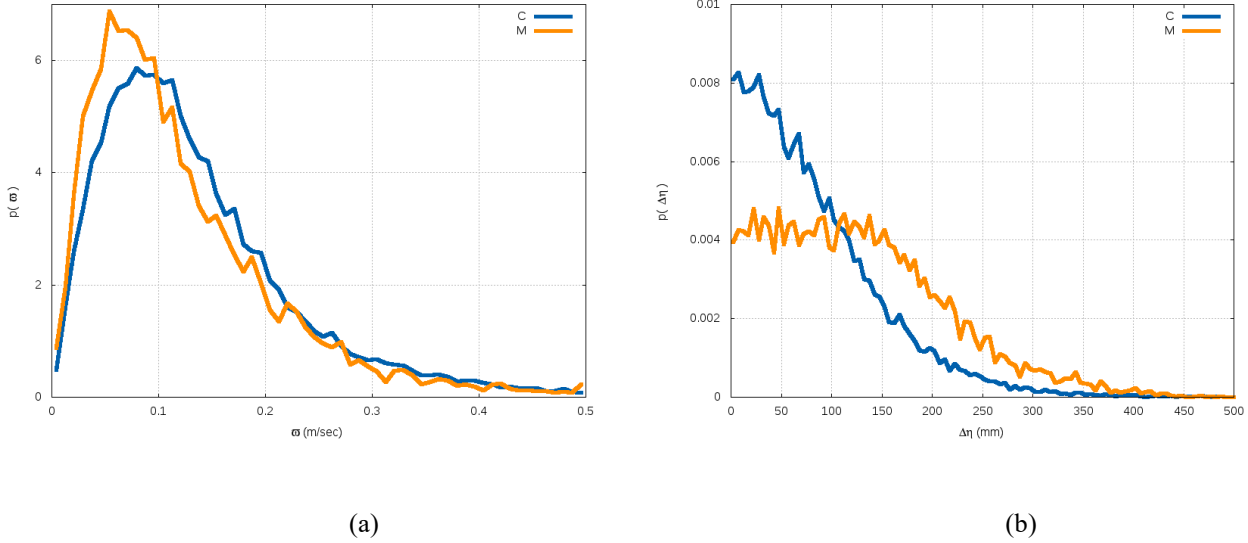


Fig. 3: Empirical distribution of (a) velocity difference (b) height difference of peers for dyads in coalitional (C) and mating (M) relation.

compute the conditional probability that a given set of observations come from a dyad in a particular social relation.

Suppose that from a pair of pedestrians (p_i, p_j) we gather a set of observations at time t and denote it by $\Sigma(t) = \{\delta(t), v_g(t), \omega, \Delta\eta\}$. Let us denote their social relation by r , where the possible values of r are coalitional C and mating M . We compute the probability that the observation set Σ , gathered at time t , comes from a dyad in social relation of r , $P_t(r|\Sigma)$, as follows,

$$P_t(r|\Sigma) = \frac{P_t(\Sigma|r)P_t(r)}{P_t(\Sigma)} \quad (1)$$

Here, $P_t(r|\Sigma)$ is the posterior probability that the dyad comes from relation r given the observation set Σ . In addition, $P_t(\Sigma|r)$ is the likelihood term and $P_t(r)$ is the prior probability of social relation.

While computing the likelihood, we assume that the four kinds of observables $\Sigma(t) = \{\delta(t), v_g(t), \omega, \Delta\eta\}$ are independent. This assumption enables expressing the likelihood term using the following product,

$$P_t(\Sigma|r) = P_t(\delta|r)P_t(v_g|r)P_t(\omega|r)P_t(\Delta\eta|r) \quad (2)$$

For each conditional probability in Eq. 2, we use the empirical distributions. Namely, we shuffle the dataset and randomly select a subset of the pairs to build the probability density functions.

As for an initial value for our prior belief, $P_0(r)$, we adopt an equal probability to avoid any bias. Thus,

$$P_0(r) = (0.5 \quad 0.5), \quad (3)$$

since we have two possible cases for social relation.

As time elapses, we propose updating (or not) the prior as in Eq. 4, where the parameter α defines the rate of update.

$$P_t(r) = \alpha P_0(r) + (1 - \alpha)P_{t-1}(r) \quad (4)$$

Regarding the update, we contrast three cases as follows:

- (i) Update priors to the last computed value (i.e. the posterior) at every step.
- (ii) Update priors using a linear combination of the initial value and last computed probability value
- (iii) No update on the priors

The 3 cases described above can be realized using $\alpha = \{0, 0.5, 1\}$, respectively.

The term, $P_t(\Sigma)$, which is called the marginal likelihood, is not necessary to be explicitly computed. Specifically, we make use of the fact that a particular pair comes either from a C or M relation and thus the sum of the posterior probabilities, which are scaled by the same term in Eq. 1, need to sum up to 1.

6. Results

In practice, we randomly choose 30% of the pairs and use their trajectories to build the probability density functions in Eq. 2. The remaining 70% are used to test the ability of our estimation method to recognize relation of dyads outside the training set (of course, the general applicability of the method should be tested in future on different environments and cultural settings). Moreover, repeating this validation procedure 20 times, we compute the mean and standard deviations of performance values to investigate the sensitivity (i.e. dependence) of the observables on training set. By randomly picking 30% of the entire samples and repeating this procedure 20 times, the probability that a particular sample is not used for training falls below 10^{-3} .

From the recognition rates presented in Table-1, it is observed that coalitional relation is recognized with a somewhat higher rate for all values of α , which could be due to the imbalance of samples in the dataset as given in Section-3 (and possibly on the nature of the observable pdfs, e.g. standard deviations). Moreover, taking a fixed and unbiased prior performs slightly better than applying an update. In addition, the effect of random shuffling is regarded to be minute, which suggests that the observables are stable across samples and the method is resilient to changes in training set. All in all, the proposed method achieves significant accuracy considering the challenge of the problem.

Table 1: Recognition performance (%) for varying α .

α	C	M
0	88.5 ± 2.1	73.4 ± 5.0
0.5	88.1 ± 2.1	79.1 ± 3.8
1	87.1 ± 2.3	81.3 ± 4.1

7. Conclusions

This study describes a method to identify social relation between members of a pedestrian group. We particularly focus on dyadic groups belonging to a coalitional or mating relation. Several observables are derived from individual and group trajectories in addition to height difference of the peers. A recognition algorithm, which uses these data as features, is proposed. Running it over the entire trajectory updating the estimation of social relation in a probabilistic manner at every sampling step, recognition rates are computed. On the average, coalitional relation is detected with 87% and mating relation with 81% accuracy, when the prior is not updated. We believe this is the first study to recognize social relation from trajectory and height information.

Acknowledgements

This work was partially supported by JST-Mirai Program Grant Number JPMJMI17D4, Japan. This paper is based on results obtained from a project commissioned by the New Energy and Industrial Technology Development Organization (NEDO).

References

1. M. Schultz, L. Rößger, H. Fricke, and B. Schlag, "Group dynamic behavior and psychometric profiles as substantial driver for pedestrian dynamics," in *Pedestrian and Evacuation Dynamics 2012*, pp. 1097–1111, Springer, 2014.
2. C. von Krüchten, A. Schadschneider, "Empirical study on social groups in pedestrian evacuation dynamics," *Phys A: Stat Mech Appl.* 2017;475:129–141.
3. J. Shao, C Change Loy, X Wang, "Scene-independent group profiling in crowd," In: *CVPR*. Columbus, OH; 2014. p. 2219–2226.
4. F. Zanlungo, Z. Yücel, D. Brscic, T. Kanda, and N. Hagita, "Intrinsic group behaviour: dependence of pedestrian dyad dynamics on principal social and personal features," *arXiv preprint arXiv:1703.02672*, 2017.
5. C. McPhail, R. Wohlstein, "Using film to analyze pedestrian behavior," *Sociological Methods & Research* 1982;10:347–375.
6. A. P. Fiske, "The four elementary forms of sociality: framework for a unified theory of social relations.," *Psychological review* , vol. 99, no. 4, p. 689, 1992.
7. M. S. Clark and J. Mills, "Interpersonal attraction in exchange and communal relationships.," *Journal of personality and social psychology* , vol. 37, no. 1, p. 12, 1979.
8. E. B. Foa and U. G. Foa, "Resource theory," in *Social exchange* , pp. 77-94, Springer, 1980.
9. D. B. Bugental, "Acquisition of the algorithms of social life: A domain-based approach.," *Psychological bulletin* , vol. 126, no. 2, p. 187, 2000.
10. V. Ramanathan, B. Yao, L. Fei-Fei, "Social role discovery in human events," *CVPR 201*, pp. 2475-2482, IEEE.
11. G. Wang, A. Gallagher, J. Luo, D. Forsyth, D. , "Seeing people in social context: Recognizing people and social relationships," *ECCV 2010*, pp. 169-182, Springer.
12. Z. Yücel, F. Zanlungo, T. Ikeda, et al. "Deciphering the crowd: modeling and identification of pedestrian group motion," *Sensors*. 2013;13(1):875– 897.
13. F. Zanlungo, D. Bršćić, and T. Kanda, "Spatial-size scaling of pedestrian groups under growing density conditions," *Physical Review E*, vol. 91, no. 6, p. 062810, 2015.
14. ATR-IRC, "Dataset: Pedestrian tracking with group annotations," <http://www.irc.atr.jp/sets/groups/> , (accessed January, 2018).
15. D. Bršćić, T. Kanda, T. Ikeda, and T. Miyashita, "Person tracking in large public spaces using 3-d range sensors," *IEEE Transactions on Human-Machine Systems* , vol. 43, no. 6, pp. 522-534, 2013.
16. Cohen, Jacob. "A coefficient of agreement for nominal scales." *Educational and psychological measurement* 20.1 (1960): 37-46.
17. Fleiss, Joseph L. "Measuring nominal scale agreement among many raters." *Psychological bulletin* 76.5 (1971): 378.
18. Krippendorff, Klaus. "Reliability in content analysis." *Human communication research* 30.3 (2004): 411-433.
19. Gustafsson, A and .Lindenfors, P, "Latitudinal patterns in human stature and sexual stature dimorphism", *Annals of Human Biology*, 2009; 36(1), 74-87.
20. Goodman, Steven N., and Jesse A. Berlin. "The use of predicted confidence intervals when planning experiments and the misuse of power when interpreting results." *Annals of internal medicine* 121.3 (1994): 200-206.
21. D. Bršćić, F. Zanlungo, and Takayuki Kanda. "Modelling of pedestrian groups and application to group recognition." *Information and Communication Technology, Electronics and Microelectronics (MIPRO)*, 2017 40th International Convention on. IEEE, 2017.

Experimental Study on Variation Strategies for Complex Social Pedestrian Groups in Conflict Conditions

Xiaolei Zou¹, Xiaoyi Qu², Ruihua Xu³

¹College of Transportation Engineering, Tongji University
4800# Cao'an Road, Shanghai, China
zouxiaolei@tongji.edu.cn

²College of Public Safety Management, Shanghai Open University
288# Guoshun Road, Shanghai, China
quxy@shtvu.edu.cn

³College of Transportation Engineering, Tongji University
4800# Cao'an Road, Shanghai, China
zouxiaolei@tongji.edu.cn
rhxu@tongji.edu.cn

Abstract - The paper concentrates on an experimental study of the variation strategies of complex social pedestrian groups in conflict conditions. We tracked the trajectories of group members and analysed the configuration of both the complex group and its subgroups when the groups walked through a narrowing passage, passed by an obstacle or faced counter flows. We summarized the variation strategies of complex groups when they faced these conflict conditions. The effect of groups on the crowd was also studied. It was found that groups could have significant effect on self-organization of the crowd. The results in the paper could be applied in modelling pedestrian group decision and behaviour and analysing crowd dynamics.

Keywords: variation strategies, complex social pedestrian groups, group behavior, self-organization, conflict conditions

1. Introduction

In our previous studies, complex social pedestrian groups with more than 5 members are proved to be composed of simple subgroups with 2-3 members [1] and the complex groups always keep regular structures in free pedestrian flow [2]. The studies of other researchers also showed that facts [3,4]. But how do the groups variate and reorganize when they face conflict conditions? In this paper, we made a further experimental study on variation strategies for complex social pedestrian groups.

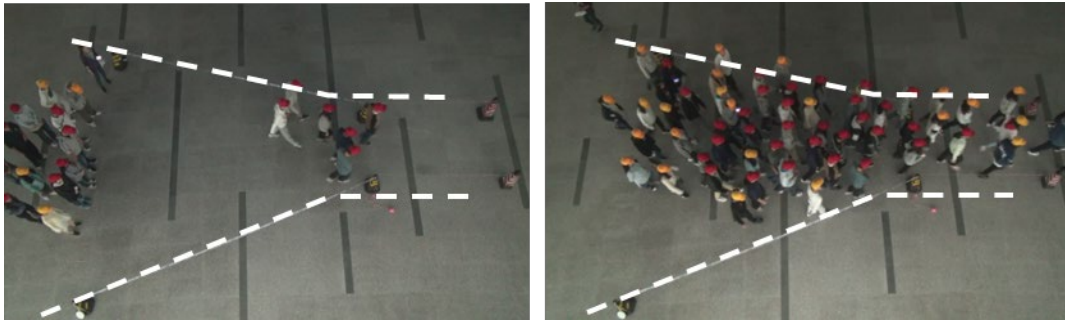
The paper concentrates on the variation strategies of complex social pedestrian groups in conflict conditions. We summarized the variation strategies of complex groups when they walked through a narrowing passage, passed by an obstacle or faced counter flows. We also studied the effect of groups on the crowd and found that groups could have significant effect on self-organization of the crowd.

2. Controlled Experiments on Group Behavior

From 2014 to 2016, we conducted a series of experiments on social pedestrian group behavior in Tongji University, Shanghai. Some of the experiments took place on October 27th and 28th with 60 student participants divided into complex social groups with 5-7 members in the following scenes:

(1) Group behavior and dynamics of crowd evacuation in the narrowing passage

In order to observe and test the behavior of complex groups with 5-7 members, the groups were asked to walk through a passage, the length of which was 8m and the width gradually narrowed from 3 m to 1.5 m. The groups kept walking for 5 meters after they passed the bottle neck. The scenes of both single groups and the crowd walking through the passage were conducted to observe the intragroup behaviour and intergroup interactions, which is shown in Fig.1.



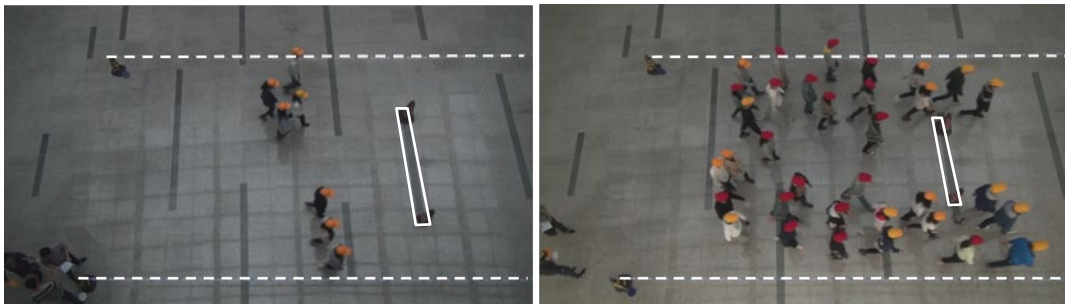
(a) Scene of a single group

(b) Scene of the crowd

Fig. 1: Scenes of groups and crowds walking through the narrowing passage and bottle neck

(2) Obstacle avoidance behavior of groups and crowds

In this experiment, 3m, 1.5m and 0.8m wide obstacles were set separately in a 6m wide passage. Groups with 5-7 members were asked to walk through the passage in sequence to test the strategies of the obstacle avoidance behavior of the groups. In order to test the mutual influence of groups, crowds with groups were asked to go through the passage as well. See Fig. 2.



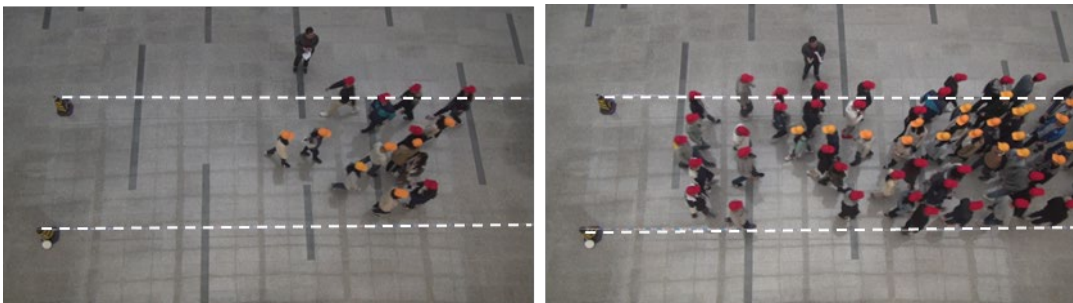
(a) A single group passing by the obstacle

(b) The crowd passing by the obstacle

Fig. 2: Experiments for obstacle avoidance behavior of groups and crowds

(3) Group behavior in bidirectional counter flows

The width of the passage was set to 6m and 3m, and groups with 5-7 members were asked to walk through the passage oppositely in sequence to test the variation strategies of the groups when they passed by each other. Bidirectional counter flows with groups and without groups were also asked to walk through the passage to test the impact of group behaviour on the evacuation of bidirectional counter flows. In addition, experiments for two vertical conflict streams walking across each other and bidirectional counter flows walking across the bottle neck were conducted as well.



(a) Two groups passing by each other

(b) Bidirectional counter flows in the passage



(c) Vertical conflict flows walking across each other

(d) Bidirectional counter flows in the bottle neck

Fig. 3: Experiments for group and crowd behavior in conflict conditions

3. Strategies for Variation of groups in Narrow Space and Conflict

We developed a visualization tool for group structure and trajectory analysis. By tracking and analysing the movement of the groups when passing narrowing passage and avoiding static obstacles, we summarized the variation strategies for group patterns.

3.1. A visualization tool for group structure and trajectory analysis

The visualization tool for group structure and trajectory analysis was developed in the environment of Visual Studio with C# and Python. It provides a visualized way for observing the structure variation of moving complex groups and calibrating the group structure, and also the functions for speed and spatial distribution analysis for group members.

As shown in Fig. 4, trajectories of all the members of a complex group can be drawn. After setting the relationships of the members and subgroups in several key frames, the logical structure of the group for each moment can be expressed with colored dots and lines. The logical structure includes the location and connection of members, the barycenter of the complex group and subgroups, as well as the connection of subgroups. The connections between group members and subgroups are expressed with symbol expressions (See Reference [2]). All of the expressions and spatial locations of members can be deduced automatically and stored in time series.

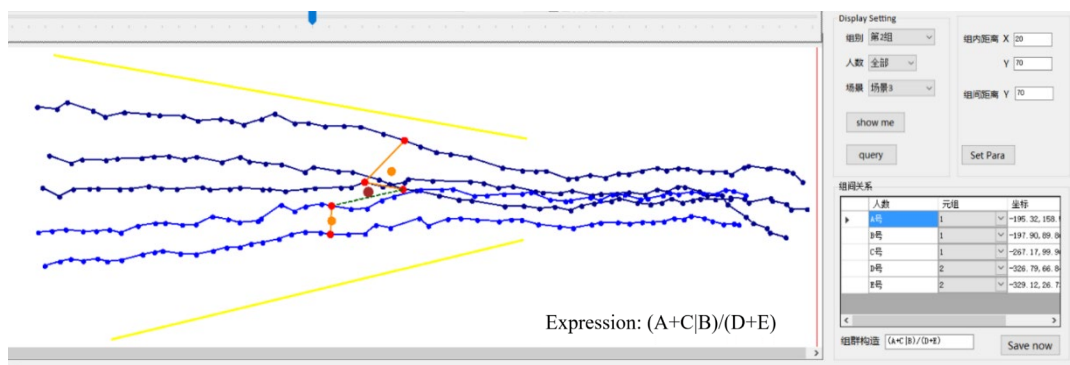


Fig. 4: A screen shot for the tool for dynamics visualizing analysis

3.2. Strategies for Variation of Groups When Passing Narrowing Passage

In scene 1, the motion of 61 complex groups with 5 members were tracked. The groups started walking in a free pattern (see Reference [2]) with their members aligned. We numbered the members from left to right in the group and plot the trajectories of all members of the tested groups together into one figure and plot the trajectories of all subgroups together into another. Fig. 5 shows that the groups experience the

process of free walking, space compression, congestion and expansion during passing through the narrowing passage. In the state of free walking, boundaries of the distribution of group members are relatively clear, which means that group members intend to keep a comfortable private space from 50-60cm in free walking. It is entirely consistent with our earlier research [5]. In other states, the distribution areas of the members overlap, which means that the structure and configuration of the groups vary in order to keep the private space of the members. Fig.6 shows that the trajectories of subgroups align parallel to the walking direction when the passage is wide enough and overlap others when the passage becomes narrow.

Fig. 5 and Fig. 6 tell that both the group members and the subgroups vary their position in the group to adapt to the width of passage. What strategies for variation do groups adopt when the space becomes limited and how do they reorganized after they go out of the bottleneck?

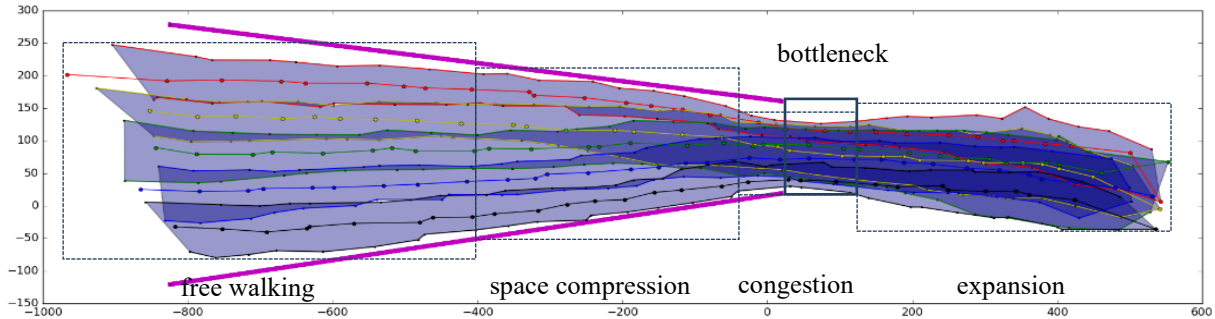


Fig. 5: Distribution of group members during passing through the narrowing passage

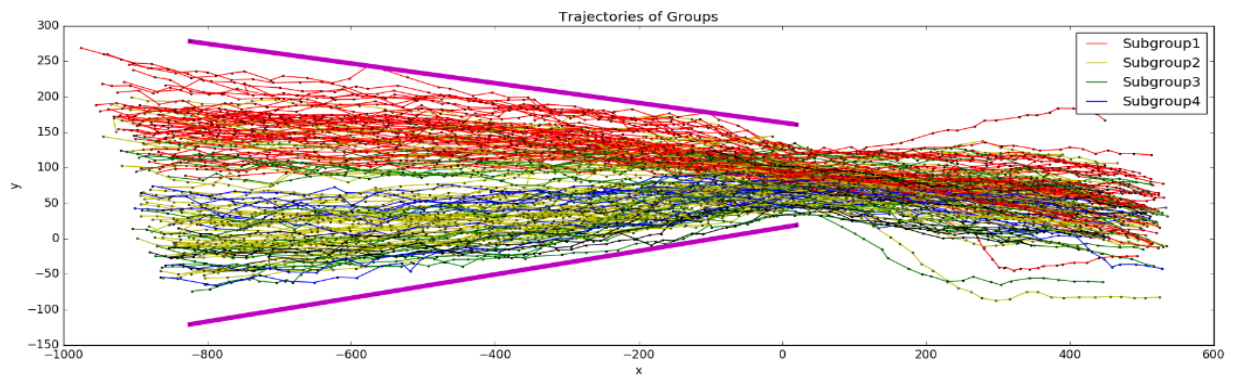


Fig. 6: Trajectories of subgroups

By analysing the trajectories of the members and social connections of them, we estimated the strategies of variation of the groups in two aspects, the constancy of the composition of members and the stability of the configuration of the groups.

At the beginning, the complex groups are naturally composed with subgroups and individuals. Approximately 63.9% of the complex groups are composed of 2 subgroups, which is the common structure of the 5-member groups (see Reference [1]). And 85.2% of the complex groups spread in free pattern and simple pattern (see Reference [2]). The structures and patterns of the groups are consistent with the natural group features observed in our previous field studies from 2014 to 2016 in the massive long-distance striding (see Reference [2]).

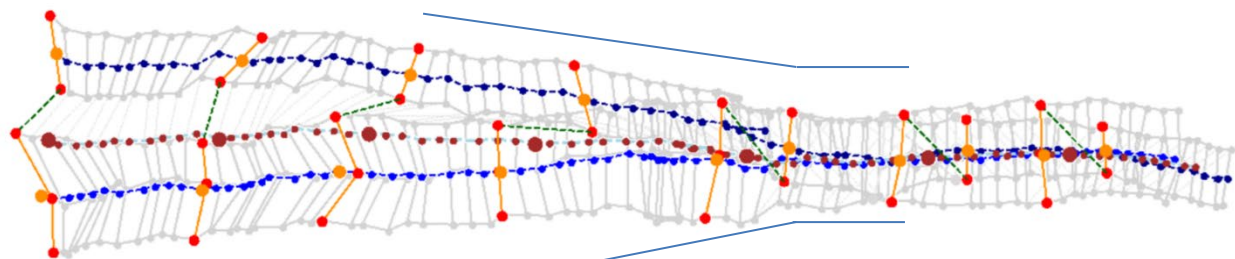
While the groups walk from the wide side to the narrow side as shown in Fig. 1(a), the vertical space to the walking direction space narrows and most of the groups keep constant subgroup members, with a proportion of 77.1% of the tested ones. The constant groups adopt two main strategies. One is giving priority to keep the subgroup configuration by maintaining stable relative positions of members within the subgroup but changing the relative positions of the subgroups, and the other is giving priority to keep the complex group configuration by maintaining stable relative position of the subgroups within the complex

group but changing the configuration of its subgroups. The data shows that 70.2% of the constant groups preferred to keep stable configurations of subgroups, which makes 54.1% of all the complex groups.

Fig. 7(a) shows one of the complex groups with 2 subgroups walking through the passage using strategy of keeping subgroup configuration. None of the subgroups changes its structure or configuration when it arrives at the bottleneck. The expressions for group members remains $(A+B)$ and $(C+D+E)$. But one subgroup accelerates while the other decelerates. The expression for subgroups changes from $a+b$ to $a|b$. The whole complex group keeps its configuration stable after it go out of the bottleneck.

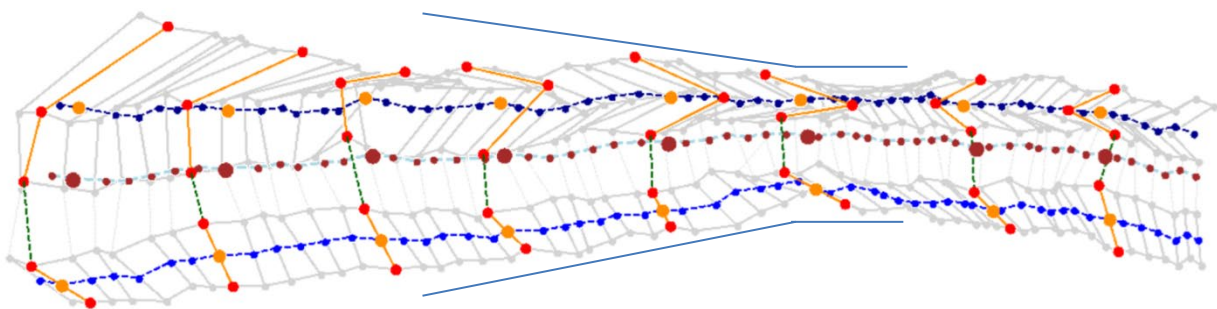
Fig. 7(b) shows one of the complex groups with 2 subgroups walking through the passage using strategy of keeping the complex group configuration. The two subgroups walk at the same speed and keep the configuration stable when they arrive at and go out of the bottleneck with a symbol expression of $a+b$. But the subgroups compress their space and change the configuration.

After walking out of the bottleneck, the complex groups have enough space and can walk freely. However, most of them do not reorganize to their original structure but keep their new configuration. 84.8% of the groups who use strategy of keeping subgroup configuration do not reorganize. They walk with a simple pattern with 2 rows and keep the whole group walking freely and the subgroup members communicating easily. And 71.4% of the groups who use strategy of keeping the complex group configuration do not reorganize but most of them spread to a free pattern to keep enough space for walking and communication.



$$(A+B)+(C+D+E) \longrightarrow (A+B)|(C+D+E) \longrightarrow (A+B)|(C+D+E)$$

(a) Strategy of keeping subgroup configuration



$$(A/B+C)+(D\E) \longrightarrow (A/B\C)+(D+E) \longrightarrow (A/B\C)+(D+E)$$

(b) Strategy of keeping complex group configuration

Fig.7: Variation strategies in narrow passages

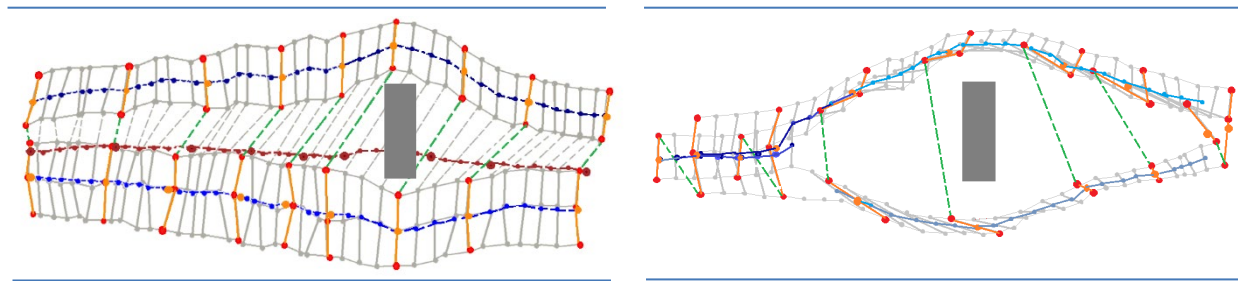
3.3. Strategies for Variation of Groups When Avoiding Obstacles

Motion of 66 complex groups with 5 members were tracked by the tool in scene 2. In the experiments, two common initial patterns (See Reference [2]) of the groups were considered, the free pattern and the

simple pattern. In free pattern, the group members aligned in one row and the simple pattern the members aligned in two rows.

From the data we got, splitting is the main strategy for variation when groups passed by the obstacle. 94.1% of free pattern groups and 83.2% of simple pattern groups split into two clusters to go through the sidewalks no matter how wide the obstacles are. But a significant difference occurs with the splitting strategy between the two patterns. When free pattern groups pass by the obstacle, the main strategy of splitting is to keep the configuration of the subgroups. It is observed that 84.3% of the subgroups keep their configuration while splitting, 9.2% of them vary their configuration and only 7.1% split and regroup into new subgroups. When simple pattern groups pass by the obstacle, the main strategy of splitting is to split the subgroups. 73.2% of the complex groups split their subgroups when passing a 0.6m wide obstacle and 67.3% split their subgroups when passing a 1.2m wide obstacle.

Although the splitting strategies are different, almost all subgroups return to their original configuration after passing the obstacles and most of the complex groups reorganize to their original structure no matter which strategy they choose for passing by the obstacles. Fig. 8 shows the examples of splitting strategies of most of the free pattern and simple pattern complex groups.








(a) splitting strategies of most of the free pattern (b) splitting strategies of most of the simple pattern

Fig.8: Variation Strategies in obstacle avoidance

3.4. Variation Strategies When Facing a Counter Group

In scene 3, two complex groups with 5-7 members walked oppositely from in the passage and passed by each other. 46 groups were tested in a 5m wide passage and 44 tested in a 3m wide passage. As shown in Table 1, most groups choose passing through or finger cross and break the group configuration while keeping less than half of the configuration of subgroups.

Table 1: Passing and Variation Strategies for counter groups

Passage width	Passing Strategies			Variation Strategies	
	Passing round	Passing through	Finger cross	Breaking group	Breaking subgroup
3m					
3m	18.8%	25.0%	56.2%	73.7%	31.8%
5m	5.3%	10.5%	89.5%	92.3%	50.7%

4. Mutual influence between the Groups on the Crowd

In scene 1, crowds with complex groups of 5-7 members were asked to walk through the narrowing passage (Fig. 1(b)) for 5 times as well as the crowds with only individuals for contrast. In scene 2, crowds with complex groups of 5-7 members were asked to walk through the passage and pass by the obstacle (Fig. 2(b)) for 10 times as well as the crowds with only individuals. In scene 3, counter flows and vertical

crossing flows with complex groups and with only individuals were studied. In this way, we wanted discover the mechanism of mutual influence between the Groups on the Crowd in conflict conditions.

4.1. Influence of the Crowd on the Groups in Strategies Choosing

Variation strategies of the groups are affected by the crowd. In scene 1, the proportion of keeping constant subgroup members is 78.9%, which is quite similar to the single group experiments. But because of the disturbance and influence from other groups and individuals, it is much more difficult for the groups to keep configuration of the whole group and subgroup. 73.3% complex groups change their configuration and 78.1% of the subgroups change their configuration. In scene 2, the proportion of group splitting is 82.6%, which is similar to the single group experiments. And 81.4% of the subgroups change their configuration because of the influence of the crowd. In both scenes, the variation of the complex and subgroups happen simultaneously and the group members arrange in the complicated pattern.

The results show that the groups do not have significant effect on crowd evacuation in narrow passage and bottle neck in respect of evacuation time. The evacuation time for crowds composed with groups and with only individuals are nearly the same, approximately 27-29s in scene 1 and 20s in scene 2.

Groups do not have obvious effect on crowd in sidewalk choosing when passing by the obstacle, but it seems that single groups make slightly better decision than the crowds do. When groups pass by the obstacle in sequence, the linear correlation between the pedestrian number and sidewalk width are stable and obvious, for instance, 33.5% of the members choose the narrower sidewalk which has 1/2 width of the wider one. While the crowds pass by the obstacle, 40.7% of the pedestrians choose the narrower sidewalk in different experiment rounds, which shows that single groups could make better decision than the crowd to split into the sidewalks with a higher walking efficiency and lower density.

4.2. Effect of Groups on the Self-organization

Groups have significant effect on self-organization in counter flows by decrease the number of lanes and widen each lane. In a 6m wide passage, 60 people were divided into two clusters to form counter flows. In counter flows with groups, 3-5 lanes were observed while 8-10 lanes were observed in counter flows with only individuals (See Fig. 9). The data in 3 m wide passage was 3-4 vs 4-5. Groups increase the average width of the lanes from 0.7m to 1.5m. It is precisely the width of a 3-member subgroup (see reference [5]). So the subgroups following in rear of a lane can keep its configuration better.

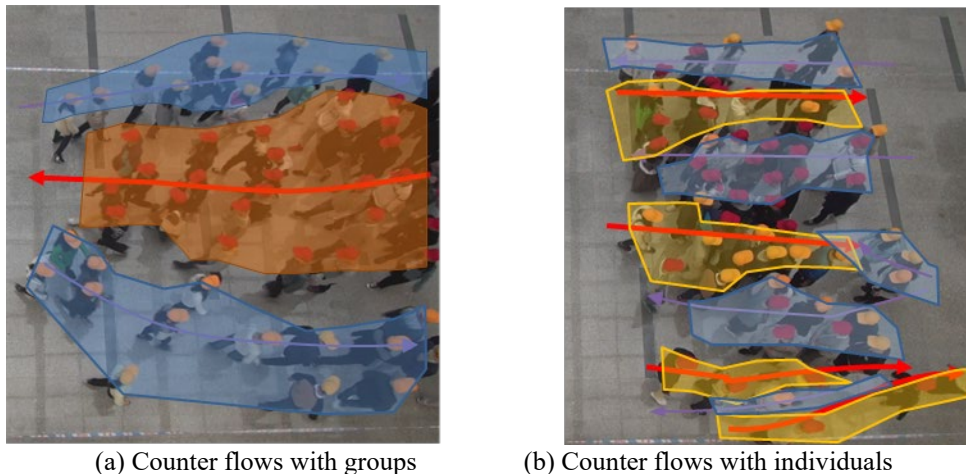
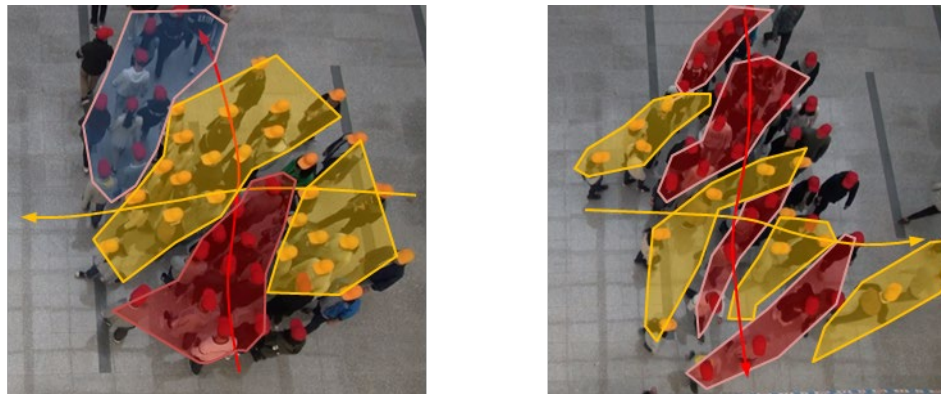


Fig.9: Effect of groups on counter flows

Groups also have significant effect on the self-organization in vertical cross flows by decrease the number of lanes and widen each lane at the cross. Groups increase the average width of the lanes from 0.6m to 1.3m. It is approximately the width of a subgroup with 2-3 members.



(a) Vertical cross flows with groups

(b) Vertical cross flows with individuals

Fig.10: Effect of groups on vertical cross flows

5. Conclusion

In this paper, we studied the variation strategies of complex groups as well as the mutual influence between the groups and the crowd when they walked through a narrowing passage. The strategies of keeping configuration of complex groups and subgroups in narrowing passage, the strategies of splitting the groups when passing by the obstacle, and the strategies of breaking the groups and reorganizing could be applied in modelling pedestrian group decision and behavior. The study of the effect of groups on self-organization of the crowd is new in this field.

More work should be done in comparison of the walking velocity and evacuation efficiency under different strategies. Whether the effect of groups on self-organization is positive for crowd evacuation should be tested with detailed dynamic analysis.

Acknowledgements

The work was supported by Natural Science Foundation of China, Grant No. 51208381, and Scientific Research Funding for Youth Science Fund Project. The work was also supported in part by Natural Science Foundation of China, Grant No. 71271153. The key laboratory of road and traffic engineering of the Ministry of Education provided the support for the experiments. We are grateful to Jiajun Huang, Mengru Xi and the students from Tongji University for conducting and participating in the experiments.

References

- [1] Jia'an Xi, Xiaolei Zou, Zhuo Chen, Jiajun Huang, Multi-pattern of Complex Social Pedestrian Groups, *Transportation Research Procedia* 2, 2014: pp. 60-68.
- [2] Jiajun Huang, Xiao-lei Zou, Xiaoyi Qu, Jie Ma, Ruihua Xu. A Structure Analysis Method for Complex Social Pedestrian Groups with Symbol Expression and Relationship Matrix, *Conference of Pedestrian Evacuation Dynamics 2016*: pp. 283-289.
- [3] Francesco Zanlungo, Takayuki Kanda. Do walking pedestrians stably interact inside a large group? Analysis of group and sub-group spatial structure. *Proceedings of the Annual Meeting of the Cognitive Science Society 2013*: pp. 3847-3852.
- [4] M. Moussaïd, N. Perozo, S. Garnier, D. Helbing, and G. Theraulaz The walking behaviour of pedestrian social groups and its impact on crowd dynamics. *PLoS ONE*, 2010, 5(4): e10047.
- [5] Xiaolei Zou, Xiaoyi Qu, Ruihua Xu. Data-driven modeling on spatial pattern and private space of pedestrian groups. *Proceedings of The 11th International Conference of Chinese Transportation Professionals*. 2011: pp. 2102-2108.

Measuring social influence and group formation during evacuation process

Adriana Balboa, Arturo Cuesta, Daniel Alvear

University of Cantabria

Los Castros, Santander, Spain

balboaa@unican.es; cuestaar@unican.es; alveard@unican.es

Abstract - Evacuees are likely to respond and move forming groups. However specific data about grouping is generally unavailable and the relationship between response and movement times and specific groupings are unknown. Using a simple method, we measure behavioural cohesion of occupants during evacuation processes. The case study involves using the method in a bus station, a sport centre and a library. Results suggest that proximity (visual/verbal contact) is an important factor but not decisive in the formation of evacuation groups. Social ties and whether occupants share a target and/or an activity before the alarm are also deemed to be important factors. This study provides an exciting opportunity to advance our knowledge of social influence and group formation during evacuation.

Keywords: Collective behaviour; Evacuation groups; Behavioural cohesion; Social influence; Evacuation process

1. Introduction

Primary questions concerning collective behaviour during the evacuation process include how individuals reach a consensus and form groups and how this impacts life safety. It is known that individuals are influenced by others. This can also happen in response to ambiguous threat cues [1]. Collective behaviour can occur whenever people are confused or do not know what to do. Individuals work together to redefine the situation and propose a new set of actions, which is the product of the milling and keynoting process [2]. Several studies have shown that people behaviour in emergencies tends to be cooperative [3, 4]. The common identity in response to the same threat would explain this. Evidence and theories support the idea that individuals form a group before evacuating and then continue their evacuation together until they reach safety [5].

Despite collective behaviour being important, most current evacuation models simulate agents as if they were not influenced by others. One agent can start the evacuation while others remain in the same room/place. In other words, no social influence is represented. There are methods for modelling the collective behaviour. However, to the authors' knowledge, this is not supported by empirical data. A quantitative method to measure collective behaviour in evacuees proposed in [6] is here applied to three evacuation scenarios to test its validity.

2. Method

2.1. Formulation

Collective evacuation behaviour denotes a reduction in the behavioural variability of individuals. Let X be a continuous behavioural random variable. Hence, the smaller the statistical dispersion of the variable X intragroup, compared to the statistical dispersion of the same variable X in all groups, the greater the collective behaviour. This can be expressed by the following statistical hypothesis:

$$\begin{aligned} H_0: UCV_i < LCV_t \\ H_1: UCV_i \not< LCV_t \end{aligned} \tag{1}$$

Where UCV_i is the upper confidence interval for the coefficient of variation (CV) of X variable for the i -th potential evacuation group defined as a number of people who are located, gathered or classed together before the evacuation and LCV_t is the lower confidence interval for the coefficient of variation (CV) of X variable for all the potential groups. There are various methods for estimating the confidence interval for a population CV [7, 8]. We propose to use the Median Modified Miller Estimator (Med Miller) [9, 10] and the Median Modified Curto and Pinto's with iid assumption (Med C&P) [11] since skewed distributions are likely to be obtained and the variability can be measured in terms of the median rather than the mean. If the null hypothesis fails to reject, then we have preliminary evidence of collective behaviour among the members of the potential group. Then, we can go a step beyond and measure the behavioural cohesion of group members by:

$$\gamma_{B_i} = 1 - \frac{CV_i}{CV_t} \quad (2)$$

Where CV_i is the coefficient of variation of the X variable in the i -th group and CV_t is the coefficient of variation of the same X variable of all groups in the evacuation scenario. The higher the γ_{B_i} coefficient the higher the cohesion (i.e. a value of 1 represents a perfect synchronization of group members). It is also possible to introduce a new variable ($\tilde{\gamma}_B$) to characterize the degree of behavioural cohesion for a given evacuation scenario:

$$\tilde{\gamma}_B = \frac{1}{n} \sum_{i=1}^m n_i \cdot \gamma_{B_i} \quad (3)$$

Where n is the number of occupants in the evacuation scenario, m the number of evacuation groups in the evacuation scenario and n_i the number of members for the i -th group.

2.2. Cases of study

The case study involves three evacuation scenarios: 1) a bus station, 2) a sports centre and 3) a library. These scenarios represent different geometries, population distribution and activities performed by people before the evacuation.

The first scenario consisted of an evacuation experiment in an underground bus station in Madrid, Spain. In total 18 trials were conducted to analyse the people response to a terrorist attack. However, only one of these trials is analysed in this paper. In total 74 participants took part in the trial (average age 40.4 range 19-67). Between 6 and 9 participants were randomly assigned to the 10 boarding gates (see Fig. 1). The second scenario involved an unannounced evacuation drill in a sports centre at the University of Cantabria, Spain involving 78 naive students. Fig. 2 shows the distribution of occupants within the building before the alarm. The third scenario comprises an unannounced evacuation drill in a library of the Faculty of Economics and Business at the University of Cantabria, Spain with 33 naive students. Fig. 3 shows the initial distribution of the students in the library before the alarm.

The potential groups for the analysis were predefined by authors according to their initial location within the building i.e. occupants were likely to interact with each other and/or whether they share a target and/or an activity before the alarm. Video-cameras were used for the data collection. The following variables were considered to measure the group behaviour of the bus station and the sports centre: the response time (t_{res}) defined as the time from the sounding of the alarm to deliberate evacuation movement (s) and the exit time (t_{exit}) defined as time from the sounding of the alarm to leaving the building by an exit (s). For the library, only the response phase of evacuation was measured (i.e. we did not have enough time to cover the exits with the video-cameras). The variables measured were: the recognition time (t_{rec}) defined as the time from the sounding of the alarm to the first response action such as collect belongings, shutdown laptop, etc. (s) and the response time (t_{res}) the same as above. The defined variables were measured manually using an image processing software frame by frame. Datasets were transcribed into a spreadsheet for further analysis.

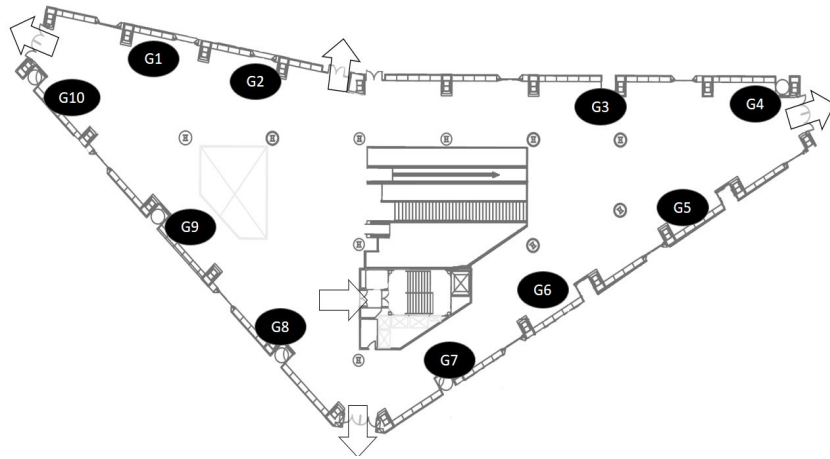


Fig. 1: Initial distribution of participants in the bus concourse before the alarm (G1=6; G2=7; G3=6; G4=8; G5=7; G6=6; G7=9; G8=9; G9=7 and G10=9). All participants were waiting told to act as if they were waiting for the bus.

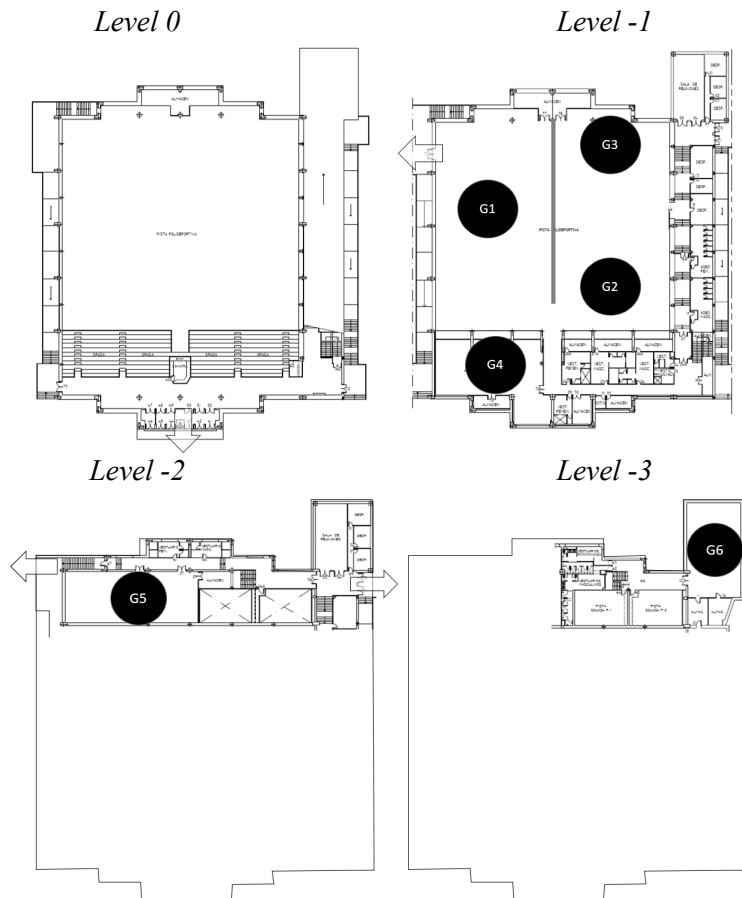


Fig. 2: Initial distribution of occupants in the sports centre before the alarm (G1=11 occupants playing football; G2=9 occupants playing badminton; G3=11 occupants working out Cross Fit; G4=32 occupants in the gym; G5=6 occupants dancing and G6=9 occupants doing yoga).

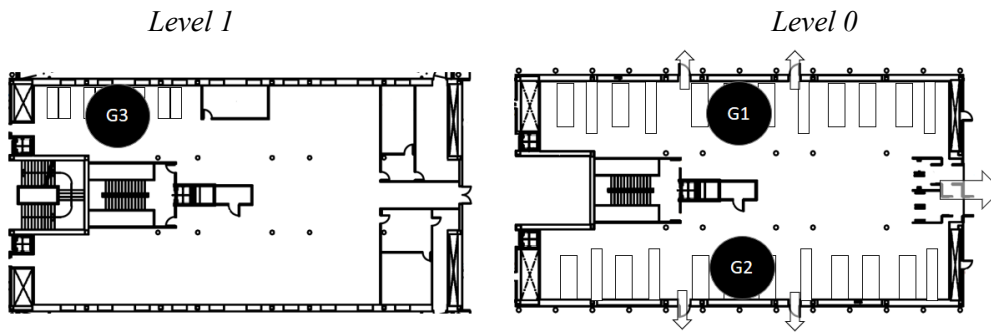


Fig. 3: Initial distribution of occupants in the library before the alarm (G1=10; occupants reading; G2=10 occupants reading; G3=13 occupants using computers).

3. Results

The aim of this section is to determine quantitatively the collective behaviour of evacuees involved in the three different evacuation scenarios. It should be noted that people reached a consensus decision regarding the direction of evacuation in the bus station and the sport centre i.e. people from the same predefined group used the same exit. This is a *conditio sine qua non* for the application of the proposed method. Fig. 4 shows the maximum, minimum and mean values of the measured variables for each potential group allowing a preliminary visual information of the current analysis.

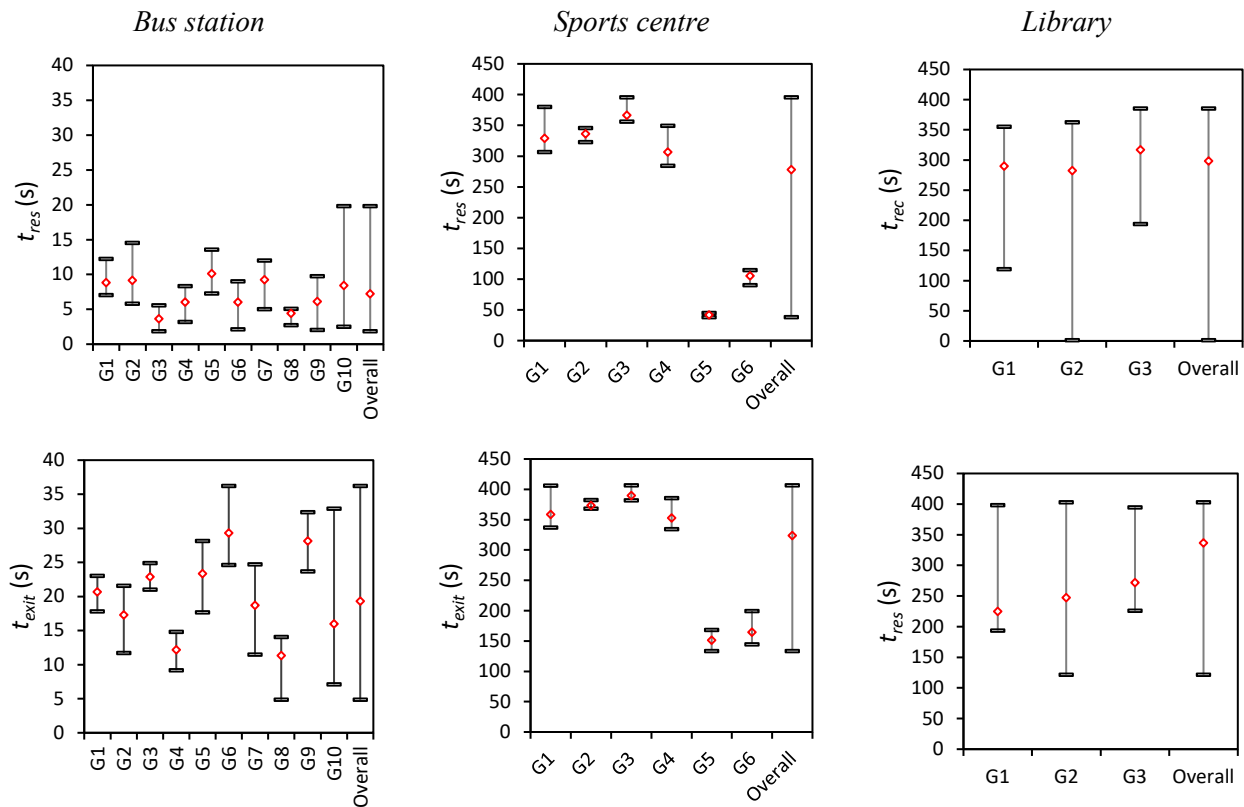


Fig. 4: Range and mean values of the variables measured for each potential group of the three evacuation scenarios.

The variability relative to the mean of data observed in the bus station differs from potential group to potential group (for t_{res} $CV_{G1}=0.23$; $CV_{G2}=0.37$; $CV_{G3}=0.45$; $CV_{G4}=0.25$; $CV_{G5}=0.26$; $CV_{G6}=0.41$; $CV_{G7}=0.27$; $CV_{G8}=0.18$; $CV_{G9}=0.40$; $CV_{G10}=0.74$ and for t_{exit} $CV_{G1}=0.10$; $CV_{G2}=0.17$; $CV_{G3}=0.06$; $CV_{G4}=0.17$; $CV_{G5}=0.19$; $CV_{G6}=0.15$; $CV_{G7}=0.20$; $CV_{G8}=0.24$; $CV_{G9}=0.10$; $CV_{G10}=0.60$). The data collected reveals in general low variability relative to the mean in the sport centre during the response phase (for t_{res} $CV_{G1}=0.06$; $CV_{G2}=0.02$; $CV_{G3}=0.03$; $CV_{G4}=0.06$; $CV_{G5}=0.37$; $CV_{G6}=0.08$) and the movement phase (for t_{exit} $CV_{G1}=0.06$; $CV_{G2}=0.01$; $CV_{G3}=0.02$; $CV_{G4}=0.04$; $CV_{G5}=0.11$; $CV_{G6}=0.09$). By contrast, the behaviour of people in the library during the response phase is found to have higher variability in relation to the mean (for t_{rec} $CV_{G1}=0.31$; $CV_{G2}=0.40$; $CV_{G3}=0.20$ and for t_{res} $CV_{G1}=0.23$; $CV_{G2}=0.29$; $CV_{G3}=0.16$).

Whereas the coefficient of variation (CV) is a measure that provides information of the dispersion of probability distributions, and therefore the behavioural variability among evacuees, it is not sufficient to determine whether participants responded together (as a group) and maintained cohesion with neighbours during the evacuation movement. Hence, the proposed method is applied. In the first step, the statistical test (see section 2.1) was conducted to provide a *prima facie* evidence of collective behaviour among evacuees. Results of statistical tests are displayed in Table 1. In regard to the bus station, the null hypothesis failed to reject for 3 potential groups (Med Miller $p = 0.35 \pm 0.12$) and 4 potential groups (Med C&P $p = 0.43 \pm 0.13$) during the response phase (t_{res}). For the movement phase of evacuation (t_{exit}) the null hypothesis failed to reject for 7 potential groups (Med Miller and Med C&P $p = 0.66 \pm 0.01$). In the sport centre the null hypothesis failed to reject for 5 potential groups (Med Miller and Med C&P $p = 0.90 \pm 0.007$) for the response phase (t_{res}) whereas all potential groups failed to reject the null hypothesis during the movement phase (t_{exit}). The behaviour of evacuees in the library had more variability and the null hypothesis rejected during the response phase (t_{rec}) and (t_{res}).

Table 1: Statistical tests results $H_0: UCV_i < LCV_i$ ($\alpha=0.05$).
Cells in F-grey mean a preliminary evidence of collective behaviour.

Scenario	Potential group	N	Med Miller		Med C&P	
			t_{res}	t_{exit}	t_{res}	t_{exit}
Bus station	G1	6	R	F	F	F
	G2	7	R	F	R	F
	G3	6	R	F	R	F
	G4	8	F	F	F	F
	G5	8	R	R	R	R
	G6	6	R	F	R	F
	G7	9	F	F	F	F
	G8	9	F	R	F	R
	G9	7	R	F	R	F
	G10	9	R	R	R	R
			t_{res}	t_{exit}	t_{res}	t_{exit}
Sports centre	G1	11	F	F	F	F
	G2	9	F	F	F	F
	G3	11	F	F	F	F
	G4	32	F	F	F	F
	G5	6	R	F	R	F
	G6	9	F	F	F	F
			t_{rec}	t_{res}	t_{rec}	t_{res}
Library	G1	10	R	R	R	R
	G2	10	R	R	R	R
	G3	13	R	R	R	R

R= Reject; F= Fail to reject

The second step of the methodology involves the application of Eq. (2) which allow us to measure the behavioural cohesion of evacuees and therefore confirm whether they behave as a unit or not. Fig. 5 shows the γ_{B_i} values produced. Note that the null hypothesis of collective behaviour fails to reject for the cases with γ_{B_i} values >0.50 with a region of uncertainty between 0.44 and 0.50. As explained above, the closer the γ_{B_i} to 1 the more behavioural cohesion of the group members. Values between 0.50 and 0.75 denote cohesion while values between 0.75 and 1 represent a strong behavioural cohesion among evacuees.

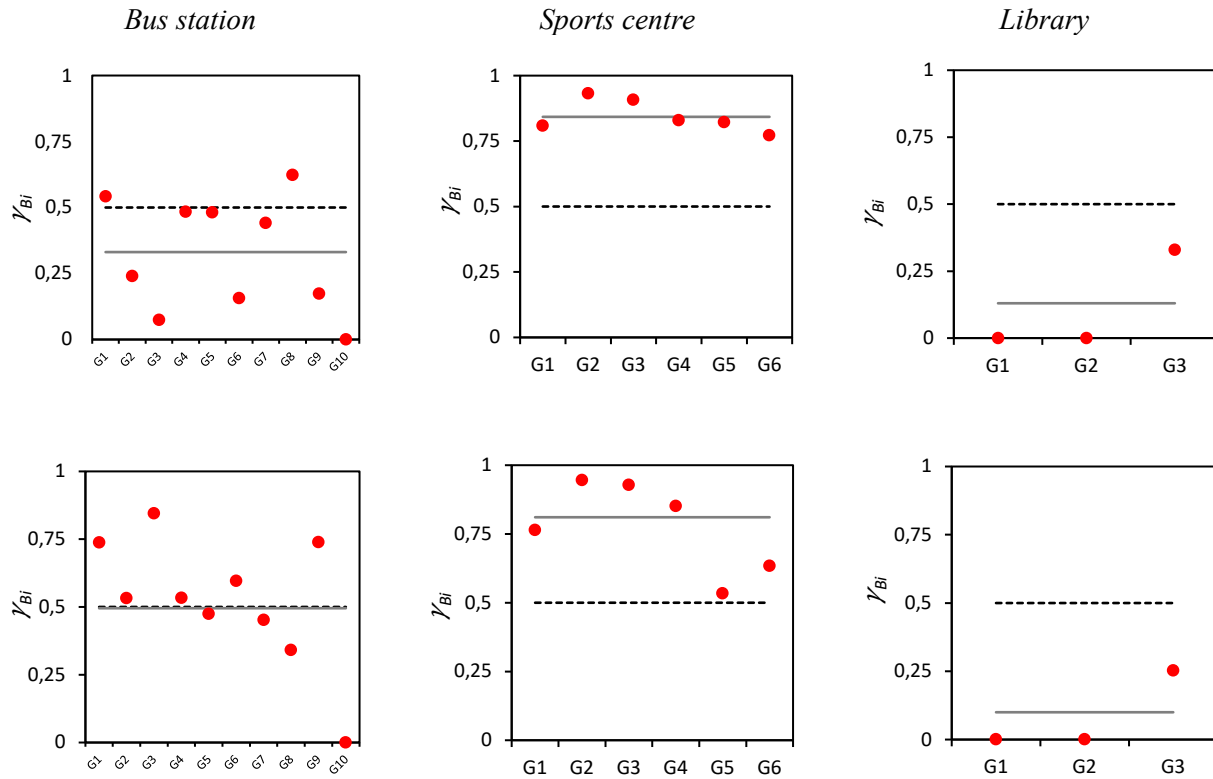


Fig.5. γ_{B_i} values for t_{res} variable during the evacuation. Dashed line is the minimum threshold for group behavioural cohesion ($\gamma_{B_i} = 0.5$) and line in grey is the weighted coefficient to characterize the degree of behavioural cohesion of the evacuation scenario.

In the bus station, the behavioural cohesion during the response phase was found in two groups (G1=0.54; G8=0.62). Other potential groups produced values close to 0.5 (G4=0.48; G5=0.48; G7=0.44). However, these values are considered in a region of uncertainty. The behavioural cohesion during the movement phase of evacuation was confirmed in more groups G1 (0.73), G2 (0.53), G3 (0.84), G4 (0.53), G6 (0.59) and G9 (0.73). Despite some responded individually, evacuees tended to assume the speed of the slowest member or increasing their speed to maintain the cohesion.

In the sport centre, a different process was observed. Results in Fig. 5 confirm that the response of evacuees was very close to each other (G1=0.81; G2=0.93; G3=0.91; G4=0.83; G5=0.82; G6=0.77). Note that groups G1, G2, G3 and G4 were warned by staff members. Groups G5 and G6 started evacuation by themselves and produced a decrease in the behavioural cohesion (from 0.82 to 0.53 in G5) and (from 0.77 to 0.63 in G6) due to the long distances the occupants had to cover to leave the building, but they still kept united.

Based on results in Fig. 5, no behavioural cohesion in evacuees was found in the library. Despite some students were in small groups before the alarm (two or three friends), they behaved independently during the response phase of evacuation. Some started evacuation activities and some others ignored the alarm, and continued reading or using computers, as they did not recognize the alarm relevant to their situation. It should be noted that these occupants needed the staff intervention to physically undertake evacuation activities. Furthermore, all people in the library performed different tasks before starting the purposive evacuation movement such as shutting down laptops, packing work items, packing/collecting personal belongings, putting on jackets, moving to another location to perform an action. The time spent on these tasks varied considerably (G1 mean 46.81 s and standard deviation 19.37 s; G2 mean 47.61 s and standard deviation 32.80 s; G3 mean 25.12 and standard deviation 19.77 s) thus increasing the variability in the response phase of evacuation.

4. Discussion

Groups are likely to emerge during evacuation. However very little is still known about how and why this happens. For example, we do not know what the actual influence of collective behaviour on decision making and actions performed by people during evacuation process is. Based on the fact that consensus and uniformity denote a reduction in the behavioural variability, we have proposed a possible approach to identify evacuation groups and measure the behavioural cohesion of group members. The presented method is expected to improve our understanding of the conditions in which such behaviours take place.

An illustrative case study has been presented through the analysis of three evacuation scenarios: a bus station, a sports centre and a library involving 185 evacuees divided in 19 potential evacuation groups. We confirmed the presence of collective behaviour in the bus station and the sport centre in 60% and 100% of potential evacuation groups respectively. Contrary to expectations, no evidence of collective behaviour was found in the library. Despite having visual and verbal contact, occupants responded individually and performed different tasks before start evacuation (collecting belongings, shutting down lab tops, etc.) thus increasing the behavioural variability. This suggests that proximity could be important but not always a key factor in collective evacuation behaviour. Social ties, whether occupants share activities before the evacuation and/or the type of alarm could be also important factors to consider. This is an example of the importance of using the proposed method. For instance, implementing the same pre-evacuation time distribution to all occupants could be a good approach for the evacuation analysis of a library but potentially unrealistic in other evacuation scenarios where some groups are likely to emerge during evacuation.

The main contribution of this paper is suggesting the use of Eq. (2) as a fast and simple approach to conduct a preliminary assessment of collective behaviour for any evacuation scenario. If $\gamma_{B_i} > 0.50$ the collective behaviour can be confirmed and the higher the γ_{B_i} value the higher the behavioural cohesion in evacuees. Values from 0.50 to 0.75 denote a high cohesion while values > 0.75 represent a very strong behavioural cohesion in evacuees. It is worth to remind that an ideal value of 1 would represent a perfect synchronization on people actions.

Care is required however when using the proposed method as it has a number of limitations. The first limitation is that the identification of the potential groups for the analysis relies on the analyst. A plausible approach could be, for instance, the specific location (room, zone, area, queue, etc.), the proximity where occupants are likely to interact (verbal and/or non-verbal communication) and/or whether they share a target before the alarm. The second limitation is that the members of the potential group should use the same exit, when analysing the movement phase of evacuation. The third limitation is that the number of members in the potential evacuation group should be higher enough to calculate the coefficients of variation (i.e. more than 5). The fourth limitation is that the results are very sensitive to divergent behaviours of individuals (extreme values). For instance, given a defined group, it only takes an individual who acts separately to discard behavioural cohesion although the rest of group members behave as a group. This limitation may be solved through the application and inclusion of *outliers* detection methods. Nevertheless, this is very complicated for small sample sizes ($N = [5-25]$).

Acknowledgements

The authors would like to thank the European Union for the LETS-CROWD project received funding from the Horizon 2020 Research and Innovation Programme under the grant agreement N° 740466 and the Spanish Ministry of Economy and Competitiveness for DEFENDER Project Grant, Ref: BIA2015-64866-R, co-funded by ERDS funds.

References

- [1] B. Latane, and J.M. Darley, “Group inhibition of bystander intervention emergencies”, *Journal of Personality and Social Psychology*, vol. 10, pp. 215-221, 1968.
- [2] R. H. Turner and L. M. Killian. *Collective Behaviour*. Englewood Cliffs, NJ: Prentice Hall, Inc., 1987.
- [3] B. E. Aguirre, D. Wenger and G. Vigo, “A test of the emergent norm theory of collective behaviour”, *Sociological Forum*, vol. 13, no. 2, pp. 301-320, 1998.
- [4] E. L. Quarantelli, “The Nature and Conditions of Panic”, *American Journal of Sociology*, vol. 60, no. 3, pp. 267– 275, 1954.
- [5] E. Kuligowski, “Human Behaviour in Fire”, in *SFPE Handbook of Fire Protection Engineering*, 2016, pp. 2070-2114.
- [6] A. Cuesta, O. Abreu and D. Alvear, “Methods for measuring collective behaviour in evacuees”, *Safety Science*, vol. 88, pp. 54-63, 2016.
- [7] W. Panichkitkosolkul, “Asymptotic confidence interval for the coefficient of variation of Poisson distribution: a simulation study”, *Maejo International Journal of Science and Technology*, vol. 4, pp. 1–7, 2010.
- [8] M. Gulhar et al., “A comparison of some confidence intervals for estimating the population coefficient of variation: a simulation study”, *Statistics and Operations Research Transactions*, vol. 36, no. 1, pp. 45–68, 2012.
- [9] G. E. Miller, “Asymptotic test statistics for coefficients of variation”, *Communications in Statistics-Theory Methods*, vol. 20, no. 10, pp. 3351–3363, 1991.
- [10] G. E. Miller and Karson, “Testing the equality of two coefficients of variation”, *American Statistics Association: Proceedings of the Business and Economic Section*, Part I, pp. 278–283, 1977.
- [11] J. D. Curto and J. C. Pinto, “The coefficient of variation asymptotic distribution in the case of non-iid random variables”, *Journal of Applied Statistics*, vol. 36, no. 1, pp. 21–32, 2009.

The influence of physical and mental constraints to a stream of people through a bottleneck

Paul Georg¹, Jette Schumann², Maik Boltes², Stefan Holl², Anja Hofmann¹

¹Bundesanstalt für Materialforschung und –prüfung, 12205 Berlin, Germany
paul.georg@bam.de; anja.hofmann@bam.de

²Forschungszentrum Jülich GmbH, 52425 Jülich, Germany
j.schumann@fz-juelich.de; m.boltes@fz-juelich.de; st.holl@fz-juelich.de

Abstract - Understanding movement in heterogeneous groups is important for a meaningful evaluation of evacuation prediction and for a proper design of buildings. The understanding of interactions and influencing factors in heterogeneous groups on key performance figures is fundamental for a safe design. This contribution presents results of experimental studies on movement of a crowd through a bottleneck involving participants with and without disabilities. High precise trajectories of the attendees extracted from video recordings were used to calculate density and velocity of the participants. Besides the well-established fundamental diagram new insights into the individual relation between density and velocity are discussed. A complex structure and considerate behaviour in movement implicates a strong influence of the heterogeneity on key performance values of safe movement.

Keywords: human behaviour, egress, pedestrians with disabilities, evacuation, engineering data

1. Introduction

Many studies to investigate pedestrians' movement, their decision making, navigation and behaviour have been carried out during the last years [1-3]. Yet those studies mainly have analysed the movement of young and able-bodied participants in homogeneous groups. Thus, the studies do not represent circumstances in real life with a wide variety of individual limitations on moving. Empirical data sets involving people with disabilities are needed for a proper modelling and validation of heterogeneous pedestrian streams. Up to now only a few studies involving people with disabilities have been carried out and commonly focus on the unimpeded walking speed [4-8].

This contribution presents results of large-scale studies carried out in an interdisciplinary research-project "SiME - Safety for people with physical, mental or age-related disabilities" considering persons with body-, mental- or age-related disabilities as well as heterogeneous populations in evacuation planning. The experimental design and calculation methods are described in Sec. 2. The results will be discussed in Sec. 3 and lastly we conclude in Sec. 4.

2. Method

The characteristics of movement in heterogeneously composed populations are insufficiently described so far. Meanwhile, reduction of restrictions by disabilities is societal consensus and is connected to an old discussion about equal access vs equal egress [10]. The research project SiME focuses on safety in inclusive societies. As a part of this project, the relationship between inhomogeneity in groups and pedestrians' movement is studied. Twelve studies with more than 145 single runs and overall 252 participants with different difficulties and without any disabilities were performed in 2017 in a large hall in Wermelskirchen, Germany. One of these studies investigated the influence of body-related disabilities on the walking behaviour in groups.

2.1. Study setup

The main focus of this paper are two configurations comparing the movement of the crowd through a bottleneck with and without participating wheelchair users. The experimental setup is sketched in Fig. 1. Each run was carried out twice with the same boundary conditions and was captured by eight high definition cameras mounted at the ceiling of the hall more than 6 m above ground.

In the first study approx. 10 % were of the population as wheelchair users (82 participants without disabilities and seven wheelchair users at a mean age of 37 ± 16); the second study was performed without any participants with disabilities (69 participants at a mean age of 32 ± 16).

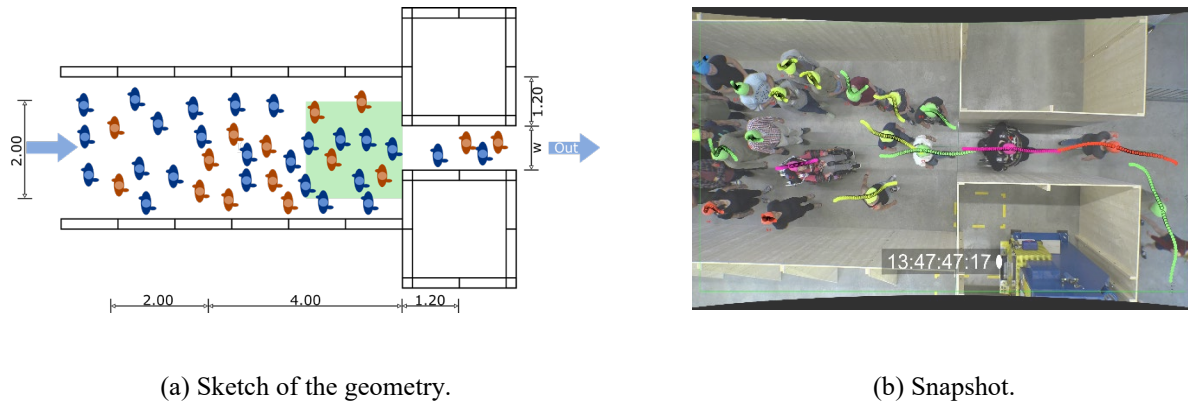


Fig 1: Geometrical setup of the study (left) and snapshot (right) of a study with wheelchair users and tracked individual positions for a bottleneck width of 0.9 m.

All attendees were asked to move directly and quick through the bottleneck but without pushing each other. Participation was voluntary for everybody and a cancellation of participation without any negative consequences at any time was possible. All participants have been paid for participation by 25, 00 € per half a day. Only anonymous data were used for the studies. The ethics committee of the University of Wuppertal has approved the project. No ethical concerns were mentioned.

2.2. Data extraction

The passageway through the geometry setup was captured by cameras and processed by a software developed for automatic extraction of attendees' trajectories, PeTrack [11]. For extracting individual positions at every frame, the positions of the coloured caps were detected and tracked (for example see Fig. 1(b) with the position of participants highlighted one second in the past and future).

To improve the tracking quality of the individual positions the participants were asked to wear a coloured cap encoding different ranges of body heights. Before the experiments the height of each participant was measured and the corresponding coloured cap was chosen. It was ensured, that the colours did not occur in the observation area. The unique colour coded pixel area was approximated by an ellipse, which centre represents the position of a participant. The centre of the coloured area was auto corrected by taking the perspective view into account [12] resulting in trajectories for all participants. By neglecting the individual height information and using an average body height (for one colour), the trajectories represent the projected path in x and y-direction on the ground.

We assume a coherent area of pixels in the middle of the coloured hats as body centre of a participant, so the resulting trajectories represent positions of the head projected on the ground. All resulting trajectories were checked and corrected manually. For more details we refer to [11].

2.2. Calculation methods

To quantify characteristics of participants' movement the Voronoi method is used to calculate density and velocity [9, 13]. Density and velocity were analysed in a rectangular measurement area of 2 x 2 m

centred in front of the bottleneck entrance (green dotted area in Fig. 2). Calculations were performed using *JPSreport* (part of the *JuPedSim*-Framework [14]).

3. Analysis and results

To compare attendees' movement considering participants with disabilities, we analysed movement data from studies with and without wheelchair users. Fig. 2 shows trajectories for two runs with a bottleneck width of 0.9 m. Based on these trajectories, movement characteristics such as density, velocity and flow at any time and position are calculated.

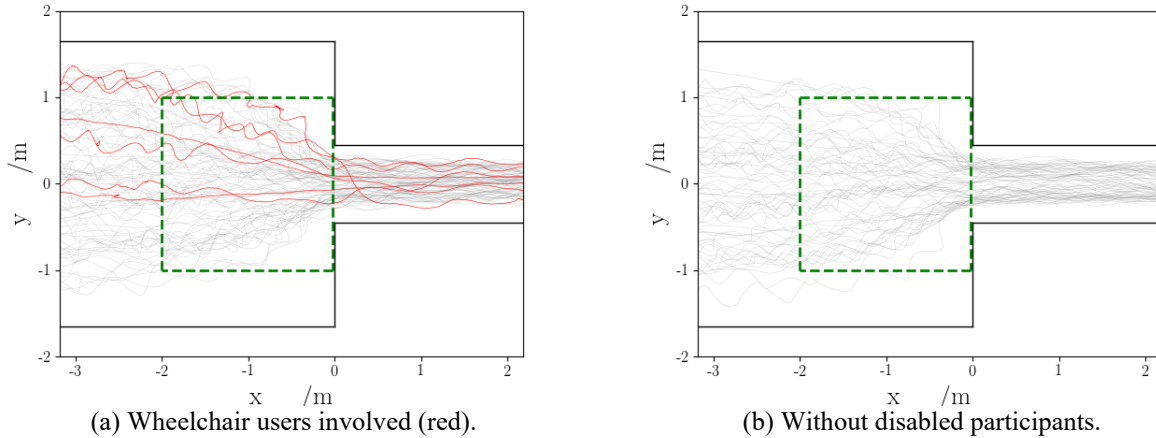


Fig 2: Attendees' trajectories from studies with wheelchair users (red) and without (grey) disabilities passing the bottleneck (width = 0.9 m). Measurement area for calculating speed and density is represented by the green dotted rectangle.

The time-dependent development of density and velocity is characterised by medium densities (mean density: with wheelchair users $1.50 \pm 0.72 /\text{m}^2$, without wheelchair users: $1.93 \pm 0.94 /\text{m}^2$) and significant slow individual velocities (mean velocity: with wheelchair users: $0.35 \pm 0.23 \text{ m/s}$, without wheelchair users: $0.37 \pm 0.23 \text{ m/s}$). Taking into account that the studies are conducted for short time periods a significant percentage of the run is sensitive from start and end conditions. It is common to use the steady part of a run for further analysis which is independent to start and end conditions [15, 16].

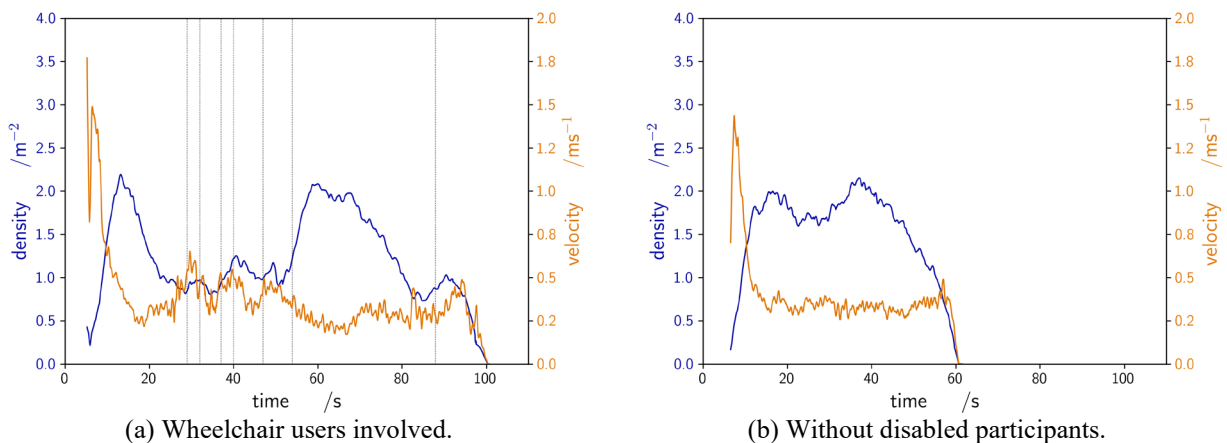


Fig 3: Time series for the development of density and velocity for two runs with and without wheelchair users. The time of entrance of a wheelchair user in the bottleneck is indicated by black dotted vertical lines. Steady states can be hardly defined by the relative stable stage of the curves.

For both runs the density increases at the beginning of the run and decreases at the end. Development of density in the study without wheelchair users fluctuates slightly in the middle of the run. The characteristic of the run considering wheelchair users is significantly different: density and velocity are characterised by strong fluctuations. In this case, density and velocity are influenced by other events than start or end conditions and boundaries. The presence of wheelchair users becomes important and causes significant fluctuations in time development of density and flow. Fluctuations occur when a wheelchair user reaches the entrance of the bottleneck (see Fig. 3(a)). Wheelchair users may cause a rapid decrease of density and indicate more fluctuations of mean movement speeds in the measurement area located in front of the bottleneck. To consider this striking fluctuations in the analysis (e.g. in density-speed-relations, see Fig. 5), data over the entire time-interval is considered.

The fluctuations observed in the time series are also exhibited in the representation of the trajectories in space and time (see Fig. 4). We can show, that participating wheelchair users tend to favour stop-and-go waves. Furthermore, it was observed that non-disabled participants reduced their movement speed in a long distance to the bottleneck entrance and refrained from overtaking. Wheelchair users act as slow-moving obstacles and lead to an anticipation of movement (social behaviour).

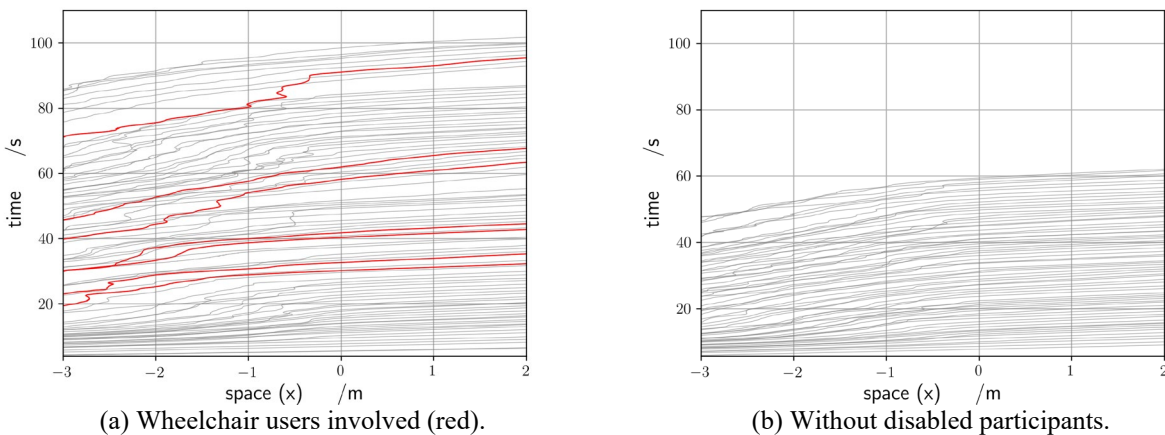


Fig 4: Time-space-relations for two runs with and without wheelchair users. Participating wheelchair user (red lines) lead to an occurrence of stop-and-go waves.

To gain a deeper understanding the fundamental relationship between density and velocity is analysed (see Fig. 5). We found values for participants in wheelchairs in all areas of the speed-density-relation, especially in density-areas $\leq 3.0 /m^2$. It is striking that density and velocity are not dependent. So surprisingly the expected three basic domains free flow, bound flow and congestion [17, 18] are not observed. A plateau of velocities is formed for densities above $\geq 1.0 /m^2$. Such plateaus are known from ordering effects in bidirectional flows [19, 20]. Even if a wheelchair user reaches the bottleneck, their neighbours anticipate individual velocity and stop passing. Participants interact and solve priority of movement by communication.

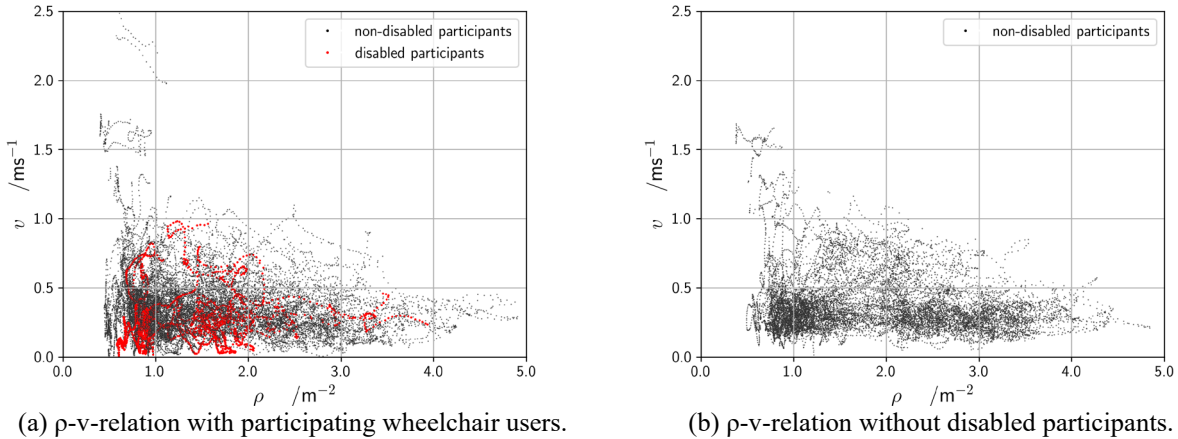


Fig 5: Individual speed-density-relation for a run with wheelchair users. Individual densities and velocities for wheelchair users are coloured in red.

This behaviour can be interpreted as stop-and-go-waves as a result of slow-moving obstacles prior the bottleneck (see the increasing inhomogeneity prior to the bottleneck-entrance in Fig. 4). Social norms, individual behaviour and degrees of freedom in movement as well as the influence of technical assistance devices and accompanying persons may affect the passageway. Further on, the impact of disabilities on movement differs: those who are in a wheelchair may be able to roll with a high unimpeded movement speed, but may characterised by a delayed acceleration because of the inertia of the wheelchair.

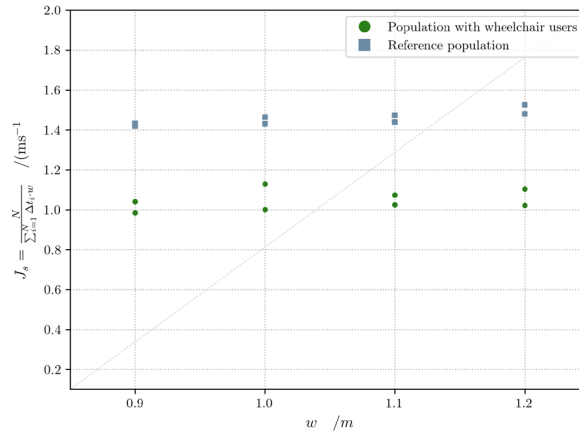


Fig 6: Comparison of specific flows for studies considering a subpopulation with wheelchair users in a bottleneck defined by different width w . The specific flow J_s here is defined as the ratio of the cumulative number of participants to the sum of all individual time headways at the bottleneck entrance.

The specific flow J_s through the bottleneck comparing the presence and absence of wheelchair users is presented in Fig 6. For the reference population we observed slightly higher but comparable values as previously published (e.g. see [1]) with a slight linear tendency. In case of participations of wheelchair users, a reduced specific flow was observed which is mainly caused by the defensive manoeuvring in the pedestrian flow.

3. Conclusions

A series of well-controlled laboratory studies on movement through a bottleneck participating wheelchair users and participants without disabilities was analysed. Movement of the crowd was recorded with high-definition cameras and precise trajectories of all participants were extracted automatically. Relations between individual density and velocity calculated with the Voronoi method were presented. Usually expected relation between density and velocity was not observed: the movement speed in heterogeneous groups depends not only on pedestrians' density but also on singular events like communication in front of the bottleneck, considerate behaviour or anticipation of social norms. This leads to significant fluctuations in speed and density and indicates the importance of social behaviour on the performance of a facility. The presented results contribute to empirical data of pedestrian dynamics and arise a lot of questions regarding the complexity of movement in heterogeneous social groups.

Acknowledgements

Part of this work has been performed within the research program Safety for people with physical, mental or age-related disabilities (SiME) supported by the German Federal Ministry of Education and Research - BMBF (FKZ starting on 13N13946). Paul Geörg thanks the SFPE Foundation for financial support with the Dr. Guylène Proulx, OC Scholarship.

References

- [1] A. Seyfried *et al.*, “New Insights into Pedestrian Flow Through Bottlenecks,” *Transportation Science*, vol. 43, no. 3, pp. 395–406, 2009.
- [2] J. Zhang and A. Seyfried, “Quantification of Bottleneck Effects for Different Types of Facilities,” *Transportation Research Procedia*, vol. 2, pp. 51–59, 2014.
- [3] S. P. Hoogendoorn and W. Daamen, “Pedestrian Behavior at Bottlenecks,” *Transportation Science*, vol. 39, no. 2, pp. 147–159, 2005.
- [4] K. E. Boyce, T. J. Shields, and G. W. H. Silcock, “Toward the Characterization of Building Occupancies for Fire Safety Engineering: Capability of Disabled People to Negotiate Doors,” *Fire Technology*, vol. 35, no. 1, pp. 68–78, 1999.
- [5] G.-Y. Jeon, J.-Y. Kim, W.-H. Hong, and G. Augenbroe, “Evacuation performance of individuals in different visibility conditions,” *Building and Environment*, vol. 46, no. 5, pp. 1094–1103, 2011.
- [6] J. G. Sørensen and A. S. Dederichs, “Evacuation characteristics of visually impaired people - a qualitative and quantitative study,” *Fire and Materials*, vol. 39, no. 4, pp. 385–395, 2013.
- [7] M. S. Sharifi *et al.*, “Analysis of Walking Speeds Involving Individuals with Disabilities in Different Indoor Walking Environments,” *Journal of Urban Planning and Development*, vol. 142, no. 1, p. 4015010, 2016.
- [8] K. Christensen, S. Collins, J. Holt, and C. Phillips, “The Relationship Between the Design of the Built Environment and the Ability to Egress of Individuals with Disabilities,” *Review of Disability Studies*, vol. 2, no. 3, pp. 24–34, 2006.
- [9] J. Zhang and A. Seyfried, “Comparison of intersecting pedestrian flows based on experiments,” *Physica A: Statistical Mechanics and its Applications*, vol. 405, pp. 316–325, 2014.
- [10] C. Kindler, J. G. Sørensen, and A. Dederichs, “Evacuation of mixed populations from trains on bridges,” in *Bridge maintenance, safety, management, resilience and sustainability: Proceedings of the sixth International Conference on Bridge Maintenance, Safety and Management, Stresa, Lake Maggiore, Italy, 8-12 July 2012*, F. Biondini and D. M. Frangopol, Eds., Boca Raton: CRC Press, 2012, pp. 1573–1579.
- [11] M. Boltes and A. Seyfried, “Collecting pedestrian trajectories,” *Neurocomputing*, vol. 100, pp. 127–133, 2013.
- [12] M. Boltes *et al.*, “Influences of Extraction Techniques on the Quality of Measured Quantities of Pedestrian Characteristics,” in *Proceedings of the 8th International Conference on Pedestrian and Evacuation Dynamics: PED2016*, Hefei, China, 2016, pp. 540–547.

- [13] B. Steffen and A. Seyfried, “Methods for measuring pedestrian density, flow, speed and direction with minimal scatter,” *Physica A: Statistical Mechanics and its Applications*, vol. 389, no. 9, pp. 1902–1910, 2010.
- [14] U. Kemloh, M. Chraibi, and J. Zhang, “Jülich Pedestrian Simulator: JuPedSim,” User's Guide Version 0.7, 2015.
- [15] W. Liao *et al.*, “Measuring the steady state of pedestrian flow in bottleneck experiments,” *Physica A: Statistical Mechanics and its Applications*, vol. 461, pp. 248–261, 2016.
- [16] W. Liao *et al.*, “Experimental Study on Pedestrian Flow through Wide Bottleneck,” *Transportation Research Procedia*, vol. 2, pp. 26–33, 2014.
- [17] A. Seyfried, B. Steffen, W. Klingsch, and M. Boltes, “The fundamental diagram of pedestrian movement revisited,” (*Journal of Statistical Mechanics: Theory and Experiment*, vol. 2005, no. 10, pp. P10002, 2005.
- [18] S. Holl, M. Boltes, and A. Seyfried, “Level of safety concept for major events,” in *Traffic and Granular Flow '15*, V. Knoop and W. Daamen, Eds.: Springer-Verlag New York Inc, 2016.
- [19] J. Zhang and A. Seyfried, “Empirical Characteristics of Different Types of Pedestrian Streams,” *Procedia Engineering*, vol. 62, pp. 655–662, 2013.
- [20] A. John, A. Schadschneider, D. Chowdhury, and K. Nishinari, “Collective effects in traffic on bi-directional ant trails”, *Journal of theoretical biology*, vol. 231, no. 2, pp. 279–285, 2004.

Evacuation characteristics of preschool children through bottlenecks

Jun Zhang, Hongliu Li, Yanghui Hu, Weiguo Song

State Key Laboratory of Fire Science, University of Science and Technology of China
Jinzhai Road 96, Hefei, Anhui, P. R. China
junz@ustc.edu.cn; wgsong@ustc.edu.cn

Abstract - Pedestrian movement through bottlenecks have been widely studied from various aspects to understand the effects of bottlenecks on the pedestrian flow. However, few attentions have been paid to the movement characteristics of preschool children, who show obvious differences behaviour compared to adults due to the poor balance and understanding of danger especial under emergencies. In this study, we focus on the evacuation characteristics of preschool children through bottlenecks with laboratory experiments. From all the experiment, we do not observe clear lane formation process from the trajectories diagrams. It is found that the first arrive first out principle does not work in the situation with competition. Compared to adults, children are more likely to fall and hard to be controlled during movement, which is very dangerous in emergencies. The highest speed for the preschool children can beyond 3 m/s and is depend on the location in the crowd for each individual. For a given number of evacuees, the total evacuation time firstly decreases a linear with the increasing the bottleneck width and then keeps a constant if nobody falls down during the movement. Falling down of children will increase the evacuation time incredibly. The findings will be beneficial for the evacuation drill design in kindergarten as well as the facility design for young children.

Keywords: bottleneck, pedestrian flow, competition, preschool children evacuation

1. Introduction

It is reported that 26.1% of the population in the world are children aged from 0 to 14 years and 17.85% are kids aged 0-9 [1]. There are of great difference between children and adults in movement behaviours as well as psychological characteristics. Children prefer to behave with temporary feelings and desires instead of rational thinking. Especially for kids, their behaviours are usually not purposeful and easily affected by the surrounding environment. For example, kids aged 2-5 years are forming their control scheme of their own bodies and prefer to open their arms to keep balance. Most of them do not follow the desired direction [2]. Under emergencies, children face higher risks and might need more assistance than adults do due to their poor balance ability and poor understanding of danger. Besides, with the developed society, more and more children stay in kindergartens or day-care centres for both parents have to work outside. Thus, it is significant to consider the children evacuation dynamics when designing buildings for kids like kindergartens or children's amusement parks in order to reduce the risk of casualties.

Bottleneck is a common geometry in most of pedestrian facilities. When a large group of discrete bodies passes through a narrow exit, they might accumulate in front of the exit since the narrow exit restrict their movement [3]. Several stamped disasters happened because of the congestion in front of bottleneck. Hence, pedestrian flow through bottleneck has attracted increasing attention from researchers and several well-controlled experiments have been performed in the last decades [4-11]. Pedestrian movement through bottleneck is influenced by several factors including the geometry of the bottleneck (length, width and location), the initial distribution of pedestrians and sociological effects [8]. The impact of bottleneck lengths, widths and shapes on the flow has been investigated widely with different objects such as pedestrians, sheep herds or mice [3]. It is found that appropriate bottleneck shape can improve the traffic effectiveness and the wider the bottleneck the greater the flow [8, 11]. There is a linear decline of

the specific flux with increasing width when only one person can pass the bottleneck at a time and a constant value for larger bottleneck widths [6, 7, 9, 12, 13]. The bottleneck width shows strong influence on the density and velocity inside the bottleneck but less on them in front of the bottleneck [6]. There are severe differences between upstream and downstream of a bottleneck. Pedestrians' movements upstream are guided by the traffic state information of bottleneck ahead while their movements downstream are ruled by the physical restrictions of local conditions [14]. Different opening width, population composition and light intensity show influence on capacity of emergency doors [15]. Paradoxical phenomena like faster-is-slower effect can be observed from flow through bottlenecks [3, 5, 16-18]. Some researchers study pedestrian counterflow through bottlenecks and point out that bottleneck width has clear influence on the process of lane formation and wider bottleneck width can reduce passing time [19]. While some researchers thought that wide bottlenecks have few impacts on formation of lanes inside the bottleneck and the number of lanes does not show clear impact on the relations between flow and bottleneck width [4].

Even though there are studies on pedestrian flow through bottlenecks, most of data is related to the movement of adults. Up to now, very few studies on the children movement can be found, especially for preschool children [2, 20, 21]. Some researchers found that the speed of 3-5 years old children on the stairs was low and tended to grow when they can use handrails or walk hand in hand [2]. When kids are familiar to surroundings, they show higher walking speeds in spiral stairs and lower speeds on horizontal plane. During evacuation, they are keen to run and their speed can be higher than that of adults [21, 22]. Compared to adults, higher densities and flow of children through doors were observed [20, 21]. Lack of data and special behaviour characteristics of kids determines the necessity to study children's evacuation characteristics through bottlenecks.

In this study, preschool children experiments were performed to investigate the impact of the width of bottlenecks on children's evacuation process. The remainder of the paper is as following. In section 2, the experiment setup is briefly described. Section 3 shows the main results from the experiment analysis and the concluding remarks are made in section 4.

2. Experiment Setup

Totally 16 runs of experiment were performed in a kindergarten in Yueyang City, Hunan Province in China in Jan. 2018. The participants were 32 preschool children in the kindergarten with the age of 3-5 years old: 14 girls and 18 boys. The height of them ranges from 0.95m to 1.25m with the average of 1.06m, while their weight is from 14.8kg to 33.1kg with a mean value of 19.3kg. Fig. 1 shows the sketch of the experimental scenarios and two snapshots during the experiment. Two types of bottleneck, normal and funnel-shaped exit, were considered to study the influence of the shape of bottleneck on pedestrian flow. For each type of bottleneck, eight runs were performed by changing the width of exit from 0.4m to 1.1m at 0.1m intervals. Especially for the funnel shaped bottleneck, the cone angle α was fixed as 45° and only the width of outer edge of the bottleneck was changed. The geometry of the experimental scenario was built with plastic security fences (height: 75cm) and tables (size: 120×60×50 cm). In this case, the effective width of the bottleneck is larger than expected value especially for narrow situations, since both the fences and tables are shorter than the children. The upper part of the body can move outside the bottleneck, which can be seen from the snapshot.

Each child was given a yellow or blue hat during the experiment for quick extraction of their trajectories automatically afterward. Before each run of the experiment, all the children assembled orderly in the waiting area 5m far away from the bottleneck and were told to leave the exit like in an evacuation drill when the experiment start, which was organized by the kindergarten teachers. When everything was ready, one of our managing staff gave command "Ready! Go!" and the experiment started. During the experiment we asked the children to leave the bottleneck as fast as they can. As a result, competitive behaviours were observed and some children always wanted to leave the exit firstly. Especially in front of the bottleneck nobody let others overtake them and they always tried their best to leave the exit, even push-and-pull behaviour occurred sometimes. Since we considered several safety issues and prepared well in advance, the experiment was performed safely and smoothly finally. The whole experiment was

recorded by two cameras (a HD camera with the resolution of 1920 x 1080 pixels, frame rate of 25fps and a sports camera GoPro Hero 4) mounted on the roof of a three-floor building. Before and after the experiment, we calibrated the camera and the whole scenario twice based on the operation instruction of the software PeTrack to extract the trajectories precisely. Finally, we extracted all the trajectories from video recordings of HD camera. Moreover, all quantitative analysis following is based on these trajectories.

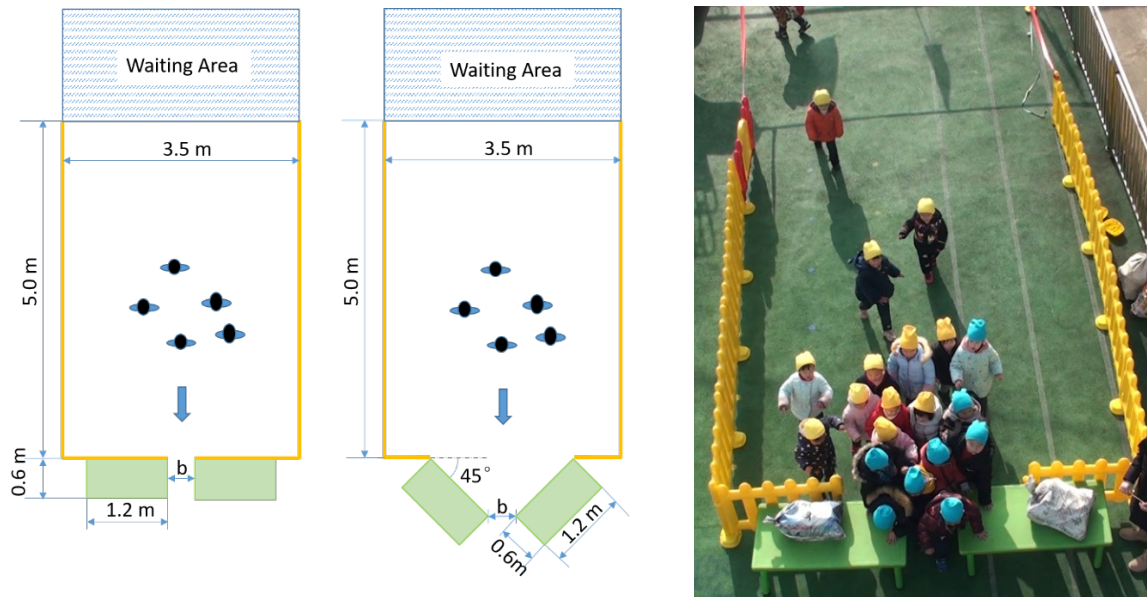


Fig. 1: Illustration of the experiment scenarios and a snapshot.

3. Results and Analysis

3.1. Trajectories

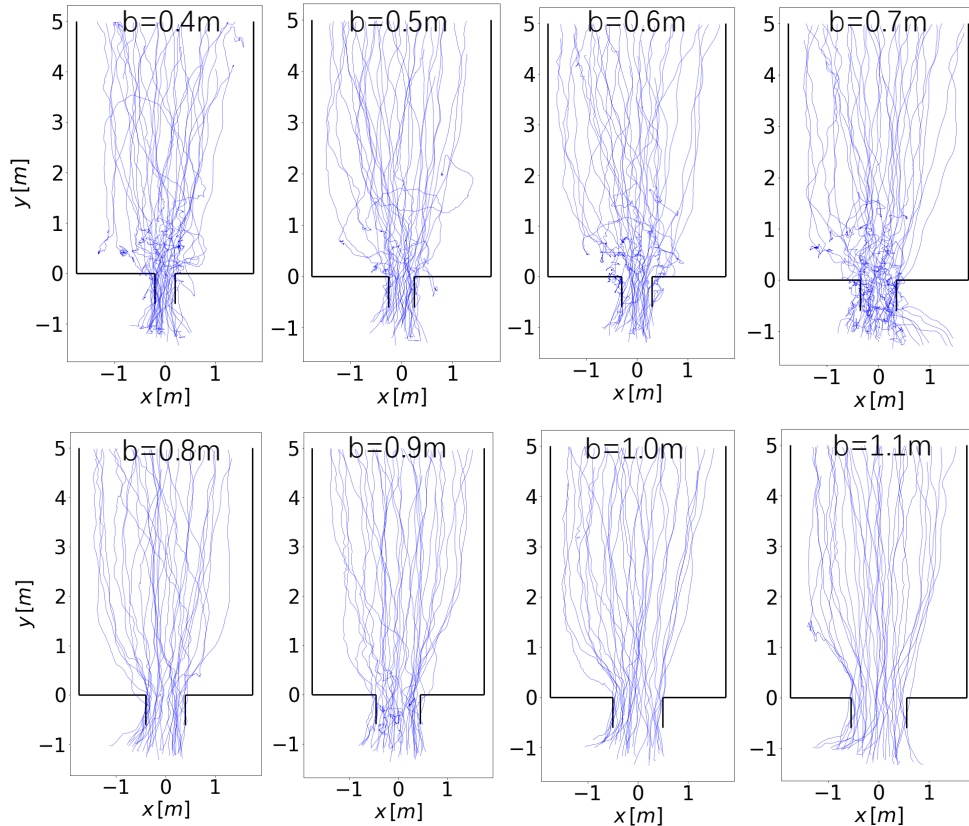


Fig. 2: Trajectories of all children in the experiment.

In Fig. 2 all paths taken by the children passing through bottlenecks of varying widths are overlaid. Firstly, we can examine the process of lane formation, which is considered as a typical self-organization phenomenon and is often discussed in previous experiments for pedestrian movement in narrow corridors. However, unlike the results in [8], the process is not apparent from the trajectories in this experiment. The motivation of the movement can be one main reason for the difference. Pedestrians in other experiments move in normal speed with collaborative and gentle way. However, children tried to leave the bottleneck as soon as possible by run and competitive behaviours exist in this experiment. In this case, they less consider to follow the behaviours or paths of others around them. For $b < 0.8\text{m}$, serious congestion formed very quickly after the experiment started and children movement at bottleneck is chaotic. The trajectories near the bottleneck oscillate obviously due to the strong competition. Some child squeeze through the boundary of the bottleneck with the upper body on the table. That is the reason why some trajectories are out of boundary in the figure. Especially for the scenario with $b = 0.7\text{m}$, the trajectories inside bottleneck also show strong oscillations. That is because some children fall down outside the bottleneck and become obstacles. For $b > 0.8\text{m}$, less congestion occurred due to insufficient participants and children can pass through the bottleneck nearly freely. The trajectories are smoother compared to the other four runs. From video recording, we can observe lanes sometimes in the corresponding runs during the experiment. However, from the trajectories it is not as obvious as that in [8], where there are about 250 participants in the experiment. It does not mean that the lane can be observed from the trajectory if we have more participants, because more participants may lead to serious congestion around the bottleneck and the situation will be similar to $b < 0.8\text{m}$.

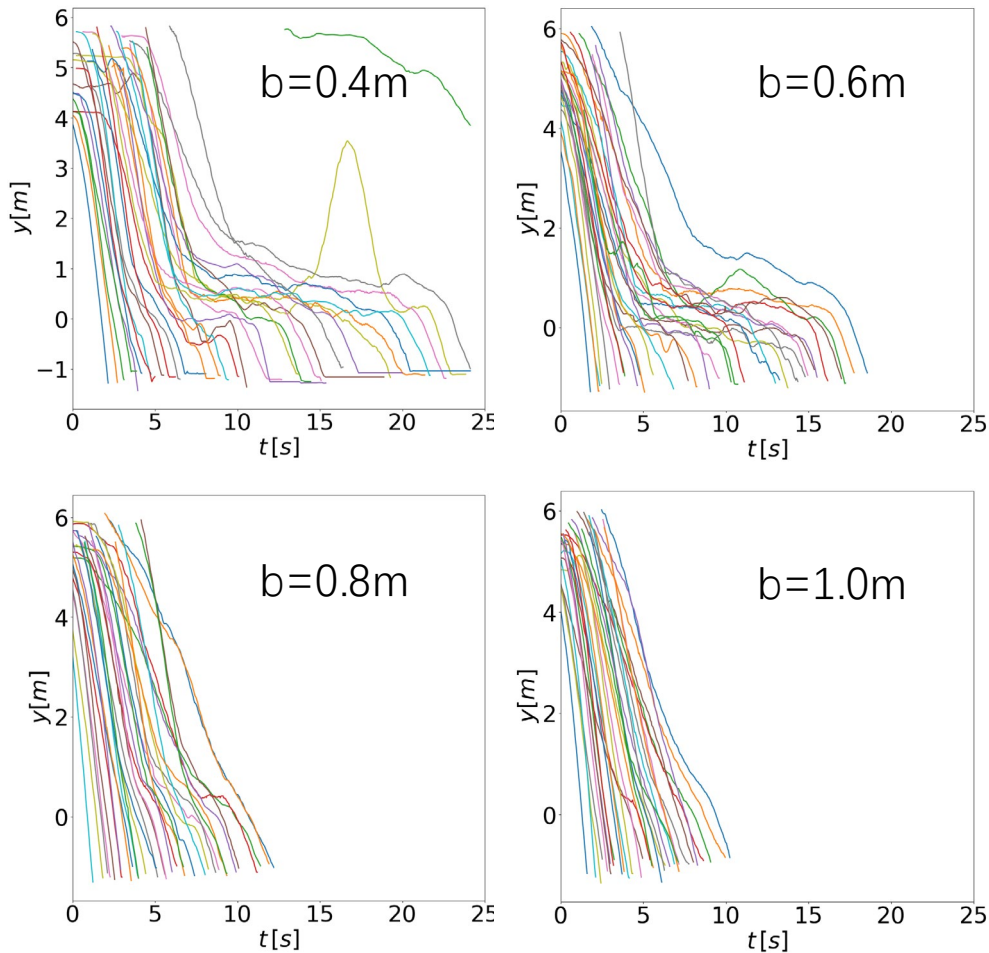


Fig. 3: Time space diagrams for four different scenarios. Here we focus on the movement towards the bottleneck (y direction).

Fig. 3 shows the time-space diagrams for four different scenarios. We focus on the movement towards the exit and thus y direction is considered. It is obvious that both the total evacuation time and the number of children under stop state decrease with the increasing bottleneck width. For the first few children, they leave the experiment scenario with relatively free speed without stop. For the other children, they firstly accelerate and then decelerate when congestions occur around the bottleneck. At the same time, there are children under both stop and movement state. Several intersections for the curves from stopping and moving children mean that the children pass through the bottleneck without obeying the “first come first out” principle under competitive conditions. The aggressive child always pushes away others to leave firstly and the children closely behind can then follow his path easily. For example, in Fig. 4 left, the child in the circle stopped at the corner and cannot leave for a long time because the one with black coat and his followers pushed her. Besides, poor balance and hard to be controlled can be two obvious properties of children compared to adults. They are more likely to fall even without push and pull from others. Once a child falls down, several children behind will fall down also. In this case, even if you ask them stop, nearly nobody cares about the command (See Fig. 4 right). In other word, for the safety of children movement, the best way is to take methods that can avoid or decrease falling down especially under emergency.



Fig. 4: Two snapshots from the experiment. Left: the child in the circle was pushed and cannot leave the bottleneck for a long time even if she arrives there earlier. Right: children are hard to be controlled. When there are children fall down, others behind don't stop move forward even if the organizers ask them stop during the experiment.

3.2. Evacuation Time

In this section, we focus the evacuation speed and time of the 32 children in the experiment. Fig. 5 shows the evolution of speed for each child along the movement direction from two runs with bottleneck width of 0.4 m and 1.0 m. It can be seen that the influence of the bottleneck on the speed can extend to 2 m away under the experiment condition. Of course, this range may change for different number of evacuee and different distance to waiting area. The children accelerate from zero to the maximal speed in the area from the waiting area to $y = 2$ m. The bottleneck width shows less influence on the movement of the children in the area. Then they decrease to a lower speed from $y = 2$ m to the bottleneck. The minimum speed is around zero for the scenario with $b = 0.4$ m, whereas it is about 0.5 m/s for the run with $b = 1.0$ m. Not only the maximal speed but also the minimal speed varies in a wide range for different children based on their location in the crowd. The maximal speed for the first few children can be over 3 m/s and reach 4 m/s, whereas it is lower than 1 m/s for the ones at the end. In any case, it is obvious that the minimal speed appears at the bottleneck $y = 0$ m, which means the bottleneck do have influence on pedestrian movement even it is very weak for wide bottleneck. Besides, the periodic oscillation of the speed around a certain value for each individual is due to the alternation of the two legs. The frequency of the oscillation agrees well with that of two legs. That is also the reason why less oscillation is observed for high speed.

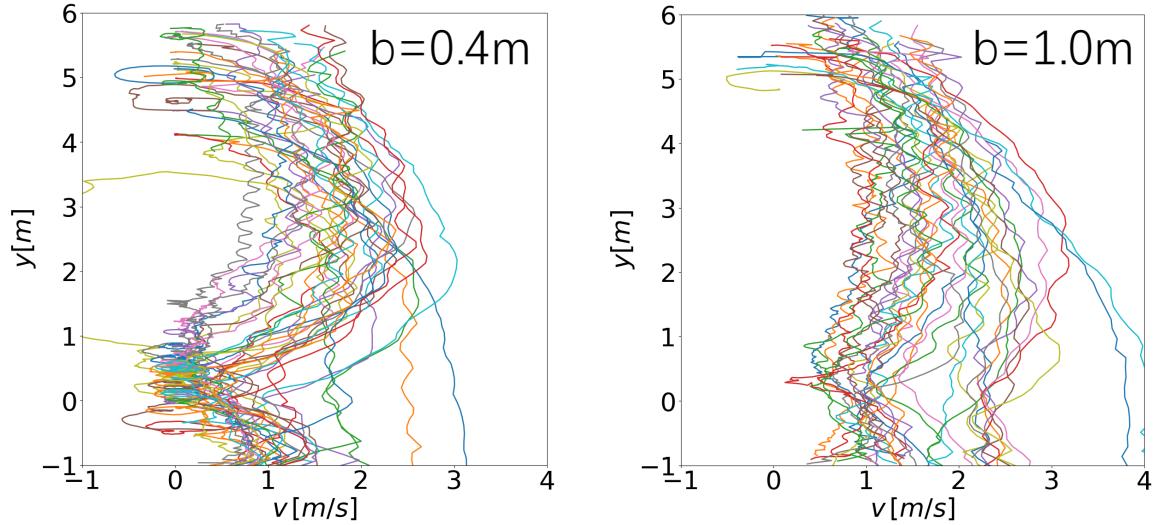


Fig. 5: The evolution of speed over space in different runs.

Even if the speed of each children shows apparent difference over space and time, from Fig. 6 we can see that the total evacuation time decrease linearly with the bottleneck width and then keeps a constant even in the competitive situations. For the given number of evacuees, increase of the width of bottleneck does not always have influence on the total evacuation time, for example the two scenarios with $b = 1.0$ m and 1.1 m. Especially, the evacuation time for $b = 0.7$ m is the longest one over all the experiment. That is because several children fall down outside the bottleneck and affect the movement of others behind.

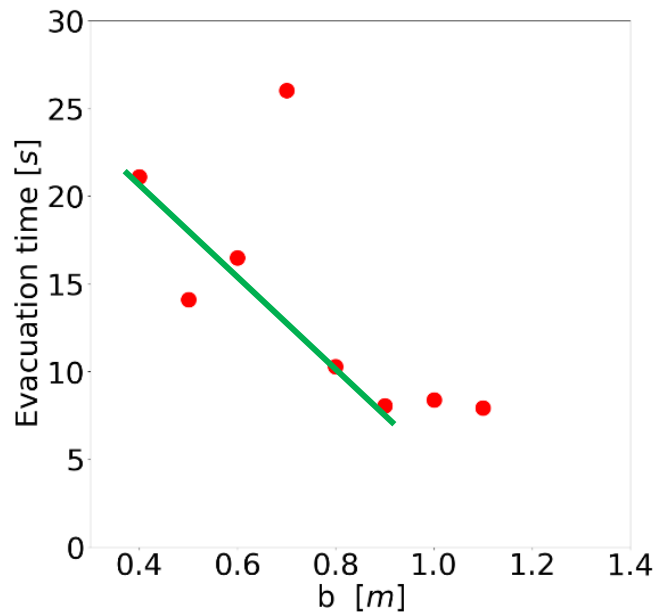


Fig. 6: The relation between the total evacuation time and bottleneck width.

4. Conclusion

In this work, we mainly focus on evacuation characteristics of young children through a bottleneck experimentally. Totally 32 kids with the age of 3-5 years old in a kindergarten participated in 16 runs experiment by changing the width of bottleneck from 0.4 m to 1.1 m at 0.1m intervals. The trajectories of each child are extracted from video recordings by using the software Petrack. The trajectories are

relatively smooth when the bottleneck width is larger than 0.8 m, whereas serious oscillations are obvious in narrow bottleneck scenarios. The process of lane formation is not observed in all widths of bottleneck under competitive conditions, which is different from previous studies in normal movement without pushing. From time-space diagram, stop-and-go state is observed. It is found that the first arrive first out principle does not work anymore. The aggressive children will push or pull others to leave earlier. Unlike adults, it is more likely to fall down for preschool children and they are much harder to be controlled during movement. Even in the situation that some children fall down and block the path, the children behind continue moving forward without following the new instructions from outside. The evacuation speed varies over the whole space and shows great dependency on the location in the crowd. The highest individual speed reaches over 3 m/s for the children in front of the crowd. The total evacuation time displays a linear relation with the bottleneck width b for $b < 0.9$ m and then keeps a constant for $b > 0.9$ m. For the given number of evacuees, increasing bottleneck width does not always decrease the evacuation time. However, falling down of children increases the total evacuation time incredibly.

Acknowledgements

The authors acknowledge the foundation support from the National Natural Science Foundation of China (Grant No. 71704168), from the Anhui Provincial Natural Science Foundation (Grant No. 1808085MG217) and the Fundamental Research Funds for the Central Universities (Grant No. WK2320000040).

References

- [1] U. NATIONS. (2017). World Population Prospects 2017. Available: <https://esa.un.org/unpd/wpp/Download/Standard/Population/>
- [2] V. Kholoshevnikov, D. Samoshin, and A. Parfenenko, "Pre-school and school children building evacuation," in *Proceedings of the Fourth International Symposium on Human Behaviour in Fire*, 2009, pp. 243-254.
- [3] I. Zuriguel et al., "Clogging transition of many-particle systems flowing through bottlenecks," *Sci Rep*, vol. 4, p. 7324, Dec 4 2014.
- [4] T. Rupprecht, W. Klingsch, and A. Seyfried, "Influence of Geometry Parameters on Pedestrian Flow through Bottleneck," pp. 71-80, 2011.
- [5] A. Garcimartin, D. R. Parisi, J. M. Pastor, C. Martin-Gomez, and I. Zuriguel, "Flow of pedestrians through narrow doors with different competitiveness," (in English), *Journal of Statistical Mechanics-Theory and Experiment*, Apr 2016.
- [6] W. Liao, A. Seyfried, J. Zhang, M. Boltes, X. Zheng, and Y. Zhao, "Experimental Study on Pedestrian Flow through Wide Bottleneck," *Transportation Research Procedia*, vol. 2, pp. 26-33, 2014.
- [7] T. Kretz, A. Grünebohm, and M. Schreckenberg, "Experimental study of pedestrian flow through a bottleneck," *Journal of Statistical Mechanics: Theory and Experiment*, vol. 2006, no. 10, pp. P10014-P10014, 2006.
- [8] J. Liddle, A. Seyfried, W. Klingsch, T. Rupprecht, A. Schadschneider, and A. Winkens, "An experimental study of pedestrian congestions: influence of bottleneck width and length," *arXiv preprint arXiv:0911.4350*, 2009.
- [9] A. Seyfried and A. Schadschneider, "Empirical Results for Pedestrian Dynamics at Bottlenecks," (in English), *Parallel Processing and Applied Mathematics, Part II*, vol. 6068, pp. 575-+, 2010.
- [10] A. Seyfried, B. Steffen, A. Winkens, T. Rupprecht, M. Boltes, and W. Klingsch, "Empirical Data for Pedestrian Flow Through Bottlenecks," (in English), *Traffic and Granular Flow '07*, pp. 189-+, 2009.
- [11] L. Sun, W. Luo, L. Yao, S. Qiu, and J. Rong, "A comparative study of funnel shape bottlenecks in subway stations," *Transportation Research Part A: Policy and Practice*, vol. 98, pp. 14-27, 2017.
- [12] A. Seyfried, O. Passon, B. Steffen, and M. Boltes, "new sights into pedestrian flow through bottlenecks," *Transportation Science*, vol. 43, August 2009.
- [13] T. Masuda, K. Nishinari, and A. Schadschneider, "Critical bottleneck size for jamless particle flows in two dimensions," *Phys Rev Lett*, vol. 112, no. 13, p. 138701, Apr 4 2014.

- [14] D. Duives, W. Daamen, and S. Hoogendoorn, "Anticipation Behavior Upstream of a Bottleneck," *Transportation Research Procedia*, vol. 2, pp. 43-50, 2014.
- [15] W. Daamen and S. Hoogendoorn, "Capacity of doors during evacuation conditions," *Procedia Engineering*, vol. 3, pp. 53-66, 2010.
- [16] D. Helbing, I. Farkas, and T. Vicsek, "Simulating dynamical features of escape panic," *Nature*, vol. 407, no. 6803, p. 487, 2000.
- [17] H. Oh and J. Park, "Main factor causing "faster-is-slower" phenomenon during evacuation: rodent experiment and simulation," *Sci Rep*, vol. 7, no. 1, p. 13724, Oct 20 2017.
- [18] J. M. Pastor et al., "Experimental proof of faster-is-slower in systems of frictional particles flowing through constrictions," *Phys Rev E Stat Nonlin Soft Matter Phys*, vol. 92, no. 6, p. 062817, Dec 2015.
- [19] X.-d. Liu, W.-g. Song, and W. Lv, "Empirical Data for Pedestrian Counterflow through Bottlenecks in the Channel," *Transportation Research Procedia*, vol. 2, pp. 34-42, 2014.
- [20] A. R. Larusdottir and A. S. Dederichs, "Evacuation of Children: Movement on Stairs and on Horizontal Plane," *Fire Technology*, vol. 48, no. 1, pp. 43-53, 2010.
- [21] A. R. Larusdottir and A. S. Dederichs, "Evacuation Dynamics of Children – Walking Speeds, Flows Through Doors in Daycare Centers," pp. 139-147, 2011.
- [22] A. Cuesta and S. M. V. Gwynne, "The collection and compilation of school evacuation data for model use," (in English), *Safety Science*, vol. 84, pp. 24-36, Apr 2016.

Analysis of Built Environment Influence on Pedestrian route choice behavior in Dutch Design Week using GPS Data

Yanan Liu, Dajuan Yang, Bauke de Vries, Harry J.P. Timmermans

Built Environment

Eindhoven University of Technology

Eindhoven, the Netherlands

y.liu.1@tue.nl, d.yang@tue.nl, b.d.vries@tue.nl, H.J.P.Timmermans@tue.nl

Abstract - Visitors not only have specific destinations targeting the Dutch Design Week (DDW) exhibitions distributed all over the city, but also visit the city in between exhibition activities. The mixed environment makes modeling behavior of DDW visitors more complex than shoppers and tourists only. This research pays special attention to the influence of built environment on pedestrian route choice. The built environment includes building and transportation infrastructure. GPS tracking data and social demographic information were collected during the event. Multinomial logit model and path size logit model are used to analysis route choice behavior. The results show that some built environment factors have significant influence on route choice. Shops are more attractive for aged visitors. Females prefer shorter routes more. In big event, the alternative routes with more sharing links could increase the possibility to choose.

Keywords: Pedestrian route choice; Built environment; GPS data

1. Introduction

The Dutch Design Week (DDW) 2017 attracted around 335,000 visitors from both the Netherlands and other countries during a week with more than around 610 exhibitions in 110 locations spread over the city Eindhoven. Due to specific travel purposes, visitors normally have specific destinations targeting the DDW exhibitions. Meanwhile, they might also visit the city for taking a break, a meal or a touring in between exhibition activities. The mixed environment makes modeling behavior of DDW visitors more complex than shoppers and tourists only. Will visitors' behavior be influenced by city built environment, except by exhibitions' location? In this perception we research how the exhibitions and city built environment together influence visitors' route choice becomes the interest. Except the OD (original and destination place) and trip character, the shops, transportation facilities and other built environment besides the route may also attract them to change their visiting route and destination. In this paper, we will pay special attention to the route choice between different exhibitions. Knowing how the built environment influences on pedestrian behavior can help the event organizer distribute the exhibitions and facilities more efficiently. Thus, visitors can visit more exhibitions and have a better experience.

For pedestrian behavior, traditionally researchers have mainly focused on socio-demographic characteristics and trip characteristics [1, 2]. The most well studied aspects are age, gender, speed, formation of groups, shy away distance, travel purpose and walking direction [3, 4]. Pedestrians may also be influenced by their own lifestyles, OD and attitudes [5, 6, 7]. Recently, from both transportation planning field and public health field, the built environment has gained increasing attention. Built environment represents the real city, containing urban facilities, buildings, transport infrastructure and designs to the entities [8]. It has been proved that built environment has significant some influence on pedestrian behavior [9, 10]. It consists of land use patterns, the distribution across space of activities and the buildings that house them, the transportation system, the physical infrastructure such as network characteristics as well as the service provided by the system, urban design, and the arrangement and appearance of physical elements [2, 11, 12, 13].

For route choice, factors may be divided into four categories: network characteristics [11], route characteristics [12, 2, 13], personal characteristics [1] and trip characteristics (Crow, 1998). Cross effects between items of these categories have been identified. Most pedestrian route choice models are based on shortest route calculations. These route choice models are based on shortest routes in time, formulating deterministic shortest path-based methods, stochastic shortest path-based methods, and constrained enumeration methods [14, 15].

Many visitors gather in the city area with numbered exhibitions. Different people will travel between two exhibitions or two activity points (stopping more than 15 minutes). So except the shortest path, there may also have other alternative routes between two exhibitions or two activity points. These alternative routes may have different built environment alongside the routes. These differences of built environment and visitors' choices can help us understand the influence of built environment on route choice.

This research will focus on modeling DDW visitors' route choice behavior. Considering walking route choice only, the model will take into consideration the effects of socio-demographic characteristics and the built environment in the city.

2. Method

2.1 Data

Two types of data were collected for this study, which are built environment data and DDW visitors' route choice data. The built environment data includes locations of exhibitions and information of DDW special facilities which can be accessed from the website of DDW, building information, land use patterns, transport system and the physical infrastructure. The information is imported from the latest Open Street Map. Then the links map was built. Each link indicate one segment of street and has its built environment information in the attribute table. Table 1 describes the variables in the Multinomial Logit Model and Path Size Logit Model.

Table 1 Variable Distributions

Variables	Description
Exhibition acreage /number	Average exhibition acreage on one link (unit, 100m ² per exhibition). Total exhibition acreage on one link divide total exhibition numbers on this link.
Exhibition types	From the official website of DDW, include Design management, Design education, Food design Graphic design, Industry design, Products design, Space design, Service design, Textile & Fashion
Coffee & Restaurant	Number of coffee shop and restaurant besides one link
Shops	Retail and grocery shop number besides one link
Bus stop	If this link has a bus stop (city bus and DDW bus) or not.
Rent bikes	If this link has a place to rent a bike (city bike and DDW bike) or not.
Car parking	If this link has a car parking or not.
<i>exhPS_k</i>	Length of one link
<i>PS_k</i>	Common path size for one route in the choice set

To collect DDW visitors' route choice behavior data, GPS loggers were used. We selected 4 days out of 7 days (both weekdays and weekend) during the DDW and distributed the GPS loggers randomly to the visitors at an exhibition ticket office near Eindhoven central railway station. We access visitors who come by train, bus, car, bike, walk and other ways. Only travelers with a DDW ticket were asked to join the survey. The GPS logger is small and light, has a button which means it is on and recording the location. It records a location coordinate every 5 seconds. A pencil-paper questionnaire was prepared to collect socio-demographic information, such as age, gender, visiting times for DDW, and familiarity with Eindhoven. The investigator turned on the GPS logger after respondent finished the paper questionnaire. The respondent can put it in a bag, pocket or other places. They were requested to give back the GPS logger at the central railway station.

2.2 GPS post processing

The collected GPS data were exported as csv files in GPS Photo Tagger. Then the csv files were imported in QGIS (Quantum Geographic Information System). The real observed GPS data is shown as Figure 1. The activity with stopping more than 15 minutes were recognized as one stop.

The routes between the activity stops were gotten manually. As the pedestrian walking ways have a high density in the city area and the signal of GPS logger were influenced by the high buildings, the GPS data often went too far from the route links on the map. Programing about matching GPS data to real routes in the links map were not suitable in this situation.

2.3 Choice set generation

Moreover, the modeling of route choice behavior using revealed choice data normally have to deal with generating a reasonable choice set. There are many well-used methods to identify the alternative routes which are feasible, such as K-shortest path [16], link elimination and penalty [17], branch and bound, simulation and labeling approach [18]. These methods consider more about the route character itself, but less about the city built environment besides the route. However, for pedestrians on streets, especially in the big event, route choice maybe influenced by the buildings, shops, activities and others in the city environment. As so far, there is no any perfect method to study the relationship between built environment and pedestrian route choice. So we can't calculate the alternative routes according to any methods and models.

To get the alternative routes, according to the GPS data, we found many visitors traveled between the same two locations. So observed different routes between two locations can be captured. These different routes could be considered as potential alternative routes for any traveler who walk from the origin location to the destination. In this research, we assume the alternative routes are a combination of the shortest route between two locations and routes chosen by all visitors who passed the same two locations.

The shortest route in this research is calculated based on the shortest distance. As most exhibitions were located in the pedestrian walking area in the city center, and some roads were also closed, so most of the visitors could walk freely, without influence by traffic lights or other limitations. Thus, in the shortest path calculating, we don't consider the elimination and penalty.

2.4 Discrete choice modeling framework

2.4.1 Multinomial logit model

The multinomial logit model is estimated on a subset of alternatives [19]. Conditional maximum likelihood estimation is used. The probability function is

$$P_{kn} = \frac{\exp(V_{kn})}{\sum_{l \in C} \exp(V_{ln})} \quad (1)$$

where V_{kn} is the utility of route k on individual n , V_{ln} is the utility of route l in choice set C on individual n , P_{kn} is the probability of individual n to choose route k .

2.4.2 Path size logit model

According to the choice set generation, many alternative routes gather in the limited city area. So, the alternative routes may be overlapped, and share some common links. The commonality can make errors with the utility of alternative routes. So, here we use Path Size Logit Model to measure the similarity in the utility function [20]:

$$P_k = \frac{\exp(V_k + \beta_{PS} \cdot \ln PS_k)}{\sum_{l \in C} \exp(V_l + \beta_{PS} \cdot \ln PS_l)} \quad (2)$$

$$PS_k = \sum_{a \in \Gamma_k} \frac{L_a}{L_k} \cdot \frac{1}{\sum_{l \in C} \delta_{al}} \quad (3)$$

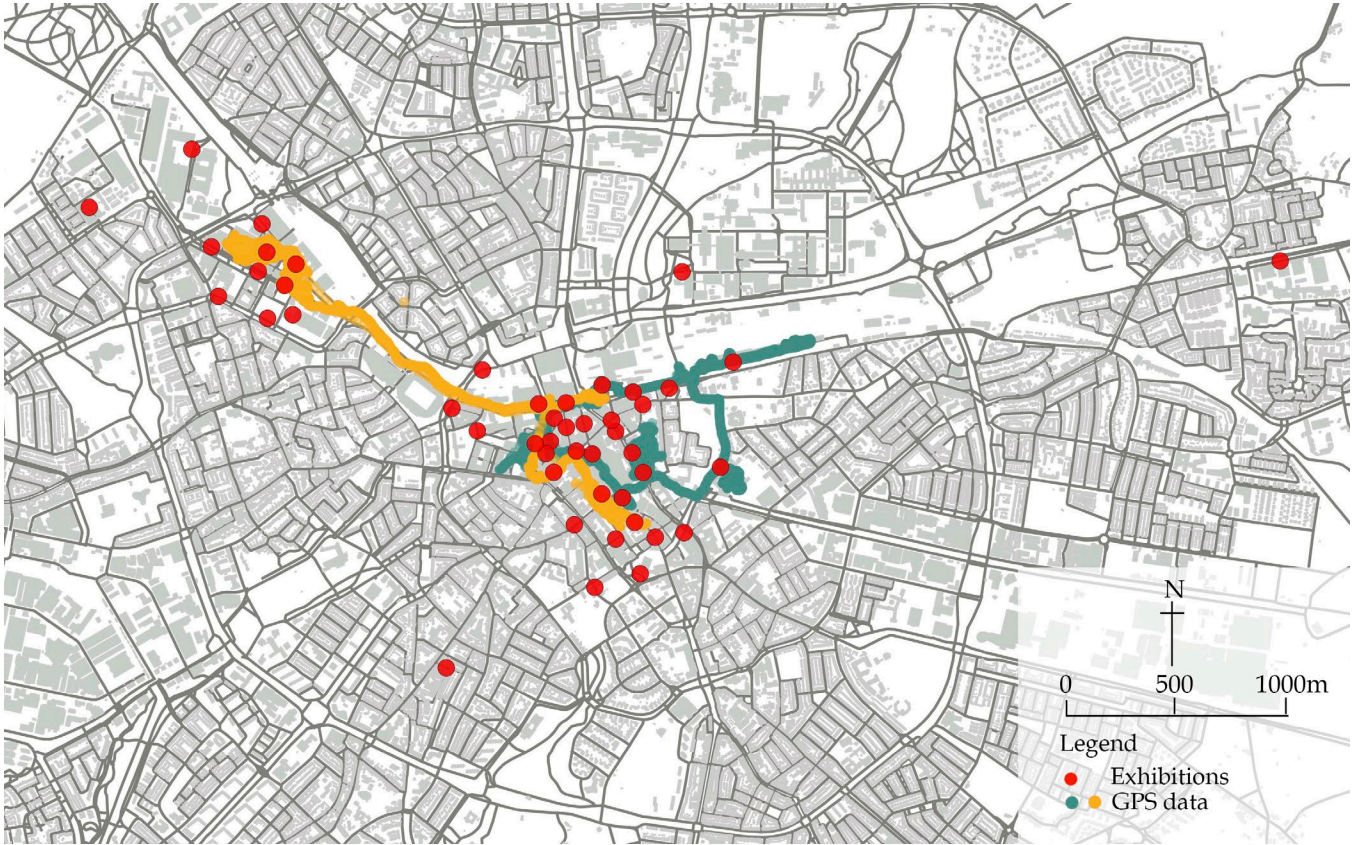


Figure 1 GPS data and exhibitions

where PS_k and PS_l are the commonality factors, L_a and L_k are the path size of routes k and l , Γ_k is the set of links in alternative k , C is the choice set for decision maker, L_k is the length of route k , L_a is the length of link a , δ_{al} is the link-path incidence dummy, equal to one if route l uses links a and zero otherwise, and β_{ps} is a parameter to be estimated.

The commonality factor PS_k expresses similarity of all links in the route and the ratio between link and route lengths. It should decrease when the overlapping between the routes increases. The commonality factor in equations (2) through (3) are always positive, between 0 and 1. Consequently, the estimated parameter β_{ps} should be positive to express the reduction of the utility of paths with common links with respect to other routes. Also, for unique paths the arguments of the logarithms are equal to one and the commonality factors with log are null [21].

3. Results

3.1 Descriptive statistics

In total 296 groups (565 persons) of visitors joined the GPS data collection. The distribution of their socio-demographic information and planned visiting information is shown in Table 2. Attribute “age” was collected personally in one visiting group. But attribute “familiar and visiting times” were collected by group, not personally. “Familiarity” means how familiar the visitors feel with Eindhoven. “Visit times” is about how many times the visitor have been to DDW before. The respondents are almost equally distribute between female and male. Respondents’ age from 19 to 30 years old occupied more than half which indicates that DDW attracts young adult the most. About 63.2% respondents are more or less familiar with Eindhoven. And about half of these respondents have been to the DDW in the past. These respondents somehow know about the routes and built environment. It reduces the randomness in the model about their rout choice.

Table 2 Distribution of Socio-demographic Information from DDW Respondents

Gender		Female 59.3%	Male 40.7%	Sum 565 (persons)
Age(years)	0-18	2.5%	1.8%	4.3%
	19-30	40.5%	29.2%	69.7%
	31-50	8.0%	5.3%	13.3%
	≥51	8.3%	4.4%	12.7%
Familiar with Eindhoven				Sum 296 (groups)
	Not at all	-	-	36.8%
	Slightly	-	-	20.6%
	Somewhat	-	-	11.5%
	Moderately	-	-	20.3%
Extremely	-	-	10.8%	
Visiting times	0	-	-	54.7%
	1-2	-	-	25.7%
	3+	-	-	19.6%

3.2 Multinomial Logit Model estimation

The estimated parameters for variables in the visitors' route choice model appear in Table 3. It includes built environment variables and interaction between built environment and social demographic information. R-project was used to perform the choice model estimation.

The result of the goodness of fit of the Multinomial Logit Model is described based on rho square. The null log likelihood value is -1832.0 and the final log likelihood after including all variables is -1623.0. Value of rho-square is 0.1140. Adjusted rho-square is 0.1599.

Length enters the model in log form. It performs better than original length. The estimated parameter is -0.7378, which is negative and significant. It indicates that visitors prefer shorter routes. This is reasonable. The estimated result of interaction of length and female is -0.8147, which is negative and significant. It means that females prefer shorter routes more than males. For the result of interaction of shops and females, we found that the parameter is not significant. It shows that females in DDW have no significant preference on routes with more shops. This is somehow opposed with the cliches. Moreover, we found that aged visitors prefer routes with more shops. As shown in **Table 3**, the result is +0.0428, positive and significant. What's more, aged visitors are more attracted by routes with larger exhibitions. The result of interaction of exhibition acreage/number and age is 0.0077, which is positive and significant.

Table 3 Multinomial Logit Model Estimation Results

	Estimate	Std. Error	t-value	Pr(> t)
Exhibition acreage /number	-0.0260	0.0204	-1.2758	0.2020
<i>Exhibition acreage /number* age</i>	0.0077	0.0038	2.0137	0.0440
Design management	-0.0497	0.2500	-0.1989	0.8423
<i>Design management* visit times</i>	0.1489	0.0616	2.4165	0.0157
<i>Design management* familiarity</i>	-0.2124	0.0781	-2.7191	0.0065

Design education	0.0236	0.2318	0.1018	0.9189
Food design	0.0160	0.2200	0.0725	0.9422
Graphic design	0.0543	0.3364	0.1613	0.8718
Industry design	-0.5829	0.2550	-2.2860	0.0223
Products design	-0.0053	0.2318	-0.0228	0.9818
Space design	0.1605	0.2527	0.6350	0.5254
Service design	0.2612	0.2104	1.2414	0.2145
Textile & Fashion	0.3589	0.3186	1.1263	0.2600
Coffee & Restaurant	-0.0452	0.0745	-0.6068	0.5440
Shops	-0.0867	0.0884	-0.9813	0.3265
<i>Shop*age</i>	0.0428	0.0167	2.5575	0.0105
Bus stop	0.3925	0.2417	1.6236	0.1045
Rent bikes	1.2400	1.1807	1.0502	0.2936
Car parking	0.1054	0.1725	0.6111	0.5411
lnlength	-0.7378	0.3997	-1.8461	0.0649
<i>lnlength* female</i>	-0.8147	0.3538	-2.3024	0.0213

Most of the exhibition types have no significant influence on the route choice, except design management and industry design. And the type of design management has different influence on visitors with more visit times and high familiarity. This is shown in Table 3. The result of interaction of design management and visit times is +0.1489, which is positive and significant. The result of interaction of design management and familiarity is -0.2124, which is negative and significant. Visitors with more visiting experience prefer routes with more design management. However, visitors with high familiarity with Eindhoven don't prefer routes with more design management.

As to other built environment variables, coffee, restaurant, bus stops and car parking have no significant influence on route choice. The results can be seen in Table 3.

According to the statement above, shops and exhibitions have significant and positive influence on visitors. Then, we can get that built environment exactly have significant influence on route choice.

3.3 Path Size Logit Model estimation

Table 4 shows the estimated results of Path Size Logit Model with built environment variables and social demographic information. R-project was used to perform the choice model estimation.

The result of the goodness of fit of the Path Size Logit Model is described based on rho square. The null log likelihood value is -1832.0 and the final log likelihood after including all variables is -1572.4. Value of rho-square is 0.1417. Adjusted rho-square is 0.1881.

Length also enters the model in log form. However, the result of length is not the same with result in Table 3. The estimated result is positive and not significant. It somehow means length has no obvious influence on route choice. After interaction with female, the result is negative and significant. It's the same with result in Table 3. Female still prefer shorter routes.

Aged visitors prefer routes with more shops. It's shown in Table 4. The estimated result of interaction of shops and age is +0.0440, which is positive and significant. The result of interaction of rent bikes and familiarity is -0.6525, which is negative and significant. Visitors with high familiarity with Eindhoven prefer routes without service of renting bikes. Because the streets with renting bike points were usually too crowded with visitors who were going to rent a bike during the event.

The same with result of Multinomial Logit Model, most of the exhibition types have no significant influence on the route choice, but except design management, industry design and products design.

And the type of design management also has different influence on visitors with more visit times and high familiarity. This is shown in Table 4. The result of interaction of design management and visit times is +0.1394, which is positive and significant. The result of interaction of design management and familiarity is -0.2126, which is negative and significant. These results are almost the same with result of Multinomial Logit Model in Table 3. Moreover, the result of interaction of products design and age is -0.1174, which is negative and significant. Aged visitors don't like routes with more products designs.

According to the statement above, shops and exhibitions have significant and positive influence on visitors. Then, according to the two models' results, we can get that built environment exactly have significant influence on route choice.

However, the estimated parameter of $\ln PS_k$ is negative, means routes with more sharing links have a high probability to be chosen by visitors. It's against with the common accepted result of Path Size Logit Modelling theory. This may be caused by the different preconditions in this research. The objects in this research are pedestrians. And their route choices happened in the big event. As stated in last part, the influence factors may be multiple, not only the route characters, but also the city built environment. These may make the results be different from other researches using Path Size Logit Model.

Table 4 Path Size Logit Model Estimation Results

	Estimate	Std. Error	t-value	Pr(> t)
Exhibition acreage /number	-0.0253	0.0208	-1.2173	0.2235
Design management	-0.0466	0.2507	-0.1861	0.8524
<i>Design management* visit times</i>	0.1394	0.0620	2.2494	0.0245
<i>Design management* familiarity</i>	-0.2126	0.0788	-2.6984	0.0070
Design education	0.1202	0.2405	0.4998	0.6172
Food design	-0.0325	0.2241	-0.1451	0.8847
Graphic design	0.1319	0.3395	0.3885	0.6976
Industry design	-0.5920	0.2599	-2.2780	0.0228
Products design	0.0160	0.2349	0.0683	0.9456
<i>Products design* age</i>	-0.1174	0.0459	-2.5552	0.0106
Space design	-0.0625	0.2561	-0.2441	0.8072
Service design	0.3379	0.2194	1.5398	0.1236
Textile & Fashion	0.4209	0.3249	1.2955	0.1952
Coffee & Restaurant	-0.0494	0.0765	-0.6456	0.5185
Shops	-0.0668	0.0888	-0.7523	0.4519
<i>Shop*age</i>	0.0440	0.0169	2.6117	0.0090
Bus stop	0.3853	0.2414	1.5965	0.1104
Rent bikes	1.4093	1.2405	1.1360	0.2560

<i>familiarity</i>	-0.6525	0.3211	-2.0323	0.0421
Car parking	0.1406	0.1756	0.8008	0.4233
lnlength	0.2254	0.4159	0.5419	0.5879
<i>lnlength*</i> <i>female</i>	-0.8911	0.3622	-2.4604	0.0139
<i>lnPS_k</i>	-1.4457	0.1502	-9.6232	0.0000

The result in Table 4 shows that more sharing links can increase the utility of this route. Routes with more sharing links are more close to each other. We assume that the exhibitions on these routes may have accumulative synergic effects. As the visitors came for exhibitions mainly, the exhibition maybe an important factor. However, the estimated result of exhibition acreage/number is negative and not significant. The correlation of exhibition acreage/number and $lnPS_k$ is also not significant. The exhibitions seem to be not the reason which causes the unreasonable parameter of $lnPS_k$.

To check if routes with more sharing links really have a higher utility for visitors, the correlation of $lnPS_k$ and appearing times of each routes is calculated. The appearing times of each routes are from the observed GPS data. It means how many times a route was traveled by all visitors. A route with higher appearing times is more popular for the visitors. The calculated correlation is -0.3783. They have a lower correlation. Somehow, it indicates that more popular routes have more sharing links. This can explain the result of $lnPS_k$ to some extent.

The result in this research, is different with the route choice in daily situations. In daily situations, each individual's ODs are seldom the same. The popularity of the alternative routes in one choice set have no significant difference usually. Thus, the appearing times of each route traveled by individuals are similar. So, it could not be recognized that routes with more sharing links are more popular in daily situations. However, in the big event DDW, a lot of visitors gathered in the limited area. Many visitors had the same ODs. The appearing times of routes had significant difference. There were some popular routes. According to the GPS data, in one choice set, the highest appearing times of one alternative route can be 74, the lowest times can be 1. The big difference between the alternative routes makes different popularity. More popular routes usually have more sharing links. So, the route choice utility of sharing links in big event could be different with daily situations. When the individuals sharing more common ODs and links, the common factor could increase the utility of the route. This is also mentioned in Frejinger's research [22]. The estimated negative result of $lnPS_k$ captures an attractiveness for overlapping paths.

4. Discussion

The Multinomial Logit Model and Path Size Logit model estimated in this study indicates that pedestrian route choice in big event is influenced by other factors, not only by route characters. In this research, visitors care more about the built environment, like exhibitions and shops. In total, visitors, especially female visitors prefer shorter routes. However, according to the variety built environment factors, length of rout is not the most important factor for visitors.

The model estimated coefficients give insights into relationship between built environment and route choice in big event. And it also helps to know the relationship between the event and the city. Different distribution of event's facilities in the city could generate different pedestrian behaviors. Different pedestrian behaviors could make different influence on the city. Better distribution plan of the event facilities combined with the city environment could give the visitors better experience.

As this research recorded visitors' routes in one visiting group. Most of the visitors traveled with others. The final observed route choice might be influenced by all group members. But, we don't know the weight of different members working on the final decision. In these research, we only consider the interaction relationship between social demographic information and route choice. A better way to analysis the group members and the route choice need to be generated.

The reason why the sign of PS_k is not reasonable needs more analysis. More empirical studies need to be estimated.

Acknowledgements

We thank the organization of Dutch Design Week; Alice, Ming Yuan, Maxi, Soheil, Tashin and Kim, the coordinator of the data collection effort; Sunghoon, research supporting. The author, Yanan Liu holds a scholarship from the China Scholarship Council.

References

- [1] Verlander, N.O. & B.G. Heydecker, "Pedestrian route choice: An empirical study," In: Proceedings of Seminar F of the PTRC European Transport Forum, pp. 39–49, September 1997.
- [2] Crow, "ASVV: Recommendations for Traffic Provisions in Built-Up Areas", Report 15, January 1998.
- [3] Carstens, R.L. & S.L. Ring, "Pedestrian capacities of shelter entrances, Traffic Engineering", vol. 41(3), pp. 38–43, 1970.
- [4] Daamen, W. & Hoogendoorn, S.P., "Controlled experiments to derive walking behavior", European Journal of Transport and Infrastructure Research, 3 (1), pp. 39-59, 2003.
- [5] Vale, D.S., Saraiva, M. & Pereira M., "Active accessibility: A review of operational measures of walking and cycling accessibility", The Journal of Transport and Land Use, 9(1), pp. 1-27, 2016.
- [6] Townsend, C. & Zacharias, J., "Built environment and pedestrian behavior at rail rapid transit stations in Bangkok", Transportation, 37, pp. 317-330, 2010.
- [7] Bagley, M.N. & Mokhtarian, P.L., "The impact of residential neighborhood type on travel behavior: A structural equations modeling approach", The Annals of Regional Science, 36, pp. 279-297, 2002.
- [8] Saelens B.E., & Handy, S.L., "Built environment correlates of walking: a review", Medicine & Science in Sports & Exercise, vol. 40(7), pp. 550–566, 2008.
- [9] Robert Cervero, Kara Kockelman, "Travel demand and the 3Ds: density, diversity and design", Pergamon Transpn Res, 2(3), pp. 199-219, 1997.
- [10] Owen, N., Humpel, N., "Understanding Environmental Influences on Walking: Review and Research Agenda", American Journal of Preventive Medicine, vol.27(1), pp. 67-76, 2004.
- [11] Seneviratne, P.N. & J.F. Morrall, "Analysis of factors affecting the choice of route of pedestrians. Transportation Planning and Technology", vol. 10 (2), pp. 147–159, 1985.
- [12] Ciolek, M.T., "Spatial behaviour in pedestrian areas", Ekistics, vol. 45 (268), pp. 120–121, 1978.
- [13] Bovy, P.H.L. & E. Stern, "Route Choice: Wayfinding in Transport Networks", Kluwer Academic Publishers, Dordrecht, 1990.
- [14] Ben-Akiva M., Bierlaire M., "Discrete Choice Methods and their Applications to Short-Term Travel Decisions", In: Hall R.W. (eds) Handbook of Transportation Science, International Series in Operations Research & Management Science, Springer, Boston, MA. 23, 1999.
- [15] Antonini, G., Bierlaire, M., and Weber, M., "Discrete choice models of pedestrian walking behavior," Transportation Research Part B, vol. 40(8), pp. 667-687, September 2006.
- [16] Bellman, R., "On a routing problem", Quarterly of Applied Mathematics, vol.16 (1), 87-90, 1958.
- [17] Prato, C.G., Bekhor, S., "Applying branch & bound technique to route choice set generation", Transportation Research Record, pp.19-28, 1985.
- [18] Ramming, S., "Network knowledge and route choice". Ph.D. Thesis, Massachusetts Institute of Technology, Cambridge, USA, 2002.
- [19] Frejinger, E., Bierlaire M., Ben-Akiva, M., "Sampling of alternative for route choice modeling", Transportation Research Part B, vol 43, pp.984-994, 2009.
- [20] Ben-Akiva, M.E., Bierlaire, M., "Discrete choice methods and their applications to short term travel decisions", In: Hall, R.W. (Ed.), Handbook of Transportation Science. Kluwer, Dordrecht, The Netherlands, pp.5-34, 1999.
- [21] Carlo G. P., "Route choice modeling: past, present and future research directions," Journal of Choice Modelling, vol. 2(1), pp. 65-100, 2009.
- [22] Frejinger, E., Bierlaire, M., "Capturing correlation with subnetworks in route choice models", Transportation Research Part B, vol(41), pp. 363-378, 2007.

The Modelling of Pedestrian Vehicle Interaction for Post-Exiting Behaviour

Peter J Lawrence, Veronica Pellacini, Edwin R Galea

Fire Safety Engineering Group, University Of Greenwich,
Old Royal Naval College, London, UK

P.J.Lawrence@gre.ac.uk; V.Pellacini@gre.ac.uk; E.R.Galea@gre.ac.uk

Abstract - During a major evacuation of high capacity buildings, such as a tower block or transportation hub, the emergency services will need to consider the safety of the people within the vicinity of the emergency. However, in general, when assessing the safety of a building for evacuation only the behaviour within the building is considered. One method of assessing this is to utilise a computer based simulation tool. This research outlines a number of developments required to simulate the impact of traffic on the evacuation process in an urban environment in relation to post-exiting behaviour. It uses a unique data set and model capabilities for representing pedestrian-vehicle interaction post-evacuation, which also considers the impact of time pressures on decision making. In addition, a number of software developments and pedestrian behaviours are identified for bridging the behavioural gaps when interfacing an emergency pedestrian model with a traffic simulation.

Keywords: Pedestrian, Vehicle, Post-exiting behaviour, Road crossing, Time pressure

1. Introduction

The standard practice when assessing a building evacuation is that people are considered to have reached a place of safety once they have exited the building, which is typically used to calculate a required safe egress time [1]. However, in real emergencies, for example, the Holborn station fire and the Paddington station false alarm [2], the emergency services will need to also consider the safety of pedestrians within the vicinity of the facility [3]. In these cases, people will be evacuating into an urban environment where the road network and pedestrian space will impact people trying to clear the area or reach a place of safety, such as an assembly location.

The work presented here extends the building evacuation modelling domain to include the road network outside the facility being modelled as well as key behaviours in pedestrian-vehicle interaction. These developments are an attempt to model people's post-exiting behaviour, while in the vicinity of an emergency. The objective of this work is to answer the research question, what behaviours need to be implemented in a computer model to simulate people interacting with vehicles after exiting from a building in an emergency?

The developments include pedestrian behaviours such as selecting whether to use a pedestrian crossing, crossing behaviour within or outside (i.e. jaywalking) a designated crossing area, along with different strategies for how to cross, for example crossing each lane of traffic in stages. Furthermore, these behavioural developments investigate how time pressure may play a role in decision making associated with pedestrian road crossing, something which is not currently considered by other pedestrian evacuation models, which include vehicles [4]-[6]. In addition, the necessary behavioural developments to facilitate the coupling of building EXODUS [7][8] to a third-party vehicle evacuation model for the simulation of urban scale evacuations are discussed.

2. Vehicle and Pedestrian Models

There are a number of models which simulate pedestrian interaction with vehicles, such as LEGION [6], VISSIM [4] and MATSIM [5]. However, these models do not consider psychological factors such as the time pressure a person might feel during an actual emergency situation (i.e. a fire). Furthermore, they consider pedestrians crossing only at designated locations (pedestrian crossings) and do not at

non-designated locations, as suggested by Wang [9] and rolling gap behaviours [10], which can be used if the pedestrian is considered a risk-taker [11][12][13].

Other research has been carried out looking at developing a framework for integrating fire, pedestrian and vehicle models for Wildland-Urban Interfaces [14]. While others have considered the vehicles as stationary obstacles for the evacuation [15]. The model presented here takes the recommendations identified by Schroeder [16] and Wang [9]. It then extends these ideas further with information from an online survey [17] to build a unique set of behaviours for representing how people might interact with vehicles in an emergency situation after evacuating from a building.

The cognitive behaviours for pedestrian road crossing included in this research cover the decision making process of whether to cross the road or not (gap acceptance model) and where to cross (at a pedestrian crossing or not). In addition, the methods employed to reach such decisions are considered. For further information on previous studies on pedestrian crossing behaviours related to cognitive aspects, see [18] and [19].

3 Vehicle Modelling

The main focus of the research developments within the evacuation model are on the pedestrian behaviours. Therefore, the primary purpose of the vehicle modelling is to provide interaction events for the pedestrians, so that pedestrian-vehicle interaction can take place. The vehicle modelling capability is limited to straight sections of the road network. The intention is to link these sections of the road network into a third-party vehicle model at a later date, when it is necessary to model the macro simulation of the road network. To allow for testing and development, without a third-party vehicle model, building EXODUS has been adapted to generate vehicles at specific locations in the model, at a user definable exponential rate [9] using a fuzzy logic car following model [20]. The road network can be imported from OpenStreetMap data [21], together with crossing information.

4 Pedestrian and Vehicle Interaction

The main simulation objectives of this research is to model people evacuating to a place of safety outside a building in an urban setting, where this place of safety is remote from the building itself. In these situations it is possible for people to come into contact with traffic and cross roads to leave the current area to reach the place of safety. For the crossing behaviour, a pedestrian crossing choice model has been developed which takes into account the pedestrian's distance from the pedestrian crossing, the type of crossing, time pressures, road type and traffic conditions and directions.

In the model, simulated people or agents, can select to cross a road at pedestrian crossing locations or at any point along the road. If an agent does not choose to use any of the available crossings, a probabilistic gap acceptance model is used which utilises the data from a number of previous studies [9][16][22], see Section 4.4. The gap acceptance model allows the pedestrian agent to choose to cross all lanes, when safe to do so, in one go, known as double gap [11] or one stage crossing [13]. Alternatively, if the agent is identified as a risk-taker, they may choose to cross lane by lane, rather than crossing all lanes in one go, sometimes waiting in the middle of the road, known as rolling gap [10] or risk-taker [11] crossing behaviour.

4.1 Where to Cross

Since the model is intended to be used to simulate people in emergency situations, a time pressure factor needs to be considered [23]. Furthermore, Chu et al [24] states a time pressure factor is important, because it has an influence on where and when people may cross a road. However, none of the models surveyed, as part of this research, were found to include such a feature. When examining other models there was lack of information regarding under what circumstances their data was collected, such as traffic conditions or there was vagueness regarding the travel distances involved. Therefore, the data needed for the crossing behaviour was collected using an online survey. The survey covered pedestrian crossing type,

route choice, traffic conditions, and how this could be impacted if the person was in a hurry, see reference [17].

From the data collection, analysis probabilities were derived depending on the origin and destination position for the condition *busy* and *light traffic* and for each combination of *rush* and *no rush*.

The derivation of these curves will be discussed in a following article, however an example is shown in Figure 1 to indicate the data type employed and the method used. In Figure 1 the distance of the position of the agent from the pedestrian crossing is on the x-axis while each line is for a different distance of the destination distance (bus stop) from the pedestrian crossing. For example, in Option 1, the probability to use the pedestrian crossing, starting at 40m and arriving at 30m (light grey line, Figure 1) in busy traffic rush is around 60%. Similar probability curves were obtained for the other options, Figure 4, which are discussed later in the paper.

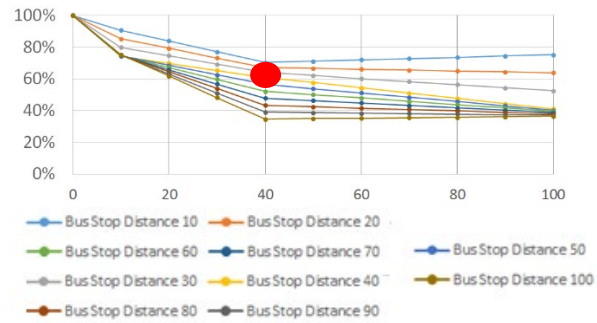


Figure 1 Distribution of Probabilities to use the Zebra crossing (Option 1) in a two way road with busy traffic and rush.

4.2. Modelling Crossing Behaviour

Agents in EXODUS are modelled using a fine network of nodes therefore, the pavement area around the road network is discretised in this fashion. In EXODUS the nodes are linked by a system of arcs. The road network area is represented by a network of links and vertices, as in OpenStreepMap [25], with polygonal areas representing the area of each road segment and separate polygons for junctions [21]. A road segment is defined as any straight section of the road network.

While pedestrian agents move using the *fine nodal* model on the pavement area, on the road, they move using a continuous spatial movement algorithm utilising the hybrid spatial capabilities in EXODUS [26]. A continuous spatial movement algorithm was selected for the road area as it consists of a well-defined region and provides greater flexibility for crossing at arbitrary angles. Since the agents need to be aware of approaching vehicles and other pedestrian agents on the road, a traffic lane based collision avoidance algorithm tied to the road network is utilised. In contrast, the fine nodal model is optimised more for checking for collisions (conflicts algorithm [7]) within a locality of adjacent nodes, which is around 0.5 to 0.7 metres. Furthermore, a typical vehicle can travel the distance of several fine nodes during a single EXODUS time step when travelling more than 6m/s (21.6km/h), which prevents the utilisation of the nodal spatial representation for the road network without an increase to the EXODUS clock rate. This would in turn require recalibration to the fine node conflict resolution algorithm [7].

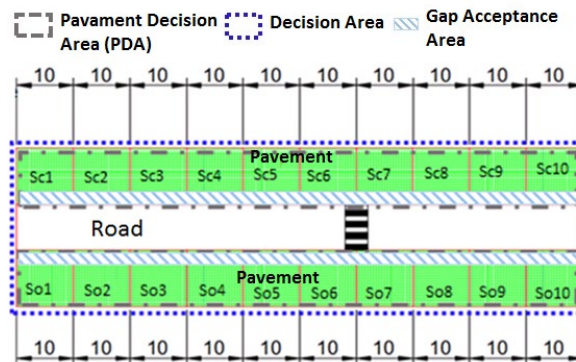


Figure 2 Pavement Area Allocation Types

When the simulation is initialised, the *Gap Acceptance* and *Pavement Decision* Areas, see Figure 2, are automatically identified. The *Gap Acceptance Area* consists of any nodes directly adjacent to the road and is defined as the region on the pavement where agents can choose to initiate crossing the road, i.e. identify if there is a sufficient gap in the traffic to be able to start to cross the road. The *Pavement*

Decision Area (PDA) is a user definable area on either side of the road (divided in *Origin* and *Destination* cells 10m wide by default, Figure 3) where agents consider the possibility of crossing the road.

During the simulation whenever an agent enters, changes their objective or starts responding in a *PDA*, the model's "Where To Cross" algorithm is utilised. Firstly, it determines whether the agent's projected path will require them to cross the road. If the agent needs to cross the road to achieve their objective, the behaviour algorithm will then identify the agent's *Origin* and *Destination* pavement cells and nodes, depicted in Figure 3. The *Destination Cell* is the cell on the opposite side of the pavement, to the agent, which is nearest to the agent's final objective (Target Destination), e.g. an assembly area or exit.

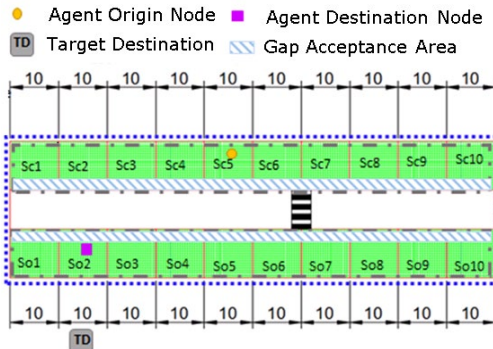


Figure 3 Selection of Target Destination

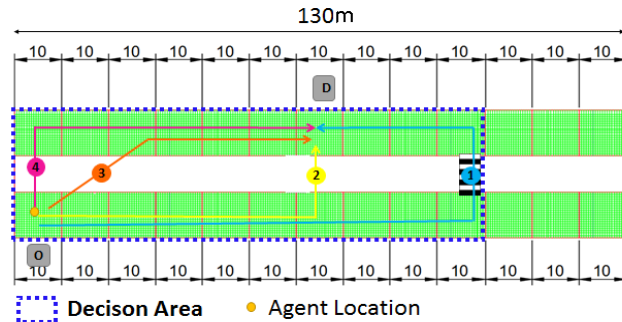


Figure 4 Possible Crossing Options from Agent's Current Origin Cell O to D their Destination.

The *Where To Cross Algorithm* calculates the agent's *Decision Area*, default length 100m towards the crossing, and assesses the likelihood for each possible route (Figure 4), being selected. The route selected is based on traffic levels and crossing type, if present, and whether the pedestrian agent is assessed as having urgency (rush, no-rush) and their origin and destination location. The probability of selecting each route, Figure 4, is calculated by linear interpolation [27] using the diagram as shown in Figure 1. The urgency parameter (rush, no rush) is a user define variable.

4.3 Gap Acceptance (When to Cross)

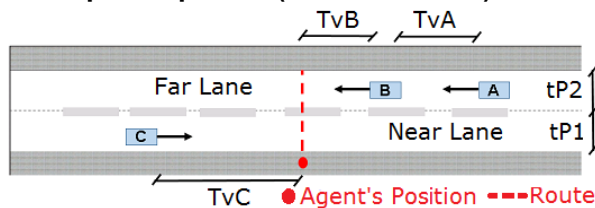


Figure 5 Gap Acceptance Parameters (two way)

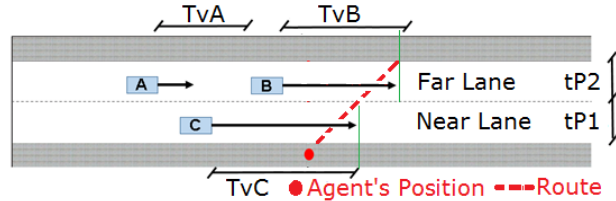


Figure 6 Diagonal Gap Acceptance Model (two way)

When a pedestrian agent enters the *Gap Acceptance Area* of the pavement and has chosen to Cross the Road (e.g. Options 3 and 4, Figure 4) they will assess the possibility of crossing the road, utilising a *Gap Acceptance Model*. The *Gap Acceptance Model* allows the agent to choose to cross all lanes, when safe to do so, in one go, known as double gap [11] or one stage crossing [13]. Alternatively, they may choose to cross lane by lane, known as rolling gap [10] or risk-taker [11], which is selected if the agent is consider as a risk-taker. The percentage of the population which is considered as a risk-taker is a user definable value. How to categorise risk-takers for mixed populations of different age and ability is left for further research.

When an agent looks to cross the road they consider vehicles in the near and far lane, only the nearest vehicle in the near lane and the first two vehicle in the far lane are considered. The key parameters are shown in Figure 5, for perpendicular crossing, and diagonal crossing in Figure 6. The Tv_A ,

parameter, time gap in seconds between vehicles A and B in the far lane plus TvB and TvC the time in seconds for vehicles C and B to reach the agent's location (first gap near and far).

The pedestrians will use the *Double Gap Model* if they are identified as risk-averse; hence, will try to cross only when safe to cross both lanes in one go. This is when both the times to cross the first lane ($tP1$) and the second lane ($tP2$) are less than the vehicle gap in the near lane (TvC) and in the far lane (TvB). If this condition is met a probability is calculated to accepting this gap.

The *Rolling Gap Model* is used when the agent is considered a risk-taker. In this case the time to cross the first lane ($tP1$) is less than the near gap (TvC) but the time to cross the second lane is greater than the first gap far (TvB) the agent will look at the second gap far (TvA). If this condition is met a probability is calculated to accepting the near gap. If the gap is accepted, the agent will cross the first lane, then when they reach the middle of the lanes, the gaps in the far lane is reassessed. Hence the behaviour modelled is where the agent will cross the first lane and then optionally wait in the middle before continuing if in the second instance the far gap is not accepted.

If a pedestrian agent fails to cross within the time specified by their patience attribute (1-30 seconds) [7] they will reassess *Where to Cross* and may choose to move further along the pavement and attempt to cross at a different location. When a pedestrian agent reaches a pavement *Origin/Destination* cell where a *Pedestrian Crossing* is located, and have chosen to use the crossing, they will move and wait at a location as near as possible the space in front of the crossing, i.e. the nearest EXODUS free *fine node* location adjacent to the pedestrian crossing.

In the model the Crossing acts as an *agent* which either allows the pedestrian or vehicles to pass, the decision to cross is not left to the individual agents. In the model currently two types of crossings have been implemented *Zebra* (Pedestrian Controlled) and a Signalised one.

5. Demonstration Case

These behaviours are demonstrated on a large transport hub, namely a train station, where the occupants have been instructed to head towards a place of safety away from the building. Since the focus of the demonstration case is on the crossing behaviours, only a section of the station will be considered, where the occupants evacuate through a main exit into the street. Once outside, they will have to cross a busy road to reach the designated assembly area.

There are three scenarios, which are examined, two cases where there is a road between the station exit and the assembly area that the people will need to cross. For comparison a base case is also given, where the road is removed and people stay on a paved surface to reach the assembly area, *Scenario 1*. The population in all three scenarios is 2098 with a response time of 0 to 30 seconds. In Table 1 a summary of the key model parameters are summarised.

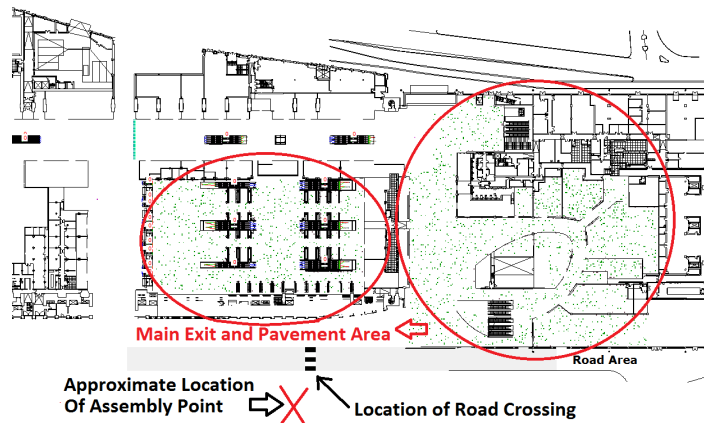


Figure 7 Station Area being evacuated. The Red Circles indicate where the people assigned to use the Main Exit and Assembly Point are initially located within the station.

Table 1 Simulation Characteristics

Scenario	Road	Crossing	Distances
1	No	None	Exit to Assembly Location 61m
2	Yes	Zebra	Exit to Crossing 35.5m. Crossing to Assembly
3	2 Lanes (8.5m wide) Traffic Busy[29]	Signalised (Red 15s, Red Amber)	

	Risk Takers 50%, in rush (100%)	3.5s, Green 30s, Amber 3.5s) [28]	Location 29.5m
--	---------------------------------	--------------------------------------	----------------

In each of the two road crossing scenarios different pedestrian crossings types will be considered, an un-signalised *Zebra Crossing*, Scenario 2, and a signalised pedestrian type crossing, Scenario 3. Figure 7 shows the geometry of the station area being evacuated, the assembly location together with road area being modelled and crossing location.

5.1 Results Analysis and Limitations

Each of the three scenarios was run a total of 50 times, which was sufficient to get 95% Confidence Interval on the mean simulation time at a tolerance of 5%, Figure 8 shows the base case *Scenario 1* after 90 seconds, where agents are starting to assemble outside the station. Figure 9 depicts Scenario 3 after 120s.

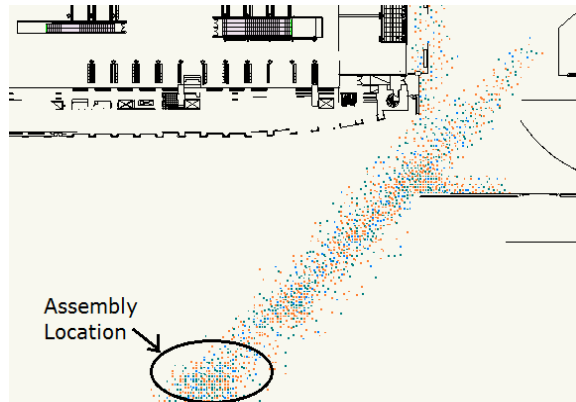


Figure 8 Scenario 1 - Assembly of agents when no road is present (90 seconds into simulation)

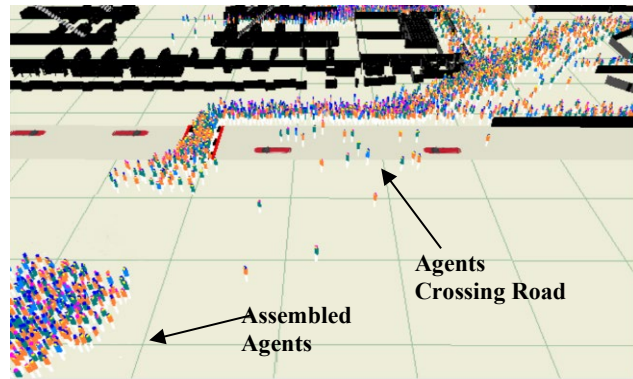


Figure 9 Scenario 3 - Agents Crossing at Signalised crossing (120 Seconds). Signals showing red to traffic.

The summary results of the three scenarios are shown in Table 2. The main observation here is that scenarios 1 and 2 mean assembly times are relatively close when compared to Scenario 3, the *Signalised Crossing*. This is further confirmed when looking at the evacuation curves of scenarios 1 and 2, Figure 10, which show a similar pattern.

Table 2 Simulation Results

Scenario	Assembly Time (s) Mean \pm SD (95 % CI)	Distance Travelled (m) Mean [Range]	Percentage Using Crossing Mean [Range]
Scenario 1	239.4 \pm 3.1 (238.6 to 240.3)	138.62 [47.05, 234.20]	N/A
Scenario 2	280.1 \pm 4.1 (278.9 to 281.2)	161.65 [59.84, 243.10]	91.29% [90.3, 92.5]
Scenario 3	625.9 \pm 16.6 (621.4 to 630.6)	173.59 [59.71, 263.30]	95.20% [94.27, 96.4]

The reason why the evacuation times and profile from *Scenario 2, Zebra Crossing*, is closer to, *Scenario 1*, is that once the agents start to use the *Zebra Crossing*, the traffic flow is effectively blocked. This allows the agents to proceed continuously across the road, until everyone from the station has evacuated and crossed the road, see the profile of *Zebra Crossing* usage Figure 10. Only once everyone has crossed the road can the traffic then continue. This means the impact of the road delaying people reaching the assembly areas is only impacted by the additional travel distance required to use the *Zebra Crossing* to reach the assembly area, see Table 2.

Looking at the crossing usage profile for the *Signalised Crossing*, see Figure 10 it can be seen that there is a stepped profile, unlike the *Zebra Crossing*, Figure 10. This means the time for the agents to cross the road is interrupted at intervals of approximately 22 seconds (i.e. time to go from green to red, then back to green). Once the traffic signal has completed its red cycle the agents have around 30 seconds to cross the road. This cycle of stop and go, has an effect on the agents' movement, which increases

congestion on the pavement area, as can be seen when comparing Figure 8, where there is no crossing, to Figure 9, with the signalised crossing.

Furthermore, it is evident that a higher than expected proportion of the pedestrians who use the crossing (around 90%), in both the *Signalised* and *Zebra Crossing* cases. This percentage is greater than the one shown in Figure 1. This is most likely due to the position of the crossing being located towards the assembly area. Furthermore, when the pavement is congested, agents have difficulty moving towards the edge of the pavement to cross the road. This means they re-evaluate the probability of where to cross, hence increasing the likelihood of the agents moving towards the pedestrian crossing.

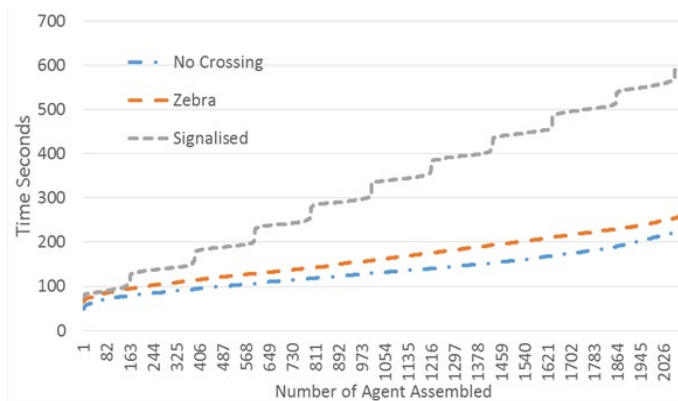


Figure 10 Scenario Evacuation Curves – Time to Assemble

The model has not been fully calibrated, only basic functional testing and verification has been performed so far. Since no model validation has yet

been carried out, the results can only be considered as indicative. The probability of crossing the road is mainly based on the pedestrian agent's distance from the pedestrian crossing, traffic and time pressure and does not consider the crowd density on the pavement. In crowded situations people are probably more likely to cross outside the pedestrian crossing to escape congestion. So further research could be focused on whether the crowd density could also be factored into the agent's crossing decision, this would likely have an impact on the results presented in the demo case presented here.

Further work will be looking at the above limitations as well as examining the impact on the model of varying the likelihood of crossing outside the pedestrian crossing. This will be done in addition to investigating how to connect the crossing and evacuation model to a third-party vehicle model, for example SUMO [30], which is one such model under consideration.

6. Conclusions and Final Remarks

This research has incorporated a number of key model developments and behaviours that are required to simulate the interactions of pedestrians with vehicles after exiting from a building during an emergency, which represents a unique effort to bridge the evident behavioural gaps identified in the integrations of emergency pedestrian models with traffic simulations. This work allows agents to decide when and where to cross a road once they have evacuated from a building during an emergency, incorporating psychological factors that affect their decision process. Further work is required for calibration and to examine the sensitivity of the various model crossing parameters, before moving onto model validation.

Acknowledgements

Part of this research was funded under a University of Greenwich VC Scholarship.

References

- [1] H.J. Hurley et al. (Ed.), *SFPE Handbook of Fire Protection Engineering*, Springer, New York, 5th edition, ISBN: 978-1-4939-2564-3, 2016.
- [2] London Fire Brigade, (April 2015) Holborn fire shows how complex London can be says capital's fire chief [Online] Available: http://www.london-fire.gov.uk/news/LatestNewsReleases_holbornfireshowshowcomplex.asp, [Accessed: 7/01/2018].
- [3] HSG154, *Managing crowds safely, A guide for organisers at events and venues*, (Second edition), ISBN 978 0 7176 1834 7, 2000.

- [4] L.D. Han, F. Yuan, “Evacuation modeling and operations using dynamic traffic assignment and most desirable destination approaches”, in Proceedings of the 84th Annual Meeting Transportation Research Board, Washington, DC, USA, November 2005.
- [5] G. Lämmel, H. Klüpfel, K. Nagel, “The MATSim Network Flow Model for Traffic Simulation Adapted to Large-Scale Emergency Egress and an Application to the Evacuation of the Indonesian City of Padang in Case of a Tsunami Warning”, Chapter 11, pages 245-265, Emerald Group Publishing Limited, DOI:10.1108/9781848557512-011, 2009.
- [6] LEGION, (2017) Pedestrian and Traffic Simulation Integrated Into a Single Software Application [Online], Available: (<http://www.legion.com/pedestrian-traffic-simulation-integrated-into-a-single-software-application>), [Accessed: 3 Jan 2018].
- [7] E Galea, M Owen, P Lawrence, “The EXODUS Model”, Fire Engineers Journal, pp.26-30, July 1996.
- [8] E.R. Galea, P.J. Lawrence, L. Fillippidis, D. Blackshields, D. Cooney, “buildingEXODUS V 6.1 Theory Manual”, Fire Safety Engineering Group, University of Greenwich, 2012.
- [9] T. Wang, Study of Pedestrian - Vehicle Interaction Behaviour by Microscopic Simulation Modelling, Doctoral Thesis, University of Southampton, Faculty of Engineering and the Environment, 2012.
- [10] M. Brewer, K. Fitzpatrick, J. Whitacre, D. Lord, D, “Exploration of Pedestrian Gap-Acceptance Behavior at Selected Locations”, Transportation Research Record, 1982(1), 132–140. doi:10.3141/1982-18, 2006.
- [11] L. Song, M.C. Dunne and J.A. Black, “Models of Delay and Accident Risk to Pedestrians, Transportation and Traffic Theory”, Proceedings of the Twelfth International Symposium, Elsevier Science, 2003.
- [12] D. Sun, S. Ukkusuri, R. Benekohal, S. Waller, “Modeling of motorist-pedestrian interaction at uncontrolled mid-block crosswalks”, Proceedings of 82nd Annual Meeting of the Transportation Research Board, Urbana, November 2002.
- [13] M. Paul and P. Rajbonshi, “A Comprehensive Review on Pedestrian Gap Acceptance at Unsignalized Road” International Journal of Engineering Research & Technology (IJERT), Vol. 3 Issue 11, November-2014, ISSN: 2278-0181, November 2014.
- [14] E. Ronchi, S. Gwynne, G. Rein, R. Wadhvani, P. Intini and A. Bergstedt, "e-Sanctuary: Open Multi-Physics Framework for Modelling Wildfire Urban Evacuation", Fire Protection Research Foundation Report, FPRF-2017-22, December 2017.
- [15] P. Alvarez, V Alonso, “Using microsimulation software to model large-scale evacuation scenarios. The case of Sangiesa and the Yesa dam collapse”, Safety Science, Vol. 106 Pages 10-27, <https://doi.org/10.1016/j.ssci.2018.02.021>, 2018.
- [16] B.J Schroeder, “A Behavior-Based Methodology for Evaluating Pedestrian-Vehicle Interaction at Crosswalks”, Doctoral Thesis North Carolina State University, Department of Civil Engineering, 2008.
- [17] V. Pellacini, (2016), “Pedestrian Behaviour Survey”, Fire Safety Engineering Group, University of Greenwich [Online] Available: <https://fseg.gre.ac.uk/surveys>, [Accessed: 2 Feb 2018].
- [18] A. Dommes, V. Cavallo J. Dubuisson, I. Tournier, F. Vienn, “Crossing a two-way street: comparison of young and old pedestrians”, Journal of Safety Research, vol. 50, pp27-34, 2014.
- [19] X. Zhuang, C Wu, “Pedestrians' crossing behaviors and safety at unmarked roadway in China”, Accident Analysis & Prevention, vol. 43, pp. 1927-1936, 2011.
- [20] M. McDonald, J. Wu and M. Brackstone, “Development of a Fuzzy Logic Based Microscopic Motorway Simulation Model”, in Proceedings of the IEEE Conference on Intelligent Transportation Systems (ITSC97), Pages 82-87 Boston, USA, DOI: 10.1109/ITSC.1997.660454, 1997.
- [21] P.J. Lawrence, L. Flippidis, A. Veeraswamy, E. Galea E, “Utilising OpenStreetMap for Urban Evacuation Analysis”, in Proceedings of the 24th GIS Research UK (GISRUK 2016) conference, University of Greenwich, March 2016.
- [22] G. Yannis, N. Technical, “Pedestrian gap acceptance for mid-block street crossing”, in Proceedings of the 12th World Conference for Transportation Research, pages 1–11, 2010.
- [23] R. Fahy, G. Proulx, “Panic and Human Behaviour in Fire”, Proceedings of the 4th International Symposium on Human Behaviour in Fire Cambridge, UK: Robinson College, 2009.
- [24] X. Chu, M. Guttenplan. M Baltés, “Why People Cross Where They Do” Transportation Research Record: Journal of the Transportation Research Board, 160(03), January 2004.
- [25] OpenStreetMap (2018) OpenStreetMaps [online], Available: <https://www.openstreetmap.org>, [Accessed: 27 April 2018].
- [26] N. Chooramun, P. Lawrence, E. Galea E, “Evacuation simulation using Hybrid Space Discretisation and Application to Large Underground Rail Tunnel Station”, Physical Sciences Reviews, Vol. 2, Issue 7, DOI:10.1515/psr-2017-0001, Aug 2017.
- [27] V. Airault, S. Espie, “Behavioural model of the pedestrian interaction with road traffic”, Association of European Transport and Contributors, 2005.
- [28] R. Walker, M. Winnett, A. Martin, J. Kennedy, “Puffin Crossing Operation and Behaviour Study”, Transport Research Laboratory project report for the London Road Safety Unit, Transport for London, 2005.

- [29] J. Hine, “Assessing the impact of traffic on behaviour and perceptions of safety using an in-depth interview technique”, *Journal of Transport Geography*, 4(3), 179–197, 1996.
- [30] D. Krajzewicz, J. Erdmann, M. Behrisch, and L. Bieker, “Recent Development and Applications of SUMO - Simulation of Urban Mobility” *International Journal On Advances in Systems and Measurements*, 5 (3&4):128-138, December 2012.

Modelling and Simulation of Urban Mobile Agents for Analyzing Mixed Flows in Urban Pedestrian Space

Toshiyuki Kaneda¹, Masahiro Shohmitsu¹, Wataru Sasabe¹, Yuanyuan Liu^{1,2}

¹Graduate School of Engineering
Nagoya Institute of Technology
Nagoya, Japan

²College of Architecture and Urban Planning
Tongji University
Shanghai, China

kaneda@nitech.ac.jp; mshr.shoh3@gmail.com;
sw130cl@gmail.com; liuyuanyuan330@gmail.com

Abstract - Since the 1990s, complex systems research has been developing agent simulations to explain the phenomena observed in urban spaces. In recent years, agent-based modelling has often been employed to successfully simulate pedestrian behaviour. In such studies, explanations using pedestrian counter flow phases have appeared sporadically. Most state-of-the-art models, however, do not generally consider mobile agents other than pedestrians or counter flows in at least two directions. In this paper, we consider agents such as pedestrians, vehicles, wheelchairs, bicycles and so on in urban pedestrian space (UPS), which we call urban mobile agents (UMAs). The aim of this research is to develop a simulation platform to support urban simulation research. The models of rule-based UMAs that we have been developing are used to analyze the micro-meso behaviours of the mixed flows in UPS. The content of this class of agent includes the pedestrian agent as per the simplified agent simulation of pedestrian flow (sASPF) rules as well as the vehicle agent and bicycle agent in the UPS, including a wheelchair agent in the coming research. Using these models, we explore the following approaches: (a) theoretical analyses of phase transitions such as laminar flow formation or blockade of pedestrian counter flows, with clarification of the relationship between the degree of pedestrian global density and the bias of the diagonal stepping probability, which is the right or left selection probability of avoidance behaviour; (b) the implementation of obstacle avoidance rules in the sASPF pedestrian agent model, and their comparison with published evacuation experiment results, so as to evaluate the performance of the obstacle avoidance function; (c) the development of a vehicle agent model to simulate pedestrian-vehicle mixed flow at a crossroads assuming a disaster scenario; (d) the development of a bicycle agent model by extending sASPF rules; and (e) consideration of a conceptual framework for interaction fields representing heterogeneous agent mixed flows, including vehicle, bicycle, pedestrian and wheelchair agents.

Keywords: pedestrian agent, vehicle agent, bicycle agent, urban pedestrian space, implicit interaction assumption

1. Introduction

We aimed to represent and simulate spatial behaviours resulting from the micro-actions of urban mobile agents (UMA) such as humans, wheelchairs, bicycles, and vehicles in an urban pedestrian space (UPS) such as pedestrian pavement, open space, and so forth, and develop an integrated simulation platform that will form the basis for urban simulation research. As its basic model, simplified agent simulation of pedestrian flow (sASPF) [6] includes a pedestrian agent, which was developed by applying a simplified set of behaviour rules.

In this paper, we address the pedestrian agent in our sASPF project by showing the results of the performance tests, explain the simulation performance at a crossroads of vehicle-pedestrian mixed flow, refer to modelling of a bicycle agent that performs by prediction, and consider the types of interaction systems that characterize the situations specified in the simulations.

The features of our sASPF project include the following:

- UMA is rule-based, so the behaviour of an agent is described by rules. These are expected to have advantages over difference equation systems such as the social force model [1] and cellular automata models [2,3] in terms of readability of actions, calculation of time and interactions between various models. These are useful for urban simulation research.
- Although the spatial representation of UPS uses a two-dimensional continuous space with a 0.4 m unit scale, the time representation uses a discrete step of 1/3 second due to the abstraction of practical expressions and computational simplifications.
- Regarding the behaviour rule of the agent, the antecedent "others assessment" is applied in the "discrete" sight field grid, and the subsequent result is given as a stochastic "micro-action".
- Our simulation model runs on agent-based modelling and simulation software, artisoc [8] that adopts random sequential updating (RSU) as a conflict-resolution method that takes into account interactions between agents.

2. sASPF project, a simplified rule-based urban mobile agent simulation

Here, we describe the pedestrian agent model that plays the role of the “primal actor” on UPS and its basic performance. Note that this section contains some of the findings of our previous research.

2.1. Pedestrian agent, the first and basic component of the sASPF project

The sASPF project uses a new pedestrian agent that we developed by simplifying our previous ASPF model, including six basic behaviour rules, eight slow-down rules, four avoidance rules, to simulate pedestrian behaviours [4, 5]. A pedestrian agent in the sASPF project uses 8 behavior rules, including diagonal stepping, whereas 18 behaviour rules were applied to represent pedestrian behaviours in the ASPF model. Each agent has a position (x,y) and walking direction θ on the base space (two-dimensional Euclid plain). The agent also has a sight field grid (with unit scale e of 0.4 m, which is proximate to the shoulder width of an adult man) as the x-axis is set as the walking direction (see Fig. 1).

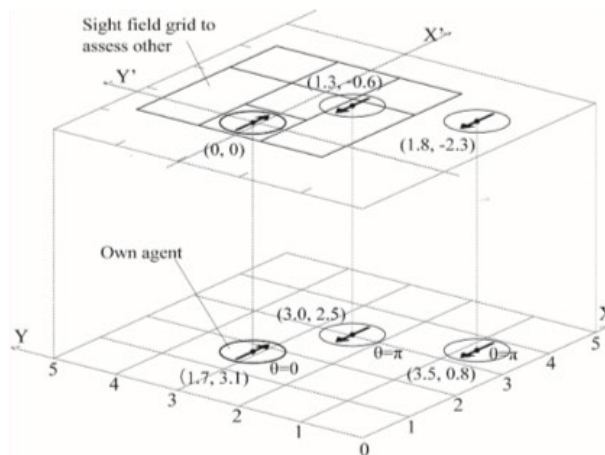
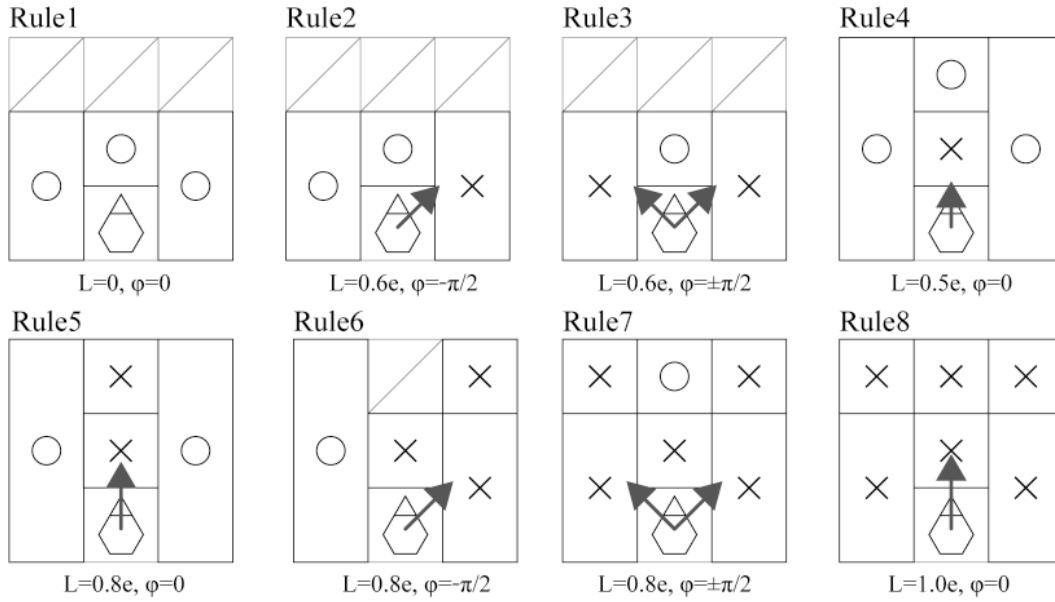


Fig. 1: Sight field grid of pedestrian agent in the sASPF project .

In each step, one behavioural rule is applied from the rule set corresponding to the locations of other agents or obstacles within its own sight field grid. During each step, the agent transforms the position by the given motion vector according to the applied rule, which specifies a stepping distance L and diagonal stepping angle φ in its relative polar coordinate representation, or $(L\cos(\theta+\varphi), L\sin(\theta+\varphi))$ in the xy -coordinate on the base space (see Fig. 2).

The direction of the relative grid θ takes a real value of $[0, 2\pi)$ [5], but in this paper we deal with one-way flows and counter flows and so treat the two directions as $\theta = 0$ or π .



- Apply the first rule that fulfills the antecedent by scanning inside this rule set in turn
- O: Occupied, X: Non-Occupied. Unit Length $e = 0.4$ mtr
- Diagonal stepping direction in Rule3 and Rule7 is determined by random with probability p .

Fig. 2: The behavioural rule set of a pedestrian agent in the sASPF project.

2.2. Basic performance tests of pedestrian flows

Figures 3 and 4 summarize our basic performance tests [6]. In the test results of one-way flows, our results appear to be a nice fit to the measured value up to a density of 3 people/m², and this model is suitable for dealing with pedestrian flow simulations in the noncontact situation. We also analyzed phase transitions of counter flows theoretically. Our results confirmed that phase transitions occurred for a range of biases of the diagonal stepping probability, from 50:50% to 60:40%, and the global density from 0.4 to 1.4 agents/m². It is worth noting that, in this model, different phase transition patterns appeared in the counter flow due to the slight probabilistic differences in the pedestrian micro-motive, i.e., avoidance directions.

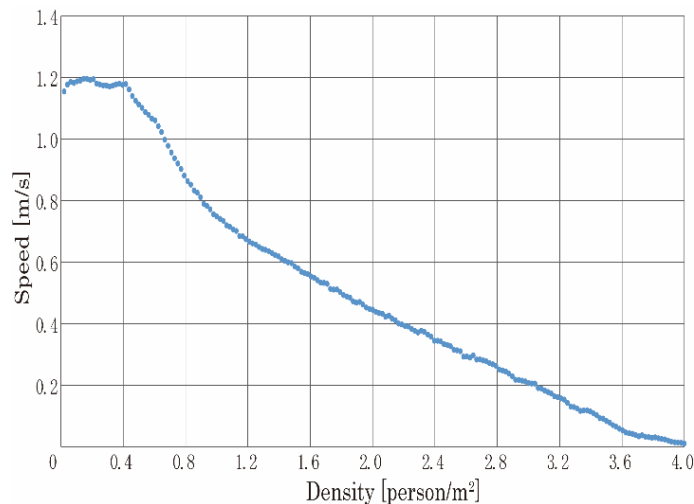


Fig. 3: Fundamental diagram, or performance of pedestrian agent simulations: density-speed graph in one-way flow.

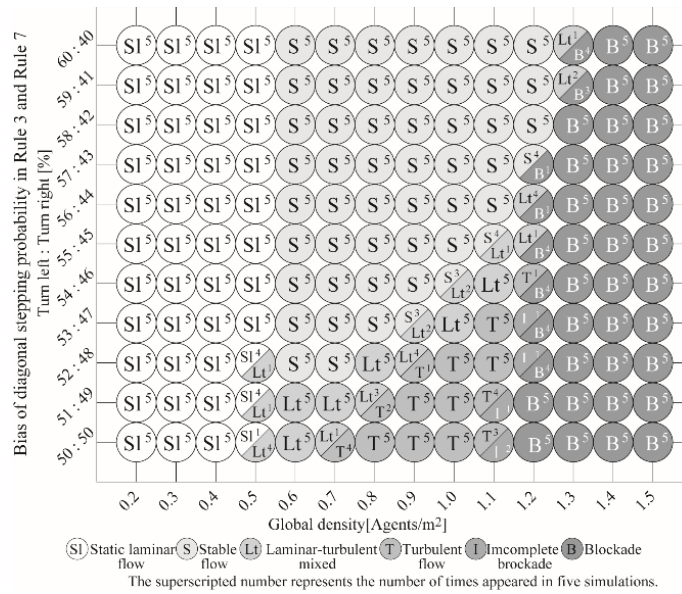


Fig. 4: Performance of pedestrian agent simulations: phase distribution map of counter flows [6].

2.3. Performance test of pedestrian flows with fixed obstacles laid out

In this subsection, we discuss the validity of our pedestrian agent model, assuming a practical situation such as an evacuation from a city after an earthquake. Here, the subject of the data-fitting consists of the results of a classic evacuation experiment conducted by the Fire and Disaster Prevention Science Centre of Japan in 1983 [7]. In this experiment, the performance of pedestrian flows in situations where cars were left on a crossroad was recorded. We added a large obstacle avoidance rule whereby an agent looks ahead up to $10e (=4.0 \text{ m})$ and changes direction to the short side when coming upon a row of obstacles, and then returns to the original direction just after avoiding the obstacle. Fixed obstacles representing stationary vehicles were laid out on a map that reproduced the crossroads of the evacuation experiment (hereafter, reproduction map: Fig. 5), and a total of 127 pedestrian agents were divided into two similar-sized groups walking through the area.

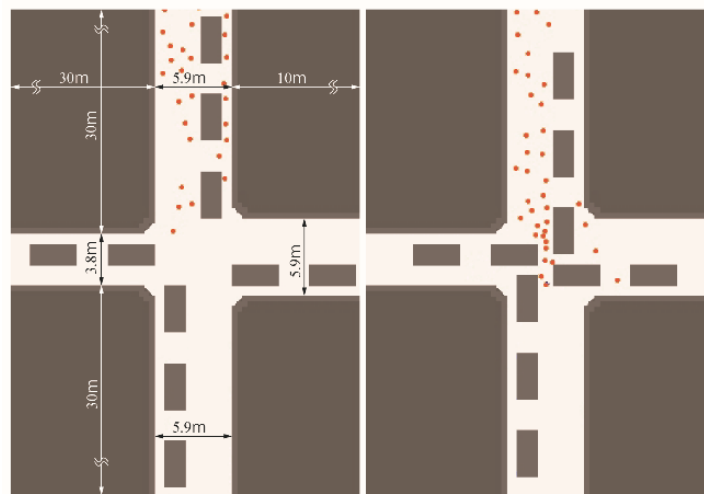


Fig. 5 Layout settings on a crossroad with fixed obstacles and their snapshots in the one-way simulation cases. (Left: Layout 1; Right: Layout 2)

Table 1: Comparisons between experimental data and simulations in evacuation situations.
(Added to [7])

Data in experiment				
Obstacles Ped'n Layout Flow Pattern	Layout1	Layout2	No Obstacle	Max. / Min.
One Way	1.20	1.20	—	1.00
Counter	1.00	0.80	1.10	1.38
Max. / Min.	1.20	1.50	—	
Simulation results				
Obstacles Ped'n Layout Flow Patter	Layout1	Layout2	No Obstacle	Max. / Min.
One Way	1.09	1.04	—	1.05
Counter	1.01	0.87	1.11	1.28
Max. / Min.	1.08	1.20	—	

(Average Waking Speed [m/s])

The fixed obstacles were laid out in three ways: the two obstacle patterns as shown in Figure 5 and one with no layout of fixed obstacles. Two pedestrian flows were prepared: a one-way flow and counter flows. In the one-way flow, one group of agents moved from the north to the south end, and after all of them had left the map, the other group started moving from the south to the north end; in the counter flows, the two groups appeared from the north and south ends concurrently and moved to the opposite ends.

For the five cases created by combining the three fixed obstacle layout patterns and the two pedestrian flow patterns (as the combination of no layout of fixed obstacles and one-way flow are self-explanatory, this case was excluded), the simulation was repeated 10 times for each case, and the average speed of the pedestrian agents was measured.

Table 1 shows the results of the evacuation experiment and simulations run on the reproduction map. The counter flows of the simulations showed a similar tendency to those in the experiment for all patterns (layout 1, layout 2, and no obstacle). In the one-way flow, compared to the experiment, layout 1 and layout 2 had lower values, but the maximum/minimum values were similar. Therefore, we can conclude that the changes to the average speed resulting from the modified pattern combinations were fitted approximated.

3. Pedestrian-vehicle mixed flow simulations

Here, we introduce a simple vehicle agent model, and then explain the simulation of mixed-vehicle flow as an example of the interactions between heterogeneous agents on the UPS.

3.1. Situation setting: Design of an interaction system between heterogeneous agents

Here, let us consider another evacuation situation in which we simulate the mixed flow of light vehicles and pedestrians immediately after an earthquake under the following two assumptions: many pedestrians and few vehicles, and with an application order of micro-motion of Pedestrian (Pd) > Vehicle (Vl). Then, we make every agent model judge other agents' motions based on their current position, assuming that the relative speed is sufficiently slow for both.

3.2. Vehicle agent model in the sASPF project

We developed a vehicle model to simulate pedestrian-vehicle mixed flows. The model included 20 agents, each of which measured 5e wide and 7e long (hereinafter, 2.0 m × 2.8 m vehicle agent). A vehicle agent recognizes other agents, including pedestrians and vehicles, within a forward range of 7e wide and 20e (=8.0 m) long on the sight field grid, and moves by accelerating or decelerating. The vehicle moves straight and the steering wheel is not used. At this time, the upper speed limit is set to 2.4 m/s, indicating a situation where progress is slow, and it is difficult to confirm the road conditions. If there is at least one

obstacle, such as a moving vehicle in this sight field grid, the vehicle will decelerate by $0.98 \text{ m/s}^2 (=1G)$; otherwise it will accelerate by $0.98 \text{ m/s}^2 (= 1G)$.

3.3. Pedestrian-vehicle mixed flow simulations at a crossroads

In this section, we describe simulations on a crossroads map (Fig. 6), which we created by referring to a standard double-lane trunk road. To run simulations under disaster conditions, fixed obstacles representing rubble were laid out on the footpaths. The pedestrian agents appear from the north or south end to maintain a set global density and move towards the south or north end.

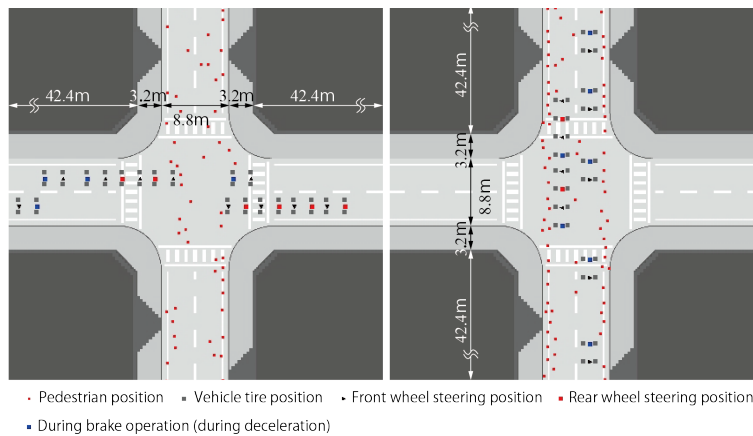


Fig. 6: Snapshots of pedestrian-vehicle mixed flows at a crossroads.
(Left: Cut-across case; Right: Move-along case)

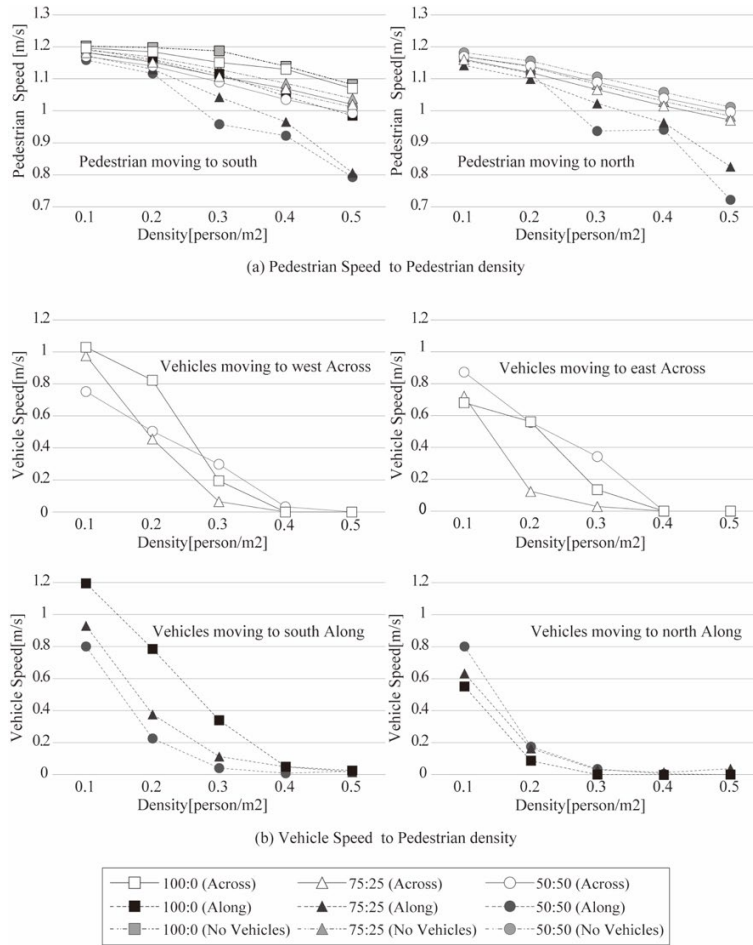


Fig. 7: Density-speed graphs of pedestrians and vehicles in the simulations.

The vehicle agents keep appearing on the map until we reach a maximum of 10 agents. The vehicle agents move in three patterns (Fig. 6): agents appear from the east and west ends and cut across the pedestrian agents; they appear from the north and south ends and move north or south along with the pedestrian agents; or no vehicle agents appear.

The pedestrian agents appearing from the north and south ends were set in three ratios at 25% intervals: 100:0%, 75:25%, and 50:50%. Five patterns of pedestrian agent global density were set from 0.1 to 0.5 agent/m² at 0.1 intervals. Combining these eight patterns with three patterns of the direction of vehicle agent movement resulted in 45 cases, each of which was simulated five times to measure the average speeds of the pedestrian agents and vehicle agents, and the number of vehicle agents that passed the intersection.

Attention was paid to the average speed of pedestrian agents (Fig. 7). When the direction of vehicle agent movement was analyzed, the average speed values were high, in the order of no vehicle, cutting across from east and west, and moving between north and south. In particular, in the case of north/south movement, as the global density of pedestrian agents increases, the range of the average decrease in speed widens. When analyzing the appearance ratio of pedestrian agents, the average speed values tended to be high, in the order of 100:0%, 75:25%, and 50:50%.

Next, we focused on the average speeds of the vehicle agents (Fig. 7). When we compared the vehicles moving north and south, the south-moving vehicles had high average speed values, in the order of 100:0%, 75:25%, and 50:50%. However, the order was reversed in the case of the north-moving vehicles. This was affected by a few factor. For example, in 100:0%, the south-moving vehicles could advance by following the south-moving pedestrian agents, while the north-moving vehicles advancing in the opposite direction to the south-moving pedestrian agents were likely to experience a decrease in their

average speed. In conclusion, our project can show another type of density-speed fundamental diagram in the case of a mixed flow of pedestrian and vehicles.

4. Modelling bicycle agent as the third UMA component

Here, we take the case of a bicycle as an example of another type of agent in UMA and discuss our model.

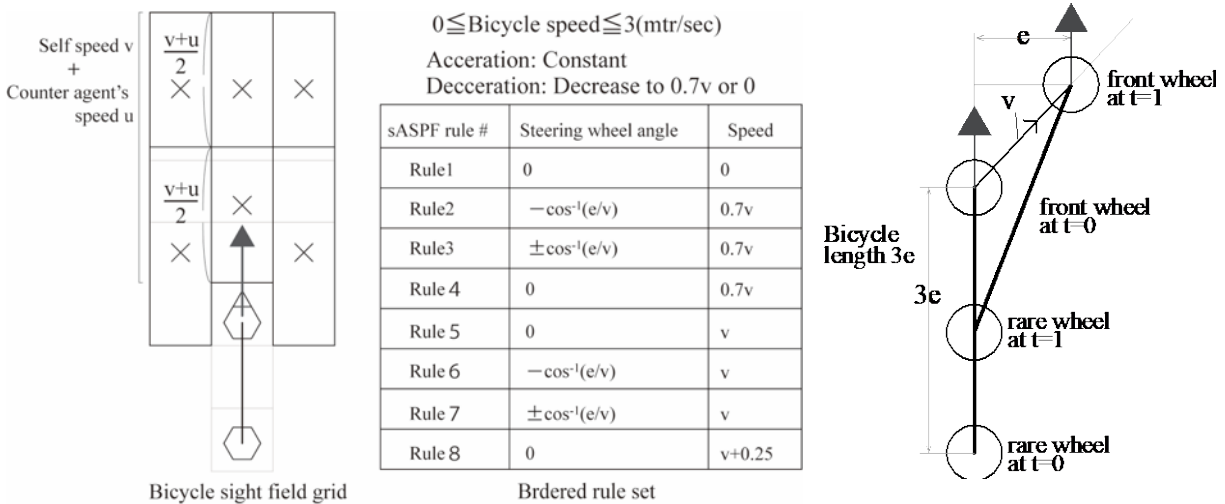


Fig. 8: Bicycle agent model in sASPF project. (Left and center: sight field grid and behavioural rule set; Right: behaviours of front and rear wheels of the bicycle agent)

When modeling our bicycle agent by applying sASPF, we set its centre on the front wheel, over the handle. Under the given advancing direction, the frontward limit of the sight field grid has a length of $2e$ for the pedestrian agent. However, the limit for the bicycle agent is the sum of the agent's own speed and the speed of the other agent, which is the relative speed and is variable for both speeds (Fig. 8). In the case of agents proceeding in the same direction, we only consider their own speeds.

Here, the applied behaviour rule determines the handle angle and the speed. Bicycle agents have speed as an internal state, and we assume a constant acceleration in Rule 8, deceleration in Rules 2, 3 and 4, and stop in Rule 1. Regarding the handle angle, although the direction at the beginning of the step goes straight ahead, it advances by changing the angle according to the action rule and returns to going straight again at the end. The rear wheel follows the front wheel (right in Fig. 8).

5. Situation characterized by implicit interaction assumptions

Here, we discuss the importance of introducing the notion of "situation" when considering the practical uses of simulations dealing with heterogeneous UMAs on UPS.

Although interactions between agents initially include implicit interaction assumptions, these are rarely treated consciously in the case of homogeneous agent flows. However, under heterogeneous agent flows, many interaction assumptions are considered. As these are assumed to characterize various situations, it is necessary to discuss the classification in advance.

In the system consisting of four types of agents of vehicle (VI), bicycle (By), pedestrian (Pd) and wheelchair (Wc), when focusing on many/few vehicles and many/few pedestrians, the four situations (Many, #, Many, #), (Few, #, Many, #), (Many, #, Few, #) and (Few, #, Few, #) can be considered on the 4-tuple of the VI, By, Pd and Wc agents (# means the wildcard). Among these, a typical example of the first is the evacuation situation immediately after an earthquake, the second is a fireworks festival fair

venue, the third is a road in a developing country, and the fourth is a road for both cars and pedestrians in a residential area.

Furthermore, the speeds of these models of transport are in the order vehicles (Vl), bicycles (By), pedestrians (Pd) and wheelchairs (Wc, which assumes elderly people as riders), but in urban pedestrian space in developed countries, the priority of these micro-actions is in the reverse order. This is due to traffic restrictions in daily life, and the manners of individuals. We can describe these situations as (1, 2, 3, 4) and (4, 3, 2, 1) of the priority rank on the 4-tuple, respectively, with the former as Anarchy and the latter as Organized. There are also various intermediate types between these two polar opposite cases, called Designed. If we consider one, two or three agents instead of four types of agents, 64 types of situations ($=24 + 24 + 12 + 4$) can be considered.

Here, it is the priority of micro-action that specifies the characteristics of the interaction system, thus the simulation algorithm is expressed as the priority of classification rank of RSU and the presence / absence of positional prediction of the opposite agent. Position prediction means that, when two opposing relative speeds are greater than a threshold value, the higher priority side determines its own action from the current position of the opponent, while the other side uses the future position, which they predict. If the priority is the same, we predict the position of both. For example, consider a situation in which a car is traveling on a roadway at a high speed and a pedestrian crosses the roadway in front of it. In the case of car priority, the pedestrian side predicts the future position of the car and decides its own movement, whereas the car decides the motion based on the current position of the pedestrian. However, in the case of pedestrian priority, the vehicle side predicts the future position of the pedestrian and decides its own motion, and the pedestrian side decides the motion based on the current position of the car. We used a variable length of sight field grid based on the speed of the bicycle agent in the previous section, but we believe that this is the only possible model representation.

6. Conclusion

We explained the principle and characteristics of the sASPF project, which we are developing as an integrated simulation platform for modelling various urban mobile agents in urban pedestrian space. This project is being developed with urban simulation research in mind.

(1) In the sASPF project, the micro-motions of all UMAs, including pedestrian agents, is calculated by a rule-based system in two-dimensional continuous space. Therefore, it is possible to construct a model that is both practical and computationally efficient. Moreover, according to the performance test, there is no reason why fitting with the measured value within the density of the non-physical contact situations is also inadequate. We carried out theoretical analyses of phase transitions of pedestrian counter flows. The results confirmed that phase transitions occurred for a range of biases in the diagonal stepping probability, from 50:50% to 60:40%, and the global density from 0.4 to 1.4 agent/m².

(2) We also presented an overview of pedestrian-vehicle mixed flow simulations at a crossroads in a disaster slowing situation, as a case of heterogeneous agents. A vehicle agent model was implemented to simulate pedestrian-vehicle mixed flows assuming a disaster situation. The results showed the same tendency for both pedestrian and vehicle agents: the speed of motion decreased as the number of the other agents in the counter flow increased. It is also noticeable that the average speed values are higher when vehicle agents cut across pedestrian agents than when moving from north and south. A vehicle agent moving against pedestrian agents is likely to experience a decrease in its average speed instead of moving past them.

(3) Furthermore, a trial model of a bicycle agent was illustrated as a natural extension of the pedestrian agent in our sASPF project. This bicycle agent is an example of a model for determining the micro-motion based on the relative speed, that is, the predicted position of another agent.

(4) We pointed out that there is an implicit interaction assumption that cannot be avoided when simulating heterogeneous agent flows. On the other hand, the solution principle that we referred to is to determine the order of priority of the micro-actions of various agents according to the situation of the simulation target. When the relative speed threshold is exceeded, the subordinate agent uses the predicted position of the dominant agent to determine their micro-motion. In other words, we discussed the need for

introducing an appropriate interaction system according to each of the situations considered, and the priority of the micro-motion characterizes the "situation" of the simulation target.

The authors do not have space to mention the wheelchair agent in this paper but are planning to publish it to another paper.

Acknowledgements

This work was partially supported by JSPS KAKENHI Grant Number 18H03825

References

- [1] D. Helbing, I.J. Farkas, et al, "Simulation of Pedestrian Crowds in Normal and Evacuation Situations," in *Pedestrian and Evacuation Dynamics*, 2001, pp. 21-58.
- [2] M. Muramatsu, T. Irie, T. Nagatani, "Jamming transition in pedestrian counter flow," *Physica A*, vol. 267, pp. 487-498, 1999.
- [3] M. Fukui and Y. Ishibashi, "Self-Organized Phase Transitions in Cellular Automaton Models for Pedestrians," *Journal of the Physical Society of Japan*, vol.68, no.8 (8), pp. 2861-2863, 1999.
- [4] T. Kaneda, T. Yoshida, Y. He, et al, "Adding Higher Intelligent Functions to Pedestrian Agent Model," in *Pedestrian and Evacuation Dynamics 2008*, pp. 529-535, 2010.
- [5] T. Kaneda and O. Okayama, "A Pedestrian Agent Model Using Relative Coordinate Systems," *Agent-Based Approaches in Economic and Social Complex Systems IV*, vol. 3, pp. 63-70, 2007.
- [6] M. Shomitsu and T. Kaneda, "Simulation Analyses on Phase Transition in Counter Flow Situations by Using a Pedestrian Agent Model with Simplified Behavior Rules," *Aij Journal of Technology and Design*, vol. 23, no. 54, pp. 721-724, 2017-6.
- [7] Firefighting Disaster Prevention Science Center, *Evacuation simulation system R&D report (3)*, pp. 33-43, pp. 135-145, 1983.
- [8] Kozo Keikaku Engineering Inc.: <https://www.kke.co.jp/en/>

An Artificial Neural Network Framework for Pedestrian Walking Behavior Modeling and Simulation

Peter M. Kielar, André Borrmann

Chair of Computational Modeling and Simulation, Technische Universität München
Arcisstrasse 21, Munich, Germany
peter.kielar@tum.de; andre.borrmann@tum.de

Abstract – Movement behavior models of pedestrian agents form the basis of computational crowd simulations. In contemporary research, a large number of models exist. However, there is still no walking behavior model that can address the various influence factors of movement behavior holistically. Thus, we endorse the use of artificial neural networks to develop walking behavior models because machine learning methods can integrate behavioral factors efficiently, automatically, and data-driven. In this paper, we support this approach by providing a framework that describes how to include artificial neural networks into a pedestrian research context. The framework comprises 5 phases: data, replay, training, simulation, and validation. Furthermore, we describe and discuss a prototype of the framework.

Keywords: Pedestrian Simulation, Framework, Artificial Neural Network, Walking Behavior

1. Introduction

The research on pedestrian walking properties identified various influence factors on movement behavior. Researchers apply these findings and develop operational models that describe peoples' walking behavior [1, 2, 3, 4]. In computational crowd simulation, operational models are used as low-level behavior units. These models predict the movement of pedestrians in crowd simulation; thus are concerned with microscopic interactions of pedestrians. Microscopic aspects comprise, for example, how the velocity of pedestrians changes in different density situations. In general, the goal of microscopic behavior simulations is to identify macroscopic (emerging) movement patterns [5, 6] for crowd behavior predictions.

Most walking models define equations to calculate pedestrian movement behavior [7, 8, 9, 10]. Typically, the models' equations are fully designed by the researchers. However, the research on walking behavior discusses various influence factors on movement behavior. The challenging task is to combine all of these behavior aspects into consistent and valid equations that can predict operational behavior accurately. However, contemporary research still did not find the optimal behavior model. The large number of existing walking models in the pedestrian dynamics literature point to this subtle issue. Thus, an individually designed model might not be an optimal solution to model operational behavior. A promising approach to overcome this issue is the application of machine learning methods that derive models based on data. This means that the modeling of the agents' walking behavior is delegated to a machine learning method and is not directly carried out by a researcher. To evaluate this concept, we developed a framework that embeds the artificial neural network (ANN) methodology in the pedestrian research domain. We also provide an example implementation of the framework and an ANN.

2. Related work

This research provides an approach for the application of ANNs in operational behavior modeling. However, literature shows that the application of ANN in operational behavior modeling is not new.

The authors of [12] apply a multi-layer perceptron ANN for training a cellular automaton model. The ANN models the influence of the terrain altitude on the cellular automaton rules. This means that the ANN model alters the probability of choosing a cell. The data that is used to train the ANN was acquired

by a virtual experiment. The input of the ANN is the relative position of the agent as well as the terrain altitude and the cell-coverage in proximity to the pedestrian.

In the research of [11], a multi-layer perceptron ANN is used to model the operational behavior of pedestrians in continuous space for a bidirectional flow at a crosswalk. The input data comprises the features of the agent’s movement and perception. The output of the ANN estimates the horizontal and vertical velocity of a pedestrian agent for the next simulation time step. The training data was acquired via camera and augmented by an artificial agent sensing data. The sensing data comprises the relative distance and velocity of the 5 nearest pedestrians in front of a pedestrian agent.

These papers showed that it is possible to apply ANNs in a pedestrian dynamics environment to simulate operational behavior.

Here, we define a framework that embeds an ANN for walking behavior modeling and simulation. This framework is a useful guideline for pedestrian dynamics researchers that like to include ANNs in their methods. Thus, we are concerned with providing an ecosystem for implementing ANN approaches.

3. Integrating artificial neural networks in pedestrian research

In this section, we provide the details on the developed framework and discuss a prototype implementation of the method. In this context, we also show a case study using data from a laboratory experiment.

3.1. Framework overview

The framework comprises multiple phases. Figure 1 gives an overview of the phases and the process. The first phase is the data phase. In the data phase laboratory or standardized field experiments are conducted to provide pedestrian movement data. The processed data is given to the replay phase. Here, a pedestrian simulation uses the experiment trajectory data and augments it to provide additional information of pedestrians. The augmented data samples are given to an ANN for training. The trained ANN is integrated as operational model into the pedestrian simulator in the simulation phase. The simulator uses the model to realize operational behavior in test cases. In the validation phase, well-known methods for model validation are applied to evaluate the capabilities of the developed ANN model.

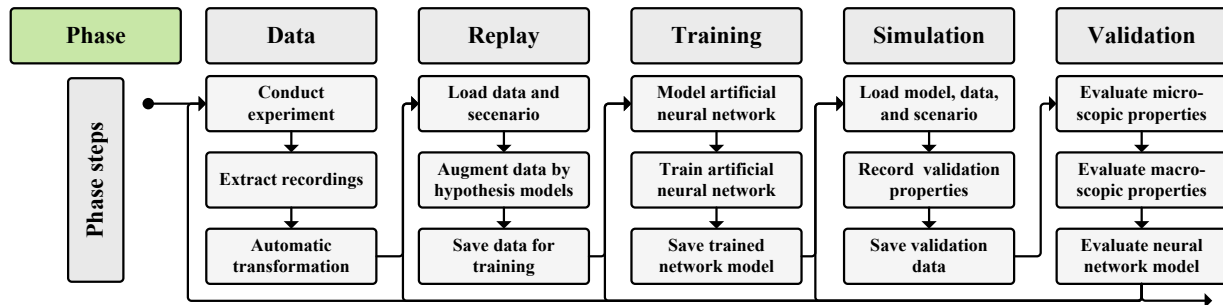


Fig. 1: The workflow of the framework. Five phases provide the basis of the concept. Each phase has three steps and is applied in a different technological and mathematical context. It is possible to restart the process at any given previous phase in case a phase indicates issues.

3.2. Data phase

The data phase comprises experimental studies and the automatic transformation of the experiments’ trajectory data into a format which is processible by pedestrian simulators. For details on pedestrian experiments and video-based trajectory acquisition, we point to [13, 24]. We used the trajectory data of the laboratory experiments UG 140 [13] and applied an automatic transformation for the pedestrian simulator MomentUM [3, 14]. However, some data of these series were omitted because the natural flow of the participants were intentionally changed in the experiment. Such noisy data would influence

the ANN training results negatively. In addition to the participants' movement data, the geometrical layout of the experiment is needed. The layout mostly includes the boundaries and obstacles.

Our tests with the data phase and the training of the ANN showed that we can improve the training phase later on if additional information beyond the participants' trajectories are given. We identified that the shoulder positions, the velocity, and the head-direction can improve the ANN training. Regarding the layout of the experiment, it is highly beneficial to identify the height of obstacles. If the height is not given, the agent might appear to overlap with the walls, which is not true for small obstacles.

3.3. Replay phase: basis

In this phase, the movement of the participants of the laboratory experiments is replayed in a pedestrian simulation. This is done to compute additional information based on the egocentric perspective of the participants. These information are basically data that a person can acquire from his or her visual perception but cannot be captured by a top-down camera. This data augmentation enables to enrich the input data set for training an ANN. For the replay phase, we use the pedestrian simulation framework MomenTUM.

Walking behavior is only a single aspect of the rich characteristic of pedestrian dynamics. For example, we can identify queuing and navigation behavior as additional mechanisms of pedestrian behavior [3, 19]. Operational behavior, which is in focus here, is heavily related to tactical behavior, memory, and perception (see Fig. 2). Therefore, a realistic simulation of operational behavior uses additional information beyond the movement properties that can be extracted by data of a typical movement experiment.

The augmentation of the data is done by classical models. These classical (bottom-up) design models implement assumptions of aspects of pedestrian behavior without machine learning methods. Here, we name these models hypothesis models. In the following section, we give details of the hypothesis models and data augmentations of our prototype implementation of the framework.



Fig. 2: A simplified visualization of the basic building blocks of pedestrian behavior. Operational behavior is directly dependent on the perception, memory, and tactical aspects of this pedestrian behavior architecture [1, 2, 3, 4, 14]. Memory, perception, and tactical information cannot be acquired easily in the data phase.

3.4. Replay phase: hypothesis models

The trajectory data of the experiments is used to guide the movement of the agent through the replay. If not given, we need and compute the current velocity of an agent for each time step. The velocity can be computed using the positions over time. We can extract the head direction of the participations if the laboratory experiments include markers for this. However, if no head-direction is given, the velocity vectors are a good substitution.

A tactical or navigation model define a walking target in the visible space of a pedestrian agent. The walking target comprises at least a target position for the agent [19]. Unfortunately, the walking target cannot be determined from experimental video data because they do not provide the egocentric goal-directed intentions that guide people into a direction. A tactical hypothesis model has to provide an

assumption of how the participants determine a walking target. We apply a graph-based model that includes a graph-generation schema and a routing method [18]. This provides sufficient detail for our purpose. It is important to note that the model should not provide a fixed position as input for an ANN but an egocentric perspective towards the walking target. This is realized by computing the relative angle and distance to the walking target position that is given by the navigation model. A schematic overview of the navigation hypothesis model is given in Fig.3 a).

The perception model should provide perceptual information for each computed time step in the replay phase. Models that apply a sweep-line method are sufficient for this purpose. However, the accuracy of the underlying grid and the stepwise angle change for the sweep have direct influence on the training success later on. Regardless of the realization of the perception model, it must provide egocentric information of the agent view. This would be the distance and the relative direction angle of a perceived object or free area. An overview of the applied perception model is given in Fig. 3 b).

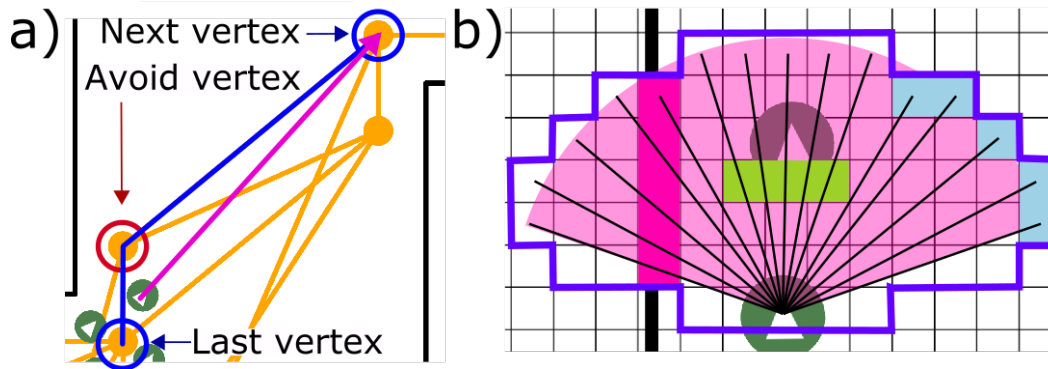


Fig. 3: Examples of how the navigation a) and perception b) hypothesis models. a) the navigation hypothesis model operates on a routing graph (orange). The agent's walking target is the next visible vertex alongside the graph towards the agent's destination (top blue circle). The agent avoids simple vertex hopping (red circle) alongside the graph. This method guides operational behavior to be goal directed. b) the perception hypothesis model is based on a perception arc (light pink) that originates in an agent. However, we avoid numerical inaccuracies and generate a fixed number of perceptual points. Thus, we identify all border cells of a circle. The border cells are the destinations of perception rays that start from the agent's position. If a ray hits a target or its destination it extracts data, e.g. the distance to the collision cell. The parameters of the perception model in our prototype framework is an arc of 120° , a perception distance of 5.0 m, and a cell size of 0.1 m.

3.5. Replay phase: output data

The simulation framework MomenTUM exports the data of the replay phase for each agent and for each time step. All exported data items form part of the training data. We marked the relative heading-change and the velocity magnitude of the training data as training ground truth variables. Thus, the ANN will use the training data as exercise information to predict the ground truth variables. The training data comprises the last velocity, the last heading-change, the current distance to the walking target, and the relative direction to the walking target of an agent. Furthermore, the perception information of the object closest to the agent will be used. Here, the information is the distance and the relative angle to the closest object.

Each data set is generated for each agent and each time step. The time step discretization is 0.04 seconds, a value that is based on the time resolution of the video data. The time step is an important value because it shapes the classification set due to the velocity and heading change measuring points. We tested different time steps in values from 0.08 to 0.52, but could find benefits in higher values; thus, we used 0.04 seconds.

An important aspect of the reply phase is the handling of data that is not available from the experiments. These situations arise when participations are outside of the view of the camera in the experiments. Here, pedestrians are missing in the replay but exist in reality. This means that if a

pedestrian agent in the replay is close to the boundary of the camera range, this agent may miss to perceive other agents that are outside of cameras view. These kind of situation must be avoided for data quality. A solution is to ignore trajectory data points of the experiment that are closer to the camera boundaries as the perception distance of an agent.

3.6. Training phase

For the purpose of applying the ANN in pedestrian dynamics, the input and the output data of the ANN are highly important aspects. We believe that these interfaces incorporate most pedestrian domain-knowledge and are crucial for an ANN to be able to learn pedestrian operational behavior. Thus, the given prototype ANN is a case study of how to approach the application of ANNs in a pedestrian dynamics context and therefore will cover only minor aspects of pedestrian movement behavior.

For our prototype ANN definition, we followed the approach of [11] and modeled a multi-layer perceptron ANN. We used TensorFlow and its Python API [15]. The ANN's goal is to compute a joint classification of each agents' egocentric velocity magnitude and movement direction change. Thus, we did not compute a regression. A regression showed to be highly inaccurate due to noise in the training data. We decided on the hyper-parameter, data processing, and the ANN architecture as follows:

- We normalized the input data of the replay phase in the range [0.0, 1.0].
- The number of training data points for each agent and each time step of the replay data is 6, which define the number of input neurons.
- Based on the data by UG 140 [13], we extracted 38599 training samples that provide a time sampling discretization of the pedestrian walking behavior of 0.04 seconds. Furthermore, we extended the data to 77198 samples by flipping all data regarding the walking axis of each individual agent.
- The number of output neurons is defined by the joint classification of velocity and movement direction change pairs. For our prototype, we define 2 velocity classes and 41 movement direction change classes. However, we ignore all classes that cover less than 0.5% of the data to avoid noise. Thus, we actually have 6 classes, which cover 97.92% of the data and define the number of output neurons.
- Furthermore, we oversampled classes [25] due to imbalanced data.
- The activation function in the last layer is a Softmax function [21]. This function computes the most likely class based on the last hidden layer output and set the value of the output neuron that represents this class to 1.0, otherwise 0.0. The loss value for optimizing the network is computed by a cross entropy that is applied on the Softmax output.
- The number of hidden layers is 2 and the number of neurons for each hidden layer is set to 60.
- The activation function in the hidden layers is a leaky ReLu [20] with alpha and the initial weights between neurons that are connected with these functions are in range of a normal distributed in]0.0, 0.1].
- A bias neuron that is initialized with 0.0 is given for each matrix multiplication between layers.
- We applied 150 epochs, a mini batch size of 1000, and 5% dropout on all connections of the ANN that applied a leaky ReLu activation function. We randomized input data but homogenized the class occurrences in the training and evaluation data. The training and evaluation split is set 90% to 10%.
- We used the ADADELTA Optimizer [23] for the training.

The design and architectural parameters of the applied multi-layer perceptron ANN are the proposed approach to model ANN that is supposed to learn operational pedestrian behavior. This is therefore an example of the wide range of possible network solutions. The literature provides a rich body of research and information of how to train an ANN and which ANN architecture might be useful for specific applications [21, 22]. We point to the literature for further reading as the focus of this paper is to provide a framework that embeds an ANN in a pedestrian dynamics context.

3.7. Simulation phase

The simulation phase comprises the automatic integration of the trained ANN model into a pedestrian simulator and to run test simulations. We used the built-in method of TensorFlow to store the trained ANN model and the TensorFlow Java API to import the model into MomenTUM.

In the simulation phase, a set of standardized test scenarios should be used to calculate validation data for the ANN model. However, for the initial purpose to check whether the ANN model is able to provide basic operational pedestrian behavior, we applied the scenarios of the training data. Here, the trajectory data provides the start positions of the agents in the test simulations. From the starting position of each agent, the ANN will guide the agents' operational behavior. The hypothesis models are used to generate the perceptual and navigation data for each pedestrian for each time step. This data and the movement information of an agent are given to an embedded ANN as input information. The agent's ANN predicts the operational behavior for the next time step by a classification. The simulator translates the predicted class into new velocity magnitude and body rotation for each agent for each time step.

3.8. Validation phase

The validation phase comprises a microscopic and macroscopic validation and applies the data of the trajectory and layout data of scenarios used in the simulation phase.

The microscopic validation checks whether the individual behavior of the pedestrian agents are correct. This includes two aspects. The first aspect is to validate if a pedestrian shows physically impossible behavior. For example, this happens if pedestrian slip through walls or if the body rotation is extreme. The second aspect addresses fundamental pedestrian behavior properties. These are for example whether pedestrian proactively avoid other pedestrians.

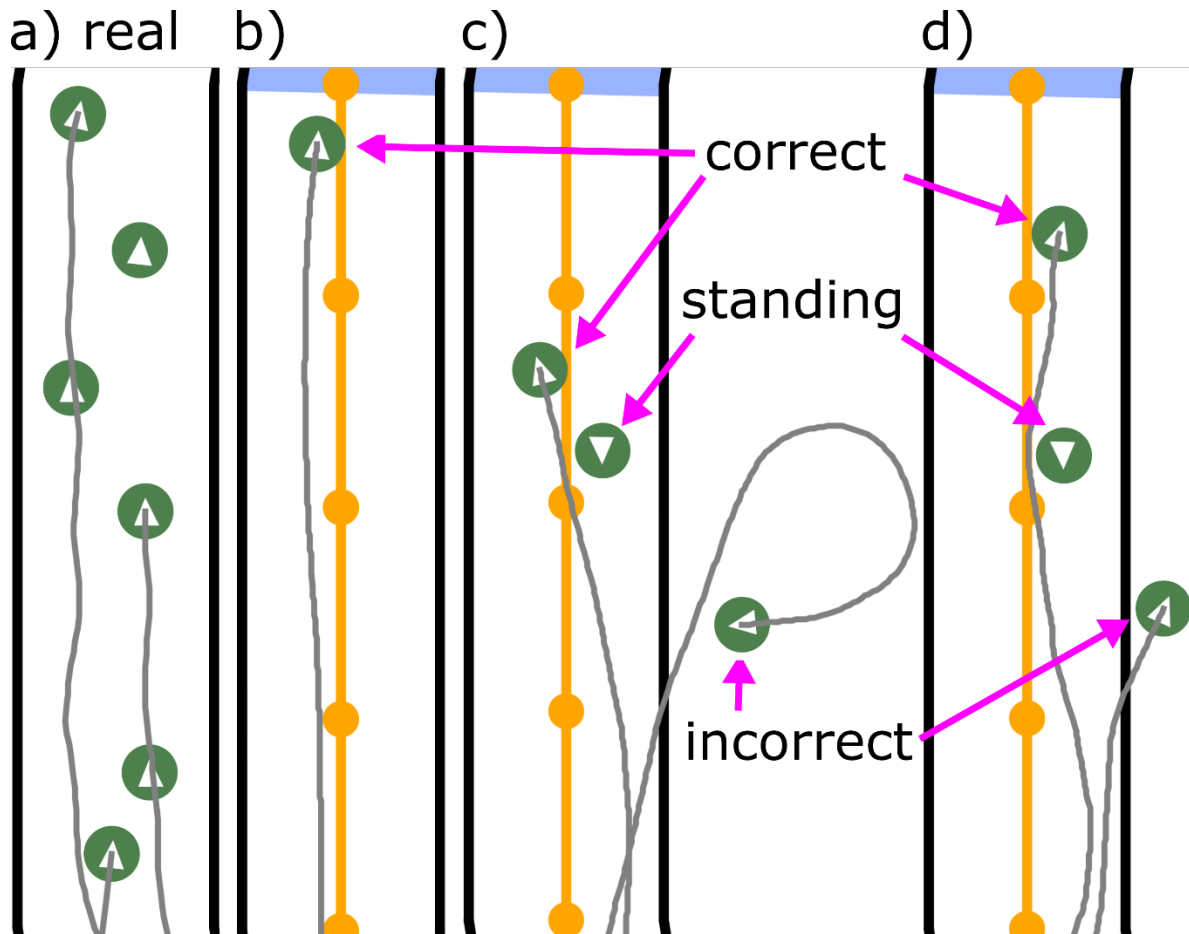


Fig. 5: a) a visualization of the experimental data of UG 140 [13]. b) a single ANN controlled pedestrian walking alongside the corridor. c) two ANN controlled pedestrians walking alongside the corridor and a single pedestrian standing still. Here, the ANN provides corrected behavior for first pedestrian but incorrect for the second. This situations can be seen quite often with the given ANN. d) is similar to c). Here, the situation is reversed, the first pedestrian is capable to avoid the standing person and reach the goal but the other agent behaves incorrect. This indicates that the behavior is not stable but a good starting point for further improvements.

The macroscopic validation is scenario dependent and compares emerging patterns of the simulation and the real pedestrian movement of an experiment. Here, one method is to compare the fundamental diagram that can be extracted by real and simulated trajectory data. Another example is to evaluate whether lane formation occur in the simulation and the experiments.

If the validation of the ANN model does not provide qualitative and quantitative operational pedestrian behavior, one has to repeat the framework process at one of the previous phase. Here, the identification of the root cause of model issues is highly dependent on the experiences regarding the combination of machine learning and pedestrian dynamics. For example, the ANN structure, the experimental data, or the hypothesis models could be insufficient.

In our prototype application of the proposed framework, we evaluated the microscopic properties of the ANN model of Sec. 3.6. Figure 4 shows snapshots of a replay and diverse results for the scenario UG 140 [13]. Some of the predicted trajectories provide realistic behavior but some violate the physical properties of pedestrian walking. We identified that we miss to train the ANN with a large data basis of balanced and standardized trajectory data. This would have improved the results. Nonetheless, we could show that the ANN framework for pedestrian operational behavior modeling and simulation is a promising method.

4. Conclusion, discussion and further research

In this paper, we provided a framework that integrates artificial neural networks (ANNs) into a pedestrian simulation context. The framework gives guidelines of how to embed an ANN based pedestrian walking model into a pedestrian simulation workflow. The framework defines 5 phases: data, replay, training, simulation, and validation. Furthermore, we discussed a prototype implementation of our framework and a model that uses the framework to simulate operational behavior of agents by a data-driven ANN.

The described approach has two important advantages. The first is that researcher can avoid individually designed mathematical models of pedestrian walking. The diverse influence factors on pedestrian walking behavior are complex and a bottom-up defined behavior model might not cover all walking behavior aspects that are hidden in experimental data. Using the developed framework, researchers can delegate the walking behavior modeling to an ANN. The second advantage it that one can define hypothesis models that support the ANN walking model. Hypothesis models augment experimental data as input for the ANN. Thus, hypothesis models provide a method for behavior and cognition hypothesis testing. For example, the perception model that augments the data in the replay phase plays a mandatory role for the ANN to be able to learn and generalize the movement behavior. We could use a perception model that includes attention aspects. This model may improve or worsen the learning capabilities of the ANN because the model may or may not capture important features of pedestrian perception. This will give evidence whether assumptions of the hypothesis model is well-chosen or insufficient for pedestrian dynamics.

We showed that the ANN framework is a promising approach. However, the developed prototype ANN is not reliable and needs improvement. Future research will focus on the application of a broad range of experimental data to further test and improve the ANN framework. The most important aspect of the ANN approach is to have a large data basis of realistic pedestrian trajectories in normal situations. The moderate success of the prototype ANN of this work can be reduced to the limited data and imbalanced data classes. Further, we will also test different hypothesis models and will evaluate ANN architectures for

pedestrian dynamics applications. Another promising improvement is to use eye-tracking methods on the participations in the experiments [17]. This technology will provide additional data and will improve the perceptual and navigational hypotheses. If high quality and automatically evaluable eye-tracking data is given, research could replace the hypothesis models with a machine learning approach.

References

- [1] S. P. Hoogendoorn, and P. H. L. Bovy, „Pedestrian route-choice and activity scheduling theory and models”, *Transportation Research Part B: Methodological*, vol. 38, no. 2, pp. 169-190, 2004.
- [2] M. Bierlaire, and T. Robin, „Pedestrians Choices” in *Pedestrian Behavior: Models, Data Collection and Applications*, H. Timmermans, Ed. Emerald Group Publishing, 2009, pp. 1-26.
- [3] P. M. Kielar, „Kognitive Modellierung und computergestützte Simulation der räumlich-sequenziellen Zielauswahl von Fußgängern“, Ph.D. Dissertation, Technische Universität München, 2017.
- [4] P. M. Kielar and A. Borrmann, „Spice: A Cognitive Agent Framework for Computational Crowd Simulations in Complex Environments“, *Autonomous Agents and Multi-Agent Systems*, DOI: 10.1007/s10458-018-9383-2, 2018.
- [5] D. Helbing, L. Buzna, A. Johansson, and T. Werner, „Self-organized pedestrian crowd dynamics: Experiments, simulations, and design solutions“, *Transportation Science*, vol. 39, no. 1, pp. 1-24, 2005.
- [6] A. Portz, and A. Seyfried, „Analyzing Stop-and-Go Waves by Experiment and Modeling“, in *International Conference on Pedestrian and Evacuation Dynamics*, 2010, pp. 577-586.
- [7] D. Helbing, and P. Molnár. „Social force model for pedestrian dynamics“, *Physical Review E*, vol. 51, no. 5, pp. 4282-4286, 1995.
- [8] M. Moussaïd, D. Helbing, and G. Theraulaz, „How simple rules determine pedestrian behavior and crowd disasters“, *Proceedings of the National Academy of Sciences*, vol. 108, no. 17, pp. 6884-6888, 2011.
- [9] J. Pettré, D. Wolinski, and A.-H. Olivier, „Velocity-Based Models for Crowd Simulation“, in *International Conference on Pedestrian and Evacuation Dynamics*, 2014, pp. 1065-1078.
- [10] V. J. Blue., and J. L. Adler, „Cellular automata microsimulation for modeling bi-directional pedestrian walkways“, *Transportation Research Part B: Methodological*, vol. 35, no. 3, pp. 293-312, 2001.
- [11] Y. Ma, E. W. M. Lee, and R. K. K. Yuen, „An Artificial Intelligence-Based Approach for Simulating Pedestrian Movement”, *IEEE Transactions on Intelligent Transportation Systems*, vol. 17, no. 11, pp. 3159-3170, 2016.
- [12] P. Shao, „A more realistic simulation of pedestrian based on cellular automata,” in *IEEE International Workshop on Open-source Software for Scientific Computation*, 2009, pp. 24-2.
- [13] C. Keip and K. Ries, „Dokumentation von Versuchen zur Personenstromdynamik“, Technical Report, Project Hermes, 2009.
- [14] P. M. Kielar, D. H. Biedermann, and A. Borrmann, „MomenTUMv2: a modular, extensible, and generic agent-based pedestrian behavior simulation framework“, Technical Report, Technische Universität München, 2016.
- [15] M. Abadi et al., „TensorFlow: Large-Scale Machine Learning on Heterogeneous Systems“, Whitepaper, <https://www.tensorflow.org/>, 2015.
- [16] W. Shao and D. Terzopoulos. „Autonomous pedestrians“, *Graphical Models*, vol. 69, no. 5-6, pp. 246-274, 2007.
- [17] S. Schwarzkopf, et al., „What Lab Eye Tracking Tells us about Wayfinding: A Comparison of Stationary and Mobile Eye Tracking in a Large Building Scenario“, in *International Workshop Eye Tracking for Spatial Research in conjunction with COSIT*, pp. 31-36, 2013
- [18] P. M. Kielar, D. H. Biedermann, A. Kneidl, and A. Borrmann, „A Unified Pedestrian Routing Model for Graph-Based Navigation Built on Cognitive Principles“, *Transportmetrica A: Transport Science*, vol. 14, no. 5, pp. 406-432, 2017.

- [19] P. M. Kielar and A. Borrmann, „Coupling Spatial Task Solving Models to Simulate Complex Pedestrian Behavior Patterns“, in *International Conference on Pedestrian and Evacuation Dynamics*, 2016, pp. 229-235.
- [20] A. L. Maas, A. Y. Hannun, and Y. Ng. Andrew, “Rectifier nonlinearities improve neural network acoustic models”, in *Proc. ICML*, vol. 30, no. 1, pp. 3-11, 2013
- [21] C. M. Bishop, *Machine learning and pattern recognition*, Springer, 2006.
- [22] M. A. Nielson, *ANNs and Deep Learning*, Determination Press, 2015.
- [23] M. D. Zeiler, „ADADELTA: An Adaptive Learning Rate Method”, arXiv:1212.5701, 2012.
- [24] S. Holl, „Methoden für die Bemessung der Leistungsfähigkeit multidirektional genutzter Fußverkehrsanlagen“, Ph.D. dissertation, Bergische Universität Wuppertal, 2016
- [25] H. He and E. A. Garcia, “Learning from imbalanced data”, *IEEE Transactions on knowledge and data engineering*, vol. 21, no. 9, pp. 1263-1284, 2009

A Method for Joint Estimation of Homogeneous Model Parameters and Heterogeneous Desired Speeds

Fredrik Johansson

Swedish National Road and Transport Research Institute (VTI)
Box 8072, 402 78 Gothenburg, Sweden
fredrik.johansson@vti.se

Abstract – One of the main strengths of microscopic pedestrian simulation models is the ability to explicitly represent the heterogeneity of the pedestrian population. Most pedestrian populations are heterogeneous with respect to the desired speed, and the outputs of microscopic models are naturally sensitive to the desired speed; it has a direct effect on the flow and travel time, thus strongly affecting results that are of interest when applying pedestrian simulation models in practice. An inaccurate desired speed distribution will in most cases lead to inaccurate simulation results. In this paper we propose a method to estimate the desired speed distribution by treating the desired speeds as model parameters to be adjusted in the calibration together with other model parameters. This leads to an optimization problem that is computationally costly to solve for large data sets. We propose a heuristic method to solve this optimization problem by decomposing the original problem in simpler parts that are solved separately. We demonstrate the method on trajectory data from Stockholm central station and analyze the results to conclude that the method is able to produce a plausible desired speed distribution under slightly congested conditions.

Keywords: Pedestrian simulation, Desired speed, Social force model, Calibration, Estimation

1. Introduction

Microscopic simulation is a powerful tool to evaluate or compare infrastructure design or control strategies. One of its strengths is the ability to explicitly represent the heterogeneity of the pedestrian population in the model. Most pedestrian populations are heterogeneous with respect to the desired speed; the speed that a pedestrian is striving to keep but is often unable to keep due to surrounding pedestrians.

The outputs of microscopic models are sensitive to the value of the desired speed; it has a direct effect on the flow and the travel time in most scenarios, thus strongly affecting results that are of interest when applying pedestrian simulation models in practice. An inaccurate desired speed distribution will in most cases lead to inaccurate simulation results.

The desired speed is often not directly observable, since in any situation with significant congestion, most pedestrians are unable to keep their desired speed. A proxy for the desired speed is the free flow speed; the speed that the pedestrians walk at in absence of any interactions with other pedestrians. The free flow speed is directly measurable, and in most microscopic models the free flow speed of an individual pedestrian is equal to its desired speed. However, since the population present when free flow occurs may have a different desired speed distribution than the population present when congestion occurs, observations of the free flow speed distribution may provide an inaccurate estimate of the desired speed distribution during the congested conditions of interest. This may occur even if the same individuals are present both during free flow and congested conditions due to variations of individual desired speeds over time.

Investigations of pedestrian speeds have been performed since at least the fifties, when controlled experiments were performed and observations in the London Underground were made, resulting in an estimated free flow speed of 1.6 m/s [1]. A modern investigation of a similar kind was performed in Hong Kong, reporting a free flow speed of around 1.3 m/s, but with significant variations between walking

areas with differing characteristics [2]. Numerous similar studies have been performed, see [3] for an overview. A common reference of the free flow speed is [4], who reports a value of 1.34 m/s, which also happens to be the average of the values reported by the studies reviewed by [3]. Measurements of free speed *distributions* dates back to at least the seventies through observations of low density conditions [5]. More recently, the free speed distribution was estimated in controlled experiments, also by only considering low density observations [6], [7]. These desired speed estimates were improved in [3], which corrects for that the data is censored; an estimate based only on free pedestrians in partly congested traffic will be biased since pedestrians with a high desired speed have a larger probability to be constrained. However, this method depends on a classification of observed pedestrians into constrained or freely walking, respectively. For vehicular traffic this classification can be circumvented by considering observations partly censored [8], but this method is hard to apply to pedestrian traffic due to the lack of clearly defined lanes.

In this paper we propose a method to estimate the desired speed distribution by treating the desired speeds as model parameters to be adjusted in the calibration together with other model parameters. The method is based on the calibration methods previously applied in [9]–[11] to calibrate the Social Force Model (SFM) [12]. Also here, we demonstrate the proposed method by calibrating the SFM, but both the proposed method and the previously applied methods can also be used to calibrate similar models.

The optimization problem of the proposed method is similar to the one in [9]: simulations are performed for each observed pedestrian, while letting the surrounding pedestrians move exactly according to the observations. The deviations of the simulated trajectories from the observed ones are used to define the objective of a minimization problem with the model parameters as decision variables.

In [9] the desired speed of each pedestrian is set to the maximum observed instantaneous speed of that pedestrian, while in [10] it is set to a certain percentile of the observed instantaneous speeds of the pedestrian. As noted in [9], this works well for low density condition. However, the desired speed is underestimated when fast pedestrians start to get delayed. A biased estimate of the desired speed may lead to biased estimates also of the other parameters, due to interdependence between parameters; a too small desired speed may for example be partly compensated by lowering the relaxation time.

The method in [11], on the other hand, treats the desired speeds as calibration parameters, adjusting them together with the parameters that are common to all pedestrians. This results in an optimization problem with dimension proportional to the number of observed pedestrians, which dramatically increases the solution time with increasing size of the data set. This was not a problem in [11], due to the use of a data set from controlled experiments with a relatively small number of subjects. However, for naturalistic data sets with thousands of pedestrians the computational cost becomes problematic.

We propose a heuristic solution approach to this optimization problem that decomposes the problem into one problem for the model parameters that are assumed to be constant over the population, here called homogeneous parameters, and a set of one-dimensional problems, one for the desired speed of each pedestrian. These problems are solved alternately until the improvement is negligible. In this way, instead of having a problem with dimension proportional to the number of observed pedestrians, we get a number of one-dimensional problems proportional to the number of pedestrians and a problem with dimension equal to the number of homogeneous parameters. This implies that the method is feasible for large data sets for which the optimization problems would be prohibitively costly to solve directly. Intuitively, this decomposition is possible since the optimal desired speeds are not too strongly dependent on the homogeneous parameters, and the optimal homogeneous parameters are only slightly affected by each desired speed.

2. Method

This paper presents a method to jointly estimate homogeneous parameters and heterogeneous desired speeds. The method is expected to be applicable for most microscopic models with continuous space representation, but for concreteness and since the exact definition of the desired speed depends on the model considered, a specific version of the SFM is considered.

2.1. Simulation model

The simulation model considered in this study is based on the version of the SFM presented by [9]. The acceleration $\ddot{\mathbf{x}}_i$ of agent i is given by a sum of forces dependent on the surroundings,

$$\ddot{\mathbf{x}}_i = \frac{1}{\tau}(\mathbf{v}_i - \dot{\mathbf{x}}_i) + \sum_j \frac{1 + \cos \varphi_{ij}}{2} \mathbf{F}_{ij}, \quad (1)$$

where the desired velocity \mathbf{v}_i , is given by some route choice model or as input data; φ_{ij} is the angle between the direction of motion of the affected agent i and the direction toward the affecting agent j . When applying the model in simulations, a stochastic term is usually included in addition to the systematic terms above; however, only the systematic effect is calibrated, in line with [9]. Also, a force from static obstacles is necessary to include, however, the observed area does not include any obstacles, see section 3. The social force, \mathbf{F}_{ij} , exerted on agent i by agent j is given as the gradient of a potential V of the form

$$V = F\sigma \exp\left(-\frac{1}{2\sigma} \sqrt{\left(r_{ij} + \left|\dot{\mathbf{r}}_{ij} T\right|\right)^2 - \left(\dot{r}_{ij} T\right)^2}\right), \quad (2)$$

where σ is the range scale and F the strength of the force, T is the anticipation time, and \mathbf{r}_{ij} the relative position of the affecting agent. In total, this model contains five parameters: the relaxation time τ , the social force strength F , the social force range scale σ , the anticipation time T , and the desired speed v .

2.2. The calibration problem

For application of microscopic pedestrian simulation models for predictive purposes, the goal of the calibration is in general to find parameter values that result in a model that can predict traffic under conditions and environments that are similar, but not identical, to some observed reference situation. To achieve this the parameters are adjusted such that the output of the model becomes sufficiently similar to the observed reference traffic. We call this the calibration of the model, and this is the focus of the present study, while the subsequent test of the predictive power of the model through comparison with independent data, that is the validation, is not considered.

As noted above, the model has five parameters that correspond to various properties and preferences of the simulated pedestrians. However, some, or all, of these properties and preferences may vary over the population, so in principle we would like to estimate the multivariate distribution of the parameters over the population. This is, however, an immense task requiring large amounts of data. We will here undertake the simpler task of estimating the distribution of only the desired speed, under the assumption that the remaining parameters are homogeneous, that is all agents have the same value of the parameters. An important observation is that the distribution of the desired speed under the assumption of homogeneous remaining parameters is not necessarily the same as the marginal distribution of desired speed when all parameters vary over the population.

We formulate the calibration problem as an optimization problem, minimizing some error function that quantify the difference between the model output and the reference data,

$$\min_{v_i, \theta} \sum_{i=1}^N E_i(v_i, \theta), \quad (5)$$

where N is the number of trajectories in the data set, E_i is an error function that quantify the difference between the simulated trajectory of agent i and the observed trajectory of the corresponding pedestrian, and θ is the set of homogeneous parameters, that is, $\theta = (\tau, F, \sigma, T)$.

A significant difficulty here is that the dimensionality of the solution space of problem (5) is $N + 4$, that is, the dimensionality is proportional to the number of observed trajectories. For a modest number of observed trajectories problem (5) is tractable, but as the number of trajectories in the data set increases the problem quickly becomes computationally too costly to solve directly.

2.3. Objective function

The error function E_i quantify the fit of individual simulated trajectories to the observed data. Many versions have been used in the literature; here we consider the integrated Euclidian distance between the observed trajectory and the trajectory obtained by simulating an agent with the same initial conditions and environment as the observed pedestrian. That is, the agent is simulated in presence of agents moving exactly according to the observed trajectories. This is similar to the approach taken by e.g. [9], [10]. Furthermore, it is assumed that the desired destination of the agent is the end of the observed trajectory. The simulation is executed for a certain time T_{sim} , and is then restarted with the agent reset to a position at the observed trajectory. This is repeated K_i times, to avoid promoting parameter values that steer back the agent toward the observed trajectory from a position deviating from it.

The error function thus becomes

$$E_i(v_i, \theta) = \sum_{k=0}^{K_i} \int_{t_i^k}^{t_i^k + T_{sim}} \left| \mathbf{x}_i^k(v_i, \theta; t) - \mathbf{X}_i(t) \right| dt, \quad (6)$$

where $\mathbf{x}_i^k(v_i, \theta; t)$ and $\mathbf{X}_i(t)$ are the simulated and observed positions at time t , respectively; and $t_i^k, k = 0, 1, \dots, K_i$ are the starting times for each of the short simulations.

2.4. Optimization method

As mentioned above, problem (5) is computationally too costly to solve directly for large data sets. This is due to the combination of the large dimensionality of the solution space and that the objective function is very unlikely to be convex, likely to have multiple local minima, and is likely to be non-smooth and even discontinuous at some points. We therefore propose a method similar to the coordinate descent class of optimization methods, see e.g. [13], to solve the problem.

The proposed method can be summarized as:

0. Obtain initial estimate of the desired speed distribution by heterogenous calibration.
1. Minimize the sum of the error functions with respect to the homogeneous parameters θ , keeping the desired speeds at the values obtained in previous step.
2. Separately minimize each error function E_i with respect to v_i , keeping the homogeneous parameters at the values obtained in previous step.
3. Go to step 1 if improvement in the error is above some threshold.

In the initial step, step 0, the problems

$$\min_{v_i, \theta_i} E_i(v_i, \theta_i), \quad i = 1, 2, \dots, N, \quad (7)$$

are solved separately. This gives an initial estimate of the desired speed distribution. The values of θ_i , on the other hand are highly uncertain, since most trajectories separately contain too little information to obtain meaningful values of all the parameters. We also use the solutions of (7) to remove any trajectories

with a value of $E_i^* = \min_{v_i, \theta_i} E_i(v_i, \theta_i)$ above a threshold corresponding to an average deviation of 0.1 m from the observed trajectory from further use in the calibration procedure, since such trajectories are likely affected strongly by factors external to the model. If included, these trajectories could promote values of the parameters that compensate for such external effects. The threshold was chosen rather high to only sort out strongly deviating trajectories.

In step 1, the problem

$$\min_{\theta} \sum_{i=1}^N E_i(v_i, \theta), \quad (8)$$

is solved, with v_i according to the result of the previous iteration of step 2 (or step 0 if it is the first iteration). This problem has a computationally costly objective function requiring the simulation of each of the agents representing the observed pedestrians, and the solution space has a dimensionality equal to the number of homogeneous parameters; four in the case of the model used as an example here. This makes problem (8) a costly problem, especially for more complex (realistic) models with more parameters. However, the calculation of the objective is suitable for parallelization since it is a sum. The result of solving problem (8) is a set of values for the homogeneous parameters θ .

Step 2 consists of solving the set of N one dimensional problems

$$\min_{v_i} E_i(v_i, \theta), \quad i = 1, 2, \dots, N, \quad (9)$$

where the homogeneous parameters θ have the values obtained from step 1. These problems are one dimensional and can be solved in parallel, and thus computationally cheap compared to problem (8) and if treated carefully it is likely that the global minimum of each problem can be found.

Since the objective function of the problem for the homogeneous parameters is likely to contain discontinuities (when a small shift in the value of a parameter leads to that the agent passes another agent on the other side compared to without the parameter shift), a derivative free optimization algorithm is preferable. In the demonstration of the method we apply a genetic algorithm in line with [9]–[11], since this also can handle the existence of a large set of local minima.

The advantage of the proposed method over trying to directly solve problem (5) is that it reduces the hard problem (5) to the much simpler problems (7-9). However, there is no guarantee that the method will find the global minimum of problem (5), so careful analysis of the results is required to check that the results are reasonable.

3. Case

We now demonstrate the proposed method on trajectory data collected at Stockholm central station during the afternoon peak through manual annotation of video recordings [14]. The annotation was made by estimating the center of mass of the pedestrian by the point half way between their feet when they were maximally separated or together. This annotation method almost completely removes the swaying problem encountered when tracking the heads of the pedestrians but is slightly more labor intensive.

The observed area is approximately four by six meters, located in the middle of a wide passage, with dominating flows in the direction along the longer sides of the observed area. There are no fixed obstacles in, or directly adjacent to, the observed area. The data consists of 1841 trajectories, of which 1705 remain after the filtering related to equation 7, and the flow aggregated over 15 min intervals varies in the range 1980-3960 pedestrians per hour. To improve the solution time of problem (8), bounds on the homogeneous parameters are introduced according to: $\tau \in [0.01, 2]$ s, $F \in [0.01, 5]$ m/s², $\sigma \in [0.01, 3]$ m, $T \in [0, 3]$ s.

3.1. Results

The result of the calibration in terms of the optimal values of the homogeneous parameters are given in table 1, together with corresponding values from two similar studies, and the resulting desired speed distribution is presented in figure 1. The estimated parameters do not deviate strongly from the results of the previous studies. The anticipation time estimated here is a bit high compared to the other studies and it seems to be compensated by a lower value of the range scale of the social force. The mean of the desired speed distribution is 1.25 m/s, its support is between 0.46 m/s and 3.0 m/s, and its standard deviation is 0.29 m/s.

Table 1: Estimation results from the present study and from the literature for comparison.

Study	τ [s]	F [m/s ²]	σ [m]	T [s]
This study	0.72	0.58	0.45	2.0
Johansson et al. (2009) [10]	0.25	0.59	0.60	1.3
Zanlungo et al. (2011) [11]	1.2	0.80	0.62	1.7

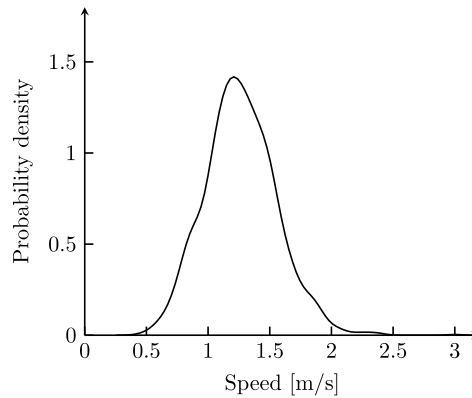


Fig. 1: A kernel density estimate of the estimated desired speed distribution.

3.2. Analysis

Since there is no proof that the proposed method converges to the global solution of problem (5), some analysis of the solution is provided here. In figure 2 the solution progress of the genetic algorithm used to solve problem (8) is displayed for the first, second, fifth and last iterations of the proposed method. As can be seen, 50 generations seem sufficient for the genetic algorithm, and the progress after the second iteration of the procedure is negligible.

To the right in figure 2 the sensitivity of the objective functions to perturbations in each of the homogeneous parameters around the best found solution is presented. The objective is clearly sensitive to perturbations in all parameters except the anticipation time. That the data contain limited information on the anticipation time is expected due to the size of the observed area. If two agents are walking toward each other, each at a speed of say 1.3 m/s, and the anticipation time is 2 s, the agents will start reacting to each other at a distance approximately equal to the length of the observed area.

The clear increase of the objective in the direction of each homogeneous parameter is an indication that the procedure may indeed have found the optimum, but it is far from certain. Also, even though the increase is clear it is rather small, indicating that either the data only contain limited information on the parameters, or that the parameters really should be heterogeneous over the population. In the case of strong heterogeneity over the population, the found solution would be a compromise and a shift in either direction would improve the fit for some trajectories and worsen it for others, thus giving a relatively flat objective.

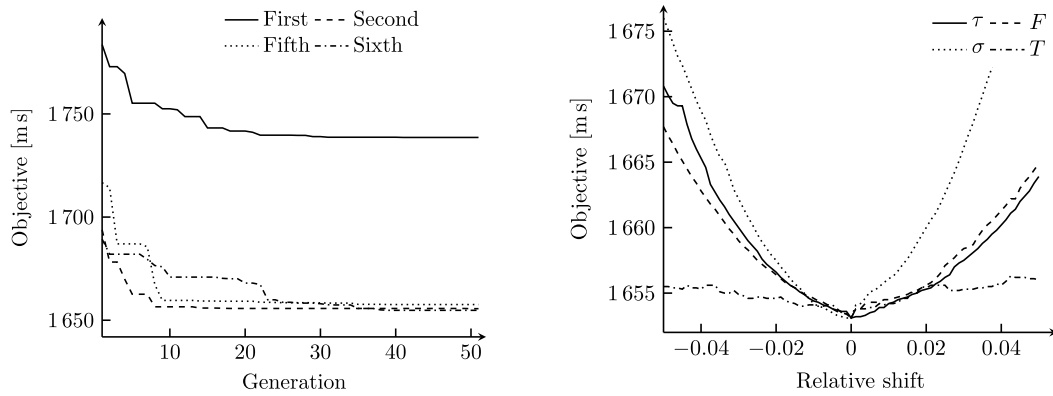


Fig. 2: Left: The solution progress of problem (8) for the first, second, fifth, and last iteration of the proposed solution procedure. Right: The sensitivity of the objective function to changes in the homogeneous parameters. The changes are relative to the widths of the feasible interval for each parameter.

To investigate the interdependence between the desired speed and the homogeneous parameters, the relative change in the solutions of a sample of the problems (9) to changes in each of the homogeneous parameters from the best found solution are presented in figure 3. Note that the presented relative change in the desired speed is the absolute relative change. This shows that the estimated desired speed indeed is dependent on the values of the homogeneous parameters, at least for some of the trajectories, even though this dependence is rather weak.

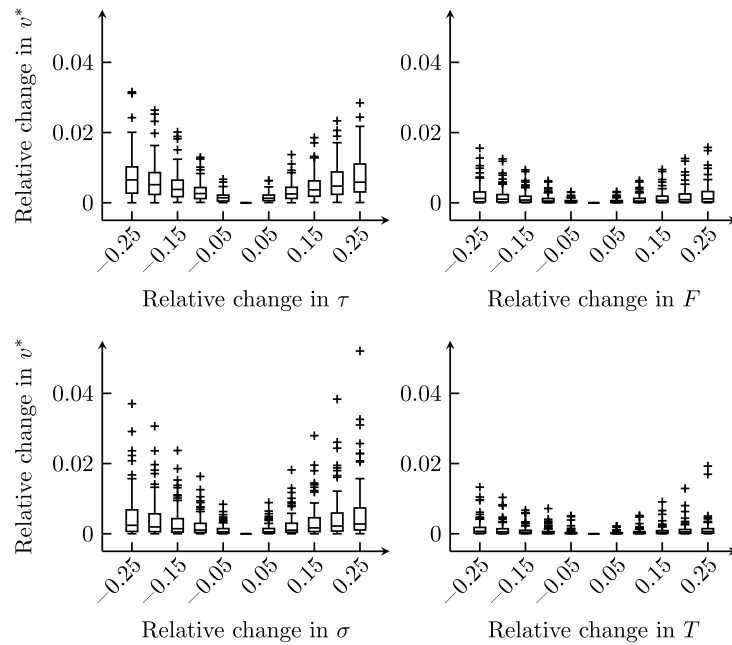


Fig. 3: The sensitivity of the estimated desired speed, of a random sample of 100 pedestrians, to changes in the homogeneous parameters.

The dependence is clearly stronger for the relaxation time and the range scale of the social force, than for the social force strength and the anticipation time. This seems reasonable, since an agent with a high value of the desired speed will tend to perform smaller evasive maneuvers than an agent with a low

value of the desired speed, due to the stronger desired force for a given directional change due to an interaction with another agent. A similar effect is obtained by decreasing the relaxation time or the range scale of the force, so it is reasonable to expect an interdependence between the desired speed and these two parameters.

5. Discussion and conclusions

We conclude that the method is able to estimate a desired speed distribution in slightly congested conditions that seems plausible, while further studies are needed to evaluate the accuracy and robustness of the estimation of the remaining, homogeneous, parameters. Also, it may be worth noting that the proposed method relies heavily on the use of individual trajectories, and it is hard to see any version of the method that does not, and the method thus has the drawbacks of any trajectory-based method. There is a risk that observed pedestrians close to the border of the observed area might be affected by pedestrians outside the observed area. However, this risk is reduced by removal of trajectories deviating too strongly after the solution of eq. 7. An important topic for future research is to verify the method against synthetic data and test for how high densities it is capable to estimate the desired speed distribution.

Acknowledgements

The research presented in this paper was funded by the Swedish Traffic Administration (TRV 2013/13329 and TRV 2016/32495).

References

- [1] B. Hankin and R. Wright, "Passenger flow in subways," *OR*, vol. 9, no. 2, pp. 81–88, 1958.
- [2] W. H. Lam and C. Cheung, "Pedestrian speed/flow relationships for walking facilities in Hong Kong," *Journal of transportation engineering*, vol. 126, no. 4, pp. 343–349, 2000.
- [3] W. Daamen, "Modelling Passenger Flows in Public Transport Facilities," Ph.D. dissertation, TU Delft, 2004.
- [4] U. Weidmann, "Transporttechnik der fußgänger," IVT, Institut für Verkehrsplanung, Transporttechnik, Strassen-und Eisenbahnbau, 1992.
- [5] L. Henderson, "The statistics of crowd fluids," *Nature*, vol. 229, pp. 381–383, 1971.
- [6] W. Daamen and S. P. Hoogendoorn, "Controlled experiments to derive walking behaviour," *European journal of transport and infrastructure research EJTIR*, 3 (1), 2003.
- [7] W. Daamen and S. P. Hoogendoorn, "Experimental research of pedestrian walking behavior," *Transportation Research Record: Journal of the Transportation Research Board*, vol. 1828, no. 1, pp. 20–30, 2003.
- [8] S. Hoogendoorn, "Unified approach to estimating free speed distributions," *Transportation Research Part B: Methodological*, vol. 39, no. 8, pp. 709–727, Sep. 2005.
- [9] A. Johansson, D. Helbing, and P. K. Shukla, "Specification of the social force pedestrian model by evolutionary adjustment to video tracking data," *Advances in Complex Systems*, vol. 10, no. SUPPL. 2, pp. 271–288, 2007.
- [10] A. Johansson, "Data-Driven Modeling of Pedestrian Crowds," Ph.D. dissertation, Technische Universität Dresden, 2009.
- [11] F. Zanlungo, T. Ikeda, and T. Kanda, "Social force model with explicit collision prediction," *Europhysics Letters*, vol. 93, no. 6, p. 68005, 2011.
- [12] D. Helbing and P. Molnár, "Social force model for pedestrian dynamics," *Physical Review E: Statistical, nonlinear and soft matter physics*, vol. 51, pp. 4282–4286, 1995.
- [13] S. J. Wright, "Coordinate descent algorithms," *Mathematical Programming*, vol. 151, no. 1, pp. 3–34, Jun. 2015.
- [14] M. Lagervall and S. Samuelsson, "Microscopic Simulation of Pedestrian Traffic in a Station Environment: A Study of Actual and Desired Walking Speeds," Master's Thesis, Linköping University, Communications and Transport Systems, The Institute of Technology, 2014.

Analysis on Alighting and Boarding Movement Laws in Subway Using Modified Social Force Model

Feng CHEN^{1,2}, Yongxin GAO³, Zijia WANG⁴, Yan LIU⁵

^{1,3-5}School of Civil Engineering, Beijing Jiaotong University
Beijing, China

First author: fengchen@bjtu.edu.cn; second author: 13115312@bjtu.edu.cn

²Beijing Engineering and Technology Research Center of Rail Transit Line Safety and Disaster
Prevention

Beijing, PR China

Abstract - This paper presents a multi-agent simulator based on social force model to simulate each passenger's boarding and alighting behavior both in a train and on a platform seamlessly. Passengers can be divided into three types: to board, alight and stay in train. They have different individual attributes and follow different walking rules. Due to the characteristics of subway environment and passengers' behavior in boarding and alighting, some adjustment and improvement were made to the basic social force model: (1) In some cases during the process of boarding and alighting, the driving force targeting to destination needs to be doubled, and the repulsion force between two agents needs to be reduced. (2) Passengers who stay in the train show quite different movement from the usual pedestrian. They usually want to remain still, unless they are in front of the door. To describe their behaviors, we introduced a tangent detour force. The scope of the interaction between agents is extended and some passengers out of the visual field also should be counted. (3) Divide the repulsive force between an agent and an obstacle into the frontal force and convex corner force. These two forces have different spheres of influence and calculation methods. The agents could exhibit reasonable intelligence and diversity during alighting and boarding.

Keywords: multi agent; micro-simulation; alighting and boarding movement; subway station; social force model

1. Introduction

Passengers' boarding and alighting is an inevitable event in a subway system. With the short departure interval of trains (less than 2 minutes in some lines), limited dwell time and large passenger flow, a well-ordered organization of boarding and alighting is essential to guarantee the trains' departure without delay.

The existing research mainly focused on the survey and statistics of time [1-4], but did not cover the influencing factors and mechanisms of boarding and alighting. In addition, there is insufficient attention to modeling the process of alighting and boarding. [5] modeled this process by Cellular Automata Model, but the passengers who stay in the car were not taken into consideration. And due to the mesh generation of the CA model, the passengers' walking path is very mechanical, which was far from the actual situation. [6, 7] did similar work by the Potential Model, but failed to fully describe the behavior characteristics of different passengers.

To solve these problems, this paper presents a multi-agent simulator based on social force model to simulate each passenger's boarding and alighting behavior both in a train and on a platform seamlessly. Passengers can be divided into three types: to board, alight and stay in train. They have different individual attributes and follow different walking rules. The agents could exhibit reasonable intelligence and diversity during alighting and boarding.

2. Model

2.1 Passenger behaviour during alighting and boarding

There are three components of passengers in the model: the alighting passenger moving from the car to the platform, the boarding passenger moving from the platform to the car through the doors, and the staying on-board passengers (through-standees).

The whole process of alighting and boarding can be divided into four stages.

Stage I : Before a train arrives at a station. The alighting passengers queue up beside the door at the platform, and the passengers get ready to get off and move towards the door.

Stage II : A train arrives at the station and the door opens, alighting passengers start to get off while boarding passengers wait in queue beside the door. This stage will last until the last alighting passengers get out of the train.

Stage III: The boarding passengers start to get on.

Stage IV: The door closes and the train runs to the next station. The boarding passengers and the through-standees may adjust their positions in the train slightly for comfort. Then, they will go into a balanced state.

It is also a common phenomenon that the boarding passengers crowd around the door, hurrying to board, and hamper alighting ones. So, stage 2 and 3 may have some overlap, or even run simultaneously.

2.2 Social force model

According to the social force model (SFM), the system is updated at every time step and each of the passengers in simulation system can move to a new position at each discrete time step $t \rightarrow t+1$ according to a driving force. In the following, we describe a social force model for pedestrian motion dynamics by considering personal motivations and environmental constraints.

2.2.1. Desired Force

Desired force reflects the desire of a passenger to move to a target. It can be defined as Equation 1.

$$\vec{F}_{i,t}^{\text{seek}} = m_i \frac{1}{\tau} (v_i^0 \vec{e}_{i,t} - \vec{v}_{i,t}) \quad (1)$$

where $\vec{F}_{i,t}^{\text{seek}}$ the desired force of agent i at time t , m_i is the mass, v_i^0 is the velocity that the pedestrian i wants to achieve, $\vec{e}_{i,t}$ is the normalized vector pointing to the direction where the pedestrian i wants to go, $\vec{v}_{i,t}$ is the pedestrian current velocity, and τ is the time relaxing constant.

The boarding passengers would be driven by this force only in stage III; the alighting passengers would be driven from stage II, until they leave the platform. It is assumed that the through-standees are not driven by a desired force in the train. But one case is exceptional. If a through-standee was located near the door, he would be greatly disturbed by the alighting and boarding passengers. Therefore, for comfort, he would take the initiative to change his position so that other passengers can get on and off smoothly. Therefore, a restricted zone is set up in front of each door inside the train. The through-standees would be driven by a desired force when they enter the restricted zones.

In case of huge amount of passengers, it may be difficult to get off/on and sometimes passengers need to surge forward to achieve their goals. To reflect their strong wishes to get off/on, the desired force should be modified as equation 2 in the following two cases: (1) the desired force of an alighting passenger should be doubled from Stage II until he goes out of the car and leaves the door with a distance of 0.5m. The distance of 0.5m is taken because of the gap between the train and the platform, and the passenger's body size. (2) The desired force of a boarding passenger should be doubled when he is near the door, that is, in a range of 0.5 m outside the door and 0.125 m inside the door.

$$\vec{F}_{i,t}^{\text{seek}} = 2 * \vec{F}_{i,t}^{\text{seek}} \quad (2)$$

2.2.2. Social Force

In SFM, the exclusive force between pedestrians, $\vec{F}_{i,t}^{\text{social}}$, is expressed as a net force of the psychological exclusive force, $\vec{F}_{i,j,t}^{\text{social repulsive}}$, the physical extrusion pressure, $\vec{F}_{i,j,t}^{\text{pushing}}$, and the friction force, $\vec{F}_{i,j,t}^{\text{friction}}$, as shown in equation 3. The latter two exist only when pedestrians i and j have physical contact. The psychological repulsion is modified with density and direction, as shown in equation 4 and 5.

$$\vec{F}_{i,t}^{\text{social}} = f_{\text{density},i} * \sum f_{\text{direction},i,j} * \vec{F}_{i,j,t}^{\text{social repulsive}} + \sum \vec{F}_{i,j,t}^{\text{pushing}} + v_{ij,t}^{\tau} \sum \vec{F}_{i,j,t}^{\text{friction}} \quad (3)$$

$$f_{\text{density},i} = 0.3(1 - D_{i,t}) \quad (4)$$

$$f_{\text{direction},i,j} = \lambda + 0.5(1 - \lambda)(1 + \cos \alpha_{t,i,j}) \quad (5)$$

where $f_{\text{density},i}$ and $f_{\text{direction},i,j}$ are the correction factor of density and direction, $v_{ij,t}^{\tau}$ is the relative velocity in tangent direction of passengers i and j , λ is direction weight, $\alpha_{t,i,j}$ is the angle between the current position of passengers i, j and the current target point of pedestrian i . $D_{i,t}$ is the utilization of space around pedestrian i , $D_{i,t} = \sum_{k=1}^{N_{i,t}} A_k / A_i^{\text{visual}}$, it is the ratio of total area of passenger in the vision field and the area of vision field (A_i^{visual}), $D_{i,t} \leq 1$. The number of passengers in the vision field is $N_{i,t}$ and the horizontal projection area of pedestrian k is A_k .

The alighting passenger needs to cross through the waiting boarding passengers, who are lined up on both sides of the door. There is a narrow space left for alighting passengers, so they have less psychological exclusion with the queued boarding passengers. The waiting passengers on both sides can be regarded as a virtual wall and the psychological exclusive force between an alighting passenger i and a boarding passenger in queue j could be set as zero in the direction parallel to the train. In the direction perpendicular to the train, the psychological exclusive force should be halved, as shown in equation 6.

$$\begin{aligned} F_{y,i,j,t}^{\text{social repulsive}} &= 0 \\ F_{x,i,j,t}^{\text{social repulsive}} &= F_{x,i,j,t}^{\text{social repulsive}} / 2 \end{aligned} \quad (6)$$

The carriage is always crowded, moving slowly, and it is normal to make physical contact with other passengers. So passengers have reduced expectation of personal space. The social force works in a much smaller scope, with the view angle of 180 degree and the radius of 0.5m, as the blue region in Figure 1a.

In addition to the passengers in the vision field, other passengers (the red agent in Figure 1a) who have physical contact with passenger i also make a social force, though they are out of the vision field.

Sometimes, a through-standee may get in the way of an alighting/boarding passenger behind him. In real life, the alighting/boarding passenger would remind the through-standee by physical contact or verbal communication. In order to solve this dilemma, the range of social force for a through-standee is expanded to 0.3 m behind him, as shown in Figure 1b.

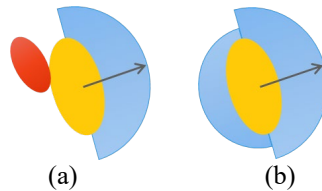


Fig. 1: The scope where social force worked

2.2.3. Centripetal Force

Deadlock occurs when a through-standee and an alighting passenger are in some special relative position. To solve this problem, the centripetal force (equation 7) is introduced in this paper.

Agent i (the red one in Fig. 2) would make a tangential detour driven by the centripetal force if agent j (the yellow one in Fig. 2) is in the current walking area of agent i and the distance of agent i, j is smaller than 0.5m.

In summary, a passenger could be driven by an exclusive force from other passengers, and sometimes a centripetal force as well as.

$$\vec{F}_{i,t}^{\text{centri}} = m_i * v_{i,t}^2 / r_{i,j} \quad (7)$$

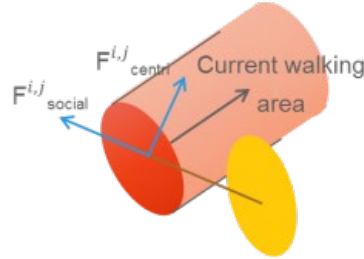


Fig. 2: Centripetal force

2.2.4. Wall Force

According to the relative position of a passenger and the walls, the repulsive force between them should be calculated in different ways. In the first case, passenger i is close to and in front of a wall (agent 1,2,3 in Fig. 3a), he would be driven by a repulsive force $\vec{F}_{i,t}^{\text{wall_front}}$, defined in equation 8. Similar to social force, the working scope of wall force is less than other scenes such as a passage. In our model, we set it as 0.3m.

In the second case, passenger i is close to a convex corner of an obstacle (agent 4 in Fig. 3a), the repulsive force could be defined as equation 9. In a carriage, such convex corners are the lateral corners of seats. The detour repulsive force has not been considered in other SFM. This can cause a larger overlap between the agent and the seat in a crowded carriage, as shown in Fig. 3b, which is unrealistic. As observed in metro trains, passengers show weak rejection to the seat corner, and they often walk close to such corner. Therefore, the detour repulsive force works with the distance of 0.2m.

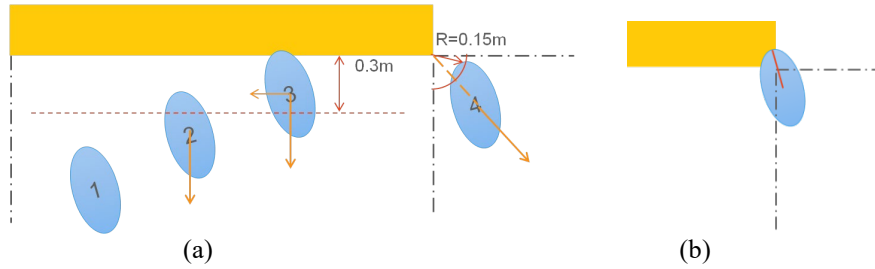


Fig. 3: Centripetal force

$$\vec{F}_{i,t}^{\text{wall_front}} = \vec{F}_{i,w,t}^{\text{social repulsive}} + \vec{F}_{i,w,t}^{\text{pushing}} + v_{i,w,t}^{\tau} * \vec{F}_{i,w,t}^{\text{friction}} \quad (8)$$

$$\vec{F}_{i,t}^{\text{wall_corner}} = \vec{F}_{i,w,t}^{\text{social repulsive}} + \vec{F}_{i,w,t}^{\text{pushing}} \quad (9)$$

where $\vec{F}_{i,w,t}^{\text{social repulsive}}$ is the psychological repulsion between pedestrians i and wall w , $\vec{F}_{i,w,t}^{\text{pushing}}$ and $\vec{F}_{i,w,t}^{\text{friction}}$ are the extrusion force and friction force when pedestrian i makes a contact with wall w , $v_{i,w,t}^{\tau}$ is the tangent velocity of passengers i in direction of wall, if the tangent velocity is 0, then the friction force would be 0.

A passenger may be driven by several forces from different walls at the same time. In our simulation, only the nearest wall or corner is considered. This is consistent with the passengers' strategy of giving priority to solving the most urgent situation in real life.

3. Simulation

The simulation program is developed by C++, which is an object-oriented programming language. In the simulation system, personal characteristics (body size, mass, expected speed, etc.) are considered with certain random distributions. The alighting passengers, the boarding passengers and the through-standees are marked by a property variable. In the visual interface, they are represented as red, blue and green respectively. The simulator could record the kinematic parameters of each agent during simulation in the individual level, such as passenger ID, location coordinates, speed, force and local density, as well as the key points in time of different groups. In the light of these data, we can capture some characteristics of their activities both on platforms and in the trains, as shown in Fig. 4.

Based on the micro-simulation model developed in this paper, simulation experiments that include a wide range of alighting and boarding group sizes and ratios were run. The evacuation simulation experiments indicate that the flow rate of the vehicle door is varied with passengers' expected speed, the number of evacuees and the passing time, rather than a constant. The local velocity outside the door can explain 90% variation of the flow rate. When the desired speed is less than 1.5 m/s, the maximum and average speed of getting through the door can be stabilized at 1m/s and 0.8m/s, respectively. Beyond that, the greater the desired speed, the higher the get-through speed.

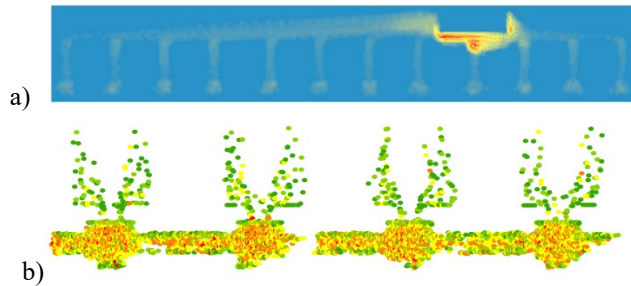


Fig. 4: (a) Congestion of alighting passengers near staircase. (b) Density distribution of the boarding passengers.

Passengers' movement follows the principle of "get off and then on". It is an important issue to tell the time when stage II finished and stage III starts. Based on the observation in metro stations, stage III would begin if there is no alighting passengers in a range of 0.5m around the door. Due to the uncertainty of passenger attributes and behaviour, for each door, the start time of stage III may be slightly different and it needs to make a dynamic identification.

The movement parameters of agents are updated by Gear method. Due to the limited motor ability of passengers, the velocity at any time should be less than the expected speed. To avoid some sudden and huge changes in the movement parameters caused by great force, the acceleration and one-step displacement should also be restricted. In addition, the volume compression of the human body cannot exceed the limit value (20%). An agent should remain in place when he is not driven by any force.

The alighting and boarding process occurs at a typical island platform. There are two sets of escalators/stairs connecting with the underground hall, as shown in Fig. 6. It is assumed that passengers have no preference for these two sets of escalators/stairs and they would choose the nearest one. As the platform is symmetrical, we simulate only half of the platform on one side. This scenario is also applicable to the analysis of side platforms.

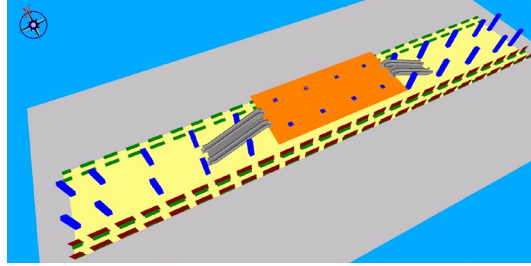


Fig. 3: The simulated island platform

The model was verified in the view of three aspects: the value of extrusion pressure of alighting passengers while getting on the train; the duration of alighting/boarding with different density; the relationship between velocity and density. Simulation experiments denote the model considered basic motivation and dynamic conditions and show perfect performance in the calibration run for the validation.

4. Discussion

This section explores the impact of some certain structural facilities and organizational measures on the movement of alighting and boarding. To evaluate the effectiveness of these design and managing measures, an index evaluation system was established in terms of comfort, smoothness and efficiency.

4.1. Waiting Area

The waiting area of the platform is usually marked as yellow or white waiting lines. Boarding passengers would queue up according to the marked position and their queue locations determine the available space for the alighting passengers. To find out the most suitable queuing position, five groups of simulation experiments were conducted and a control group was set up.

The longer the distance between the two waiting lines in front of a door, the higher the efficiency of getting off that was reached. But when the distance is longer than 10 cm, the efficiency is almost constant.

According to human perception of pressure, physical extrusion pressure is divided into four levels, as shown in Table 1. The closer the two queue lines, the greater the force will be, and the longer the force worked. And this may lead to discomfort. It is already quite comfortable in the case of 10 cm outward from the door.

Therefore, queuing up outward 10 cm from the door would achieve both efficiency and comfort.

Table 1: Duration of physical extrusion pressure in the process of alighting.

physical extrusion pressure	20 cm inward	10 cm inward	align with the door	10 cm outward	20 cm outward	30 cm outward
175 N-247 N	49.50 s	23.41 s	10.37 s	2.84 s	1.9 0s	0.17 s
247 N-600 N	7.49 s	2.36 s	0.90 s	0.13 s	0.1 0s	0
600 N-2500 N	15.02 s	3.79 s	1.52 s	0.21 s	0.12 s	0
>2500 N	7.6 0s	1.29 s	0.35 s	0.11 s	0.04 s	0

4.2. Pillar on Platform.

The existence of a pillar on the platform leads to low efficiency, with longer time to get off. This is mainly because of the low speed and increased crowd density between the pillar and the door. U is smoothness of speed, defined as equation 10. The doors near pillars have larger values of U , which means that the passengers suffer more interference.

$$U = \frac{1}{N} \sum_{\alpha} \frac{\overline{(\vec{v}_{\alpha} - \vec{v}_{\alpha})^2}}{(\vec{v}_{\alpha})^2} \quad (0 \leq U \leq 1) \quad (10)$$

where $\overline{v_\alpha}$ is pedestrian's space speed (m/s), which means the ratio of distance to time in a certain space, and \vec{v}_α is pedestrian's instantaneous speed (m/s), which means the speed of a pedestrian through a certain point.

4.3. Handrail in Train

Inside a carriage, a handrail may be built in the seat area or the door area, or both. Simulation experiments show that the handrail has little influence on the time of alighting and boarding. The difference is within 5%, less than 1 second, which can be neglected.

Considering the complexity of the facilities and the environment, pedestrians do not always walk the shortest distance. Distance curve coefficient is defined as the ratio of walking distance l to the shortest linear distance d , indicating smoothness and stability:

$$R = \frac{l}{d} \quad (11)$$

Investigation of passengers' alighting process indicate that the value of R is in the range of [1.2~2.6]. A handrail in the door area (Fig. 5 shows the passenger path) can make lower value of R , while a handrail in the seat area has little influence. Compared with the car equipped with handrails in both areas, the R value of a car with a handrail only in the door area could reduce by 1.4%, and for a car with a handrail only in the seat area, 4% reduced. So, the handrail is disadvantageous for the passenger's walking path. But it can help passengers maintain balance. Therefore, it is recommended to replace the handrail by a suspended handle.

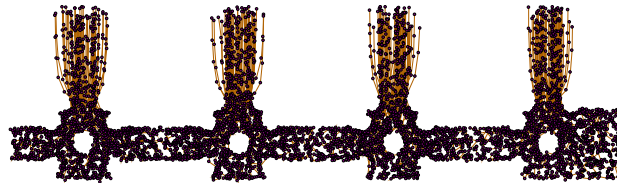
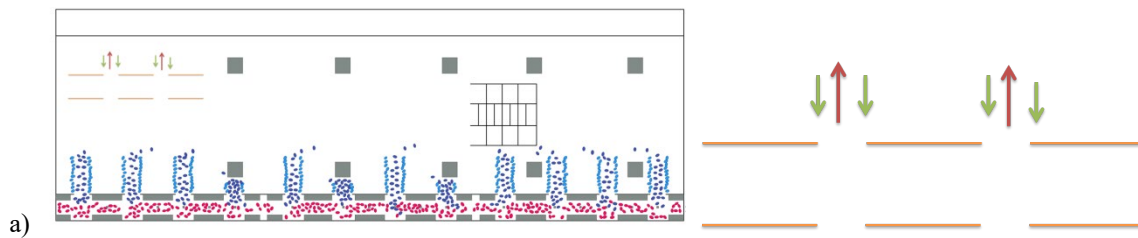


Fig. 5: The simulated island platform

4.4. Separated Alighting and Boarding

Finally, we put forward a creative organization mode to minimize the disturbance between alighting and boarding passengers. The two movements were separated (Fig. 6b) and would take place in the two adjacent vehicle doors simultaneously. In Fig. 6b, the average drop time is reduced by 2.5 seconds; passengers can leave the platform faster through the stairs, reduce queuing and congestion; the distance curve coefficient is decreased by 38%. Therefore, this measure has better performance in general.



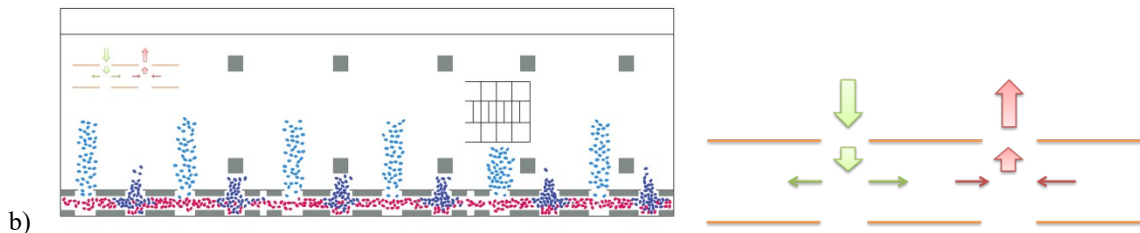


Fig. 6: (a) "Get off and then on" at the same door. (b) Boarding and alighting movements are separated by the adjacent door, with less conflict, more comfortable and more efficient.

5. Conclusion

We developed a multi-agent model in micro-level to simulate passenger movement in boarding and alighting. It has good performance, even in some complex scenes, and provides an effective method for design and passenger organization in metro stations. The model presented in the paper exhibits a range of complex, collective phenomena. It also captures individual characteristics and collective group behaviors during the processes of alighting and boarding movement that were once difficult to model. The agents appear to exhibit reasonable intelligence and diversity during the process of alighting and boarding, which includes some characteristics of actual persons. Field data and simulation output show the validity of this model to emulate passenger movement. Some measures to make passengers get on and off trains smoothly were proposed in three aspects. The first one is the way of queuing up on the platform before getting on. The second aspect is the structure facilities, specifically, the vertical handrail in train and the pillar on platform. Finally, we put forward a creative organization mode to minimize the disturbance between alighting and boarding passengers. The two movements were separated and would take place in the two adjacent vehicle doors simultaneously. However, calibration and validation of the simulation model presented in the paper have limited field data and experiments. Further research has to be done to perform more observations and extend the calibration and validation of the model. Further study of the model should include the collective behavior of passenger distribution on the platform, changing target doors and other detailed behavior that may influence alighting and boarding performance.

Acknowledgements

The research leading to this paper received a funding from the Beijing Municipal Science & Technology Commission. The project ID is Z171100002217011.

References

- [1] Thoreau, Roselle, et al. "Train design features affecting boarding and alighting of passengers." *Journal of Advanced Transportation* 50 (2017).
- [2] Holloway, C., et al. "Effect of vertical step height on boarding and alighting time of train passengers." *Proceedings of the Institution of Mechanical Engineers Part F Journal of Rail & Rapid Transit* 230.4 (2016).
- [3] Fernandez, Rodrigo; Zegers, Pablo; Weber, Gustavo. "Platform height, door width and fare collection on public transport dwell time." *Transportation research record* vol. 2143, pp. 59-66 (2010).
- [4] Xenia Karekla, and Nick Tyler. "Reduced dwell times resulting from train–platform improvements: the costs and benefits of improving passenger accessibility to metro trains." *Transportation Planning & Technology*. vol. 35.5, pp. 525-543 (2012).
- [5] Zhang, Qi, B. Han, and D. Li. "Modeling and simulation of passenger alighting and boarding movement in Beijing metro stations." *Transportation Research Part C*. vol. 16.5, pp. 635-649 (2008).
- [6] Tomomi Kamizuru , Tomoyuki Noguchi , Norio Tomii. "Dwell Time Estimation by Passenger Flow Simulation on a Station Platform based on a Multi-Agent Model." *6th International Conference on Railway Operations Modelling and Analysis - RailTokyo*.pp:154 (2015).

- [7] Yamamura, Akiyoshi. "Dwell Time Analysis in Urban Railway Lines using Multi Agent Simulation. "
(2012).

Concept of a Decision-Based Pedestrian Model

Cornelia von Krüchten¹, Andreas Schadschneider^{1,2}

¹Institut für Theoretische Physik, Universität zu Köln
Zülpicher Str. 77, 50937 Cologne, Germany
cvk@thp.uni-koeln.de; as@thp.uni-koeln.de

²Institut für Physikdidaktik, Universität zu Köln
Gronewaldstr. 2, 50931 Cologne, Germany

Abstract – We develop a decision-based model for pedestrian dynamics which is an extension of the Stochastic Headway Distance Velocity (SHDV) model for single-file motion to two dimensions. The model is discrete in time, but continuous in space. It combines perception, anticipation and decision-making with the simplicity and stochasticity that are characteristic for cellular automaton models. The basic concept is discussed and preliminary results show that the model yield realistic trajectories and fundamental diagrams.

Keywords: Modelling, Perception, Decision-Based model, Distance-to-Collision, SHDV model

1. Introduction

Research on pedestrian dynamics and crowd movement is generally based on two aspects: first, empirical and experimental observations provide direct insights and allow for an unmediated investigation. However, since experiments cannot be performed for any arbitrary situation due to ethical, financial or practical reasons, modelling and simulation help to analyse a wide variety of scenarios and to understand the underlying general mechanisms of pedestrian dynamics.

Over the years, model development has given rise to many different modelling approaches that can be roughly classified considering their fundamental properties (see e.g. [1, 2]). For now, we will focus on microscopic models that describe the individual behaviour and interaction of particles that represent the pedestrians. This class again contains different approaches. The group of acceleration-based models includes social-force models that are usually continuous in space and time and deterministic, based on [3]. They consider intrinsic and extrinsic forces due to the environment and surrounding pedestrians that directly influence the motion. By contrast, rule- or decision-based models are mostly stochastic and discrete in space and time. Using this approach, often realized as cellular automaton models, the agents' movement is determined by certain rules that consider the local environment and current situation of the pedestrian (see e.g. [4, 5, 6]). Therefore, cellular automata (CA) models are rather simple, however, the spatial discretisation can lead to unwanted artefacts. A third group describes velocity-based models for which the velocity of the pedestrian is determined based on environment and interaction.

In this contribution, we want to present a modelling approach that combines several aspects of different model types. In Sec. 2, the general concept and idea of this approach is presented, whereas Sec. 3 mainly focuses on the concrete execution. Sec. 4 approaches first few simulation results.

2. Model concept

As a basis, this model combines continuous space with discrete time. Discrete time steps, as they are used in cellular automaton models, provide the opportunity for laying down simple rules that directly determine the pedestrians' behaviour. In CA models this simplicity is gained at the expense of artefacts due to a lack of spatial resolution. Integrating continuous space as in forced-based models, allows arbitrary values for position and velocity. This approach of combining continuous space with discrete time steps is

already used in some models, see e.g. [7-13]. However, since the potential of this approach has not been fully explored yet, this model is supposed to be a first step in this direction.

The basic concept of the model is shown in Fig. 1. In each time step, a pedestrian takes a decision about his or her velocity for the next step. In this model, speed and direction of motion are determined separately and rely on cognition, e.g. the so-called distance-to-collision which is again directly determined by the environment of the agent and his/her own goals.

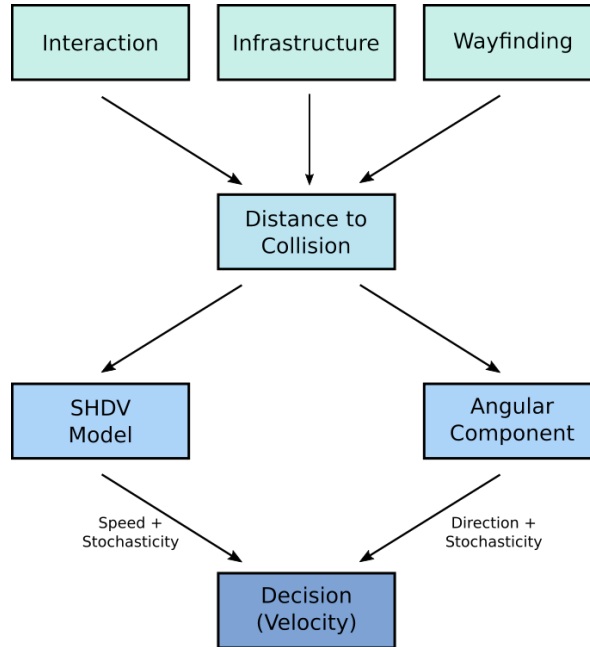


Fig. 1: Concept of the decision-based model: the environment including infrastructure, wayfinding and interaction determines the distance-to-collision which acts as a basis for the calculation of the velocity, namely speed and direction. These components include stochasticity to consider unknown mechanisms.

The environment of a pedestrian is perceived visually and consists of the infrastructure like walls, exits, etc., and other pedestrians the respective agent might interact with. Considering all these elements, the agent calculates the distance to a potential collision in a certain direction. Since anticipation was shown to be potentially crucial for pedestrian dynamics [14, 15], the distance-to-collision is not determined for this respective moment in time, but for the next time step, assuming uniform and linear movement of the agent itself as well as the other pedestrians. This quantity is then used as an input parameter for the calculation of speed and direction.

Since a pedestrian is assumed to prefer directions in which a collision with an infrastructure element or other pedestrians is at least unlikely, the distance-of-collision helps to weight the potential directions. Therefore, it is used to calculate a probability distribution for all directions. Moreover, the distance-to-collision also influences the speed of the pedestrian. In this case, it acts as an input parameter for the Stochastic Headway Dependent Velocity (SHDV) model [12] that correlates the distance headway of a pedestrian with his/her speed. It also includes a stochastic element that reduces the velocity of an agent additionally.

The stochasticity that is found in both speed and angular component of the velocity represents the limited knowledge about cognitive processes of pedestrians and shall cover underlying mechanisms that cannot be simulated or that are not fully understood.

3. Realization

In contrast to many other approaches, we explicitly take into account the spatial extension of the pedestrians. They are modelled by a circle with radius $r = 0.15$ m and are assumed to use cognitive abilities to move within the given environment. This behaviour includes several aspects that are explained separately in the following.

3.1 Perception and visual field

Visual perception is a commonly used approach in heuristic or perception-based models, see e.g. [13, 16-18]. In this model, each pedestrian perceives his or her environment via a visual field of range d_{vf} and an expanse of 2ϕ . Only walls or pedestrians that lie within the visual field are perceived and considered for the calculation. In the visual field, pedestrians and walls or other obstacles cover a certain angular range that depends on the relative position and orientation to the perceiving agent (see Fig. 2). These ranges are then less preferable to be chosen for the direction of the velocity since the corresponding distance-to-collision is smaller than in angular ranges without any imminent obstacles. Considering all elements of the environment and all pedestrians results in an angular distribution of distances-to-collision that can be used to determine the direction for the next time step.

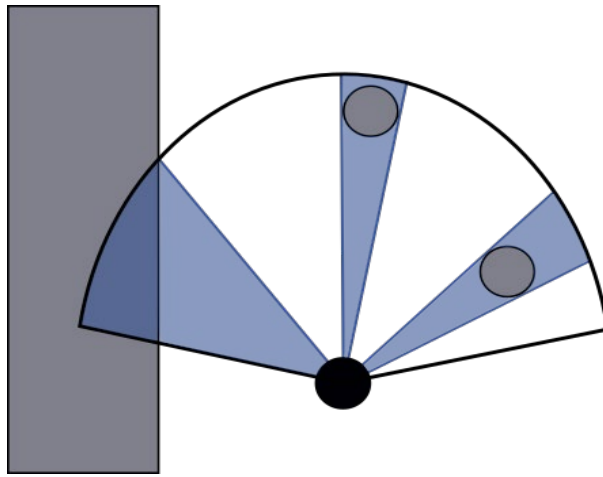


Fig. 2: Each pedestrian (black circle) has a visual field that can be partially covered by walls (left) or other pedestrians (grey circles). Directions chosen within these ranges are less likely.

3.2 Anticipation and distance-to-collision

In several model approaches, anticipation concepts are realised using the time or the distance to an imminent collision, see e.g. [8, 17, 19-21]. In this model, the anticipated distance-to-collision is calculated for each pedestrian that is perceived in the visual field of the agent. The agent assumed the he/she itself as well as the other pedestrian will move with the same speed and direction as in the previous step, leading to a uniform, linear motion. Then the distance-to-collision is calculated based on these anticipated positions with consideration of the extension of the bodies. Relying on anticipation shall help to consider the current direction of motion when taking the decision on the direction for the next step.

3.3 Determination of direction of motion

The determination of the angular component of the velocity is based on different aspects. First, each pedestrian is assigned a target position he or she wants to reach during the simulation. Therefore, for each time step the direction α_t towards the target is determined. The final target angle is then calculated with a Gaussian distribution with mean α_t and standard deviation $s = 0.05$. Using this stochasticity includes that a pedestrian does not always choose the perfect angle to make the simulation results more realistic. At this point the pedestrian considers the presence of walls etc. If the target direction eventually resulted in a

collision with the infrastructure, the pedestrian would choose an intermediate target for his/her current calculation that is given by the surrounding walls and obstacles. How exactly this intermediate target is situated could be determined in more general settings by using different route choice or wayfinding procedures.

In the presence of other pedestrians, the preferred direction must be changed. During the perception phase the relative distances and orientations of all pedestrians to the respective agents are determined. This leads to an angular distribution of distances-to-collision. For angular ranges that are not covered by any pedestrians, the distance-to-collision is set to the maximum visual range d_{vf} . When divided by this maximum range, each angle within the visual field is assigned a positive value for the distance-to-collision within 0 and 1. This quantity can then be used as a measure of probability that the respective direction is chosen for the next time steps. Therefore, if a pedestrian i is perceived by an agent in the direction α_i and a respective distance-to-collision d_i , the probability for the agent choosing this direction for the next timestep is given by $p_i = d_i/d_{vf}$. Summing over all pedestrians results in an angular probability distribution $P(\alpha)$ that is positive and stepwise constant. Then, according to this distribution, the direction is calculated that can be understood as an “interaction angle” (in order to distinguish it from the target angle).

Due to the stochastic nature of the collision avoidance procedure, large changes of direction could occur from one time step to another. To avoid this, a concept of inertia in case of interaction is applied. If the environmental situation has not changed compared to the previous time step, the pedestrian should keep the direction of rotation for the next time step. That means, if a pedestrian has chosen to turn left to avoid a collision in the previous time step, and there were no pedestrians exiting or entering the visual field, he or she should turn left again, i.e. chose any arbitrary direction on his left side. Only if the situation has changed during the last time step, there is no such restriction.

If an interaction angle is chosen, the distance-to-collision in this direction is again determined considering both environment and pedestrians. This distance is then compared to the distance-to-collision (considering infrastructure and pedestrians) in the direction to the target. Then, out of these two directions the one with the highest distance-to-collision is chosen to be the direction of velocity.

3.5 Determination of speed

The distance-to-collision resulting from the determination of the direction acts now as the input parameter for the determination of the absolute value of the velocity. Here, one relies on the SHDV model [12] that was originally developed for single-file motion. In this model, the velocity of an agent depends linearly on his/her headway distance h in one dimension which is replaced by the distance-to-collision in the two-dimensional case (see also Fig. 3):

$$v(h) = \begin{cases} 0 & h \leq d \\ \alpha(h - d) + v_{min} & d < h < d_c \\ v_{max} & d_c \leq h \end{cases} \quad (1)$$

with v_{max} and v_{min} representing the maximum and minimum velocity, respectively, d being a lower threshold and d_c being a higher threshold resulting from $d_c = d + 1/\alpha(v_{max} - v_{min})$. For a headway distance below d , a pedestrian stands still, with a headway distance that is larger as d_c he or she moves freely with maximum velocity. α is the slope of the increasing headway-velocity function.

As a stochastic element, a slow-to-start rule [22] is additionally introduced. Pedestrians whose speed was zero in the last timestep stand still for the next time step with a probability p_0 , with probability $1 - p_0$ they move with a speed according to (1).

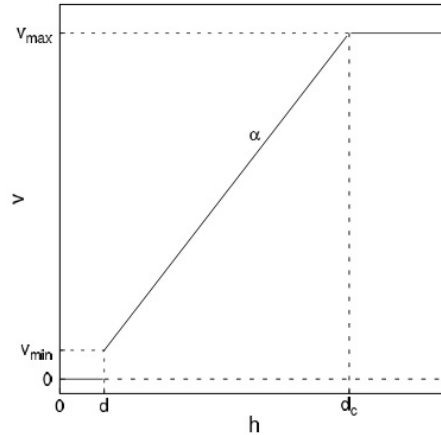


Fig. 3: Headway-velocity function of the SHDV model. The velocity increases linearly with the headway distance without exceeding the free-flow velocity v_{\max} and being 0 for distances that are smaller than the lower threshold d (from [12]).

4. First preliminary results

To assess if the approach described above can reproduce realistic pedestrian dynamics, the model is tested with some simple scenarios. First, we simulated two-person-interactions without additional influence by the infrastructure; second, we measured a fundamental diagram for pedestrian motion in a corridor.

All simulations are performed with a time step of $\Delta t = 0.3$ s and parallel update. The maximum range of the visual field is set to $d_{vf} = 8.0$ m. The parameters for the determination of speed are chosen as $v_{\max} = 1.2$ m/s, $v_{\min} = 0.1$ m/s, $\alpha = 0.5$ and $p_0 = 0.5$, as in [12]. Compared against the original SHDV model, the lower threshold d was reduced to 0.15 m to compensate the explicit consideration of the pedestrians' extension.

The scenarios are not meant to be used for calibration or optimization. To approach the characteristics of the modelled dynamics we used reasonable values for the model parameters such as radius and lower threshold.

4.1 Two-person-interaction

Fig. 4 shows trajectories of simple scenarios with two pedestrians that pass in a free area. All situations were simulated with a visual field extension of $2\varphi=170^\circ$.

In the first scenario, a pedestrian walking from the bottom to the top passes another pedestrian that stands in the middle of the room. As soon as the walking agent perceives the presence of the other pedestrian, it starts to avoid the collision. The trajectory during the avoidance phase is not as smooth as it is wanted to be. This indicates that the applied concept of inertia is not strong enough to suppress larger deviations of the turning angle. Moreover, since the trajectories in Fig. 4 are specific realizations of a stochastic process without any averaging, the simulations do not result in smoothed trajectories.

In Fig. 4 (b), two pedestrians pass on their way to the opposite site of the room. Since the pedestrian coming from the top (dashed green line) turns early enough, the other pedestrian can walk nearly unaffected through the room.

The last Fig. 4 (c) shows two pedestrians coming from the lower edges walking towards the opposite edges. As in (b), one pedestrian can nearly maintain the optimal route, because the other agent gives way. The temporal dimension cannot be shown in this depiction, therefore we would like to emphasise that the agents do not collide, but pass the position where the trajectories cross at different times.

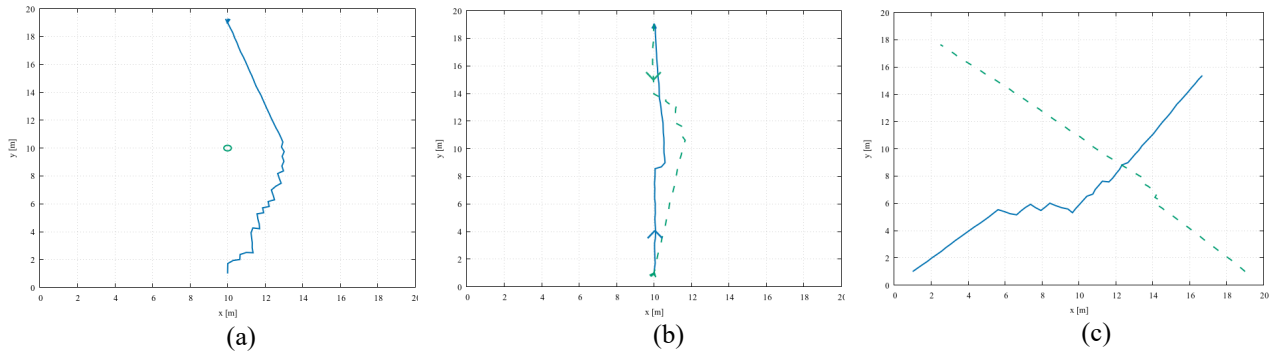


Fig. 4: Simple two-person-interaction scenarios: (a) a pedestrian walks bottom up with passing a standing pedestrian, (b) two pedestrians walking bottom up (blue solid line) / top down (green dashed line, the arrows show the respective direction of motion), (c) two pedestrian walking diagonally bottom down with left to right/vice versa. Since time is not depicted in this plot, it should be emphasised that the pedestrians do not collide in (c).

4.2 Fundamental diagram of single file motion

As a second test, we simulated the situation the SHDV model was originally developed for. The pedestrians walked in single-file motion, that means without any overtaking, in a corridor of length $L = 26.0$ m and width $B = 0.8$ m with periodic boundary conditions. The density was measured globally by the number of agents in the corridor. Because of the extension of the pedestrians the maximum number of agents was by comparison to the SHDV model decreased from 70 to 60. The simulation started with inhomogeneous initial conditions, meaning that all pedestrians were placed at the beginning of the corridor with a minimal distance of 3 cm. Since backward motion is forbidden in single-file motion, the pedestrians were forced to walk towards their target when the interaction angle exceeds $0.9 \times \pi/2$. Additionally, the range in which other pedestrians can be perceived was set to $2\varphi = 1.25 \times \pi$. All simulations were performed for 600 s, measuring over the last 100 s.

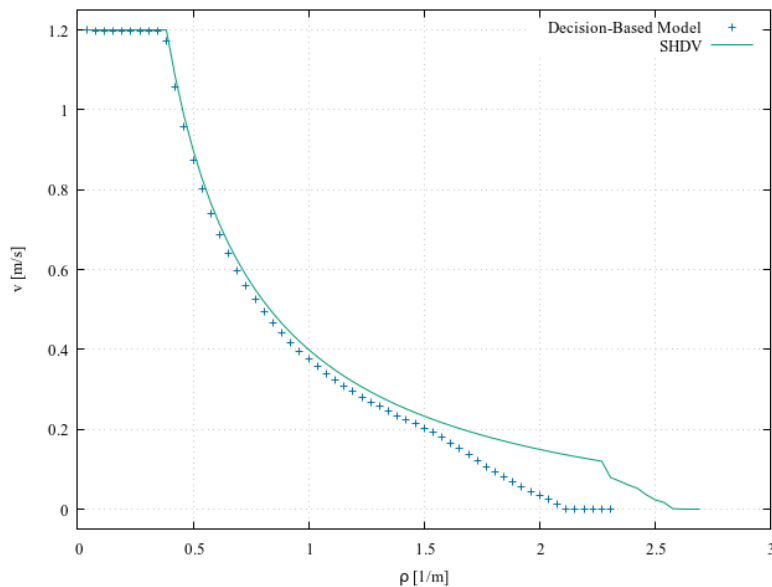


Fig. 5: Comparison of fundamental diagrams for single-file motion of the SHDV model and the decision-based approach. ρ is the global density, and v the averaged velocity. In general, the velocities in the decision-based model are lower than these of the SHDV model, the deviation increases with density.

The fundamental diagram in Fig. 5 shows the global density against the averaged velocity. The progress of the curve fits qualitatively to the fundamental diagram of the SHDV model. However, the velocities of the decision-based model are lower than the velocities measured with the SHDV model. The origin for these deviations, especially for large densities, lies probably in the consideration of a finite extension of pedestrians. In the SHDV model, pedestrians were treated as point-like particles and an effective extension was introduced by the headway-velocity function.

5. Conclusion

The new modelling approach presented in this contribution is based on the combination of continuous space and discrete time and relies on cognition and perception. It is an extension of the one-dimensional SHDV model to two dimensions by adding an angular component to the pedestrians' velocity.

In each time step, a pedestrian perceives its environment visually and determines the distance-to-collision for different directions. In doing so, the agents consider the infrastructure as well as other pedestrians. Based on this information the pedestrians take a decision about their velocity for the next time step. The direction of motion is determined by the pedestrians' individual target and their interaction strategy. In order to avoid collisions, a probability distribution for all potential directions is calculated based on the distance-to-collision. Therefore, directions that may lead to a collision are less likely to be chosen for the next time step. Once a direction is chosen, the distance-to-collision in this direction is used as an input parameter for the dynamics of the SHDV model. So, the speed for the next time steps depends linearly on the distance-to-collision.

Using stochastic elements in the determination of direction and speed covers unknown underlying mechanisms and shall make the simulation results more realistic.

The model was tested with simple scenarios. In the two-person-interaction, it is shown that the model provides realistic trajectories, even if the inertia component of the collision avoidance must be improved. Comparing the fundamental diagram for single-file motion to the results of the SHDV model, it is shown that the model yields similar results. However, due to the extension of the pedestrians that is explicitly considered in this model, the averaged velocities are lower than in the SHDV model. This effect becomes even more significant for large densities. So far, the model has not been calibrated with empirical data. For the preliminary investigations reasonable parameter values were used without any optimization procedure.

Acknowledgements

Financial support by Deutsche Forschungsgemeinschaft (DFG) under grant SCHA 636/9-1 and Bonn-Cologne Graduate School of Physics and Astronomy (BCGS) is gratefully acknowledged.

References

- [1] A. Schadschneider, W. Klingsch, H. Klüpfel et al., "Evacuation dynamics: empirical results, modelling and applications," in *Encyclopedia of Complexity and Systems Science*, R.A. Meyers, Ed. New York: Springer, 2009, pp. 3142-3176.
- [2] A. Schadschneider, M. Chraïbi, A. Seyfried et al., „Pedestrian dynamics – from empirical results to modelling”, to appear in *Crowd Dynamics, Volume 1 – Theory, Models, and Safety Problems*, L. Gibelli and N. Bellomo, Ed. Springer.
- [3] D. Helbing and P. Molnár, "Social force model for pedestrian dynamics," *Phys. Rev. E*, vol. 51, pp. 4282-4286, 1995.
- [4] M. Fukui and Y. Ishibashi, "Jamming transition in cellular automaton models for pedestrians," *J. Phys. Soc. Japan*, vol. 68, pp. 3738-3739, 1999.
- [5] V. Blue and J. Adler, "Cellular automata microsimulation of bidirectional pedestrian flow," *Transp. Res. Rec.*, vol. 1678, pp. 135-141, 2000.
- [6] C. Burstedde, K. Klauck, A. Schadschneider and J. Zittartz, „Simulation of pedestrian dynamics using a two-dimensional cellular automaton,” *Phys. A*, vol. 295, pp. 507-525, 2001.

- [7] K. Yamamoto, S. Kokubo and K. Nishinari, „Simulation for pedestrian dynamics by real-coded cellular automata (RCA),” *Phys. A*, vol. 379, pp. 645-660, 2001.
- [8] I. Karamouzas and M. Overmars, „A velocity-based approach for simulating human collision avoidance,” in *Intelligent Virtual Agents*, Springer, 2010, pp. 180-186.
- [9] G. Baglietto and D.R. Parisi, „Continuous-space automaton model for pedestrian dynamics,” *Phys. Rev. E*, vol. 83, no. 056117, 2011.
- [10] Z.-M. Fang, W. Song, X. Liu et al., „A continuous distance model (CDM) for single-file pedestrian movement considering step-frequency and length,” *Phys. A*, vol. 391, pp. 307-316, 2012.
- [11] M.J. Seitz and G. Köster, „Natural discretization of pedestrian movement in continuous space,” *Phys. Rev. E*, vol. 86, no. 046108, 2012.
- [12] C. Eilhardt and A. Schadschneider, „Stochastic headway dependent velocity model for 1d pedestrian dynamics at high densities,” *Transp. Res. Proc.*, vol. 2, pp. 400-405, 2014.
- [13] W. Kang and Y. Han, „A simple and realistic pedestrian model for crowd simulation and application,” *arXiv:1708.03080*, 2017.
- [14] S. Nowak and A. Schadschneider, “Quantitative analysis of pedestrian counterflow in a cellular automaton model,” *Phys. Rev. E*, vol. 85, no. 066128, 2012.
- [15] Y. Suma, D. Yanagisawa and K. Nishinari, “Anticipation effect in pedestrian dynamics: modelling and experiments,” *Phys. A*, vol. 391, pp. 248-263, 2012.
- [16] G. Antonini, M. Bierlaire and M. Weber, “Discrete choice models of pedestrian walking behavior,” *Transp. Res. B*, vol. 40, pp. 667-687, 2006.
- [17] M. Moussaïd, D. Helbing and G. Theraulaz, “How simple rules determine pedestrian behavior and crowd disasters,” *PNAS*, vol. 108, pp. 6884-6888, 2011.
- [18] M. Zhou, H. Dong, F.-Y. Wang et al., “Modeling and simulation of pedestrian dynamics behavior based on a fuzzy logic approach”, *Information Sciences*, vol. 360, pp. 112-130, 2016.
- [19] A. Johansson, “Constant-net-time headway as a key mechanism behind pedestrian flow,” *Phys. Rev. E*, vol. 80, no. 026120, 2009.
- [20] P. Degond, C. Appert-Rolland, M. Moussaïd et al., “A hierarchy of heuristic-based models of crowd dynamics,” *J. Stat. Phys.*, vol. 152, pp. 1033-068, 2013.
- [21] M. Asano and T. Iryo and M. Kuwahara, “Microscopic pedestrian simulation model combined with a tactical model for route choice behaviour,” *Transp. Res. C*, vol. 18, pp. 842-855, 2010.
- [22] R. Barlovic, L. Santen, A. Schadschneider and M. Schreckenberg, “Metastable states in cellular automata for traffic flow,” *Europ. Phys. J. B*, vol. 5, pp. 793-800, 1998.

Pedestrian collision avoidance with a local dynamic goal

Rafael F. Martin¹, Daniel R. Parisi^{1,2}

¹Instituto Tecnológico de Buenos Aires, Lavardén 315, C. A. de Buenos Aires, Argentina

²Comisión Nacional de Investigaciones Científicas y Técnicas (CONICET), Argentina.

ramartin@itba.edu.ar; dparisi@itba.edu.ar

Abstract - We present here a general formalism for equipping simulated pedestrians with an avoidance mechanism. The central idea is to use a short-range target which is adjusted dynamically depending on the environment and thus modulating the desired velocity of the agent. This formulation can be implemented over any type of existing pedestrian model, being force-based or rule-based. As an example, we implement a simple instance of the formulation which is adjusted to reproduce previous reported and available experimental data of collision avoidance in scenarios of low density. The proposed minimal model shows good agreement with the real trajectories and other macroscopic observables.

Keywords: pedestrian simulation, steering, navigation, collision avoidance.

1. Introduction

In the simulation of pedestrian movements, the collision avoidance mechanisms are a key issue. The algorithm performing this task should be both, computationally efficient and realistic. In the case of social force models [1, 2], the basic avoidance is provided by the repulsive social force acting on the particle. This “social” force is an artificial force and may produce collateral effects [3, 4]. More advanced avoidance models consider future positions, try to anticipate a collision and apply an evasive force on the center of mass of the particles [5]. Other variant consist in applying a decision layer based on the optimization of a cost/energy function before the compute of the “social” force [6,7].

However, one important ingredient of force based models is the driving force which aims the particle toward a long-distance and fixed goal. This concept of a goal or target seems to be very general which is present, not only in force based models, but also in off-lattice cellular automata models [8]. In the real system of free pedestrian (without contact), the only force acting on the agents is the driving force, which is the locomotion mechanism that self-propels the individual. All steering maneuvers are performed through changes in the propulsion direction. This fact was already considered [9-12] and inspired us to postulate (Sec. 2) a new family of models that only use the particle propulsion in order to avoid collisions with obstacles or other moving particles without resorting to fictitious forces or mechanisms.

This framework is independent of the type of low-level model being force-based, rule-based or other. For example, it could be implemented on the Social Force Model [1, 2], by replacing the social force with a variable desired velocity that takes into account the possible future collisions [13].

Under this approach, the problem lies in postulating the heuristics required for computing the variable desired velocity depending on the environment. As in the traditional pedestrian theoretical

models, any arbitrary heuristics can be proposed (for example, [11, 14]) and then the free parameters could be tuned in order to obtain simulated trajectories that approach experimental micro or macroscopic data.

In this work, as an application example of this new family of general models, we propose a simple implementation of a navigation model in diluted systems (Sec. 2.1). Then, we use it to reproduce three different scenarios (a pedestrian avoiding a fixed obstacle, two pedestrian who initiate at 90° relative at the supposed collision point and two groups of two pedestrians each with a potential collision at 90 degrees). In each scenario we compare the simulated trajectories with real ones obtained in experiments performed in an empty parking lot [10] adjusting the only two free parameters in the model. As product of this adjust we obtain simulations with good agreement with experimental trajectories.

2. The model

Our general framework, postulated that particle i , with position \mathbf{x}_i , has of a temporary and short-range goal ($\mathbf{g}_i^t(t)$) which is dynamically placed depending on the environment. When the path to the fixed goal is free of any future collision, thus the temporary goal will be aligned with it. In other case, $\mathbf{g}_i^t(t)$ will produce a detour in the trajectory in order to avoid all kind of collisions.

The environment is defined by the fixed long-distance goal (\mathbf{g}_i); the positions (\mathbf{x}_j) and the relative velocities (\mathbf{v}_j^{rel}) of the nearest neighbors and obstacles. We denote this general function as \mathbf{H} (Eq. (1)) and a graphic representation of the quantities involved are presented in Fig. 1.

$$\mathbf{g}_i^t(t) = \mathbf{H}(\mathbf{x}_i(t), \mathbf{x}_j(t), \mathbf{v}_i(t), \mathbf{v}_j(t), \mathbf{g}_i) \quad (1)$$

In its general form $\mathbf{g}_i^t(t)$ determines the avoidance direction, but also it has a magnitud that could be used for adjusting the speed of the agent.

The function \mathbf{H} is completely general and, of course, it can take any form. Note that some previous works, have presented particular implementations, calling to this kind of approach “cognitive heuristic” [11, 15].

It is important to remark, that this general formulation does not depend on the type of low-level operational model, being force-based or rule-based. In other words, the general heuristic that determines the placement of a local and dynamic goal could be defined for any kind of pedestrian dynamics model, no matter if it is first-order, second-order or other.

2.1. A possible instance of function \mathbf{H}

As a test bed for the formulation we present in this work a minimal implementation of the function \mathbf{H} . Only some simple configurations in a diluted pedestrian system are considered, which corresponds to the experimental data of avoiding a fixed obstacle and pedestrian collisions in 90° crossing [10]. Under this conditions, it was observed that only steering maneuvers are performed, without abrupt changes in the speed [10]. Thus, we make the approximation that the local dynamic goal is represented by $\hat{\mathbf{n}}_i^t$ that is the unit vector pointing in the direction of ($\mathbf{g}_i^t(t)$). This versor, only alters the direction of the desired velocity, keeping a constant speed.

Each simulated pedestrian i , has an associated radius r_i that is used for collision predictions. The particle velocity is designated by $\mathbf{v}_i(t)$ and has constant magnitud v_i . Following the notation of Fig.1 and Fig. 2, \mathbf{g}_i is the fixed global target.

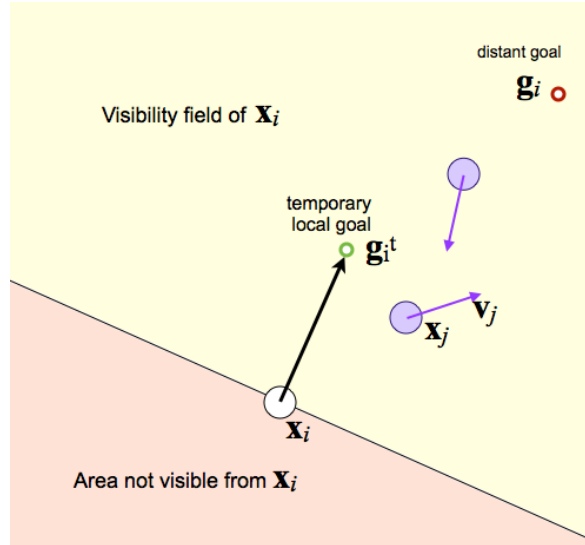


Fig. 1: Basic quantities of the general framework defining the environment of particle i and the placement of the temporary local goal.

When the particle at \mathbf{x}_i detects a future collision with any other particle or obstacle, our minimal implementation propose to calculate the temporary goal (\mathbf{g}_i^t) as a weighted sum of two versors with origin at \mathbf{x}_i : a) \mathbf{n}_i^g , the one pointing toward the final goal (\mathbf{g}_i); and b) \mathbf{n}_i^a , the one pointing toward a temporal avoidance goal (\mathbf{g}_i^a):

$$\mathbf{g}_i^t(t) = s_a(d_c)\mathbf{n}_i^a + [1 - s_a(d_c)]\mathbf{n}_i^g \quad (2)$$

where d_c is the distance from $\mathbf{x}_i(t)$ to the future position at collision time $\mathbf{x}_i(t_c)$ and the weighting factor are given by a sigmoid function

$$s_a(x) = \frac{1}{1+e^{[a(x+b)]}} \quad (3)$$

being b an offset that makes $s_a(0) = 0.99$; and the parameter $a > 0$ is the inverse of avoidance length determining the distance at which the particle's velocity is influenced by a potential collision. This function (Eq. 3) tends to zero when distance x tends to infinity and it tends to one when x tends to zero. The above described quantities are presented in Fig. 2.

One more definition is needed in order to complete the proposed avoidance mechanism, which is the positioning of the avoidance goal \mathbf{g}_i^a . To this end, we first consider the direction from particle at $\mathbf{x}_i(t)$ toward its final goal \mathbf{g}_i . Then, we take the segment at minimum distance from this line to the particle (or obstacle) j . The unit vector \mathbf{n}_j^p is then defined passing from particle j perpendicular and pointing opposite to the line joining \mathbf{x}_i with its fixed goal \mathbf{g}_i . In Fig. 2 we illustrate this quantities.

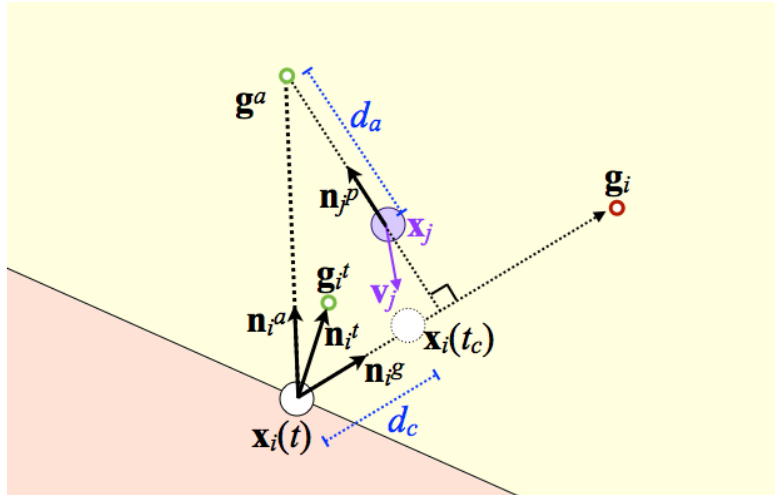


Fig. 2: Placement of the temporary goal and related quantities in a simple particular implementation of the general framework proposed for collision avoidance of simulated pedestrians.

Mathematically, Eq. (4) define the position of the avoidance goal \mathbf{g}_i^a , (for short, we use the notation $\mathbf{g}_i^a = \mathbf{g}^a$ and $\mathbf{n}_j^p = \mathbf{n}^p$)

$$\mathbf{g}^a(\mathbf{x}_i, \mathbf{x}_j, \mathbf{v}_i, \mathbf{v}_j, \mathbf{g}_i) = \begin{cases} \mathbf{x}_j + d_a \mathbf{n}^p & \text{if } |\mathbf{v}_j| \neq 0 \\ \mathbf{x}_j - d_a \mathbf{n}^p & \text{if } |\mathbf{v}_j| = 0 \end{cases} \quad (4)$$

where d_a is a parameter determining the distance between the avoidance goal (\mathbf{g}^a) and the position of particle j (see Fig. 2)

To understand the spirit of this avoidance target we can think that in the case in which the obstacle is fixed ($\mathbf{v}_j=0$) the simulated agent will decide to avoid it by the closest points perpendicular in the direction to its global target. In the very particular case of perfect alignment (agent-obstacle-target), \mathbf{n}^p is defined such us $\mathbf{n}^p \cdot \mathbf{n}^g < 0$, where the subindex 1 and 2 indicates the cartesian coordinates. This last condition produce that the agent go through the right side.

In the case in which the the obstacle is a mobile pedestrian ($\mathbf{v}_j \neq 0$), \mathbf{g}_i^a is positioning at the opposite side with respect to the motion of the potential colliding agent because of the definition of \mathbf{n}^p (see Fig.2).

Now, having calculated \mathbf{g}_i^a , we can obtain \mathbf{g}_i^t from Eq. (2) and then compute the dynamically-adjusted desired velocity as $\mathbf{v}_i^d(t) = v \mathbf{n}_i^t(t)$, being v the constant desired speed and the unitary vector, pointing in the direction to the temporal goal, defined as $\mathbf{n}_i^t(t) = \frac{\mathbf{g}_i^t(t)}{|\mathbf{g}_i^t(t)|}$.

Finally, the evolution of particles is given in the present implementation based on a first order model

$$x_i(t + \Delta t) = x_i(t) + v_i(t)\Delta t \quad (5)$$

where

$$v_i(t) = \frac{[v_i^d(t) + v_i(t - \Delta t)]}{2} \quad (6)$$

This mean value of the velocity is taken in order to give some inertia to the movement of agents, which could be increased by taking a higher time lag ($v_i(t - k\Delta t)$).

The presented minimal model only considers trajectories with constant speed corresponding to diluted systems. Thus, a natural limitation is that avoiding maneuvers with drastic changes in the speed will not be well reproduced. However, we should notice that this simple model is shown just as an example of the general framework outlined at the beginning of Sec. 2, which does not have this limitation as an infinity number of heuristics or models, that suit this framework, could be proposed.

3. Results

3.1. Simulated scenarios

The studied scenarios of potential collisions are inspired by the low density cases studied experimentally in [10,15]. In particular the ones sketched in Fig. 3.

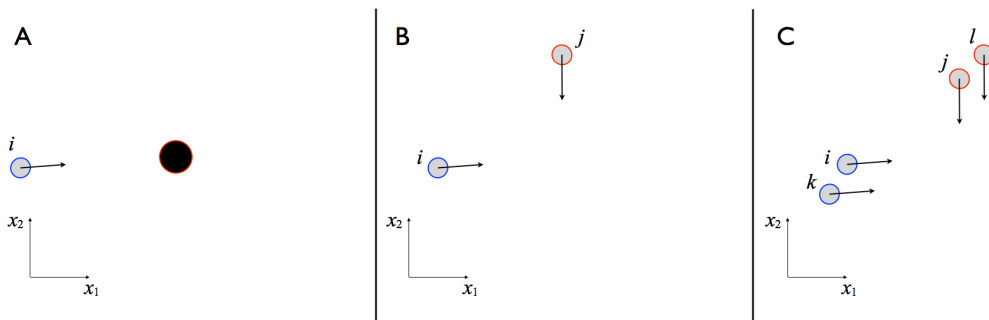


Fig. 3: Configuration of the 3 scenarios studied with the model compared with experiments [10,13]. (A) one pedestrian avoiding a fixed obstacle. (B) and (C) all moving pedestrians.

In order to synchronize the simulation with the experimental data, a value of $\Delta t = 1/30$ s was chosen in all simulations which is the frame rate of the processed videos. The final goals of all pedestrians are placed in the opposite side of the initial positions. The radius of all moving pedestrians were set to $r = 0.3$ m and $r = 0.45$ m for the obstacle. The constant speed v selected for each particle it was took as the mean speed of the corresponding experimental particles.

3.2. Simulations vs. experimental data

From the minimal model described in Sec. 2.1, the free variables that can be tuned in order to

approach experimental data are the parameters a (Eqs. 2 and 3) and d_a (Fig.2). In all cases we compare the simulated and experimental trajectories one by one. For the case of 4 pedestrians (Fig. 3C) a macroscopic property is also used as benchmark.

First, we consider the simple case of one pedestrian avoiding an obstacle as shown in Fig. 3A. For each particular experimental trajectory, a search in the (a, d_a) space can be performed. In order to do that, we choose as measure of error the mean absolute distance between both trajectories ($\langle E \rangle$). The Fig. 4 shows an example of this search (Fig. 4A) and the resulting trajectory compared with the experimental one (Fig. 4B). The best parameter values found in this case are $a = 0.5 \text{ m}^{-1}$, $d_a = 0.9 \text{ m}$. It can be observed that the main difference between both trajectories is the swing of the experimental one, not taken into account by the model. However, this would not be difficult to consider by adding a sinusoidal modulation to the desired velocity, with amplitude and frequency corresponding to the mechanism of walking by taking steps. In order to keep the model simple, we neglect this correction in the present work.

The next scenario, analyzed corresponds to the one shown in Fig. 3B, i.e.: two walking pedestrians with trajectories at 90° . We take a particular set in which can be observed that one of the agents decides not to make any avoidance maneuver, while the other change his/her velocity. Thus in the simulation we set the parameter $a \gg 1$ for the former pedestrian and only adjust the parameters of the avoiding one. The result of this simulation and the comparison with the corresponding experimental trajectories can be seen in Fig.5A. The parameters found for particle j are $a = 6 \text{ m}^{-1}$, $d_a = 0.3 \text{ m}$.

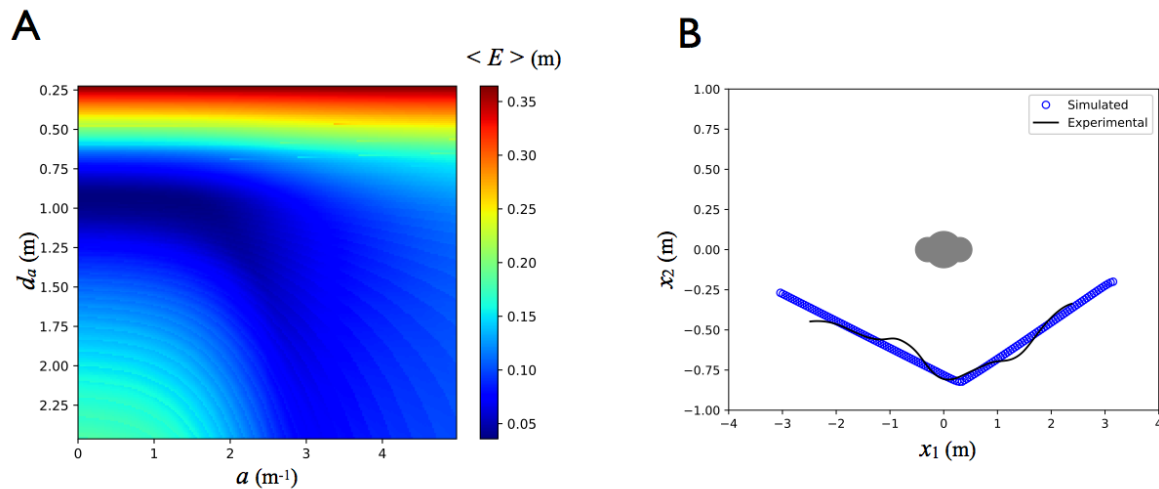


Fig. 4: Simulation of scenario shown in Fig.3A. (A) Parameter search. (B) Experimental and simulated trajectories.

Finally, the configuration shown in Fig.3C is considered. The potential collision of two against two pedestrians at 90° which is generally achieved keeping each group of two people together (Fig. 5B). On the other hand, in some cases the four trajectories are interlaced (one group split) as shown in Fig. 5C.

Besides describing trajectories in agreement with the experimental ones, another macroscopic observable is considered: the minimum distance between each pair of potential colliding particle (d_{min}). It was measured from experiments that in the scenarios given by Fig.5B and C, this minimum distance is $d_{min} = 1.07 \pm 0.37 \text{ m}$, where the error is one standard deviation. Similar values can be obtain with the minimal model: $d_{min} = 1.05 \pm 0.35 \text{ m}$. The trajectories displayed in Fig.5 and the corresponding minimum distance can be obtained by the model by setting its parameters in the range: $a \in [0.5,6] \text{ m}^{-1}$ and $d_a \in [0.5,2] \text{ m}$. Furthermore, the same range of parameters are able to approach the average d_{min} of

all the available trajectories: experimental $d_{min} = 1.10 \pm 0.40\text{m}$ and simulated $d_{min} = 0.97 \pm 0.45\text{m}$.

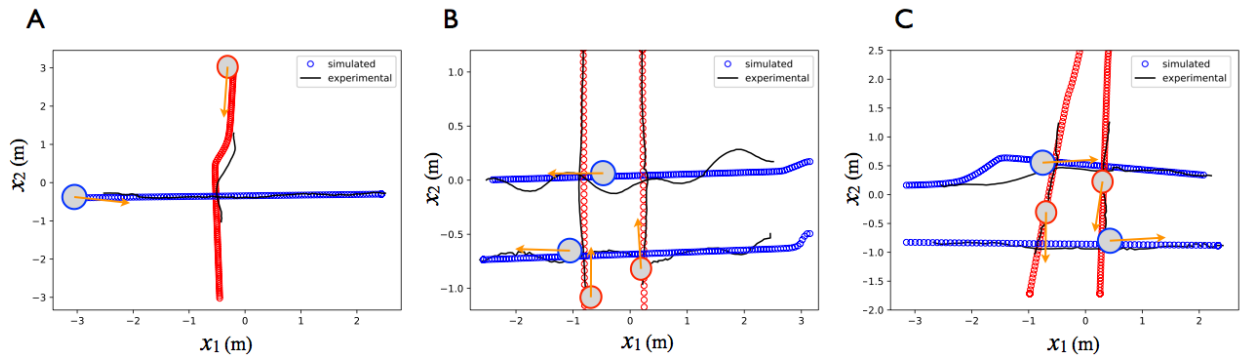


Fig. 5: Simulated vs. experimental trajectories in the displayed configurations.

4. Conclusion

In summary, we have proposed a general framework for collision avoidance which is valid for any kind of operational-level model being second order or first order. As an application example we present a minimal model which allows navigation in dilute systems. Simulations reproduced experimental trajectories of pedestrians avoiding 90° potential collisions and one pedestrian avoiding one fixed obstacle. Also, the minimum distance between avoiding agents are in good agreement with experiments.

As a next step, it must be defined the transition from diluted to congested state of the system, in which avoidance mechanisms shut down (or reduce drastically), in particular, the presented model could tend to the "Contractile Particle Model" [8] when density became high enough.

The present contribution is a step forward in the pursuit of efficient and realistic large-scale pedestrian simulation models and we expect that a new family of models can be created.

Acknowledgements

The authors acknowledge financial support via project PID2015-003 (Agencia Nacional de Promoción Científica y Tecnológica, Argentina; Instituto Tecnológico de Buenos Aires; Urbix Technologies S.A.).

References

- [1] Helbing, D. and Molnar, P., "Social force model for pedestrian dynamics". Physical review E, vol. 51(5), pp. 4282, 1995.
- [2] Helbing, D., Farkas, I. and Vicsek, T., "Simulating dynamical features of escape panic". Nature, vol. 407, no. 6803, pp.487, 2000.
- [3] Lakoba, T.I., Kaup, D.J. and Finkelstein, N.M., "Modifications of the Helbing-Molnar-Farkas-Vicsek social force model for pedestrian evolution". Simulation, vol. 81, no. 5, pp. 339-352, 2005.
- [4] Parisi, D.R., Gilman, M. and Moldovan, H., "A modification of the social force model can reproduce

- experimental data of pedestrian flows in normal conditions". *Physica A: Statistical Mechanics and its Applications*, vol. 388, no. 17, pp. 3600-3608, 2009.
- [5] Karamouzas, I., Heil, P., Van Beek, P. and Overmars, M.H., "A predictive collision avoidance model for pedestrian simulation". In *International Workshop on Motion in Games* (pp. 41-52). Springer, Berlin, Heidelberg, Nov., 2009.
- [6] S. Shin, J. Suh, and H. Yeo, "Development of ecm-based microscopic pedestrian movement model," in *16th International IEEE Conference on Intelligent Transportation Systems (ITSC 2013)*, pp. 249–254, IEEE, 2013.
- [7] H. Xi, S. Lee, and Y.-J. Son, "An integrated pedestrian behavior model based on extended decision field theory and social force model," in *Human-in-the-Loop Simulations*, pp. 69–95, Springer, 2011.
- [8] Baglietto, G. and Parisi, D.R., "Continuous-space automaton model for pedestrian dynamics". *Physical Review E*, vol. 83, no. 5, pp. 056117, 2011.
- [9] Qian-Ling, W., Yao, C., Hai-Rong, D., Min, Z. and Bin, N., "A new collision avoidance model for pedestrian dynamics". *Chinese Physics B*, vol. 24, no. 3, pp. 038901, 2015.
- [10] Parisi, D.R., Negri, P.A. and Bruno, L., "Experimental characterization of collision avoidance in pedestrian dynamics". *Physical Review E*, vol. 94, no. 2, pp. 022318, 2016.
- [11] Moussaïd, M., Helbing, D. and Theraulaz, G., "How simple rules determine pedestrian behavior and crowd disasters". *Proceedings of the National Academy of Sciences*, vol. 108, no. 17, pp.6884-6888, 2011.
- [12] S. J. Guy, S. Curtis, M. C. Lin, and D. Manocha, "Least-effort trajectories lead to emergent crowd behaviors," *Physical review E*, vol. 85, no. 1, p. 016110, 2012.
- [13] W. Qian-Ling, C. Yao, D. Hai-Rong, Z. Min, and N. Bin, "A new collision avoidance model for pedestrian dynamics" *Chinese Physics B*, vol. 24, no. 3, p. 038901, 2015.
- [14] M. J. Seitz, N. W. Bode, and G. Köster, "How cognitive heuristics can explain social interactions in spatial movement," *Journal of The Royal Society Interface*, vol. 13, no. 121, p. 20160439, 2016.
- [15] Seitz, M.J., Bode, N.W. and Köster, G., "How cognitive heuristics can explain social interactions in spatial movement". *Journal of the Royal Society Interface*, vol. 13, no. 121, pp. 20160439, 2016.
- [16] <http://ped.fz-juelich.de/extdb>

The difference between individuals and social groups in multidirectional movement

Yanghui Hu, Jun Zhang*, Weiguo Song*

State Key Laboratory of Fire Science
University of Science and Technology of China
No.96, JinZhai Road Baohe District, Hefei, China
huyang1@mail.ustc.edu.cn; junz@ustc.edu.cn; wgsong@ustc.edu.cn

Abstract - Social groups exhibit some degree of social cohesion that is more than a simple collection or aggregation of individuals. The study on behaviours of social groups is essential to gain a deeper understanding on pedestrian dynamics. In this paper, the crowd movement among individuals and social groups are studied by performing a series of multidirectional pedestrian flow experiments under laboratory condition. Interestingly, we found that the speed of individual is not always higher than that of social groups. Pedestrians try to use different strategies to arrive their destination. With different strategies, their speed and movement time show different properties. These findings may provide basis for facility design and evacuation plan.

Keywords: Social group; Individual; Pedestrian dynamic; Speed; Movement time

1. Introduction

The studies on human safety and pedestrian dynamics are growing rapidly in recent years. The comprehensive understanding on pedestrian dynamics is essential for crowd management and facility design. The major component of the crowd is social groups [1-4]. However, most of previous studies focused on individuals but only a few works consider the influence of social groups in a crowd on pedestrian dynamics.

Speed is one of the basic parameters for describing pedestrian dynamics. Many researchers have pointed out that the velocity of social groups is smaller than that of individuals. Moussaid et al. took an observation and found that the walking speed of pedestrians decreased linearly with the increasing of group size [3]. Zanlungo et al. concluded that three-person groups walked slower than two-person groups, and the latter walked slower than individual pedestrians [5]. Li et al. observed that the average velocity of group members ($v=1.072$ m/s) was smaller than that of individuals ($v=1.15$ m/s) from a field study [6]. Gorrini et al. focused the impact of different densities on pedestrian velocity [7, 8]. They found that the walking speed of social groups was slower than that of individuals in both low and high densities. Zhao et al. found that the walking speed of individuals was significantly faster than that of dyads both in low and high densities in a subway station [9]. However, from control experiments Wagnlid et al. found that the speed of male dyads was larger than that of male individuals [10]. From these studies, it seems that there is no consensus on the speed difference between social groups and individuals.

Besides, under the same situations individuals and social groups may choose different walking path due to their different flexibility and synergy. Gorrini et al found that the walk path of individual was 4% longer than that of social group through observation [8]. Besides, they noticed that the walk path of adult individuals was longer than that of adult dyads and elderly dyads [11]. Zhao et al. found no difference of the walking path between individuals and social groups in low densities from an observation in a subway station in Beijing. However, under high density situations dyads trended to walk in a more straight way compared to individual [9].

Furthermore, most of these results are obtained from uni- or bidirectional flow. In daily life, we often encounter with multidirectional flow, for example, in the atrium of shopping malls, train stations

and subway stations and so on. In these locations, pedestrians come from different directions and go to different destinations. To investigate the difference between social groups and individuals, we carried out experiments to study the difference between social groups and individuals under multidirectional flow.

2. Experiment Setup

The experiment was carried out in November 2017 in the University of Science and Technology of China, Anhui, China. The experiment scenario is a circle with the radius of 5m which is used to form multidirectional flows [11]. Fig. 1 shows the sketch of the experiment scenario and a snapshot of the experiment (the red pedestrians represent the individuals and the blue pedestrians represent the social groups). In this paper, we only consider pairs as social group since the proportion of pair is larger than 50% of crowd in most case [1-4]. In this paper, a special relationship that is the strong paired relationship between pairs was adopted. For each pair, they were asked to keep in physical touch (arm in arm) with each other in the experiment. At the beginning of the experiment, participants stood on the border of the circle (cross standing between social groups and individuals in theory) and individuals separated different groups uniformly. The destination of each pedestrian is the opposite circle arc through the centre of the circle. Pedestrians were asked to reach their destination as quickly as possible in each run with the same instruction. During the movement, they can freely choose their preferred manner to avoid collision with other participants to arrive at their destinations. In total, 72 participants took part in the experiment. They are all undergraduate students from University of Science and Technology of China and 18-24 years old. Six runs were performed with different numbers of participants. In each run, the numbers of social groups and individuals are the same (except scenario 01 where the number of individual is one more than that of social groups). The ratio of boys to girls is close to one and thus we ignored the impact of gender and age on the results. The details of the experiment are shown in Table 1.

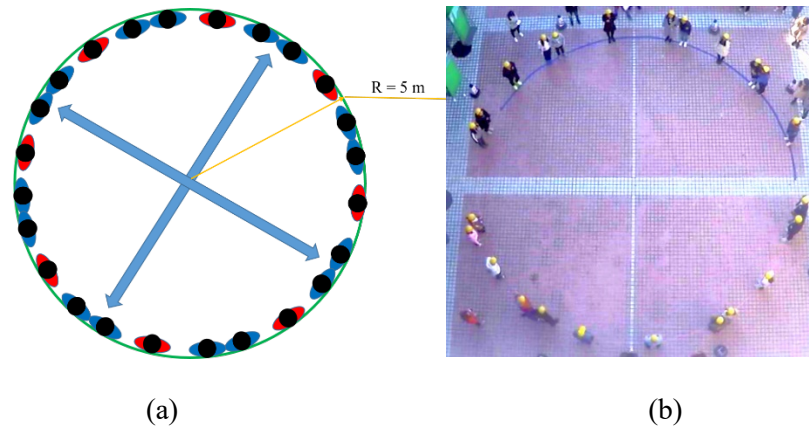


Fig. 1: (a) The schematic illustration of the scenario and (b) a snapshot of the experiment.

Table 1. The details of the experiment.

Scenario	Pedestrians number	Number of social groups	Number of individuals
01	13	4	5
02	24	8	8
03	36	12	12
04	48	16	16
05	60	20	20
06	72	24	24

Two cameras were fixed on the 5th floor of a building to record the whole experiment. The trajectories of pedestrians were automatically extracted from video recordings using the software PeTrack

[12]. Finally, the trajectories of the whole experiment were corrected manually. The frame rate of the trajectories data corresponds to 25 fps.

3. Trajectories

Based on high precision tracking of PeTrack, the characteristics of pedestrians including trajectories, velocity and density can be determined. Due to the head swing of the pedestrian, the trajectories display the periodic change and cannot show the real position of the body. We smooth the trajectories according to the step frequency which is about 2 Hz. We use 1 s as the smoothing window and calculate the average value as the x and y coordinate. Results show that it can eliminate the effect of head swing well. We draw the trajectories of pedestrians for run 1 to run 6 in Fig 2. The red lines represent the individuals and the blue lines represent the trajectories of social groups.

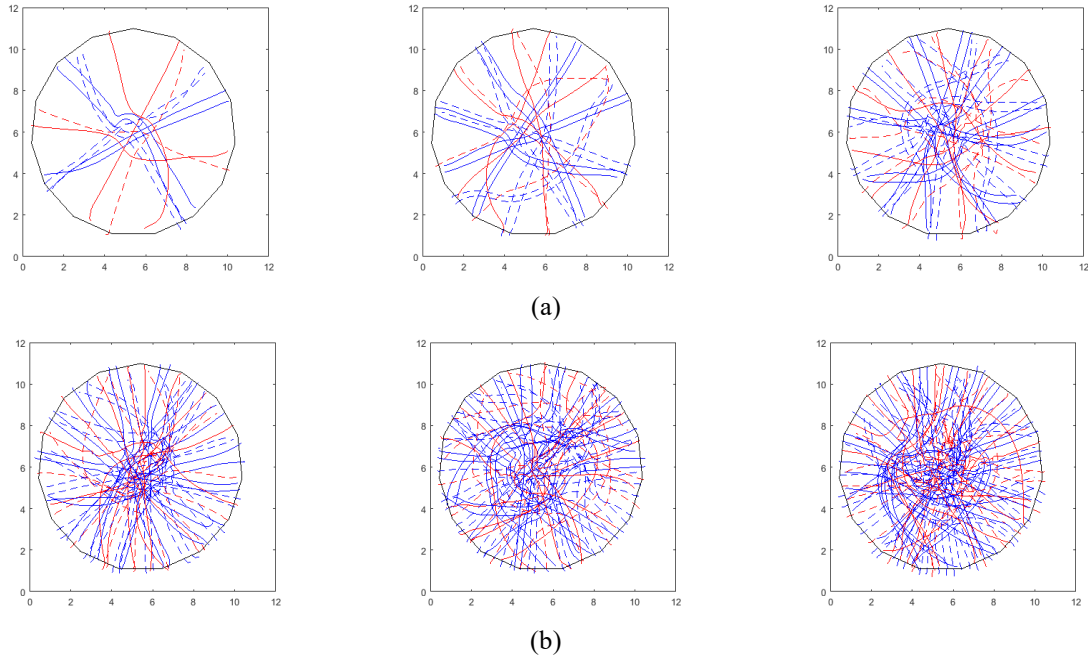


Fig. 2. The trajectories of (a) scenario 01 to 03 (b) scenario 04 to 06.

From the figures, we can see that social group move together and they keep a relative small interpersonal distance. In low density, the walk path is more orderliness and few detour phenomenon appears. Pedestrians can get through the central area straight. However, with the increase of participants, the trajectories of pedestrians becomes complicated gradually. The trajectories in central area (area 2 which will be explained below) is seriously crossed and obvious detour behaviour appears in the experiment. Serious congestion occurred in the central area and pedestrian are stuck in the area and cannot move quickly. In order to reach the target quickly, some pedestrians made a detour.

4. Data Analysis Method

The instantaneous velocity $\bar{v}_i(t)$ is defined as below:

$$\bar{v}_i(t) = \frac{\sqrt{[x_i(t+\Delta t'/2) - x_i(t-\Delta t'/2)]^2 + [y_i(t+\Delta t'/2) - y_i(t-\Delta t'/2)]^2}}{\Delta t'} \quad (1)$$

where $x_i(t)$ and $y_i(t)$ are the x and y coordinates of pedestrian i at time t and $\Delta t' = 0.4 s$ is used in this paper.

The average velocity $v(t)$ is calculated by equation (2):

$$v(t) = \frac{\sum_i \|\bar{v}_i(t)\|}{N(t)} \quad (2)$$

The global density ρ is calculated by equation (3):

$$\rho = \frac{N}{A} \quad (3)$$

where N is pedestrian number in measurement area, $A = 28.26 \text{ m}^2$ is the size of the measurement area.

The walk path is calculate by equation (4):

$$S = \sum_{i=t_0}^{t_D} \sqrt{(x_{t=i+1} - x_{t=i})^2 + (y_{t=i+1} - y_{t=i})^2} \quad (4)$$

where t_0 and t_D is the origin and destination time of pedestrian, $x_{t=i}$ and $y_{t=i}$ are the x and y coordinate of pedestrian at time i, $x_{t=i+1}$ and $y_{t=i+1}$ are the x, y coordinate of pedestrian at time i+1.

5. Results and Discussion

5.1. The average speed of pedestrians

To investigate pedestrian speed in different scenarios, we calculate average speed of each pedestrian by equation 1 and 2 and results are shown in figure 3.

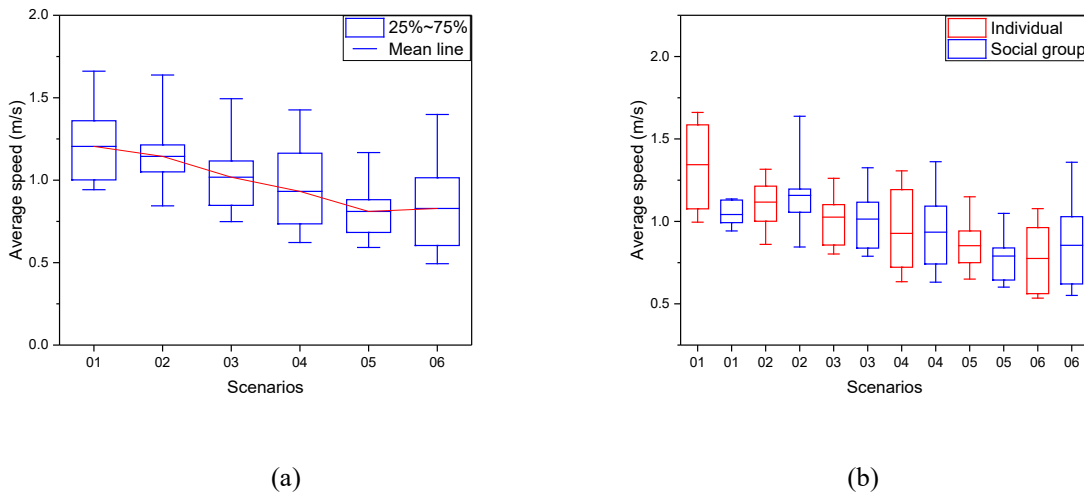


Fig 3. The average speed of (a) different scenarios and (b) of social group and individual.

As shown in Figure 3(a), with the increasing number of pedestrians in the experiment, the average speed decreases. Since the probability of collision between pedestrians increases with the increasing density in the central area, most of pedestrians have to decrease the walking speed to avoid the conflict with others.

The average speeds of individuals and social groups in different runs are shown in Fig 3. The speed of individual is not always higher than that of social groups. This is contrary to the findings of [7, 8] who found that individuals are more flexible than social groups and the latter have a negative influence on the speed of crowds. The influence of social group on pedestrian speed should be deeply investigated.

5.2. The walk path of pedestrians

Fig 4 shows the length of the walk path of pedestrians in movement, which increases with pedestrian number. Pedestrians need to walk further to get their destination when there are more pedestrians. Fig 4 (b) shows walk path of social group and individual in different runs. We notice that the walk path of individual is larger than the walk path of social group in each scenario. This conclusion is coincide with the result of Gorrini [8] and Zhao [9]. Due to the flexibility of individual, the walk path of individual is larger than that of social group.

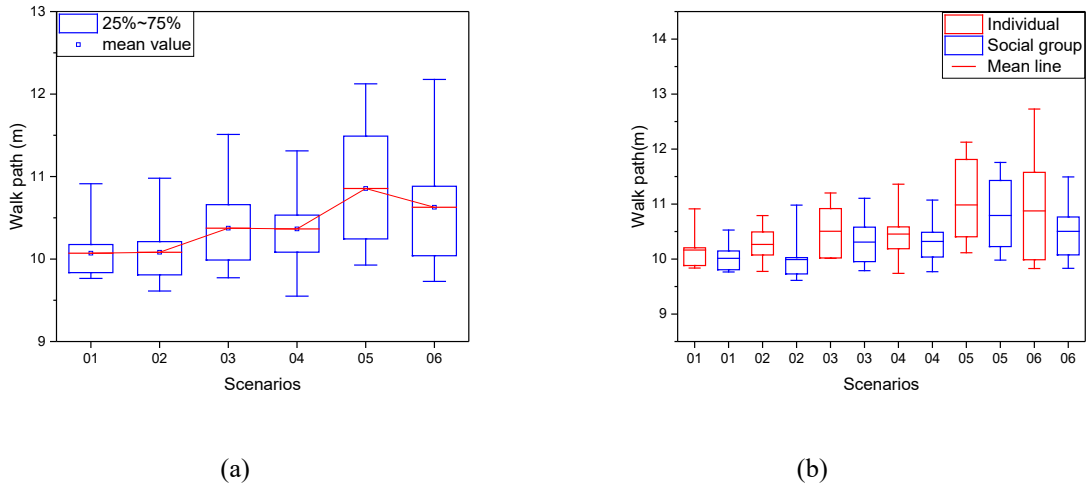


Fig 4. The walk path (a) in different scenarios and (b) of social group and individual.

5.3. Strategies of pedestrians

By analyzing the factors influencing the speed and movement time further, we find that pedestrians adopt different strategies in the process of multi-directional movement. To avoid collisions with others, pedestrians mainly adopt three different strategies in the video recordings: a) decelerating the speed, b) waiting in situ and letting others go first, c) making a detour. We use pedestrian speed and DC value to classify these strategies into six strategies: 1) Straight - Movement in Steady speed (S-MS), 2) Straight - Movement with Deceleration (S-MD), 3) Straight - Movement with Waiting (S-MW), 4) Curve - Movement in Steady speed (C-MS), 5) Curve - Movement with Deceleration (C-MD), 6) Curve - Movement with Waiting (C-MW).

We define a Detour Coefficient (DC) value to represent the detour probability of pedestrians during the movement. The DC value is defined as:

$$DC = \left(\frac{\sum_{t=t_0}^{t_D} \sqrt{(x_{t+1}-x_t)^2 + (y_{t+1}-y_t)^2}}{\sqrt{(x_D-x_0)^2 + (y_D-y_0)^2}} - 1 \right) \times 100\% \quad (9)$$

where x_t and y_t are x and y coordinates of pedestrians at time t, x_{t+1} and y_{t+1} are x and y coordinate of pedestrians at time t+1, x_0 and y_0 are x and y coordinates of pedestrians at origin position, x_D and y_D are x and y coordinates of pedestrians at destination positions.

During the experiment, the scenario can be approximately divided into two areas where pedestrians show different movement states: 1) the free movement state area: pedestrians move freely and less influenced by others in this area. This area contains two processes, a) at the beginning of the experiment, the self-accelerating process of the pedestrian from standstill to movement, b) at the end of the experiment, the self-deceleration process of the pedestrian from movement to standstill. 2) Congested movement area: congestion occurs in this area due to the accumulation of pedestrians and their speeds are influenced by each other. To facilitate the calculation, we divide the experiment scenario into two parts. Area 1 is a circle with the radius of 3m and locates at the center of the experimental site. Moreover, area 1 is the rest of experimental site. From data analysis, we find that there is no difference in speed and movement time between pedestrians in area 1. Here we focus on the movement of pedestrian in area 2.

Under normal condition, pedestrian will choose the shortest path in movement [13, 14]. However, under certain circumstances, such as crowded pedestrians, they will make a detour to reach their destination quickly in order to avoid conflicts with other pedestrians and waiting others due to the congestion. Firstly, we divide pedestrians into two categories based on the DC value: 1) $DC < 5\%$ straight movement 2) $DC > 5\%$ curve movement (detour). We find that in the 166 groups (an individual is regarded as one group), 55.4% (92 groups) move along straight and 44.6% (74 groups) along curves. This

is consistent with the shortest path principle in our normal life that most of people prefer to move straight. After manual verification, the 5% DC value is used as a standard to divide pedestrians into straight movement and curve movement, the accuracy of the detour criterion is as high as 90%.

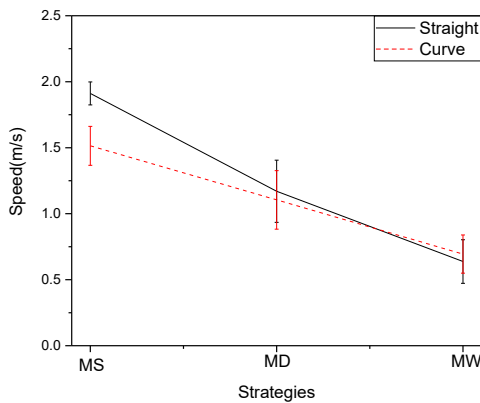
Secondly, we divide the pedestrians into three classes according to the speed variation ratio. 1) Movement in Steady speed (MS): the speed variation ratio is less than 25%. 2) Movement with Deceleration (MD): the speed variation ratio is larger than 25%. The minimal speed is larger than 0.3 m/s. 3) Movement with Waiting (MW): the speed variation ratio is larger than 25%. The minimal speed is smaller than 0.3 m/s. In this paper, we think the pedestrian is waiting for others when the speed is less than 0.3 m/s.

The classify basis and proportion of different strategies are shown in table 2.

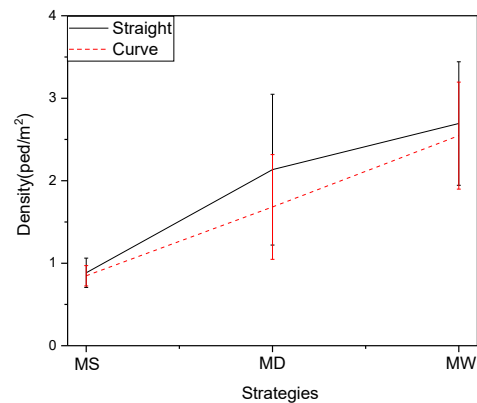
Table 2: The classify basis and proportion of different strategies.

Strategies	DC value	Speed variation ratio $\frac{v_{max} - v_{min}}{v_{max}}$	v_{min} (m/s)	Proportion
Straight – Movement in Steady speed (S-MS)	< 5%	< 25%	> 0.3	2.4%
Straight – Movement with Deceleration (S-MD)	< 5%	> 25%	> 0.3	18.1%
Straight – Movement with Waiting (S-MW)	< 5%	> 25%	< 0.3	34.9%
Curve - Movement in Steady speed (C-MS)	> 5%	< 25%	> 0.3	1.8%
Curve - Movement with Deceleration (C-MD)	> 5%	> 25%	> 0.3	22.9%
Curve - Movement with Waiting (C-MW)	> 5%	> 25%	< 0.3	19.9%

We plot average speed, density and movement time of different strategies in figure 6.



(a)



(b)

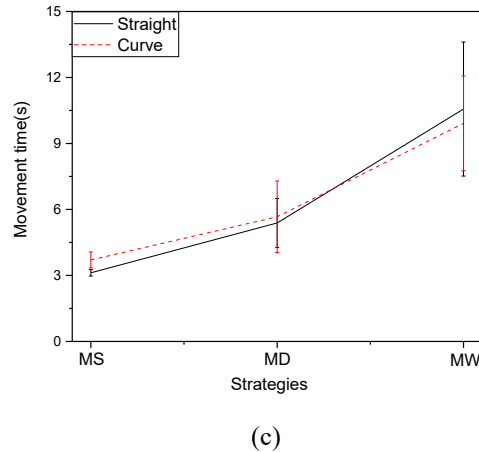


Fig. 6: (a) the average speed (b) average density and(c) movement time of different strategies.

As can be seen from Fig 6, in six strategies, the MS strategy leads to a higher speed, lower density than and the shortest movement time during the movement. However, this strategy is only observed when the number of participants is small. When the number of pedestrian increases, there is no enough space for them to get through the congested areas in high speed and thus the MS strategy does not work anymore. Due to the change of directions in movement along curve, pedestrian speed of C-MS strategy is smaller than that of S-MS. Owing to the increase of the movement path, the movement time is slightly larger than that of S-MS. However, the density of pedestrians who select the straight movement strategy is larger than that of curve movement strategy. The detour strategy keeps pedestrians away from crowded areas, which results in a lower density and a lower probability of collision with other pedestrians. There is little difference in speed and movement time between S-MD strategy and C-MD strategy. However, the density under C-MD strategy is obviously lower than that under S-MD strategy. It shows that detour strategy is beneficial to keep a certain distance with other pedestrians and to avoid overcrowding between pedestrians. Compared with S-MW strategy, under C-MW strategy pedestrian has higher speed, lower density and shorter movement time. Therefore, curve strategy (detour) is beneficial to improve the movement efficiency in our experiment.

5. Conclusion

We conducted a series of experiments with different number of pedestrians to investigate the difference between individuals and social groups in multidirectional crowd movement. We analyse the trajectories, speed and movement time of pedestrians. The results indicate that the speed difference between individual and social group changes based on different conditions. The length of pedestrian walk path increases with the pedestrian density. Moreover, the walk path of social group is shorter than that of individual. Social group do have influence on pedestrian dynamics. We find different strategies for pedestrians to reach their destinations and the speed, density and movement time for different strategies are different. The experiment shows that detour is beneficial in multidirectional movement.

Acknowledgements

The authors acknowledge the foundation support from the National Natural Science Foundation of China (Grant No. 71704168), from Anhui Provincial Natural Science Foundation (Grant No. 1808085MG217) and the Fundamental Research Funds for the Central Universities (Grant No. WK2320000040).

References

- [1] M. L. Federici, A. Gorrini, L. Manenti, and G. Vizzari, "Data collection for modeling and simulation: case study at the university of milan-bicocca," in *International Conference on Cellular Automata*, 2012, pp. 699-708: Springer.
- [2] C. H. Jazwinski and C. H. Walcheski, "At the mall with children: Group size and pedestrian economy of movement," *Environment and Behavior*, vol. 43, no. 3, pp. 363-386, 2011.
- [3] M. Moussaïd, N. Perozo, S. Garnier, D. Helbing, and G. Theraulaz, "The walking behaviour of pedestrian social groups and its impact on crowd dynamics," *PloS one*, vol. 5, no. 4, p. e10047, 2010.
- [4] M. Schultz, C. Schulz, and H. Fricke, "Passenger dynamics at airport terminal environment," in *Pedestrian and Evacuation Dynamics 2008*: Springer, 2010, pp. 381-396.
- [5] F. Zanlungo, D. Bršćić, and T. Kanda, "Spatial-size scaling of pedestrian groups under growing density conditions," *Physical Review E*, vol. 91, no. 6, p. 062810, 2015.
- [6] X. Li, S. Xiong, P. Duan, S. Zheng, B. Li, and M. Liu, "A study on the dynamic spatial-temporal trajectory features of pedestrian small group," in *Dependable Computing and Internet of Things (DCIT), 2015 2nd International Symposium on*, 2015, pp. 112-116: IEEE.
- [7] A. Gorrini, S. Bandini, and M. Sarvi, "Group dynamics in pedestrian crowds: Estimating proxemic behavior," *Transportation Research Record: Journal of the Transportation Research Board*, no. 2421, pp. 51-56, 2014.
- [8] A. Gorrini, S. Bandini, and G. Vizzari, "Empirical investigation on pedestrian crowd dynamics and grouping," in *Traffic and Granular Flow'13*: Springer, 2015, pp. 83-91.
- [9] P. Zhao, L. Sun, L. Cui, W. Luo, and Y. Ding, "The walking behaviours of pedestrian social group in the corridor of subway station," in *Proceedings of the 2016 Pedestrian and Evacuation Dynamics Conference*, 2016.
- [10] J. Wagnild and C. M. Wall-Scheffler, "Energetic consequences of human sociality: walking speed choices among friendly dyads," *PloS one*, vol. 8, no. 10, p. e76576, 2013.
- [11] J. R. Dyer *et al.*, "Consensus decision making in human crowds," vol. 75, no. 2, pp. 461-470, 2008.
- [12] M. Boltes, A. Seyfried, B. Steffen, and A. Schadschneider, "Automatic extraction of pedestrian trajectories from video recordings," in *Pedestrian and Evacuation Dynamics 2008*: Springer, 2010, pp. 43-54.
- [13] Y. Guy, "Pedestrian route choice in central Jerusalem," *Department of Geography, Ben-Gurion University of The Negev, Beer Sheva (in Hebrew)*, 1987.
- [14] P. Seneviratne and J. Morrall, "Analysis of factors affecting the choice of route of pedestrians," *Transportation Planning and Technology*, vol. 10, no. 2, pp. 147-159, 1985.

Parameter Calibration in Crowd Simulation Models using Approximate Bayesian Computation

Nikolai W.F. Bode

Department of Engineering Mathematics, University of Bristol
Merchant Venturers Building, BS8 1YB, Bristol, UK
nikolai.bode@bristol.ac.uk

Abstract - Simulation models for pedestrian crowds are a ubiquitous tool in research and industry. It is crucial that the parameters of these models are calibrated carefully and ultimately it will be of interest to compare competing models to decide which model is best suited for a particular purpose. In this contribution, I demonstrate how Approximate Bayesian Computation (ABC), which is already a popular tool in other areas of science, can be used for model fitting and model selection in a pedestrian dynamics context. I fit two different models for pedestrian dynamics to data on a crowd passing in one direction through a bottleneck. One model describes movement in continuous-space, the other model is a cellular automaton and thus describes movement in discrete-space. In addition, I compare models to data using two metrics. The first is based on egress times and the second on the velocity of pedestrians in front of the bottleneck. My results show that while model fitting is successful, a substantial degree of uncertainty about the value of some model parameters remains after model fitting. Importantly, the choice of metric in model fitting can influence parameter estimates. Model selection is inconclusive for the egress time metric but supports the continuous-space model for the velocity-based metric. These findings show that ABC is a flexible approach and highlights the difficulties associated with model fitting and model selection for pedestrian dynamics. ABC requires many simulation runs and choosing appropriate metrics for comparing data to simulations requires careful attention. Despite this, I suggest ABC is a promising tool, because it is versatile and easily implemented for the growing number of openly available crowd simulators and data sets.

Keywords: Pedestrian dynamics, Simulation model, Parameter calibration, Statistical Analysis, Approximate Bayesian Computation.

1. Introduction

Simulation models for pedestrian crowds are a widely used tool [1]. The dynamics these models produce are controlled by parameters that capture the preferred speed of pedestrians or the strength of interactions between pedestrians, for example [1]. As many models are intended to be used or are already used to investigate real world scenarios, a key challenge is to calibrate model parameters, such that simulations produce realistic behaviour [2]. In addition, robust approaches for calibrating parameters facilitate a fair comparison of the predictive potential or goodness of fit across different models [3].

A range of approaches for calibrating model parameters have been suggested [2,4-8]. They compare models to empirical data at a microscopic level (e.g. trajectories [5]) or at a macroscopic level, where summary statistics for simulations and data are compared (e.g. pedestrian flows [2]). For specific models, it is sometimes possible to formulate a likelihood function linking model and data via probability distributions [6]. However, for most simulation models it is not practical to find explicit, closed-form probability distributions for simulation outcomes. Thus, parameter calibration typically uses an objective function that measures the difference between data and simulations via measures derived from microscopic data [5,7,8]. Parameter estimates are found by optimising the objective function. While this approach is valid, it has three major shortcomings. First, this approach yields point-estimates for parameters and provides no information on the uncertainty associated with estimates. Second, this approach is not suited for model comparison, where the relative quality of different models in describing data is established. The objective function does provide a goodness of fit measure, but it is not clear how

differences in model complexity (i.e. number of model parameters) should be accounted for when comparing this measure across models. Third, all numerical optimization procedures are liable to getting stuck in local optima, meaning that the true optimal solution may not be found.

In this contribution, I propose an alternative approach for pedestrian model calibration using Approximate Bayesian Computation (ABC), that is already widely used in other fields of science (e.g. [9]). I show how this flexible framework avoids the issues mentioned above and I demonstrate for representative simulation models that even for simple scenarios (e.g. unidirectional flow through one bottleneck), parameter estimates are associated with substantial uncertainty.

2. Methods

To demonstrate the parameter calibration and model selection approach based on Approximate Bayesian Computation (ABC), I consider two different simulation models and two different approaches for comparing simulations to data. In the following, I first describe the two models, then I outline the ABC approach and finally I provide details on model fitting and selection.

2.1. Microscopic Pedestrian Simulation Models

I consider two microscopic models that are derived from popular models in the literature. As this work is intended as a demonstration of principle only, I do not wish to make any claims about the overall quality of either model or similar models.

The first model is a derivative of a popular simulation model that describes the movement of pedestrians in continuous space [10]. To save space, I do not provide a detailed description of this model, but all details can be found in previous work [11]. Briefly, pedestrian-pedestrian and pedestrian-wall interactions are captured in force vectors acting on simulated pedestrians. The movement preferences of simulated pedestrians, e.g. towards a target and away from walls, is encoded in a discrete floor field [11]. Models of this type are commonly referred to as ‘‘Social Force models’’ and I thus refer to this model as ‘‘SF model’’ here. I fit the values of five parameters of this model, keeping the remaining parameters fixed at default levels that have been specified previously [11]. The fitted parameters are the preferred speed of pedestrians, v^0 , coefficients determining the strength of psychological interactions between pedestrians (A, B) and coefficients regulating the strength of physical pedestrian-pedestrian and pedestrian-wall interactions (k, κ). The nomenclature for these parameters is identical to the one used in previous work [11].

The second model is a cellular automaton model that describes the movement of pedestrians in discrete space on a lattice grid with square cells of side-length 0.4m. It is very loosely based on previous work [12]. The model is deliberately kept very simple to provide a contrast to the complex SF model. Let F_{ij} denote the value of cells of a static floor field that encodes the movement preferences of pedestrians in the same way as the floor field used for the SF model. The same algorithm as for the SF model is used to construct F_{ij} (see [11]). The indices i and j denote the rows and columns of the lattice grid. Furthermore, let M_{ij} be a matrix that takes value 1 if cell (i, j) of the lattice grid that pedestrians move on is occupied by a pedestrian or a wall and 0 otherwise. The positions of all simulated pedestrians are updated synchronously in fixed time steps of length δt seconds. Simulated pedestrians move to cells within the Moore neighbourhood of their current position according to probabilities P_{ij} that are computed as follows:

$$P_{ij} = \frac{([1 + F_{ij}][1 - M_{ij}])^S}{C} \quad (1)$$

S is a model parameter that captures how strongly simulated pedestrians respond to gradients in the floor field F_{ij} and C is a normalising constant that ensures the P_{ij} sum to 1 over the Moore neighbourhood for any given simulated pedestrian. Eq. (1) ensures that simulated pedestrians cannot move onto walls or grid cells that are already occupied by other pedestrians. If the procedure above leads to a conflict

between two or more simulated pedestrians moving onto the same grid cell, only the simulated pedestrian with the highest value of P_{ij} associated with this cell is moved and the others remain stationary. I fit two parameters of this model: S and δt . The former parameter controls how strongly simulated pedestrians respond to gradients in the floor field and the latter parameter controls the update rate and thus the maximum attainable speed of simulated pedestrians. As this model is a cellular automaton, I refer to it as “CA model”.

The simulation scenario I consider throughout is one where 70 simulated pedestrians exit a square 10mx10m room through a single bottleneck that is 1.2m, 1.6m or 2.0m wide and 0.4m deep. Pedestrians are considered to have left the room once they have passed through the bottleneck and simulated pedestrians are removed from the simulation once they have moved 1.0m away from the bottleneck after leaving the room.

The next section describes the general principles of the model fitting approach before section 2.3 details how the SF and the CA model are fitted to data.

2.2. Approximate Bayesian Computation

ABC is a likelihood-free statistical model fitting technique [9]. Instead of an explicit likelihood function, model simulations are used in the model fitting procedure. In its simplest form, ABC consists of five steps that are described below (Fig. 1).

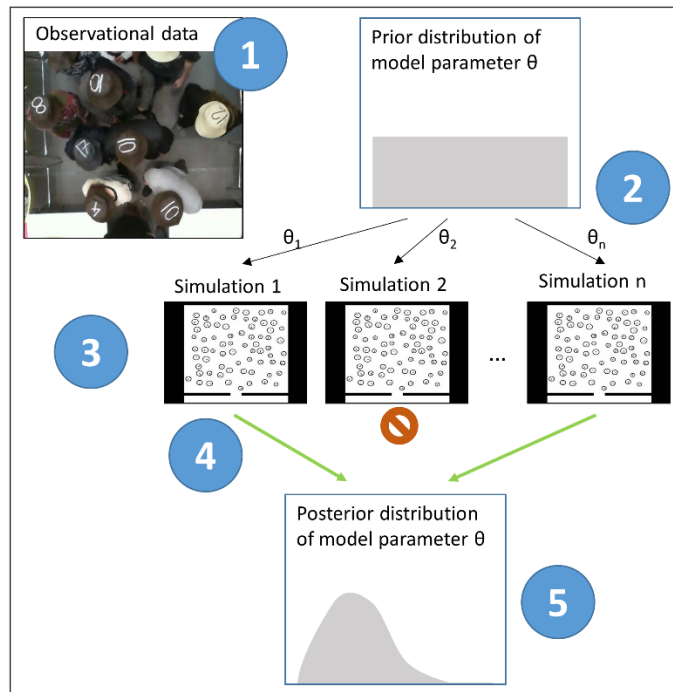


Fig. 1 Illustration of Approximate Bayesian Computation. Steps 1-5 labelled in the figure are explained in the text.

- (1) Obtain measures of interest from data. These could be microscopic or macroscopic measures.
- (2) For a given model, decide on a prior distribution for model parameters, θ . In Fig. 1 we assume no prior knowledge about θ and therefore use uniform or flat distributions. θ can be a vector including multiple parameters.
- (3) Draw n samples, θ_1 to θ_n from the prior distribution and use them to perform model simulations.
- (4) Compute the measure of interest from (1) for simulations and use a distance function and a tolerance ϵ to decide if a model simulation is sufficiently similar to the data.

- (5) Approximate the posterior distribution of θ with the parameter values accepted in (4) – θ_1 and θ_n in Fig. 1.

This process works for different measures of interest (e.g. pedestrian flow, fundamental diagram, trajectories), as long as a suitable distance function linking data to simulation can be found (step 4 above). Provided the tolerance ε is chosen small enough and enough simulations are performed (large n), ABC will find an accurate estimate of the posterior parameter distribution [9]. The posterior parameter distribution indicates both the most likely parameter values (e.g. mean or mode of posterior) and the uncertainty associated with it (e.g. variance of posterior). A particularly useful feature of ABC is that it can be used to compare the quality of models in explaining data. If ABC is performed for different models on the same data using the same value of ε , then the rate at which parameters are accepted into the posterior distribution (step 4) for each model can be used to approximate the Bayes Factor – a commonly used measure for model selection [9]. Model complexity, i.e. the number of parameters a model has, is inherently accounted for in ABC [9].

2.3. Model Fitting and Model Selection

For model calibration I focus on the simple benchmark scenario of unidirectional flow through one bottleneck, as already indicated above. For this scenario, experimental data including the trajectories of all pedestrians within a measurement area in front of the bottleneck is publicly available (data published in [13], available on <http://ped.fz-juelich.de/db/>). As already described above, I consider bottleneck widths of 1.2m, 1.6m and 2.0m.

The model fitting procedure requires a measure recorded from the experimental data that can be used to compare data and simulations. I use two different measures to investigate the robustness of the model fitting procedure.

The first measure I use is the time it takes 30 pedestrians to pass through the bottleneck after the first 10 pedestrians have exited, denoted ΔT_{10}^{40} (Fig. 2a). The measured times for the experimental data are 9.68s, 7.64s and 5.20s for the bottleneck widths 1.2m, 1.6m and 2.0m, respectively. This measure presents a crude approximation of the pedestrian flow. I focus on data close to the start of experiments and simulations to avoid artefacts caused by transient effects, such as changes in behaviour at the end of experiments. For comparison with simulations, I compute the Euclidean distance between the times obtained from the data and from simulations.

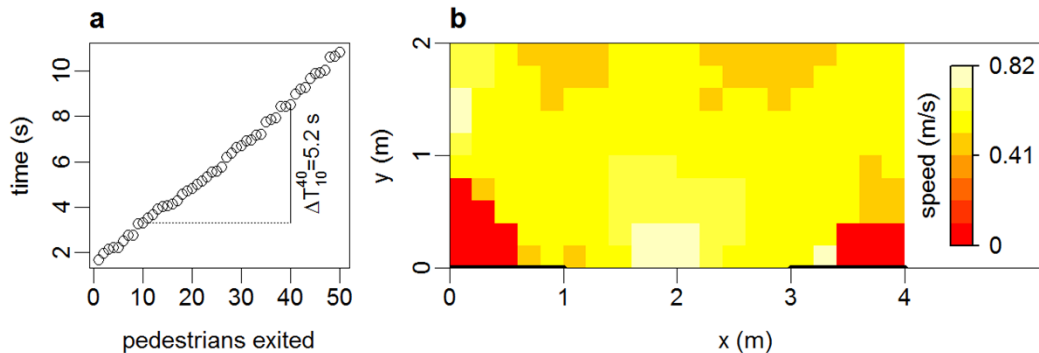


Fig. 2: Measures used to compare experimental data to simulations. Panel (a) shows the time it takes 30 pedestrians to pass through the bottleneck, after the first 10 pedestrians have exited. Panel (b) shows the field of the average speed directed at the bottleneck centre in a measurement area in front of the bottleneck. The data shown is for a bottleneck width of 2m. The centre of the bottleneck is located at $(x, y) = (2, 0)$. See text for details.

The second measure I use is recorded over the same time interval as the first measure (i.e. between the 10th and the 40th pedestrian passing through the bottleneck). This measure is inspired by work which suggests that the variation of average pedestrian velocities at different locations in front of bottlenecks is

informative for the overall dynamics [14]. It is measured on a 4m by 2m grid located in front of the bottleneck that consists of square cells of side-length 0.2m. For each grid cell, individuals located inside the cell are considered and the average of the component of their velocity that is directed towards the centre of the bottleneck is recorded (Fig. 2b). In other words, the measure captures how fast pedestrians are moving towards the centre of the bottleneck at different locations in front of the bottleneck. Fig. 2b shows a V-shaped funnel of this speed field, suggesting that movement speeds towards the bottleneck are not homogeneous in space. For comparison with simulations, I compute the Euclidean distance between speed fields obtained from experimental data and from corresponding simulations and average over the three bottleneck widths.

For both distance measures, I fit the two models by performing simulations with 70 pedestrians for 1,000,000 samples from the prior distribution for each bottleneck width. For the distance measure based on exit times I then use a tolerance of $\varepsilon = 2s$ to obtain posterior parameter distributions. For the distance measure based on the field of speeds directed towards the exit, I use a tolerance of $\varepsilon = 10m/s$ to obtain posterior parameter distributions. I use flat priors (i.e. uniform distributions) for all parameters and the range of values for the prior distributions is detailed in section 3 below.

3. Results and Discussion

All posterior parameter distributions for the SF model differ substantially from the uniform prior distributions (Fig. 3). This change between the prior and posterior parameter distributions indicates the information we gain about the parameter values from the data using ABC model fitting procedure. For all parameters and in particular for A (Fig. 3a), the posterior distribution indicates that a substantial level of uncertainty associated with the estimate of the parameter remains (consider the spread of the distribution). Decreasing the ABC acceptance threshold ε and increasing the number of simulations performed in ABC, may address these issues to some extent, but some uncertainty for parameter estimates will always remain, reflecting inherent variability in simulations.

Comparing the posterior distributions obtained from fitting the model using the two different distance measures between data and simulations (egress time and speed field) reveals that the choice of distance measure can have a substantial effect on the parameter estimates and therefore on model calibration. For example, while the estimate for parameter k is robust to the choice of distance measure in the ABC model fitting (Fig. 3d), the mean of parameter v^0 is shifted with model fitting using the speed field leading to a lower estimate of v^0 , on average. This shows that fitting the SF model to one feature of data does not necessarily lead to the best fit for other aspects of data (see e.g. discussion in [15] for a different model). This is not a surprising insight for complex models, but I suggest the ABC model fitting approach is useful for investigating such differences in several ways. First, the posterior parameter distributions indicate how parameter estimates differ for model fits that use different distance measures. Second, when using ABC, several distance measures can be combined, as desired, depending on the context. For example, multiple different measures could be combined in a weighted sum or otherwise to provide a new distance measure that takes more aspects of the data into account. Third, ABC provides a rigorous approach for comparing the quality of different models, depending on what distance measure is used (see below).

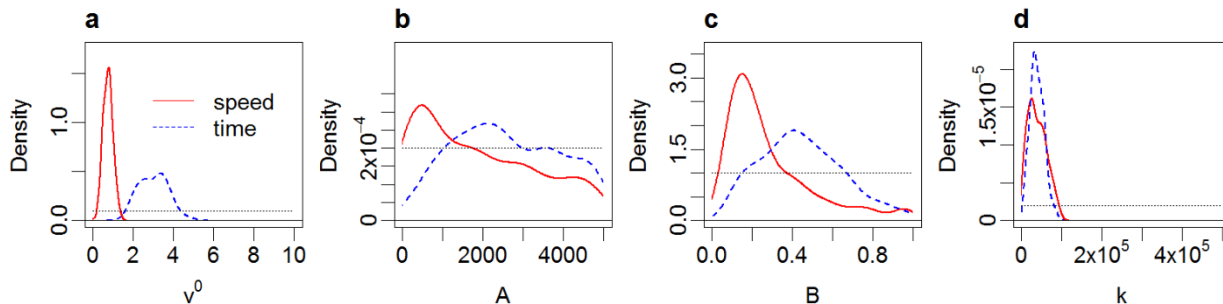


Fig. 3: Marginal posterior distributions for parameters in the SF model. The solid red line indicates the posterior obtained using the speed field distance measure, the dashed blue line shows the posterior obtained using the egress time distance measure and the dotted horizontal line indicates the uniform prior distribution. Due to spatial constraints, I only report the marginal posterior distributions for four of the five fitted model parameters here.

ABC model fitting for the CA model provides qualitatively similar insights (Fig. 4). Posterior distributions indicate the evidence on parameters we gain from the data. The value of δt is identified with high certainty (highly peaked posterior, Fig. 4a) for both distance measures, while we learn little about the value of S when considering egress times (equivalently, S does not affect egress times substantially), but there is comparatively little uncertainty about S when considering the speed field (Fig. 4b). This also shows that as for the SF model, using different distance measures when fitting the CA model leads to different posterior distributions for parameters.

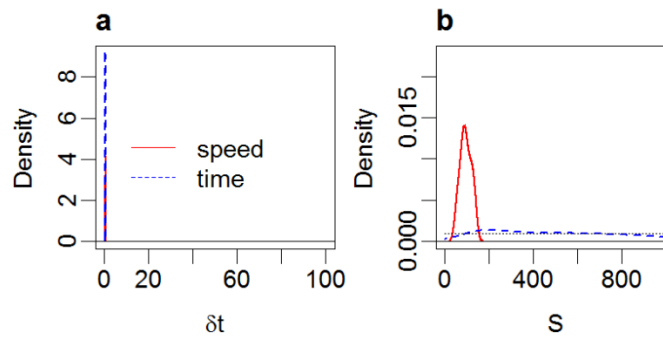


Fig. 4: Marginal posterior distributions for parameters in the CA model. The solid red line indicates the posterior obtained using the speed field distance measure, the dashed blue line shows the posterior obtained using the egress time distance measure and the dotted horizontal line indicates the uniform prior distribution.

When choosing acceptance thresholds ε in ABC, values that are as small as possible while still leading to meaningful approximations of the posterior parameter distributions are desired. Table 1 shows that the acceptance rates for samples from the prior are low for both models, but Figs 3 and 4 show that posterior distributions can still be estimated. To compare the relative quality of the SF and CA model in explaining the data, the Bayes Factor between the two models can be approximated from the rate at which samples from the prior distribution are accepted into the posterior distribution in ABC [9]. This approach for comparing the quality of models implicitly takes model complexity (i.e. number of model parameters) into account. I compute the Bayes Factor (BF) between the SF and the CA model. Therefore, positive values of $\log(BF)$ indicate support for the SF model and vice-versa. If the BF is close to zero, it is difficult to distinguish between the two models. I adopt a commonly used scale for interpreting $2\log(BF)$ values which suggests that only absolute values larger than 2 indicate positive evidence for either model [16].

Table 1: ABC acceptance rates for the two models and the two distance measures between data and simulations used. The Bayes Factor (BF) can be approximated as the fraction of the two ABC acceptance rates [9]. I compute the BF between the SF and the CA model. Thus, positive values of $\log(BF)$ indicate support for the SF model.

	SF model	CA model	$2\log(\text{Bayes Factor})$
Acceptance rate egress time	2.21×10^{-4}	5.46×10^{-4}	-1.80
Acceptance rate speed field	2.75×10^{-4}	2.20×10^{-5}	5.04

Table 1 shows that fitting models using the egress time measure leads to a negative value of $2\log(BF)$ which would indicate that the CA model is better supported by the data than the SF model.

However, as the absolute value of $2\log(BF)$ is lower than 2, the model selection using the egress time measure is inconclusive. In contrast, model fitting using the speed field measure leads to a positive value of $2\log(BF)$ that is larger than 2, which indicates positive evidence in favour of the SF model.

These findings suggest that the CA model can capture egress times as well as the SF model, but that the SF model outperforms it in capturing the fine-scale patterns encoded in the speed field. More generally, the contrasting outcomes of model selection for the two measures I used in model fitting indicate that model selection does not always provide a clear outcome. It is possible that different models are suitable for describing different aspects of pedestrian dynamics. If this was the case, which model to select or prefer would then depend on the context and the intended use of the model. As already discussed above, it is also possible to combine different distance measures in ABC to take multiple features of data into account.

4. Conclusion

In summary, my contribution aims to demonstrate that ABC is a useful and flexible approach for pedestrian model calibration. ABC provides parameter estimates, indicates the uncertainty associated with the estimates and can be used for model selection. In addition, ABC is an excellent tool to highlight the difficulties of model calibration and model selection in pedestrian dynamics.

On the one hand, my findings demonstrate that ABC provides a flexible approach to fit models for pedestrian dynamics to data and to compare the relative quality of models for explaining data. On the other hand, it is important to note that the success of ABC relies on two main components. First, ABC requires a suitable quantitative measure to compare data and simulations. I have demonstrated the use of two different measures here. The differences in model fitting and selection results depending on the measure used highlight the importance of carefully deciding how to compare data and simulations. Second, ABC requires many numerical simulations of models. How many simulations are needed depends on the prior information available. When starting without much prior information (as I demonstrate here with flat priors), millions of simulations are needed. The availability of information, e.g. on a narrow range of values parameters can take, or even information on the most likely parameter values, will reduce the required number of simulations for ABC model drastically. For confined scenarios, like the bottleneck scenario I consider here, it is feasible to run large numbers of simulations. However, if little prior information is available and models are to be fitted to data from highly complex scenarios (e.g. involving many pedestrians or entire buildings), the high number of simulations required may become prohibitive. One way to approach such scenarios could be to initially fit models to subsets of the scenario investigated (e.g. only considering part of a building or crowd) or ideally to separate data and to subsequently use the posterior parameter distributions from this model fitting as prior distributions in model fitting.

In addition to being flexible, I suggest ABC is a useful addition to the model calibration and model selection efforts in pedestrian dynamics because once a simulator for a given model is available, it is very easily implemented. As model simulators are increasingly being made openly available [17-19], I believe now is a good time to introduce ABC into the field of pedestrian modelling.

References

- [1] D.C. Duives, W. Daamen, and S.P. Hoogendoorn. "State-of-the-art crowd motion simulation models." *Transp. Res. Part C*, vol. 37, pp. 193-209, 2013.
- [2] W. Liao, J. Zhang, X. Zheng, and Y. Zhao. "A generalized validation procedure for pedestrian models." *Simul. Model. Pract. Theor.*, vol. 77, pp. 20-31, 2017.
- [3] M. Chraïbi, T. Ensslen, H. Gottschalk, M. Saadi, and A. Seyfried. "Assessment of models for pedestrian dynamics with functional principal component analysis." *Physica A*, vol. 451, pp. 475-489, 2016.

- [4] D. Wolinski, S.J Guy, A - H. Olivier, M. Lin, D. Manocha, and J. Pettré. "Parameter estimation and comparative evaluation of crowd simulations." *Comput. Graph. Forum*, vol. 33, no. 2, pp. 303-312. 2014.
- [5] S. Seer, C. Rudloff, T. Matyus, and N. Brändle. "Validating social force based models with comprehensive real world motion data." *Transp. Res. Proc.*, vol. 2, pp. 724-732, 2014.
- [6] R. Lovreglio, E. Ronchi, and D. Nilsson. "Calibrating floor field cellular automaton models for pedestrian dynamics by using likelihood function optimization." *Physica A*, vol. 438, pp. 308-320. 2015.
- [7] M. Li, Y. Zhao, L. He, W. Chen, and X. Xu. "The parameter calibration and optimization of social force model for the real-life 2013 Ya'an earthquake evacuation in China." *Safety Sci.*, vol. 79, pp. 243-253, 2015.
- [8] W. Zeng, P. Chen, G. Yu, and Y. Wang. "Specification and calibration of a microscopic model for pedestrian dynamic simulation at signalized intersections: A hybrid approach." *Transp. Res. Part C*, vol. 80, pp. 37-70, 2017.
- [9] T. Toni, D. Welch, N. Strelkowa, A. Ipsen, and M.P.H. Stumpf. "Approximate Bayesian computation scheme for parameter inference and model selection in dynamical systems." *J. R. Soc. Interface*, vol. 6, no. 31, pp. 187-202, 2009.
- [10] D. Helbing, I. Farkas, and T. Vicsek. "Simulating dynamical features of escape panic." *Nature*, vol. 407, no. 6803, pp. 487, 2000.
- [11] N.W.F. Bode, and E.A. Codling. "Human exit route choice in virtual crowd evacuations." *Anim. Behav.*, vol. 86, no. 2, pp. 347-358, 2013.
- [12] C. Burstedde, K. Klauck, A. Schadschneider, and J. Zittartz. "Simulation of pedestrian dynamics using a two-dimensional cellular automaton." *Physica A*, vol. 295, no. 3, pp. 507-525, 2001.
- [13] J. Little, A. Seyfried, W. Klingsch, T. Rupperecht, A. Schadschneider, and A. Winkens. "An experimental study of pedestrian congestions: influence of bottleneck width and length" in *Proceedings of International Conference on Traffic and Granular Flow 2009*, Shanghai, China, 2009.
- [14] A. Garcimartín, J.M. Pastor, C. Martín-Gómez, D. Parisi, and I. Zuriguel. "Pedestrian collective motion in competitive room evacuation". *Sci. Rep.*, vol. 7, no. 1, pp. 10792, 2017.
- [15] I. von Sivers, and G. Köster. "Dynamic stride length adaptation according to utility and personal space". *Transp. Res. Part B*, vol. 74, pp.104-117, 2015.
- [16] R.E. Kass, and A.E. Raftery. "Bayes factors". *J. Am. Stat. Assoc.*, vol. 90, no. 430, pp.773-795, 1995.
- [17] F. Albrecht, B. Degenhart, F. Dietrich, M. Gödel, B. Kleinmeier, G. Köster, M. Laubinger, D. Lehmborg, J. Schöttl, S. Schuhbäck, M. Seitz, S. Stemmer, I. von Sivers, M.T. Parente, and B. Zönnchen. (2018, May 31). Vadere [Online]. Available: <http://www.vadere.org/>
- [18] E. Andresen, M. Chraibi, A. Graf, D. Haensel, W. Liao, U. Kemloh, M. Osterkamp, A. Portz, O. Schmidts, B. Schröder, D. Shhikhalev, A. Tordeux, J. Zhang, A. Schumacher, N. Sohre, and Y. Xiao. (2018, May 31). JuPedSim [Online]. Available: <http://www.jupedsim.org/>
- [19] S. Curtis, A. Best, and D. Manocha. (2018, May 31). Menge [Online]. Available: <http://gamma.cs.unc.edu/Menge/>

Movement Characteristics of Processions

Petros Polichronidis and Michael Schreckenberg

Physik von Transport und Verkehr/Universität Duisburg-Essen

Lotharstr. 1, 47057 Duisburg, Germany

petros.polichronidis@uni-due.de; michael.schreckenberg@uni-due.de

Abstract – Processions are a scientifically not much investigated traffic system. Recent studies found that the first participant in the Cologne Rose Monday parade has a remarkable higher travel time than the last participant. The velocity profiles of the participants are explained by the constant moving vehicle driving ahead of the parade leaving the pathway and partly due to a spatial contraction of the parade during the procession. This contribution compares the traffic kinematics of the Cologne Rose Monday parade in Germany with other processions (*Schuetzenausmarsch Hanover 2017*, *Niederrheinischer Kinderkarnevalsumzug 2018*). The kinematics of these processions were analysed based on GPS data from participants. Their kinematics differ from those of the Cologne Rose Monday parade. In general, the observations depend on the size of a procession, the length of its pathway, the composition of the procession and especially on the catching up behaviour, of the participants, when gaps occur in front of them. Furthermore, we examine the influence of the pathway on the traffic flow. This can be used to choose a parade's pathway avoiding flow reducing infrastructure characteristics like traffic area transitions, narrow curves etc. In summary, this work extends the understanding of the kinematics of processions. It can serve as a basis upon which the parade's movement can be predicted and so the duration of such events can be estimated better.

Keywords: Transportation, GPS data, random processes, parades, processions

1. Introduction

Processions are a subject of little attention in the literature so far. In particular, there is, to our knowledge, no analysis and modeling based on empirical data of the kinematics of processions. One of the few works dealing with traffic at street parades or carnivals has been published by M. Batty, J. DeSyllas and E. Duxbury [1]. They describe the impact of the route of the parade and the entire event on the surrounding traffic. In particular, simulations are used to check how traffic can be influenced by a modified parade route. In this context, we recently published a study in which a detailed data analysis of the kinematics of the Cologne Rose Monday procession is presented [2]. We developed a cellular automaton based parade group model for processions as a modified Nagel-Schreckenberg model. The statistical analysis of the kinematics of the Cologne Rose Monday procession carried out on the basis of provided GPS data from 2014, brought out characteristics of the movement that can be qualitatively reproduced by the parade group model.

An essential observation is that the foremost participants in this procession move along the pathway much faster than those at the lead. This is particularly interesting as one would normally expect the opposite, since it is a matter of a traffic system that is predominantly influenced by stop-and-go or congested traffic. This is exemplarily shown for the data set from 2014 in figure 1a. This phenomenon can be partly explained by the constantly moving leader driving ahead of the parade, leaving the pathway. Figure 1b illustrates the velocity of the whole processions averaged over time. The red line indicates the time point at which the leader of the parade leaves the pathway at the end. After its egress, a considerable increase of the velocity is observed. The quantitatively unidentified proportion of the velocity increase is due to the spatial contraction of the entire parade. The distances between the individual participants, with which they are deployed in the area in front of the path start, are not maintained during the parade. As a result, the passing by took about four hours at the end and about five hours at the beginning of the pathway in 2014.

In this contribution, we compare our earlier results with the kinematics of two other processions, the Marksmen’s parade 2017 in Hanover and the *Niederrheinischer Kinderkarnevalszug 2018* in Duisburg-Hamborn/Marxloh. At first, the methodology of the GPS measurement is described. Then an overview of general features of processions is given and afterwards the results of the data analysis are presented. Subchapter 4.1 describes the influence of the infrastructure on the dynamics of the Cologne Rose Monday parade from 2014. The velocity dependencies of the other mentioned parades are shown in subchapter 4.2.

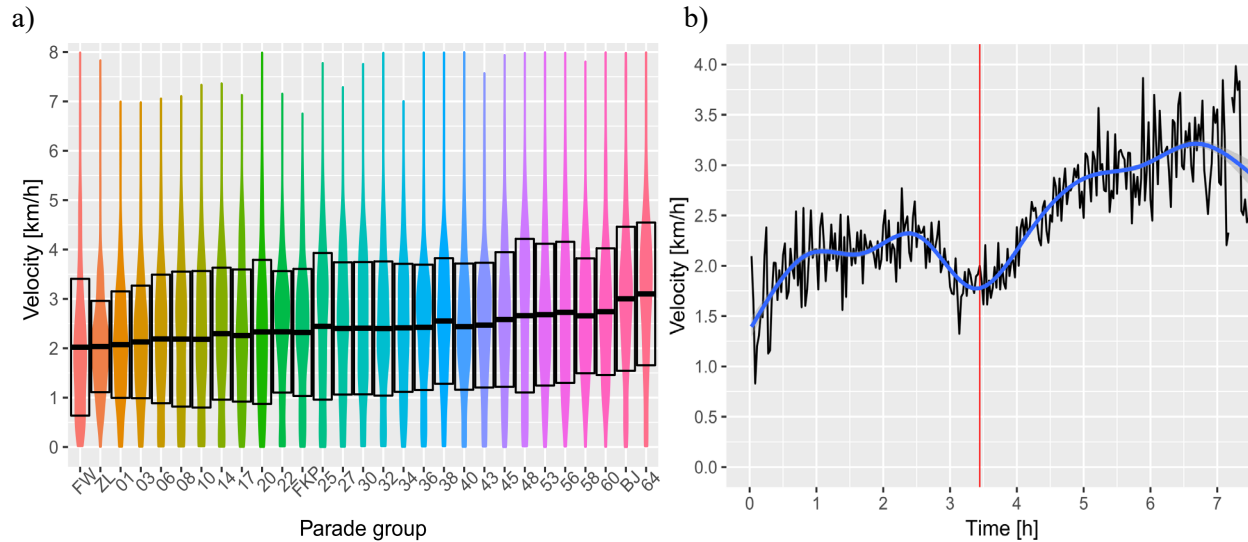


Fig. 1: a) Velocity distributions specifically colored for each GPS equipped parade group in the Cologne Rose Monday parade 2014. The boxes describe the standard deviation and the wide middle lines the mean values of the distributions. b) Velocity-time diagram: The black line represents the average velocity and the blue line an interpolated course. The width of the shaded area around the blue line corresponds to the quality of the interpolation. The red vertical line marks the time point at which the fire truck (leader) leaves the parade route. After this moment, the average velocity of the procession increases. [2]

2. GPS-Measurement/Methodology

The GPS Data required for the analysis of the traffic dynamics of the Cologne Rose Monday parade were provided by the *Festkomitee Kölner Karneval von 1823 e.V.* In 2014, 30 parade groups out of 65 were equipped with a GPS device so that the movement of the whole procession can be studied. The temporal resolution of this measurement was 30 seconds. For the collection of the traffic data of the *Marksmen’s Parade in Hanover* and the *Niederrheinischer Kinderkarnevalszug* we used the GPS data logger *Columbus V-990*, logging the data with a temporal resolution of 1 second. The recording of the parade’s movement was performed with 8 devices in equidistant placements in the procession.

In narrow streets with partly tall buildings, the accuracy of positioning has been reduced due to blocked or reflected GPS signals, as described in [3]. Due to the lateral inaccuracy of the GPS measurement, a map-matching was performed. Since the true position in the map should be known for the analysis of the GPS data, the map-matching algorithm is used to match the measured positions with a one-dimensional route in the road network of the city of Cologne, Hanover and Duisburg-Hamborn/Marxloh. The aim of these widely used map-matching algorithms is to determine coordinates of the recorded data corresponding to the actual positions of the GPS carrier most likely [4]. However, due to the transversal inaccuracy of the measurement, a change of the spatiotemporal order of the measuring points occurs. In addition, this order is disturbed by the orthogonal projection on narrow curves and at locations where the inaccuracy of the GPS measurement is bigger than the distance between two pathway sections. To filter only the data points with decent quality, an algorithm was developed that identifies the misprojected data points.

3. Characteristics of Processions

The kinematics of processions exhibit characteristics that differ from common road traffic. In general, the traffic flow of a system can be distinguished between interrupted and uninterrupted flows. In the case of an uninterrupted flow, the kinematics depend mainly on the roadway characteristics and the interactions between vehicles or traffic participants. On the other hand, traffic control systems (e.g. traffic signals, etc.) characterize interrupted traffic flows. However, processions mostly take place on a one-dimensional route and do not experience any kind of controlled flow interrupt. The movement dynamics are dominated by interactions of the participants with the infrastructure, visitors and the preceding participants. In the following, we will give an overview of the involved characteristics.

3.1. Boundary conditions

A procession can be classified regarding the kind of boundary condition. The major part exhibits open boundaries, which means that the parade's pathway has a start and a finish. Thus participants run the pathway down only once. In contrary, processions with periodic boundary conditions let the participants run the pathway several times down along a full circle. The weakest or slowest participant dominates the kinematics in a heterogeneous composited procession with periodic boundaries. Due to lack of data for processions with periodic boundaries, we study in the course of this contribution only processions with open boundary conditions.

3.2. Leader of a procession

Processions are commonly led by a participant who prescribes a specific velocity for the following parade. In the case of the Cologne Rose Monday parade the leader is a fire truck, whose gear ratio is capable to drive at three different, low velocities. The travel times of this truck have been measured on a test track of 1000 m and the velocities were calculated. The fire truck can drive in first gear at 1.428 km/h, in second gear at 2.068 km/h and in the third gear at 2.307 km/h. The leader in the *Niederrheinischer Kinderkarnevalsumzug* is likewise a specially adjusted carnival float capable to constantly prescribe a low velocity. The Marksmen's parade in Hanover whereas is headed by a public person by feet. This cannot hold a constant velocity by its very nature is contrary to an idling mixture supply. The velocity behaviour of the parade's leader is therefore either constant or varying and yet a variation of the velocity prescription can be reasoned or inherently chaotic.

3.3. Pathway, composition

The infrastructure of a parade essentially influences the dynamics of the procession. There are sections along the parade's path where participants have to adjust their speed for different reasons. Such places are exemplarily due to the festive activities along the pathway. Those are where the grandstands, party trucks, areas with high visitor numbers are located and a strong parader-visitor-interaction is observed. The interludes of the dancing groups are normally performed in front of the visitors, which gather increasingly on the grandstands and the load platforms of the trucks. There are also sections where the float drivers need to be extra careful because they come very close to buildings and sections, where the pathway width is only a little wider than the widest float. In the Cologne Carnival procession in front of the *Hotel Mondial*, there is a cobblestone paved road with a slope. The equestrian coaches cannot drive this part of the route, as long as the preceding group is still on this section. They wait at the intersection until they can pass through the section without interruption. A stop on the slope carries the risk of overloading the horses. There are several such sections on the path, which act as flow-reducing bottlenecks.

Further important properties of a procession are the length of the parade and its pathway. The parade route length of the Cologne Rose Monday parade is 7.6 km [5], of the Marksmen's parade in Hanover 3 km and the *Niederrheinischer Kinderkarnevalszug* in Duisburg-Hamborn 3.2 km long. If the pathway is shorter than the parade itself, the first participants already pass the end of the route, while the last participants are still waiting for their entry at the beginning of the path. Due to the absence of the velocity-prescribing leader, the adopted velocities mainly depend on the parade's composition and the paraders' behaviour..

Processions partially differ considerably in their composition (see table 1). In the case of demonstrations or protests and Corpus Christi processions, all participants move by foot, whereas in the case of the *Niederrheinischer Kinderkarnevalszug*, almost only motorized participants are taking part along with a few music and foot groups.

Table 1: Composition of the studied processions. The data for the Marksmen's parade and the Kinderkarnevalszug is based on observations from video recordings.

Participants	Cologne Rose Monday Parade 2014 [5]	Marksmen's parade Hanover 2017	Niederrheinischer Kinderkarnevalsumzug 2018
Persons in foot groups	3276	5302	400
Persons in music groups	3130	2828	125
Horses	328	35	0
Coaches	54	7	0
Cars	67	16	2
Trucks/tractors	85	17	22

Essentially, the participants can be classified in terms of their acceleration and braking ability. Typically, pedestrians are assumed to be able to accelerate to their targeted speed instantaneously, as well as decelerate from it to $v = 0$ km/h. While they are on the move, their velocity besides physiological factors (age, gender, size, fitness) is limited because of the leading participants. In comparison to this disordered movement of the groups on foot, the participants in the music corps keep a predetermined stepping frequency by the marching music. As a result, a music group moves along as a contiguous foot group in a correlated manner, without changing the gaps between the musicians significantly.

In order to be able to assess the dynamics of the procession as a whole, it is inessential to consider the behaviour of the individual participants and thus the composition of the parade. The types of processions discussed in this article take place on festive occasions, such as the *Rheinische Carnival* or Marksmen's parades in Germany. The behaviour of the participants in these processions differs and causes the kinematics of these procession types to differ.

While participants in the Cologne Rose Monday parade are encouraged not to allow gaps or to close them immediately, the participants in past-marches on Marksmen's parades as well as in military parades march orderly in lockstep or goose step through streets and squares. The marching music helps the effort to maintain the organized, steady and rhythmic walking forward. The correlated motion in a Marksmen's parade, as well as in military parades, mainly depends on the following details.

To start the move, the general gives the marching orders. Shortly thereafter, the music corps start to play the marching music and on the second beat, the first step is taken in the collective. The foot group starts and follows the rhythm of the commander. His group follows him in the cadence prescribed by him - also against the rhythm of the music. Usually, in a Marksmen's parade, some foot groups follow before the next music corps follows. Ideally, the music groups are synchronized with the music. If a synchronization of the bands is not possible, subsequent bands are just beginning to play, when the preceding music group has finished their playing. To intercept deviations, a so-called *Spiess* runs alongside each foot group to maintain order and to correct the participants. This *Spiess* has a particular importance in the movement of Marksmen's parades He ensures that the gaps between the parade groups, between the individual foot and music groups and between the ranks of the individual participants in the groups are maintained. The formation in the groups is ordered by body size. By tending to take larger steps, the bigger persons run a little faster and usually have to be "reminded" to keep their distance more often.

4. Results

4.1. Influence of the pathway on the kinematics

In this subchapter, the effect of the parade's pathway on the kinematics of the Cologne Rose Monday procession is described. The data is explored with respect to conspicuous route sections, where the procession adopts velocities above or below average velocities. For this purpose, the variance of velocity along the pathway is considered for all years. Since the parade route was not changed over the years for which data sets were provided, a correlated behaviour of the variances is observed. Therefore, the following figures give an exemplary overview of the distribution of obstructive sections along the pathway from 2014. The four dominant peaks in Fig. 2 are explained in table 2 in more detail.

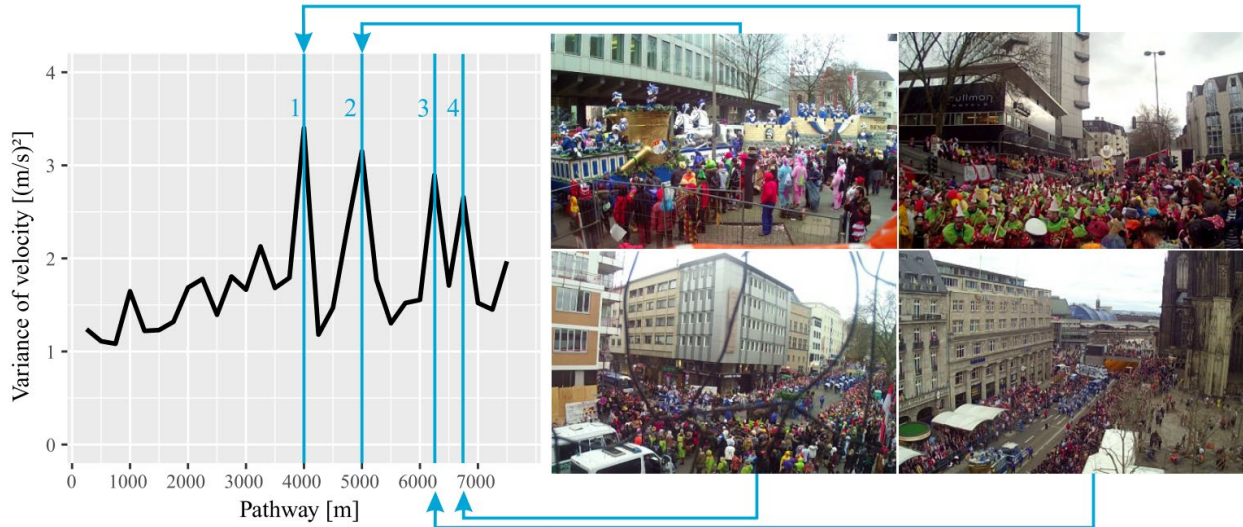


Fig. 2: Variance of the speed versus the travel path for the data set from 2014: The blue lines mark the maxima correlated for 2014 and 2016. The right pictures illustrate the corresponding local situation.

For the calculation of the variance, the path was divided into averaging intervals of 250 m. Because of the functional rule of the variance, only conclusions about the modulus of change is possible. However, it is probable that the local maxima observed here are solely indicative of velocity drops. This is based on observations in video recordings and in the participation in the event itself, as well as on statements of the festive committee of the Cologne Carnival, who described these sections in advance as flow reducing. Table 2 briefly describes the locations represented by vertical lines in Figure 2. In addition to the numbering and position indication, the main cause of the obstacles in these areas is described.

Table 2: Position and description of the main flow reducing sections along the Cologne Rose Monday parade's pathway

No.	Position [m]	Description
1	4000	Due to the large number of stands and party trucks, the number of visitors is particularly high. Since the path in this area is only demarcated from the visitors by means of barrier tape, they crowd onto the path and narrow the pathway width. In this state, the section acts like a bottleneck. The photo shows the parade and the audience, a clear demarcation is not recognizable.

2	4950	In this section, the route winds along some narrow curves through the area at the <i>Appellhofplatz</i> and in front of the <i>Vier-Scheiben-Haus</i> . There are sections, where the road width is not sufficient so that it is heaped up to form ramps on sidewalks. In particular, float with excess length must be ranked very cautiously here. The corresponding picture shows two large floats passing through the bottleneck.
3	6250	At the illustrated curve in the area of the street <i>Am Hof</i> , the route has a slope. On this slope draft horses with carriages must not stop, because the starting is very difficult for draft horses. Therefore, the carriages should wait at the curve until the ascent or the next 100 m are free. In addition, the road is paved with cobblestone, which is slippery in the rain. These features naturally lead to a traffic jam.
4	6750	The parade route leads along the <i>Trankgasse</i> to the main station forecourt. There, it forms a traffic area transition from the street to traffic areas intended exclusively for pedestrians. The high sidewalk (20 - 30 cm) is bridged by a ramp and must be driven carefully by the drivers.

4.2. Analysis of the velocities in the Marksmen's parade Hanover 2017 and the Niederrheinischer Kinderkarnevalsumzug 2018

In this subchapter, the analysis of the kinematics of the Marksmen's parade 2017 in Hanover and the *Niederrheinischer Kinderkarnevalsumzug 2017* in *Duisburg-Hamborn* is presented. Figure 3 illustrates the dependency of the averaged parade velocity against time. For this, the arithmetic average of all velocities was calculated over a time interval of 10 seconds. This course is shown in Figure 3 by the black curve.

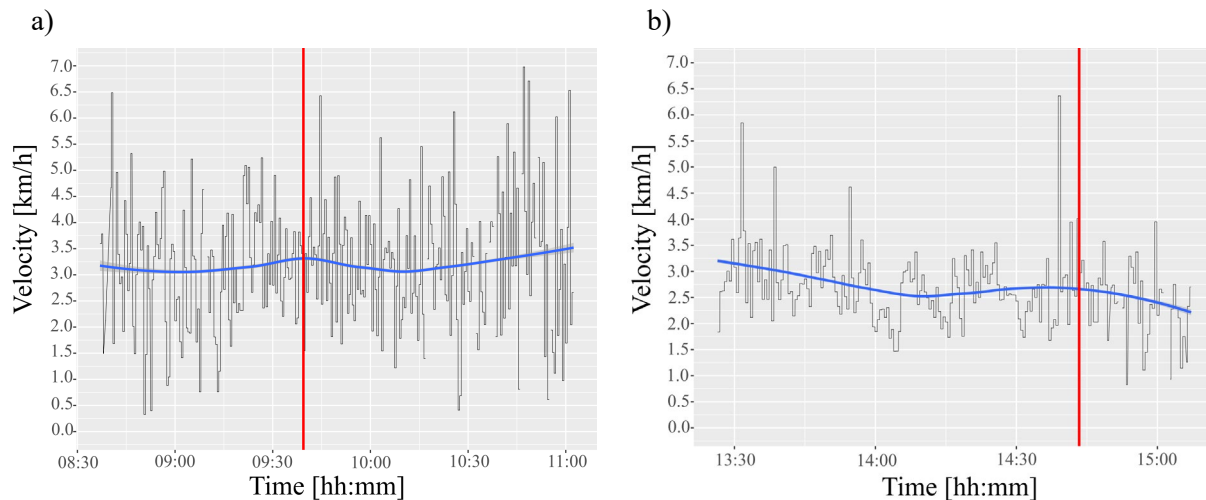


Fig. 3: Velocity-time diagram of the studied parades; a) Hanover Marksmen's parade 2017, b) Niederrheinischer Kinderkarnevalsumzug 2018: The black line represents the over a time interval of 10 seconds averaged velocity and the blue line an interpolated course. The red vertical line marks the time point at which the leader of the parade leaves the route. After this moment, the velocity increases in a) not considerably, in b), the velocity continues its decrease during the whole procession.

The blue, superimposed line shows an interpolation of the determined values and the associated gray, shaded area around the blue curve corresponds to the degree of accuracy of the interpolation. The red line, as in Figure 1b, corresponds to the time point at which the leader of the parade reaches the end of the pathway. Up to the outlet of the leader, the velocity is kept nearly constant. The pageant experiences up to this point, a minimal increase in velocity. After this time, the average speed of the parade decreases. Based on this illustration it can be asserted that the missing velocity prescribing leader causes no increase, but in

fact a change in the velocity of the following. This is due to the effort of the participants to move in order and uniformly, rather to close up the ranks. This behaviour is indicative of arising gaps, which are indeed observed in video recordings of the parade.

Figure 3 b) depicts a similar illustration to Figure 3 a). Due to the brevity of the procession (both temporal and spatial), the exit of the leader can be observed relatively late. The course of the average speed as a function of time shows a monotonous decrease towards later times. In particular, no increase in velocity is observed after the leading participant has left the pathway. Rather, the declining behaviour continues. It is noteworthy that the parade comes to a standstill at approximately 14:00 h. The velocity breakdowns within the last half hour are due to arising congestion in the dissolution area, after the end of the path. That at the end of the path the remaining sweets are handed out and disproportionately many people are waiting there accordingly, is a generic feature of carnival parades. For example, with a length of 10 km, the pageant in Cologne has to be properly disbanded, as experience has shown that this is responsible for persistent congestion on the parade's route.

Table 2: Duration of each procession presented in this contribution calculated for sections at the start the end of the pathway. The parade in Cologne shows a remarkable change of the procession's duration. The duration of the Marksmen's parade in Hanover does not change plainly, whereas in the case of the parade in Duisburg-Hamborn, an increase of the duration is observed.

		Cologne Rose Monday parade 2014	Marksmen's parade Hanover 2017	Niederrheinischer Kinderkarnevalszug 2018
Duration of procession	Start	5 h 06 min	1 h 29 min	0 h 18 min
	End	4 h 10 min	1 h 23 min	0 h 24 min
Relative Contraction		22.4 %	7.2 %	- 33.3 %

5. Conclusion

In this contribution, we presented a GPS-data-based kinematic analysis of different processions. We analysed the influence of the pathway on the kinematics of the Cologne Rose Monday procession. A number of sections can be identified as flow-reducing bottlenecks. The observed obstructions can be assumed generic for the procession types described here. We further outlined general aspects of processions and executed the data analysis in this context. It is shown that in the case of the Marksmen's parade in Hanover the behaviour of the participants influences the kinematics of the whole procession significantly. Kinematical differences are observed that partially depend on the parade-length/pathway-length ratio and partially on the individual composition of the parades. Although the Marksmen's parade is longer than its pathway, no considerable increase in velocity is observed after the parade leader has left the route. The average velocity of the parade in Duisburg, whose length is smaller than the pathway, shows a decrease. The analysis of the processions presented here prompts that different behavioral patterns of participants can be presumed in processions. It would be interesting to have a systematic study of the rules according to which groups of people move in a regular procession. This would further improve the understanding of the movement of processions.

Acknowledgements

We would like to thank the *Festkomitee Kölner Karneval 1823 e.V.* for providing the GPS data of the Cologne Rose Monday parade, as well as the many discussions contributing significantly to the development of this work. Furthermore, we are very grateful to the event management of the city Hanover, in particular Mr. Ralf Sonnenberg, who let us put our GPS devices on the Marksmen's parade. Finally, yet importantly, we would like to thank the parade chief of the *Niederrheinischer Kinderkarnevalszug*,

Karlheinz Müller and his associated carnival society *1. Große Karnevalsgesellschaft Rot-Weiß Hamborn-Marxloh* for their kind cooperation.

References

- [1] M. Batty, J. Desyllas, and E. Duxbury, “The discrete dynamics of small-scale spatial events: agent-based models of mobility in carnivals and street parades,” *Int. J. Geographic. Inf. Sci.*, vol. 17, no. 7, pp. 673-697, 2003.
- [2] P. Polichronidis, D. Wegerle, A. Dieper, and M. Schreckenberg, “Traffic dynamics of carnival processions,” *EPL (Europhysics Letters)*, vol. 121, no. 6, 2018.
- [3] L. Wang, P. D. Groves, and M. K. Ziebart, “Multi-Constellation GNSS Performance Evaluation for Urban Canyons Using Large Virtual Reality City Models,” *Journal of Navigation*, vol. 65, no. 3, pp. 459-476, 2012.
- [4] C. A. Scott and C. R. Drane, “Increased accuracy of motor vehicle position estimation by utilising map data: vehicle dynamics, and other information sources” in *Vehicle Navigation and Information Systems Conference*, Yokohama, Japan, 1994, pp. 585-590.
- [5] Festkomitee des Kölner Karnevals von 1823 e.V. (2018, May 10). Rosenmontagszug [Online]. Available: <https://koelnerkarneval.de/zuege/#zug-in-zahlen>

Noise-Induced Stop-and-Go Dynamics in Pedestrian Single-file Motion

Andreas Schadschneider¹, Antoine Tordeux²

¹ Institut für Theoretische Physik, Universität zu Köln, 50937 Köln, Germany
as@thp.uni-koeln.de

² Institut für Sicherheitstechnik, Bergische Universität Wuppertal, 42119 Wuppertal, Germany
tordeux@uni-wuppertal.de

Abstract - Stop-and-go waves are a common feature of vehicular traffic and have also been observed in pedestrian flows. Usually the occurrence of this self-organization phenomenon is related to an inertia mechanism. It requires fine-tuning of the parameters and is described by instability and phase transitions. Here, we present a novel explanation for stop-and-go waves in pedestrian dynamics based on stochastic effects. By introducing coloured noise in a stable microscopic inertia-free (i.e. first order) model, pedestrian stop-and-go behaviour can be described realistically without requirement of instability and phase transition. We compare simulation results to empirical pedestrian trajectories and discuss plausible values for the model's parameters.

Keywords: Pedestrian single-file motion, stop-and-go dynamics, first-order microscopic models, coloured noise, simulation

1. Introduction

Stop-and-go waves in traffic flow have been studied for several decades [1-3] (see [4,5] for reviews). Curiously, congested flows self-organise in waves of slow and fast traffic (stop-and-go) instead of streaming homogeneously. Stop-and-go dynamics which can not be explained by disturbance due to the infrastructure are observed in road traffic, bicycle and pedestrian movements [6] both in reality as well as in experiments [7]. Besides its scientific interest, such self-organisation phenomena impact transportation networks in terms of safety, economy, and comfort.

In modelling, stop-and-go behaviour can be analysed with microscopic, mesoscopic (kinetic) and macroscopic models based on non-linear differential systems (see for instance [8-10]), but also with discrete models like cellular automata. The models based on systems of differential equations have homogeneous equilibrium solutions that can become unstable for certain values of the parameters. The stable cases describe homogeneous dynamics whereas in unstable cases periodic or quasi-periodic solutions describe non-homogeneous dynamics. In the latter case, potentially stop-and-go waves can occur after fine-tuning of the parameters.

Phase transition and instability in self-driven dynamical systems far from equilibrium are commonly observed in physics, theoretical biology or social science [11-15]. In vehicular traffic, typical continuous models are inertial second order systems based on relaxation processes. Stop-and-go dynamics and matching to Korteweg–de Vries (KdV) and modified KdV soliton equations occur when the inertia of the vehicles exceed critical values [8,16,17]. Empirical evidence for phase transitions in traffic, like hysteresis or capacity drop, has been observed in real data as well as during experiments [2,7]. Yet the number of phases and their characteristics remain actively debated [18].

Some studies describe pedestrian stop-and-go dynamics by means of, as traffic models, instability and phase transitions [19-22]. However, to our knowledge, empirical evidence for phase transitions and instability has not been observed for pedestrian flow. Pedestrian dynamics shows no pronounced inertia effect since human capacity nearly allows any speed variation at any time. Furthermore, pedestrian motion does not show mechanical delays. Nevertheless, stop-and-go behaviour is observed at congested density levels [6,23].

In this work, we propose a novel explanation of stop-and-go phenomena in pedestrian flows as a consequence of stochastic effects. We first present statistical evidence for the existence of Brownian noise in pedestrian speed time-series. Then a microscopic model composed of a minimal deterministic part for the convection and a relaxation process for the noise is proposed and analysed. Simulation results show that the stochastic approach allows describing realistic pedestrian stop-and-go dynamics without instability and fine-tuning of the parameters.

2. Stochastic first order model

Stochastic effects can have various roles in the dynamics of self-driven systems [24]. Generally speaking, the introduction of white noise in models tends to increase the disorder in the system [12] or prevents self-organisation [25]. Coloured noises can affect the dynamics and generate complex patterns [26,27]. Coloured noise has been observed in human response [28,29]. Pedestrian as well as driver behaviours result from complex human cognition. They are intrinsically stochastic in the sense that the deterministic modelling of the driving, i.e. the modelling of the human cognition composed of up to 10^{11} neurons [30], is not possible. Furthermore the behaviour of drivers and pedestrians can be influenced by various factors, e.g. environment, experience, culture, psychology, etc. Stochastic effects and noises are the main emphases of many pedestrian or road traffic modelling approaches (see, e.g., white noises [31, 17], pink-noise [32], action-point [33], or again inaccuracies or risk-taking behaviour [34,35]).

In Fig. 1 statistical evidence for the existence of Brownian noise in a time series of pedestrian speeds is presented. Brownian noise has a power spectral density (PSD) proportional to the square of the inverse noise frequency $1/f^2$. A characteristic linear tendency is observed independent of the density (see [36] for further details). Such a noise with exponentially decreasing time-correlation function can be described by using the Ornstein-Uhlenbeck process (see e.g. [37]).

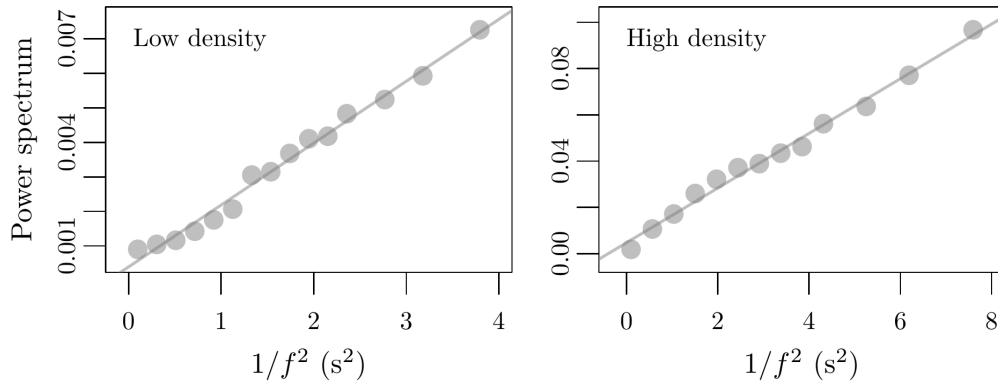


Fig. 1: Periodogram power spectrum estimate for the speed time-series of pedestrians at low and high density. The power spectrum shows the characteristic $1/f^2$ behaviour of Brownian noise.

We denote in the following $x_k(t)$ the curvilinear position of the pedestrian k at time t . Pedestrian $k+1$ is the predecessor of k . The model is the Langevin equation

$$\begin{aligned} dx_k(t) &= V(x_{k+1}(t) - x_k(t))dt + \varepsilon_k(t)dt \\ d\varepsilon_k(t) &= -\frac{1}{\beta} \varepsilon_k(t)dt + \alpha dW_k(t) \end{aligned}$$

Here $V: s \rightarrow V(s)$ is a differentiable and non-decreasing optimal velocity (OV) function for the convection [8], while $\varepsilon_k(t)$ is a noise described by the Ornstein-Uhlenbeck stochastic process. In the following, an

affine function $V(s)=(s-l)/T$ is used with T the time gap between the agents and l their size. (α, β) are positive parameters related to the noise. α is the volatility while β is the noise relaxation time. $W_k(t)$ is a Wiener process. The homogeneous solution is stable for any positive values of the parameters in the deterministic case where $\alpha=0$. Note that alternatively, the model can be defined as a special stochastic form of the Full Velocity Difference model [38].

3. Simulation results

We have performed simulations using an explicit Euler-Maruyama numerical scheme with time step $\delta t=0.01$ s. The parameter values are $T=1$ s, $l=0.3$ m, $\alpha=0.1$ $\text{ms}^{-3/2}$ and $\beta=5$ s. Such values are close to the statistical estimates for pedestrian flow [36]. The length of the system is $L=25$ m, corresponding to the experimental situation, and the boundary conditions are periodic.

Simulations from jam initial conditions are carried out for systems with $n=25, 50$ and 75 agents with the stochastic model and the unstable deterministic optimal velocity model introduced in [39]. The trajectories during the first 120 s are presented in Fig. 2 while the mean time-correlation functions for the distance spacing in stationary states (i.e. for large simulation time) are presented in Fig. 3. The peaks of the time-correlations match for both stochastic and deterministic models, i.e. the frequency of the stop-and-go waves are the same. A wave propagates backward in the system at a speed $c=-l/T$ while vehicles travel in average at the speed $v=(L/n-l)/T$. In agreement with the theory, the wave period is $L/(v-c)=nT$.

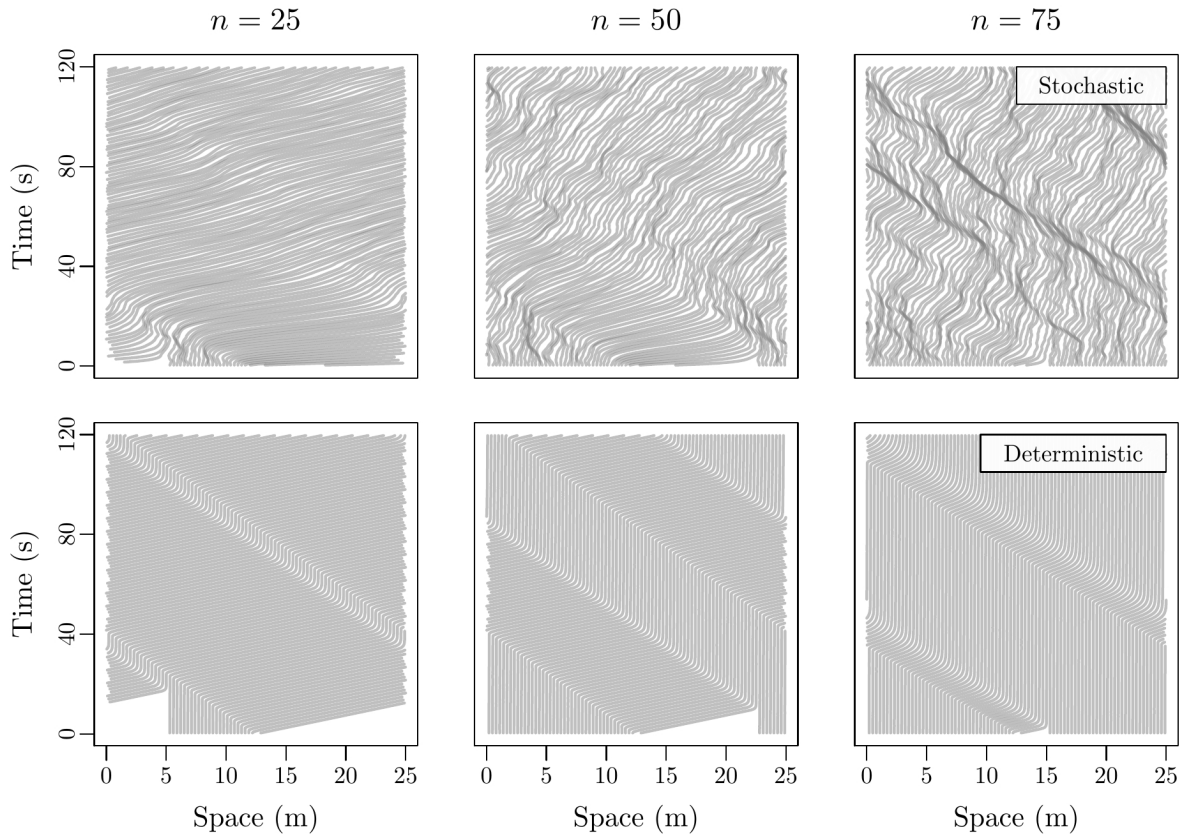


Fig. 2: Simulated trajectories for different density levels with the stochastic model presented in the paper (top panel) and the deterministic model with instability and phase transition introduced in [39] (bottom panels).

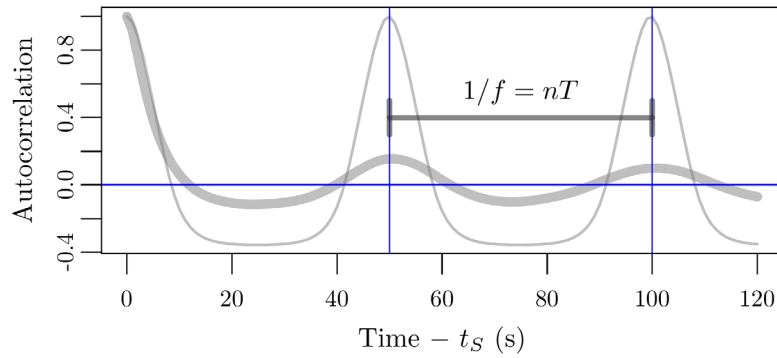


Fig. 3: Mean time-correlation function in stationary states of the distance spacing for the stochastic model (bold curve) and the deterministic model introduced in [39] (thin curve). The same period $1/f = nT$ for the stop-and-go waves is observed. The simulation time to consider the system stationary is $t_S = 2 \cdot 10^5$.

Numerical experiments are carried out for different values of the noise parameters α and β . In Fig. 4, the trajectories of 50 agents are presented for $\alpha = 0.05, 0.1$ and $0.2 \text{ ms}^{-3/2}$ while $\beta = 1.25, 5$ and 20 s . The values are chosen such that the amplitude of the noise is constant. For small β the noise tends to be white and unstable waves emerge locally and disappear (see Fig. 4, left panel). For large relaxation times β , the noise autocorrelation is high and stable waves with large amplitude occur (Fig. 4, right panel). The parameters of the noise influence the amplitude of the time-correlation function, but not the frequency that only depends on the parameters n and T , see Fig. 5.

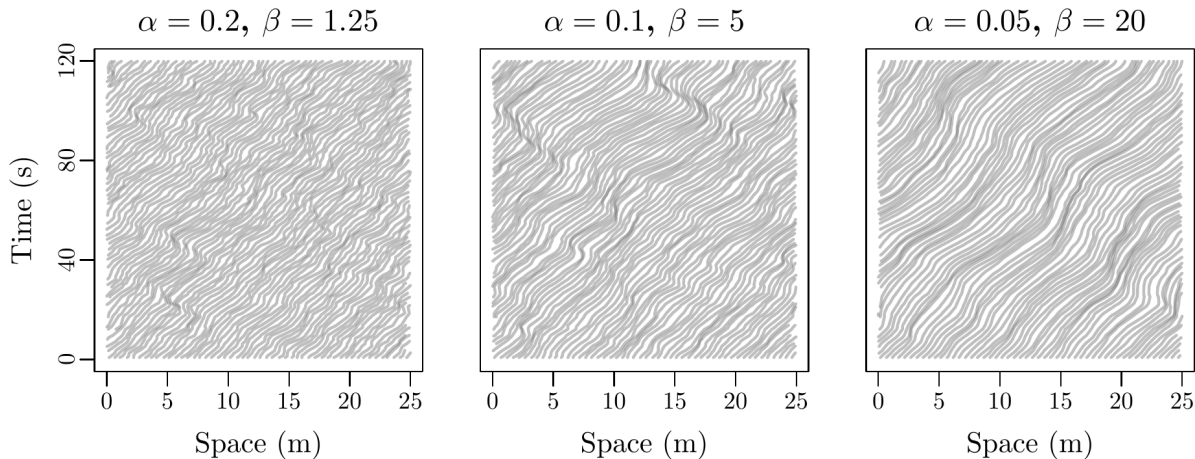


Fig. 4: Simulated trajectories for $n=50$ agents and different values of the noise parameters (units: α in $\text{ms}^{-3/2}$, β in s). The initial configuration is homogeneous.

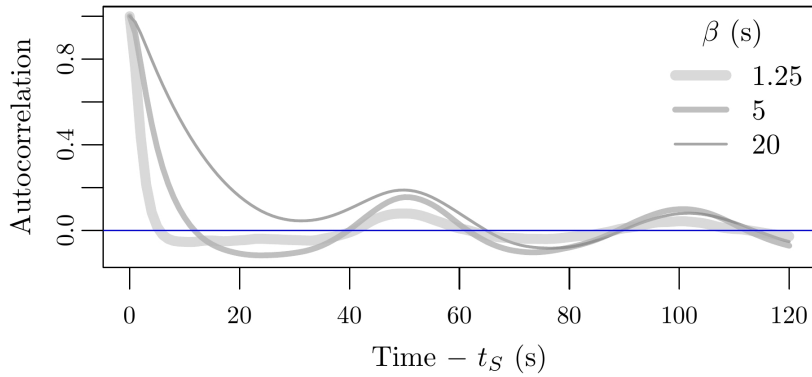


Fig. 5: Mean time-correlation function of the distance spacing in the stationary state for different values of the noise parameters. The frequency of the waves only depends on n and T . The simulation delay time is $t_s=2 \cdot 10^5$ s.

In Fig. 6, real trajectories for experiments with 28, 45 and 62 participants (see [36]) and simulations with the stochastic model are compared. The simulations are in good agreement with the empirical data. Stop-and-go waves appear for semi-congested ($n = 45$) and congested ($n = 62$) states, while free states ($n = 28$) seem homogeneous in both empirical data and simulation.

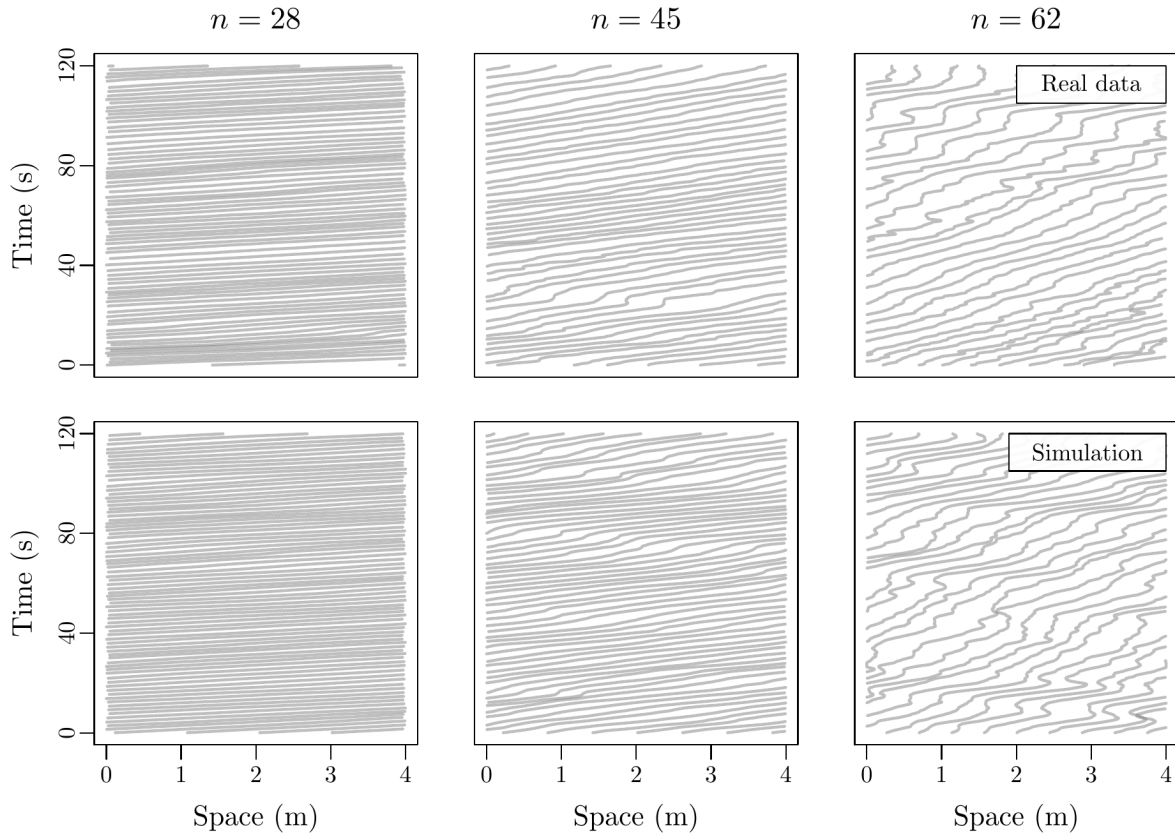


Fig. 6: Empirical (top panels) and simulated (bottom panels) trajectories for different densities. The initial configuration is homogeneous in both the real experiments and the simulations.

4. Conclusions

We have proposed an alternative explanation for stop-and-go phenomena in pedestrian flows. In our stochastic approach, they are the consequence of a coloured noise in the dynamics of the speed. The oscillations in the system occur as a consequence of the perturbations introduced by the noise. This mechanism qualitatively describes stop-and-go waves, especially when the system is weakly damped. The approach differs from classical deterministic traffic models with inertia. Here stop-and-go occurs due to instability and phase transitions to periodical dynamics. These basic differences between the two routes to stop-and-go behavior are summarized in Fig. 7.

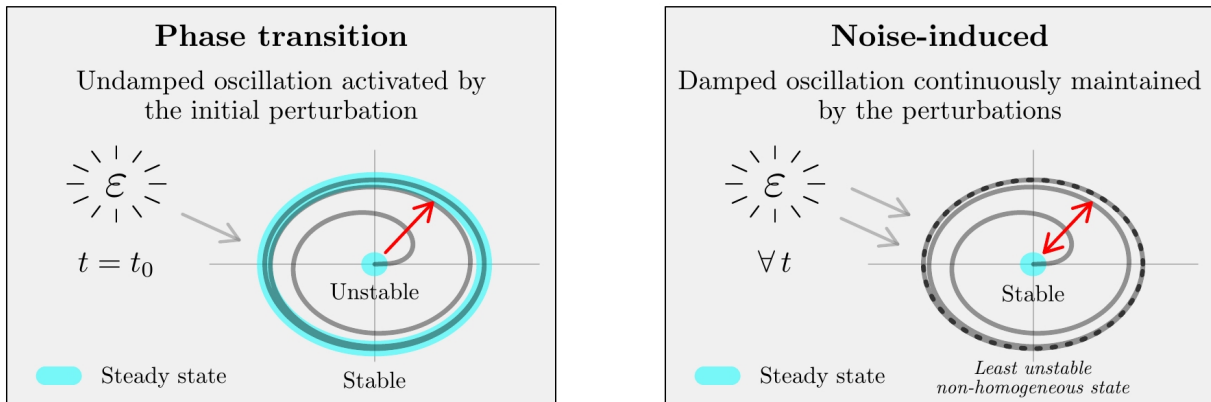


Fig. 7: Illustrative scheme for the modelling of stop-and-go dynamics with phase transition in the periodic solution (left panel) and the noise-induced oscillating behaviour (right panel).

We have identified two mechanisms based on relaxation processes for the description of stop-and-go waves. In the novel stochastic approach, the relaxation time is related to the noise and is estimated to approximately 5 s [36]. The parameter corresponds to the mean time period of the stochastic deviations from the phenomenological equilibrium state. Such a time can be large, especially when the deviations are small and the spacings are large. In the classical inertial approaches, the relaxation time is interpreted as the driver/pedestrian reaction time and is estimated by around 0.5 to 1 s. Technically, such a parameter can not exceed the physical time gap between the agents (around 1 to 2 s) without generating unrealistic (collision) behaviour and has to be set carefully.

The goal of the present study was to develop a realistic model for the description of pedestrian streams, but a toy model to demonstrate an alternative mechanism for the formation of stop-and-go waves. The results are relevant also for the interpretation of empirical and experimental data. In future studies, the effects of more realistic interactions, heterogeneities etc. need to be elucidated.

Acknowledgements

The authors thank Prof. Michel Roussignol for his help in the formulation of the model. Financial support by the German Science Foundation (DFG) under grant SCHA 636/9-1 is gratefully acknowledged.

References

- [1] Herman, R., Montroll, E., Potts, R., Rothery, R.: Traffic dynamics: analysis of stability in car-following. *Op. Res.* 7(1), 86–106 (1959).
- [2] Kerner, B.S., Rehborn, H.: Experimental properties of phase transitions in traffic flow. *Phys. Rev. Lett.* 79, 4030–4033 (1997).
- [3] Orosz, G., Wilson, R.E., Szalai, R., Stépán, G.: Exciting traffic jams: Nonlinear phenomena behind traffic jam formation on highways. *Phys. Rev. E* 80(4), 046,205 (2009).
- [4] Chowdhury, D., Santen, L., Schadschneider, A.: Statistical physics of vehicular traffic and some related systems. *Phys. Rep.* 329(4-6), 199–329 (2000).
- [5] Kerner, B.: *The Physics of Traffic*. Springer (2004).
- [6] Zhang, J., Mehner, W., Holl, S., Boltes, M., Andresen, E., Schadschneider, A., Seyfried, A.: Universal flow-density relation of single-file bicycle, pedestrian and car motion. *Phys. Lett. A* 378(44), 3274–3277 (2014).
- [7] Sugiyama, Y., Fukui, M., Kikushi, M., Hasebe, K., Nakayama, A., Nishinari, K., Tadaki, S.: Traffic jams without bottlenecks. Experimental evidence for the physical mechanism of the formation of a jam. *New J. Phys.* 10(3), 033,001 (2008).
- [8] Bando, M., Hasebe, K., Nakayama, A., Shibata, A., Sugiyama, Y.: Dynamical model of traffic congestion and numerical simulation. *Phys. Rev. E* 51(2), 1035–1042 (1995).
- [9] Helbing, D., Treiber, M.: Gas-kinetic-based traffic model explaining observed hysteretic phase transition. *Phys. Rev. Lett.* 81, 3042–3045 (1998).
- [10] Colombo, R.: Hyperbolic phase transitions in traffic flow. *SIAM J. Appl. Math.* 63(2), 708–721 (2003).
- [11] Ben-Jacob, E., Schochet, O., Tenenbaum, A., Cohen, I., Czirok, A., Vicsek, T.: Generic modelling of cooperative growth patterns in bacterial colonies. *Nature* 368, 46–49 (1994).
- [12] Vicsek, T., Czirók, A., Ben-Jacob, E., Cohen, I., Shochet, O.: Novel type of phase transition in a system of self-driven particles. *Phys. Rev. Lett.* 75, 1226–1229 (1995).
- [13] Bussemaker, H., Deutsch, A., Geigant, E.: Mean-field analysis of a dynamical phase transition in a cellular automaton model for collective motion. *Phys. Rev. Lett.* 78, 5018–5021 (1997).
- [14] Buhl, J., Sumpter, D.J.T., Couzin, I.D., Hale, J.J., Despland, E., Miller, E.R., Simpson, S.J.: From disorder to order in marching locusts. *Science* 312, 1402–1406 (2006).
- [15] Hermann, G., Touboul, J.: Heterogeneous connections induce oscillations in large-scale networks. *Phys. Rev. Lett.* 109, 018,702 (2012).
- [16] Muramatsu, M., Nagatani, T.: Soliton and kink jams in traffic flow with open boundaries. *Phys. Rev. E* 60, 180–187 (1999).
- [17] Tomer, E., Safonov, L., Havlin, S.: Presence of many stable nonhomogeneous states in an inertial car-following model. *Phys. Rev. Lett.* 84, 382–385 (2000).
- [18] Treiber, M., Kesting, A., Helbing, D.: Three-phase traffic theory and two-phase models with a fundamental diagram in the light of empirical stylized facts. *Transport. Res. B: Meth.* 44(89), 983–1000 (2010).
- [19] Portz, A., Seyfried, A.: Modeling Stop-and-Go Waves in Pedestrian Dynamics. . In: *Lect. Notes Comp. Sci.*, vol. 6068, pp. 561–568 (2010).
- [20] Moussaïd, M., Helbing, D., Theraulaz, G.: How simple rules determine pedestrian behavior and crowd disasters. *Proc. Nat. Acad. Sci.* 108(17), 6884–6888 (2011).
- [21] Kuang, H., Fan, Y., Li, X., Kong, L.: Asymmetric effect and stop-and-go waves on single-file pedestrian dynamics. *Procedia Eng.* 31, 1060 – 1065 (2012).
- [22] Lemercier, S., Jelic, A., Kulpa, R., Hua, J., Fehrenbach, J., Degond, P., Appert-Rolland, C., Donikian, S., Pettr, J.: Realistic following behaviors for crowd simulation. *Comput. Graph. Forum* 31(2pt2), 489–498 (2012).

- [23] Seyfried, A., Portz, A., Schadschneider, A.: Phase coexistence in congested states of pedestrian dynamics. In: *Lect. Notes Comp. Sci.*, vol. 6350, pp. 496–505 (2010).
- [24] Hänggi, P., Jung, P.: *Colored Noise in Dynamical Systems*, pp. 239–326. John Wiley & Sons, Inc. (2007).
- [25] Helbing, D., Farkas, I., Vicsek, T.: Freezing by heating in a driven mesoscopic system. *Phys. Rev. Lett.* 84(6), 1240–1243 (2000).
- [26] Arnold, L., Horsthemke, W., Lefever, R.: White and coloured external noise and transition phenomena in nonlinear systems. *Z. Phys. B* 29(4), 367–373 (1978).
- [27] Castro, F., Sánchez, A.D., Wio, H.S.: Reentrance phenomena in noise induced transitions. *Phys. Rev. Lett.* 75, 1691–1694 (1995).
- [28] Gilden, D., Thornton, T., Mallon, M.: $1/f$ noise in human cognition. *Science* 267(5205), 1837–1839 (1995).
- [29] Zgonnikov, A., Lubashevsky, I., Kanemoto, S., Miyazawa, T., Suzuki, T.: To react or not to react? Intrinsic stochasticity of human control in virtual stick balancing. *J. R. Soc. Interface* 11(99) (2014).
- [30] Williams, R., Herrup, K.: The control of neuron number. *Annu. Rev. Neurosci.* 11(1), 423–453 (1988).
- [31] Helbing, D., Molnár, P.: Social force model for pedestrian dynamics. *Phys. Rev. E* 51(5), 4282–4286 (1995).
- [32] Takayasu, M., Takayasu, H.: $1/f$ noise in a traffic model. *Fractals* 01(04), 860–866 (1993).
- [33] Wagner, P.: How human drivers control their vehicle. *Eur. Phys. J. B* 52(3), 427–431 (2006).
- [34] Treiber, M., Kesting, A., Helbing, D.: Delays, inaccuracies and anticipation in microscopic traffic models. *Phys. A* 360(1), 71–88 (2006).
- [35] Hamdar, S., Mahmassani, H., Treiber, M.: From behavioral psychology to acceleration modeling: Calibration, validation, and exploration of drivers cognitive and safety parameters in a risk-taking environment. *Transp. Res. B-Meth.* 78, 32 – 53 (2015).
- [36] Tordeux, A., Schadschneider, A.: White and relaxed noises in optimal velocity models for pedestrian flow with stop-and-go waves. *J. Phys. A* 49(18), 185,101 (2016).
- [37] Lindgren, G., Rootzen, H., Sandsten, M.: *Stationary Stochastic Processes for Scientists and Engineers*. Taylor & Francis (2013).
- [38] Jiang, R., Wu, Q., Zhu, Z.: Full velocity difference model for a car-following theory. *Phys. Rev. E* 64, 017,101 (2001).
- [39] Tordeux, A., Seyfried, A.: Collision-free nonuniform dynamics within continuous optimal velocity models. *Phys. Rev. E* 90, 042,812 (2014).

Tsunami evacuation facility choice behavior model in flat area and rias area considering possibility to remain at home

Hiroyuki Yoshihara, Tatsuya Kishimoto

Graduate School of Science and Technology, Keio Univ.
Yokohama City, Japan

Abstract - The tsunami associated with the Great East Japan Earthquake that occurred on March 11, 2011 caused enormous damage to the coast of the Pacific Ocean. Since the occurrence of the Great Earthquake, it is urgent to develop tsunami evacuation countermeasures against the great tsunamis caused by the large earthquake that is expected to occur in the future in the country and coastal municipalities. In this study, we used logit model to estimate each parameters about the relationship between evacuees and buildings in flat area and rias area by using the evacuation behavior survey data of the Great East Japan Earthquake in 2011. The estimated results show that “whether the evacuation destination is home or not” is important when people choose the tsunami evacuation destination. Moreover, by comparing the moving in flat area and in rias area the difference between them becomes clear. By using these models, it enables to estimate the home selection probability in flat area and rias area.

Keywords: Tsunami, Evacuation behavior, Tsunami evacuation facility, Logit Model

1. Research background and purpose

The Great Tsunami associated with the Great East Japan Earthquake that occurred on March 11, 2011 caused enormous damage to the coast of the Pacific Ocean. Since the occurrence of the Great East Japan Earthquake, it is urgent to develop tsunami evacuation countermeasures against the tsunami caused by the large earthquake that is expected to occur in the future in the country and coastal municipalities.

A tsunami evacuation plan was formulated on the premise of evacuation to the nearest facility on the land side by foot. [1] However, it is clear that some people evacuate by car or stay at home without choosing to evacuate from the survey targeting Ojimachi City, Chiba Prefecture and Natori City, Miyagi Prefecture. [2] [3] In addition, there were characteristics of the evacuation destination selection due to differences in topography such as flat and rias. [4] The purpose of this research is to clarify the characteristics of the actual evacuation behavior of the coastal community residents at the time of the occurrence of the tsunami, by modeling the evacuation facility choice behavior of evacuees at the time of the Great East Japan Earthquake.

Specifically, we modeled the actual evacuation facility selection behavior at the time of the Great East Japan Earthquake using a multinomial logit model, and identified influential factors. Then, we calculated the home selection probability and clarified the evacuation difficulty area. We analyzed these in the topography of the flat area and the rias area and applied it to the regions where there is a possibility of the tsunami damage in the future, which helps the tsunami evacuation plan. Therefore, it is significant to compare and analyze the results.

2. Evacuation behavior in target area

The target areas are areas having sufficient number of samples for each municipality. In flat areas, they are Sendai City, Natori City, Iwanuma City, Watari-cho, Yamamoto-cho, and in rias area they are Ofunato City, Rikuzentakada City, Kesenuma City. The evacuation behavior data for modeling the evacuation behavior to the evacuation facility are GIS data of “Reconstruction Support Survey Archive”.

These are the point data of the evacuation place obtained by the questionnaire survey by the investigator's interview, and the polyline data of the evacuation route on the day of the Great East Japan earthquake disaster. The interview is carried out by the Ministry of Land, Infrastructure and Transport. The data set includes 20,503 routes of 10,603 people who suffered flood damage by the tsunami in 49 municipalities in 6 prefectures of Aomori, Iwate, Miyagi, Fukushima, Ibaraki and Chiba. Fig. 1 shows target areas in flat area and in rias area.

In order to create models with high versatility, we defined subjects for analysis as follows. We focused on evacuation behaviors in the coastal area by restricting the start of movement to within 1 km from the tsunami inundation area. We focused on the pure tsunami evacuation behavior by limiting the purpose of movement to "for evacuation from the tsunami" and "to go to shelter ". We focused on evacuees who move by walking and by car, since 90% or more of people walked or used a car on the day of the Great East Japan earthquake disaster. We eliminated the secondary evacuation after the tsunami by limiting the end time of the evacuation to the time before the tsunami maximum wave arrival time. The end of the movement was limited to home, designated evacuation shelters, facilities where more than two evacuated, since samples evacuated to a place that only a specific individual recognizes as an evacuation destination, such as an office or an acquaintance house among the evacuees of the tsunami, is not highly versatile as compared with other destinations. Therefore, in flat area, 439 routes are defined as above (route 100 of Sendai city, 128 routes of Natori City, 51 routes of Iwanuma City, 80 routes of Watari-cho, 80 routes of Yamamoto-cho) and, in rias area, 359 routes are defined as above (89 routes of Ofunato City, 49 routes of Rikuzentakada City, 221 Route of Kesennuma City).

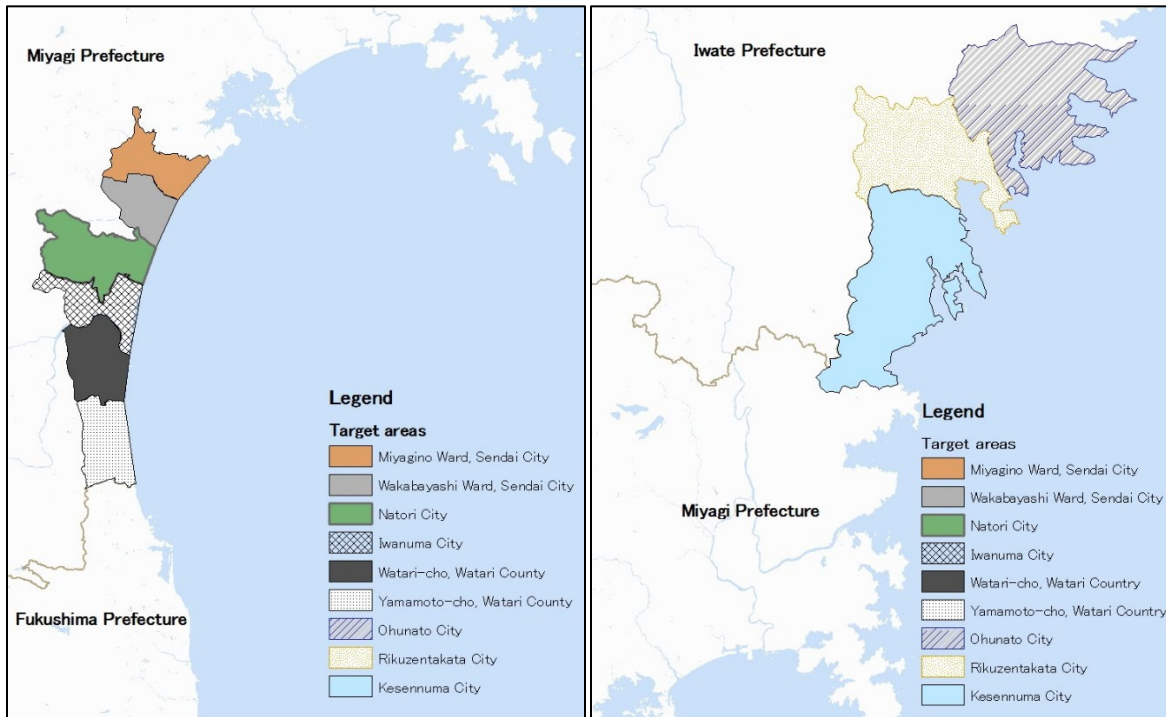


Fig. 1: Target areas in flat area (left) and in rias area (right)

3. Evacuation behavior in target area

We estimate parameters of utility function using a multinomial logit model. The selection probability P_{ij} and the utility U_{ij} of the utility function are defined as follows when each evacuee selects the evacuation facility as the evacuation destination.

We consider the behavior that individual i select target j of J selection targets. The utility U_{ij} is expressed as Equation (1) when each object j is selected by individual i . At this time, each individual i selects the largest utility among the objects. However, the utility U_{ij} is not a definite value, but it varies in various situations.

$$U_{ij} = V_{ij} + e_{ij} \quad (1)$$

V_{ij} is the utility function, and e_{ij} is the probabilistic variable. The logit model assumes that the probability term e_{ij} follows the Gumbel distribution, and the probability P_{ij} that individual i selects object j can be expressed by Equation (2).

$$P_{ij} = \frac{\exp(V_{ij})}{\sum_{j=1}^J \exp(V_{ij})} \quad (2)$$

The utility function V_{ij} is determined by 1) the evacuation direction for the coastline, 2) the evacuation direction for the riverbank line, 3) the evacuation distance from the refugee to the evacuation facility, 4) the construction area of the evacuation facility, 6) the altitude of the evacuation destination, 7) the designated evacuation shelter dummy, and 8) the home dummy. Table. 1 shows factors to consider in determining V_{ij} .

In this research, we consider the psychological utility $\alpha_1 \sin \theta_{iwj}$, $\alpha_2 \sin \theta_{icj}$ due to the relationship between the direction of the tsunami's attack and the evacuation direction. Assuming that the tsunami attacks from the sea side, we consider the psychological utility so that the utility is high in evacuation to the land side in the opposite direction and the utility is low in the case of evacuation to the sea side. Specifically, we set the angle between the coastline and the straight line from evacuee i to evacuation facility j as θ_{iwj} in case of evacuation on foot and θ_{icj} in case of evacuation by car. α_1 and α_2 are coefficients.

As the tsunami runs along the river, we consider the psychological utility $\beta_1 \sin \varphi_{iwj}$, $\beta_2 \sin \varphi_{icj}$ due to the evacuation direction from the river. In the same way as the evacuation direction from the ocean, specifically, the angle between the river line and the straight line from the evacuee i to the evacuation facility j is set to φ_{iwj} in case of evacuation on foot and φ_{icj} in case of evacuation by car. β_1 and β_2 are coefficients. Here, θ_{iwj} , θ_{icj} , φ_{iwj} , and φ_{icj} are the angle ($-90^\circ \leq \theta \leq 90^\circ$) formed by the straight line from the evacuee to the evacuation facility and the parallel line from the evacuee to the coastline or the river line, so the utility value becomes the maximum at 90 degrees and becomes the minimum at -90 degrees.

Since it is desirable to complete the evacuation as soon as possible from the occurrence of the earthquake, we consider the psychological utilities $\gamma_1 D_{iwj}$, $\gamma_2 D_{icj}$ due to the evacuation distance from the evacuees to the evacuation facility. The evacuation distance on walking is set as D_{iwj} (m), the evacuation distance by car is set as D_{icj} (m). γ_1 and γ_2 are coefficients. Here, the evacuation distance is defined as the straight distance between the evacuation start point and the evacuation arrival point.

Since the planar size of the evacuation facility is thought to affect the evacuation facility choice behavior, we set the utility $\delta \ln(S_j)$ by the building area S_j . δ is a coefficient. Since the vertical height of the evacuation facility is thought to affect the evacuation facility choice behavior, we set the utility $\varepsilon \ln(F_j)$ by the building floor F_j . ε is a coefficient. In this case, taking into consideration the characteristic that the utility value is nonlinear, we use natural logarithm of the building area and the building floor in the model expression. [5]

When evacuating from the tsunami, it is important to evacuate to a place with high altitude. Therefore, we set the utility μA_j by the altitude A_j of the evacuation destination. μ is a coefficient.

Whether it is a designated evacuation facility set by each municipality is an important factor. Therefore, we introduce the dummy variable R_j . It is 1 if the evacuation destination is a designated evacuation facility, otherwise it is 0, and we set the utility ρR_j . ρ is a coefficient.

In evacuation behaviors during the Great East Japan Earthquake, whether a refugee is at home is an important factor in the evacuation, since a certain number of evacuees have chosen their homes as evacuation destinations. Therefore, we introduce a dummy variable H_j . It is 1 if the evacuation destination is at home, otherwise it is 0, and we set the utility σH_j . σ is a coefficient. Since the attribute at home differs depending on the evacuees, when H_j is 1, we set all other utility values is 0. the utility function V_{ij} is determined whether the evacuation destination is at home or not.

By using the above factors variables, we formulated the utility function V_{ij} . It can be expressed by Equation (3).

$$V_{ij} = \begin{cases} \alpha_1 \sin \theta_{iwj} + \beta_1 \sin \varphi_{iwj} + \gamma_1 D_{iwj} \\ + \delta \ln(S_j) + \varepsilon \ln(F_j) + \mu A_j + \rho R_j (\text{by walking}) \\ \\ \alpha_2 \sin \theta_{icj} + \beta_2 \sin \varphi_{icj} + \gamma_2 D_{icj} \\ + \delta \ln(S_j) + \varepsilon \ln(F_j) + \mu A_j + \rho R_j (\text{by car}) \\ \\ \sigma H_j (\text{home evacuation}) \end{cases} \quad (3)$$

We obtained estimated values (maximum likelihood estimate) of the coefficients $\alpha_1, \alpha_2, \beta_1, \beta_2, \gamma_1, \gamma_2, \delta, \varepsilon, \mu, \rho, \sigma$ from the data on the evacuation facility selection by GIS data of “Reconstruction Support Survey Archive”. The estimated value is a coefficient that maximizes the simultaneous occurrence probability L^* by Equation (4). To maximize L^* is equivalent to maximizing $L = \ln L^*$, so we obtained the value that maximizes L .

$$L = \ln L^* = \sum_{j=1}^J \ln P_{ij} \quad (4)$$

Table. 1 Factors to consider in modeling

Factors	Transportations	Utility function
Direction from the sea[$\sin \theta$]	Walking	$\alpha_1 \sin \theta_{iwj}$
	Car	$\alpha_2 \sin \theta_{icj}$
Direction from the river [$\sin \varphi$]	Walking	$\beta_1 \sin \varphi_{iwj}$
	Car	$\beta_2 \sin \varphi_{icj}$
Distance[m]	Waking	$\gamma_1 D_{iwj}$
	Car	$\gamma_2 D_{icj}$
Facility area[$\text{LN}(\text{m}^2)$]		$\delta \ln(S_j)$
Facility floor[$\text{LN}(\text{floor})$]		$\varepsilon \ln(F_j)$
Facility altitude[m]		μA_j
Designated evacuation facility dummy(0,1)		ρR_j
Home dummy(0,1)		σH_j

In addition to the estimated value of the coefficient, we tested the estimation model by the t value, the likelihood ratio ρ^2 , and the hit rate as well. [6]

Table.2 shows the estimation results of the parameters. In order to raise the hit rate, we eliminated parameters with low significance level by setting β_1, β_2 in the flat area model to 0 and α_1, β_2 in the rias area model to 0. In the flat area, the likelihood ratio is 0.547, the hit rate is 53.2%, in the rias area the likelihood ratio is 0.521, the hit rate is 13.5%. In addition, all the estimated parameters satisfy the

significance level of 10%. Both the flat area and the rias area model are accurate models in terms of the likelihood ratio, the hit rate and the significance level of each parameter.

$\alpha_1, \alpha_2, \beta_1, \delta, \varepsilon, \mu, \rho, \sigma$ are positive values and γ is negative for both flat and rias area. We found that people tended to choose the designated facility which is close and with high altitude and floor, large area, and away from the sea and the river or home according to situations. In the comparison between the flat area and the rias area, we can understand that the parameter of the evacuation direction in the flat area is larger than that in the rias area from the values of α_1, α_2 , and β_1 , and it influences the evacuation facility choice behavior. Moreover, we can understand that the importance of the designated evacuation facility and the home is greater in the flat area than in the rias area from the values of ρ and σ , and it is easier to select the designated evacuation facility and the home as the evacuation destination.

Table. 2 Modeling results

Transportations	Factors	Parameters	Flat areas		Rias areas	
Walking	direction from the sea[sin θ]	α_1	1.45	***		
Car		α_2	1.35	***	0.305	**
Walking	direction from the river [sin φ]	β_1			0.127	**
Car		β_2				
Walking	distance[m]	γ_1	-0.00349	***	-0.00354	***
Car		γ_2	-0.000990	***	-0.00238	***
	facility area[LN(m ²)]	δ	0.105	*	0.224	***
	facility floor[LN(floor)]	ε	0.303	*	0.248	*
	facility altitude[m]	μ	0.0385	***	0.0268	***
	designated evacuation facility dummy(0,1)	ρ	1.25	***	0.734	***
	home dummy(0,1)	σ	4.25	*	2.30	*
Likelihood ratio(ρ^2)			0.547		0.521	
Hitting percentage(%)			53.2		13.5	

4. Estimation of home selection probability

Using the model, we estimated the home selection probability of each mesh divided into target areas by 100m. Despite the fact that home evacuation is dangerous in the evacuation behavior of the tsunami, since the utility of home selection is large in the actual evacuation behavior, it is very important to estimate the home selection probability. Fig. 2 shows the home selection probability and death rate of the flat area. The correlation coefficient of Pearson between the home selection probability and the death rate in the target area in the flat area is 0.428, and it is a considerably positive correlation. If the mortality rate can be calculated in smaller unit than the postal code area, the correlation coefficient would become larger. According to Fig. 2, the home selection probability exceeds 40% in the area facing the ocean, and the death rate also has a high value of 10% or more there. It is considered as one reason that many designated evacuation facilities are located in places far from the sea. We think that it is necessary to install a tsunami temporary evacuation building etc. that can withstand high tsunamis in the coastal area.

Fig. 3 shows the home selection probability and death rate of the rias area. The correlation coefficient of Pearson between the home selection probability and the death rate in the target area in the rias area is 0.291, and it is a slight positive correlation. Therefore, even in the rias area, areas with high home selection probability tend to be easily damaged by the tsunami. As you can see from Fig. 3, unlike the flat area, the home selection probability is higher near the river at upstream areas of the river than the area facing the sea. This means that the arrangement of designated evacuation facilities is not catching up

with the tsunami going up highly along the river in the rias area. Therefore, it is necessary to install a tsunami temporary evacuation building along not only the coastal area but also the river.

In Chapter 3, the actual tsunami evacuation behavior at the time of the Great East Japan Earthquake can be modeled by dividing it into two topographies of the flat area and rias area. We apply this model to areas where tsunami damage is expected due to the Nankai Trough Earthquake. The Nankai Trough Earthquake is a large earthquake that is expected to occur in Japan in the future. The target areas are Kamakura City, Kanagawa Prefecture facing the Sagami Bay in the flat area and Owase City, Mie prefecture facing Owase Bay in the rias area. The population and the predicted tsunami height due to the Nankai Trough Earthquake in Kamakura City and Owase City is similar to those in the target areas in the Great East Japan Earthquake. From Fig. 4, in Kamakura City, home selection probability is high on both sides of Sagami Bay coast. From Fig. 4, in Owase City, the home selection probability is high at the inundation area along the Owase Bay coast and along the river. Tsunami evacuation facilities need to be installed to the upstream part of the river, considering the characteristic that not only the coast but also the tsunami goes up along the river. Since the distribution of home selection probability is similar to the features of the target areas in flat area and the rias area at the time of the Great East Japan Earthquake, we think that measures need to be taken promptly.

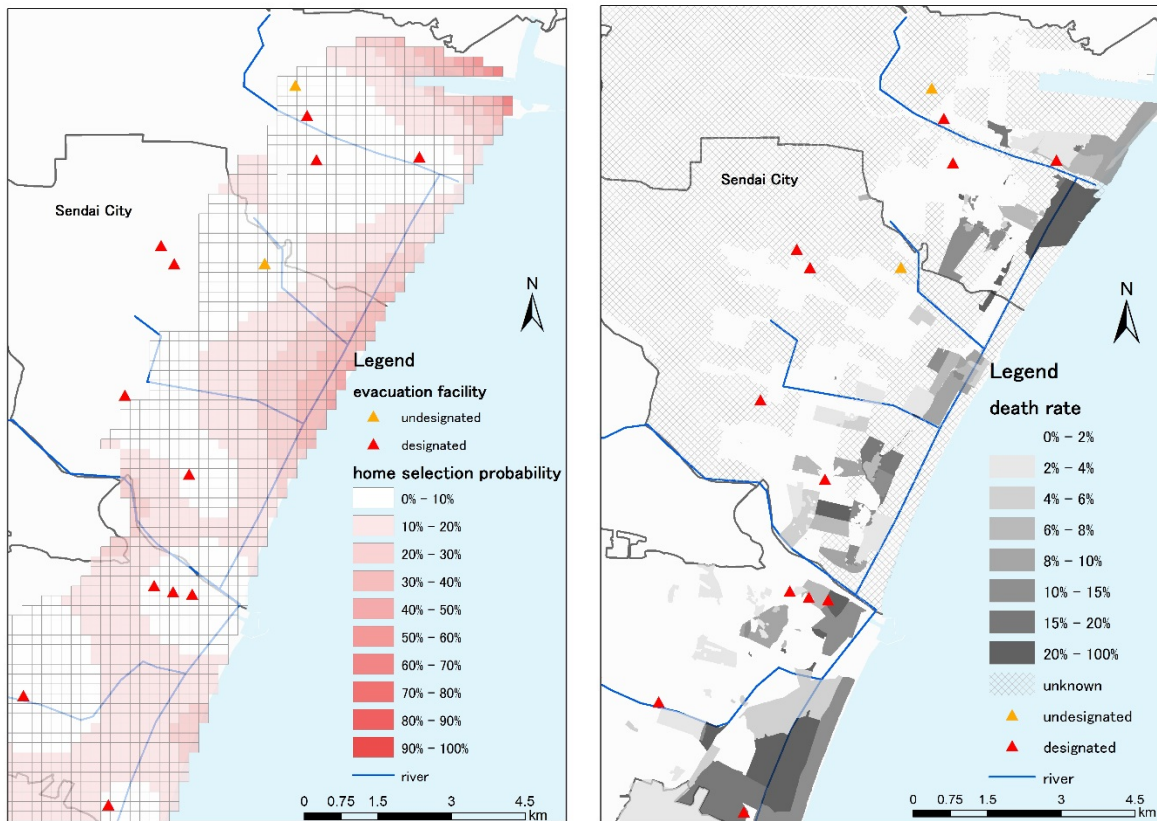


Figure. 2 Home choice probability (left) and death rate (right) in flat areas

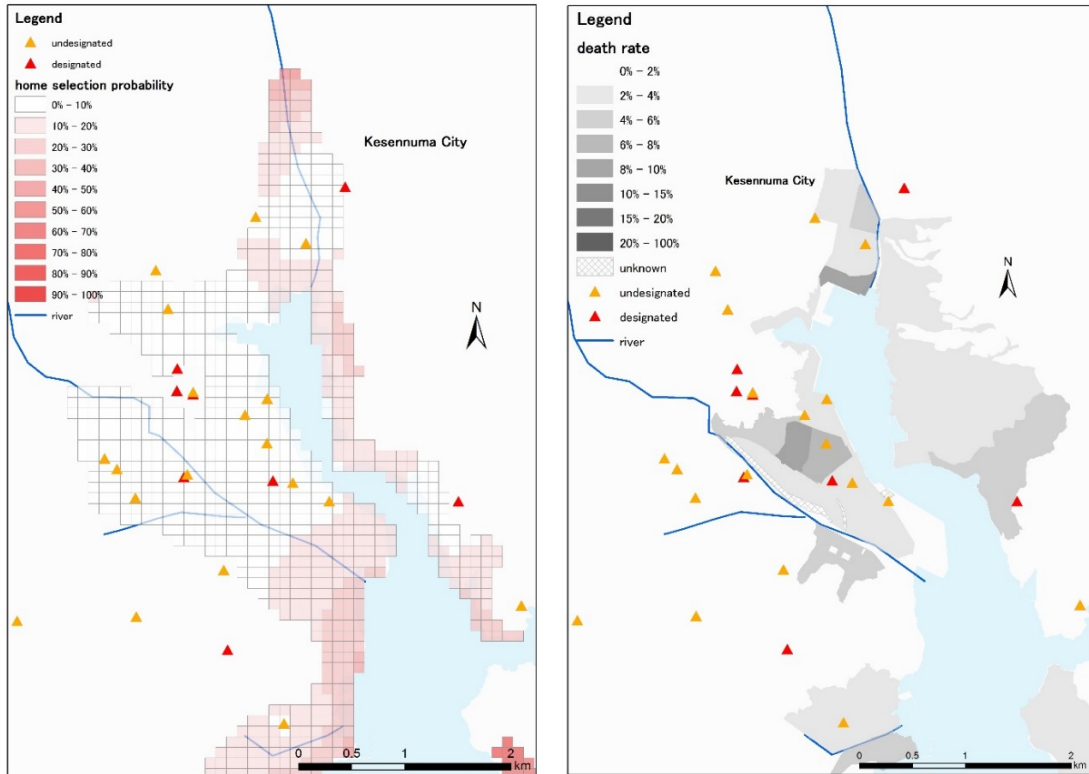


Figure. 3 Home choice probability (left) and death rate (right) in rias areas

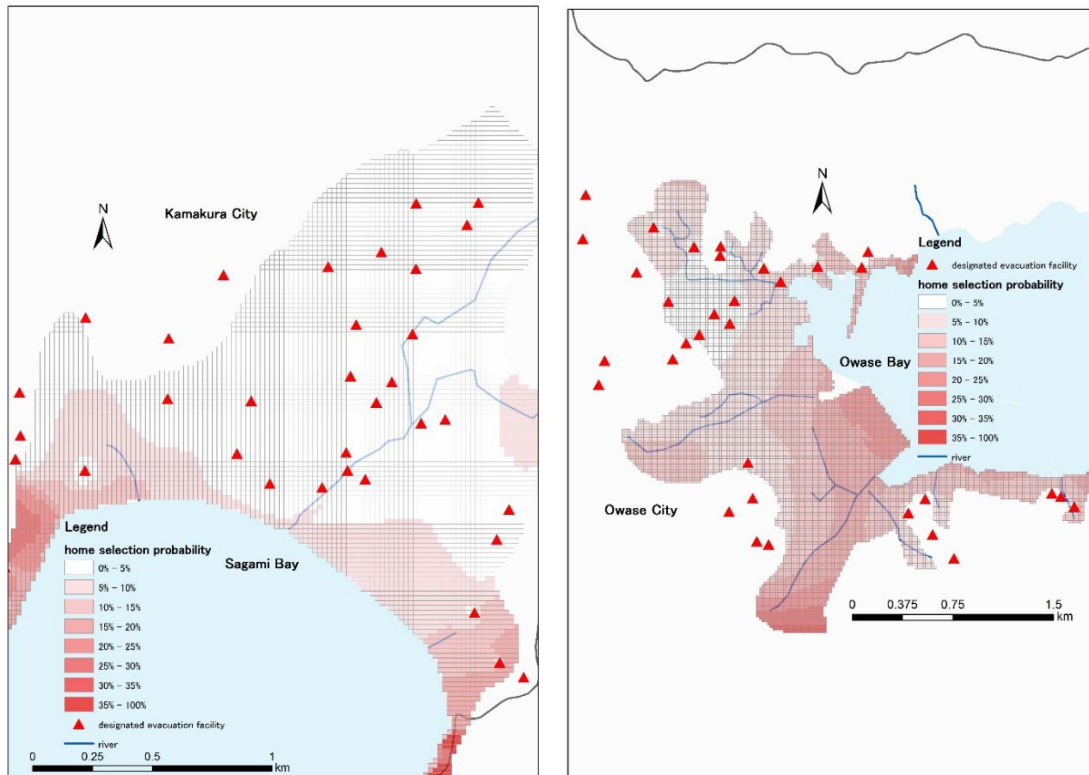


Figure. 4 Home choice probability in Kamakura (left) and in Owase (right)

5. Conclusion

We analyzed the characteristics of the tsunami evacuation behavior by East Japan great earthquake by geography through a logit model with the reconstruction support survey archive.

In addition, we clarified evacuation difficulty areas through estimation of home selection probability. As a result, we were able to grasp where to evacuate facilities. We would like to make use of the findings obtained in this research to actual evacuation plans in preparation for the tsunami damage caused by the Nankai Trough massive earthquake.

As a future work, it is desirable to apply the findings obtained in this research to a wider range. Also, in this study, we proposed a region to expand evacuation facilities considering the home selection probability, but we have to simulate the case where the evacuation facility is newly established in the area and plan the placement method more quantitatively. In order to show how to arrange evacuation facilities in the evacuation plan, it is necessary to consider evacuation plans of evacuation behaviors and evacuation places / evacuation facilities. Furthermore, in planning the arrangement of evacuation facilities, it should be considered in relation to evacuation behaviors based on the characteristics of coast topography.

References

- [1] T. Yamada, M. Sasaki, T. Kishimoto, “The sphere of evacuation facility based on the facility choice behavior model”, *AIJ J. Technol.*, vol. 22, no. 51, pp. 825-830, 2016
- [2] T. Isagawa, “Residents’ Attitude towards Tsunami Evacuation after the Great East Japan Earthquake Questionnaire surveys before and after the earthquake at Onjuku, Chiba prefecture which experienced small tsunami”, *Institute Social Safety Science*, vol. 12, no. 4, pp. 263-277, 2012
- [3] H. Muurakami, “A study on fatality and factors affecting evacuation delay in Natori City hit by the 2011 Great East Japan Earthquake and Tsunami”, *Journal of social safety science*, vol. 24, pp. 101-110
- [4] T. Yamada, T. Kishimoto, “Choice behavior model of refuge building selection during a tsunami coastal areas”, *J. Archit. Plann.*, *AIJ*, vol. 80, no. 707, pp. 125-133, 2015
- [5] R. Kimura, H. Hayashi, S. Tatsuki, K. Tamura, “Psychologically defined life reconstruction processes of disaster victims in the 1995 Hanshin-Awaji Earthquake”, *Journal of social safety science*, vol. 6, pp. 241-250, 2004
- [6] R. Alvarez, M. Camacho, G. Perez-Quiros, “Aggregate versus disaggregate information in dynamic factor models”, *International Journal of Forecasting*, vol. 32, no. 3, pp. 680-694, 2016

Modelling Emergency Evacuation of Classroom with Different Age Profiles

Lakshmi Devi Vanumu¹, Aditya Arya², Hari Krishna Gaddam³, K. Ramachandra Rao⁴

^{1,2,3,4} Indian Institute of Technology, Delhi

Hauz Khas, New Delhi, India

lakshmiddevivanumu@gmail.com; aditya.arya.civil@gmail.com; harikrishnagaddam@gmail.com;
rrkalaga@civil.iitd.ac.in

Abstract - Evacuation characteristics of pedestrians can be captured under two different conditions - one in immediate and another in non-immediate. The safe and quick evacuation of pedestrians from a building in any situation depends on pedestrian and building characteristics. Understanding the behaviour of pedestrians in emergency situations such as earthquake or fire accident helps in designing buildings for safe evacuation. In view of the limited research on this problem in the Indian subcontinent, this study aims to capture the pedestrian flow characteristics in emergency situations by conducting several experiments in a classroom environment. As a part of the experimental study, the students were instructed to behave as if they were in an emergency evacuation situation. Data was collected on pedestrians with different age profiles such as high school, under graduate and post graduate students considering various scenarios that includes different door widths. Several factors such as number of pedestrians, width of the door, average age of the pedestrians, Body Mass Index, proportion of females, number of students and classroom capacity are considered and their influence on evacuation characteristics was analysed. Based on the observations, an evacuation model has been developed using least square error method. Results show that the variables such as door width and number of students are crucial in representing evacuation time of the classroom. It was found that the relationship between total evacuation time (TET) and door width is represented by power function. This is contrast to the findings of existing literature which shows that the relationship between flow and door width is linear. Our results are best supported by the fact that the TET is exponentially varying with door width till a particular value and remains constant for further increase in door width which is realistic in nature. It is anticipated that the results of the study would provide guidelines to various agencies on managing evacuations. This can also lead to suggestions on optimization of layouts while designing various building access facilities in an academic environment.

Keywords: Emergency Evacuation, Classroom, Total Evacuation Time, Pedestrian flow characteristics, Experiments

1. Background

Understanding the evacuation behaviour of pedestrians during emergency situations is important to prepare evacuation management strategies. Due to the lack of experience and being new to the situation, evacuees tries to get out of the risk zone as quickly as possible where available exits gets crowded and restricts proper evacuation. Most of the researchers studied the pedestrian evacuation characteristics in emergency situations by conducting several experiments in laboratory under controlled conditions.

Yang et al., [1] tried to find the difference between the real world experiments and simulations. They used video recordings of the May 12, 2008, Wenchuan magnitude 8.0 earthquake in southwest China. From the results, it was observed that the relation between the arrival time and the order of the person arriving shows a nonlinear variation, which is different from simulated exercises in which this relation appears linear. Daamen and Hoogendoorn [2] conducted laboratory experiments on large scale in order to find emergency door capacity at the time of evacuation. In their study, experimental research was carried out to gather information on capacity of door at the time of emergency evacuations. Many aspects contributing to the emergency door capacity like door width, composition of population and conditions at the time of evacuation were considered. This study also concluded that the 'faster-is-slower' effect was not achieved even after pushing has increased in the experiment. Heliövaara et al., [3] studied the evacuees' exit selection under different behavioural objectives where two exits located asymmetrically in a corridor. The results suggest that the members of an evacuating crowd may not be able to make optimal

decisions when assessing the fastest exit to evacuate. Another outcome of this study was that the egress time of the whole crowd turns out to be shorter when the evacuees behave egoistically instead of behaving cooperatively. Chen et al., [4] conducted several experiments to examine the route choice behaviour of pedestrians during evacuation of a class room having two exits. They proposed a microscopic pedestrian model based on cellular automata. The simulation results shows that the evacuation time is linearly increasing with the number of pedestrians. Li et al., [5] used social force model to simulate the emergency evacuation of a classroom during Ya'an earthquake of China in 2013. Authors tried to understand the behaviour of pedestrians in real-life emergency situation. Further, they calibrated and optimized the parameters of social force model by using a differential evolution algorithm. Bernardini et al., [6] propose an innovative database for earthquake evacuation models based on previous studies. The quantities such as speed, acceleration and distance from the obstacles were also provided. The results demonstrate how people prefer moving with an average speed of about 2.3 to 3 m/s. Moreover, fundamental diagrams obtained during earthquake emergency conditions show how, density values being equals, speeds and flows are higher in comparison to previous studies (in particular: fire evacuation and evacuation drill). Cuesta and Gwynne [7] in their study provided the data related to five evacuation experiments from the same school where Children from 4 to 16 years old were involved in the drills. A number of different performance data-sets were collected: pre-evacuation times, travel speeds, route use and evacuation arrival curves etc. Nicolas and Marcelo [8] also aimed to study the impact of behaviour of pedestrians while evacuating through the narrow exit. They aimed to study the effect of polite vs selfish behaviour of pedestrians on the process of evacuation of the heterogeneous crowd and to establish a link between complexities of humans with this behaviour. The results show that there was no collision when selfish participants were nil and with increase of selfish participants soft collision and pushing increased. It was also found that selfish behaviour of certain people is not good for rest but it enhanced the rate of flow. In summary, they found that the global flow rate enhanced monotonically with increase in selfish agents and hence supporting 'faster-is-faster' effect. Concurrently stronger intermittency is displayed in evacuation with high selfish agents. Gu et al., [9] analyse school students' emergency evacuation behaviour in earthquakes using data extracted from videos of real emergency evacuation. Comparison between students behaviour under normal and emergency conditions were studied using regression models. The analysis revealed that student's behaviour in normal conditions is linear whereas in emergency it is convex. However, reaction time is lower than those observed in other studies and 'faster-is-slower' effect has not been observed. Li et al., [10] study proposed a stair-unit model to depict the topologies of a stairwell and the results were compared with the real evacuation drills. The outcomes proved the consistency of the proposed model in representing the real behaviour. Han and Liu [11], in their paper introduced the information transmission mechanism into the social force model to simulate pedestrian behaviour in an emergency, especially when most pedestrians were unfamiliar with the evacuation environment. Results show that the pedestrians can choose the correct direction of movement with the help of information transmission mechanism and that the new model can represent the actual pedestrian behaviour during an emergency evacuation.

Based on the literature review, it can be stated that the number of studies in the field of evacuation characteristics of pedestrians in emergency situations are very few. The gaps in this research are two-fold. Firstly, the effect of physical characteristics of pedestrians such as age, gender, weight etc. on emergency evacuation in class room case has not been studied. Secondly, there is no published literature on this aspect in the Indian context. Thus it would be difficult to suggest any significant changes which can improve the efficiency of evacuations in the Indian scenario. These are the main reasons that emphasise on the need of a further detailed study of evacuation plans during disasters. Evacuation of pedestrians in closed or restricted environments is affected by several major and minor factors. As we delve into the minute details, the number of factors increases and the study becomes more complex. The aim of this study is to offer a simplified but fairly accurate analysis of pedestrian flow characteristics in closed space environments in the disaster situations with an impending evacuation. For this study, the factors that had a major effect on the pedestrian movement such as age, gender, number of pedestrians, door width etc. were considered and studied in detail. The rest of the factors were kept at a generalized level, for example, we

can assume that due to lack of experience, majority of human beings are ill-prepared in such situations and head to the nearest exit as quickly as possible in a chaotic manner.

2. Methodology

The first phase of this study deals with the experimental setup and data extraction, while the second phase deals with the model development. Further this study considered the individual characteristics of students such as gender, age, evacuation time, number of students, speeds along with different classroom characteristics such as area of the classroom, number and placement of exits, desk and chair arrangements.

As a part of this study, seventeen experiments have been carried out in a classroom environment with different age groups of pedestrians and varying door widths. The data collected from these experiments was used to analyse the pedestrian evacuation characteristics and for the model development. The data was collected at two different places (University class room and public school class room, Delhi, India), in order to consider different age groups of pedestrians, Post-graduate (PG), Under-graduate (UG) and higher secondary school) with all possible scenarios were considered. The higher secondary school classrooms consist of movable tables and chairs on a level floor. There was only one exit provided at the entrance of the classroom. The PG and UG classrooms consist of arrangement of movable tables and chairs on a level floor with two exits. In all these experiments, students were instructed to evacuate the room from the shortest path to the exit. The evacuees were informed about the evacuation procedure before conducting the study and asked them to behave as if they were in an emergency situation. The data collection for the study was performed using video graphic technique. Videos were recorded from convenient vantage points (Fig. 1) and then data was extracted using MATLAB[®] based tool (Singh et al. [12]). Data analysis was carried out using Microsoft Excel and R statistical tool (R Core Team [13]). Snapshots and evacuation time details of 6th grade class room and undergraduate class room are shown in Fig.2. The data from the evacuation experiments such as flow, composition, individual travel times, individual speeds and total evacuation times were obtained and used in developing the relationship between evacuation time and characteristics of evacuees. Individual speeds of pedestrians followed normal distribution. From Fig. 2(b) it can clearly be seen that when both the doors were open, the evacuation time was less compared to other scenarios. Similarly, for UG class room, it was observed that (Fig. 2(d)) when both the exits were open, the time taken by students to evacuate the room was lowest. The details of evacuation experiments are given in Table 1. In first set of experiments, forty three students and thirty six students from sixth and ninth grade respectively have participated. There was only one exit provided at the entrance of the classroom. In second set of experiments, students from Indian Institute of Technology Delhi have participated. In the experiments, thrity eight students from UG and twelve students from PG classes were involved. In all the above experiments (both school and Univeristy) the classrooms consist of movable tables and chairs on a level floor with exits.

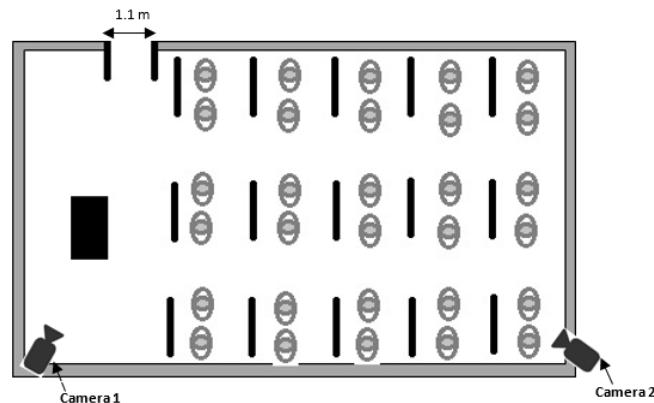
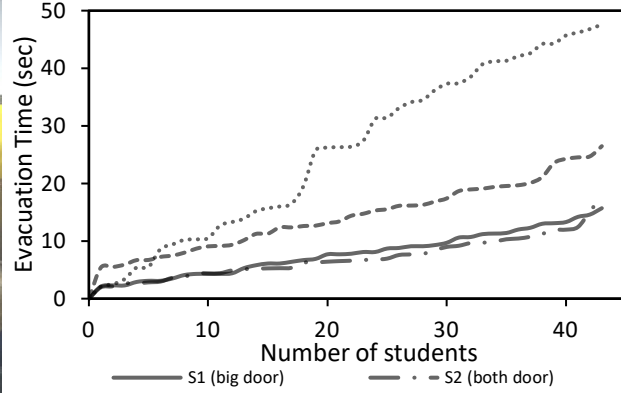


Fig. 1: Schematic representation of Grade 6th and 9th class rooms during experiments



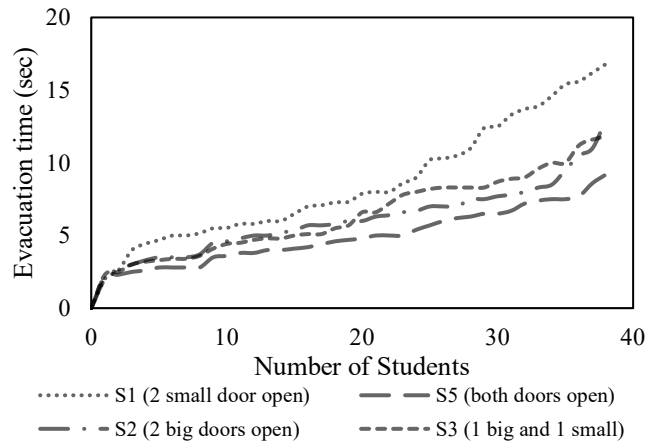
(a)



(b)



(c)



(d)

Fig. 2: (a) Snapshot of 6th Grade classroom (b) Cumulative evacuation times for different door widths for 6th Grade classroom; (c) Snapshot of the undergraduate class room (d) Cumulative evacuation times for different door widths for undergraduate class room (In Fig.2 (b): big door = 0.8 m, both doors = 1.1 m, small door = 0.3 m, In Fig.2 (d): two small door = 1.2 m, both doors = 3.0 m, two big doors = 1.8 m, 1 big and 1 small = 1.5 m)

Table 1: Details of the evacuation experiments

S.No	Grade / class	Class occupancy (class room capacity)	Door width (m)	Age distribution (μ^*, σ^*)	Proportion of women	Average BMI [#]	Class room area (sq.m)	Total Evacuation time (sec)	Speed distribution (μ^*, σ^*)
1	6 th	43 (50)	0.8	11.14, 0.41	41.80	20.1	46.65	15.70	0.93, 0.29
2	6 th	43 (50)	1.1	11.14, 0.41	41.80	20.1	46.65	17.76	1.01, 0.27
3	6 th	43 (50)	0.3	11.14, 0.41	41.80	20.1	46.65	47.60	0.36, 0.26
4	6 th	43 (50)	0.8	11.14, 0.41	41.80	20.1	46.65	26.47	0.50, 0.15
5	9 th	36 (48)	1.1	14.56, 0.56	41.66	19.2	46.2	14.21	0.99, 0.23
6	9 th	36 (48)	1.1	14.56, 0.56	41.66	19.2	46.2	12.64	1.10, 0.32
7	9 th	36 (48)	0.3	14.56, 0.56	41.66	19.2	46.2	33.03	0.51, 0.27
8	9 th	36 (48)	1.1	14.56, 0.56	41.66	19.2	46.2	31.60	0.45, 0.16

9	UG&	38 (60)	1.2	23.80,1.20	10.50	22.5	87.86	16.80	0.93,0.38
10	UG	38 (60)	1.8	23.80,1.20	10.50	22.5	87.86	13.00	1.26,0.42
11	UG	38 (60)	1.5	23.80,1.20	10.50	22.5	87.86	11.80	1.23,0.34
12	UG	38 (60)	1.5	23.80,1.20	10.50	22.5	87.86	12.30	1.43, 0.32
13	UG	38 (60)	3.0	23.80,1.20	10.50	22.5	87.86	9.20	1.53,0.38
14	PG ⁺	12 (30)	1.2	25.42, 6.76	33.30	22.7	38.97	9.00	0.89,0.25
15	PG	12 (30)	1.8	25.42, 6.76	33.30	22.7	38.97	5.77	1.03,0.20
16	PG	12 (30)	1.5	25.42, 6.76	33.30	22.7	38.97	6.00	0.99, 0.22
17	PG	12 (30)	3.0	25.42, 6.76	33.30	22.7	38.97	7.20	1.33, 0.66

* μ =mean, σ =standard deviation; # BMI = Body Mass Index, &UG=Under Graduate, + PG=Post-Graduate,

2.1. Model Development

Several factors including number of pedestrians, width of the door (m), average age of pedestrians, BMI, proportion of females, class occupancy and classroom capacity were considered and their influence on evacuation characteristics were analysed. Correlation matrix between these factors was obtained. From the matrix (Fig.3), it was found that the BMI and average age are highly correlated with each other. Thus in the model development only one variable out of the two should be considered. It also shows a good correlation between evacuation time, door width, class occupancy, and BMI. Further, it is also evident that the total evacuation time of the class room is highly correlated with the door width and class occupancy i.e. number of students in the class room. Therefore the door width and class occupancy are the variables considered for model development. Based on the observations, an evacuation model (Eq. 1) was developed using least square error method ($R^2 = 0.80$).

$$\text{Total Evacuation time (s)} = -6.22 + 6.67 \text{ Door width}^{-1.22} + 3.6 \ln(\text{class occupancy}) \quad (1)$$

Results show that variables such as door width and number of students are crucial in representing evacuation time of the classroom. It was found that the relationship between total evacuation time (TET) and door width is represented by power function (Eq.1, Fig 4). This is contrast to the findings of Liao et al. [14], which shows that the relationship between flow and door width is linear. Our results are best supported by the fact that TET is exponentially varying with door width till a particular value and henceforth remains constant for further increase in door width which seems somewhat realistic.

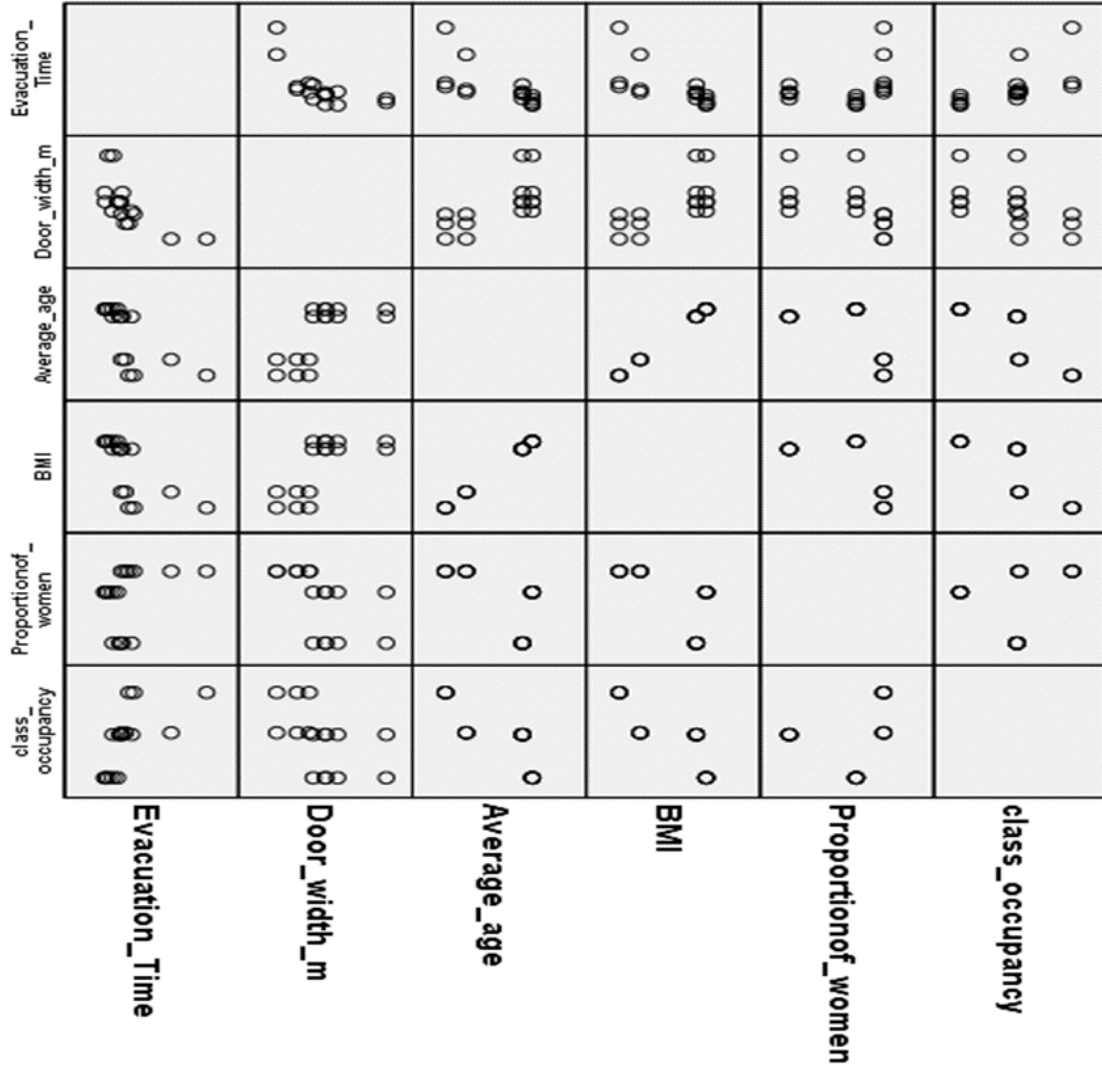


Fig.3: Correlation Matrix between different variables in the experiment

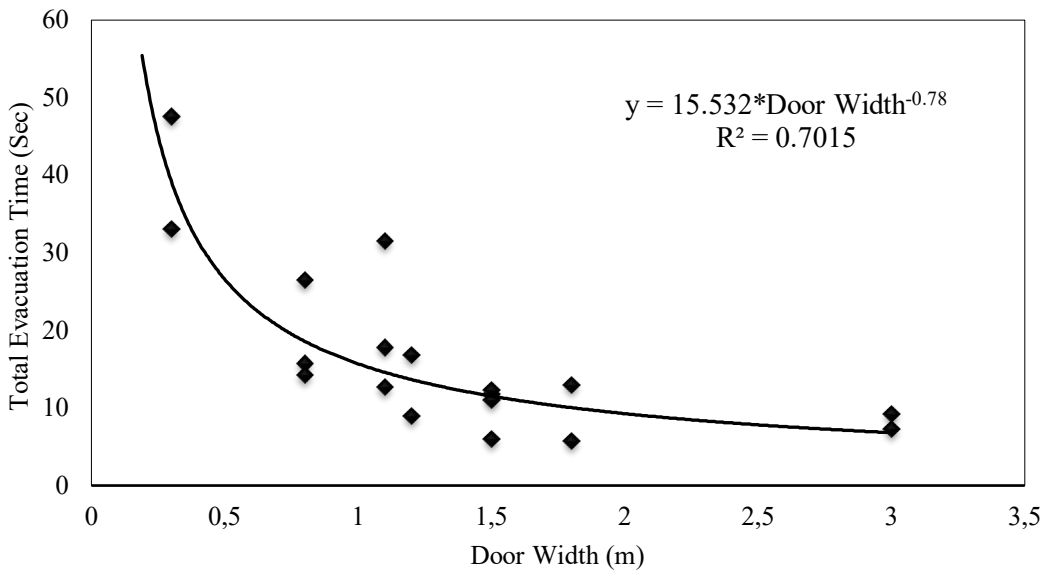


Fig.4: The relationship between total evacuation time of the students and door width

3. Conclusion

Based on the evidence presented and the data analysis, the following conclusions were drawn from the study:

1. Door width, class occupancy or number of students in the class room shows significant effect on the total evacuation time (TET) of the evacuees. A non-linear relationship is observed between total evacuation time and door width where TET is exponentially decreases up to a particular door width and remains constant afterwards. It was observed that the bottleneck situation leads to increase the pushing and crushing between the pedestrians. Further, ‘faster-is-slower’ effect behaviour was also observed in the evacuation experiments.
2. The experiments were conducted on different age profiles in various class rooms. The results show that the age has little or no effect on the outcomes. However, this result cannot be generalised, whereas more variation in the age might have significant effect on the evacuation time.
3. It was found there is an inadequacy in the evacuation guidelines where they are good at improving safety but lacking in quick evacuation from the school building. These are evacuation route maps in the class rooms. More experimental studies are required to provide safety guidelines for the educational environment especially at school level.
4. It is anticipated that the results of this study could formulate better guidelines to various agencies on managing evacuations. This can also lead to suggestions on optimization of layouts while designing various building access facilities in an academic environment.

Acknowledgements

This research did not receive any specific grant from funding agencies in the public, commercial, or not-for-profit sectors. The authors would like to thank the Principal, Lancers Convent Public School, New Delhi for necessary permissions to conduct the evacuation drills.

References

- [1] X.Yang, Z.Wu and Y.Li, “Difference between real-life escape panic and mimic exercises in simulated situation with implications to the statistical physics models of emergency evacuation: The 2008 Wenchuan earthquake,” *Phys. A Stat. Mech. its Appl.*, vol.390, no.12, pp.2375-2380, 2011.
- [2] W.Daamen and S. Hoogendoorn, “Calibration of Pedestrian Simulation Model for Emergency Doors for Different Pedestrian Types,” *Proc. Trans. Res. Board 91st Ann. Meet.*, Washington D. C., USA, 2012.
- [3] S.Heliövaara, J. M.Kuusinen, T.Rinne, T.Korhonen and H.Ehtamo, “Pedestrian behavior and exit selection in evacuation of a corridor—An experimental study,” *Saf. Sci.*, vol.50, no.2, pp.221-227, 2012.
- [4] L. Chen, R. Y. Guo and N.Ta, “Simulation and experimental results of evacuation of pedestrian flow in a classroom with two exits,” *Acta Phy. Sin.*, vol.62, Issue (5): 050506, 2013. doi: 10.7498/aps.62.050506
- [5] M. Li, Y.Zhao, L.He, W.Chen and X.Xu, “The parameter calibration and optimization of social force model for the real-life 2013 Ya’an earthquake evacuation in China,” *Saf. Sci.*, vol. 79, pp.243-253, 2015.
- [6] G.Bernardini, E.Quagliarini, and M. D’Orazio, “Towards creating a combined database for earthquake pedestrians’ evacuation models,” *Saf. Sci.*, vol.82, pp.77-94, 2016.
- [7] A.Cuesta, and S. M. V. Gwynne, “The collection and compilation of school evacuation data for model use,” *Saf. Sci.*, vol. 84, pp.24-36, 2016.

- [8] A.Nicolas and N.Marcelo, “Influence of selfish and polite behaviours on a pedestrian evacuation through a narrow exit : A quantitative characterisation,” *arXiv* : 1608 . 04863v2 [physics . soc-ph], vol.18. 2016.
- [9] Z. Gu, Z.Liu, N.Shiwakoti, and M.Yang, “Video-based analysis of school students’ emergency evacuation behavior in earthquakes,” *Int. J. Disaster Risk Reduct.*, vol.18, pp. 1-11, 2016.
- [10] W.Li, Y.Li, P.Yu, J.Gong, S.Shen, L.Huang and J.Liang , “Modeling, simulation and analysis of the evacuation process on stairs in a multi-floor classroom building of a primary school,” *Phys. A Stat. Mech. its Appl.*, vol.469, pp.157-172, 2017.
- [11] Y.Han, and H.Liu, “Modified social force model based on information transmission toward crowd evacuation simulation,” *Phys. A Stat. Mech. its Appl.*,vol.469, pp.499-509, 2017.
- [12] M. K Singh, H.K.Gaddam, L.D.Vanumu, and K.R.Rao. “Traffic Data Extraction Using MATLAB® Based Tool,” TPMDC Int. Conf., IIT Bombay, 2016.
- [13] R Core Team. R: “A language and environment for statistical computing,” R Foundation for Statistical Computing, Vienna, Austria. 2015. URL <https://www.R-project.org/>.
- [14] W. Liao, A.Tordeux, A.Seyfried, M.Chraibi, K.Drzycimski, X.Zheng, and Y.Zhao, “Measuring the steady state of pedestrian flow in bottleneck experiments,” *Phys. A Stat. Mech. its Appl*, vol.461, pp.248-261, 2016.

Interdependence of flows when merge in rail tunnel evacuations

Adriana Balboa, Daniel Alvear, Orlando Abreu

University of Cantabria
Los Castros s/n, Santander, Spain
balboaa@unican.es; alveard@unican.es; abreuo@unican.es

Abstract – The understanding of merging flows during evacuation can have important implications for rail tunnels safety. This paper explores the interdependence of the merging of flows coming from the walkway with those exiting the train. Eight train exit configurations were tested using a mock-up of a rail car exit and a lateral walkway involving 77 participants (mean age 48; standard deviation 15; range 18-74). New measurements and data processing methods are proposed allowing statistical analysis to be performed. The results provide quantitative evidence of the preferences between flows. We found that the bias in the evacuation was slightly in favour of the walkway when train exit was at 0 m in height. Contrary to expectations a moderate dominance of walkway flow was observed at 0.8 m in height. Less variation was found for the train exit at 1.2 m in height with a clear priority of walkway flow. This happened despite deference behaviours performed by participants, i.e. people stopped to help those entering from the rail car. This novel contribution aims to provide a new method for those involved in development and validation of new and current evacuation modelling tools and those who want to improve their understanding of merging behaviour during evacuation in rail tunnels.

Keywords: Merging flows, evacuation, experimental data set, rail tunnels.

1. Introduction

Emergency evacuations of rail vehicles (trains, metro) inside tunnels are complex processes. Rail tunnels are unique environments with their own specific characteristics such as long evacuation distances and lateral walkways with no natural light [1]. These characteristics may increase the risk to passengers in case of evacuation since the available time to escape can be short. In such conditions, an appropriate design and an effective evacuation strategy can save lives. In this sense, computer modelling permits rail tunnel evacuation to be evaluated. This involves advantages such as the reduction of the actual trials and the increase of the number of scenarios in the analysis.

Simulation models can provide consistent and accurate results when reliable inputs are used [2, 3]. The potential of such analyses is clear [4, 5, 6, 7]. Nevertheless, data on rail evacuation is scarce. Some references in the literature describe the performance of evacuees in rail tunnels including train exit flow rates [8, 9, 10, 11], walking speeds under smoke conditions [12, 13] and on a tunnel walkway [14] and even exit strategies adopted by people to overcome the height of train exits [10].

However, less attention has been paid to merging conditions between rail car exits and the walkway and, therefore, very little is still known about this process. As suggested by [8], there is a need to determine the cause and effect relationship between the population density inside the tunnel and the flow rate capacity of a train exit, as this is expected to have a significant influence on the total evacuation time.

This paper aims to contribute to the existing body of work by analysing the merging process and how this impacts evacuation in rail tunnels. The main scope is to provide rail operators, authorities, researchers, engineers, designers, model developers and model users with a method to determine the interdependence of flows when merging to better understand this process and its impact on life safety.

2. Method

The proposed method is applied to evacuation experiments conducted in an indoor sports court at the University of Cantabria (Spain). A full-scale mock-up was used representing a train exit and a lateral walkway (see Figures 1 and 2). It was built flexible enough to change the height of the train exit area (h) and width (w_t) as well as the walkway width (w_w). As Table 1 shows, eight exit configurations were analysed involving 16 trials.

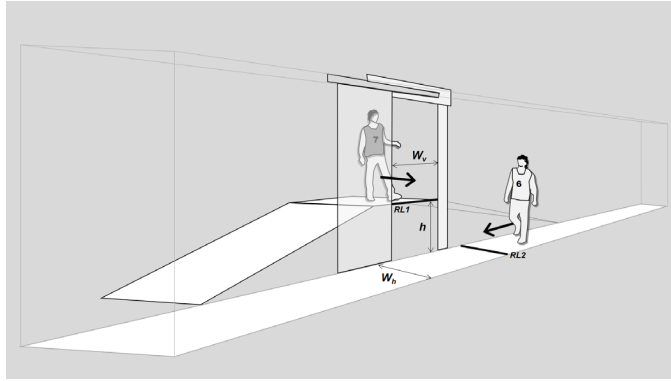


Fig. 1. Experimental mock-up.



Fig. 2. Layout and participants during a trial.

Table 1: Characteristics of trials conducted.

Test	Initial location		Variable of interest		
	Red group	Yellow group	h (m)	w_t (m)	w_w (m)
1	Rail car	Walkway	0	0.8	1.2
2	Walkway	Rail car	0	0.8	1.2
3	Rail car	Walkway	0	1.2	1.2
4	Walkway	Rail car	0	1.2	1.2
5	Walkway	Rail car	0	0.8	0.8
6	Rail car	Walkway	0	0.8	0.8
7	Walkway	Rail car	0	1.2	0.8
8	Rail car	Walkway	0	1.2	0.8
9	Rail car	Walkway	0.8	0.8	0.8
10	Walkway	Rail car	0.8	0.8	0.8
11	Rail car	Walkway	0.8	0.8	1.2
12	Walkway	Rail car	0.8	0.8	1.2
13	Walkway	Rail car	1.2	1.2	1.2
14	Rail car	Walkway	1.2	1.2	1.2
15	Walkway	Rail car	1.2	1.2	0.8
16	Rail car	Walkway	1.2	1.2	0.8

In total 77 participants were used. A deliberate recruitment process was conducted to meet future passenger demographics¹. Therefore, ageing population was selected (mean age 48; standard deviation 15; range 18-74) with 48 % female and 52 % male. No children were allowed. Participants were asked to carry backpacks (21 %) or handbags (62 %).

Participants signed a Consent Informed Form before the experiment. They were randomly divided into two groups: red group (39) and yellow group (38). One group was initially located on the train and another group formed a queue at the entrance of the walkway. A whistle was then used to start the trial. The trial finished when the last participant left the walkway. The initial location of the groups was switched for the next trial.

¹ Eurostat population projections: http://ec.europa.eu/eurostat/statistics-explained/index.php/People_in_the_EU_%E2%80%93_population_projections

Video cameras were placed at the top of the walkway to gain an overhead view of the merging area (see Figure 2). Video recordings, collected at a frequency of 29.97 frames/s, were manually analysed using an image processing software. The specific frame when the body of each participant crossed a reference line (for both participants from the train exit and walking through the walkway) was noted and then transcribed into a spreadsheet. The reference lines were the rail car exit and a line on the walkway floor located 0.6 m before the rail car exit. A new variable was considered namely the instantaneous specific flow (\hat{f}_s) defined as the time interval between two participants, coming from the same location train or walkway, that cross a reference line divided by its effective width:

$$\hat{f}_s = \frac{1}{\Delta t_{i,i-1} * w_{ef}} \quad (1)$$

Where $\Delta t_{i,i-1}$ is the time interval between an individual and the next one who crosses a reference line and w_{ef} is the effective width. This new variable can be easily derived from the measured time intervals. The advantage is the possibility to produce statistical samples instead of using constant values. It is important to note that the use of flow rates (constant values) tends to average the personal hesitations leading to a simple representation of the actual passenger rail car exit flow [15]. Therefore, passengers' exiting processes could be considered as a random variable that depends on passengers (abilities, behaviour, baggage, etc.), design (exit, walkway) and how they behave in response to it [16]. Nevertheless, care should be taken when using the proposed measurements. Very short time intervals between two subjects produce higher values (i.e. outliers). There are methods for the extreme values (lower and upper bound) definition and elimination of outliers to deal with this problem. Data samples of time spent by each participant to cross a line of reference are likely to be skewed [15], being necessary to calculate the medcouple, which is a robust measure of skewness introducing a correction to the Tukey Test [17].

The aim of the proposed method is to determine the interdependence between flows when merging. This involves the assumption that the flow from the train and the flow from the walkway are related and mutually dependent. In total 32 independent samples of instantaneous specific flow during the merging process were collected. The samples from the train exit and the walkway derived from the same trial were combined keeping the original order of access to the merging area. A novel way of data clustering was applied to explore the interdependence of flows when merging. In Clustering A, clusters were defined as groups of participants interacting each other. In Clustering B, clusters were defined as time intervals during the merging period. Since clustering is not an automatic task but an iterative process, we selected different groups of participants for Clustering A (6, 8 and 10 participants) and for Clustering B we selected different time intervals (5, 7.5 and 10 s). The mean value of the instantaneous specific flows was calculated separately and paired samples (train - walkway) were obtained for each cluster. The data points of the means were then plotted according to the height differential of the train exit. This allowed us to explore the mutual relationship between flows produced in the three different evacuation conditions (train exit height of 0, 0.8 and 1.2 m). Finally, a least-square linear regression through the origin was employed to represent the interdependence of flows [18].

3. Results

Figure 3 shows the interdependence of flows when merging process occurs for Clustering A and Figure 4 shows the results produced by Clustering B. The x-axis corresponds to the walkway flow and y-axis corresponds to train exit flow. The straight line in the figures is the reference line, with a slope equal 1, used to show no reciprocal influence between flows (i.e. it represents a 50:50 merging ratio). The slopes of the lines illustrate the interrelation between both flows. Although results varied among clusters, the same pattern was found. Some previous studies detected differences in merging for several configurations at the same height [19]. We found that height conditions that represent evacuation in rail tunnels also have impact on merging process. As Figures 3 and 4 shows, all regression lines (dashed

lines) were below the reference line (straight line) denoting a walkway priority. However, this priority varied according to the height of the train exit.

From the Figures 3 and 4 it is possible to see a slight priority of walkway flow over the train flow (slope lines 0.87-0.97) with no height differential of the train exit ($h = 0$ m). The slope lines when $h = 0.8$ m (Clustering A 0.79-0.92 and Clustering B 0.81-0.84) suggests a moderate dominance of walkway flow over the train exit flow. However, a clear priority of the walkway flow was found when $h = 1.2$ m denoted by the low values of the slope lines (0.53- 0.65 and 0.53-0.63 in Clustering A and B respectively). It is apparent from results in Figures 3 and 4 that the higher the height differential of the rail car exit, the more dominance of the walkway flow.

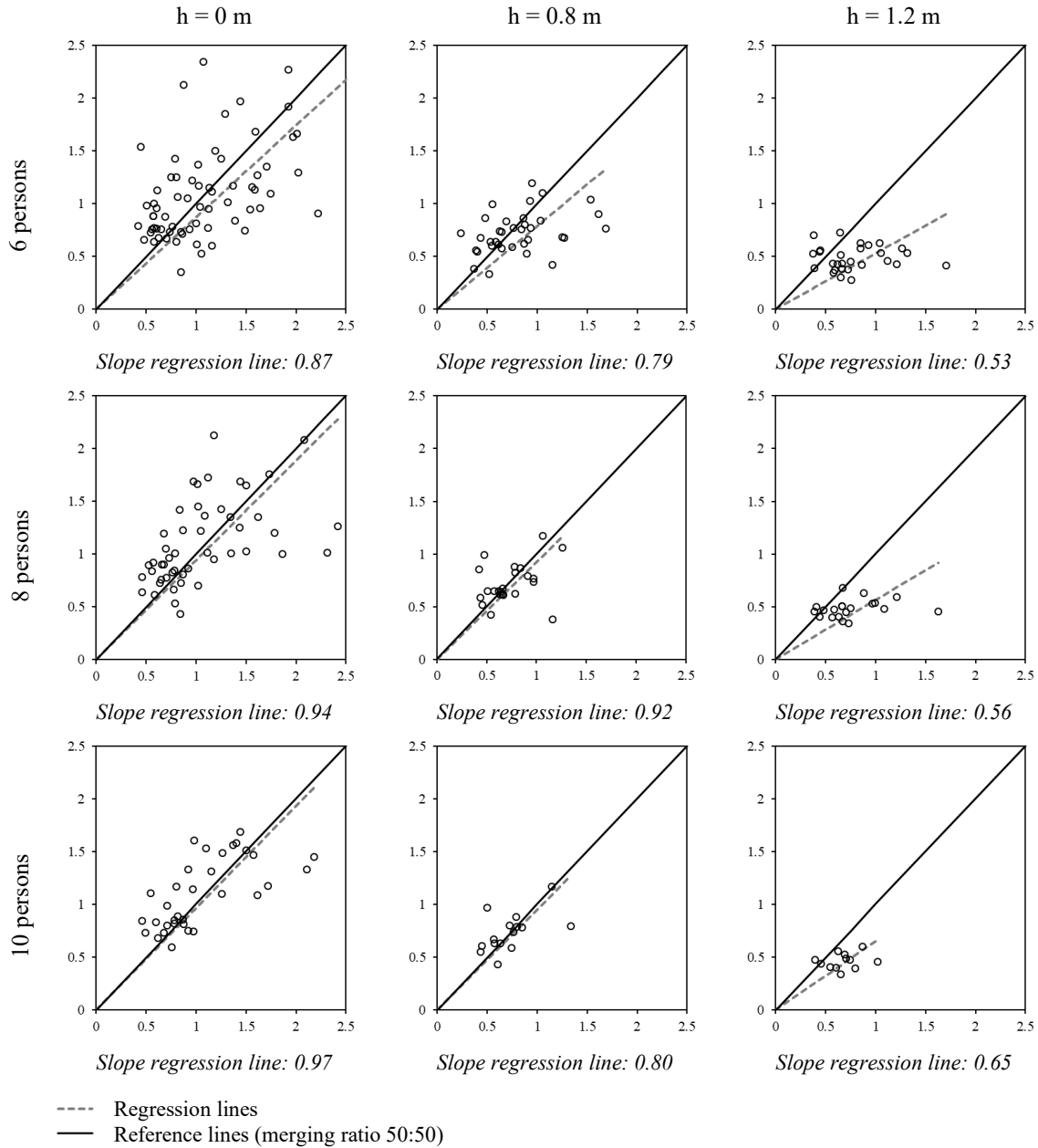


Fig. 3. Clustering A. Interdependence between walkway flow (x-axis)-train exit flow (y-axis) in [per/s m].

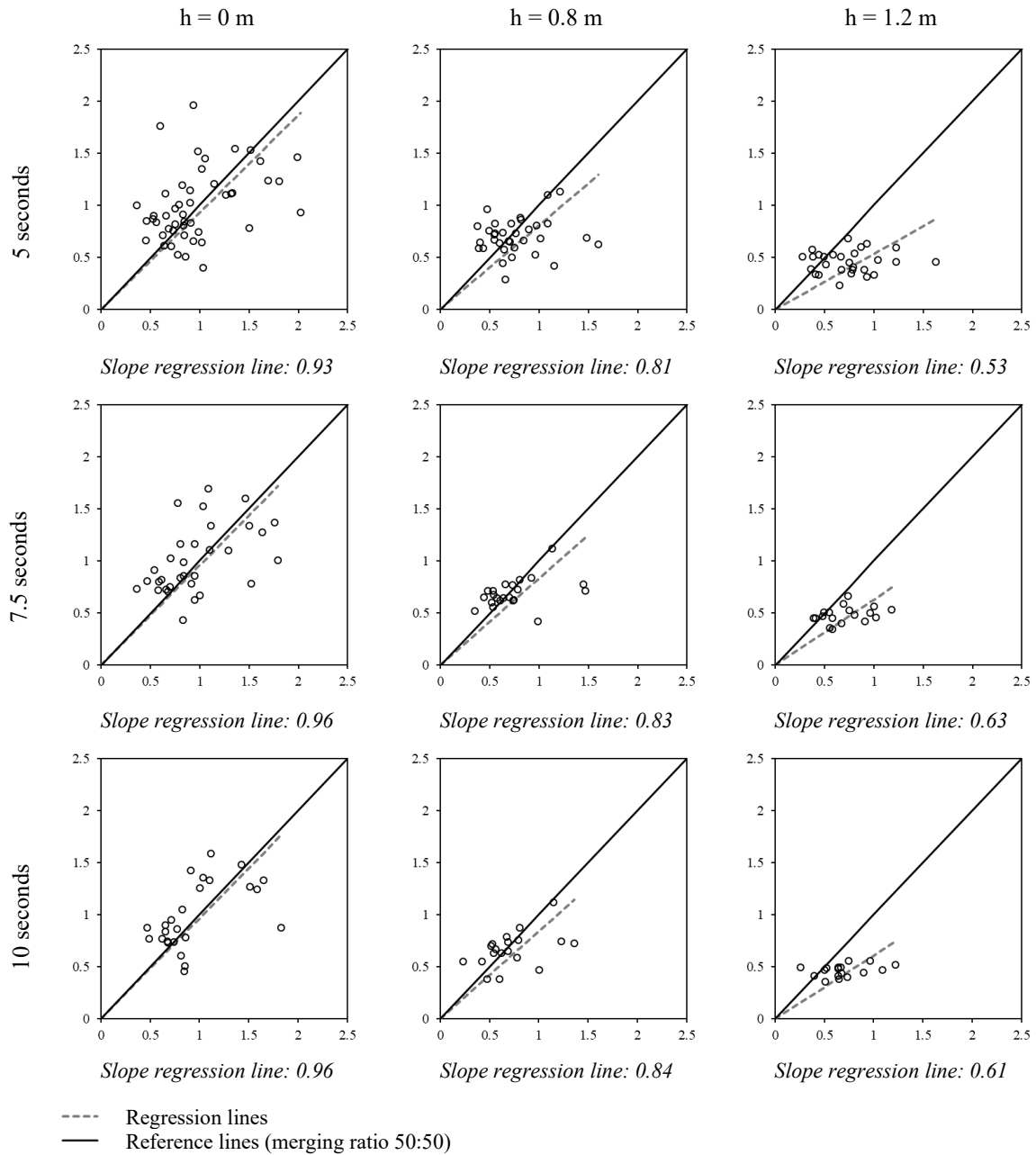


Fig. 4. Clustering B. Interdependence between walkway flow (x-axis)-train exit flow (y-axis) in [per/s m].

4. Discussion

In reviewing the literature, no data was found on the interaction between the flow from those coming from the walkway and the flow from those exiting the train in rail tunnel evacuations. This paper proposes a way to determine the interdependence between such flows. Datasets from rail car evacuation experiments were analysed. The experiments were conducted in a mock-up of a rail car exit and a lateral walkway allowing eight train exit configurations to be analysed. A representative sample of future rail

transport population was used. New measurements were proposed to obtain random flow samples for the statistical analysis. The idea behind the presented analysis is that merging flows are mutually dependent.

Paired samples of the mean values derived from both flows were compared through a linear regression analysis. Three different train exit conditions were examined depending on the height differential of the train exit: no height differential, 0.8 m and 1.2 m. With no height differential, a balance between merging flows was observed (i.e. train participants and walkway participants almost equally accessed to the merging area). With higher height differential (0.8 m and 1.2 m) walkway participants were observed performing deference behaviours such as reducing their walking speed, waiting until they had enough space to access the merging area and/or stopping to help those entering from the rail car (i.e. given their hands and/or using their bodies as support). Despite these observations, our findings confirm a walkway flow priority over the train flow.

These findings may have important implications for rail tunnels design and the definition of appropriate evacuation procedures. In general, there is a lack of homogeneity in evacuation design requirements for rail tunnels. For instance, the minimum lateral walkway width recommended ranges from 0.80 m [20] to 1.45 m [21]. There is also a lack of detail in some other requirements such as the height between the train floor and the walkway, barely suggested or omitted. Results suggest a walkway as high as the train floor to facilitate an effective evacuation from rail vehicles even when merging occurs. It is important to note that, some participants (by 7.69 % and 26.32 % of participants for $h = 0.8$ m and $h = 1.2$ m respectively) decided to withdraw because of the rail car exit height. A key aspect is the availability of sufficiently detailed, comprehensive and relevant data to analyse the impact of merging process on different evacuation strategies. It should be mentioned that evacuation models are now requiring distributions to produce probabilities of outcomes [5]. In fact, current evacuation models for passenger trains use distributions to represent the exiting performances of passengers [2, 3, 15]. Our research supports this by the use of a new random variable (the instantaneous specific flow) derived from a straightforward measurement method. It is argued that results produced can be used as a reference to conduct a more detailed analysis by using evacuation modelling. For instance, a model user could configure the model by implementing the relation of dependence between the merging flows and explore different evacuation strategies (i.e. number of exits available to reduce the merging points, giving priority to the passengers that are closer to the fire, etc.).

Although this paper can provide some support for further analyses, caution must be applied as the findings may not be generalized. Despite the mock-up was flexible enough to reproduce different exit configurations, different factors were not present during the experiment (i.e. visibility conditions, collective behaviours, crew procedures, etc.). Future work, which takes these factors into account, will need to be undertaken preferably in real tunnel environments.

Acknowledgements

The authors would like to thank the Ministry of Economy, Industry and Competitiveness (MINECO) for funding the SIGNAL project on the frame of the Subprogram RETOS-COLABORACIÓN 2016 call (Ref -RTC-2016-5474-4) as well as the European Union through ERDF funding under the objective of Strengthening Research, Technological Development and Innovation.

References

- [1] E. Ronchi, P. Colonna, J. Capote, D. Alvear, N. Berloco, and A. Cuesta, “The evaluation of different evacuation models for assessing road tunnel safety analysis”, *Tunnelling and Underground Space Technology*, vol. 30, pp. 74-84, 2012.
- [2] J. Capote, D. Alvear, O. Abreu, and A. Cuesta, “Analysis of evacuation procedures in high speed train fires”, *Fire Safety Journal*, vol. 49, pp. 35-46, 2012a.

- [3] J. Capote, D. Alvear, O. Abreu, A. Cuesta and V. Alonso, “A stochastic approach for simulation human behavior during evacuation process in passenger trains”, *Fire Technology*, vol. 48, pp. 911-925, 2012b.
- [4] A. Cuesta, D. Alvear, O. Abreu, and D. Silió, “Real-time stochastic evacuation models for decision support in actual emergencies”, in *IAFSS Fire Safety Science*, New Zealand, 2014, vol. 11, pp. 1063-1076.
- [5] A. Cuesta, O. Abreu, and D. Alvear, “Future challenges in evacuation modelling”, in *Evacuation Modeling Trends*, Ed. Springer International Publishing, 2016, pp. 103-129.
- [6] W. L. Wang and T. Y. Jacqueline Lo, “A Simulation Study on Passenger Escape in Rail Tunnels”, *Procedia Engineering*, vol. 71, pp. 552-557, 2014.
- [7] B. V. Weyenberge and X. Deckers, “Development of a risk assessment method for fire in rail tunnels”, in the *7th International Conference Tunnel Safety and Ventilation*, Graz, 2014, pp. 180-189.
- [8] K. Fridolf, D. Nilsson and H. Frantzych, “The flow rate of people during train evacuation in rail tunnels: Effects of different train exit configurations”, *Safety Science*, vol. 62, pp. 515-529, 2014a.
- [9] K. Fridolf, D. Nilsson and H. Frantzych, “Evacuation of a Metro Train in an Underground Rail Transportation System: Flow Rate Capacity of Train Exits, Tunnel Walking Speeds and Exit Choice”, *Fire Technology*, vol. 52, pp. 1481-1518, 2016.
- [10] M. Oswald, H. Kirchberger and C. Lebeda, “Evacuation of a high floor metro train in a tunnel situation: experimental findings”, in *Fourth International Conference on Pedestrian and Evacuation Dynamics, PED 2008*, Springer, University of Wuppertal, Germany, 2008, pp. 67–81.
- [11] A. Norén, and J. Winér, “Modelling Crowd Evacuation from Road and Train Tunnels-Data and design for faster evacuations”, Report 5127, Dept. of Fire Safety Engineering, Lund University, Sweden.
- [12] M. Seike, N. Kawabata and M. Hasegawa, “Experiments of evacuation speed in smoke-filled tunnel”, *Tunnelling and Underground Space Technology*, vol. 53, pp. 61-67, 2016.
- [13] H. Frantzych and D. Nilsson, “Evacuation experiments in a smoke filled tunnel”, in *Proceedings of 3rd International Symposium Human Behaviour in Fire*, Belfast, United Kingdom, 2004, pp. 229–238.
- [14] V. Lundström, J. Ahlfont and D. Nilsson, “The effect of raised walkway design on evacuation behaviour in rail tunnels”, in *IAFSS Fire Safety Science*, New Zealand, 2014, vol. 11, pp. 1091-1102.
- [15] E. R. Galea, D. Blackshields, K. M. Finney and D. P. Cooney, “Passenger Train Emergency Systems: Development of Prototype railEXODUS Software for U.S. Passenger Rail Car Egress”, Final Report, U.S. Department of Transportation Federal Railroad Administration.
- [16] S. Gwynne, E. Kuligowski, J. Kratchman and J. A. Milke, “Questioning the linear relationship between doorway width and achievable flow rate”, *Fire Safety Journal*, vol. 44, pp. 80–87, 2009.
- [17] J. W. Tukey, *Exploratory Data Analysis*. Reading (Addison-Wesley), Massachusetts, 1977.
- [18] J. G. Eisenhauer, “Regression through the Origin”, *Teaching Statistics*, vol. 25, pp. 76 – 80, 2003.
- [19] L. Lian, X. Mai, W. Song, Y. K. K. Richard, Y. Rui and S. Jin, “Pedestrian merging behavior analysis: An experimental study”, *Fire Safety Journal*, vol. 91, pp. 918-925, 2017.
- [20] European Commission, “Concerning the technical specification for interoperability relating to ‘safety in railway tunnels’ of the rail system of the European Union”, *Official Journal of the European Union*, Commission Regulation (EU), no. 1303/2014, 2014.
- [21] Fire in Tunnels, “Fire Safe Design-Rail Tunnels”, *European Thematic Network Fire in Tunnels*, Technical report part 2. [Online]. Available:

https://www.iroads.co.il/sites/default/files/imce/fit_-_fire_in_tunnels_-_part_2.pdf

Bridging the gap

Why we need to enhance current simulation models

Kneidl Angelika

accu:rate GmbH

Rosental 5, Munich, Germany

ak@accu-rate.de

Abstract - Many models that simulate evacuations are state of the art and provide realistic insight to their users. However, simulating everyday situations, such as visitor flow through a museum or passenger flow through an airport, presents marked challenges; existing models reach their limit here. This contribution will introduce and highlight the gap between existing egress models and the difficulties found simulating, for instance, passenger flow or capacity analysis.

Keywords: pedestrian simulation model enhancements, agent-based behaviour, persona approach, simulation of everyday situations

1. Introduction

Over the last few decades, a variety of different pedestrian simulation models have been developed. These models range from the physics-inspired Social Force Models ([3]), to Cellular Automaton [5] that have their origin in traffic simulation, and agent-based models that base their ideas on computer game engines ([1], [6]). In between, many hybrid models combine aspects of each approach. Each of these models have their strengths and weaknesses. [11] present a thorough overview of existing models.

Since the 90s, the number of use-cases for such models has grown beyond evacuation analyses: the more advanced the models, the more the demand from practitioners.

This work was inspired from the S²UCRE research project (www.s2ucre.de): Here, we try to predict the short-time future from video footage. Since we only get aggregated data and have to extract individuals, modelling of behaviours is essential to a most realistic result. This context refers to only as one example – current simulation models need to be improved to model crowds more realistically.

In this paper, impetus to develop existing simulation models towards market needs shall be provided.

2. State-of-the-Art Models: What are they capable of and what we need

To model pedestrian behaviour most accurately, models should consider different layers of intent [6]:

The strategy layer describes a pedestrian's motivation for movement. For instance: a commute to work, hurrying to a meeting, or a stroll through a museum. This layer should not be modelled explicitly. Rather, it helps derive simulation parameters, such as speed or torso size.

The navigational layer describes how pedestrians move from their current position to a location that is not visible to them.

The locomotion layer models the stepping (or in some models sliding) of a pedestrian. It determines the best (though not necessarily optimal) next position based on, typically, a destination.

On top of these layers, behavioural characteristics must be taken into account. In microscopic pedestrian simulations, individuals are often described as just that: individual. However, it is well understood that people socialize with one another, resulting in behaviour that might not otherwise appear. Common examples are grouping behaviours and queues (e.g. [7], [8], [9]). Further, we learn from psychologists and

sociologists that there are many more stimuli that influence our behaviour. [12] speak of Human Factors. There are four main factors they refer to:

- The environment / infrastructure we are moving in
- Any impacts (e.g. weather, fire, surroundings)
- Occasion (what is the reason for gathering or moving? This is the analogous to the strategy layer and thus for the choice of parameters)
- Humans (affiliation: what role am I on the occasion, e.g. family, security, friend...)

To include these factors, common simulation models must be extended. Furthermore, we have found that patterns describing individual mannerisms (e.g. politeness, impatience, anxiousness) and urges (e.g. needing the toilet, hunger, thirst) should be considered in modern simulation tools as well.

Naturally, these behaviours must not play a role in evacuation simulations, but must feature in business-as-usual simulations.

There exists already work which tries to cope with psychological factors and suggest models, like the PECS Model [13], PMServ[14] or a concurrent hierarchical state machine [15]. The PECS model is capable of modelling physical, emotional, cognitive and social factors and originates in Operations Research. The MACES (Multi-Agent Communication for Evacuation Simulation) in combination with PMServ (psychological representation with memory data in combination with a short-term memory system) is an architecture to integrate a psychological model into crowd simulations [14]. The authors of [15] propose a concurrent hierarchical finite state machine for modelling pedestrian behavioural tendencies.

These existing models try to model the complex interrelations between cognition, psychology and movement. They are only theoretical and academic approaches not set into practice so far and consist of very complex models. For practitioners, the objective is a simple model to integrate complex human behaviour. Thus, in the following chapter the most important aspects from a practitioners' point of view are addressed in order to narrow down the complexity.

3. Needs from practitioners' point of view

The requirements and wishes of the commercial sector are varied. Some of them are beyond the abilities of simulation models, but we have identified numerous gaps that can be closed by modern tools.

3.1. How can we apply realistic avoidance behaviour for agents when it comes to counter-flows?

Common simulation models tackle this situation with repelling and attracting forces. That is, agents walking against me are more repellent than agents who walk with me. Manifesting these phenomena as parameters and forces, simulation models can reproduce the observed lane formation that occurs when agents are in counter-flow. Still, with high densities, agents get stuck. In Fig. 1, different results for different repulsion setups are shown.

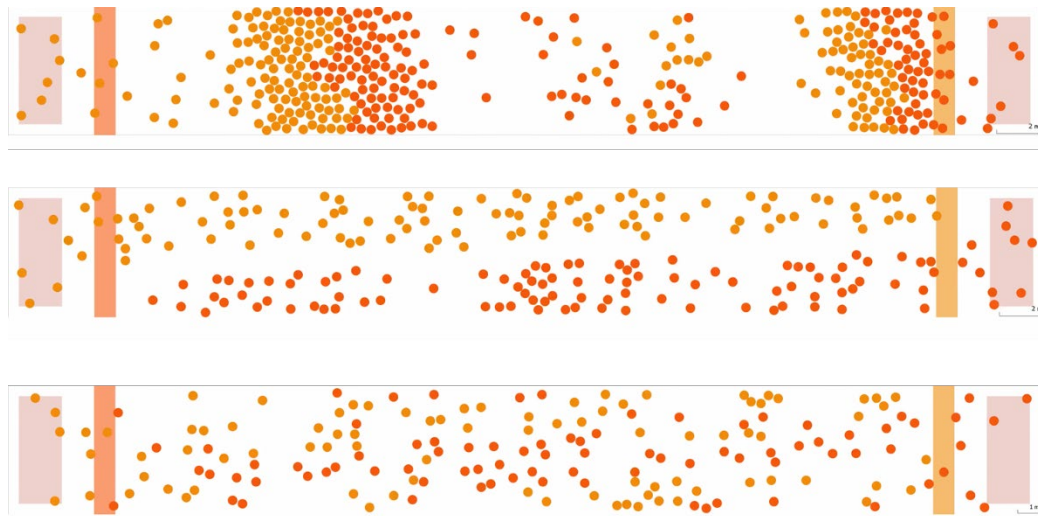


Fig. 1 Different results of counter-flow and lane formation: The upper figure shows results of very low counterflow repulsion resulting in blockage, the middle picture with a very high value where clear lanes occur, the lower picture shows a moderate repulsion.

The different outcomes in Fig. 1 show the challenge quite well: the same situation with the exact same number of agents lead to different results and lane formations when changing the repulsiveness of counter-flow agents. Does it make sense to model counter-flows by adding repellent values or might it be better to model the behaviour of agents instead? The observed counter-flow patterns form due to behaviour of individuals: Some people are more polite and offer room for one another and even step back to let others pass whereas some people really try to squeeze through a crowd. By applying individual behaviours to agents, such counter-flow formations may evolve more or less intense depending on the agent types one would model and thus patterns would evolve from individuals' behaviours instead of forces that are applied on all pedestrians the same way.

3.2 How can we teach agents Generalized Knowledge [2]?

When modelling and simulating complex buildings, agents must “know” patterns of behaviour, which are learnt over time. I.e. if you are in a hospital, you do not need to search for an exit in a patient room, as you know there won't be an exit there; corridors will most likely guide you to an exit. An example of applying this knowledge is given in Fig. 2. Here, the agent chooses the shortest path (left) whereas in the right picture, he uses the knowledge that rooms won't lead to exits.

This implicit knowledge should be integrated into simulation models in order to present more realistic results – not only in emergency situations. First approaches have already been realized by [2]. Nevertheless, we may be able to extract semantic information from building information model, and use this extra layer of information in the simulation tools. Individual agents can then use semantic data uniquely to make decisions. But to what extent could these data be used? How much knowledge has everyone and how much does he make use of it? These are open questions to be answered when integrating knowledge into simulation tools.

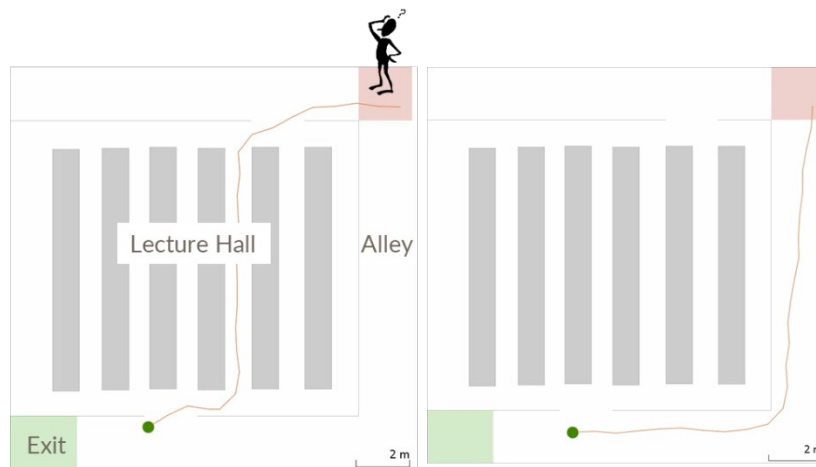


Fig. 2 Example of Generalized Knowledge: left, the agent has no generalized knowledge and walks through a lecture hall, since this is the shortest and fastest path; right, the agent walks along the corridor.

3.3 What measures can we take to simulate correct behaviour in front of bottlenecks?

Whenever many people share limited space, at some point bottlenecks may occur. Behaviour in front of bottlenecks depends on human factors, such as: *Am I in a hurry? What situation am I in? Can I see why a congestion has occurred?* As a consequence, queuing and waiting behaviour depends on the situation and the people involved in that situation. We have to ascertain which factors most influence behaviour in front of bottlenecks. Is it an intrinsic personal attitude that lets someone be more polite versus being more pushy, or are there extrinsic factors, such as the situation and possible danger that you face? Or is it a combination of both? How can these factors be translated into parameters we can use as input to our simulation models?

Another aspect is the decision on how long a pedestrian would queue for a certain point of interest, like a toilet or a ticket office. When would a person rethink and re-decide not using that facility but maybe search for another one? Same holds true for attractions one has to queue for.

A common approach to these issues is to tag certain environments as attractive or not. As such, people avoid or prefer certain areas depending on the attractiveness. However, this does not allow individual preferences or states. We therefore need to focus more on modelling individual human factors than labelling areas with an attractiveness.

Many models do not take the above behaviours into account but instead use statistics. We believe the integration of a persona model [10], defining a scale of urges and preferences would lead to greater realism and widen the purview of pedestrian simulation tools.

A key factor in these approaches however, is to generate an appropriate validation method, such that the quality of the model is assured.

4. The road onwards: Integrating Machine Learning?

This paper gives an overview on the gap between current state-of-the-art models and commercial consumer needs. As shown, pedestrian simulation applications have varied requirements. Tackling these requirements represents challenges for research: integration of results from psychological studies in order to be able to focus on agents and their individual behaviours. Until now, computers need a very specific set of rules, whereas psychologists and sociologists tend to give more vague answers and tendencies. New methods for tackling this discrepancy could be found in machine learning. When using such techniques, video input data can serve as training data and certain questions like “*Where will a crowd move towards?*” or “*Do people use restrooms in the first floor more likely than in the second floor?*” addressed.

Integrating such new methods into a hybrid model, where we use a Persona model for modelling certain aspects like the motivation of pedestrians plus some basic characteristics like patience, preferences, mobility, grouping in combination of “learned” patterns from crowds may lead to a new generation of simulation models that are able to bridge the gap.

Acknowledgements

This work was funded by the German Federal Ministry of Education and Research through the project S2UCRE (grant number 13N14464).

References

- [1] Funge, John and Tu, Xiaoyuan and Terzopoulos, Demetri, “Cognitive Modeling: Knowledge, Reasoning and Planning for Intelligent Characters”, Proceedings of the 26th annual conference on Computer graphics and interactive techniques, p-29-38, 1999
- [2] Andresen, E., M. Charaibi, A. Seyfried, “A Representation of Partial Spatial Knowledge: A Cognitive Map Approach for Evacuation Simulations”, *Transportmetrica A: Transport Science*, pp.1-18, 2018
- [3] Moussaïd, M. & Helbing, D., How simple rules determine pedestrian behavior and crowd disasters, *Proceedings of the National Academy of Sciences*, 2011, 108, 6884-6888
- [4] Helbing, D. & Molnár, P., Social Force Model for Pedestrian Dynamics *Physical Review E*, 1995, 51, 4282-4286
- [5] Blue, V. & Adler, J., Cellular Automata Microsimulation of Bidirectional Pedestrian Flows, *Transportation Research Record: Journal of the Transportation Research Board*, 1999, 1678, 135-141
- [6] Reynolds, C., Steering Behaviors for Autonomous Characters, *Game Developers Conference*, 1999
- [7] Köster, G.; Treml, F.; Seitz, M. & Klein, W., Validation of crowd models including social groups, *Proceedings of the 6th International Conference on Pedestrian and Evacuation Dynamics*, 2012
- [8] Moussaïd, M.; Perozo, N.; Garnier, S.; Helbing, D. & Theraulaz, G., The Walking Behaviour of Pedestrian Social Groups and Its Impact on Crowd Dynamics, *PLoS ONE*, 2010, 5, e10047
- [9] Köster, G. & Zönnchen, B., Queuing at Bottlenecks Using a Dynamic Floor Field for Navigation, *Transportation Research Procedia* , 2014, 2, 344 – 352
- [10] C. Schaefer, R. Zinke, L. Kuenzer, G. Hofinger, and R. Koch, “Applying Persona method for describing users of escape routes?” in *The Conference on Pedestrian and Evacuation Dynamics 2014 (PED2014)*, 2014, pp. 636–641.
- [11] D. C. Duives, W. Daamen, and S. P. Hoogendoorn, “State-of-the-art crowd motion simulation models,” *Transportation Research Part C: Emerging Technologies*, vol. 37, pp. 193–209, 2013
- [12] G. Hofinger, R. Zinke, and L. Künzer, “Human Factors in Evacuation Simulation, Planning, and Guidance,” *Transportation Research Procedia*, vol. 2, pp. 603–611, 2014
- [13] B. Schmidt: *Modelling of Human Behaviour: “The PECS Reference Model.” AAI Technical Report FS-01-02*, 2001
- [14] N. Pelechano, K. O’Brien K. B. Silverman, N. Badler, “Crowd Simulation Incorporating Agent Psychological Models, Roles and Communication“, *First International Workshop on Crowd Simulation*, 2005
- [15] P. Kielar, O. Handel, D. Biedermann, A. Borrmann: “Concurrent hierarchical finite state machines for modeling pedestrian behavioral tendencies.” *Transportation Research Procedia* 2 (2014) 576 – 584, 2014

Determination of pedestrian's personal space in mass religious gatherings - A case study of Kumbh Mela

Ms. Aparna P M, Ms. Karthika P Sobhana, Dr. Ashish Verma

Department of Civil Engineering

Indian Institute of Science

Bangalore, India

aparna.pras@gmail.com; pskarthika@iisc.ac.in; ashishv@iisc.ac.in

Abstract-Personal space can be defined as the physical distance between two individuals in a social environment. It varies from person to person depending on culture and context and there are significant individual differences too. Studying personal space includes the ability to recognize the various zones of involvement and the activities, relationships, and emotions associated with each zone. This paper tries to formulate and define personal space in high density crowd situations in Kumbh Mela, one of the world's largest mass religious gatherings. Video data of pilgrims taking part in the Panchkroshi Yatra, a religious walkathon which is a part of KumbhMela, is used for the analysis of factors affecting personal space. To identify the thresholds of personal space, walking speed of individuals, gender, presence of luggage and the number of males and females surrounding an individual have been considered. It is found that the average speed of the individual, the group size, and the gender ratio of group members have a significant effect on the personal space of an individual. Also, it is observed that the personal space follows an asymmetrical pattern rather than a symmetrical pattern.

Keywords: Inter-personal distance, Personal space, Mass religious gatherings, Stampede, Psychology

1. Introduction

Personal space is defined as the immediate space available to an individual for exercising his movements without causing discomfort to oneself and his/her immediate neighbour. Most of the literature on personal space either treats the personal space as circular in nature on the lines of [2] or studies the personal space intrusions at a psychological level from a medical perspective. [9] has defined personal space as the flight zone of a human with respect to other humans and the person steps away to reinstate the margin of safety when their personal space is violated. The complexity of personal space comes from the fact that its dimensions are affected by many factors like the context, personal relation, status, gender, culture, intentions etc. The concept of personal space is rooted in zoology and ecology [5], but it is an entirely different concept from that of territory.

In this study, our aim is to understand and define the concept of personal space in a mass religious gathering, especially at high density conditions. Kumbh Mela, where an expected 100 million people visits the area in a span of one month, is taken as the study scenario. The event exhibits different crowd scenarios ranging from low density single file movement to a tightly compressed torrent of pedestrians. The crowd scenario studied here consists of pedestrian flow in a confined space, where masses of people are trying to get to the destination with a defined purpose.

While moving in a dense crowd, pedestrians adjust both speed and step length in such a way as to avoid collisions and to preserve their personal space. Personal space invasion is likely to increase physiological stresses and therefore individuals tend to maintain personal space zones to protect themselves. As far as a mass religious gathering is concerned, it is important not to have personal space intrusions since it can leave a threat for potential stampede, which may be caused due to possible

aggression. This study, thus, ascertains how behavioural and psychological aspects affect crowd situations, and the relevance of studying interpersonal distances in the context of mass religious gatherings.

The upcoming section discusses the motivation behind pursuing the study. Data used for the study as well as analysis of personal space intrusions is discussed in Section 3. The last section concludes with the important findings of the study.

2. Background and Motivation

Humans tend to maintain a certain distance from others as they are walking. This interpersonal distance is important as it creates a protective buffer zone in a human mind. It is natural to feel discomfort when other people intrude upon this safe bubble. It is more pronounced when the intruders are strangers. This feeling of uneasiness causes psychological stress and in the case of a mass gathering where it is unavoidable, this uneasiness can cause defensive reflexes. It is imperative that these local disturbances do not affect the crowd and result in unfortunate incidents.

Over the last four decades, anthropologists and psychologists theorized that personal space was a zone maintained by individuals to keep others at a comfortable distance during different social interactions ([5],[12], [2]). Studies have also concentrated on personal space as a protective zone during locomotion that provides sufficient time to perceive environmental hazards, plan gait adaptations, and execute them. There are no studies about the way people use space in high density crowds.

The effect of intercultural differences on personal space has received a fair attention from fields like social psychology, where the aim is to understand the differences in personal space between different ethnic groups. [4] interviewed people from different cultural backgrounds and shows that Anglo Saxons, and Asians uses larger personal space than Caucasians or Latinos.[2] described personal space as the region surrounding an individual where a person can touch or hold or grasp others with their arms extended, this is generally a distance of 45-75cm. [10] found that proxemic distance is greater in the rear (~120cm) than in the front and on the sides (~60cm each) using an experiment conducted with students. While [1] found that personal space is bigger in the front than in the rear, which even drops to zero in the rear if test subjects are not allowed to move their heads ([8],[11]).

[6] hypothesizes that as the number of pedestrians increases, interpersonal distances reduce, and the walking group follows an inverted U-shape. Also, as the number of pedestrians increases, the number of direction changes while walking increases. However, most of the work reported is in situations of low density. The spatial pattern of the groups with respect to the alignment within the group, group size, group composition, and the effect of these proxemic variables on walking speed is investigated by [3]. It is observed that higher walking speeds are correlated with the mis-alignment within the groups. > formation, stair disposition, < formation prevailed more in groups compared to the aligned spatial arrangement. It is also noted that males preserve more interpersonal distance when compared to females. However, majority of these studies refrain from using locations of excessive social density, and hence fail to study the effect of changes in density on personal space violations and walking behavior.

[7] explores the possibility of using a virtual environment rather than a physical experimental setup to study the personal space of adults while they were trying to circumvent a cylindrical obstacle in their path. However, most of the existing literatures study personal space within a laboratory setup, with controlled experimental conditions. The situation is vastly different in field where hundreds of people walk for long distances in extreme weather conditions, and the slightest provocation can result in unforeseen incidents. Therefore, the main focus of this paper is to understand the shape of personal space around an individual in a field setting, and to ascertain if it is symmetrical in nature. Further, an attempt is

made to understand the variables that are likely to influence the personal space intrusions in Kumbh Mela.

3. Data description and analysis

3.1 Data description

Video data of pilgrims moving in the Ambodhya Stretch, which is a part of Panchkroshi Yatra, spanning five days was analysed. It is an annual religious walkathon where pilgrims take a circuitous route of 118 km around the city covering many temples and finally take a holy bath in the sacred river, in a limited span of five days. Fig 1 shows the screenshots of the study section.



Fig. 1: Snapshot of the study section (Ambodhya stretch)

A 15 minutes long video of unidirectional flow was observed, and a total of 102 groups were identified for analysis. The Traffic Data Extractor developed by IIT Bombay was used to track pedestrians. A central person was identified and then all the persons who were in the immediate vicinity of the central person were also identified. A group is then defined as this collection of central person and the surrounding persons.

The central person within each group, gender of the central person and his/her neighbours, and the presence of luggage was additionally noted down. Of these 726 persons, 538 were females (74.10%) and 188 were males (25.89%) and out of those people, 569 persons were carrying luggage (78.37%). The entire sample was segregated into two groups; female centric group, and male centric group. Of this, almost 85% of the female centric group, and 55% of male centric group had head baggage.

In many literatures, personal space is also perceived as a protective zone during walking: it allows people to perceive dangers and adapt their walking strategies to alleviate those hazards. Here, personal space is defined as the immediate space surrounding a person and enclosed by boundaries created by his/her immediate neighbours. This is based on the hypothesis that in a large mass religious gathering as Kumbh Mela, people are aware of the magnitude of the gathering. In such high densities, the concern to personal space intrusion would be the immediate surrounding rather than the people at the periphery. It is also hypothesized that the shape of the personal space would not be circular, mostly because the pedestrian flow is unidirectional.

3.2 Analysis and Results

A group of pedestrians are identified from video, with the aim to analyze the personal space requirements of the pedestrian positioned at the centre of each group. The analysis of the personal space bubble as defined by the space around the central person is done from the time the central person enters the frame till the time the person exits the frame. The personal space around a person mostly follows an oblong asymmetrical pattern rather than a symmetrical one. This could be the result of the unidirectional flow of pedestrians along the walkway as hypothesized earlier. It is necessary to preserve a larger distance in the front rather than rear to ensure a comfortable walking gait. It is also observed that the central person tries to maintain the initial distance with all neighbours as they continue to walk through the section.

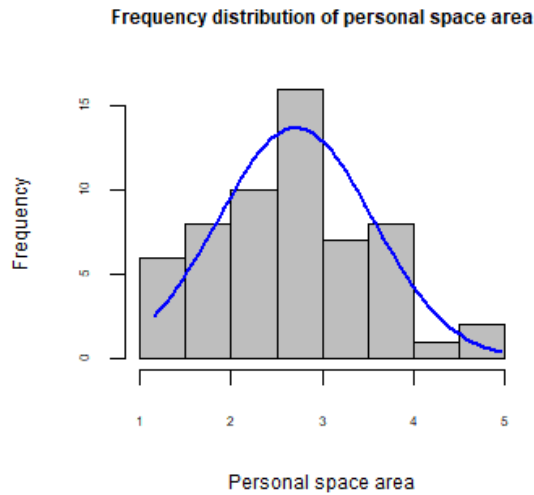


Fig. 2: Histogram of personal space area

Average personal space area of an individual is calculated as the area of the polygon obtained by connecting the coordinates of immediate neighbours. Fig 3 shows the frequency distribution of personal space area. The personal space follows a normal distribution with a mean value of 2.71m^2 . Personal space area ranges from 1.15m^2 to 4.96m^2 . The effect of the individual's average speed, the number of neighbours, gender of the central person, ratio of same gender to the opposite gender in the group members, and presence of luggage on the personal space is modelled using linear regression. The parameter estimates, and t-stats are presented in Table 1.

Table 1: Regression model parameter estimates

Explanatory variable	Parameter estimate	Significance level
Constant	-2.61 (-3.63)	***
Average speed of individual	2.79 (4.62)	***
Number of immediate neighbours	0.51 (7.08)	***
Opposite gender to same gender indicator	0.62 (3.12)	**

Presence of head luggage	0.20 (1.04)	-
R ²	0.60	
Adjusted R ²	0.52	
Number of observations	60	

Based on the t-statistics obtained, it could be concluded that all the parameter estimates, except for head luggage, are found to be statistically significant at 95% confidence level, as all the t-stats are found to be greater than the t_{crit} value of 1.96. As per the model, the average speed parameter estimate gives the marginal impact of the variable on the personal space, given everything else remains the same. For every unit increase in average speed, the personal space is expected to increase by 2.79 units, *ceteris paribus*. The gender of the central person was found to be negative, which indicates that females are willing to stay closer when compared to males. The same result has been reported from previous studies conducted in experimental settings. Head luggage was found to be insignificant. However, the variable is retained in the model as the authors feel that the variable contributes to a great extent in deciding the personal space. Another variable considered was an indicator variable which indicates the ratio of number of group members with opposite gender (with respect to the central person) to the number of group members with same gender. This variable was found to be significant and it indicates that people try to maintain a larger personal space when opposite gender dominates the surrounding group.

However, the personal space requirements are likely to differ if the surrounding people are familiar. In such large gatherings, people may come together and stay as a group. Also, familiarity implies that they move around together. However, identifying such groups from video data is a difficult task. Common indicators used in identifying people belonging to a group include hand holding, eye contact, sharing a luggage between each other, or holding on to the same child. These interchanges between people are used as indicators but extracting such information even under medium density conditions is not trivial. In the recent past, clustering techniques have been employed to detect abnormal crowd flow patterns [14], group trajectories [13], and detection and tracking of dense crowds. The popularity of cluster analysis is that technique can cluster objects such that the members of each cluster are closer to each other than members of other cluster.

Here, social groups are identified through clustering technique. The trajectory information is used to identify social groups in each frame using K-means clustering technique, a standard clustering approach. In this clustering technique, the data points are grouped into k -clusters (where k is the defined number of clusters). Here, the clustering is done by minimizing the Euclidean distance between the data points and the corresponding centroids. However, the clustering is sensitive to the initial position of cluster centroids. The optimal number of clusters is determined using the elbow method, where the point of inflection in the plot of sum of squared errors (SSE) for each value of k is taken to be optimal- k . Further, social groups identified as per the visual observations are used to validate the identified clusters. Voronoi diagrams are constructed to delineate the clusters visually, such that each cell in the region corresponds to one social group. Such proximity diagrams are used quite frequently, wherein each of the cells is convex polygons, and this is further used to identify the personal space within each cell/group. Figure 3 shows the identified clusters for a few sample frames.

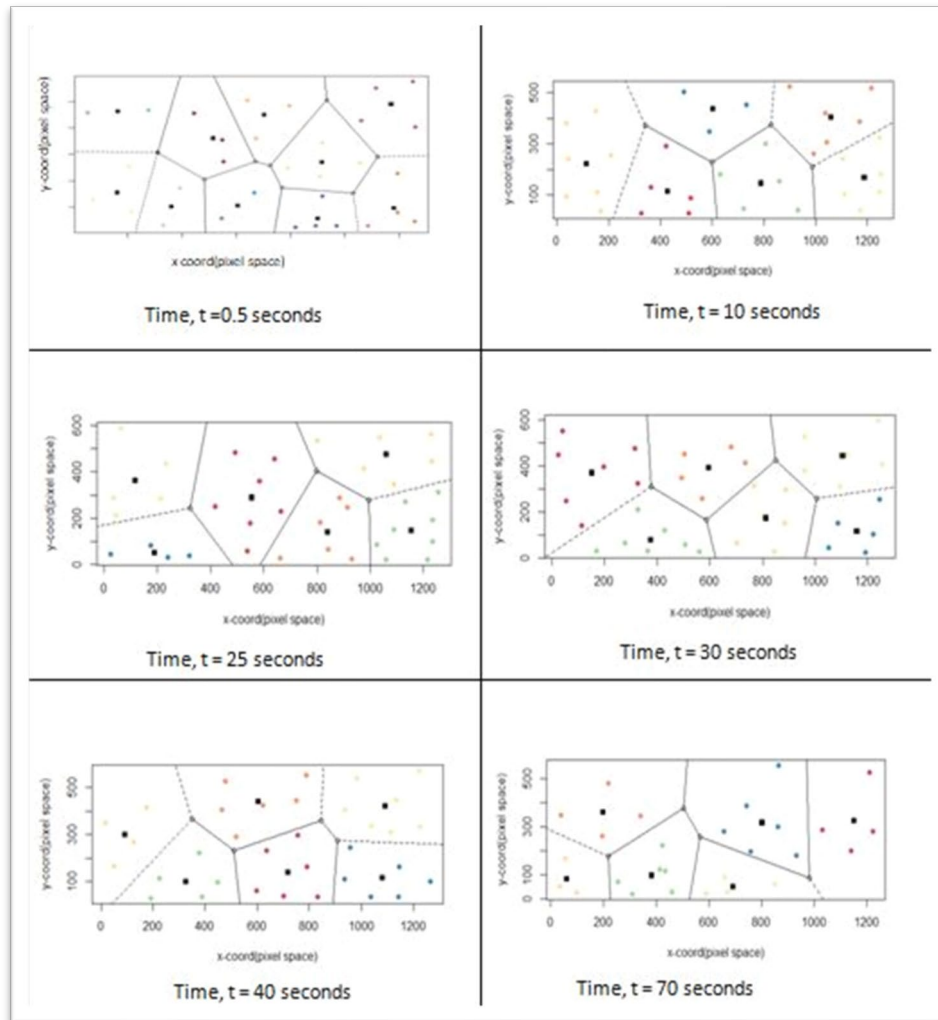


Fig. 3: Voronoi plots of clusters for different time frames

Groups obtained are categorized as female-dyads, female-triads, female-quartets, and male-triads. It is seen that there is significant difference in the mean personal space requirements of all-female groups compared to all-male groups. (female-dyads: 0.26m, female-triads: 0.23m, female-quartets: 0.23m, and male-triads: 0.16m). This could be the result of several factors including the nature of the event, the crowd being female-dominated, and due to the differences between experimental and field conditions.

4. Conclusion

The aim of this study was to define and understand the concept of personal space in a mass religious gathering. The analysis of trajectories of groups of people around a central person revealed that the shape of the bubble surrounding a person, i.e. the personal space is not symmetrical in nature. The bubble tapers in the longitudinal direction while maintaining approximately the same distance laterally on either side. This refutes the assumptions of circular personal space as reported in earlier literatures, especially in situations of medium density. It is also noted that as walking speed increases, personal space increases. This could in turn be the result of lower densities, which permit people to walk at a higher pace. A new insight from this study is the effect of the dominant gender group on the personal space.

There is a lot of heterogeneity in the way people perceive personal space across different cultures and different backgrounds. In Kumbh Mela, a mix of urban, rural, and foreign population, either singly or in groups of different sizes, participate in multiple religious activities together. This heterogeneity reflects in how individuals set rules of personal space for themselves. For this reason, it is extremely challenging to model the personal space as perceived by an individual. It is in this context that the results from this study can be used as inputs to simulate pedestrian behaviour in large crowds.

Further work would include studying the variation of personal space in different locations and varying densities. Group composition is found to influence personal space. Taking this forward, the work can be extended to study the interrelation between group behavior and personal space in higher densities.

Acknowledgements

The work reported in this paper is part of the project titled “The Kumbh Mela Experiment: Measuring and Understanding the Dynamics of Mankind's largest crowd,” funded by the Ministry of Electronics and IT Ministry of Communication and Information Technology, Government of India (MITO-0105), Netherlands Organization for Scientific Research, NWO (Project no. 629.002.202), and Robert Bosch Center for Cyber Physical Systems, Indian Institute of Science, Bangalore. (Grant No. RBCO001). The authors also express their gratitude towards Kumbh Mela administration and government of Madhya Pradesh, India for providing constant support and official permissions to carry out research work and establish Indo-Dutch collaboration research camp at Kumbh Mela 2016.

The authors also acknowledge the help rendered by Mr Abhinav Gyan, intern at IISc Bangalore, during data extraction for this study.

References

- [1] L. A. Hayduk, “The shape of personal space: An experimental investigation.,” *Canadian Journal of Behavioural Science/Revue canadienne des sciences du comportement*, vol. 13, no. 1, pp. 87–93, 1981.
- [2] E. T. Hall, “The Hidden Dimension,” *Leonardo*, vol. 6, no. 1, p. 94, 1973.
- [3] M. Costa, “Interpersonal Distances in Group Walking,” *Journal of Nonverbal Behavior*, vol. 34, no. 1, pp. 15–26, Apr. 2009.
- [4] C. Beaulieu, “Intercultural Study of Personal Space: A Case Study,” *Journal of Applied Social Psychology*, vol. 34, no. 4, pp. 794–805, 2004.
- [5] R. Sommer, “Studies in Personal Space,” *Sociometry*, vol. 22, no. 3, p. 247, 1959.
- [6] A. Frohnwieser, R. Hopf, and E. Oberzaucher., “Human Walking Behavior – The Effect of Pedestrian Flow and Personal Space Invasions on Walking Speed and Direction”, *Human Ethology Bulletin*, vol. 28, no. 3, pp. 20-28, 2013.
- [7] M. Gérin-Lajoie, C. L. Richards, and B. J. Mcfadyen, “The Negotiation of Stationary and Moving Obstructions during Walking: Anticipatory Locomotor Adaptations and Preservation of Personal Space,” *Motor Control*, vol. 9, no. 3, pp. 242–269, 2005.
- [8] L. A. Hayduk, “The permeability of personal space.,” *Canadian Journal of Behavioural Science/Revue canadienne des sciences du comportement*, vol. 13, no. 3, pp. 274–287, 1981.
- [9] M. S. Graziano and D. F. Cooke, “Parieto-frontal interactions, personal space, and defensive behavior,” *Neuropsychologia*, vol. 44, no. 6, pp. 845–859, 2006.
- [10] R. C. Newman and D. Pollack, “Proxemics in deviant adolescents.,” *Journal of Consulting and Clinical Psychology*, vol. 40, no. 1, pp. 6–8, 1973.
- [11] L. A. Hayduk and S. Mainprize, “Personal Space of the Blind,” *Social Psychology Quarterly*, vol. 43, no. 2, p. 216, 1980.

- [12] K. B. Little, "Personal space," *Journal of Experimental Social Psychology*, vol. 1, no. 3, pp. 237–247, 1965.
- [13] R. Sharma, and T. Guha, "A trajectory clustering approach to crowd flow segmentation in videos", *2016 IEEE International Conference on Image Processing (ICIP)*, 2016.
- [14] Ma, Jian, and Weiguo Song. "Automatic Clustering Method of Abnormal Crowd Flow Pattern Detection." *Procedia Engineering* 62 ,509-18. 2013

Understanding Crowd Dynamics in Processions during Mass Religious Gatherings

A case study of Shahi Snan in Kumbh Mela

H Gayathri¹, Siddhartha Gulhare², Ashish Verma^{3*}

¹Research Scholar, ² ex- Project Associate

Department of Civil Engineering,
Indian Institute of Science (IISc), Bangalore 560012, India
gayuhariharan@gmail.com; siddharthagulhare89@gmail.com

³ Associate professor, Department of Civil Engineering and
Robert Bosch Centre for Cyber Physical Systems,
Indian Institute of Science (IISc),
Bangalore 560012, India
ashishv@iisc.ac.in

*(Corresponding Author)

Abstract - Large people gatherings in public places exhibit crowd dynamics that are quite complex. Such mass events with high densities are fraught with potentially serious consequences if not understood and managed properly. In mass religious processions, the participants in the crowd are emotional and mostly impulsive and often crowd disasters occur due to the behaviour of the crowd. These events have great potential to cause safety hazards to the people. This paper attempts to narrate the typical situations of crowd dynamics observed in the Kumbh Mela procession-2016 and to describe the characteristics of the crowd that have not been reported in literature so far but have a significant impact on the crowd. Extreme crowd pressures resulting in individual loss control due to psychological and physiological factors, heterogeneity in the crowd, group behaviour and their induced competitiveness, unexpected behaviour exhibited due to the motivation behind participating in such procession makes it a typical crowd concentrated event to study the potentially critical dynamics of crowd. Physical and psychological forces acting on the people and their resulting dynamics of crowd in the Kumbh Mela procession 2016 lead to serpentine behaviour, which can possibly lead to crowd crushes, or any such crowd risk situations. Therefore, the characteristics of crowd participating in the Kumbh Mela procession have to be clearly understood so that it helps in better planning and well-organized movement patterns.

Keywords: Group Behaviour; Pedestrian; Mass religious gatherings; Crowd risk; India

1. Introduction

Crowds are extremely complex systems. Large number of people gather in places like temples, mosques, shopping malls, bus and train stations, etc. and in places of particular attractions or events that take place like sports events, concerts, theatres, religious gatherings, carnivals (melas), processions, etc. Each crowd is a unique phenomenon and the nature of the crowd is difficult to generalize. In a mass procession, the participants in the crowd are emotional and mostly impulsive and often crowd disasters occur due to the behaviour of the crowd. At high densities, there is the potential for overcrowding which could result in personal injuries due to the role of situational influences. Therefore understanding the complex crowd dynamics in such mass processions is a crucial step towards eliminating the crowd disasters.

There have been several studies on how crowd disasters happen. The inadvertent body contacts between pedestrians induce high forces that propagate along the direction in which they exert (Ma et al, 2013, Kolli, 2014, Dave, 2014, Fruin, 1993, Helbing et al, 2007, Moussaid et al, 2011). In addition, many studies have revealed that people mostly come in groups at leisure places like shopping malls, football events, etc. (Coleman & James 1961, Aveni 1977, Moussaid et al 2010 and Cheng & Yarlagaadda 2014). Pedestrian groups generally develop patterns (Strogatz et al, 2005, Moussaid et al, 2010, Miguel, 2015) and thereby reduces the travel time (Koster et al, 2011). In mass religious processions like Kumbh Mela, people participate with a common objective of taking a dip in a river believing it. These goal-oriented

crowds are concerned about the safety of their affiliated members and so mostly consists of groups. A questionnaire survey conducted by the authors in Kumbh Mela-2016 revealed that 95% of surveyed people came in groups. Many researchers also study the competitiveness between members in crowd (Kretz, 2007, Fruin JJ, 1993, Darwin, 1871). When large number of people gather and move in a constrained environment with common goals, they find themselves in dangerous conditions.

Many processions that happened across the world have resulted in life-threatening disasters due to the unexpected behaviour of the crowd. Some of the examples of crowd disasters in processions are funeral procession in Moscow (Pozner and Vladimir, 1990), crowd crush in Shia procession (“Reaction to Iraq stampede”, BBC News, 31 August 2005), crowd crush in Varanasi religious procession (“Varanasi: Deadly stampede at Hindu procession”, CNN International Edition, 16 October 2016) and crowd crush in Kumbh Mela procession (“The worst stampede in Allahabad in 1954, killing 800”, The Guardian, 28 August 2003). Crowd crush often occur when a majority of people in an event with mass gathering tries to move towards a central attraction (Dave, 2014). These crowd concentrated events have a great potential to cause safety hazards to the people. Therefore finding a sensible description of the various aspects of crowd behaviour and its characteristics in mass processions with high degree of complexities involved is an important issue. Nevertheless, this has to be understood to provide opportunities to change crowd dynamics and to avoid any adverse effects in future events.

2. Qualitative analysis- A case study of Shahi Snan

Shahi Snan (royal holy bath) is the major event of Kumbh Mela festival, which takes place on predetermined dates. During this time, river Kshipra is the point of central attraction, as it is believed to wash the sins of all previous births. Before taking bath, there goes a long procession of saints and their disciples from various ascetic orders. Several saints come in the procession sitting on horses and decorated chariots drawn by their disciples. Uniquely, Kumbh Mela is one mass religious event that gives opportunity to study all the typical situations of crowd dynamics observed in such events. The scenario of crowd is very different. (Gayathri et al, 2017). This work attempts to study the situations in Kumbh Mela procession 2016 that may lead to crowd disasters in future events and recommendations/solutions to prevent such disasters in future are suggested. In Kumbh Mela-2016 Shahi Snan, as per the government, 2.5 million people visited the city (Economic Times, May 09, 2016). Fig. 1 shows the GPS trace of a participant during shahi snan procession in Kumbh Mela-2016.



Fig. 1: GPS trace of participant during Shahi Snan procession in Kumbh Mela-2016

The shahi snan procession-2016 is a well-planned event. The saints travel in their tractor-drawn chariot and their respective disciples would follow them. It was planned in such a way that the tractor-drawn chariots would control the crowd situation at macroscopic level to some extent. Also, since people spend time in bathing in the ghat area, the inflow is to be curtailed from time to time in such a way that the rate of people entering the ghat is less than or equal to the rate at which they are exiting the ghat.

In order to avoid overcrowding in the ghat area, the chariots will have to wait at the ghat entrance and will be allowed to enter at certain intervals. The planned scenario for the procession is depicted in Fig. 2.

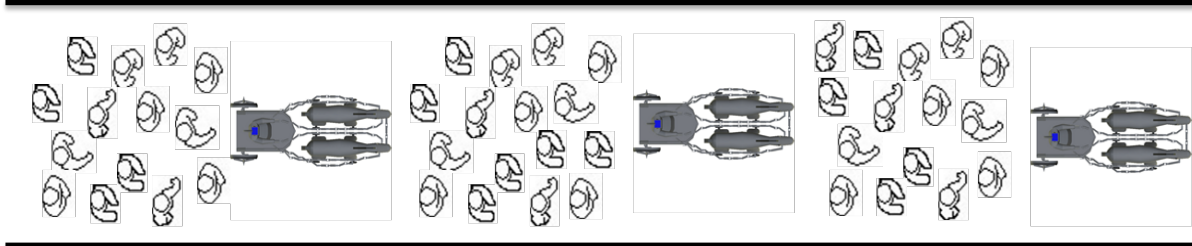


Fig. 2: Representation of planned scenario for the procession

3. Observed crowd characteristics in Kumbh Mela procession-2016

The actual situation observed in Kumbh Mela procession-2016 was different from the planned scenario. On the day of procession, saints and disciples from 13 akhadas participated in the procession. The pilgrims gathered in their respective saints' camp from late evening. The procession started as planned but with a delay of 2 hours due to which the pilgrims became impatient. The delay is believed to be due to some rituals in some akhadas. A team including authors joined and observed the procession. The team members walked alongside the procession carrying GPS devices and head mount camera and visually observed the impact of the event on the crowd as they moved forward towards the ghat for holy dip. Snapshots of Shahi Snan procession in Kumbh Mela 2016 is shown in Fig. 3.



Fig. 3: Snapshots of Shahi Snan procession

As the procession began, the camps started leaving the akhadas one after another. As the procession started with a delay, people became impatient and tried to exit their camps and join the procession with high desirable speed. Near the front gate of one of the camps (Niranjani Akhara) people recognized that the other camp people were trying to overtake them and so they tried to increase their speed rapidly. The front gate of the camp was narrow and this created a bottleneck effect near the gate which resulted in pushing. People at the rear end, unaware of the situation at the front, kept moving while those in the front experienced severe distress. The smaller densities at the rear end allowed people to move freely but those at the front were immobile and under extreme pressure. Therefore, people started behaving aggressively as their urge to move forward as quickly as possible towards the ghat to take holy dip increased and the spiritual gain that they derive from the rare occasion being with their saints, made them feel like they are privileged.

As the crowd progressed towards the destination, the density became high. Some people who don't belong to the akhada and do not hold a permission to participate in the procession tried to enter the procession and overtake the pilgrims and saints from sides to reach the ghat to take holy dip. Therefore, the pilgrims started to take the holy dip as a 'chance to gain' and more likely as a competition to reach the ghat as quick as possible. Therefore, a cooperative behaviour, which is very important in mass gatherings like Kumbh procession to avoid crowd risk situations, was missing. This competitiveness of crowd only

added instability in the crowd leading to decrease in flow rate and resulted in altruism among people in groups. They had the desire to overtake others and move forward and so tried to find out gaps in the crowd to sneak through. This added complexity to the crowd. The actual situation witnessed in the Kumbh Mela procession 2016 is depicted in fig. 4. Pedestrians in red indicates serpentine group and blue indicates people who try to overtake along the sides.

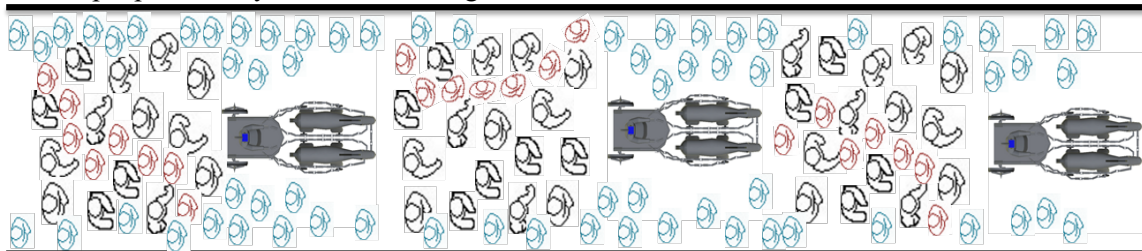


Fig. 4: Representation of actual situation observed in the procession

Some people followed their saints and moved along the crowd but some people tried to sneak through the crowd to reach the ghat as early as possible. They overtook others including the saints' tractor drawn chariots to reach the ghat entrance. Security personnel using temporary barricades stopped people 100 m before the ghat entrance and allowed them to enter the ghat at suitable intervals to avoid overcrowding at the ghat section. The saints were allowed to enter first and the pilgrims were stopped near the ghat entrance and allowed at regular intervals. The people at the rear end, unaware of the situation ahead, kept moving forward even when the flow is stopped and this increased the density at the rear end. Some impatient pedestrians tried to overtake the crowd and reach the ghat entrance. Also people from sides tried to merge with the crowd and this lead to high densities near the entrance resulting in stop and go waves propagating in the opposite direction. Interaction of these factors lead to a peculiar type of behaviour in groups called serpentine behaviour.

3.1. Serpentine behaviour

Crowd as an entity is dominated by uniform moods and feelings (Canetti, 1984). In mass religious processions, individuals in a crowd try to move forward deliberately towards their goal. This deliberate movement towards achieving their goal results in emergence of some kind of pattern or structure. Majority of the people attending such processions come in groups consisting of family members, friends, and longtime affiliated members. Group behaviour dominates such religious processions. Kumbh Mela has been notoriously known for families losing their loved ones in large crowd. Hence group members stay together. Two kinds of group behaviour were observed: Groups subdivide into smaller subgroups/free forming groups but as a whole remain in proximity to each other (very regular group behaviour as described in literature); group size varying between 3-8 pedestrians, consisting of very close members (such as women and children) remain in very close proximity and rarely break away from their groups. Members of group stay close to each other with physical contact (by holding hands) and behave as a single large unit of various shapes like serpentine chain, clusters with vulnerables in the middle. These groups try to stay together and do not allow others to penetrate through and thus restricting the differential movement of others in crowd. Therefore this increases the crowd risk by clogging and thereby reducing the efficiency at the exit.

However, it is practically not possible for the group members in the procession to form loops, circles, walk in horizontal direction or any other type of group patterns as the density is very high and all the members in the crowd try to overtake each other. In such cases, during overtaking, one member leads the group and others follow as shown in fig. 5. This Serpentine Behaviour is a special case of group behaviour. The attractive force between leader-follower and repulsive force from other pedestrians lead to formation of flexible chain of member trying to percolate through the crowd. When the distance between the people in the crowd is more, attractive forces dominates. As the distance decreases, repulsive forces are created. This phenomenon ensures that group stays together. During serpentine movement, members hold hands or place their hands on shoulder and do not allow others to penetrate through it. As more and

more groups continue to form serpentine chains to overtake and move forward, they get compressed against each other with very little breathing space. This behaviour creates an inadvertent body contact with other members in the crowd creating a compressive force on them resulting in pushing. Therefore, presence of large serpentine chain increases the crowd risk.

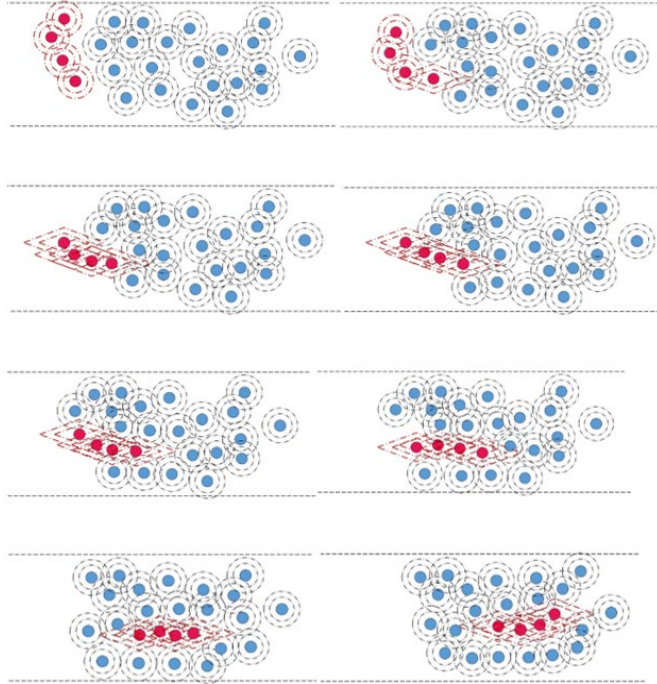


Fig. 5: Serpentine behaviour observed in crowd

4. Modelling serpentine behaviour

4.1. Basic concept of Helbing's social force model

Helbing's social force model (Helbing and Molnar, 1995) is slightly modified to include the overtaking and serpentine behaviour of pedestrians. Helbing has considered the following four types of forces acting on a pedestrian i .

1. Acceleration force towards goal = \vec{f}_i^0
- $$\vec{f}_i^0 = \frac{v_i^0 \vec{e}_i - \vec{v}_i}{\tau_i} \quad (1)$$

where,

v_i^0 and \vec{v}_i are the desired and actual speeds of pedestrian i

τ_i is the relaxation time

\vec{e}_i is the desired direction of pedestrian i

$$\vec{e}_i = \frac{\vec{r}_i^k - \vec{r}_i(t)}{\|\vec{r}_i^k - \vec{r}_i(t)\|}$$

where, \vec{r}_i^k is $\vec{r}_i(t)$ are the desired position and actual position of pedestrian i at time t .

2. Repulsive force from other pedestrian $j = \vec{f}_{ij}$

$$\vec{f}_{ij}(\vec{r}_{ij}) = -\nabla_{\vec{r}_{ij}} V_{ij}[d(\vec{r}_{ij})] \quad (2)$$

This force is a monotonically decreasing function of d (private sphere within which if other pedestrians enter, repulsive effect is created), where,

\vec{r}_{ij} is the position of i with respect to j and is calculated as $\vec{r}_{ij} = \vec{r}_i - \vec{r}_j$

V_{ij} is the repulsive potential

$$3. \text{ Repulsive force from obstacle } B = \vec{f}_{iB}$$

$$\vec{f}_{iB}(\vec{r}_{iB}) = -\nabla_{\vec{r}_{iB}} U_{iB}[\|\vec{r}_{iB}\|] \quad (3)$$

where, \vec{r}_{iB} is the position of i with respect to boundary.

$$4. \text{ Attractive force from obstacles/pedestrians } \alpha = \vec{f}_{i\alpha}$$

(Ignored in this study for simplicity)

Therefore, resultant force $\vec{f}_i = \vec{f}_i^0 + \vec{f}_{ij} + \vec{f}_{iB} + \vec{f}_{i\alpha}$

4.2. Forces acting on pedestrians while overtaking

The following are the three types of forces acting on a pedestrian i when he tries to overtake j (refer fig. 6).

1. Acceleration force towards goal = \vec{f}_i^0
2. Repulsive force while overtaking pedestrian j (aligned with ij) = \vec{f}_{ioj}
3. Repulsive force from obstacle B = \vec{f}_{iB}

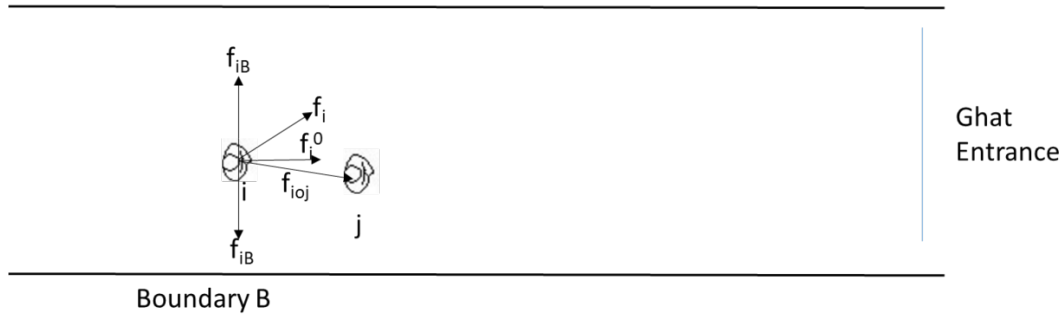


Fig. 6: Forces acting on pedestrians while overtaking

For overtaking, within the private sphere of pedestrian j, speed of i should be greater than speed of j

$$v_i > v_j$$

Pedestrian may try to overtake either on left or right side of pedestrian j (Tamura et al 2012)

$$r_{\delta L} = r_j + d_{\delta 1} e_i + d_{\delta 2} e_{\frac{1}{i}}$$

$$r_{\delta R} = r_j + d_{\delta 1} e_i - d_{\delta 2} e_{\frac{1}{i}}$$

where,

e_i and $e_{\frac{1}{i}}$ are the desired direction and unit normal to desired direction

$d_{\delta 1}$ and $d_{\delta 2}$ are longitudinal and lateral distance between pedestrian j and the next desired position of i

$$e_i(t) = \text{desired direction} = \frac{\vec{r}_{\delta L}^k - \vec{r}_i(t)}{\|\vec{r}_{\delta L}^k - \vec{r}_i(t)\|} \text{ or } \frac{\vec{r}_{\delta R}^k - \vec{r}_i(t)}{\|\vec{r}_{\delta R}^k - \vec{r}_i(t)\|}$$

Based on the position, repulsive force \vec{f}_{ioj} is calculated using equation (2)

Other force calculations would remain the same as social force model.

$$\text{Resultant force } \vec{f}_i = \vec{f}_i^0 + \vec{f}_{ioj} + \vec{f}_{iB}$$

4.3. Forces acting on pedestrians in serpentine chain

The following are the four types of forces acting on pedestrians in serpentine chain (refer fig. 7)

1. Acceleration force towards goal = \vec{f}_i^0
2. Repulsive force from other pedestrian $j = \vec{f}_{ij}$
3. Repulsive force from obstacle $B = \vec{f}_{iB}$
4. Attractive force from other pedestrian within group when there are n number of members in a group = $\vec{f}_{i_2 i_1}, \vec{f}_{i_3 i_2} \dots \vec{f}_{i_n i_{n-1}}$

Within the serpentine group, the first member leads the group whereas the other members follow their previous member. This following behaviour is introduced as their sub goals with position γ , which is set behind their respective follower. The sub goal is the attractive force exerted on other pedestrians within the chain. If the number of members in chain is n , then there are m sub goals where $n-1 = m$ for simplicity. As seen in fig 7, the first member, also known as the leader, will have \vec{f}_{ij} or \vec{f}_{ioj} whereas the followers in the chain will have $\vec{f}_{i_2 i_1}, \vec{f}_{i_3 i_2}, \vec{f}_{i_4 i_3}, \vec{f}_{i_5 i_4}$ and $\vec{f}_{i_6 i_5}$ respectively.

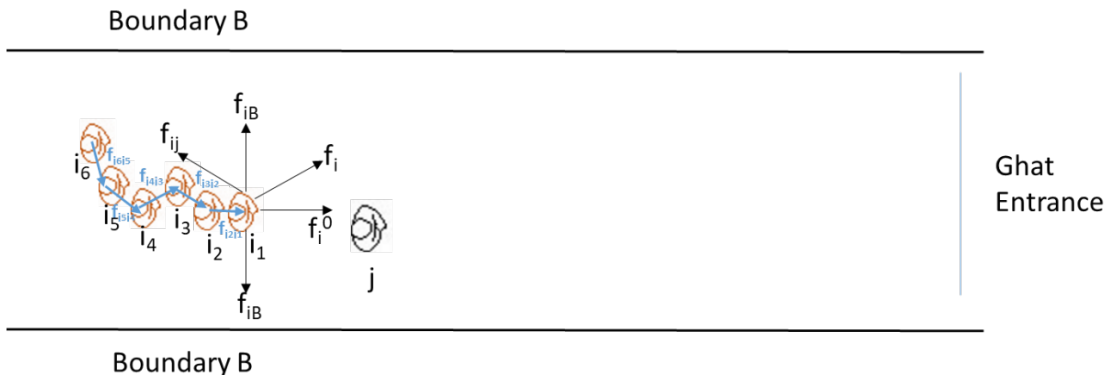


Fig. 7: Forces acting on pedestrians in serpentine chain

Position of $\gamma_1 = r_{\gamma_1} = r_{i_1} - d_{i_1 \gamma_1} e_{i_1}$

Therefore, in general, position of $\gamma_m = r_{\gamma_m} = r_{i_n} - d_{i_n \gamma_m} e_{i_n}$

$$\vec{f}_{i_2 i_1}^{\gamma_1} = \frac{v_{i_2}^{\gamma_1} * \vec{e}_{i_2} - \vec{v}_{i_2}}{\tau_{i_2}}$$

$$\vec{f}_{i_n i_{n-1}}^{\gamma_m} = \frac{v_n^{\gamma_m} * \vec{e}_{i_n} - \vec{v}_{i_n}}{\tau_{i_n}}$$

where,

$\vec{f}_{i_n i_{n-1}}^{\gamma_m}$ is the attractive force from pedestrian i_{n-1} to i_n with i_n 's sub goal position γ_m in the serpentine chain

$v_n^{\gamma_m}$ and \vec{v}_{i_n} is the desired and actual velocity of i_n with i_n 's sub goal position γ_m in the serpentine chain

\vec{e}_{i_n} is the desired direction of pedestrian i_n in the serpentine chain

τ_{i_n} is the relaxation time of i_n in the serpentine chain

Repulsive force from obstacles \vec{f}_{iB} is common for all pedestrians in the serpentine chain and remains the same as social force model.

Resultant force $\vec{f}_{i_1} = \vec{f}_i^0 + \vec{f}_{ij} + \vec{f}_{iB}$ (i_1 - the first member in the chain)

In case of overtaking, $\vec{f}_{i_1} = \vec{f}_i^0 + \vec{f}_{ioj} + \vec{f}_{iB}$

Resultant force for the other members (followers) in the chain $\vec{f}_{i_n} = \vec{f}_i^0 + \vec{f}_{i_n i_{n-1}}^m + \vec{f}_{iB}$

5. Recommendations

The following are some of the recommendations/suggestions for the event planners and organisers for better management of crowd to avoid circumstances leading to crowd crush and other crowd risk situations.

1. The acceptable level of crowd density should be clearly defined.
2. All Akharas should inform the authorities about the expected number of people likely to participate in the procession from their side.
3. Keeping the above numbers in consideration the flow should be managed in such a way that there is no chaotic movement. (For example, in 2016 Kumbh Mela, near the ghat entrance, the saints were allowed first and the pilgrims were barred from entering. This led to an unstable equilibrium).
4. A proper briefing on the route, ascetic order that the participants need to follow, and the order in which the camps join the procession (ash-smearad sadhus, saints in tractor-drawn chariots, pilgrims) should be provided to participants by the organizers well before the start of the processions.
5. Procession routes should be free from soft boundaries or temporary barricades as they can lead to dangerous situations. The pilgrims should be kept moving to the maximum possible extent by rerouting or by any other strategies, so that the flow is not stopped. This can help in avoiding potential situations leading to crowd crush.
6. The organizers must ensure that the procession starts without any delay. Delayed start is the reason why people started behaving aggressively and tried to push each other to exit their respective camps. Proper information should be provided to people if any delay is unavoidable.
7. Organizers should allow only akhara members to participate in the processions. One suggestion is to issue tickets or badges to the participants so that others do not try to enter the crowd. Others should not be allowed to participate or cross over through the procession.
8. The security personnel should locally control the flow of the procession. Scenarios where people from other camp try to break the flow and overtake should not be allowed with the help of security personnel.
9. The crowd behaviour and its movement should be monitored continuously. Loudspeakers, or any public announcement systems should be used to communicate with the crowd.
10. CCTV monitoring of the crowd along the procession route should be done to identify hazard points and initiating corrective actions.

6. Summary and Conclusion

The characteristics of crowd in the procession adds complexities to the dynamics of crowd. Most of the people who participate in the procession come in groups with their affiliated members due to the fear of getting lost or hurt in the crowd. Waiting time due to delay triggers these sleep-deprived people's mind psychologically but still they stay motivated to complete the procession as they consider this as a rare opportunity and feel like they are privileged to be with their saints. This waiting time induces people to exhibit competitive behaviour. Due to this, some people try to percolate through the crowd holding hands of their group members and forming a chain thus exhibiting serpentine behaviour. This causes pressure building in the surroundings and triggers a complex avoidance maneuver in the crowd. As one person starts overtaking, others try to act in the same manner thereby breaking the organized flow.

Therefore, the sense of individuality is almost removed in the crowd. This herding behaviour develops an unstable flow pattern. In addition, the speed of people trying to overtake from the sides is higher than the people walking along the procession. The interaction between people who walk faster and

slower than the average speed creates an unstable equilibrium in the crowd. All these behaviours lead to situations of crowd risks and suitable measures have to be taken so as to avoid these crowd risks leading to crowd disasters. To model the forces exerted on pedestrians forming serpentine chain, Helbing's social force model is slightly changed to the context of this study.

Many studies have been done to understand pedestrian crowd dynamics and most of them are limited to kinematics of crowd. However, crowd dynamics is a highly complex system. High-density crowds have an enormous potential for overcrowding which could lead to dangerous situations. This paper attempted to highlight the crowd characteristics in high-density event, which have not been captured so far but have a significant impact on crowd behaviour associated with risk. A better understanding of these crowd characteristics will help to increase the efficiency and mitigate the risks in mass events.

Specific recommendations on how to dissipate the forces exerted due to overtaking and serpentine behaviour require detailed research. In addition, only the social forces acting on the pedestrians in the serpentine chain have been considered in this study. Psychological forces, which are predominant in such religious procession, also have a huge impact on crowd and is worth further research.

Acknowledgments

The work reported in this paper is part of the project titled “The Kumbh Mela Experiment: Measuring and Understanding the Dynamics of Mankind's largest crowd,” funded by the Ministry of Electronics and IT Ministry of Communication and Information Technology, Government of India (MITO-0105), Netherlands Organization for Scientific Research, NWO (Project no. 629.002.202), and Robert Bosch Center for Cyber Physical Systems, Indian Institute of Science, Bangalore. (Grant No. RBCO001). The authors also express their gratitude towards Kumbh Mela administration and government of Madhya Pradesh, India for providing constant support and official permissions to carry out research work and establish Indo-Dutch collaboration research camp at Kumbh Mela 2016.

References

1. “The worst stampede was in Allahabad in 1954, killing 800”. The Guardian, 28 August 2003
2. “Varanasi: Deadly stampede at Hindu procession”, CNN International Edition, 16 October 2016
3. Canetti, E, “Crowds and Power”, Farrar, Straus and Giroux, New York, NY, USA, 1984
4. Cheng L, Yarlagaadda R, Fookes C, Yarlagaadda P (2014) “A review of pedestrian group dynamics and methodologies in modelling pedestrian group behaviours” *World Journal of Mechanical Engineering* Vol. 1(1). pp. 002-013.
5. Coleman J S & James J (1961) “The equilibrium size distribution of freely-forming groups” *Sociometry*, vol.24, pp-36 – 45.
6. Helbing D and Molnar P(1995) “Social Force Model for Pedestrian Dynamics,” *Physical Review E*, vol. 51, no5, pp.4282-4286
7. Darwin C (1871) “The Descent of Man and Selection in Relation to Sex” John Murray, London 1st edition, <http://darwin-online.org.uk/>
8. Dave R K (2014) “Crowd Management and Public Safety in India-A new policy initiative”, *ICT2014*, Org 1476577876.
9. Fruin J J (1993) “The Causes and Prevention of Crowd Disasters” *First International Conference on Engineering for Crowd Safety*, London, England.
10. Gayathri H, Aparna P M, Verma A (2017) “A review of studies on understanding crowd dynamics in the context of crowd safety in mass religious gatherings”, *International Journal of Disaster Risk Reduction* Volume 25, pp 82-91
11. Helbing D, Johansson A, Al-Abideen HE Habib Z (2007) “Crowd turbulence: the physics of crowd disasters” *The Fifth International Conference on Nonlinear Mechanics (ICNM-V)*, Shanghai.

12. Koster G, Seitz. M, Treml. F, Hartmann. D, Klein. W (2011) “On modeling the influence of group formations in a crowd”, *Contemporary Social Science* 6, 397-414.
13. Kretz T (2007), “Pedestrian Traffic Simulation and Experiments” PhD thesis, Universität Duisburg-Essen
14. Ma J, Song W G, Lo S M and Fang Z M (2013) “New insights into turbulent pedestrian movement pattern in crowd-quakes”, *Journal of Statistical Mechanics: Theory and Experiment*, Volume 2013.
15. Miguel A F (2015) “Key Mechanisms behind Pedestrian Dynamics: Individual and Collective Patterns of Motion” *Diffusion Foundations*, Vol. 3, pp. 153-164.
16. Moussaid M, Helbing D, Theraulaz G (2011) “How simple rules determine pedestrian behaviour and crowd disasters” *Proceedings of the National Academy of Sciences of the United States of America*, vol. 108, no. 17, 6884–6888
17. Moussaid M, Perozo N, Garnier S, Helbing D, Theraulaz G (2010) “The walking behaviour of pedestrian social groups and its impact on crowd dynamics”, *PloS one* 5 (4). e10047.
18. Pozner, Vladimir (1990) “Parting with Illusions”, Atlantic Monthly Press, 324pp.
19. Strogatz S H, Abrams D M, McRobie A, Eckhardt B, Ott E (2005) “Crowd synchrony on the Millennium Bridge”, *Nature* 438, pp. 43-44, <http://dx.doi.org/10.1038/438043a>
20. Sindhu K (2014), “Multi-Agent Management of Crowds to Avoid Stampedes in Long Queues”, MS thesis, Center for Data Engineering, International Institute of Information Technology, Hyderabad
21. Tamura Y, Phuoc Dai Le, Hitomi K, Chandrasiri N P, Bando T, Yamashita A and Asama H (2012) “Development of Pedestrian Behaviour Model Taking Account of Intention,” 2012 IEEE/RSJ *International Conference on Intelligent Robots and system (IROS)*, pp. 482-387

Investigating pedestrians' obstacle avoidance behaviour

Abdullah Alhawsawi^{1,2}, Majid Sarvi¹, Milad Haghani¹, Abbas Rajabifard¹

¹Transport Engineering Group, School of Engineering
Department of Infrastructure Engineering
The University of Melbourne
Victoria 3010 Australia

aalhawsawi@student.unimelb.edu.au¹; majid.sarvi@unimelb.edu.au¹
milad.haghani@unimelb.edu.au¹; abbas.r@unimelb.edu.au¹

²Hajj and Umrah Institute, Umm Al-Quran University,
Makkah, KSA,
E:anhawsawi@uqu.edu.sa

Abstract - Modelling and simulating pedestrian motions are standard ways to investigate crowd dynamics aimed to enhance pedestrians' safety. Movement of people is affected by interactions with one another and with the physical environment that it may be a worthy line of research. This paper studies the impact of speed on how pedestrians respond to the obstacles (i.e. Obstacles avoidance behaviour). A field experiment was performed in which a group of people were instructed to perform some obstacles avoidance tasks at two levels of normal and high speeds. Trajectories of the participants are extracted from the video recordings for the subsequent intentions:(i) to seek out the impact of total speed, x and y-axis (ii) to observe the impact of the speed on the movement direction, x-axis, (iii) to find out the impact of speed on the lateral direction, y-axis. The results of the experiments could be used to enhance the current pedestrian simulation models.

Keywords: (Evacuation, Modelling, and Simulation, Crowd dynamic, Motion, Obstacle avoidance)

1. Introduction

Modelling and simulating the interaction of people around the physical environment are important issues in the study of crowd dynamics. The key issue is to design and build safe venues wherever crowd management rules are applied. For example, large gathering venues, schools, theatres, mosques, railway stations and alternative places are designed to have an entry and exit point.

Using physical obstacles is a common crowd control and management tool to navigate pedestrian flows. These include crowd control barricades, line management systems, entry control systems, temporary fencing and barriers. It's widely accepted that these measures facilitate, particularly in increasing the security in mass events [4]. According to Oksana [4], crowd control should think about several details to organize a safe and secure indoor or outdoor event.

Understanding the way in which obstacles size will affect pedestrian behaviour is important in nowadays, which can provide better evacuation management plan, comfort, and safety for the crowd. Investigating the effects of the obstacles in human behaviour have commonly used in many crowd simulation models. Crowd simulation models assist in predicting the crowd threats and in doing so reduce the deaths that may occur [1]. Many researchers had focused on the interaction of human behaviour, characteristics and phenomena in a complex geometrical environment to find the most common variables that led to the death or injury [2-8].

Many models are developed to explain the interaction of people, e.g., physical primarily based models [9], Social force model [10, 11], social cellular automaton [12-14]. Per people may well be delineated as Newton-like particles driven by forces [2]. These particles describe the interaction amongst the crowd. Several researchers have used these models due to promising results or well-acceptance. There are some delusive results found in these models, like interaction forces or geometries environment associated with the relative position of people.

Factors affecting how pedestrians respond to the environment or to others are in the beginning stages and not fully understood, and more human experiments are needed [15]. To do that, several experimental studies have been conducted on how pedestrians avoid obstacles [15] and collisions during their movements [15-19] using the recent technological approach of image processing to extract the trajectories [20]. The trajectories of the participants were extracted from recorded videos and analysed in two different levels of speeds, normal and high. Therefore, this paper studies the impact of speed on how pedestrians respond to the obstacles (i.e. obstacles avoidance behaviour).

A field experiment was performed during which a group of people were instructed to perform some obstacles avoidance tasks at two levels of normal and high speeds. Trajectories of the participants are extracted from the video recordings for the following intentions: (i) to find the impact of total speed (ii) to observe the impact of the speed on the movement direction, (iii) to find out the impact of speeds on the lateral direction. The results of the experiments could be used to enhance the current pedestrian simulation models.

2. Related works

2.1. Microscopic models

In microscopic models, each pedestrian in a crowd is treated as an individual agent holding a certain area during each time instant. These models are able to offer valuable insight over a wide range of behavioural inputs. The microscopic models deal with all the factors that take the pedestrians towards their goals or destination by respecting the interaction between pedestrians. Such models provide a more realistic description of pedestrian movements. In the most recent microscope models, individuals avoid obstacles, by avoiding collisions based on their positions [10].

The physical based models were studied and developed by [11] Helbing and Molnar. The model has been widely used in indoor environments, particularly in emergency and panic conditions [1]. This model provides better capabilities to design a strategic plan for the evaluation of pedestrians. In this model, an optimal acceleration is determined based on totally different physical force to apply the motion equations; then the simulation will be updated from time to time based on different steps and models, social force - models [11]. Therefore, this model can facilitate to provide better results to attain the aims of this study.

Social force model (SFM) is one of the most frequently used models in microscopic pedestrian studies. With the help of the self-stopping mechanism, a modification for upgrading this method is done day by day. The forces in the social model are not related to the pedestrian's personal environment but incorporated with an individual's performance to complete a certain action [8]. The basic concept of this model is motivating pedestrians to reach their goals. But the main assumption force for this model is that each agent has his/her own goals to reach a certain point at the target time.

2.2. Factors behaviour

The basic dynamics of the crowd activity may be characterized and influenced by numerous factors involving movement, speed, interactions. Based on the various situations, design, planning layout can be determined. Some of the several factors may include social factors, physical factors, and psychological factors [21]. The physical aspects of an individual are the most important attribute in the simulation process. It is essential that the simulation model incorporates these factors to ascertain human behaviour and patterns [22].

3. Methods

An experiment has been performed to grasp the behaviour of pedestrians throughout their movement through obstacles within the sports centre at the University of the Melbourne on 06/03/2017. The experiment procedure was approved by the Engineering Human Research Ethics Advisory Group. The experiment involved over 110 students of both genders moving in 120 m² area of square shape. The age group was limited to 21-25 years.

The movement of the participants was recorded at 50 frames per seconds by a video camera straddled at the experiment site. Special software, PeTrack [20], was used for tracking the position of participants. The program parameters were calibrated according to the experimental environments in the field. The program was set at the colour matchup mode and instructed to them to wear yellow and green beanies. The software provided a mass trajectory file of each experiment as the raw output data, based on which the subsequent analyses are performed [24].

The objective of this study is to examine the characteristics of individuals walking through several obstacles sizes and to evaluate the impact of an obstacle on human moving speed and on the individual's movement behaviours during high and low-density conditions. The data was collected from these experiments with a group of people walking and running through several sizes of the obstacles with different desired speeds scenarios, as shown in Table 1. The participants were ordered to enter a 50 cm size door and visit the opposite aspect bypassing obstacles with different sizes (1.2, 2.4, 3.6, 4.8 meters wide). In Fig.1. an extracted trajectory from the interface of the tracking software on and the trajectories in X (the Moving Direction) and Y (Lateral Direction) for all the participants from one door size of 50 cm and different obstacles sizes (a) Walking 1.2 m. (b) Running 1.2 m. (c) Walking at 2.4 m. (d) Running 2.4 m. (e) Walking 3.6 m (f) Running 3.6 m. (g) Walking 4.8 m (h) Running 4.8 m.

Table 1: Experiments scenarios

Entrance door size	50 (cm)	
Speed	Walking	Running
Obstacle Size	1.2 m (a)	1.2 m (b)
	2.4 m (c)	2.4 m (d)
	3.6 m (e)	3.6 m (f)
	4.8 m (g)	4.8 m (h)

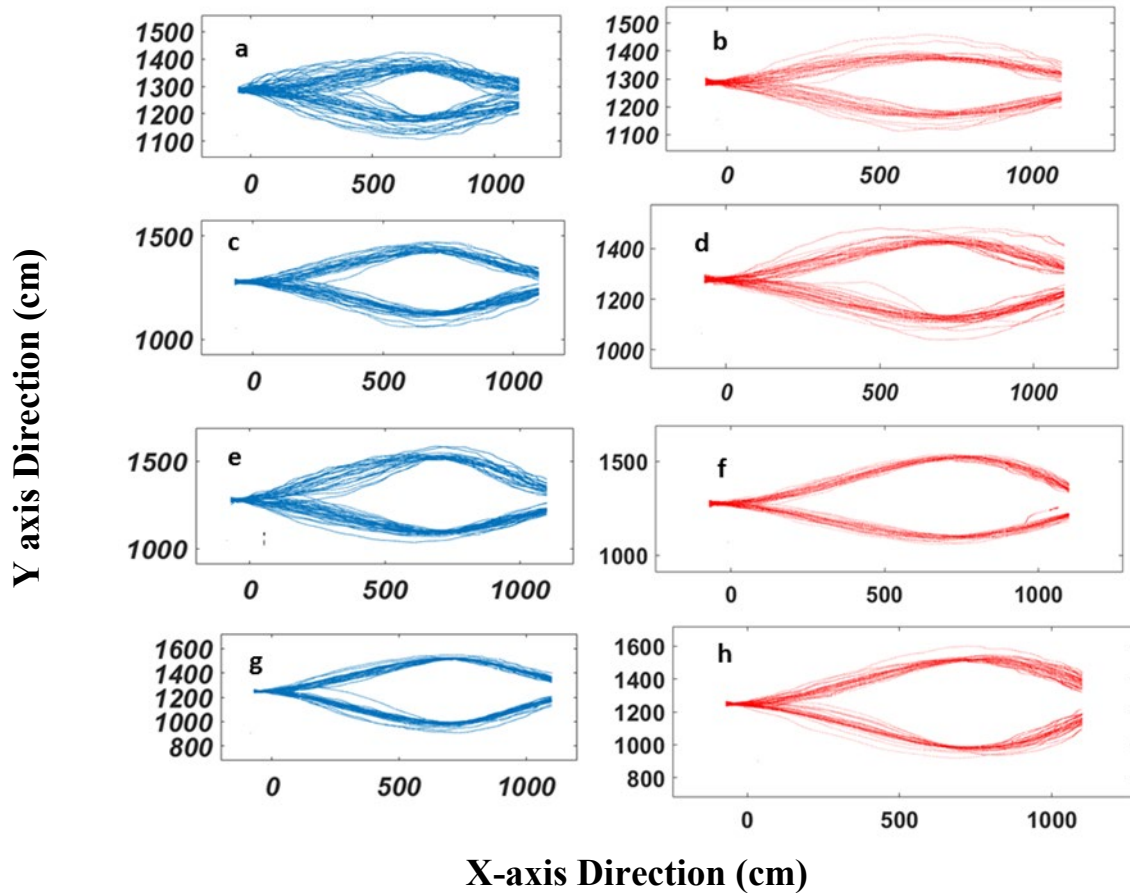


Fig. 1: Trajectories in X and Y direction for all the participants from one door size 50 cm and different obstacles sizes (a) Walking 1.2 m. (b) Running 1.2 m. (c) Walking at 2.4 m. (d) Running 2.4 m. (e) Walking 3.6 m (f) Running 3.6 m. (g) Walking 4.8 m (h) Running 4.8 m.

4. Results

4.1. Total speed

From the analysis of the extracted trajectories for all the participants, we have applied a method for measuring pedestrian speed in the direction with minimal scatter [23]. Then by averaging the area at every 10 cm managed to get all measurement within the whole area. A total speed (**x and y-axis**) was measured by applying the average speed in an ascertained area [23]. As can be seen in Fig 2. Walking speed was not significantly affected when participants moved towards the different obstacles ranged from the narrowest obstacle to the widest, as showing in fig 2 (a, b, c, and d) the total speed is not affected by the obstacles in the walking. The averages total waking speed in scenario (a) is 1.22 (m/s), (b) is 1.30 (m/s), (c) is 1.18 (m/s), and (d) is 1.31 (m/s). Obstacle had a more significant impact when subjects were running as showing in fig 2 (a, b, c and d). The total speed in scenario (a) is 2.66 (m/s), (b) is 2.16 (m/s), (c) is 2.55 (m/s), and (d) is 2.41 (m/s). From the results, walking speed has no significant variation in the walking scenarios (a, b, c, and d) which means moving towards different sizes of the obstacles is not affected by walking speed or obstacles had no significant impact when they were walking. On the other hand, the trends and patterns of speed in the running speed experiments as shown in (a, b, c, and d) had both changes meaning moving towards the different size of the obstacles affected the running speed. In summary, the results indicate that different obstacles size does not affect the participants while walking, but it does affect while the participants are running.

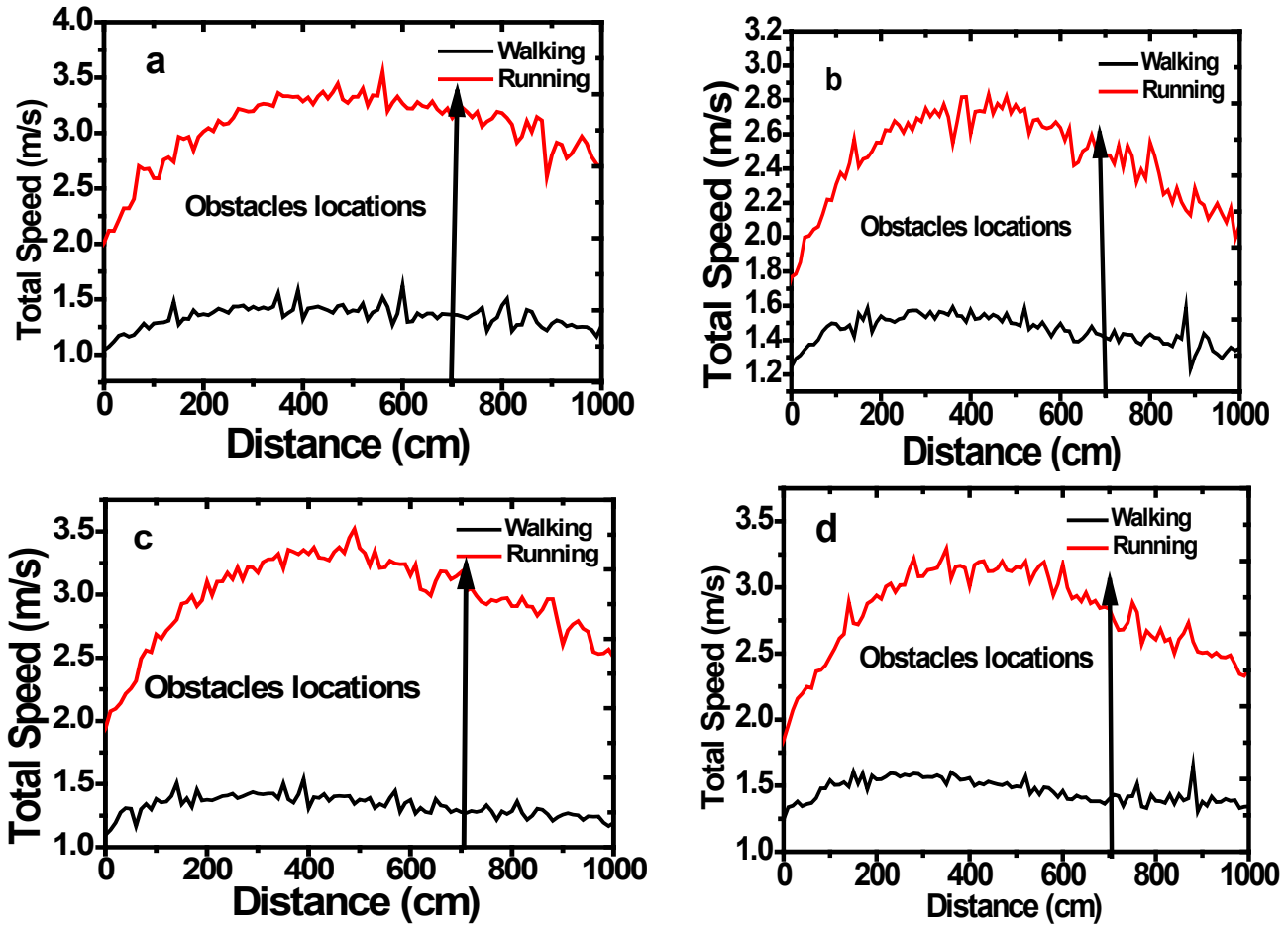


Fig. 2: Comparison of the total speed in (low vs high -speed) for difference obstacle size ((a) 1.2m, (b) 2.4m, (c) 3.6m, (d) 4.8m).

In Fig-3, we tend to additionally compare the impact of the size of the various obstacle in each low (a) high (b) speeds to visualize however the pedestrians responded to the various obstacles at the microscope level. The results show that in the low and high speeds, obstacle had an impression regardless of the speed. Most of the previous studies showed that there is no impact on walking. However, this study shows that even in low-speed condition, as shown in Fig 3 (a), there is an impact in both experiments. In low speed (a) experiments, obstacles had a less impact. Walking speed toward (1.2 and 3.6 (m)) obstacles have few speed changes that of (2.4 and 4.8(m)). In contrast, in the high-speed experiments in fig 3, (b) obstacle had a more impact, running speed toward (2.4 (m)) has few speed changes than that of (1.2, 3.6, 4.8(m)), therefore, more investigation is needed. In summary, results indicated that the total velocities are affected by the size of the different obstacle in both experiments walking and running.

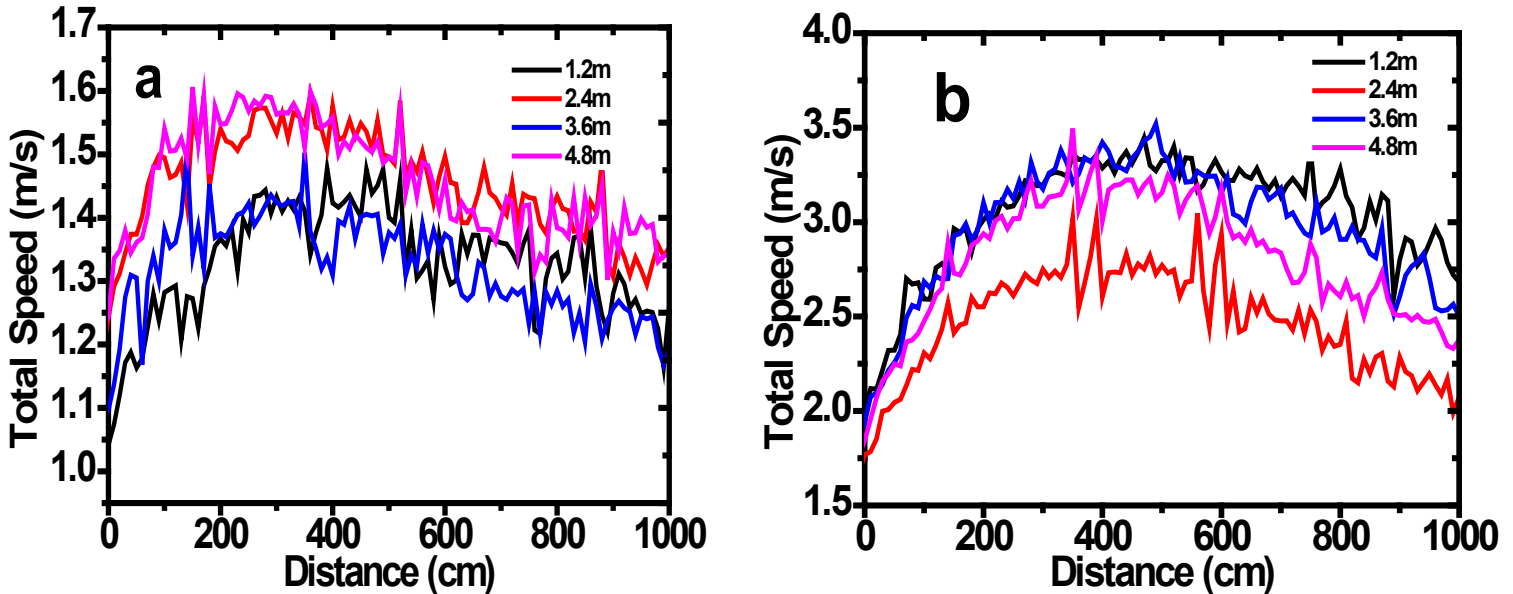


Fig. 3: Comparison of the total speed in all (low (a) and high (b)-speed) for difference obstacle size (1.2m, 2.4m, 3.6m, 4.8m.).

4.2. Speed in the Lateral Direction

In Fig 4, we also compared different speeds in low and high-speed experiments in the lateral direction. Obstacles had an impact on both cases. Walking and running velocities had the same impact when participants moved toward the different obstacles in the lateral direction (Y) axis. The obstacles arranged from the smaller obstacle to the largest, as shown in Fig 4 (a, b, c and d). In both experiments, the initial velocities have the same trends and patterns, they start to increase, then the speed drops down at the obstacles' locations, then the speed starts to increase to go back to the same trends and patterns. Our interpretation for that drop is that people are anticipating a collision point around them at the obstacle locations hence they would try to avoid the collision by dropping down their speed. In Fig 5, we compared, the low and high-speed experiments walking Fig 5 (a) and running Fig 5 (b) speeds to investigate more about the drop-down speeds at the location of the obstacle. The result shows that walking velocities had no impact when participants moved toward different obstacles. This means all the drop-down velocities are at the same point as shown in Fig 5 (a). In the running experiments, the drop-down velocities points are changed from point to another point based on the size of the obstacle as shown in Fig 5 (b). In Fig 6, we investigate the drop-down points by comparing the averages speed within the lateral direction, our results show a linear increased of the speed with the rise of the size of the obstacle in the path of the participants in low and high - speed experiments. The averages speed was impacted scientifically rise of the speed with obstacles size raised in low-speed experiments. However, in high-speed experiments, the averages speed had more affected when the participants were passing obstacles 3.6 -m and 4.8- m compared to the low speed -experiments, that was the reason for the previous drop-down points in Fig 5 (a) and (b). Therefore, high-speed experiments have more affected than low -speed experiments. In summary, the participants were affected by all the obstacles size at each experiment (walking and running).

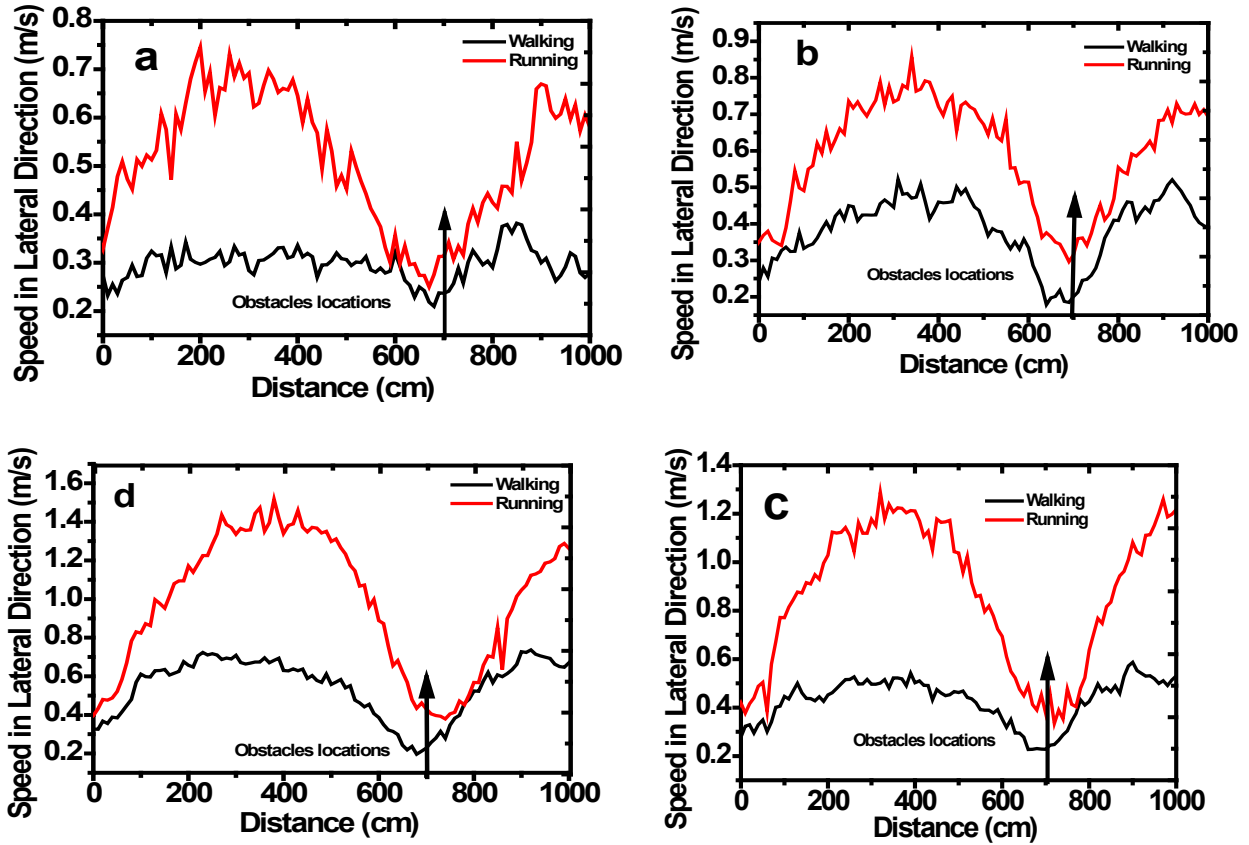


Fig. 4: Comparison of the speed - in (low- high) in the Lateral Direction (Y) axis, for difference obstacle size ((a) 1.2m, (b) 2.4m, (c) 3.6m, (d) 4,8m).

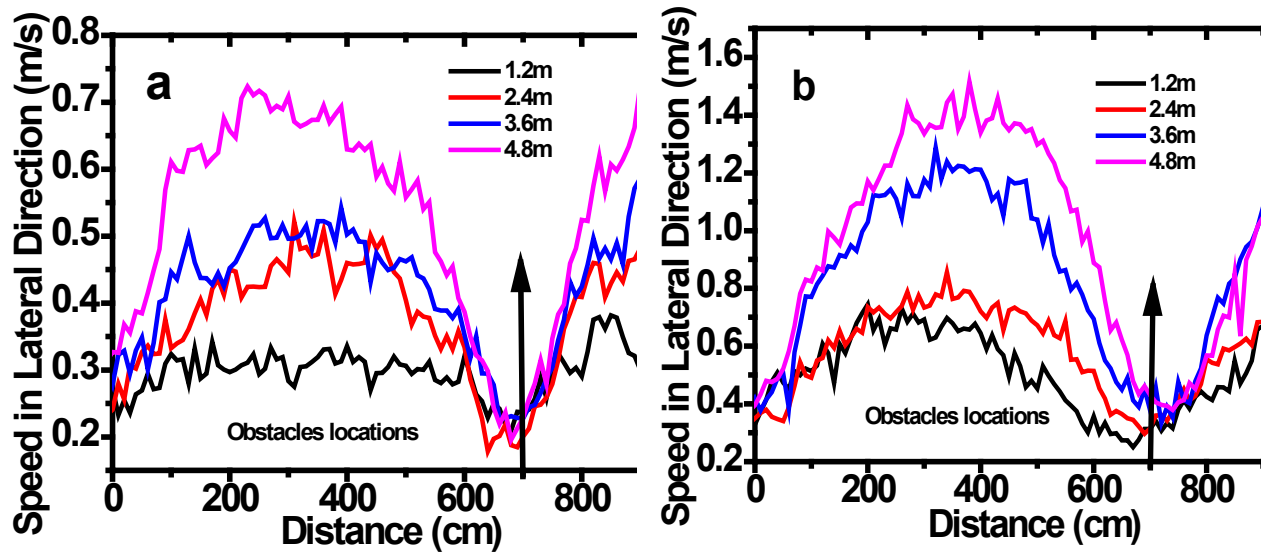


Fig. 5: Comparison of the Lateral speed in all (low (a) and high (b)-speed) for difference obstacle size (1.2m, 2.4m, 3.6m, 4,8m,).

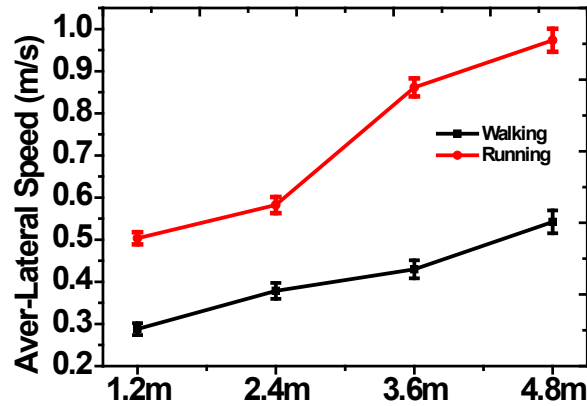
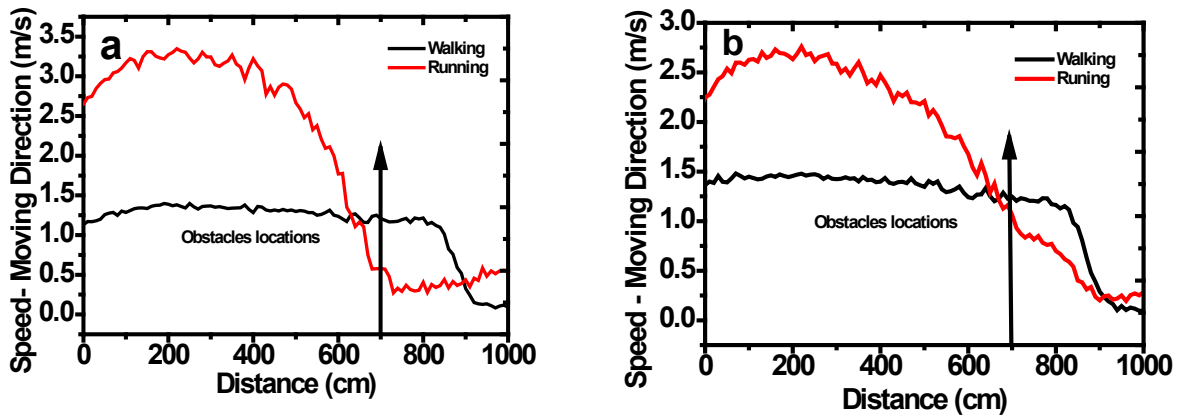


Fig. 6: Comparison of the Ave- speed in lateral speed - in (low-high) in the Lateral Direction (Y) axis, for difference obstacle size.

4.3. Speed in the Movement Direction

In this section Fig 7, we have a tendency to additionally compared the various speeds within the x-direction. It is found that obstacle had no impact on walking. There are similar trends and patterns for the velocities within the walking experiments in all eventualities (see Fig 7). However, obstacle had a lot of prevalent impact throughout running experiments. Running speed has a lot of affected within the trends and patterns in running experiments as shown in Fig 7 (a, b, c, and d) concluding moving toward completely different size of the obstacles is affected by running speed. Also, in Fig 8, we compared the effect of the size of the various obstacles in both experiments in the moving direction (X) axis, low (a) and high (b) speed to see how the pedestrians will respond to the different obstacles at the microscope level. The results show that within the low and high speed at Fig 8 (a and b) walking and running velocities are stricken by completely different obstacles. In low speed (a) experiments, walking speed have an impacted when participants moved toward the different obstacles. Walking speed toward (1.2 and 3.6 (m)) obstacle have few speed changes compared to that of 2.4 and 4.8- (m). However, within the high-speed experiments (b), running speed toward (2.4 and 4.8 (m)) has few speed changes compared to 1.2 and 3.6-(m) obstacle.



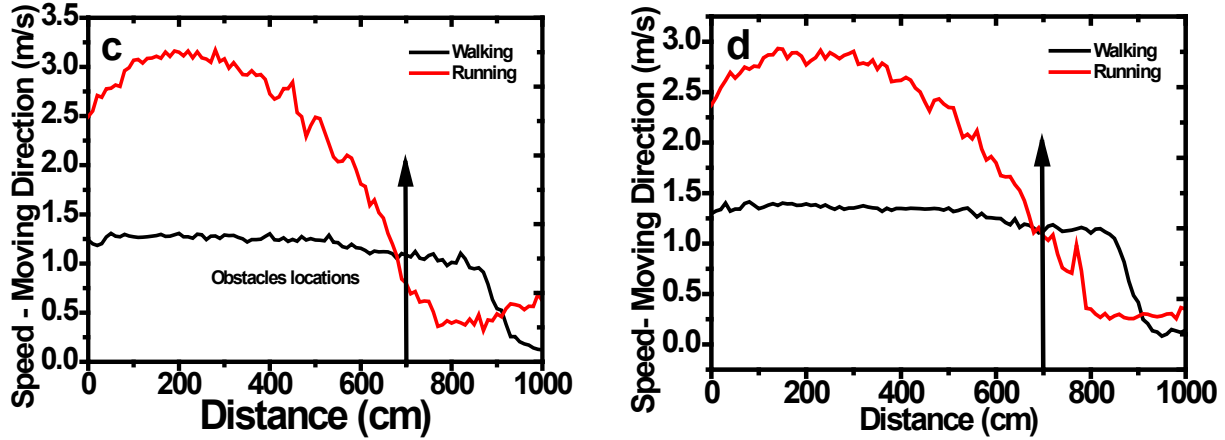


Fig. 7: Comparison of the speed - in (low Vs high) in the Moving Direction (X) axis, for difference obstacle size ((a) 1.2m, (b) 2.4m, (c) 3.6m, (d) 4,8m).

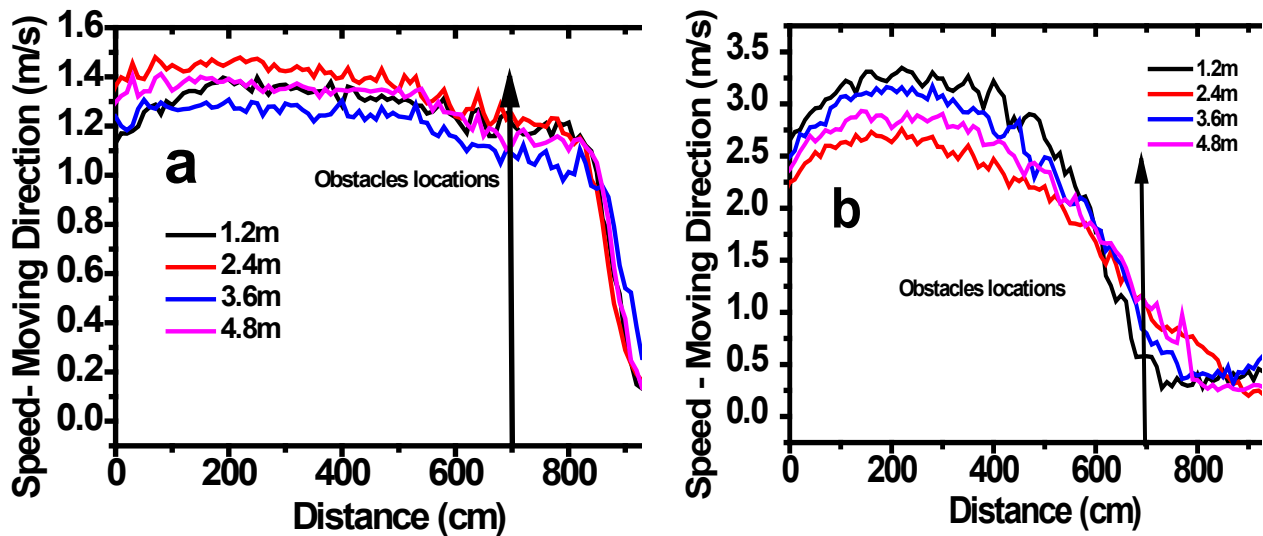


Fig.8: Comparison of the speed - in All (low (a) high (b)) in the Moving Direction (X) axis, for difference obstacle size (1.2m, 2.4m, 3.6m, 4,8m)

5. Conclusion

We experimentally investigated the walking characteristics of individuals through several obstacle sizes to evaluate the impact of an obstacle on human moving speed for both walking and running. We centred totally on the impact of the overall speed, speed within the moving direction, lateral speed. Our results show that obstacle had no vital impact on the overall speed once the participants were walking, in contrast, this impact was obvious for high-speed experiments (i.e. running). Results showed that obstacles would have an impact on lateral movements and it varies based on the speed of pedestrians.

References

1. Shiwakoti, Sarvi, Burd and Rose, Animal dynamics based approach for modelling pedestrian crowd egress under panic conditions. Transportation Research Part B, 45 (9), pp. 1433-1449, 2011.

2. Bandini, S., S. Manzoni, and G. Vizzari, *Crowd behaviour modelling: From cellular automata to multi-agent systems*. Multi-Agent Systems: Simulation and Applications. CRC Press, Boca Raton, 2009: p. 204-230.
3. Boltès, M., et al., *Experimentation, data collection, modelling and simulation of pedestrian dynamics*. 2014, Jülich Supercomputing Center.
4. Duives, D.C., W. Daamen, and S.P. Hoogendoorn, *State-of-the-art crowd motion simulation models*. Transportation research part C: emerging technologies, 2013. **37**: p. 193-209.
5. Luo, L., et al. *Modeling Gap Seeking Behaviors for Agent-based Crowd Simulation*. in *Proceedings of the 29th International Conference on Computer Animation and Social Agents*. 2016. ACM.
6. Singh, H., et al., *Modelling subgroup behaviour in crowd dynamics DEM simulation*. Applied Mathematical Modelling, 2009. **33**(12): p. 4408-4423.
7. Teknomo, K., Y. Takeyama, and H. Inamura, *Microscopic pedestrian simulation model to evaluate "lane-like segregation" of a pedestrian crossing*. arXiv preprint arXiv:1610.00749, 2016.
8. Teknomo, K., Y. Takeyama, and H. Inamura, *Review on microscopic pedestrian simulation model*. arXiv preprint arXiv:1609.01808, 2016.
9. Braun, A., et al. *Modeling individual behaviours in crowd simulation*. in *Computer Animation and Social Agents, 2003. 16th International Conference on*. 2003. IEEE.
10. Dias, Sarvi, Shiwakoti and Burd *Turning angle effect on emergency egress*. *Transportation Research Record, Issue2312, 2012*
11. Shiwakoti and Sarvi. *Understanding pedestrian crowd panic: A review on model organisms approach*. Journal of Transport Geography, 2013, Vol 26.
12. Bandini, S., S. Manzoni, and G. Vizzari, *Crowd behaviour modelling: From cellular automata to multi-agent systems*. Multi-agent systems: simulation and applications, 2009: p. 301-324.
13. Schadschneider, A., *Cellular automaton approach to pedestrian dynamics-theory*. arXiv preprint cond-mat/0112117, 2001.
14. Wolfram, S., *Statistical mechanics of cellular automata*. Reviews of modern physics, 1983. **55**(3): p. 601.
15. Gao, Y., et al. *Experimental study on pedestrians' collision avoidance*. in *Intelligent Control and Automation (WCICA), 2014 11th World Congress on*. 2014. IEEE.
16. Borenstein, J. and Y. Koren, *Histogramic in-motion mapping for mobile robot obstacle avoidance*. IEEE Transactions on Robotics and Automation, 1991. **7**(4): p. 535-539.
17. Frank, G. and C. Dorso, *Room evacuation in the presence of an obstacle*. Physica A: Statistical Mechanics and its Applications, 2011. **390**(11): p. 2135-2145.
18. Patla, A.E., et al., *Visual control of locomotion: strategies for changing direction and for going over obstacles*. Journal of Experimental Psychology: Human Perception and Performance, 1991. **17**(3): p. 603.
19. Zhang, X., et al., *Extended social force model-based mean shift for pedestrian tracking under obstacle avoidance*. IET Computer Vision, 2016. **11**(1): p. 1-9.
20. Boltès, M. and A. Seyfried, *Collecting pedestrian trajectories*. Neurocomputing, 2013. **100**: p. 127-133.
21. Gorrini, A., et al. *An empirical study of crowd and pedestrian dynamics: the impact of different angle paths and grouping*. in *Transportation Research Board, 92nd Annual Meeting*. 2013.
22. Xu, P.-j. and K.-c. Cao, *Review of Research on Simulation Platform Based on the Crowd Evacuation*, in *Advanced Computational Methods in Life System Modeling and Simulation*. 2017, Springer. p. 324-333.
23. Steffen, B. and A. Seyfried, *Methods for measuring pedestrian density, flow, speed and direction with minimal scatter*. Physica A: Statistical mechanics and its applications, 2010. **389**(9): p. 1902-1910.
24. *Shahhoseini, Z., M. Sarvi, and M. Saberi, Pedestrian crowd dynamics in merging sections: Revisiting the "faster-is-slower" phenomenon*. Physica A: Statistical Mechanics and its Applications, 2018. **491**: p. 101-111.

A MARKOV-CHAIN ACTIVITY-BASED MODEL FOR PEDESTRIANS IN OFFICE BUILDINGS

Sanmay Shelat¹, Winnie Daamen¹, Bjorn Kaag², Dorine Duives¹, Serge Hoogendoorn¹

¹Department of Transport and Planning, Delft University of Technology
Stevinweg 1, Delft, The Netherlands
s.shelat@tudelft.nl

²Argosonic, The Netherlands

Abstract - As the number of people working in office buildings increases, there is an urgent need to improve building services, such as lighting and temperature control, within these buildings to increase energy efficiency and well-being of occupants. A pedestrian behaviour model that simulates office occupants' movements and locations can provide the high spatial and temporal resolution data required for the testing, evaluation, and optimization of these control systems. However, since most studies in pedestrian research focus on modelling specific actions at the operational level or target situations where movement schedules do not have to be modelled, a pedestrian behaviour model that can simulate complex situations over long time periods is missing. Therefore, this paper proposes a tactical level model to generate occupant movement patterns in office buildings. The Markov-chain activity-based model proposed here is data parsimonious, flexible in accepting different levels of information, and can produce high resolution output. The mathematical properties of the methodology are analyzed to understand their impact on the final results. Finally, the tactical level pedestrian behaviour model is face validated using a case study of an imaginary office with a simple layout.

Keywords: pedestrians; tactical behaviour level; offices; buildings; activity-based; Markov-chain

1. Introduction

Around the world, as more people work in office buildings, these buildings consume a large proportion of resources for building services, such as lighting and temperature control. Therefore, these services need to be researched and evaluated to optimize their performance, for which occupant behaviour data, such as their spatio-temporal distribution within the building, is required. A pedestrian behaviour model that simulates the movements of office occupants can generate this data for various situations without expensive implementation of test sensors in the real-world and minimal privacy concerns. However, most pedestrian studies focus on the operational behaviour level [1] and those that do model a broader picture either assume a movement schedule or model situations where the sequence of movements is already known. To obtain pedestrian locations over long periods of time in complex situations, the tactical behaviour level, where pedestrian itineraries are constructed, must be modelled alongside the operational level. Hence, the next step in pedestrian research is to develop a model that integrates the different behaviour levels [2]. For this, the tactical behaviour level which schedules movements deserves greater attention than it has received.

The few approaches in literature for scheduling pedestrian movements can be divided into (i) activity-based, (ii) location-based, and (iii) random-access models. In the first category, movements take place because pedestrians have to perform activities at different locations. Activity episodes are generated and scheduled for pedestrians. A location choice model is used to assign each activity episode in the itineraries to a location to form movement schedules. Tabak [3] presented the most detailed model of pedestrian behaviour in offices but, like other models in this category, it has been critiqued for its complexity and extensive data requirements. In the next two categories, movement occurs for

movement's sake and pedestrians are directly assigned a sequence of locations to visit, making these models less intuitive than activity-based ones. Location-based models generate individual movements using stochastic models with the aim of reproducing location-based statistics, such as occupancy or transition sequences. A common method in location-based models is to divide the area modelled into zones and use them as states of Markov-chains that are assigned to every pedestrian. The Markov-chains are then simulated in discrete time steps and a movement is generated whenever a pedestrian transitions to another zone [4, 5]. These models are much less complex and data intensive than the previous category. However, unlike activity-based models, the running time and complexity of location-based models depends on the resolution of the zones and the size of the area modelled. Finally, random-access models use random walks that do not consider locations or activities but depend on the overall spatial configuration to simulate movements [6]. However, they are generally not applicable for situations that are process driven or buildings that are highly programmed and, therefore, not useful for scheduling movements in office buildings.

This paper proposes a tactical level model of pedestrian behaviour in office buildings that is data parsimonious, flexible in accepting different amounts of information, and can produce high resolution output; thus combining the advantages of activity- and location-based approaches whilst overcoming their limitations. The focus here is on the scheduling of movements while other decisions at this level, such as route and activity location choice, are simplified with assumptions that office occupants are familiar with the building and indifferent to activity locations, which is reasonable given the types of activities to be performed (e.g. getting coffee) [7]. Furthermore, unlike previous studies [5, 8, 9] the mathematical properties of the stochastic process used in the model are analysed to understand their effect on the final results. The methodology and its analysis are presented in section 2. In order to face validate the model, a simple case study of an imaginary office is carried out in section 3, followed by the conclusions in section 4 which note model limitations and relevant future work.

2. Methodology

To combine the advantages of the activity- and location-based approaches, the Markov-chain location-based model (henceforth, the Wang model) proposed in [5] is adopted in an activity-based framework. The Wang model is similar to many models in its category in that it divides the building into zones which are used as states in the Markov-chains assigned to each occupant, and these Markov-chains are simulated to generate movements. However, recognizing that defining each transition matrix element in every agent's Markov-chain is data-intensive, the authors of the Wang model propose a novel method that derives these probabilities from profiles consisting of only two variable sets per agent; thus, considerably reducing the number of inputs required to model multi-zone, multi-occupant scenarios. Other studies [8, 9] have used the Wang model to develop occupancy simulation software because of its simplicity and data parsimony.

However, certain limitations prevent the Wang model from being used to simulate pedestrian movements. Being a location-based model, it is not robust against building size and cannot use high spatial resolutions. Furthermore, all movements between zones are assumed to take place in a single time step which lowers the temporal resolution to maintain feasibility of the assumption (a 5 minute time step is used in [5]). These limitations are resolved by adopting the Wang model in an activity-based framework (section 2.2) and adding complementary models (section 2.4). Additionally, their novel method of generating transition matrices is improved by linearizing the optimization problem (section 2.2) and analysing its impact on the final results through simulation (section 2.3).

2.1. Activity Classification

Since activities have different properties, they cannot all be generated and scheduled with the same methodology. Thus, to make the activity-based framework possible, a classification of activities is created such that each category contains activities with similar properties whilst all categories together allow representing the full range of activities occurring in various situations [3, 10]. These categories are further

grouped according to their association with a time-of-day (time-dependent or time-independent) and these groups each have their own scheduler.

Time-dependent activities include *planned* and *time-window* activities, which, respectively, have a fixed starting time or a fixed time window within which they may be performed. Planned activities (e.g., meetings) have priority over all other activity types, whereas time-window activities (e.g., arrivals, lunch) have a higher priority than time-independent activities but may be skipped if they cannot be executed in their time window due to planned activities. These activities are modelled using an *Event Scheduler*. Time-independent activities include recurrent and continuous activities. Recurrent activities are related to occupants' physiological processes [3] (e.g., taking breaks, getting a drink, visiting the restroom) which may be assumed to have a regular recurrence time. It is assumed that these activities are not undertaken in the middle of time-dependent activities, such as meetings. Continuous activities (e.g., working at one's desk), which have the lowest priority, are performed when no other activity is being performed. They do not have a fixed starting time, duration, or period and are the default activity to which occupants return when they are unable to execute other activities. The *Markov-chain Scheduler*, which is a modification of the Wang model, is used to simulate time-independent activities.

2.2. Markov-Chain Scheduler

The methodology used to generate and schedule time-independent activities is based on first-order, discrete time, finite-space ergodic Markov-chains. Instead of the zones, to adopt the Wang model in an activity-based framework, time-independent activities are used as the states of the Markov-chains. Eq. 1 describes the memoryless characteristic of Markov chains with states S indicating that the state of the chain, X , at time t , is only dependent on the state in the previous time-step. Combining p_{ij} 's for all i and j into matrix form creates a transition matrix P , where each element (p_{ij}) indicates the probability of going from the row state (i) to the column state (j). Eq. 2 gives an example of an n -state transition matrix.

$$P\{X_t = j | X_0 = m, X_1 = k, \dots, X_{t-1} = i\} = P\{X_t = j | X_{t-1} = i\} = p_{ij}, \quad \forall i, j, \dots, m, n \in S. \quad (1)$$

$$P = \begin{bmatrix} p_{11} & \dots & p_{1n} \\ \vdots & \ddots & \vdots \\ p_{n1} & \dots & p_{nn} \end{bmatrix} \text{ s. t. } \sum_{j=1}^n p_{ij} = 1; \quad \forall i, j \quad p_{ij} \geq 0. \quad (2)$$

The model uses two inputs to generate the transition matrix for each occupant. The first input is the average continuous duration of time (also called expected sojourn time) the agent spends in a state, that is, a time-independent activity. For large values of t , (i.e., $t \rightarrow \infty$) the expected sojourn time (τ_i) in a state converges to a limiting value which can be used to derive the diagonal elements of the transition matrix as shown in Eq. 3. The second input is the proportion of time spent in a state, that is performing a time-independent activity. For $t \rightarrow \infty$, this value – the probability of being in a state, which describes, in essence, the overall percent of time a Markov-chain spends in a given state – also converges to a limit. This probability distribution over all the states of a Markov-chain is called the stationary probability distribution (π) (Eq. 4). By definition, the stationary probability distribution can be calculated as the left eigenvector (normalized to 1) of the transition matrix (Eq. 5). For recurrent activities, such as getting a coffee, it is more convenient to use the average time between two episodes of the activity, that is the away time of a state (α_i). This variable is also observed to tend to a limit which can be used to derive the stationary probability values of those states (Eq. 6).

$$E(\tau_i) = \frac{1}{1-p_{ii}} \Rightarrow p_{ii} = 1 - \frac{1}{E(\tau_i)}. \quad (3)$$

$$\pi = [\pi_1, \pi_2, \dots, \pi_n] \text{ s. t. } \sum_{i=1}^n \pi_i = 1; \quad \forall i \quad \pi_i \geq 0. \quad (4)$$

$$\pi = \pi \cdot P. \quad (5)$$

$$E(\alpha_i) = E(\tau_i) \cdot \left[\frac{1}{\pi_i} - 1 \right] \Rightarrow \pi_i = \frac{E(\tau_i)}{E(\tau_i) + E(\alpha_i)}. \quad (6)$$

For each occupant, a transition matrix is derived by setting up a constrained linear least-squares problem. Linearization increases the speed of the model considerably, thus, reducing the model's running time. The system of linear equations is derived from the following conditions: (i) the relation between the stationary probability distribution and the transition matrix (Eq. 5); (ii) the fact that the sum of columns of a row in the transition matrix sum to 1 (Eq. 2); (iii) the known values of the diagonal elements of the transition matrix (Eq. 3); and (iv) the constraint that all transition elements are non-negative values (Eq. 2). Thus, for an n -state Markov chain, the system of equations consists of $2n$ equations, formed by the first two conditions, which are solved for $n(n - 1)$ variables that represent the elements of the $n \times n$ transition matrix (given that the diagonal elements are known from the third condition). Eq. 7 shows the system of linear equations used for the constrained linear least-squares problem and Eq. 8 shows the setup of the problem.

In order to generate the transition matrix, MATLAB's constrained linear least-squares solver *lsqlin* is used to solve Eq. 8 for x – the array of unknown transition matrix elements. Similar to [5], the problem proposed in Eq. 8 is under-determined, and thus, it has either no solutions or an infinite number of solutions. Since a unique solution is not already defined, the linear problem can accept increasing amounts of information through additional linear constraints of the form $Cx \leq d$ or upper and lower bounds for x in the constrained least-squares problem. This additional information can be in the form of complementary observations, such as the tendency to perform one activity after another. Incorrect solutions are discarded by setting a tolerance value of 10^{-10} on the objective function value of *lsqlin*, which should ideally be zero. Furthermore, since this method uses ergodic Markov-chains, a check is made to detect and remove states with zero stationary probability (i.e., activities that are never performed by an occupant) when generating a transition matrix. After the generation, null rows and columns corresponding to those states are added to maintain consistency with other transition matrices.

Once the transition matrix is generated, a simulation of the Markov chain is carried out by starting from a random initial state (activity) and then choosing the next state at every time step using the transition probabilities from the current state. This simulation returns a sequence of time-independent activities for the occupant. Thus, doing both, generating activity episodes with durations and scheduling them. The next section analyses how the under-determined nature of the problem impacts the final results.

2.3. Transition Matrix Generation Analysis

Since the problem setup in Eq. 8 is under-determined, the same inputs will result in more than one transition matrices (if any). This could mean that if the solver resulted in a different transition matrix, the end results could be quite different. However, while the problem setup in the previous section is, strictly speaking, only true for expected values at $t \rightarrow \infty$, the Markov-chains are simulated for a maximum time period of a day, which is approximately 500 time steps if each time step is a minute (500 minutes \sim 8 hours \sim 1 working day). Hence, the limited time simulations add stochasticity to the results, which could mean that the existence of different transition matrix solutions may not, ultimately (i.e., post-simulation), make a difference. To check this, a three-state situation is considered. Four Markov-chains are obtained from the same inputs and simulated 1000 times for 500 time steps. The transition probability observed from the simulation (i.e., the simulated transition probabilities) between all the states are recorded for each run and plotted as an histogram with different colours representing the four Markov-chains (Fig. 1). Additionally, to understand the impact of the input values on the simulated transition probabilities the sojourn time values are varied – the bottom figure of Fig. 1 has 10 times the sojourn time values of the top figure. The diagonal elements are similar in Fig. 1 for all four Markov-chains in both figures as they are fixed by the input (see Eq. 3).

$$A = \begin{bmatrix} 0 & \dots & \dots & \dots & 0 & \pi_2 & 0 & \dots & \dots & 0 & \dots & \pi_n & 0 & \dots & \dots & 0 \\ \pi_1 & 0 & \dots & \dots & 0 & 0 & 0 & \dots & \dots & 0 & \dots & 0 & \pi_n & \dots & \dots & 0 \\ 0 & \pi_1 & 0 & \dots & 0 & 0 & \pi_2 & 0 & \dots & 0 & \dots & 0 & 0 & \pi_n & \dots & 0 \\ \vdots & \vdots & \vdots & \vdots & \vdots & \vdots & \vdots & \vdots & \vdots & \vdots & \vdots & \vdots & \vdots & \vdots & \vdots & \vdots \\ 0 & \dots & \dots & \dots & \pi_1 & 0 & \dots & \dots & 0 & \pi_2 & \dots & 0 & \dots & \dots & \dots & 0 \end{bmatrix}_{2n \times n(n-1)}$$

$$b = \begin{bmatrix} (1-p_{11})\pi_1 \\ (1-p_{22})\pi_2 \\ \vdots \\ (1-p_{nn})\pi_n \end{bmatrix}_{2n \times 1}$$

$$x = \begin{bmatrix} p_{12} \\ p_{13} \\ \vdots \\ p_{1n} \\ p_{21} \\ p_{23} \\ \vdots \\ p_{2n} \\ \vdots \\ p_{n1} \\ p_{n2} \\ \vdots \\ p_{nn-1} \end{bmatrix}_{n(n-1) \times 1} \quad (7)$$

$$\min \|Ax - b\|_2 \text{ s. t. } x \geq 0. \quad (8)$$

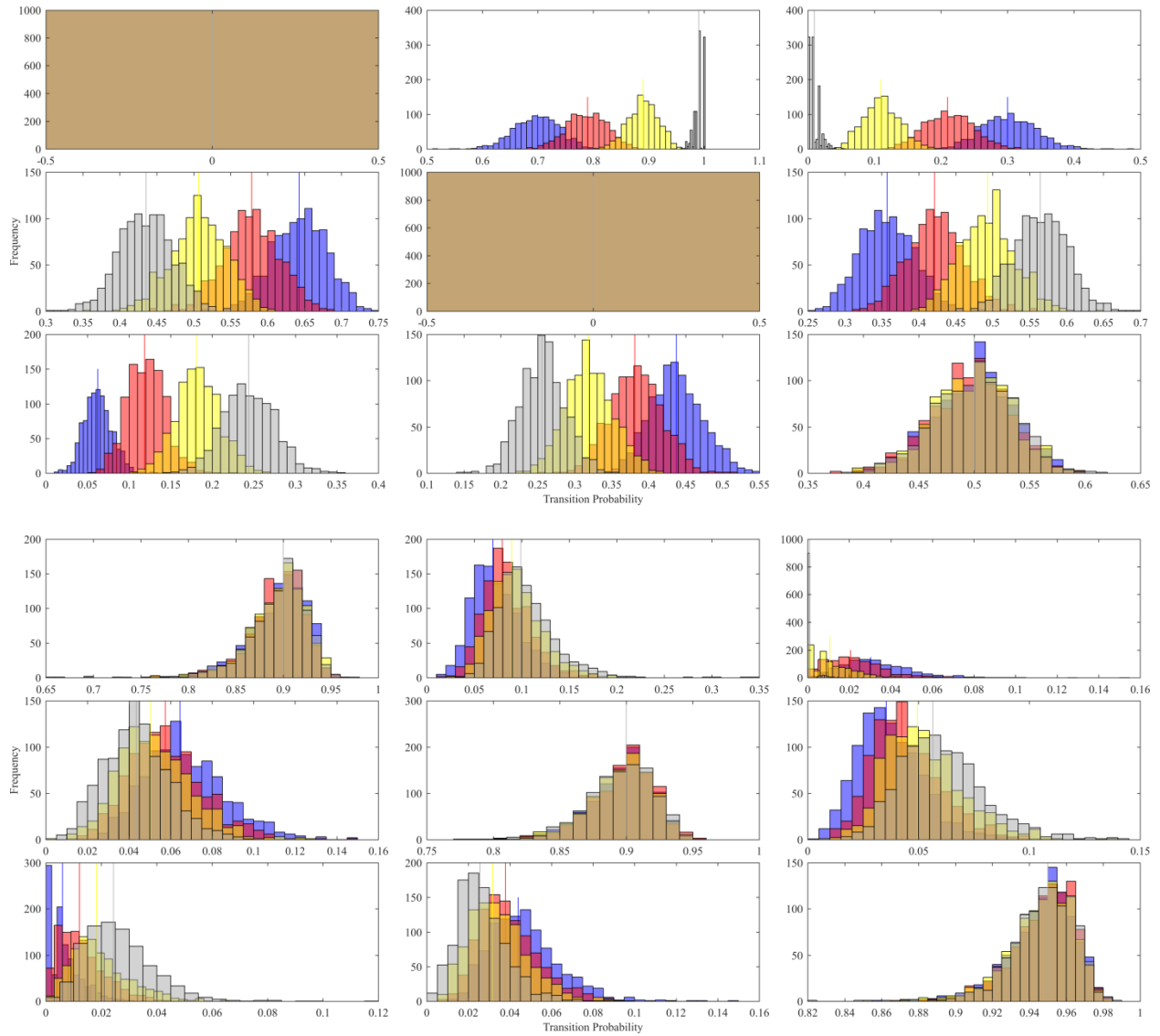


Fig. 1: Histograms of transition probabilities observed from simulation of four (differentiated by colour), 3-state Markov-chains generated using the same stationary probability (π) and sojourn time (τ) inputs.

Top: $\pi = [0.25 \ 0.35 \ 0.40]$, $\tau = [1 \ 1 \ 2]$; bottom: $\pi = [0.25 \ 0.35 \ 0.40]$, $\tau = [10 \ 10 \ 20]$. Note, the x-axis scales differ.

For smaller values of sojourn times (Fig. 1, top) the differences in the transition matrices can be clearly observed in their simulated transition probabilities, but the differences are much less when the sojourn times are multiplied by 10 (Fig. 1, bottom). This increase in sojourn times reduces the scale of the distributions of transition probabilities to other states, that is, corresponding to the increase in sojourn times the mean values of the transition probabilities to the other states have reduced by 10. Thus, the differences in the transition probabilities of different Markov-chains are less clear. Thus, for states with a high sojourn time, in absolute terms, the transitions from that state will produce similar results for different transition matrices while those with a low sojourn time will be impacted more strongly by the transition matrix choice.

2.4. Complementing Schedulers

While the Markov-chain scheduler gives a sequence of time-independent activities performed by an occupant, other schedulers are needed to obtain a complete schedule of an occupant's movements through a day. Complementing the Markov-chain scheduler, are three different supporting schedulers: (i) event scheduler, (ii) movement scheduler, and (iii) re-scheduler. Each of these schedulers is accompanied by a location choice model that decides where activities will be performed. Fig. 2 shows the schedulers within the general framework of the movement scheduler for pedestrians (occupants) in office buildings.

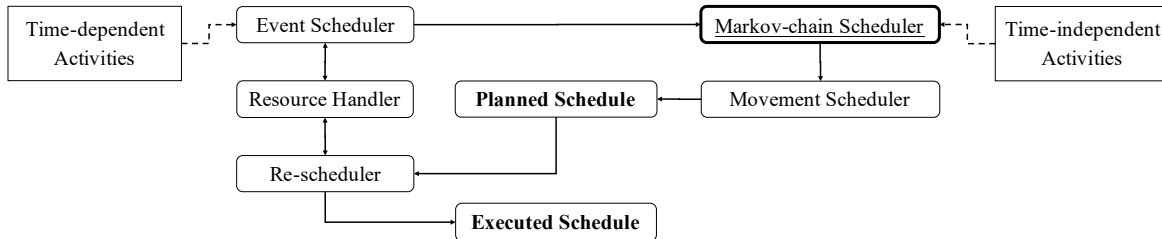


Fig. 2: Framework of the occupant movement scheduler. Single-headed arrows indicate the flow of the movement scheduler; double-headed arrows show interacting parts.

First, the event scheduler is used to schedule time-dependent (first planned and subsequently time-window) activities that anchor the itinerary. Activities such as meetings or arrivals and departures may be generated by sampling from aggregated observations such as meeting room booking data and occupancy sensor data, or expectations of the same. For planned activities, the event scheduler interacts with a resource handler to check the availability of a location chosen by the location choice model before reserving it. Once the schedule is anchored with time-dependent activities, such as a meeting and a lunch break, gaps in the itinerary have to be filled. Since the Markov-chain scheduler derivation holds strictly true only for a large number of time steps, instead of simulating the Markov-chain for the time period of each gap individually, it is simulated for the total period of all the gaps in the itinerary. This long sequence of time-independent activities is then split up to fill in the gaps. The location choice model is used to assign locations where each activity will be performed. Simultaneously, between each activity, the movement scheduler assigns the time required to move from one location to another; thus, developing the planned schedule for a day. Finally, when executing the planned schedule, dynamic updates are required; for example, when a pedestrian discovers that a chosen location is occupied and has to choose a new location, or has to skip an activity because all locations are occupied, or when a delay in starting time of an activity requires shifting the schedule. Location availability is checked by the re-scheduler by interacting with the resource handler before updating schedules based on feedback from the operational level model to result in the final executed schedule.

3. Case Study

A case study of an imaginary consultancy office with a simple layout (Fig. 3) and 18 employees is conducted to face validate the model output. Amongst the 18 employees are 1 manager, 4 senior

engineers, 12 junior engineers, and 1 receptionist. All occupants with the same role are assigned the same input profile (stationary probabilities or away times and sojourn times of states). Occupants are assumed to perform the following activities: continuous – being at their desk; recurrent – going to the toilet, getting a drink, taking a break; time-window – arrival, departure, lunch; and planned – meeting. This simple set of activities represents all four categories and is likely to be performed by occupants of most offices.

In order to carry out the first step towards model validation, the following three simulated measures are used: (i) break durations, (ii) time between two episodes (away time) of getting coffee, and (iii) desk occupancy. The first two indicators are compared against the distributions expected from the limiting behaviour of Markov-chain based models while the desk occupancy is judged qualitatively against expected patterns. All measures are calculated as the aggregated output of 10 simulations of the model, that is, 10 days of occupant movements in the imaginary office.

As expected for Markov-chain based models, both distributions show features of exponential distributions. For 10 simulations, the mean break duration is found to be 9.3 minutes while the mean away time for coffee is 84.6 minutes. While the former is close, both values underestimate the true input sojourn times of 10 minutes and 120 minutes respectively. A possible reason for the lower simulated duration may be the splitting of activities from the Markov chain agenda while filling the gaps in the event schedule. Splitting activities would reduce their average duration.

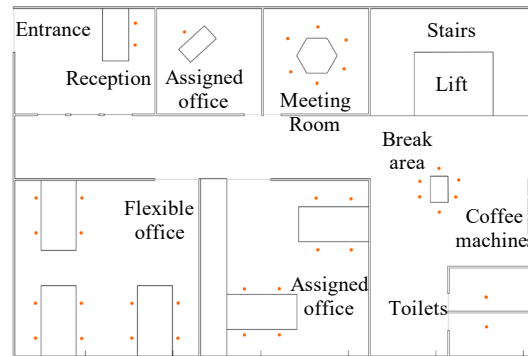


Fig. 3: Layout of the imaginary office used in the case study

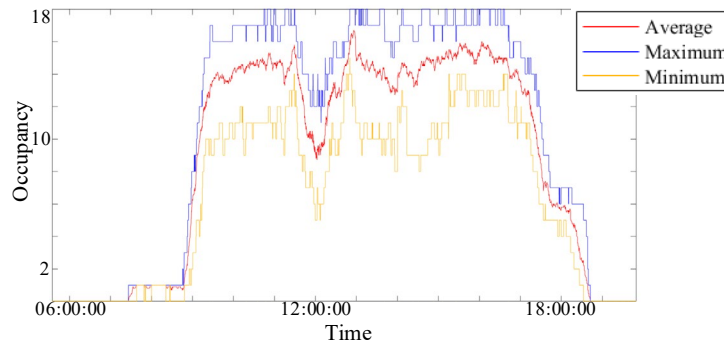


Fig. 4: Minimum (yellow), maximum (blue), and average (red) desk occupancy levels (y-axis) versus time (x-axis) across 10 days

Desk occupancy describes the number of office occupants who are at their desk at a given moment. It is an important parameter for lighting and temperature controls in office buildings because these building services are based on the presence of people in certain areas. Fig. 4 shows the maximum, minimum, and average desk occupancy in a day over 10 simulations. Clear patterns of arrivals at 09:00, lunch break near 12:00, and departures from 16:30 and onwards can be observed. Moreover, the desk occupancy fluctuates throughout the day indicating the natural patterns of people moving about in the

office. While these fluctuations seem to be random, as one would expect, the individual activities indeed follow a pattern as indicated by the distributions of the durations of the activities and their away times.

4. Conclusions

While most previous studies have focussed on the operational behaviour level and have not been able to model complex situations for long periods of time, this paper present a tactical behaviour level model that is able to do that. The model can be used to model pedestrian behaviour in office buildings and optimize building services therein. The tactical behaviour level model uses an activity-based framework which produces the high spatial and temporal resolution movement patterns required for testing and optimizing building services in office buildings while the Markov-chain methodology keeps the model data parsimonious and flexible in accepting increasing amounts of information. Furthermore, the paper analyses the transition matrix generation methodology closer than other studies, revealing that using higher temporal resolution – that is, increasing absolute sojourn times – reduces the effect of its under-determined nature on the final result. Finally, the case study of an imaginary office indicates that the model's results could represent movement patterns in an office building.

Despite the advantages of the model proposed here, it has some limitations which could be paths for future studies. To build connections with several studies on workplace interactions in the field of architecture (e.g. [11]), environment-induced activities – activities induced by the current spatial position of the occupant must be modelled. For example, an occupant may find themselves in sight of a colleague and decide to have an unplanned discussion. Furthermore, currently only the first steps towards model validation have been carried out. Therefore, future studies could focus on quantitative validation of the model.

References

- [1] S. P. Hoogendoorn, "Normative Pedestrian Flow Behavior: Theory and Applications," Delft University of Technology 2001.
- [2] A. Schadschneider, H. Klüpfel, T. Kretz, C. Rogsch, and A. Seyfried, "Fundamentals of pedestrian and evacuation dynamics," in *Multi-Agent Systems for Traffic and Transportation Engineering*: IGI Global, 2009, pp. 124-154.
- [3] V. Tabak, "User simulation of space utilisation," Eindhoven University Press 9068146149, 2008, vol. PhD.
- [4] C. Liao, Y. Lin, and P. Barooah, "Agent-based and graphical modelling of building occupancy," *Journal of Building Performance Simulation*, vol. 5, pp. 5-25, 2011.
- [5] C. Wang, D. Yan, and Y. Jiang, "A novel approach for building occupancy simulation," *Building Simulation*, vol. 4, pp. 149-167, 2011.
- [6] A. Penn and A. Turner, "Space syntax based agent simulation," presented at the 1st International Conference on Pedestrian and Evacuation Dynamics, University of Duisburg, Germany, 2001.
- [7] E. Andresen, D. Haensel, M. Chraïbi, and A. Seyfried, "Wayfinding and Cognitive Maps for Pedestrian Models," in *Traffic and Granular Flow '15*, Cham, 2016, pp. 249-256: Springer International Publishing.
- [8] X. Feng, D. Yan, and T. Hong, "Simulation of occupancy in buildings," *Energy and Buildings*, vol. 87, pp. 348-359, 2015.
- [9] Y. Chen, T. Hong, and X. Luo, "An agent-based stochastic Occupancy Simulator," *Building Simulation*, journal article pp. 1-13, 2017.
- [10] G. Zimmermann, "Modeling and Simulation of Individual User Behavior for Building Performance Predictions," presented at the Proceedings of the 2007 Summer Computer Simulation Conference, San Diego, California, 2007.
- [11] K. Sailer and I. McCulloh, "Social networks and spatial configuration—How office layouts drive social interaction," *Social Networks*, vol. 34, no. 1, pp. 47-58, 2012/01/01/ 2012.

Incorporation of elevator evacuation from a specific floor – A numerical study of an office building

Johanna Hammarberg¹, Håkan Niva², Axel Mossberg³

¹Briab – Brand & Riskingenjörerna AB
Stockholm, Sweden

johanna.hammarberg@briab.se

²Briab – Brand & Riskingenjörerna AB
Malmö, Sweden

hakan.niva@briab.se

³Brandskyddslaget AB
Stockholm, Sweden

axel.mossberg@brandskyddslaget.se

Abstract: This paper investigates evacuation from a specific floor plan to determine if elevators can replace one of the escape routes consisting of a staircase without lengthening the evacuation times. This study specifically studies evacuation from one single office floor with 360 and 540 occupants, designed as one fire compartment with an area of 2800 m². To specify the occupants' willingness to use the elevator for evacuation from different floors, three different functions are used. These functions are modified to include more floors and are used to derive different distributions for the proportion using staircases and elevators, by simulations in Pathfinder. Two setups are studied. First, three staircases are used for evacuation. Secondly, one staircase is replaced with five evacuation elevators with capacity for eight occupants, and one elevator for sixteen occupants. For these setups, evacuation is studied from the 2nd, 8th, 16th, 25th and 50th floor. In addition to the studied functions, distributions that minimize the evacuation time for each floor are derived from the simulations. These distributions give the shortest possible evacuation times. The distributions are then compared to evacuation simulations from the first setup, only utilizing the three staircases. The results show that for the elevators to fully replace a staircase, between 45-60 % of the floor occupants need to use the elevators when the occupant count is 360, and 43-50 % when the number of occupants is 540. However, these values are dependent on floor number. Compared to the functions studied, the optimal percentage is significantly higher for lower floors, becoming closer to the functions as they increase with higher floor numbers. For each distribution on every floor, queuing time was also studied. Based on the results from the calculations, the study concludes that six evacuation elevators could replace one staircase on the studied office floor. However, this result relies on a certain percentage of the occupants using elevators for evacuation.

Keywords: elevator evacuation, evacuation modelling, pathfinder, evacuation, numerical study

1. Introduction

As urbanization increases, it is becoming more difficult to accommodate the need of living- and workspace within the cities. As a response to this, more focus is being put into constructing more high-rise buildings. However, this development can lead to other issues, for example ensuring safe evacuation for the parts of the population that are not able to use the staircases by themselves. This could be solved by incorporating evacuation elevators in the building's evacuation strategy. However, to what extent the evacuation elevators will be used is still an unsolved issue. The main issue is the fact that people have been taught not to use elevators in case of a fire. When buildings are constructed in such a way that the evacuation strategy involves elevators, it may therefore be necessary to review people's approach and behavior in this matter. This issue is further complicated by the contradicting fact that people are used to evacuate the way that they entered the building, and in high-rise buildings the common way to enter would be with an elevator. The advantages that evacuation elevators offer makes it a relevant area to study further.

Since the terrorist attack on the World Trade Center, the focus on elevator evacuation strategies has increased within the fire research community [1]. Connected to this, awareness for robust and reliable

elevator systems has been raised [2]. The solution with elevator evacuation is still relatively uncommon, as there are several challenges where more research is needed. Validation of the evacuation elevators' capacity and overcoming the general population's perception of elevator usage during evacuation are some of these challenges [3, 4].

Queuing is something that usually occurs when people evacuate. In case of evacuation from high-rise buildings, queues can form when using stairs or elevators as an escape route. By queuing and prolonging the evacuation procedure, evacuees can be exposed to fire or smoke if the queuing occurs in the fire compartment where the fire started. Queuing can also lead to unrest and stressful situations if the evacuees are standing in line for too long.

Incorporating elevators in a building evacuation strategy is not only a matter of psychology and occupant flows. It is mainly a regulatory issue, as buildings always must follow the local regulations. Also, it is unlikely for elevator evacuation to be incorporated in buildings as a non-mandatory add-on to the fire safety as the cost of this installation might be quite substantial. In Sweden, there is a possibility to use evacuation elevators to replace one of the otherwise mandatory staircases that are built if equal evacuation safety can be proved. In order to prove this, the efficiency of elevator evacuation needs to be examined further.

Several previous studies have investigated the efficiency of elevator evacuation, but with the focus on total evacuation of a building, i.e. the evacuation of all occupants from every floor [2, 5, 6]. However, no studies have been found on how elevator evacuation affects the evacuation procedure from a single floor or fire compartment. In Sweden, the building regulations on fire safety do not include a provision to study the effects of a total evacuation but the evacuation of each fire compartment and floor needs to be secured separately. Because of this, this study investigates under what circumstances a number of evacuation elevators can replace a staircase for certain evacuation scenarios when studying a single office floor.

The study presented in this paper specifically studies the evacuation from one single office floor, designed as one fire compartment. One main factor of the study was the percentage of occupants in the building that would have to use the elevators depending on which floor that was evacuated. However, the effect of changing capacities and velocities for the elevators, and other more technical specifications are also briefly studied.

2. Method

The simulation software used in this study was Pathfinder, which is a commonly used evacuation tool developed by Thunderhead Engineering. In order to specify the occupants' willingness to use the elevator for evacuation from different floors, three different functions were used and incorporated in the simulations [3, 7, 8]. These functions are given as 1-3 below. These three functions were developed in different studies with the help of questionnaires to investigate the connection between which floor occupants were located on and how many of them were willing to evacuate with elevators. Simulations were done once per floor per function.

$$P = 0.84 * F + 1.05 \quad 5 < F \leq 24 \quad (1) \text{ Andersson and Jönsson [3]}$$

$$P = 1.14 * F + 5.3 \quad 5 \leq F \leq 60 \quad (2) \text{ Heyes [7]}$$

$$P = 0.320 * \ln F - 0.4403 \quad 5 \leq F \leq 55 \quad (3) \text{ Kinsey [8]}$$

In these functions, P is the percentage of occupants using elevators for evacuation from the floor and F is the floor number being evacuated.

The functions were slightly modified to create three different evacuation scenarios for each studied floor. The functions were essentially extended to incorporate a larger range of floors. Function 1 was extended to be valid up to floor number 50 (from 24 in the original reference) and all three functions were assumed to have the same percentage of elevator usage on floor number two as for floor number five. The simulations used most of the program's standard settings [9], though occupant movement speed (1.3 m/s) and person flow rate through openings (1.1 p/sm) were modified to be in line with the recommendations in the Swedish building regulation [10].

During the simulations, the evacuation of only one floor at a time was studied. This is the standard evacuation procedure for Swedish office buildings. The drawing in Fig. 1 was imported into Pathfinder where an estimated office environment with obstacles such as furniture, separating walls and pillars was

drawn out. In the figure, the white area corresponds to the floor area where the occupants are placed at the beginning of the simulation. The floor area is about 2800 m².

The studied office floor has several escape routes. As shown in Fig. 1, there are three staircases; left, centre and right. The central staircase has an adjacent elevator lobby with six elevators and three entrance points. Five of the six elevators are of the same size and have capacity for eight people, the sixth having twice this capacity. The staircases and the elevator lobby make up their own fire compartments and in order to reach the staircase in the middle occupants have to go through the elevator lobby. The floor area in the elevator lobby is approximately 60 m² and the floor area in the two staircases on the sides are about 15 m² each. The floor area of the central staircase is about 6 m². Each staircase has a width of 1.2 meters, which is the required width of escape routes for fire compartments with more than 150 persons in the Swedish building code.

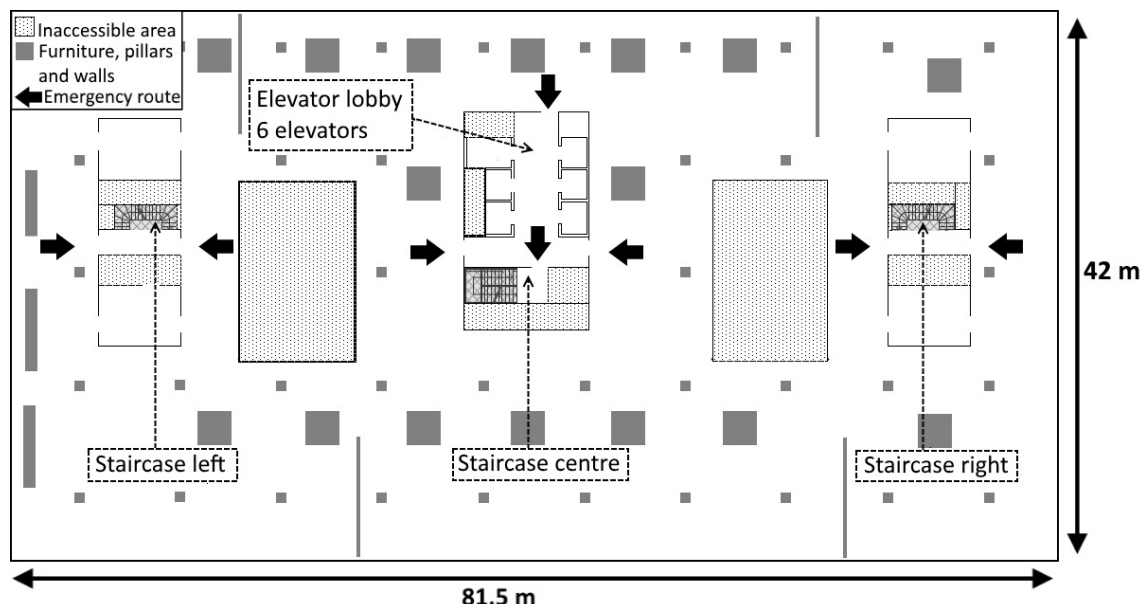


Fig. 1: Floor blueprint with items of significance.

The simulations studied evacuation from five different floors, i.e.: 2nd, 8th, 16th, 25th and the 50th floor. This could also be regarded as the number of floors which the elevators would need to travel to get people to another safe floor, not necessarily the entrance floor. Two types of behaviors were used to define what emergency exit the occupants could use. One behavior only allowed for elevators to be used, and the other only allowed for stairs to be used. This made it possible to control what percentage of the occupants were going to use the elevators and the stairs.

To find out which values would be used for the elevators in Pathfinder, a few questions were sent to KONE via a contact form on the company's website. The values used were for “regular elevators” and are shown in Table 1. The delay between closing the elevator doors in the simulations until it begins to move was identified to be about 2.5 seconds by studying the elevators in the simulations. It was therefore not a setting chosen by the authors.

Table 1: Used elevator parameters.

Parameter	Used values
Maximum occupants	8 and 16
Elevator velocities	1.6, 3, 4 and 10 m/s (depending on floor number)
Elevator acceleration	800 mm/s ²
Time for doors to open and close	5 s (total time for opening and closing)
Time between door closure and elevator movement	2.5 s

In the first simulations, the evacuation of 360 occupants from the floor was studied. Additionally, simulations were performed with 540 people evacuating from the floor, which meant an increase of 50 %. 540 was the allowed number of occupants on the floor according to the Swedish building code [11].

An assumption was made that as soon as occupants using the stairs reached the floor below, they were no longer part of the simulation as they had reached a safe zone. This meant that the simulation did not study the time it took to exit the building completely as this was deemed to give no further value to the study. This also means that factors like fatigue that can affect the evacuation from tall buildings were disregarded.

Two different evacuation setups were studied. In the first setup, the three staircases were used for evacuation. In the second setup, the centre staircase was replaced with six evacuation elevators. For these setups, evacuation was studied from the different floors mentioned above.

In addition to the different distributions mentioned above, “optimal” distributions for each floor were derived from the simulations. These “optimal” distributions were the ones giving the shortest possible evacuation times. These distributions were then compared to evacuation simulations from the first setup, only utilizing the three staircases. The reason that these distributions differ for different floors are explained by the fact that the elevator parameters differ according to Table 1 above and also that the travel distance for the elevator varies. The purpose with this comparison was to investigate if the six evacuation elevators could theoretically replace one staircase without lengthening the evacuation times.

The queuing time was also studied for the case with 360 occupants. The queuing time for elevator usage was the time from the first person who entered one elevator until the last person entered the elevator and the door closed. In occasional cases of evacuation from floor 25 and 50, 1-2 people did not fit with the last elevator round and had to wait for the last elevator to return, which could take up to 50 seconds. It was then assumed that those occupants actually took place in one of the last elevators as it was considered to be a more realistic situation. At most, the occupant density in the elevator lobby was as high as 3.2 persons per square meter in the simulations. This was calculated by Pathfinder and was not a factor that the study was heavily focused on, meaning it was not further investigated. The queuing time for staircase usage was the time from the moment a small queue was formed at the stairs, when people slowed down by those who were in front, until the last occupants could enter the first step of the staircase.

Queuing time for 540 occupants was not studied due to time constraints. Furthermore, the three studied distributions were not applied to the scenarios with 540 occupants, for similar reasons.

3. Results

The evacuation simulations show that in order to replace a staircase with evacuation elevators, the percentage using the elevators need to be increased in the lower floors, see Fig. 2, assuming that the distributions from the previous studies are correct. With the optimal distributions of evacuation elevator usage, the evacuation times from the floor are similar to when only staircases were used.

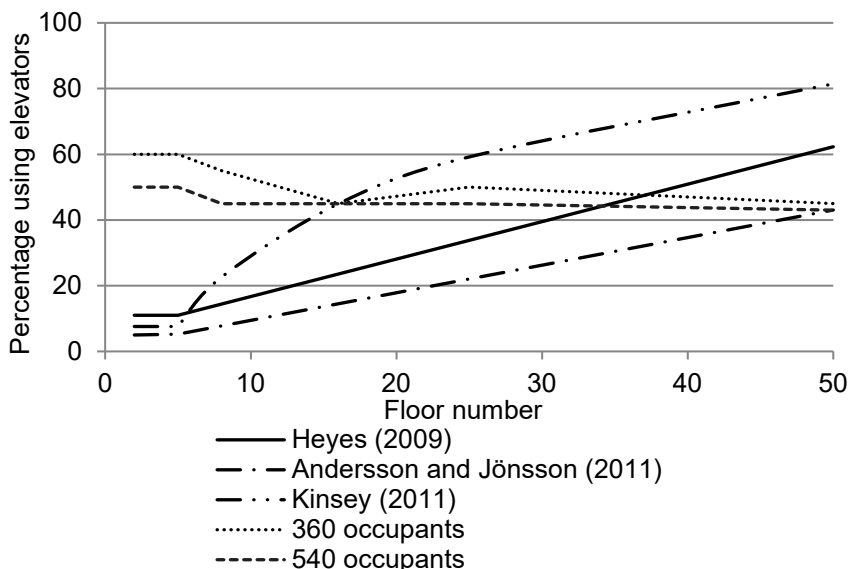


Fig. 2: Optimal distributions compared to correlations on elevator usage from different floors.

The simulations show that for 360 occupants, approximately 45-60 % of the evacuees need to use the elevators for each floor to acquire similar evacuation times as if only using the staircases. When the number of occupants increases to 540, between 43-50 % of the evacuees need to use the elevators in order to get equivalent times as the staircase solution. This is also indicated by the results in Fig. 2, which shows that the scenarios with 540 occupants evacuating from the floor gives a slightly lower optimal percentage of evacuees using the elevator.

Results from the simulations with 360 occupants show that queuing times for the evacuation elevators increase significantly for some of the functions when the floor that was evacuated was higher up in the building. This is natural, as the elevator usage also increases with floor number in the correlations. However, the significance of the difference with these solutions have previously not been quantified. These results are shown in Fig. 3. Note that the evacuees did not change evacuation route, regardless of waiting/queuing times.

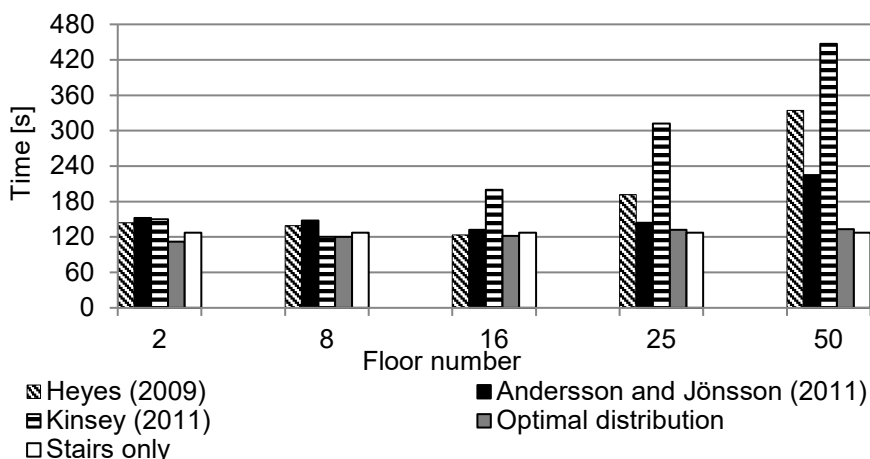


Fig. 3: Queuing times for the different correlations and floors studied for 360 occupants. Here, the maximum queuing time during the simulation is displayed.

The results also show that as the studied floor number increases, the required time for all occupants to reach another fire compartment generally decreases, with one major exception, as shown in Fig. 4. In general, this is because of the increasing elevator usage and the available occupant capacity of the elevator lobby. When elevator usage increases, it takes less time for the occupants to reach a new fire compartment since some of those who previously were queuing to the staircases now can enter the elevator lobby instead. The exception to this is with function 3 (Kinsey, [8]) on floor 50, which has the highest elevator usage of around 80 %. Here, the capacity of the elevator lobby is not enough to accommodate for the high number of occupants using the elevators, which leads to queuing to the lobby

while the staircases are free of queues instead. In all simulations it was concluded that if the optimal distributions were applied, the results were similar to when only staircases were used for evacuation.

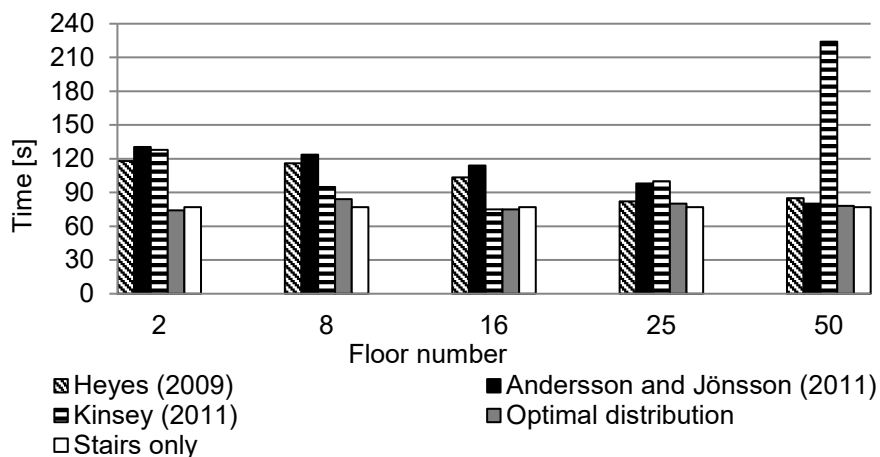


Fig. 4: Time until all 360 occupants had reached the next fire compartment.

When the number of occupants was increased to 540 and simulations were done to study how well the optimal distributions for 360 occupants could be directly applied to the increased number of occupants, the results show that the distributions are not directly applicable for different number of occupants, as seen in Fig. 5. The difference in the time it took for the occupants using elevators to evacuate compared to the ones using staircases is significant. Therefore, new distributions were developed, which can be seen in Fig. 2. This indicates that, in this case, the number of occupants impacts the optimal distribution of elevator usage.



Fig. 5: Optimal distributions for 360 occupants applied to 540 occupants, showing the difference in evacuation time for elevator and staircase users.

With the optimal distributions for 540 occupants developed the same way as before, Fig. 6 shows a comparison of the evacuation scenarios with elevators and stairs to the scenarios when only the staircases were used. With the exception of evacuation from the 2nd floor, the results show similar required time for the occupants to reach the next fire compartment. With the optimal distributions, the required time for evacuating the 2nd floor was around 30 seconds shorter than when only staircases were used.

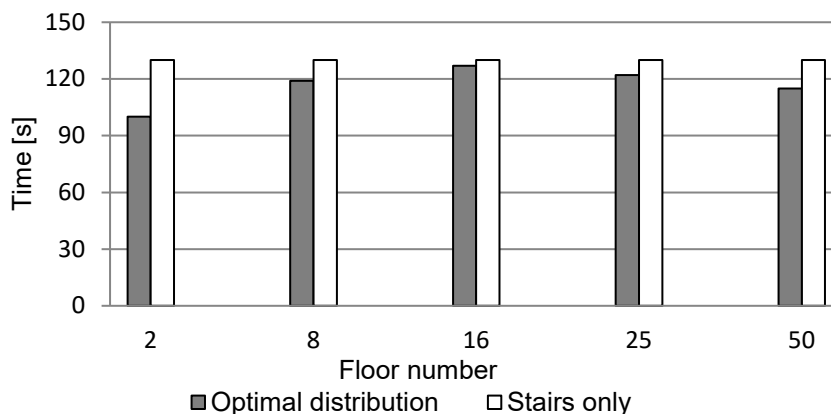


Fig. 6: Comparing the time until all 540 occupants had reached the next fire compartment, using optimal distributions and only the staircases.

4. Discussion

The optimal distributions for the most efficient evacuation proved to be more constant than the distributions of occupants' willingness to use elevators from previous studies, which increased with higher floors. There seem to be breakpoints where a higher proportion than expected from the previous studies need to evacuate by elevator on lower floors in order for the elevators to be effective. Similarly, with higher floors, a higher number of staircase usage would be needed in order for the elevator solution to be more effective.

Naturally, when the number of occupants increased from 360 to 540, time to another fire compartment increased too. When the simulations were made for 540 occupants the same distributions as for the scenarios with 360 occupants were used. This showed that time to another fire compartment for the scenarios with elevators increased and did not give the same results as for 360 occupants. Occupant times to reach another fire compartment for the stairs were similar at the lower floors, but at higher floor levels this time increased. In order for the scenarios with evacuation elevators and the scenarios with only stairs to be completed at the same time with 540 occupants, a smaller proportion should use the elevators than indicated in the distributions for the 360 occupants. In summary, this result implies that with a change of occupant number, new optimal distributions need to be derived in order to find the optimal evacuation procedure.

When the optimal distributions for 360 and 540 occupants were compared with the scenarios when only the stairs were used, the evacuation times were similar. This means that the elevators used for the simulations can replace the staircase for this specific floor.

As Fig. 6 shows, the time for the optimal distributions for 540 occupants are always slightly lower than the time to use only stairs. This could indicate that if increasing the occupant number, the evacuation can be more effective if one staircase is replaced with six elevators. However, this needs more studies to be concluded.

5. Conclusions

Based on the results from the performed calculations, the study concludes that one staircase on the studied office floor could be replaced with six evacuation elevators. However, this result relies on 45-60 % or 43-50 % of the occupants using elevators for evacuation, for 360 and 540 occupants respectively. These distributions represent optimal distributions between the elevator and stair users in the studied evacuation situations.

When compared to functions derived in previous studies on human behavior connected to elevator evacuation, these results pose certain challenges, i.e., on lower floors, the number of occupants using the evacuation elevators needs to be increased in order for the solutions to be equivalent. This means that on these floors, the usage of the elevators needs to be promoted. However, at higher floor numbers, the problem is the opposite, as too many occupants are willing to use the evacuation elevators. Here, the stairs may need to be promoted in order for the evacuation to be as effective as possible. The results of this study highlight the importance to further study how to incentivize occupants to use both elevators and stairs in high-rise buildings.

This study relates to the layout of the certain office building used. Therefore, the results cannot be directly translated to other buildings. However, the conclusions mentioned above can be assumed to be general indications to expect in any building utilizing elevators for evacuation. Hence, the study highlights the importance of dealing with these problems in the fire safety design.

References

- [1] D. Nilsson and A. Jönsson, "Design Evacuation Systems for Elevator Evacuation in High-rise Buildings," *Journal of Disaster Research*, vol. 6, pp. 600-609, 2011.
- [2] E. Ronchi and D. Nilsson, "Modelling total evacuation strategies for high-rise buildings," *Building Simulation*, vol. 7, no. 1, pp. 73-87, 2014.
- [3] J. Andersson and A. Jönsson, "Evacuation in High-rise Buildings - An analysis of risk perception," Lund University, Lund, 2011.
- [4] M. Arnqvist and J. Olsson, "Emergency elevators as a means of egress – An analysis of the possibility to use elevators when designing emergency egress systems," Lund University, Lund, 2010.
- [5] J. H. Klote, "A Method for Calculation of Elevator Evacuation Time," *Journal of Fire Protection Engineering*, vol. 5, no. 3, pp. 83-95, 1993.
- [6] E. Kuligowski, "Elevators for Occupant Evacuation and Fire Department Access," Kuala Lumpur, 2003.
- [7] E. Heyes, *Human Behavior Considerations in the Use of Lifts for Evacuation from High Rise Commercial Buildings*, Canterbury: University of Canterbury, 2009.
- [8] M. J. Kinsey, "Vertical transport evacuation modelling," University of Greenwich, Greenwich, 2011.
- [9] Thunderhead Engineering, "Pathfinder User Manual," Thunderhead engineering, New York, 2014.
- [10] Boverket, "BBRAD 3," Boverket, Karlskrona, 2013.
- [11] Boverket, "BFS 2014:3," Boverket, Karlskrona, 2014.

Thermodynamics of a gas of pedestrians: theory and experiment

Claudio Feliciani¹, Francesco Zanlungo², Katsuhiko Nishinari^{1,3}, Takayuki Kanda^{2,4}

¹ Research Center for Advanced Science and Technology, The University of Tokyo
4-6-1 Komaba, Meguro-ku, Tokyo 153-8904, Japan
feliciani@jamology.rcast.u-tokyo.ac.jp

² Advanced Telecommunications Research Institute International
2-2-2 Hikaridai Seika-cho, Sorakugun, Kyoto 619-0288, Japan

³ Department of Aeronautics and Astronautics, Graduate School of Engineering, The University of Tokyo
7-3-1 Hongo, Bunkyo-ku, Tokyo 113-8656, Japan

⁴ Department of Social Informatics, Graduate School of Informatics, Kyoto University
36-1 Yoshida-Honmachi, Sakyo-ku, Kyoto 606-8501, Japan

Abstract - In this paper, we perform an experiment on the interaction of pedestrians in a chaotic environment and investigate the possibility to study its results using a thermodynamic model. In contrast to simple single-file unidirectional scenarios, where only distance and time are relevant to adjust walking speed, bidirectional cases are much more complex since pedestrians can perform evading manoeuvres to avoid collisions. To better understand collision avoidance in a bidimensional environment we designed a set of experiments where people need to move chaotically for the whole time. Trajectories of moving pedestrians were obtained by tracking their head position, but a method to obtain body orientation failed, thus limiting reliable information on average quantities, i.e. average density and speed. By analysing those data, we showed that equations for thermodynamic processes can be used to describe pedestrian dynamics from medium densities or a state where interaction distances are very small. To allow combining low density cognitive aspects of collision avoidance with semi-random motion at medium densities we also developed a microscopic simulation model inspired by physics. Results show that, after calibrations, the simulation model allows to reproduce the fundamental diagram of different studies despite the very simple rules implemented. This shows that describing the statistical nature of specific crowds requires a relatively small set of rules and research should focus on cognitive/psychological aspects which are essential for understanding crowds of people.

Keywords: chaotic motion, collision avoidance, potential-based model, simulation, crowd experiment

1. Introduction

Studies considering single-lane unidimensional pedestrian motion already showed, both theoretically and experimentally, that headway distance and collision time are related to the formation of jam. When pedestrians are unable to adjust their distance from the preceding person, they need to stop, leading to a queue which propagates opposite to the walking direction. This fundamental mechanism of collision avoidance is also found in similar collective systems [1], with car traffic being the most prominent.

For the unidirectional case, it has been shown that there is a typical relationship between pedestrian density and walking speed and this property has been often referred to as the fundamental diagram (Figure 1). In the unidirectional case, the speed-density fundamental diagram can be described using a monotonic function and many authors have proposed equations which allow a mathematical description [2]. From a practical aspect, the flow-density representation, where flow is typically computed by multiplying density and speed, is more interesting. The particularity of the flow-density representation lies on its non-monotonic nature, which allows to recognize the density region where congestion starts occurring as a peak.

In reality, pedestrian crowds are bidimensional entities and collision avoidance does not only occur by adapting speed and distance from other pedestrians, but evading manoeuvres (like overtaking) are also possible. When bidirectional flows are considered, then emerging structures (in the specific organized

lanes) are formed as a result of coordination between groups of pedestrians moving in opposite directions. When even more complex forms of motion are considered, such as crosswalks, scramble crossings or random walk, then understanding how people avoid each other and what is the typical density at which motion starts being obstructed becomes very difficult.

In fact, when the fundamental diagram is plotted for the bidirectional case a quite different shape is obtained in the flow-density representation, but it is still possible to observe the typical elements recognized in the unidirectional case (see Figure 1). If more complex (multidirectional) streams are considered, it is remarkable to notice that the peak observed in the flow disappears (at least for medium densities as the ones considered in Figure 1).

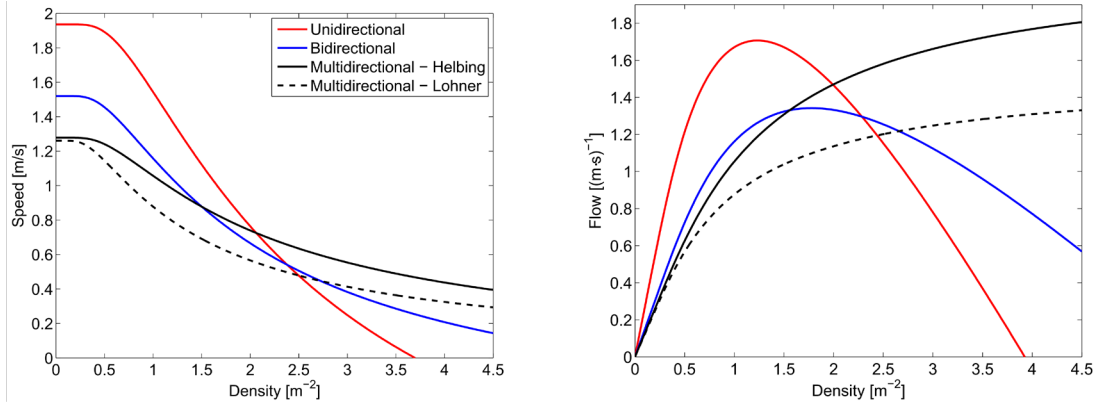


Fig. 1: Speed-density and flow-density fundamental diagrams from different studies considering pedestrian motion in specific environments. The Weidmann equation [3] is used to fit experimental data of each study [4,5,6,7]. Absolute speed is taken here and flow is defined as the product of speed and density.

The above discussion leads to two important considerations: (i) the typical definition of flow as the product of density and (absolute) speed possibly only holds for unidirectional (or similar) cases and (ii) complex bidimensional crowds need to be considered in vectorial manner, with collision avoidance being a combination of distance, speed and collision angle (or an equivalent quantity).

2. Experiment

To study collision avoidance and related aspects in a real environment we designed an experiment in which pedestrians need to walk continuously in a very chaotic scenario where emergent structures cannot form. Experimental setup and procedures will be provided in this section (for details see [8]).

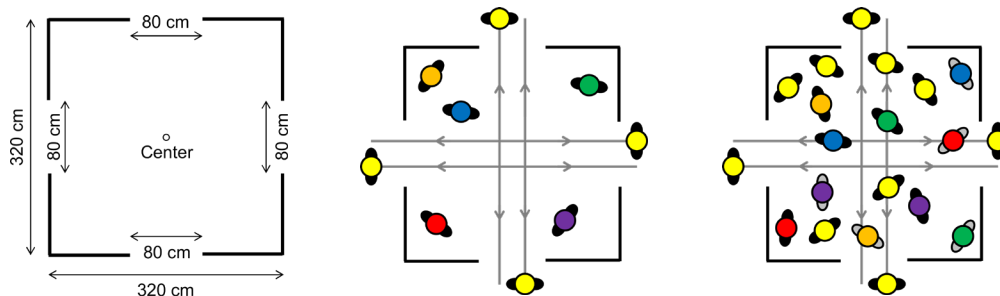


Fig. 2: Room dimensions and schematic representation of the experimental principle for low and medium densities.

A room (whose dimensions are given in Figure 2) has been created using band partitions. An entrance was located in the middle of each side to allow pedestrians entering/leaving the room before, during and after the experiments. For each execution a fixed number of participants was allowed into

the room and was asked to continuously walk without a specific aim for the whole length of the experiment. Although we predicted that the above instruction would result in a continuous chaotic motion, we were afraid that, in the long run, some emergent structures would appear (in the specific we wanted to avoid that people would start moving in a circle to reduce collisions). To make sure that it would be impossible to get organized in whatever way, we asked to some of the participants to continuously cross the room in four different directions. Crossing pedestrians would enter the room, cross it taking the shortest possible path, shortly step outside the exit on the opposite side, turn themselves by 180 degrees and then cross the room again in the opposite direction. Crossing pedestrians are indicated using lines in Figure 2.

Two different strategies were used to change the density inside the room. In a first set of experiments (configuration A) we gradually increased both the number of people inside the room and the ones continuously crossing it, thus ensuring that the ratio between both roles was maintained constant. In the second set of experiments (configuration B), we kept the number of crossing pedestrians constant at four (i.e. one for each direction) and we only increased the number of participants wandering inside the room. The number of pedestrians for each role and the resulting density are given in Table 1.

Table 1: Experimental procedure and number of participants in each run.

Configuration A: wandering/crossing ratio fixed				Configuration B: crossing number fixed			
Wandering	Crossing	Total	Density	Wandering	Crossing	Total	Density
5	0	5	0.49 m ⁻²	5	0	5	0.49 m ⁻²
5	4	9	0.88 m ⁻²	6	4	10	0.98 m ⁻²
10	8	18	1.76 m ⁻²	11	4	15	1.46 m ⁻²
15	12	27	2.64 m ⁻²	16	4	20	1.95 m ⁻²
20	16	36	3.52 m ⁻²	21	4	25	2.44 m ⁻²
				26	4	30	2.93 m ⁻²
				31	4	35	3.42 m ⁻²
				36	4	40	3.91 m ⁻²

After having participants ready at their initial positions, a loud “start” signal was given and people started walking. After roughly two minutes a “stop” signal was given, allowing them to stop and rest.

A camera was fixed 5.5 m above the ground pointing right at the centre of the room. Videos from the experiments were later analysed using PeTrack [9] software to gain trajectories of the participants using the caps as marker. Frames taken during different experiments are given in Figure 3.

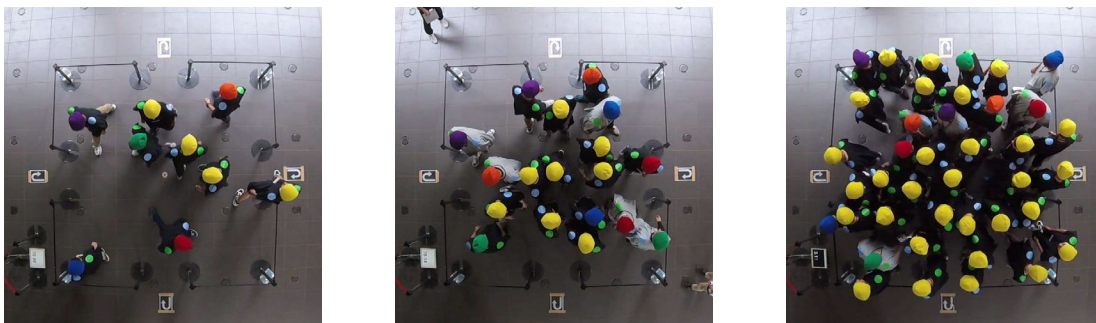


Fig. 3: Examples of snapshots taken during the experiment at low, medium and high densities.

In an attempt to collect body orientation to allow a more detailed analysis on the mechanisms of collision avoidance, we also added some markers on the shoulders, which are visible as small dots in Figure 3. Unfortunately, shoulder markers became covered most of the time due to the geometrical location of the camera and the wide-angle lens employed. While it would still be possible to obtain body orientation by

combining head and a single shoulder position at low densities, at high density the obstruction became very frequent and, in some cases, both markers became invisible.

As a consequence, we had to limit our analysis on the trajectories gained by tracking the position of the head, which, while accurate enough to obtain condensed information such as average speed or density, it does not provide sufficient accuracy to allow obtaining the orientation of the body by derivation (in addition, orientation of the body is not necessarily corresponding to the angle created by the trajectory).

3. Experimental results and discussion

As already discussed earlier, since the fundamental diagram represents a widely studied property of pedestrian motion, our experimental analysis will focus on considering the speed-density relation and the equation which can be used to describe the particular scenario considered in this study. The speed-density fundamental diagram is presented in Figure 4 for the two different experimental configurations given in Table 1.

To allow a more accurate estimation of density, Voronoi cells have been used to account for the reduction in density observed when crossing pedestrians briefly step out from the room (for this reason densities given in Table 1 are not exactly the same of Figure 4). Speed has been simply computed by considering the whole crowd and excluding the speed-up and slow-down periods occurring after the “start” and “stop” signals were given (i.e. only steady-state conditions are studied).

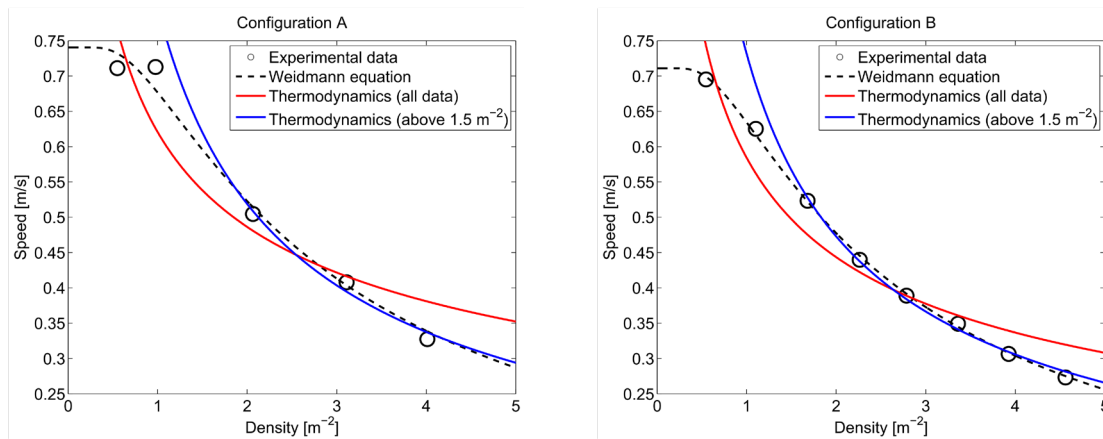


Fig. 4: Fundamental diagram of pedestrian motion in a chaotic scenario with proposed fitting functions.

The Weidmann equation [3] has been often used to describe the speed-density relationship of human crowds and has been therefore chosen as the first candidate to fit experimental data. The general form of the Weidmann equation describing speed v in function of density ρ is given by:

$$v = v_0 \left(1 - e^{-k \left(\frac{1}{\rho} - \frac{1}{\rho_{max}} \right)} \right) \quad (1)$$

where v_0 is the free walking speed, ρ_{max} the maximum density and k an empirical parameter. Although the number of points for case A is limited, it is seen that in both cases the Weidmann equation allows for an accurate description of the reduction in speed resulting from the increase of density.

Given the nature of our experiment and previous research indicating that pedestrian crowds can be modelled based on equations from gas dynamics [10,11], we also tried to use simple equations obtained from thermodynamics. By introducing density into the ideal gas law and combining it with the expression defining thermodynamic transitions in a polytropic process, it is possible to show that density ρ and temperature T in two separate states (1 and 2) are satisfying the following equality:

$$\frac{T_1}{T_2} = \left(\frac{\rho_1}{\rho_2}\right)^{m-1} \quad (2)$$

where m is the polytropic index, specifying the conditions under which the thermodynamic process occurs, and that we consider as a model parameter since the nature of such thermodynamic process is not clear for pedestrians. Now, defining a reference state 0, it is possible to describe the variation of temperature in a polytropic process according to:

$$T = T_0 \left(\frac{\rho}{\rho_0}\right)^{m-1} \quad (3)$$

with T_0 and ρ_0 being the temperature and density at the reference state. Since the average of the squared gas velocity is proportional to the temperature, we may assume (for modelling purposes) that an expression substituting T with v may allow to describe the speed-density relationship of our experiments.

As shown in Figure 4, such an expression does not allow a sufficiently good representation of the experimental results, which may be a consequence of the overly simple model considered in this first modelling attempt. However, by excluding low density points (where thermodynamic velocity goes to infinity) a much better fitting (eventually even better than the Weidmann equation) is achieved.

The reasons which could explain the contrasting results obtained by considering the different set of points is related to the range of interaction and the obvious diversity between gas and humans (which, in contrast to particles, do perform collision avoidance to avoid dumping into each others). In brief, the very different results obtained by excluding low density points show that collision avoidance is a long-range interaction and cannot be modelled with overly simple short-range thermodynamics. This also shows that a model specific for humans is required for low density scenarios characterized by long-range interactions.

4. Simulation model

Inspired by our (partial) success in reproducing the experimental data with a simple thermodynamical model, we have considered the possibility of describing the results of our experiments using a microscopic “particle gas” (molecular dynamics) model [10], i.e. a simulation model in which pedestrians are explicitly represented in a continuous space and inter-pedestrian interactions are modelled using physical forces.

Theoretical or simulation models aiming to describe the motion of active matters have been already proposed in the past [11,12], but comparison with experimental data has been more difficult to perform due to the lack of experiments with comparable conditions. Although in this work we will not attempt any theoretical analysis in which the macroscopic (thermodynamical) crowd properties are derived from the microscopic dynamics using statistical mechanics methods, to let the possibility of realising such a program, we will explicitly use a Hamiltonian model on which statistical mechanics approaches may be applied. The goal of such a simulation model is not to exactly reproduce pedestrian trajectories observed in experiments but rather show what are the minimal requirements to be satisfied to see similar behaviours, and more in general to investigate the correspondence between microscopic interaction rules and macroscopic statistical properties such as the fundamental diagram.

In such a model, we would assume that pedestrian behaviour may be modelled using a potential depending only on relative distance. More explicitly, we would need at least three potentials: one describing attraction to a point of interest; one describing physical interactions; and one describing collision avoidance. Nevertheless, although the potential concerning physical interactions is definitely relevant to introduce the finite volume effects present in high density crowds, for simplicity’s sake we will ignore it in the following discussion.

A relatively simple Hamiltonian model describing the remaining two behaviours was introduced in [13]. Its departure from the usual gas of physical particles lies in the assumption that pedestrians may have a limited field of view (for simplicity’s sake, a cone with a fixed aperture angle α and radius r_v centred

on the pedestrian velocity) and perform collision avoidance only towards those pedestrians that fall in their field of view. This leads to a Non-Newtonian dynamics, a term that we use to mean that the dynamics does not follow the third (action-reaction) law of dynamics. Interestingly, this Non-Newtonian model can still be analytically treated in the two-body case, and, although the explicit solution is cumbersome, it is easy to show that the system is dissipative.

Numerical simulations show that in the N-body problem the system converges, for any given initial condition (excluding a measure 0 set) to a "frozen" state with zero kinetic energy. A way to avoid this "freezing" of the system is to provide pedestrians with "memory", i.e. to allow them to remember the position of the other pedestrians for a short time τ after they have left the field of view.

For reasons of space we cannot reproduce here a detailed analytical and numerical treatment of the model. Readers may refer to [13] for an introduction to the model and to [14] for a full treatment. A statistical mechanics treatment of a Non-Newtonian model of pedestrian dynamics is performed in [15].

5. Comparison between experimental and numerical results

In [13,14] a throughout analysis of the dependence on field of view extension and memory of the statistical properties of this system had been performed. Nevertheless, the original work made no reference to the concept of crowd density, which is crucial for our current purpose. We may introduce the concept of density by fixing the radius R of the self-consistent KV charge distribution [14] so that we have $A = \pi R^2 = 9$ square meters (in line with our experimental setting), varying the number of simulated pedestrians and defining density as the ratio between the pedestrian number and the area A . In this way, for each set of model parameters, we may obtain a fundamental diagram by plotting how the average pedestrian velocity varies with density.

As in [13,14], the potential describing the attraction to the point of interest is a 2D harmonic potential

$$U(r) = K/2 r^2 \quad (4)$$

which means that the point of attraction is the centre of the self-consistent charge area. To differentiate between ordered and disordered velocity, we computed the projection of the pedestrian velocity towards the centre (point of attraction) and plotted the system speed as the average of the absolute value of the latter radial velocity (this method applies only for Fig. 5 and 6), and the flow as the product of speed and density.

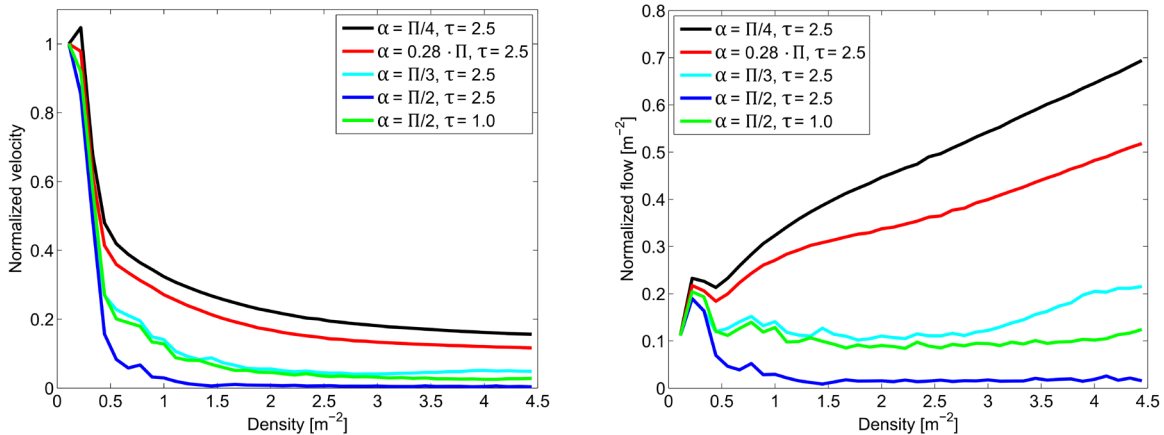


Fig. 5: Normalized fundamental diagrams for different set of parameters.

As shown in the results of Figure 5, for a large set of parameters the system has a non-zero (radial or ordered) velocity for moderate and high density, as observed experimentally in our work and reported in other studies [6,7].

Studying the (radial or ordered) flow, we see a transition in parameter space from a flow with a maximum for low density to a constant flow and finally a concave monotonic function similar to the experimentally observed one. For intermediate parameters we see a convex growth range as reported for high density in [7].

Encouraged by these results, we tried to explicitly investigate the parameter values that minimise the difference between the flow in the model and in the experimental data of the current work and of [6,7].

Each different data-set presents a different “free speed”, i.e. the speed that is observed (or extrapolated) in the zero-density limit. In the microscopic model, such velocity is the average velocity of a system with a single pedestrian, which is determined by the constant K in Eq. (4). For this reason, to replicate the flow of each data-set we would need to change the value of K but this would introduce a new parameter. A simple way to avoid this is to study *normalised flow*, i.e. to divide the flow by the free speed, and optimise (using a Genetic Algorithm) on these data that have, by definition, the same low density limit.

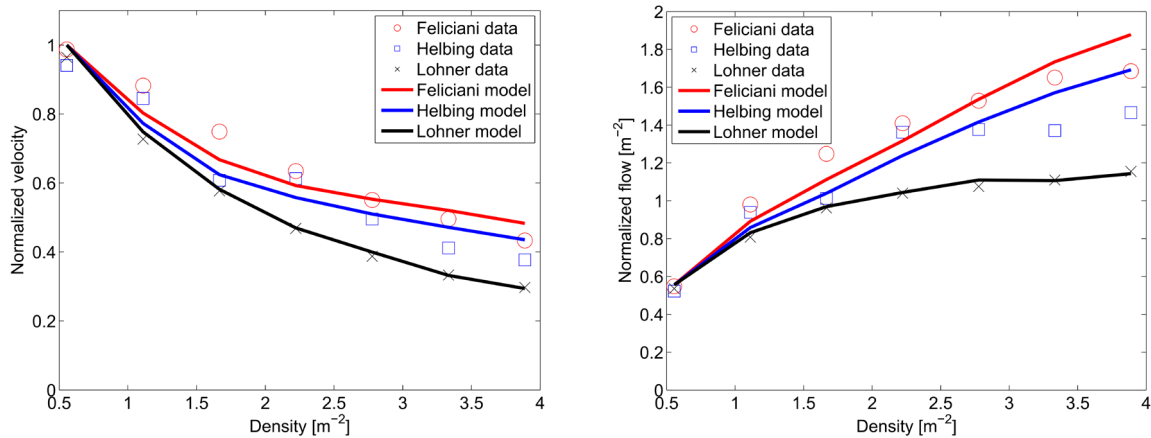


Fig. 6: Comparison between experimental data and numerical model simulation using normalized quantities of different authors for chaotic-like motion. Feliciani refers to the data of this study where configurations A and B have been unified considering their similarities (and to make results easier to read).

Figure 6 compares the velocity (left) and flow dependence (right) between the model and the original data for each data set. The parameters that minimise the difference between the flow in the model and in the observed data are: Lohner $\alpha = 0.72$, $\tau = 3.70$ and $r_v = 1.39$ [7]; Helbing $\alpha = 0.02$, $\tau = 4.53$ and $r_v = 2.71$ [6] and Feliciani $\alpha = 0.06$, $\tau = 4.66$ and $r_v = 4.55$ [8]. We may observe that the model reproduces extremely well the fundamental diagram observed in [7], while the agreement with the other two data-sets is less good.

6. Conclusion

This study presented the results from an experiment where people need to move in chaotic way trying to reduce collisions. Our simple analysis showed that there are similarities with physical systems and in particular thermodynamic laws for gases may help describing the transitions occurring when density is increased as a sort of thermodynamic process. However, since humans do perform mostly long-range collision avoidance to avoid colliding with other people, such similarities hold true only for packed crowds where evading manoeuvres are very difficult but often necessary (thus a short-range interaction).

A numerical model inspired from physics but also including elements typical of human cognitions partially helped improving the results at low densities by including a mechanism of collision avoidance where people (or particles) are able to see and remember motion of others. However, results showed that while it is possible to reproduce with good accuracy datasets from similar studies, the model reproduced with less accuracy the experimental data presented in this work.

The conclusions from the above remarks assume therefore a dual nature. On one side, our study showed that even a very simple model may clarify the basic mechanisms that lead to the emergence of the statistical behaviour of pedestrians and help in the development of more realistic models. In particular, when people move in a very chaotic context and influence of the environment is minimal, a very simple model may be sufficient to describe the overall behaviour.

On the other side, we also showed the limits of modelling pedestrians as physical entities, thus implying, as some author [16] already pointed out, that cognitive and/or psychological knowledge is required to correctly reproduce the behaviour of pedestrians in simulations. Realistic and more complex simulation models should therefore focus on psychological crowd phenomena, which are the leading cause to the different behaviour between humans and physical particles.

Acknowledgements

This work was financially supported by JST-Mirai Program Grant Number JPMJMI17D4, JSPS KAKENHI Grant Number 25287026 and the Doctoral Student Special Incentives Program (SEUT RA). It is also partially based on results obtained from a project commissioned by the New Energy and Industrial Technology Development Organization (NEDO).

References

- [1] J. Zhang, W. Mehner, S. Holl, M. Boltes, E. Andresen, A. Schadschneider, A. Seyfried, “Universal flow-density relation of single-file bicycle, pedestrian and car motion”, *Physics Letters A*, vol. 378, no. 44, pp. 3274-3277, 2014.
- [2] A. Gupta, N. Pundir, “Pedestrian flow characteristics studies: A review”, *Transport Reviews*, vol. 35, no. 4, pp. 445-465, 2015.
- [3] U. Weidmann, “Transporttechnik der fussgänger“, *ETH Zürich*, vol. 90, 1992.
- [4] J. Zhang, W. Klingsch, A. Schadschneider, A. Seyfried, “Ordering in bidirectional pedestrian flows and its influence on the fundamental diagram“, *J. Stat. Mech. Theor. Exp.*, vol. 2012, no. 2, 2012.
- [5] S. J. Older, “Movement of pedestrians on footways in shopping streets”, *Traffic Engineering and Control*, vol. 10, no. 4, 1968.
- [6] D. Helbing, A. Johansson, H. Z. Al-Abideen, “Dynamics of crowd disasters: An empirical study”, *Phys. Rev. E*, vol. 75, no. 4, 2007.
- [7] R. Lohner, B. Muhamad, P. Dambalmath, E. Haug, “Fundamental diagrams for specific very high density crowds“, *Collective Dynamics*, vol. 2, pp. 1-15, 2018.
- [8] C. Feliciani, K. Nishinari, “Measurement of congestion and intrinsic risk in pedestrian crowds”, *Transp. Res. Part. C Emerg. Technol.*, vol. 91, pp. 124-155, 2018.
- [9] M. Boltes, A. Seyfried, “Collecting pedestrian trajectories”, *Neurocomputing*, vol. 100, pp. 127-133, 2013.
- [10] D. Helbing, P. Molnar, “Social force model for pedestrian dynamics”, *Phys. Rev. E*, vol. 51, no. 5, 1995.
- [11] S. Hoogendoorn, P. Bovy, “Gas-Kinetic Modeling and Simulation of Pedestrian Flows”, *Transp. Res. Rec.*, no. 1710, pp. 28-36, 2000.
- [12] S. C. Takatori, J. F. Brady, “Towards a thermodynamics of active matter”, *Phys. Rev. E*, vol. 91, no. 3, 2015.
- [13] G. Turchetti, F. Zanlungo, B. Giorgini, “Dynamics and thermodynamics of a gas of automata“, *EPL (Europhys. Lett.)*, vol. 78, no. 5, 2007.
- [14] F. Zanlungo (Adviser G. Turchetti), “Microscopic dynamics of Artificial life systems”, Dissertation Thesis for the Ph.D. in Physics, Bologna University, 2007.
- [15] F. Zanlungo, T. Ikeda, T. Kanda, “Potential for the dynamics of pedestrians in a socially interacting group”, *Phys. Rev. E*, vol. 89, no. 1, 2014.
- [16] A. Templeton, J. Drury, A. Philippides, “From mindless masses to small groups: Conceptualizing collective behavior in crowd modeling”, *Rev. Gen. Psychol.*, vol. 19, no. 3, 2015.

Towards Real-Time Monitoring of the Hajj

Muhammad Baqui and Rainald Löhner

CFD Center/George Mason University
4400 University Avenue, MS 4c7, Fairfax, VA 22030, USA
mbaqui@gmu.edu; rlohner@gmu.edu

Abstract – An automated approach to explore the fundamental properties of high-density pedestrian traffic is outlined. The framework operates on video or time lapse images captured from surveillance cameras. For pedestrian velocity extraction, the framework incorporates cross-correlation based Particle Image Velocimetry (PIV) techniques. For pedestrian density estimation, the framework relies on the Machine Learning technique of the Boosted Regression Trees. The information collected from images in pixel coordinates are transformed to world coordinates with a pin-hole camera based projective transformation technique. The framework has been tested with high density crowd images acquired during the Muslim religious event, the Hajj. Accuracy and performance of the framework are reported.

Keywords: Crowd Monitoring, Particle-Image Velocimetry, Machine Learning, Hajj

1. Introduction

Every year millions of Muslims congregate to perform the Hajj. Managing pedestrian safety and comfort for crowds of this size presents formidable challenges. As recently as 2015 hundreds of people lost their lives in an unfortunate accident during the Hajj [1]. Since surveillance cameras are widely used, studying video or time lapse photos from these cameras may provide valuable insights on the dynamics of high-density pedestrian traffic. The aim of this work is to enable automatic processing of these images and the extraction of quantifiable information. More specifically, the current work provides ways for obtaining velocity and density information from surveillance camera images. The framework relies on the Particle Image Velocimetry (PIV) [2] technique for pedestrian velocity extraction and a trained Machine Learning model for obtaining density. After obtaining velocity and density in the image/pixel coordinates, these are transformed to physical units (meters) in world coordinates through projective geometry (perspective correction).

The rest of the paper is organized as follows: in Section 2 a brief description is provided for the current state of research with image processing of crowd images. In Section 3 the theoretical aspects of the framework are discussed followed by Section 4, where the experiments and results are reported on the accuracy of the framework. In Section 5, some potential applications of the data are presented and finally conclusions are drawn on Section 6.

2. Background

Image processing and computer vision techniques have been used to analyze various aspects of pedestrian dynamics, namely walking behavior, crowd monitoring, head counting, trajectory extraction etc. In recent times, Maurin et al. [3] have constructed a crowd monitoring system based on optical flow, segmentation, and Kalman filter. Nedevschi et al. [4] also constructed a detection and collision avoidance scheme from video data based on Kalman Filtering. The results presented in both of these studies are promising. However, a major limitation of these frameworks is that they are not designed to handle high density crowds.

In order to obtain pedestrian density from a given image, the first step would be to get a headcount of the people in that image. Machine learning models have been shown to be effective in order to achieve

this. The crowd counting has often been formulated as a regression problem in machine learning. A regression model would output a predictive headcount once it is trained properly. Ma et al. [5] have developed a counting model based on Gaussian process regression. Idrees et al. [6] have constructed a Support Vector Regressor that has been trained with more than one feature (image gradients, Fourier peaks and interest point based samplings).

For obtaining pedestrian speed, Optical Flow [7] is arguably the most popular. The optical flow technique resolves the pedestrian velocities per pixel. As a result, the processing time becomes quite high for surveillance camera images which often have resolutions close to 5760x3840 pixels. The PIV technique that being widely used in the fluid dynamic community can be used to extract pedestrian velocities in a much faster rate. The PIV technique was developed in the mid 80's [8], and has recently found its use in other fields. For example, Vanlanduit et al. [9] have used PIV for metal fatigue experiments and Sveen et al. [10] applied it to the study of water waves. The application of PIV in audio speaker performance can be found in Rossi et al. [11]. From the review of relevant literature, it is apparent that by combining machine learning techniques with Optical Flow or PIV speed detection, one can conveniently create an automated framework that would monitor crowd properties and provide quantifiable information which could be used to make decisions on crowd management such as impending danger.

3. Materials and Methods

This section outlines a brief description of the theoretical aspects of the crowd monitoring framework. Crowd velocity extraction from PIV is discussed in section 3.1, crowd counting through boosted regression trees is discussed in section 3.2 and image-to-world coordinate transformation is discussed in section 3.3.

3.1 PIV

The PIV technique takes a sequence of time lapse photos that are being separated by a small time-gap (typically fractions of seconds). Initially the photos are divided into smaller blocks known as the interrogation spots. Afterwards, for each interrogation spot, cross correlation is performed. The cross-correlation computes component wise inner product. The inner product is generally computed in the frequency domain through convolution. Operating in frequency domain enables much faster processing time compared to regular (direct) correlation. In Figure 1, a sample input image and correlation surface can be seen.

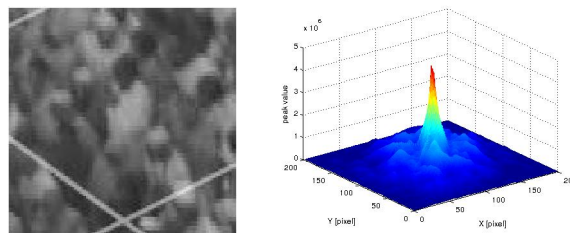


Fig 1. Input image and corresponding PIV correlation surface

3.2 Head counting

Head counting or pedestrian counting is the first step for the density estimation. The machine learning model formulated for head counting uses Histogram of Oriented Gradients (HOG) [12] as image features and manual annotations as ground truth. The machine learning model solves a regression problem following the gradient boosting algorithm [13]. Input to the machine learning model consists of image segments with pedestrians in it and output would be approximate counts of the number of people. To achieve the final counts, the machine learning model operates in two stages. In step 1, image features

are extracted via HOG and in the subsequent step, the regression model is trained with the HOG features and ground truth counts.

3.2.1 Feature Extraction via HOG

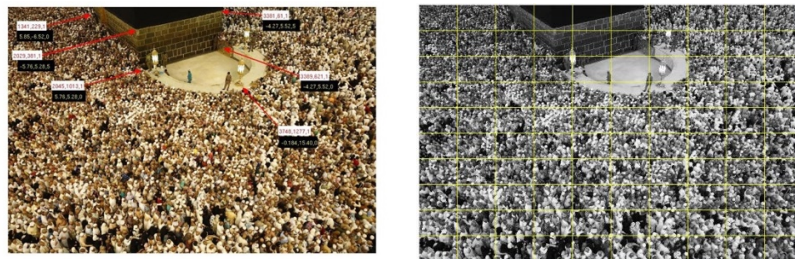
The HOG feature creates a histogram of images edges based on their orientation. The input image segment is first divided into 8x8 pixel blocks. For each block, image gradient is calculated. If the input image is an RGB image, it is first converted to Gray scale image (0-255 gray level values) in order to reduce the influence of illumination effects. Then gradients are calculated in a block wise fashion. Afterwards, these gradients are collected into 9 orientation bins. The final outcome is a histogram of this gradients. More information on its application to crowd counting can be found in [14].

3.2.2 Regression Model Construction

The regression model is constructed with HOG features of the input images and their corresponding ground truth counts. The model input has the form of $([x_{11}, x_{12}, x_{13}, \dots, x_{1m}], y_1), ([x_{21}, x_{22}, x_{23}, \dots, x_{2m}], y_2), \dots, ([x_{n1}, x_{n2}, \dots, x_{nm}], y_n)$, where n is the number of training samples (100 in this case) [Figure 2(b)] and m is the dimension of the HOG histogram (68600 in this case). The goal of the regression model is to formulate an approximate function $F, (x_{nm} \rightarrow y)$ that minimizes dissimilarity between the ground truth and the model prediction in a stage wise fashion by formulating trees (regression trees). After the model is being trained, if an input image is given, the model will first compute the HOG features of the input image and with the HOG features, the regression model approximates a head count of pedestrians in the image. More details of the approach can be found in [14] and [15].

3.3 Image to World Transformation

The pedestrian speed obtained through PIV comes in pixel coordinates. Also, for the density calculation, the counts obtained through Machine Learning need to be divided by the image area. As the images are not taken from an orthogonally posed camera, converting of these pixels to meters/centimeters becomes a challenge. The coordinate transformation technique involved here operated on a few landmark points for which pixel and world coordinates are known. In Figure 2 (a), these landmark points along with their pixel and world coordinates can be seen. Since the pedestrians are moving along a 2D plane, an equation of this plane is formulated in the image and world coordinates. Later, an intersection of any pixel point with this plane is determined. This intersection point is then converted to 3D coordinate with camera intrinsic parameters. These intersection points can be pixel locations of pedestrians or PIV displacements. More details of the approach can be found in [15].



(a) Landmark Points

(b) Perspective cells

Fig 2. Landmark points and cells used for image to world transformation

4. Experiments and Results

In this section, the results are presented for the numerical experiments undertaken in order to investigate the performance of the framework in real world application. In section 4.1, the dataset used for the study is presented. In sections 4.2 to 4.4, accuracy results are presented for velocity extraction, head counting and image-to-world coordinate transformation.

4.1 Dataset

As the paper title implies, the focus of the study is the Muslim event, the Hajj. The Sahn area of the Hajj constitute the gathering (Figure 3) where people move circularly around the kaaba (black building), this is called tawafs. The study focuses two different camera images. A sample frame from the second camera can be seen in Figure 3(a). These images are taken from Closed Circuit Television camera (CCTV) located at the facility. As part of the training and testing of the machine learning model, 600 image segments were manually annotated. Some annotations can be seen in Figure 3(b).

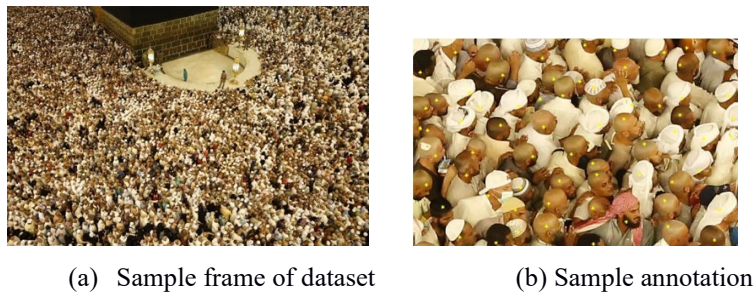


Fig 3. Sample frames of dataset and manual headcounting annotation

4.2 Velocity Extraction

The velocity vectors obtained from PIV processing of crowd images can be seen in Figure 4. Figure 4 (a) depicts the vectors of the entire image while Figures 4 (b) and (c) show vectors from two selected portions of Figure 4 (a). As can be seen from the magnified sections [Figure 4(b) and (c)] that the vectors are not streamlined. This is a result of high density. The predominant flow in this location is circular. However due to high density, some density waves appear that results in the chaotic patterns of the vectors.

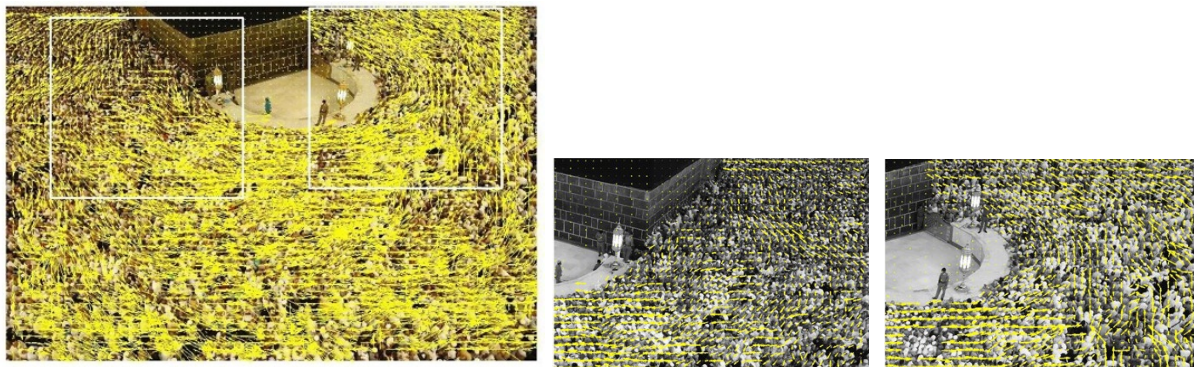


Fig 4. PIV velocity vectors of hajj crowds. Smaller images depict the vectors more clearly

To check the accuracy of the PIV velocity extraction, a number of methods have been undertaken. One of them is to manually track some random people at random locations of an image. In Table 1, the

results are listed for 6 random locations with PIV and manual tracking. It was found that the maximum error was about 16%.

4.3 Head counting Results

The head counting from images are needed to obtain density. In Table 2, the results are presented for the Machine Learning model vs the ground truth counts for 6 different images of both datasets. As can be seen from the table (Table 2) the countings are close to each other.

Table 1 PIV displacement and ground truth comparison

Actual dx (pixel)	PIV dx (pixel)	Actual dy (pixel)	PIV dy (pixel)	%Error
-3	-2.52	3	2.73	12.43
-3	-3.89	5	4.08	3.32
-8	-6.87	3	2.39	14.86
-5	-4.28	4	4.14	7.08
4	3.08	-2	-2.14	16.13
8	7.55	2	1.72	6.09

Table 2. Comparison between Machine Learning count and ground truth count

Test set number	Frame number	Machine Learning model count	Ground truth count	%Error
1	5	2949	2910	1.34
1	6	3024	3263	7.32
1	8	2981	2816	5.58
2	4	4449	4451	0.0004
2	10	4564	4686	2.60
2	20	4423	4729	0.6

As mentioned earlier in section 3.2, for head counting, the input image is being divided into 100 smaller sub images i.e. image cells [Figure 2(b)]. The Machine Learning model provides predictive counts for each of this smaller image cells. In Figure 5, the blue dots represent the predictive headcount from Machine Learning model while the error bars indicate difference between the ground truth counts and the predictive counts. It can be seen that from cells 0 to 50, the headcounts vary quite a bit. This is because of the camera angle (camera perspective). The effect diminishes in the cells from 50-99. However, Table 2 indicates that the cumulative counts are close to the ground truth counts. So, the perspective is not severely affecting the overall counts.

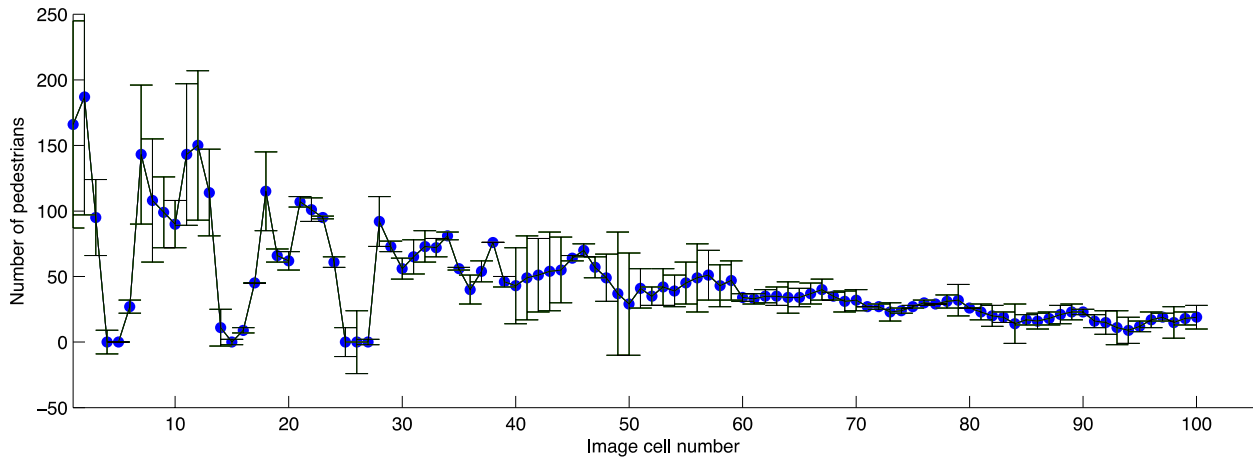


Fig 5. Machine Learning model and ground truth count difference for one test image

4.4 Coordinate transformation results

The results of this transformation process for 4 different coordinate points can be seen in Table 3. It can be seen that the projected points are not very far from the world coordinates.

Table 3. Comparison between transformed image coordinates (to world) and actual world coordinates

World x (m)	World y (m)	World z (m)	Projected x (m)	Projected y (m)	Projected z (m)	Difference in person width
1.77	15.35	0.0	2.54	14.65	0.0008	2.08
-1.84	15.40	0.0	-0.183	15.39	0.0008	2.02
5.85	-6.52	0.0	4.09	-6.31	0.0008	3.54
-4.27	5.52	0.0	-4.87	5.18	0.0008	1.37

4.5 Processing Time:

Compute time plays a key role in real-time processing applications. The framework outlined in this study has two components (PIV processing and Head counting) where timings are critical. To process two frames of the second dataset (Figure 3) took 32.79 seconds. The timing includes the PIV processing and head counting combined. The experiments are performed in a 4-core laptop with 1.8 GHz processor and 8 GB main memory. So, in terms of compute power requirement, the framework is not very demanding. However, as more cameras are incorporated in the processing, the demand for compute power will go up. GPU processing may offer a simple solution to this.

5. Application

When fundamental properties (density and velocity) of a crowd are known they can be incorporated into a fundamental diagram. Furthermore, they can also be used to obtain pedestrian distribution in future time. These applications are briefly explained in this section.

5.1. Fundamental Diagram

The fundamental diagram (speed vs density plot) for images from dataset 2 are shown in Figure 6. The fundamental diagrams are rare to find for high density flows considering the risks associated in conducting experiments in such conditions.

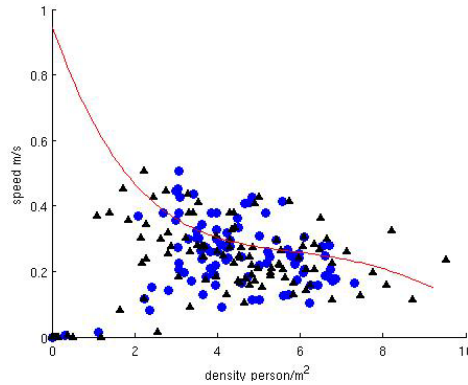


Fig 6. The fundamental diagram obtained from dataset 2 images. Blue dots are ground truth density and black triangles are predictive density. The solid line is from Predechenskii and Milinski [16]

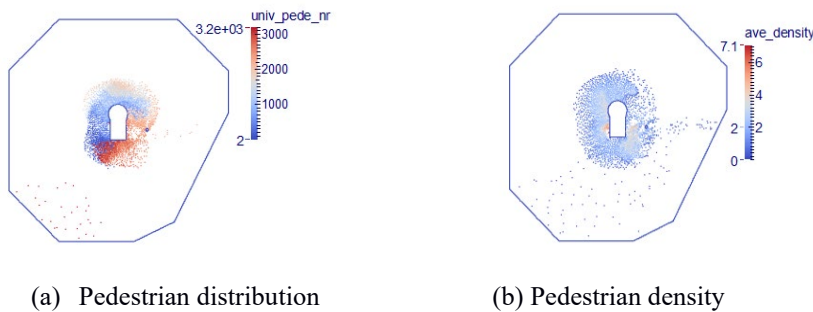
The proposed framework can provide as an alternative approach in obtaining empirical results for high density crowds. The fundamental diagram of Figure 6 also graphically outlines the difference of density values obtained from the Machine Learning model and ground truth counts.

5.2. Predicting Future State of Crowd

Microscopic models such as PEDFLOW [17] take pedestrian density and speed as input and can approximate pedestrian distribution at future times. The current framework can enable the microscopic models to approximate a more accurate distribution of pedestrians through a more accurate input. In Figure 7, three images of the Kaaba premises are shown that gives a whole 360-degree coverage of the facility. The PEDFLOW approximation of pedestrian distribution and pedestrian density at 4 seconds in future can be seen in Figure 8. Although the approach is currently in its infancy, such an application possesses a great promise in high density crowd monitoring and accident prevention.



Fig 7. Input images processed with PIV for speed and machine learning for density as input to PEDFLOW



(a) Pedestrian distribution

(b) Pedestrian density

Fig 8. The PEDFLOW simulation results at 4 secs in future

6. Conclusions and Outlook

The study addresses two critical challenges of high-density pedestrian traffic: real-time monitoring and estimation of future state (accident/congestion). In the case of real-time monitoring, the proposed PIV technique can be considered as a faster alternative of optical flow; while for future state estimation, the PEDFLOW model combined with inputs from PIV (speed) and machine learning model (density) provides a useful tool to the safety personnel managing/monitoring the crowd. The accuracy of the framework is reported for the crowd of Makkah. The main challenge lies in the scarcity of ground truth datasets in order to make the model more general. As of right now, there are only a handful of datasets for machine learning based crowd counting and their generalization ability is limited. An alternative to the scarcity of datasets could be to model individual crowd events separately and study them individually. This the route that the authors have taken in this study.

References

- [1] S. Almukhtar and D. Watkins, “How One of the Deadliest Hajj Accidents Unfolded,” *The New York Times*, 05-Sep-2016.
- [2] R. J. Adrian and J. Westerweel, *Particle Image Velocimetry*. Cambridge University Press 558, 2010.
- [3] B. Maurin, O. Masoud, and N. P. Papanikolopoulos, “Tracking all traffic: computer vision algorithms for monitoring vehicles, individuals, and crowds,” *IEEE Robot. Autom. Mag.*, vol. 12, no. 1, pp. 29–36, Mar. 2005.
- [4] S. Nedeveschi, S. Bota, and C. Tomiuc, “Stereo-Based Pedestrian Detection for Collision-Avoidance Applications,” *IEEE Trans. Intell. Transp. Syst.*, vol. 10, no. 3, pp. 380–391, Sep. 2009.
- [5] Z. Ma and A. B. Chan, “Crossing the Line: Crowd Counting by Integer Programming with Local Features,” *IEEE Conf. Comput. Vis. Pattern Recognit.*, vol. 1063–69/13, pp. 2535–2546, 2013.
- [6] H. Idrees, I. Saleemi, C. Seibert, and M. Shah, “Multi-source multi-scale counting in extremely dense crowd images,” in *Proceedings of the IEEE Conference on Computer Vision and Pattern Recognition*, 2013, pp. 2547–2554.
- [7] B. Lucas and T. Kanade, “An iterative image registration technique with an application to stereo vision,” *Proc. Int. Jt. Conf. Artif. Intell.*, pp. 674–679, 1981.
- [8] R. J. Adrian and C. S. Yao, “Development of Pulsed Laser Velocimetry (PLV) For Measurement of Turbulent Flow,” in *In Symposium on Turbulence*. X.B. Reed Jr., G.K. Patterson ed, 1984, pp. 170–184.
- [9] S. Vanlanduit, J. Vanherzeele, R. Longo, and P. Guillaume, “A digital image correlation method for fatigue test experiments,” *Opt. Lasers Eng.*, vol. 47, no. 3, pp. 371–378, 2009.
- [10] J. K. Sveen and A. E. Cowen, “Quantitative Imaging Techniques and Their Application to Wavy Flows, In PIV and Water Waves,” *World Sci.*, 2004.
- [11] M. Rossi, E. Esposito, and E. P. Tomasini, “PIV Application to Fluid Dynamics of Bass Reflex Ports,” in *Particle Image Velocimetry*, Springer, 2007, pp. 259–270.
- [12] N. Dalal and B. Triggs, “Histograms of oriented gradients for human detection,” in *Computer Vision and Pattern Recognition, 2005. CVPR 2005. IEEE Computer Society Conference on*, 2005, vol. 1, pp. 886–893.
- [13] J. H. Friedman, “Greedy function approximation: a gradient boosting machine,” *Ann. Stat.*, pp. 1189–1232, 2001.
- [14] M. Baqui, “Automated Monitoring of High Density Crowd Events,” 2018.
- [15] P. Dollár, *Piotr’s image and video Matlab Toolbox (PMT)*, <https://pdollar.github.io/toolbox/>. 2013.
- [16] V. M. Predtechenskii and A. I. Milinskii, *Planning for foot traffic flow in buildings*. National Bureau of Standards, US Department of Commerce, and the National Science Foundation, Washington, DC, 1978.

- [17] R. Löhner, “On the Modeling of Pedestrian Motion,” *Appl Math Model.*, vol. 34, no. 2, pp. 366–382, 2010.

A Case for Identity Hierarchies in Simulating Social Groups

Platt A.¹, Kneidl A.²

^{1,2}accu:rate GmbH

Rosental 5, Munich, Germany

ak@accu-rate.de; ap@accu-rate.de

Abstract – By considering previous empirical studies in group dynamics, modelling designs for pedestrian simulators and psychological and sociological theories of crowd behaviour, we briefly present a hierarchical, identity-based approach to simulating pedestrian social groups.

Keywords: Group modelling; Social identity; Simulation; Pedestrian modelling; Hierarchical structure

Social and emergent group behaviour in crowds has garnered enough attention that [1] present a review of research. The review provides a consolidation of and comment on empirical studies, most notably the prevalence of groups within crowds and some consistent phenomena: the ‘V-shape’ and the lower walking speed of groups compared to individuals (see e.g. [2], [3], [4] for further studies).

As with any simulation practice however, there is a struggle between empirical intricacy (in a universe of infinite parameters) and programmatic simplicity. There is strong evidence that heuristics robustly map cognition to action¹, see [5] who suggest cognitive heuristics do not seek optimality but sufficiency through the use of an “*adaptive* [heuristic] *toolbox*”. These ideas have been proposed and discussed extensively by [6] (also [11]). They hierarchically structure their heuristics, based on the concept of least-effort (e.g. [7, 8]). That is, heuristics are attempted successively; the heuristic of least effort is attempted first, then the second, until some goal is realized or postponed. In this way, environmental stimuli cause *implicit* changes in agent behaviour as a direct result of ‘cognitive’ functions. This approach lends itself to tackling emergent lane formation (e.g. [10]) and other phenomena where environmental conditions alter behavioural motives (as appose to environmental conditions directly acting on agents).

Exploiting and deriving heuristics, and even hierarchical heuristic toolboxes, is paramount to developing a meaningful group model. The questions for practitioners are: “*what kind of information is used by the pedestrian?*” and “*how is this information processed to adapt the walking behavior?*” [11].

The Social Identity Model of Deindividuation Effects (SIDE) may provide assistance. SIDE presents an agent with one or more social identities and a personal identity, each of which influences to a greater or lesser extent the behaviour of the agent [13]. SIDE traces its routes to observations in emergent, antisocial behaviour in crowds and mass gatherings (e.g. [14])², however the conceptual distinction between social and personal identities seems both theoretically plausible (given its allegiance to the well-established social categorization theory [15]) and pragmatically useful. [16] already consider such identities to model helping behaviour amongst strangers during emergencies. However, we propose that it is SIDE’s emphasis on the *salience* of social and personal identities, and the resultant *partial*-deindividuation (employed here as shared behavioural approaches) that should also be utilized in social group models.

As noted in the literature (e.g. [2], [3], [4]), group behaviour is dependent on both intrinsic properties of an agent: sex, age and mobility, and extrinsic properties of the group’s relationship: family vs. friends, male friends vs. female friends etc. By considering an agent’s personal and social identities, and hierarchically structuring these identities, such factors may be more easily confronted.

¹ In fact, [12] suggests analogies are used before-the-fact; we anticipate how things might be based on previous, analogous “patterns and statistical regularities”, before marrying our anticipations to reality. Use of such analogies and “context frames” could be considered, in an admittedly loose sense, heuristic-based perception (as an extension to heuristic-based action).

² This is pertinent given [17]’s research report; evidently caution should be taken in determining social (identity) norms.

In introducing personal and social identities to agent-based modelling, two main questions arise. First: under what circumstances do these identities manifest? That is, what is the salience of a particular identity at any one time? (There are critiques of SIDE that particularly target its abstract notion of anonymity [18]). Second: in what manner do social and personal identities manifest within the agent? We consider only this second obstacle, in the hope that the first is, if not solved, less elusive.

As described in the PECS architecture [19], to adequately represent cognitive mechanisms, perceptions must be filtered, and internal states retrieved. Each agent is prescribed one or more identities. At time-step t , the identities filter environmental input and are measured for their salience. The motivations and goals of each identity are then retrieved (representing the internal states of an agent). Via some weighting procedure, the motivation or goal most pertinent to the agent at t is selected as action determining, and the relevant heuristic toolbox then employed (see Fig. 1). (Note that people’s differing “self-motion cues” and cognitive maps [e.g. 21, 22], and given the ‘many-motivations, one goal; many-goals, one motivation’ phenomenon [20], means motivation must be addressed separately to goal-pursuance.) It is this weighting procedure, we propose, that could unveil the nuances of group behaviour.

At a finer level, the specific effects of social and personal identity variables are open to investigation. [1] present some of the latest methodologies, in particular, the popular communication heuristic prescribed by [9]. We may also consider the empirical investigation of [23], which suggests an ellipse of minimum area shapes groups. [24] suggest a distinction between in-group cohesion and in-group sociality. Considering cohesion independently allows us to introduce agents’ personal (identity) and social (identity) space requirements, e.g. [25]. Whilst [26] set-out a means of in-group imitation by considering Social Comparison Theory: in our context, certain identities are shared or copied amongst in-group members. Note also that by deriving variables that traverse social and personal identities, the salience of a specific identity at any one time will bear no influence on an agent’s base-level functioning. In any case, the modular framework prescribed by [6] should include empirically reflective heuristics that manage the wishes of distinct and interactive agent identities.

In attempting to simulate pedestrian behaviour, practitioners have struggled to encompass the widely varying and deeply complex dynamics of social groups. It is hoped this identity-based approach could aid future projects in binding many available methodologies and theories in group dynamics modelling.

This work was funded by the German Federal Ministry of Education and Research through the project S2UCRE.

References

- [1] Cheng L, Yarlagadda R, Fookes C, Yarlagadda P (2014) A review of pedestrian group dynamics and methodologies in modelling pedestrian group behaviours. World Journal of Mechanical Engineering Vol. 1(1), pp. 002-013.
- [2] Costa M (2009) Interpersonal Distances in Group Walking. J Nonverbal Behav (2010) 34:15-26
- [3] Feng Y, Dewei L (2016) An Empirical Study and Conceptual Model on Heterogeneity of Pedestrian Social Groups for Friend-group and Family-group. Pedestrian and Evacuation Dynamics 2016, Collective Dynamics pp. 402-407

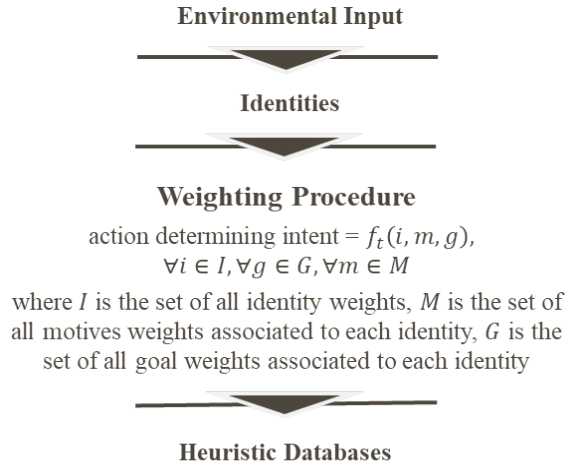


Fig.1: Environmental stimuli influence an agent’s prescribed identities. They alter the salience of each identity’s motives and goals. A weighting procedure (function f) determines over all motives and goals which is the most influencing, and thus which heuristic (toolbox) to employ.

- [4] Zanlungo F, Yücel Z, Brščić D, Kanda T, Hagita N (2017) Intrinsic group behaviour: Dependence of pedestrian dyad dynamics on principal social and personal features. *PLoS ONE* 12(11): e0187253
- [5] Gigerenzer G (2008) Why Heuristics Work. *Perspectives on Psychological Science*, Vol. 3, No. 1.
- [6] Seitz M, Bode N, Köster G (2016) How cognitive heuristics can explain social interactions in spatial movement. *Journal of Royal Society Interface*, August 2016, vol. 13, Issue 21, DOI:10.1098/rsif.2016.0439
- [7] Shah A, Oppenheimer D (2008) Heuristics Made Easy: An Effort-Reduction Framework. *American Psychological Association, Psychological Bulletin*, 2008, Vol. 134, No. 2, 207–222
- [8] Garbarino E, Edell J (1997) Cognitive effort, affect, and choice. *J. Consum. Res.* 24, 147–158
- [9] Moussaïd M, Perozo N, Garnier S, Helbing D and Theraulaz G (2010) The walking behaviour of pedestrian social groups and its impact on crowd dynamics. *PLoS ONE* 5(4): e10047
- [10] Helbing D, Buzna L, Johansson A, Werner T (2005) Self-Organized Pedestrian Crowd Dynamics: Experiments, Simulations, and Design Solutions. *Transportation Science* 39: 1-24
- [11] Moussaïd M, Helbing D, Theraulaz G (2011) How simple rules determine pedestrian behavior and crowd disasters. *PNAS* April 26, 2011. 108 (17) 6884-6888
- [12] Bar M (2007) The proactive brain: Using analogies and associations to generate predictions. *Trends in Cognitive Sciences*, Volume 11, Issue 9, September 2007, pp. 372
- [13] Reicher S, Spears R, Postmes T (1995) A Social Identity Model of Deindividuation Phenomena. *European Review of Social Psychology* 6(1):161-198
- [14] Reicher, S. D. (1984a). The St. Pauls riot: an explication of de limits of crowd action in terms of a social identity model. *European Journal of Social Psychology*, 14, 1–21
- [15] Turner J, Ontaro R (1999) The psychology of the social self: Social identity, personality and the self-concept: A self-categorization perspective, Chapter 1. *Psychology Press, Taylor and Francis Group*
- [16] Sivers I, Templeton A, Köster G, Drury J, Philippides A (2014) Humans do not always act selfishly: social identity and helping in emergency evacuation simulation. *Proceedings of Conference on Pedestrian and Evacuation Dynamics 2014, Transportation Research Procedia* 2 585-593
- [17] Drury J, Cocking C (2007) The mass psychology of disasters and emergency evacuations: A research report and implications for practice
- [18] Moral-Toranzo F, Canto-Ortiz J, Go´mez-Jacinto L (2005) Anonymity effects in computer-mediated communication in the case of minority influence. *Computers in Human Behavior* 23 (2007) 1660–1674
- [19] Schmidt B (2001) Modelling of Human Behaviour: The PECS Reference Model. *AAAI Technical Report FS-01-02*
- [20] Kielar P, Handel O, Biedermann D, Borrmann A (2014) Concurrent hierarchical finite state machines for modeling pedestrian behavioral tendencies. *Transportation Research Procedia* 2 (2014) 576 – 584
- [21] Golledge R, Jacobson R, Kitchin R, Blades M (2000) Cognitive Maps, Spatial Abilities, and Human Wayfinding. *Geographical Review of Japan* Vol. 73 (Ser. B), No. 2, 93-104, 2000
- [22] Etienne A, Jeffery K (2004) Path Integration in Mammals. *HIPPOCAMPUS* 14:180 –192
- [23] Krüchten C, Schadschneider A (2007) Empirical study on social groups in pedestrian evacuation dynamics. *Physica A: Statistical Mechanics and its Applications*, vol. 475, pp. 129-141
- [24] Jaklin N, Kremyza A, Geraerts R (2015) Adding Sociality to Virtual pedestrian Groups. *Proceedings of Conference: 21th ACM Symposium on Virtual Reality Software and Technology*
- [25] Frohnwieser A, Hopf R, Oberzaucher E (2013) Human Walking Behaviour – The Effect of Pedestrian Flow and Personal Space Invasions on Walking Speed and Direction. *Human Ethology Bulletin* 28 (2013):3 20-28, Brief Reports
- [26] Fridman N, Kaminka G (2007) Towards a Cognitive Model of Crowd Behavior Based on Social Comparison Theory. *Proceedings of the 22nd national conference on Artificial intelligence – vol. 1* pp. 731-737

A new framework for high-resolution pedestrian data processing using rule-based algorithms and real-time alarm systems

Michael Moos¹, Basil Vitins², Mirwais Tayebi³,
Lukas Gamper⁴, Julia Wysling⁵, Uri Schtalheim⁶

^{1,2,3,4,5,6}ASE AG
Zurich, Switzerland
michael.moos@ase.ch

Abstract - Pedestrian flows and densities have increased in recent years within transport-related public facilities such as train stations, as well as in private buildings such as shopping centers, event halls or convention centers. Increasing flows and high densities often raise comfort, safety, operational and delay issues; and therefore, require pedestrian flow optimization, intervention or even revised regulation. Recent technological advances enhanced pedestrian sensing; however, they disregard adaptive data capture, processing, and strategic communication within reasonable time, or real-time, such as tactic occupancy or density alarms trigger rules. Content of this research is twofold. First, new data capturing and processing advances of recent technological developments are combined in an integral software and hardware-based framework. Second, applied methods highlight projects and experiences on both pedestrian research and on existing and operating pedestrian facilities. Based on the described, two-sided approach, proposed framework is able to fulfil high safety and comfort standards of facilities such as train stations, retail facilities or event halls. In this research, past semi-automatic video analysis processing of pedestrian behavioral studies is replaced with combined sensor and data processing system within proposed framework. In train stations of major operators, real-time pedestrian observation increases safety levels on station platforms. Tactic algorithms and alarm trigger schemes enable on-time surveillance, e.g. at overcrowded floor levels in shopping centers for escalator or door closure. Sensor data is used to train models for underpass pedestrian flow regarding path choice and fundamental diagram. In retail, queue length, trajectory analysis and floor occupancy are determined for economic, comfort as well as safety evaluation. Using trajectory classification, movement and dwell time is analyzed for staff and visitors separately (see Figure 1).

Keywords:

Video Analysis, Realtime Monitoring, Alarming, Model Calibration, Trajectory Classification

1. Introduction

Recent population growth in many countries increase densities in public spaces such as public transportation and its demands; e.g. London already has special schemes for their underground lines such as temporarily closed stations for boarding passengers. Technological developments have enabled sensing for precise movement captures, including fast data processing such as image recognition. Infrastructure operators require reliable sensing technologies and highly aggregated and selected data to provide security, comfort and functionality to their infrastructure. Infrastructure usage increases and demand gets closed to the limits.

There is a gap recognized between sensing technologies with their large and raw data output, and corresponding evaluation and application requiring aggregated data for end users. The goal of this study is therefore a generic framework proposition to cover such high and specialized requirements. The framework is adaptive in areas, environments (indoor, outdoor) and relies on generic data capturing, processing and visualization chain. New advance in sensing can therefore be used for operation purposes.

2. Data Capturing

Various technologies capture pedestrian movements. Most relevant technologies rely on video analysis, laser sensing, WiFi and Bluetooth signal detection. Video and laser rely on light waves and can capture precise images. In comparison to image processing, WiFi capturing is less adequate, since often only about 20% and 40% of all persons carry at least one active WIFI device. For indoor applications, video-based sensors are the most established while in outdoor applications, laser-based sensors have advantages, especially with little ambient light or weather-related influence. For indoor and outdoor, sensors are usually mounted on the ceiling for vertical detection to increase precision. This strategy is important, especially in situations with high densities where pedestrians are hidden between each other (example see Figure 1).

Pedestrian sensing can mainly be divided into 3 categories. Initially, pedestrian analysis was limited in counting persons crossing a virtual counting line. Later, area-based measurement evolved for advanced evaluations. By defining not just a virtual line, but a virtual area, many more applications became possible like waiting time or queue length in certain, user-defined areas (rectangles). In recent years, sensors were developed which were capable to record trajectories, enabling precise person tracking.

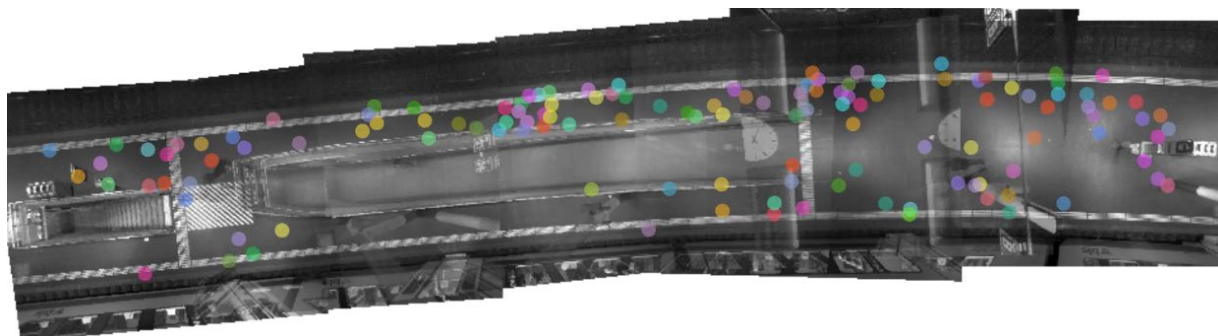


Figure 1. Example top-down view of a video based pedestrian sensor. The image shows waiting travelers on a swiss railway platform. The goal of this application is the evaluation of passovers of the white barrier line.

3. Applications

3.1 Real-Time Monitoring

In real-time monitoring, a dashboard with all necessary information is often used for analysis. Dashboards are synchronized with live measurements from sensor protocols. A parallel running, permanent system control is essential for reliability. Notifications must appear immediately in case of component failure or irregularities. Depending on the sensing area, dangerous pedestrian situations (e.g. high densities) not only require a dashboard for overview but also the possibility of alarming staff using text messages or internet capable devices. In recent years, many such devices have been released like smart light bulbs or speakers. Pedestrian data are essential to many IoT applications requiring efficient data processing. These not only apply on security but also the signaling for staff, when large queues arise in sales. Using rule-based algorithms, customized thresholds are defined for alarm and notification triggering.

3.2 Analytics

Major challenge in analytics includes information extraction and processing from large-scale raw data. Often, aggregation becomes essential regarding time and space. While aggregation is trivial for frequency-based information (e.g. time series), aggregation of combined space and time-related information is more demanding (e.g. dwell time) and often not well-defined. Trajectory-based data even allow many more possibilities like trajectory classification and origin-destination extraction. Figure 2

shows an example of trajectory classification. Movement and dwell time is analyzed separately for staff and visitors, leading to new insights at the planning of store layouts. In this example, trajectories were classified regarding the position of origin and termination.

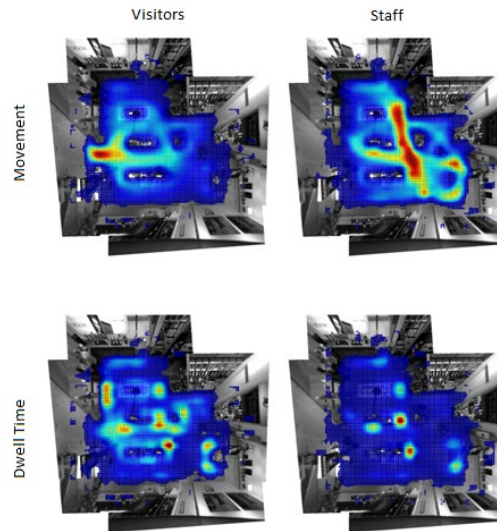


Figure 2. Using trajectory classification, movement and dwell time is analyzed for staff and visitors separately.

3.3 Flow Models

Data monitoring for pedestrian movement can be costly for complete floor area coverage. Necessary measurements can be drastically reduced when adding pedestrian flow models. This approach is most effective in transport applications like train stations, where shortest path assumptions apply. In all situations, high-resolution pedestrian data is crucial in model calibration. Data capturing and model calibration are used iteratively for high reliability in pedestrian flow prediction.

5. Conclusion

In the previous decade, image processing and sensing technologies were the most challenging subject in pedestrian movement analysis. Today, these issues have mostly been solved. With that, the extraction of information from data has become the most essential part in the area.

The proposed framework closes existing gaps between the raw data output of high-end sensing technologies and the required information by the wide range of end users. Key strategy is the two-sided approach of real-time monitoring for instant notification and intelligent data aggregation and visualization for long term analytics. With the proposed framework, a wide range of possible applications are covered not only for researchers but also management.

References

- [1] J. Thureau, J. Van den Heuvel, M. Ofwegen, N. Keusen and S. Hoogendoorn „Influence of pedestrian density on the use of the danger zone at platforms of train stations”, Conference on Traffic and Granular Flow, Washington DC, July 2017.
- [2] D. Helbing and A. Johansson “Pedestrian, Crowd and Evacuation Dynamics”, Encyclopedia of Complexity and Systems Science, vol. 16, pp. 6476-6495, 2010.
- [3] T. Kretz, “Pedestrian traffic: on the quickest path”, J.Stat. Mech. Theor. Exp., vol. 03, pp. 1-13, 2009.
- [4] A. Johansson, D. Helbing and P.K. Shukla, “Specification of the social force pedestrian model by evolutionary adjustment to video tracking data”, Adv. Compl. Syst., vol. 10, pp. 271-288.
- [5] S. Buchmueller and U. Weidmann, Parameters of pedestrians, pedestrian traffic and walking facilities, Schriftenreihe, vol. 132, ETH Zurich, 2007.
- [6] D. Duives, W. Daamen and S. Hoogendoorn “Quantification of the level of crowdedness for pedestrian movements”, Physica A Stat. Mech. Appl., vol. 427, June 2015.

Agent Based Modelling and Simulation of Pedestrian Crowds in Panic Situations

Mohammed M. Alrashed & Jeff S. Shamma

King Abdullah University of Science and Technology (KAUST)
Computer, Electrical and Mathematical Science and Engineering Division (CEMSE)
Thuwal, Saudi Arabia 23955-6900
mohammed.alrashed@kaust.edu.sa jeff.shamma@kaust.edu.sa

Abstract - The increasing occurrence of panic stampedes during mass events has motivated studying the impact of panic on crowd dynamics. Understanding the collective behaviors of panic stampedes is essential to reducing the risk of deadly crowd disasters. In this work, we use an agent-based formulation to model the collective human behavior in such crowd dynamics. We investigate the impact of panic behavior on crowd dynamics, as a specific form of collective behavior, by introducing a contagious panic parameter. The proposed model describes the intensity and spread of panic through the crowd. The corresponding panic parameter impacts each individual to represent a different variety of behaviors that can be associated with panic situations such as escaping danger, clustering, and pushing. Simulation results show contagious panic and pushing behavior, resulting in a more realistic crowd dynamics model.

Keywords: Pedestrian crowd simulation; Agent based models; Multiagent systems.

1. Introduction

The rising frequency of mass events has led to an increase in the risk of crowd stampedes. Despite the tremendous effort of authorities, critical situations keep recurring. The lack of understanding of panic within stampedes still causes hundreds of fatalities each year, not to mention the scarce methodical studies of crowd panic behavior. In crowd stampedes, panic is an essential factor that influences crowd behavior. Panic contagion is a type of herding behavior, where panicking individuals tend to cause social contagion and lead to jamming and life-threatening overcrowding [4, 5]. Moreover, biological studies indicate the role of panic in the change of human reactions, decision-making, and behaviors [2].

Motivated by these circumstances, we develop an agent-based model that uses a panic parameter that can be contagious among pedestrians to influence their behaviors. Furthermore, we introduce aggressive pushing behaviors that cause body collisions and stampedes. The model can simulate the motion of pedestrians and reproduce observed features of crowd dynamics such as lane formation, oscillations at bottlenecks, dynamics at intersections, and transition to uncoordinated movement due to clogging. Moreover, the model can include panic contagion among pedestrians, where the value of the panic parameter of one agent is impacted by the panic parameter value of other nearby agents in a dynamic manner. A direction for future work is the degree to which this model represents actual panic in a crowd through verification and validation to real data of crowd panic behavior.

2. Methods

Pedestrian crowd dynamics are generally predictable in high-density crowds where pedestrians cannot move freely. Thus pedestrian crowd dynamics give rise to self-propelling interactions between pedestrians. Although every pedestrian has personal preferences, the motion dynamics can be modelled as a social force in such crowds [1]. These forces are representations of internal preferences and objectives to perform certain actions or movements.

The proposed model will be presented as an extension of the work in [1]. It uses a blend of physical forces and socio-psychological factors to simulate crowd dynamics. Our goal is to introduce contagious panicking and pushing behavior by introducing proportional–integral dynamics, based on control theory, and a panic parameter with contagion.

In our model, every agent has P_i as a panic parameter, whose value ranges from zero to one. The initial value for panic parameter is always zero. However, it increases because of external stimuli in the surrounding environment. The value of the panic parameter is also impacted by the neighboring agent. The spread of panic is modelled as follows:

$$P_i^+ = c_i \left(z_i P_i + \sum_{j \in r_{si}} P_j w_j \right) + (1 - c_i) Q_i \quad (1)$$

where c_i is a constant that represents relative weight of the environment effects versus social influence. Similarly, w_j is a constant used to weigh the panic influence caused by the agents in the neighboring area of agent i , defined by a circle centered at the position of the agent with radius r_{si} . The constant z_i represents personal confidence in an agent's own judgment of the situation. In other words, $1 - z_i$ represents the amount of influence by the other agents in the vicinity of agent i , where $\sum_{j \in r_{si}} w_j + z_i = 1$, and Q_i is a variable representing external stimuli in the surrounding environment such as fire or smoke, life-threatening overcrowding, power outage in a crowded public site.

Our proposed model builds on the microsimulation Helbing model from [1]. To introduce aggressive pushing behaviors to the Helbing model, we added auxiliary states in order to overcome repulsive interaction forces. We propose the following acceleration equation:

$$\frac{dv_i}{dt} = u_i + \frac{1}{m_i} (\sum_{j(\neq i)} f_{ij} + \sum_w f_{iw}) \quad (2)$$

$$u_i = k_{Pi} e_i + f(P_i) \cdot k_{Ii} \int_0^t e_i dt \quad (3)$$

where repulsive interaction forces f_{ij}, f_{iw} keep a separating distance from other pedestrian's, j , and walls, w ; $e_i = v_i^0 - v_i$ represents the error between the desired velocity, v_i^0 , and the actual velocity, v_i ; and m_i is mass. The function $f(P_i)$ is an increasing function of the panic parameter and weighs the effect of the cumulative integrator action. The increase of $f(P_i)$ leads to the increase in following the desired velocity and hence the behavior to push and to cross the crowd. The constants k_{Pi}, k_{Ii} are agent proportional–integral controller parameters. It is also possible to have parameters such as maximum and nominal velocity depend on panic as well [3]. The proportional and integrator constants reflect the strength of the agent. In other words, they represent how fast an agent change its states: the bigger the constant, the faster the change. However, the interaction forces will be kept unchanged as in the Helbing model.

3. Results and Discussion

The introduction of contagious panic has a significant impact on crowd dynamics. A simulation of a fire evacuation of 400 agents in two connecting rooms was conducted in order to explore the effect of panic in the crowd dynamics as a specific form of collective behavior (see Figure 1). We used the fire and spreading smoke in the left room as the environmental source of panic Q_i . The simulation result shows panic spreading over to the crowd in the right room causing transition to uncoordinated movement due to pushing behavior at the exit. The stampede at the exit causes significant delay in the evacuation time and leads to a greater number of casualties. Video of the simulation is available at [6].

The simulation results shows panicking agents tend to push other agents to increase their chance of survival or to open ways among the crowd. To explore the effect of the added auxiliary states and for the sake of comparison, a simulation of 50 agents in a closed room is conducted both for our model and the Helbing model. In the simulation, one agent (we will refer to it as agent-red) tries to push other agents in its way in order to cross the crowd, while the other 49 agents try to maintain their positions. The environmental source of panic parameter Q_i is fixed to zero for all agents, as well as c_i for all the agents, which means that panic from agent-red is not contagious. For the Helbing model, pushing behavior is described by increasing the desired velocity. Therefore, the maximum desired velocity of 10 m/s was given to agent-red. The simulation shows that agent-red was unable to cross the crowd, although the other agents are not pushing. On the other hand, the proposed model was able to exhibit new pushing behaviour by introducing panic-dependent integrator action. Furthermore, for the same simulation agent-red with panic parameter fixed equal to one was able to cross the crowd, although it was given a desired velocity of only 5 m/s. The simulation results are available as video at [6].

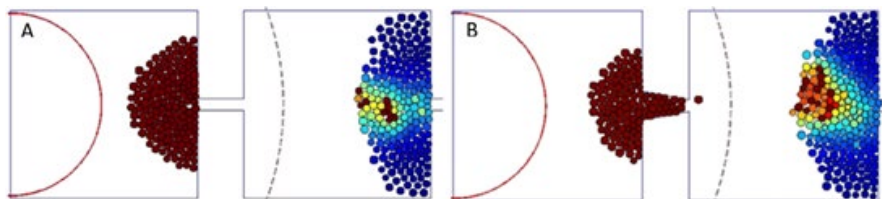


Fig. 1: Panic spreading over to the crowd in the second room.
(A) Zero degrees angle corridor, (B) 10 degrees angle corridor.

We can improve the safety of buildings and facilities by optimizing the boundaries in order to improve the pedestrian flows. Bottleneck boundaries influence pedestrian flows in a crucial way and we can improve the flows by smoothing corners and using funnel shapes. Our objective was to investigate the optimal angle of the funnel shape (see Figure 1). An evacuation simulation of 200 agents with fixed door size and different corridor angles from zero to thirty-five was used to determine an optimal angle. The simulation showed that pressure localization depends on corridor angle. As the angle increases, the pressure moves from the entrance of the corridor to the exit. For the corridor with zero angle, we can see the pressure on an agent in the entrance of the corridor is high. On the other hand, for the corridor with the angle of thirty we can see the pressure on the agent in the exit of the corridor is very high. The results of this simulation show a significant improvement in evacuation time and reduction in the pressure can be achieved by using corridor angle of 10 degrees. The simulation results are available as video at [6].

Acknowledgements

The research reported in this publication was supported by funding from King Abdullah University of Science and Technology (KAUST).

References

- [1] D. Helbing, I. Farkas, and T. Vicsek, “Simulating dynamical features of escape panic.” *Nature*, vol. 407, no. 6803, pp. 487–490, Sep. 2000.
- [2] M.A. Staal, “Stress, Cognition, and Human Performance: A Literature Review and Conceptual Framework”, Ames Research Center, Moffett Field, California, NASA/TM—2004–212824.
- [3] M. Alrashed, *Agent Based Modelling and Simulation of Pedestrian Crowds in Panic Situations*, (master dissertation) KAUST.

- [4] Bosse, Tibor, et al. "Agent-based analysis of patterns in crowd behaviour involving contagion of mental states." International Conference on Industrial, Engineering and Other Applications of Applied Intelligent Systems. Springer, Berlin, Heidelberg, 2011.
- [5] Elzie, Terra, et al. "Panic that spreads sociobehavioral contagion in pedestrian evacuations." Transportation Research Record: Journal of the Transportation Research Board 2586 (2016): 1-8.
- [6] https://www.youtube.com/channel/UCXPNS0in-q2-JFyT3vz_Nnw/videos

Application of Ensemble Kalman Filter to Pedestrian Flow

Fumiya Togashi¹, Takashi Misaka², Rainald Löhner³, Shigeru Obayashi⁴

¹Applied Simulations Inc.

10001 Chartwell Manor Cr., Potomac, MD 20854, USA

fumiya.togashi@gmail.com

²Frontier Research Institute for Interdisciplinary Science, Tohoku University

2-1-1 Katahira, Aoba-ku, Sendai 980-8577, Japan

misaka@edge.ifs.tohoku.ac.jp

³George Mason University

4400 University Dr., Fairfax, VA 22030, USA

rlohner@gmu.edu

⁴Institute of Fluid Science, Tohoku University

2-1-1 Katahira, Aoba-ku, Sendai 980-8577, Japan

obayashi@ifs.tohoku.ac.jp

Abstract - We adopted the Ensemble Kalman Filter (EnKF) methodology in our computational simulation code for pedestrian flows. The EnKF, which is a type of data assimilation methodology, has been developed in the field of weather forecast where the atmospheric condition varies hour by hour. The EnKF estimates the parameters or boundary/initial conditions in the numerical model based on the updated measured data. We considered the EnKF a promising tool for the simulation of pedestrian flows, which are notoriously difficult to predict. In this study, two scenarios were conducted to confirm the usefulness of the EnKF. The first case was unidirectional pedestrian flow in straight corridors, and the second case was Mataf scenario at the Kaaba in Mecca. Needless to say, the second scenario was very challenging because of the number of pilgrims and the degrees of freedom. In each scenario, we conducted the numerical simulation using the original parameter set and then applied the EnKF to improve the accuracy of the simulation.

Keywords: Computational Crowd Dynamics, Ensemble Kalman Filter, Data Assimilation, Pedestrian flow

1. Introduction

During the past decade, research on pedestrian and traffic flows has attracted a lot of attention [1, 2]. With the aid of supercomputers, one can consider a large number of scenarios in a short period of time. However, human behavior has individual variability, so typical models end up having many empirical parameters. Generalization of these parameters, which determine the human behavior that is ultimately simulated, could be very challenging to determine as they vary depending on circumstances (age group, cultural characteristics, etc.). The aim of the present study is to determine these parameters in an efficient and automatic way from experiments. One promising candidate for such an automatic parameter estimation is the Ensemble Kalman Filter (EnKF) methodology [3, 4]. In this study, our objective is to confirm the usefulness of the EnKF in estimating the proper parameters based on the updated observation data (see [7] for a detailed description).

2. Ensemble Kalman Filter (EnKF)

EnKF is a type of sequential data assimilation methodology which has been developed from the Kalman Filter [5]. In the Kalman Filter, the model is integrated forward in time and, whenever the observation data become available, it is used to update the model prediction before the integration continues. The methodology is often used in the field of weather forecast. The detail of implementation can be found in many references [3, 4].

3. Application of EnKF and Result

In this study, the experiment of unidirectional flow in straight corridors was utilized as the observation data. A total of 28 runs were performed in corridors with widths of 1.8m, 2.4m, and 3.0m. The details of exit and entrance width in the experiment setting can be found in ref [6]. Figure 1 shows the snapshots from the experimental run. In the experiment, averaged pedestrian density, velocity in the corridors, and evacuation time (time until the last pedestrian reached the exit) were measured. Numerical simulations were conducted for all 28 runs. Figure 2 shows the blueprint of the numerical simulation and the computed result. The pedestrians are represented by the dots in the numerical simulation. The comparisons of the evacuating time between the experiment (green) and the computations (blue) are shown in Figure 3. The focus was on improving the input parameters for the worst case: run 28.

EnKF was applied to improve 8 empirical parameters, namely, desired pedestrian velocity, variability of velocity, relaxation time to achieve desired velocity, variability of relaxation time, variability of pedestrian radius, pushiness (min/max), and comfort zone. The measured pedestrian density and velocity were utilized as the observation data for EnKF. 20 parameter sets were prepared as the initial ensemble members. The total computational time was a few hours using a laptop, or about 7 minutes using 576 cores of the SGI ICE X system. The filtering processes took a few seconds.

After applying EnKF, the new parameter set was applied to all 28 cases. The evacuation time comparisons of all runs were shown in Fig. 3 as red dots. Remarkably, using the new parameters improved the computed evacuation times for all of the runs.

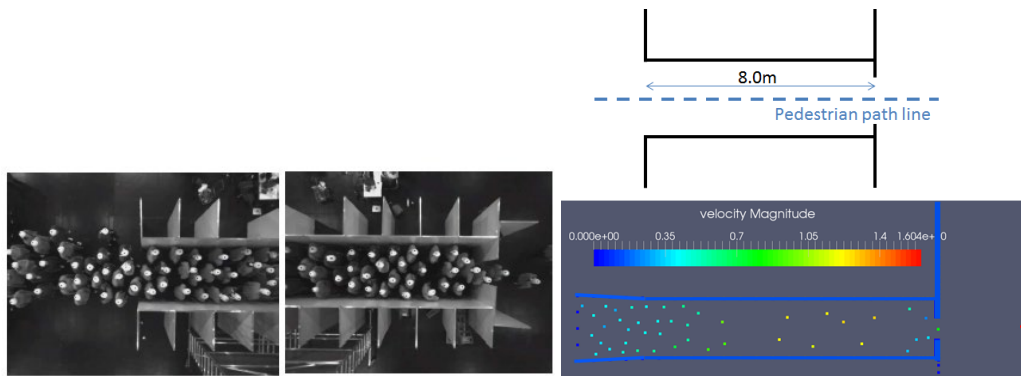


Fig. 1: Left: Snapshots from one run of the experiment. Fig. 2: The blueprint and snapshot of the numerical simulation

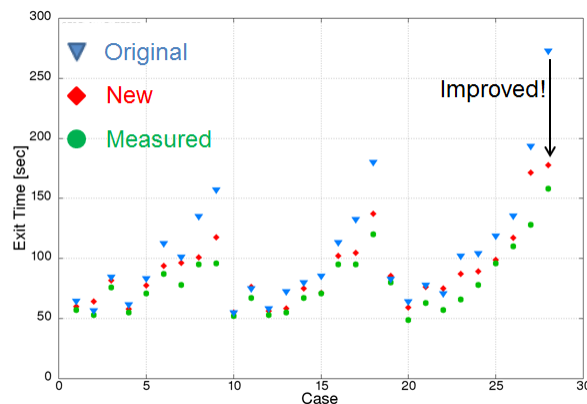


Fig. 3: Comparison of evacuating time of all 28 runs between the experiment (green) and the computed results using the original parameters (blue), and using the estimated parameters (red)

4. Mataf at the Kaaba in Mecca

In the second case, the real observation data of pilgrims around the Kaaba was utilized to improve the accuracy of the numerical simulation. In addition to the 8 parameters which were handled in case 1, two more parameters were added for improvement: the pilgrim's will force and tolerance to high densities. 32 parameter sets were prepared as the initial ensemble members. The total computational time was about 20 hours using 576 cores of the SGI ICE X system. Figure 7 shows the snapshot of the numerical simulation using the estimated parameter set by the EnKF and the comparison of the pilgrim density along the distance from the Kaaba for the observation, the computed result using the original parameter set, and the computed result using the estimated parameter set. The computed result using the estimated parameter sets by the EnKF shows an excellent agreement with the observation.

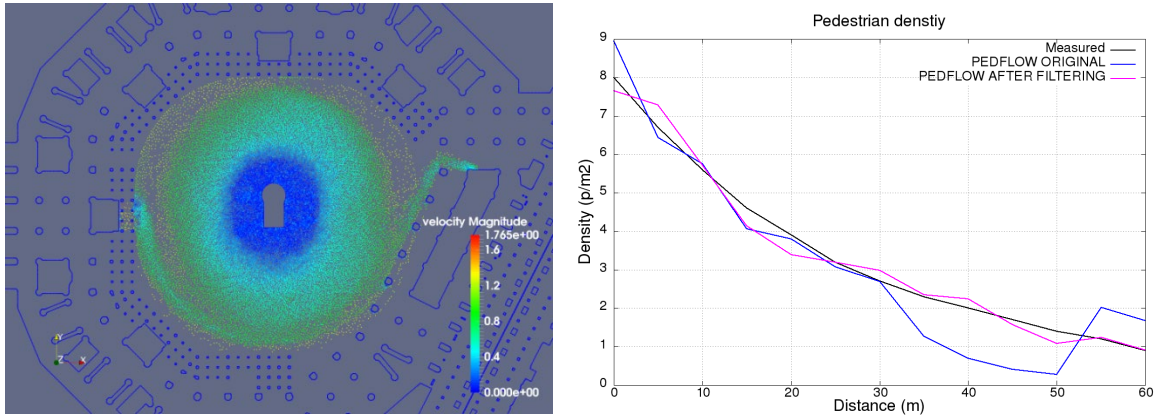


Fig. 6: (Left) Snapshot of the numerical simulation of pilgrims around the Kaaba using the new parameter set. (Right) Comparison of the pilgrim density along the distance from the Kaaba between the observation (black) and the computation using the original parameter set (blue), and the computation using the estimated parameter set (magenta)

5. Conclusion

EnKF was applied to estimate the empirical parameters required by the pedestrian and crowd dynamics simulation code PEDFLOW [7]. The new runs using the estimated parameter set provided much closer results to the experimental data than the results using the original parameters.

The advantage of the EnKF is the capability of dynamically utilizing the observation data. Parameters, initial conditions, and boundary conditions are updated whenever the new observation data is available. Thus the accuracy of the numerical simulation keeps improving along the environmental conditions such as season, weather, time, temperature, etc.

The application of EnKF to pedestrian flow simulation will be a useful approach for future pedestrian flow simulations.

References

- [1] The Conference on Pedestrian and Evacuation Dynamics, a biannual Conference; 2016 edition was in Hefei, China; see (W. Song, J. Ma and L. Fu eds.), University of Science and Technology Press, Hefei, China (2016).
- [2] Helbing, Dirk, et al. "Simulation of pedestrian crowds in normal and evacuation situations." *Pedestrian and evacuation dynamics* 21.2, pp. 21-58, 2002
- [3] E. Kalnay, "Atmospheric Modeling, Data Assimilation and Predictability," New York: Cambridge University Press, 2003
- [4] G. Evensen, "The ensemble Kalman filter: Theoretical formulation and practical implementation," *Ocean Dynamics* 53, pp. 343-367, 2003

- [5] Kalman, Rudolph Emil. "A new approach to linear filtering and prediction problems." *Journal of basic Engineering* 82.1, pp. 35-45, 1960
- [6] J. Zhang, D. Britto, M. Charaibi, R., Löhner, E. Haug, B. Gawenat, "Quantitative validation of PEDFLOW for description of unidirectional pedestrian dynamics," *Transportation Research Procedia*, 2, pp. 733-738, 2014
- [7] F. Togashi, T. Misaka, R. Löhner, S. Obayashi. "Using Ensemble Kalman Filter to Determine Parameters for Computational Crowd Dynamics Simulations," *Engineering Computations* 35, 7, 2612-2628, 2018

Congestion in Computational Evacuation Modelling

Volker Schneider¹, Rainer Könecke²

^{1,2}IST GmbH

Feuerbachstraße 19, 60325 Frankfurt, Germany
v.schneider@ist-net.de; r.koennecke@ist-net.de

Abstract - The time-based analysis of egress scenarios is a long-standing and well-established method to evaluate occupant safety. It is based on the necessary condition that the required egress time is smaller than the available egress time. The former is derived by the application of evacuation models, the latter by calculation of smoke and heat spread in the case of a fire incident. In the calculation of required egress time the time-dependent development of occupant density and consequently the emergence of congestion often play a crucial role. There is a demand to evaluate the development of local occupant density and jam situations independent of the above time-based criterion. This is for example reflected in national guidelines and standards. It is however difficult to obtain general valid evaluation criteria for congestion due to the multitude of influencing parameter and the highly situation-dependent nature of the accompanying boundary conditions. In addition, prediction of localization and duration of congestion may differ from model to model if applied to equal scenarios. Furthermore, close inspection reveals the difficulty to define proper terms for a quantitative definition of congestion. This issue is further analysed in this paper based on three case studies.

Keywords: evacuation, modelling, congestion, egress movement, numerical simulation

1. Introduction

For buildings and areas of special size or complexity in combination with a large number of occupants, computational evacuation modelling is often applied to support approval procedures or design processes. Criteria for the time-based analysis of the egress process can be straightforward derived based on the concept of required egress time versus available egress time. More difficult is the assessment of situations involving congestion [1]. This issue is for example addressed in the German Guideline Fire Protection Engineering [2] and in the current work on E DIN 18009-2 that is scheduled to be published next year [3], [4]. Guideline and norm will provide technical definitions and evaluation criteria to assist fire engineers, designers and authorities. The three case studies summarized in this paper will contribute to the characterisation and evaluation of congestion by presenting numerical simulations and respective empirical data.

2. Benchmark cases for congestion analysis

The first example consists of a series of plain benchmark cases. For these, a comparison of microscopic simulations using the ASERI evacuation model [5] and macroscopic calculations is performed. By variation of initial and boundary conditions with respect to geometry and population, relevant parameter for the formation and evaluation of congestion e.g. at exits or in front of stairs are developed. This leads to suggestions for the definition and classification of jam situations, including definitions for stand-still times and methods for analysing local occupant density. A statistical analysis is performed, as described exemplary in figure 1. This graphical representation describes the number of people in a jam in front of a descending stair that are affected by a certain reduction of unrestricted walking speed or stand-still for at least a certain time interval.

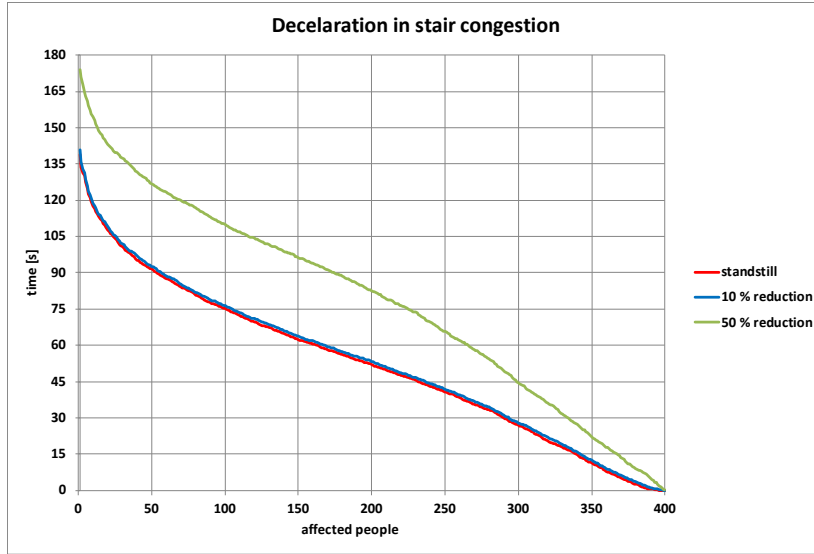


Fig. 1: Distribution of reduced walking speed in congestion scenarios

3. Evacuation of an Auditorium

The second case is the evacuation of an auditorium – a scenario documented in the guideline [2] that is presently updated for the next revised edition scheduled for 2019. Numerical studies applying several evacuation models show some differences that include also the localization of congestion along the available egress paths. Table 1 shows the escape times and localizations of congestion as derived by the various models.

Table 1: Calculated escape times and congestion characteristics [2]

Model	first escape route		second escape route	
Capacity analysis (SFPE)	304 s	Entrance door	298 s	Emergency exit
Predtetschenski & Milinski	295 s	Aisle stairways Foyer stairs	318 s	Aisle stairways
buildingEXODUS	382 s	Aisle stairways	266 s	Aisle stairways
PedGo	348 s	Aisle stairways Foyer stairs Main exits	276 s	Aisle stairways Emergency exit
FDS+Evac	373 s	Aisle stairways Main exits	239 s	Aisle stairways
ASERI	324 s	Aisle stairways Main exits	311 s	Aisle stairways Emergency exit

4. Empirical flow data for a large ice hockey arena

The last case covers a monitored ingress and egress situation inside a large ice hockey arena. Starting at first admittance and ending after the last spectators had left the arena, the inflow, outflow and the distribution on the spectators on a grandstand where monitored by cameras above the playing field and counted by supporters. The snapshot in figure 2 taken from one of these videos illustrates the situation shortly after the final whistle. Two examples of the evaluation of the counting are added (figure 3). The first one shows the dwell time (yellow curve) for the grand stand and the temporary outflow (blue curve) with peaks at the breaks of the game. The second graph presents total inflow and outflow. This data will be used for a more detailed analysis of the formation and decomposition of jams.



Fig. 2: Egress from an ice hockey arena - © IST GmbH

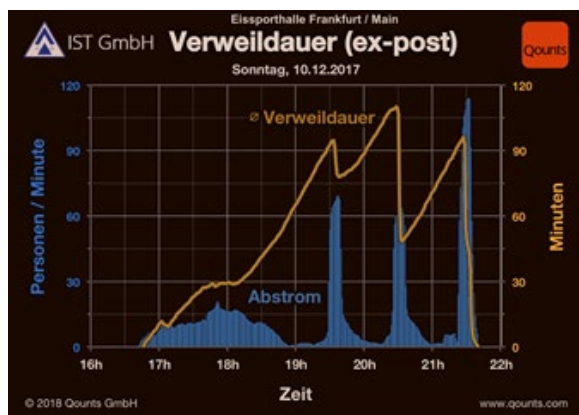


Fig. 3: Dwell time (Verweildauer), inflow (Zustrom) and outflow (Abstrom) for the grand stand during an ice hockey match - © Qounts GmbH

Acknowledgements

The authors wish to thank Stefan Leitmannslehner (Qounts GmbH, Göttingen) for the data monitoring and analysis presented in section 4.

References

- [1] V. Schneider, “Räumungssimulationen – Genügen Räumungszeiten für eine Bewertung der Personensicherheit?” in *Proceedings of the vfdb Jahresfachtagung 2016*, Stuttgart, Mai 2016.
- [2] D. Hosser (Ed.), “Guideline Fire Protection Engineering” vfdb Technical Report TR 04-01, November 2013.
- [3] A. Seyfried, G. Jäger, M. Kitzlinger, B. Schröder, “Normierung von Personenstromsimulationen in DIN 18009-2” in *Proceedings of the Braunschweiger Brandschutztag 2015*, September 2015.
- [4] J. Wiese, “Personenstromsimulationen nach E DIN 18009-2” in *Proceedings of the vfdb Jahresfachtagung 2018*, Duisburg, Mai 2018.
- [5] V. Schneider, “Application of the individual-based evacuation model ASERI in designing safety concepts” in *Proceedings of the 2nd Int. Symp. on Human Behaviour in Fire*, Boston, March 2001.

Decentralized Control for Self-driving Cars That can Freely Move on Two-dimensional Plane

Takeshi Kano¹, Mayuko Iwamoto², Daishin Ueyama³

¹Research Institute of Electrical Communication, Tohoku University, Sendai, Japan
tkano@riec.tohoku.ac.jp

²Interdisciplinary Faculty of Science and Engineering, Shimane University, Matsue, Japan
miwamoto@riko.shimane-u.ac.jp

³Faculty of Engineering, Musashino University, Tokyo, Japan
d.ueyama@gmail.com

Abstract – In the current traffic rules, cars have to move along lanes and to stop at red traffic lights. However, in the future when all cars become completely driverless, these traffic rules may vanish and cars may be allowed to move freely on two-dimensional plane by avoiding others like pedestrian flow. This innovation could greatly reduce traffic jams. In this study, we propose a decentralized control scheme for future self-driving cars that can freely move on two-dimensional plane, based on the social force model widely used as the model of pedestrian flow. The performance of the proposed scheme is validated via simulation. Although this study is still conceptual and does not consider realistic details, we believe that it paves the way to developing novel traffic systems.

Keywords: Decentralized control, Self-driving cars, Social force model, Pedestrian flow

1. Introduction

Technologies for self-driving cars have been developed within the framework of the conventional traffic rules in which cars have to move along lanes and to stop at red traffic lights. However, these traffic rules, which limit traffic flow and often cause traffic jams, may not be necessary in the future when all cars become completely driverless, because self-driving cars will be able to move more accurately than cars driven by humans. It is expected that traffic jams will be greatly reduced if self-driving cars move freely on two-dimensional plane by avoiding others like pedestrian flow.

In this study, we propose a decentralized control scheme for future self-driving cars that can freely move on two-dimensional plane. Because this study looks ahead to distant future, we employ minimal assumptions, rather than consider realistic and detailed problems, to capture the essence of the control. Social force model [1,2], a simple model of pedestrian flow, would be a suitable platform for considering this problem. We construct the control scheme by improving the social force model and demonstrate that the simulated self-driving cars can move fast, smoothly, and safely.

2. Model

In the social force model [1,2], each pedestrian on a two-dimensional plane is regarded as a circular particle with the radius of r , and its time evolution is described as

$$m\ddot{\mathbf{x}}_i = a(v_0\mathbf{e}_i - \dot{\mathbf{x}}_i) + \sum_{j \neq i} (\mathbf{f}_{ij}^{\text{phys}} + \mathbf{f}_{ij}^{\text{soc}}) + \sum_b (\mathbf{f}_{ib}^{\text{phys}} + \mathbf{f}_{ib}^{\text{soc}}), \quad (1)$$

where m is the mass of the particle, \mathbf{x}_i is the position of the particle i , \mathbf{e}_i is the unit vector that represents the direction particle i wants to move, v_0 is the target speed, and a is a positive constant. The second and third terms on the right-hand side denote forces generated by the interaction with the other particles and that with the environment, *e.g.*, walls, respectively. Superscripts “phys” and “soc” for these forces denote physical and social forces, respectively. Details are provided in [1,2].

The model of self-driving cars proposed here is also described in the same form as Eq. (1). Here, whereas the social force originates from psychological effect, *i.e.*, desire to avoid others, in the case of pedestrian flow [1,2], it is redefined as the control input to self-driving cars and is designed based on the

prediction of future motion of itself and nearby cars (see Steps 1—4 below). Note that the basic idea of the design is similar to our previous work on the decentralized control of traffic signals [3].

The social force (control input) $\mathbf{f}_{ij}^{\text{soc}}$ in the proposed model is calculated according to the following 4 steps ($\mathbf{f}_{ib}^{\text{soc}}$ can be calculated in a similar manner as $\mathbf{f}_{ij}^{\text{soc}}$):

Step 1: Each car detects the relative position and velocity of cars within the distance R from itself every time interval Δt .

Step 2: Based on the information obtained in Step 1, each car predicts the future motion of cars within the distance R from itself. Because the interaction terms (the second and third terms on the right-hand side) in Eq. (1) are hard to predict, the equation in which the interaction terms are omitted from Eq. (1),

$$m\ddot{\mathbf{x}}_i = a(v_0\mathbf{e}_i - \dot{\mathbf{x}}_i), \quad (2)$$

is solved numerically for duration T , wherein the initial position and velocity of the cars are the same as those obtained in Step 1 (Fig. 1).

Step 3: Based on the numerical calculation performed in Step 2, the expected time until the distance between cars i and j takes a minimum value or until car j collides car i , τ_{ij} , is derived (Fig. 1). Here, $\tau_{ij} = 0$ when the distance is expected to increase monotonically, and $\tau_{ij} = T$ when the distance is expected to decrease monotonically without any collision. Further, the expected distance between cars i and j after the time interval τ_{ij} , $\hat{d}_{ij}(\tau_{ij})$, is also derived.

Step 4: The social force $\mathbf{f}_{ij}^{\text{soc}}$ is derived according to the following equation:

$$\mathbf{f}_{ij}^{\text{soc}} = -A \exp\left(-\frac{d_{ij} - 2r}{B}\right) \mathbf{n}_{ij} - C \left(1 - \frac{\tau_{ij}}{T}\right) \hat{d}_{ij}(\tau_{ij})^{-\mu} \hat{\mathbf{n}}_{ij}(\tau_{ij}), \quad (3)$$

where A , B , C , and μ are positive constants, and d_{ij} is the distance between cars i and j . The unit vectors \mathbf{n}_{ij} and $\hat{\mathbf{n}}_{ij}(\tau_{ij})$ are given by

$$\mathbf{n}_{ij} = \frac{\mathbf{x}_j - \mathbf{x}_i}{|\mathbf{x}_j - \mathbf{x}_i|},$$

$$\hat{\mathbf{n}}_{ij} = \frac{\hat{\mathbf{x}}_j(\tau_{ij}) - \hat{\mathbf{x}}_i(\tau_{ij})}{|\hat{\mathbf{x}}_j(\tau_{ij}) - \hat{\mathbf{x}}_i(\tau_{ij})|}, \quad (4)$$

where $\hat{\mathbf{x}}_i(\tau_{ij})$ is the expected position of car i after the time interval τ_{ij} (Fig. 1). The first and second terms on the right-hand side in Eq. (3) denote the exclusive volume effect and the avoidance force based on the prediction, respectively. The term $(1 - \tau_{ij}/T)\hat{d}_{ij}(\tau_{ij})^{-\mu}$ in Eq. (3) was introduced because the avoidance force should be large when the distance between cars i and j is expected to become small in near future. Note that the proposed model is consistent with the original social force model [1,2] when $A > 0$ and $C = 0$.

3. Simulation

Simulation of the proposed model was performed. The deflection angle of \mathbf{e}_i was set to be random and did not vary during the simulation. The periodic boundary condition was employed. The performance was evaluated by the following indices E_1 , E_2 , and E_3 :

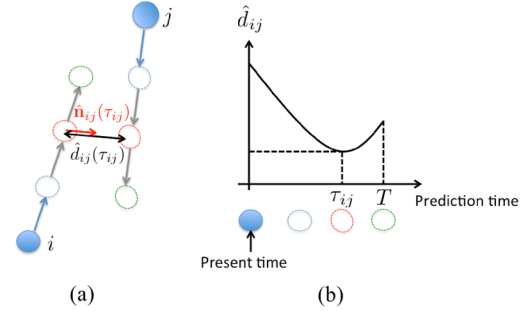


Fig. 1: Schematic of the proposed control scheme. (a) Based on the present position and velocity of the cars (blue filled circles and arrows, respectively), their future trajectories are estimated by calculating Eq. (2) (blue, red, and green dashed circles). (b) Schematic of the time evolution of the distance between cars i and j for the situation shown in (a).

$$\begin{aligned}
 E_1 &= \frac{\sum_{k=1}^n \sum_{i=1}^N (\dot{\mathbf{x}}_i(k) \cdot \mathbf{e}_i)}{v_0 n N}, \\
 E_2 &= \frac{\sum_{k=1}^n \sum_{i=1}^N |\ddot{\mathbf{x}}_i(k)|^2}{n N}, \\
 E_3 &= \frac{\sum_{k=1}^n \sum_{i=1}^N |\mathbf{f}_{ij}^{\text{phys}}(k)|}{n N},
 \end{aligned} \tag{5}$$

where k is the time step, n is the maximal time step, and N is the number of particles. Index E_1 is large when cars move fast in the direction they want to move, while indices E_2 and E_3 are small when cars move smoothly and safely, respectively.

The result when parameters A and C are varied with the other parameters fixed is shown in Fig. 2. It is found that E_1 increases as A decreases and C increases (Fig. 2(a)), while E_3 decreases as A and C increase (Fig. 2(c)). In contrast, E_2 is small in the area where A is small and C is around 3.0 [m⁴ kg s⁻²].

White and yellow arrows in Fig. 2 point the parameter regions where “speed”, “smoothness”, and “safety” are well-balanced for the proposed model ($A > 0$, $C > 0$) and for the original social force model ($A > 0$, $C = 0$) [1,2], respectively. It is clear that the performance is better for the proposed model than for the original social force model ($E_1 = 0.85$, $E_2 = 140.7$ [m² kg s⁻⁴], and $E_3 = 53.0$ [m kg s⁻²] at the region where the white arrows point, while $E_1 = 0.71$, $E_2 = 428.5$ [m² kg s⁻⁴], and $E_3 = 233.0$ [m kg s⁻²] and at the region where the yellow arrows point). Thus, the avoidance force based on the prediction, which was newly introduced, plays a crucial role for enabling self-driving cars to move fast, smoothly, and safely.

4. Conclusion

We proposed a decentralized control scheme for future self-driving cars that can freely move on two-dimensional plane, based on the social force model. We demonstrated via simulations that cars with the proposed control scheme can move fast, smoothly, and safely. It should be noted that this study is still conceptual and does not consider realistic issues (e.g., calibration of parameters to realistic values of current cars *etc.*). However, we believe that our new concept becomes a breakthrough for developing novel traffic systems. Finally, we would like to note that the model proposed here could be also used as the model of pedestrian flow because pedestrians change their path by predicting the movement of their nearby pedestrians. Hence, we believe that this study contributes to the field of pedestrian and evacuation dynamics.

Acknowledgements

The authors would like to thank Prof. Akio Ishiguro and Prof. Takashi Akamatsu of Tohoku University for their helpful suggestions.

References

- [1] D. Helbing and P. Molnár, “Social force model for pedestrian dynamics”, *Phys. Rev. E*, vol. 51, pp. 4282-4286, 1995.
- [2] D. Helbing, “Traffic and related self-driven many-particle systems”, *Rev. Mod. Phys.*, vol. 73, pp. 1067-1141, 2001.
- [3] T. Kano, Y. Sugiyama, and A. Ishiguro, “Autonomous decentralized control of traffic signals that can adapt to changes in traffic”, *Collective Dynamics*, vol. 1, A5, pp. 1-18, 2016.

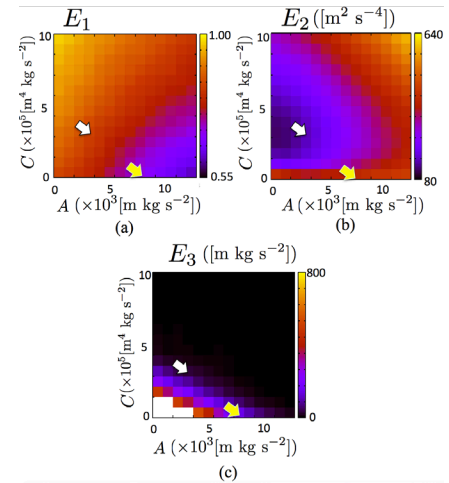


Fig. 2: Values of E_1 , E_2 , and E_3 when parameters A and C are varied are shown in (a), (b), and (c), respectively. White areas in (c) denote the areas in which $E_3 \geq 800$ [m kg s⁻²]. Explanations for the white and yellow arrows are provided in the main text.

Efficient Quantification of Model Uncertainties When De-boarding a Train

Florian Künzner¹, Tobias Neckel¹, Hans-Joachim Bungartz¹, Felix Dietrich², Gerta Köster³

¹Technical University of Munich, Department of Informatics
Munich, Germany

florian.kunzner@tum.de, tobias.neckel@tum.de, bungartz@tum.de

²Johns Hopkins University, Department of Chemical and Biomolecular Engineering,
Baltimore, MD, USA

felix.dietrich@jhu.edu

³Munich University of Applied Sciences
Munich, Germany

gerta.koester@hm.edu

Abstract - It is difficult to provide live simulation systems for decision support. Time is limited and uncertainty quantification requires many simulation runs. We combine a surrogate model with the stochastic collocation method to overcome time and storage restrictions and show a proof of concept for a de-boarding scenario of a train.

Keywords: Pedestrian dynamics, uncertainty quantification, surrogate models

1. Introduction

When trying to assess whether or not the passengers of a train can safely de-board onto an already over-full platform a safety officer faces a number of uncertainties. Chief among them are the initial numbers of passengers on the train and on the platform. By varying uncertain parameters in a computer simulation, one can, in principle quantify their effect [1] as demonstrated in [2] for the evacuation of a train. One obtains probability distributions of quantities of interest, in our case, the number of passengers on the platform. If this number exceeds a threshold, the safety officer might want to evacuate the platform. Uncertainty quantification would tell how likely this event is, given the initial passenger distributions (see Fig. 1 left).

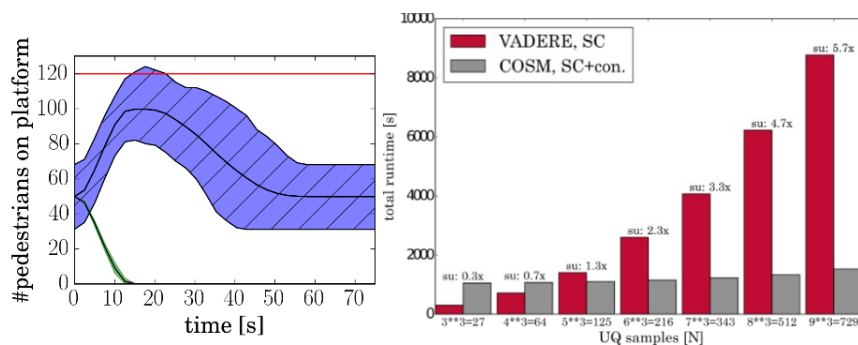


Fig. 1: Left: Mean and standard deviations of passengers on (green) and off (blue) the train. Right: total runtime of stochastic collocation for the original model compared to stochastic collocation for COSM.

With this approach, the computer scientist faces two problems: Simulation time and storage costs. Sampling the parameter space means that a usually very complex simulation program runs many times,

which makes the process slow. The resulting data which includes, for example, trajectories of individual pedestrians over time is high dimensional, expensive to store and hard to retrieve from its vast storage space. For the safety officer, this means that the results come too late to act.

2. The Closed Observable Surrogate Model (COSM)

To overcome the speed and storage barriers, we propose a low dimensional surrogate model that captures the dynamic of the original data and that allows observation of the quantity of interest. Thus, one can investigate the surrogate instead of the original model. As a further plus, techniques that reduce the number of samples for uncertainty quantification [3], but depend on prior choices for the distribution of uncertain parameters, can be applied on the surrogate, without having to re-sample the original model. Stochastic collocation [4] is such a technique.

The solution we offer here, the Closed Observables Surrogate Model, is based on theoretical work in [5, 6]. It reduces storage requirements in the very costly time domain, by using time-delayed embedding of the original data to ensure that the output can be uniquely constructed. This means that we initially increase the model's dimensionality, see Fig. 3 (right). Consequently, we need to strip away redundant dimensions. For this, we employ a manifold learning technique: Diffusion Maps [7]. The reduction allows efficient storage and reloading of the surrogate model. Through interpolation, one can access data points in areas that were not simulated beforehand. Fig.2 shows how a quantity of interest, the number of passengers on a train, is computed based on the original data and on the surrogate for different uncertain parameter pairs (initial number of persons on platform; initial number of persons on train). An interpolation is constructed for $(\#platform; \#train) = (75; 60)$, which matches data explicitly simulated for these initial values very well.

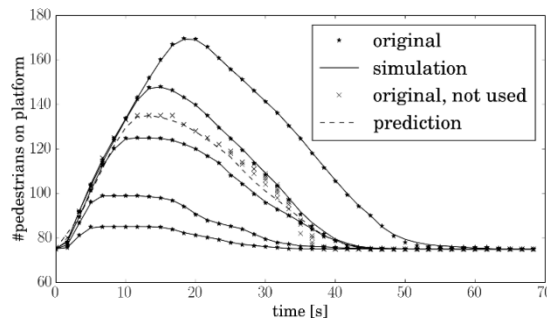


Fig. 2: Comparison of a quantity of interest (number of pedestrians on the platform) computed with the original simulation result (solid) and with the surrogate (dashed).

The next step is to combine the Closed Observables Surrogate Model with stochastic collocation [4]. The final combined method is illustrated in Fig. 3 (left). In the train example, the final combined method delivers results close to a classic Monte Carlo approach [4] that repeatedly samples the original model, and that we use as a benchmark. The new approach is much faster: Even in our small example, with only three uncertain parameters (initial number of initial pedestrians on the platform, initial number of pedestrians on the train, mean free flow velocity) we achieve a speed-up factor of about six for $9^3=27$ samples. The runtime for the surrogate does not increase significantly with the number of samples (see Fig. 1 (right)).

3. Conclusion

Fast and cheap surrogate models to reproduce simulation data or measured data are constructed using time delayed embedding for uniqueness and diffusion maps for subsequent order reduction. The gain in speed and storage efficiency allows studying the effect of uncertain parameters on safety relevant quantities of interest, such as the number of passengers in a critical location. Stochastic collocation further reduces the number of samples. With the combined speed-up we come closer to the goal of supporting decision making

in a live situation. We presented a sample application as proof of concept. To be useful to end users, the methods, which are not trivial to implement, must be made accessible through libraries and frameworks.

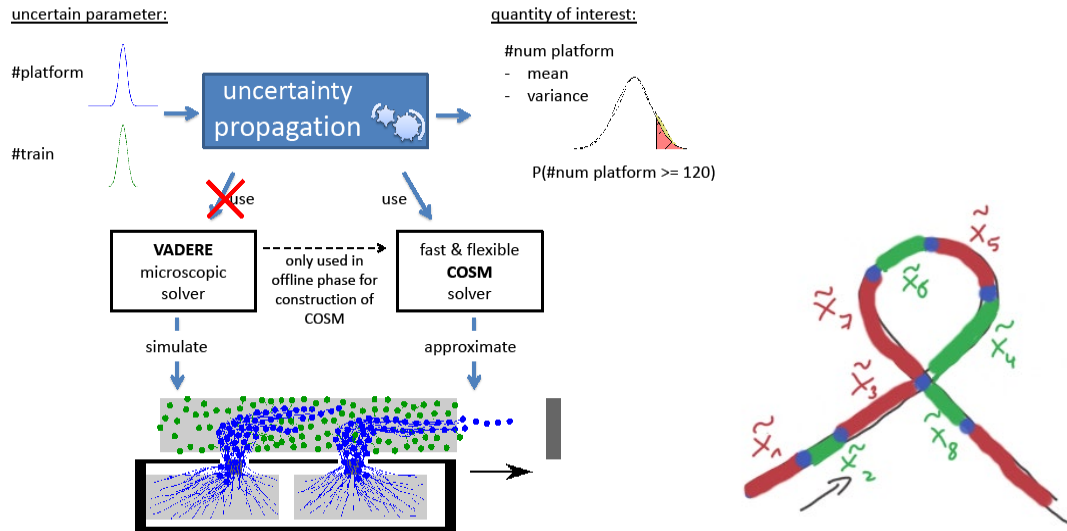


Fig. 3: Left: Simulation of the de-boarding process, and uncertainty quantification, including the construction of a surrogate model. Right: Illustration of time-delayed embedding to recover uniqueness of a dynamic on a string.

Acknowledgements

This work was funded by the German Federal Ministry of Education and Research through the project OPMOPS (grant 13N14562) and by DFG through the project QUEST. The authors acknowledge support by the Faculty Graduate Center CeDoSIA of TUM Graduate School at Technical University of Munich, and the research office FORWIN at Munich University of Applied Sciences, Germany.

References

- [1] Iaccarino, G., “Quantification of uncertainty in flow simulations using probabilistic methods,” Report on *VKI Lecture Series*, Sept. 8-12, pp. 1-30, 2008.
- [2] Von Sivers I. et al., “Modelling social identification and helping in evacuation simulation,” *Safety Science*, vol. 89, pp. 288-300, 2016.
- [3] Smith, R.C., “Uncertainty Quantification: Theory, Implementation, and Applications,” *SIAM Computational Science and Engineering*, 2014.
- [4] Xiu, D. and Karniadakis, G.E., “The Wiener–Askey polynomial chaos for stochastic differential equations,” *SIAM Journal on Scientific Computing*, vol. 24(2), pp.359–718, 2002.
- [5] Dietrich et al., “Numerical model construction with closed observables,” *SIAM Journal on Applied Dynamical Systems*, vol. 15, pp. 2078-2108, 2016.
- [6] Dietrich et al., “Fast and flexible uncertainty quantification through a data driven surrogate model,” *International Journal of Uncertainty Quantification*, vol. 8, pp. 175-192 2018.
- [7] Coifman, R.R. and Lafon, S., “Diffusion maps, Applied and Computational Harmonic Analysis,” vol. 21(1), pp. 5-30, 2006.

Empirical Findings from an Ascending Stair Evacuation Exercise in a Subway Station

Helmut Schrom-Feiertag¹, Thomas Matyus¹, Martin Stubenschrott¹, Stefan Seer¹

¹ Center for Mobility Systems, AIT Austrian Institute of Technology GmbH

Giefinggasse 2, 1210 Vienna, Austria

{Helmut.Schrom-Feiertag, Thomas.Matyus, Martin.Stubenschrott, Stefan.Seer}@ait.ac.at

Abstract - Crowd simulations have proven to be a valuable numerical tool for evacuation analysis. There is series of research and empirical evacuation studies for infrastructures and buildings. In contrast to research on evacuation via descending stairs, little attention has been given to ascending stairs, but they are an important criterion, especially in subway stations with high passenger frequencies. In this paper, we present the findings from an evacuation exercise in a subway station with long ascending stairs. The empirical findings showed an increasing walking time on the ascending stairs during evacuation. Also, the flow rate differs with higher flow rates at the beginning of the stairs and lower values at the end of the stairs. The mechanism behind these results has still to be investigated, but the findings already provide an interesting basis for modelling and validating evacuation simulations over long ascending stairs.

Keywords: pedestrian, emergency evacuation, subway station, ascending stair, empirical study

1. Introduction

Crowd simulations have proven to be a valuable numerical tool for the investigation of the evacuation performance for different infrastructures and buildings in the case of an emergency [1], [2]. Such crowd simulation models can only fully exploit their potential if they are based on an empirical basis [3]. Due to its unforeseeable occurrence, data from real emergency evacuations is hard to collect. Thus, evacuation experiments, either announced or unannounced, with scripted scenarios have been conducted and their results published in literature [4]–[10]. The focus of these evacuation experiments ranges from particular infrastructure elements, e.g. staircases [5]–[7], to route-choice behaviour [8] and walking behaviour at bottlenecks [9]. In the view of subway stations with long ascending stairs, the publication of [10] is to be emphasized here. In [10] the challenges of long ascending stairs are considered and a comprehensive literature review was carried out. They found that the influence of physical exhaustion on walking speed on long staircases and escalators had already been investigated in previous studies, but it was neither determined when physical exhaustion begins to affect walking speed nor to what extent. In addition, mainly young and healthy persons were involved in experiments, which must also be considered when utilizing the results. For a better understanding it is therefore necessary to carry out further investigations.

2. Evacuation Scenarios

The emergency evacuation exercise was carried out at a subway station in Vienna in December 2017. The station was chosen for two reasons, 1) it is closely located to a soccer stadium and hence used by large numbers of passengers at events, and 2) it is one of the deepest stations with a height difference of 23.2 meters below ground level. The station is equipped with a staircase with a width of 2.4 meters at both ends and an additional escalator with three lanes on one side.

The scenarios for the emergency evacuation exercise were designed to represent a peak occupancy as it can occur during the morning peak or in the context of nearby events (e.g. soccer game). Furthermore, the occurrence of technical limitations in the station building, e.g. due to regulations or because of maintenance work, was considered and only one escalator lane was available but switched off and stood still. The

elevators were also not available for evacuation, as they are reserved for the rescue services in the event of an emergency. Another simplification for the evacuation scenario was that all participants in the front half of the platform left the station via the front exit over the ascending staircase or ascending escalator and the participants in the rear half to the rear exit with only one staircase.

The exercise was executed in two scenarios with 560 participants each. In the first scenario the front half of the train and in the second scenario only the rear half of the train was filled with the full capacity of 420 persons and in addition 140 persons waited according to the scenario on the front or rear half on the platform. Immediately after the train had arrived and the doors were open the participants started to evacuate. The evacuation exercise was recorded with video cameras for analysis. Video screenshots taken at the platform, at the staircase and on the escalator, are shown in Fig. 1.

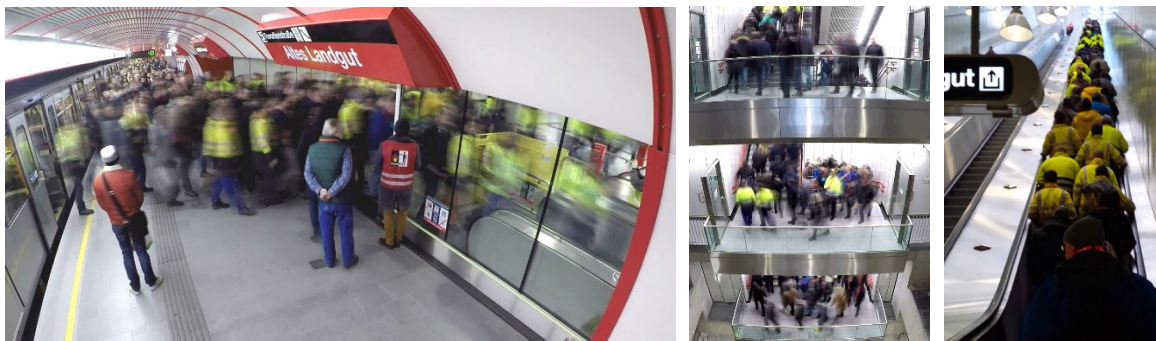


Fig. 1: Video screenshots showing people (left) leaving the train over the platform to the front escalator and staircase, (centre) on the staircase and (right) on the long ascending escalator.

Results

The time for evacuation, walking times, pedestrian flow rates and densities for both staircases and the escalator were manually extracted from the recorded video footage. Fig. 2 shows the results for scenario 2 with a single ascending staircase to illustrate the empirical findings. In Fig. 2a, the decreasing number of persons inside the station over the evacuation duration can be seen. The orange line shows the number of people still on the platform at the lower level and the blue line shows the number of people still in the station and decreases over time until everyone has left the station. At time 273 seconds or 57 percent of the total duration the platform level is cleared (t_{platform}) and all persons are either on the staircase or have already left the station. After the total evacuation time of 483 seconds (t_{station}) everyone has left the station through the exit on the surface. At first glance, the orange and blue lines appear parallel, but the evaluation of the walking times based on the difference between these two lines along the x-axis shows that the blue line has a flatter course.

Fig. 2b shows the walking times and walking speeds on the staircase. For each participant the time entering the staircase (x-value) and the duration on the stairs (y-value) is shown. The continuous increase in walking time from 112 seconds to 220 seconds over the duration of the evacuation should be emphasized here. The average walking time is 189 seconds. The total length of the path over the stairs was 112 meters and was divided into 10 stair segments with in total 156 steps and 57 meters length connected by 9 stair landings with total length 48 meters and a final 7 meters stretch towards the exit. Overall, a level difference of 23.2 meters was overcome. The calculated speeds are in a range of 0.5 to 1.1 m/s. The average walking speed with 0.6 m/s is within the range of the studied literature in [10] ranging from 0.27 to 0.75 m/s.

In Fig. 2c the pedestrian flow measured at the beginning of the stairs and at the exit is shown. For better visual representation the values are smoothed using a sliding window with a 15 seconds interval. The beginning of the staircase represents a bottleneck where the flow rate initially increases rapidly to a maximum value of 1.16 Persons per meter per second (P/ms) and then fluctuates around the average of 0.86 P/ms. The flow rate at the exit rises slowly until it reaches the range around the average of 0.57 P/ms and oscillates around that value. The flow at the exit was clearly smaller than at the beginning of the stairs. Just in front of the stairs, the crowd density was in average 2.5 Persons/m² without strong variations.

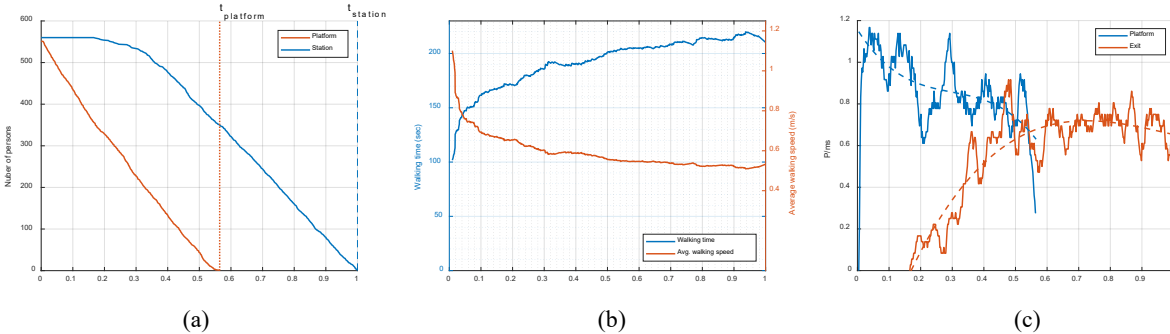


Fig. 2: Course of (a) number of persons on platform (orange line) and inside station during evacuation (blue line), (b) walking times (blue) and walking speeds (orange) from entering the stairs until leaving the building and (c) flow rates at the beginning (blue) and at end of stairs (orange).

4. Conclusion

The empirical findings showed that after 483 seconds the station was evacuated over long ascending stairs, whereby a distance of 174 meters and a level difference of 23.2 meters was overcome. While the average walking time was 189 seconds and the average walking speed 0.6 m/s, a steady increase of walking time from 112 to 220 seconds and decrease of walking speed from 1.1 to 0.5 m/s on the ascending stairs was observed. Also, the flow rate differs with higher flow rates at the begin of the stairs, in average 0.86 P/ms and lower values at end of the stairs with an average of 0.57 P/ms. It seems that after congesting at the begin of the stairs the people start to keep a greater distance from each other and the crowd spreads out along the stairs. The mechanism behind these results and how strong physical exhaustion plays a role has still to be investigated, but the findings already provide an interesting basis for modelling and validating evacuation simulations over long ascending stairs.

References

- [1] S. Gwynne, E. Kuligowski, and D. Nilsson, "Representing evacuation behavior in engineering terms," *J. Fire Prot. Eng.*, vol. 22, no. 2, pp. 133–150, May 2012.
- [2] D. C. Duives, W. Daamen, and S. P. Hoogendoorn, "State-of-the-art crowd motion simulation models," *Transp. Res. Part C Emerg. Technol.*, vol. 37, pp. 193–209, 2013.
- [3] A. Schadschneider, W. Klingsch, H. Klüpfel, T. Kretz, C. Rogsch, and A. Seyfried, "Evacuation Dynamics: Empirical Results, Modeling and Applications," in *Encyclopedia of Complexity and Systems Science*, R. A. M. Ph. D, Ed. Springer New York, 2009, pp. 3142–3176.
- [4] M. L. Isenhour and R. Löhner, "Validation of a Pedestrian Simulation Tool Using the NIST Stairwell Evacuation Data," *Transp. Res. Procedia*, vol. 2, pp. 739–744, Jan. 2014.
- [5] S. Burghardt, A. Seyfried, and W. Klingsch, "Performance of stairs – Fundamental diagram and topographical measurements," *Transp. Res. Part C Emerg. Technol.*, vol. 37, pp. 268–278, 2013.
- [6] R. D. Peacock, "Building Occupant Evacuation," *NIST*, 25-May-2010. [Online]. Available: <https://www.nist.gov/el/fire-research-division-73300/building-occupant-evacuation>. [Accessed: 08-Feb-2018].
- [7] E. Ronchi, P. A. Reneke, E. D. Kuligowski, and R. D. Peacock, "An analysis of evacuation travel paths on stair landings by means of conditional probabilities," *Fire Saf. J.*, vol. 65, pp. 30–40, 2014.
- [8] M. Stubenschrott, T. Matyus, H. Schrom-Feiertag, C. Kogler, and S. Seer, "Route-Choice Modeling for Pedestrian Evacuation based on Infrastructure Knowledge and Personal Preferences," presented at the Transportation Research Board 96th Annual Meeting, Washington, DC, 2017.
- [9] S. Hoogendoorn, W. Daamen, and P. Bovy, "Extracting Microscopic Pedestrian Characteristics from Video Data," in *TRB 2004 Annual Meeting*, 2004.
- [10] J. Norén, M. Delin, and K. Fridolf, "Ascending Stair Evacuation: What do We Know?," *Transp. Res. Procedia*, vol. 2, pp. 774–782, Jan. 2014.

Experimental Investigation of Pedestrian Dynamics in Circle Antipode Experiments

Yao Xiao, Rui Jiang, Ziyou Gao, Xingang Li, Yunchao Qu

School of Traffic and Transportation, Beijing Jiaotong University,

Beijing, China

xiaoy@bjtu.edu.cn

Abstract - To explore the pedestrian motion navigation and conflict reaction mechanisms in practice, we organized a series of circle antipode experiments. In the experiments, pedestrians are uniformly initialized on the circle and required to leave for their antipodal positions simultaneously. On the one hand, a conflicting area is naturally formulated in the center region due to the converged shortest routes, so the practical conflict avoidance behaviors can be fully explored. On the other hand, the symmetric experimental conditions of pedestrians, e.g., symmetric starting points, symmetric destination points, and symmetric surroundings, lay the foundation for further quantitative comparisons among participants. The pedestrian trajectories in the experiments are recognized and rotated, and several aspects, e.g., the trajectory space distribution, route length, travel time, velocity distribution, and time-series, are investigated. It is found that: (1) Pedestrians prefer the right-hand side during the experiments; (2) The route length follows a log-normal distribution, the route potential obeys an exponential distribution, and travel time as well as speed are normally distributed; (3) Taking the short routes unexpectedly cost pedestrians plenty of travel time, while detours seem to be time-saving.

Keywords: Circle antipode experiment, pedestrian trajectories, experiment analysis, pedestrian dynamics

1. Introduction

The circle antipode experiment has been applied as a simulation scene [1-3], but very limited attention is paid to the performance of pedestrians in reality. In the circle antipode experiments, pedestrians are uniformly initialized on a circle, and they are required to reach the antipodal positions. The first significant feature of the experiment is that the shortest routes intersect at the center of the circle, and a crowded area is generally formulated in the center zone. In this case, a pedestrian has to deal with the conflicts with other pedestrians and pass through the crowded area in front. The ability to deal with the situations of conflicts and congestions is a fundamental and core problem in pedestrian research, and here the practical handling ability of conflicts and collisions could be revealed. Another significant but rarely mentioned feature is that each pedestrian has a symmetric initial position and a symmetric destination position in the experiment. In other words, except for the heterogeneity of pedestrians themselves, each pedestrian faces a symmetric experimental condition. Based on it, the results of pedestrian trajectories could be used to maximum possible extent, and more quantitative investigations are possible. Finally, with the development of the video recognition technology and other trajectory recognition technologies in recent years, obtaining the precise trajectories of pedestrians even in crowded situations is not so difficult as before. The achievement of the precise pedestrian trajectories provides more detailed characteristics of microscopic pedestrian behaviors. In summary, the access to the trajectories of the circle antipode experiments provides more possibilities for quantitatively investigating the performance of pedestrians in a challenging conflicting situation.

2. Experiments

Up to 64 participants (31 females, 33 males) were involved in the experiment, and they were students from the university and aged 18 to 28. The experiments were conducted on two circles of radii of 5m and 10 m, respectively (Figure 1). For each circle, experiments with four pedestrian counts (8, 16, 32, 64) were carried out, each of which was repeated four times. With these specific number of participants (e.g.,

$8=64/2^3$), it is convenient to formulate a symmetric experimental situation for all the participants based on the existing 64 surface marks in practice. In addition, more videos about the experiments can be found on our website, <http://pedynamic.com/circle-antipode-experiments/>.

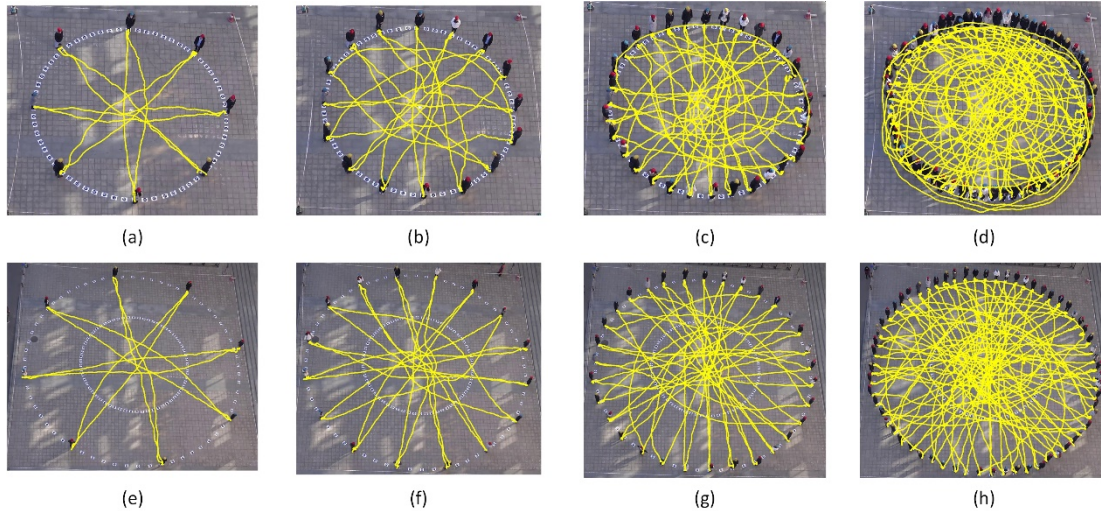


Figure 1. Original trajectories in the circle experiments. The yellow curves represent the trajectories on the ground. (a)-(d) 8, 16, 32, 64 pedestrians in the circle of 5m. (e)-(h) 8, 16, 32, 64 pedestrians in the circle of 10m.

3. Results

To make the most of the specific symmetric distribution features, the original route trajectories are respectively rotated around the center of the circle until the starting point of the route and the left end of the circle are overlapped. Since the destination of each pedestrian locates at the antipodal position of the starting point, the destination should also be consistent.

3.1 Side Preference

Though investigation on the spatial distribution of trajectories, it is found that the probabilities of trajectories in the right side semi-circle are greater than those in the left side semi-circle (Figure 2). That is to say, pedestrians prefer to detour from the right side in our experiments. Past studies [4-5] suggested that the side preference could be interpreted as a cultural bias, and the right side preference in China agrees with our experimental results. What's more, the circle antipode experiments can be regarded as quantitative measurement for side preference.

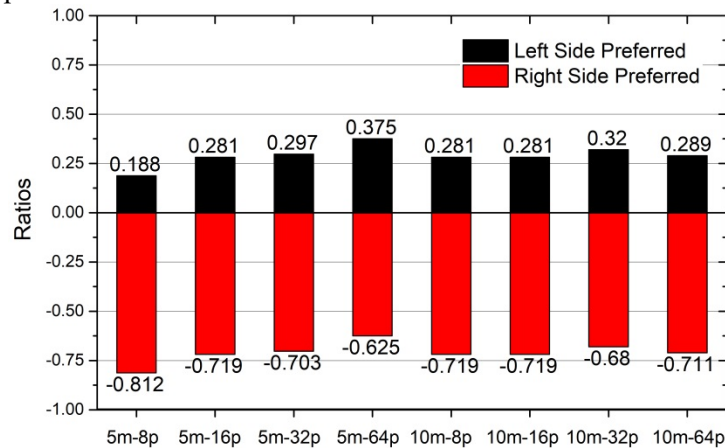


Figure 2. Trajectory distribution in left/right side semicircle

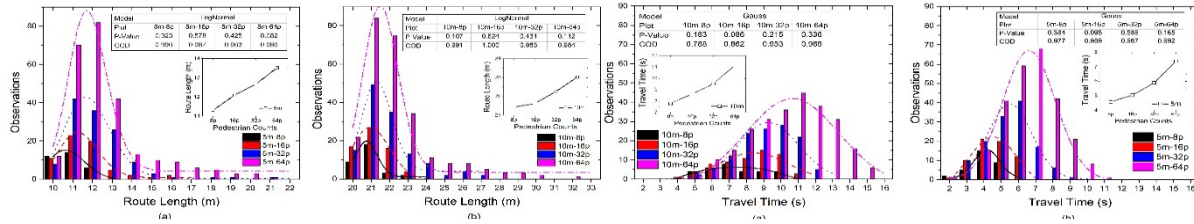


Figure 3. Distributions of the route length and travel time. (a) 5m experiments. (b) 10m experiments.

3.2 Distribution of route length and travel time

The mean values and distributions of the route length are illustrated in Figure 3. The route lengths cover from 10m to 21m in the 5m experiments, while from 20m to 33m in the 10m experiments. On the whole, there is a peak value in each distribution, and the peak value generally exists at the left side of the data range and a long tail exists at the right side. Considering the special shape of the route length distribution, the log-normal distribution is introduced to fit it. In the hypothesis test, the null hypothesis is that the route length distribution follows a log-normal distribution, and the significant level is set as 5%. The results of the non-parametric test show that the p-values in all experiments are greater than 0.05 (see Figure 4), so the null hypothesis cannot be rejected and the route length obeys a log-normal distribution. Besides, the coefficients of determination (COD) further prove the goodness of fitting.

The mean values and distributions of travel time are illustrated in Figure 3. In the experiments, the mean travel time increases with increasing pedestrian counts. The growing pedestrian counts make the circle more crowded and more pedestrians have to detour or slow down, hence the travel time increases. The travel times cover from 2 seconds to 11 seconds in the 5m experiments, while from 3 seconds to 16 seconds in the 10m experiments. Each distribution has a peak value which increases with increasing pedestrian counts. The normal (Gauss) distribution is introduced to fit it. The normality tests (Figure 5) and the COD prove that the travel time distribution follows a normal distribution.

References

- [1] Van den Berg J, Lin M, Manocha D. Reciprocal velocity obstacles for real-time multi-agent navigation., IEEE International Conference on Robotics and Automation; 2008: 1928-1935.
- [2] Ondřej J, Petré J, Olivier A-H, Donikian S. A synthetic-vision based steering approach for crowd simulation. ACM Transactions on Graphics; 2010; 29: 123.
- [3] Golas A, Narain R, Curtis S, Lin MC. Hybrid Long-Range Collision Avoidance for Crowd Simulation. IEEE Trans Vis Comput Graph. 2014;20(7):1022-1034.
- [4] Helbing D, Buzna L, Johansson A, Werner T. Self-organized pedestrian crowd dynamics: Experiments, simulations, and design solutions. Transportation Science. 2005;39(1):1-24.
- [5] Moussaïd M, Helbing D, Garnier S, Johansson A, Combe M, Theraulaz G. Experimental study of the behavioural mechanisms underlying self-organization in human crowds. Proc Biol Sci. 2009;276(1668):2755-2762.

Network-Based Continuous Space Representation for Describing Pedestrian Movement in High Resolution

Wataru Nakanishi¹, Takashi Fuse²

¹Tokyo Institute of Technology
2-12-1-M1-20 Ookayama Meguro, Tokyo, Japan
nakanishi@plan.cv.titech.ac.jp

²The University of Tokyo
7-3-1 Hongo Bunkyo, Tokyo, Japan
fuse@civil.t.u-tokyo.ac.jp

Abstract - A concept of network-based continuous space representation is proposed and applied to the sequential map matching problem with simulation data assuming pedestrian movement. The concept allows for dealing with situations that the resolution of network representation is not high enough to describe the pedestrian movement considering the observation accuracy. The experiment showed that the proposed concept worked well in the example of pedestrian movement along with the sidewalk by estimation of accurate positions.

Keywords: road network, offset, continuous space, general state space model, map matching

1. Introduction

Map matching is the method to specify the sequence of road network travelled by people by using the sequential measurement of positioning data. A large number of studies on map matching method have been accumulated [1] mainly focusing on vehicle trajectory estimation. Generally, the road network is given in advance as the GIS (Geographic Information System) data (Fig. 1, left), and the positioning data are obtained by GNSS (Global Navigation Satellite System) (Fig. 1, centre). Such methods might be also useful for pedestrian trajectory estimation. For example, estimation of pedestrian behaviour in high-resolution is expected to advance the facility placement along the street. Since devices such as smartphones are moving with individuals while sequentially performing GNSS positioning, expectations for map matching, which is a prerequisite for utilising data obtained there, are increasing.

When capturing the walking trajectory in high resolution, it does not exist directly above the road network. The conventional map matching method, in which measurement coordinates are matched onto the network, has a problem from this viewpoint. In other words, in most methods, the coordinates of the road network as the matching destination are treated as lines having no width and always being on the correct coordinates. This means that the measuring device exists only above the links constituting the network and the map matching problem is corresponding the obtained data including the observation error to the correct position or link of the original network (red line of Fig. 1, right). This is because the application of the conventional map matching is mainly vehicle trajectory and can be regarded that the observation error is much larger than the representation error of the network itself.

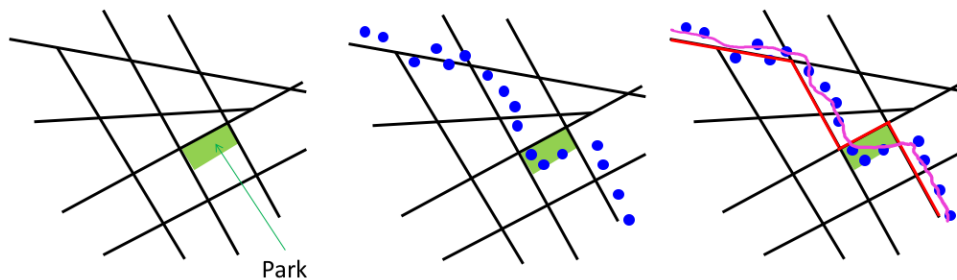
However, it may not always hold true in the present and future situation due to following two reasons. First, let us take pedestrian movement as an example and consider a road with a width of tens of meters. Then, on one hand, pedestrians pass through sidewalks on both sides. On the other hand, this road is represented by a single link drawn in the centre. At this time, the observation error about 10 [m] is as large as the error of restoring the coordinates observed by a pedestrian in the sidewalk to the link existing in the centre of the road (pink line of Fig. 1, right). Second, the positioning accuracy will get higher due to the increase of the number of satellites. Then, even if a device is located close to the link, the representation error is still not ignorable. An illustration of this scenario is shown in Fig. 2. Nevertheless,

considering that behaviour analysis is conducted by describing a route on a network for route choice and traffic assignment problem, trajectory of movement is desired to be associated with a network.

Therefore, in this study, a concept of network-based continuous space representation is proposed to explicitly consider errors of network on continuous space. In this concept, pedestrian positions are represented by the combination of link and offset. This representation has the following two advantages. First, different from the conventional methods, the estimated positions by map matching can be any position, not limited to that just above the road link. Second, the pedestrian trajectory as the matching result is still a sequence of road network, which allows for easy applications for behaviour analyses. The proposed method is applied to the sequential map matching problem with simulation data assuming pedestrian movement.

2. Continuous Space Representation Using Network

A Bayesian approach, utilised to cope with uncertainty of observation in the existing studies [2,3], is employed to describe sequential map matching problem. Similar to them, whole model structure is a form of general state space model. Here, a set of latent variables at time instance t is called state vector \mathbf{x}_t and a set of observed variables is called observation vector \mathbf{y}_t . Dynamics of state vector, called system model is a conditional probability $p(\mathbf{x}_{t+1}|\mathbf{x}_t)$, and observation process, called observation model is a conditional probability $p(\mathbf{y}_t|\mathbf{x}_t)$. The core of the proposed concept is the definition of these components (Fig. 3 and 4). Given a road network, any position in continuous space is defined as $\mathbf{x}=(l,d)$, where l indicates a link and d indicates a offset from the corresponding link l . Observation is defined as $\mathbf{y}=(x,y,\sigma)$, where x and y are observed coordinates and σ is obtained measurement accuracy. Sequential map matching is to estimate the posterior of \mathbf{x} as following,



(left) Black lines represent road network (links) with park; (centre) blue dots represent GNSS observations; (right) red lines represent matching result of conventional methods (a sequence of links), and pink lines represent the expected matching results of the proposed method. Walking on sidewalks and across the park can be estimated by this continuous representation.

Fig. 1. Road network, GNSS observation and map matching

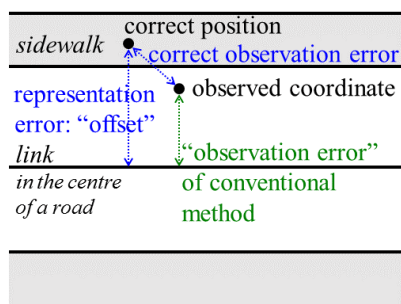


Fig. 2. Basic concept for continuous space representation

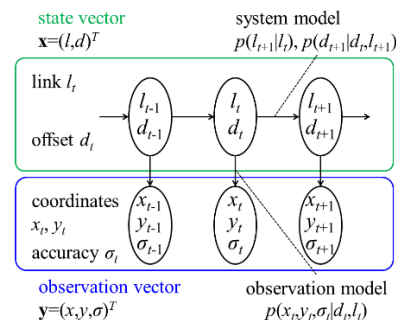


Fig. 3. Space state modelling

$$p(\mathbf{x}_t | \mathbf{y}_{1,2,\dots,t}) \propto p(\mathbf{y}_t | \mathbf{x}_t) p(\mathbf{x}_t | \mathbf{y}_{1,2,\dots,t-1}) = p(\mathbf{y}_t | \mathbf{x}_t) \int p(\mathbf{x}_t | \mathbf{x}_{t-1}) p(\mathbf{x}_{t-1} | \mathbf{y}_{1,2,\dots,t-1}) d\mathbf{x}_{t-1} \quad (1)$$

Actual form of state vector is considered as a conditional probability of offset d on link l , $p(\mathbf{x})=p(l,d)=p(d|l)p(l)$. $p(d|l)$ is defined according to the features of each link (Fig. 5). Then, system model is a combination of $p(l_{t+1}|l_t)$ and $p(d_{t+1}|d_t, l_{t+1})$. The former, link choice model, is treated as Markov transition model. For example, the probability of transition is defined referring to the expected staying time in the same link. The latter, offset dynamics is as follows.

$$p(d_{t+1} | d_t, l_{t+1}) \propto (1-\alpha) p(d_{t+1} | d_t) + \alpha p(d_{t+1} | l_{t+1}) \quad \text{if } l_{t+1} = l_t, \quad p(d_{t+1} | d_t, l_{t+1}) = p(d_{t+1} | l_{t+1}) \quad \text{otherwise} \quad (2)$$

where $p(d_{t+1}|d_t)$ describes a similarity of offset in successive time instances (considered to be random walk), and α is a weight of two components. In addition, observation model at any time instance is as follows (Fig. 4).

$$p(x, y, \sigma | l, d) \propto 1 - \frac{|\hat{d} - d|}{\sigma^2} \quad \text{if } |\hat{d} - d| \leq \sigma, \quad p(x, y, \sigma | l, d) = 0 \quad \text{otherwise} \quad (3)$$

where $p(d_{t+1}|d_t)$ describes a similarity of offset in successive time instances (considered to be random walk), and α is a weight of two components. In addition, observation model at any time instance is as follows (Fig. 4). where \hat{d} is the shortest distance between (x,y) and l . At last, calculation procedure is explained. Given posterior at time instance t , first calculate the predictive distribution of l_{t+1} using Markov transition model. Then, calculate d_{t+1} using equation (2). After obtaining $\mathbf{y}_{t+1}=(x_{t+1},y_{t+1},\sigma_{t+1})$, calculate equation (3) and then equation (1), the posterior at time instance $t+1$. The estimated distribution of link (the marginal distribution) and the estimated offset distribution given link $l=a$ are as follows.

$$p(l_t | \mathbf{y}_{1,2,\dots,t}) = \int p(l_t, d_t | \mathbf{y}_{1,2,\dots,t}) dd_t = \int p(\mathbf{x}_t | \mathbf{y}_{1,2,\dots,t}) dd_t \quad (4)$$

$$p(d_t | l_t = a, \mathbf{y}_{1,2,\dots,t}) = p(d_t, l_t = a | \mathbf{y}_{1,2,\dots,t}) / p(l_t = a | \mathbf{y}_{1,2,\dots,t}) \quad (5)$$

Particle filter [4,5] is employed to calculate the integrals.

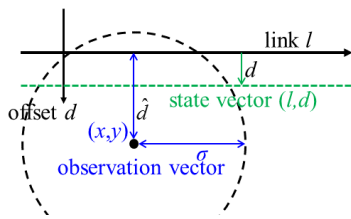


Fig. 4. State and observation vector

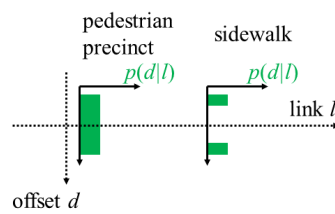


Fig. 5. Various types of $p(d|l)$

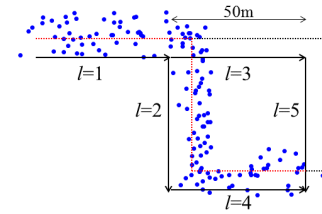


Fig. 6. Virtual network

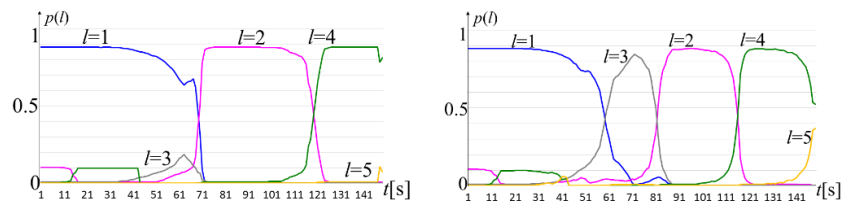


Fig. 7. Estimated link (left: $d|l \sim N(-10, 2^2)$, right: $d|l \sim N(0, 10^2)$)

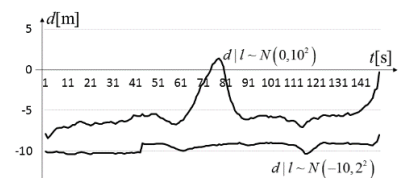


Fig. 8. Estimated offset

3. Application to Simulation Data

The proposed method is applied to simulation data on several virtual network with several parameter settings. Overall, the proposed method works well in both estimating the correct link and the amount of offset. One example of network is shown in Fig. 6. Road network is represented by black solid lines and the length of each link is 50[m]. However, pedestrian actually moves along sidewalks (red dashed lines), which are located at $d=-10$ of each link. Observation coordinates are generated by a pedestrian moves 1[m/s] along the link 1, 2 and 4 in this order with accuracy of $\sigma=5$ [m]. In this way, a set of observation is obtained from $t=1$ to 150 (shown by blue dots in Fig. 7). Two distributions of $p(d|l)$, the component of state vector, are assumed as $d|l \sim N(-10, 2^2)$ and $d|l \sim N(0, 10^2)$. The former corresponds the situation that the information of sidewalk is included and the latter the conventional method. In this setting, the estimated results are shown in Fig. 7 and 8. The former distribution is superior in both estimating link and offset; in the latter setting, the wrong link $l=3$ and offset about $d=0$ are estimated around $t=70$.

4. Conclusion

The sequential map matching with network-based continuous space representation was proposed and applied to simulation data assuming pedestrian movement. The experiment showed that the proposed method worked well in the example of pedestrian movement along with the sidewalk.

Acknowledgements

This work was supported by JSPS KAKENHI Grant Number JP15K18131.

References

- [1] M. A. Quddus, W. Y. Ochieng, and R. B. Noland, "Current map-matching algorithms for transport applications: State-of-the art and future research directions," *Transp. Res. Part C*, Vol.15, no.5, pp.312-328, 2007.
- [2] W. Kim, G. Jee and J. Lee, "Efficient use of digital road map in various positioning for ITS," *Proc. of IEEE Symposium on Position Location and Navigation*, 2000.
- [3] T. Hunter, R. Herring, P. Abbeel and A. Bayen, "Path and travel time inference from GPS probe vehicle data," *Proc. of the Neural Information Processing Systems Foundation (NIPS)*, 2009.
- [4] N. Gordon, D. Salmond, and A. Smith, "Novel approach to nonlinear / non-Gaussian Bayesian state estimation," *Radar and Signal Processing, IEE Proc. F*, Vol.140, no.2, pp.107-113, 1993.
- [5] G. Kitagawa, "Monte Carlo filter and smoother for non-Gaussian nonlinear state space models," *Journal of Computational and Graphical Statistics*, Vol.5, no.1, pp.1-25, 1996.

Experimental study on mixed traffic flow of bicycles and pedestrians

Ning Guo¹, Rui Jiang², SC Wong³, Qing-Yi Hao⁴, Shu-Qi Xue², Yao Xiao², Chao-Yun Wu⁴

¹School of Automotive and Transportation Engineering, Hefei University of Technology
230009, Hefei, P.R. China
guoning_945@126.com

² Key Laboratory of Transport Industry of Big Data Application Technologies for Comprehensive Transport,
Ministry of Transport, Beijing Jiaotong University
100044, Beijing, P.R. China
rjiang@ustc.edu.cn

³ Department of Civil Engineering, The University of Hong Kong
Pokfulam Road, Hong Kong, P.R. China

⁴ School of Mathematics and Computational Science, Anqing Normal University
246133, Anqing, P.R. China

Abstract - The mixed flow of bicycles and pedestrians is frequently observed on bicycle-pedestrian-shared roads. Unfortunately, studies on dynamics of this kind of mixed flow are very limited. This paper reports an experimental study of this kind of mixed traffic flow with equal numbers of pedestrians and cyclists asked to walk/ride in a ring-shaped track. In the uni-/bi-directional flow scenarios, pedestrians and bicycles moved in the same/opposite direction. Under both scenarios, bicycles and pedestrians formed their own lanes. Pedestrians walked in the inner lane and cyclists rode in the outer lane. Widths of both the pedestrian lane and the bicycle lane were more uniform in bidirectional flow. The pedestrian flow rate is larger in the unidirectional flow scenario than in the bidirectional flow scenario. In contrast, at low densities, the bicycle flow rate is essentially the same under the two scenarios. When the density is large, the bicycle flow rate becomes larger in the unidirectional flow scenario. Comparing the two modes, pedestrian flow rate is smaller/larger than bicycle flow rate at small/large densities under both scenarios.

Keywords: mixed flow; pedestrian flow; bicycle flow; lane formation

1. Introduction

Slow traffic includes walking and cycling. Comparing to car traffic, the slow traffic has the advantage of convenience, flexibility and no pollution. The slow traffic is indispensable, and its development has effect on the whole transportation system. In recent years, the studies of pedestrian traffic flow or bicycle traffic flow have drawn wide attention in fields of physical science and engineering respectively [1~4].

In China, with the rapid development of motorization, many bicycle lanes have been converted into motor lanes. As a result, bicycles have to share the lanes with pedestrians. Chen and Xie [5] developed a traffic conflict model on urban pedestrian-bicycle road, showing that the increment of path width helps to reduce conflict intensity between cycles and pedestrians. Xie [6] analysed the traffic characteristics and conflicts on cycle-pedestrian shared path, and provided a quality description of level of service on shared-use path. Yu et al. [7] found that the service level of bicycle-pedestrian mixed traffic flow improves with the road width, and the proportion of pedestrian affects the bicycle movement significantly. However, the self-organized process and flow dynamics of the mixed flow of bicycles and pedestrians have not been investigated. In this paper, an experimental study on bicycle/pedestrian mixed traffic flow is performed. The experiment concerns both unidirectional flow and bidirectional flow scenario. The lane formation phenomenon has been observed under both scenarios. The fundamental diagrams have been investigated.

2. Experimental setup

The experiments were conducted in a ring-shaped track with inner radius 8m and external radius 11 m. 160 participants took part in the experiments. They were requested to walk/ride in the same direction or opposite directions. After 3-5 minutes, pedestrians were asked to turn around to walk, and cyclists went on riding anti-clockwise. Six runs of experiment were performed. Chronologically, the participant numbers were as follows: 80 pedestrians+80 bicycles (unidirectional flow first), 40 pedestrians+40 bicycles (bidirectional flow first), 70 pedestrians+70 bicycles (unidirectional flow first), 50 pedestrians+50 bicycles (bidirectional flow first), 60 pedestrians+60 bicycles (unidirectional flow first), and finally 80 pedestrians+80 cyclists (bidirectional flow first).

3. Experimental results

In both the unidirectional flow or bidirectional flow, pedestrians and bicycles segregate into their own lanes very quickly at any densities. Pedestrians walked in the inner lane, and cyclists rode in the outer lane (see Fig.1). In the bidirectional flow scenario, both pedestrians and cyclists avoided each other actively. Pedestrians usually walked individually, or two pedestrians walk side by side (Fig.1b). It was seldom been observed that three or more pedestrians walked side by side. Therefore, widths of both the pedestrian lane and the bicycle lane were rather uniform in the bidirectional flow. In contrast, in the unidirectional flow, pedestrians cared less about bicycles behind them. It was frequently observed that three or more pedestrians walked side by side. The red box in Fig.1a shows a typical situation where five pedestrians walked side by side. As a result, the width of pedestrian lane was not uniform. Consequently, the width of bicycle lane was not uniform, either. For example, see the situation indicated by yellow box, where bicycles occupy the whole cross section of the track.



Fig. 1: Snapshots of 80 pedestrians + 80 bicycles experiment. (a) unidirectional flow, (b) bidirectional flow.

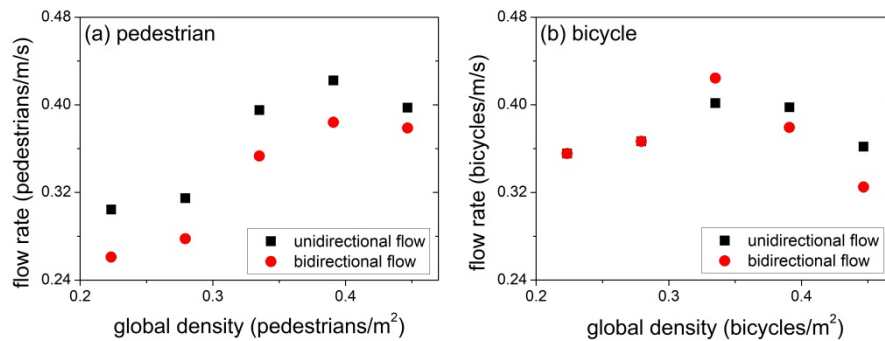


Fig. 2: Comparison unidirectional flow and bidirectional flow. (a) pedestrian flow, (b) bicycle flow in the mixed flow. Average values in 80 pedestrians + 80 bicycles experiment.

Next, we study the fundamental diagram of the flow rate versus the global density. Fig.2 compares pedestrian/bicycle flow rate in the unidirectional flow with the bidirectional flow. Fig.2a shows that the maximum pedestrian flow rate was achieved at $\rho \approx 0.389$ pedestrians/m² under both scenarios. Moreover, the pedestrian flow rate in unidirectional flow was always larger than that in bidirectional flow. Fig.2b shows that the maximum bicycle flow rate was achieved at $\rho \approx 0.333$

bicycles/m² under both scenarios. At low densities, bicycle flow rates were essentially the same under the two scenarios. At high densities, bicycle flow rate in the unidirectional scenario became larger. However, the maximum bicycle flow in bidirectional flow was larger than that in unidirectional flow.¹

Fig.3 compares the flow rate of pedestrian and bicycle in uni- and bi-directional flow. The bicycle flow rate is larger at low densities, but smaller at high densities under both scenarios.

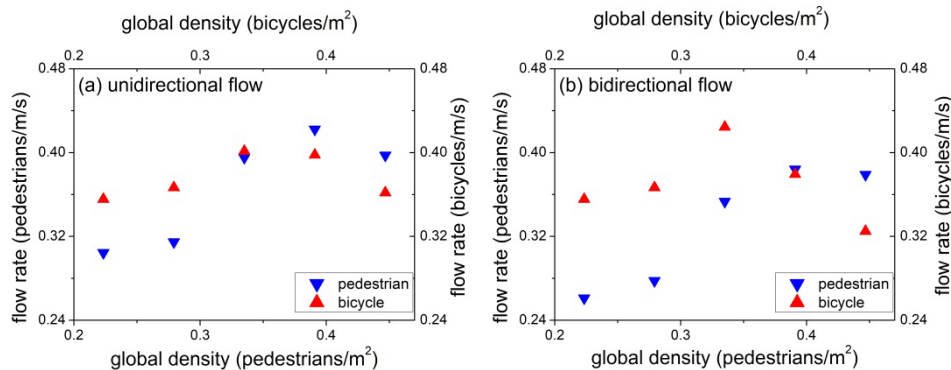


Fig. 3: Fundamental diagram of mixed flow of pedestrians and bicycles. (a) unidirectional flow, (b) bidirectional flow. Average values in 80pedestrians+80 bicycles experiment.

4. Conclusion

In this paper, we have experimentally studied the mixed flow of pedestrians and bicycles. It is found that bicycles and pedestrians formed their own lanes. Widths of both pedestrian lane and bicycle lane were more uniform in bidirectional flow. The fundamental diagrams of pedestrian/bicycle flow under uni-/bi-directional scenarios have been investigated. In future work, more runs of experiments with more participants and different proportion of pedestrian/bicycle should be carried out. Moreover, it is necessary to propose models to simulate the mixed flow.

Acknowledgements

This work is supported by the National Key R&D Program of China (No. 2017YFC0803300), the National Natural Science Foundation of China (Grants No.71621001, 71631002, 71371175), and the Beijing Natural Science Foundation (Grant No. 9172013).

References

- [1] D. Helbing, I. Farkas, T. Vicsek, "Simulating dynamical features of escape panic," *Nature*, vol. 407, pp. 487-490, 2000.
- [2] D. Helbing, L. Buzna, A. Johansson, T. Werner, "Self-organized pedestrian crowd dynamics: experiments, simulations, and design solutions," *Transp.Sci.*, vol. 39, pp. 1-24, 2005.
- [3] F.P.D. Navin, "Bicycle traffic flow characteristics: Experimental results and comparisons," *ITE J.*, vol. 64, pp. 31-36, 1994.
- [4] R. Jiang, M.B. Hu, Q.S. Wu, W.G. Song, "Traffic dynamics of bicycle flow: Experiment and modelling," *Transport. Sci.*, vol. 51, pp. 998-1008, 2017.
- [5] J. Chen, Z.Q. Xie, "Cycle traffic conflict model on urban pedestrian-bicycle paths," *J. Jilin Univ.*, vol. 39, pp. 121-125, 2009. (in Chinese)
- [6] Z.Q. Xie, "link operational characteristics and resources optimization allocation of bicycle-pedestrian shared-use paths", Nanjing: Southeast University, 2009. (Dissertation in Chinese)
- [7] H. Yu, J. Chen, Z.Q. Xie, "Level of service model on urban cycle-pedestrian road," *Urban Transport of China*, vol. 10, pp. 75-79, 2012. (in Chinese)

¹ Only one run of the experiment was performed at this density. More experiments are needed for validation.

Extracting Crowd Velocities at High Density

Muhammad Baqui and Rainald Löhner

CFD Center/George Mason University
4400 University Avenue, MS 4C7, Fairfax, VA 22030, USA
mbaqui@gmu.edu; rlohner@gmu.edu

Abstract – Velocity is a fundamental property of foot traffic flow. Monitoring the change of velocity patterns at high pedestrian densities may provide valuable insights on foot traffic dynamics. In this paper, a closer look is taken to explore the capability of the Particle Image Velocimetry (PIV) technique on extracting crowd velocities from surveillance camera images. Experiments are performed to report the accuracy of pedestrian velocity extraction with PIV. Quantitative accuracy is reported with manual tracking of pedestrians, surveying correlation misses at different window sizes and compute times. The results indicate that the PIV algorithm can be a good candidate for velocity extraction in real-time.

Keywords: Particle Image Velocimetry (PIV), Crowd Monitoring, Pedestrian Flow, Surveillance

1. Introduction

Particle Image Velocity or PIV is a widely used technique in experimental fluid dynamics [1]. Recently, a number of studies have been able to apply the technique outside the domains of fluid dynamics [2], [3]. Some preliminary studies have also been performed on crowd velocity extraction [4]. However, the scope and limitations of the PIV technique for crowd velocity extraction is still not thoroughly known. The objective of the current work is to analyse the PIV velocity extraction from both the qualitative and quantitative accuracy perspectives. The PIV application may also be suitable for real-time velocity extraction for its superior timing compared to the Optical Flow technique [5]. The study focuses on the processing of images acquired from a dense crowd event known as the Hajj. In order to properly process these images, an automated background detection and camera angle perspective correction approach have also been implemented.

The paper is organized as follows: Section 2 outlines the PIV, background removal and perspective correction techniques. Section 3 provides results on the PIV accuracy and timings. Finally, conclusions are drawn in Section 4.

2. Materials and Methods

A brief description is provided of the methods involved in crowd image processing. The PIV technique is discussed in section 2.1, followed by automated background removal in section 2.2 and perspective correction in section 2.3.

2.1. Particle Image Velocimetry(PIV)

The Particle Image Velocimetry (PIV) technique takes a sequence of two images that are separated by a small time-gap and produces vectors indicating the direction of movement. It operates in two stages: 1) Cross correlation and 2) Sub pixel displacement estimation. To facilitate the processing, the input image is being divided into smaller sub images called interrogation spots (spot size). The cross-correlation operation produces one correlation surface per interrogation spot with a single peak at the centre. In Figure 1, a sample interrogation spot and the corresponding correlation surface can be seen.

Once the correlation surface is obtained, the next step is to fit a Gaussian between the central peak and its neighbouring peaks. The Gaussian fit produces the pixel displacements with sub pixel accuracy [6].

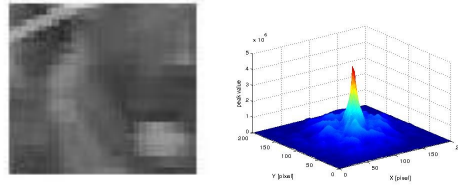


Fig. 1: Input image and corresponding correlation surface from PIV cross correlation

2.2. Background Removal

The surveillance camera images can come in various settings. As image noise is typically high, the background removal is important. Here, for background removal, some representative sections of the background are collected during pre-processing. Then, during operation, a chi-square based distance function is evaluated for each interrogation spot. If the interrogation spot exceeds a threshold of distance (greater than 0.84) then it is considered as background. The results for automated background removal can be seen in Figure 2. More details can be found in [6].

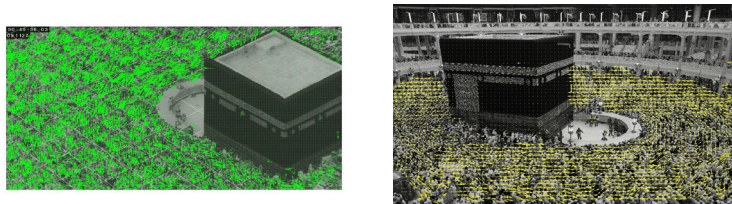


Fig. 2: Velocity vectors after PIV processing with automated background removal

2.3. Correction of Perspective

In real life, the surveillance cameras are not mounted orthogonally to the direction of crowd movement. As a result, different portions of the image will correspond to different displacement values in physical units. A correction scheme is applied to rectify the issue that is based on pin-hole camera and projective geometry [6].

3. Experiments and Results

Results of the accuracy and timings of the PIV technique in obtaining crowd velocities are presented in this section. In section 3.1 the accuracy results are reported and in section 3.2 the compute times are presented.

3.1. Quantitative Accuracy

Quantitative accuracy is reported through finding correlation misses varying spot window sizes and manual tracking of pedestrians.

3.1.2. Correlations Miss

Successful correlation is dependent on optimal spot window size. In order to process crowd images, 150x150 pixels wide spot windows were chosen. During experiments, it was found that when the spot size is increased from 2x2 pixels, the correlation misses start to decrease. Beyond a window of 40x40 pixels, no misses at all were found.

3.1.1. Manual Tracking of Pedestrians

The movement of pedestrians at 6 random locations were manually tracked and displacements were compared with PIV displacements. Results can be seen in Table 1.

Table 1 PIV displacement and ground truth comparison

Actual dx (pixel)	PIV dx (pixel)	Actual dy (pixel)	PIV dy (pixel)	%Error
-3	-2.52	3	2.73	12.43
-3	-3.89	5	4.08	3.32
-8	-6.87	3	2.39	14.86
-5	-4.28	4	4.14	7.08
4	3.08	-2	-2.14	16.13
8	7.55	2	1.72	6.09

3.2. Compute Time

Table 2 shows the results of timings for PIV and Optical Flow in processing crowd images of various sizes. The experiments are performed in a 4-core laptop with 1.8 GHz processor and 8 GB main memory.

Table 2 Compute time results of PIV and Optical Flow

Image Size (pixel)	Optical Flow (sec)	PIV (sec)
576x384	51.46	0.0469
288x192	20.26	0.0286
5760x3840	-	2.92

4. Conclusion

PIV technique has been able to successfully extract pedestrian velocities from surveillance camera images. It also has superior timing compared to the Optical Flow technique. However, more experiments are needed in various image illumination levels and different camera angles in order to see what possible limitations this technique is susceptible to.

References

- [1] R. J. Adrian, "Particle-Imaging Techniques for Experimental Fluid-Mechanics," *Annu. Rev. Fluid Mech.*, vol. 23, pp. 260–304, 1991.
- [2] S. Vanlanduit, J. Vanherzeele, R. Longo, and P. Guillaume, "A digital image correlation method for fatigue test experiments," *Opt. Lasers Eng.*, vol. 47, no. 3, pp. 371–378, 2009.
- [3] M. Rossi, E. Esposito, and E. P. Tomasini, "PIV Application to Fluid Dynamics of Bass Reflex Ports," in *Particle Image Velocimetry*, Springer, 2007, pp. 259–270.
- [4] J. Ma, W. Song, S. M. Lo, and Z. Fang, "New insights into turbulent pedestrian movement pattern in crowd-quakes," *J. Stat. Mech. Theory Exp.*, vol. 2013, no. 02, p. P02028, 2013.
- [5] M. Baqui and R. Löhner, "Real-time crowd safety and comfort management from CCTV images," in *Real-Time Image and Video Processing 2017*, 2017, vol. 10223, p. 1022304.
- [6] M. Baqui, "Automated Monitoring of High Density Crowd Events," PhD Thesis, George Mason University, 2018.

Follower-Leader Concept in Microscopic Analysis of Pedestrian Movement in a Crowd

Jana Vacková¹, Marek Bukáček²

^{1,2}FNSPE, Czech Technical University in Prague

Břehová 7, Prague, Czech Republic

janca.vackova@fjfi.cvut.cz; marek.bukacek@fjfi.cvut.cz

Abstract - This paper presents a microscopic analysis of factors influencing pedestrian movement and interactions with their surroundings for two considered modes: independent movement influenced only by the surrounding conditions and synchronized movement based on following another pedestrian. This study analyses which of these effects prevail in different phases of the movement. The results show that the significant value of correlation between pedestrian velocity and corresponding individual density is observed mainly during approaching the crowd. Contrarily, in the segment of pedestrian trajectory which corresponds to movement inside the crowd, correlation between the velocity of a follower and a leader is more important. This confirms that the pedestrian behaviour in a crowd is a complex field.

Keywords: pedestrian dynamics, egress experiment, correlation, individual density, follow-the-leader.

1. Introduction

The prediction of a pedestrian's velocity is one of the most crucial tasks for evacuation and egress modelling. Naturally, pedestrians react to the conditions in their surroundings and interact with others. Velocity-density dependency represents one of the most popular diagrams in this field [4]. Nevertheless, having discussed in [2], the shape of this relation significantly differs with the phase of the motion.

Social interaction may be categorized as social interactions between friends, colleagues or family members and the crowd interaction that is not driven by any prior intention, but only the temporal purpose. In this paper, we put aside the social level and focus only to individuals. The concept of correlations between velocities of the nearest neighbors in a specific angle was studied in [5], the results were interpreted on group level. In this study, all conclusions will be provided on individual level.

Similarly to [2], the Pearson correlation coefficient $R(\rho_{\omega_\alpha}, v_\alpha)$ is used to measure the strength of a pedestrian's α reaction expressed by their velocity v_α to their surroundings described by an individual density ρ_{ω_α} . Rolling window with memory time $\tau = 1.56$ s enables to watch a progress in time. Moreover, the same technique visualizes the correlation $R(v_\alpha, v_\beta)$ which expresses the relation of a pedestrian and their nearest predecessor ('leader') β .

This study is based on the egress experiment summarized in [1]. Pedestrians randomly entered the room by one of three entrances, walked to the opposite wall and left the room by one exit. By controlling input flow, different conditions from free flow to congestion in the exit area were achieved.

2. Pedestrian velocity, individual density and correlation

The velocity of a pedestrian is calculated as usual using central differences of space coordinates. There are many ways to enumerate the density, in details [3]. We use the concept introduced in [2], where each pedestrian α contributes by their individual density distribution $p_\alpha(\mathbf{x})$ to the density distribution for the whole area $p(\mathbf{x})$. In other words, every single pedestrian is considered to be a source of density distribution (a cone was picked as the best shape).

Fig. 1, Left shows the trend of these variables for one chosen trajectory. The trend of their velocity and the individual density indicates short free flow phase followed by gradual joining a crowd

characteristic by the decrease in velocity with increasing density. These trends dramatically changed since the pedestrian fully entered the crowd – their velocity reaches almost zero and starts growing as the pedestrian adapts to new conditions.

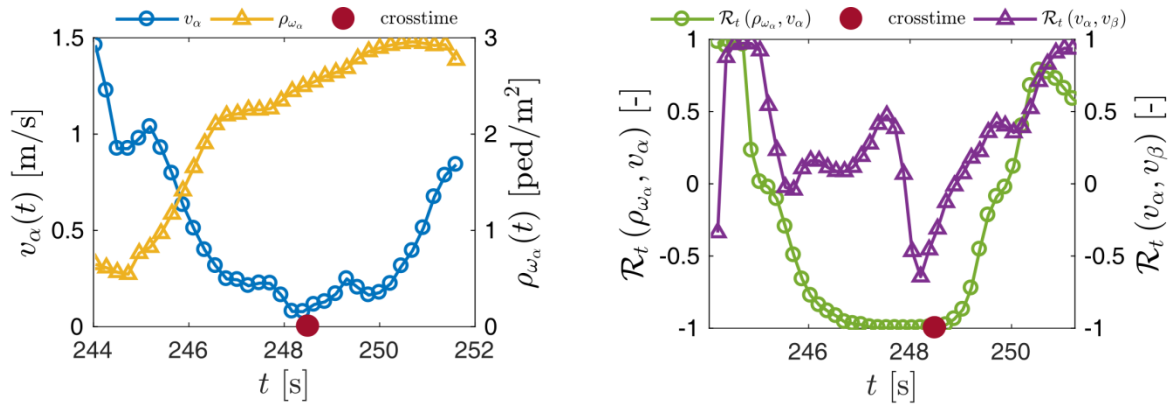


Fig. 1: Left: Velocity (blue circles) and individual density (yellow triangles) for pedestrian α . The time of the approach of pedestrian β to the pedestrian α at a distance of **0.75 m** (crosstime) is visualized by the red point. Right: The correlation of density and velocity for pedestrian α (green circles), the correlation of velocities for pedestrians α and leader β .

The behaviour of the pedestrian in free flow is not quite controlled by either local density or response to a certain leader (Fig. 1, Right). The positive correlation of velocity and density indicates competitive behaviour when the occurrence of another pedestrian motivates participants to move faster. Moreover, the positive correlation between the velocities for pedestrians α and β indicates that both are affected by the same environmental effects.

While approaching and joining the crowd, velocity of any pedestrian is strongly related to their individual density – significant negative correlation is observed in Fig. 2, Left, where curves are plotted at the normalized time t_N (for each pedestrian $t_N = 0$ and $t_N = 1$ corresponds to the entry and exit time, respectively). The joining the crowd phase was observed for t_N between 0.2 and 0.6.

Although this correlation is sensitive to all possible deviations, it is obvious that the most paths were fully joined the crowd in t_N from 0.5 to 0.7 and then the expected negative correlation completely turned positive – despite the increasing individual density, the velocity is slowly growing. An explanation of this phenomenon including the flow conservation law is described in [2].

As this phenomenon represents just a coincidence, not causality, there is no prediction power of such dependence. The model of increasing velocity based just on increasing density is not applicable; it is necessary to look at this particular part of movement in a detail.

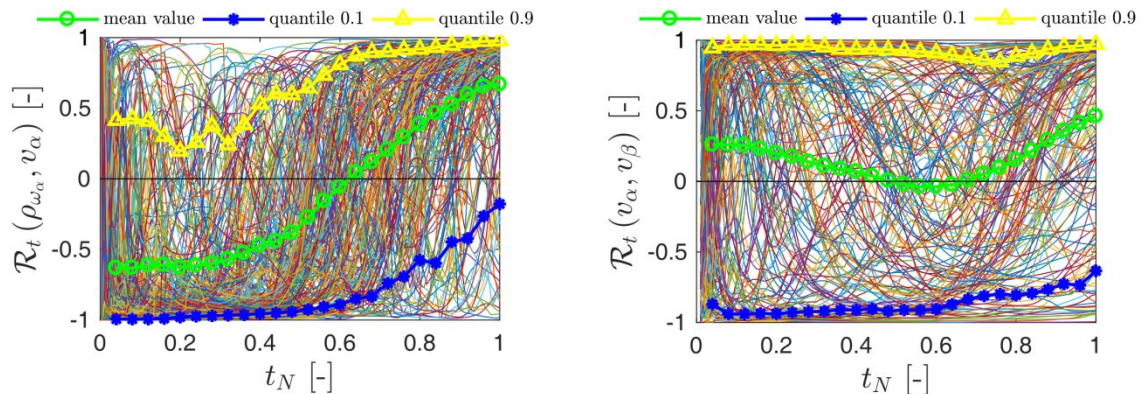


Fig. 2: Correlation between individual density and velocity (Left) and between follower and leader velocities (Right) - for each pedestrian corresponding to travel time $\in (7, 15)$ s and mean occupancy $\in (7, 15)$ ped. Mean value (green line with circles), lower (blue line with stars) and upper (yellow line with triangles) decile are visualized. All plotted with respect to normalized time t_N .

3. Follower-leader concept

The studied crowd at the exit area has an internal structure similar to a multi-row chaotic queue; therefore the pedestrian standing behind someone else often just copies the movement of a predecessor. To explain this behaviour, simple follow-leader model inspired by vehicular traffic might be developed.

The intended algorithm selects suitable candidates to be a leader for each pedestrian with respect to their distance and direction. As a result of that, the movement of so-called follower might be modelled (predicted) using information of the movement of their leader.

In this proof-of-concept study, the pedestrian β is defined as a leader for pedestrian α from the point in time when α approaches β at a distance 0.75 m according to our assumption that β is closer to the exit than α . As shown in Fig. 1, Right, the correlation of such leader's and follower's velocity increases shortly after crosstime, and it is followed by the mentioned changes in the trend of velocity-density correlation. Furthermore, this phenomenon seems to be global – the Fig. 2, Right demonstrates that the mean correlation of leader's and follower's velocities significantly grows in the crowd part of the egress process.

It is worth noting that a leader for one pedestrian can be at the same point in time a follower for another, and, although the leader and the follower have the same goal, there does not have to be any psychological link between them. This approach is not related to controlled evacuation models, where leaders are often defined in advance and have a special role during an evacuation.

However, no behaviour pattern is universal for all pedestrians. Similar to heterogeneity in velocity, aggressiveness or path selection, heterogeneity in the behaviour inside crowd might be introduced as well.

3. Conclusions

This article investigates the correlation of pedestrian velocity and individual density during the whole process of passing a room. As shown, the expected negative velocity-density correlation holds only in the phase of approaching the crowd. To predict the velocity of an individual, we introduced the follow-leader concept to replace a velocity-density dependency by leader-follower velocity dependency. The definition of a leader is individual and based just on the position in the room and the velocity that enables automatic detection. The provided correlation study proved the competency of such an approach that can be formulated as movement model on microscopic scale.

Acknowledgements

Research presented in this work has been supported by the Grant SGS18/188/OHK4/3T/14 provided by the Ministry of Education, Youth, and Sports of the Czech Republic (MŠMT ČR).

We would like to thank GAMS team members, namely Pavel Hrabák and Matěj Kotrba, for significant help with organizing the experiment. All experiment participants approve for the experimental data to be stored, used and published for academic purposes.

For more details see our webpage <http://gams.fjfi.cvut.cz/topics/pedstrian-dynamics/>.

References

- [1] M. Bukáček and P. Hrabák and M. Krbálek, “Microscopic Travel Time Analysis of Bottleneck Experiments,” *Transportmetrica A: Transport Science*, 2018.
- [2] M. Bukáček and J. Vacková, “Evaluation of pedestrian density distribution with respect to the velocity response,” in *Traffic and Granular Flow*, 2017, submitted.
- [3] B. Steffen and A. Seyfried, “Methods for Measuring Pedestrian Density: Flow, Speed and Direction with Minimal Scatter,” *Physica A* 389(9): 1902 -- 1910, Elsevier, 2010.
- [4] A. Schadschneider and D. Chowdhury and K. Nishinari, *Stochastic Transport in Complex Systems*. Elsevier, 2010.
- [5] J. Poryzcki and J. Was and L. Hedayatifar and F. Hassanibesheli and K. Kulakowski, “Velocity correlations and spatial dependencies between neighbors in a unidirectional flow of pedestrians,” *Physical review E*, 2017.

Forecasting Visitors' behaviour in Crowded Museums

Caterina Balzotti¹, Maya Briani², Alessandro Corbetta³, Emiliano Cristiani²,
Marina Minozzi⁴, Roberto Natalini², Sara Suriano⁵, Federico Toschi^{2,3}

¹Dipartimento di Scienze di Base e Applicate per l'Ingegneria, Sapienza Università di Roma, Rome, Italy

²Istituto per le Applicazioni del Calcolo, Consiglio Nazionale delle Ricerche, Rome, Italy

³Department of Applied Physics, Eindhoven University of Technology, Eindhoven, The Netherlands

⁴Galleria Borghese, Rome, Italy

⁵Dipartimento di Matematica, Sapienza Università di Roma, Rome, Italy

Abstract - In this paper we tackle the issue of measuring and understanding the visitors' dynamics in a crowded museum in order to create and calibrate a predictive mathematical model. The model is then used as a tool to manage, control and optimize the fruition of the museum. Our contribution comes with one successful use case, the Galleria Borghese in Rome, Italy.

Keywords: pedestrian modelling, complex behaviour, floor usage, data acquisition, museums.

1. Introduction

Operating public facilities such as museums, which come as intricate assemblies of rooms, entails a complex technological issue: the optimization of the floor usage. This aims at ensuring that visitors' flows develop safely and comfort levels are maintained at all times. Overall, a successful floor usage optimization demands different capabilities, namely monitoring, forecasting, and, ultimately, steering the visitors' dynamics.

Monitoring and forecasting involve a mixture of challenges: the first demands continuous and reliable data acquisition, the second requires complexity reduction, modelling and the understanding of some psychological aspects of crowd motion.

In this contribution we tackle the issue of forecasting the visitors' dynamics and create a predictive mathematical model for the visitors' behaviour in a museum. Our model is aimed at enhancing the guests' experience, and particularly at preventing under- and over-occupied areas.

2. The 'Galleria Borghese' in Rome

Our contribution comes with one successful use case: the optimization of the visitors' dynamics at Galleria Borghese in Rome, Italy. Galleria Borghese is one of the most famous museums in the world, unique with regard to Bernini's sculptures and Caravaggio's paintings. The museum receives more than 500,000 visitors per year, which is quite a large number considering the small size of the exhibition space.

The museum has several historical, artistic and architectural constraints which limit its usability. In addition, the two floors of the museum have different capacity limits (because of the different escape routes), and the artworks cannot be exposed to excessive temperature and humidity variations.

Currently, the visits are organized as follows. Tickets must be booked in advance, and two hours are given to stay in the museum. A small percentage of tickets, called "last minute", are instead sold at the moment. At the end of each period of visit, people are invited to leave, and the museum empties completely. Visits are not organized - on purpose - through an obligatory exhibition path (i.e. a predetermined sequence of rooms). Moreover, the circular structure of the building makes the visit not a one-way route: visitors tend to come back several times to the same rooms (the density of the artworks is so high that one can miss completely some pieces on the first visit) and some effort must be done to find the stairway which connects the lower with the upper level.

The main goal of this research is to increase the number of visitors per day while keeping the number of people within the limits and under an acceptable comfort level at any time. The control variables of the museum are the maximum number of sold tickets, the opening hours, the maximum duration of the visit, the maximum number of guided groups allowed at the same time, and others.

3. Methods

3.1. Data acquisition

Presence data were collected manually, simply counting the passages of people moving from one room to another in the whole museum. This was done for four turns of visit during four days, by means of a specifically designed smartphone app. The app, connected to a database, was able to record the data (including the direction of the movement) and its timestamp in real time. Such measurements allowed us to get the number of people in each room at each time. The duration of the visit of each room was also measured from a sample of visitors (about 500).

3.2. Mathematical model

The complex behaviour of visitors inside the museum makes the prediction of the path of each single visitor almost impossible. On the contrary, it is feasible to predict the movements of the visitors as a whole. For this reason, although our model treats the visitors' motion individually, we do not consider the problem of tracking single persons. Rather, we adopt an "Eulerian" point of view, being interested only in the number of people present in every room at all times, and the flows of people through museum's doors. The visitors' dynamics deploy over an undirected graph representing the museum rooms, see Fig. 1. Thus, while each room is simplified as a graph node, connections among different rooms, such as doors or staircases, define the edges of the graph.

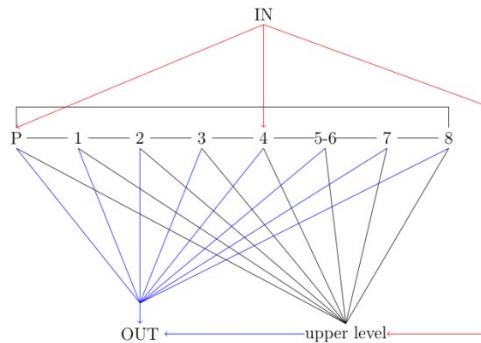


Fig. 1: Graph representing the connections among the rooms of the museum. Numbers 1-8 denote the eight rooms of the lower level, 'P' is the entrance hall. The museum has three access points (red lines). For simplicity, all rooms at the upper level are unified in a single node and we assume that exit and upper level can be accessed by any room.

Initially visitors are placed in a waiting room (IN, cf. Fig. 1). The time spent in this room is computed accordingly to a specific probability distribution function, in order to take into account that people do not all enter together (because ticketing requires a few seconds) and that some people arrive late. Once the visitor is in a room, the algorithm assigns the room visit time (RVT), i.e. the desired duration of the stay in that room, sampling a normally distributed random variable shaped in accordance to measured data. The RVT is then modified based on the current degree of congestion of the room (slight congestion increases the RVT, high congestion decreases it) and based on the number of times that room was already visited (known rooms are visited more rapidly, and no room can be visited more than three times). Once the visit of the room is completed, the visitor moves to another room. Among the connected rooms, the choice is random, with higher probability to move to yet unvisited or less visited locations. The probability to change floor, instead, is proportional to the number of visited rooms in the current floor

(but the upper level can be visited only once). When the whole museum is visited or the time allowed for visit is over, the visitor leaves the museum (moves to OUT, cf. Fig. 1).

A calibration of the model parameters allowed us to get the result shown in Fig. 2: The model is able to reproduce nicely the occupancy over time, both in the whole museum and in the two floors separately.

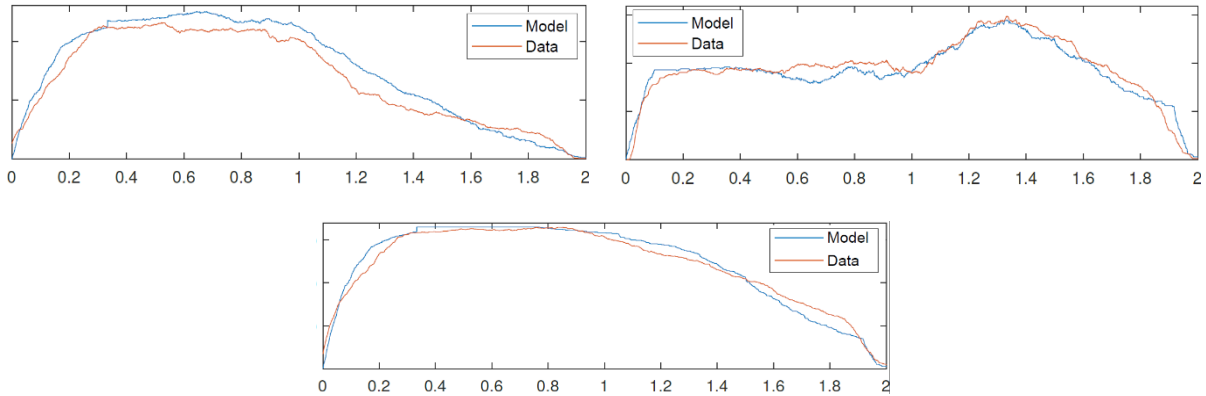


Fig. 2: Profile of the number of visitors as a function of time (0-2h, i.e. a single turn) computed by the model and compared with measured data (top-left: lower level, top-right: upper level, bottom: whole museum). Exact numbers are not made public by the museum.

3. Results

In this section we report the results of the simulations corresponding to three scenarios, see Fig. 3. In the first one we reproduce the strategy currently employed in the museum. Every 2h (from 9 a.m. to 7 p.m.) 360 visitors enter the museum, 270 of them begin the visit from the lower level, while 90 begin from the upper level. At the end of the turn, visitors are invited to leave.

In the second scenario, we test the same entrance strategy (270+90) but we drop the forced exit, i.e. people are free to stay more than two hours. As it can be seen, the overall occupancy is not larger than the first scenario. This is plausible since we observed that two hours are enough for most people and, in the first scenario, about 5 minutes are lost in emptying and re-filling the museum again.

In the third scenario, the strategy resulted from a gradient-based optimization algorithm. The goal was to maximize the number of visitors per day under two constraints: the maximum number of visitors allowed in the lower level and in the upper level. The two control variables were the number of people beginning the visit from the lower and the upper level respectively. Moreover, people enter every hour, with no forced exit after two hours. Initially, 140+90 people enter the museum, then 190+0 people enter every hour until the final turn, when 250+30 people go in. In this way we are able to reduce significantly the congested period at the upper level (see Fig. 2 top-right, around 1.3h), to avoid dead periods and, most important, increasing by 40 the total number of visitors per day.

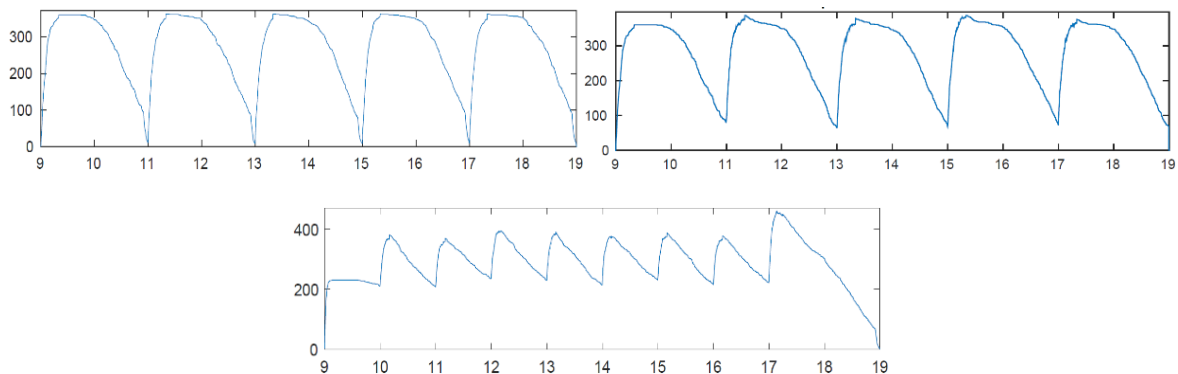


Fig. 3: Number of visitors in the whole museum as a function of the hour of the day (top-left: first scenario, top-right: second scenario, bottom: third scenario). In the second and third scenario the museum is never empty.

Human stampedes at mass gatherings: An overview

Lakshmi Devi Vanumu¹, Laxmikant², K.Ramachandra Rao³

^{1,2,3} Department of Civil Engineering, Indian Institute of Technology, Delhi
Hauz Khas, New Delhi, India
lakshmiddevivanumu@gmail.com; kumar.laxmikant24@gmail.com
rrkalaga@civil.iitd.ac.in

Abstract - The main aim of this study is to present an overview of human stampedes and to identify the major triggering factors with respect to the type of events leading to number of fatalities and injuries. Considering major crowd incidents, the stampedes were categorized based on location, triggering factor, type of event and year of occurrence. This paper lists a total of 137 stampedes occurred all over the world between the years 1883 and 2017. The details include the name and type of event, location of the event, number of injuries and fatalities, probable reason for the stampede and type of reliable source. Stampedes are classified based on type of events as religious, sports, entertainment, festival, political and others. Among all types of events, religious gatherings cause 64% of total fatalities and 51% injuries. The triggering factors are identified as rumours, fire, structural failure, narrow passage, overcrowding and others. Out of all the triggering factors mentioned above, narrow passage causes about 27% fatalities followed by overcrowding and rumours with 23 and 21% respectively. The majority of injuries caused by overcrowding turn out to be 35%. It is also observed that the frequency of stampede occurrences increasing since 1980. This study can be considered as an initial step in giving an overview of human stampedes, which would help to prepare a framework based on the past experiences. Further, it can give better insights for large-scale crowd management and to minimize the loss of human lives in future.

Keywords: Human stampedes, Triggering Factors, Fatalities, Injuries

1. Background

Human stampedes can occur at mass gatherings due to several reasons such as high crowd densities, physical and psychological problems of humans and crowd management issues etc. which leads to injuries and fatalities. Few researchers have addressed the need of studying human stampedes. Based on the number of deaths and injuries, Ngai et al., [1] proposed a logarithmic scale ranging from Class I to V to classify the human stampedes. This unique categorization may help the researchers and scientists to understand the characteristics of stampedes for systematic investigation and further analysis. Illiyas et al., [2] identified that majority of human stampedes occurred in India are in religious gatherings. Ngai et al., [3] tried to estimate the degree of underreporting of human stampedes in India by using two different methods. For a systematic investigation of epidemiological characteristics of stampedes, they have emphasized the need of an international standardized database that can record the human stampedes occurring all over the world. Alaska et al., [4] highlighted that the crowd control measures such as use of crowd simulation models, video monitoring, modification of transport system etc. were adopted during Hajj played a crucial role in improving the safety. The current study made an attempt to present an overview of human stampedes and to identify the major triggering factors with respect to the type of events leading to number of fatalities and injuries.

2. Analysis

Data related to human stampedes were collected from various sources such as reports, journal publications, different search engines etc. After a thorough review of literature, the stampedes were categorized based on location, triggering factor, type of event and year of occurrence. A total of 137 stampedes occurred all over the world between the years 1883 and 2017 were considered in this paper. The details include the name and type of event, location of the event, number of injuries and fatalities, probable reason for the stampede, and type of reliable source. Stampedes are classified based on type of

events as religious, sports, entertainment, festival, political and others. Among all types of events, religious gatherings cause 64% of total fatalities and 51% injuries. Further, it is observed that most of the peak values in Fig.1 representing the fatalities and injuries occurred in different years are related to various religious events. This observation is in concurrence with the findings of [5] reporting that majority of the stampedes occurred in India and Saudi Arabia. Some of the major stampedes were described in table 1. The triggering factors are identified as rumours, fire, structural failure, narrow passage, overcrowding and others. Out of all the triggering factors mentioned above, narrow passage causes about 27% fatalities followed by overcrowding and rumours with 23 and 21% respectively. The majority of injuries caused by overcrowding turn out to be 35%. Proportion of fatalities with respect to type of event and impact of triggering factors on number of injuries, fatalities are shown in Fig.2.

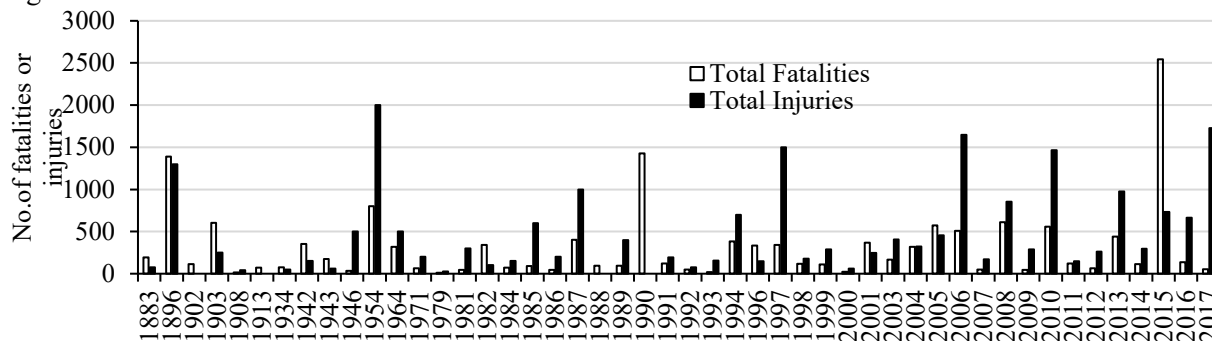


Fig. 1: Total number of fatalities and injuries with respect to year of all the events

Table 1: Description of some major stampedes

S. No	Name of the Event	Year	Country	Location	Fatalities	Injuries	Type of Event	Triggering factor
1	Nicholas Coronation	1896	Russia	Moscow	1389	1300+	Festival	Rumour
2	Iroquois Theatre Fire	1903	United States	Chicago	602	250	Entertainment	Fire
3	Peru Stampede	1964	Peru	Lima	318	500	Sporting ingress	Tear Gas
4	Hajj	1987	Saudi Arabia	Mina, Mecca	402	1000	Religious	Conflict b/w people
5	Hajj	1990	Saudi Arabia	Mina, Mecca	1426	-	Religious	Narrow Passage
6	Hajj	1994	Saudi Arabia	Mina, Mecca	270	200	Religious	Overcrowding
7	Wai Stampede	2005	India	Wai, Maharashtra	267	200	Religious	Wet Floor
8	Mandhar Devi temple	2005	India	Satara, Maharashtra	258	200	Religious	Fire
9	Hajj	2006	Saudi Arabia	Mina, Mecca	380	1000	Religious	Overcrowding
10	Naina Devi Temple	2008	India	Himachal Pradesh	163	48	Religious	Rumour
11	Phnom Penh	2010	Cambodia	Phnom Penh	347	395	Entertainment	Rumour
12	Sabarimala	2011	India	Pullumedu, Kerala	102	100+	Religious	Narrow Passage
13	Hajj	2015	Saudi Arabia	Mina, Mecca	2431	427	Religious	Narrow Passage
14	Puttingal Devi temple	2016	India	Kerala	106	383	Religious	fire

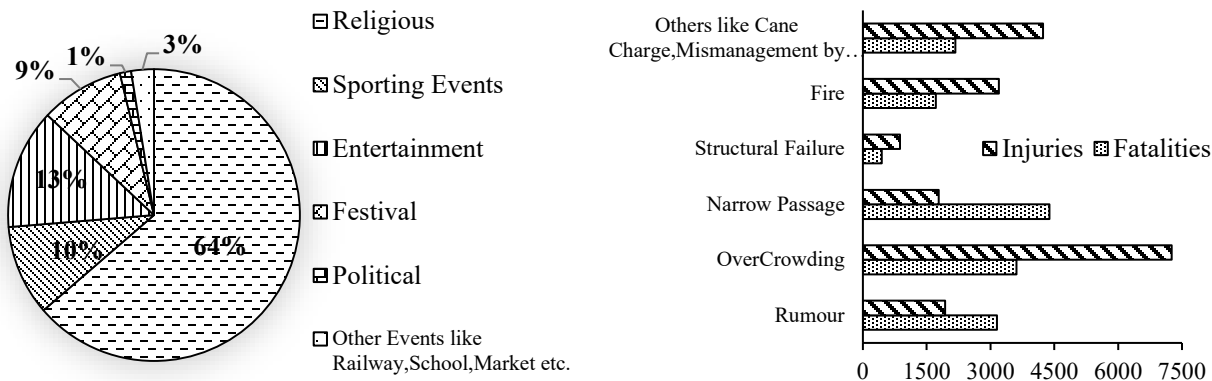


Fig. 2: (a) Distribution of fatalities with respect to type of event (b) Influence of triggering factors on injuries and fatalities.

3. Conclusion

The study presents an overview of human stampedes occurred all over the world. It is observed that the frequency of stampede occurrences increasing since 1980 and most of the stampedes are happened in religious gatherings. The major triggering factors in various stampedes were identified as narrow passage, overcrowding and rumours. This study can be considered as an initial step in giving an overview of human stampedes, which would help to prepare a framework based on the past experiences. Further, it can give better insights for large-scale crowd management and to minimize the loss of human lives in future.

References

- [1] K.M. Ngai, F.M. Burkle, A. Hsu and E.B. Hsu, "Human stampedes: a systematic review of historical and peer-reviewed sources," *Disa. Med. Pub. Health Pre.*, vol.3, no.4, pp.191-5, 2009.
- [2] F.T. Illiyas, S.K. Mani, A.P. Pradeepkumar, K. Mohan, "Human stampedes during religious festivals: A comparative review of mass gathering emergencies in India," *Int. Jour. Dis. Risk. Red.*, vol.5, pp.10-18, 2013.
- [3] K.M. Ngai, W.Y. Lee, A. Madan, S. Sanyal, N. Roy, F.M. Burkle Jr and E.B. Hsu, "Comparing two epidemiologic surveillance methods to assess underestimation of human stampedes in India," *PloS. Cur.*, vol.23, no.5, 2013.
- [4] Y.A. Alaska, A.D. Aldawas, N.A. Aljerian, Z.A. Memish and S. Suner, "The impact of crowd control measures on the occurrence of stampedes during mass gatherings: the Hajj experience," *Travel. Med. Inf. Disease.* vol.15, pp.67-70, 2017.
- [5] Y.H. Hsieh, K.M. Ngai, F.M. Burkle and E.B. Hsu, "Epidemiological characteristics of human stampedes," *Disa. Med. Pub. Health Pre.*, Vol.3, no.4, pp.217-23, 2009.
- [6] Hoseinpourfard, Mohammadjavad, G. Mostafa, T. Shahram, A. Ali and I. Morteza. "The Emergence of Hajj Stampedes: Lessons for Draw near in the Islamic Values in Hajj Trauma Centers Accreditation." *Trauma. Mon.* Published online 2016.
- [7] E.B. Hsu and F.M. Burkle, "Cambodian Bon Om Touk stampede highlights preventable tragedy," *Prehospital. Dis. Med.*, vol.27, no.5, pp.481-2. 2012.
- [8] S. Parkash. (2016, April 10). Brief Report on Reconnaissance Study of Puttingal Temple Fire Incident Paravur, Kollam District, Kerala State 10.13140/RG.2.1.1782.4249.
- [9] A tragedy remembered NFA Journal July/August 1995.
- [10] India disaster report (2011, June). National Institute of Disaster Management.

Influence of Obstacles on the Use of the Danger Zone on Railway Platforms

Jasmin Thurau¹, Nicolas Keusen²

¹SBB AG, Technologic Asset Management
Hilfikerstrasse 3, 3000 Bern 65, Switzerland

jasmin.thurau@sbb.ch

²BAV, Dept. of Security
Ittigen, Switzerland

Nicolas.Keusen@bav.admin.ch

Abstract - Growing passenger numbers and the lack of space available led to research on pedestrians' behaviour on railway platforms in Switzerland. By using stereo sensors, pedestrians' tracks were collected on a platform in the train station of Bern. The analysis of pedestrians stepping into the danger zone showed clearly that obstacles have a large influence on the frequencies of pedestrians using the danger zone. By presenting four hypotheses the effect of obstacles on pedestrians' use of the danger zone on train station platforms is investigated.

Keywords: railway platforms, pedestrian behaviour, use of danger zone, influence of obstacles

1. Introduction

Passenger numbers grew significantly within the last years and are expected to increase further in the future. This trend results in more crowded platforms and, especially during peak hours, the capacity of platforms is nearly reached.

Latest research analysed the relation between pedestrian density on platforms and the number of pedestrians entering the danger zone [1]. Thurau et al. (2017) show that there is still further research needed when defining the maximum number of passengers allowed on platforms. By using highly accurate sensor data [2], this paper focuses on where pedestrians on railway platforms tend to use the danger zone more often.

For this paper the Swiss definition of the danger zone is used (Fig. 1). It is defined as follows: The danger zone is the area next to the tracks, which shouldn't be used by passengers when no train occupies or a train drives through the station. The safety zone is the area which shall be used by passengers for movements and waiting. The danger zone starts with the safety line, which itself is still within the safety zone.

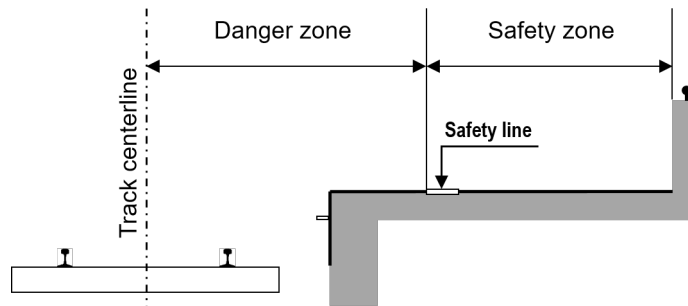


Fig. 1 Definition of the danger zone

2. Hypotheses

In order to analyse the influence of obstacles on railway platforms on the use of the danger zone, the following hypotheses have been presented:

H1: Next to obstacles the number of people stepping into the danger zone is significantly higher than in areas without any obstacles.

H2: The share of people using the danger zone rises when the safety zone gets smaller.

H3: The duration of people using the danger zone is significantly higher next to obstacles than in areas without any obstacles nearby.

H4: The average walking speed of pedestrians using the danger zone decreases with an increase of time people use the danger zone.

H1 and H2 are derived from the idea that less space for overtaking, due to obstacles or other pedestrians, leads to a higher number of pedestrians stepping into the danger zone [3].

Under the assumption that safety zones are similarly crowded, H3 is based on the thought that overtaking pedestrians next to larger obstacles require longer distances within the danger zone, in comparison to short obstacles [3].

H4 results from the idea that pedestrians use the danger zone for the shortest possible time period and therefore speed up for overtaking. Pedestrians that do not realize the potential threat when being within the danger zone do not change their walking speed, as they do not make a difference between both platform zones.

3. Analysis

3.1 Data collection and data set

In order to investigate the hypotheses, tracking data of pedestrians on a railway platform in the train station of Bern, Switzerland is used. The data is collected with high precision sensors [2]. The data was aggregated to x- and y-coordinates per person per second. Basic characteristics per pedestrian, such as walking speed, were calculated. By combining this data with information describing the presence or absence of trains on the tracks, it was possible to select only the situations when pedestrians were using the danger zone without a train occupying the track. These situations are considered as potentially unsafe and are therefore relevant for the investigation of the hypotheses. The analysis is based on data for weekdays and day time (6am to 8pm) for the month of September 2016 (21 weekdays). The number of trains is 2 to 4 per hour and track.

Fig. 2 shows the sensor equipped area of platform 3/4 in Bern. It consists of a shorter obstacle (staircase) to the left (zone 1), a longer obstacle (ramp) in the middle (zone 2) and small obstacles to the right (zone 5). Zone 3 represents the zone where passengers enter or leave the platform by using the ramp; zone 4 has no obstacles. In the following the platform is going to be separated in the middle, parallel to the tracks, so that zone 1 at track 3 is named 1.3, zone 2 at track 4 is named 2.4 and so on.

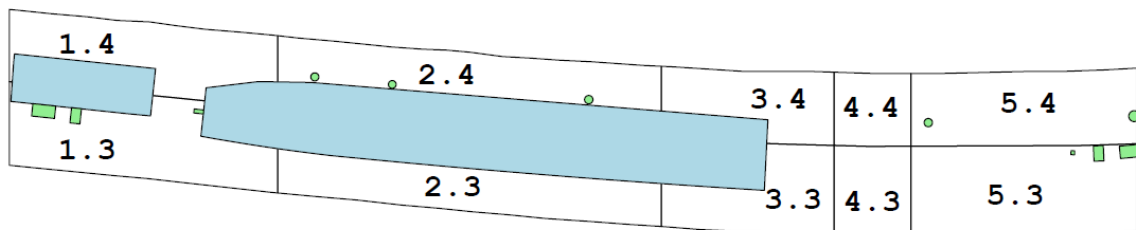


Fig. 2 Platform layout Bern - tracks 3 and 4

For the analysis of hypothesis 1, 2 and 4 the platform is separated into zones of 1m length. This results into zones from 1.3 until 60.3 at track 3 and 1.4 to 60.4 at track 4, as 60 meters length of the platform is equipped with sensors.

3.2 Results for H1 & H2: number of uses and share of people using the danger zone

H1 and H2 can't be rejected: The analysis shows a higher number of uses of the danger zone next to obstacles. Overall results for both tracks show a median number of uses of the danger zone during

daytime at weekdays of 7.19 uses per hour in zones with less than 2m safety zone. For safety zones wider than 2m the median is 3.65, which is significantly lower. Table 1 shows detailed results including upper and lower quartile. The median share of people using the danger zone next to obstacles and with smaller safety zones (11%) is significantly higher than the share of people using the danger zone at wider safety zones (3%). The lower quartile of small safety zones (9%) is higher than the upper quartile of wider safety zones (4%).

Table 1 number and share of uses of the danger zone with different width of safety zone

	uses of the danger zone			share of people using the danger zone	
	< 2m	> 2m		< 2m	> 2m
width of safety zone			width of safety zone		
upper quartile	9.5	5.5	upper quartile	15%	4%
median	7.19	3.65	median	11%	3%
lower quartile	5.76	2.58	lower quartile	9%	2%

3.2 Results for H3: duration of use of the danger zone

H3 can't be rejected: The highest median duration of people's use of the danger zone was measured in zone 2.3, this is the zone next to the ramp, representing the smallest safety zone on the platform. The results for zone 2.4 are the second highest, although the safety zone is slightly smaller (see Table 2). The reason might be the lower frequency of use of this side of the ramp. This shows that additional factors, such as person density, influence pedestrians use of the danger zone (see also [1]).

Table 2 duration of use of danger zone with different width of safety zone [s]

zone	average duration in danger zone										< 2m	> 2m
	1.3	1.4	2.3	2.4	3.3	3.4	4.3	4.4	5.3	5.4		
average width of safety zone	2.68m	2.22m	1.73m	1.72m	2.67m	2.44m	4.10m	3.30m	4.04m	3.33m		
upper quartile	2.13	0.86	20.14	6.10	6.72	1.33	9.69	4.50	3.45	1.02	12.55	3.16
median	1.41	0.46	14.53	4.53	3.50	0.67	4.00	3.25	2.27	0.59	9.79	2.27
lower quartile	0.86	0.25	10.66	3.06	1.72	0.33	1.81	2.00	1.31	0.34	7.74	1.59

3.2 Results for H4: walking speed and duration in danger zone

Data reliability is not high enough to calculate the duration within the danger zone per person. The overall time of any person in the danger zone can be computed, but not the duration of use of the danger zone for a certain ID. Therefore, speed and distance of a certain ID can't be compared, but analysis of H3 was possible.

4. Conclusion

It is shown that the available width of the safety zone clearly influences number, share and duration of use of the danger zone by pedestrians. It can be found that at around two meters safety zone we can find a different behaviour of pedestrians regarding the use of the danger zone. This parameter needs further analysis, especially at different train stations. In the next step, a model including the width of the safety zone and the person density shall be developed.

References

- [1] J. Thureau, J. van den Heuvel, N. Keusen, M. van Ofwegen und S. Hoogendoorn, „Influence of Pedestrian Density on the Use of the Danger Zone at Platforms of Train Stations“, Bern / Utrecht, 2017.
- [2] J. van den Heuvel, J. Thureau, M. Mendelin, R. Schakenbos, M. van Ofwegen und S. Hoogendoorn, „An application of new pedestrian tracking sensors for evaluating platform safety risk at Swiss and Dutch train stations“, Utrecht / Bern, 2017.
- [3] N. Keusen et al., „Safety Distances on Platforms“, Bern, 2011.

Modeling Environmental Operative Elements in Agent-Based Pedestrian Simulation

Luca Crociani¹, Giuseppe Vizzari¹, Stefania Bandini^{1,2}

¹Complex Systems and Artificial Intelligence research center
University of Milano-Bicocca, Milano, Italy
{name.surname}@unimib.it

²Research Center on Advanced Science and Technology,
The University of Tokyo, Tokyo, Japan

Abstract - Models for pedestrian simulation are employed on a day-to-day basis for supporting the design and planning of the built environment in normal and evacuation situations. One of the aspects that are least investigated in the community, probably because it is considered closer to technology transfer than to research, is the modelling of operational elements of the simulated environment. The present paper briefly describes an agent-based approach to the representation of operative elements of the environment with particular attention to the mechanisms of interaction between these active objects and pedestrians.

Keywords: agent-based simulation, environment, operative elements

1. Modelling Operative Elements of Pedestrians' Environment

Models for pedestrian simulation are employed on a day-to-day basis for supporting the design and planning of the built environment in normal and evacuation situations. Discrete modeling approaches are characterized by good computational properties (in particular the possibility to exploit parallel computing architectures) while preserving reasonable precision in the simulation of pedestrian dynamics. The Floor Field approach [1], originally proposed for Cellular Automata pedestrian models, represents a very general mechanism for managing operational level aspects of pedestrian dynamics in discrete modeling approaches. There are several extensions of the approach, for instance representing the effect of groups in the simulated pedestrian population [2][3], but also for the management of aspects that are difficult to incorporate within a discrete setting, like heterogeneous walking speeds [4][5], and particular shapes of the simulated environment (such as situations in which pedestrians perform circular movements [6]). It is important to notice that there are also extensions of this modeling approach that employ annotations to the discrete structure of the environment for the management of spatial information supporting tactical level decisions [7].

One of the aspects that are least investigated in the community, probably because it is considered closer to technology transfer than to research, is the modeling of operational elements of the simulated environment. We adopt this broad term to describe particular objects that are situated in the environment that is being modeled and simulated that influence the behavior of pedestrians by altering their velocity, due to the fact that they partly hinder a smooth movement, require pedestrians to perform some action to proceed, or that they purportedly limit overall flow, but that can also influence tactical level choices, for instance due to the fact that unbalanced queues can form as a consequence of their presence. A typical example of these objects is represented by turnstiles/ticket gates, but also resource distributors (e.g. ATMs). These objects are often crucial elements of the simulated scenarios, especially within the transportation area, and alternative numbers and arrangement of these elements is sometimes entirely motivating the simulation project.

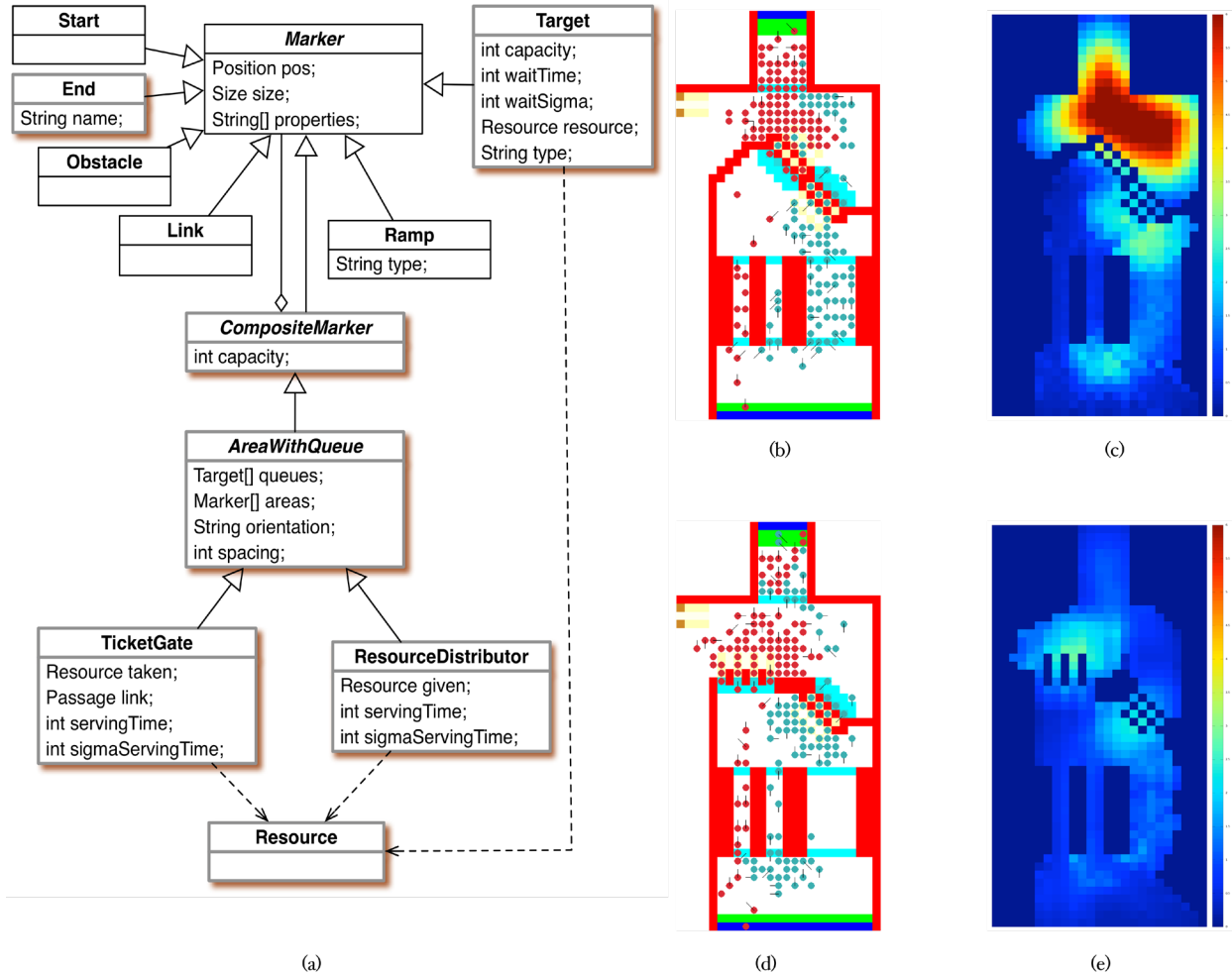


Figure 1- UML class diagram describing the organization of markers related to operative elements (a), and screenshots of alternative spatial arrangements (b and d) and cumulative mean densities (c and e).

The management of this kind of object within a pedestrian simulation models requires a more thorough consideration of the role of agents' environment [8][9], that is something more than a simple container of pedestrians, limiting their movements due to the presence of obstacles. The approach adopted for this work extends a model for operational and tactical level decisions (described in [7]) to represent and manage turnstiles and resource distributors. In particular, the environment in which agents are situated includes markers (their organization is shown in Figure 1a), that are particular sets of cells that play a role in supporting different aspects of agents' decisions and behaviors: these markers are in fact instrumental in the generation of floor fields, guiding pedestrian navigation at operational level, but they also compose higher level knowledge about the structure of the environment, owned by each agent. Within this context, some markers influence in an even deeper way agents' actions, in the vein of [10], leading them to form queues in front of distributors of objects that are necessary to carry out some specific actions (i.e. tickets to pass through a turnstile) or gates that require passing agents to provide an object (the above mentioned ticket) and that can also limit the overall flow of pedestrians, causing delays that can be calibrated to reflect real-world situations. These objects clearly influence both the tactical level decisions (i.e. "if I need to pass through a certain turnstile I need a ticket, so I have to go to a distributor first") as well as pushing agents to adopt some operational level alterations of their behavior (i.e. yield some turns of action to adapt to the

maximum throughput flow associated to a certain turnstile), therefore cooperating with agents and performing a regulation function [11].

2. Achieved Results

Validation experiments based on “unit tests” (i.e. measuring the overall flow of pedestrians within a corridor with a single turnstile) have been performed also with the aim of actually calibrating some parameters of objects like turnstiles, also with the aim of supporting forms of verification tests as suggested by [12]. We also considered a more complicated example scenario, presenting most typical elements of a transport station but in a much smaller scale, to support a comparison among alternative arrangements for the same number of operative elements within a small entrance to a transit station, as shown in Figure 1b-Figure 1e. The effect of different position and arrangement of turnstiles has a significant effect on spatial utilization patterns, depicted in terms of cumulative mean density, qualitatively showing how this kind of object could be relevant to generate what-if scenarios fully exploiting pedestrian simulation models.

3 Conclusions and Future Works

The adopted approach represents a way to model and implement operative elements of pedestrians’ environment within an agent-based framework, and it also represents a starting point for modelling additional and potentially more complicated elements, such as elevators: the latter would require the definition of additional mechanisms for the operative element per se (in particular for the specification of the way the elevator responds to requests from different floors), but also potentially additional behavioural patterns for pedestrians (for instance to manage the social norms governing the process of exiting and boarding).

References

- [1] C. Burstedde, K. Klauck, A. Schadschneider, and J. Zittartz, “Simulation of pedestrian dynamics using a two-dimensional cellular automaton,” *Phys. A Stat. Mech. its Appl.*, vol. 295, no. 3–4, pp. 507–525, Jun. 2001.
- [2] G. Vizzari, L. Manenti, and L. Crociani, “Adaptive Pedestrian Behaviour for the Preservation of Group Cohesion,” *Complex Adapt. Syst. Model.*, vol. 1, no. 7, 2013.
- [3] F. Müller, O. Wohak, and A. Schadschneider, “Study of Influence of Groups on Evacuation Dynamics Using a Cellular Automaton Model,” *Transp. Res. Procedia*, vol. 2, pp. 168–176, Jan. 2014.
- [4] A. Kirchner, H. Klüpfel, K. Nishinari, A. Schadschneider, and M. Schreckenberg, “Discretization effects and the influence of walking speed in cellular automata models for pedestrian dynamics,” *J. Stat. Mech. Theory Exp.*, vol. 2004, no. 10, p. P10011, Oct. 2004.
- [5] S. Bandini, L. Crociani, and G. Vizzari, “An approach for managing heterogeneous speed profiles in cellular automata pedestrian models,” *J. Cell. Autom.*, vol. 12, no. 5, 2017.
- [6] K. Shimura, S. D. Khan, S. Bandini, and K. Nishinari, “Simulation and evaluation of spiral movement of pedestrians: Towards the tawaf simulator,” *J. Cell. Autom.*, vol. 11, no. 4, pp. 275–284, 2016.
- [7] L. Crociani, A. Piazzoni, G. Vizzari, and S. Bandini, “When reactive agents are not enough: Tactical level decisions in pedestrian simulation,” *Intelligenza Artif.*, vol. 9, no. 2, pp. 163–177, Dec. 2015.
- [8] D. Weyns, A. Omicini, and J. Odell, “Environment as a First Class Abstraction in Multiagent Systems,” *Auton. Agents Multi-Agent Syst.*, vol. 14, no. 1, pp. 5–30, 2007.
- [9] A. Helleboogh, G. Vizzari, A. Uhrmacher, and F. Michel, “Modeling dynamic environments in multi-agent simulation,” *Auton. Agent. Multi. Agent. Syst.*, vol. 14, no. 1, pp. 87–116, 2007.
- [10] S. Paris and S. Donikian, “Activity-Driven Populace: A Cognitive Approach to Crowd Simulation,” *IEEE Comput. Graph. Appl.*, vol. 29, no. 4, pp. 34–43, 2009.
- [11] S. Bandini and G. Vizzari, “Regulation Function of the Environment in Agent-Based Simulation,” in *Environments for Multi-Agent Systems III, Third International Workshop, E4MAS 2006, Hakodate, Japan, May 8, 2006, Selected Revised and Invited Papers*, 2007, vol. 4389, pp. 157–

- 169.
- [12] E. Ronchi, E. D. Kuligowski, P. A. Reneke, R. D. Peacock, and D. Nilsson, “The Process of Verification and Validation of Building Fire Evacuation Models,” Gaithersburg, MD, Nov. 2013.

Multiscale Pedestrian Dynamics and Infection Spread Model for Policy Analysis

Sirish Namilae^{1*}, Pierrot Derjany¹, Dahai Liu¹ Anuj Mubayi² and Ashok Srinivasan³

¹Embry-Riddle Aeronautical University
Daytona Beach, Florida, USA

²Arizona State University
Tempe, Arizona, USA

³University of West Florida
Pensacola, Florida, USA

*namilae@erau.edu

Abstract - In this paper, we present a formulation for a multiscale model combining a social force based pedestrian movement including collision avoidance and a stochastic infection dynamics framework to evaluate the spread of multiple infectious diseases during air travel. We apply the multiscale model to evaluate pedestrian movement strategies that can reduce infection spread during air travel. The results are presented for airport lounge and airplane boarding and deplaning. Use of parallel computing to evaluate the vast parameter space created due to stochasticity and discretionary pedestrian behavior is addressed

Keywords: Pedestrian dynamics, Infectious disease spread, Air travel

1. Introduction

Public transportation in general and air travel in particular have been identified as leading factors in the spread of infectious diseases; there is direct evidence for air travel related spread of infections such as influenza [1], SARS [2], measles [3] and norovirus [4]. Pedestrian movement within an airport and in airplanes is key to understanding and estimating the casual contacts between passengers and thereby understanding the infectious disease spread.

We have formulated a multiphysics computational model [5, 6] that incorporates particle dynamics based pedestrian movement of travelers in transit hubs (e.g. airports), contact analysis and stochastic infectious disease spread, to frame and analyze transportation policies that can mitigate infectious disease spread. The high economic and public perception costs on the transportation sector due to pandemic events necessitates policy that addresses mitigation. We utilize this multiscale model for policy design to develop strategies that mitigate spread.

2. Model Formulation

In order to first determine the number of pedestrian-pedestrian and pedestrian-surface contacts, we model the dynamics of mobile pedestrians incorporating interactions with other pedestrians and stationary objects, like walls and chairs, as particles. The motion of pedestrians interacting with other pedestrians and stationary particles evolves through molecular dynamics-based social force formulation [7]. The force \bar{f}_i acting on pedestrian i (or particle) can be defined as:

$$m_i \frac{dv_i}{dt} = \frac{m_i}{\tau} (\bar{v}_o^i(t) - \bar{v}^i(t)) + \sum_{j \neq i} \bar{f}_{ij}(t) \quad (1)$$

with pedestrian position at a given time obtained by integration as $r_i(t) = \int v_i dt$ where $\bar{v}_o^i(t)$ is the desired velocity of pedestrian and $\bar{v}^i(t)$ is the actual velocity, m_i is the mass and τ is the time constant. The momentum generated by a pedestrian's intention results in a self-propulsion force that is balanced by a repulsion force $\bar{f}_{ij}(t)$.

We also introduce location dependence to the desired velocity in the self-propulsion term as: $\bar{v}_o^i(t) \cdot \hat{e}_1 = (v_A + \gamma_i v_B) \left(1 - \delta / (\bar{r}_i \hat{e}_1 - \bar{r}_k \hat{e}_1)\right)$. Here \hat{e}_1 is the direction of desired motion. v_A and $\gamma_i v_B$ are the deterministic and stochastic components of desired velocity, δ is a distance constant such that at distance δ between pedestrian i and k the desired velocity of pedestrian i is zero. The $\gamma_i v_B$ term accounts for walking speed variations due to age group and gender [8]. We also introduce path determination and obstacle avoidance into our model to create a realistic representation of pedestrian motion.

Given the trajectory of pedestrians over time, the number of contacts of passenger i at time t can be evaluated as: $m_{i,t} = \sum r_{ij} \cdot \lambda_{ij}$, where $\lambda_{ij} = 0$ if $r_{ij} > x$ and $\lambda_{ij} = 1/r_{ij}$ if $r_{ij} < x$. r_{ij} is the distance between pedestrian i and j , and x is a virus specific distance parameter. The probability that the susceptible pedestrian i at time t will become infected is computed by multiplying the number of contacts, $m_{i,t}$, with the respective transmission probability of each contact of pedestrian i at time t . Eventually the number of infected individuals will be counted for each time.

Consider a population of size N consisting of $I(t)$ infected and $S(t)$ susceptibles at time t . A susceptible can become infected when coming into direct contact with an infected. However, the newly infected cannot be infective during the start of the incubation period of the illness. Moreover, the infection spread initiates due to the insertion of i_c^0 infectives initially ($t_0=0$) at their “ c ” days of infection, out of “ d ” incubation days. The probability that an infectious individual in the crowd meets other individuals is m_i/N . Denote by p_c the probability that a contact between a susceptible and an infective results in infection of the susceptible. The number of newly infected by infective i at time t , a discrete variable is a Poisson probability distribution, with mean $m_i(t-1) \cdot p_c \cdot [S_i(t-1)/N]$. Therefore, the number of people infected at time t is obtained by:

$$I(t) = \text{Poisson} \left(\sum_{c=1}^d \sum_{i=1}^{i_c^0} m_i(t-1) \cdot p_c \cdot (S_i(t-1) / N) \right) \quad (2)$$

Where m_i is the number of contact of susceptibles with the infectious traveller i and p_c the infection transmission probability.

3. Results and Discussion

Figure 1 shows the evolution of pedestrians at airport gate while (a) boarding, (b) deplaning and (c) at airport security check. The evolution of the particles is based on above formulation. We however perform numerous simulations using parallel algorithms on a supercomputing cluster to account for discretionary events and stochasticity in parameters like pedestrian speed. Aggregated information of pedestrian contacts from these simulations is used for modeling infectious disease spread based on Eq. 2 above. The contacts are defined based on time proximity and time spent. For example, for a contact based infectious disease like Ebola, a contact radius within touching distance (1 m) is used for the simulations while a larger contact radius of 2.1 m is used for diseases spread through aerosols like H1N1 influenza. This is based on studies that indicate fine particle spread over this distance due to expiratory events like coughing [9]. The probability of infection for different diseases is estimated based on viral shedding e.g. The H1N1 viral RNA level in nasal, oral or ocular shedding is used to construct corresponding probability profiles [10].

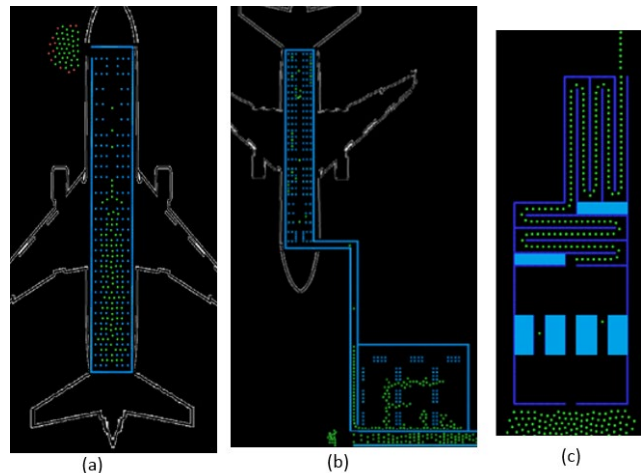


Fig 1. Simulation snapshots for pedestrian movement for (a) deplaning (b) boarding (c) security check

The combined pedestrian dynamics – infection spread model is then used for parametric analysis of strategies that mitigate infectious disease spread. An example of the policy study is the effect of airplane size and layout on the disease spread. Does transporting same number of people using large or small airplanes help reduce spread? How does this change for diseases transmitted via coarse droplets (e.g. Ebola) Vs fine aerosols (e.g. SARS)? What effect does pedestrian movement during boarding and deplaning have in this conjunction? We find that smaller airplanes are more effective in reducing the number of contacts compared to larger airplanes. Figure 3 provides a comparison between different airplanes and different infectious diseases (Ebola, SARS and H1N1 influenza) for enplaning airplanes of different sizes when one infected passenger in an unknown location is traveling. Such maps can be effective in analysing policies for infection reduction. We have studied similar strategies for queue shape, the size of airport gate and various boarding and deplaning schemes. The final poster will show the variations of infection spread for various strategies.

4. Conclusion

A multiscale computational model incorporating pedestrian dynamics and infection spread is presented. The model is used to study infection mitigation strategies for air travel.

Acknowledgements

Department of Transportation, Center for Advanced Transportation Mobility and National Science Foundation PRAC grant for partially supporting different parts of the research.

References

- [1] M.R. Moser, T.R. Bender, H.S. Margolis, G.R. Noble, A.P. Kendal, and D.G. Ritter, An outbreak of influenza aboard a commercial airliner. *American Journal of Epidemiology*, 110, (1), 1979, pp.1–6.
- [2] S.J. Olsen, H.L. Chang, T.Y. Cheung, A.F.Y. Tang, T.L. Fisk, S.P.L. Ooi, and J. Lando, Transmission of the severe acute respiratory syndrome on aircraft. *New England Journal of Medicine*, Vol. 349, No.25, 2003, pp. 2416–2422.
- [3] K. Nelson, K. Marienau, C. Schembri and S. Redd, 2013. Measles transmission during air travel, United States, December 1, 2008–December 31. *Travel Medicine and Infectious Disease*, Vol. 11, No.2, 2011, pp. 81–89.
- [4] M.A. Widdowson, R. Glass, S. Monroe, R.S. Beard, J.W. Bateman, P. Lurie, and C. Johnson, Probable transmission of norovirus on an airplane. *Jama*, Vol. 293, No.15, 2005, pp. 1855–1860.
- [5] S. Namilae, A. Srinivasan, A. Mubayi, M. Scotch and R. Pahle, Self-propelled pedestrian dynamics model: Application to passenger movement and infection propagation in airplanes, *Physica A* Vol. 465, 2017, 248–260
- [6] S. Namilae, P. Derjany, A. Mubayi, M. Scotch and A. Srinivasan, Multiscale Model For Infection Dynamics During Air Travel. *Physical review E* Vol 95, (2017), 052320
- [7] D. Helbing, and P. Molnár, Social force model for pedestrian dynamics, *Physical Review E*, vol. 51, Jan. 1995, pp. 4282–4286.
- [8] J. Zębala, P. Ciepka, and A. Reza, Pedestrian acceleration and speeds. *Problems of Forensic Sciences*, Vol.91, 2012, pp. 227-234.
- [9] J.K. Gupta, C.H. Lin and Q. Chen, Flow dynamics and characterization of a cough, *Indoor Air*, vol. 19, 2009, pp. 517–525.
- [10] S.C. Paquette et al Influenza Transmission in the Mother-Infant Dyad Leads to Severe Disease, Mammary Gland Infection, and Pathogenesis by Regulating Host Responses, *PLOS Pathogens*, vol. 11, Aug. 2015.

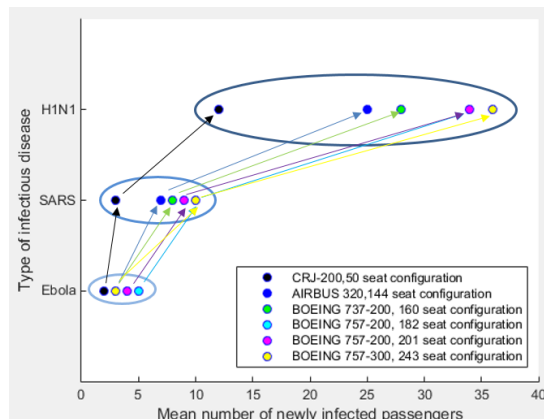


Fig 2. Policy analysis map for airplane size effect on different infectious diseases.

Pedestrian Evacuation Modelling with Dynamics Congestion Avoidance

Zongzhi Wang¹, Tao Chen²

^{1,2}Institution of Public Safety Research

Tsinghua University, Beijing, China

zongzhiwang@hotmail.com; chentao.a@tsinghua.edu.cn

Abstract – With the development of computer technology, pedestrian simulation becomes an efficient method to analyse evacuation efficiency under various scenarios. Some important and common behaviour of pedestrians, congestion detection and avoidance, which is seldom considered in pedestrian simulation complicatedly, are discussed in this paper. A modified cellular automata model considering dynamic congestion detection and avoidance is proposed and applied to simulate two different scenarios to demonstrate the effect of congestion avoidance behaviour, which have a significant improvement on evacuation efficiency. The accuracy and efficacy of this model is verified through the comparison result which is conducted through commercial software, Pathfinder. The modified model shows that with the consideration of congestion avoidance behaviour properly, the evacuation efficiency is improved approximately 40% than the model proposed by this paper, without the consideration of congestion avoidance behaviour.

Keywords: Pedestrian dynamics, Pedestrian simulation, Emergency evacuation, Cellular automata, Congestion avoidance

1. Introduction

Pedestrian evacuation simulation is an efficient method to analyse emergency evacuation plan. The intrinsic requirement to improve the accuracy of simulation is to establish movement rules that reflect actual pedestrian behaviour. The impediments to high evacuation efficiency in an evacuation mainly are some ‘congestion points’, for example, exit doors or narrow corridors. Previous research was conducted in this domain and some inspiring methods were introduced.

While analysing information transmission toward crowds, a social force model considering exit density of pedestrian was built, simulating a four exits square room (Han, Liu. 2017^[1]). A modification of an existing cellular model was proposed with experiments conducted in a classroom with obstacles (Liu, et al. 2009^[2]), taking into consideration of the influence of occupant density around exits. Cellular automata model was employed and modified by researchers to simulate pedestrians’ velocity change with different neighbourhood density (Pereira, et al. 2013^[3]). Research leading by the same researcher (Pereira, et al. 2017^[4]) modified his cellular automata model with introduction of adjust field, the value of which is relevant to congestion nearby and the willingness of congestion avoidance is determined by the weight of adjust field.

More researchers have conducted relevant research on congestion avoidance behaviour, including analysis on the relationship between crowd density and movement velocity (Fang, et al. 2003^[5]), modelling the response of behaviour on the presence of other pedestrian (Antonini, et al. 2006^[6]), application of Voronoi diagram to calculate the detour direction (Yunchao, Qu. 2018^[7]), and the consideration of panic mentality under congestion situation (Jinhuan, Wang. 2015^[8]).

2. The Principles of the modified cellular automata model

Cellular automata model is a discrete model used to simulated pedestrian movement widely. Evaluation area is divided into lattices or cells while pedestrians are viewed particles occupied a single cell at a time, who follow movement rules, in the form of moving probabilities to transfer to neighbour cells.

2.1. Movement Probability Equations

Movement probability equations are the most important part of a cellular automata model, of which the equations provide the description of certain human behaviour. Mainly based on Pereira and other researchers' model, the movement probability of pedestrian is presented as following equation.

$$p_{ij} = N\xi_{ij}exp(K_s S_{ij})exp(K_d D_{ij})exp(\delta_a K_a A_{ij}) \quad (1)$$

Where, N is the normalization factor; ξ_{ij} denotes the factor which determines whether the cell $\{i, j\}$ is available for a pedestrian; S_{ij} denote the value of static field, which measures the prior movement preference of a pedestrian; K_s denotes the sensitive parameter of static field; D_{ij} denotes the value of dynamic field; K_d denotes the sensitive parameter of dynamic field; A_{ij} denotes the value of adjust field, which measures the movement preference when the primary exit is jammed; K_a denote the sensitive parameter of adjust field; δ_a is an indicator of congestion situation, of which the calculation method is discussed in the next section.

2.2. Congestion Detection and Avoidance Method

The imitation of congestion detection and avoidance behaviour of pedestrian is accomplished by the introduction of a quasi-ant colony algorithm combined with the adjust field. Mentioned in Eqs. (1) and previous section, δ_a is a binary variable that submit to some rules to indicate a congestion being detected. . φ , representing “pheromone”, is calculated as Eqs. (2) shown.

$$\varphi_t = \lambda \times \varphi_{t-1} + x \quad (2)$$

Where, λ denotes the decay parameter of pheromone; x denotes the number of people in detection area. δ_a follows these rules:

$$\delta_a = \begin{cases} 0 \rightarrow 1, & \varphi_t > threshold_h \\ 1 \rightarrow 0, & \varphi_t < threshold_l \end{cases} \quad (3)$$

The value of $threshold_h$ is always higher than the value of $threshold_l$ indicating pedestrians' cognition are always lag behind actual information.

3. Simulations and Results

Based on Eqs. (1) – (3), two scenarios are established to test the validity and availability of the model, and one of the strengths of the proposed model is tested as well, that due to the introduction of ‘pheromone’ and δ_a , the congestion detection indicator, complex scenario which include more than one congestion point, can be analysed easily.

3.1. Illustration of Scenarios

Two artificial scenarios are designed and developed through cellular automata model, and the schematic illustrations of them as well as alternative routes are shown in Fig.1.

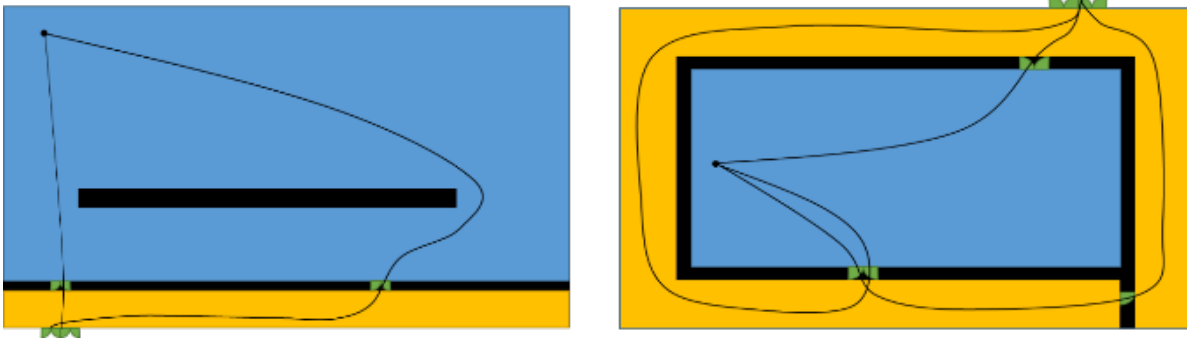


Fig.1: The schematic illustrations of the artificial scenarios

3.2 Verification of the modified model

The accuracy of the model is testified through the comparison of the result with the simulation output or commercial software Pathfinder on the less complicate scenario in which the evacuation area is rebuilt with the detour exit sealed, which represents the least complex condition for illustration convenience. The result of validation is shown in Fig.2.

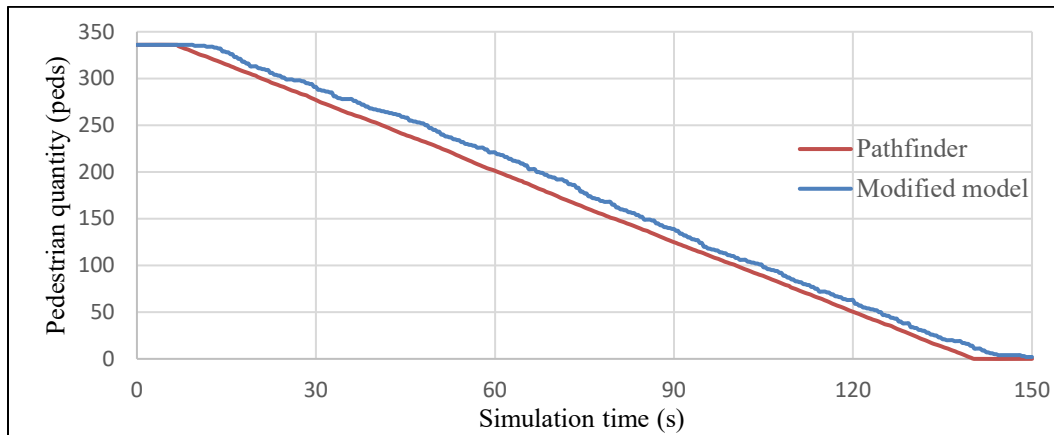


Fig.2: The results of modified model and Pathfinder on same scenario without congestion avoidance behaviour

After the adjustment of the parameters of modified model, the evacuation efficiency error between each result is within the range of 5% or 15 pedestrians.

3.3. Brief illustrations of simulations

The simulation result is ideal that significant improvement on evacuation efficiency are displayed in both scenarios with the introducing of adjust field. Part of the results are shown in Fig.3. The first row images show the evacuation process without the consideration of congestion avoidance behaviour, and therefore, the sensitive parameter of adjust field is set as 0. The second row images show the imitation of congestion avoidance behaviour, and the evacuation efficient is improved significantly if pedestrians make a detour to avoid congested exit or corridor. Pedestrians detect congestion situations and make decisions dynamically, and thus they may alter their routes according to the situation promptly.

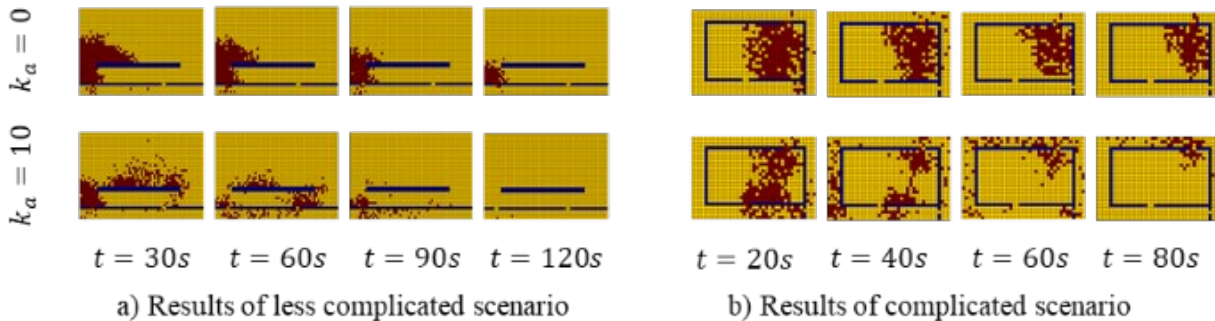


Fig.3: The results of simulation of modified CA model

4. Conclusion

Emergency evacuation which takes place in human intensive facility faces impediments of congestion problems. In an ideal condition, pedestrians would make decisions on whether choosing the nearest evacuation route, or moving around when the nearest route is congested. This paper proposed a modified cellular automata model to simulate congestion avoidance behaviour of pedestrians. With the introduction of quasi-ant colony algorithm and adjust field in cellular automata model, the modified model is capable of imitation congestion detection and avoidance behaviour dynamically, while the analysis of complex scenarios can be conducted easily. In two examples proposed in previous section, this model output ideal results that the congestion avoidance behaviour is imitated properly while the evacuation efficiency is improved at 35% or 43% maximum, respectively, then the model without congestion avoidance behaviour.

Acknowledgements

The authors appreciate the projects 71373139 and 71673163 supported by NSFC of China.

References

- [1] Y. Han, and H. Liu, "Modified social force model based on information transmission toward crowd evacuation simulation," *Physica A: Statistical Mechanics and its Applications*, vol. 469, pp. 499-509, 2017.
- [2] S. Liu, L. Yang, T. Fang, and J. Li, "Evacuation from a classroom considering the occupant density around exits," *Physica A: Statistical Mechanics and its Applications*, vol. 388(9), pp. 1921-1928, 2009.
- [3] L. A. Pereira, L. H. Duczmal, and F.R.B. Cruz, "Congested emergency evacuation of a population using a finite automata approach," *Safety Science*, vol. 51, pp: 267-272, 2013.
- [4] L. A. Pereira, D. Burgarelli, L. H. Duczmal, and F.R.B. Cruz, "Emergency evacuation models based on cellular automata with route changes and group fields," *Physica A: Statistical Mechanics and its Applications*, vol. 473, pp: 97-110, 2017
- [5] Fang, Z., S. M. Lo, and J. A. Lu. "On the relationship between crowd density and movement velocity." *Fire Safety Journal* vol. 38, no.3, pp: 271-283, 2003.
- [6] G. Antonini, M. Bierlaire, and M. Weber, "Discrete choice models of pedestrian walking behavior." *Transportation Research Part B: Methodological* vol. 40, no.8, pp: 667-687, 2006.
- [7] Y. Qu, Y. Xiao, J. Wu, T. Tang, and Z. Gao, "Modeling detour behavior of pedestrian dynamics under different conditions." *Physica A: Statistical Mechanics and its Applications* vol. 492, pp: 1153-1167, 2018.
- [8] J. Wang, L. Zhang, Q. Shi, P. Yang, and X. Hu, "Modeling and simulating for congestion pedestrian evacuation with panic." *Physica A: Statistical Mechanics and Its Applications* vol. 428, pp: 396-409, 2015.

Using Agent-based Simulation for Safety: Fact-finding about a crowd accident to improve public space design

Yuanyuan Liu^{1,2}, Toshiyuki Kaneda¹

¹Graduate School of Engineering
Nagoya Institute of Technology
Nagoya, Japan

²College of Architecture and Urban Planning
Tongji University
Shanghai, China

liuyuanyuan330@gmail.com; kaneda@nitech.ac.jp

Abstract – With the growing city density and large gatherings happening all over the world, crowd safety has become a new topic. This research discusses how to diagnosis and improve crowd safety in urban public space by analysing a real crowd accident that happened in Shanghai in 2014 using an agent-based simulator. Fact-finding analysis shows that insufficient capacity of the whole area, density difference in bottleneck stairs and lack of separation measurements in front of bottleneck stairs are the main causes of the accident. According to the media query towards the original space plan, we made two alternative plans in the bottleneck area and tested their performances.

Keywords: crowd accident, agent-based simulation, city design, disaster prevention, crowd management

1. Introduction

Traditional architectural design follows various codes and regulations, and in terms of crowd safety capacity and evacuation speed are mainly taken into consideration. The analysis of various crowd accidents indicated that even in a public space that fully meets the design criteria an accident can occur because of the avoidance or competitive behaviour of pedestrians. However, in urban public space, even such criteria are scarce. Since the 1990s, experimental and quantitative analysis about pedestrian counter flows were occasionally conducted. This paper focuses on characterizing a real case with a multi-direction flow at a stair bottleneck and its potential solution and addresses the pressure inside crowds.

2. Diagnosis space for fact finding — 2014 Shanghai Bund Stampede

2.1. Overview of the situation

The Shanghai Bund Waterfront is a linear area along the Huangpu River that occupies an area of 3.1 km² (Fig. 1, left). This area has 3 different elevations of 3.5m, 4.7m and 6.9m corresponding to the pedestrian street, Chen Yi Square and the viewing platform. The viewing platform is built on top of a flood defense wall and is considered to be the best viewing location. Chen Yi Square has its highest density from East Nanjing Road where visitors come from subway. The crowd accident happened on 31 December, 2014 at 23:35pm, on the stairs on the north-east corner connecting the square to the viewing platform, when people gathered for the New Year countdown. The stairs have 17 steps, 6.2m in width, with no separation in the middle, thus tightening the crowds from the square and forming a bottleneck. The tragedy caused 36 deaths and 49 injuries. The following January, the investigation report was released [1], and the accident details became clear (Table. 2). It is noteworthy that a few minutes before the accident happened, people moving upwards and downwards constantly collided and stalemated in the middle of the stairs, and then formed a liquid-like ‘wave’ [1] [4].

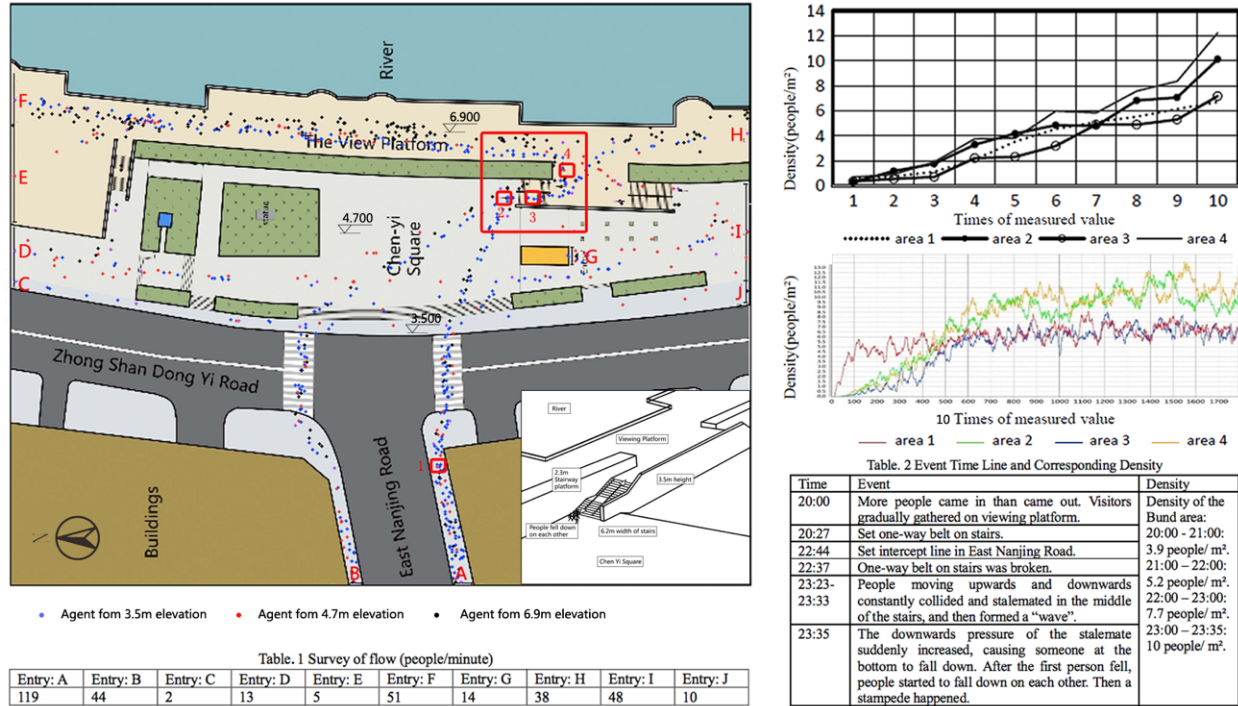


Fig. 1: Density analysis for fact finding.

2.2. Simulation model setting

In our simulation model, space is divided into 40cm cells and one step is set as 0.5 seconds. The simulation area has 10 entries/exits marked as A to J (Fig. 1, left). Agents move following the shortest path rule and 36 pedestrian rules in ASPFver.4.0 (Agent Simulator of Pedestrian Flows, Kaneda et al.), including 6 basic behavior rules, 1 pattern cognition rule, 4 avoidance rules, 3 high density flow rules, 1 pattern cognition rule and 14 wall avoidance rules [3]. Four density measurement areas are shown in red rectangles in Fig. 1. A pedestrian inflow survey was conducted between 15:00 and 16:00 on a September weekend. Survey data is shown in Table 1.

2.3. Experiment 1: Characterising the density growth at the stairs bottleneck

On the accident night, the density was around 4 people/m² at 20:00 and gradually increased until the stampede happened. Two groups of stairs in the accident area have a scissor shape and people moving upwards and downwards are on the right. To characterize the density growth in this complex mixed flow area, we timed the surveyed flow-in value from 1 to 10 times. The result (Fig. 1, top right) shows that: (1) The change of density in area 2 follows the density in area 4. This means the pressure on the platform is often higher than the stairs and the square, which leads to a downward pressure. Video observation shows that the accident more likely happened because significant pressure suddenly pushed people down rather than because someone fell, leading to a domino effect [4]. (2) The growth pattern of the platform density (area 4) shows stage character: it goes through a stable period from 4 to 5, then sharply increases to 6. This means that flow control measurements of the bottleneck area should start when the density is 2 or 3.

2.4. Experiment 2: Simulation for fact finding

In experiment 2, we conducted the simulation with 10 times flow-in value, which is closest to the actual accident (Fig. 1, center right). The result shows that the density on the platform (area 4) and in front of the stairs (area 2) is relatively higher than the density on the stairs. A possible reason is that pedestrian flows from five different directions met at the top of the stairs, forming a high-density mixed crowd. On the square in front of the stairs, pedestrian flows from three different directions also formed a high-density mixed crowd, but the density was relatively lower than the platform. Enormous downward

pressure caused balance loss and suddenly pushed down the people on the stairs. Adding separation measures in mixed-flow areas will be a solution.

3. Test alternative space plans

3.1. Two alternative space plans

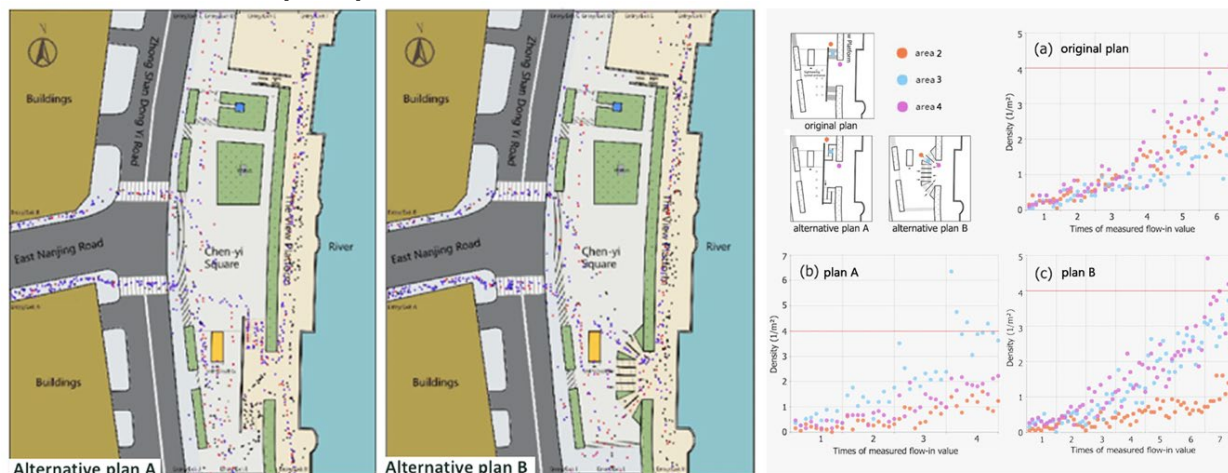


Fig. 2: Density measurement of original plan and alternative space plans.

Shanghai Bund Waterfront underwent landscape transformation in 2010, expanding pedestrian activity space by 40% percent [2]. After the accident, two major questions about the stairs bottleneck were posed: (1) Are the stairs too steep? (2) Would it be better to open the bottleneck area? Regarding these questions, we made two alternative plans and tested their performance (Fig. 2, left). Plan A changed the stairs with two one-direction slopes, and plan B is an open plan without bottleneck.

3.2. Experiment 3: Performance test

In experiment 3, we timed the measured flow-in value in the original space plan and two alternative plans to observe the density change in three measurement areas (Fig. 2, right). The experiments stop when any measurement area reaches 4 people/m². The result shows that in unextreme density: (1) The ability to allow more people into the square while maintaining a relatively pleasant density: plan B > original plan > plan A. (2) In plan B and the original plan, the platform reaches risk density first. In plan A, the slope reaches risk density first. When it comes to the preventive measures, the former should be conscious of the pressure difference while the latter should prevent squeeze.

4. Conclusion

In this paper, we quantitatively analysed the bottleneck in a crowd accident and evaluated the possibility of improvement. The pressure caused by the density difference between people is notable, and in current agent-based models, high density scenarios often fail by lacking the ability to present it.

References

- [1] Bund Chen Yi Square Crowd Accident Fact-Finding Committee, *Fact-Finding Report on Bund Chen Yi Square Crowd Accident* (in Chinese), 2015.
- [2] W. Xi and W. Xu, "Remodel Classic, the Centenary Shanghai Bund: Detailed Plan of the Urban Design & Site Plan of Shanghai Bund Waterfront," *Urbanism and Architecture*, pp. 42-45, 2011-2.
- [3] T. Kaneda, T. Yoshida, Y. He, et al, "Adding Higher Intelligent Functions to Pedestrian Agent Model," *Pedestrian and Evacuation Dynamics 2008*, pp. 529-535, 2010.
- [4] Southern Metropolis Daily. (2015. January 1). [Online]. Available: https://v.youku.com/v_show/id_XODYxODcxODUy.html

Pedestrian flow characteristics through bends: Effects of angle and desired speed

Jiahua Zhang¹, Charitha Dias², Majid Sarvi³, Miho Iryo-Asano⁴

^{1,2}Institute of Industrial Science/The University of Tokyo

4-6-1 Komaba, Meguro-ku, Tokyo, Japan

zhangjh@iis.u-tokyo.ac.jp; cdias@iis.u-tokyo.ac.jp

³Department of Infrastructure Engineering/The University of Melbourne

Building 176, Victoria 3010, Melbourne, Australia

majid.sarvi@unimelb.edu.au

⁴Graduate School of Environmental Studies/Nagoya University

Environmental Studies Hall, Furo-cho, Chikusa-ku, Nagoya, Japan

iryu@nagoya-u.jp

Abstract - This study quantitatively described how the desired speed, which may reflect the emergency level, and the angle of bend affect the pedestrian flow by comparing fundamental diagrams derived from trajectory data collected through laboratory experiments. Results showed that the slow running (≈ 2.8 m/s speed) can increase the maximum flow through a bend by around 60 % compared to normal walking (≈ 1.4 m/s speed) regardless of the turning angle. Further, it was found that the turning angle of the bend has a stronger negative impact on the moving speed of crowds under running conditions. Compared to the turning angle, congestion level seemed to have a minor impact on the average moving speed through the bends. On the other hand, for 90° and 180° bends, the variations of the speed were observed to decrease with the increase of density which indicated that although congestion level deteriorated the flow conditions at bends, it homogenized the collective moving speed of pedestrians.

Keywords: Pedestrian flow, Pedestrian turning behaviour, Fundamental diagram, Crowd experiment

1. Introduction

As experimentally verified in previous studies [1-2], corridors with bends are inefficient for crowd movements and could become bottlenecks under emergency as well as normal conditions. Therefore, when public spaces are planned and designed, attention should be paid to such locations. As a first step, this study aims to quantitatively describe how the desired speed and the angle of bend affect the pedestrian flow characteristics by comparing fundamental diagrams derived from trajectory data. On one hand, the measurement results from this experiment could be used to estimate the capacity of bends with different angles under different situations (i.e., normal or evacuation); on the other hand, the findings from this study could also be beneficial for the validation and calibration of crowd simulation models.

2. Experiment Setup

The data used for this study were collected from an experiment conducted at Monash University in October 2013 [2]. Trajectory data for walking through a straight (0°) and different angled (45° , 90° and 180°) corridors (corridor width is 1.5 m) were collected under two different desired speed levels, i.e., normal speed walking (individual speed ≈ 1.4 m/s) and slow speed running (individual speed ≈ 2.8 m/s). Around 55 individuals participated in this experiment and each experiment scenario was repeated 3 times. Initial conditions were kept similar for all these experiments. Fig. 1 shows the experiment setup and a snapshot during one experiment scenario. The positions of each pedestrian's head were manually tracked at 0.12 s intervals from video recordings to obtain trajectories of individuals.

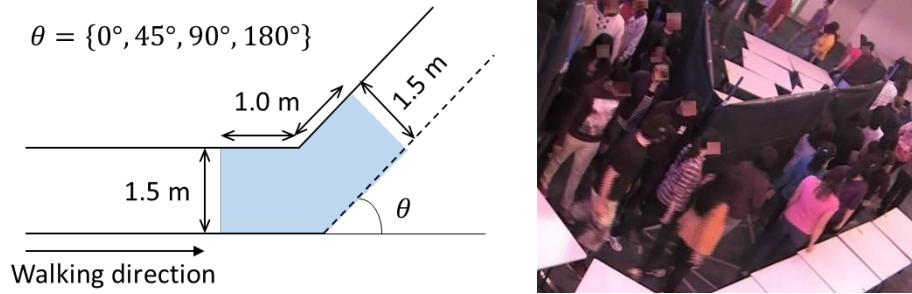


Fig. 1 Experiment setup (left) and one snapshot (right).

3. Measurement Method

This study adopted Voronoi diagram method to calculate pedestrian traffic variables since it was reported to be able to reduce the density scatter and at the same time improve the resolution of data with higher sampling rate [3]. The basic idea of this method is that at each frame or during a short enough time period, a Voronoi cell area, A_i , can be obtained for each person i . Then, the density and velocity for a measurement area can be defined as:

$$\rho_{xy} = 1 / A_i \text{ and } v_{xy} = \|\vec{v}_i(t)\| \quad \text{if } (x, y) \in A_i \quad (1)$$

$$\langle \rho \rangle_v = \frac{\iint \rho_{xy} dx dy}{|A|}, \quad \langle v \rangle_v = \frac{\iint v_{xy} dx dy}{|A|} \quad (2)$$

Where ρ_{xy} and v_{xy} are the density and speed within voronoi cell A_i respectively. $|A|$ is the measurement area and in this study it was specified as 1 m range from the inner turning point at both sides shown as blue shadowed region in Fig. 1. $\vec{v}_i(t)$ is the instantaneous speed of person i and it is calculated using the displacement during adjacent time instants from trajectory data. Finally, the flow is obtained by multiplying the Voronoi density $\langle \rho \rangle_v$ and speed $\langle v \rangle_v$.

4. Flow Characteristics

By applying the Voronoi diagram method, the density-flow relations for different angles and desired speeds were derived as shown in Fig. 2. Firstly, it can be seen that only the free flow regime of fundamental diagram was observed and therefore, the capacity of the bend cannot be accurately estimated. However, still it can be observed that the maximum flow for running scenarios (≈ 2.5 ped/m/s) was significantly higher than that for walking scenarios (≈ 1.5 ped/m/s). This indicates that slow speed running could probably increase the efficiency of bends by around 60% compared to normal speed walking. Secondly, the regression lines without intercept were drawn to compare the impact of turning angle on the moving speed. Since the slope of the regression line can be approximately considered as the average moving speed of pedestrians, the change rate of slope therefore represents the influence of angle. It can be calculated that from 0° to 90° , the slope dropped about 20% for each 45 degrees under running scenarios while only 11% for walking scenarios. Also from 0° to 180° , the slope decreased 50% for running but 35% for walking. These differences imply that turning angle has a stronger negative impact on the average moving speed of the crowd under running or evacuation conditions.

Further, we used the criterion of Fruin [4] to divide the congestion levels and separately compared average speed and standard deviation under each level of service as presented in Table 1. It can be observed that the speed under three LOSs didn't show a consistent and significant transition which may suggest that compared to the turning angle, congestion level had a minor impact on the moving speed through bends. On the other hand, for 90° and 180° bends, the standard deviations continuously decreased with the deterioration of level of services. This indicates that at right-angle and U-turn corridors, high congestion level would homogenize the moving speed of the crowd by restricting individual's freedom of choosing his or her desired speed.

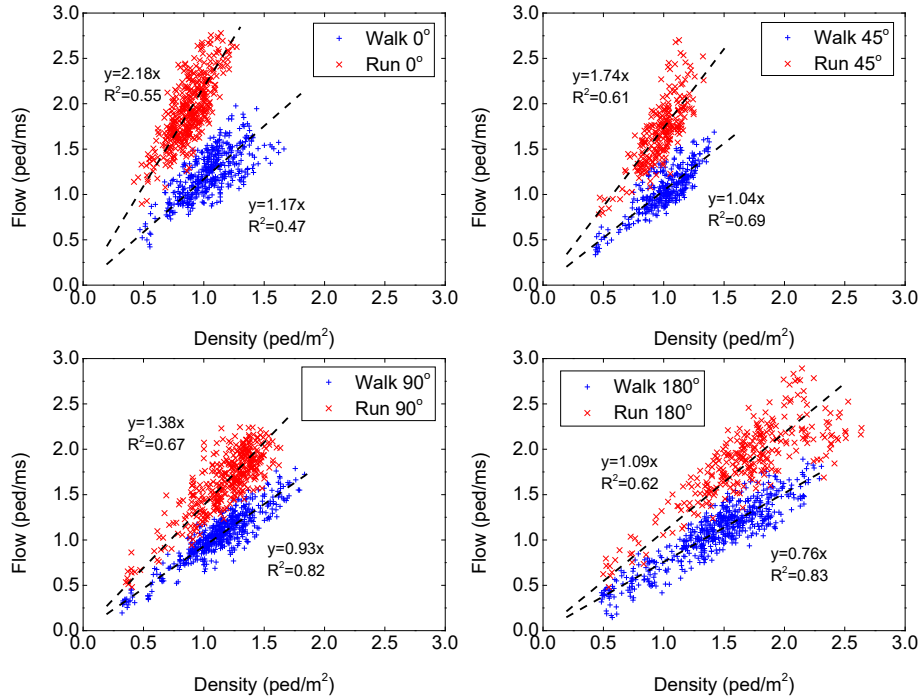


Fig. 2 Comparison of flow-density relations at bends.

Table 1: Average moving speed (m/s) and its standard deviation (STDEV, m/s) under different levels of service.

Scenario	Walk 0°	Walk 45°	Walk 90°	Walk 180°	Run 0°	Run 45°	Run 90°	Run 180°
LOS C	1.24	0.98	0.90	0.71	2.35	1.72	1.57	1.25
(STDEV)	(±0.22)	(±0.13)	(±0.15)	(±0.20)	(±0.30)	(±0.19)	(±0.27)	(±0.19)
LOS D	1.22	1.06	0.94	0.73	2.19	1.73	1.47	1.20
(STDEV)	(±0.17)	(±0.15)	(±0.10)	(±0.14)	(±0.29)	(±0.22)	(±0.22)	(±0.17)
LOS E	1.15	1.04	0.93	0.76	2.15	1.76	1.37	1.12
(STDEV)	(±0.18)	(±0.12)	(±0.09)	(±0.09)	(±0.15)	(±0.23)	(±0.15)	(±0.14)

4. Conclusions

This study quantitatively investigated the flow characteristics of the crowds moving through bends with different turning angles at two desired speed levels. We found that larger turning angle significantly reduced the moving speed under running conditions compared to walking and the maximum flow when pedestrians were walking was around 60% of that when they were running. On the other hand, compared to turning angle, congestion level at bends was observed to have a minor impact on the moving speed although it cut down the variations of speed by restricting the movement freedom of individuals.

References

- [1] C. Dias, M. Sarvi, N. Shiwakoti, O. Ejtemai and M. Burd, "Examining the Impact of Different Turning Angles on the Collective Egress of Crowds", *Journal of Transportation Safety & Security*, vol. 6, no. 2, pp. 167-181, 2014.
- [2] C. Dias, M. Sarvi, O. Ejtemai and M. Burd, "Elevated desired speed and change in desired direction: effects on collective pedestrian flow characteristics", *Transp Res Rec*, vol. 2490, pp. 65-75, 2015.
- [3] B. Steffen and A. Seyfried, "Methods for measuring pedestrian density, flow, speed and direction with minimal scatter", *Physica A*, vol. 389, no. 9, pp. 1902-1910, 2010.
- [4] J. Fruin, *Pedestrian planning and design*. New York: Metropolitan Association of Urban Designers and Environmental Planners, 1971.

Pedestrian Models for Robot Motion

Francesco Zanlungo¹, Florent Ferreri¹, Jani Even^{1,2}, Luis Yoichi Morales³, Zeynep Yücel⁴,
Takayuki Kanda^{1,2}

¹ATR IRC, Kyoto, Japan

zanlungo@atr.jp, florent@atr.jp, even@atr.jp, kanda@atr.jp,

²Kyoto University, Kyoto, Japan

³Nagoya University, Nagoya, Japan

morales_yoichi@coi.nagoya-u.ac.jp

⁴Okayama University, Okayama, Japan

zeynep@okayama-u.ac.jp

Abstract - We discuss the development of a robot system able to replicate human group motion and show how a pedestrian model may be converted to a robot control system in order to achieve this goal.

Keywords: robotics, collective behavior, collision avoidance, potential-based model

1. Introduction

The deployment of autonomous mobile robots in public environments is an open problem, a subject of a large set of research studies, but whose complete solution is still far ahead. One of the main problems is related to how to attain safe and efficient navigation inside a human crowd [1-8]. “Social robots” (robots interacting with humans in the humans’ natural environment) are intended to assist or accompany people, or just perform their duties in the same environment in which humans are present, and thus need to understand and possibly replicate pedestrian behaviour, so that they may move safely inside the crowd, and be perceived as safe by the humans. An important class of these social robots is represented by small size autonomous vehicles (such as automatic wheelchairs), whose task is to transport people or goods. Group behaviour is an important component of crowd dynamics, and thus of crucial importance to all the mobile social robots, and in particular to those supposed to move along humans (including vehicles transporting them). For this reason, such robots may need to move as part of a pedestrian group [9-10].

Researchers in the social robotics field may thus take advantage from behaviour models developed in the field of pedestrian and crowd simulation, although applying a pedestrian model to a robot system may not be trivial, due to the differences in scope between the two fields (while in crowd dynamics the task is to reproduce in a realistic but computationally fast way the behaviour of a large amount of humans, in robotics the task is to move in a safe way one or at most a few robots).

In recent years we have been working actively both in the development of pedestrian models and in their application to robot systems. In this work we would like to share some of the knowledge attained in this field, first describing a specific application (side by side motion of an autonomous robot and a human), and then by presenting a general recipe for converting an acceleration based pedestrian model to a robot control system, while taking in consideration the differences in motion and perception between a robot and a human, and the difference in scope between crowd modelling and robot applications, and while focusing in particular on group motion. Finally, we discuss the differences between acceleration-based models and cost function models and discuss how potential based models may be converted into cost functions for robot operation.

2. Side by side

In cost function methods (or utility as the negative of cost), a set of features is selected based on data from pairs of people walking side by side and a cost function is minimized. In a previous work, a cost function composed of eight features was proposed to model how an agent moves side by side with a partner [11]. The considered features were: velocity magnitude, angular velocity and acceleration (motor

features); relative distance, relative angle and relative velocity (social features); distance and angle towards (sub-)goals (environmental features). To implement the cost function a prediction grid containing possible future locations of each agent was used, and the cost of each cell for each agent was computed by summing each different feature with proper weights. Finally, the location that minimizes the cost of the double anticipation is selected. The implementation of the system is shown in Fig. 1 (left).



Fig 1: Left: implementation of side by side walk. Right: group motion implemented in a 3 robot system.

3. Converting a pedestrian model to a control system

We may assume that in an acceleration based pedestrian model (“social force model” [12]), the dynamics of a pedestrian is given by

$$\mathbf{a} = \mathbf{f}_{\text{drag}} + \mathbf{f}_{\text{group}} + \mathbf{f}_{\text{ped}} + \mathbf{f}_{\text{obs}} \quad (1)$$

The terms on the right [13], correspond to a drag force that makes pedestrians walk at their preferred speed in the direction of their goal (possibly a local goal determined by a path planner) \mathbf{f}_{drag} , to a term that makes the pedestrians walk as members of a social group $\mathbf{f}_{\text{group}}$, to a term that makes the pedestrians avoid collisions with other pedestrians \mathbf{f}_{ped} , and to a term used to avoid collisions with non-human obstacles \mathbf{f}_{obs} .

We typically face three problems when applying such an equation to a non-holonomic robot.

1. Eq. 1 assumes obstacles to be polygonal lines (walls), and pedestrians interact with their closest points, while in robot systems obstacles are usually expressed as laser scan points.
2. Acceleration has to be converted to a (v, θ) command, v being the linear velocity and θ the angular velocity of the robot.
3. The velocity and acceleration limitations of the robots have to be taken in consideration.

In [14], we show in detail how to deal with the above problems, and present the results obtained when our recipe is applied to the collision and group models of [13], [15], both in a simulated environment (Fig. 2) and as an actual mobile robot implementation in a controlled laboratory environment (Fig. 1 on right).

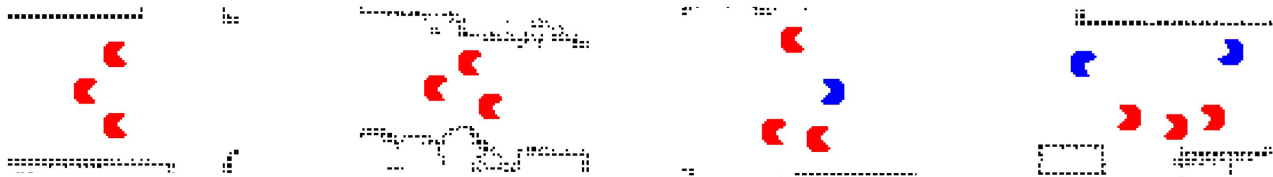


Fig 2: From left to right: simulated robot behaviour in free space, narrow space and while avoiding collisions with pedestrians.

4. Cost Function

In side by side walking, a cost function approach, rather than an acceleration based one, was used. The former approach is often preferred in robotics, because it allows to explicitly avoid forbidden and dangerous areas. As stated in [14], a security check may be applied after the acceleration model provides the new velocity command, but as a result the motion of the robot may not reflect the output of the pedestrian model. When the acceleration of the pedestrian model is provided as the gradient of a potential, as for the group model [13], it is straightforward to include such a potential directly in the cost function. Nevertheless, velocity dependent collision avoidance models are not always derived from a potential. In our future work, we will combine the collision avoidance model to the path planner before passing it to the cost function, and apply this method to a simulated 3 robots system.

This work is partially based on results obtained from a project commissioned by the New Energy and Industrial Technology Development Organization (NEDO), and partially supported by JSPS KAKENHI Grant Number JP16K21719..

References

1. E. Pacchierotti, H. I. Christensen, and P. Jensfelt, “Evaluation of passing distance for social robots,” in ROMAN 2006. IEEE, 2006, pp. 315–320.
2. T. Kanda, M. Shiomi, Z. Miyashita, H. Ishiguro, and N. Hagita, “A communication robot in a shopping mall,” IEEE Transactions on Robotics, vol. 26, no. 5, pp. 897–913, 2010.
3. M. Shiomi, F. Zanlungo, K. Hayashi, and T. Kanda, “Towards a socially acceptable collision avoidance for a mobile robot navigating among pedestrians using a pedestrian model,” International Journal of Social Robotics, vol. 6, no. 3, pp. 443–455, 2014.
4. A. Garrell and A. Sanfeliu, “Cooperative social robots to accompany groups of people,” The International Journal of Robotics Research, vol. 31, no. 13, pp. 1675–1701, 2012.
5. S. Thrun, M. Bennewitz, W. Burgard, A. B. Cremers, F. Dellaert, D. Fox, D. Hahnel, C. Rosenberg, N. Roy, J. Schulte et al., “Minerva: A second-generation museum tour-guide robot,” in Robotics and automation, 1999, vol. 3. IEEE, 1999.
6. H.-M. Gross, H. Boehme, C. Schroeter, S. Müller, A. König, E. Einhorn, C. Martin, M. Merten, and A. Bley, “Toomas: interactive shopping guide robots in everyday use-final implementation and experiences from long-term field trials,” in IROS 2009. IEEE, 2009, pp. 2005–2012.
7. H. Huttenrauch and K. S. Eklundh, “Fetch-and-carry with cero: observations from a long-term user study with a service robot,” in Robot and Human Interactive Communication, 2002. 11th IEEE International Workshop on. IEEE, 2002, pp. 158–163.
8. W. Burgard, A. B. Cremers, D. Fox, D. Hähnel, G. Lakemeyer, D. Schulz, W. Steiner, and S. Thrun, “The interactive museum tour guide robot,” in Aaai/iaai, 1998, pp. 11–18.
9. Y. Morales, N. Kallakuri, K. Shinozawa, T. Miyashita, and N. Hagita, “Human-comfortable navigation for an autonomous robotic wheelchair,” in IROS 2013. IEEE, 2013, pp. 2737–2743.
10. Y. Kuno, N. Shimada, and Y. Shirai, “Look where you’re going [robotic wheelchair],” IEEE Robotics & Automation Magazine, vol. 10, no. 1, pp. 26–34, 2003.
11. N. H. Yoichi Morales, Takayuki Kanda, “Walking together: Side by side walking model for an interacting robot,” Journal of Human-Robot Interaction, vol. 3, no. 2, pp. 50–73, 2014.
12. D. Helbing, I. Farkas, and T. Vicsek, “Simulating dynamical features of escape panic,” Nature, vol. 407, no. 6803, pp. 487–490, 2000.
13. F. Zanlungo, T. Ikeda, and T. Kanda, “Potential for the dynamics of pedestrians in a socially interacting group,” Physical Review E, vol. 89, no. 1, p. 012811, 2014.
14. F. Zanlungo, Z. Yücel, F. Ferreri, J. Even, L. Y. M. Saiki, and T. Kanda, “Social group motion in robots,” in International Conference on Social Robotics. Springer, 2017, pp. 474–484.
15. F. Zanlungo, T. Ikeda, and T. Kanda, “Social force model with explicit collision prediction,” EPL (Europhysics Letters), vol. 93, no. 6, p. 68005, 2011.

Social Force Modeling of the Pedestrian Motion in the Mataf

Rainald Löhner¹, Eberhard Haug², Britto M.²

¹Center for Computational Fluid Dynamics
George Mason University, Fairfax, VA, USA
rlohner@gmu.edu

²SL Rasch
Kesslerweg 22, Oberaichen, Germany
britto.muhamad@sl-rasch.de, haugfmly@club-internet.fr

Abstract - Two models for the motion in the Mataf of the Holy Mosque of Makkah that are applicable to any so-called social force or agent-based model are presented. The first model assigns a desired distance to the Kaaba to each pilgrim. The second model assumes that pilgrims desire to get as close as possible to the Kaaba until a tolerable density is reached. Both models are realistic: image data shows behaviours of both types. The models are very simple to incorporate into any computational crowd dynamics code, and yield results that correlate surprisingly well with observed data.

Keywords: Pedestrian Modeling, Social Force Model, Crowd Dynamics, Kaaba, Hajj

1. Introduction

One of the obligatory rites of Muslim pilgrims visiting Makkah is the sevenfold circumambulation of the Kaaba at the center of the Holy Mosque - the so-called Mataf. During the peak holy seasons of Ramadan and Hajj millions of pedestrians perform this rite, leading to congestion and, in some cases, worrisome densities. The motion of pedestrians in the Mataf has been the focus of much modeling effort over the last years. Unfortunately, at this point there does not exist a reliable predictive model for this motion. This should not come as a surprise: after all, at every instance a pilgrim is taking decisions based on many factors: faith, social and cultural background, current anemic and fitness state, the surrounding crowd, climate, etc. Following the observation that 'all models are wrong, but some are useful', the present effort was directed at developing improved social force models for this type of motion/rite. Starting from a series of empirically based assumptions, two models were derived in a systematic manner. The first model assumes that pilgrims want to perform the Tawaf at a certain **distance** from the Kaaba. Video footage shows that even when there are very few pilgrims, some pilgrims do not venture close to the Kaaba, implying that this model is not unrealistic. The second model assumes that pilgrims want to get as close as possible to the Kaaba when performing the Tawaf but have a limited **tolerance for high density**. This implies that they will stop trying to get closer to the Kaaba if the density is above a certain threshold. Video footage shows that even when there are very many pilgrims, some pilgrims keep trying to get to the Kaaba or very close to it, i.e. are not afraid of high densities.

2. Model 1: Desired Distance from Kaaba

The first model assumes that pilgrims want to perform the Tawaf at a certain distance from the Kaaba. Video footage shows that even when there are very few pilgrims, some pilgrims do not venture close to the Kaaba, implying that this model is not unrealistic. The desire to stay at a certain distance from the Kaaba is modeled by assigning to each pilgrim a ‘desired distance’ d_d . The inward or outward force is then a function of the difference in desired distance d_d and actual distance d from the Kaaba.

3. Model 2: Tolerated Density

The second model assumes that pilgrims want to get as close as possible to the Kaaba when performing the Tawaf but have a limited tolerance for high density. This implies that they will stop trying to get closer to the Kaaba if the density is above a certain threshold. Video footage shows that even when there are very many pilgrims, some pilgrims keep trying to get to the Kaaba or very close to it, i.e. are not afraid of high densities. The desire to stay in regions where pilgrim density is below a certain threshold is modeled by assigning to each pilgrim a ‘threshold density’ ρ_0 . The inward or outward force is then a function of the difference between the local density ρ and the threshold density ρ_0 .

4. Examples

Both models were implemented into PEDFLOW [1-3], a typical pedestrian flow and crowd dynamics simulation tool based on a mix of social force and agent-based approaches. In order to discern the relative merit and performance of the two models, the Mataf motion was computed with the maximum number of simplifying assumptions that still reflect reality.

a) Geometry: The Great Mosque in Makkah has been undergoing construction for the last decade, so the areas where pilgrims can walk and pray are constantly changing. However, the geometry chosen closely reflects the actual dimension and areas expected in the next decade.

b) Entry/Exit Points: Pilgrims are assumed to enter through one entry into the central patio (the so-called Sahn) and exit through one area. From a series of exploratory simulations it was found that the crowd motion patterns that form are almost unaffected by the actual form of entry into and exit from the Sahn as long as there is enough space for pilgrims to move through.

c) Sunnah Prayer: A part of the actual pilgrimage rite that was left out was the post-Mataf prayer. Pilgrims remain in the general area of the Sahn and pray before exiting. As these prayer areas were not clearly defined for the geometry chosen, they were omitted.

d) Demographics: Only one demographic type was considered, with a desired velocity of $v_d=1.5\pm 0.25$ m/sec, a relaxation time of $t=0.5\pm 0.05$ sec, and radius of $r=0.25\pm 0.05$ m.

e) Constant Influx: The influx of pedestrians was set to $f = 9$ p/sec = 32,400 p/hr, constant for the duration of the simulation. This is considered typical of high holidays.

As stated before, more realism and complexity could easily have been added, but it would not have been helpful to elucidate the relative merits of the models proposed.

4.1 Distance Preference

The case was first run with the model based on a desired distance. Figure 1 shows the average density, average velocity, number of pedestrians and density vs distance from the Kaaba at $T = 15,000$ sec. Note that the velocities are only displayed in the range $0 < |v| < 1$ in order to clarify the regions with slower motion. Note the unrealistically low average values for the density close the Kaaba obtained with the model, as well as the low density regions close to the left part of the Kaaba. Nevertheless, the ‘flow pattern’ is much better than that obtained with many other approaches we tried to date.

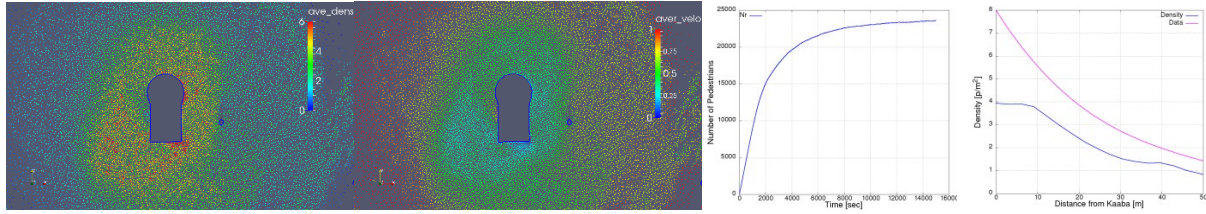


Figure 1: Average Density and Velocity, Number of Pedestrians and Density vs Distance from Kaaba

4.2 Density Preference

The same case was then run with the model based on a desired density. Figure 2 shows the average density, average velocity, number of pedestrians and density vs distance from the Kaaba at $T=10,000$ sec. As before, the velocities are only displayed in the range $0 < |v| < 1$ in order to clarify the regions with slower motion. Note the high values of density close to the Kaaba obtained with the model, which correlate well with observed data.

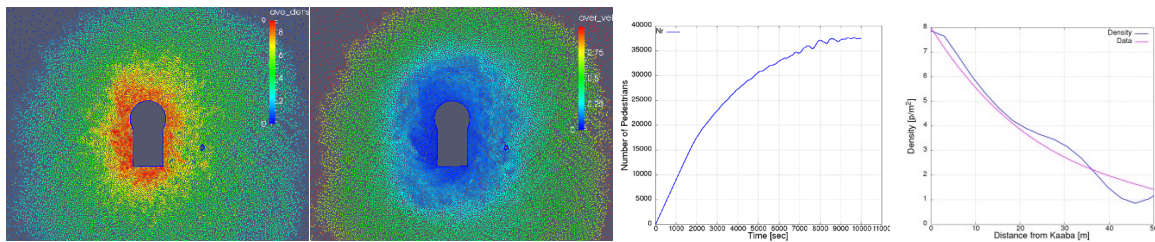


Figure 2: Average Density and Velocity, Number of Pedestrians and Density vs Distance from Kaaba

5. Conclusions and Outlook

Two models for the motion in the Mataf that are applicable to any so-called social force model were presented. The first model assigns a desired distance to the Kaaba to each pilgrim. The second model assumes that pilgrims desire to get as close as possible to the Kaaba until a tolerable density is reached. Both models are realistic: image data shows behaviours of both types. The second model offers the advantage of being self-regulating and thus more robust. If the density increases too much, the pilgrims move further away from the Kaaba and the simulation proceeds without problems while still being realistic. Both models are very simple to incorporate into any computational crowd dynamics code, and yield results that correlate well with observed data.

As in all such cases, it is tempting to overinterpret the results obtained. Both behaviours (desired distance, density threshold) are observed in the field. What percentage will opt for any of these goals remains an open question.

References

- [1] R. Löhner, “On the Modeling of Pedestrian Motion,” *Appl. Math. Modelling* 34, 2, 366-382 (2010).
- [2] R. Löhner, E. Haug, C. Zinggerling and E. Onate, “Real-Time Micro-Modeling of City Evacuations,” *Comp. Part. Mech.* 5, 71-86 (2018).
- [3] R. Löhner, B. Muhamad, P. Dambalmath and E. Haug, “Fundamental Diagrams for Specific Very High Density Crowds,” *Collective Dynamics* 2 (2018).

Toward dynamical crowd control to prevent hazardous situations

Tomoichi Takahashi

Department of Information Engineering
Meijo University
Nagoya, Japan

Keywords: *evacuation guidance, crowd control, prevention planning, promotion signage, simulation and validation*

1. Introduction

It is common for large crowds to gather to attend games, exhibitions, political rallies, and other events. Thus, careful designs and operational plans are made to ensure the safe, secure, and efficient movement of people in these crowded environments. However, the congestion created by large crowds has resulted in hazardous incidents across the world (e.g., those during the Hajj pilgrimage, gatherings at Mecca, and the Akashi fire festival) [1][2].

In 2011, the Tokyo Fire Department conducted a study on fire-prevention plans at large subway terminal stations [3]. The study surveyed 400 people who responded to questions such as “What points do you feel anxious about in emergency situations?” and “How do you behave when a fire occurs?” The survey revealed that the majority of people in unfamiliar places follow the guidance provided by public announcement (PA) systems and the people around them.

Figure 1 displays photos captured at Tokyo rail terminals after a snowfall in January 2018. People returned home early to avoid potential troubles resulting from the snowfall. The number of people present at the terminals was larger than the allowable transportation capacity. People consequently filled the terminals, causing the railroad companies to restrict entrance. However, people remained disciplined under this duress for several hours in part because they were able to ascertain the causes of the congestion and could access information through their cellular telephones.



Figure 1. Crowded terminals (2018. Jan.22)

Developments in information technology (IT) can provide new means to disseminate public information, thus changing human behavior in situations of danger and duress. In this paper, we propose a crowd control and evacuation guidance (CCEG) management system using digital promotional signage

(PS) to demonstrate the effects of crowd control via simulations.

2. Providing information and guidance

2.1 Preliminary studies

Figure 2 depicts signs often seen in public spaces across the world. The first image shows signs indicating the direction in which emergency exits can be found. The second image shows a wall-mounted evacuation plan and map. The exit sign (ES) and map are considered to be good methods for prompting evacuations. However, people seem to travel without paying attention to these signs unless unexpected events occur and the guidance contents are fixed.



Figure 2. Evacuation guidance media at a terminal

We conducted a survey to determine whether people sufficiently notice signs during everyday life. This study involved two questionnaire surveys (i.e., test A and test B), which were conducted at a subway mall in 2016 (Figure 3). The subway mall is located underground and contains fourteen exits leading to the surface and adjacent buildings. The test subjects were different groups of students at our university. We asked these subjects to walk normally in the mall along the route displayed in Figure 3 on different days. At the end of the route, the subjects were asked to recall the number and locations of any ESs or digital PS they saw.



Figure 3. Underground shopping mall (black line indicates the route traveled by participants)

In test A, participants were asked to retrace their paths and attentively count the number of ESs and digital PS. This exercise corresponded to real emergency situations in which evacuees would search for guidance. Such an event was staged during test B; so seven additional PS locations were included.

Table 1 indicates the number of signs that were spotted along the route shown in Figure 3. The results demonstrate the following:

- Participants noticed a maximum of 28% of the ES locations when they traversed the route as usual, but detected nearly three times as many when asked to pay attention.
- There was little difference in the perception rates between the proportion of ESs and PS noticed.
- People unconsciously noticed a higher proportion of PS during the unexpected staged event.

This indicates that PS functions as ESs during emergency situations. Thus, an increased number of signs can guide more people to proper evacuation routes.

Table 1. Survey on ES awareness

Test	Sign	Number of signs	Number and rate awareness	
			unaware(forth)	Attentive(back)
A	ES	36	9.3 (26%)	30.8 (86%)
	PS	5	1.4 (28%)	4.0 (80%)
B	ES	36	6.0 (16%)	-
	PS	12*	9.0 (75%)	-

(*Seven PSs were added for an unexpected event)

2.2 New guidance systems proposals

PSs have recently been used for promotions and advertising in public spaces. Figure 4 shows an image of our CCEG management system. The first figure shows everyday use in which PS is used to display promotional contents. The second figure shows our CCEG concept in which the PS is used to display contents suitable for emergencies. In this concept, the role of the PS changes to that of an ES. That is, the PS displays messages intended to guide people to safety. To accomplish this, data from video camera feeds are sent to crisis-management centers, proper evacuation routes are planned for emergencies, and PS messages are then displayed to provide proper information based on these plans.

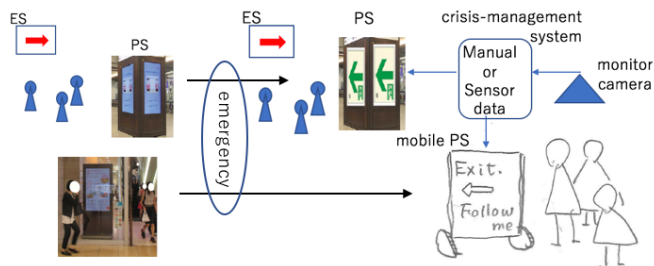


Figure 4. Crowd control management system using PS

3. Validation via agent-based simulations

3.1 Simulation scenarios

It is necessary to show the effectiveness of the CCEG before it is practically applied. The agent-based social simulation (ABSS) is an appropriate testing method for this.

The CCEG's effectiveness was validated by simulating crowd behavior at the subway mall through the TENDENKO ABSS system (Figure 3). Agents perceived the surrounding data and selected an action from a prescribed set at every step of the simulation [4].

An alarm was first sounded through the PA system. A verbal warning indicated the following: "Fire near exit number one; evacuate from exit number seven." This message was sent to all agents, who were assumed to have begun following the instructions. However, behavior becomes unpredictable during emergencies. Individual movement creates congestion, and evacuation efficiency is reduced. To increase efficiency, PS is used to display proper directions and information about evacuation routes according to manuals and sensor data. Agents within 10m of the PS can view these messages.

3.2 Simulation validation

The crowd evacuation simulation is a type of social simulation. The validation of these simulation tools has been a highly important issue, and a number of questions have been raised as a result of the associated testing methods. The following questions were suggested according to the quantitative/qualitative attributes of behavioral uncertainty, which are essential during ABSS experiments [5]:

- Q1. How do we ascertain whether a tool is sufficiently accurate?
- Q2. Which and how many tests should be performed to assess the accuracy of the model's predictions?
- Q3. Who should perform the tests (e.g., the model's developers, users, or a third party)?

These questions should be answered for users who will employ the simulation results when making practical decisions.

3.3 Simulation parameters

Personal behavior was simulated according to the following three changing parameters:

p is the rate at which agents follow PS guidance. Reports from the Great West Japan Earthquake of 2011 indicated that some agents evacuated immediately, but others did not [6]. This parameter is indicative of how human behavior differs according to the individual and their surrounding environment.

n is the number of people present at the mall. They are uniformly distributed throughout this location.

s is the number of PS locations used as ESs during emergencies. PS positions were selected to form test B.

Simulations were executed in which $n = \{1000, 4000, 7000, 10000\}$, $p = \{30\%, 50\%, 70\%, 100\%\}$, and $s = \{4, 6, 8\}$. The population density of $n = 4000$ is equal to one person per $1m^2$. This number corresponds to crowd status during commuting hours. Figure 1 depicts a crowd congestion status of $n = 10000$.

Two message display modes were compared:

Default mode: At the time of the first PA announcement, the PS display was changed to "Go to the nearest exit. The exit number is X."

Congestion mode: When congestion occurred, the PS display changed to "Go to the nearest exit; the number is X." Two

sign-change policies were tested to ascertain the effects of individuals detecting the congestion status:
policy 1 employs population density per square meter; policy 2 uses the changes in population density

4. Simulation and decision-making analyses

4.1 Effects of increasing the amount of PS

Figures 5 and 6 show the simulation results for $n = 4000$. The first and second charts in Figure 5 correspond to simulations containing no signs and a default simulation mode of $p=30\%$. The vertical axis in each graph represents the evacuation rate (i.e., the rate of individual evacuation). The horizontal axis in each graph represents simulation time. The graphs show that evacuation rates improved according to the amount of PS, even with low p .

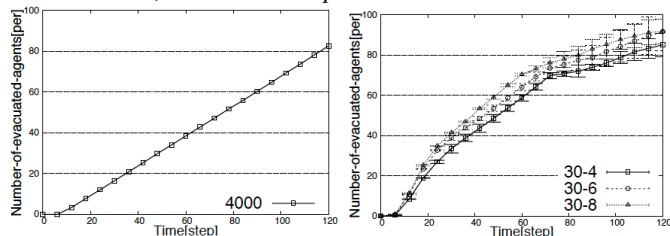


Figure 5. Improved evacuation rate ($n=4000$ and $s=8$) (Legend numbers are p - s , e.g., 30-4 corresponds to a simulation of $p=30\%$ with four PS locations.)

4.2 The effects of introducing congestion

The first and second charts in Figure 6 correspond to the default and congestion modes (policy 1), respectively. Both graphs indicate that the evacuation rates were improved with increased p . Higher evacuation rates are shown on the right-side chart compared to the corresponding rates on the left-side chart. This indicates that adaptive evacuation guidance improved the state of congestion, and consequently the evacuation rate.

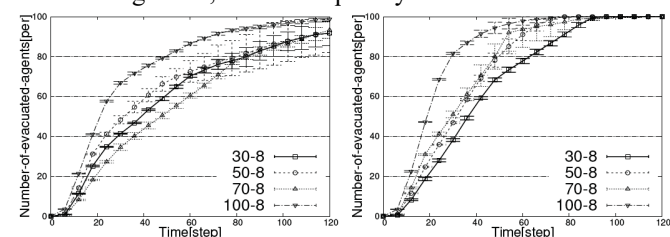


Figure 6. Improved evacuation rate ($n=4000$ and $s=8$)

4.3 Effects of congestion status detection

Figure 7 shows the results of comparing the two policies for $p = 70\%$. The first and second charts depict $n=4000$ and 10000 . The p1 graph in the first chart corresponds to the legend indicating 70-8 in the second chart of Figure 5. Policy 2 indicates better results as steps advance for both $n=4000$ and 10000 . This indicates that the ways of evacuation detection improves evacuation rates.

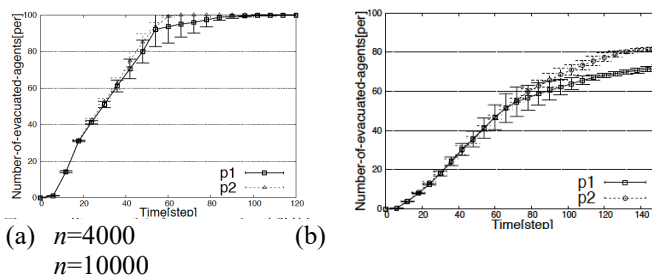


Fig. 7 Evacuation rate ($p=0.7$ and $s=8$). p1 and p2 in the legends correspond to policy1 and policy2, respectively.

5. Discussion and summary

Technological advancements influence how we access information and provide data. New media formats will affect human behavior during emergencies in ways that we can only assume at present. This means that there is little data to prove the effects of the new technology.

This study proposed a CCEG management system to prevent hazardous crowd situations. This system adopted the PS media format as a new disaster prevention method for future disasters. The effects of PS on evacuation rates were simulated through ABSS and disaster simulations should be designed to ascertain the behaviors of study targets in addition to the features of the field before the results are used during policy creation.

These simulations indicated that an increased number of signs prompted evacuations and that sign contents affected evacuation behaviors. Such validating approaches involving field simulations designed to study human behaviors will be important for assessing new disaster-prevention technologies.

6. Acknowledgements

The authors would like to thank Katsuki Ichinose for conducting the simulations. This work was supported by JSPS KAKENHI Grant Number 16K01291.

REFERENCES

- [1] C. Tunasar, "Analytics driven master planning for mecca: Increasing the capacity while maintaining the spiritual context of hajj pilgrimage". 2013 Winter Simulations Conference (WSC) (pp. 241-251). IEEE
- [2] Akashi City: Fire festival (in japanese), <http://www.city.akashi.lg.jp/anzen/anshin/bosai/kikikanri/jikochosa/index.html>
- [3] Tokyo Fire Department. Fire evacuation simulation at big terminal station (in japanese), <http://www.tfd.metro.tokyo.jp/hp-youbouka/fukugouterminalanzen/>
- [4] M. Okaya, T. Takahashi: Effect of guidance information and human relations among agents on crowd evacuation behavior, 6th International Conference on Pedestrian and Evacuation Dynamics Programme (PED2012).47-48, 2012, July
- [5] Averill, J. D., et.al. (2005). Occupant behavior, egress, and emergency communications (Draft). U.S. Department of Commerce, National Institute of Standards and Technology. Gaithersburg, MD: National Institute of Standards and Technology. Retrieved from https://ws680.nist.gov/publication/get_pdf.cfm?pub_id=909233
- [6] Cabinet Office Government of Japan. Prevention Disaster Conference, the Great West Japan Earthquake and Tsunami. Report on evacuation behavior of people. <http://www.bousai.go.jp/kaigirep/chousakai/tohokukyokun/7/index.html>

Virtual Reality approaches for evacuation simulation of various disasters

Naohiro Takeichi ¹, Takeshi Katagiri ², Harumi Yoneda ³, Shusaku Inoue ⁴,
Yusuke Shintani ⁵

¹ Advanced Design Department/Takenaka Corporation, Tokyo, Japan
takeichi.naohiro@takenaka.co.jp

^{2,3,4,5} Research and Development Institute/Takenaka Corporation, Chiba, Japan
katagiri.takeshi@takenaka.co.jp; nishimura.harumi@takenaka.co.jp; inoue.shuusaku@takenaka.co.jp;
shintani.yuusuke@takenaka.co.jp

Abstract - This paper presents a virtual reality (VR) system of evacuation in the cases of various disasters. We considered a combination of disasters under realistic scenarios. Disaster simulations by numerical models were imported into the VR system to express a realistic situation. Not only disaster experts but also designers and non-professionals are able to share realistic experiences for escape from the disasters. This system is useful for performance-based design, planning of escape, disaster prevention, evacuation drill etc. The VR system consists of Building Information Modelling, physical simulation models for disasters and human behaviour's simulation.

Keywords: virtual reality, multi-agent dynamics, performance-based design, serious gaming, CFD, BIM

1. Introduction

It is difficult for usual people to imagine real situations in buildings under disasters like earthquake, tsunami, storm tide, fire, etc. Because of that, they often delayed in starting evacuation in emergencies. For example, in case of tsunami after a big earthquake, people have to go to high ground or upper floors when they feel ground shaking. In other hand, people immediately move downstairs to go outside in case of fire. How to escape from disasters depends on types of them. Habitants and crowd handlers have to judge the best way to evacuate in an emergency. Planners, designers and engineers have to design buildings to support them. However those experts also lack knowledge and experience of the disasters.

To help them, various disasters simulations and their evacuation models have been developed so far. Although each single hazard or human behaviour have been studied, but simulations for complex of hazards and their evacuation are still insufficient to let designers imagine realistic situations. In actual disasters, several hazards happen in same time and people have to consider them.

To solve the problem, we have tried to integrate disasters and evacuation simulations, and visualize the results on single VR system, named "maXim". [1]

2. Contents of Virtual reality

Building data is based on Building Information Model (BIM). Modelling approaches of simulations are based on as below:

Human behaviour:	multi-agent dynamics
Seismic response:	real-time physical dynamics of gaming technology
Tsunami:	Flood dynamics by Navier-Stokes with Volume of Fluid Methods
Fire & smoke:	Computational Fluid Dynamics (CFD)

Under scenarios assuming disasters, hazards and human behaviours are simulated by each simulator and the logs of simulations are installed into the virtual space. The VR can be expressed by PC monitor, head mount display, and dome theatre. (Fig. 1.)

For convenience of the paper, only the outline of each simulation will be described.

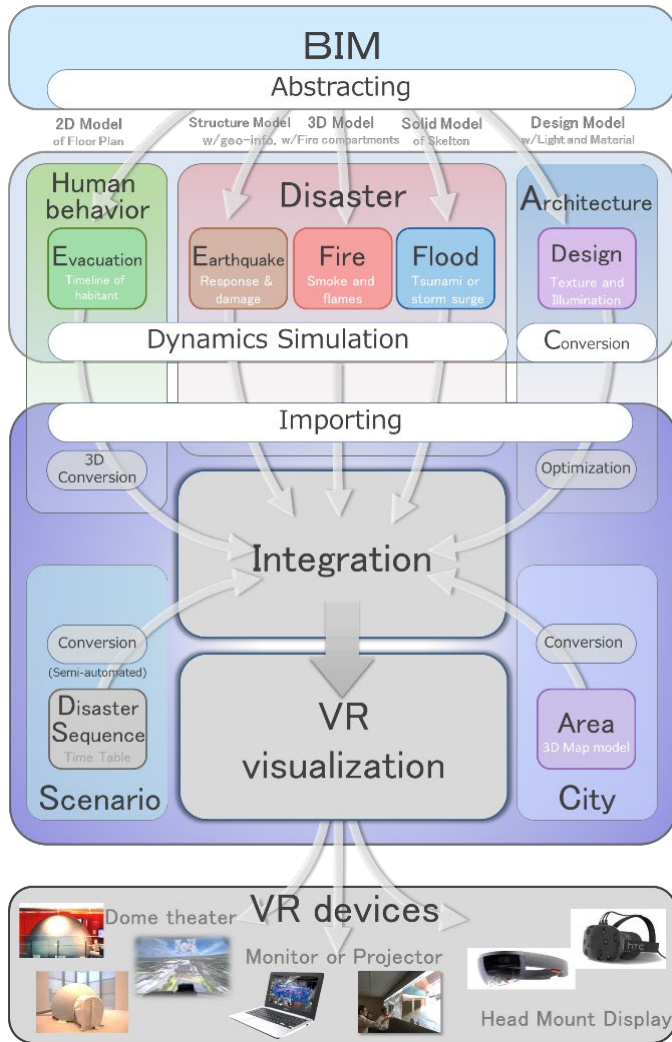


Fig.1. Frame of virtual reality under disasters



Fig. 2. Scene of evacuation in an office building.



Fig. 3. Virtual evacuation drill

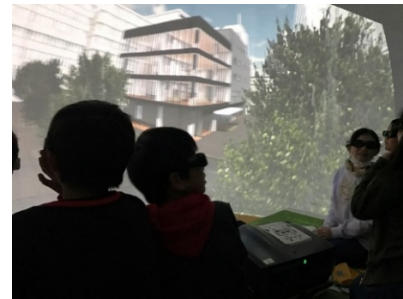


Fig. 4. Virtual reality in the dome theatre

2.1. Human behaviour – multi-agent simulation

Multi-agent simulation “SimTread” has been developed as a pedestrian simulation system following a straightforward, highly user-definable pedestrian and spatial model. Unlike network and mesh models, this pedestrian model is a multi-agent system, where an individual pedestrian is modelled as an agent, and the spatial model is based on actual coordinates; this enables the direct representation of plans.[2]

The crowd characteristics represented by this system have been evaluated through test cases by measuring the flow rate, a primary indicator of crowd evaluation [3][4].

2.2. Seismic response

The behaviours of furniture during earthquake are calculated with real-time physical dynamics of gaming technology by using physics engines named physX in Unity. Where, the floor response that is obtained by simulation with another structural model is imported.

We modelled furniture as rigid bodies attached colliders and joint constraints. We gave the values of weight and centre of mass and material properties such as coefficients of friction and bounciness to each model. Since material properties are given to each object not between the objects, the selection of the combine function affects simulation [5]. As physX is a commercial engine, the implementation details are unknown. We determined these values by reference to simulations and experiments that we conducted.

2.3. TSUNAMI - numerical methodology

Flow-3D is a general-purpose CFD package that is used to solve transient and three dimensional flow problems. It was developed by Flow Science, Inc., and has a comprehensive track record in CFD modelling. Though, the application in modelling tsunami on building is a new attempt. Flow-3D is developed based on the fractional volume of fluid (VOF) free surface tracking method. Under this method, cells are defined with a value between zero and one for empty to fully filled cells with fluid. For partially filled cells, the slope of the free surface is determined by an algorithm that uses the surrounding cells to define a surface angle and a surface location. This method allows the steep fluid slopes to be defined and it is applicable to describe the breaking wave in tsunami.

The model used in this research is an incompressible and viscous flow model. Flow-3D employs the finite difference method to solve the fluid equations of motion. The computational domain is defined in a fixed rectangular grid [6].

2.2. Fire & Smoke - FDS

Fire and smoke simulation was conducted by using Fire Dynamics Simulator (FDS) [7] developed by National Institute of Standards and Technology (NIST). FDS solves numerically a large eddy simulation form of the Navier-Stokes equations with an emphasis on smoke and heat transport from fires.

The 3D model of the rooms was imported from the BIM data automatically using third party pre-processing tool of FDS. The calculation conditions such as mesh, material properties, and boundary conditions etc. were set into the model. The fire source was also set in the model based on the fire scenario. The fire behaviour such as smoke movement and flame shapes were calculated. Virtual Reality System imported the calculation results such the temperature, the velocity, the transmission in each cell as at each time step.

3. Conclusions

The VR system can simulate earthquakes, tsunamis, fires and evacuation from them under realistic scenario by PC monitor, head mount display, and dome theatre.

Not only researchers and professionals, but also ordinary citizens without technical knowledge can experience virtual escape from the hazards that is useful for performance-based design, planning of escape, disaster prevention, evacuation drill etc. (Fig. 3, 4.)

References

- [1] Sample movies: <https://www.youtube.com/watch?v=Vm7rFCUCYuk>
<https://www.youtube.com/watch?v=iURFNcBbJy4>
- [2] T. Kimura, N. Takeichi, et al; Representing crowds using a multi-agent model-Development of the SimTread pedestrian simulation system, Japan Architectural Review, volume 2, pp.101-110, Jan. 2019
- [3] Tomonori Sano, Yoshiyuki Yoshida, Naohiro Takeichi, Takeshi Kimura, Yoshikazu Minegishi; Experimental Study of Crowd Flow Passing through Simple-shaped Room and Validation for an Evacuation Simulator, Pedestrian and Evacuation Dynamics 2011p.587 – 599, 2011
- [4] Akihide Jo, et al; Analysis of crowd flow capacity through a door connected to a crowded corridor., The Conference on Pedestrian and Evacuation Dynamics 2014 (PED2014), Transportation Research Procedia, vol.2, pp.10-18, 2014.10
- [5] Unity: Unity User Manual (2018.1)/ Physics/ 3D Physics Reference/ Physic Material/
<https://docs.unity3d.com/2018.1/Documentation/Manual/class-PhysicMaterial.html> (2018.5.17)
- [6] Shusaku Inoue and Yasunori Mizushima; Simulation of three-dimensional Tsunami inundation into the inside of a building, 10th International Conference on Urban Earthquake Engineering, March 1-2, 2013, Tokyo Institute of Technology, Tokyo, Japan
- [7] K. McGrattan, et al, Fire Dynamics Simulator Technical Reference Guide Volume 1: Mathematical Model, NIST Special Publication, 2017

Vulnerable People in Microscopic Evacuation Modelling

Rainer Könnecke¹, Volker Schneider²

^{1,2}IST GmbH

Feuerbachstraße 19, 60325 Frankfurt, Germany
r.koennecke@ist-net.de; v.schneider@ist-net.de

Abstract - Computational evacuation modelling as a part of approval procedures or design processes is sometimes concerned with vulnerable people requiring special attention. This vulnerability can be based on external circumstances or on individual characteristics. Microscopic methods are well suited to deal with such specific determinants by their ability to model individual movement and certain behavioural aspects. By reference to case studies the possibilities of up-to-date individual evacuation models to cover egress scenarios including vulnerable people are discussed. The selected examples demonstrate that the evacuation of vulnerable people often depends more on the modelling of individual behaviour rather than on a very detailed description of individual characteristics. Group formation and the guidance or assistance of other people will have a strong impact on the evacuation process and thus require special modelling techniques and respective calibration and validation efforts guided by empirical studies.

Keywords: mobility restrictions, microscopic modelling, vulnerable people, egress movement, guided evacuation

1. Introduction

Computational evacuation modelling as a part of approval procedures or design processes is sometimes concerned with vulnerable people requiring special attention. This vulnerability can be based on external circumstances, as in the first sample case, or on individual characteristics as presented in the second example. Both case studies include numerical simulations with the microscopic evacuation model ASERI [1] and [2]. For the second example, the results of the numerical simulations can be compared to corresponding empirical data.

2. Train Evacuation inside a Tunnel

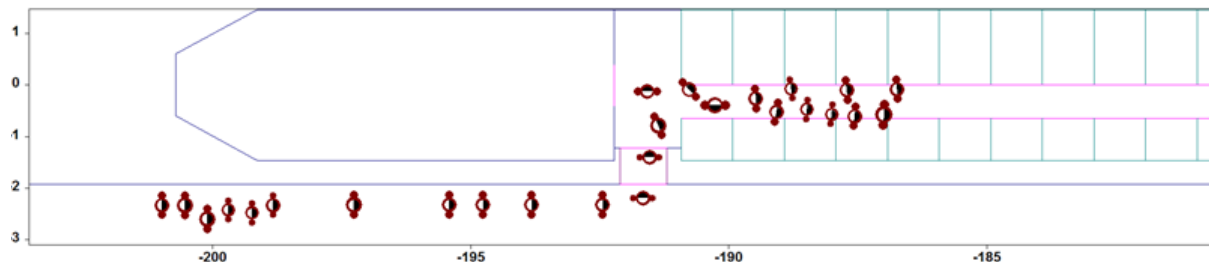


Fig. 1: Snapshots from an ASERI simulation for train evacuation inside a tunnel

This sample application of egress from a train refers to an unscheduled stop within a tunnel, requiring controlled evacuation of the coaches. The evacuation concept requires that only certain specified exits of the coaches are used for egress. Further limitations or prioritizations are posed by the cause of the evacuation, e.g. a fire inside a coach. The goal of such an egress study is the optimization of the details of

the evacuation procedure. Conductors are present at the coach exits to assist the evacuees. Furthermore, conductors will guide the passengers within the train to the available exits, thus establishing a controlled evacuation. A possible evacuation concept is based on a phased evacuation coach by coach. The passengers within one coach are guided by a conductor to the appropriate exit, while the other passengers are waiting until it is their turn to start egress guided by a conductor. The special features covered by the ASERI evacuation model are the phased evacuation of groups of passengers within the narrowness of the coaches and the process of exiting the coach inside a tunnel. The latter requires the negotiation of a considerable height from exit level to the tunnel surface. This requires empirical data to establish the order of magnitude of the exit flow and a sensitivity analysis to cover the uncertainties of the sparse empirical data available. Figure 1 shows a detail from such a train egress simulation.

3. School Evacuation including Wheelchair Users

Evacuation exercises performed at a German academic high school with focus on the vertical assisted movement of wheelchair users were investigated in [3]. Two scenarios were monitored: scenario 1 (reference scenario) consists of 49 pupils and 3 teachers without mobility restrictions, scenario 2 includes in addition two wheelchair users.

The exercises involved one staircase of the school connecting three classrooms from the upper storey to the foyer at ground level. The stair has two intermediate landings. There are two larger stairs (12 steps each) and one small stair to the foyer (4 steps). Step width is 29,5 cm, step height 17 cm. Stair width is 1,61 m with handrails reducing the width to 1,46 m.

Three exercises were performed for scenario 1 and four exercises for scenario 2. It was therefore not an unannounced evacuation drill. The occupants of the three classrooms were alarmed at the same time by portable radiophones. They were instructed to leave behind all bags and similar items and to egress at normal pace. The pupils that assisted the wheelchair users were not assigned in advance and thus were different for the individual exercises of scenario 2.

Table 1: Egress time for the evacuation exercises

scenario	exercise 1	exercise 2	exercise 3	exercise 4
1	79 s	73 s	74 s	
2	94 s	120 s	123 s	118 s

Table 1 lists the evacuation times from starting signal until the last pupil has reached the foyer. For scenario 1, a smooth flow was observed on the stairs (figure 2), resulting in egress times for the three exercises very close to each other. For scenario 2, there is a substantial difference between exercise 1 and the other three exercises. The shorter egress time of 94 s is explained by the fact, that in exercise 1 the wheelchairs were carried straight downstairs without any pausing on the landings. Whereas in the other exercises the wheelchairs were dropped on the landings and pushed to the next flight of stairs. In most cases (7 from 8) the wheelchairs were transported by three assistants – two in front and one behind (figure 3). In one case, four assistants did transport the wheelchair downstairs. In all exercises the wheelchair users left the classroom prior to the other pupils. The further movement of the wheelchair users did vary in the four exercises. In exercise 2-1, one wheelchair was transported first, then the main flow of pupils and the second wheelchair last. In the other three exercises both wheelchairs were transported after the main flow of pupils. For these cases the wheelchair users took waiting positions in the upper floor outside the classrooms.

Scenario 1 and 2 were also simulated using the microscopic evacuation model ASERI with its feature to model independent movement of wheelchair users and assisted vertical transport of wheelchairs [2]. The size of the wheelchairs had been derived from the actual wheelchair sizes used in the exercises. The results for scenario 1 (no reaction time) vary between 76 s and 81 s (10 runs), with smooth flow on the stairs as observed during the exercises. For scenario 2, the egress time varies between 94 s and 105 s (19 runs). The simulations for scenario two did not include explicit waiting positions for the wheelchair users and are thus representative for exercise 2-1. The

wheelchair users in the numerical simulation move towards the tread of stairs and are then immediately assisted by two helpers at the side of the wheelchair to assist vertical transport.

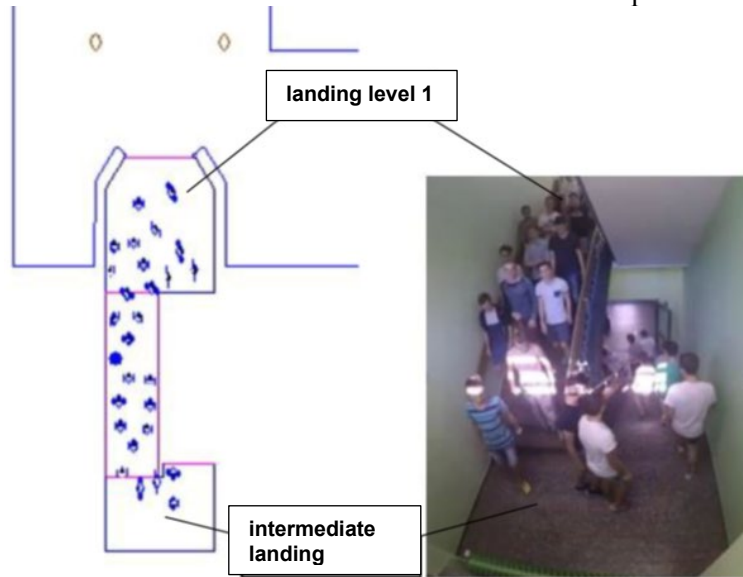


Fig. 2: Snapshots from exercise 1-3 (right) and corresponding ASERI simulation (left) - © J. Melles [3]



Fig. 3: Snapshot from exercise 2-3 - © J. Melles [3]

4. Conclusion

It is demonstrated that microscopic methods are well suited to deal with egress modelling of scenarios including vulnerable people. Example 1 shows the capability of the ASERI evacuation model to describe highly organized phased evacuation in constricted surroundings. The empirical data presented in the second case can be matched very well with the corresponding calculations.

Additional empirical data, including an evacuation drill in a large office building with vertical evacuation of wheelchair users with the help of evacuation chairs, will be used for further validation of the ASERI evacuation model with respect to the modelling of heterogeneous groups.

Acknowledgements

The authors wish to thank Julian Melles (IfB Ingenieurgesellschaft für Brandschutz mbH Bad Kreuznach) for his permission to include parts from his master thesis in this paper.

References

- [1] V. Schneider, “*Application of the individual-based evacuation model ASERI in designing safety concepts*” in *Proceedings of the 2nd Int. Symp. on Human Behaviour in Fire*, Boston, March 2001.
- [2] V. Schneider and R. Könnecke, “*Occupants with mobility impairments and social groups in design calculations*” in *6th Int. Symp. on Human Behaviour in Fire*, Cambridge, September 2015.
- [3] J. Melles, “*Datenerfassung für die Entfluchtungssimulation für mobilitätseingeschränkte Personen mittels Ingenieurmethoden im Brandschutz*,” Master Thesis Hochschule Darmstadt, 29.09.2017.

Organization

CONFERENCE CHAIR:

Anne Dederichs (RISE Research Institutes of Sweden, Technical University of Denmark)

ORGANIZING COMMITTEE:

Anne Dederichs (RISE Research Institutes of Sweden, Technical University of Denmark)

Åse Svensson (Lund University)

Lena Hiselius (Lund University)

Fredrik Rosén (RISE Research Institutes of Sweden)

Kaisa Kaukoranta (RISE Research Institutes of Sweden)

SCIENTIFIC COMMITTEE:

Steve Gwynne (National Research Council, Canada, Ottawa)

Erica Kuligowski (NITST)

Guy Theraulaz (University Toulouse)

Paola Goatin (INRIA, France)

Aoife Hunt (Movement Strategies, UK)

Daniel R. Parisi (Buenos Aires Institute of Technology, Argentina)

Amir Sobhani (ARRB Group, Australia)

Keith Still (Manchester Metropolitan University, United Kingdom)

Guy Théraulaz (University of Toulouse, France)

Iker Zuriguel (Universidad de Navarra, Pamplona, Spain)

Ai Sekizawa, Japan

Tomonori Sano, Japan

Bryan Hoskins, USA

Cecile Appert-Rolland, France

Jean Michel Auberlet, France

Stefania Bandini, Italy

Nikolai Bode, UK

Henrique Braga, Brazil

Tao Chen, China

Mohcine Chraïbi, Germany

Arturo Cuesta

Winnie Daamen, Netherlands

Maria Davidich, Germany

Serge Hoogendoorn, Netherlands

Anders Johansson, UK

Gerta Köster, Germany

Tobias Kretz, Germany

Laura Künzer, Germany

Jian Ma, China

Katsuhiko Nishinari, Japan

Majid Sarvi, Australia

Andreas Schadschneider, Germany

Armin Seyfried, Germany

Weiguo Song, China
Paul Townsend, UK
Giuseppe Vizzari, Italy
Jaroslaw Was, Poland
Kwok Kit Richard YUEN, China
Jun Zhang, Germany
Aldis Larusdottir, Iceland
Rita Fahy, USA
Poul Hjorth, Denmark
Peter Thompson, UK

EDITORS:

Anne Dederichs
Andreas Schadschneider
Gerta Köster

STEERING COMMITTEE:

Armin Seyfried
Winnie Daamen
Weiguo Song
Andreas Schadschneider



Organised by

RISE Research Institutes of Sweden
2018 | P O Box 857 | SE-501 15 Borås | SWEDEN
<https://www.conferencemanager.dk/ped2018>